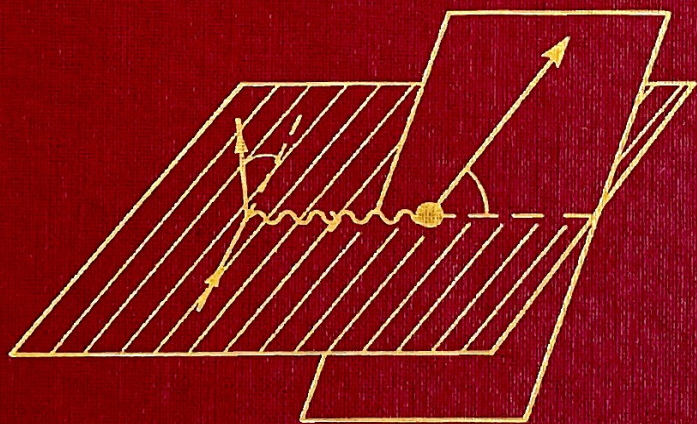


THEORETICAL NUCLEAR PHYSICS

Nuclear Reactions



Herman Feshbach

BIBLIOTHÈQUE EPFL LIBRARY
ÉLIMINÉ DISCARD

THEORETICAL NUCLEAR PHYSICS

2000

THEORETICAL NUCLEAR PHYSICS

Nuclear Reactions

HERMAN FESHBACH

Massachusetts Institute of Technology
Cambridge, Massachusetts



A Wiley-Interscience Publication

JOHN WILEY & SONS, INC.

New York / Chichester / Brisbane / Toronto / Singapore

BIBLIOTHÈQUE
ÉLIMINÉ
EPFL LIBRARY
DISCARD

2A.103²

104392

BIBLIOTHÈQUE
BÂTIMENT DES SCIENCES PHYSIQUES
Université de Lausanne

In recognition of the importance of preserving what has been written, it is a policy of John Wiley & Sons, Inc., to have books of enduring value published in the United States printed on acid-free paper, and we exert our best efforts to that end.

Copyright © 1992 by John Wiley & Sons, Inc.

All rights reserved. Published simultaneously in Canada.

Reproduction or translation of any part of this work beyond that permitted by Section 107 or 108 of the 1976 United States Copyright Act without the permission of the copyright owner is unlawful. Requests for permission or further information should be addressed to the Permissions Department, John Wiley & Sons, Inc.

Library of Congress Cataloging in Publication Data:

Feshbach, Herman.

Theoretical nuclear physics : nuclear reactions / Herman Feshbach.
p. cm.

“A Wiley-Interscience publication.”

Includes bibliographical references and index.

ISBN 0-471-05750-9

1. Nuclear reactions. 2. Scattering (Physics) I. Title.

QC794.F43 1991

539.7'5—dc20

91-4668

CIP

Printed in the United States of America

10 9 8 7 6 5 4 3 2 1

Printed and bound by Courier Companies, Inc.

To Amos de Shalit, Friend and Colleague

CONTENTS

PREFACE	xi
----------------	-----------

I INTRODUCTORY REVIEW	1
------------------------------	----------

1. Introduction / 1
2. Nomenclature and Elementary Kinematics / 6
3. Classification of Reactions / 10
4. Direct and Compound Nuclear Reactions / 22
5. Multistep Direct Reactions / 29
6. Statistical Doorway State Reactions / 34
7. Statistical Theory of Multistep Direct and Multistep Compound Reactions / 39
8. Direct Nuclear Reactions and Specificity / 40
9. Reactions with "Exotic" Projectiles / 58
10. Specificity and Symmetry / 61
11. Densities, Correlations, and the Direct Reactions / 67

II MULTIPLE SCATTERING	74
-------------------------------	-----------

1. Introduction / 74
2. Qualitative Results / 77
3. Optical Model Potential / 84
4. Formal Theory of Multiple Scattering / 90
5. The Semiclassical Approximation / 103
6. Center-of-Mass and Pauli-Principle Correlations, Fermi Motion / 121
7. Some Kinematics / 125

8. An Example: Proton–Nucleus Scattering / 132
- Appendix A / 142
- Appendix B: Correlations / 145

III FORMAL THEORY OF NUCLEAR REACTIONS **149**

1. Introduction / 149
2. Formal Theory / 157
3. Derivation of the Optical Model Potential / 172
4. Intermediate Structure, Doorway State Resonances, and Giant Resonances / 179
5. Projection Operators and Antisymmetrization / 195
6. Alternative Reaction Formalisms / 209
7. Summary / 225
- Appendix. The Boundary Condition Model for Nuclear Reactions / 226

IV RESONANCE AND THE STATISTICAL THEORY OF NUCLEAR REACTIONS **231**

1. Introduction / 231
2. Isolated Resonances; Interference with the Prompt Amplitude / 234
3. Properties of the Widths, Threshold Behavior of Cross Sections, Cusps / 242
4. Overlapping Resonances / 248
5. Level Density / 260
6. Spacing of Energy Levels; Width Distributions / 286
7. Statistical Theory of Nuclear Reactions / 296
8. Effect of the Direct Reactions on the Statistical Theory / 314
9. Applications of the Statistical Theory / 321

V ELASTIC AND INELASTIC SCATTERING **333**

1. Introduction / 333
2. The Single-Channel Optical Model / 336
3. Charge Exchange Reactions: Optical Model Description / 396
4. Inelastic Scattering / 407
5. The Interaction Potentials / 436
6. Comparison with Experiment / 445

VI TRANSFER REACTIONS **455**

1. Introduction / 455
2. The DWA Amplitude / 463
3. Applications / 475
4. The Deuteron–Nucleus Interaction / 488
5. Overlap Wave Function / 492
6. Three-Body Model / 494

VII MULTISTEP REACTIONS	505
1. Introduction / 505	
2. Coupled Channels and Higher-Order DWA / 509	
3. Applications / 517	
4. Coupled-Channel Born Approximation (CCBA) and Transfer Reactions / 522	
5. Statistical Direct and Compound Multistep Reactions / 524	
6. Applications / 541	
7. Summary / 551	
Appendix / 552	
VIII HEAVY IONS	554
1. Introduction / 554	
2. Fusion / 570	
3. Deep Inelastic Scattering / 588	
4. Quasi-Elastic Scattering / 602	
5. Heavy-Ion Resonances / 613	
6. Diffusion Theory / 633	
7. The Lorentz, Boltzman, Uhlenbeck, and Uehling (LBUU) Method / 644	
8. The Time-Dependent Hartree-Fock Method / 658	
IX HIGH-ENERGY NUCLEAR PHENOMENA	679
1. Introduction / 679	
2. Electron Scattering / 684	
3. Medium-Energy Proton-Nucleus Scattering / 740	
4. Proton ^4He Elastic Scattering and the Effect of Isobar Excitation / 755	
5. Reactions Induced by Medium-Energy Protons / 757	
6. The $(p, 2p)$ Reaction / 764	
7. Relativistic Heavy Ions / 767	
8. Collisions at Ultrarelativistic Energies / 787	
X PION AND KAON INTERACTIONS WITH NUCLEI	803
1. Introduction / 803	
2. Pion-Nucleon System / 806	
3. Pion-Nucleus Scattering / 818	
4. Kaon-Nucleus Interaction / 859	
APPENDIX A SCATTERING THEORY	906
APPENDIX B CROSS SECTIONS; VECTOR AND TENSOR POLARIZATIONS	917
BIBLIOGRAPHY	922
INDEX	951

PREFACE

The development of the experimental and theoretical understanding of nuclear reactions is one of the more important achievements in physics during the last half of this century. It is an achievement which has been largely unrecognized or celebrated, even by the nuclear physicists themselves. It was accomplished without detailed knowledge of the underlying governing nuclear forces. Nevertheless, through ingenious use of physical principles and analogies and through the synergism of experiment and theory, a coherent and powerful methodology has evolved, one capable of interpreting the wide range of experimental nuclear studies and providing at the same time insights into the nature of the nuclear Hamiltonian. We have learned to distinguish and treat various types of reactions. We have learned how a reaction proceeds, which reactions and projectiles are most suitable for probing the structure of the nucleus, how the various degrees of freedom of nuclear systems such as the giant resonances manifest themselves in reactions, what the influence the Pauli principle is, when statistical methods are applicable touching in this way on nonequilibrium statistical mechanics, and so on. The power of these procedures is revealed when new areas of interest come under study, for one finds that one can apply them, adjusted for the new circumstances and in a suitable range of kinematic parameters, to obtain a quantitative understanding. This is not meant to imply that the theory is complete. As nuclear physicists become involved with quark-gluon degrees of freedom, new procedures, which may or may not be generalizations, may be required. The incorporation of relativity and of quantum fields form major challenges. But we do have a firm, well-understood base from which to begin.

These results are not of value only for nuclear collisions. They are valid and

have been applied to collisions between atoms, between molecules, and to collisions of these systems with electrons and photons. Some have recently become of interest to students of mesoscopic systems. It is this universal applicability which gives nuclear reactions its seminal importance.

Following the introductory Chapter I, Chapters II and III (Multiple Scattering and the Formal Theory of Nuclear Reactions) set the stage for the applications which follow. These two chapters provide the theoretical foundation which in the subsequent chapters is generalized and approximated as needed. Chapter IV (Compound Nuclear Resonances) deals with reactions involving long interaction times, while Chapter V and Chapter VI consider the limiting short interaction time reactions as seen in elastic and inelastic scattering and in particle and cluster transfer. In Chapter IV statistical approximations are introduced, while in Chapter V and Chapter VI the optical model and single-step direct reactions play dominant roles. Reactions involving interaction times which are intermediate, neither so long as those which prevail in the resonance region nor so short as implied by the single-step direct interactions, are considered in Chapter VII. This chapter is concerned with coupled equations and the statistical multistep compound and direct theories, which can be thought of as an approximate way of solving systems of many coupled equations. Chapters II through VII provide a formalism, together with examples, which enables one in principle to deal with most nonrelativistic reactions. This account of course reflects my own personal point of view and experience.

Chapters VIII through X differ in character from the earlier chapters in that they deal with subjects rather than with reaction types. Examples of the use of the analysis of the preceding chapters and generalizations thereof, as well as in some cases special methods which have been proved to be of value, are described. Chapter VIII considers heavy-ion reactions, Chapter IX reactions with high energy projectiles including electrons, nucleons, and heavy ions briefly, and Chapter X the interaction of pions and kaons with nuclei.

It is not possible to be complete or up to date. After all, the *Treatise on Heavy Ion Science*, edited by D. A. Bromley, consists of four large volumes and even it is not complete. A selection had to be made. In each case I try to present an overview of the subject together with a number of topics which I think are important and which in addition illustrate concepts and methods described in the earlier chapters. It is my hope that this will make the current literature and review articles accessible to the reader.

I have assumed a good understanding of nonrelativistic quantum mechanics, especially of scattering theory. A summary of that theory is presented in an appendix. The appendix also contains a general formalism for polarization phenomena. In the main body of the book only the polarization variables which occur in the scattering of spin-1/2 particles by spin-zero systems are discussed in detail.

The reader will find many references to the book with de Shalit entitled *Theoretical Nuclear Physics: Nuclear Structure*. That book has been reissued (with some major errors removed) in a paperback edition in the Wiley Classics Library (1990).

No attempt has been made to determine priorities. In view of the enormous relevant literature this just by itself would be a major project. The bibliography contains references to publications which I found useful and to papers referred to in the text. At the beginning of most sections I have listed the principal references I have consulted and/or review papers which provide a more detailed discussion of the subject of the section.

A number of people have been of great help to me. I particularly want to thank Viki Weisskopf, a dear friend and teacher, for his inspiring example and for the many years we have spent together discussing physics and plotting to do our share in improving the human condition: Peace rather than war, mutual respect rather than bigoted hostility. I owe much to Arthur Kerman with whom I collaborated on several papers on nuclear reactions. I want to thank my friends who took time out from their busy lives to read and comment on most of this volume: A. Gal, read Chapters I to IV; M. Baranger, Chapter IV; Norman Austern, Chapters VI to VIII; A. Molinari, Chapter IX; and F. Lenz, Chapter X. T. Matsui read the sections in Chapter IX on high energy heavy-ion reactions. I am grateful to E. Moniz for supplying me with a preliminary version of his review article on pion physics with F. Lenz, to L. Ray for his advice on the proton–nucleus discussion in Chapter IX, and to J. Negele for several helpful suggestions. The supportive atmosphere of the MIT Center for Theoretical Physics, the friendship I have enjoyed with its faculty for many years, and the wide range of available expertise within the group and in the MIT Department have been of inestimable value as I pursued the writing of this book for more than a decade while undertaking and carrying out many other responsibilities. Roger Gilson helped to prepare most of the manuscript for publication. I am indebted to him for his thoughtful and expert assistance.

Most importantly I want to thank my wife, Sylvia, who for more than fifty years has been my companion and friend. Her understanding and encouragement were essential ingredients in executing and completing this project.

THEORETICAL NUCLEAR PHYSICS

CHAPTER I

INTRODUCTORY REVIEW

1. INTRODUCTION

Nuclear reactions present an extraordinarily rich and diverse set of phenomena. They are the principal source of information regarding nuclear systems. Their discovery and investigation are made possible because of the large number of projectiles available, each of which can interact with nearly all the stable nuclei, because of the precision with which the energy and general quality of the projectile beams can be controlled, because of the sensitivity of the detectors, and because of the theoretical framework available for the analysis of the data obtained.

A list of elementary particles most of which can and have served as projectiles is given in Table I.10.1 in deShalit and Feshbach (74). The strongly interacting projectiles of interest include the elementary bosons, such as the pion and kaon; the elementary baryons, such as the nucleons; the antiprotons and strange baryons; and an expanding number of the atomic nuclei, ranging from the deuteron to uranium. Clearly, these projectiles provide a wide range in mass, charge, isospin, strangeness and internal structure. Electromagnetic probes include γ -rays and charged particles such as the electron, the muon, the α -particle, and heavy ions—to mention those that have been used for this purpose. Reactions in which electron or muon neutrinos (or antineutrinos) are projectiles or are produced are used to study the effects of the weak interactions. These interactions are also responsible for symmetry violations, which are investigated by means of reactions sensitive to parity conservation or time-reversal invariance.

In most cases the projectiles are stable or have a relatively long life. The question arises: Can the interactions of very unstable particles whose lifetimes

are very short, such as the π^0 ($\tau \sim 0.83 \times 10^{-16}$ s), the ρ ($\tau \sim 4.3 \times 10^{-24}$ s), or the Δ ($\tau \sim 5.7 \times 10^{-24}$ s), be studied? The distances these particles travel before decay is far too small for it to be possible to prepare a beam. The distance between the source and the target is, under ordinary circumstances, far too large. However, this distance can be reduced if the source is inside the target for π^0 or inside a nucleus for the ρ meson or the Δ . In the first case, the π^0 can travel a distance on the order of the interatomic distances in matter before decaying. In the second, the ρ (or Δ) produced by the interaction of an energetic particle with a nucleon inside a target nucleus will live long enough to interact with a neighboring nucleon and thus permit a measure of the ρ -nucleon cross section.

An important measure of the quality of an experimental arrangement is the energy resolution that can be obtained. The first excited state of nuclei varies in energy above the ground state from a few MeV in light nuclei to a few tens of keV in rotational nuclei. These energy spacings decrease as one goes to higher excitation energies. As one can see from compound nuclear resonances observed with neutrons, near the separation energy the spacing is on the order of eV. To investigate reactions in which only a particular state of the final residual nuclei is excited, it is necessary to have a sufficiently good energy resolution, $\Delta E/E$, where ΔE is the effective uncertainty in our knowledge of the value of the energy. To observe states that are separated by the order of 10 keV, the value of $\Delta E/E$ for, say, a 10-MeV beam energy is on the order of 10^{-3} , while for 100 MeV it is 10^{-4} and for 1 GeV it is 10^{-5} . Eventually, as the level spacing becomes too small, it becomes impossible to resolve levels and one obtains cross sections that are averages over a number of levels.

Energy resolution is also required to observe resonances and other structure in the energy dependence of the cross section. Clearly, their unambiguous identification and their investigation become possible only if ΔE is less than the width of the resonance or, more generally, less than the range in energy over which interesting structure is present.

Energy resolution on the order of several parts in 10^5 has been achieved with primary beams of charged particles produced directly by accelerators. In Fig. 1.1 an extreme example is shown, demonstrating resolution on the order of 100 eV achieved for proton beams of about 2 MeV. Figure 1.2 illustrates an example of a similar resolution achieved with high-energy electron beams. Energy resolution of secondary beams of particles, such as neutrons, pions, and γ -rays, produced when a primary charged particle beam collides with nuclei, is steadily improving. The development of semiconductor detectors such as lithium-drifted germanium has been particularly useful for γ -ray detection (Fig. 1.3), while the development of electronics capable of picosecond timing has been of great value for the determination of neutron energies by the time-of-flight method. Better secondary beams and better precision can be obtained as well by increasing the intensity of the primary beam. Some facilities of this type have recently been built.

These improvements in the control of projectile beams and the detection of

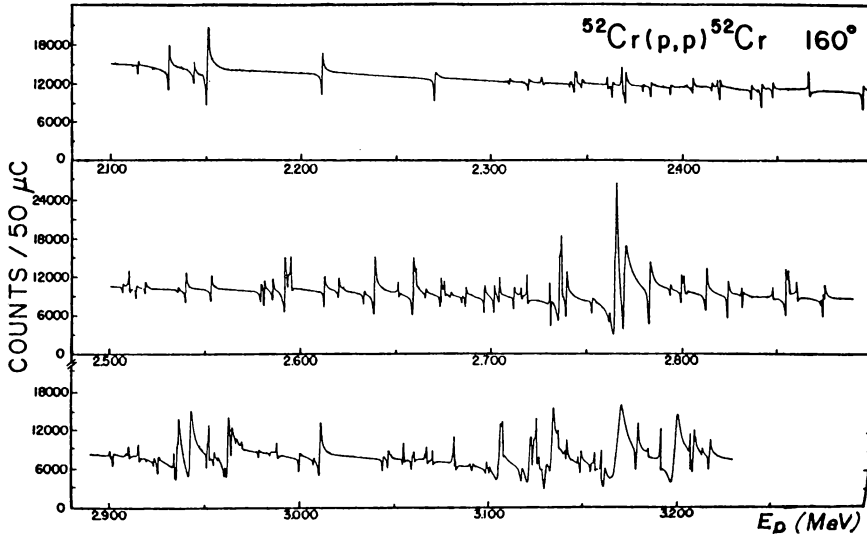


FIG. 1.1. High-energy resolution ($\Delta E \sim 100 \text{ eV}$) achieved for proton beams for proton energies of a few MeV. [From Moses, Newson, et al. (71).]

reaction products make possible the discovery of relatively rare phenomena such as narrow isobaric analog resonance, observation of the structure of the broad giant electric dipole resonance (Fig. 1.4), and elucidation of nuclear structure as exemplified by the study of nuclei in the lead region, to cite a few examples.

A large variation in the energy of the projectiles, which has been substantially expanded in recent years, is possible, permitting the study of nuclear reactions under a variety of kinematic circumstances. For the most part (there are a few exceptions) the energies of projectiles employed have been less than a few GeV, although beams of nuclei with energies of 200 GeV per nucleon have recently become available.

Perhaps the most important insight to be gained from this discussion of the capabilities presently available to experimental nuclear physics is that they make it possible to conduct a systematic study of an entire class of phenomena, observing its dependence on the Z and A values and the structure of the target nucleus; the properties of the projectile, including its charge, mass, isospin, hypercharge, and structure; and on the projectile energy. Such multipronged investigations are necessary in strong interaction physics to unravel the various structural and dynamical elements determining the course of a reaction.

Nuclear theory plays an important role in this process. Its principal achievement in this regard has been to furnish a framework permitting a dynamical interpretation of the experimental data and the extraction of nuclear structure information. Calculations to predict nuclear reactions, based directly

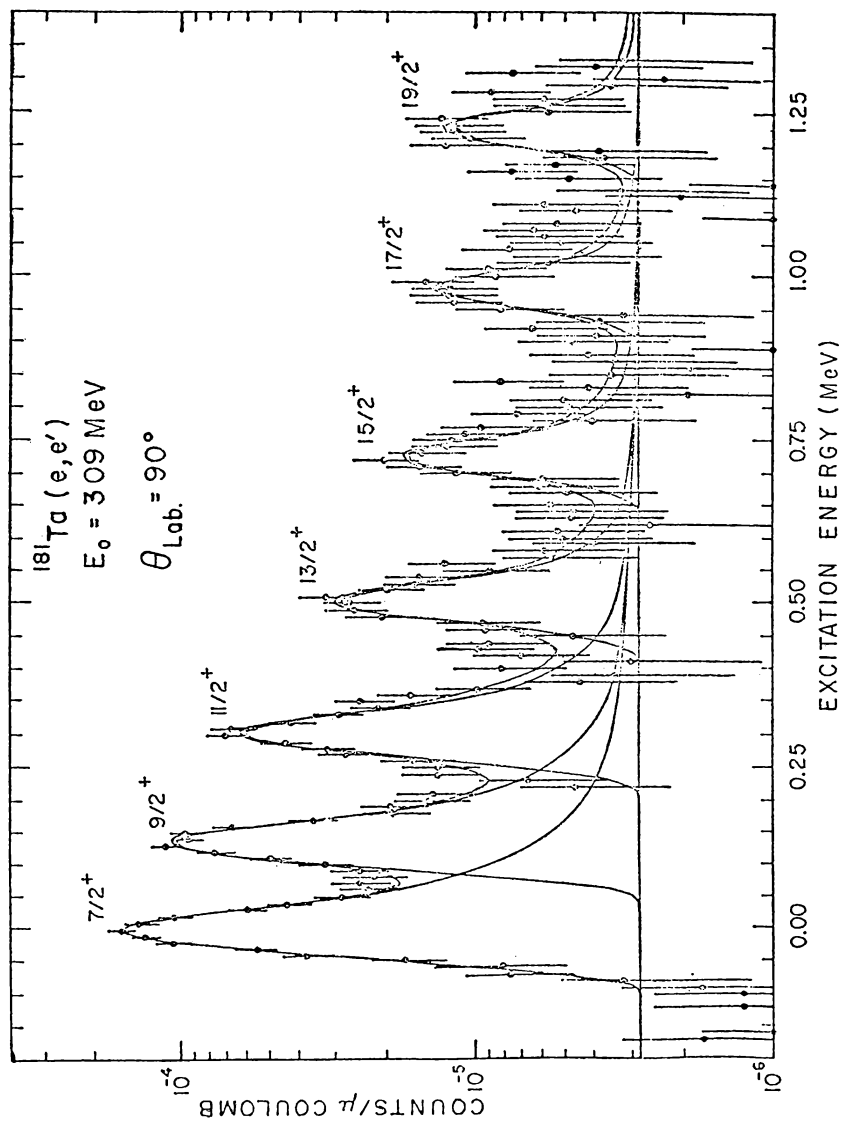


FIG. 1.2. High-energy resolution achieved with electron beams. [From Bertozzi (82).]

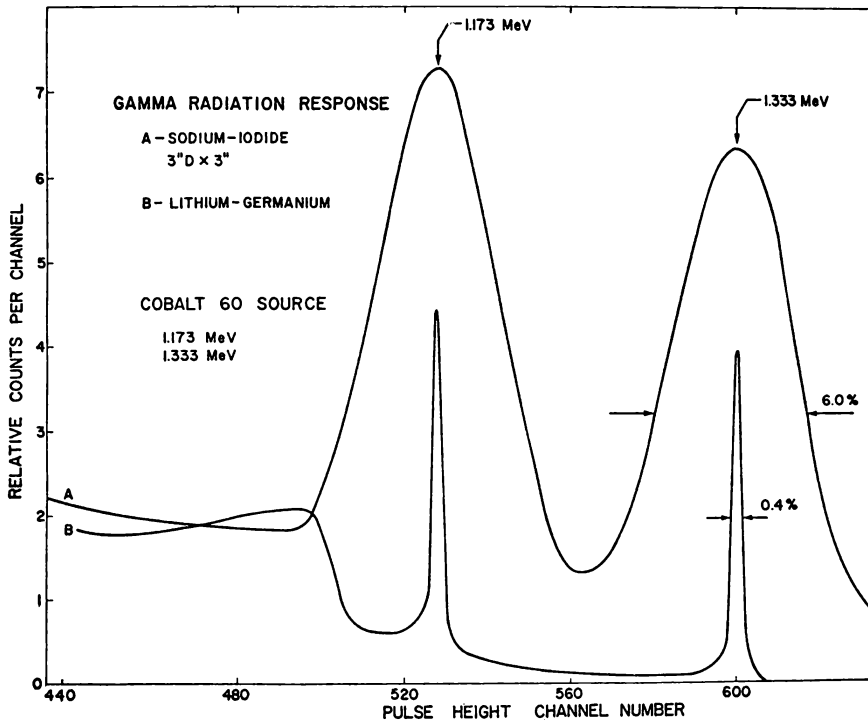


FIG. 1.3. Gamma-ray energy resolution obtained with (A) a sodium iodide detector and (B) a lithium-germanium detector. [(From Bromley).]

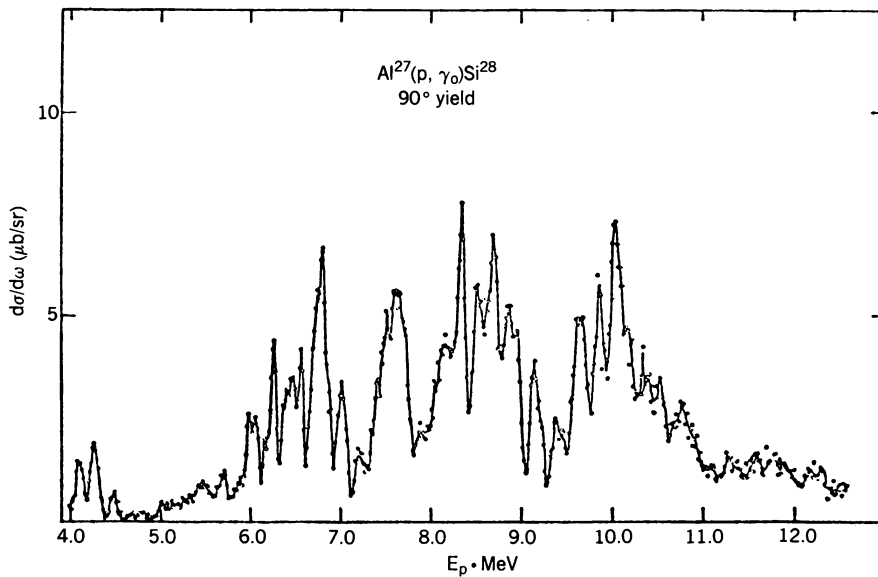


FIG. 1.4. Giant resonance structure. [(From Singh, Segel, et al. (1965).)]

on the underlying nucleon–nucleon forces, called the microscopic theory, have been rather few. However, as our understanding of the many-body problem grows, it may be expected that the methods used to predict the properties of nuclear matter and the low-lying states of finite nuclei will be extended to the “many-body problem in the continuum,” which is just another way of describing nuclear reactions.

2. NOMENCLATURE AND ELEMENTARY KINEMATICS

Nuclear reactions involve the collision of an *incident projectile* with a *target nucleus*. As a consequence, the *initial system* is transformed into the *final system*, consisting of the *products of the reaction*. Symbolically,

$$a + X \rightarrow Y + b + c + \dots \quad (2.1)$$

where a is the incident projectile, X the target nucleus, and Y the *residual nucleus*. A more succinct notation is often used: $X(a, bc, \dots)Y$. The initial system is typically a two-body system. The target nucleus is in its ground state, while the incident projectile is generally stable or sufficiently long-lived. The final system may consist of several particles, so that one speaks of two-body, $X(a, b)Y$; three-body, $X(a, bc)Y$; and so on, final states. The residual nucleus or any of the emergent particles may be in its ground state, or it may be excited. The latter condition will be indicated by an asterisk.

The words *initial* and *final* describe the system when its constituents are spatially separated and noninteracting. The interacting system is referred to as the *compound system*. When the initial system is brought together so as to be interactive, it forms the compound system, which eventually comes apart into various possible final states. When a compound system lives a sufficiently long time so that it has well-defined quantum numbers such as energy, angular momentum, parity, and so on, the compound system is referred to as the *compound nucleus* and the corresponding long-lived state as the *compound nuclear state*.

In describing these reactions several conservation principles are employed. *Conservation of charge* and *baryon number* are directly applicable to the reaction equation, (2.1). The value of the total charge and the baryon number in the final state must equal their values in the initial state. The baryon number B is defined by the equation

$$B = A - \bar{A} \quad (2.2)$$

where A represents the number of baryons and \bar{A} is the number of antibaryons. *Conservation of nucleons* is the special case of conservation of baryons appropriate for most nuclear reactions which do not usually involve strange particles or antibaryons. Generally, the baryon number and charge are known

for the initial system. Under these circumstances, observation of these numbers for a part of the final system (e.g., the emergent particles) immediately determines their values for the remainder of the system (e.g., the residual nucleus).

Conservation of charge and baryon number are considered absolute conservation principles, as indicated by the very long bounds to the lifetimes of the electron and proton. Moreover, the magnitudes of the charge of the electron and the proton are known to be equal to a very high accuracy. Other conservation rules are not as strongly obeyed. As has already been discussed in deShalit and Feshbach (74), because of the action of the electromagnetic field, isospin is not conserved. Hypercharge is not conserved in the weak interactions that induce the decay of strange particles, such as

$$\Lambda^0 \rightarrow p + \pi^-$$

However, it does appear to be conserved in the strong interactions. Violation of the *conservation of lepton number* [see deShalit and Feshbach (74), Chapter IX] has not been observed (e.g., the $\mu \rightarrow e + \gamma$ reaction has not been seen), but it is not as firmly established as the conservation of baryon number and charge.

Space-time symmetries and their corresponding conservation principles must also be preserved in nuclear reactions. Linear and angular momentum as well as energy are conserved. Parity is conserved and time-reversal invariance is valid for both the strong and electromagnetic interactions, which play the principal roles in nuclear reactions. The weak interactions, which lead to parity nonconservation in the hadron-hadron interaction [see deShalit and Feshbach (74), Chapter IX], or the neutral current of the Salam-Weinberg standard model, which leads to weak parity conservation violations in the electromagnetic interaction, have very little effect on nuclear reactions. Unless we are specifically investigating the weak interactions, there is no need to consider their effects.

There are some simple consequences of these invariance principles that it will be convenient to develop now. In most circumstances the target nucleus is stationary.[‡] The colliding beams experiment, for which both the *target* and *projectile* are moving, is an exception. But so far this device has been used only for proton-proton, proton-antiproton, and electron-positron collisions. One can expect that heavy-ion colliding beams will become available in the future. The reference frame in which the target nucleus is at rest is referred to as the *laboratory frame*. Quantities associated with it will be designated by a subscript *L*.

From conservation of momentum we know that in the absence of any external forces the total momentum of the system is unchanged during collision and that its center of mass moves with a constant velocity. It is therefore convenient to use a uniformly moving coordinate system in which the center of mass is at rest. The position of the center of mass **R** with respect to an arbitrary reference

[‡]The target is, in fact, not at rest because of thermal motion. This is of importance for reactions induced by slow neutrons.

frame for a projectile of mass m and velocity \mathbf{v}_1 striking a target of mass M and velocity \mathbf{v}_2 is given nonrelativistically by

$$\mathbf{R} = \frac{m\mathbf{r}_1 + M\mathbf{r}_2}{m + M}$$

where \mathbf{r}_1 and \mathbf{r}_2 are the positions of the projectile and the target, respectively, with reference to some fixed origin. The velocity of the center of mass is

$$\mathbf{V} = \frac{m\mathbf{v}_1 + M\mathbf{v}_2}{m + M}$$

In the laboratory frame of reference ($v_2 = 0$)

$$\mathbf{V}_L = \frac{m\mathbf{v}_1}{m + M} = \frac{\mathbf{p}_L}{m + M} \quad (2.3)$$

where \mathbf{p}_L is the momentum of the projectile. In the center-of-mass frame, $\mathbf{V} = 0$, so that $\mathbf{p}_1 = -\mathbf{p}_2$. Thus the center-of-mass frame can be referred to as a *zero-momentum frame*. The relations between the momentum and energy in the two frames, laboratory and zero-momentum, are needed. The two physical situations are compared in Fig. 2.1. In the figure, p is the common magnitude of \mathbf{p}_1 and \mathbf{p}_2 . The center-of-mass frame is moving to the right with the velocity \mathbf{V}_L . Hence

$$\mathbf{p}_L = \mathbf{p} + m\mathbf{V}_L$$

or using (2.3),

$$\mathbf{p} = \frac{M}{m + M} \mathbf{p}_L \quad (2.4)$$

Thus the kinetic energy in the center-of-mass frame, E , and the kinetic energy

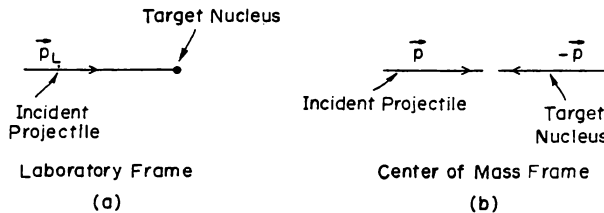


FIG. 2.1

in the laboratory frame, E_L , are related by

$$E = \frac{M}{m + M} E_L \quad (2.5)$$

Finally,

$$E = \frac{1}{2\mu} p^2 \quad (2.6)$$

where μ is the reduced mass:

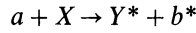
$$\mu = \frac{Mm}{M + m}$$

The energy of the center of mass in the laboratory frame,

$$E_{cm} = \frac{m}{m + M} E_L$$

remains constant and is thus not available for the reaction.

The final and initial systems are related by the conservation principles. It is most useful at this point to discuss some of the consequences of the conservation of momentum and energy for two-body final states as illustrated in Fig. 2.2. The reaction is



where the asterisks indicate the possibility that the residual nucleus, Y , and the emergent particle, b , might be excited. In the center-of-mass frame, the energy

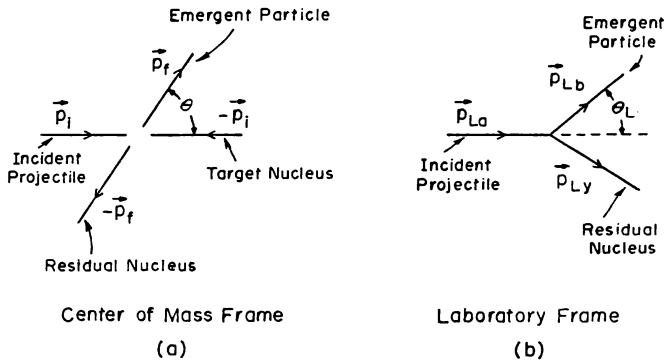


FIG. 2.2

of the initial system is, in the nonrelativistic limit, $(m_a + m_x)c^2 + T_i$, where the first two terms give the rest energy and T_i is the kinetic energy (2.6), with the momentum \mathbf{p} equal to the initial momentum \mathbf{p}_i . The energy of the final system is, similarly,

$$(m_b + m_Y)c^2 + \varepsilon_b + \varepsilon_Y + T_f$$

where ε_b and ε_Y are the excitation energies of the particle b and nucleus Y , respectively. The value of the momentum p_f can be obtained from T_f using (2.6). Conservation of energy requires that the energies of the initial and final systems be equal. Hence

$$T_f - T_i \equiv Q_{fi} = (m_x + m_a - m_Y - m_b)c^2 - \varepsilon_b - \varepsilon_Y \quad (2.7)$$

where Q_{fi} , referred to as the *Q value*, gives the kinetic energy *released* by the reaction. If Q_{fi} is positive, the reaction will proceed even if T_i , the initial kinetic energy, is zero. The reaction is then said to be *exothermic*. If Q_{fi} is negative, T_i must at least equal $|Q_{fi}|$, the *threshold energy*, before the reaction can proceed. The reaction is then *endoergic*. In a typical case, the masses are known, and the emergent particle is not excited ($\varepsilon_b = 0$). Then by measuring Q_{fi} the value of ε_Y , the excitation energy of the residual nucleus, can be determined.

Of course, in practice, laboratory energies are measured directly and it sometimes is useful to express the energy difference $T_f - T_i$ as given by (2.7) in laboratory-frame variables. It is an easy matter to obtain Q_{fi} by applying conservation of momentum and energy in the laboratory frame. The result is

$$Q_{fi} = T_{Lb} + \frac{1}{2m_Y}(\mathbf{p}_{La} - \mathbf{p}_{Lb})^2 - T_{La} \quad (2.8)$$

or

$$Q_{fi} = \frac{1}{m_Y}[(m_Y + m_b)T_{Lb} - (m_Y - m_a)T_{La} - 2\sqrt{m_a m_b T_{La} T_{Lb}} \cos \theta_L] \quad (2.9)$$

where θ_L is defined in Fig. 2.2. The mass m_Y may be eliminated using its approximate value $m_x + m_a - m_b$. Since Q_{fi} depends only on intrinsic energies [see (2.7)], its value is independent of the angle θ_L . Thus T_{Lb} must vary with angle θ_L so as to cancel out the explicit θ_L dependence in the right-hand side of (2.9). The angle variation of T_{Lb} can be obtained from (2.9) by solving for T_{Lb} in terms of Q_{fi} .

3. CLASSIFICATION OF REACTIONS

Each of the projectiles can induce reactions of various kinds. We begin with the examples schematically illustrated in Fig. 3.1. This gives the energy spectrum

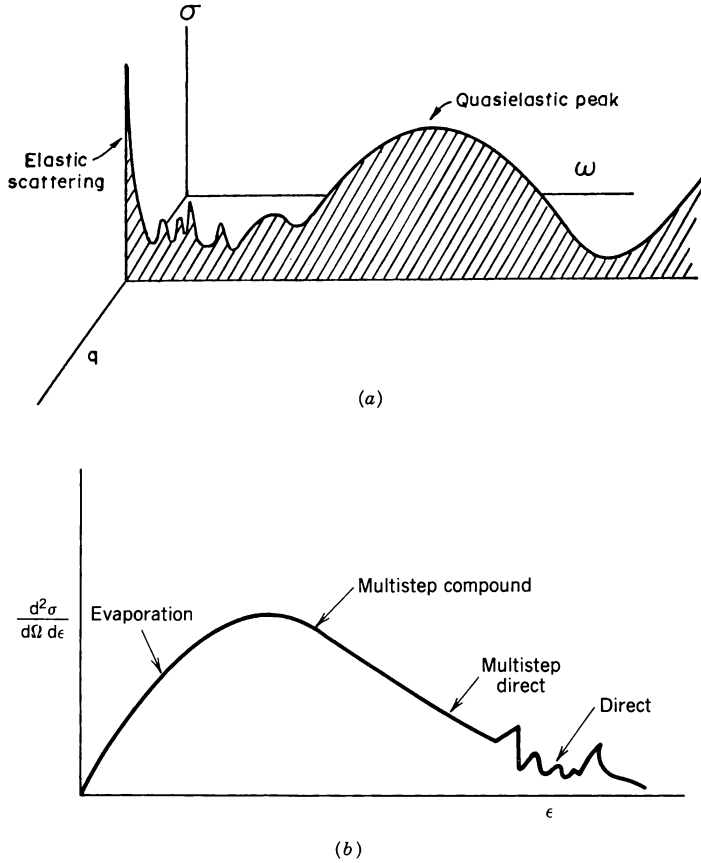


FIG. 3.1. (a) Energy spectrum of a particle scattered with a momentum transfer $\hbar q$ and an energy loss $\hbar\omega$; (b) energy spectrum of a nucleon emitted with an energy, ϵ , as the consequence of a reaction.

of a projectile scattered with a given momentum transfer $\hbar q$ and energy transfer $\hbar\omega$ in the center-of-mass reference frame, where

$$\mathbf{q} = \mathbf{k}_i - \mathbf{k}_f \quad \mathbf{p}_{i,f} = \hbar \mathbf{k}_{i,f} \quad (3.1)$$

and

$$\hbar\omega = E_i - E_f \quad (3.2)$$

where E_i and E_f are the energies of the target and residual nuclei, respectively. The peak in the intensity for zero energy loss is produced by *elastic scattering*, designated by $X(a, a)X$. Elastic scattering is defined to be a collision in which the colliding particles only change their direction of motion, and possibly spin

orientation if they have spin. None of the kinetic energy of the system is used to excite the colliding systems internally; that is, $Q_{fi} = 0$. The projectile and the target nucleus remain in their ground state, simply changing their direction of motion as illustrated in Fig. 3.2 but not the magnitudes of their momenta. The cosine of the angle of scattering, θ , is given by $\hat{\mathbf{k}}_i \cdot \hat{\mathbf{k}}_f$. It is related to \mathbf{q} as follows:

$$q = 2k \sin \frac{1}{2} \theta \quad (3.3)$$

where k is the common magnitude of \mathbf{k}_i and \mathbf{k}_f .

If both or either the projectile and target nucleus are complex, *inelastic scattering* can occur with the excitation of either or both, as indicated by $X(a, a^*)X^*$. The reaction is endoergic. The sharp peaks for nonzero values of ω in Fig. 3.1a correspond to the excitation of sharp discrete levels in, for example, the target nucleus. Figure 3.2 still applies, but in contrast to elastic scattering, p_i no longer equals p_f . The energy transfer $\hbar\omega$ equals the excitation energy ε , so that

$$\hbar\omega \equiv \varepsilon = \frac{1}{2m} (p_i^2 - p_f^2) \quad (3.4)$$

where it has been assumed that the change in the kinetic energies of the target can be neglected. Relation (3.3) is replaced by

$$q^2 = (k_i - k_f)^2 + 4k_i k_f \sin^2 \frac{1}{2} \theta \quad (3.5)$$

Since ε is fixed, the magnitude of k_f does not vary with angle. However, the value of q , for a given ε , does vary with angle, increasing as θ increases. The significance of q can be seen from the Born approximation, which states that the amplitude for the process will be proportional to

$$\int e^{-i\mathbf{k}_f \cdot \mathbf{r}} V(\mathbf{r}) e^{i\mathbf{k}_i \cdot \mathbf{r}} d\mathbf{r} = \int e^{i\mathbf{q} \cdot \mathbf{r}} V(\mathbf{r}) d\mathbf{r}$$

where V is the effective potential which induces the transition, elastic or inelastic as the case may be. V will generally depend on the properties of the nuclear systems undergoing the transition. We see that the reaction will serve as a probe

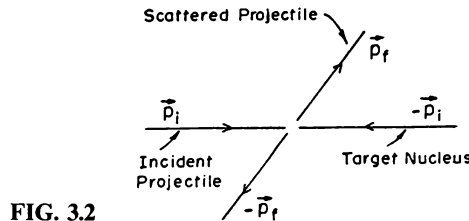


FIG. 3.2

of $V(r)$ for distances on the order of \hbar/q . Thus the larger the q , the more sharply the short-range properties of V are probed.

For larger energy transfers (Fig. 3.1b), the spectra lose their discrete character and become continuous. For one thing the density of levels of the target nucleus becomes so large that it is no longer possible to distinguish individual levels. It should also be realized that the approach to the continuous energy spectrum will differ with differing types of excitation. States of the excited nucleus with high angular momentum, J , will, for example, achieve the requisite high-level density at comparatively high excitation energies. At the lower energies the spectrum may thus be, effectively continuous as far as small values of J are concerned but will have a superimposed discrete character characterized by large values of J .

For sufficiently large energy transfers, those exceeding the separation energy for a nucleon, deuteron, or other fragments, the target nucleus can emit a particle. The corresponding reactions are referred to as $(p, 2p)$, $(p, p'd)$, and $(p, p'\alpha)$ when the incident particle is a proton. The final states consist of the residual nucleus; the incident proton, which has lost energy; and the particle, which has been knocked out of the target nucleus—and are thus at least three-body final states.

An important feature in this regime is a consequence of the *quasi-elastic scattering mechanism*. In quasi-elastic scattering the incident particle is assumed to collide elastically with a nucleon (or a complex cluster) within the target nucleus, the remainder of the target nucleus acting as a “spectator.” If the nucleons (or clusters) in the nucleus were at rest and free, one would see a sharp peak in the cross section at an energy loss, $\hbar\omega$, corresponding to the energy acquired by the nuclear nucleons. Using definitions (3.1) and (3.2), this implies that

$$\hbar\omega = \frac{\hbar^2 q^2}{2m} \quad (3.6)$$

where m is the mass of the nuclear nucleons (or clusters).

However, the nucleons in the nucleus move with a momentum p . In a Fermi-gas model the maximum value of p is p_F , the Fermi momentum. The conservation of momentum requires that the momentum $\hbar\mathbf{q}$ [see (3.1)] lost by the incident particle is acquired by the target nuclear nucleon of mass m^* , where m^* the effective mass, is a function of the momentum, taking into account to some extent the effect of the interaction with other nucleons in the nucleus. Therefore, more accurately,

$$\frac{p^2}{2m^*(p)} + \hbar\omega = \frac{P^2}{2m^*(P)} \quad \mathbf{P} = \mathbf{p} + \hbar\mathbf{q} \quad (3.7)$$

This equation neglects the recoil energy of the residual nucleus, whose maximum value is on the order of $\epsilon_F/(A - 1)$, where A is the mass number of the target

nucleus and ε_F is the Fermi energy. This approximation is valid only when $\hbar\omega$ and $\hbar q$ are sufficiently large. From (3.7) one obtains a relation between ω and q , neglecting the difference between $m^*(p)$ and $m^*(P)$:

$$\hbar\omega = \frac{1}{m^*} \left(\hbar \mathbf{p} \cdot \mathbf{q} + \frac{\hbar^2 q^2}{2} \right) \quad (3.8)$$

Hence $\hbar\omega$ is bounded as follows:

$$\frac{p_F \hbar q}{m^*} + \frac{\hbar^2 q^2}{2m^*} > \hbar\omega > \frac{-p_F \hbar q}{m^*} + \frac{\hbar^2 q^2}{2m^*} \quad (3.9)$$

The free nucleon peak at $(\hbar q)^2/2m$ is shifted to $\hbar^2 q^2/2m^*$. Moreover, it spreads out, acquiring a width of the order of $\hbar p_F q/m^*$ as a consequence of the internal motion of the nucleons of the target nucleus. It should be noted that the peak energy depends on the angle θ between the initial and final momenta, \mathbf{p}_i and \mathbf{p}_f , in a characteristic way. This fact can be used to differentiate the quasi-elastic peak from others. The energy difference $\hbar\omega = Q_{fi}$ for inelastic excitation, for example, does not vary with the center-of-mass angle θ [see (2.7)].

Problem. Discuss how these conclusions are changed because of a possible difference between $m^*(p)$ and $m^*(P)$.

The presence of the quasi-elastic peak is shown in Fig. 3.1a. Its shape depends, at least in the noninteracting Fermi-gas or shell model, on the distribution of momenta within the nucleus or more generally on the state of the struck particle. The energy of the emergent particle is not given by $p^2/2m^*$ since that is its energy relative to the bottom of the potential well, as shown in Fig. 3.3. The observed energy is $p^2/2m^* - \varepsilon_b$, where ε_b is the binding energy, the minimum energy required to remove the struck nucleon from the nucleus.

Some experimental results for the $(e, e'X)$ cross section, in which only the inclusive cross section in which only the emerging electron and not X is observed, are shown in Fig. 3.4. The solid lines give the fit obtained with the quasi-elastic mechanism using the Fermi-gas model of the target nucleus. The values of ε_b

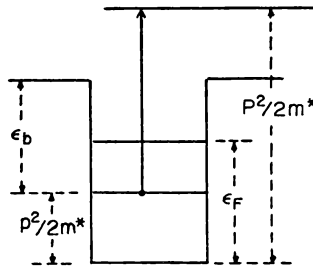


FIG. 3.3. Quasi-elastic scattering.

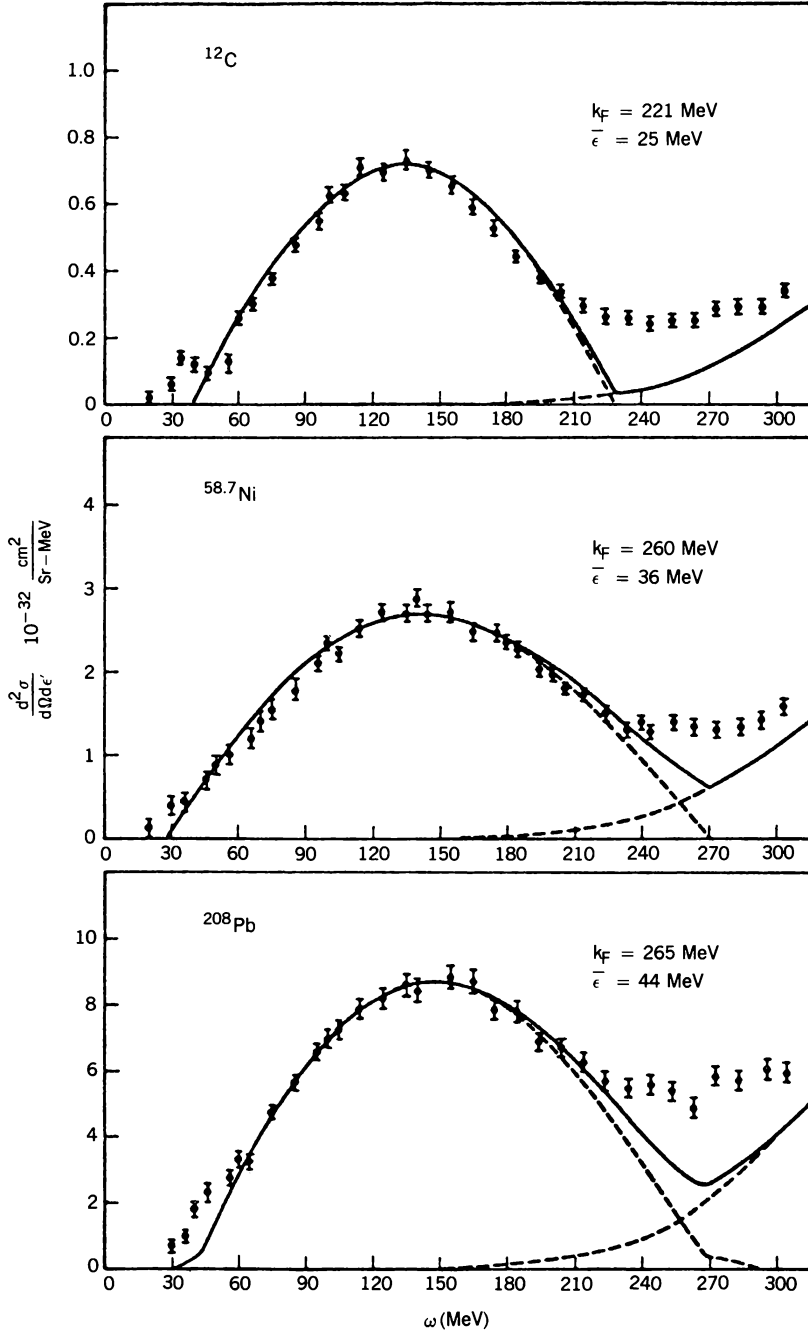


FIG. 3.4. Quasi-elastic scattering of electrons. The solid lines are calculated using a Fermi-gas nuclear model. [From Moniz et al. (71).]

and p_F are indicated in the figure and are also given in Table I.15.1 in deShalit and Feshbach (74).

More information can be obtained if the emergent proton in the (e, ep) and $(p, 2p)$ reactions are also detected in a coincidence experiment. In these experiments it becomes possible to determine ε_p for different single-particle orbitals and to obtain information on the momentum distributions for each.

In Figs 3.1a and 3.4, note the minimum at the low- $\hbar\omega$ end of the inelastic spectrum, lying between the quasi-elastic peak and the region where discrete levels are excited. This minimum is a consequence of the competition with the many other reactions that can occur in this region. At the upper end of the peak, we see that the spectrum shows a rise that is not predicted by the Fermi-gas model. This is a consequence of pion production.

Reactions in which the residual nuclei differ in either their mass number A , atomic number Z , or hypercharge Y , are called *transmutations*. When the mass number does not change but the atomic number or hypercharge do change, the reactions are referred to as *charge exchange* (CEX) or *hypercharge exchange scattering* (HCEX). Examples of charge exchange reactions include the (p, n) , the $(^3\text{He}, ^3\text{H})$, and so on, reactions. With pion projectiles one can observe both single and double charge exchange reactions,

$$\begin{aligned}\pi^\pm + (Z, A) &\rightarrow \pi^0 + (Z \pm 1, A) \\ \pi^\pm + (Z, A) &\rightarrow \pi^\mp + (Z \pm 2, A)\end{aligned}$$

where (Z, A) denotes a nucleus with atomic number Z and mass number A . The second of these reactions can lead to nuclei relatively far from the “stable” valley. For example, if the target is ^{16}O , the resulting nucleus produced by the double charge exchange reaction (π^+, π^-) is ^{16}Ne .

Hypercharge exchange reactions can involve either incident kaons or the production of kaons. In the first the hypercharge of the kaon is transferred to a nucleon in the target converting, for example, a neutron into a Λ . For example,

$$K^- + {}^{12}\text{C} \rightarrow {}_{\Lambda}^{12}\text{C} + \pi^-$$

where ${}_{\Lambda}^{12}\text{C}$ consists of six protons, five neutrons, and one lambda and is referred to as a hypernucleus. Associated production can also lead to hypercharge exchange. The elementary processes can be

$$\begin{aligned}\pi^+ + n &\rightarrow K^+ + \Lambda \\ &\rightarrow K^+ + \Sigma^0 \\ &\text{etc.}\end{aligned}$$

The nuclear process corresponding to the first of these reactions is, for example,

$$\pi^+ + {}^{12}\text{C} \rightarrow {}_{\Lambda}^{12}\text{C} + K^+$$

Particle transfer reactions form a most important class of reactions leading to transmutations. The stripping (d, p) and pickup reactions (p, d) in which a neutron is transferred to or from the target nucleus played an important role in establishing the nuclear shell model. The (d, p) reaction was found to populate the single-particle neutron shell model states selectively, while the (p, d) reaction was found to be sensitive to the orbital of the neutron, which is “picked up” to form the deuteron. It proved possible in both these cases to correlate the angular distributions of the protons or deuterons in the two cases with the properties of the single-particle orbital from or to which the neutron is transferred. In Fig. 3.5 the values of l labelling each curve indicate the orbital angular momentum in question. As is apparent, the value of l can be deduced immediately from the shape of the angular distribution. Single proton transfer reactions with deuterons such as the (n, d) or (d, n) reactions are most difficult since at least until recently, neutrons have proven to be more difficult to manage. It has been necessary to turn to reactions with ^3He , such as the ($^3\text{He}, d$) or ($d, ^3\text{He}$) to investigate single proton transfer reactions.

The transfer of two neutrons is studied in the ($^3\text{H}, p$) and (p, H^3) reactions. In this case it is believed that the two neutrons transferred are in a 1S_0 state since that is for the most part their state within the ^3H nucleus. It may be expected that the pickup reaction ($p, ^3\text{H}$) reactions will proceed most vigorously when the target nucleus ground state is superconducting, being built up of precisely such correlated pairs. An example is shown in Table 3.1. This reaction is clearly useful for the discovery and study of pairing correlations.

Reactions in which a larger number of nucleons are transferred have been observed using α -particles and most recently, heavy-ion projectiles. The transfer of as many as eight nucleons has been seen; in this way the production of many new nuclei away from the stable valley has become possible.

Still another class of reactions occurs when the incident projectile is a boson. When the projectile is a photon, a pion, or a kaon, it can be absorbed by the target nucleus. This process, referred to as *absorption*, can result in the transfer of a relatively large amount of energy but with a relatively small amount of momentum transfer. This is obvious in the case of photon absorption. In that case the absorption by a single nucleon of the target nucleus is reduced since the recoil energy of the nucleon $\hbar^2\omega^2/2mc^2$ is very small compared to the energy transfer $\hbar\omega$ for photon energies $\hbar\omega \ll mc^2$. As a result, the absorption is by a pair of nucleons in which the nucleons move in antiparallel directions so that their energy can be appreciable while their net momentum is small. A similar phenomenon can occur when pions and (to some extent) kaons have small momentum, as in the case of pionic and kaonic atoms, in which π^- and K^- are captured in atomic orbits by the attractive Coulomb field of the nucleus. In that situation the momentum of the pion or kaon is small, while upon absorption by the nucleus, an energy equal to $m_\pi c^2$ or $m_K c^2$ is released. In the case of kaon absorption there is a finite probability that a hypernucleus is formed. Indeed, it was through this process that the first hypernuclei were observed.

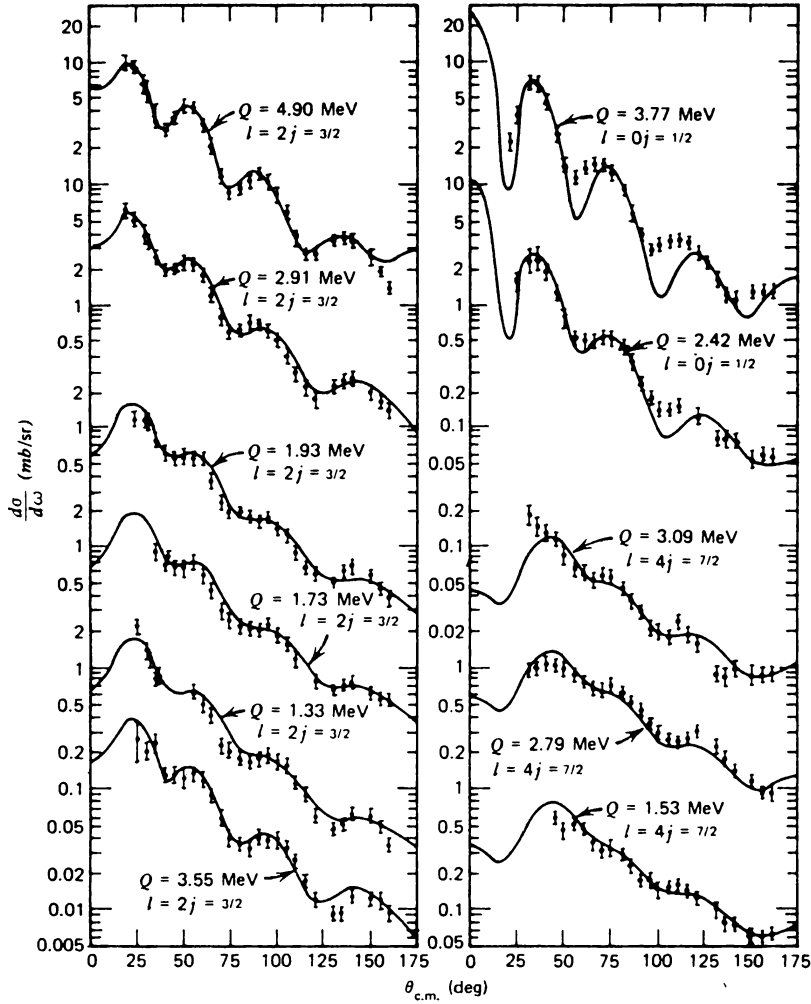


FIG. 3.5. Angular distribution for the $^{90}\text{Zr}(d, p)$ reaction with 12-MeV deuterons in which the neutron transferred to ^{90}Zr carries an orbital angular momentum of $l = 0, 2, 4$. [From Satchler (66).]

Photon absorption with the emission of a single nucleon [e.g., (γ, n)] also occurs. The underlying process may be the two-nucleon absorption, with one nucleon captured before it emerges from the nucleus. Of course, this capture *must* occur if the photon energy is below the threshold for the production of two nucleons. In that event it may become more convenient to describe the process as the excitation of the target nucleus into the continuum. The effect of the other nucleons is then contained in the high-momentum components of the single-particle wave function of the absorbing nucleon.

TABLE 3.1 Yield Y for the $^{124}\text{Sn}(t, p)$ Reaction Forming $^{126}\text{Sn}^a$

(t, p) group	E_n (MeV)	L	Y
0	0	0	100
1	1.164	2	5
2	2.070	> 2	3
3	2.185		4
4	2.236		7
5	2.377		5
6	2.659		2
7	2.732		6
8	2.905		3
9	3.439		4
10	5.226		4
11	5.282		9
12	5.313		11
13	5.762		10

Source: (Bjerregaard Hansen, et al. (69)).

^a L is the transferred angular momentum.

The inverse of photon absorption is called *radiative capture*, such as (n, γ) , (p, γ) , (π, γ) and so on. The neutron capture process, for example, is very useful for determining the presence and properties of low-lying levels of the final nucleus, which are readily connected via the electromagnetic interaction to the capturing energy region. In the neutron case, the first step in the capture of the neutron can be the formation of a compound nuclear resonance. In the proton case, the use of polarized protons[†] in the (p, γ) reaction has led to a more complete understanding of the contribution of the various multipole momenta in the giant dipole resonance region.

Fermions can be absorbed by the nucleus through the weak interactions. For the electron the process is known as K, L , and so on, capture and results in neutrino emission [see deShalit and Feshbach (74), Section IX.6]. In the case of muons [see deShalit and Feshbach (74), Section IX.18], the final state can consist of the muon neutrino and a nucleon as well, because of the large rest-mass energy of the muon.

Absorption of antiparticles such as the antiproton, \bar{p} , proceeds through the strong interactions for the most part. In the case of antiprotonic atoms in which the antiproton is in an atomic orbit about the attractive Coulomb field of the nucleus, absorption of the antiproton involves the *annihilation* process. The

[†]Polarized projectiles are indicated by boldface.

important elementary process is

$$\bar{p} + p \rightarrow (n\pi)$$

where $(n\pi)$ refers to the emission of n pions. The analogous electromagnetic system, positronium, decays by the emission of photons:

$$e^+ + e^- \rightarrow (n\gamma)$$

where n is 2 or 3, depending on the state of the positronium. Larger values of n are not easily observable because of the weakness of the electromagnetic interaction.

The inverse of boson absorption is boson *production*. When protons of sufficient energy strike a nucleus, pions can be produced, as exemplified by the reaction

$$p + (Z, A) \rightarrow (Z, A + 1) + \pi^+ \quad (3.10)$$

The threshold for this process occurs at a lower energy than the elementary processes:

$$\begin{aligned} p + p &\rightarrow n + p + \pi^+ \\ &\rightarrow d + \pi^+ \end{aligned}$$

For the first of these the kinetic energy in the center-of-mass frame is $\frac{1}{2}E_L$, whereas, with the nuclear target the kinetic energy in the same frame is $[A/(A+1)]E_L$. Roughly (neglecting differences in the neutron and proton masses, etc.), E_L for the p - p reaction must be at least $2m_\pi c^2$, while for the nuclear target the threshold energy $[1 + (1/A)]m_\pi c^2$ is considerably less. However, the cross section will be very small in this limit, since the entire target nucleus must be involved in the collision and production process. Intuitively, one would expect that the critical parameter is the ratio of the momentum transfer, $\hbar q$, to the Fermi momentum p_F . If this ratio is greater than 1, the probability of ejecting a nucleon will be correspondingly large and the probability of (3.10) occurring is reduced. If the produced pion is at rest, and if one neglects the momentum of the neutron added to the target nucleus by the reaction, this ratio becomes p_L/p_F , where p_L is the momentum of the incident proton in the laboratory frame. At threshold, nonrelativistically,

$$\frac{p_L}{p_F} = \sqrt{\frac{2mm_\pi A c^2}{(A+1)p_F^2}} \approx 2 \sqrt{\frac{A}{A+1}}$$

Since this ratio is greater than 1 for all nuclei, there will be a reduction in the cross section of process (3.10). Indeed, as soon as it becomes energetically

possible, the reaction

$$p + (Z, A) \rightarrow (Z, A) + p + \pi$$

is expected to dominate.

When the energy deposited in a nucleus is sufficiently large, as can be the case if the incident projectile is very energetic, or when the nucleus absorbs a massive particle as described above, the nucleus may break apart into several highly excited large fragments. This catastrophic event is referred to as *fragmentation*. In response to relatively minor perturbations, heavy nuclei whose stability is reduced by the repulsive electrostatic forces will fragment into two

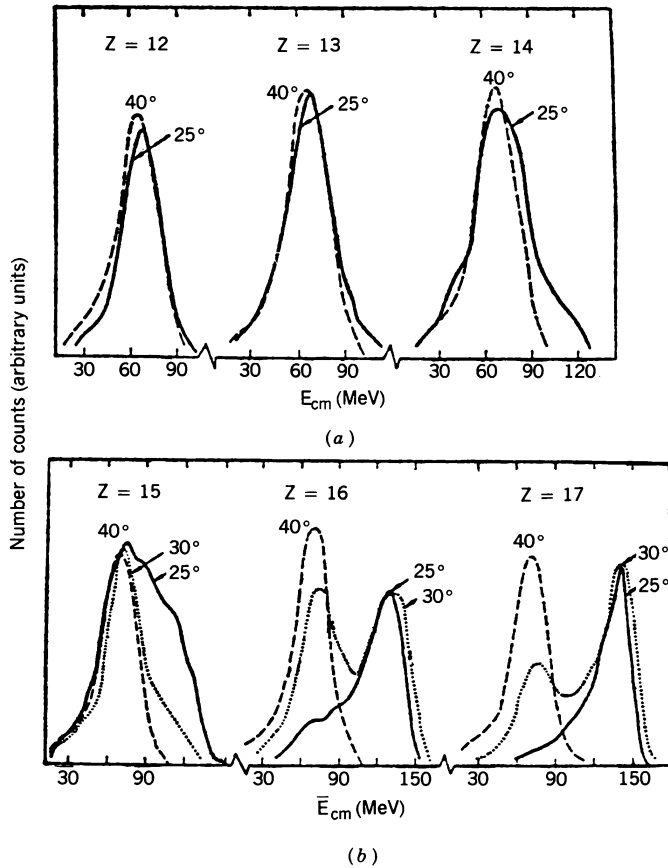


FIG. 3.6. Energy distribution of the light products in the reaction $(^{40}\text{Ar} + ^{108}\text{Ag})$: (a) for $Z = 12, 13$, and 14 the spectra are identical at 25° and 40° ; (b) for $Z = 15, 16$, and 17 , the deep inelastic process appears more clearly at 40° . [From Lefort (76).]

or more massive fragments. This process is called *fission*. *Fusion* is an inverse process in which heavy ions combine to form a single nucleus with perhaps the emission of a few light particles. Recently, a process termed *deep inelastic collision* has been discovered. It is found that in the process most of the kinetic energy available in the initial system has been transformed into internal energy. The observed kinetic energy of the final system is mostly a consequence of Coulomb repulsion. That is, it can be understood to be equal to the Coulomb energy of the two emerging nuclei making up the final system, in contact and at rest. As an example, consider the reaction $^{40}_{18}\text{Ar} + ^{108}_{47}\text{Ag}$; the energy of the argon projectile is 288 MeV. In Fig. 3.6 we plot the energy distribution of the fragments $Z = 12, 13$, and 14 at two angles, 25° and 40° . It will be seen that the energy distribution at the two angles for the various fragments is nearly identical! This is the signature for this remarkable phenomenon. The peak energy is about 72 MeV. Assuming a two-particle final state, the total energy of the final system is 78 MeV, considerably less than the 288 MeV and reasonably close to the Coulomb energy of the two final particles.

4. DIRECT AND COMPOUND NUCLEAR REACTIONS

The various processes discussed just above can proceed through a variety of mechanisms. An early differentiation was made between “direct” and compound nuclear statistical reactions. In Sections I.12 and I.13 of deShalit and Feshbach (74) it was emphasized that the two reaction types, the direct and that leading to the formation of a compound nuclear state, could be distinguished by the time delay caused by the reaction or equivalently, by the interaction time required for the completion of the reaction. The direct reaction involves a short time delay whose order of magnitude is the time it would take a projectile and/or the emergent particle simply to traverse the nucleus. As pointed out in deShalit and Feshbach (74), a short time delay is reflected in a relatively weak dependence of the cross section on energy as well as a strongly anisotropic angular distribution, indicating that the memory of the direction of motion of the projectile has not been lost in the course of the reaction. In other words, from the angular distribution it is possible to estimate the direction of motion of the incident projectile. These properties of direct reaction have led to the *single-step* description of the process referred to as the *DWA distorted wave approximation* (DWA). In a single-step process, the projectile (e.g., a proton) in *one interaction* forms the emergent particle (e.g., a deuteron). The matrix element for this process (p, d) is therefore written as a matrix element of the effective transition potential, V , acting directly on the initial state to produce the final state. If the process is $X(a, b)Y$, the initial-state vector is the product of a state vector $|a, X\rangle$, giving the dependence on the internal variables of projectile a and the target nucleus X , and the wave function $\chi_i^{(+)}(\mathbf{k}_i, \mathbf{r})$, giving the dependence on their relative coordinate \mathbf{r} with $\hbar\mathbf{k}_i$ the incident momentum. $\chi_i^{(+)}$ is a “distorted” wave in that it is not a plane wave but also takes into account the

average interaction between the projectile and the target.[‡] The plus superscript denotes the outgoing diverging wave boundary conditions satisfied by $\chi_i^{(+)}$. In terms of this description of the initial state and an analogous one for the final state, the DWA matrix element giving the amplitude for a direct reaction is proportional to

$$\int d\mathbf{r} [\chi_f^{(-)}(\mathbf{k}_f, \mathbf{r})]^\dagger \langle b, Y | V | a, X \rangle \chi_i^{(+)}(\mathbf{k}_i, \mathbf{r}) \quad (4.1)$$

In this equation $\chi_f^{(-)}$ is the wave-function describing the relative motion of the final constituents, subject to the converging wave boundary condition. In the $X(p, d)Y$ case, $\chi_i^{(+)}$ describes the dependence on the relative p - X coordinate, while $\chi_f^{(-)}$ is the wave function for the dependence on the relative d - Y coordinate. The single-step nature of the process is indicated by the linear dependence of the matrix element on the potential, V . This “theory” can give excellent agreement with the appropriate experiment, as exemplified by Fig. I.12.1 in deShalit and Feshbach (74).

The compound nuclear resonance involves a very long interaction time, as can be seen directly from the very rapid variation of the cross section with energy, as indicated by its width, Γ [see Fig. I.12.3 in deShalit and Feshbach (74)]. The resonance demonstrates the presence of a nearly bound state of the compound nucleus, with well-defined quantum numbers such as energy, angular momentum, and parity—the compound nuclear state, whose lifetime is given by (\hbar/Γ) . Clearly, the excitation of the compound nucleus state cannot be described in terms of a single-step process. Rather, the incident projectile completely loses its identity, amalgamating with the target nucleus to form a compound nuclear state. The compound nuclear state lives for a finite (rather than an infinite) time because it can decay by emitting a variety of products. If the particle emitted is identical with the incident projectile, the process is elastic or inelastic scattering. If the particle emitted is *not* identical with the incident projectile, the reaction is a transmutation. If interference with the direct reaction is unimportant, the angular distribution of a reaction product is symmetrical about 90° . It is thus no longer possible to ascertain the direction of motion of the incident projectile, although its line of motion is determined.

The isolated compound nuclear resonance is a spectacular phenomenon. However, it can be observed in only a comparatively limited energy range. As soon as the excitation energy increases sufficiently, the density of resonances and the variety of accessible exit channels will become so large that it becomes most unlikely that an isolated compound nuclear resonance will be present. Rather, the resonances will overlap, their presence being reflected by fluctuations in the energy dependence of the cross section away from a smooth average. In this regime it becomes necessary to use statistical measures such as averages

[‡]The quantities, the effective transition potential, and the average projectile–target nucleus interaction are discussed and described in Chapter VI.

over the fluctuations and mean-square deviations from the average. This theory is referred to as the *statistical theory of compound nuclear reactions*.

The principal assumption of this theory rests on the insight that the wave function for the system is very complex, consisting of a large number of components (e.g., the overlapping resonances). The amplitudes, both in magnitude and phase, of each of these vary rapidly as the energy changes. The assumption is made that these amplitudes are random variables. The expression for the reaction cross section, depending on the square magnitude of reaction amplitude, will therefore depend on bilinear products of this set of random variables. Upon averaging, the cross products of the random variables will vanish. This result follows from the assumption that the phase of each component amplitude is random. We provide a detailed discussion of the consequences of this approach in Chapter IV.

Problem. Let $f = \sum_{n,m} A_n(E_i)B_m(E_f)$, where A_n and B_m are random variables. Show that $\langle |f|^2 \rangle = [\sum_n |A_n(E_i)|^2][\sum_m |B_m(E_f)|^2]$.

For the present purposes it will suffice to quote the results that follow exactly for the collision of spinless systems producing spinless reaction products, and that follow approximately for reactions involving particles with spin. The average cross section for exciting a specific level in the residual nucleus is

$$\langle \sigma_{if}(E_f) \rangle = \sigma_c(i; E_i) \frac{A_f(E_f)}{\sum_a A_a(E_a)} \quad (4.2)$$

This result is an expression of the *Bohr independence hypothesis*. The cross section factors into two terms. The first, $\sigma_c(i; E_i)$, gives the cross section for forming the compound system when the available center-of-mass energy is E_i and the quantum numbers describing the target nucleus are symbolized by i . The second factor, depending only on the final energy, is a branching ratio giving the probability that the compound nucleus will decay to a particular final state.

An approximate argument (which turns out to yield the correct result!) provides the form for A_f . A more precise discussion is given in Chapter IV. We assume incorrectly (why?) that detailed balance is valid for the reaction considered above. For spinless systems, detailed balance states that

$$E_i \langle \sigma_{if}(E_f) \rangle = E_f \langle \sigma_{fi}(E_i) \rangle \quad (4.3)$$

Inserting (4.2) into this equation yields

$$A_f(E_f) \sim E_f \sigma_c(f; E_f)$$

Hence

$$\langle \sigma_{if}(E_f) \rangle = \frac{\sigma_c(i; E_i) E_f \sigma_c(f; E_f)}{\sum_a E_a \sigma_c(a; E_a)} \quad (4.4)$$

Generally, in the energy region where this formula is to be applied, the final states of the residual nucleus form a continuum, or the individual states are not resolvable. Suppose that the density of states at the excitation energy of the residual nucleus U_{fi} is $\omega_0(U_{fi})$. Then the spectrum $\langle d\sigma_{if}/dE_f \rangle$ is given by

$$\left\langle \frac{d\sigma_{if}}{dE_f} \right\rangle = \sigma_c(i; E_i) \frac{\mu_f E_f \sigma_c(f; E_f) \omega_0(U_{fi})}{\sum_a \mu_a \int dE_a E_a \sigma_c(a; E_a) \omega_0(U_{ai})} \quad (4.5)$$

where μ_a is the reduced mass for the possible final systems. This formula applies approximately to systems with spin if ω_0 is the density of levels with zero total spin. The value of the excitation energy, U_{fi} , is given by

$$U_{fi} = E_i + Q_{fi} - E_f \quad (4.6)$$

where Q_{fi} is the Q of the reaction [see (2.7)].

Despite the approximations involved in deriving (4.5), it has proved to be of great utility, in part because it gives a very definite prescription for determining an average cross section. The cross section for forming the compound nucleus can readily be calculated from the optical model obtained from fitting elastic scattering cross sections and angular distributions. In the short-wavelength limit for a strongly absorbing nucleus and a neutral projectile, it is given roughly by $\pi R^2(1 - \langle V \rangle/E)$, where R is the *nuclear radius*, that is, the radius of the potential acting between the target (residual nucleus) and the projectile (emitted particle) and $\langle V \rangle$ is the average strength of that potential.

Some consequences of (4.5) are immediately clear. The ratio

$$\frac{d\sigma_{if}/dE_f}{\sigma_c(i; E_i) E_f \sigma_c(f; E_f)}$$

depends only on the excitation energy U_{fi} , that is, only on the difference $E_i - E_f$ and not on either E_i and E_f separately. This assumes that the denominator on the right-hand side of (4.5) is insensitive to E_i . This is to be expected when there are many channels into which the compound system can decay. Moreover, it is possible to extract the level density ω_0 , which is traditionally (Chapter IV) parametrized as follows:

$$\omega_0(U) = C e^{2\sqrt{a}U} \quad (4.7)$$

The empirical values of a for a number of nuclei are shown in Fig. 4.1. As one can see, the density of states rises very rapidly as the excitation energy U increases.

The function $\omega_0(U)$, where U is given by (4.6), can be expanded about the

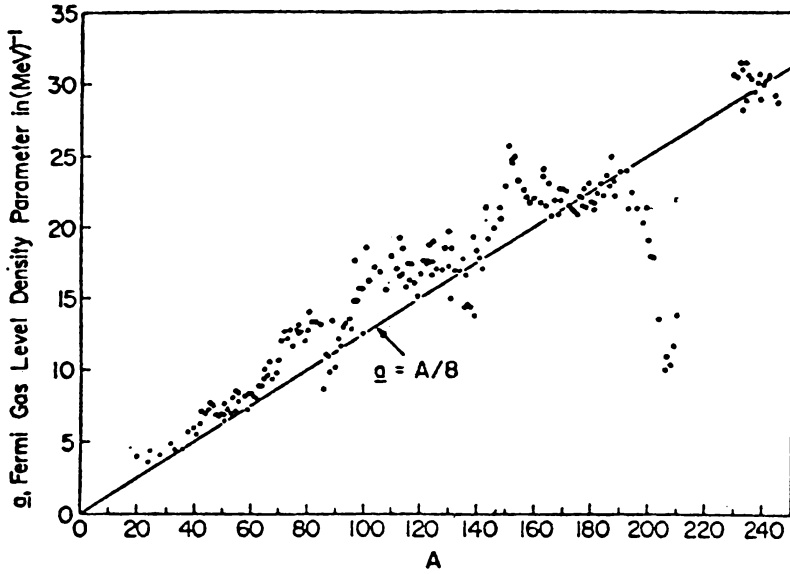


FIG. 4.1. Level density parameter a versus A . The straight line corresponds to $a = A/8$ and dark points are experimental determinations. [From Lefort (76).]

maximum excitation energy for the nucleus, $(E_i + Q_{fi}) \equiv U_M$,

$$\omega_0(E_i + Q_{fi} - E_f) = C e^{2\sqrt{aU_M}} e^{-E_f/T(U_M)} \quad (4.8)$$

where

$$T(U_M) = \sqrt{\frac{U_M}{a}} \quad (4.9)$$

T is referred to as the *nuclear temperature*,[†] given in energy units. The energy spectrum (4.5) becomes, as far as its dependence on E_f is concerned,

$$\left\langle \frac{d\sigma_{if}}{dE_f} \right\rangle \sim E_f \sigma_c(f; E_f) e^{-E_f/T} \quad (4.10)$$

[†]One can obtain a more general formula by postulating

$$\omega_0 = e^{S(U)}$$

Expanding $S(U)$ about U_M yields

$$\omega_0(U) = e^{S(U_M)} e^{-E_f/T} \quad T^{-1} = \left(\frac{\partial S}{\partial U} \right)_{U=U_M}$$

This formula is similar to that which gives the energy distribution of molecules evaporated from condensed matter. It suggests the picture that the incident particle deposits energy in the system, which then heats to a temperature T and then evaporates. For this reason the low-energy part of the spectrum for which (4.10) is valid is often referred to as the evaporation and/or the *equilibrium region*. An example of the determination of the temperature from experiment is shown in Fig. 4.2.

The angular distribution of the reaction products in the evaporation region is predicted to be spherical. The derivation of this result employs the assumption that the excitation of the residual nucleus will populate levels with all possible values of and directions of the angular momentum. However, in the case of some systems, particularly those involving the collision of heavy ions, for which large angular momenta are selectively populated, isotropy will no longer be predicted. We shall postpone the discussion of that case to Chapter VIII.

The dependence of the density of levels on angular momentum in the residual nucleus has been derived by Bloch (54) using the independent particle model for the nucleus: The z component of the total angular momentum M (z is in an arbitrary direction) is obtained by adding up the z components of the angular momentum of each of the nucleons making up the residual nucleus. Presuming these components to be random, the probability distribution for a given total $M (\geq 0)$ is given by the central limit theorem as

$$F(M) \sim e^{-M(M+1)/2\sigma^2}$$

where σ is the dispersion and $M(M+1)$ rather than M^2 has been put into the exponent. The density of levels with a value of angular momentum equal to I , ω_I , is given by $F(I+1) - F(I)$ since the M component of the angular momentum in the range $(I-1, I)$ must be projected from total angular momenta greater than $I-1$ and less than I . Approximately,

$$F(I-1) - F(I) \sim -\frac{\partial F(I)}{\partial I} dI = \frac{2I+1}{2\sigma^2} e^{-I(I+1)/2\sigma^2} dI \quad (4.11)$$

Hence

$$\omega_I = \frac{(2I+1)\omega_0}{\sqrt{8\pi\sigma^3}} e^{-I(I+1)/2\sigma^2} \quad (4.12)$$

where the dependence on σ in the coefficient of the exponential has been chosen so that

$$\sum_I \frac{2I+1}{\sqrt{8\pi\sigma^3}} e^{-I(I+1)/2\sigma^2} \approx 1$$

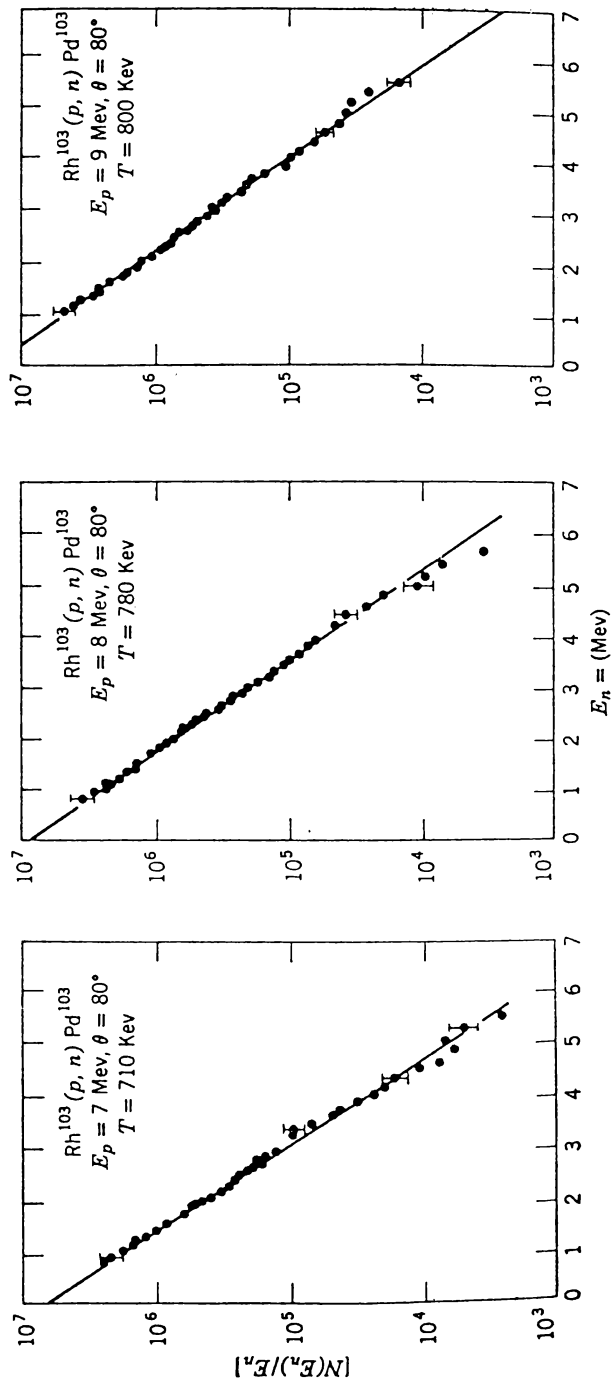


FIG. 42. Spectrum of neutrons from the $\text{Rh}(p, n)$ reaction at a neutron emission angle of 80° .
[From Holbrow and Barschall (63).]

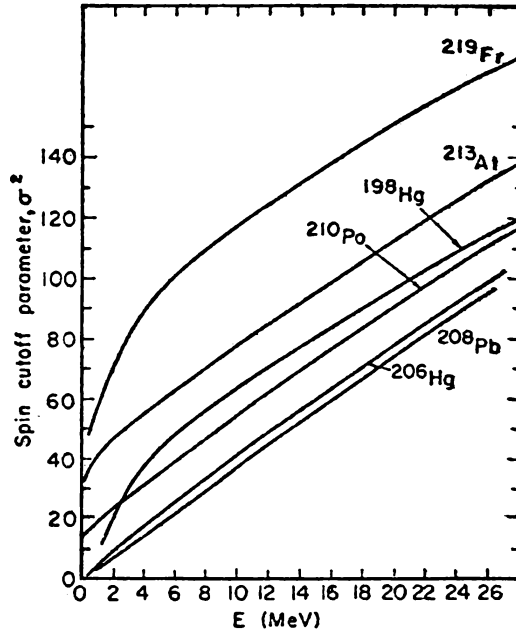


FIG. 4.3. Theoretical spin cutoff parameters σ^2 as a function of excitation energy for nuclei in the ^{208}Pb region (40). The calculations have been performed on the basis of the Nilsson diagram. [From Huizenga and Moretto (72).]

Theoretical values of σ as a function of mass number are shown in Fig. 4.3. Equation (4.5) (for spin-dependent systems) and the isotropy of the reaction products is derived under the assumption that $\omega_I \simeq (2I + 1)\omega_0$, that is, neglecting the exponential in (4.12), an assumption that fails for the collision of heavy ions. This exponential factor expresses the fact that for a given number of nucleons, the number of ways one can construct a total angular momentum, I , from the individual nucleon angular momenta must eventually decrease as I increases.

5. MULTISTEP DIRECT REACTIONS

A wide variety of nuclear reactions cannot be described either as a single-step direct process, that is, by the DWA approximation (4.1), or as a compound nuclear resonance reaction, as extended by the statistical theory of nuclear reactions [see (4.5)]. In terms of Fig. 3.1*b* giving a typical energy spectrum of particles emerging at a given angle (or of the corresponding residual nuclei), the region of validity of these two descriptions is limited to the high-energy region for the direct single-step process, while the statistical compound nuclear process is limited to the low-energy end. The latter domain is characterized by

spherical angular distributions and rapid fluctuations in the energy dependence of the cross section, symptomatic of long interaction times. The direct reaction involves short interaction times and thus is characterized by anisotropic angular distributions and a slowly varying energy dependence of the cross section.

However, in the energy region between high and low energies, large deviations from the predictions of these two mechanisms are found. For example, in Fig. 5.1 the $^{197}\text{Au}(\alpha, xn)$ cross section integrated over angles are compared with the statistical compound theory [see (4.5)] for α -particle energies ranging from 20 to over 70 MeV. Clearly, a rapidly growing discrepancy appears in each of the cross sections shown in the figure.

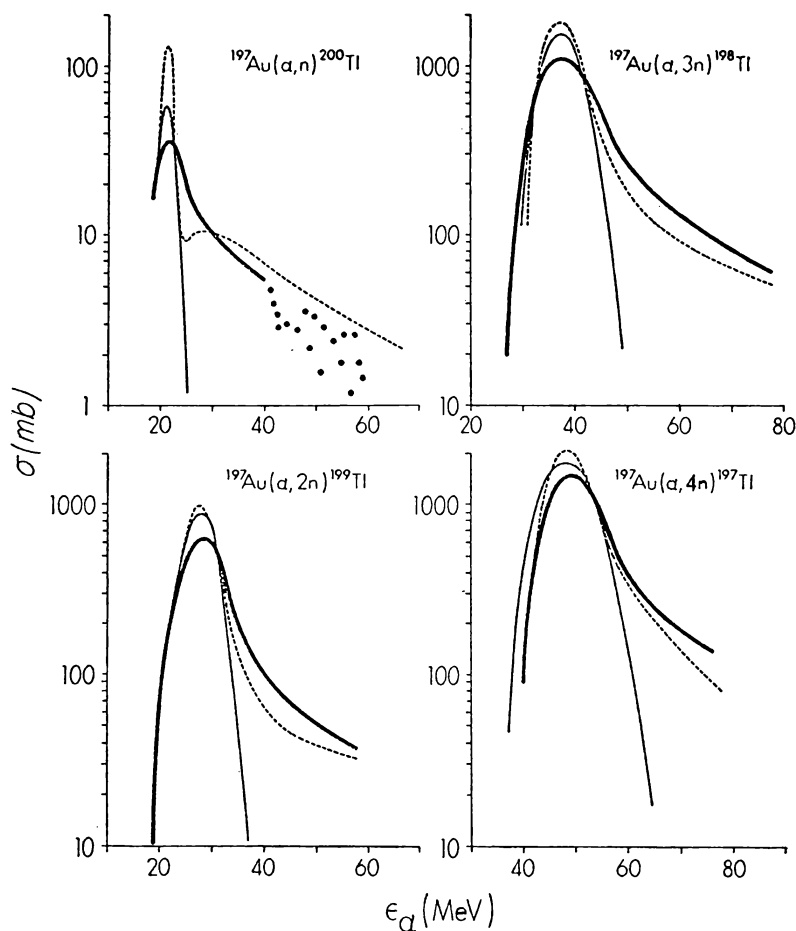


FIG. 5.1. Calculated and experimental excitation functions for the reactions $^{197}\text{Au}(\alpha, xn)$. The heavy solid curves represent experimental yields. The thin solid curves represent equilibrium statistical model calculations. [From Blann (72).]

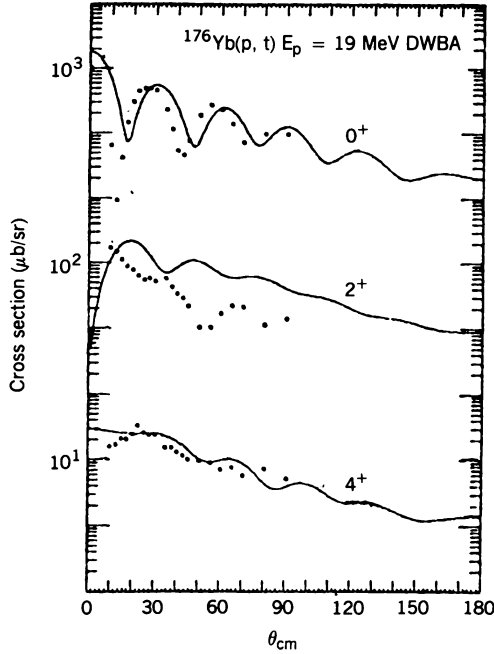


FIG. 5.2. Experimental data for the reaction $^{176}\text{Yb}(p, t)$ compared with the single-step DWA calculation (solid line). [From Ascuitto, Glendenning, and Sørensen (72).]

The single-step direct process can fail to describe reactions at the high-energy end of the spectrum, as illustrated by the reaction $^{176}\text{Yb}(p, t)^{174}\text{Yb}$. In Fig. 5.2 the DWA is compared with the experimental result and does not provide an explanation of the angular distribution for the excitation of the 2^+ state by a wide margin.

Both the statistical compound and the direct reaction theories are limiting descriptions, the former involving very long interaction times, the latter, very short reaction times. It is now necessary to retreat from these extremes and consider processes involving intermediate interaction times.

In the case of direct reactions, the procedure to be used is rather obvious. The single-step reaction is described in terms of the DWA. This is a perturbation theory where the perturbing interaction is, according to (4.1), given by $\langle b, Y | V | a, X \rangle$. The amplitude given by (4.1) is an approximation to the more precise amplitude to be obtained from the coupled equations

$$[E_i - T - V_{\text{opt}}(a, X)]\psi(a, X) = \langle a, X | V | b, Y \rangle \psi(b, Y) \quad (5.1a)$$

$$[E_f - T - V_{\text{opt}}(b, Y)]\psi(b, Y) = \langle b, Y | V | a, X \rangle \psi(a, X) \quad (5.1b)$$

where $V_{\text{opt}}(a, X)$ is the optical potential between the target X and projectile a

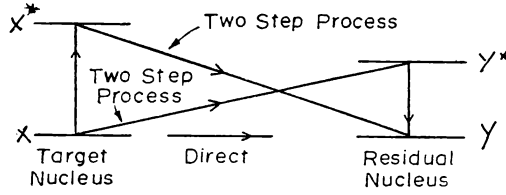


FIG. 5.3

and T is the kinetic energy operator for their relative motion. The amplitude equation (4.1) is obtained by dropping the terms on the right of (5.1a).

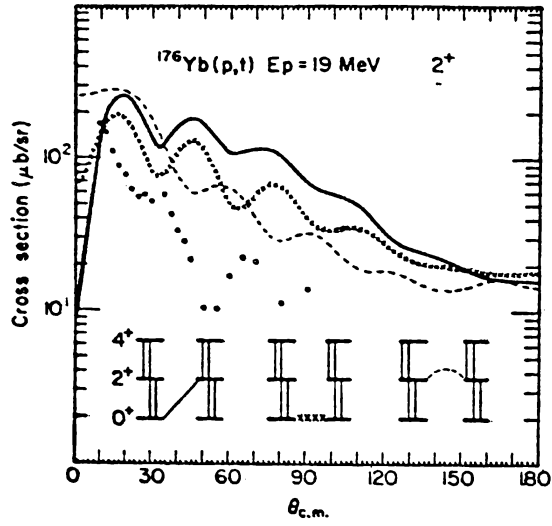
However, this result still leaves out possibly important physical processes, consequences of the polarizability of the target (residual) nucleus by the projectile (emergent particle). For example, the target nucleus and/or the residual nucleus may be excited, permitting the reaction to the final state to proceed by several interfering routes, as indicated in Fig. 5.3. In addition to the one-step process, there are several two-step amplitudes. In one, the target nucleus is excited and then makes the transition to the final state of the residual nucleus; in another, the transition is from the initial target nucleus to an excited state of the residual nucleus which in the second step of the process is deexcited. In a reaction such as $(^3\text{H}, p)$, in which several nucleons are transferred, interference between the direct route and one in which the nucleons (neutrons in the example) are transferred one at a time is possible. Indeed particle transfer can play a role even in the case of an inelastic scattering (p, p') reaction. It might be the case that the two-step process $X(p, d)Z(d, p')X^*$ is important for some special reason. For example, a collective state (or set of collective states) of nucleus Z might be accessible in the energy, charge, and angular momentum range under investigation.

The two-step process illustrated in Fig. 5.3 is described by the following equations:

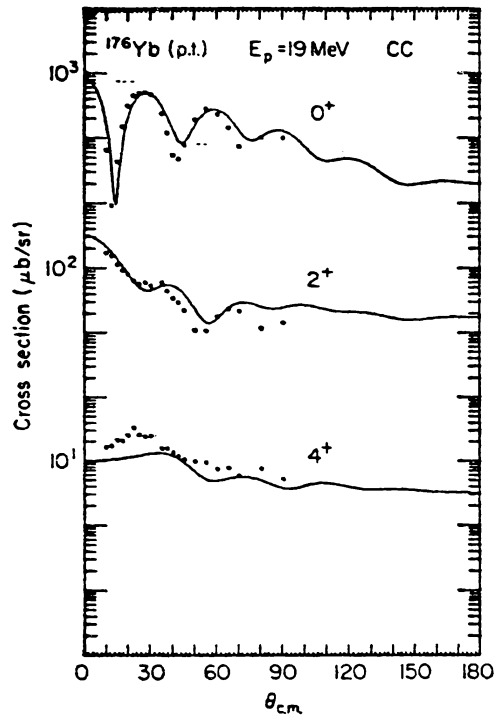
$$[E_i - T - V_{\text{opt}}(a, X)]\psi(a, X) = \langle a, X | V | a, X^* \rangle \psi(a, X^*) + \langle a, X | V | b, Y \rangle \psi(b, Y) + \langle a, X | V | b, Y^* \rangle \psi(b, Y^*) \quad (5.2a)$$

$$[E_i - T - \varepsilon_x - V_{\text{opt}}(a, X^*)]\psi(a, X^*) = \langle a, X^* | V | a, X \rangle \psi(a, X) + \langle a, X^* | V | b, Y \rangle \psi(b, Y) \quad (5.2b)$$

FIG. 5.4. (a) Cross sections for the 2^+ state that correspond to the individual transfer processes shown. Note that the direct and indirect routes are comparable in magnitude. Each of these overestimate the cross section and interfere destructively to produce the final result. (b) Cross sections for members of the ground band of ^{174}Yb . Calculations include all transitions connecting all three states in both nuclei. The 0^+ curve was normalized to the data and the same normalization was used for the other two. [From Ascuitto, Glendenning, and Sørensen (72).]



(a)



(b)

$$[E_f - \varepsilon_y - T - V_{\text{opt}}(b, Y^*)]\psi(b, Y^*) = \langle b, Y^* | V | a, X \rangle \psi(a, X) \\ + \langle b, Y^* | V | b, Y \rangle \psi(b, Y) \quad (5.2c)$$

$$[E_f - T - V_{\text{opt}}(b, Y)]\psi(b, Y) = \langle b, Y | V | a, X \rangle \psi(a, X) \\ + \langle b, Y | V | a, X^* \rangle \psi(a, X^*) + \langle b, Y | V | b, Y^* \rangle \psi(b, Y^*) \quad (5.2d)$$

The *coupled-channel Born approximation* (CCBA) follows the prescription dictated by the arrows in Fig. 5.3. It is obtained by putting the right-hand side of (5.2a) equal to zero, retaining only the terms in $\psi(a, X)$ on the right-hand side of (5.2b) and (5.2c).

Note that the optical potential $V_{\text{opt}}(a, X)$ in (5.2a) is not identical to the $V_{\text{opt}}(a, X)$ of (5.1a). The optical potential takes into account, in an average way, the effects of channels that are not explicitly considered. Since these differ for the two cases (5.2a) and (5.1a), the corresponding $V_{\text{opt}}(a, X)$ cannot be equal.

Obviously, the number of coupled equations can be made infinitely large. Practically, what one should do is to take into account the couplings that are felt to be most important for some physical reason; even then there may be a great number of equations. Under these circumstances it often proves more appropriate to use a statistical approach. The statistical theory of multistep direct processes is discussed below.

As an example of the use of multistep processes, consider the reaction discussed earlier, $^{176}\text{Yb}(p, t)^{174}\text{Yb}$ to the 2^+ state in the residual nucleus. By including the excitations of the ^{176}Yb ground-state band up to 4^+ and the ^{174}Yb ground-state band, we see in Fig. 5.4 that the theoretical predictions now follow the experimental results much more completely than in the single-step DWA theory case. In particular, in the transition routes illustrated in the figure, ground state to ground state with subsequent transition to the 2^+ , and excitation of the ground state in the target nucleus to the 2^+ followed by a two-particle transfer to the 2^+ of the residual nucleus, were especially important, as important as the direct excitation.

6. STATISTICAL DOORWAY STATE REACTIONS

We consider now that portion of the spectrum which borders on the low-energy region dominated by the evaporation process. A clue to the mechanism involved is provided by the experiments of Grimes, Anderson, et al. (71) shown in Fig. 6.1. The reaction is $^{59}\text{Co}(p, n)^{59}\text{Ni}$. The ordinate is the excitation energy of the residual nucleus ^{59}Ni , so that a large U value corresponds to small neutron energies. As expected from evaporation theory, the lowest-energy neutrons had an isotropic angular distribution. However, as the energy of the neutrons increases, the angular distribution became anisotropic but remained symmetric around 90° . Eventually, this symmetry also disappeared, as indicated on the figure. We pay special attention to the regime in which the angular

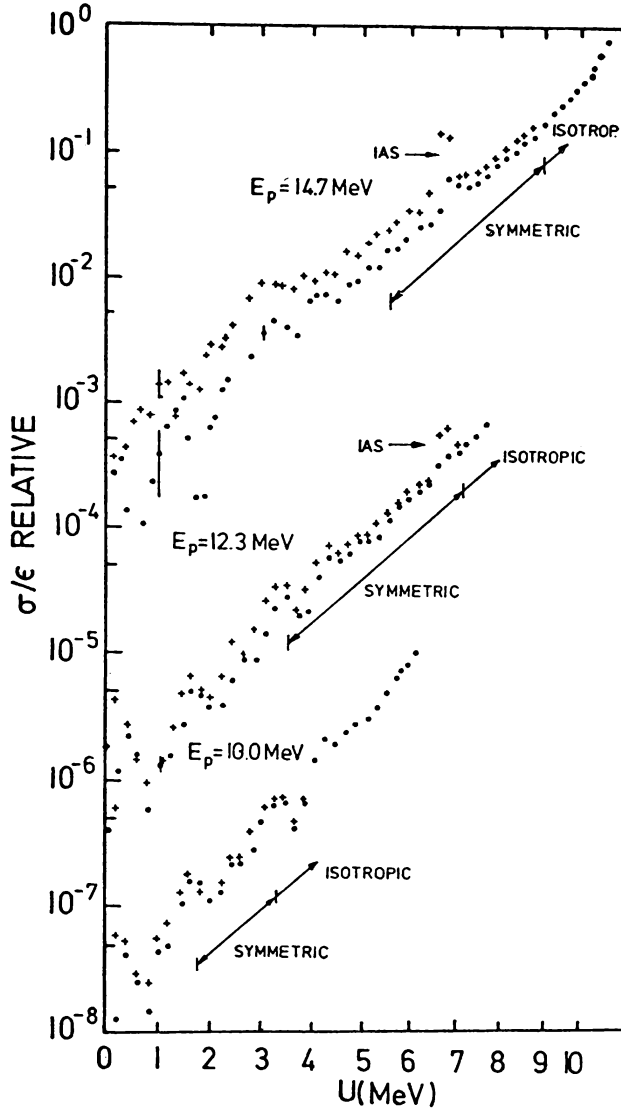


FIG. 6.1. Neutron spectrum for the $^{51}\text{V}(p, n)^{51}\text{Cr}$ reaction. U is the excitation energy of the residual nucleus. [From Grimes, Anderson, et al. (71).]

distribution is symmetric but no longer isotropic. An examination of all the data reveals that in this excitation region, there are a greater number of higher-energy neutrons than would have been predicted from evaporation theory using the state density Equation (4.7). The symmetry about 90° suggests a statistical mechanism analogous to that discussed in the preceding section involving compound nuclear resonances, and indeed, Grimes, Anderson, et al.

(71) propose that the resonances now involved are the doorway state resonances. A statistical theory of such doorway state nuclear reactions had been suggested earlier and used explicitly by Block and Feshbach (63).

The concept of the doorway state and the doorway state resonances is described briefly in deShalit and Feshbach (74, pp. 99–104), with particular attention being paid to the isolated doorway state such as the isobar analog state [which by the way, is visible in the data of Grimes, Anderson, et al., (71) shown in Fig. 6.1)]. In the present context, we shall be energy averaging over a number of doorway state resonances, again using the random-phase assumption of Section 4.

The importance of the doorway state in the present context should, in retrospect, not have been surprising. It seems rather obvious that the interaction time for reactions leading to the domain lying between the low-energy part of the spectrum of Fig. 3.1*b* with its long interaction time and the high-energy end with its short interaction time is intermediate, lying between these two extremes. The intermediate range of interaction times corresponds exactly with the domain in which doorway states should be of importance. As expressed in deShalit and Feshbach (74, p. 99), a cross section can have energy dependence, that is, “structure,” which varies (1) over a scale on the order of the compound nuclear width Γ_{CN} , which applies to the evaporation region; (2) over the much broader scale of the single-particle width Γ_{SP} , which applies to the direct reaction region; and (3) over an intermediate scale Γ_d , which is appropriate for the region lying between:

$$\Gamma_{SP} \gg \Gamma_d \gg \Gamma_{CN}$$

The interaction times, τ , vary inversely, so that

$$\tau_{dir} \ll \tau_d \ll \tau_{evAP} \quad (6.1)$$

The dynamical mechanism responsible for the intermediate structure presumes the existence of simple excitations of the system. A simple *example* is shown in Fig. 6.2. The well and the black dots represent schematically the shell

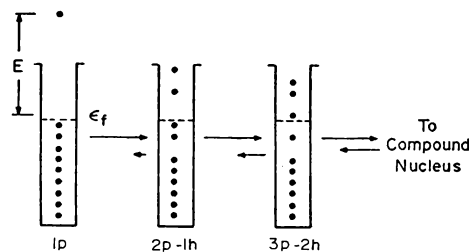


FIG. 6.2. Successive steps in a nuclear reaction leading to the formation of α compound nucleus. [From Blann (73).]

model potential and particle filling levels of that potential, respectively. The incident particle is shown with an incident energy E . It is readily able to excite, via an assumed two-body residual nucleon–nucleon potential, two-particle-one-hole states ($2p-1h$), which are next in complexity to the incident channel, which in this language is a one-particle ($1p$) state. The two-body residual potential acting on the ($2p-1h$) hole states can mix these, can return the system to the simpler $1p$ state, or can generate ($3p-2h$) states of still higher complexity. In this way a description of the components of the states of the system in terms of a hierarchy based on increasing complexity can readily be formulated. Obviously, if it is appropriate for the system in question, a model other than the shell model might be used and a different set of definitions would be involved in defining the hierarchy of complexity. It is necessary, perhaps to emphasize that this choice of model is *not* a matter of convenience. It is a statement regarding the nature of the excitations of the system.

To emphasize that point, we replace Fig. 6.2 by Fig. 6.3, in which the set of states next in complexity to the incident channel have been labeled as doorway states and the remaining states have been grouped together in the box entitled “states of higher complexity.” The word *doorway* was originally suggested by Block and Feshbach (63) to indicate an additional assumption employed to give the partition of Fig. 6.3 a dynamical significance. That assumption states that with the system starting in the incident channel to excite the states of higher complexity (the third stage in the figure) it is first necessary for the system to involve states of lower complexity, that is, the doorway states. This assumption implies that if the probability of forming doorway states from the incident channel is small, the probability of forming compound nuclear states will be reduced correspondingly. The doorway state assumption can be stated analytically: The matrix elements of the Hamiltonian between the incident channel and the second boxes in Fig. 6.3 are assumed to be zero. This assumption can be justified for the case of the shell model hierarchy classification for a two-body residual interaction. It is not expected that this assumption is obeyed exactly.

We are now ready to exploit the interaction time differences expressed by (6.1). It permits energy averaging over a range ΔE , which is large compared to Γ_{CN} but still small compared to Γ_d , thus preserving the intermediate structure associated with doorway states but smoothing out the fluctuations caused by the compound nuclear state resonances. The average cross section for a doorway state resonance reaction $i \rightarrow f$, *omitting the effects of spin and direct reactions*

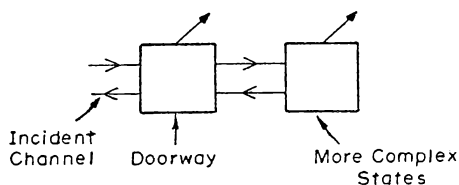


FIG. 6.3

for simplicity is

$$\sigma_{if} = \frac{\pi}{k^2} \frac{\Gamma_{di}^\dagger \Gamma_{df}^\dagger}{(E - E_d)^2 + (\frac{1}{2}\Gamma_d)^2} \quad (6.2)$$

In this formula, Γ_{di}^\dagger is the width measuring the probability of forming the doorway state from the incident channel i , while Γ_{df}^\dagger , the *escape width*, is proportional to the probability that the doorway state will decay into the final channel. Equation (6.2) resembles the expression for the cross section for the same process proceeding through a *compound nuclear resonance*. With the same assumptions as those which apply to (6.2), that cross section is given by

$$\sigma_{if} = \frac{\pi}{k^2} \frac{\Gamma_{\lambda i} \Gamma_{\lambda f}}{(E - E_\lambda)^2 + (\frac{1}{2}\Gamma_\lambda)^2} \quad (6.3)$$

where E_λ is the resonance energy, Γ_λ its width, and $\Gamma_{\lambda a}$ are the partial widths proportional to the probability that a system in the resonant state, denoted by the subscript λ , will decay into channel a . The width of the resonance Γ_λ when the resonance is isolated is related to the partial widths as follows:

$$\Gamma_\lambda = \sum \Gamma_{\lambda a} \quad (6.4)$$

The corresponding relation does not hold for the doorway state width Γ_d . It is not just the sum of Γ_{da}^\dagger . The physical reason is that the doorway state can decay not only into the open channels but also can make a transition into a more complex state, as indicated by Fig. 6.3, and one must add in the width for this process. Therefore,

$$\Gamma_d = \sum_a \Gamma_{da}^\dagger + \Gamma_d^\dagger \quad (6.5)$$

where Γ_d^\dagger is called the *spreading width*.[†] It is a width that increases the doorway state width because of coupling between the doorway and more complex states. It reflects the fact that the doorway state is not an exact eigenstate of the nuclear Hamiltonian. The compound nuclear resonance would be an exact bound state if all the exit channels were closed. The doorway state would also be an exact bound state if, in addition, the probability of a transition to any more complex state were reduced to zero. In the example of Fig. 6.2, the doorway state becomes an exact bound state composed only of 2p–1h wave functions if the probability of transitions to the simpler 1p state, and to the more complex states such as the 3p–2h states, were zero.

We note that the form of the cross section for a doorway state resonance and that for the compound nuclear resonance are identical. The *only* difference

[†] Γ_w is used for this width in deShalit and Feshbach (74).

is that exhibited by (6.5): namely, the addition of the spreading width. It is thus possible to use all the results developed for the compound nuclear resonance reaction theory. It is only necessary to bear in mind the “extra” channel, the transition to more complex states, with the width Γ_d^\downarrow . In particular, it is possible to take over the results of the statistical theory of compound nuclear–nuclear reactions [see (4.5)] to obtain for the zero-spin case,

$$\left\langle \frac{d\sigma_{if}}{dE_f} \right\rangle_d = \sigma_d(i, E_i) \frac{k_f^2 \sigma_d(f, E_f) \omega_d(U_{fi})}{\sum_a \int dE_a k_a^2 \sigma_d(a; E_a) \omega_d(U_{ai}) + 2\pi^2 \langle \Gamma_d^\downarrow \rangle \omega_d} \quad (6.6)$$

In this expression, σ_d is the cross section for the formation of a doorway state, ω_d the density of doorway states, and $\langle \Gamma_d^\downarrow \rangle$ the average spreading width. Although the density of doorway states can be large, it is generally much smaller than the density of compound nuclear states. All the quantities appearing in (6.6) depend on the initial energy and the other quantum numbers for the incident channel, since these features are decisive in determining the nature of the doorway states. The corresponding quantities in (4.5) are not dependent on the initial state since the full complexity of the compound nuclear states is achieved only after many steps beyond the doorway stage, at which stage the memory of the incident situation has become very faint. One important conclusion that can now be drawn is that the Bohr independence hypothesis [see (4.2)] is not valid for the statistical doorway state reactions.

7. STATISTICAL THEORY OF MULTISTEP DIRECT AND MULTISTEP COMPOUND REACTIONS

The system of equations, (5.2) describes a comparatively simple situation. However, as the energy of the projectile increases, the excitations of larger numbers of intermediate states become more probable, with the consequence that the number of coupled equations required for an adequate account of the reaction increases rapidly. One can question the usefulness of solving these even if it were practical and even if the coupling potentials were well known. A more fruitful approach—one that proves to be insightful—asks for statistical quantities (as discussed in Section 4) such as energy-averaged cross sections. Such a theory is referred to as the *statistical theory of multistep direct reactions*.

Similar remarks apply to the generalization of the statistical theory of doorway state reactions. In such a development, the stages beyond the primary doorway stage play an important role and thus must be considered explicitly (see Fig. 7.1). Each stage contains wave functions of a given degree of complexity, as discussed in Section 6. Emission into the reaction channel is possible at each stage, as indicated. The statistical theory of doorway state reactions considers emission only at the doorway stage, while the compound nucleus resonance reaction involves emission far down the chain. With so many steps involved in

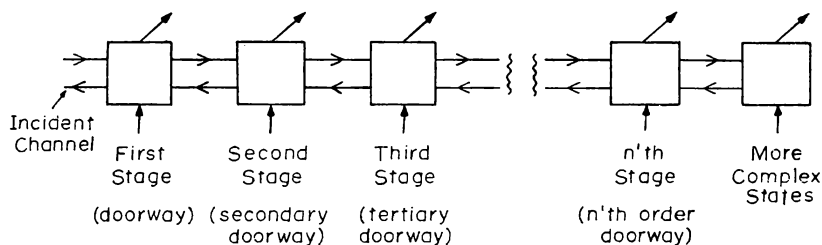


FIG. 7.1

the latter case, it is not surprising that the nature of the initial state is not important for the emission process, thus recovering the Bohr independence hypothesis. Since this chain of stages (Fig. 7.1) can be used to describe the compound nucleus, the reaction type is designated the *multistep compound reaction* to which the adjective “statistical” is added if statistical assumptions are employed in evaluation of the reaction cross sections. As might be expected from the results for the statistical theory of doorway state reactions discussed in Section 6, the statistical theory of multistep compound reactions predicts an angular distribution symmetric about 90° .

This cross section must be added to that obtained for the statistical multistep direct reaction. The latter, with some approximation, can be described as a sequential series of one-step energy-conserving direct reactions. The cross section then consists additively of the contributions from each possible value, n , of the number of steps. However, for a given energy of the emerging particle, there is a most probable value of n , depending on the average energy loss per single-step direct reaction. The angular distribution will generally be anisotropic and asymmetrical. If the angular distribution for the single-step process peaks in the forward direction with the angular width $\delta\theta$, the statistical multistep direct reaction process is predicted to lead again to a forward peak, but the width would now be given by $\sqrt{n} \delta\theta$.

8. DIRECT NUCLEAR REACTIONS AND SPECIFICITY

Much of the present-day understanding of nuclear structure, particularly the properties of low-lying states, has been gained from the study of nuclear reactions, particularly the single-step direct type. For this purpose it is necessary to understand the dynamics of nuclear reaction, while at the same time methods must be developed that permit the extraction of nuclear structure information. These two objectives are inextricably involved. Nevertheless, it has proved possible to accomplish both despite the fact that these reactions are governed by the strong interactions. Playing an essential role has been the ability to study the various processes systematically, varying the targets, the projectiles, and projectile energy and exploiting the wide variety of reactions described in Section 3.

The key has been what is termed the *specificity* of, particularly, the direct nuclear reactions [see deShalit and Feshbach (74, p. 72)]. *Specificity* refers to the ability of these nuclear reactions to excite specific types of nuclear states preferentially or to probe particular nuclear properties. Specificity can be a consequence of a property of the projectile, that is, its charge, mass, spin, and so on, and/or it can be a consequence of a property of the initial and final nuclear states connected by the reaction. Generally, specificity can be exhibited for experiments in which specific final states are observed rather than an average over a group of final states appropriate for the statistical models. This requirement calls for precision experiments involving beams and detection equipment with excellent energy resolution. Obviously, observation of particular final states is less easily performed. As the excitation energy increases, the density of levels increases and the energy separation between the levels decreases. By and large this has the consequence that it is in the transition to low-lying states, for which the existence of specificity is most easily observed. This limitation can be violated if a particular reaction mechanism selects out a particular type of state for which the density of states is not very large, even if the excitation energy is high. An example is the excitation of states with a very large angular momentum by heavy-ion projectiles. Another is the excitation of isobar analog states, whose existence is a consequence of the approximate conservation of isospin. Incidentally, the excitation of single states permits the use of conservation principles that help not only to identify the mechanism involved but also to determine the nature of the states excited.

The importance of the single-step direct reaction in this context should be emphasized. As we have described repeatedly, the excitation of complex states will generally require multistep processes. However, multi-step processes do not usually play an important role in the excitation of simple modes of motion.

On the other hand, single-step direct reactions preferentially excite simple modes of motion of nuclei. For example, the stripping (d, p), which adds a neutron to the target nucleus, and the pickup (p, d) reaction, which removes a neutron, are sensitive to the single-particle aspects of nuclei and are thus particularly useful for shell model studies. The added neutron in the first example will be placed in an empty single-particle orbital, producing a particular state of the residual nucleus. The contributions to this cross section from multistep processes will generally be relatively small.

A. Angular Momentum and Coulomb Barriers

Specificity depends on several factors. The one first realized historically is concerned with the probability that a projectile can penetrate to where a nuclear reaction can take place. The most familiar barrier to penetration is the *Coulomb barrier*, present because of the electrostatic repulsion between the positively charged nucleus and the positively charged projectile. This barrier is illustrated in Fig. 8.1. It can be expected that if the energy of the system is well below the peak (see curve A in the figure), the particle will not be able to penetrate and

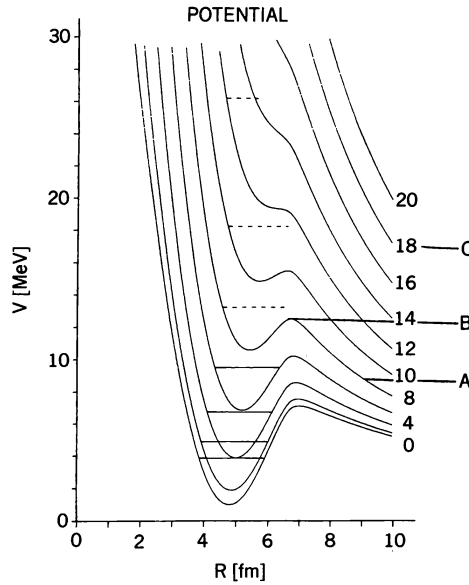


FIG. 8.1. Real potential for ^{12}C – ^{12}C scattering. [From Scheid, Fink, and Müller (73).]

nuclear reactions will be improbable. On the other hand, when the energy is near the top of the barrier or above (see curves B and C in the figure), penetration will readily be accomplished. The barrier energy is given roughly by

$$E_B = \frac{zZe^2}{R}$$

where ze is the projectile charge, Ze the charge of the target nucleus, and R the distance between the centers of the projectile and target when touching. Replacing R by $1.2(A_T^{1/3} + A_p^{1/3})$ fm, where A_T is the mass number of the target and A_p of the projectile, this formula becomes

$$E_B = 1.22 \frac{zZ}{A_T^{1/3} + A_p^{1/3}} \quad \text{MeV} \quad (8.1)$$

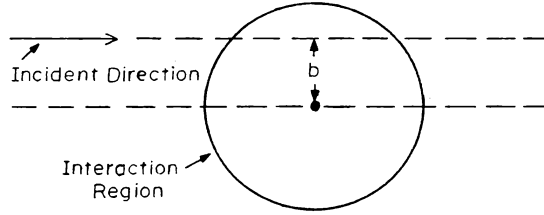
Some representative values are given in Table 8.1.

Another barrier to penetration is the *angular momentum barrier*. Classically, the system, consisting of an incident projectile of momentum p and target nucleus at rest, will have an angular momentum given by pb , where b is the *impact parameter* (see Fig. 8.2). If the *interaction radius*, that is, the distance between the centers of the interacting projectile and target nucleus beyond which nuclear reactions become improbable, is R , the maximum angular

TABLE 8.1

Nucleus	Coulomb Barrier Energy for Protons ^a (MeV)	Coulomb Barrier Energy for α -Particles ^a (MeV)
$^{27}_{13}\text{Al}$	3.97	6.96
$^{64}_{29}\text{Cu}$	7.07	12.62
$^{108}_{47}\text{Ag}$	9.95	18.06
$^{179}_{72}\text{Hf}$	13.28	24.30
$^{238}_{93}\text{U}$	15.59	28.80

^aIn the radius formula $1.2(A_T^{1/3} + A_p^{1/3})$ the factor 1.2 is determined empirically by charged particle reactions. It can, in fact, be as large as 1.5 in some cases, reducing the values above by the ratio $1.2/1.5 = 0.8$.

**FIG. 8.2**

momentum of the system that can contribute to a reaction is pR . Therefore, nuclear reactions will involve angular momenta lh , satisfying

$$l \lesssim \frac{pR}{\hbar} \lesssim kR \quad k \equiv \frac{p}{\hbar} \quad (8.2)$$

Numerically (and nonrelativistically) for light projectile.

$$kR = 0.22R(A_p E)^{1/2} \quad (8.3)$$

where R is expressed in fermis, A_p is the projectile mass number, and E is the projectile energy in MeV. For a given energy E the more massive particle carries more angular momentum, so that a heavy-ion projectile is capable of transmitting a relatively larger angular momentum to the target nucleus. In fact, it is in this way (i.e., by heavy-ion collisions) that the very high spin states referred to earlier are excited.

The phrase *angular momentum barrier* emphasizes that kR gives a rough upper bound to the angular momentum which can be involved in a nuclear reaction. Quantum mechanically, the probability for a nuclear reaction falls rapidly but not immediately to zero when the angular momentum kR is exceeded. The angular momentum barrier makes its appearance explicitly as an effective repulsive potential (the centrifugal potential) in the radial Schrödinger equation describing the relative radial motion of projectile and target. The ratio of this centrifugal potential energy to the total energy E evaluated at the interaction radius R is

$$\frac{\hbar^2}{2mE} \frac{l(l+1)}{R^2}$$

which must be less than 1 if the centrifugal barrier is to be penetrated easily. On introducing the variable k , this condition becomes

$$l(l+1) \lesssim (kR)^2 \quad (8.4)$$

which is just the quantum-mechanical equivalent of (8.2).

Roughly, the probability for a nuclear interaction is proportional to the probability that the incident particle will arrive at the nuclear surface. For neutral particles such as the neutron, the incident amplitude for a wave carrying angular momentum $l\hbar$ is proportional to the spherical Bessel function of order l , $j_l(k_i r)$, where k_i is the incident momentum divided by \hbar . The corresponding probability evaluated at the nuclear radius R is $j_l^2(k_i R)$, which for small $k_i R$ is on the order of $(k_i R)^{2l}$. The fact that this quantity approaches zero for small k_i is simply the expression of inequality (8.4).

The effect of the Coulomb barrier is given for small values of $k_i R$ by multiplying the neutral penetration factor by one depending on the dimensionless parameter η_i :

$$\eta_i = \frac{zZe^2}{\hbar v_i} = \frac{E_B R}{\hbar v_i} \quad (8.5)$$

where ze is the projectile charge, Ze the target nucleus charge, and v_i the incident velocity. One obtains for the penetration factor

$$C_l^2(\eta_i)(k_i R)^{2l}$$

where

$$C_l^2 = \frac{2^{2l}}{[\Gamma(2l+1)]^2} [l^2 + \eta_i^2][l(l-1)^2 + \eta_i^2] \cdots [1 + \eta_i^2] \frac{2\pi\eta_i}{e^{2\pi\eta_i} - 1} \quad (8.6)$$

The last factor is the value of C_l^2 for $l=0$, C_0^2 . This factor goes to zero rapidly

TABLE 8.2

η	$C_0^2(\eta)$
0	1.000
0.2	0.500
0.4	0.222
0.6	0.089
0.8	0.033
1.0	1.18×10^{-2}
2.0	4.38×10^{-5}

as the barrier energy increases or as the incident velocity decreases, as can be seen from Table 8.2, indicating the strong effect of the Coulomb repulsion. Similar factors $(k_f R)^{2l}$ and $C_l^2(\eta_f)(k_f R)^{2l}$ are present in the cross section for endoergic reactions, for which the emergent particle's momentum can approach zero.

B. Inside the Nucleus

Finally, we come to the question of how far a projectile will travel inside the nucleus once it penetrates the barrier. More precisely, how soon will the incident projectile leave the incident channel, that is, the elastic scattering channel? Empirical evidence indicates that the absorption of neutrons and protons in the nuclear interior is weak. It is, however, very strong for composite systems such as deuterons, α -particles, or heavy ions because these "dissolve" inside the nuclear interior and do not preserve their identity. Thus the composite particles do not penetrate a great distance into the nucleus and tend to be more sensitive to surface properties of nuclei and to excite surface states. The proton does not show such selectivity since it can penetrate the nuclear interior. This is illustrated in Fig. I.10.3 in deShalit and Feshbach (74), where one sees a marked difference in the number of levels excited in inelastic proton scattering compared to inelastic deuteron scattering. In the latter case one would expect a preference for the excitations of the vibrational modes of a nucleus [see deShalit and Feshbach (74, p. 471)].

Let us illustrate these remarks with simple examples. Neutrons and γ -rays are uncharged and thus do not have to penetrate the Coulomb barrier. Neutrons of low kinetic energy are thus the appropriate projectiles to be employed for the study of these states of the *compound nucleus*, formed by the neutron and target nucleus, whose excitation energy is near the separation energy of the neutron. It is in this region that an enormous number of compound nuclear resonances have been found. These are nearly bound states of the compound nucleus. [see Figs. I.12.2 and I.12.3 in deShalit and Feshbach (74); note the neutron energies.]

At very low energies, these resonances must, according to (8.4), be $l = 0$ resonances. As the energy increases, it becomes possible to excite $l = 1$ resonances

and at higher energies $l = 2$ resonances, and so on. For example, for the target nucleus, ^{64}Cu , kR is $\sqrt{2}$ for 1.8 MeV neutrons. It equals $\sqrt{6}$, appropriate for the $l = 2$ case for 5.4 MeV. Of course, both $l = 1$ and $l = 2$ resonances will make their appearance long before these values are reached. Their presence can be demonstrated by, for example, examining the angular distributions of elastically scattered neutrons at and near the resonant energy.

γ -Rays may be used to excite the target nucleus by absorption and in principle could be used to study any of the nuclear states. However, the angular momentum barrier plays a role. If a photon of energy $\hbar\omega$ is absorbed at a distance R from the center of the nucleus, it can transmit an angular momentum of $\hbar\omega R/c$, so that

$$l \lesssim \frac{\hbar\omega R}{\hbar c} = kR \quad k \equiv \frac{\omega}{c}$$

Since $\hbar c = 197.32 \text{ MeV fm}$, it is clear that for photon energies up to the order of a few tens of MeV, the photon absorption process will be dominated by the $l = 1$ (i.e., dipole) mode. Quadrupole and higher multipoles will also be absorbed, but the cross sections will be considerably smaller. This effect is clearly visible in the long-wavelength limit. In that limit the transition probability [see (VIII.5.35) deShalit and Feshbach (74)] is proportional to $(kR)^{2j+1}$, where j is the multipole order, so that the transition probability decreases rapidly with increasing j . It is, of course, no accident that the most readily observable gamma-induced reaction, the giant resonance seen in all nuclei [see pp. 48 and 491–503 in deShalit and Feshbach (74)], is a dipole resonance.

A major problem with the use of uncharged particles is the difficulty to measure and control them. The use of lithium-drifted germanium counters has vastly improved the detection of γ -rays, while in recent years the development of nano- and picosecond circuitry, together with the availability of more intense neutron sources, has changed the situation in neutron physics with regard to, for example, the study of (n, n') , (n, γ) , and $(n, n'X)$ reactions.

C. Electron Excitation

Since electrons are negatively charged, they are attracted by the positively charged target nucleus. The importance of elastic electron scattering for determination of the nuclear charge density has been emphasized in deShalit and Feshbach (74, pp. 3–7). Here the excitation of nuclear levels by electrons is discussed briefly. We shall consider *only* the effect of the Coulomb interaction:

$$V = \sum_{\text{prot}} \frac{e^2}{|\mathbf{r} - \mathbf{r}_i|} \quad (8.7)$$

where the sum is taken over all the protons in the nucleus and \mathbf{r} is the electron

coordinate. There are other terms involving the magnetic-type interaction and the interaction with exchange currents.

It is, of course, one of the great advantages of using the electron as a probe that the interaction is well known. In addition, the interaction is relatively weak, so that one can use the Born approximation.[†] For simplicity, we shall use the nonrelativistic form, which is incorrect for the high-energy electrons used. However, to some extent, it will be possible to correct for this error in the course of the calculation. The Born approximation inelastic amplitude is

$$f_{fi} = -\frac{1}{4\pi} \frac{2m}{\hbar^2} \int \dots \int e^{-i\mathbf{k}_f \cdot \mathbf{r}} \Phi_f^*(1, 2, \dots, A) \sum_{\text{prot}} \frac{e^2}{|\mathbf{r} - \mathbf{r}_i|} \Phi_i(1, 2, \dots, A) \times e^{i\mathbf{k}_i \cdot \mathbf{r}} d\mathbf{r} d(1) \dots d(A-1) \quad (8.8)$$

or

$$f_{fi} = -\frac{1}{4\pi} \frac{2m}{\hbar^2} \sum_{\text{prot}} \int e^{-i\mathbf{k}_f \cdot (\mathbf{r} - \mathbf{r}_i)} e^{i\mathbf{k}_i \cdot (\mathbf{r} - \mathbf{r}_i)} \frac{l^2}{|\mathbf{r} - \mathbf{r}_i|} d\mathbf{r} \int \dots \int e^{-i\mathbf{k}_f \cdot \mathbf{r}_i} e^{i\mathbf{k}_i \cdot \mathbf{r}_i} \times \Phi_f^*(1, 2, \dots, A) \Phi_i(1, 2, \dots, A) d(1) \dots d(A-1)$$

where Φ_f and Φ_i are the final and initial states of the nucleus, respectively. Since all the particles are identical, each of the terms in the sum is numerically identical. Therefore, with a change of variable,

$$f_{fi} = -\frac{1}{4\pi} \frac{2m}{\hbar^2} \int e^{i\mathbf{q} \cdot \boldsymbol{\xi}} \frac{Ze^2}{\xi} d\xi \langle \Phi_f | e^{i\mathbf{q} \cdot \mathbf{r}_1} | \Phi_i \rangle$$

where

$$\mathbf{q} = \mathbf{k}_i - \mathbf{k}_f \quad (8.9)$$

and \mathbf{r}_1 is the coordinate of one of the protons in the target nucleus. The first factor is the nonrelativistic Born approximation for the elastic scattering of an electron by a point nucleus of charge Ze . We shall replace it by the exact relativistic elastic scattering amplitude. Hence

$$f_{fi} = f_e(\mathbf{q}) \bar{\rho}_{fi}^{(c)}(\mathbf{q}) \quad (8.10)$$

where $\bar{\rho}_{fi}^{(c)}$ is

$$\bar{\rho}_{fi}^{(c)} \equiv \langle \Phi_f | e^{i\mathbf{q} \cdot \mathbf{r}_1} | \Phi_i \rangle$$

[†]For nuclei with large Z one must take the Coulomb distortion of the electron wave function into account. This will, however, not change the qualitative nature of the results obtained here.

$\bar{\rho}_{fi}^{(c)}(\mathbf{q})$ is the *form factor* for the transition. It is the Fourier transform of the transition charge density

$$\rho_{fi}^{(c)}(\mathbf{r}_1) = \int d(2) \cdots d(A-1) \Phi_f^*(1, 2, \dots, A) \Phi_i(1, 2, \dots, A) \quad (8.11)$$

and

$$\bar{\rho}_{fi}^{(c)}(\mathbf{q}) = \int e^{i\mathbf{q}\cdot\mathbf{r}_1} \rho_{fi}^{(c)}(\mathbf{r}_1) d\mathbf{r}_1 \quad (8.12)$$

It is the last quantity that is determined by experiment.

The transition will involve an angular momentum change of j and thus those components of $e^{i\mathbf{q}\cdot\mathbf{r}_1}$ that carry at least that amount of angular momentum will

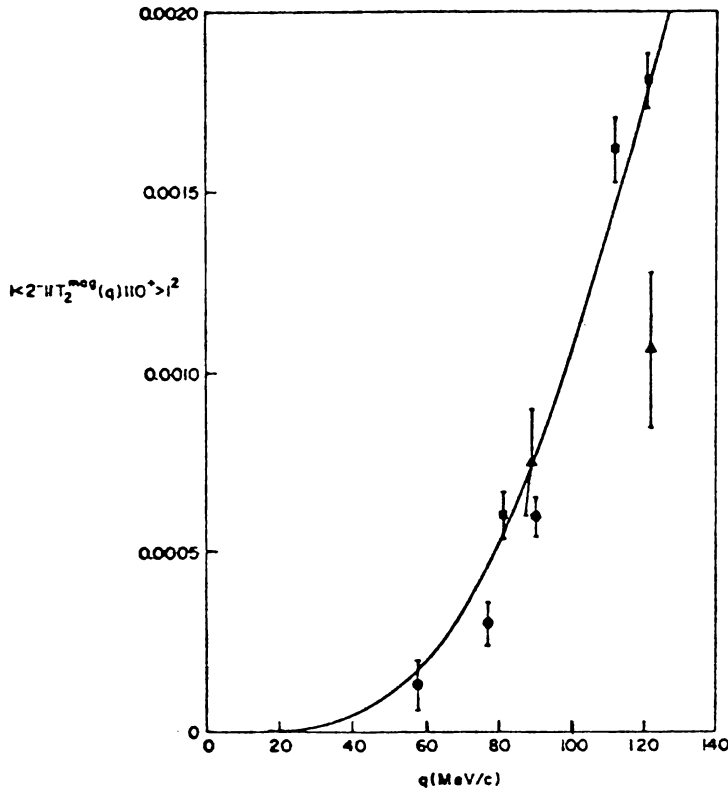


FIG. 8.3. Square of the magnetic form factor for the 2^- , $T = 1$ state at 20.76 MeV in ^{12}C . The theoretical calculation divided by 2 is compared with experiment. [From deForest and Walecka (66).]

survive the integration, that is

$$\bar{\rho}_{fi}^{(c)}(\mathbf{q}) = \sum_{l \geq j} (2l+1) i^l \int j_l(qr_1) P_l(\cos \vartheta_1) \rho_{fi}^{(c)}(\mathbf{r}_1) d\mathbf{r}_1$$

For not too large q , the first term in this sum dominates:

$$\bar{\rho}_{fi}^{(c)}(\mathbf{q}) \sim (2j+1) i^j \int j_j(qr_1) P_j(\cos \vartheta_1) \rho_{fi}^{(c)}(\mathbf{r}_1) d\mathbf{r}_1 \quad (8.13)$$

$$\sim \frac{i^j q^j}{(2j-1)!!} \int r_1^j P_j(\cos \vartheta_1) \rho_{fi}^{(c)}(\mathbf{r}_1) d\mathbf{r}_1 \quad (8.14)$$

The integral gives the *transition electric multipole moment*. The characteristic dependence on q^j of (8.14) is a reflection of the angular momentum barrier penetration. However, in contrast with the radiative case, for which q is limited to ω/c , where $\hbar\omega$ is the excitation energy, q in the electron inelastic scattering case can be varied from the minimum value of ω/c to a maximum available at back angles given by $(k_f + k_i) \approx 2E/\hbar c$, where E is the electron energy. It thus is possible to use inelastic electron scattering to map out $\bar{\rho}_{fi}^{(c)}(q)$ over a wide range in q , and therefore $\rho_{fi}^{(c)}(r)$, the γ -ray-induced transition providing only $\bar{\rho}_{fi}^{(c)}(\sim 0)$. It should be noted that the dependence q^j helps to identify the multipole moment (but not its electric or magnetic nature), as illustrated by Fig. 8.3.

D. Coulomb Excitation

As implied by the term *barrier*, the Coulomb and angular momentum barriers generally reduce the probability of a nuclear reaction as demonstrated by (8.4) and (8.6). However, this assumes that the reactions are induced by short-range forces. This assumption fails for the Coulomb force. A heavy ion of moderate energy passing at some distance from the target nucleus can still excite the nucleus through the action of the Coulomb force. This mechanism is referred to as *Coulomb excitation*. It is more effective the larger the atomic number of the heavy-ion projectile. By proper choice of the projectile and energy, one can adjust the distance of closest approach so that the projectile does not come too close to the nucleus, so that whatever excitation is observed is caused by the changing electric field associated with the motion of the projectile. Coulomb excitation will preferentially excite levels that have a high probability for γ -emission and indeed has been the method of choice for investigating the rotational spectrum of deformed nuclei [see deShalit and Feshbach (74, p. 412)]. A rough estimate of the Coulomb excitation cross section can be obtained using the Weiszäcker–Williams approximation. This approximation, which becomes increasingly valid as the projectile energy increases, replaces an incident charged

projectile by an equivalent beam of photons with a spectrum given by

$$dn(\omega) = \frac{2Ze^2}{\pi} \frac{d\omega}{\hbar v \omega} \quad (8.15)$$

where v is the velocity of the projectile. The cross section is then given by multiplying this spectrum by the cross section for the absorption of a γ -ray of energy $\hbar\omega$. Using (VIII.8.1) from deShalit and Feshbach (74), assuming zero width for the excited state, one obtains the following for the excitation cross section:

$$\sigma = (4\pi)^2 \frac{Ze^2}{\hbar v} \frac{e^2}{\hbar c} \frac{j+1}{j(2j+1)[(2j+1)!!]^2} k^{2j-2} B(\sigma_j; i \rightarrow f) \quad (8.16)$$

This formula should be considered of qualitative validity only in view of the shortcomings of the Weiszäcker–Williams approximation in the energy range in question. It does show the direct connection of the Coulomb excitation cross section with the B coefficients.

The Coulomb field exerted by a heavy ion is very strong. Evaluating the field of a heavy ion of charge z at the target nuclear radius R_T , one finds that the force F on a target nucleus, mass number A_T , and charge Ze is

$$F = \frac{zZe^2}{R_T^2} \simeq \frac{zZ}{A_T^{2/3}} \text{ MeV/fm} \quad (8.17)$$

For a ^{64}Cu projectile incident on ^{208}Pb , $F = 68 \text{ MeV/fm}$. Such a strong force permits multiple excitations; that is, the target nucleus while excited can be excited once more and the process can be repeated during the course of the collision. This means that the target nucleus will be in one of this chain of possible excited states for a finite time, with the consequence that the properties of such a state can be investigated. In this way the quadrupole moments of excited states have been measured.

E. Surface Reactions

As we stated earlier, composite particle projectiles do not penetrate the target because of absorption. These reactions thus probe the surface of the nucleus. The fact that only the surface is involved means that the important incident angular momenta are in the neighborhood of $p_i R$, where p_i is the initial momentum of the projectile, while the angular momentum carried off by the emerging projectile is $p_f R$, where p_f is the final momentum. Hence it will be most probable to excite the target to a level whose angular momentum differs from the ground state by qR , where $q = |\mathbf{p}_i - \mathbf{p}_f|$. This implies a maximum in

the angular distribution at an angle determined by

$$\hbar\Delta J = qR$$

or

$$1 - \cos \theta_M = \frac{(\hbar\Delta J/R)^2 - (p_i - p_f)^2}{2p_i p_f} \quad (8.18)$$

This angle becomes larger as the angular momentum change ΔJ increases. Since, classically, qR must be larger than $\hbar\Delta J$, the cross section is zero classically for $qR < \hbar\Delta J$. This phenomenon is illustrated in Fig. I.11.2b of deShalit and Feshbach (74), in which the angular distribution for the inelastic excitation of various levels in ^{58}Ni by α -particles is shown. One sees that the first peak (excluding a possible peak at 0°) occurs at greater angles as l , the angular momentum of the levels, increases. The angles θ_M predicted from (8.18) are 6.2° , 9.2° , and 12.1° , which compare with 10° , 15° , and 17° experimentally. One also observes a drop in the cross section as one decreases the angle for the $l = 3$ and 4 cases.

The angles predicted from (8.18) are not quite correct since the reduction in momentum that occurs because of the Coulomb repulsion was not taken into account. The Coulomb reduced momentum, p_c , is related to the momentum p (either the incident or final momentum) by

$$p_c = p \left(1 - \frac{zZe^2}{ER} \right)^{1/2} \quad (8.19)$$

where E is the energy. Then using $(p_c)_i$ and $(p_c)_f$ in (8.18) instead of p_i and p_f gives values of θ_M equal to 10.4° , 15.5° , and 20.3° , which compare more favourably with the experimental values. Of course, these simple predictions are substantially modified by quantum-mechanical effects as well as by the effects of the interaction with the target.

An indication of the narrow range in orbital angular momenta involved in reactions of this type is shown in Fig. 8.4. In this case of α -particle inelastic scattering by ^{24}Mg at $E = 84 \text{ MeV}$, the behavior of imaginary parts of the radial integrals involved in the calculation of the cross section for the process is plotted as a function of the average $\bar{l} = (l_i + l_f)/2$, where l_i is the angular momentum of the incident wave and l_f of the emergent wave. We see that most of the radial integral is concentrated in the region $\bar{l} = 18 \pm 2$. This is in reasonably close agreement with pR/\hbar , which for the R of 3.841 fm used in these calculations equals 15.2 . One also notes a very strong oscillation in the angular distribution (see Fig. 8.5). This is the case because the reaction occurs only at the surface, with the consequence that the α -particle is diffracted by the target. Typically, the angular distribution is proportional to $[j_l(qR)]^2$ (j_l is the spherical Bessel

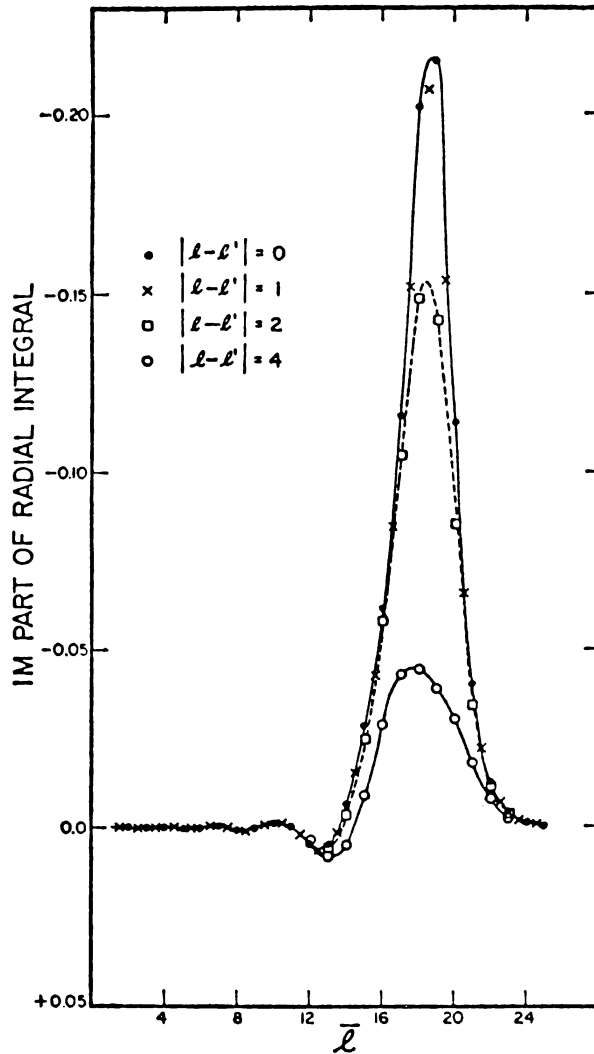


FIG. 8.4. Localization of the radial integrals for $\text{Mg}^{24}(\alpha, \alpha')$. [From Austern (70).]

function; see Appendix A). Indeed, as pointed out in Chapter I of deShalit and Feshbach (74, p. 79), this phenomenon can be used to determine R , the effective radius for the reaction being studied.

F. Stripping and Pickup

As discussed earlier, the stripping and pickup reactions result in the deposition (stripping) or removal of a neutron (pickup) from a single-particle orbit. Since

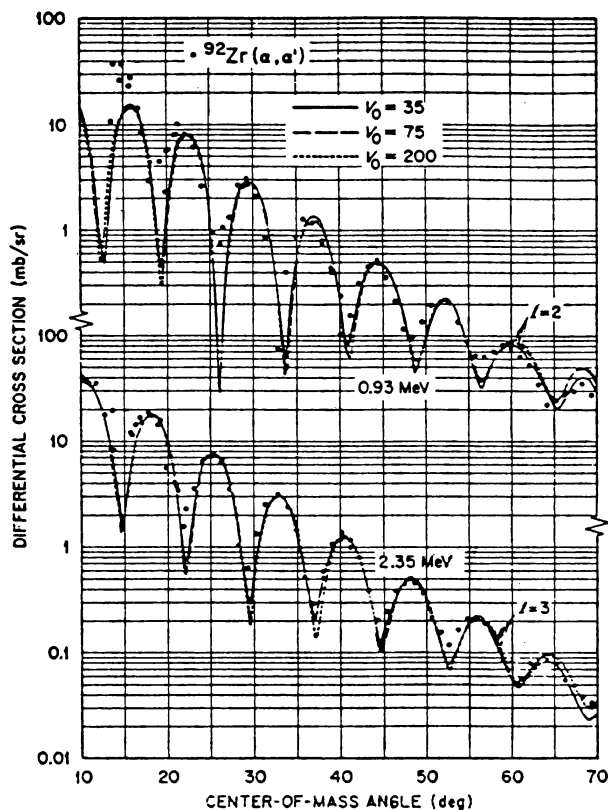


FIG. 8.5. Comparison of the DWA theory with experimental data for $\text{Zr}^{92}(\alpha, \alpha')$ at 65 MeV bombarding energy. The energies and angular momenta of the Zr^{92} excited states are given on the graph. [From Austern (70).]

the deuteron is strongly absorbed, the cross section will be largest if the single-particle wave-function is appreciable at the nuclear surface. For this reason the valence neutrons are generally involved. For example, in the $^{40}\text{Ca}(d, p)^{41}\text{Ca}$ reaction of Fig. I.12.1 in deShalit and Feshbach (74), the neutron can go into the $1f_{7/2}$ orbit or higher orbits. However, the state in ^{41}Ca that is excited is generally not pure $\phi(f_{7/2})\Psi_T(^{40}\text{Ca})$ but will have other components. As a consequence, before comparison with experiment is possible, the magnitude of the cross section calculated using (4.1) must be multiplied by a factor, the *spectroscopic factor*, less than unity. The spectroscopic factor gives the probability of finding the final system in the state $\phi(f_{7/2})\Psi_T(^{40}\text{Ca})$. One of the results of the measurement is the energy of the state in question, so that one can map out the energy of the single-particle (or quasi-single-particle) states for a large variety of nuclei. The results are shown in Fig. 8.6.

Neutrons are also added to or removed from a target nucleus by the (n, γ)

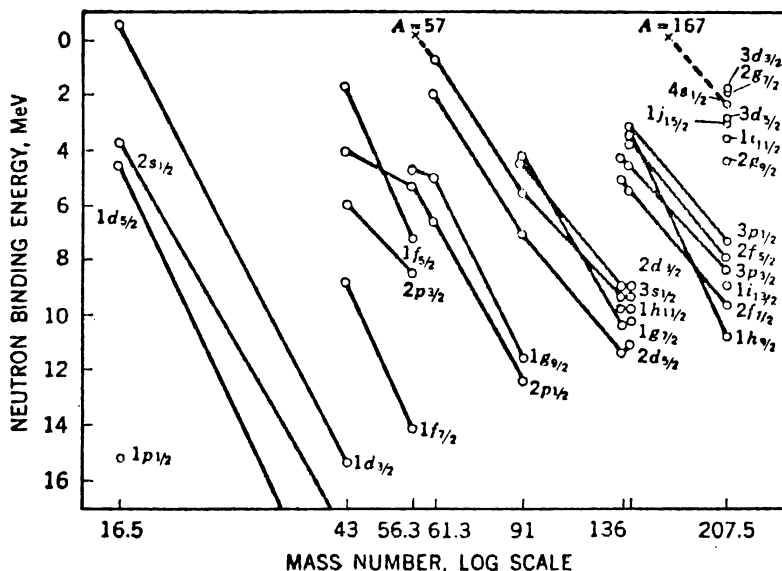


FIG. 8.6. Energies of neutron orbits in various single-particle and single-hole nuclei. Small corrections for symmetry energy have been applied to correct the data to the line of beta stability. [From Cohen (71).]

and (γ, n) processes, respectively. By choosing the appropriate γ -ray energy, one can select some of the states populated by (d, p) or (p, d) reactions. The comparison between the two sets of reaction is informative both as to the nature of the reactions and the states excited. The neutron absorbed is usually a low-energy neutron limiting the angular momentum of the quantum numbers of the compound nucleus. The (γ, n) reaction, on the other hand, is not limited to the removal of neutrons in surface orbitals as is the (p, d) reaction.

The pickup process, (p, d) , may be discussed in similar terms. The neutron that is "picked up" is, for the following reason, again a surface neutron in the sense that its wave function peaks at the surface. If the deuteron is made too deeply within the nuclear interior, it will be absorbed before it can escape from the nucleus. Hence surface production will be more visible.

As the energy increases the deuteron will eventually have a large enough mean free path that its production in the interior of the nucleus will be observable. In that case the state of the residual nucleus will, in shell model terminology, be a hole state.[†] Observations of such states by this method have been made. We mentioned earlier another method of observing single hole states by the (γ, n) reaction and by quasi-elastic scattering of energetic electrons or protons

[†]The reader should recall that the definition of a hole state depends on the "vacuum" chosen. For example, the removal of a neutron from ^{18}O could be described as leaving a hole state in ^{18}O or leaving a $2p-1h$ state with an ^{16}O core.

in the $(e, e'p)$ or $(p, 2p)$ reaction, respectively. A comparison of the results obtained with these various methods will provide information on the reaction mechanisms involved as well as the nature of the excited state.

For the stripping and pickup processes, it is important to realize that the single-particle or single-hole states that are probed are surface states not only in configuration space but also in momentum space; that is, for the most part we are dealing with states near the Fermi momentum p_F . Much the same can be said of the excitations induced by other composite particles. The vibrations seen with inelastic α -particles are, for the most part, coherent linear combinations of one-particle-one-hole states, but the major contributions come from states close to p_F .

G. Examples of Direct Reactions

The stripping and pickup reactions are archetypes of the use of direct reaction to study nuclear structure. By choosing the appropriate projectile and energy, it becomes possible to study a wide variety of nuclei and excitations. We earlier mentioned the use of the $(^3\text{He}, d)$ and $(d, ^3\text{He})$ reactions to study single-particle proton states and the $(^3\text{H}, p)$ and $(p, ^3\text{H})$ to study “superconducting” nuclei by the transfer of two neutrons coupled in a 1S_0 state. Inelastic proton and neutron scattering will study the formation of $1p-1h$ states.[‡]

H. Heavy Ions

The availability of heavy ions greatly increases the variety of projectiles and the range of possible transfers of particles from and to the heavy ions and the target nuclei. The transfer of α -particles is conveniently studied using ^6Li projectiles, for example. The nuclei ^{17}O and ^{18}O are useful projectiles for the study of single- and two-neutron transfers. Heavier nuclei are neutron rich and thus facilitate the transfer of many neutrons and the consequent formation of new nuclei approaching more closely those nuclei that are unstable against neutron emission. On the other hand, the same process can lead to the formation of multiparticle-hole states.

In the case of heavy-ion projectiles, it is often the case that the single-step direct description is inadequate and one must turn to the multistep direct processes. Virtual excitation of the low-lying levels in both the projectile and target nucleus can play a role. The sequential transfer of nucleons, resulting in

[‡]We repeat a caveat. The independent-particle model description of nuclei is oversimplified. The ground state of ^{16}O , for example, consists of the independent-particle state marking the completion of the p -shell but also $2p-2h$ and $4p-4h$ components, to mention the most likely. These are essential for proper descriptions of the correlations in the ground state. It is convenient to adopt the terminology of Chapter VII in deShalit and Feshbach (74) and refer to the more complete description of single-particle states as *quasi-single-particle* states and the states obtained by inelastic excitation as *quasi-particle-hole* states.

a many-nucleon transfer, can compete with the transfer of the entire cluster as a single-step process.

Because heavy ions are composite, they generally do not penetrate deeply into the target nucleus. Most of the transfer reactions discussed above occur close to the nuclear surface, and thus the heavy ions serve as probes of the surface. The effectiveness of heavy ions in this respect is accentuated by their very short wavelength, which is given by

$$\lambda = \frac{4.56}{(AE)^{1/2}} \quad \text{fm} \quad (8.20)$$

where A is the projectile mass, E its energy in MeV, and λ is in fermis. For example, if an electrostatic accelerator of the van de Graaf type has an effective terminal voltage of 20 MV, a ^{32}S ion stripped of half its electrons will acquire an energy of 5 MeV per nucleon. Under these circumstances λ equals 6.4×10^{-15} cm! This very short wavelength permits the use of classical mechanics for the discussion of the motion of a heavy ion. Second, it demonstrates the possibility of using a heavy ion as a probe of the surface structure of the target with considerable spatial resolution.

An example of the discussion above is provided by the interaction of ^{16}O ions with ^{60}Ni . The angular distribution, shown in Fig. 8.7, shows rapid oscillations at small angles. This effect can be understood by examining the classical orbits of the ^{16}O ion in the field of the ^{60}Ni nucleus taking the nuclear interaction as well as the Coulomb interaction into account (see Fig. 8.8). It will be observed that orbit 1 above the grazing orbit, g , and orbit 3 give rise to identical scattering angles; in the latter case the nuclear interaction plays an essential role. However, it might be expected that orbit 3 would not be of much importance because of the absorption that takes place in passing through the surface region of the target nucleus. To explain the observations, this expectation must be incorrect. In the surface region involved in the small-angle scattering (and one can be quite specific about that region because of the short wavelength involved), the absorption must be weak, an important conclusion that so far seems to be valid for a variety of heavy-ion reactions.

The procedure employed to obtain the foregoing conclusion is of general interest. It is familiar from *physical optics*, where characteristically the wavelength of light is very much smaller than the dimensions of the components of the optical system. In physical optics the motion of the incident plane wave is "broken up" into the behavior of rays, which is calculated by the methods of classical mechanics. Each ray follows the classical orbit illustrated in Fig. 8.8. The phase of the wave along each ray is obtained by calculating the optical path length given by

$$\int n ds$$

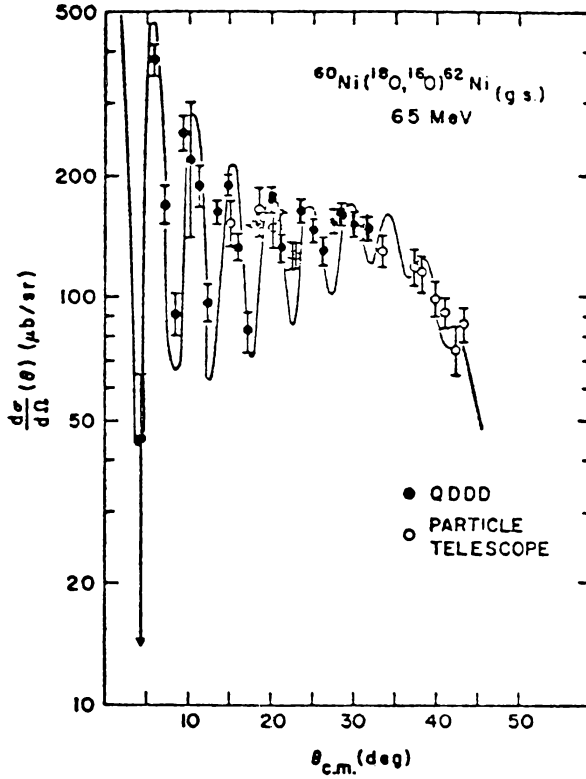


FIG. 8.7. Angular distribution corresponding to the $^{60}\text{Ni}(^{18}\text{O}, ^{16}\text{O})^{62}\text{Ni}(\text{g.s.})$ transition to the ground state of ^{62}Ni measured at an incident laboratory energy of 65 MeV compared with a DWA theoretical prediction. [From LeVine, Baltz, et al. (74).]

where n is the effective index of refraction

$$n = \sqrt{1 - \frac{V}{E}}$$

By this means it is possible to construct a final wavefront, which, of course, will no longer be a plane wave.

The crucial point in the analysis of the small-angle $^{16}\text{O} + ^{58}\text{Ni}$ scattering is that different rays, 1 and 3 in Fig. 8.8, have the same angle of scattering. The amplitude at infinity is obtained by adding the *amplitude* of each of these two contributions. The rapid oscillations reflect the fact that as the angle of scattering changes, the net value of the amplitude will fluctuate as the relative phase of the two contributions changes. Constructive interference will give rise to the peaks and destructive interference to the valleys. For these oscillations to be observable, the magnitude of the contributing amplitudes must be comparable.

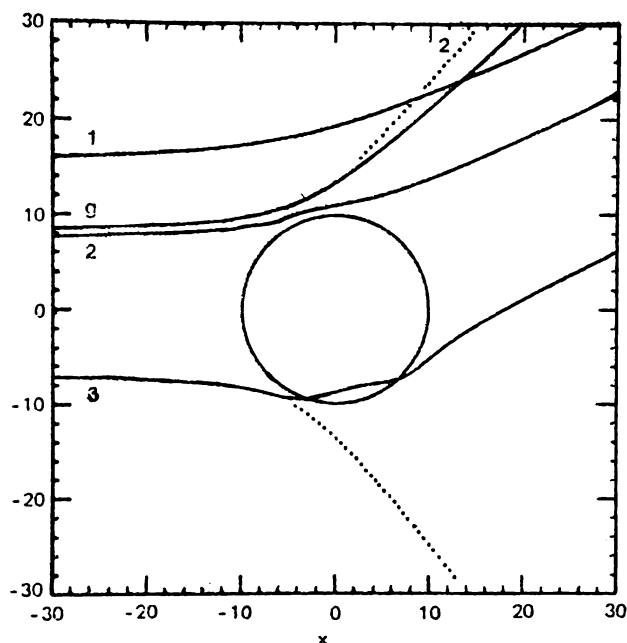


FIG. 8.8. Four classical orbits are plotted, three of which (1,2,3) scatter to the same angle. The grazing orbit is *g*. The circle marks the half-value of the Woods-Saxon nuclear potential. The orbits are for 100 MeV lab energy ^{18}O scattered by ^{120}Sn . Dotted lines show pure Coulomb orbits. The scale is in Fermi's [From Glendenning (75).]

This is possible only if the absorption in the surface region is not large, the conclusion noted earlier in this discussion.

9. REACTIONS WITH "EXOTIC" PROJECTILES

We have commented earlier on the reactions that can be induced by the exotic projectiles (π , K , \bar{p} , etc.). Their theoretical description does bring in some unique features that need to be addressed. For example, a pion interacting with a nucleon can form a Δ , the excited state of the nucleon. Therefore, an important intermediate state—a doorway state—which is formed in a pion-nucleus collision, is a Δ -hole state. The properties of the Δ -hole state are critically important for an understanding of pion-induced reactions and pion production. In pion production a Δ is formed in the collision of a nucleus with the incident projectile. The Δ then decays into a nucleon plus a pion. Because the Δ -hole state is generally a coherent combination of states with differing orbits for the Δ and for the hole, a single-step DWA direct reaction description will not suffice. Note that the π^+ couples strongly to the proton and weakly to the neutron in forming the Δ . The reverse is exhibited by the π^- , so that

pion–nucleon interaction is sensitive to the neutron and proton distributions. The double charge exchange reaction (see p. 16) requires the intervention of at least two nucleons and therefore is sensitive to the nucleon–nucleon correlations inside the nucleus.

When a kaon is incident on the target nucleus, it becomes possible to produce a Λ via the elementary reaction.



If the Λ is captured by the nucleus, a hypernucleus will be formed. Capturing the Λ in a well-defined state is most likely if the nucleus does not fragment. Fragmentation can occur if the recoil momentum of the nucleon in the nucleus exceeds the Fermi momentum, which is on the order of 250 MeV/c for all but the lightest nuclei. [However, see Dalitz and Gal (76), who give a more stringent condition.]

A zero-momentum transfer is possible for the (K^-, π^-) reaction, for example [Podgoretsky (63); Feshbach and Kerman (66)]. In the elementary reaction equation (9.1), consider the case in which the neutron is at rest and the pion is observed in the forward direction. We shall now show that there is an incident kaon momentum for which the Λ produced is at rest. Under these circumstances conservation of energy and momentum (the momentum p of the kaon and the momentum of the pion are equal) requires

$$\sqrt{c^2 p^2 + m_K^2 c^4} + m_N c^2 = m_\Lambda c^2 + \sqrt{c^2 p^2 + m_\pi^2 c^4}$$

It is a simple matter to solve this equation for the kinetic energy of the incident kaon:

$$E_K - m_K c^2 = \frac{(m_K + m_N - m_\Lambda - m_\pi)(m_K + m_N - m_\Lambda + m_\pi)c^2}{2(m_\Lambda - m_N)}$$

Inserting the value of the masses yields a kinetic energy of about 231 MeV and a momentum of 531 MeV/c. At this energy the Λ produced will be at rest. In Table 9.1, the recoil Λ momenta, p_Λ , is given for a range of incident kaon momenta. Note that p_Λ equals the momentum transfer. Moreover, for a given kaon momentum, departure from the forward direction for the π^- increases the momentum transfer.

TABLE 9.1

$p_K(\text{MeV}/c)$	0	400	531	700	1000	2000
$p_\Lambda(\text{MeV}/c)$	250	40	0	40	75	130

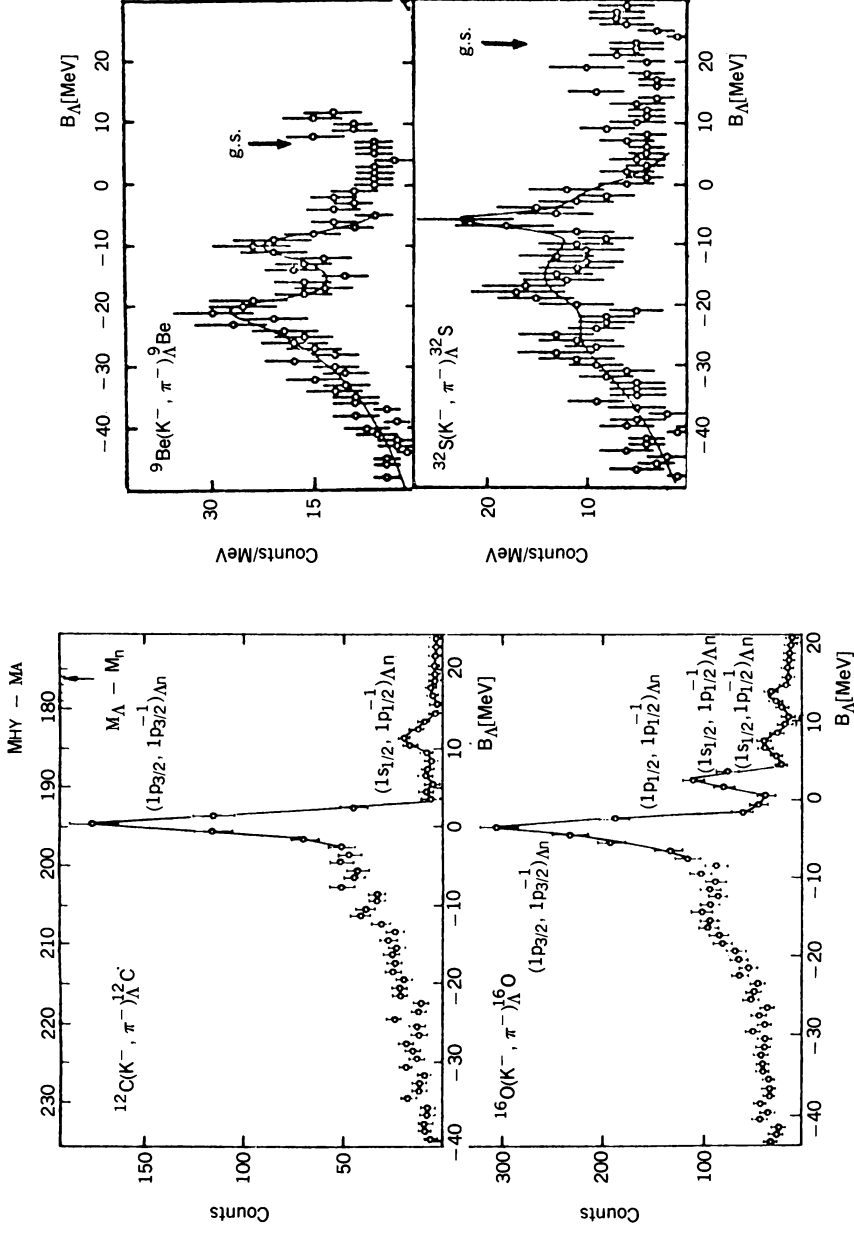


FIG. 9.1. Pion spectra obtained from the (K^-, π^-) reaction on ^{12}C , ^9Be , ^{16}O , and ^{32}S plotted as a function of the Λ binding energy, B_Λ . [From Brückner, Granz, et al. (76, 78).]

These results suggest that if a K^- in the momentum range sufficiently close to 531 MeV/c strikes a nucleus, it will be possible for the kaon to “strangeness exchange” with a nucleon, with the emergent pion going off in the forward direction, the Λ remaining behind and forming a hypernucleus in a definite state. One would expect a large cross section in this kaon momentum range, with the cross section being small elsewhere. This effect has been observed in a number of nuclei. In Fig. 9.1 we show the results obtained for $^{12}\text{C}(K^-, \pi^-)^{12}_{\Lambda}\text{C}$ and $^{16}\text{O}(K^-, \pi^-)^{16}_{\Lambda}\text{O}$ (at $p_K = 715$ MeV), where the pions are observed in the forward direction [Brückner, Granz, et al. (76, 78)]. A strong peak with a sizable cross section is clearly seen, confirming the existence of a direct strangeness exchange process.

The peaks are labeled by the orbit occupied by the Λ and the resulting neutron-hole. The major peaks are substitutional. The $p_{3/2}$ peak in ^{16}O consists of a Λ in a $p_{3/2}$ orbit about the host nucleus ^{15}O in a $p_{3/2}$ state, while in the $p_{1/2}$ case the ^{15}O is in a $p_{1/2}$ state. The splitting in ^{15}O between these two states is 6 MeV, with a maximum amount of 0.3 MeV which can be ascribed to the Λ spin-orbit interaction. It is therefore very small. The DWA calculation of Boussy (77) confirms this result. The Λ -nucleus spin-orbit potential is thus very much smaller than in the nucleon-nucleus case. Later experiments in which γ -ray transitions between hypernuclear energy levels were observed in a $(K^-, \pi^- \gamma)$ coincidence measurement. [May et al. (81)] confirmed this result.

We also note that an $(s_{1/2})_{\Lambda}(p_{3/2}^{-1})_n$ state is found. This illustrates an important point. In a hypernucleus, the Λ with a mass (1115.6 MeV) similar to the nucleon and indeed a member of the SU(3) octet ($n, p, \Lambda, \Sigma^{\pm}, \Sigma^0, \Xi^-, \Xi^0$) does not need to satisfy the Pauli exclusion principle with respect to the nucleons in the nucleus. It can enter regions of configuration and momentum space forbidden to the nucleons. For example, the state $(s_{1/2})_n(p_{3/2}^{-1})_n$ is forbidden by the exclusion principle, but a Λ in the $s_{1/2}$ orbital about the ^{15}O host is allowed. From the point of view of the study of nuclear structure, the Λ in a hypernucleus acts as a baryonic probe, thereby providing another and quite different way to study nuclear properties.

10. SPECIFICITY AND SYMMETRY

The isolation of a given mode of interaction, which is one of the essential elements helping to ensure specificity, is greatly aided by symmetry requirements. These lead to selection rules that must be satisfied by the reaction. On the other hand, by studying the appropriate nuclear reactions and observing the selection rules, one can help determine the symmetries of the underlying elementary particle interactions and the accuracy with which they are satisfied. The discovery of parity nonconservation is a notable example of the use of nuclear properties for this purpose.

There are two kinds of symmetry of interest, intrinsic and space-time. The first is exemplified by charge, isospin, and strangeness. The second leads to such

overall conservation principles as conservation of linear and angular momentum, parity, and energy. Dynamically, the space-time properties of the fields that interact with nuclei are of fundamental importance. Since the vector potential (\mathbf{A}, ϕ) transforms as a 4-vector, the electromagnetic field couples with the 4-vector nuclear charge current (\mathbf{J}, ρ) and thus serves as a probe of these nuclear properties. This coupling is required by Lorentz invariance of the Lagrangian, giving the interaction term $\mathbf{j} \cdot \mathbf{A} - \rho \phi$. The selection rules for electromagnetic transitions given in Chapter VIII of deShalit and Feshbach (74) are direct consequences of the transformation properties of \mathbf{A} and ϕ . On the other hand, if the selection rules are known, it becomes possible to deduce these transformation properties.

In actual practice the transformation properties of the electromagnetic fields are used to identify the spins and parities of the levels of a nucleus by observing transitions induced by γ -rays, by the Coulomb field of heavy ions, or by the inelastic scattering of electrons.

Once these quantum numbers are established by, for example, observation of electromagnetic transitions, it becomes possible, by observing the transitions induced by another field, to determine its transformation properties. For example, nuclei can be used as “filters” that distinguish among the various symmetries of the weak interactions [Chapter IX of deShalit and Feshbach (74)]. In β -decay, by choosing the appropriate decaying nucleus and the appropriate final state, one can examine separately the Fermi and Gamow–Teller interactions. The superallowed $O^+ \rightarrow O^+$ transitions of isospin $T = 1$ nuclei [see deShalit and Feshbach (74, p. 788)] involve only the Fermi matrix element, $\langle \psi_f | \tau^\pm e^{i\mathbf{q} \cdot \mathbf{r}} | \psi_i \rangle$, while the decay of ${}^6\text{He}$ into ${}^6\text{Li}$, from a spin 0 state to a spin 1, involves only the Gamow–Teller interaction, $\langle \psi_f | \tau^\pm \boldsymbol{\sigma} e^{i\mathbf{q} \cdot \mathbf{r}} | \psi_i \rangle$.

It is possible using neutrino-induced reactions [e.g., (ν, e^-)] and appropriate initial and final nuclear states, to select out various components of the weak interaction and obtain their momentum dependence. The results for the Fermi and Gamow–Teller matrix elements obtained from β -decay mentioned above involve only low momenta (i.e., small q) values. The selection rules for the neutrino-induced process are given in Table IX.17.2, of deShalit and Feshbach (74). By choosing appropriate initial and final states in the reaction, one can select out various combinations of terms in the Hamiltonian equation (IX.17.15).

Pion reactions can be used to explore the nature of the transition axial vector currents. For example, in a (γ, π) or (π, γ) reaction, the coupling to the nucleons must involve transition axial nuclear currents because of the pseudoscalar nature of the pion. The leading term of the (γ, π) reaction amplitude near threshold is proportional to

$$\left\langle \psi_f \left| \sum_i \tau^\pm \boldsymbol{\sigma}_i \cdot \mathbf{E} \phi \right| \psi_i \right\rangle$$

where \mathbf{E} is the electric field associated with the γ -ray and ϕ is the pion field wave function. We see that the Gamow–Teller combination is involved, while

the axial current is given by $\sum_i \tau_i^\pm \sigma_i$. The connection of the pion transition to the weak interaction is not in retrospect surprising because of the relation between the axial current and the pion field given by PCAC [see (IX.14.4) of deShalit and Feshbach (74)]. Similarly, the (K, π) reactions can probe the transition and exchange strangeness currents.

Intrinsic symmetries will also provide selection rules that select reaction modes. Strictly speaking, isospin is not conserved in nuclear reactions because the Coulomb interaction violates isospin conservation. However, the effects of Coulomb force, such as the Coulomb barrier on either the incident channel or on the exit channel or both, can be taken into account. One may then ask: Upon making this correction, will the remaining features of the reaction conserve isospin? In other words, is the effect of the Coulomb field (or other isospin breaking interactions) of importance only when the projectile approaches the target or when the emergent particle leaves the residual nucleus? The answer appears to be that isospin is usually conserved in one-step direct reactions once the external effects of the Coulomb field are taken into account. However, the question of whether isospin is conserved in multistep processes is more difficult to answer in general. One would expect it to hold if there are only a few steps involved but that as the number of steps increases it would begin to fail. The expectation that isospin is conserved in direct processes relies on the long range of the Coulomb potential, which as a consequence has small nondiagonal matrix elements connecting states of differing isospin. The Coulomb potential can have substantial diagonal elements, giving rise to substantial energy shifts (the *Coulomb energy*). An excellent example of this effect is seen in the isobar analog state, which differs substantially in energy from its parent state because of the Coulomb interaction but whose wave function is hardly affected because its nondiagonal matrix elements between states of differing isospin are small [see the discussion on p. 102 of deShalit and Feshbach (74)]. However, in the multistep processes one has the possibility that the isospin (conservation) violation accumulates after a number of steps and become appreciable. It should also be borne in mind that the effect of the isospin violating interaction depends not only on the magnitude of the nondiagonal matrix element but also on the density of final states; the greater their number at the right energy, the greater the probability of a transition. The relevant additional fact is that the density of levels goes up very rapidly with the number of steps. It thus seems likely that if a reaction involves more than a few steps, isospin is probably not conserved. We would, for example, not expect isospin conservation in the evaporation part of the spectrum. This is indeed observed.

A rather striking example of the breakdown of isospin conservation occurs in the (α, γ) process. The α -particle has zero isospin, while the γ -ray can be considered for the energy domain under investigation to have unit isospin. The process therefore involves a change $\Delta T = 1$ between the initial and final nuclei. Under these circumstances, the process $^{28}\text{Si}(\alpha, \gamma_0)^{32}\text{S}$ leading to the ground state of ^{32}S is isospin forbidden, whereas $^{30}\text{Si}(\alpha, \gamma_0)^{34}\text{S}$ is allowed. But, in fact, the cross section for the first of these is larger than the cross section for

the second! The explanation seems to be that a number of steps must be involved as the system proceeds from the capture of the α -particle to the final release of the γ -ray.

Isospin symmetry is broken because of the interaction carried by the electromagnetic field. That interaction can be considered to be transmitted by the interchange of the photon by the interacting systems. When we extend our considerations to include the strange particles, isospin symmetry is extended to the SU(3) symmetry. If isospin symmetry were exact, the masses of the neutron and proton would be identical. If SU(3) symmetry were exact, the masses of the neutron, proton, Λ , $\Sigma^{(+,0,-)}$, and $\Xi^{(-,0)}$ would be identical. They are not. The Λ -proton mass difference, for example, is 177.3 MeV. This symmetry breaking (in addition to the electromagnetic variety described above) is thought to be a consequence of the mass of the strange quark, which differs from that of the up and down quarks. Recall that the proton consists of two up quarks and one down quark, while the Λ is made up of an up, a down, and a strange quark. Symmetry breaking of the baryon-baryon forces occurs because the kaons and pions are massive; the forces they transmit have a finite range given by their Compton wavelength, which is on the order of 0.4 and 1.4 fm, respectively. It is clear that in contrast with the Coulomb potential, the differences between the nuclear matrix elements of the forces generated by pion and kaon exchange will not be small and thus SU(3) symmetry is broken. However, it is possible, as in the Coulomb case, that the nondiagonal matrix elements between states specified by SU(3) quantum numbers are small. In that event, SU(3) analog states would exist.

We conclude this section with two examples of the impact of symmetry on nuclear reactions. Spatial symmetries in the angular distribution of reaction products can be a consequence of the statistics satisfied when the projectile and target are *identical*. The simplest case is provided by the elastic scattering of a ^{12}C nucleus by another ^{12}C nucleus. This system obeys Bose statistics; that is, the wave function of the system must be symmetric with respect to the exchange of the two ^{12}C nuclei. The wave function for the system can be written as follows:

$$\phi(\xi_a)\phi(\xi_b)\chi(\mathbf{R}_a - \mathbf{R}_b)$$

where $\phi(\xi_a)$ is the wave function describing the ^{12}C particle and ξ_a represents all the internal coordinates. The wave function χ describes the relative motion of the two nuclei, depending only on the center of mass \mathbf{R}_a and \mathbf{R}_b of each of the particles. From the Bose symmetry it follows that

$$\chi(\mathbf{R}_a - \mathbf{R}_b) = \chi(\mathbf{R}_b - \mathbf{R}_a)$$

Hence asymptotically,

$$\begin{aligned} \chi(\mathbf{R}_a - \mathbf{R}_b) \rightarrow \frac{1}{\sqrt{2}} [e^{ik \cdot (\mathbf{R}_a - \mathbf{R}_b)} + e^{-ik \cdot (\mathbf{R}_a - \mathbf{R}_b)}] \\ + [f(\theta) + f(\pi - \theta)] \frac{e^{ik|\mathbf{R}_a - \mathbf{R}_b|}}{|\mathbf{R}_a - \mathbf{R}_b|} \end{aligned} \quad (10.1)$$

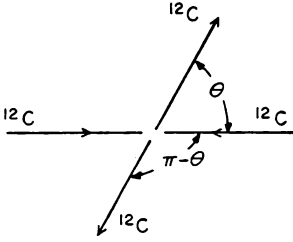


FIG. 10.1

where

$$\cos \theta = \frac{\mathbf{k} \cdot (\mathbf{R}_a - \mathbf{R}_b)}{k|\mathbf{R}_a - \mathbf{R}_b|}$$

The scattering amplitude

$$f(\theta) + f(\pi - \theta) \quad (10.2)$$

is symmetric about 90° , which simply reflects the identity of the two ^{12}C nuclei, as can be seen in Fig. 10.1. It is not possible to determine which of the two ^{12}C nuclei scattered through the angle θ and which through the angle $(\pi - \theta)$. The plus sign between the two amplitudes is a consequence of the Bose statistics obeyed by the ^{12}C nuclei. Fermi statistics implies the opposite sign.

More generally, Bose statistics imply that the only even-parity wave functions enter into the incident wave [see the first two terms in (10.1), which describe the incident wave for a two-body Bose system], and therefore (assuming conservation of parity) *only even-parity wave functions are to be found in the emerging wave*. This conclusion applies not only to elastic scattering but also to reactions. Thus in the $^{12}\text{C}(^{12}\text{C}, \alpha)^{20}\text{Ne}$ reaction, as a consequence of the Bose statistics of ^{12}C , only even-parity states of the $\alpha + ^{20}\text{Ne}$ system are generated.

These arguments are readily generalized to particles with spin. Nuclei with an odd number of nucleons obey Fermi statistics, while even- A nuclei obey Bose statistics. A simple example is the scattering of identical spin- $\frac{1}{2}$ particles, such as protons or ^{17}O nuclei. One can classify the spin states of the system as singlet and triplet, the first of which is odd under exchange, the second even. To satisfy the requirements of Fermi statistics, the spatial wave function for the singlet state should be even under exchange, whereas for the triplet state the spatial wave function is odd. The former then has even parity, the latter odd parity, so that for the triplet state the scattering amplitude has the form

$$f(\theta) - f(\pi - \theta)$$

and is zero at $\theta = \pi/2$.

A general theorem derived, for example, by C. N. Yang deals with the maximum complexity to be expected in an angular distribution. Consider, for simplicity, the collision of a spinless system by a spinless, target leading to

spinless products. The maximum angular momentum L_i brought in by the incident wave that will make significant contributions to the collision is determined by the Coulomb and angular momentum barriers. The limit imposed by the latter is approximately

$$L_i \sim k_i R$$

where k_i is the incident wave number and R is the radius determined by the range of the interaction. Similarly, there will be a limit to angular momentum of the final system given by L_f . The theorem states that when the angular distribution is decomposed into Legendre polynomials P_L , the maximum value of L will be the minimum of the two values $2L_i$ and $2L_f$. The theorem can readily be understood on the basis of the information content of both the

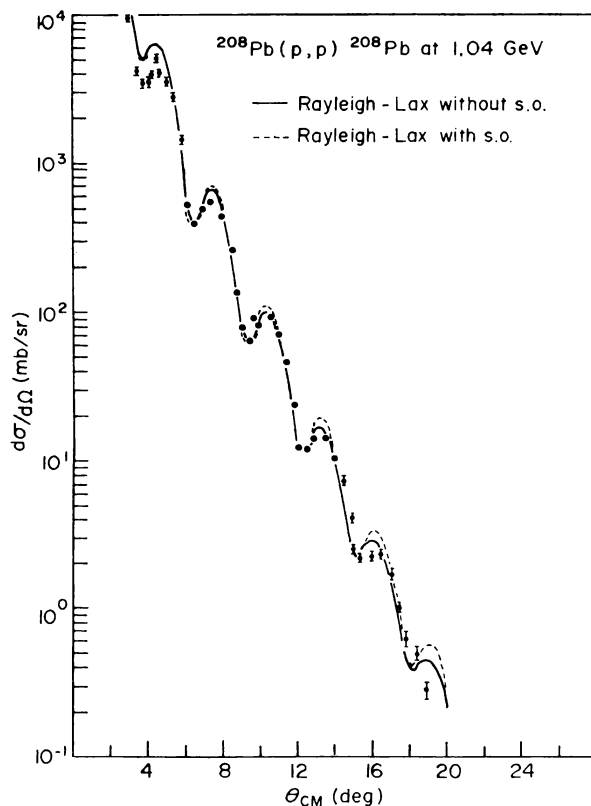


FIG. 10.2. Comparison of experimental angular distribution for the elastic scattering of 1.04-GeV protons by ^{208}Pb with the predictions employing the Rayleigh-Lax potential with and without spin-orbit (s.o.) terms. The density-dependent Hartree-Fock densities are used. [From Boridy and Feshbach (77).]

incident and emerging waves. For example, if the highest-order Legendre polynomial entering in the incident wave is P_{L_i} , the incident direction is defined with an uncertainty of $O(1/L_i)$. The collision process cannot reduce this uncertainty, so that the maximum order of the Legendre polynomials in the emerging amplitude certainly cannot exceed L_i . The angular distribution involves the square of the amplitude and thus the limit of $2L_i$ is obtained. When spin is introduced the theorem now states that the maximum value of L is the minimum of $2L_i$, $2L_f$, and $2J$, where J is the maximum value of the total angular momentum of the system entering in the reaction. A simple consequence of this discussion is that the angular distribution for the elastic scattering will exhibit oscillations whose period is greater than or on the order of $1/kR$. At very high energies or for strongly absorbed particles the oscillations are of the order of $(1/kR)$ (see Fig. 10.2).

Problem. Prove that the only states of a spin-zero nucleus that can be excited by the forward ($\theta = 0$) inelastic scattering of α -particles are the natural parity states, 0^+ , 1^- , 2^+ , ..., $J^{(-1)^J}$,

11. DENSITIES, CORRELATIONS, AND THE DIRECT REACTIONS

In the preceding sections and in Sections I.12 to I.15 of deShalit and Feshbach (74), we have reviewed some of the elementary concepts that are useful for the understanding of nuclear reactions. We have seen how by choosing the appropriate experimental parameters—target, projectile and its energy, type of reaction, excitation energy of residual nucleus, energy resolution, and angular definition that can be obtained with the detection apparatus—one can select the type of final state excited and determine its properties. These detailed studies for a wide range of experimental parameters are essential for a deep and broad understanding of the properties of nuclei. In this final section we discuss the long-range goals of nuclear reaction studies, which go beyond the discovery of the “simple” degrees of freedom, the nuclear normal modes of motion.

A principal goal is the determination of the nuclear Hamiltonian, that is, the detailed description of the forces that determine nuclear structure and the interaction of nuclei with a variety of particles, and the form to which these reduce for the nuclear normal modes. The energy spectrum of a nucleus is very useful in this respect. The Hamiltonian of Chapter VI in deShalit and Feshbach (74), for example for rotational deformed nuclei, was in the long run mostly, but not entirely, justified by the observed rotational energy spectrum. But, in addition, properties of the nuclear wave function such as the B coefficients for radiative transition probabilities provided important supporting evidence. If we wish to go beyond the model Hamiltonian, much more information on the nuclear wave function is required; in fact, if we knew the nuclear wave function for one state with “infinite” accuracy, it would be possible to determine the nuclear Hamiltonian.

Interestingly, the one-step direct reactions provide the most direct information on the nuclear wave function. Perhaps the most outstanding example is the use of elastic and inelastic electron scattering to determine the charge and current density inside nuclei.

Formally, the amplitude for a transition of a target nucleus with wave function Ψ_T to the residual nucleus with wave function Ψ_R can always be cast into the form

$$\mathcal{T}_{RT} = \langle \Psi_R | \hat{\mathcal{T}} \Psi_T \rangle \quad (11.1)$$

The operator $\hat{\mathcal{T}}$ depends on the coordinates of the problem, including positions, momenta, spins, and isospins, and on the state of the incident projectile and the emergent particle. As is apparent from the form of (11.1), the observation of the transition will yield information on the overlap Ψ_T with Ψ_R , its nature depending on whether $\hat{\mathcal{T}}$ is a one-body, a two-body, or a more general, many-body operator. When the residual and target nucleus have the same mass number, that is, when scattering occurs, for example, in the (p, p) or (p, p') reaction, and when $\hat{\mathcal{T}}$ is a one-body operator[†] as regards its dependence on target nucleons,

$$\hat{\mathcal{T}} = \sum_i \hat{\mathcal{T}}(i) \quad (11.2)$$

(presuming symmetry), Equation (11.1) becomes

$$\hat{\mathcal{T}}_{RT} = \sum_i \int \Psi_R^*(1, 2, \dots, A) \hat{\mathcal{T}}(i) \Psi_T(1, 2, \dots, A) d(1) \dots$$

where the integration refers to summation over spin and isospin and integration over spatial coordinates. The center-of-mass motion of the residual and target nuclei will be included in the operator $\hat{\mathcal{T}}$ so that Ψ_R and Ψ_T depend only upon internal coordinates. The spatial integrations are then over $3(A-1)$ coordinates. The remaining three coordinates are those of the center of mass. Using the symmetry of $\hat{\mathcal{T}}$ and the wave functions, one finds that

$$\mathcal{T}_{RT} = A \int \Psi_R^*(1, \dots, A) \hat{\mathcal{T}}(1) \Psi_T(1, \dots, A) d(1) \dots$$

or

$$\mathcal{T}_{RT} = A \int \rho_{RT}^{(1)} \hat{\mathcal{T}}(1) d(1) \quad (11.3)$$

[†]More generally $\hat{\mathcal{T}} = \sum_{i,i'} \hat{\mathcal{T}}(i|i')$. This form leads to more complicated results which we discuss later [see (11.10)].

where $\rho_{RT}^{(1)}$ is the density matrix:

$$\rho_{RT}^{(1)} = \int \Psi_R^*(1, 2, \dots, A) \Psi_T(1, 2, \dots, A) d(2) \dots \quad (11.4)$$

The experiment can provide the values of \mathcal{T}_{RT} (more precisely $|\mathcal{T}_{RT}|^2$) as a function of energy, momentum transfer, and finally, energy transfer if the scattering is inelastic. From that one hopes to deduce $\rho_{RT}^{(1)}$ or at least to compare with \mathcal{T}_{RT} computed using a $\rho_{RT}^{(1)}$ based on theory and/or other experiments. Elastic electron scattering can be used to determine the charge density of a number of nuclei. The density refers to the diagonal value of $\rho_{RT}^{(1)}$, $\rho_{TT}^{(1)}$. Similarly, inelastic electron scattering can be used to determine nondiagonal elements of $\rho_{RT}^{(1)}$.

Problem. Prove that when $\hat{\mathcal{T}} = \sum_{i,i'} \hat{\mathcal{T}}(i'|i)$, $\mathcal{T}_{RT} = A \text{tr} \rho_{RT}(i|i') \hat{\mathcal{T}}(i|i')$, where the trace is carried out with respect to spin, isospin, and spatial coordinates.

Obviously, the question arises of when the operator $\hat{\mathcal{T}}$ is a one-body operator. It clearly has that character when the underlying interaction between the projectile and target is weak or electromagnetic in character, for then first-order perturbation theory may be applied. It also has that character for *single-step* direct reactions. Generally, $\hat{\mathcal{T}}$ for a multistep direct or compound nuclear reaction is a many-body operator.

There are several types of densities: matter density, charge density, spin density, and spin-isospin density. The latter describes the probability per unit volume of finding a particular particle (i.e., neutron or proton) with a particular spin orientation at a point within the nucleus. Equation (11.4) for $\rho_{RT}^{(1)}$ is just the matter density. It is convenient to rewrite it and ρ_{RT} as the matrix element of the operator $\hat{\rho}(\mathbf{r})$:

$$\hat{\rho}(\mathbf{r}) = \frac{1}{A} \sum \delta(\mathbf{r} - \mathbf{r}_i) \quad (11.5)$$

where \mathbf{r}_i is the coordinate of a nucleon and

$$\rho_{RT}^{(1)}(\mathbf{r}) = \langle \Psi_R | \hat{\rho} | \Psi_T \rangle \quad (11.6)$$

The expression for the charge density $\hat{\rho}^{(e)}$ is

$$\hat{\rho}^{(e)}(\mathbf{r}) = \frac{1}{A} \sum_i \frac{1}{2} [1 + \tau_3(i)] \delta(\mathbf{r} - \mathbf{r}_i) \quad (11.7)$$

while the spin and spin-isospin density operators are

$$\hat{\rho}_\alpha^{(s)}(\mathbf{r}) = \frac{1}{A} \sum_i \sigma_\alpha(i) \delta(\mathbf{r} - \mathbf{r}_i) \quad (11.8)$$

$$\rho_{\alpha\beta}^{(\sigma\tau)}(\mathbf{r}) = \frac{1}{A} \sum_i \sigma_\alpha(i) \tau_\beta(i) \delta(\mathbf{r} - \mathbf{r}_i) \quad (11.9)$$

The diagonal ground-state values of $\hat{\rho}^{(c)}$ are quite well known. Its nondiagonal values and the matrix elements of $\hat{\rho}^{(\sigma)}$ are now in the process of being determined by elastic and inelastic electron scattering. Further information is also provided by the scattering of high-energy protons and pions by nuclei.

Equation (11.2) provides an accurate representation of one-body operators only if the interaction between the projectile and the target nucleon is sufficiently weak. For the strong interactions, (11.2) is replaced by

$$\hat{\mathcal{T}} = \sum_{i',i} \hat{\mathcal{T}}(i'|i) \quad (11.10)$$

and $\hat{\rho}_{RT}$ now becomes a matrix not only with respect to the subscripts R and T but also with regard to space [see (III.4.4) in deShalit and Feshbach (74)]:

$$\rho_{RT}(i|i') = \int \Psi_R^*(i, 2, \dots) \Psi_T(i', 2, \dots) d(2) \dots \quad (11.11)$$

The spatial matrix properties of this full $\rho_{RT}(i'|i)$ can be exploited to obtain nuclear information of even greater subtlety than, say, that obtained from $\hat{\rho}^{(c)}$. For example, take the diagonal

$$\rho(i'|i) \equiv \rho_{TT}(i'|i) \quad (11.12)$$

It can be considered as a Hermitian matrix in i' and i , and as a consequence, can be diagonalized. The procedure will be described later (see p. 203). For the moment it is sufficient to state the result:

$$\rho(i'|i) = \sum_\lambda \psi_\lambda^*(i') \psi_\lambda(i) \kappa_\lambda \quad (11.13)$$

The functions $\psi_\lambda(i)$ are orthogonal and can be normalized. They are the best single-particle wave functions for the description of the target, at least as far as the reactions leading to the determination of $\rho(i'|i)$ are concerned.

One-particle transfer reactions such as (p, d) or $(p, 2p)$ are frequently used to determine the properties of single-particle wave functions. The analog of ρ_{RT} for this case is

$$S_{RT}(1) = \int \Psi_R^*(2, 3, \dots, A) \Psi_T(1, 2, \dots, A) d(2) \dots \quad (11.14)$$

Clearly, if Ψ_T differed from Ψ_R by the addition of one orbital to a Slater determinant, $S_{RT}(1)$ would be proportional to the corresponding single-particle

wave function. The square magnitude of the constant of proportionality gives the probability that Ψ_T consists of Ψ_R and a particle in a particular single-particle state and is known as the spectroscopic factor. If Ψ_R is a complex combination of excitations, this constant will be small, and in the absence of other effects originating in $\hat{\mathcal{T}}$, the cross section will be reduced. The cross section for one-particle transfer reactions tends to be largest when the shell model description is most applicable.

Returning to scattering, two-particle density matrices [see (III, 4.9) in deShalit and Feshbach (74)] appear when the operator $\hat{\mathcal{T}}$ is a two-body operator:

$$\hat{\mathcal{T}} = \sum_{i < j} \hat{\mathcal{T}}(i, j) \quad (11.15)$$

The resultant \mathcal{T}_{RT} is then

$$\mathcal{T}_{RT} = \frac{1}{2}A(A-1) \int \Psi_R^*(1, 2, \dots, A) \hat{\mathcal{T}}(1, 2) \Psi_T(1, 2, \dots, A) d(1) \dots$$

or

$$\mathcal{T}_{RT} = \frac{1}{2}A(A-1) \int \rho_{RT}^{(2)}(1, 2) \hat{\mathcal{T}}(1, 2) d(1) d(2)$$

where

$$\rho_{RT}^{(2)}(1, 2) = \int \Psi_R^*(1, 2, 3, \dots, A) \Psi_T(1, 2, 3, \dots, A) d(3) \dots \quad (11.16)$$

The corresponding operator is

$$\hat{\rho}^{(2)}(\mathbf{x}, \mathbf{y}) = \frac{2}{A(A-1)} \sum_{i < j} \delta(\mathbf{x} - \mathbf{r}_i) \delta(\mathbf{y} - \mathbf{r}_j) \quad (11.17)$$

The pair correlation function $C^{(2)}(x, y)$ is defined by

$$C^{(2)}(\mathbf{x}, \mathbf{y}) = \hat{\rho}^{(2)}(\mathbf{x}, \mathbf{y}) - \hat{\rho}(\mathbf{x}) \hat{\rho}(\mathbf{y}) \quad (11.18)$$

It has the property

$$\int C^{(2)}(\mathbf{x}, \mathbf{y}) d\mathbf{x} = \int C^{(2)}(\mathbf{x}, \mathbf{y}) d\mathbf{y} = 0 \quad (11.19)$$

since

$$\int \hat{\rho}^{(2)}(1, 2) d(1) = \hat{\rho}^{(1)}(2)$$

Pair correlations for both elastic and inelastic scattering will be present whenever the interactions are sufficiently strong. They therefore can play an important role for hadron interactions with nuclei. Some information on the diagonal

ground-state two-body density is available from the calculation of the binding energy of nuclei [see (III.4.11) in deShalit and Feshbach (74)].

Spin and isospin components of the correlation function can be obtained through the use of appropriate operators. The operator

$$\hat{\rho}_{s=0}^{(2)} = \frac{2}{A(A-1)} \sum_{i < j} \delta(\mathbf{x} - \mathbf{r}_i) \delta(\mathbf{y} - \mathbf{r}_j)^{\frac{1}{4}} (1 - \boldsymbol{\sigma}_i \cdot \boldsymbol{\sigma}_j) \quad (11.20)$$

gives the probability density of finding a pair of nucleons at \mathbf{x} and \mathbf{y} in the singlet ($S = 0$) state. Similarly,

$$\hat{\rho}_{S=1, T=0}^{(2)} = \frac{2}{A(A-1)} \sum_{i < j} \delta(\mathbf{x} - \mathbf{r}_i) \delta(\mathbf{y} - \mathbf{r}_j)^{\frac{1}{4}} (3 + \boldsymbol{\sigma}_i \cdot \boldsymbol{\sigma}_j)^{\frac{1}{4}} (1 - \boldsymbol{\tau}_i \cdot \boldsymbol{\tau}_j) \quad (11.21)$$

gives the probability density of finding a pair of nucleons at \mathbf{x} and \mathbf{y} in the spin triplet ($S = 1$) and isospin singlet ($T = 0$) state. These will appear in \mathcal{T}_{RT} if the two-body operator $\hat{\mathcal{T}}(1, 2)$ has a spin and isospin structure which necessarily will appear in the form exemplified by (11.20) and (11.21).

Two-body transfer reactions [e.g., $(p, {}^3\text{H})$] will provide information on the two-body wave functions since it will involve overlap integrals of the form

$$S_{RT}^{(2)}(1, 2) = \int \Psi_R^*(3, 4, \dots, A) \Psi_T(1, 2, 3, 4, \dots, A) d(3) \dots \quad (11.22)$$

Deviations of $S_{RT}^{(2)}(1, 2)$ from the product of single-particle wave functions, which might be obtained from single-particle transfer reactions (11.14), would reflect the presence of correlations in the wave function Ψ_T . In the case of the $(p, {}^3\text{H})$ reaction, there is a pronounced sensitivity to correlations in which the two neutrons ($T = 0$) are in a 1S_0 state.

Generally, correlations may be needed to describe a process when the strong interactions are involved. Highly accurate studies with the weak and electromagnetic interactions could in principle provide information on the correlations—that is, if the accuracy required second-order perturbation theory in order to obtain a sufficiently precise prediction. For strong interactions, the multistep processes will generally be sensitive to correlations. This can most easily be seen in the high-energy limit, for which it is possible to picture the reaction as preceeding by a number of collisions between the nucleons in the target and the projectile. Clearly, if two such collisions are important, the consequences will depend on the pair correlations in the target; if three, the triple correlations will be relevant; and so on.

We can extend this discussion to include third- and higher-order density matrices and correlations. We have, however, already shown that a principal result of the study of reactions will be the determination of properties of the wave functions of the target and residual nuclei. If it were possible to carry out

all the indicated evaluations (it is probably not necessary or desirable to carry out all of them), one would determine the nuclear wave function and thereby the nuclear Hamiltonian, which is the ultimate goal of the study of nuclear structure. We are a very long way indeed from carrying out this ambitious task, and the description given above is almost certainly overidealized. The outstanding example of the application of this analysis is the use of elastic and inelastic electron scattering to determine the charge and current density inside nuclei. More recently, high-energy proton scattering by nuclei has begun to achieve similar results for the matter density.

Problem. Define $\hat{\rho}^{(3)}(\mathbf{x}, \mathbf{y}, \mathbf{z})$. Show that the third-order correlation function is

$$\begin{aligned} C^{(3)}(\mathbf{x}, \mathbf{y}, \mathbf{z}) = & \rho^{(3)}(\mathbf{x}, \mathbf{y}, \mathbf{z}) - \rho(\mathbf{x})\rho^{(2)}(\mathbf{y}, \mathbf{z}) - \rho(\mathbf{y})\rho^{(2)}(\mathbf{x}, \mathbf{z}) \\ & - \rho(\mathbf{z})\rho^{(2)}(\mathbf{x}, \mathbf{y}) + 2\rho(\mathbf{z})\rho(\mathbf{y})\rho(\mathbf{x}) \end{aligned}$$

Show that $\int C^{(3)} d\mathbf{x} = 0$.

CHAPTER II

MULTIPLE SCATTERING

1. INTRODUCTION

Considerable simplifications in the theory describing the reactions induced by a projectile incident on a nucleus become possible when the energy of the projectile is sufficiently high. In this limit, the projectile in passing through the nucleus can be considered to undergo successive collisions with the target nucleons—hence the term *multiple scattering*. In the lowest approximation, each of these collisions is treated as a two-body (projectile–target nucleon) collision. One can thereby relate the transition amplitude for the processes induced by the collision with the nucleus to the transition amplitude for those induced by the collision of the projectile with the individual nucleons making up the nucleus. The complex many-body problem is thus reduced to a simpler two-body one, although it must be borne in mind that the projectile–nucleon collision occurs in an “environment” produced by the other nucleons in the nucleus, sometimes referred to as *spectators*.

For this approximation to be accurate, it is necessary for the nucleus to be sufficiently dilute so that the projectile encounters only one target nucleon at a time. The range of the force between the projectile and nucleon should therefore be small compared to the distance $2r_0$ between the nucleons. A second condition requires that the wavelength of the projectile be small compared to the distance between the nucleons of the nucleus:

$$kr_0 \gg 1 \quad (1.1)$$

where $k = 1/\lambda$. If the wavelength is so long that this condition is not satisfied,

a collision with one nucleon will necessarily involve its neighbors and thus it cannot be regarded as a two-body collision. It will be recognized that an essential part of these conditions is the requirement that the projectile is “on the energy shell” between collisions; that is, between collisions the energy is kinetic, $\hbar^2 k^2/2m$. One can readily take into account a *constant* potential energy, $-V$, in the region between collisions where the energy is then $(\hbar^2 k^2/2m) + V$.

Under these circumstances the projectile wave proceeds through the nucleus, producing at each target nucleon a scattered wave. These scattered waves for elastic scattering will be coherent and in the forward direction will interfere constructively, leading to a scattering amplitude proportional to the number of nucleons, A , in the target. The cross section in the forward direction will be proportional to A^2 . For larger angles of scattering the cross section will decrease as the angle of scattering or equivalently the momentum transfer, q , increases. The relevant parameter can be determined by the following considerations.

When an incident projectile collides elastically with a target nucleon, it will impart a momentum transfer q and therefore an energy $\hbar^2 q^2/2M$ to the target nucleon. However, at small angles, that energy is not sufficient to lift the nucleon out of the Fermi sea. There must be further collisions of the struck target nucleon with the other nucleons, so that finally the nucleus recoils as a whole. For that to occur, the uncertainty in position of the struck nucleon, \hbar/q must be larger than the size of the nucleus. Hence, roughly

$$\frac{\hbar}{q} > R \quad (1.2)$$

where R is the nuclear radius. Or since for elastic scattering

$$q = 2p \sin \frac{1}{2}\theta$$

inequality (1.2) becomes

$$2kR \sin \frac{\theta}{2} < 1 \quad (1.3)$$

For angles greater than those satisfying (1.3), \hbar/q will be less than R and only part of the nucleus will be involved. Thus the nucleus will not be able to recoil as a whole and the elastic scattering amplitude will be reduced, falling from its $\theta = 0$ value.

When these conditions are satisfied, one can, for example, obtain the elastic scattering amplitude for the collision of the projectile by the target nucleus in terms of the nuclear density, and of the two-body (projectile–nucleon) scattering amplitude. This result is of great power since it permits the determination of the nuclear density from experiments using a variety of projectiles that probe different spin-, isospin-, and momentum-dependent components of the nuclear density.

The importance of the approximations involved must, of course, be evaluated. A detailed discussion is given in Section 4. For the present we note that the conditions described above are never exactly satisfied since there is a finite probability that the separation of two target nucleons will be so small that the potentials between the projectile and the target nucleons will overlap and/or that the projectile wavelength will not be sufficiently small. In that event the projectile will interact with at least two of the target nucleons simultaneously. The transition amplitude for projectile–nucleus reactions will then depend not only on the density of target nucleons but also on their spatial correlation. One such correlation is induced by the Pauli exclusion principle and has the scale given by $1/k_F$, so that nucleons separated by less than this distance can no longer be considered as independent [see Chapter III in deShalit and Feshbach (74)]. Other correlations will be a consequence of the nuclear forces acting between the target nucleons. The scales in this case are the various ranges characterizing the nucleon–nucleon potential. The strength of, for example, the pair correlation is given by the number of target nucleons, multiplied by the probability of a nucleon finding another within a distance r_c (\equiv scale length of the correlation). The latter factor is given by $(r_c/R)^3$, so that the correlation effect is of the order of

$$A\left(\frac{r_c}{R}\right)^3 = \left(\frac{r_c}{r_0}\right)^3 \quad (1.4)$$

using $R = r_0 A^{1/3}$. It is thus difficult to observe correlation lengths much smaller than r_0 . (For a more quantitative result, see Appendix A.)

Another approximation we shall often use in this chapter asserts that the projectile passes through the nucleus in so short a time that the target nucleons are essentially stationary. This approximation, referred to as the *frozen nucleus approximation*, is valid for sufficiently high projectile energy. The characteristic time, τ_n , for target nucleon motion can be obtained from the zero-point motion of the nucleon of amplitude r_0 . The corresponding momentum is \hbar/r_0 with energy $\Delta E = \hbar^2/2Mr_0^2$. The time τ_n is then

$$\tau_n \sim \frac{\hbar}{\Delta E} = \frac{2Mr_0^2}{\hbar} \quad (1.5)$$

The time required for the projectile to pass a target nucleon is

$$\tau_p = 2r_0 \frac{E_p}{p_p c^2} \quad (1.6)$$

where E_p and p_p are the energy, including the rest mass and momentum of the projectile, respectively. The ratio τ_n/τ_p needs to be much greater than 1 if the

frozen approximation is to be valid:

$$\frac{\tau_n}{\tau_p} = k_p r_0 \frac{Mc^2}{E_p} \quad (1.7)$$

In the limit $E_p \gg M_p c^2$, this ratio becomes $Mc^2 r_0 / \hbar c$, which is much larger than unity. In the nonrelativistic limit, one obtains for the ratio, $k_p r_0 M / M_p$. Thus if the projectile is a nucleon, inequality (1.7) becomes identical with (1.1).

Under the frozen nucleus approximation the transition amplitude $\hat{\mathcal{T}}$ is a function of the position, spin, and so on, of each of the target nucleons that prevail at the time the projectile passes through the target:

$$\hat{\mathcal{T}} = \hat{\mathcal{T}}(\mathbf{r}_1, \mathbf{r}_2, \dots, \mathbf{r}_A) \quad (1.8)$$

The transition amplitude to be compared with experiment is obtained by taking appropriate matrix elements of $\hat{\mathcal{T}}$ with respect to the target nucleus states. For elastic scattering that amplitude is

$$\mathcal{T}_{ii} = \langle \Psi_i | \hat{\mathcal{T}} | \Psi_i \rangle \quad (1.9)$$

where Ψ_i is the target nucleus wave function. For inelastic scattering, it is

$$\mathcal{T}_{fi} = \langle \Psi_f | \hat{\mathcal{T}} | \Psi_i \rangle \quad (1.10)$$

where Ψ_f is the final target nucleus state. This approximation is called *adiabatic*.

2. QUALITATIVE RESULTS[†]

Much of the physics of multiple scattering can be understood at a qualitative level by studying a simple case. In this example the target nucleus is taken to be a system of nucleons which is so dilute that the probability the projectile will undergo two collisions with a target nucleon is small. The frozen nucleus approximation will be used so that the target nucleons will be considered as being fixed during the course of the collision.

Under these circumstances the transition amplitude $\hat{\mathcal{T}}$ will be given by a sum of amplitudes emanating from each of the target nucleons:

$$\hat{\mathcal{T}} = \sum_n t(\mathbf{k}_f, \mathbf{k}_i; \mathbf{r}_n) \quad (2.1)$$

where t is the projectile–nucleon amplitude giving the scattering of a projectile with incident momentum $\hbar \mathbf{k}_i$ and final momentum $\hbar \mathbf{k}_f$ by a target nucleon at \mathbf{r}_n .

[†]Lax (51).

We now must make use of an important theorem relating the amplitude $t(\mathbf{k}_f, \mathbf{k}_i, \mathbf{r}_n)$ with the amplitude of a scatterer located at the origin $t(\mathbf{k}_f, \mathbf{k}_i; 0)$. Toward this end, compare the integral Schrödinger equations appropriate to these two situations:

$$\psi(\mathbf{r}; \mathbf{r}_n) = e^{i\mathbf{k}_i \cdot \mathbf{r}} - \frac{1}{4\pi} \int \frac{e^{ik|\mathbf{r}-\mathbf{r}'|}}{|\mathbf{r}-\mathbf{r}'|} V(\mathbf{r}' - \mathbf{r}_n) \psi(\mathbf{r}'; \mathbf{r}_n) d\mathbf{r}' \quad (2.2a)$$

$$\psi(\mathbf{r}; 0) = e^{i\mathbf{k}_i \cdot \mathbf{r}} - \frac{1}{4\pi} \int \frac{e^{ik|\mathbf{r}-\mathbf{r}'|}}{|\mathbf{r}-\mathbf{r}'|} V(\mathbf{r}') \psi(\mathbf{r}'; 0) d\mathbf{r}' \quad (2.2b)$$

where V is the scattering potential. In the first of these equations introduce a shift of the origin:

$$\mathbf{r}' - \mathbf{r}_n = \mathbf{s}' \quad \mathbf{r} - \mathbf{r}_n = \mathbf{s}$$

One obtains

$$\psi(\mathbf{s} + \mathbf{r}_n; \mathbf{r}_n) = e^{i\mathbf{k}_i \cdot \mathbf{s}} e^{i\mathbf{k}_i \cdot \mathbf{r}_n} - \frac{1}{4\pi} \int \frac{e^{ik|\mathbf{s}-\mathbf{s}'|}}{|\mathbf{s}-\mathbf{s}'|} V(\mathbf{r}') \psi(\mathbf{s}' + \mathbf{r}_n; \mathbf{r}_n) d\mathbf{s}'$$

Comparing this equation with (2.2b) yields immediately the important result

$$\psi(\mathbf{s} + \mathbf{r}_n; \mathbf{r}_n) = e^{i\mathbf{k}_i \cdot \mathbf{r}_n} \psi(\mathbf{s}; 0) \quad (2.3)$$

Thus the shift in the origin results only in a change in phase, a consequence of translational invariance of the Schrödinger equation (2.2a). From (2.2a) we obtain

$$\begin{aligned} t(\mathbf{k}_f, \mathbf{k}_i; \mathbf{r}_n) &= \int e^{-i\mathbf{k}_f \cdot \mathbf{r}'} V(\mathbf{r}' - \mathbf{r}_n) \psi(\mathbf{r}'; \mathbf{r}_n) d\mathbf{r}' \\ &= e^{-i\mathbf{k}_f \cdot \mathbf{r}_n} \int e^{-i\mathbf{k}_f \cdot \mathbf{s}'} V(\mathbf{s}') \psi(\mathbf{s}' + \mathbf{r}_n; \mathbf{r}_n) d\mathbf{s}' \end{aligned}$$

Using (2.3) it follows that

$$t(\mathbf{k}_f, \mathbf{k}_i; \mathbf{r}_n) = e^{i(\mathbf{k}_i - \mathbf{k}_f) \cdot \mathbf{r}_n} t(\mathbf{k}_f, \mathbf{k}_i; 0) \quad (2.4)$$

One corollary of this equation will be important for later discussion. We leave it as a problem.

Problem. Let $t(\mathbf{r}, \mathbf{r}'; \mathbf{r}_n)$ be defined by

$$t(\mathbf{r}, \mathbf{r}'; \mathbf{r}_n) \equiv \iint e^{i\mathbf{k}_f \cdot \mathbf{r}} t(\mathbf{k}_f, \mathbf{k}_i; \mathbf{r}_n) e^{-i\mathbf{k}_i \cdot \mathbf{r}'} \frac{d\mathbf{k}_f}{(2\pi)^3} \frac{d\mathbf{k}_i}{(2\pi)^3} \quad (2.5a)$$

Show that

$$t(\mathbf{r}, \mathbf{r}'; \mathbf{r}_n) = t(\mathbf{r} - \mathbf{r}_n, \mathbf{r}' - \mathbf{r}_n; 0) \quad (2.5b)$$

We can now return to (2.1). Using (2.4), it becomes

$$\begin{aligned} \hat{\mathcal{T}} &= t(\mathbf{k}_f, \mathbf{k}_i) \sum_n e^{i\mathbf{q} \cdot \mathbf{r}_n} \\ \mathbf{q} &\equiv \mathbf{k}_i - \mathbf{k}_f \\ t(\mathbf{k}_f, \mathbf{k}_i) &\equiv t(\mathbf{k}_f, \mathbf{k}_i; 0) \end{aligned} \quad (2.6)$$

Finally, the elastic scattering transition amplitude is

$$\mathcal{T}_{el}(\mathbf{k}_f, \mathbf{k}_i) = t(\mathbf{k}_f, \mathbf{k}_i) \langle \Psi_i | \sum_n e^{i\mathbf{q} \cdot \mathbf{r}_n} \Psi_i \rangle$$

Using the antisymmetry of the wave function Ψ_i , this becomes

$$\mathcal{T}_{el}(\mathbf{k}_f, \mathbf{k}_i) = A t(\mathbf{k}_f, \mathbf{k}_i) \tilde{\rho}(\mathbf{q}) \quad (2.7)$$

where

$$\tilde{\rho}(\mathbf{q}) = \int e^{i\mathbf{q} \cdot \mathbf{r}_1} \rho(\mathbf{r}_1) d\mathbf{r}_1$$

and

$$\rho(\mathbf{r}_1) = \int |\Psi_i(\mathbf{r}_1, \mathbf{r}_2, \dots)|^2 d\mathbf{r}_2 \dots \quad (2.8)$$

$$\int \rho(\mathbf{r}_1) d\mathbf{r}_1 = 1 \quad (2.9)$$

From (2.9) it follows that the Fourier transform of the density, $\tilde{\rho}(\mathbf{q})$, is unity at $\mathbf{q} = 0$, that is, for scattering in the forward direction. Generally, as described in the preceding section, $\tilde{\rho}$ will drop rapidly with increasing scattering angle. (Note that $|q| = 2k \sin \frac{1}{2}\theta$, where θ is the scattering angle.) For example, if

$$\rho(\mathbf{r}) = \left(\frac{3}{2\pi}\right)^{3/2} \frac{1}{R^3} e^{-(3/2)(r^2/R^2)} \quad (2.10)$$

which satisfies (2.9) and

$$R^2 = \int \rho(\mathbf{r}) r^2 d\mathbf{r}$$

so that R is the root-mean-square radius, then

$$\tilde{\rho}(\mathbf{q}) = e^{-q^2 R^2/6} = e^{-(2/3)k^2 R^2 \sin^2(1/2)\theta} \quad (2.11)$$

We note the rapid decrease in $\tilde{\rho}(\mathbf{q})$ and therefore of the scattering transition amplitude, (2.7), as the scattering angle, the energy, or the size of the system increases. The quantity $\tilde{\rho}(\mathbf{q})$ is referred to as the *form factor*.

According to (1.10), the inelastic transition amplitude is given by

$$\mathcal{T}_{fi}(\mathbf{k}_f, \mathbf{k}_i) = t(\mathbf{k}_f, \mathbf{k}_i) \langle \Psi_f | \sum_n e^{i\mathbf{q} \cdot \mathbf{r}_n} \Psi_i \rangle \quad (2.12a)$$

or

$$\mathcal{T}_{fi} = A t(\mathbf{k}_f, \mathbf{k}_i) \tilde{\rho}_{fi}(\mathbf{q}) \quad (2.12b)$$

where $\tilde{\rho}_{fi}(\mathbf{q})$ is the Fourier transform of the transition density:

$$\tilde{\rho}_{fi}(\mathbf{q}) = \int e^{i\mathbf{q} \cdot \mathbf{r}_1} \rho_{fi}(\mathbf{r}_1) d\mathbf{r}_1 \quad (2.13)$$

and

$$\rho_{fi}(\mathbf{r}_1) = \int \Psi_f^*(\mathbf{r}_1, \mathbf{r}_2, \dots) \Psi_i(\mathbf{r}_1, \mathbf{r}_2, \dots) d\mathbf{r}_2 \dots \quad (2.14)$$

Note that $\mathcal{T}_{fi}(\mathbf{k}_f, \mathbf{k}_i)$ is zero whenever q is zero because of the orthogonality of Ψ_f and Ψ_i . As a consequence, \mathcal{T}_{fi} at small q will be proportional to some power of q .

Further insight is obtained from examination of the total angular distribution for inelastic scattering summing over all possible final states:

$$\sum_f \frac{d\sigma_{\text{tot}}^{(\text{inel})}}{d\Omega} = \frac{2\pi}{\hbar} (\rho_f/j_i) \sum_f |\mathcal{T}_{fi}|^2 = \frac{m^2}{(2\pi)^2 \hbar^4} \frac{k_f}{k_i} \sum_f |\mathcal{T}_{fi}|^2 \quad (2.15)$$

where the projectile wave functions appearing in \mathcal{T}_{fi} are asymptotically plane waves of unit amplitude and m is the reduced mass of the projectile–nucleus system. ρ_f is the density of final states and j_i is the incident current density. Inserting (2.12a) into (2.15) and summing over the final states one obtains

$$\sum_f \frac{d\sigma_{\text{tot}}^{(\text{inel})}}{d\Omega} = \frac{m^2}{(2\pi)^2 \hbar^4} \left\langle \frac{k_f}{k_i} |t(\mathbf{k}_f, \mathbf{k}_i)|^2 \right\rangle_{\text{av}} \sum_f \langle \Psi_i | \sum_n e^{-i\mathbf{q} \cdot \mathbf{r}_n} \Psi_f \rangle \langle \Psi_f | \sum_m e^{i\mathbf{q} \cdot \mathbf{r}_m} \Psi_i \rangle \quad (2.16)$$

The factor in front of the sum is the cross section for projectile–nucleon scattering except that the projectile–nucleon reduced mass is replaced by projectile–nucleus reduced mass. We shall return to this point later.

Making use of the completeness of the final states Ψ_f the sum in (2.16) may be performed. A sum rule is obtained:

$$\sum_f \frac{d\sigma_{\text{tot}}^{(\text{inel})}}{d\Omega} = \frac{m^2}{(2\pi)^2 \hbar^4} \left\langle \frac{\mathbf{k}_f}{\mathbf{k}_i} \middle| t(\mathbf{k}_f, \mathbf{k}_i) \right|^2 \rangle \sum_{\text{av } n, m} (\langle \Psi_i | e^{i\mathbf{q} \cdot (\mathbf{r}_m - \mathbf{r}_n)} \Psi_i \rangle - \langle \Psi_i | e^{i\mathbf{q} \cdot \mathbf{r}_m} \Psi_i \rangle \langle \Psi_i | e^{-i\mathbf{q} \cdot \mathbf{r}_n} \Psi_i \rangle)$$

Using the antisymmetry of the wave function Ψ_i , the sum is readily shown to equal

$$\begin{aligned} & \sum_{n, m} (\langle \Psi_i | e^{i\mathbf{q} \cdot (\mathbf{r}_m - \mathbf{r}_n)} \Psi_i \rangle - \langle \Psi_i | e^{i\mathbf{q} \cdot \mathbf{r}_m} \Psi_i \rangle \langle \Psi_i | e^{-i\mathbf{q} \cdot \mathbf{r}_n} \Psi_i \rangle) \\ &= A + A(A-1)\tilde{\rho}(\mathbf{q}, -\mathbf{q}) - A^2\tilde{\rho}(\mathbf{q})\tilde{\rho}(-\mathbf{q}) \end{aligned} \quad (2.17)$$

where

$$\tilde{\rho}(\mathbf{q}, -\mathbf{q}) = \int e^{i\mathbf{q} \cdot (\mathbf{r}_1 - \mathbf{r}_2)} \rho(\mathbf{r}_1, \mathbf{r}_2) d\mathbf{r}_1 d\mathbf{r}_2 \quad (2.18)$$

and

$$\rho(\mathbf{r}_1, \mathbf{r}_2) \equiv \int |\Psi_i(\mathbf{r}_1, \mathbf{r}_2, \mathbf{r}_3, \dots)|^2 d\mathbf{r}_3 \dots \quad (2.19)$$

The quantity $\rho(\mathbf{r}_1, \mathbf{r}_2)$ is the diagonal two-body density giving the probability density to find a nucleon in the range $d\mathbf{r}_1$ at \mathbf{r}_1 and another in the range $d\mathbf{r}_2$ at \mathbf{r}_2 . To obtain the correlation density, one must subtract the probability that obtains when the two particles are independent, $\rho(\mathbf{r}_1)\rho(\mathbf{r}_2)$. Thus

$$C(\mathbf{r}_1, \mathbf{r}_2) = \rho(\mathbf{r}_1, \mathbf{r}_2) - \rho(\mathbf{r}_1)\rho(\mathbf{r}_2) \quad (2.20)$$

Note that

$$\int C(\mathbf{r}_1, \mathbf{r}_2) d\mathbf{r}_1 = 0 = \int C(\mathbf{r}_1, \mathbf{r}_2) d\mathbf{r}_2 \quad (2.21)$$

The Fourier transform of C is

$$\tilde{C}(\mathbf{q}_1, \mathbf{q}_2) = \int e^{i\mathbf{q}_1 \cdot \mathbf{r}_1 + i\mathbf{q}_2 \cdot \mathbf{r}_2} C(\mathbf{r}_1, \mathbf{r}_2) d\mathbf{r}_1 d\mathbf{r}_2 \quad (2.22)$$

From (2.21)

$$\tilde{C}(\mathbf{q}_1, 0) = \tilde{C}(0, \mathbf{q}_2) = 0 \quad (2.23)$$

Asymptotically, $C(\mathbf{r}_1, \mathbf{r}_2)$ should vanish since for large $|\mathbf{r}_1 - \mathbf{r}_2|$, the nucleons are expected to be independent, so that

$$C(\mathbf{r}_1, \mathbf{r}_2) \rightarrow 0 \quad \text{as } |\mathbf{r}_1 - \mathbf{r}_2| \rightarrow \infty \quad (2.24)$$

In terms of the function C , the right-hand side of (2.17) is

$$A + A(A-1)\tilde{C}(\mathbf{q}, -\mathbf{q}) - A|\rho(\mathbf{q})|^2$$

so that

$$\sum_f \frac{d\sigma_{\text{tot}}^{(\text{inel})}}{d\Omega} = \frac{m^2}{(2\pi)^2 \hbar^4} \left\langle \frac{k_f}{k_i} |t(\mathbf{k}_f, \mathbf{k}_i)|^2 \right\rangle_{\text{av}} [A(1 - |\rho(\mathbf{q})|^2) + A(A-1)\tilde{C}(\mathbf{q}, -\mathbf{q})] \quad (2.25)$$

We see immediately the expected result that this cross section vanishes as $q \rightarrow 0$. As already indicated [see (1.4)] and to be shown in more detail below, $\tilde{C} \sim 1/A$, so that $\langle d\sigma_{\text{tot}}^{(\text{inel})}/d\Omega \rangle_{\text{av}} \sim A$. This result is to be contrasted with the elastic scattering cross section, which according to (2.7), is proportional to A^2 . The latter is a consequence of the constructive interference of the waves scattered by the target nucleon in the forward direction. For this reason, the elastic scattering is referred to as *coherent scattering*. The inelastic cross section is referred to as *incoherent scattering* since proportionality of the cross section to A can be interpreted as addition of the cross sections, rather than the amplitude, for each target nucleon.

An important consequence of this discussion of inelastic scattering is that it will be easier to observe the correlation term at the larger angles, $qR \sim 1$, and in the inelastic scattering.

A simple model of $\rho(\mathbf{r}_1, \mathbf{r}_2)$ will serve to illustrate some of these points. We take

$$\rho(\mathbf{r}_1, \mathbf{r}_2) = N e^{-(1/2)\alpha^2(r_1^2 + r_2^2)} [1 - e^{-(1/2)\beta^2(\mathbf{r}_1 - \mathbf{r}_2)^2}] \quad (2.26)$$

The correlation is carried by the second term in parentheses. It disappears as $|\mathbf{r}_1 - \mathbf{r}_2| \rightarrow \infty$. Moreover, $\rho(\mathbf{r}_1, \mathbf{r}_2)$ goes to zero as $|\mathbf{r}_1 - \mathbf{r}_2| \rightarrow 0$, simulating the effect of a hard core and/or the Pauli exclusion principle. The parameter α is $O(1/R)$ and β is $O(1/r_c)$, where r_c is the correlation length, so that

$$\beta \gg \alpha \quad (2.27)$$

except for the smallest nuclei. N is a normalization factor determined by the condition

$$\iint \rho(\mathbf{r}_1, \mathbf{r}_2) d\mathbf{r}_1 d\mathbf{r}_2 = 1$$

Note that

$$\rho(\mathbf{r}_1) = \int \rho(\mathbf{r}_1, \mathbf{r}_2) d\mathbf{r}_2$$

has a contribution from the correlation term in β :

$$\begin{aligned} \rho(\mathbf{r}) &= N \frac{(2\pi)^{3/2}}{\alpha^3} \left[e^{-(1/2)\alpha^2 r^2} - \left(\frac{\alpha^2}{\alpha^2 + \beta^2} \right)^{3/2} e^{-(1/2)[(\alpha^2 + 2\beta^2)/(\alpha^2 + \beta^2)]\alpha^2 r^2} \right] \\ &\xrightarrow{\beta \gg \alpha} N \frac{(2\pi)^{3/2}}{\alpha^3} \left[e^{-(1/2)\alpha^2 r^2} - \left(\frac{\alpha}{\beta} \right)^3 e^{-\alpha^2 r^2} \right] \end{aligned} \quad (2.28)$$

The second term in brackets has a shorter range than the first term. The normalization factor is

$$N = \frac{\alpha^6}{(2\pi)^3 \{1 - [\alpha^2/(\alpha^2 + 2\beta^2)]^{3/2}\}} \xrightarrow{\beta \gg \alpha} \frac{\alpha^6}{(2\pi)^3 [1 - (1/\sqrt{8})(\alpha^3/\beta^3)]} \quad (2.29)$$

It is straightforward to evaluate the Fourier transforms:

$$\begin{aligned} \tilde{\rho}(\mathbf{q}) &= \frac{1}{1 - [\alpha^2/(\alpha^2 + 2\beta^2)]^{3/2}} \left\{ e^{-q^2/2\alpha^2} - \left(\frac{\alpha^2}{\alpha^2 + 2\beta^2} \right)^{3/2} e^{-(1/2)q^2[\alpha^2 + \beta^2]/\alpha^2(\alpha^2 + 2\beta^2)} \right\} \\ &\xrightarrow{\beta \gg \alpha} \frac{1}{1 - (1/\sqrt{8})(\alpha^3/\beta^3)} \left(e^{-q^2/2\alpha^2} - \frac{1}{\sqrt{8}} \frac{\alpha^3}{\beta^3} e^{-q^2/4\alpha^2} \right) \end{aligned} \quad (2.30)$$

and

$$\begin{aligned} \tilde{\rho}(\mathbf{q}_1, \mathbf{q}_2) &= \frac{1}{1 - [\alpha^2/(\alpha^2 + 2\beta^2)]^{3/2}} \left\{ e^{-(q_1^2 + q_2^2)/2\alpha^2} \right. \\ &\quad \left. - \left(\frac{\alpha^2}{\alpha^2 + 2\beta^2} \right)^{3/2} e^{-(1/2)[1/\alpha^2(\alpha^2 + 2\beta^2)][\alpha^2(q_1^2 + q_2^2) + \beta^2(\mathbf{q}_1 + \mathbf{q}_2)^2]} \right\} \end{aligned} \quad (2.31)$$

Finally,

$$\begin{aligned} \tilde{C}(\mathbf{q}_1, \mathbf{q}_2) &\xrightarrow{\beta \gg \alpha} -\frac{\alpha^3}{\sqrt{8}\beta^3} [e^{-(1/2)(q_1^2 + q_2^2)/\alpha^2} + e^{-(1/4)\alpha^2\beta^2[\alpha^2(q_1^2 + q_2^2) + \beta^2(\mathbf{q}_1 + \mathbf{q}_2)^2]} \\ &\quad - (e^{-q_1^2/4\alpha^2 - q_2^2/2\alpha^2} + e^{-q_1^2/2\alpha^2 - q_2^2/4\alpha^2})] \end{aligned} \quad (2.32)$$

We see directly that for $\beta \gg \alpha$, \tilde{C} is on the order of $(r_c/R)^3$, so that $\tilde{C} \sim 1/A$. $\tilde{C}(\mathbf{q}_1, \mathbf{q}_2)$ goes to zero as \mathbf{q}_1 or \mathbf{q}_2 go to zero. Note also that for large \mathbf{q}_1 and

\mathbf{q}_2 the decrease of \tilde{C} is governed by the parameters $1/\alpha^2$, $1/2\alpha^2$ and when $\mathbf{q}_1 + \mathbf{q}_2 = 0$, by $1/2\beta^2$. This last case will provide the smallest asymptotic rate of decrease since $1/\beta^2 \ll 1/\alpha^2$. The sum rule, (2.25), depends on $\tilde{C}(\mathbf{q}, -\mathbf{q})$:

$$\tilde{C}(\mathbf{q}, -\mathbf{q}) \xrightarrow{\beta \gg \alpha} -\frac{\alpha^3}{\sqrt{8}\beta^3} [e^{-q^2/\alpha^2} + e^{-q^2/2\beta^2} - 2e^{-(3/4)(q^2/\alpha^2)}], \quad (2.33)$$

which at large angles is dominated by the second term.

3. OPTICAL MODEL POTENTIAL[†]

The preceding discussion assumes that the projectile wave incident on each target nucleon is the incident plane wave. In fact, the incident wave is composed of that plane wave together with the waves that have been generated by scattering from all the other nucleons of the target nucleus. The discussion in Section 2 is thus invalid if the probability for secondary and multiple scattering, that is, rescattering of wave generated by a previous scattering, is important. When that is the case, the wave incident on a target nucleon consists of a linear superposition of plane wave so that (2.1) is replaced by

$$\mathcal{T}_{el} \equiv \langle \Psi_i | \hat{\mathcal{T}} | \Psi_i \rangle = \sum_n \int \frac{d\mathbf{k}}{(2\pi)^3} \langle \Psi_i | t(\mathbf{k}_f, \mathbf{k}; \mathbf{r}_n) \Psi_i \rangle \tilde{\chi}_n(\mathbf{k})$$

or

$$\mathcal{T}_{el} = A \int \frac{d\mathbf{k}}{(2\pi)^3} \int d\mathbf{r}_n \rho(\mathbf{r}_n) t(\mathbf{k}_f, \mathbf{k}; \mathbf{r}_n) \tilde{\chi}_n(\mathbf{k}) \quad (3.1)$$

where $\tilde{\chi}_n(\mathbf{k})$ is the probability amplitude for a plane wave of momentum \mathbf{k} to be incident on the n th target nucleon. We now introduce $t(\mathbf{r}, \mathbf{r}'; \mathbf{r}_n)$ by inverting the Fourier transform, (2.5a), and using (2.5b) as well, so that

$$\mathcal{T}_{el} = A \int \frac{d\mathbf{k}}{(2\pi)^3} \int \rho(\mathbf{r}_n) d\mathbf{r}_n \int d\mathbf{r} \int d\mathbf{r}' e^{-i\mathbf{k}_f \cdot \mathbf{r}} t(\mathbf{r} - \mathbf{r}_n, \mathbf{r}' - \mathbf{r}_n) e^{i\mathbf{k} \cdot \mathbf{r}'} \tilde{\chi}_n(\mathbf{k}) \quad (3.2)$$

The integral over \mathbf{k} yields directly the incident wave in coordinate space:

$$\chi_n(\mathbf{r}') = \int \frac{d\mathbf{k}}{(2\pi)^3} e^{i\mathbf{k} \cdot \mathbf{r}'} \tilde{\chi}_n(\mathbf{k}) \quad (3.3)$$

[†]Lax (51).

so that (3.2) can be rewritten

$$\mathcal{T}_{el} = A \int d\mathbf{r} e^{-i\mathbf{k}_f \cdot \mathbf{r}} \int d\mathbf{r}' \left[\int d\mathbf{r}_n t(\mathbf{r} - \mathbf{r}_n, \mathbf{r}' - \mathbf{r}_n) \rho(\mathbf{r}_n) \right] \chi_n(\mathbf{r}') \quad (3.4)$$

We now make the approximation that $\chi_n(\mathbf{r}')$ is independent of n and can be written $\chi(\mathbf{r}')$. This is not exact since the linear combination of waves incident on the n th nucleon, (3.1), should not include the effect of the wave coming from the n th nucleon itself. However, if the number of nucleons is sufficiently large, the error should be small. When χ_n is replaced by χ , the resulting amplitude is identical to that which would be obtained from a Schrödinger equation with the nonlocal energy-dependent optical model potential $V^{(\text{opt})}(\mathbf{r}, \mathbf{r}')$:

$$V^{(\text{opt})}(\mathbf{r}, \mathbf{r}') = A \int d\mathbf{r}_n t(\mathbf{r} - \mathbf{r}_n, \mathbf{r}' - \mathbf{r}_n) \rho(\mathbf{r}_n) \quad (3.5)$$

Its Fourier transform is

$$\begin{aligned} \tilde{V}^{(\text{opt})}(\mathbf{k}, \mathbf{k}') &= \iint d\mathbf{r} d\mathbf{r}' e^{-i\mathbf{k} \cdot \mathbf{r}} V^{(\text{opt})}(\mathbf{r}, \mathbf{r}') e^{i\mathbf{k}' \cdot \mathbf{r}'} \\ &= A \tilde{\rho}(\mathbf{k} - \mathbf{k}') \tilde{t}(\mathbf{k}, \mathbf{k}') \end{aligned} \quad (3.6)$$

In using (3.6) it has been the practice to structure $\tilde{t}(\mathbf{k}_f, \mathbf{k}_i)$ as follows:

$$\tilde{t}(\mathbf{k}_f, \mathbf{k}_i) = t_E(\mathbf{q}) \quad \mathbf{q} = \mathbf{k}_i - \mathbf{k}_f \quad (3.7)$$

where E , the projectile energy, is treated as a parameter. Under these circumstances

$$\begin{aligned} t(\mathbf{r}, \mathbf{r}'; \mathbf{r}_n) &= \delta(\mathbf{r} - \mathbf{r}') \frac{1}{(2\pi)^3} \int e^{-i\mathbf{q} \cdot (\mathbf{r} - \mathbf{r}_n)} \tilde{t}_E(\mathbf{q}) d\mathbf{q} \\ &\equiv \delta(\mathbf{r} - \mathbf{r}') t_E(\mathbf{r} - \mathbf{r}_n) \end{aligned} \quad (3.7')$$

The optical potential then becomes local:

$$\begin{aligned} V^{(\text{opt})}(\mathbf{r}', \mathbf{r}) &= \delta(\mathbf{r} - \mathbf{r}') V_E^{(\text{opt})}(\mathbf{r}) \\ V_E^{(\text{opt})}(\mathbf{r}) &= A \int d\mathbf{r}_n t_E(\mathbf{r} - \mathbf{r}_n) \rho(\mathbf{r}_n) \end{aligned} \quad (3.8)$$

This is the form of the high-energy multiple scattering optical potential found in the literature [Lax (51), Kerman, McManus, and Thaler (59)]. Its Fourier transform is

$$\tilde{V}_E^{(\text{opt})}(\mathbf{q}) = \int e^{i\mathbf{q} \cdot \mathbf{r}} V_E^{(\text{opt})}(\mathbf{r}) d\mathbf{r} = A \tilde{t}_E(\mathbf{q}) \tilde{\rho}(\mathbf{q}) \quad (3.9)$$

Both (3.5) and (3.8) demonstrate that within the limits of the approximations employed to obtain them, that high-energy elastic scattering experiments provide a probe, symbolized by the transition matrix $t(\mathbf{k}_f, \mathbf{k}_i)$ characteristic of the projectile–nucleon scattering, to study the one-body density $\rho(r)$. Each projectile, whether a nucleon, α -particle, pion, and so on, will be sensitive to different aspects (i.e., spin and isospin dependence) of ρ so that by combining experiments one may be able to obtain a complete description of ρ .

Even in the approximate form, (3.5) and (3.8), the transition amplitude for all values of \mathbf{k}_f and \mathbf{k}_i needed to obtain $V^{(\text{opt})}$ cannot be determined directly from experiment since one would have to know $\tilde{t}(\mathbf{k}_f, \mathbf{k}_i)$ for $k_f \neq k_i$. The procedure generally used takes a functional form for $\tilde{t}_E(\mathbf{q})$ fitted to experimental data and using that form extrapolates to values “off the energy shell” (i.e., $k_f \neq k_i$). A commonly used form is

$$\tilde{t}_E(\mathbf{q}) = B(E)e^{-b(E)q^2} \quad (3.10)$$

This procedure leads to minor errors, for the following reason. For larger nuclei, only values of $\tilde{t}_E(\mathbf{q})$ near $q = 0$ will enter importantly into the optical potential. The reasons follow. The scale of $\tilde{\rho}(\mathbf{q})$ is $1/R$ (R = nuclear radius). For infinite nuclei $\tilde{\rho}(\mathbf{q})$ is proportional to $\delta(\mathbf{q})$, while the scale of \tilde{t} is $1/r_N$, where r_N is the range of nuclear forces. Hence $\tilde{t}(\mathbf{q})$ falls off with increasing q much more slowly than $\tilde{\rho}(\mathbf{q})$. In the relatively small momentum transfer range in which $\tilde{\rho}$ differs from zero, there is no difficulty in obtaining the requisite $\tilde{t}(\mathbf{q})$ from experiment.

For very large nuclei (i.e., nuclear matter), (3.9) becomes

$$\tilde{V}_E^{(\text{opt})}(\mathbf{q}) = A\tilde{t}_E(0)\tilde{\rho}(\mathbf{q})$$

and

$$V_E^{(\text{opt})}(\mathbf{r}) = A\tilde{t}_E(0)\rho(\mathbf{r}) \quad (3.11)$$

The imaginary part of $V_E^{(\text{opt})}$ can be related to λ , the mean free path of the projectile in nuclear matter. We note that

$$\frac{2m}{\hbar^2} \text{Im } V_E^{(\text{opt})} = \frac{2m}{\hbar^2} A\rho \text{Im } \tilde{t}_E(0) = -4\pi A\rho \text{Im } f(0^\circ) = -A\rho k\sigma_T \quad (3.12)$$

where in the last step we have made use of the relationship between the imaginary part of the elastic scattering amplitude at 0° , $f(0^\circ)$, and the total cross section:

$$\sigma_T = \frac{4\pi}{k} \text{Im } f(0^\circ) \quad (3.13)$$

From the Schrödinger equation one has

$$(k_R + ik_I)^2 = \frac{2m}{\hbar^2} E - \frac{2m}{\hbar^2} V^{(\text{opt})} \quad (3.14)$$

where k_R and k_I are the real and imaginary part of k , respectively. Inserting (3.11), using (3.12), and assuming that $k_R \gg k_I$ leads to

$$k_R^2 = \frac{2m}{\hbar^2} (E - V_R^{(\text{opt})})$$

and

$$\frac{2m}{\hbar^2} V_I^{(\text{opt})} = -2k_R k_I \simeq -2k k_I$$

Hence, using (3.12),

$$k_I = \frac{1}{2} A \rho \sigma_T \quad (3.15)$$

and the mean free path, λ ,

$$\lambda = \frac{1}{2k_I} = \frac{1}{A \rho \sigma_T} \quad (3.16)$$

a familiar result. (See Chapter V, p. 354, for a derivation that takes into account the important effect of the properties of the medium in which the collisions occur.)

The optical potential bears a simple relation to the results obtained in Section 2 for the scattering amplitude [see (2.7)]. Equation (2.7) is the first Born approximation amplitude using the optical model potentials, (3.5) or (3.8). The Schrödinger equation with these potentials takes into account the distortion of the incident plane wave by the nucleon medium. The Schrödinger equation also develops an amplitude that satisfies unitarity, which is not the case for the first Born approximation. From equation (3.8) [rather than (3.5)] is often pointed to as justification for the *folding potential* described in Chapter V, to which the reader can turn for further discussion.

The foregoing derivation of the optical model potential fails under two circumstances. First, it fails if three-body forces are important [Austern (83)], for then the scattering cannot involve one nucleon at a time with the projectile on the energy shell between collisions. It also fails, even when only two-body forces are acting, when the target nucleons are too close to each other. In that event, a double scattering in which the projectile is not on the energy shell after the first scattering becomes possible, in contradiction to the postulated

conditions for the validity of (3.5) and (3.9). The importance of this process depends on the probability that the target nucleons are sufficiently close to each other, that is on the correlation function. If the energy deficiency is ΔE , the lifetime of the system is $\hbar/\Delta E$ and the distance traveled by the projectile is $\hbar v/\Delta E$. By the end of this time interval a second collision restoring the system to the energy shell is necessary, so that $\hbar v/\Delta E$ must be on the order of the correlation length r_c . As ΔE increases, the correlation length to which the experiment is sensitive decreases, so that the projectile must go farther off the energy shell to see smaller correlation lengths.

One can take account of these collisions in which two of the target nucleons are close together by considering multiple scattering as involving a series of scattering from two target nucleons rather than from one target nucleon as assumed in the earlier discussion. It is intuitively clear that in that case (3.8)[‡] is replaced by

$$V^{(\text{opt})}(\mathbf{r}, \mathbf{r}') = A(A-1) \int d\mathbf{r}_n \int d\mathbf{r}_m t^{(2)}(\mathbf{r}, \mathbf{r}'; \mathbf{r}_n, \mathbf{r}_m) \rho(\mathbf{r}_n, \mathbf{r}_m) \quad (3.17)$$

In this equation $t^{(2)}$ is the transition amplitude for the scattering of the projectile by two target nucleons located at \mathbf{r}_n and \mathbf{r}_m . It is generally a nonlocal operator. [It is left to the reader as a problem to derive (3.17) using an analysis following that which led to (3.8).] The two-particle density $\rho(\mathbf{r}_n, \mathbf{r}_m)$ can, according to (2.20), be written as follows:

$$\rho(\mathbf{r}_n, \mathbf{r}_m) = \rho(\mathbf{r}_n)\rho(\mathbf{r}_m) + C(\mathbf{r}_n, \mathbf{r}_m) \quad (2.20)$$

where [cf. (2.21)]

$$\int C(\mathbf{r}_n, \mathbf{r}_m) d\mathbf{r}_n = 0 = \int C(\mathbf{r}_n, \mathbf{r}_m) d\mathbf{r}_m \quad (2.21)$$

Consider the term generated when the first term of (2.20) is inserted into (3.17):

$$A(A-1) \int d\mathbf{r}_m \int d\mathbf{r}_n \rho(\mathbf{r}_n) t^{(2)}(\mathbf{r}, \mathbf{r}'; \mathbf{r}_n, \mathbf{r}_m) \rho(\mathbf{r}_m)$$

This term describes the independent scattering of the projectile by nucleons at \mathbf{r}_n and \mathbf{r}_m . This is precisely what the optical potentials (3.5) and (3.8) were designed to describe. Hence this term is already contained in (3.8). The term arising from the correlation in (2.20) is

$$A(A-1) \int d\mathbf{r}_n \int d\mathbf{r}_m C(\mathbf{r}_n, \mathbf{r}_m) t^{(2)}(\mathbf{r}, \mathbf{r}'; \mathbf{r}_n, \mathbf{r}_m) \quad (3.18)$$

[‡]The more complex equation, (3.5), could equally well be generalized.

Using (3.8) to describe the scattering from the two-particle system, one obtains

$$t^{(2)}(\mathbf{r}, \mathbf{r}'; \mathbf{r}_n, \mathbf{r}_m) = \frac{1}{2}t(\mathbf{r} - \mathbf{r}_n)\delta(\mathbf{r} - \mathbf{r}') + \frac{1}{2}t(\mathbf{r} - \mathbf{r}_m)\delta(\mathbf{r} - \mathbf{r}') \\ + \Delta t^{(2)}(\mathbf{r}, \mathbf{r}'; \mathbf{r}_n, \mathbf{r}_m) \quad (3.19)$$

The first two terms are obtained from (3.8); the last is the nonadditive contribution obtained when the scattering from the two-body system is obtained more precisely. Inserting into (3.18) and using (2.21), (3.18) becomes

$$A(A-1) \int d\mathbf{r}_n \int d\mathbf{r}_m C(\mathbf{r}_n, \mathbf{r}_m) \Delta t^{(2)}(\mathbf{r}, \mathbf{r}'; \mathbf{r}_n, \mathbf{r}_m)$$

The revised optical potential taking into account the possibility that two of target nucleons can be close together is

$$V^{(\text{opt})}(\mathbf{r}, \mathbf{r}') = A \int d\mathbf{r}_1 \rho(\mathbf{r}_1) t(\mathbf{r} - \mathbf{r}_1) \delta(\mathbf{r} - \mathbf{r}') \\ + A(A-1) \int d\mathbf{r}_1 \int d\mathbf{r}_2 C(\mathbf{r}_1, \mathbf{r}_2) \Delta t^{(2)}(\mathbf{r}, \mathbf{r}'; \mathbf{r}_1, \mathbf{r}_2) \quad (3.20)$$

It is generally not possible to obtain $\Delta t^{(2)}$ for the necessary ranges of \mathbf{r}_1 and \mathbf{r}_2 from experiment. Therefore, to complete (3.20), a method for calculating $\Delta t^{(2)}$ must be given. One might numerically solve the problem of projectile/two-nucleon scattering in the frozen nucleus approximation [Sparrow (75)] or one can provide an approximation [Feshbach, Gal, and Hüfner (71); Chaumeaux, Layly, and Schaeffer (78)], which permits a ready evaluation of this term. By taking the Fourier transforms of the $C \Delta t^{(2)}$ term, one can verify that because of the properties of $\tilde{C}(\mathbf{q}_1, \mathbf{q}_2)$ [see (2.32)], the magnitude of that term is on the order of $(r_c/R)^3$ ($\sim 1/A$) multiplied by the magnitude of $\Delta t^{(2)}(\mathbf{q}_1, \mathbf{q}_2)$. The first factor reduces the A dependence of $V^{(\text{opt})}$ to a linear one. The second is expected to be small at high energies since most of the scattering by the two-body system will be given by the first two terms of (3.19). One therefore expects the second term in (3.20) to be small compared to the first term (see Appendix B of this chapter). However, because of interference of the first and second term, the latter may become visible especially at high momentum transfers, where the precipitous decrease of the first term will be modified by the presence of the second.

One should note the differing origin of the correlation function present in (2.25) and (3.20). In (2.25) we are concerned with the inelastic cross section. There is no interference and only $\tilde{C}(\mathbf{q}, -\mathbf{q})$ makes its appearance. Only single scattering is present in the amplitude, \tilde{C} making its appearance as a consequence of squaring the transition amplitude and summing over all final states. The conclusion reached in Section 2, that \tilde{C} will not be visible in the elastic scattering,

must be modified because as has been emphasized, interference of the first and second terms in (3.20) may make the correlation-dependent term visible.

4. FORMAL THEORY OF MULTIPLE SCATTERING[†]

The intuitive considerations of the preceding sections need to be put on a firmer footing in which a more accurate result is derived, with the approximations clearly stated and methods for the calculation of corrections indicated. In this section we employ the formalism developed by Kerman, McManus, and Thaler (59) [here called the KMT method; see also Feshbach, Gal, and Hufner (71)], which in turn is based on the analysis by Watson (53, 57, 58) and Lax (51) of the multiple scattering problem.

Formally, the multiple scattering problem can be stated as follows. Let the potential acting between the incident projectile and the target nucleus be a sum of two-body interactions, v_i , including spin and isospin dependence acting between the projectile and the i th target nucleon:

$$V = \sum_{i=1}^A v_i \mathcal{A} \quad (4.1)$$

where \mathcal{A} is the antisymmetrization operator operating on the target nucleons, thus guaranteeing that only those wave functions for the target system that satisfy the Pauli principle will enter into the discussion. When the projectile consists of nucleons, we shall assume that the Pauli principle acting between the projectile nucleons and the target nucleons need not be enforced [Takeda and Watson (55)]. Physically, this seems reasonable (unless the collision leads to a large energy loss), for one can identify the projectile after collision by its large energy. However, there have been some criticisms of this procedure [Picklesimer and Thaler (81)].

The goal of the multiple scattering theory is to relate the transition matrix, \mathcal{T} , for the projectile–nucleus collision to the transition matrix, t , for the projectile–nucleon collision. From (4.1), \mathcal{T} satisfies

$$\mathcal{T}(E) = \sum_{i=1}^A v_i \mathcal{A} + \sum_{i=1}^A v_i \frac{\mathcal{A}}{\alpha} \mathcal{T}(E) \quad (4.2)$$

where

$$\alpha = E^{(+)} - K - H_N \quad (4.3)$$

and H_N is the target nucleus Hamiltonian; K is the kinetic energy of the incident projectile relative to the center of mass of the target nucleus. On the other hand,

[†]Kerman, McManus, and Thaler (59); Feshbach, Gal, and Hufner (71); Feshbach (81).

the t matrix satisfies, for scattering from the i th nucleon,

$$t_i(E) = v_i + v_i \frac{1}{E^{(+)} - K_0} t_i(E) \quad (4.4)$$

where K_0 is the kinetic energy operator in the projectile–nucleon system.

As a first step, one introduces an operator τ which is the transition matrix for the averaged two-body interaction $(1/A)\sum_1^A v_i \mathcal{A}$:

$$\tau = \frac{1}{A} \sum_1^A v_i \mathcal{A} + \frac{1}{A} \sum_1^A v_i \frac{\mathcal{A}}{\alpha} \tau \quad (4.5)$$

τ is a many-body operator closely related to t_i . This relationship is made more explicit by introducing τ_i defined by

$$\tau = \frac{1}{A} \sum \tau_i \quad (4.6)$$

Then

$$\tau_i = v_i \mathcal{A} + v_i \frac{\mathcal{A}}{\alpha} \tau \quad (4.7)$$

which should be compared with (4.4). τ_i may be considered as the effective two-body operator in the nuclear medium. The latter's presence is indicated by the antisymmetrization operator \mathcal{A} as well as by the nuclear Hamiltonian in the operator α^{-1} . Equation (4.7) takes into account the contribution to the scattering amplitude generated by the i th nucleon of the waves emanating from all the other nucleons, as indicated by the presence of the operator τ on the right-hand side.

We can now use (4.5) to eliminate v_i from (4.2) for τ . This elimination is essential if v_i is singular. Toward that end, rewrite (4.5) as follows:

$$\sum_i v_i \mathcal{A} = \left(A - \sum_i v_i \frac{\mathcal{A}}{\alpha} \right) \tau$$

and replace $\sum v_i \mathcal{A}$ in (4.2) by the right-hand side:

$$\mathcal{T} = \left(A - \sum_i v_i \frac{\mathcal{A}}{\alpha} \right) \tau + \left(A - \sum_i v_i \frac{\mathcal{A}}{\alpha} \right) \tau \frac{1}{\alpha} \mathcal{T}$$

Using (4.5) [**Problem.** Prove (4.8)]

$$\tau \frac{1}{\alpha} \sum_i v_i \mathcal{A} = \sum_i v_i \frac{\mathcal{A}}{\alpha} \tau \quad (4.8)$$

this equation becomes

$$\mathcal{T} = A\tau + A\tau \frac{1}{\alpha} \mathcal{T} - \tau \frac{1}{\alpha} \left(\sum_i v_i \frac{\mathcal{A}}{\alpha} + \sum_i v_i \mathcal{A} \frac{1}{\alpha} \mathcal{T} \right)$$

or

$$\mathcal{T} = A\tau + (A-1)\tau \frac{1}{\alpha} \mathcal{T} \quad (4.9)$$

Define \mathcal{T}' by

$$\mathcal{T} \equiv \frac{A}{A-1} \mathcal{T}' \quad (4.10)$$

Then

$$\mathcal{T}' = (A-1)\tau + (A-1)\tau \frac{1}{\alpha} \mathcal{T}' \quad (4.11)$$

We thus obtain the remarkable result that the scattering induced by $\sum_i v_i$ can equally well be considered as a consequence of the effective interaction $(A-1)\tau (= [(A-1)/A] \sum \tau_i)$. The effect of the Pauli principle is now contained within the operator τ , while the transition matrix \mathcal{T} is to be obtained from the solution of (4.11) by multiplication by the factor $A/A-1$ according to (4.10).

With this result it now becomes possible to introduce the “frozen” nucleus approximation with some improvement upon its formulation as given in Section 2. We return to the Schrödinger equation equivalent to (4.11):

$$[E - K - H_N - (A-1)\tau]\Psi = 0 \quad (4.12)$$

and derive an equation for the open-channel component of Ψ . That component will at least contain the elastic channel, but it can as well contain other channels of interest. Toward this end we introduce a projection operator P which when applied to any wave function such as Ψ will yield the open-channel component of interest. P is given by

$$P = 0\rangle\langle 0 + 1\rangle\langle 1 + \dots \quad (4.13)$$

where $0\rangle$ is the state vector for the ground state of the target nucleus, $1\rangle$ the first excited state, and so on. The number of terms included is determined by the physics of the phenomena under study. Here the emphasis is on elastic and inelastic scattering. The projection operator Q complementary to P is defined by

$$Q \equiv 1 - P \quad (4.14)$$

The following relationships will be needed:

$$P^2 = P \quad Q^2 = Q \quad PQ = QP = 0 \quad (4.15)$$

We also define the symbols τ_{PQ} , τ_{PP} , and τ_{QQ} :

$$\begin{aligned} \tau_{PQ} &\equiv P\tau Q & \tau_{QP} &= Q\tau P \\ \tau_{PP} &\equiv P\tau P & \tau_{QQ} &= Q\tau Q \end{aligned}$$

The Schrödinger equation (4.12) can be replaced by a pair of coupled equations for $P\Psi$ and $Q\Psi$, where $P\Psi + Q\Psi = \Psi$:

$$[E - K - (H_N)_{PP} - (A - 1)\tau_{PP}](P\Psi) = (A - 1)\tau_{PQ}(Q\Psi) \quad (4.16a)$$

$$[E - K - (H_N)_{QQ} - (A - 1)\tau_{QQ}](Q\Psi) = (A - 1)\tau_{QP}(P\Psi) \quad (4.16b)$$

Solving the second equation formally for $(Q\Psi)$ and substituting in the first equation yields

$$\left[E - K - (H_N)_{PP} - (A - 1)\tau_{PP} - (A - 1)\tau_{PQ} \frac{1}{E - K - (H_N)_{QQ} - (A - 1)\tau_{QQ}} (A - 1)\tau_{QP} \right] P\Psi = 0 \quad (4.17)$$

thereby deriving an effective Hamiltonian and in particular an effective potential for the subspace projected by P . Equation (4.17) is exact. The first-order term in the effective potential, $(A - 1)\tau_{PP}$, is supplemented by a second-order term involving τ twice, which describes the system making the transition from the space projected by P to the complementary space projected by Q , propagating in \mathcal{Q} space followed by a transition back to the space projected by P . The Schrödinger equation iterates this process. Equation (4.17) is exact, but it is in a form that is suitable for approximation. For example, the frozen nucleus approximation is obtained by replacing $(H_N)_{QQ}$ by an average excitation energy $\bar{\epsilon}$ and $(A - 1)\tau_{QQ}$ by a first approximation to the two-body projectile-nucleus optical model Hamiltonian. Hence

$$\begin{aligned} V_{\text{opt}} &\simeq (A - 1)\tau_{PP} + (A - 1)\tau_{PQ} \frac{1}{E - K - \bar{\epsilon} - V^{(1)}} (A - 1)\tau_{QP} \\ &= (A - 1)\tau_{PP} + (A - 1)^2 \tau_{PQ} \frac{Q}{E - K - \bar{\epsilon} - V^{(1)}} \tau_{QP} \end{aligned} \quad (4.17')$$

where $V^{(1)}$ is the first-order potential [given by (4.30)] still to be derived. In writing the second of the equations we have used the fact the propagator no

longer depends on the target nuclear coordinates, depending only on the projectile coordinates relative to the nucleus center of mass. To proceed further we must elucidate the relation between τ_i and t_i .

The first approximation replaces (4.4) by

$$t_i \simeq v_i + v_i \frac{1}{\alpha} t_i \quad (4.18)$$

This involves adding H_N to the denominator of the propagator to obtain $1/\alpha$. This may not be a serious error under the assumption that E is large. Since we shall eventually replace H_N by some average value, this error can be compensated to some extent by shifting the energy in (4.4). For a further discussion of this point, see Appendix A at the end of this chapter, where it is shown that the error is of the order of $1/A$. Note also that (4.4) is in the projectile–nucleon center-of-mass system, whereas (4.18) is in the projectile–nucleus frame, very close for the heavier nuclei to the laboratory frame.

Using (4.18), one can eliminate v_i in (4.7) for τ_i . From (4.18),

$$v_i = \left(1 - v_i \frac{1}{\alpha}\right) t_i$$

Substituting in (4.7) gives

$$\begin{aligned} \tau_i &= \left(1 - v_i \frac{1}{\alpha}\right) t_i \mathcal{A} + \left(1 - v_i \frac{1}{\alpha}\right) t_i \frac{\mathcal{A}}{\alpha} \tau \\ &= t_i \mathcal{A} + t_i \frac{\mathcal{A}}{\alpha} \tau - t_i \frac{1}{\alpha} \left(v_i \mathcal{A} + v_i \frac{\mathcal{A}}{\alpha} \tau\right) \end{aligned}$$

where the equation

$$v_i \frac{1}{\alpha} t_i = t_i \frac{1}{\alpha} v_i$$

has been used. This equation follows from (4.18). Using (4.7), the equation for τ_i becomes

$$\tau_i = t_i \mathcal{A} + t_i \frac{1}{\alpha} (\tau - \tau_i)$$

The equation for τ is then

$$\begin{aligned} \tau &= \frac{1}{A} \sum t_i \mathcal{A} + \frac{1}{A} \sum t_i \frac{1}{\alpha} (\tau - \tau_i) \\ &= \frac{1}{A} \sum t_i \mathcal{A} + \frac{1}{A} \sum t_i \frac{\mathcal{A} - 1}{\alpha} \tau_i \end{aligned} \quad (4.19)$$

where the following relation has been used:

$$\tau = \mathcal{A}\tau_i \quad (4.20)$$

and it is assumed that the operators are acting on antisymmetrized wave functions. It is important to replace the propagator $(1/\alpha)[=1/(E^{(+)} - K - H_N)]$ by $1/\tilde{\alpha}$, which takes the effect of the nuclear medium more completely in account:

$$\tilde{\alpha} = E^{(+)} - K - H_N - (A - 1)\tau \quad (4.21)$$

These two propagators are related by

$$\frac{1}{\alpha} = \frac{1}{\tilde{\alpha}} + \frac{1}{\alpha} - \frac{1}{\tilde{\alpha}} = \frac{1}{\tilde{\alpha}} + \frac{1}{\alpha}(\tilde{\alpha} - \alpha)\frac{1}{\tilde{\alpha}}$$

or

$$\frac{1}{\alpha} = \frac{1}{\tilde{\alpha}} - \frac{1}{\alpha}(A - 1)\tau\frac{1}{\tilde{\alpha}} \quad (4.22)$$

But we need $(\mathcal{A} - 1)/\alpha$ and this is, from (4.22),

$$\frac{\mathcal{A} - 1}{\alpha} = \frac{\mathcal{A} - 1}{\tilde{\alpha}} \quad (4.23)$$

which follows from the equation $(\mathcal{A} - 1)\mathcal{A} = 0$ and (4.20). Inserting this result in (4.19), we have

$$\tau = \frac{1}{A} \sum_i t_i \mathcal{A} + \frac{1}{A} \sum_i t_i \frac{\mathcal{A} - 1}{\tilde{\alpha}} \tau_i \quad (4.24)$$

providing the desired relation between τ and t_i . [It is the analog of the Bethe–Goldstone equation stated in Chapter III of deShalit and Feshbach (74).] One can now solve this equation for τ by successive approximations. In the first order, obtained by dropping the second term on the right-hand side of (4.24),

$$\tau \sim \frac{1}{A} \sum_i t_i$$

or

$$\tau_i \sim t_i \quad (4.25)$$

To second order obtained by using this result in (4.24),

$$\tau = \frac{1}{A} \sum_i t_i \mathcal{A} + \frac{1}{A} \sum_i t_i \frac{\mathcal{A} - 1}{\tilde{\alpha}} t_i \quad (4.26)$$

or

$$\tau = \frac{1}{A} \sum t_i + \frac{1}{A^2} \sum_{i,j} t_i \frac{1}{\bar{\alpha}} t_j - \frac{1}{A} \sum t_i \frac{1}{\bar{\alpha}} t_i \quad (4.26')$$

where we have used $\mathcal{A}t_i = (1/A) \sum t_j$. We can now calculate the effective potential operator \hat{V}_{opt} , the optical model potential $\hat{V}_{\text{opt}} = P \hat{V}_{\text{opt}} P$. From (4.17),

$$\begin{aligned} \hat{V}_{\text{opt}} &= (A-1)\tau + (A-1)^2 \tau \frac{Q}{\bar{\alpha}} \tau \\ &= (A-1)\tau + (A-1)^2 \tau \frac{1}{\bar{\alpha}} \tau - (A-1)^2 \tau \frac{P}{\bar{\alpha}} \tau \end{aligned}$$

where

$$\bar{\alpha} = E - K - \bar{\epsilon} - V^{(1)} \quad (4.27)$$

One now inserts approximation (4.26') into \hat{V}_{opt} , making the additional approximation of replacing $\bar{\alpha}$ everywhere by $\bar{\alpha}$. The result is

$$\hat{V}_{\text{opt}} = \frac{A-1}{A} \sum t_i + \frac{A-1}{A} \sum_{i \neq j} t_i \frac{1}{\bar{\alpha}} t_j - \frac{(A-1)^2}{A^2} \sum_{i,j} t_i \frac{P}{\bar{\alpha}} t_j \quad (4.28)$$

This is the principal result of the multiple scattering formalism as developed by Kerman, McManus, and Thaler (59). Its extension to third order has been given by Ullo and Feshbach (74). There are three major approximations made in deriving (4.28). They are, in major part, high-energy approximations in that they become increasingly valid as the energy increases. That assertion depends in turn upon appropriate behaviour of the matrix elements of t_i and H_N with increasing momentum transfer, \mathbf{q} , and energy. What is required is that these matrix elements decrease rapidly enough with these increasing q and E so that the magnitude of $t_i(1/\bar{\alpha})$ is sufficiently small to ensure convergence of the series for \hat{V}_{opt} , the first two orders of which are given by (4.28). This limitation can be avoided to a great extent if one were to solve the analog of the Bethe-Goldstone equation, (4.24) more exactly (i.e., adapting the independent pair approximation) rather than use a small perturbation approximation.

In the case of elastic scattering, $P = 0 \rangle \langle 0$, and

$$V_{\text{opt}} = \langle 0 | \hat{V}_{\text{opt}} | 0 \rangle \quad (4.29)$$

and $(H_N)_{PP} = 0$. The first-order optical model potential is thus

$$V_{\text{opt}}^{(1)} = \frac{A-1}{A} \langle 0 | \sum t_i | 0 \rangle = (A-1) \langle 0 | t_1 | 0 \rangle \quad (4.30)$$

The transition matrix t_i is generally a nonlocal operator because of the presence of the second term in the Lippman–Schwinger equation, (4.4). In coordinate space it therefore has the form $\langle \mathbf{r} - \mathbf{r}_1, \frac{1}{2}(\mathbf{r} + \mathbf{r}_1) | \hat{t} | \mathbf{r}' - \mathbf{r}'_1, \frac{1}{2}(\mathbf{r}' + \mathbf{r}'_1) \rangle$, where, to be specific, we have used relative coordinate and center-of-mass coordinates for a *nucleon projectile*. The generalization to other projectiles is straightforward. Conservation of momentum determines the dependence on center-of-mass coordinates:

$$t_1 = \delta(\frac{1}{2}(\mathbf{r} + \mathbf{r}_1) - \frac{1}{2}(\mathbf{r}' + \mathbf{r}'_1)) t(\mathbf{r} - \mathbf{r}_1, \mathbf{r}' - \mathbf{r}'_1) \quad (4.31)$$

Then

$$\begin{aligned} V_{\text{opt}}^{(1)}(\mathbf{r}, \mathbf{r}') &= (A-1) \int d\mathbf{r}_1 \int d\mathbf{r}'_1 \Psi^*(\mathbf{r}_1, \mathbf{r}_2, \dots) t_1 \Psi(\mathbf{r}'_1, \mathbf{r}_2, \dots) d\mathbf{r}_2 \dots \\ &= (A-1) \int d\mathbf{r}_1 \int d\mathbf{r}'_1 K(\mathbf{r}_1, \mathbf{r}'_1) t(\mathbf{r} - \mathbf{r}_1, \mathbf{r}' - \mathbf{r}'_1) \delta(\frac{1}{2}(\mathbf{r} + \mathbf{r}_1) - \frac{1}{2}(\mathbf{r}' + \mathbf{r}'_1)) \end{aligned} \quad (4.32)$$

where $K(\mathbf{r}_1, \mathbf{r}'_1)$ is the one-body density matrix for the ground-state target nucleus

$$K(\mathbf{r}, \mathbf{r}') = \int d\mathbf{r}_2 \dots \Psi^*(\mathbf{r}, \mathbf{r}_2, \dots) \Psi(\mathbf{r}', \mathbf{r}_2, \dots) \quad (4.33)$$

In momentum space (4.32) becomes

$$\tilde{V}_{\text{opt}}^{(1)}(\mathbf{k}, \mathbf{k}') = \int d\mathbf{r} \int d\mathbf{r}' e^{-i\mathbf{k} \cdot \mathbf{r}} V_{\text{opt}}^{(1)}(\mathbf{r}, \mathbf{r}') e^{i\mathbf{k}' \cdot \mathbf{r}'} \quad (4.34)$$

Introducing Fourier transforms for K and t

$$K(\mathbf{r}, \mathbf{r}') = \frac{1}{(2\pi)^6} \int d\mathbf{s} \int d\mathbf{s}' e^{i\mathbf{s} \cdot \mathbf{r} - i\mathbf{s}' \cdot \mathbf{r}'} \tilde{K}(\mathbf{s}, \mathbf{s}') \quad (4.35)$$

and

$$\tilde{t}(\boldsymbol{\kappa}, \boldsymbol{\kappa}') = \int d\boldsymbol{\rho} \int d\boldsymbol{\rho}' e^{-i\boldsymbol{\kappa} \cdot \boldsymbol{\rho} + i\boldsymbol{\kappa}' \cdot \boldsymbol{\rho}'} t(\boldsymbol{\rho}, \boldsymbol{\rho}') \quad (4.36)$$

Equation (4.34) becomes (use relative and center-of-mass integration variables)

$$\tilde{V}_{\text{opt}}^{(1)}(\mathbf{k}, \mathbf{k}') = \frac{A-1}{(2\pi)^3} \int d\mathbf{s} \int d\mathbf{s}' \tilde{K}(\mathbf{s}, \mathbf{s}') \tilde{t}\left(\frac{\mathbf{s} + \mathbf{k}}{2}, \frac{\mathbf{s}' + \mathbf{k}'}{2}\right) \delta(\mathbf{s} - \mathbf{k} - (\mathbf{s}' - \mathbf{k}')) \quad (4.37)$$

The interpretation of this equation is instructive. The projectile brings in a

momentum of \mathbf{k}' , the target nucleon $-\mathbf{s}'$. Upon scattering the projectile acquires a momentum of \mathbf{k} , the target nucleon, $-\mathbf{s}$. The delta function ensures that the momentum transferred to the projectile, $(\mathbf{k} - \mathbf{k}')$, is balanced by the amount transferred to the target nucleon $(\mathbf{s} - \mathbf{s}')$. The \tilde{t} matrix gives the amplitude for a transition from relative momentum $\frac{1}{2}(\mathbf{s}' + \mathbf{k}')$ to $\frac{1}{2}(\mathbf{s} + \mathbf{k})$. Equation (4.37) takes into account the motion (sometimes referred to as the Fermi motion) of the nucleons in the target nucleus.

As a final development we consider the consequences of the assumption that $t(\mathbf{r}, \mathbf{r}')$ is local [see (3.7')],

$$t(\mathbf{r}, \mathbf{r}') = \delta(\mathbf{r} - \mathbf{r}')t(\mathbf{r}) \quad (4.38)$$

upon the first-order potential, (4.32). The evaluation is straightforward. One finds that $V_{\text{opt}}^{(1)}(\mathbf{r}, \mathbf{r}')$ is local:

$$V_{\text{opt}}^{(1)}(\mathbf{r} - \mathbf{r}') = \delta(\mathbf{r} - \mathbf{r}')v_{\text{opt}}^{(1)}(\mathbf{r}) \quad (4.39)$$

where

$$v_{\text{opt}}^{(1)}(\mathbf{r}) = (A - 1) \int d\mathbf{r}_1 \rho(\mathbf{r}_1) t(\mathbf{r} - \mathbf{r}_1) \quad (4.40)$$

In momentum space

$$\begin{aligned} \tilde{v}_{\text{opt}}^{(1)}(\mathbf{q}) &= \int e^{i\mathbf{q} \cdot \mathbf{r}} v_{\text{opt}}^{(1)}(\mathbf{r}) d\mathbf{r} \\ &= (A - 1) \tilde{\rho}(\mathbf{q}) \tilde{t}(\mathbf{q}) \end{aligned} \quad (4.40')$$

Equation (4.39) is in agreement to order $1/A$ with the result obtained by intuitive arguments in Section 3 [see (3.9)]. In making this comparison, one should bear in mind that the scattering amplitude obtained using the potential equation (4.39) must be multiplied by the factor $(A/A - 1)$, according to (4.10), in order to obtain the full \mathcal{T} matrix. Thus the intuitive result and the first-order result just obtained will give the same amplitude in the Born approximation. Further discussion is postponed until the second-order term of (4.28) is evaluated.

We first express the second-order term in coordinate space assuming t_i to be a local operator [see (3.7')]

$$\langle \mathbf{r} | t_i | \mathbf{r}' \rangle = \delta(\mathbf{r} - \mathbf{r}') t(\mathbf{r} - \mathbf{r}_i)$$

Then

$$\begin{aligned} V_{\text{opt}}^{(2)}(\mathbf{r}, \mathbf{r}') &= \langle 0, \mathbf{r} | \hat{V}_{\text{opt}}^{(2)} | 0, \mathbf{r}' \rangle \\ &= (A - 1)^2 \int d\mathbf{r}'' \int d\mathbf{r}''' \left\{ \frac{1}{A(A - 1)} \langle 0 | \sum_{i \neq j} \delta(\mathbf{r} - \mathbf{r}'') t(\mathbf{r} - \mathbf{r}_i) \langle \mathbf{r}'' | \frac{1}{\tilde{\alpha}} | \mathbf{r}''' \rangle \right. \\ &\quad \times \delta(\mathbf{r}''' - \mathbf{r}') t(\mathbf{r}' - \mathbf{r}_j) | 0 \rangle \\ &\quad \left. - \frac{1}{A^2} \langle 0 | \sum_i \delta(\mathbf{r} - \mathbf{r}'') t(\mathbf{r} - \mathbf{r}_i) | 0 \rangle \langle \mathbf{r}'' | \frac{1}{\tilde{\alpha}} | \mathbf{r}''' \rangle \langle 0 | \sum_j \delta(\mathbf{r}''' - \mathbf{r}') t(\mathbf{r}' - \mathbf{r}_j) | 0 \rangle \right\} \end{aligned}$$

Using the antisymmetry of the target nuclear wave function and performing the integrations over \mathbf{r}'' and \mathbf{r}''' , one obtains

$$\begin{aligned} V_{\text{opt}}^{(2)}(\mathbf{r}, \mathbf{r}') &= (A-1)^2 \{ \langle 0 | t(\mathbf{r} - \mathbf{r}_1) t(\mathbf{r}' - \mathbf{r}_2) | 0 \rangle - \langle 0 | t(\mathbf{r} - \mathbf{r}_1) | 0 \rangle \langle 0 | t(\mathbf{r}' - \mathbf{r}_2) | 0 \rangle \\ &\quad \times \langle \mathbf{r} | \frac{1}{\alpha} | \mathbf{r}' \rangle \\ &= (A-1)^2 \int d\mathbf{r}_1 \int d\mathbf{r}_2 t(\mathbf{r} - \mathbf{r}_1) \langle \mathbf{r} | \frac{1}{\alpha} | \mathbf{r}' \rangle t(\mathbf{r}' - \mathbf{r}_2) [\rho(\mathbf{r}_1, \mathbf{r}_2) - \rho(\mathbf{r}_1)\rho(\mathbf{r}_2)] \end{aligned}$$

or

$$V_{\text{opt}}^{(2)}(\mathbf{r}, \mathbf{r}') = (A-1)^2 \int d\mathbf{r}_1 \int d\mathbf{r}_2 t(\mathbf{r} - \mathbf{r}_1) \langle \mathbf{r} | \frac{1}{\alpha} | \mathbf{r}' \rangle t(\mathbf{r}' - \mathbf{r}_2) C(\mathbf{r}_1, \mathbf{r}_2) \quad (4.41)$$

Clearly, $V_{\text{opt}}^{(2)}$ is a nonlocal energy-dependent potential involving a scattering by a target nucleon at \mathbf{r}_2 , a propagation from \mathbf{r}' to \mathbf{r} , and a second scattering by a target nucleon at \mathbf{r}_1 . The correlation function measures the probability of a target nucleon being present at \mathbf{r}_1 and another at \mathbf{r}_2 . Comparing (4.41) with the intuitive derivation of (3.20), one can identify the $\Delta t^{(2)}$ of that equation (to order $1/A$).

$$\Delta t^{(2)}(\mathbf{r}, \mathbf{r}'; \mathbf{r}_1, \mathbf{r}_2) = t(\mathbf{r} - \mathbf{r}_1) \langle \mathbf{r} | \frac{1}{\alpha} | \mathbf{r}' \rangle t(\mathbf{r}' - \mathbf{r}_2) \quad (4.42)$$

We also restate (4.41) in momentum space, as this is the form in which one finds it in the literature:

$$\begin{aligned} \tilde{V}_{\text{opt}}^{(2)}(\mathbf{k}, \mathbf{k}') &= (A-1)^2 \int \frac{d\mathbf{k}''}{(2\pi)^3} \int \frac{d\mathbf{k}'''}{(2\pi)^3} [\tilde{t}(\mathbf{k}'' - \mathbf{k}) \langle \mathbf{k}'' | \frac{1}{\alpha} | \mathbf{k}''' \rangle \tilde{t}(\mathbf{k}' - \mathbf{k}''')] \\ &\quad \times \tilde{C}(\mathbf{k}'' - \mathbf{k}, \mathbf{k}' - \mathbf{k}''') \end{aligned} \quad (4.43)$$

where

$$\tilde{C}(\mathbf{q}, \mathbf{q}') = \int d\mathbf{r}_1 \int d\mathbf{r}_2 e^{i\mathbf{q} \cdot \mathbf{r}_1 + i\mathbf{q}' \cdot \mathbf{r}_2} C(\mathbf{r}_1, \mathbf{r}_2) \quad (4.44)$$

A posteriori, it appears that the multiple scattering series for the optical potential is an expansion in terms of correlation functions of increasing order. The first-order term depends on the density, the second in the pair correlation. Ullo (74) has evaluated the third-order term and has shown that to $O(1/A)$, $V_{\text{opt}}^{(3)}$ depends on the triple correlation function $C^{(3)}(\mathbf{r}_1, \mathbf{r}_2, \mathbf{r}_3)$ lending support to this surmise.

Problem. Show that the triple correlation function is given by

$$\begin{aligned} C^{(3)}(\mathbf{r}_1, \mathbf{r}_2, \mathbf{r}_3) &= \rho^{(3)}(\mathbf{r}_1, \mathbf{r}_2, \mathbf{r}_3) - \rho^{(2)}(\mathbf{r}_1, \mathbf{r}_2)\rho(\mathbf{r}_3) - \rho^{(2)}(\mathbf{r}_1, \mathbf{r}_3)\rho(\mathbf{r}_2) \\ &\quad - \rho^{(2)}(\mathbf{r}_2, \mathbf{r}_3)\rho(\mathbf{r}_1) + 2\rho(\mathbf{r}_1)\rho(\mathbf{r}_2)\rho(\mathbf{r}_3) \end{aligned}$$

Show that

$$\int C^{(3)}(\mathbf{r}_1, \mathbf{r}_2, \mathbf{r}_3) d\mathbf{r}_1 = C(\mathbf{r}_2, \mathbf{r}_3)$$

The separation into density- and correlation-dependent contributions $V_{\text{opt}}^{(1)}$ and $V_{\text{opt}}^{(2)}$ must be modified when the spin dependence of the two-body transition operators is taken into account. Here it will suffice to give an example. The complete treatment is given in Lambert and Feshbach (73) and Parmentola and Feshbach (82). Suppose that the incident projectile is a nucleon and that

$$t(\mathbf{r} - \mathbf{r}_i) = t^{(0)}(\mathbf{r} - \mathbf{r}_i) + t^{(s)}(\mathbf{r} - \mathbf{r}_i) \boldsymbol{\sigma} \cdot \boldsymbol{\sigma}_i$$

Then for a spin 0 target nucleus,

$$\begin{aligned} V^{(1)}(\mathbf{r}, \mathbf{r}') &= (A-1) \langle 0 | t(\mathbf{r} - \mathbf{r}_1) | 0 \rangle \delta(\mathbf{r} - \mathbf{r}') \\ &= (A-1) \langle 0 | t^{(0)}(\mathbf{r} - \mathbf{r}_1) | 0 \rangle \delta(\mathbf{r} - \mathbf{r}') \end{aligned}$$

so that $t^{(s)}$ does not appear in $V^{(1)}$. On the other hand, the equation for $V^{(2)}(\mathbf{r}, \mathbf{r}')$ becomes

$$\begin{aligned} V^{(2)}(\mathbf{r}, \mathbf{r}') &= (A-1)^2 \langle \mathbf{r} | \frac{1}{\alpha} | \mathbf{r}' \rangle \\ &\quad \times \{ \langle 0 | [t^{(0)}(\mathbf{r} - \mathbf{r}_1) + t^{(s)}(\mathbf{r} - \mathbf{r}_1) \boldsymbol{\sigma} \cdot \boldsymbol{\sigma}_1] [t^{(0)}(\mathbf{r} - \mathbf{r}_2) + t^{(s)}(\mathbf{r}' - \mathbf{r}_2) \boldsymbol{\sigma} \cdot \boldsymbol{\sigma}_2] | 0 \rangle \\ &\quad - \langle 0 | t^{(0)}(\mathbf{r} - \mathbf{r}_1) | 0 \rangle \langle 0 | t^{(0)}(\mathbf{r}' - \mathbf{r}_2) | 0 \rangle \} \\ &= (A-1)^2 \langle \mathbf{r} | \frac{1}{\alpha} | \mathbf{r}' \rangle \int d\mathbf{r}_1 \int d\mathbf{r}_2 \{ t^{(0)}(\mathbf{r} - \mathbf{r}_1) t^{(0)}(\mathbf{r}' - \mathbf{r}_2) C(\mathbf{r}_1, \mathbf{r}_2) \\ &\quad + \langle 0 | t^{(s)}(\mathbf{r} - \mathbf{r}_1) t^{(s)}(\mathbf{r}' - \mathbf{r}_2) \boldsymbol{\sigma}_1 \cdot \boldsymbol{\sigma}_2 | 0 \rangle \} \end{aligned}$$

To avoid some Racah algebra, assume that the target wave function is a product of a spin and of a space-dependent factor. Hence the second term becomes

$$\begin{aligned} M &\equiv \int d\mathbf{r}_1 \int d\mathbf{r}_2 \langle 0 | t^{(s)}(\mathbf{r} - \mathbf{r}_1) t^{(s)}(\mathbf{r}' - \mathbf{r}_2) \boldsymbol{\sigma}_1 \cdot \boldsymbol{\sigma}_2 | 0 \rangle \\ &= \int d\mathbf{r}_1 \int d\mathbf{r}_2 \rho(\mathbf{r}_1, \mathbf{r}_2) t^{(s)}(\mathbf{r} - \mathbf{r}_1) t^{(s)}(\mathbf{r}' - \mathbf{r}_2) \langle 0 | \boldsymbol{\sigma}_1 \cdot \boldsymbol{\sigma}_2 | 0 \rangle \end{aligned}$$

and

$$\langle 0 | \boldsymbol{\sigma}_1 \cdot \boldsymbol{\sigma}_2 | 0 \rangle = \frac{1}{A(A-1)} \sum_{i \neq j} \langle 0 | \boldsymbol{\sigma}_i \cdot \boldsymbol{\sigma}_j | 0 \rangle$$

$$\begin{aligned}
&= \frac{1}{A(A-1)} [\langle 0 | \sum \sigma_i \cdot \sum \sigma_j | 0 \rangle - 3A] \\
&= -\frac{3}{A-1}
\end{aligned}$$

Hence

$$M = -\frac{3}{A-1} \int d\mathbf{r}_1 \int d\mathbf{r}_2 \rho(\mathbf{r}_1, \mathbf{r}_2) t^{(s)}(\mathbf{r} - \mathbf{r}_1) t^{(s)}(\mathbf{r}' - \mathbf{r}_2)$$

or

$$\begin{aligned}
M &= -\frac{3}{A-1} \left[\int d\mathbf{r}_1 \rho(\mathbf{r}_1) t^{(s)}(\mathbf{r} - \mathbf{r}_1) \right] \left[\int d\mathbf{r}_2 \rho(\mathbf{r}_2) t^{(s)}(\mathbf{r} - \mathbf{r}_2) \right] \\
&\quad - \frac{3}{A-1} \int d\mathbf{r}_1 \int d\mathbf{r}_2 C(\mathbf{r}_1, \mathbf{r}_2) t^{(s)}(\mathbf{r} - \mathbf{r}_1) t^{(s)}(\mathbf{r}' - \mathbf{r}_2)
\end{aligned}$$

Define the density (but not correlation dependent) optical potential as follows:

$$\begin{aligned}
\mathcal{V}_{\text{opt}}^{(1)} &= (A-1) \int \rho(\mathbf{r}_1) t^{(0)}(\mathbf{r} - \mathbf{r}_1) d\mathbf{r}_1 \delta(\mathbf{r} - \mathbf{r}') \\
&\quad - 3(A-1) \langle \mathbf{r} | \frac{1}{\bar{\alpha}} | \mathbf{r}' \rangle \int d\mathbf{r}_1 \rho(\mathbf{r}_1) t^{(s)}(\mathbf{r} - \mathbf{r}_1) \int d\mathbf{r}_2 \rho(\mathbf{r}_2) t^{(s)}(\mathbf{r}' - \mathbf{r}_2) \quad (4.45)
\end{aligned}$$

The remainder of the optical potential $V^{(1)} + V^{(2)} - \mathcal{V}^{(1)}$ will now involve only $C(\mathbf{r}_1, \mathbf{r}_2)$ and not ρ .

The Schrödinger equation with the potential $\mathcal{V}_{\text{opt}}^{(1)}$ is equivalent to a pair of coupled equations:

$$\begin{aligned}
&[E - K - (A-1) \int d\mathbf{r}_1 \rho(\mathbf{r}_1) t^{(0)}(\mathbf{r} - \mathbf{r}_1)] \psi \\
&= i\sqrt{3(A-1)} \int d\mathbf{r}_1 \rho(\mathbf{r}_1) t^{(s)}(\mathbf{r} - \mathbf{r}_1) \phi \\
&\bar{\alpha}\phi = [E - K - \bar{\epsilon} - (A-1) \int d\mathbf{r}_1 \rho(\mathbf{r}_1) t^{(0)}(\mathbf{r} - \mathbf{r}_1)] \phi \\
&= i\sqrt{3(A-1)} \int d\mathbf{r}_1 \rho(\mathbf{r}_2) t^{(s)}(\mathbf{r} - \mathbf{r}_2) \psi \quad (4.46)
\end{aligned}$$

Equation (4.45) can be obtained by eliminating ϕ from this pair of equations and identifying the potential in the resulting single-channel Schrödinger equation. The process being described consists of two scatterings. In the first the spin of the target nucleon is flipped by the $\boldsymbol{\sigma} \cdot \boldsymbol{\sigma}_1$ term, generating the

amplitude ϕ . The spin of the target and the amplitude ψ are restored through the action of the second $\boldsymbol{\sigma} \cdot \boldsymbol{\sigma}_2$.

The magnitude of this spin effect will vary with circumstances, depending on the ratio between the first and second terms in (4.45), such as the strength of the spin-dependent amplitude compared to the spin-independent one. One can show that the ratio will decrease like $1/\sqrt{E}$ but that energy dependence may be modified by the energy dependence of $t^{(s)}$ and $t^{(0)}$. In any event, before the effects of correlations can be evaluated it is necessary to evaluate the spin- and isospin-dependent contributions which make their appearance in $V_{\text{opt}}^{(2)}$. The first order $V_{\text{opt}}^{(1)}$ does not contain all the density dependence.

The optical potential \hat{V}_{opt} of (4.28) can be used to describe reaction processes such as inelastic scattering. In that case one simply includes the inelastic channels under study in (4.13). We consider the simple case of only one inelastic channel. One then obtains a pair of coupled equations with the potential matrix

$$\langle 0 | \hat{V}_{\text{opt}}^{(1)} | 0 \rangle, \quad \langle 0 | \hat{V}_{\text{opt}}^{(1)} | 1 \rangle, \quad \langle 1 | \hat{V}_{\text{opt}}^{(1)} | 0 \rangle, \quad \text{and} \quad \langle 1 | \hat{V}_{\text{opt}}^{(1)} | 1 \rangle,$$

We have just obtained $\langle 0 | \hat{V}_{\text{opt}}^{(1)} | 0 \rangle$, which in its local form, is given by (4.39), where $\rho(\mathbf{r})$ is the density for the ground state, $|0\rangle$, of the target nucleus. The other diagonal component, $\langle 1 | \hat{V}_{\text{opt}}^{(1)} | 1 \rangle$, will have a similar structure with $\rho(\mathbf{r})$ replaced by the density function for the excited state. The new elements are the coupling potentials, which will take the form

$$V_{01} \equiv \langle 0 | \hat{V}_{\text{opt}}^{(1)} | 1 \rangle = (A-1) \int \rho_{01}(\mathbf{r}_1) t(\mathbf{r} - \mathbf{r}_1) d\mathbf{r}_1 \quad (4.47)$$

where

$$\rho_{01}(\mathbf{r}_1) = \int \Psi_0^*(1, 2, \dots) \Psi_1(1, 2, \dots) d\mathbf{r}_2 \dots \quad (4.48)$$

Note that

$$\int \rho_{01}(\mathbf{r}_1) d\mathbf{r}_1 = 0 \quad (4.49)$$

as a consequence of orthogonality of the target wave functions.

The form factors ρ_{01} , as they are sometimes called, are discussed in some detail in Chapter V. We therefore will be content with a few remarks concerning the Fourier transform $\tilde{\rho}_{01}(\mathbf{q})$:

$$\tilde{\rho}_{01}(\mathbf{q}) = \int e^{i\mathbf{q} \cdot \mathbf{r}} \rho_{01}(\mathbf{r}) d\mathbf{r} \quad (4.50)$$

From (4.49) we have

$$\tilde{\rho}_{01}(0) = 0 \quad (4.51)$$

Moreover, if the transition from $|0\rangle$ to $|1\rangle$ involves a change in angular momentum, then $\rho_{01}(\mathbf{r})$ will involve $Y_{lm}(\theta, \phi)$. Therefore, in the expansion of the plane wave $\exp(i\mathbf{q}\cdot\mathbf{r})$ in (4.50) the first term that survives is proportional to $j_l(qr)$. As a consequence, $\tilde{\rho}_{01}(q) \rightarrow q^l$ for small q . This is one of the effects of the angular momentum barrier. The Born approximation then indicates a sharp decrease in the transition amplitude as one approaches $q=0$. The effect of including distortion will not substantially modify this result, so that one expects the inelastic scattering cross section to have its maximum for $qR \sim l$ and to decrease rapidly as q becomes smaller.

For most situations the distorted wave approximation (DWA) with interaction V_{01} of (4.47) suffices. The form of V_{01} suggests the possible use of folding to describe the coupling potential (see Chapter V). The extension to include correlation effects has been carried out [Feshbach (81)] and the reader is referred to that paper for more details.

5. THE SEMICLASSICAL APPROXIMATION[†]

This procedure is applicable when the wavelength of the projectile is small compared to the size of the system and when the projectile energy is much larger than the depth of the potential in which the projectile moves. We begin by considering the problem of the scattering of a projectile by a potential well and then develop the generalization to multiple scattering.

The propagation of short-wavelength radiation is a comparatively ancient subject which has received thorough study [van de Hulst (57)]. It occurs, for example, in the design of optical instruments, where the wavelength of the light is small compared to the size of the system. It is a method developed in that connection which we shall adapt to the present problem. Consider a wave propagating through a medium with an index of refraction n . The wavefront is defined to be an equiphase surface, while points on the wavefront trace out trajectories as the wave propagates. In the approximation to be used, these trajectories are calculated in the geometrical optics approximation (infinitely short wavelength) with the phase change along the ray given by the optical path length, $\Delta\Phi$:

$$\Delta\Phi = \int nk ds$$

where the integral is taken along the trajectory. By performing this calculation for each ray it is possible in principle to construct the equal-phase wavefronts and thereby follow the propagation of a wave through the medium.

In the present context, the ray is replaced by the classical mechanical

[†]Glauber (59); Feshbach (67).

trajectory of the particle. The index of refraction is given by

$$nk = \left[\frac{2\mu}{\hbar^2} (E - V) \right]^{1/2} = (k^2 - U)^{1/2}$$

where

$$U \equiv \frac{2\mu}{\hbar^2} V \quad (5.1)$$

so that

$$\Delta\Phi = \int \sqrt{k^2 - U} \, ds \quad (5.2)$$

This approximation is thus a *semiclassical* one.

In the simplest form of the approximation it is assumed that the trajectories are straight that is, undeviated by the action of the potential and thus proceeding in the incident direction. This approximation requires that the momentum change which occurs because of the action of the potential be small compared to the initial momentum. Taking the force to be of the order of V/a , where a is an interaction length, and the time during which it acts as a/v , one obtains a momentum change of V/v . The resulting angular deflection is on the order of

$$\theta = \frac{V}{vp} = \frac{V}{2E} \quad (5.3)$$

The straight-ahead approximation is thus valid when

$$\theta \sim \frac{V}{2E} \ll 1 \quad (5.4)$$

To use the geometric approximation it is necessary that the classical trajectories be well defined. This requires that the classical momentum change V/v be larger than the quantum uncertainty in the momentum \hbar/R :

$$\frac{V}{v} \gg \frac{\hbar}{R}$$

or

$$\frac{VR}{\hbar v} = \frac{V}{2E} (kR) \gg 1 \quad (5.5)$$

We observe that this condition can be satisfied simultaneously with (5.4) only if

$$kR \gg 1 \quad (5.6)$$

Problem. Prove that the Born approximation is valid when $(V/2E)(kR) \ll 1$.

Problem. Show that in the relativistic regime (5.5) is replaced by $VR/\hbar c \gg 1$.

With the straight-ahead approximation it becomes a simple matter to calculate the phase change of a plane wave propagating in the z direction. Taking the initial phase ($z \rightarrow -\infty$) to be kz , the phase at any z is

$$\Phi(z) = kz + \int_{-\infty}^z dz' (\sqrt{k^2 - U} - k)$$

and the corresponding “plane wave” by

$$\psi = \exp \left\{ i \left[kz + \int_{-\infty}^z dz' (\sqrt{k^2 - U} - k) \right] \right\} \quad (5.7)$$

It should be noted that despite the straight-ahead approximation, ψ does describe a particle with both longitudinal and transverse momentum.

Problem. Let the solution, ψ , of the Schrödinger equation for potential scattering have the form

$$\psi = e^{iS}$$

Show that when $\nabla^2 S \ll (\nabla S)^2$,

$$(\nabla S)^2 \simeq k^2 - U$$

Derive (5.7).

We are now in a position to evaluate the elastic scattering transition matrix from ψ to the plane wave with momentum \mathbf{k}_f :

$$\begin{aligned} \mathcal{T}_{el} &= \langle \phi_f^{(-)} V \psi_i^{(+)} \rangle \\ &= \frac{\hbar^2}{2\mu} \int d\mathbf{r} e^{-i\mathbf{k}_f \cdot \mathbf{r}} U \exp \left\{ i \left[\mathbf{k}_i \cdot \mathbf{r} + \int_{-\infty}^z dz' (\sqrt{k^2 - U} - k) \right] \right\} \\ &= \frac{\hbar^2}{2\mu} \int d\mathbf{r} e^{i(\mathbf{k}_i - \mathbf{k}_f) \cdot \mathbf{r}} U \exp \left\{ i \left[\int_{-\infty}^z dz' (\sqrt{k^2 - U} - k) \right] \right\} \end{aligned} \quad (5.8)$$

To proceed further we choose the z axis to be along the direction $(\mathbf{k}_i + \mathbf{k}_f)$. This is a modification of the straight-ahead approximation. It is still assumed that the trajectories are straight lines but along the direction given by the average momentum $(\mathbf{k}_i + \mathbf{k}_f)/2$. Then $(\mathbf{k}_i - \mathbf{k}_f) \cdot \mathbf{r}$ becomes $(\mathbf{k}_i - \mathbf{k}_f) \cdot \mathbf{b}$ where \mathbf{b} is a vector

perpendicular to $\mathbf{k}_i + \mathbf{k}_f$. Evaluating this scalar product yields

$$(\mathbf{k}_i - \mathbf{k}_f) \cdot \mathbf{b} = 2 \sin \frac{\theta}{2} \cos \phi b k$$

Equation (5.8) becomes

$$\mathcal{T}_{\text{el}} = \frac{\hbar^2}{2\mu} \int dz \int d\mathbf{b} e^{2i \sin(\theta/2) \cos \phi b k} U \exp \left\{ i \left[\int_{-\infty}^z dz' (\sqrt{k^2 - U} - k) \right] \right\}$$

The integration over the orientation of \mathbf{b} yields

$$\mathcal{T} = \frac{\pi \hbar^2}{\mu} \int dz \int b db J_0(2kb \sin \frac{1}{2} \theta) U \exp \left\{ i \left[\int_{-\infty}^z dz' (\sqrt{k^2 - U} - k) \right] \right\} \quad (5.9)$$

A second approximation consistent with condition (5.4) permits the integration over z to be performed. Let

$$\Phi \equiv \sqrt{k^2 - U} - k$$

Then

$$U = -(2\Phi k + \Phi^2) \simeq -2\Phi k \quad (5.10)$$

with an error of U/k^2 or V/E . Then

$$\mathcal{T}_{\text{el}} = -\frac{2\pi \hbar^2 k}{\mu} \int b db J_0(2kb \sin \frac{1}{2} \theta) \int_{-\infty}^{\infty} dz \Phi \exp \left(i \int_{-\infty}^z \Phi dz' \right)$$

The z integration can now be performed, yielding

$$\mathcal{T}_{\text{el}} = \frac{2\pi i \hbar^2 k}{\mu} \int_0^{\infty} b db J_0(2kb \sin \frac{1}{2} \theta) (e^{ix} - 1) \quad (5.11)$$

where

$$\chi(\mathbf{b}) = \int_{-\infty}^{\infty} \Phi dz = \int_{-\infty}^{\infty} dz (\sqrt{k^2 - U} - k) \quad (5.12)$$

This derivation avoids an expansion in the exponent and therefore leads to an error linear in V/E rather than $\exp[i(V/E)]$. With (5.11) we have thus reduced the calculation of \mathcal{T}_{el} to a quadrature with an error on the order of V/E and valid in the short-wavelength limit ($kR \rightarrow \infty$) [see (5.4) and (5.5)]. The straight-line approximation used to obtain (5.9) requires, in addition, that the scattering angle θ be small as stated by (5.4). A better limit is obtained from the requirement

that the value of k occurring in the expression for $\chi(\mathbf{b})$ does not differ appreciably from the magnitude of $\frac{1}{2}(\mathbf{k}_i + \mathbf{k}_f)$. The condition that the error in $\exp(i\chi)$ be small is

$$\theta < \frac{4E}{kRV} \quad (5.13)$$

Problem. In the expression (5.7) for \mathcal{T}_{el} , take the z direction to be along the incident direction. Replacing $\exp[i(k - k \cos \theta)z]$ by unity, show that \mathcal{T}_{el} is given by (5.11) with, however, $J_0(2kb \sin \frac{1}{2}\theta)$ replaced by $J_0(kb \sin \theta)$.

The expression for the elastic scattering amplitude

$$f_{\text{el}} = -\frac{1}{4\pi} \frac{2\mu}{\hbar^2} \mathcal{T}_{\text{el}} \quad (5.14)$$

is

$$f_{\text{el}} = \frac{k}{i} \int_0^\infty b db J_0(2kb \sin \frac{1}{2}\theta) (e^{ix} - 1) \quad (5.15)$$

Further exploitation of these results to be developed in this section depends on the result to be demonstrated now, that for real U (no absorption) unitarity is approximately satisfied (this is not the case for the Born approximation); that is, the total cross section, σ_T , given in that event by the total elastic cross section,

$$\sigma_{\text{el}} = 2\pi \int |f_{\text{el}}|^2 \sin \theta d\theta \quad (5.16)$$

is equal to the cross section calculated according to the expression

$$\sigma_T = \frac{4\pi}{k} \text{Im} f_{\text{el}}(0) \quad (5.17)$$

From (5.16) and (5.15) we have

$$\begin{aligned} \sigma_{\text{el}} &= 2\pi k^2 \int_0^\infty b db \int_0^\infty b' db' \int_0^\pi \sin \theta d\theta J_0(2kb \sin \frac{1}{2}\theta) J_0(2kb' \sin \frac{1}{2}\theta) \\ &\quad \times (e^{ix(b)} - 1)(e^{-ix(b')} - 1) \end{aligned} \quad (5.18)$$

We make use of the Fourier–Bessel integral [Morse and Feshbach (53, p. 766)]

$$\int_0^\infty J_0(\kappa b) J_0(\kappa b') \kappa d\kappa = \frac{\delta(b - b')}{b}$$

Letting $\kappa = 2k \sin \frac{1}{2}\theta$, this equation becomes

$$\int_0^{\pi-i\infty} J_0(2kb \sin \frac{1}{2}\theta) J_0(2kb' \sin \frac{1}{2}\theta) \sin \theta d\theta = \frac{\delta(b-b')}{k^2 b}$$

Assuming that $(f_{el})^2$ can be neglected well before one reaches $\theta = \pi$, the integration over θ in (5.18) can be performed to yield

$$\sigma_{el} = 2\pi \int_0^\infty b db |e^{i\chi(b)} - 1|^2 \quad (5.19)$$

while from (5.17)

$$\sigma_T = 4\pi \int_0^\infty b db (1 - \operatorname{Re} e^{i\chi}) \quad (5.20)$$

As can be verified immediately, σ_T equals σ_{el} when U and therefore χ is real. The approximate satisfaction of the unitarity condition is thus demonstrated in the appropriate limit of no absorption.

When U is complex, absorption will occur. The absorption cross section σ_a can be obtained by subtracting σ_{el} , (5.19), from σ_T , (5.20):

$$\sigma_a = 2\pi \int_0^\infty b db (1 - |e^{i\chi}|^2) = 2\pi \int_0^\infty b db (1 - e^{-2\operatorname{Im} \chi}) \quad (5.21)$$

These formulas for the angle integrated cross sections [Eqs. (5.19), (5.20), and (5.21)] can be interpreted as being composed additively of contributions coming from a region between b and $b + db$ with the area of $2\pi b db$. Each contribution can be calculated as if there is an S matrix, as a function of b , given by $\exp(i\chi)$. Indeed, these results can also be obtained from the phase shift series for \mathcal{T}_{el} by taking a suitable high-energy limit. One then finds that

$$S \sim e^{2i\delta(b)}$$

where

$$\frac{1}{2}\chi(b) = \delta(b) \approx \delta_l \quad b = \frac{l + \frac{1}{2}}{k}$$

These results are very useful. Because of their simplicity, they permit a rapid evaluation of the elastic angular distributions as well as cross sections. Even in domains where they are not quantitatively valid, they yield qualitative results that are useful for orientation.

The results obtained with a square well [Feshbach (67); Bassichis, Feshbach

and Reading (71)] are instructive. From (5.15),

$$f(\theta) = \frac{iU_0}{2\kappa} \int_0^\infty b db J_0(2kb \sin \frac{1}{2}\theta) (e^{2i\kappa \sqrt{R^2 - b^2}} - 1) \quad (5.22)$$

where R is the radius of the well and

$$\kappa = \sqrt{k^2 - U_0} - k \xrightarrow{U_0 \ll k^2} -\frac{1}{2} \frac{U_0}{k}$$

The value of f at 0° is

$$f(0^\circ) = -\frac{iU_0}{2\kappa} \frac{R^2}{2} \left\{ 1 + \left[\frac{1}{2\kappa^2 R^2} - e^{2i\kappa R} \left(\frac{1}{i\kappa R} + \frac{1}{2\kappa^2 R^2} \right) \right] \right\} \quad (5.22')$$

In the limit $\kappa R \rightarrow \infty$, the optical theorem, (5.16), yields

$$\sigma_T \rightarrow 2\pi R^2 \quad (5.23)$$

As one can see from (5.20), this result can also be obtained when the absorption is so strong that e^{ix} can be neglected within the radius R . The absorption cross section is then

$$\sigma_a \rightarrow \pi R^2 \quad (5.24)$$

The angular distribution consists of two terms. The term, which is dominant near 0° generally and/or because of strong absorption, is given by the -1 term in (5.22). Note that it is the U_0 independent part of the integrand. We shall refer to it as the diffraction component, f_d . It contains that part of the scattered wave responsible for the formation of the shadow, as is immediately clear in the case of strong absorption. We find that

$$f_d(\theta) = -\frac{iU_0}{2\kappa} \int_0^R b db J_0(2kb \sin \frac{1}{2}\theta) = -\frac{iU_0}{2\kappa} R^2 \frac{J_1(2kR \sin(\theta/2))}{2kR \sin(\theta/2)} \quad (5.25a)$$

$$\rightarrow iR \frac{J_1(2kR \sin(\theta/2))}{2 \sin(\theta/2)} \quad (5.25b)$$

The angular distribution $|f_d|^2$ obtained from (5.25b) has a strong maximum at $\theta = 0^\circ$:

$$f_d(0^\circ) = \frac{ikR^2}{2} \quad (5.25c)$$

The next maximum in $|f_d|^2$ occurs at $2kR \sin(\theta/2)$ equal to about 5.2, at which point the ratio to $|f_d|^2$ at 0° is 1/57.4, demonstrating the strength of the 0° maximum.

From (5.22') the value of the deviation from $f_d(0^\circ)$ is given by

$$f_{el}(0^\circ) - f_d(0^\circ) = \frac{iU_0 R^2}{2\kappa} \left[\frac{e^{2i\kappa R}}{2i\kappa R} + \frac{1}{4\kappa^2 R^2} (e^{2i\kappa R} - 1) \right]$$

so that

$$\frac{|f_{el}(0^\circ) - f_d(0^\circ)|}{|f_d(0^\circ)|} \sim \frac{e^{-2 \operatorname{Im} \kappa R}}{|\kappa| R} \quad (5.26)$$

When $\operatorname{Im} |\kappa| R \gg 1$, the small-angle scattering is dominated by f_d . Even when the absorption is small, the diffraction amplitude will make the major contribution when

$$|\kappa| R \approx \frac{|U_0| R}{2k} \gg 1 \quad (5.27)$$

Condition (5.27) is identical with the condition (5.5) that the Born approximation fail and that the classical trajectories are well defined. It is thus satisfied in the regime for which the approximation for ψ , (5.7), is valid.

At least two conditions must be met if the semiclassical method is to be applied to obtain cross sections for larger angles of scattering. The absorption must be sufficiently strong so that one can neglect scattering from the front surface of the scatterer. This could generate amplitudes that would interfere with the incident beam creating maxima and minima characteristics of "rainbow" scattering. Second, it no longer makes sense to use the straight-line approximation for, for example, scattering to the back angles. In the spirit of the semiclassical method, one should calculate the classical trajectories and then obtain a more accurate expansion for ψ . Equation (5.7) is no longer valid. The effect of neglecting the momentum transfer is shown in Fig. 5.1. The effect of expanding the square root $\sqrt{k^2 - U_0}$ around k as used in (5.10) is shown in Fig. 5.2. Deviations from the exact result appear at $\theta \sim |V|/E$. With no absorption (Fig. 5.3) strong deviations appear even at small angles. These errors decrease in magnitude as the energy increases. For example, for scattering of 516-MeV nucleons (no absorption), the real and imaginary part of the amplitude is compared to the exact amplitude in Fig. 5.4. The semiclassical real part of the amplitude, longitudinal momentum neglected, fails after the first secondary maximum, while the imaginary part is incorrect even at 0° and increasingly beyond that point. In both cases there is agreement to within an order of magnitude with the exact results at back angles. Note that all of these examples use semilog abscissa. Figure 5.5 shows that the importance of absorption even

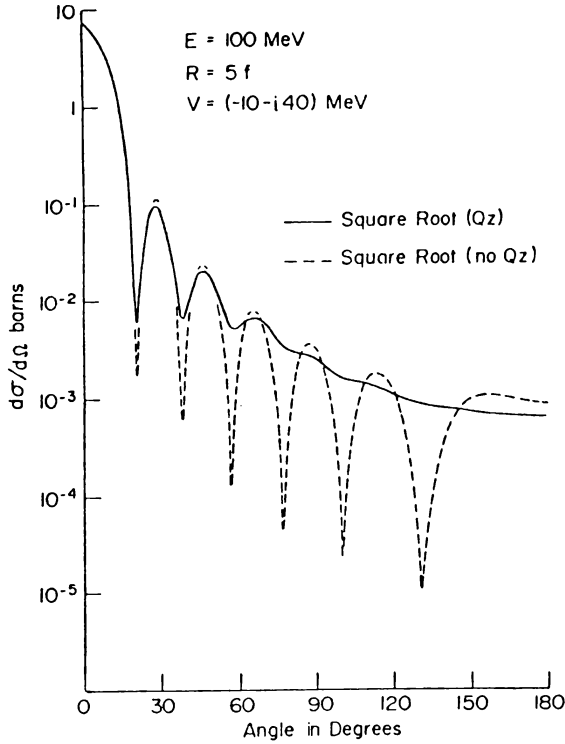


FIG. 5.1. Comparison between calculated cross sections to indicate the effect of including longitudinal momentum transfer and neglecting it, indicated by “no Q_z ” [From Bassichis, Feshbach, and Reading (71).]

at higher energies, the exact result showing the large effect of interference at back angles.

The application of the semiclassical approximation to multiple scattering is referred to as the *Glauber approximation* [Glauber (59); McCauley and Brown (58)]. We begin with the elastic amplitude, (5.11), which using (5.14) becomes

$$\hat{f}_{el} = \frac{ik}{2\pi} \int e^{i\mathbf{q} \cdot \mathbf{b}} (1 - e^{i\chi(\mathbf{b}, k)}) d\mathbf{b} \quad (5.14)$$

The scattering is from A scatterers at positions $\mathbf{r}_i (\equiv z_i, \mathbf{b}_i)$, the scattering potential being given by

$$\mathcal{V} = \sum_i V(\mathbf{r} - \mathbf{r}_i) \quad (5.28)$$

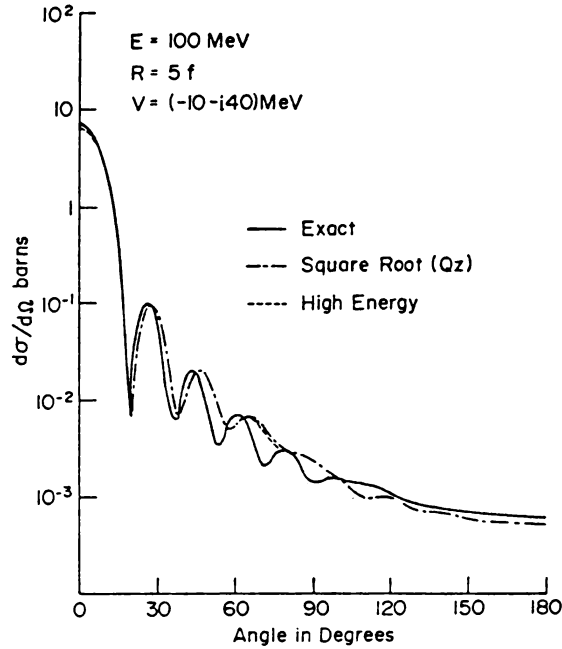


FIG. 5.2. Differential cross section for the scattering of 100-MeV nucleons by a square-well potential $5f$ in radius and potential $V = (-10 - i40)$ MeV. Comparison is made between the exact, the high-energy approximation (including the longitudinal momentum transfer indicated by “ Qz ”), and the square-root form. [From Bassichis, Feshbach, and Reading (71).]

so that the phase function χ is, according to (5.12),

$$\chi = \int_{-\infty}^{\infty} \left[\sqrt{k^2 - \sum_i U(\mathbf{r} - \mathbf{r}_i)} - k \right] dz \quad (5.29)$$

where

$$U \equiv \frac{2\mu}{\hbar^2} V$$

Expanding the square root and keeping only the first term, one obtains

$$\chi(k, \mathbf{b}) = \sum \chi_i(k, \mathbf{b} - \mathbf{b}_i) \quad (5.30)$$

$$\chi_i = -\frac{1}{2k} \int_{-\infty}^{\infty} U_i dz = -\frac{1}{\hbar v} \int_{-\infty}^{\infty} V(\mathbf{r} - \mathbf{r}_i) dz \quad (5.31)$$

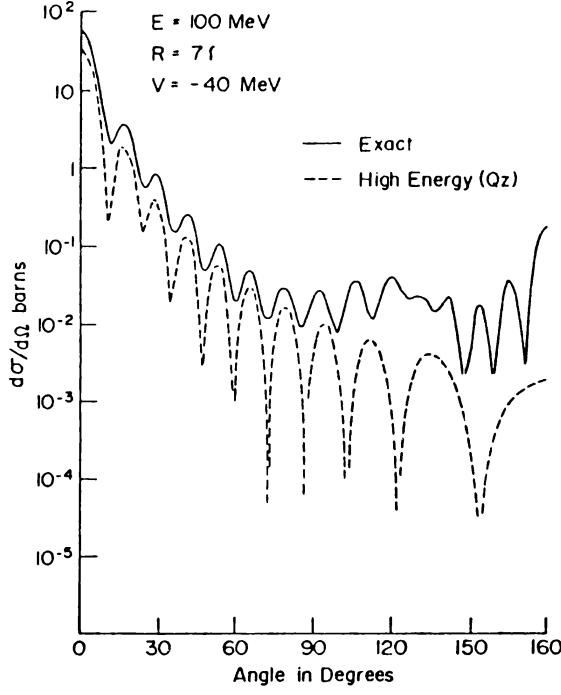


FIG. 5.3. Effect of absorption, where the radius of the square well is $7f$, the potential $V = -40$ MeV, and the incident nucleon an energy of 100 MeV. [From Bassichis, Feshbach, and Reading (71).]

so that

$$\hat{f}_{el} = \frac{ik}{2\pi} \int d\mathbf{b} e^{i\mathbf{q} \cdot \mathbf{b}} \left(1 - \prod_i e^{i\chi_i} \right) \quad (5.32)$$

Moreover, χ_i may be related to the single scattering amplitude of the projectile by a fixed-target nucleon. In the same semiclassical approximation, it is

$$f_i(\mathbf{q}) = \frac{ik}{2\pi} \int e^{i\mathbf{q} \cdot \mathbf{b}} (1 - e^{i\chi_i}) d\mathbf{b} \quad (5.33)$$

Inverting this relation gives (\mathbf{q}_\perp = vector component along \mathbf{b})

$$1 - e^{i\chi_i} = \frac{1}{2\pi ik} \int d\mathbf{q}_\perp e^{-i\mathbf{q} \cdot \mathbf{b}} f_i(\mathbf{q}) \quad (5.34)$$

where the integration is in the scattering plane containing the vectors \mathbf{k}_i and \mathbf{k}_f . The evaluation of this integral requires knowledge of $f_i(\mathbf{q})$ for nonphysical

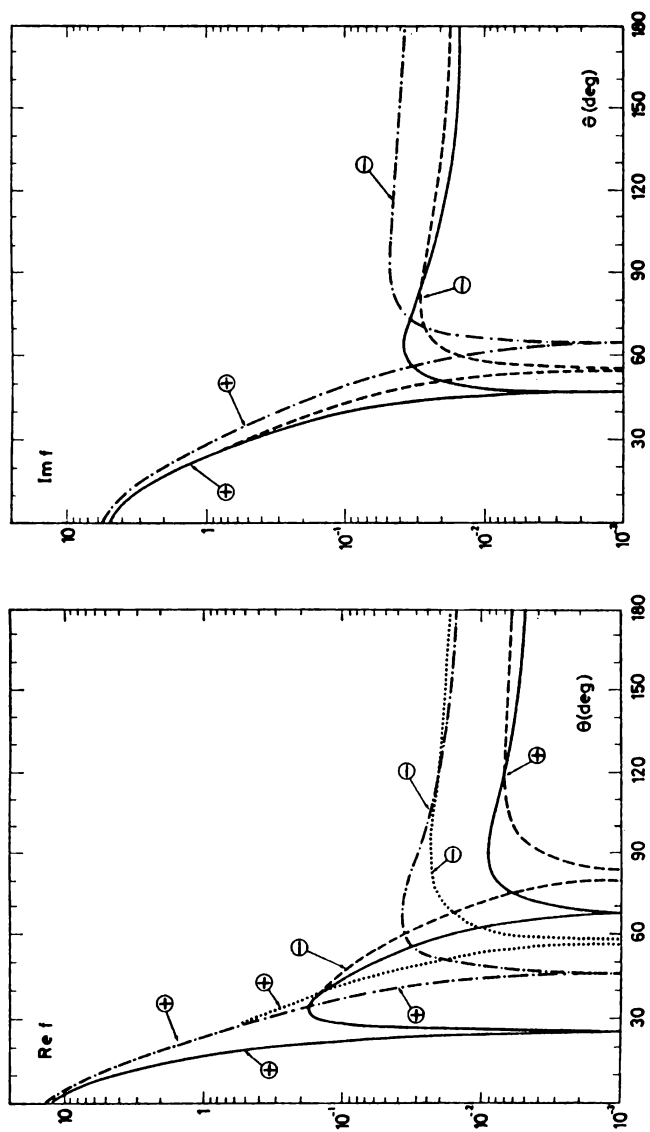


FIG. 5.4. Real and imaginary parts of the scattering amplitude induced by $-V_0(e^{-r} - 1.125 e^{-2r})/r$, where $2m/\hbar^2 V_0 = 20$ and $k = p/\hbar = 5$. The solid line gives the exact result, the dashed curve the eikonal result, the dashed-dotted curve the second Born approximation, and the dotted curve the first Born approximations. [From Joachain (75).]

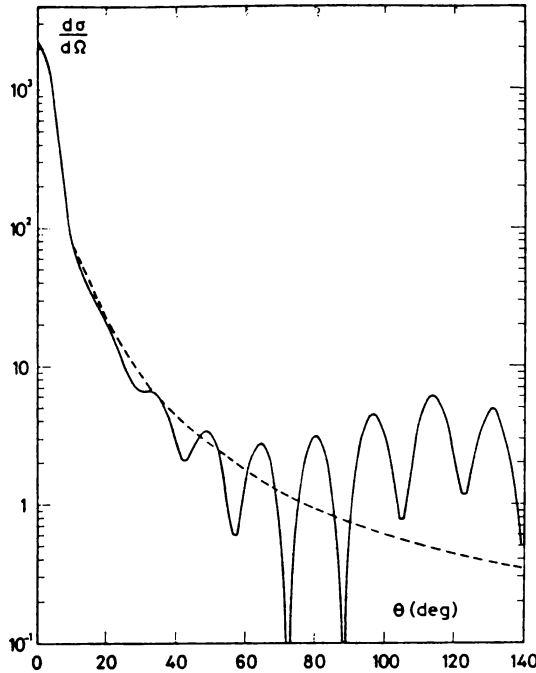


FIG. 5.5. Different cross section for a Yukawa potential, $-V_0 e^{-r}/r$, where $(2m/\hbar^2)V_0 = 250$ and $k = p/\hbar = 5$. The solid curve shows the exact result, the dashed curve the eikonal result. [From Joachain (75).]

complex values $|\cos \theta| > 1$ of the scattering angle θ , since k is fixed. However, if f_i decreases rapidly enough with increasing q , this region is not expected to contribute appreciably to the integral.

In the Glauber approximation, one starts with (5.15), postulates additivity of the phases as given by (5.30), and computes $e^{i\chi_i}$ from (5.34), avoiding any explicit mention of the scattering potential. Because of the additivity assumption, (5.30), the Glauber approximation assumes that the projectile is on the energy shell between collisions. It cannot, for example, include fully the effects of the collision of the projectile with two target nucleons (or more), since that will generally add terms in χ that depend in a nonadditive fashion on the coordinates of both target nucleons. One can immediately see the presence of such a term by expanding the square root in (5.29) to second order. Then [Feshbach (69)]

$$\chi(k, \mathbf{b}) = \sum \chi_i + \sum_{i>j} w_{ij}(\mathbf{b} - \mathbf{b}_i, \mathbf{b} - \mathbf{b}_j, z_i - z_j) \quad (5.35)$$

where

$$w_{ij} = -\frac{1}{2k^3} \int_{-\infty}^{\infty} U(\mathbf{r} - \mathbf{r}_i) U(\mathbf{r} - \mathbf{r}_j) dz$$

As a consequence, the Glauber approximation in the form given so far cannot be used to evaluate the importance of correlations. The KMT formalism does take these two-body terms into account. They appear in the second-order term (4.41), which depends on the correlation function $C(\mathbf{r}_1, \mathbf{r}_2)$.

We return to (5.32). Because of (5.34) connecting χ_i and f_i it is convenient to introduce the *profile function*

$$\Gamma_i \equiv 1 - e^{i\chi_i} \quad (5.36)$$

so that (5.32) is written

$$\hat{f}_{\text{el}} = \frac{ik}{2\pi} \int d\mathbf{b} e^{i\mathbf{q} \cdot \mathbf{b}} \left[1 - \prod_i (1 - \Gamma_i) \right] \quad (5.37)$$

The scattering amplitude is obtained by taking the matrix element of \hat{f}_{el} with respect to the ground state:

$$f_{\text{el}} = \langle 0 | \hat{f}_{\text{el}} | 0 \rangle = \frac{ik}{2\pi} \int d\mathbf{b} e^{i\mathbf{q} \cdot \mathbf{b}} \left\langle 0 \left| 1 - \prod_i (1 - \Gamma_i) \right| 0 \right\rangle \quad (5.38)$$

Note that the product, $\prod_i (1 - \Gamma_i)$, contains A factors, indicating that the target nucleons scatter the projectile nucleons only once. Expanding that product yields

$$1 - \prod_i (1 - \Gamma_i) = \sum_i \Gamma_i - \sum_{i \neq j} \Gamma_i \Gamma_j + \sum_{i \neq j \neq k} \Gamma_i \Gamma_j \Gamma_k + \cdots \quad (5.39)$$

The first term yields the single scattering, the second the double scattering, and so on, ending with the A particle scattering ($\Gamma_i \Gamma_j \Gamma_k \Gamma_l \cdots \Gamma_A$) ($i \neq j \neq k \cdots$). According to (5.38), one must now take the expectation value of (5.39) with respect to the ground states:

$$\langle 0 | 1 - \prod_i (1 - \Gamma_i) | 0 \rangle = \langle 0 | \sum_i \Gamma_i | 0 \rangle - \sum_{i \neq j} \langle 0 | \Gamma_i \Gamma_j | 0 \rangle + \cdots \quad (5.40)$$

When correlations, including those which are dynamic and those which are a consequence of the Pauli exclusion principle, are neglected, that is, using the independent-particle description for the target, (5.40) becomes

$$\begin{aligned} \langle 0 | 1 - \prod_i (1 - \Gamma_i) | 0 \rangle &= 1 - \prod_i \langle 0 | 1 - \Gamma_i | 0 \rangle = 1 - \prod_i \int \rho(\mathbf{r}_i) [1 - \Gamma(\mathbf{b} - \mathbf{b}_i)] d\mathbf{r}_i \\ &= 1 - \left[\int \rho(\mathbf{r}_i) (1 - \Gamma(\mathbf{b} - \mathbf{b}_i)) d\mathbf{r}_i \right]^A \\ &= 1 - \left[1 - \int \rho(\mathbf{r}_i) \Gamma(\mathbf{b} - \mathbf{b}_i) d\mathbf{r}_i \right]^A \end{aligned}$$

Introducing the relation between the profile function Γ and the nucleon-projectile scattering amplitude f yields

$$f_{el} = \frac{ik}{2\pi} \int d\mathbf{b} e^{i\mathbf{q} \cdot \mathbf{b}} \left\{ 1 - \left[1 - \frac{1}{2\pi ik} \int \tilde{\rho}(\mathbf{q}', 0) e^{-i\mathbf{q}' \cdot \mathbf{b}} f(\mathbf{q}') d\mathbf{q}' \right]^A \right\} \quad (5.41)$$

where $\tilde{\rho}(\mathbf{q}, 0)$ is the Fourier transform of the density with the momentum transfer along the longitudinal direction, $(\mathbf{k}_i + \mathbf{k}_f)/2$, put equal to zero.

If the binomial in (5.41) is expanded, the first surviving term in (5.41) is proportional to A , the second to $A(A-1)/2$, and so on; the term proportional to A is the contribution to the amplitude from single scattering, and the term proportional to $A(A-1)/2$ is the contribution of the scattering from two target nucleons. When the projectile-nucleon amplitude is sharply peaked in the forward direction in the laboratory system, as is the case for high-energy projectiles, one can readily see that the double scattering term has a wider angular dispersion than the single scattering term. Thus in this picture the first diffraction peak comes from the double scattering term, while the first diffraction minimum is a consequence of destructive interference between the single and double scattering terms. Equation (5.41) is a remarkably simple result that can readily be evaluated to obtain the elastic scattering amplitude. Its validity is restricted to forward scattering, which is most probable for high-energy projectiles. In view of the additivity assumption [Eq. (5.30)] it neglects correlations arising from the Pauli principle as well as those coming from the nature of the interaction. Equation (5.41) assumes that a nucleon in the target nucleus scatters the projectile only once. For these reasons it is most appropriate for a low-density target system.

When A is large, [brackets]⁴ in (5.41) can be approximated as follows:

$$\left[1 - \frac{1}{2\pi ik} \int \tilde{\rho}(\mathbf{q}, 0) e^{-i\mathbf{q} \cdot \mathbf{b}} f(\mathbf{q}) d\mathbf{q} \right]^A \rightarrow e^{i\chi_A(\mathbf{b})} \quad (5.42)$$

where

$$\chi_A = \frac{A}{2\pi k} \int \tilde{\rho}(\mathbf{q}, 0) e^{-i\mathbf{q} \cdot \mathbf{b}} f(\mathbf{q}) d\mathbf{q} \quad (5.43)$$

For large nuclei $\tilde{\rho}(\mathbf{q}, 0)$ is sharply peaked around $\tilde{\mathbf{q}} = 0$, so that

$$\begin{aligned} \chi_A &\simeq \frac{Af(0)}{2\pi k} \int \tilde{\rho}(\mathbf{q}, 0) e^{-i\mathbf{q} \cdot \mathbf{b}} d\mathbf{q} \\ &= \frac{2\pi Af(0)}{k} \int dz \rho(\mathbf{r}) \end{aligned} \quad (5.44)$$

where z is in the direction perpendicular to \mathbf{b} , that is, in the direction of $\frac{1}{2}(\mathbf{k}_i + \mathbf{k}_f)$.

The function $T(\mathbf{b})$

$$T(\mathbf{b}) = \int dz \rho(\mathbf{r}) \quad (5.45)$$

is referred to as the *thickness function*, since it gives the thickness of the target nucleus as a function of the impact parameter \mathbf{b} .

With approximation equation (5.42), (5.41) can be written

$$f_{\text{el}} = \frac{ik}{2\pi} \int d\mathbf{b} e^{i\mathbf{q} \cdot \mathbf{b}} (1 - e^{i\chi_A}) \quad (5.46)$$

which has the form to be expected from an optical potential model, (5.14). One may then calculate the total absorption cross section, σ_a , according to (5.21):

$$\sigma_a = \int d\mathbf{b} (1 - e^{-2\text{Im}\chi_A})$$

But $\text{Im}\chi_A$, in the large-nucleus approximation, is, from (5.44),

$$2\text{Im}\chi_A = \frac{4\pi A T(\mathbf{b})}{k} \text{Im}f(0) = A\sigma T(\mathbf{b}) \quad (5.47)$$

where we have used $4\pi/k \text{Im}f(0) = \sigma$, the cross section for the projectile-nucleon cross section. Therefore,

$$\sigma_a = \int d\mathbf{b} (1 - e^{-A\sigma T(\mathbf{b})}) \quad (5.48)$$

the classical result.

Once χ_A is known, (5.43), one can ask for the equivalent optical model potential, that is, the potential that will give rise to the known χ_A through the relation (5.31):

$$\chi_A(\mathbf{b}) = -\frac{1}{2k} \int_{-\infty}^{\infty} U_{\text{opt}}(\mathbf{r}) dz = -\frac{1}{\hbar v} \int_{-\infty}^{\infty} V_{\text{opt}}(\mathbf{r}) dz \quad (5.49)$$

Using the approximate expression for χ_A , (5.44), one obtains

$$U_{\text{opt}} = -4\pi A f(0) \rho(\mathbf{r}) \quad (5.50)$$

This should be compared with the result obtained using the KMT method of Section 4, which yields, according to (4.40) and using the large-nucleus

approximation,

$$U_{\text{opt}} = -4\pi(A-1)f(0)\rho(\mathbf{r})$$

Problem. One can consider (5.49) as an integral equation for U_{opt} . With the assumption $U_{\text{opt}} = U_{\text{opt}}(\mathbf{r})$, this equation may be solved. Toward this end, use r as the integration variable in (5.49), so that it becomes

$$\chi_A(b) = -\frac{1}{k} \int_b^\infty \frac{U(r)r \, dr}{\sqrt{r^2 - b^2}}$$

This is the Abel integral equation. Show that the solution is

$$U(r) = \frac{2k}{\pi} \int_r^\infty \frac{db}{\sqrt{b^2 - r^2}} \frac{d\chi_A}{db} \quad (5.51)$$

Note the result

$$\int_R^r \frac{b \, db}{\sqrt{(r^2 - b^2)(b^2 - R^2)}} = \frac{\pi}{2}$$

Discuss (5.51) using a reasonable description of χ_A .

In this section and the preceding one, we have developed two different formalisms, the KMT and the Glauber approximations, for the multiple scattering of high-energy projectiles by a target nucleus. A comparison between the two procedures is possible for the formulas for the KMT $V_{\text{opt}}^{(1)}$, (4.40), and the Glauber f_{el} , (5.41). Diagrammatically, both of these correspond to a component of the multiple scattering in which the target nucleus and the projectile are never excited, as illustrated in Fig. 5.6 for the scattering amplitude where the vertical lines indicate the presence of an interaction. The second KMT term, $V_{\text{opt}}^{(2)}$, (4.41), correspond to the contribution in which the target nucleus is excited and then deexcited, as shown in Fig. 5.7. The Schrödinger equation involving $V_{\text{opt}}^{(1)} + V_{\text{opt}}^{(2)}$ iterates the two elementary diagrams, the one shown in Fig. 5.7 and the diagram in Fig. 5.8, which is the basis for Fig. 5.6.

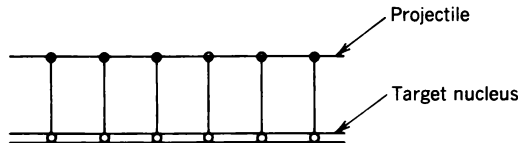


FIG. 5.6

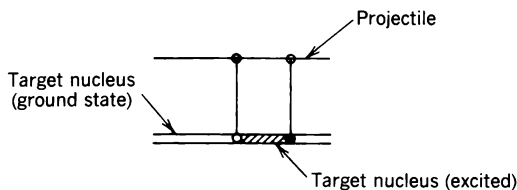


FIG. 5.7

Unfortunately, for the hope of using strongly interacting hadronic probes to study correlations, studies of the high-energy proton reactions have failed so far to reveal any easily identifiable and substantial effects (see Chapter IX) of the correlation terms in elastic scattering, so that the KMT equation (4.40) and the Glauber equation (5.41) do suffice for most purposes. For this contribution we can think of (5.41) as providing a solution to the Schrödinger equation for the optical potential. It is a convenient solution particularly for small systems, certainly more readily evaluated than a phase-shift analysis when the energy is large (unless of course the WKB method is used). It is, however, approximate and is not accurate at the larger angles or at the diffraction minima.

The effect of correlations can be introduced into the Glauber approximation by adding two-body terms to the expression for the phase-shift function χ as in (5.35). Some of the consequences of that *ansatz* have been developed [Feshbach (69)]. One of these is qualitatively important. In obtaining (5.41), correlations were neglected. In particular, $\langle 0 | \sum_{i \neq j} \Gamma_i \Gamma_j | 0 \rangle$ was placed equal to $\sum_{i \neq j} \langle 0 | \Gamma_i | 0 \rangle \langle 0 | \Gamma_j | 0 \rangle$. The difference, $\sum_{i \neq j} [\langle 0 | \Gamma_i \Gamma_j | 0 \rangle - \langle 0 | \Gamma_i | 0 \rangle \langle 0 | \Gamma_j | 0 \rangle]$, involves correlations. However, when two-body terms are included in χ , one obtains, instead, $\langle 0 | \Gamma_i \Gamma_j + i w_{ij} | 0 \rangle$, so that in discussing correlation effects one must take into account both the on-the-energy-shell effects given by $\Gamma_i \Gamma_j$ and the effect of dynamical correlations as described by w_{ij} . If one takes for w_{ij} the form given in (5.35) obtained by expanding the square root $(k^2 - U)^{1/2}$, one finds that the w_{ij} term gives the effect of the overlap of the potentials acting between the incident projectile and two of the target nucleons. In this model the effect of overlap does tend to zero with increasing energy, so that at sufficiently large energies the w_{ij} term should be relatively unimportant. The important point to be borne in mind is that it is not possible to distinguish between the correlation effects present in the ground-state wave functions and the effect of overlapping potentials. The two mechanisms give rise to indistinguishable matrix elements (except for their energy dependence).

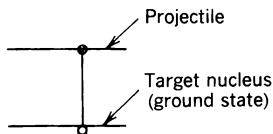


FIG. 5.8

6. CENTER-OF-MASS AND PAULI-PRINCIPLE CORRELATIONS, FERMI MOTION

A. Center-of-Mass Correlations

The effect of center-of-mass correlations is particularly important for light nuclei. It is a consequence of the conservation of momentum, which requires that the momentum of the center of mass be unchanged by the interaction between the projectile and the nucleus. This requirement is formally satisfied by target nuclear wave functions that depend only on intrinsic coordinates, that is, on

$$\mathbf{r}'_i = \mathbf{r}_i - \mathbf{R} \quad (6.1)$$

where \mathbf{r}_i is the coordinate of i th target-nucleus nucleon and \mathbf{R} is the target-nucleus center of mass. Similarly, the wave function for the projectile–nucleus system depends only on the coordinate of the projectile relative to the center of mass of the nucleus. However, it is very often the case that the model wave functions $\Psi^{(M)}$ available for the calculation of $\rho(\mathbf{r})$ and $C(\mathbf{r}, \mathbf{r}')$ (e.g., the interacting shell model wave functions) have not had their center-of-mass motion removed; that is, they are written as functions of the $3A$ coordinates \mathbf{r}_i rather than of the $3(A-1)$ coordinates \mathbf{r}'_i of (6.1). To the extent that the model wave functions are good, so that an approximate decoupling of the center-of-mass motion and the internal motion occurs, one can relate the model density and correlation functions with the exact ρ and C .

We begin with ρ and recall that

$$\tilde{\rho}^{(M)}(\mathbf{q}) = \langle \Psi_0^{(M)} | e^{i\mathbf{q} \cdot \mathbf{r}_1} \Psi_0^{(M)} \rangle \quad (6.2)$$

where the superscript (M) indicates model quantities. Introducing (6.1), one finds that

$$\tilde{\rho}^{(M)}(\mathbf{q}) = \langle \Psi_0^{(M)} | e^{i\mathbf{q} \cdot \mathbf{r}'_1} e^{i\mathbf{q} \cdot \mathbf{R}} | \psi_0^{(M)} \rangle$$

If $\Psi_0^{(M)}$ were exact, it would be a product wave function:

$$\Psi_0^{(M)} = \psi_0(\mathbf{r}'_1, \mathbf{r}'_2, \dots) \varphi_{\text{cm}}(\mathbf{R}) \quad (6.3)$$

Then $\tilde{\rho}^{(M)}(\mathbf{q})$ would factor as

$$\tilde{\rho}^{(M)}(\mathbf{q}) = \tilde{\rho}(\mathbf{q}) \tilde{\rho}_{\text{cm}}(\mathbf{q})$$

where

$$\tilde{\rho}(\mathbf{q}) = \langle \psi_0(\mathbf{r}'_1 \dots) | e^{i\mathbf{q} \cdot \mathbf{r}'_1} \psi_0(\mathbf{r}'_1 \dots) \rangle$$

and

$$\tilde{\rho}_{\text{cm}}(\mathbf{q}) = \langle \varphi_{\text{cm}} | e^{i\mathbf{q} \cdot \mathbf{R}} \varphi_{\text{cm}} \rangle \simeq \langle \Psi_0^{(M)} | e^{i\mathbf{q} \cdot \mathbf{R}} \Psi_0^{(M)} \rangle. \quad (6.4)$$

Therefore, the desired $\tilde{\rho}(\mathbf{q})$ is

$$\tilde{\rho}(\mathbf{q}) = \frac{\tilde{\rho}^{(M)}(\mathbf{q})}{\tilde{\rho}_{\text{cm}}(\mathbf{q})} \quad (6.5)$$

In case the wave functions used for $\Psi_0^{(M)}$ are constructed from single-particle harmonic oscillator wave functions, (6.3) and (6.5) are exact. [For details, see Feshbach, Gal, and Hufner (71).]

For the correlation function $\tilde{C}(\mathbf{q}, \mathbf{q}')$ we have

$$\begin{aligned} \tilde{C}^{(M)}(\mathbf{q}, \mathbf{q}') &= \frac{1}{A(A-1)} \sum_{i \neq j} \langle \Psi_0^{(M)} | e^{i\mathbf{q} \cdot \mathbf{r}_i} e^{i\mathbf{q}' \cdot \mathbf{r}_j} | \Psi_0^{(M)} \rangle \\ &= \langle \Psi_0^{(M)} | e^{i\mathbf{q} \cdot \mathbf{r}_1 + i\mathbf{q}' \cdot \mathbf{r}_2} | \Psi_0^{(M)} \rangle - \tilde{\rho}^{(M)}(\mathbf{q}) \tilde{\rho}^{(M)}(\mathbf{q}') \end{aligned} \quad (6.6)$$

Introducing the factorization, (6.3), one finds that

$$\tilde{C}^{(M)}(\mathbf{q}, \mathbf{q}') = \tilde{C}(\mathbf{q}, \mathbf{q}') \tilde{\rho}_{\text{cm}}(\mathbf{q} + \mathbf{q}') + \tilde{\rho}(\mathbf{q}) \tilde{\rho}(\mathbf{q}') [\tilde{\rho}_{\text{cm}}(\mathbf{q} + \mathbf{q}') - \tilde{\rho}_{\text{cm}}(\mathbf{q}) \tilde{\rho}_{\text{cm}}(\mathbf{q}')] \quad (6.7)$$

From this equation \tilde{C} is readily obtained, using (6.5), in terms of model quantities.

In light nuclei, the center-of-mass effect can be substantial, as illustrated by Fig. 6.1. The importance of center-of-mass correlations for elastic scattering decreasing rapidly with increasing A and is not visible for nucleon- ^{16}O scattering [Feshbach, Gal, and Hufner (71)].

B. Pauli Correlations

The Pauli exclusion principle requires that the wave function for the target nucleus be antisymmetric. As a consequence, even in the absence of a residual interaction, correlations are implied. As a first example we use a Slater determinant for a p -shell nucleus. The $1s$ and $1p$ orbitals are taken to be the harmonic oscillatory wave functions

$$\varphi_{1s}(\mathbf{r}) \sim e^{-(v/2)r^2} \quad \varphi_{1p}(\mathbf{r}) \sim r Y_{1m}(\vartheta, \varphi) e^{-(v/2)r^2}$$

One then finds that [Feshbach, Gal, and Hufner (71); Lambert and Feshbach (73)]

$$\tilde{\rho}^{(M)}(\mathbf{q}) = \left(1 - \frac{A-4}{6Av} q^2 \right) e^{-q^2/4v}$$

and

$$\tilde{C}^{(M)}(\mathbf{q}, \mathbf{q}') = \left[a_0 \frac{\mathbf{q} \cdot \mathbf{q}'}{v} + a_1 \left(\frac{qq'}{v} \right)^2 - a_2 \left(\frac{\mathbf{q} \cdot \mathbf{q}'}{v} \right)^2 \right] e^{-(q^2 + q'^2)/4v}$$

when the values of the coefficients a_n are as given in Table 6.1.

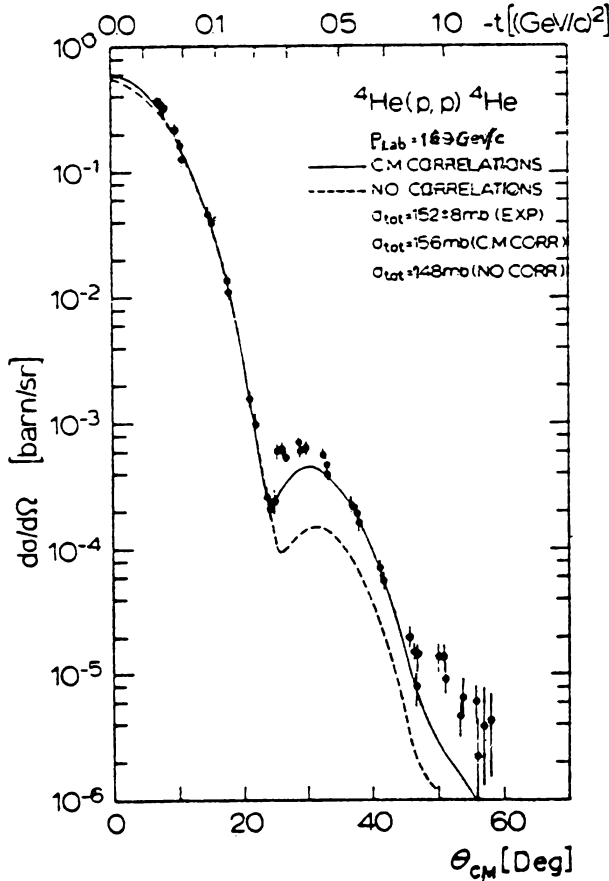


FIG. 6.1. Effect of CM correlations in p - ${}^4\text{He}$ elastic scattering. The solid line includes this effect, the dashed does not. Disregard experimental points, which have been changed substantially in later experiments. [From Feshbach, Gal, and Hufner (71).]

As indicated, the Pauli correlations for ${}^4\text{He}$ vanishes for this model wave function, as the exclusion principle has no effect. In view of the small value of the coefficients, one can expect that the Pauli correlations will have little effect on the elastic scattering. This expectation is borne but by calculations for the smaller scattering angles. However, some effects do appear beyond the first secondary maximum.

Another model appropriate for heavy target nuclei, is the Fermi-gas model. The two-body correlation for that case has been derived in Chapter II [Eq. (II.5.14)] of deShalit and Feshbach (74). This leads to the following result, after averaging over spin and isospin:

$$C(\mathbf{r}_1, \mathbf{r}_2) = -\rho(\mathbf{r}_1)\rho(\mathbf{r}_2) \frac{A}{4(A-1)} \left[\frac{3j_1(k_F|\mathbf{r}_1 - \mathbf{r}_2|)}{k_F|\mathbf{r}_1 - \mathbf{r}_2|} \right]^2 \quad (6.8)$$

TABLE 6.1

	${}^4\text{He}$	${}^{12}\text{C}$	${}^{16}\text{O}$
a_0	0	$\frac{2}{99}$	$\frac{1}{60}$
a_1	0	$\frac{1}{3564}$	$\frac{1}{120}$
a_2	0	$\frac{1}{960}$	$\frac{1}{240}$

where j_1 is the spherical Bessel function of first order. As commented on in Chapter II of deShalit and Feshbach (74), the net correlation is repulsive (Pauli repulsion); that is, it has the effect of increasing the average distance between target nucleons beyond what would be calculated from a simple product wave function. Approximating the term in brackets in (6.8) by the form (B.13) (see Appendix B at the end of this chapter) yields an effective[†] r_c of $5k_F/\sqrt{6}$, from which a length defined by (B.14) can be obtained, noting that $\beta \ll r_c$. Finally, the second-order potential can be obtained from (B.12). The effect is not small, so that Pauli correlations are of importance for the heavier nuclei. Calculations show that effects of this order of magnitude are visible at the larger angles.

C. Fermi Motion

The nucleons in the nucleus are moving. So far the discussion has assumed them to be stationary because during the passage of the projectile through the nucleus with a velocity close to c , the velocity of light, the nucleons in the target nucleus hardly move. The motion of the nucleus can be taken into account in the first-order potential $V_{\text{opt}}^{(1)}$, (4.32) or (4.37). For this purpose one needs the density matrix $K(\mathbf{r}, \mathbf{r}')$ as well as the projectile-target nucleon transition t matrix. The first is model dependent. The second involves the t matrix off the energy shell, therefore requiring a complete description of the projectile-nucleon interaction for its determination. The density matrix $K(\mathbf{r}, \mathbf{r}')$ in the independent-particle approximation is given by

$$K(\mathbf{r}, \mathbf{r}') = \sum_{\lambda=1}^A \psi_{\lambda}(\mathbf{r}) \psi_{\lambda}^*(\mathbf{r}') \quad (6.9)$$

where ψ_{λ} are the single-particle orbitals. In the Fermi-gas model

$$K(\mathbf{r}, \mathbf{r}') = \rho_0 \frac{3j_1(h_F |\mathbf{r} - \mathbf{r}'|)}{k_F |\mathbf{r} - \mathbf{r}'|} \quad (\text{Fermi-gas model}) \quad (6.10)$$

where ρ_0 is the density (A/Ω). The major effect of the Fermi motion is to introduce a nonlocality with a range of the order of $1/k_F$ into the first-order

[†]The quantities β and r_c are defined in Appendix B of this chapter.

optical potential. However, as can be seen from (4.37) and the ensuing discussion, the behavior of $K(\mathbf{r}, \mathbf{r}')$, $\mathbf{r} \neq \mathbf{r}'$ will be important only if $t(\mathbf{r}, \mathbf{r}')$, the elementary amplitude, is also nonlocal. If $t(\mathbf{r}, \mathbf{r}')$ is local, that is, proportional to $\delta(\mathbf{r} - \mathbf{r}')$ as in (4.38), only $K(\mathbf{r}, \mathbf{r}) \equiv \rho_0$ survives and there is then no impact of the Fermi motion on the first-order optical potential. We estimate that the influence of the Fermi motion is determined by the parameter $(k_F a)^2/30$, where a is the range of the nonlocality in $t(\mathbf{r}, \mathbf{r}')$. In the case of nucleon–nucleon scattering, $a \sim 0.7$ fm, so that the magnitude of the Fermi-motion term is on the order of several percent. It is clear that Fermi motion becomes more significant in the presence of long-range nonlocal elementary projectile–nucleon amplitudes.

7. SOME KINEMATICS

(a) One rather obvious requirement of importance for high-energy projectiles is the appropriate use of relativity and at the very least of relativistic kinematics. The preferred method up to recently [Goldberger and Watson (64); Kerman, McManus, and Thaler (59)] has been to insert the optical potential of Section II.4 in deShalit and Feshbach (74) into the Klein–Gordon equation. There is an ambiguity even in this simplistic procedure since one must postulate the transformation properties of the optical potential. One obtains different results, as we shall see, according to whether one presumes that the potential is the fourth component of a 4-vector or a scalar. In a recent development, a covariant description of the t matrix is used and the optical model employs the Dirac equation when the projectile is a nucleon. Use of the Dirac optical model is presented in Chapter V. In the following discussion we follow the derivation of Goldberger and Watson (64) and Kerman, McManus, and Thaler (59).

Goldberger and Watson begin with the expression of the energy in the center-of-mass frame assuming that the optical potential V is the fourth component of a four-vector. Let the energy of the system, *excluding the rest mass of the target nucleus but including the rest mass of the projectile* be \mathcal{E} . Then

$$(\mathcal{E} - V) + A mc^2 = \sqrt{m_p^2 c^4 + p^2 c^2} + A mc^2 + \frac{c^2 p^2}{2 A mc^2} \quad (7.1)$$

where the energy of the target nucleus is expressed nonrelativistically. A is the mass number of the target and m_p is the mass of the projectile. Solving this equation for p^2 to first order in V (i.e., taking $\mathcal{E} \gg V$) yields

$$\begin{aligned} c^2 p^2 &= (\mathcal{E}^2 - m_p^2 c^4) \frac{1}{1 + (\mathcal{E} - V)/A mc^2} - 2\mathcal{E} V \frac{1}{1 + (\mathcal{E} - V)/A mc^2} \\ &\simeq (\mathcal{E}^2 - m_p^2 c^4) \frac{1}{1 + \mathcal{E}/A mc^2} - 2\mathcal{E} V \frac{1}{1 + \mathcal{E}/A mc^2} \end{aligned}$$

Replacing \mathbf{p} by $\hbar/i\nabla$ yields the following Schrödinger-type equation:

$$\left[\nabla^2 + \frac{1}{\hbar^2 c^2} \left(\frac{\mathcal{E}^2 - m_p^2 c^4}{1 + \mathcal{E}/A m c^2} - 2\mathcal{E}V \frac{1}{1 + \mathcal{E}/A m c^2} \right) \right] \psi = 0 \quad (7.2)$$

The (wave number)², k^2 , which is given in the Schrödinger case by the nonrelativistic $2Am m_p E/\hbar^2(m_p + mA)$ (where $E = \mathcal{E} - m_p c^2$) is replaced by $(\mathcal{E}^2 - m_p^2 c^4)/\hbar^2 c^2(1 + \mathcal{E}/A m c^2)$. In the nonrelativistic limit ($E \ll mc^2$) the last expression reduces to the nonrelativistic value. We note that the effective potential is energy dependent. This is a result of the assumption that V is the fourth component of a 4-vector. If V is a scalar, that energy dependence is not present.

Problem. Suppose that V is a scalar. Show that the only change in (7.2) is the replacement of $\mathcal{E}V$ by $mc^2 V$. Derive the Schrödinger equation when V has two components, V_0 and V_s , where V_0 is the fourth component of a 4-vector and V_s is a scalar.

(b) The transition matrix elements, \tilde{t} , for elastic projectile–nucleon scattering are usually given with respect to the projectile–nucleon center-of-mass frame. Multiple scattering theory requires their value in the projectile–nucleus frame. The transformation between the two frames is governed by the result that

$$\sqrt{E'_1 E'_2} \langle \mathbf{p}'_1, \mathbf{p}'_2 | \hat{\mathcal{T}} | \mathbf{p}_1, \mathbf{p}_2 \rangle \sqrt{E_1 E_2} \quad \text{is an invariant} \quad (7.3)$$

In this expression (\mathbf{p}_1, E_1) , (\mathbf{p}_2, E_2) are the momentum and energy of each particle (projectile, nucleon) before collision, and (\mathbf{p}'_1, E'_1) , (\mathbf{p}'_2, E'_2) are their values after collision. The wave functions in the matrix element of $\hat{\mathcal{T}}$ are assumed to be in the form $\exp(i\mathbf{p} \cdot \mathbf{r})/\hbar$ asymptotically with unit amplitude. However, since the invariant volume in momentum space is $d\mathbf{p}/E$, the invariant normalization is given by

$$\langle \mathbf{p}' | \mathbf{p} \rangle = (2\pi\hbar)^3 \delta(\mathbf{p}' - \mathbf{p})/E$$

This condition leads immediately to the result (7.3).

Let t_{pn} be the value of the matrix element of $\hat{\mathcal{T}}$ in the projectile–nucleon center-of-mass frame, while t_{pN} is its value in the projectile–nucleus frame. From (7.3) these are related by

$$E_1 E_2 t_{pN} = \varepsilon_1 \varepsilon_2 t_{pn} \quad (7.4)$$

where E_1 and E_2 are the energies of the projectile and target nucleon, including their rest masses in the projectile–nucleus frame, and ε_1 and ε_2 are the corresponding energies in the projectile–nucleon frame. Equation (7.4) is

approximate since $E_1 \neq E'_1$, $E_2 \neq E'_2$. The equation is valid for small momentum transfers; the error is on the order of $q^2(p^2 - q^2)/m^2 E^2$. In addition, t_{Pn} is related to the scattering amplitude f in that frame by

$$t_{Pn} = -\frac{4\pi\hbar c^2}{E_0} f_{Pn} \quad (7.5)$$

where[†]

$$E_0 = \frac{1}{2}(\varepsilon_1 + \varepsilon_2) \quad (7.6)$$

Combining (7.5) and (7.4) yields

$$t_{PN} = -4\pi\hbar^2 c^2 \frac{\varepsilon_1 \varepsilon_2}{E_1 E_2} \frac{1}{E_0} f_{Pn} \quad (7.7)$$

We now relate all the energies ε_1 , ε_2 , and so on, to the energy E_L and momentum p_L of the projectile in the laboratory system. We illustrate the process for the case of ε_1 and ε_2 . In Fig. 7.1 the two situations to be compared are shown. We now form an invariant for situation (b):

$$(E_L + m_2 c^2) - c^2 p_L^2 = m_1^2 c^4 + m_2^2 c^4 + 2m_2 c^2 E_L \equiv s \quad (7.8)$$

We now calculate the same invariant using situation (a). It equals

$$(\varepsilon_1 + \varepsilon_2)^2 = 4E_0^2 = (\sqrt{m_1^2 c^4 + c^2 p_{cm}^2} + \sqrt{m_2^2 c^4 + c^2 p_{cm}^2})^2 \quad (7.9)$$

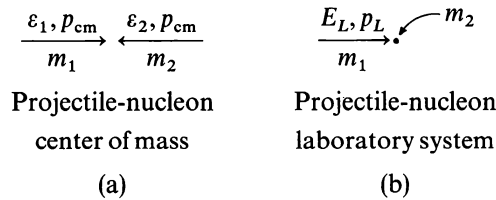


FIG. 7.1

[†]The Kerman et al. t_{KMT} is $(2\pi)^{-3} t_{Pn}$. This factor is a consequence of the differing normalizations. In the KMT case the matrix elements of \hat{t} are taken with respect to plane waves $(1/2\pi)^{3/2} e^{i\mathbf{k}\cdot\mathbf{r}}$, so that (7.5) is replaced by $t_{\text{KMT}} = -(\hbar^2 c^2 / 2\pi^2 E_0) f$. The derivation of (7.5) is similar to that of (7.2). Terms on the order of $(m_p c^2 - m_n c^2)/E_0$ and V/E_0 are neglected. The presence of E_0 in the denominator of f indicates that the assumption has been made that V transforms like the fourth component of a vector.

Equating (7.8) with (7.9) yields an equation for $c^2 p_{cm}^2$. This is readily solved to yield

$$p_{cm}^2 = \frac{m_2^2 c^4 p_L^2}{m_1^2 c^4 + m_2^2 c^4 + 2m_2 c^2 E_L} \sim \frac{m_2^2 c^4 p_L^2}{s}$$

or

$$p_{cm} = \frac{m_2 c^2 p_L}{2E_0} = \frac{m_2 c^2 p_L}{\sqrt{s}} \quad (7.10)$$

It then follows that

$$\begin{aligned} \varepsilon_1 &= \frac{m_2 E_L + m_1 c^2}{2E_0} = \frac{m_2 E_L + m_1 c^2}{\sqrt{s}} \\ \varepsilon_2 &= \frac{m_2 c^2 (E_L + m_2 c^2)}{2E_0} = \frac{m_2 c^2 (E_L + m_2 c^2)}{\sqrt{s}} \end{aligned} \quad (7.11)$$

A little manipulation will show that

$$\varepsilon_1 \varepsilon_2 = E_0^2 \left[1 - \frac{1}{(1 + m_1^2/m_2^2 + 2E_L/m_2 c^2)^2} \left(1 - \frac{m_1^2}{m_2^2} \right)^2 \right] \quad (7.12)$$

For the situations to be considered in this volume it is a good approximation to take

$$\varepsilon_1 \varepsilon_2 \simeq E_0^2 \quad (7.13)$$

equating the arithmetic mean of ε_1 and ε_2 with the geometric mean. Using the exact equation (7.12) in the discussion is not difficult, but to keep the results simple we shall employ (7.13), so that

$$t_{PN} = -4\pi\hbar^2 c^2 \frac{E_0}{E_1 E_2} f \quad (7.14)$$

We are now left with the determination of $E_1 E_2$. E_0 in terms of E_L is obtained from equating $4 E_0^2$ to the right-hand side of (7.8). The kinematic situations involved in determining E_1 and E_2 are illustrated in Fig. 7.2, where \mathcal{E}_2 is the energy of the target nucleus in the projectile–nucleus center-of-mass frame. We take

$$E_2 = \frac{\mathcal{E}_2}{A}$$

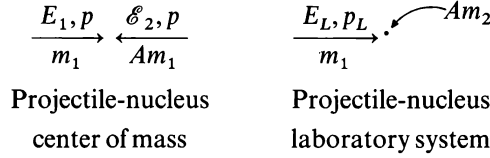


FIG. 7.2

The analysis used to obtain (7.11) can be repeated, with the result

$$E_1 E_2 = \frac{m_2 c^2 (E_L + Am_2 c^2) (Am_2 c^2 E_L + m_1^2 c^4)}{A^2 m_2^2 c^4 + m_1^2 c^4 + 2Am_2 c^2 E_L} \quad (7.15)$$

Inserting this result into (7.14) and using (7.10) yields the final result:

$$t_{PN} = -2\pi\hbar^2 c^2 \frac{k_L}{k_{cm} E_L} \frac{1 + 2E_L/AM_2 c^2 + m_1^2/A^2 m_2^2}{(1 + m_1^2 c^2/Am_2 E_L)(1 + E_L/Am_2 c^2)} f_{Pn} \quad (7.16)$$

We leave it as a problem to show that this reduces correctly in the nonrelativistic limit ($E_L = m_1 c^2$).

(c) *Breit Kinematics.* In employing (7.16) in the optical model Schrödinger equation (7.2), one must use values of f_{Pn} that cannot be obtained from the analysis of the scattering of the projectile by a free nucleon. This point becomes clear when one examines the Lippmann–Schwinger equation, corresponding to (7.2), in momentum space. The Lippmann–Schwinger equation for the transition amplitude \mathcal{T}' is

$$\mathcal{T}' = V_{\text{opt}}^{(1)} + V_{\text{opt}}^{(1)} \frac{1}{E^{(+)} - K} \mathcal{T}'$$

where K is the kinetic energy operator. Taking plane wave matrix elements of \mathcal{T}' in the projectile–nucleus coordinate frame yields

$$\langle \mathbf{k} | \mathcal{T}' | \mathbf{k}' \rangle = \langle \mathbf{k} | V_{\text{opt}}^{(1)} | \mathbf{k}' \rangle + \int \frac{d\mathbf{k}''}{(2\pi)^3} \langle \mathbf{k} | V_{\text{opt}}^{(1)} | \mathbf{k}'' \rangle \frac{1}{E^{(+)} - E(\mathbf{k}'')} \langle \mathbf{k}'' | \mathcal{T}' | \mathbf{k}' \rangle \quad (7.17)$$

For elastic projectile–nucleus scattering, the magnitude of \mathbf{k} and \mathbf{k}' are equal and the corresponding energy $E(k)$ is equal to E . Nonrelativistically, $E = \hbar^2 k^2 / 2\mu$ (μ = reduced mass). We then say that the matrix elements of \mathcal{T}' are on the energy shell. The first term on the right-hand side of (7.17) will also be on the energy shell if $V_{\text{opt}}^{(1)}$, a function of E , is also evaluated at $E = E(k)$. In the first-order theory $V_{\text{opt}}^{(1)}$ depends on the t matrix for projectile–nucleon

scattering in the projectile–nucleus reference frame, t_{pN} . The requirement that $V_{\text{opt}}^{(1)}$ is on the energy shell translates into the requirement that t_{pN} is on the energy shell and therefore can be obtained from the analysis of the experimental projectile–nucleon scattering. This last statement is valid to the extent that the kinematic regions which are allowed for projectile scattering from a free nucleon and from a nucleon embedded in the nucleus overlap. This overlap is generally not complete since the scattering from a nucleon embedded in a nucleus can involve momentum transfers $\mathbf{q} = (\mathbf{k} - \mathbf{k}')$ which are larger than those that can occur when the target nucleon is free.

To illustrate this point, suppose that the projectile is a nucleon. Then in the nucleon–nucleon center-of-mass frame each nucleon has a momentum $\mathbf{k}/2$ initially. The maximum momentum change occurs for 180° scattering, yielding a maximum value of q^2 equal to k^2 . In the laboratory frame (for simplicity we take the nucleus to be infinitely massive so that the projectile–nucleus frame and the laboratory frame are identical), q_{lab}^2 is given by $2k^2(1 - \cos \theta)$, where θ is the scattering angle. It is clear that q_{lab}^2 will exceed k^2 , the maximum q^2 for scattering by a free nucleon, for θ greater than 60° . Thus for angles greater than 60° it is no longer possible to obtain t_{pN} from the experimental t_{pN} .

Turning to the second term on the right-hand side of (7.17), the integral over \mathbf{k}'' involves values of $\langle \mathbf{k} | V_{\text{opt}}^{(1)} | \mathbf{k}'' \rangle$ that are not on the energy shell since \mathbf{k}'' can assume any magnitude. However, $V_{\text{opt}}^{(1)}$ involves the nuclear form factor $\tilde{\rho}(\mathbf{q})$, which decreases rapidly with increasing qR , where R is the nuclear radius parameter. As a consequence, the off-energy-shell contributions of $\langle \mathbf{k} | V_{\text{opt}}^{(1)} | \mathbf{k}'' \rangle$ will be small barring a singular behavior of $\tilde{t}(\mathbf{q})$ when one deviates from on-shell kinematics.

A common method for estimating off-the-energy-shell matrix elements of f_{pN} involves establishing an analytic form for t_{pN} as a function of E and \mathbf{q} [e.g., $a(E)e^{-b(E)q^2}$ often used] from the on-shell experimental data. Then one substitutes in that form, that is, treats E and q as independent variables to obtain the value of f_{pN} off-shell. This procedure presumes a smooth behavior of f_{pN} as a function of these variables.

Another method which we shall now describe resolves the problem of the overlap of the kinematic regions allowed in free nucleon–projectile scattering and that allowed in nucleus–projectile scattering. We return to (4.37):

$$\tilde{V}_{\text{opt}}^{(1)}(\mathbf{k}, \mathbf{k}') = \frac{A-1}{(2\pi)^3} \int d\mathbf{s} \int d\mathbf{s}' \tilde{K}(\mathbf{s}, \mathbf{s}') \tilde{t}\left(\frac{\mathbf{k} + \mathbf{s}}{2}, \frac{\mathbf{k}' + \mathbf{s}'}{2}\right) \delta(\mathbf{s} - \mathbf{k} - \mathbf{s}' + \mathbf{k}') \quad (4.37)$$

where

$$\tilde{K}(\mathbf{s}, \mathbf{s}') = \int d\mathbf{r} \int d\mathbf{r}' K(\mathbf{r}, \mathbf{r}') e^{-i\mathbf{s} \cdot \mathbf{r} + i\mathbf{s}' \cdot \mathbf{r}'}$$

The variables \mathbf{k} and \mathbf{k}' multiplied by \hbar are momenta in the projectile–nucleus

frame of reference. We choose a local density approximation for K :

$$K(\mathbf{r}, \mathbf{r}') = \rho \left(\frac{\mathbf{r} + \mathbf{r}'}{2} \right) e^{i(\mathbf{k}/A) \cdot \mathbf{r} - i(\mathbf{k}'/A) \cdot \mathbf{r}'} \quad (7.18)$$

In the Fermi-gas approximation equation (6.10) this amounts to replacing the $3j_1((x)/x)$ factor by its value at $x = 0$. The exponential factors in (7.18) are appropriate to the nucleon–nucleus reference frame, where \mathbf{k}' is the momentum of the nucleon and $-\mathbf{k}'$ the momentum of the nucleus. Then each nucleon in the nucleus has a momentum $-\mathbf{k}'/A$, neglecting the momentum of these nucleons with respect to the nuclear center of mass. Inserting (7.18) into the equation for $\tilde{K}(\mathbf{s}, \mathbf{s}')$ and integrating yields

$$K(\mathbf{s}, \mathbf{s}') = (2\pi)^3 \delta \left(\frac{\mathbf{Q}}{A} - \frac{\mathbf{s} + \mathbf{s}'}{2} \right) \tilde{\rho} \left(\mathbf{s}' - \mathbf{s} + \frac{\mathbf{q}}{A} \right) \quad (7.19)$$

where we have introduced

$$\mathbf{Q} \equiv \frac{\mathbf{k} + \mathbf{k}'}{2} \quad \text{and} \quad \mathbf{q} = \mathbf{k} - \mathbf{k}'$$

Inserting (7.19) in (4.37) yields a factorized expression for $\tilde{V}_{\text{opt}}^{(1)}(\mathbf{k}, \mathbf{k}')$:

$$\tilde{V}_{\text{opt}}^{(1)}(\mathbf{k}, \mathbf{k}') = (A-1) \tilde{\rho} \left(-\mathbf{q} \left(1 - \frac{1}{A} \right) \right) \tilde{t} \left(\frac{\mathbf{Q}(1 + 1/A) + \mathbf{q}}{2}, \frac{\mathbf{Q}(1 + 1/A) - \mathbf{q}}{2} \right) \quad (7.20)$$

In the Pn frame, \tilde{t} describes the elastic scattering of a nucleon with momentum $\mathbf{Q} - \mathbf{q}/2$ by a target nucleon of momentum $-\mathbf{Q}/A + \mathbf{q}/2$, with the final momenta being given by $\mathbf{Q} + \mathbf{q}/2$ and $-\mathbf{Q}/A - \mathbf{q}/2$, respectively. This is referred to as *Breit kinematics* (see Fig. 7.3). Note that for $k = k'$, $\mathbf{Q} \cdot \mathbf{q}$ equals zero, so that the energies are equal before and after the collision. Moreover, the effective kinetic energy in the laboratory frame when $k = k'$ is given nonrelativistically by

$$T_{\text{lab}}^{(\text{eff})} = \frac{1}{2m} \left[Q^2 \left(1 + \frac{1}{A} \right)^2 + \mathbf{q}^2 \right] \quad (7.21)$$

In words, the two-body scattering occurs with the Breit momenta and with the effective energy given by (7.21) when the scattering is on the energy shell. This effective energy varies with the angle of scattering.

To extrapolate $V_{\text{opt}}^{(1)}$ off the energy shell ($k' \neq k$), \tilde{t} in (7.20) is replaced by $\tilde{t}(\mathbf{q})$ evaluated at the effective laboratory energy given by (7.21), which varies with momentum transfer q . Tables of $\tilde{t}(\mathbf{q})$ are given by McNeil, Ray, and Wallace (83). The resulting potential is nonlocal, taking into account to some extent the nonlocality of the two-body transition matrix. However, as is evident from the

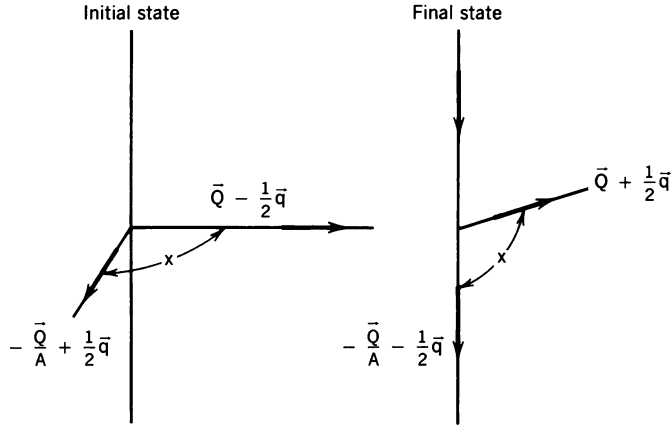


FIG. 7.3. Two vectors representing the momenta of the incident nucleon, $(\vec{Q} - \frac{1}{2}\vec{q})$, and the target nucleon, $(-\frac{1}{A}\vec{Q} + \frac{1}{2}\vec{q})$ maintain the angle between them and their magnitudes after scattering. Scattering results in a rigid rotation of the two vectors.

interpretation of (7.20) for $V_{\text{opt}}^{(1)}$, the momentum of the nucleons in the nucleus is neglected. An evaluation of the consequences of this treatment of off-shell effects has been investigated by Picklesimer, Tandy, Thaler, and Wolfe (84). Significant effects are obtained for nucleon projectile energies below 300 MeV.

Note. The relativistic generalization of (7.21) is

$$T_{\text{lab}}^{(\text{eff})} = \frac{s}{2mc^2} - 2mc^2$$

where

$$s = (E_p + E_n)^2 - \hbar^2 c^2 Q^2 \left(1 - \frac{1}{A}\right)^2$$

$$E_p^2 = \hbar^2 c^2 \left(Q^2 + \frac{q^2}{4} + \frac{m^2 c^2}{\hbar^2} \right) \quad E_n^2 = \hbar^2 c^2 \left[\left(\frac{Q}{A} \right)^2 + \frac{q^2}{4} + \frac{m^2 c^2}{\hbar^2} \right]$$

8. AN EXAMPLE: PROTON-NUCLEUS SCATTERING

We conclude this chapter with a brief description of the application of multiple scattering theory to the scattering of high-energy protons by spin-zero nuclei. The objective will be to provide a qualitative understanding rather than a definitive comparison of experiment with theory. For thorough discussions the reader should consult the papers by Chaumeaux, Layly, and Schaeffer (78) and Ray (79) (see also Chapter IX).

The starting point is the nucleon-nucleon amplitude for the scattering of the incident proton by the i th nucleon of the target nucleus, f . In the nucleon-nucleon center-of-mass frame f_{i0} has the Wolfenstein form:

$$\begin{aligned} f_{i0}(\mathbf{k}_{\text{cm}}, \mathbf{k}'_{\text{cm}}) = & A'_i + B'_i \boldsymbol{\sigma}_0 \cdot \boldsymbol{\sigma}_i + C'_i (\boldsymbol{\sigma}_0 + \boldsymbol{\sigma}_i) \cdot (\mathbf{q}_{\text{cm}} \times \mathbf{Q}_{\text{cm}}) \\ & + D'_i (\boldsymbol{\sigma}_0 \cdot \hat{\mathbf{Q}}_{\text{cm}}) (\boldsymbol{\sigma}_i \cdot \hat{\mathbf{Q}}_{\text{cm}}) + E'_i (\boldsymbol{\sigma}_0 \cdot \mathbf{q}_{\text{cm}}) (\boldsymbol{\sigma}_i \cdot \mathbf{q}_{\text{cm}}) \end{aligned} \quad (8.1)$$

The variable \mathbf{k}'_{cm} is the incident momentum of the proton in the two-nucleon center-of-mass frame, and \mathbf{k}_{cm} is the final momentum. In addition,

$$\mathbf{q}_{\text{cm}} = \mathbf{k}_{\text{cm}} - \mathbf{k}'_{\text{cm}} \quad \mathbf{Q}_{\text{cm}} = \frac{1}{2}(\mathbf{k}_{\text{cm}} + \mathbf{k}'_{\text{cm}}) \quad (8.2)$$

The vector $\hat{\mathbf{Q}}_{\text{cm}}$ is a unit vector in the direction of \mathbf{Q}_{cm} . The coefficients A'_i , and so on, in (8.1) are scalar functions of \mathbf{k}_{cm} and \mathbf{k}'_{cm} , that is, functions of $k_{\text{cm}}^2 = k_{\text{cm}}'^2$ and $\mathbf{k}_{\text{cm}} \cdot \mathbf{k}'_{\text{cm}}$. They depend on isospin as follows:

$$A' = A'_+ + \tau_0 \cdot \tau_i A'_-$$

so that

$$A'_{pn} = \langle pn | A' | pn \rangle = A'_+ - A'_- \quad A'_{pp} = A'_+ + A'_- \quad (8.3)$$

The reader should verify that (8.1) is the most general form, depending at most bilinearly on \mathbf{q}_{cm} and \mathbf{Q}_{cm} , which is rotationally, time-reversal, and space-reflection invariant. (Note that under time reversal $\mathbf{k} \rightarrow -\mathbf{k}'$.)

To use (7.16) to obtain the value of t in the nucleon-target nucleus frame, we must transform \mathbf{k}_{cm} and \mathbf{k}'_{cm} to the projectile-nucleus frame:

$$\begin{aligned} \mathbf{q} = \mathbf{k} - \mathbf{k}' = \mathbf{q}_{\text{cm}} \quad \mathbf{Q} = \frac{1}{2}(\mathbf{k} + \mathbf{k}') &\simeq \frac{k}{k_{\text{cm}}} \mathbf{Q}_{\text{cm}} \\ (\mathbf{q}_{\text{cm}} \times \hat{\mathbf{Q}}_{\text{cm}}) &= \frac{1}{k} (\mathbf{q} \times \mathbf{Q}) \end{aligned}$$

The second of these equations is valid at small angles ($\mathbf{k}' \sim \mathbf{k}$) only. Finally, using (7.16), one finds that

$$\begin{aligned} [\tilde{t}_{pN}(\mathbf{k}, \mathbf{k}')]_{i0} = & A_i + B_i \boldsymbol{\sigma}_0 \cdot \boldsymbol{\sigma}_i + C_i (\boldsymbol{\sigma}_0 + \boldsymbol{\sigma}_i) \cdot (\mathbf{q} \times \mathbf{Q}) \\ & + D_i (\boldsymbol{\sigma}_0 \cdot \mathbf{Q}) (\boldsymbol{\sigma}_i \cdot \mathbf{Q}) + E_i (\boldsymbol{\sigma}_0 \cdot \mathbf{q}) (\boldsymbol{\sigma}_i \cdot \mathbf{q}) \end{aligned} \quad (8.4)$$

where

$$\begin{aligned} A_i = \eta(E_L) \frac{k_L}{k_{\text{cm}}} A'_i \quad B_i = \eta(E_L) \frac{k_L}{k_{\text{cm}}} B'_i \quad C_i = \eta(E_L) \frac{k_L}{k k_{\text{cm}}} C'_i \\ D_i = \eta(E_L) \frac{k_L}{k_{\text{cm}} k^2} D'_i \quad E_i = \eta(E_L) \frac{k_L}{k_{\text{cm}}} E'_i \end{aligned} \quad (8.5)$$

where $\eta(E_L)$ is obtained from (7.16):

$$\eta(E_L) = -\frac{2\pi\hbar c^2}{E_L} \frac{1 + [2A/(A^2 + 1)](E_L/mc^2)}{1 + [A/(A^2 + 1)](E_L/mc^2 + mc^2/E_L)} \quad (8.6)$$

The experimental values of the coefficients in (8.1) are fitted using a Gaussian form: for example,

$$A'_{pp} = A_{pp}(0)e^{-\alpha_{pp}q^2}$$

where $A'_{pp}(0)$ and α_{pp} are complex functions of the energy.

An example of such a fit [Wallace and Alexander (80)] of the nucleon–nucleon amplitudes is given in Table 8.1 for the incident proton momentum in the laboratory frame of 1.7 GeV/c (kinetic energy 1 GeV). At that time, 1980, the only well-known proton–neutron amplitude is A'_{pn} . In the p – p case the B'_{pp} , D'_{pp} , and E'_{pp} amplitudes are poorly known. Because of these uncertainties, it has been the practice in applications to multiple scattering to neglect the B' , D' , and E' terms in (8.1) and to fit the nucleon–nucleon data with the A' and C' coefficients only. Note that the C'_{pn} term is *not* determined from nucleon–nucleon scattering but by elastic proton scattering from ^4He .

Focusing on the contributions of the A' term, one should bear in mind that $\rho(\mathbf{q})$ varies much more rapidly than $\tilde{t}(q)$, so that over a considerable range the optical potential is given by $\tilde{t}(0)\rho(\mathbf{q})$. To illustrate, take $\rho(\mathbf{q})$ to be a Gaussian

$$\tilde{\rho}(\mathbf{q}) = e^{-R^2q^2/6}$$

where R is the root-mean-square radius of the nucleus, which we shall take as roughly equal to the nuclear radius. Then the quantity to be compared with α_{pp} or α_{pn} is $R^2/6\hbar^2c^2 \sim 6A^{2/3}(\text{GeV}/\hbar c)^{-2}$. The latter is far greater than α_{pp} or α_{pn} for even light nuclei [see discussion in deShalit and Feshbach (74, 109)]. A second feature originates in the large imaginary component of A' terms. This has the consequence that the central part, V_c , of the optical potential is highly

TABLE 8.1

$A'_{pp}(0) = (-1.126 + 6.767i)(\text{GeV}/\hbar c)^{-1}$	$\alpha_{pp} = (5.08 + 0.63i)$
$A'_{pn}(0) = (-1.695 + 5.628i)(\text{GeV}/\hbar c)^{-1}$	$\alpha_{pn} = (2.93 + 0.0i)$
$B'_{pp}(0) = (-1.431 - 0.320i)(\text{GeV}/\hbar c)^{-1}$	$\beta_{pp} = (5.84 + 7.44i)$
$C'_{pp}(0) = (4.349 + 7.559i)(\text{GeV}/c)^{-2}$	$\gamma_{pp} = (3.91 + 0.596i) \times (\text{GeV}/\hbar c)^{-2}$
$C'_{pn}(0) = (-2.355 - 1.654i)(\text{GeV}/c)^{-2}$	$\gamma_{pn} = (4.00 - 2.80i)$
$D'_{pp}(0) = (.070 + 1.140i)(\text{GeV}/c)^{-1}$	$\delta_{pp} = (4.94 - 7.41i)$
$E'_{pp}(0) = (1.61.191 - 1.390i)(\text{GeV}/c)^{-3}$	$\varepsilon_{pp} = (15.6 + 1.12i)$

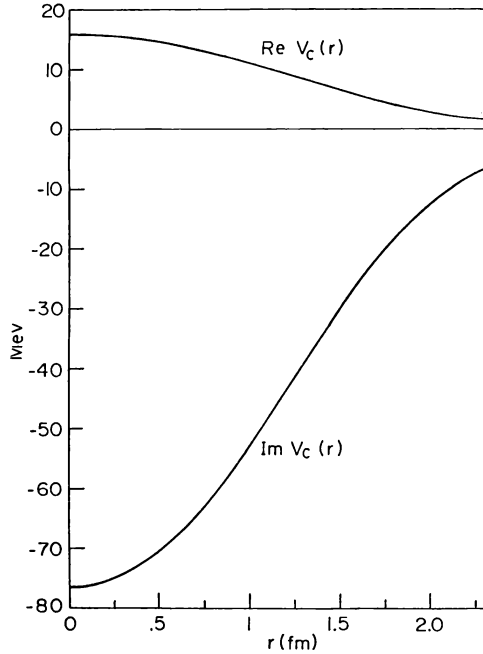


FIG. 8.1. Multiple scattering optical potential for the elastic scattering of 1-GeV protons by ^4He (central potential). [From Parmentola and Feshbach (82).]

absorptive. This is illustrated in Fig. 8.1, which gives the optical potential for 1-GeV protons in ^4He . We observe that the real part of V_c is weak and repulsive while the imaginary part is relatively large. As a consequence, the corresponding angular distribution exhibits the oscillations characteristic of Fraunhofer diffraction [$f \sim J_1(2kR \sin(\theta/2)) / 2kR \sin(\theta/2)$, Eq. (5.25b)] of the incident wave by an absorbing sphere (see Fig. 8.2). The positions of the minima of these oscillations depend only on the radius of the sphere, in the case of a sphere with a well-defined sharp radius. In the more realistic case, $\rho(\mathbf{r})$ will involve a radius parameter which will then determine the positions of the minima. Moreover, these are stable against the addition of spin-orbit contributions to the optical potential originating in the C' term of (8.1), of correlation effects, or of Coulomb terms, as demonstrated in Fig. 8.3. Chaumeaux et al. point out that the nucleon-nucleon amplitude can be changed by an overall phase which can be a function of q^2 without disturbing the fit to experiment. Such a change will, however, have an effect on the multiple scattering since the phases of the scattering amplitudes emanating from different nucleons will be modified, thereby changing the way in which they interfere (see Fig. 8.4). Note again the stability of the position of the minima.

On the other hand, a change in the density distribution has a noticeable effect, as can be seen in Fig. 8.5, where the impact of changing the neutron density is illustrated.

From this discussion it should be clear that the scattering of protons in the range 1 GeV provides a method for the determination of the neutron density within nuclei. The proton density is taken from high-energy electron scattering after removal of the finite proton charge radius in order to obtain the point proton density. Some of the results thus obtained by Ray (79) (which include important consideration of additional electromagnetic effects of which the interested reader should be aware) are given in Table 8.2.

The uncertainty in the $\Delta r_{np} (\equiv \langle r_n^2 \rangle^{1/2} - \langle r_p^2 \rangle^{1/2})$ is ± 0.05 fm. Δr_{np} is for a given nucleus, while $\Delta r_{nn'}$ is evaluated for two isotopes with differing neutron number. Examples of the deduced neutron density is shown in Fig. 8.6 for the

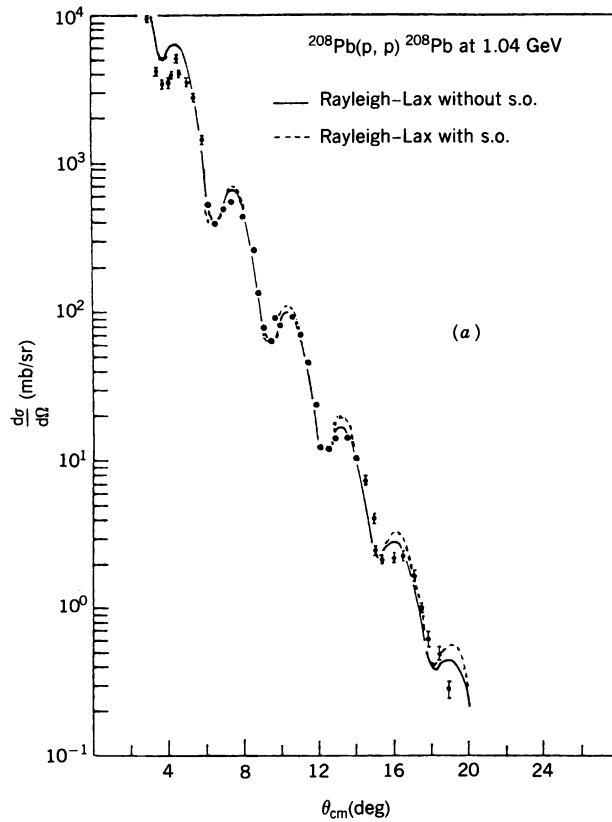


FIG. 8.2. (a) Comparison of experimental angular distribution for the elastic scattering of 1.04-GeV protons by ^{206}Pb with the predictions employing the Rayleigh-Lax potential with and without spin-orbit (s.o.) terms. The density-dependent Hartree-Fock densities are used. [From Bordy and Feshbach (77).] (b) Comparison of the angular distribution for the elastic scattering of protons by ^{16}O , ^{40}Ca , ^{58}Ni , ^{60}Ni , ^{62}Ni , ^{64}Ni , ^{90}Zr , and ^{208}Pb with predictions employing the Rayleigh-Lax potentials. The Hartree-Fock-Bogoliubov densities are used. [From Chaumeaux, Layly, and Schaeffer (78).]

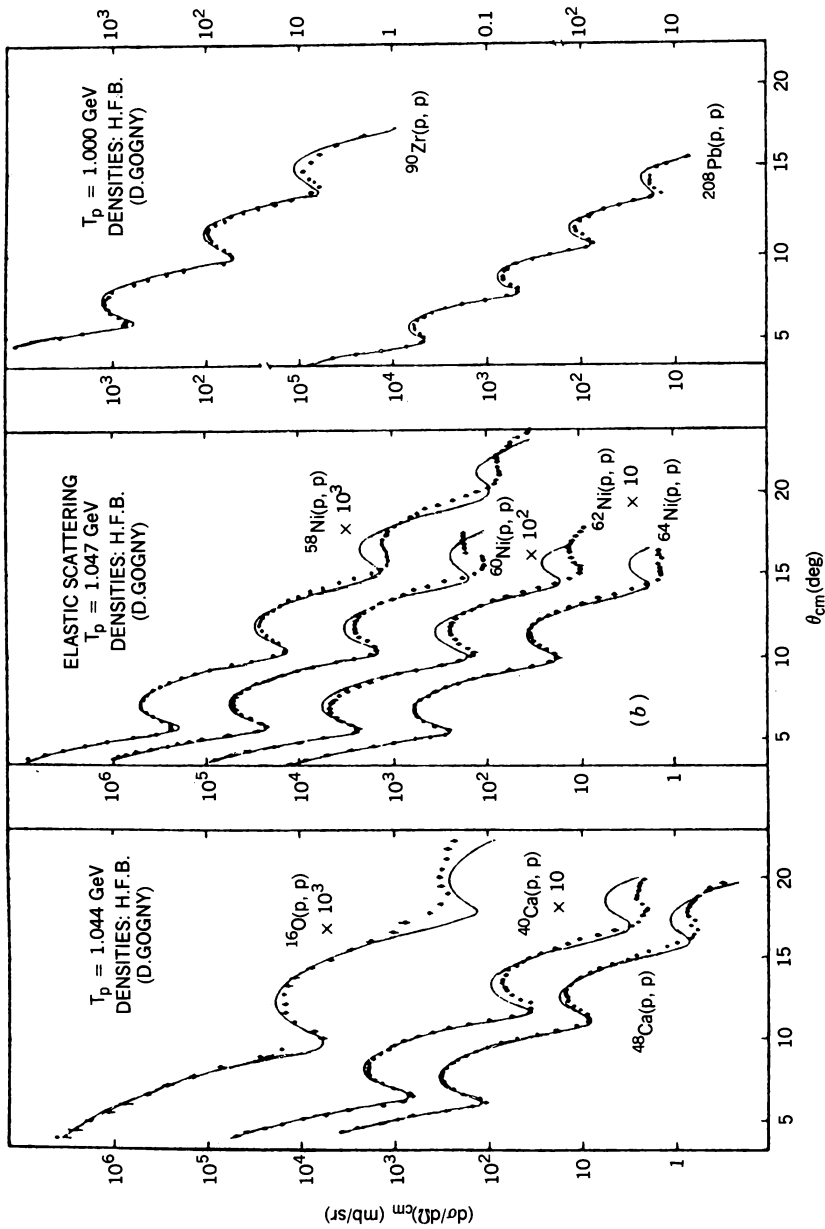


FIG. 8.2. (Continued)

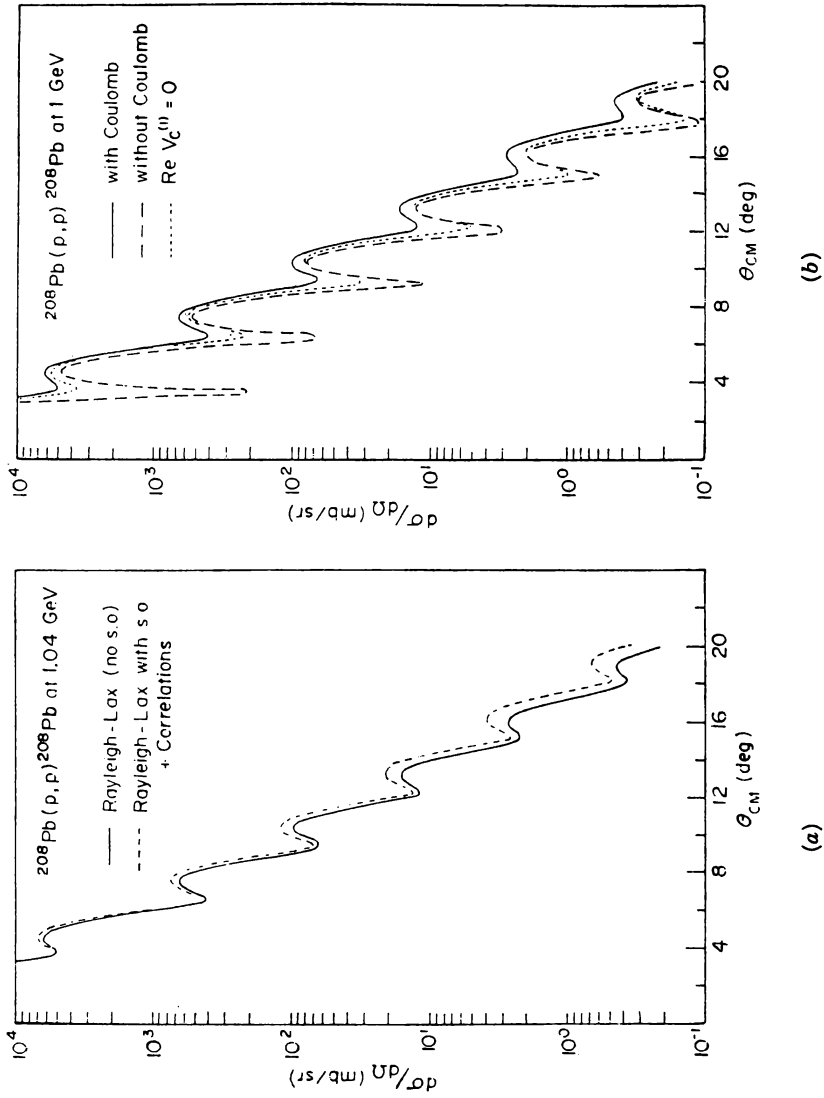


FIG. 8.3. (a) Effect of the spin-orbit interaction and correlations on the elastic scattering by ^{208}Pb ; effect of the Coulomb interaction. [From Boridy and Feshbach (77).]

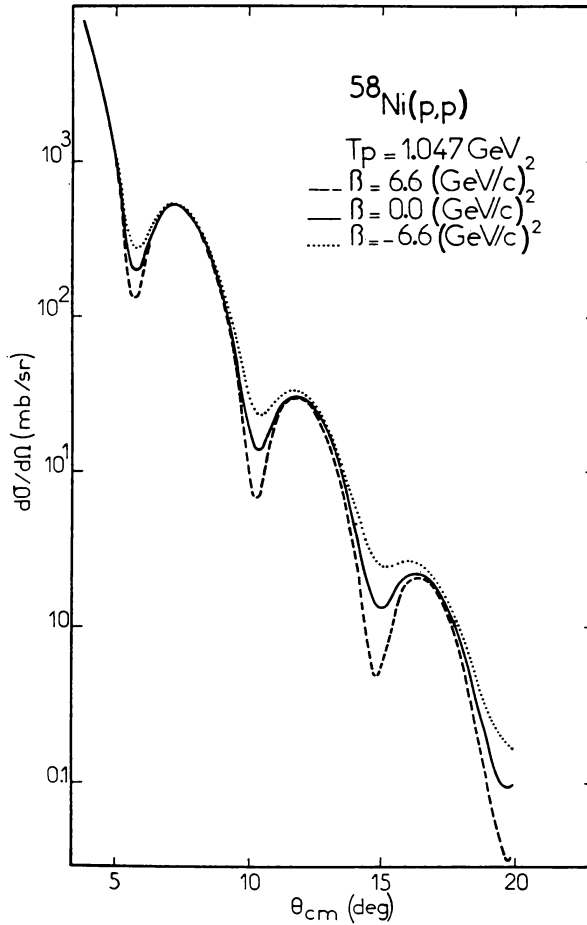


FIG. 8.4. Change of the cross section when the nucleon–nucleon amplitude is multiplied by a phase factor $e^{i\beta q^2}$ for different values of β . [From (Chaumeaux, Layly, and Schaeffer (78).)]

Ni isotopes. From Table 8.2 we see reasonable agreement with Negele's density-dependent Hartree–Fock calculation, an agreement that is also present in Fig. 8.6. The outstanding major disagreement is in the value of Δr_{nn} for the pair ^{48}Ca and ^{40}Ca .

Both Chaumeaux et al. and Ray take correlations into account. According to both authors (see Appendix B at the end of this chapter), the effects are appreciable at the larger angles. However, they are of the same order as effects arising in the uncertainties in the input data and small electromagnetic effects involving the form factor of the neutron. The effect of spin-dependent correlations, including those arising from B' , C' , D' , and E' terms, on elastic scattering have been investigated by Lambert and Feshbach (73) and Parmentola

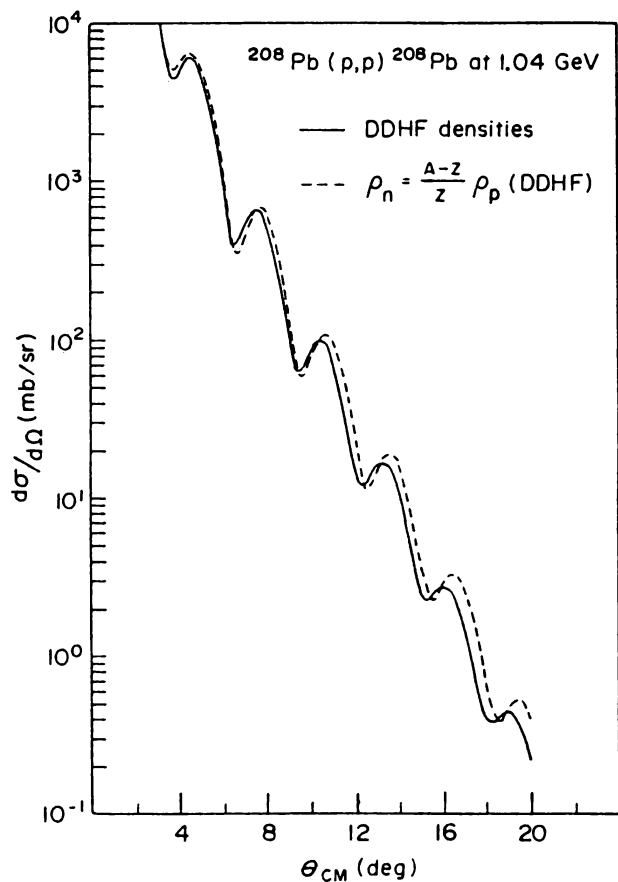


FIG. 8.5. Effect of changing the neutron density distribution. [From Boridy and Feshbach (77).]

TABLE 8.2

Nucleus	$\langle r_n^2 \rangle^{1/2}$ (fm)	$\langle r_p^2 \rangle^{1/2}$ (fm)	$\langle r_c^2 \rangle^{1/2}$ (fm)	Δr_{np}	$\Delta r_{nn'}$	DDHF	
						Δr_{np}	$\Delta r_{nn'}$
⁴⁰ Ca	3.491	3.392	3.482	0.10		-0.05	
⁴⁸ Ca	3.625	3.396	3.470	0.23	0.13 ± 0.04	0.19	0.26
⁵⁸ Ni	3.700	3.686	3.772	0.01		0.00	
⁶⁴ Ni	3.912	3.745	3.845	0.17	0.21 ± 0.02	0.13	0.18
¹¹⁶ Sn	4.692	4.546	4.619	0.15		0.12	
¹²⁴ Sn	4.851	4.599	4.670	0.25	0.16 ± 0.02	0.21	0.13
²⁰⁸ Pb	5.611	5.453	5.503	0.16		0.20	

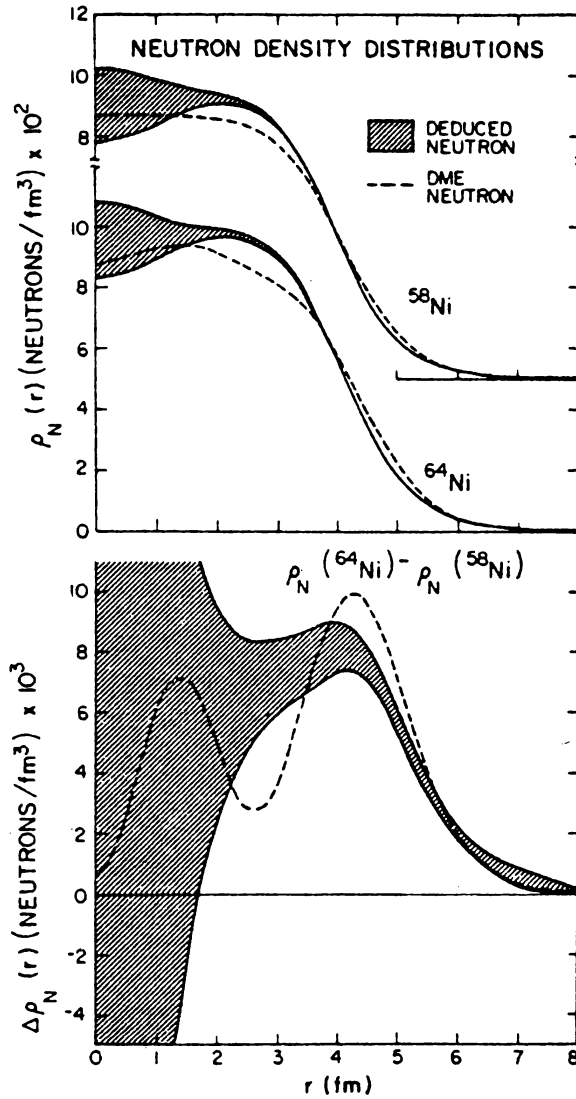


FIG. 8.6. Point neutron density distributions for $^{58,64}\text{Ni}$ deduced from second-order KMT analysis (shaded bands) and predicted by the density matrix expansion (DME) approach to Hartree-Fock theory (dashed curves). The difference between the ^{64}Ni - and ^{58}Ni -deduced neutron densities is compared with the DME prediction in the lower half of the figure. [From Ray (79).]

and Feshbach (82) for a ^4He target. These authors find that generally the influence of the B , D , and E terms is small if the nucleon–nucleon parameters of Table 8.1 are used. Chaumeaux et al. examine the spin-dependent effects of B , C , and E (D is not included) in *inelastic* scattering, pointing out quite correctly the sensitivity of the angular distribution and of the polarization to these coefficients. The results for these quantities, using coefficients A , B , C , and E quite similar to those given in Table 8.1, are less than satisfactory. But adjustments within the uncertainties can improve comparison with experiment.

APPENDIX A

In this section we apply the *optimal approximation method* of Gurvitz, Dedonder, and Amado (79) to projectile–nucleus scattering. We focus on the relationship between t_i and τ_i as given in (4.19). In the course of that derivation $\alpha_0 (\equiv E - K_0)$ of (4.4) is replaced by $\alpha (\equiv E - K_0 - H_N)$, as in (4.18). The method of Gurvitz et al. allows for an adjustment of the values of E so as to reduce the consequent error. Let

$$\bar{\alpha}_0 \equiv \varepsilon - K_0$$

and

$$\bar{t}_i = v_i + v_i \frac{1}{\bar{\alpha}_0} \bar{t}_i \quad (\text{A.1})$$

The equation for τ_i , (4.7), remains unchanged:

$$\tau_i = v_i \mathcal{A} + v_i \frac{\mathcal{A}}{\alpha} \tau_i \quad (\text{4.7})$$

The dependence of both \bar{t}_i and τ_i on v_i can be used to eliminate v_i , producing a relation between \bar{t}_i and τ_i :

$$\tau_i = \bar{t}_i \mathcal{A} + \bar{t}_i \left(\frac{\mathcal{A}}{\alpha} - \frac{1}{\bar{\alpha}_0} \right) \tau_i \quad (\text{A.2})$$

The optimal approximation will be applied to an auxiliary quantity τ'_i defined by

$$\tau'_i = \bar{t}_i + \bar{t}_i \left(\frac{1}{\alpha} - \frac{1}{\bar{\alpha}_0} \right) \tau'_i \quad (\text{A.3})$$

in terms of which

$$\tau_i = \tau'_i \mathcal{A} + \tau'_i \frac{\mathcal{A} - 1}{\alpha} \tau_i \quad (\text{A.4})$$

To second order,

$$\begin{aligned}
 \tau'_i &= \bar{t}_i + \bar{t}_i \frac{1}{\bar{\alpha}_0} (\bar{\alpha}_0 - \alpha) \frac{1}{\alpha} \tau'_i \\
 &\simeq \bar{t}_i + \bar{t}_i \frac{1}{\bar{\alpha}_0} (\bar{\alpha}_0 - \alpha) \frac{1}{\bar{\alpha}_0} \bar{t}_i \\
 &\simeq \bar{t}_i + \Delta\tau'_i
 \end{aligned} \tag{A.5}$$

We shall now show that it is possible to choose $\bar{\alpha}_0$ (by choosing ε) in a manner independent of the target nucleus, so that (A.1) describes two-body scattering and so that

$$\tau'_i = \bar{t}_i \tag{A.6}$$

and therefore in agreement with (4.26), with t_i replaced by \bar{t}_i .

To demonstrate (A.6), consider the matrix element of the second term in (A.5) ($\equiv \Delta\tau'_i$) with respect to the target nucleus and the incident and emergent projectile. Let the latter have momenta \mathbf{p} and \mathbf{p}' , respectively, while the target nucleus wave function in the momentum representation is $\psi_0(\mathbf{P}_1 - \mathbf{p}/A, \mathbf{P}_2 - \mathbf{p}/A, \dots)$, where $\Sigma \bar{\mathbf{P}}_i = \mathbf{P}$ is the total momentum of the projectile plus target. The propagator $(1/\bar{\alpha}_0)$ is taken to be diagonal in momentum space:

$$\left\langle \mathbf{p}', \mathbf{P}'_1, \mathbf{P}'_2 \dots \left| \frac{1}{\bar{\alpha}_0} \right| \mathbf{p}, \mathbf{P}_1, \mathbf{P}_2 \dots \right\rangle = \frac{\delta(\mathbf{p}' - \mathbf{p}) \delta(\mathbf{P}'_1 - \mathbf{P}_1) \delta(\mathbf{P}'_2 - \mathbf{P}_2) \dots}{\varepsilon - p^2/2\mu} \tag{A.7}$$

As a consequence, \bar{t}_i of (A.1) is diagonal in the target nucleon momenta, as v_i can only change the projectile momenta.

$$\langle \mathbf{p}', \mathbf{P}'_1, \mathbf{P}'_2 \dots | \bar{t}_i | \mathbf{p}, \mathbf{P}_1, \mathbf{P}_2 \dots \rangle = \langle \mathbf{p}' | \bar{t}_i | \mathbf{p} \rangle \delta(\mathbf{P}'_1 - \mathbf{P}_1) \delta(\mathbf{P}'_2 - \mathbf{P}_2) \dots \tag{A.8}$$

We can now proceed to evaluate the matrix element of $\Delta\tau'_i$ for elastic scattering; the incident projectile has a momentum \mathbf{p} , and the target nucleus $\mathbf{P} - \mathbf{p}$. One obtains

$$\begin{aligned}
 &\langle \mathbf{p}'; \psi_0 | \Delta\tau'_i | \mathbf{p}, \psi_0 \rangle \\
 &= \int d\mathbf{p}_1 d\mathbf{p}_2 \int d\mathbf{P}_1 \int d\mathbf{P}'_1 \dots \psi_0^* \left(\mathbf{P}'_i - \frac{\mathbf{p}'}{A}, \mathbf{P}'_2 - \frac{\mathbf{p}'}{A}, \dots \right) \\
 &\quad \times \langle \mathbf{p}' | \bar{t}_i | \mathbf{p}_1 \rangle \frac{1}{\varepsilon_1 - p_1^2/2\mu} \langle \mathbf{p}_1, \mathbf{P}'_1, \mathbf{P}'_2, \dots | \bar{\alpha}_0 - \alpha | \mathbf{p}_2, \mathbf{P}_1, \mathbf{P}_2, \dots \rangle \\
 &\quad \times \langle \mathbf{p}_2 | \bar{t}_i | \mathbf{p} \rangle \frac{1}{\varepsilon_2 - p_2^2/2\mu} \psi_0 \left(\mathbf{P}_1 - \frac{\mathbf{p}}{A}, \mathbf{P}_2 - \frac{\mathbf{p}}{A}, \dots \right)
 \end{aligned} \tag{A.9}$$

Evaluating the matrix element of $\tilde{\alpha}_0 - \alpha$ gives

$$\begin{aligned}
 & \langle \mathbf{p}_1, \mathbf{P}'_1, \mathbf{P}'_2, \dots | \tilde{\alpha}_0 - \alpha | \mathbf{p}_2, \mathbf{P}_1, \mathbf{P}_2, \dots \rangle \\
 &= \delta(\mathbf{p}_1 - \mathbf{p}_2) \left\{ \left[\varepsilon_1 - \frac{p_1^2}{2\mu} - \left(E - \frac{p_1^2}{2\mu} - \sum \frac{1}{2m} \left(\mathbf{P}'_n - \frac{\mathbf{p}_1}{A} \right)^2 \right) \right] \right. \\
 & \quad \times \delta(\mathbf{P}'_1 - \mathbf{P}_1) \delta(\mathbf{P}'_2 - \mathbf{P}_2) \cdots + \sum_n V(\mathbf{P}'_n - \mathbf{P}_n) \delta(\mathbf{P}'_1 - \mathbf{P}_1) \cdots \\
 & \quad \left. \times \delta(\mathbf{P}'_{n-1} - \mathbf{P}_{n-1}) \delta(\mathbf{P}'_{n+1} - \mathbf{P}_{n+1}) \delta(\mathbf{P}'_{n+2} - \mathbf{P}_{n+2}) \cdots \right\} \quad (\text{A.10})
 \end{aligned}$$

where the assumption has been made that the nucleons in the target nucleus move in a mean field described by a local potential V . Using the Schrödinger equation satisfied by $\psi_0(\mathbf{P}_1 - \mathbf{p}/A, \dots)$, the integration over the \mathbf{P}_n and \mathbf{p}_2 can be performed to yield

$$\begin{aligned}
 & \langle \mathbf{p}', \psi_0 | \Delta \tau'_i | \mathbf{p}, \psi_0 \rangle \\
 &= \int d\mathbf{p}_1 \int d\mathbf{P}'_1 \int d\mathbf{P}'_2 \cdots \psi_0^* \left(\mathbf{P}'_1 - \frac{\mathbf{p}'}{A}, \mathbf{P}'_2 - \frac{\mathbf{p}'}{A}, \dots \right) \langle \mathbf{p}' | \tilde{t} | \mathbf{p}_1 \rangle \\
 & \quad \times \frac{1}{\varepsilon_1 - p_1^2/2\mu} \left[\varepsilon_1 - E + \sum \frac{1}{2m} \left\{ \left(\mathbf{P}'_n - \frac{\mathbf{p}_1}{A} \right)^2 - \left(\mathbf{P}'_n - \frac{\mathbf{p}}{A} \right)^2 \right\} \right] \\
 & \quad \times \langle \mathbf{p}_1 | \tilde{t} | \mathbf{p} \rangle \frac{1}{\varepsilon_1 - p_1^2/2\mu} \psi_0 \left(\mathbf{P}'_1 - \frac{\mathbf{p}}{A}, \mathbf{P}'_2 - \frac{\mathbf{p}}{A}, \dots \right) \quad (\text{A.11})
 \end{aligned}$$

The quantity in the braces becomes $(2/A)(\mathbf{p} - \mathbf{p}_1) \cdot \mathbf{P}'_n + (1/A^2)(\mathbf{p}_1^2 - \mathbf{p}^2)$. At this point the *Breit coordinates* are introduced:

$$\mathbf{q} = \mathbf{p} - \mathbf{p}' \quad \mathbf{K} = \frac{1}{2}(\mathbf{p} + \mathbf{p}') \quad \mathbf{K} \cdot \mathbf{q} = 0, \quad \frac{1}{2}(p^2 + p'^2) = K^2 + \frac{1}{4}q^2 \quad (\text{A.12})$$

yielding

$$\begin{aligned}
 2(\mathbf{p} - \mathbf{p}_1) \cdot \mathbf{P}'_n &= 2(\mathbf{K} + \frac{1}{2}\mathbf{q} - \mathbf{p}_1) \cdot \mathbf{P}'_n \\
 &= 2(\mathbf{K} + \frac{1}{2}\mathbf{q} - \mathbf{p}_1) \cdot (\mathbf{P}'_n - \mathbf{K}) + 2(\mathbf{K} + \frac{1}{2}\mathbf{q} - \mathbf{p}_1) \cdot (\mathbf{K})
 \end{aligned}$$

By using time-reversal invariance of the integrand of (A.11) it can be shown that the first term of the equation above integrates to zero, so that no dependence on the coordinates \mathbf{P}'_n remains. As a consequence, the term in brackets in (A.11) becomes

$$\varepsilon_1 - E - \frac{\mathbf{q}^2}{8mA} + \frac{(\mathbf{p}_1 - \mathbf{K})^2}{2mA}$$

It follows from (A.11) that

$$\langle \mathbf{p}'\psi_0 | \Delta\tau'_i | \mathbf{p}\psi_0 \rangle = 0$$

if one chooses

$$\varepsilon_1 = E + \frac{q^2}{8mA} - \frac{(\mathbf{p}_1 - \mathbf{K})^2}{2mA} \quad (\text{A.13})$$

where $E = p^2/2\mu$. This choice of ε_1 is independent of the target nucleon variables \mathbf{P}_n , so that as implied by (A.7) and (A.8), \bar{t}_i is the transition amplitude for the scattering following from the Schrödinger equation:

$$\left[\frac{p^2}{2\mu} + \frac{q^2}{8mA} - \frac{(\mathbf{p}_1 - \mathbf{K})^2}{2mA} - v - \frac{p_1^2}{2\mu} \right] \phi(p_1) = 0$$

The effective energy is obtained by dropping v from this equation. One can then rewrite the term in brackets as follows:

$$\frac{p^2}{2\mu} + \frac{q^2}{8mA} - \frac{K^2}{2(mA + \mu)} - \frac{1}{2} \left(\frac{1}{\mu} + \frac{1}{mA} \right) \left(\mathbf{p}_1 - \frac{\mu}{mA + \mu} \mathbf{K} \right)^2$$

so that the effective energy is

$$E_{\text{eff}} = \frac{p^2}{2\mu} + \frac{q^2}{8mA} - \frac{K^2}{2(mA + \mu)} \quad (\text{A.14})$$

and the effective momentum operator is $\mathbf{p}_1 - [\mu/(mA + \mu)]\mathbf{K}$, so that the projectile momentum \mathbf{p} is replaced in the Schrödinger equation by $\mathbf{p} - [\mu/(mA + \mu)]\mathbf{K}$.

The development in Section 4 uses t_i rather than \bar{t}_i . In first order these two quantities will be approximately equal if the last two terms in (A.14) are small compared to the first. These ratios are on the order of μ/mA , which is appreciable only for the lightest nuclei.

The optimal approximation reduces the second-order term to zero through the choice of ε_1 given by (A.13). The question remains as to whether higher-order terms are significant. The third-order term is discussed by Gurvitz, Dedonder, and Amado (79), who conclude that it is not if t varies slowly with the energy.

APPENDIX B CORRELATIONS

The second-order optical model potential $V_{\text{opt}}^{(2)}$ given by (4.41) is nonlocal, with the consequence that its effect is difficult to evaluate analytically or even

numerically. One approximate method derived by Feshbach, Gal, and Hufner (71) [see also Feshbach (81) as well as papers written with Lambert (73), Ullo (74), and Parmentola (82)] replaces the Schrödinger equation containing $V_{\text{opt}}^{(2)}$ with a pair of coupled equations. This procedure is in any event necessary if the spin-dependent terms are to be taken into account accurately as described in the text (see p. 100). In this section further approximations valid at sufficiently high projectile energies and small momentum transfers are made which yield a local form for $V_{\text{opt}}^{(2)}$ akin to that obtained by Chaumeaux, Layly, and Schaeffer (78).

We repeat (4.41) with $\langle \mathbf{r} | 1/\bar{\alpha} | \mathbf{r}' \rangle \equiv G(\mathbf{r}, \mathbf{r}')$:

$$\int V_{\text{opt}}^{(2)}(\mathbf{r}, \mathbf{r}') \psi(\mathbf{r}') d\mathbf{r}' = (A-1)^2 \int d\mathbf{r}' G(\mathbf{r}_1, \mathbf{r}') \int d\mathbf{r}_1 d\mathbf{r}_2 t(\mathbf{r} - \mathbf{r}_1) t(\mathbf{r}' - \mathbf{r}_2) C(\mathbf{r}_1, \mathbf{r}_2) \psi(\mathbf{r}') \quad (\text{B.1})$$

We now assume that

$$C(\mathbf{r}_1, \mathbf{r}_2) = \rho(\mathbf{r}_1) \rho(\mathbf{r}_2) \gamma(\mathbf{r}_1 - \mathbf{r}_2) \quad (\text{B.2})$$

Second, we note that $t(\mathbf{r} - \mathbf{r}_1)$ is sharply peaked at $\mathbf{r} \sim \mathbf{r}_1$. Assuming that $\rho(\mathbf{r})$ varies slowly over that peak, little error is made if $\rho(\mathbf{r}_1) t(\mathbf{r} - \mathbf{r}_1)$ is replaced by $\rho(\mathbf{r}) t(\mathbf{r} - \mathbf{r}_1)$. Equation (B.1) then becomes

$$\int V_{\text{opt}}^{(2)}(\mathbf{r}, \mathbf{r}') \psi(\mathbf{r}') d\mathbf{r}' = (A-1) \rho(\mathbf{r}) \int d\mathbf{r}' G(\mathbf{r}, \mathbf{r}') \rho(\mathbf{r}') F(\mathbf{r} - \mathbf{r}') \psi(\mathbf{r}') \quad (\text{B.3})$$

where

$$F(\mathbf{r} - \mathbf{r}') \equiv \int d\mathbf{r}_1 \int d\mathbf{r}_2 t(\mathbf{r} - \mathbf{r}_1) t(\mathbf{r}' - \mathbf{r}_2) \gamma(\mathbf{r}_1 - \mathbf{r}_2) \quad (\text{B.4})$$

Note that one can show that the integral on the right-hand side of this equation is a function of $(\mathbf{r} - \mathbf{r}')$. Since the integrands in (B.4) consist of three sharply peaked functions, F itself is sharply peaked at $\mathbf{r} = \mathbf{r}'$, so that $\rho(\mathbf{r}')$ in (B.3) can be replaced by $\rho(\mathbf{r})$:

$$\int V_{\text{opt}}^{(2)}(\mathbf{r}, \mathbf{r}') \psi(\mathbf{r}') d\mathbf{r}' = (A-1)^2 \rho^2(\mathbf{r}) \int d\mathbf{r}' G(\mathbf{r}, \mathbf{r}') F(\mathbf{r} - \mathbf{r}') \psi(\mathbf{r}') \quad (\text{B.5})$$

This result could also have been obtained by using the local density approximation for second-order multiple scattering in nuclear matter. In that case it is exact, and in the case of a finite nucleus, $G(\mathbf{r}, \mathbf{r}')$ is to a good approximation $G(\mathbf{r} - \mathbf{r}')$, so that

$$\int V_{\text{opt}}^{(2)}(\mathbf{r} - \mathbf{r}') \psi(\mathbf{r}') d\mathbf{r}' = (A-1)^2 \rho^2(\mathbf{r}) \int d\mathbf{r}' G(\mathbf{r} - \mathbf{r}') F(\mathbf{r} - \mathbf{r}') \psi(\mathbf{r}')$$

The integral on the left-hand side can now be reduced to a local form using the Perey–Saxon (64) approximation, which is discussed in detail in Chapter V (p. 000). In the present case

$$\begin{aligned} \int d\mathbf{r}' G(\mathbf{r} - \mathbf{r}') F(\mathbf{r} - \mathbf{r}') \psi(\mathbf{r}') &= \int d\mathbf{s} G(\mathbf{s}) F(\mathbf{s}) \psi(\mathbf{r} - \mathbf{s}) \\ &= \int d\mathbf{s} G(\mathbf{s}) F(\mathbf{s}) e^{-\mathbf{s} \cdot \nabla_{\mathbf{r}}} \psi(\mathbf{r}) \end{aligned}$$

so that $V_{\text{opt}}^{(2)}(\mathbf{r}, \mathbf{r}')$ can be replaced by

$$V_{\text{opt}}^{(2)} = (A - 1)^2 \rho^2 \int d\mathbf{s} G(\mathbf{s}) F(\mathbf{s}) e^{-\mathbf{s} \cdot \nabla_{\mathbf{r}}} \quad (\text{B.6})$$

The Perey–Saxon approximation exploits the fact that the dominant component of $\psi(\mathbf{r})$ is the plane wave $e^{i\mathbf{k} \cdot \mathbf{r}}$. Then

$$V_{\text{opt}}^{(2)}(\mathbf{r}) \simeq (A - 1)^2 \rho^2(\mathbf{r}) \int d\mathbf{s} G(\mathbf{s}) F(\mathbf{s}) e^{-i\mathbf{k} \cdot \mathbf{s}} \quad (\text{B.7})$$

In this approximation the $V_{\text{opt}}^{(2)}$ dependence on \mathbf{r} is given by ρ^2 , in comparison with $V^{(1)}$, whose spatial dependence is determined by $\rho(\mathbf{r})$. An improved approximation for $V^{(2)}$, which may be needed when the nuclear surface plays a significant role, can be obtained by Taylor expansion of $\rho(\mathbf{r}_1)$ and $\rho(\mathbf{r}_2)$; for example, $\rho(\mathbf{r}_1)$ would be placed equal to $\rho(\mathbf{r}) + (\mathbf{r}_1 - \mathbf{r}) \cdot \nabla \rho(\mathbf{r}) + \dots$. Such corrections may be of importance in dealing with inelastic scattering.

Evaluation of the integral in (B.7) can be simplified by using the eikonal approximation for G . In zeroth order we neglect the excitation energy $\bar{\epsilon}$ and the potential energy term $V^{(1)}$:

$$G(\mathbf{s}) = G(\mathbf{b}, \zeta) \simeq G_{\text{eik}}^{(0)} = -\frac{i\alpha}{\hbar^2 c^2 k} e^{ik\zeta} \theta(\zeta) \delta(\mathbf{b}) \quad (\text{B.8})$$

where from (7.2),

$$k^2 = \frac{1}{\hbar^2 c^2} \frac{\mathcal{E}^2 - m_p^2 c^4}{1 + \mathcal{E}/Amc^2} \quad \text{and} \quad \alpha = \frac{\mathcal{E} + m_p c^2}{1 + \mathcal{E}/Amc^2} \quad (\text{B.9})$$

The energy \mathcal{E} is the energy of the system, including the rest-mass energy of the projectile but not that of the target nucleus. The function $\theta(\zeta)$ is the unit function

$$\theta(\zeta) = \begin{cases} 1 & \zeta > 0 \\ 0 & \zeta < 0 \end{cases}$$

We must still fix the ζ direction. This we take to be the direction of \mathbf{k} . One now obtains

$$\int ds G(\mathbf{s}) F(\mathbf{s}) e^{-i\mathbf{k}\cdot\mathbf{s}} = -\frac{i\alpha}{\hbar^2 c^2 k} \int d\zeta F(0, \zeta) \theta(\zeta) = -\frac{i\alpha}{2\hbar^2 c^2 k} \int_{-\infty}^{\infty} d\zeta F(0, \zeta)$$

where it has been assumed, as is usually the case, that $F(0, \zeta)$ is even in ζ . Recalling the definition of F , (B.4), the integral of $F(0, \zeta)$ can be expressed in terms of the Fourier transforms of t and γ :

$$\int F(0, \zeta) d\zeta = \left(\frac{1}{2\pi}\right)^2 \int d^2 q_{\perp} \tilde{t}(\mathbf{q}_{\perp}, 0) \tilde{t}(-\mathbf{q}_{\perp}, 0) \tilde{\gamma}(\mathbf{q}_{\perp}, 0) \quad (\text{B.10})$$

We parameterize this result by

$$\int F(0, \zeta) d\zeta = -(\tilde{t}(0))^2 l \quad (\text{B.11})$$

where l is a length. The final result for $V_{\text{opt}}^{(2)}$ is

$$V_{\text{opt}}^{(2)} = \frac{i\alpha l}{2\hbar^2 c^2 k} [(A-1)\rho(\mathbf{r})\tilde{t}(0)]^2 \quad (\text{B.12})$$

This potential is proportional to the square of $V_{\text{opt}}^{(1)}$ (4.40), when the short-range approximation is made for $t(\mathbf{r}-\mathbf{r}_1)$. A rough estimate for l is obtained by assuming the Gaussian form (see Table 8.1) for $\tilde{t}(\mathbf{q})$, $\tilde{t}(0)e^{-(\beta^2/2)q^2}$, and for $\gamma(\mathbf{r})$:

$$\gamma(\mathbf{r}) = \left(\frac{r^2}{3r_c^2} - 1\right) e^{-r^2/2r_c^2} \quad (\text{B.13})$$

the form used by Chaumeaux et al. This choice for $\gamma(\mathbf{r})$ satisfies the condition that its volume integral is zero, satisfying (2.21) when ρ can be taken to be a constant. Finally, $C(\mathbf{r})$ approaches -1 as r goes to zero. With these choices l becomes

$$l = \frac{\sqrt{2\pi}}{3} r_c \frac{1}{(1 + 2\beta^2/r_c^2)^2} \quad (\text{B.14})$$

As pointed out by Feshbach Gal, and Hüfner (71), l is reduced because of the presence of the range of the projectile-nucleon potential given by β in (B.14). Inserting typical values for r_c (~ 0.7 fm), $\beta^2 = 0.4$ fm², one finds that $l = 0.084$ and that the magnitude of $V_{\text{opt}}^{(2)}$ is small compared to $V_{\text{opt}}^{(1)}$. However, because of the dependence of ρ^2 rather than ρ , there is a greater proportion of high-momentum components which can affect the cross section for large momentum transfers.

CHAPTER III

FORMAL THEORY OF NUCLEAR REACTIONS

1. INTRODUCTION

A formal theory of nuclear reactions should provide a framework within which it is possible to describe the wide range of reaction mechanisms exhibited in nuclear collisions. It should develop, directly from the nuclear Hamiltonian, the amplitude for the rapid processes, such as the single-step direct reactions as well as for the relatively slow compound nuclear resonance reactions. It should include the intermediate structure doorway state reactions and go beyond to the multistep reactions of both the direct and compound variety. It should be possible to obtain in the high-energy limit the multiple scattering approximation of Chapter II. Finally, it should permit the application of statistical considerations and thus obtain the statistical theories of nuclear reactions applicable to the various experimental situations. It should be emphasized that the formal theory only develops a framework; a framework that provides a means for inserting the physics of the reaction under consideration. Once this is done, the theory should yield expressions that allow a direct interpretation of the experimental data in terms of well-defined parameters.

As we have emphasized, reactions can be ordered according to the time delay they involve. Time delay in a given reaction can be introduced by providing alternative mechanisms to the direct one by means of which the system can proceed to the exit channel of interest. Instead of the system proceeding in a single step to the final state, it can make a transition to another channel (or channels) and so delay the development of the final state. This possibility is shown schematically in Fig. 1.1 for the case of elastic scattering for simplicity; that is, it is assumed that the energy is so low that this is the only reaction that

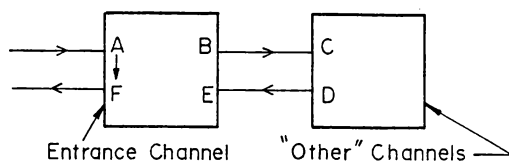


FIG. 1.1

can occur. Following the direct route the system would never leave the entrance channel. This route is symbolized by AF . But as is indicated by the figure, the time-delayed routes $ABCDEF$ can also contribute to the process. The time delay depends on the ratio of the probability of the transition from the entrance channel to the "other" channels, BC in the figure, to the probability that the system proceeds immediately to the final state, symbolized by F . However, this branching ratio is not the only parameter of importance. For example, if it were large, not only would the transition from the entrance channel be rapid but the transition back to the entrance channel would be equally quick. There would be some time delay but not necessarily a substantial one. For the latter to occur, another condition needs to be satisfied, one that inhibits the return transition.

To see what this condition is, it is necessary to decompose the other channels into a group that connect directly with the entrance channel and the remainder, as illustrated by Fig. 1.2. As indicated, the system can proceed to the doorway channels, as those channels that couple directly to the entrance channel are designated, and either proceed on to the "remaining" channels or return back to the entrance channel. The remaining channels, by definition, do not couple directly to the entrance channel. Thus a second important parameter is the ratio of the probability for the transition from the doorway channels to the remaining channels to the probability for the transition from the doorway back to the entrance channels. If this ratio is large, the time delay will be large for then the system will be trapped, spending a considerable fraction of the interaction time oscillating between the doorway channels and the remaining channels.

This time delay can be especially long at particular energies, the resonance energies, as can be seen from the following discussion. Suppose for a moment that the transition probability from the doorway channels to the entrance channel were zero. Then the system, if placed in other channels (consisting of

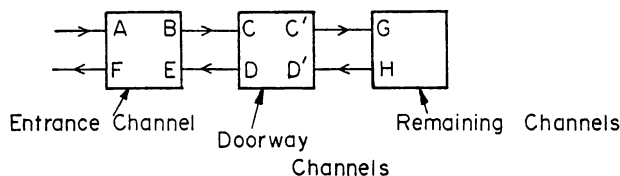


FIG. 1.2

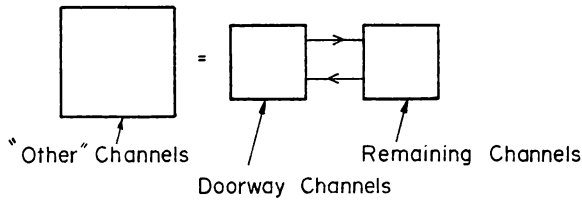


FIG. 1.3

the doorway and remaining channels), would be bound. Under these circumstances the system will oscillate between the doorway and remaining channels indefinitely but *only* at certain energies, the bound-state energies, E_b . Suppose now that the transition probability to and from the entrance channel is increased from zero. It follows that when the incident energy is correspondingly close to the binding energies E_b , a very long time delay will ensue and the system will resonate. As this transition probability increases, the resonant energy will increasingly depart from E_b , and usually the time delay will be reduced.

In summary, resonances will occur for elastic scattering when the system, restricted to other channels, as illustrated in Fig. 1.3, has bound states of positive energy, E_b . The resonance energies will be close[†] to E_b . The coupling to the entrance channel need not be small. However, if it is strong, the shift of the resonance energy from E_b will be large and the width increased, that is, the time delay shortened.

Resonance scattering of light by atoms provides a well-known example. The incident projectile is a photon of energy $\hbar\omega$, the target an atom in its ground state. This system forms the entrance channel. This channel will couple to an excited state of the atom with excitation energy ε . In the *absence* of the electromagnetic coupling by virtue of which radiation back to the ground state would occur, this excited state is bound. When the photon energy $\hbar\omega$ is close to ε , $\hbar\omega \sim \varepsilon$, a resonance in the scattering of the photon will occur in which the incident photon is absorbed by the atom and then emitted.

This effect can also be observed in the passage of monochromatic light through a medium made up of such atoms. If again $\hbar\omega \sim \varepsilon$, the index of refraction, n , will undergo a very sharp change as a function of photon energy, as illustrated in Fig. 1.4, the phenomenon being referred to as *anomalous dispersion*.

Another example, and one that more closely approaches the nuclear case, considers the interactions of a projectile (e.g., a neutron) and a target nucleus in the ground state. The incident projectile moves in a field of force exerted by the nucleus, as illustrated in Fig. 1.5a. The target nucleus shown in the same

[†]If E_b is near zero, the effect of coupling to the entrance channel can move the resonance energy to negative values. The resonance is then referred to as a negative energy resonance. This concept is useful if there is an effect of the resonance at positive energies.

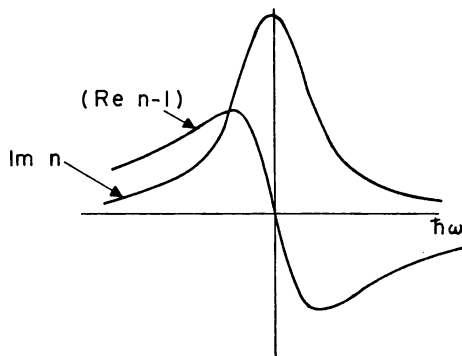


FIG. 1.4

figure consists, in the independent particle model, of nucleons, indicated by the filled circles, in the bound-state orbits. Figure 1.5a then illustrates the entrance channel. As a consequence of the interaction between the projectile and the target, a nucleon in the target is raised in energy while the incident projectile loses a corresponding amount of energy. If the excitation energy of the target is ε and the incident projectile energy is E , the energy of the projectile is $E - \varepsilon$. This situation is shown in Fig. 1.5b, where it is assumed that $E - \varepsilon$ is *negative*. The system is now bound in the sense that all the nucleons are individually bound. Of course, if the excitation energy of the target were to be returned to the projectile, it would again be unbound. But in the absence of that coupling the system is a bound one, although the *total* energy E is positive. The potential in which the projectile moves does have a bound state at $-E_b$, indicated by the line in the projectile half of the figure. According to the qualitative discussion presented earlier, when $E - \varepsilon$ is close to $-E_b$, or

$$E \sim \varepsilon - E_b$$

a resonance will occur. This example is still very far from a realistic description of the neutron-nucleus interaction, but it does contain the essential elements.

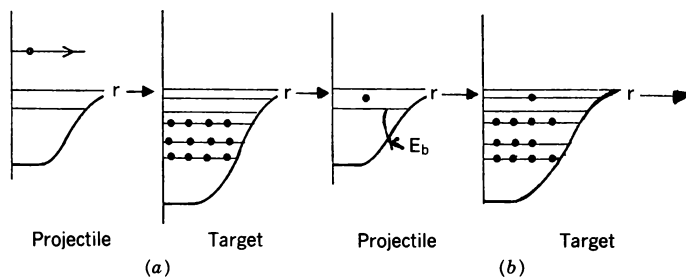


FIG. 1.5

A detailed, albeit simple example will serve to illustrate this discussion. The Hamiltonian of the system illustrated in Fig. 1.5 can be written

$$H = H_N + T + V(\mathbf{r}, \xi) \quad (1.1)$$

where \mathbf{r} is the coordinate of the incident particle and ξ represents all the independent coordinates of the nucleons in the nucleus. T is the kinetic energy operator, $V(\mathbf{r}, \xi)$ the potential energy of the projectile relative to the target center of mass, and H_N the Hamiltonian for the target nucleus, therefore depending only on ξ . Assume for simplicity that this Hamiltonian has only two eigenvalues, 0 and ε , with the corresponding normalized wave functions $\psi_0(\xi)$ and $\psi_1(\xi)$. The total wave function for the system is then

$$\Psi = \frac{1}{r} [u_0(\mathbf{r})\psi_0(\xi) + u_1(\mathbf{r})\psi_1(\xi)] \quad (1.2)$$

where u_0 and u_1 describe the projectile wave functions in the two channels Fig. 1.5a and b, respectively. Inserting this expression for Ψ in the Schrödinger equation,

$$H\Psi = E\Psi$$

and using the orthogonality of ψ_0 and ψ_1 yields a pair of coupled equations for u_0 and u_1 :

$$\begin{aligned} [E - (T + V_{00})] \frac{u_0}{r} &= V_{01} \frac{u_1}{r} \\ [E - \varepsilon - (T + V_{11})] \frac{u_1}{r} &= V_{10} \frac{u_0}{r} \end{aligned}$$

where

$$V_{ij}(\mathbf{r}) = \langle \psi_i | V(\mathbf{r}, \xi) \psi_j \rangle_\xi$$

The integrations in these matrix elements is, as indicated, over the variables ξ only. We now assume that u_0 and u_1 are spherical, that V_{00} is given by an attractive square well,

$$V_{00} = -V_0 \quad r < a$$

that

$$V_{11} = -\frac{\lambda \hbar^2}{2m} \delta(r - a) \quad \lambda = \text{constant}$$

and that

$$V_{01} = V_{10} = -\frac{A\hbar^2}{2m} \delta(r-a) \quad A = \text{constant}$$

Hence u_0 and u_1 satisfy the differential equations

$$u_0'' + (k^2 + K_0^2)u_0 = -A\delta(r-a)u_1 \quad r \leq a \quad (1.3a)$$

$$u_1'' + (-\kappa^2 + \lambda\delta(r-a))u_1 = -A\delta(r-a)u_0 \quad (1.3b)$$

where

$$\kappa^2 = \frac{2m}{\hbar^2} (\epsilon - E) \quad K_0^2 = \frac{2m}{\hbar^2} V_0$$

and

$$k^2 = \frac{2m}{\hbar^2} E$$

This selection of potentials has the merit that (1.3b) in the absence of the coupling to the entrance channel has only one bound state at $\kappa = \kappa_0$; that is,

$$v_1'' + [-\kappa_0^2 + \lambda\delta(r-a)]v_1 = 0$$

has only one bound state solution. We leave it as an exercise for the reader to show that κ_0 satisfies the equation

$$\lambda a = \frac{2\kappa_0 a}{1 - e^{-2\kappa_0 a}} \quad (1.4)$$

The right-hand side of this equation is given by the solid curve in Fig. 1.6. When $\lambda a > 1$, one solution of (1.4) exists at the intersection of the curve and

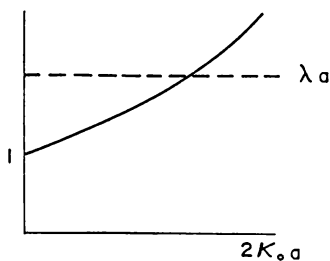


FIG. 1.6

the dashed line. As we shall see, the resonance generated by the coupled equations (1.3) will occur near the solution of (1.4)

As a first step we integrate (1.3a) and (1.3b) over a small range $a \pm \delta$. This yields

$$\begin{aligned} u'_0(a^+) - u'_0(a^-) &= -Au_1(a) \\ u'_1(a^+) - u'_1(a^-) + \lambda u_1(a) &= -Au_0(a) \end{aligned}$$

Note that

$$\begin{aligned} u_0 &= \sin Kr & r \leq a \\ u_1 &= \begin{cases} \alpha \sinh \kappa r & r \leq a \\ \alpha \sinh \kappa a e^{-\kappa(r-a)} & r \geq a \end{cases} \end{aligned}$$

where

$$K = \sqrt{k^2 + K_0^2}$$

and α is a constant to be determined. It is now a simple matter to evaluate

$$f \equiv \frac{au'_0(a^+)}{u_0(a)}$$

One obtains

$$f = Ka \cot Ka + \frac{A^2 a^2}{[2\kappa a/(1 - e^{-2\kappa a})] - \lambda a} \quad (1.5)$$

As we show in the Appendix to this chapter, resonances occur when $f = 0$. The second term in (1.5) is plotted in Fig. 1.7. Assuming that $k \ll K_0$, the first term is a constant that we take to be positive as an example. The function f equals zero at the intersection of the dashed line and the solid curve. The value of the resonance energy, E_R , is $E_R = \varepsilon - \hbar^2 \kappa_R^2 / 2m$. This is a resonance if $E_R > 0$.

The difference between κ_R and κ_0 depends on the curvature of the second term as a function of κa and the size of the first. Assuming that $\kappa_R \sim \kappa_0$, one obtains

$$\kappa_R a \simeq \kappa_0 a + \frac{\kappa_0}{\lambda} \frac{A^2 a^2}{(1 - \lambda a + 2\kappa_0 a) Ka \cot Ka}$$

This formula demonstrates that the deviation of the κ_R from κ_0 , that is, the deviation of the resonance energy from the energy of the bound state of channel

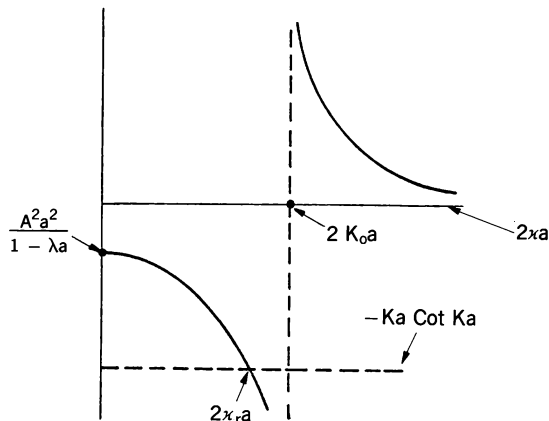


FIG. 1.7

u_1 , grows as the strength of the coupling between the channels measured by Aa increases.

The width of the resonance is shown in the Appendix to this chapter to be given by

$$\Gamma = \frac{-2\kappa a}{(\partial f / \partial E)_{E=E_R}} \quad (1.6)$$

Evaluating the derivative at κ_0 rather than at κ_R , to simplify the result, and assuming Ka to be constant yields

$$\Gamma \simeq \frac{2\hbar^2 k \kappa_0^2}{m\lambda} \frac{A^2 a^2}{[1 + (2\kappa_0 - \lambda)a](Ka \cot Ka)^2}$$

We see, as predicted, that the width increases (and the time delay decreases) as the coupling strength increases.

When E differs from E_R by an energy several times Γ , the energy variation of the cross section because of the energy variation of the second term on the right-hand side of (1.5) becomes unimportant. Of course, an effect remains, and usually the coupling to the second channel does increase the time delay.

In an actual projectile-nucleus reaction, the second channel is replaced by many channels labeled "other" channels in Fig. 1.1. There are then many bound states and correspondingly, many resonances, in contrast to the single bound state and single resonance of the coupled equations (1.3). In the next section the formalism applicable to the more complex and more realistic situation is developed.

2. FORMAL THEORY

The formal theory of nuclear reactions presented below relies on the concepts presented in the preceding section. Of course, the system to which it is applied, the compound system consisting of the projectile plus target nucleus, is much more complex than the system discussed at the end of Section 1 for which the target nucleus was assumed to have only two states, the ground state and one excited state. Nevertheless, it is possible by using projection operator techniques to rephrase the more general problem so that significant similarities to the simpler case are developed.

What we shall do is to partition all the states of the system into two sets of states. One set will contain the entrance channel and at least those channels that are involved in the prompt component of the reaction amplitude, that is, those which contribute to the direct single step as well as direct multistep processes for the reaction under consideration. This set of channels will play a role similar to that of $u_0\psi_0$ of (1.2). The second set will contain all the remaining channels (the other channels) including, necessarily, those that are bound in the absence of coupling to the first set. They play a role similar to that of $u_1\psi_1$ of (1.2).

These conditions do not constitute a precise definition of the partition. As we shall see, this lack of precision is useful since it allows the insertion of the pertinent physics of the problem into its analytical formulation. One illustration of such a partition would be helpful. Suppose that the physical process is the elastic and inelastic scattering of a pion by a nucleus (to avoid, in this illustration, the complications of the Pauli principle that would occur if the incident particle were a proton or, for that matter, any nuclear projectile). The appropriate set of states will include the entrance channel $u_0(\mathbf{r})\psi_0(\xi)$ as well as the inelastic states $u_n(\mathbf{r})\psi_n(\xi)$, where ψ_n are the states of the target nucleus, ψ_0 being the ground state, ψ_1 the first excited state, and so on; ξ are the coordinates, including spin and isospin of the nucleons making up the target. The functions $u_n(\mathbf{r})$ give the wave functions of the pion, where \mathbf{r} is the pion coordinate relative to the center of mass of the target. If the energy of the projectile is E and the excitation energy corresponding to ψ_n is ε_n , the energy associated with the pion is $E - \varepsilon_n$. If this energy is positive, the asymptotic form of the wave function u_n , $n \neq 0$, will be of the form of an outgoing wave e^{ik_nr}/r , where $k_n = [2m/\hbar^2)(E - \varepsilon_n)]^{1/2}$. Those channels for which k_n is real, that is, $(E - \varepsilon_n) > 0$, are called *open channels*. If $E - \varepsilon_n$ is less than zero, k_n is pure imaginary and the asymptotic form of u_n is proportional to $e^{ik_nr}/r = e^{-|k_n|r}/r$. These channels are referred to as *closed channels*.

Once the representation of the Hilbert space to be used is described, the next task is partition into the prompt (the first set) and delaying (the second set) components. One solution is to include all the open channels in the first set and all the closed channels in the second set. This is the partition most commonly used at relatively low projectile energies, since then the number of open channels will be small. However, even in this case it sometimes proves advantageous to include some of the closed channels in the prompt space, or vice versa, some

of the open channels in the space of the delaying channels. This option is always available.

At high projectile energies, the delaying channels become unimportant for the most part. All important channels are prompt (although there can be delayed after-effects) and the partition used in Chapter II selects for the first set just those channels that are of immediate interest (e.g., the entrance channel if elastic scattering is being studied).

The selection of the set $u_n(\mathbf{r})\psi_n(\xi)$ is not just a matter of convenience. There is an implied statement in making that choice regarding the reaction mechanism. For example, it is implicitly asserted that particle transfer channels are not important for elastic or inelastic scattering. This is, in fact, not always the case, for it can occur that by transferring a particle or cluster of particles from the projectile to the target, it is possible at some energies easily to excite a "giant" resonance of the new system formed in this way. Inelastic excitation or elastic scattering of the target would follow if inverse particle transfer back to the projectile is made. In the case of pion-nucleus collision, the list given above of the possible channels in fact omitted one significant channel that is formed when the pion is absorbed by the target nucleon, the Δ .

These examples stress the flexibility of the partition and the role of physical intuition, first, in selecting the complete set that is to be partitioned and then, in choosing the partition.

Since the nature of the representation of the Hilbert space of the problem will vary considerably, it will be useful to develop a general formalism. Toward this end let us assume that the Hilbert space of the problem is partitioned as described above into two orthogonal components, \mathcal{P} and \mathcal{Q} . The first of these, \mathcal{P} , will contain the prompt channels; the other, \mathcal{Q} , the closed channels, the exact nature of the partition depending on the physics of the reaction being considered, as described above. The projection operators P and Q project onto the subspace \mathcal{P} and \mathcal{Q} , respectively, and satisfy

$$\begin{aligned} P &= P^\dagger & Q &= Q^\dagger \\ P^2 &= P & Q^2 &= Q \\ P + Q &= 1 \end{aligned} \tag{2.1}$$

The state vector of the system, Ψ , satisfies the Schrödinger equation

$$(E - H)\Psi = 0 \tag{2.2}$$

We can now determine the equation satisfied by the prompt component of Ψ , $P\Psi$, and the time-delaying component, $Q\Psi$. Writing

$$\Psi = P\Psi + Q\Psi$$

and multiplying (2.2) from the left by P and Q yields

$$(E - H_{PP})(P\Psi) = H_{PQ}(Q\Psi) \tag{2.3}$$

and

$$(E - H_{QQ})(Q\Psi) = H_{QP}(P\Psi) \quad (2.4)$$

where

$$H_{PP} \equiv PHP, \quad H_{PQ} \equiv PHQ, \quad \text{etc.}$$

If we write

$$H = H_0 + V$$

where H_0 is the sum of the Hamiltonians for the internal degrees of freedom of the projectile and target and the kinetic energy operator for their relative motion. It is usual to restrict the class of projection operators to those for which

$$H_{PQ} = V_{PQ} \quad H_{QP} = V_{QP}$$

The analogy of (2.3) and (2.4) with (1.3) of Section 1 is rather clear. Whereas in the latter case \mathcal{P} and \mathcal{Q} contain only one component $(1/r)u_0\psi_0$ and $(1/r)u_1\psi_1$, respectively, the more general case of (2.3) and (2.4) will contain many components.

This simple partition can be used to obtain some quite general results. We can formally solve (2.4) as follows:

$$Q\Psi = \frac{1}{E^{(+)} - H_{QQ}} H_{QP} P\Psi \quad (2.5)$$

This expression includes the boundary condition that there is no incident wave in the subspace \mathcal{Q} . The $i\eta$ in $E^{(+)} = E + i\eta$, $\eta \rightarrow 0^+$, is included in case some of the open channels are in \mathcal{Q} . Substituting (2.5) in (2.3) yields

$$(E - H_{\text{eff}})P\Psi = 0 \quad (2.6)$$

where

$$H_{\text{eff}} = H_{PP} + H_{PQ} \frac{1}{E^{(+)} - H_{QQ}} H_{QP} \quad (2.7)$$

The first term on the right-hand side, H_{PP} , is associated with the prompt process. The second term describes the time-delaying effect of coupling \mathcal{P} space with \mathcal{Q} , propagation in \mathcal{Q} as given by $1/(E^{(+)} - H_{QQ})$ and then reemission into \mathcal{P} . The Schrödinger equation (2.6) iterates this process.

Problem. Referring to the discussion in deShalit and Feshbach (74, p. 648), show that \mathcal{H}_{eff} , where

$$H_{\text{eff}} = P\mathcal{H}_{\text{eff}}P$$

satisfies the integral equation

$$\mathcal{H}_{\text{eff}} = H + HQ \frac{1}{E^{(+)} - H_0} Q \mathcal{H}_{\text{eff}} \quad (2.8)$$

We see that H_{eff} is energy dependent, complex, and nonlocal. These properties are consequences of the presence of the propagator $1/(E^{+} - H_{QQ})$. Because of this, there is a dispersion-type relationship between the real and imaginary parts of \mathcal{H}_{eff} . To derive this result most simply, we express $H_{\text{eff}} - H_{PP}$ in terms of the eigenstates of the operator H_{QQ} . This operator will generally have bound eigenstates whose eigenvalues form a discrete spectrum, and unbound eigenstates whose eigenvalues form a continuous spectrum. Hence

$$\begin{aligned} H_{QQ}\Phi_s &= \mathcal{E}_s\Phi_s \quad (\text{discrete}) \\ H_{QQ}\Phi(\mathcal{E}, \alpha) &= \mathcal{E}\Phi(\mathcal{E}, \alpha) \end{aligned} \quad (2.9)$$

where α is an index which together with \mathcal{E} specifies the continuum state. These state vectors are assumed to be normalized and therefore form an orthonormal set:

$$\begin{aligned} \langle \Phi_s | \Phi_{s'} \rangle &= \delta_{ss'} & \langle \Phi_s | \Phi(\mathcal{E}, \alpha) \rangle &= 0 \\ \langle \Phi(\mathcal{E}', \alpha') | \Phi(\mathcal{E}, \alpha) \rangle &= \delta(\mathcal{E}' - \mathcal{E})\delta(\alpha - \alpha') \end{aligned}$$

Then

$$H_{\text{eff}} - H_{PP} = \sum_s \frac{H_{PQ}\Phi_s \rangle \langle \Phi_s H_{QP}}{E - \mathcal{E}_s} + \int d\alpha \int d\mathcal{E} \frac{H_{PQ}\Phi(\mathcal{E}, \alpha) \rangle \langle \Phi(\mathcal{E}, \alpha) H_{QP}}{E^{(+)} - \mathcal{E}} \quad (2.10)$$

Using the result

$$\frac{1}{E^{(+)} - \mathcal{E}} = \frac{\mathcal{P}}{E - \mathcal{E}} - i\pi\delta(E - \mathcal{E})$$

where \mathcal{P} indicates that the principal value integration should be taken and $\delta(E - \mathcal{E})$ is the Dirac delta function, we obtain

$$\text{Re}(H_{\text{eff}} - H_{PP}) = \sum_s \frac{H_{PQ}\Phi_s \rangle \langle \Phi_s H_{QP}}{E - \mathcal{E}_s} + \mathcal{P} \int \frac{d\mathcal{E}}{E - \mathcal{E}} \int d\alpha H_{PQ}\Phi(\mathcal{E}, \alpha) \rangle \langle \Phi(\mathcal{E}, \alpha) H_{QP} \quad (2.11a)$$

while

$$\text{Im}(H_{\text{eff}} - H_{PP}) = -\pi \int d\alpha H_{PQ}\Phi(\mathcal{E}, \alpha) \rangle \langle \Phi(\mathcal{E}, \alpha) H_{QP} \quad (2.11b)$$

Note that this operator is negative definite, as it must be to represent a decrease in flux in the prompt channels because of the presence of open channels in \mathcal{Q} space. Substituting (2.11b) into (2.11a) yields

$$\operatorname{Re} H_{\text{eff}} = H_{PP} + \sum_s \frac{H_{PQ}\Phi_s \langle \Phi_s | H_{QP} \rangle}{E - \mathcal{E}_s} - \frac{1}{\pi} \mathcal{P} \int \frac{d\mathcal{E}}{E - \mathcal{E}} \operatorname{Im} H_{\text{eff}}(\mathcal{E}) \quad (2.12)$$

where it is assumed that H_{PP} is real, as is usually the case.

Problem. Show that (2.12) can also be written

$$\operatorname{Re} V_{\text{eff}} = V_{PP} + \sum_s \frac{V_{PQ}\Phi_s \langle \Phi_s | V_{QP} \rangle}{E - \mathcal{E}_s} - \frac{1}{\pi} \mathcal{P} \int \frac{d\mathcal{E}}{E - \mathcal{E}} \operatorname{Im} V_{\text{eff}}(\mathcal{E}) \quad (2.13)$$

This result is the nuclear analog of the Kronig–Kramers relation between the real and imaginary parts of the index of refraction for light (see Fig. 1.4) propagating through an infinite medium. For an infinite nuclear medium there are no significant closed channels at low excitation energies, so that the second term on the right-hand side of (2.13) is essentially zero. However, at energies that permit the excitation of isobars, this term could be appreciable.

We turn next to resonances. Recall from the simple example of the preceding section [see (1.3) et seq.] that resonances are associated with the bound states of the time-delaying component of the wave function. In the present context, this is $Q\Psi$. The bound states are now given by Φ_s , with energies \mathcal{E}_s . As one can see from (2.10) for H_{eff} , rapid energy dependence of H_{eff} will occur near \mathcal{E}_s , and one would predict that rapid energy dependence and therefore a long time delay will occur for $E \simeq \mathcal{E}_s$. For E near \mathcal{E}_s , H_{eff} can be written

$$H_{\text{eff}} = \bar{H}_{PP} + \frac{H_{PQ}\Phi_s \langle \Phi_s | H_{QP} \rangle}{E - \mathcal{E}_s} \quad (2.14)$$

where all the remaining terms in the expansion (2.10) have been grouped together to form \bar{H}_{PP} , which will be assumed to have a slow energy dependence near \mathcal{E}_s . We shall see what this means after examining its consequences. Equation (2.14) is equivalent to the partition in which \mathcal{Q} contains only one state Φ_s .

The Schrödinger equation (2.6) becomes

$$(E - \bar{H}_{PP})(P\Psi) = \frac{H_{PQ}\Phi_s \langle \Phi_s | H_{QP} P\Psi \rangle}{E - \mathcal{E}_s}$$

Its formal solution is given by

$$P\Psi = \chi_i^{(+)} + \frac{1}{E^{(+)} - \bar{H}_{PP}} \frac{H_{PQ}\Phi_s \langle \Phi_s | H_{QP} P\Psi \rangle}{E - \mathcal{E}_s} \quad (2.15)$$

where $\chi_i^{(+)}$, the distorted incident wave, is the solution of

$$(E - \bar{H}_{PP})\chi_i^{(+)} = 0$$

satisfying the outgoing wave boundary condition. The \mathcal{T} matrix giving the transition amplitude is

$$\mathcal{T}_{fi} = \mathcal{T}_{fi}^{(P)} + \frac{\langle \chi_f^{(-)} | H_{PQ} \Phi_s \rangle \langle \Phi_s | H_{QP} P \Psi \rangle}{E - \mathcal{E}_s} \quad (2.16)$$

where $\mathcal{T}_{fi}^{(P)}$ is the prompt direct amplitude associated with the first term of (2.15), and $\chi_f^{(-)}$ is the solution

$$(E - \bar{H}_{PP})\chi_f^{(-)*} = 0$$

describing the final amplitude satisfying incoming wave boundary conditions. Returning to (2.15), multiply both sides by $\langle \Phi_s | H_{QP}$, yielding

$$\langle \Phi_s | H_{QP} P \Psi \rangle = \langle \Phi_s | H_{QP} \chi_i^{(+)} \rangle + \frac{\langle \Phi_s | W_{QQ} \Phi_s \rangle \langle \Phi_s | H_{QP} P \Psi \rangle}{E - \mathcal{E}_s}$$

where

$$W_{QQ} \equiv H_{QP} \frac{1}{E^{(+)} - \bar{H}_{PP}} H_{PQ} \quad (2.17)$$

Solving for $\langle \Phi_s | H_{QP} P \Psi \rangle$, one obtains

$$\langle \Phi_s | H_{QP} P \Psi \rangle = \frac{(E - \mathcal{E}_s) \langle \Phi_s | H_{QP} \chi_i^{(+)} \rangle}{E - \mathcal{E}_s - \langle \Phi_s | W_{QQ} \Phi_s \rangle}$$

Inserting this result in (2.16) yields

$$\mathcal{T}_{fi} = \mathcal{T}_{fi}^{(P)} + \frac{\langle \chi_f^{(-)} | H_{PQ} \Phi_s \rangle \langle \Phi_s | H_{QP} \chi_i^{(+)} \rangle}{E - \mathcal{E}_s - \langle \Phi_s | W_{QQ} \Phi_s \rangle} \quad (2.18)$$

This is a typical resonance formula. As expected, the resonance occurs near \mathcal{E}_s . There is an energy shift and a width that are given by the expectation value of W_{QQ} :

$$\langle \Phi_s | W_{QQ} \Phi_s \rangle = \Delta_s(E) - \frac{1}{2} i \Gamma_s(E) \quad (2.19)$$

so that

$$\mathcal{T}_{fi} = \mathcal{T}_{fi}^{(P)} + \frac{\langle \chi_f^{(-)} | H_{PQ} \Phi_s \rangle \langle \Phi_s | H_{QP} \chi_i^{(+)} \rangle}{E - E_s + (i/2)\Gamma_s} \quad (2.20)$$

Note that E_s and Γ_s are functions of E . The statement that E_s is the resonance energy assumes that their energy dependence is weak. Inserting W_{QQ} from (2.17) into (2.19) provides more explicit expressions for Δ_s and Γ_s :

$$\begin{aligned} \langle \Phi_s | W_{QQ} \Phi_s \rangle &= \left\langle \Phi_s \left| H_{QP} \frac{1}{E^{(+)} - \bar{H}_{PP}} H_{PQ} \Phi_s \right. \right\rangle \\ &= \left\langle \Phi_s \left| H_{QP} \frac{\mathcal{P}}{E - \bar{H}_{PP}} H_{PQ} \Phi_s \right. \right\rangle - i\pi \langle \Phi_s | H_{QP} \delta(E - \bar{H}_{PP}) H_{PQ} \Phi_s \rangle \end{aligned}$$

Comparing with (2.19), we see that

$$\Gamma_s = 2\pi \langle \Phi_s | H_{QP} \delta(E - \bar{H}_{PP}) H_{PQ} \Phi_s \rangle \quad (2.21)$$

Introducing a complete set of states $\chi_r^{(+)}$ of the Hamiltonian \bar{H}_{PP} at the energy E , one obtains

$$\Gamma_s = 2\pi \sum_r |\langle \Phi_s | H_{QP} \chi_r^{(+)} \rangle|^2 \equiv \sum \Gamma_{sr}(E) \quad (2.22)$$

The width Γ_s is thus the sum of *partial widths* Γ_{sr} corresponding to the decay of the state Φ_s into various possible channels with the same value of the energy E . The numerator of the resonance term in (2.20) is obviously related to these partial widths:

$$\begin{aligned} \langle \Phi_s | H_{QP} \chi_i^{(+)} \rangle &= e^{i\delta_i} \sqrt{\frac{\Gamma_{si}}{2\pi}} \equiv e^{i\delta_i} \frac{g_{si}}{\sqrt{2\pi}} \\ \langle \chi_f^{(-)} | H_{PQ} \Phi_s \rangle &= e^{i\delta_f} \sqrt{\frac{\Gamma_{sf}}{2\pi}} \equiv \frac{e^{i\delta_f} g_{sf}}{\sqrt{2\pi}} \end{aligned} \quad (2.23)$$

where δ_i gives the phase of $\chi_i^{(+)}$, that is,

$$\chi_i^{(+)} = e^{i\delta_i} F_i \quad (2.24)$$

where F_i is real. Since Φ_s is a bound-state wave function, it can be taken as real. These results, (2.22) and (2.23), upon insertion into (2.20), yield the familiar

Breit–Wigner formula[†]

$$\mathcal{T}_{fi} = \mathcal{T}_{fi}^{(P)} + \frac{1}{2\pi} e^{i(\delta_i + \delta_f)} \frac{g_{sf} g_{si}}{E - E_s + \frac{1}{2} i \Gamma_s} \quad (2.25)$$

Further properties of Γ_{sr} will be discussed later (see p. 242).

The subscript s represents all the quantum numbers required to specify the bound state Φ_s . These will certainly include its total angular momentum J and its parity Π . The resonance therefore contributes to a particular partial wave, while the prompt, direct amplitude $\mathcal{T}_{fi}^{(P)}$ will generally involve several partial waves.

Problem. Show that

$$\Delta_s = \frac{1}{2\pi} \mathcal{P} \int \frac{dE' \Gamma_s(E')}{E - E'}$$

Show that

$$\sum_s \Gamma_s = 2\pi \sum_r \langle \chi_r^{(+)} | (H - \bar{H}_{pp})^2 | \chi_r^{(+)} \rangle$$

This one resonance + direct amplitude description is exact. It is not, however, useful if the direct amplitude $\mathcal{T}_{fi}^{(P)}$ and therefore $E_s(E)$ and $\Gamma_s(E)$ vary rapidly with energy E near E_s . Generally, if the resonances arising from the bound states at \mathcal{E}_s are well separated, the direct amplitude is observed to vary slowly with energy. However, if the separation in energy D between neighboring \mathcal{E}_s is on the order or less than Γ_s , it would be necessary to remove a group of resonances in, say, an energy interval d , before the direct amplitude would become relatively constant over the energy region in the center of d . The resonances are then said to *overlap*. The formalism developed above can readily

[†]Equation (2.24) assumes that $\chi_i^{(+)}$ and $\chi_f^{(-)}$ are eigenstates of S_p , the S matrix associated with \bar{H}_{pp} , with eigenvalues $e^{2i\delta_i}$ and $e^{2i\delta_f}$, respectively. However, if they are solutions of coupled equations, that is, if the prompt space contains more than one channel, as will occur if direct inelastic or transfer reactions are energetically allowed, that will no longer be the case. It is then necessary to introduce the real orthogonal transformation M_{ia} , which connects an eigenfunction of S_p , χ_a with eigenvalues $e^{2i\Delta_a}$, with an open-channel distorted plane wave such as $\chi_i^{(+)}$. This transformation is obtained in the course of solving the prompt problem. Then (2.25) is replaced by

$$\mathcal{T}_{fi} = \sum M_{af} \left[\frac{1}{2\pi i} (1 - e^{2i\Delta_a}) \delta_{a\beta} + \frac{e^{i(\Delta_a + \Delta\beta)}}{2\pi} \frac{g_{sa} g_{s\beta}}{E - E_s + \frac{1}{2} i \Gamma_s} \right] M_{\beta i} \quad (2.26)$$

where g_{sa} gives the magnitude of $\langle \Phi_s | H_{qp} \chi_a \rangle$. Results (2.26) holds in the DWA approximation, or when only one channel is open. We shall refer to the latter as the single-channel case.

be extended to include this case [Feshbach (58,62)]. However, it will be convenient and instructive to use a different but equivalent approach.

We begin with the general expression that follows from (2.3) and the two-potential theorem:

$$\mathcal{T}_{fi} = \mathcal{T}_{fi}^{(P)} + \langle \chi_f^{(-)} | H_{PQ} Q \Psi_i \rangle \quad (2.27)$$

where we have inserted the subscript i on Ψ to indicate that it is the Ψ developed by the incident wave $\chi_i^{(+)}$. The exact expression for $Q\Psi_i$ can be obtained as follows: Solve (2.3) for $P\Psi_i$:

$$P\Psi_i = \chi_i^{(+)} + \frac{1}{E^{(+)} - H_{PP}} H_{PQ} Q\Psi_i \quad (2.27')$$

Substituting this result into (2.4) yields the inhomogeneous equation

$$(E - H_{QQ} - W_{QQ}) Q\Psi_i = H_{QP} \chi_i^{(+)} \quad (2.28)$$

where W_{QQ} is now given by

$$W_{QQ} \equiv H_{QP} \frac{1}{E^{(+)} - H_{PP}} H_{PQ} \quad (2.29)$$

Solving (2.28), one obtains

$$Q\Psi_i = \frac{1}{E - H_{QQ} - W_{QQ}} H_{QP} \chi_i^{(+)} \quad (2.30)$$

so that \mathcal{T}_{fi} becomes

$$\mathcal{T}_{fi} = \mathcal{T}_{fi}^{(P)} + \left\langle \chi_f^{(-)} \left| H_{PQ} \frac{1}{E - H_{QQ} - W_{QQ}} H_{QP} \chi_i^{(+)} \right. \right\rangle \quad (2.30')$$

The second term gives explicitly the time-delayed component that is generated by the coupling of the \mathcal{P} space to the \mathcal{Q} space. Its explicit energy dependence, as given by the propagator $[1/(E - H_{QQ} - W_{QQ})]$, can be rapid when E is near a pole of the propagator.

One can recover the result of (2.18) if \mathcal{Q} space contains only one state Φ_s satisfying (2.9). Then

$$\begin{aligned} \frac{1}{E - H_{QQ} - W_{QQ}} &= \Phi_s \left\langle \Phi_s \left| \frac{1}{E - H_{QQ} - W_{QQ}} \Phi_s \right. \right\rangle \langle \Phi_s | \\ &= \Phi_s \left\langle \frac{1}{E - \langle \Phi_s | (H_{QQ} + W_{QQ}) \Phi_s \rangle} \Phi_s \right\rangle \langle \Phi_s = \Phi_s | \frac{1}{E - \mathcal{E}_s - \Delta_s + \frac{1}{2}i\Gamma_s} \Phi_s \rangle \end{aligned}$$

where (2.19) has been used. Upon inserting this last result into (2.30'), one again obtains the Breit–Wigner formula, (2.20).

The extension of this procedure to the case of several overlapping resonances is straightforward. We simply expand \mathcal{Q} space to include just the requisite number of bound states Φ_s . That number is determined by the requirement that the energy dependence of the amplitude generated by H_{PP} in the energy interval of interest is sufficiently slow. One can then obtain the eigenvalues of the operator $H_{QQ} + W_{QQ}$ by solving the secular equation

$$\det |(E_\mu - \mathcal{E}_s)\delta_{st} - W_{st}| = 0 \quad (2.31)$$

where

$$W_{st} \equiv \langle \Phi_s | W_{QQ} | \Phi_t \rangle = \left\langle \Phi_s \left| H_{QP} \frac{1}{E^{(+)} - H_{PP}} H_{PQ} \right| \Phi_t \right\rangle \quad (2.32)$$

The eigenvalues E_μ are complex, since W_{st} is not Hermitian. The result for the isolated resonance is obtained immediately if the determinant has only one term. The eigenfunctions of $H_{QQ} + W_{QQ}$, Ω_μ , are finite linear combinations of the bound-state wave functions Φ_s which have been included in \mathcal{Q} :

$$\Omega_\mu = \sum x_s^{(\mu)} \Phi_s$$

The functions Ω_μ form a biorthogonal set with the adjoint functions $\Omega_\mu^{(A)}$:

$$\langle \Omega_\mu^{(A)} | \Omega_\nu \rangle = \delta_{\mu\nu}$$

The coefficients $x_s^{(\mu)}$ satisfy the set of linear equations

$$\sum_t [(E_\mu - \mathcal{E}_s)\delta_{st} - W_{st}] x_t^{(\mu)} = 0$$

while the corresponding coefficient for $\Omega_\nu^{(A)}$, $\tilde{x}_s^{(\nu)}$ satisfies

$$\sum_s \tilde{x}_s^{(\nu)} [(E_\mu - \mathcal{E}_s)\delta_{st} - W_{st}] = 0$$

With these results in hand it is now a simple matter to expand $1/(E - H_{QQ} - W_{QQ})$ in terms of Ω_μ and so finally obtain

$$\mathcal{T}_{fi} = \mathcal{T}_{fi}^{(P)} + \sum_\mu \frac{A_{fi}^{(\mu)}}{E - E_\mu} \quad (2.33)$$

where

$$A_{fi}^{(\mu)} = \langle \chi_f^{(-)} | H_{PQ} \Omega_\mu \rangle \langle \Omega_\mu^{(A)} | H_{QP} \chi_i^{(+)} \rangle \quad (2.34)$$

Note that the $A_{fi}^{(\mu)}$ are complex and that

$$\sum_{\mu} A_{fi}^{(\mu)} = \sum_r \langle \chi_f^{(-)} | H_{PQ} \Phi_s \rangle \langle \Phi_s | H_{QP} \chi_i^{(+)} \rangle \quad (2.35)$$

where the completeness of Φ_s has been used.

Let us for simplicity again consider a single channel, so that

$$\chi_f^{(-)} = e^{-2i\delta} \chi_i^{(+)}$$

Then

$$\sum_{\mu} A_{fi}^{(\mu)} = e^{2i\delta} \sum_s |\langle \chi_i^{(+)} | H_{PQ} \Phi_s \rangle|^2 \quad (2.36)$$

The $A^{(\mu)}$ and E_{μ} are not independent. For example, the diagonal sum rule when applied to the secular equation (2.31) yields

$$\sum_{\mu} \text{Im } E_{\mu} = \sum_s \text{Im } W_{ss}$$

Inserting the value of W_{ss} and making use of (2.36), one obtains

$$\sum_{\mu} A_{fi}^{(\mu)} = -\frac{1}{\pi} e^{2i\delta} \sum_{\mu} \text{Im } E_{\mu} \quad (2.37)$$

For isolated resonances this equality holds for each individual μ , thus reducing to (2.22), which states that the total width ($\equiv -2 \text{Im } E^{(\mu)}$) equals the sum of the partial widths that appear in the numerator of the resonance amplitude. Equation (2.37) states that this equality holds on the average, that is,

$$2\pi \sum_s |\langle \chi_i^{(+)} | H_{PQ} \Phi_s \rangle|^2 = -2 \sum_{\mu} \text{Im } E_{\mu} \quad (2.38)$$

Other relationships, such as (2.37), may be obtained from the properties of the secular equation (2.31).

Because of the relationships between $A^{(\mu)}$ and E_{μ} , the number of independent real numbers required to describe the resonance term in (2.33) is not as large as might appear. Without these connections each term involves two complex numbers, $A_{fi}^{(\mu)}$ and $E^{(\mu)}$, or four real numbers. We shall shortly derive a more economical expression in which this number of real parameters is reduced by one-half.

It is instructive at this point to show that relationship (2.37) is a consequence of the unitarity of the S matrix. For this purpose it will suffice to develop this relation for single-channel elastic scattering. Then

$$\mathcal{T} = \mathcal{T}_p + \sum_{\mu} \frac{A^{(\mu)}}{E - E_{\mu}}$$

From

$$S = 1 - 2\pi i \mathcal{T}$$

one obtains

$$S = S_p - 2\pi i \sum \frac{A^{(\mu)}}{E - E_\mu}$$

where S_p is the S matrix for the prompt process. It is convenient to introduce $\mathcal{A}^{(\mu)}$, which is defined by

$$A^{(\mu)} = S_p \mathcal{A}^{(\mu)}$$

Hence

$$S = S_p \left[1 - 2\pi i \sum \frac{\mathcal{A}^{(\mu)}}{E - E_\mu} \right]$$

To avoid obfuscating complications, consider the simple case of just two resonances,

$$\begin{aligned} S &= S_p \left[1 - 2\pi i \left(\frac{\mathcal{A}_1}{E - E_1} + \frac{\mathcal{A}_2}{E - E_2} \right) \right] \\ &= S_p \left[\frac{(E - E_1)(E - E_2) - 2\pi i \mathcal{A}_1(E - E_2) - 2\pi i \mathcal{A}_2(E - E_1)}{(E - E_1)(E - E_2)} \right] \end{aligned}$$

Unitarity, $SS^\dagger = 1$, requires that

$$(E - E_1)(E - E_2) - 2\pi i \mathcal{A}_1(E - E_2) - 2\pi i \mathcal{A}_2(E - E_1) = e^{i\lambda(E - E_1^*)(E - E_2^*)}$$

where the phase λ is to be determined. Equating coefficients of E^2 on both sides of the last equation gives $\lambda = 0$, while equating the coefficients of E yields

$$E_1 + E_2 + 2\pi i(\mathcal{A}_1 + \mathcal{A}_2) = E_1^* + E_2^*$$

so that

$$\mathcal{A}_1 + \mathcal{A}_2 = \frac{1}{\pi} (\text{Im } E_1 + \text{Im } E_2)$$

or

$$A_1 + A_2 = -\frac{1}{\pi} S_p (\text{Im } E_1 + \text{Im } E_2)$$

in agreement with (2.37).

Problem. Consider the case where several resonances contribute.

It is clear that many other relationships can be obtained by comparing coefficients of still lower powers of E . Not all of these relationships are

independent. It thus becomes important to determine the number of independent constants appearing (2.33).

The \mathcal{K} Reactance Matrix (Feshbach (67a)). Consider (2.28) once more, where, it is to be recalled, \mathcal{Q} space contains a finite number of bound states Φ_s . Expressing W_{QQ} more explicitly, (2.28) becomes

$$\left(E - H_{QQ} - H_{QP} \frac{\mathcal{P}}{E - H_{PP}} H_{PQ} \right) Q\Psi + i\pi \sum_{\gamma} H_{QP} \chi_{\gamma}^{(+)} \langle \chi_{\gamma}^{(+)} | H_{PQ} Q\Psi \rangle = H_{QP} \chi_i^{(+)} \quad (2.39)$$

where γ designates those open channels whose energy equals the initial energy, E . The wave functions for the incident state $\chi_i^{(+)}$ belong to the set $\chi_{\gamma}^{(+)}$, while $\chi_f^{(-)}$ belongs to a corresponding set of states $\chi_{\gamma}^{(-)}$. To simplify the formal manipulations it is useful to introduce the projection operator O :

$$O \equiv \sum_{\gamma} \chi_{\gamma}^{(+)} \langle \chi_{\gamma}^{(+)} | = \sum_{\gamma} \chi_{\gamma}^{(-)} \langle \chi_{\gamma}^{(-)} | \quad (2.40)$$

with

$$O^2 = 0 \quad OQ = 0$$

Also, let

$$H_{QQ} + H_{QP} \frac{\mathcal{P}}{E - H_{PP}} H_{PQ} \equiv \mathcal{K}_{QQ}$$

so that (2.39) becomes

$$(E - \mathcal{K}_{QQ})Q\Psi + i\pi H_{QO} H_{OQ} Q\Psi = H_{QO} \chi_i^{(+)} \quad (2.41)$$

where

$$H_{OQ} \equiv OHQ$$

From (2.41)

$$Q\Psi = \frac{1}{E - \mathcal{K}_{QQ} + i\pi H_{QO} H_{OQ}} H_{QO} \chi_i^{(+)}$$

Note that

$$\begin{aligned} \frac{1}{E - \mathcal{K}_{QQ} + i\pi H_{QO} H_{OQ}} H_{QO} &= \frac{1}{1 + i\pi [1/(E - \mathcal{K}_{QQ})] H_{QO} H_{OQ}} \frac{1}{E - \mathcal{K}_{QQ}} H_{QO} \\ &= \frac{1}{E - \mathcal{K}_{QQ}} H_{QO} \frac{1}{1 + i\pi H_{OQ} [1/(E - \mathcal{K}_{QQ})] H_{QO}} \end{aligned}$$

where we have made use of the operator identities

$$\frac{1}{1+AB}A = A\frac{1}{1+BA} \quad \frac{1}{XY} = \frac{1}{Y} \frac{1}{X}$$

Inserting the resulting expression for $Q\Psi$ into (2.27) yields

$$\mathcal{T}_{fi} = \mathcal{T}_{fi}^{(P)} + \left\langle \chi_f^{(-)} \left| \frac{\mathcal{K}}{1 + i\pi\mathcal{K}} \chi_i^{(+)} \right. \right\rangle \quad (2.42)$$

where

$$\mathcal{K} \equiv H_{oQ} \frac{1}{E - \mathcal{H}_{QO}} H_{Qo} \quad (2.43)$$

Note that \mathcal{K} is a finite Hermitian matrix for real E . We also note that the S matrix

$$S = 1 - 2\pi i \mathcal{T} = S_P - \frac{2\pi i \mathcal{K}}{1 + i\pi\mathcal{K}}$$

or

$$S_{fi} = \langle \chi_f^{(-)} | \chi_i^{(+)} \rangle - \left\langle \chi_f^{(-)} \left| \frac{2\pi i \mathcal{K}}{1 + i\pi\mathcal{K}} \chi_i^{(+)} \right. \right\rangle$$

Finally,

$$S_{fi} = \left\langle \chi_f^{(-)} \left| \frac{1 - i\pi\mathcal{K}}{1 + i\pi\mathcal{K}} \chi_i^{(+)} \right. \right\rangle \quad (2.44)$$

The unitarity of the S matrix can be demonstrated from this result. Note, however, that it is not immediate, but requires the use of the relation between the distorted waves $\chi_i^{(+)}$, $\chi_f^{(-)}$ and the undistorted waves.

Problem. Prove the unitarity of S_{fi} of (2.44).

To obtain a resonance expansion of \mathcal{T} , we introduce the eigenvalues κ_μ and eigenfunctions of the operator \mathcal{K} , which is Hermitian when E is real:

$$\mathcal{K} Y_\mu = \kappa_\mu Y_\mu \quad (2.45)$$

The functions Y_μ form an orthonormal set. They are also eigenfunctions of \mathcal{S} where

$$\mathcal{S} = \frac{1 - i\pi\mathcal{K}}{1 + i\pi\mathcal{K}}$$

with eigenvalues $(1 - i\pi\kappa_\mu)/(1 + i\pi\kappa_\mu)$. If we write the eigenvalues of \mathcal{S} as $e^{2i\sigma_\mu}$, we find that

$$\tan \sigma_\mu = -\pi\kappa_\mu$$

It is possible to express κ_μ in terms of e_s , the eigenvalues of \mathcal{H}_{QQ} , with corresponding eigenstates Φ_s . We note that

$$\kappa_\mu = \langle Y_\mu | \mathcal{K} | Y_\mu \rangle = \left\langle Y_\mu \left| H_{OQ} \frac{1}{E - \mathcal{H}_{QQ}} H_{QO} \right| Y_\mu \right\rangle$$

or

$$\kappa_\mu = \sum_s \frac{|\langle Y_\mu | H_{OQ} \Phi_s \rangle|^2}{E - e_s}$$

Defining the widths

$$\gamma_{\mu s}^2 \equiv 2\pi |\langle Y_\mu | H_{OQ} \Phi_s \rangle|^2$$

we obtain finally[†]

$$\kappa_\mu = \frac{1}{2\pi} \sum_s \frac{\gamma_{\mu s}^2}{E - e_s} \quad (2.46)$$

Note that $\gamma_{\mu s}$ and e_s are energy independent if the projection operator Q is chosen to be fixed with energy.

The transition matrix is then given by

$$\mathcal{T}_{fi} = \mathcal{T}_{fi}^{(P)} + \sum_\mu \langle \chi_f^{(-)} | Y_\mu \rangle \frac{\kappa_\mu}{1 + i\pi\kappa_\mu} \langle Y_\mu | \chi_i^{(+)} \rangle \quad (2.47)$$

while

$$S_{fi} = \sum_\mu \langle \chi_f^{(-)} | Y_\mu \rangle \frac{1 - i\pi\kappa_\mu}{1 + i\pi\kappa_\mu} \langle Y_\mu | \chi_i^{(+)} \rangle = \sum_\mu \langle \chi_f^{(-)} | Y_\mu \rangle e^{2i\sigma_\mu} \langle Y_\mu | \chi_i^{(+)} \rangle \quad (2.48')$$

It is often convenient to work in a representation in which S is diagonal and project to the scattering states $\chi^{(\pm)}$, as given explicitly by (2.48'). In the single-channel case the potential S matrix, $\langle \chi_f^{(-)} | \chi_i^{(+)} \rangle$, and the full S matrix are diagonal simultaneously. The resonance energies are given by the poles of (2.48'), that is, when

$$1 + i\pi\kappa_\mu = 0$$

[†]Note that κ_μ is real for real E , with poles on the real axis with positive residues. However, κ_μ is not rigorously an R function in Wigner's terminology because e_s and Φ_s are functions of the energy.

or

$$1 + \frac{i}{2} \sum \frac{\gamma_{\mu s}^2}{E - e_s} = 0 \quad (2.48'')$$

For an isolated resonance, that is, e_s takes on only one value e_1 , this equation yields the resonance energy, $e_1 - i\gamma_{\mu 1}/2$. The shift Δ_s no longer appears because of the difference between H_{QQ} and \mathcal{H}_{QQ} . To compare the result directly with (2.23), consider the case where μ is restricted to one value; that is, we consider only a single channel. There is then only one $\kappa_\mu (\equiv \kappa)$, so that

$$\mathcal{T}_{fi} = \frac{1 - e^{2i\delta}}{2\pi i} + e^{2i\delta} \frac{\kappa}{1 + i\pi\kappa} \quad (2.48''')$$

and

$$S_{fi} = e^{2i\delta} \frac{1 - i\pi\kappa}{1 + i\pi\kappa} = e^{2i(\delta + \sigma)} \quad (2.49)$$

Assuming as an example that there are only two states Φ_1 and Φ_2 in \mathcal{Q} , (2.46) yields

$$\kappa = \frac{1}{2\pi} \left(\frac{\gamma_1^2}{E - e_1} + \frac{\gamma_2^2}{E - e_2} \right)$$

and

$$\frac{\kappa}{1 + i\pi\kappa} = \frac{1}{2\pi} \frac{\Gamma E - \Lambda}{(E - e_1)(E - e_2) + (i/2)(\Gamma E - \Lambda)} \quad (2.50)$$

where

$$\Gamma \equiv \gamma_1^2 + \gamma_2^2 \quad \Lambda = \gamma_1 e_2 + \gamma_2 e_1$$

Equation (2.50) involves only four real numbers, while the resonance series (2.33) for two resonances would involve apparently four complex numbers for the single-channel case. However, as (2.50) demonstrates, there must be two independent relations between these constants. One of these is given by (2.38). The others can be derived either from the properties of the secular equation (2.31) or from the unitarity condition [see Levin and Feshbach (73)].

3. DERIVATION OF THE OPTICAL MODEL POTENTIAL

The optical model potential as originally defined [Feshbach, Porter, and Weisskopf (54)] is that single-channel potential which would generate the energy average of the elastic scattering amplitude (or the transition amplitude). The

energy average was to be taken over a domain, ΔE , which is large compared to both the width Γ of the individual resonances or fluctuations in the cross section as well as their spacing D . On the other hand, ΔE should be small compared to energies Γ_{SP} over which the potential scattering amplitude varies considerably. For nuclear potentials Γ_{SP} is of the order of several MeV, which is to be compared with the width of compound nuclear resonances, which can extend from fractions of an eV to a few hundred kilovolts.

In the context of the formalism of this chapter, the energy averaging of the transition amplitude is equivalent to an energy average of $P\Psi$, since \mathcal{P} contains the incident channel and therefore $\mathcal{T}_{fi}^{(P)}$ contains the elastic scattering amplitude. \mathcal{P} can, of course, contain all the prompt channels, so that the analysis which follows will generalize the optical model to include these prompt processes, such as the single- and multistep direct reactions.

This result for $\langle P\Psi \rangle$ can be seen directly from (2.27'), which can be written as follows:

$$P\Psi_i = \chi_i^{(+)} + \frac{1}{E^{(+)} - H_{PP}} H_{PQ} Q\Psi_i \quad (3.1)$$

Averaging both sides according to conditions outlined in the preceding paragraph yields

$$\langle P\Psi_i \rangle = \chi_i^{(+)} + \frac{1}{E^{(+)} - H_{PP}} H_{PQ} \langle Q\Psi_i \rangle \quad (3.2)$$

since the only quantity on the right side that varies with energy rapidly enough to be changed by the averaging procedure is $Q\Psi$. The transition amplitude generated by (3.2) is clearly the energy average of that generated by (3.1), as can be seen from (2.27):

$$\mathcal{T}_{fi} = \mathcal{T}_{fi}^{(P)} + \langle \chi_f^{(-)} | H_{PQ} Q\Psi_i \rangle$$

Upon averaging this quantity, one obtains

$$\langle \mathcal{T}_{fi} \rangle = \mathcal{T}_{fi}^{(P)} + \langle \chi_f^{(-)} | H_{PQ} \langle Q\Psi_i \rangle \rangle \quad (3.3)$$

To determine the optical model potential it is necessary to determine the Schrödinger equation satisfied by $\langle P\Psi \rangle$. Toward this end, we replace $Q\Psi$ in (3.2) by the result, (2.30), obtaining

$$\langle P\Psi_i \rangle = \chi_i^{(+)} + \frac{1}{E^{(+)} - H_{PP}} H_{PQ} \left\langle \frac{1}{e_{QQ}} \right\rangle H_{QP} \chi_i^{(+)} \quad (3.4)$$

where

$$e_{QQ} = E - H_{QQ} - W_{QQ} \quad (3.5)$$

Operating on both sides of (3.4) with $E^{(+)} - H_{PP}$ yields

$$(E - H_{PP})\langle P\Psi_i \rangle = H_{PQ} \left\langle \frac{1}{e_{QQ}} \right\rangle H_{QP} \chi_i^{(+)} \quad (3.6)$$

This could have been directly obtained from (2.3) since it leads directly to

$$(E - H_{PP})\langle P\Psi_i \rangle = H_{PQ} \langle Q\Psi_i \rangle \quad (3.7)$$

We now replace $\chi_i^{(+)}$ in favor of $\langle P\Psi \rangle$ by solving (3.4):

$$\chi_i^{(+)} = \frac{1}{1 + [1/(E^{(+)} - H_{PP})] H_{PQ} \langle 1/e_{QQ} \rangle H_{QP}} \langle P\Psi_i \rangle \quad (3.7')$$

so that (3.6) becomes

$$(E - H_{PP})\langle P\Psi_i \rangle = H_{PQ} \left\langle \frac{1}{e_{QQ}} \right\rangle H_{QP} \frac{1}{1 + [1/(E^{(+)} - H_{PP})] H_{PQ} \langle 1/e_{QQ} \rangle H_{QP}} \langle P\Psi_i \rangle \quad (3.7'')$$

Using the operator identity

$$B \frac{1}{1 + CAB} = \frac{1}{1 + BCA} B$$

with

$$A = \left\langle \frac{1}{e_{QQ}} \right\rangle, \quad B = H_{QP}, \quad \text{and} \quad C = \frac{1}{E^{(+)} - H_{PP}} H_{PQ}$$

one obtains

$$\begin{aligned} (E - H_{PP})\langle P\Psi_i \rangle &= H_{PQ} \left\langle \frac{1}{e_{QQ}} \right\rangle \frac{1}{1 + H_{QP} [1/(E^{(+)} - H_{PP})] H_{PQ} \langle 1/e_{QQ} \rangle} H_{QP} \langle P\Psi_i \rangle \\ &= H_{PQ} \left\langle \frac{1}{e_{QQ}} \right\rangle \frac{1}{1 + W_{QQ} \langle 1/e_{QQ} \rangle} H_{QP} \langle P\Psi_i \rangle \end{aligned}$$

Therefore, the optical model equation for $\langle P\Psi \rangle$ is

$$\left[E - H_{PP} - H_{PQ} \frac{1}{\langle 1/e_{QQ} \rangle^{-1} + W_{QQ}} H_{QP} \right] \langle P\Psi_i \rangle = 0 \quad (3.8)$$

The optical Hamiltonian is therefore

$$H_{\text{opt}} = H_{PP} + H_{PQ} \frac{1}{\langle 1/e_{QQ} \rangle^{-1} + W_{QQ}} H_{QP} \quad (3.9)$$

If $\langle 1/e_{QQ} \rangle$ were replaced by $1/e_{QQ}$, (3.9) would return to the exact form (2.7).

The term $\langle 1/e_{QQ} \rangle$ represents in an average way the impact of the omitted channels in \mathcal{Q} . Obviously, the value depends greatly on the choice of the states to be in \mathcal{P} , which should be made according to the physics of the situation being considered. Choosing only the elastic channel to be in \mathcal{P} throws all the effects of the other prompt channels into $\langle 1/e_{QQ} \rangle$. This may be what is needed if only elastic scattering and total cross section are of interest. If prompt channels exist and are included in \mathcal{P} , (3.8) becomes a set of coupled equations with complex diagonal and coupling potentials. It should not be surprising that the diagonal component of the optical potential for the elastic channel differs from that of the optical potential obtained by restricting \mathcal{P} to the elastic channel. As we shall see, H_{opt} is absorptive. As might be anticipated, the absorption is larger for the single-channel \mathcal{P} space since it must contain the effects of the channels that have been placed in \mathcal{Q} .

The reader should note that the optical model potential described in this section differs from the optical model potential derived in Chapter II. The latter is obtained by the multiple scattering approximation valid in the limit of high energies and short wavelengths. The optical model potential of this chapter is a consequence of energy averaging the fine-structure resonance. As a consequence of the averaging process, detailed information (e.g., regarding the resonances) cannot be obtained from the optical model potential and its wave function.

Averaging. It now remains to evaluate $\langle 1/e_{QQ} \rangle$. The average of any function $F(E)$ is given in terms of a normalized density $\rho(E, E_0)$ as follows:

$$\langle F(E) \rangle = \int \rho(E, E_0) F(E_0) dE_0 \quad (3.10)$$

where

$$\int \rho(E, E_0) dE_0 = 1$$

Therefore,

$$\left\langle \frac{1}{e_{QQ}} \right\rangle = \int \rho(E, E_0) \frac{1}{E_0 - H_{QQ} - W_{QQ}} dE_0 \quad (3.11)$$

Note that W_{QQ} is a function of energy but a slowly varying one, so that the only energy dependence we need to consider is the explicit one. It should be

recalled that $1/e_{QQ}$ varies rapidly with energy because of its complex poles, that is, because of resonances or fluctuations.

Two forms of $\rho(E, E_0)$ are in common use:

$$\rho(E, E_0) = \frac{\Delta}{2\pi} \frac{1}{(E - E_0)^2 + (\Delta/2)^2} \quad \text{Lorentzian} \quad (3.12)$$

$$\rho(E, E_0) = \begin{cases} \frac{1}{\Delta E} & |E - E_0| < \frac{\Delta E}{2} \\ 0 & |E - E_0| > \frac{\Delta E}{2} \end{cases} \quad \text{box average} \quad (3.13)$$

These two forms emphasize differently the resonances at a distance from E_0 , the box average giving them zero weight. It is possible to devise a family of density functions which vary from the Lorentzian to a Gaussian that is similar to the box form [Levin and Feshbach (73)]. These will give differing answers for the integral defining $\langle 1/e_{QQ} \rangle$. For the present it will suffice to discuss the consequences of the two examples above.

The Lorentzian has the advantage of analytic simplicity. Consider the Lorentzian average of $F(E)$:

$$\langle F(E) \rangle_L = \frac{\Delta}{2\pi} \int_{-\infty}^{\infty} \frac{F(E_0)}{(E - E_0)^2 + (\Delta/2)^2} dE_0$$

Assuming that $F(E_0)$ has no singularities in the upper half of the complex E plane and that it is well behaved on the infinite semicircle, it is a simple matter to evaluate the integral using the calculus of residues. One obtains

$$\langle F(E) \rangle_L = F\left(E + \frac{i\Delta}{2}\right) \quad (3.14)$$

Hence

$$\left\langle \frac{1}{e_{QQ}} \right\rangle_L = \frac{1}{E + (i\Delta/2) - H_{QQ} - W_{QQ}} \quad (3.15)$$

The effect of the averaging process is to increase the width of each resonance by Δ . Since Δ is assumed to be large compared to each of these widths, the fluctuations caused by the resonances are completely smoothed. The optical Hamiltonian, (3.9), becomes

$$(H_{\text{opt}})_L = H_{PP} + H_{PQ} \frac{1}{E - H_{QQ} + (i/2)\Delta} H_{QP} \quad (3.16)$$

To obtain the box average it is convenient to evaluate a typical term in an expansion of $1/e_{QQ}$:

$$\begin{aligned} \left\langle \frac{1}{E - E_s + i\Gamma_s/2} \right\rangle &= \frac{1}{\Delta E} \int_{E-(1/2)\Delta E}^{E+(1/2)\Delta E} \frac{dE_0}{E_0 - E_s + (i/2)\Gamma_s} \\ &= \frac{1}{\Delta E} \int_{(2/\Gamma_s)[E - E_s - (1/2)\Delta E]}^{(2/\Gamma_s)[E - E_s + (1/2)\Delta E]} \frac{x - i}{x^2 + 1} dx \end{aligned}$$

As long as

$$|E - E_s| \ll \frac{1}{2}\Delta E \quad (3.17)$$

that is, near the center of the interval,

$$\left\langle \frac{1}{E - E_s + (i/2)\Gamma_s} \right\rangle = -\frac{i\pi}{\Delta E} \quad (3.18)$$

Condition (3.17) can be rephrased to state that (3.18) is valid for resonances in an interval δE about E as long as $\delta E \ll \Delta E$. For (3.18) to be useful, the following inequalities must hold:

$$\Delta E \gg \delta E \gg \begin{cases} \Gamma \\ D \end{cases} \quad (3.19)$$

This condition is not restrictive except in the case of extraordinarily broad resonances[‡]. From (3.18) it follows that

$$\left\langle \frac{1}{e_{QQ}} \right\rangle = -\frac{i\pi}{\Delta E} \quad (3.19')$$

The optical Hamiltonian is then

$$(H_{\text{opt}})_{\text{box}} = H_{PP} - \frac{i\pi}{\Delta E} H_{PQ} \frac{1}{1 - (i\pi/\Delta E)W_{QQ}} H_{QP} \quad (3.20)$$

In both cases the optical Hamiltonian is complex. In the limit of large Δ (or ΔE) the imaginary part is negative definite, as it must be so that the optical

[‡]Equation (3.18) is not valid for resonances near the edge of the interval ΔE . This is referred to as the *edge effect*. If the edge effect is substantial one expects a sensitivity with respect to the averaging interval ΔE . Generally, experimental results are quoted when the data are insensitive to ΔE and thus (3.18) may be taken as valid for that reason. The edge effect is also present for the Lorentzian since it weights these resonances beyond $(E \pm \Delta/2)$ in a particular way.

potential is absorptive. This is expected since the elimination of the channels in \mathcal{Q} space leaves some of the flux unaccounted for.

More graphically, an energy average of the wave function is equivalent to the construction of a wave packet, whose passage time at a given space point is on the order of $(\hbar/\Delta E)$. The differing averaging densities, ρ , develop different shapes and time dependence for the wave packet. The Lorentzian, for example, leads to an exponential decay with time. As developed in deShalit and Feshbach (74, p. 91 and following), the prompt amplitude will not contain any contribution from the delayed component, whose time delay is \hbar/Γ , $\Gamma \ll \Delta E$. Thus when the incident wave strikes the nucleus, part of it passes through promptly, and part of it is delayed. The prompt amplitude does not contain the latter, so that the averaged prompt amplitude exhibits absorption. Moreover, as the width for the resonances (or fluctuations) increases, or equivalently, if it is necessary to consider a number of resonances simultaneously because they overlap, this separation in time between the delayed and time component will be reduced, raising the question of how much should be assigned to each. Clearly, if the width is on the same order as ΔE , there can be no distinction between the two and the optical potential should be real, in the absence, of course, of true inelastic processes.

The shape of the wave packet plays a critical role for this issue. $(H_{\text{opt}})_L$ does not depend on W_{QQ} and does not show this effect. On the other hand, $(H_{\text{opt}})_{\text{box}}$ does. For that case we evaluate the imaginary part of the expectation value of this potential, which is directly proportional to the absorption:

$$\begin{aligned} & \text{Im} \langle \langle P\Psi \rangle | (H_{\text{opt}})_{\text{box}} \langle P\Psi \rangle \rangle \\ &= \text{Im} \left\langle \langle P\Psi \rangle \left| \frac{-i\pi}{\Delta E} H_{PQ} H_{QP} \frac{1}{1 - (i\pi/\Delta E)[1/(E^{(+)} - H_{PP})] H_{PQ} H_{QP}} \right| \langle P\Psi \rangle \right\rangle \end{aligned} \quad (3.21)$$

where we have used (3.7'') and (3.19'). Noting that (3.7') implies that

$$\langle P\Psi \rangle = \left(1 - \frac{i\pi}{\Delta E} \frac{1}{E^{(+)} - H_{PP}} H_{PQ} H_{QP} \right) \chi_i^{(+)}$$

we can rewrite (3.21) as follows:

$$\begin{aligned} & \text{Im} \langle \langle P\Psi \rangle | (V_{\text{opt}})_{\text{box}} \langle P\Psi \rangle \rangle \\ &= \text{Im} \left\langle \chi_i^{(+)} \left| \left(1 + \frac{i\pi}{\Delta E} H_{PQ} H_{QP} \frac{1}{E^{(-)} - H_{PP}} \right) \left(\frac{-i\pi}{\Delta E} H_{PQ} H_{QP} \right) \right| \chi_i^{(+)} \right\rangle \end{aligned}$$

Assuming that $\chi_i^{(+)}$ is an eigenstate of S_P , so that

$$\chi_i^{(+)} = e^{i\delta} F$$

where F is real, one obtains

$$\begin{aligned} & \text{Im} \langle \langle P\Psi \rangle | (V_{\text{opt}})_{\text{box}} \langle P\Psi \rangle \rangle \\ &= \left\langle \chi_i^{(+)} \left| -\frac{\pi}{\Delta E} H_{PQ} H_{QP} + \pi \frac{\pi^2}{\Delta E^2} H_{PQ} H_{QP} \delta(E - H_{PP}) H_{PQ} H_{QP} \chi_i^{(+)} \right. \right\rangle \end{aligned}$$

Introducing the widths [see (2.35) and (2.22)]

$$\Gamma_s = 2\pi |\langle \Phi_s | H_{QP} \chi_i^{(+)} \rangle|^2$$

and restricting \mathcal{P} space so that it includes only $\chi_i^{(+)}$, we find that

$$\text{absorption} \sim -\text{Im} \langle \langle P\Psi \rangle | (V_{\text{opt}})_{\text{box}} \langle P\Psi \rangle \rangle \leq \left[\frac{1}{2\Delta E} \sum \Gamma_s - \pi \left(\frac{1}{2\Delta E} \right)^2 (\sum \Gamma_s)^2 \right] \quad (3.22')$$

Thus the absorption differs from zero if

$$\frac{1}{\Delta E} \sum \Gamma_s \equiv \frac{\langle \Gamma \rangle}{\langle D \rangle} \leq \frac{2}{\pi} \quad (3.22)$$

where $\langle D \rangle$ is the average spacing between resonances. This condition agrees in order of magnitude with Wigner's limit [Lane, Thomas, and Wigner (55)] and has been derived in another fashion [Feshbach (69)]. This should not be taken as a rigorous condition on a given channel strength function, as it depends on a particular choice of the averaging density. However, it does have a qualitative significance. In fact, it can be shown [Mello and Feshbach (72)] that large widths imply a strong correlation of widths with resonance energies and a hypersensitivity with regard to the choice of the averaging interval ΔE .

4. INTERMEDIATE STRUCTURE, DOORWAY STATE RESONANCES, AND GIANT RESONANCES[†]

The subjects of this section have been discussed in deShalit and Feshbach (74, pp. 99–104) and in Section I.6. It will therefore suffice to provide only a brief review before entering into the formal description.

Intermediate structure refers to an energy dependence of the cross section whose scale, Γ_d , lies between the width, Γ_{CN} , for the fine structure produced by compound nuclear resonances or Ericson–Brink fluctuations (see Chapter IV) and the width, Γ_{SP} , for the gross structure that would appear in the cross section

[†]Block and Feshbach (63); Feshbach, Kerman, and Lemmer (67).

for single-channel elastic scattering produced by a real local potential, that is,

$$\Gamma_{SP} \gg \Gamma_d \gg \Gamma_{CN} \quad (4.1)$$

To observe intermediate structure it is necessary to average the cross section (either by numerically averaging good resolution data or by using poorer, but not too poor, experimental energy resolution). In this way the fluctuations in the cross section are smoothed and larger widths become visible. The interval ΔE over which the average is made should be less than Γ_d but much greater than D , the spacing for compound nuclear levels. This process is demonstrated in Fig. I.13.7 of deShalit and Feshbach (74) for an isobar analog resonance. Conversely, intermediate structure should exhibit fine structure when examined with sufficiently good energy resolution. This is illustrated by Fig. I.1.1, which shows the fine structure associated with two isobar analog resonances at 2.77 and 3.14 MeV.

Many examples of intermediate structure have been observed. So far we have discussed the giant electric dipole resonance, the subthreshold fission cross section, and the isobar analog resonance [see deShalit and Feshbach (74, p. 99–104)]. Giant resonances generally are examples of intermediate structure. The quadrupole resonance at an excitation energy of $60/A^{1/3}$ MeV, the electric monopole mode, and the Gamow–Teller resonances are examples. The light heavy-ion system $^{12}\text{C} + ^{12}\text{C}$ exhibits intermediate structure involving many resonances, as shown in Fig. 4.1. These fragment into fine structure when examined with very high energy resolution.

All the foregoing cases involve isolated resonances. However, there will be cases in which they overlap. For these a statistical theory of the type that has been discussed briefly in Section I.6 and is discussed more fully in Chapter IV, is appropriate.

The states corresponding to these resonances have been referred to as *doorway states* and the corresponding resonances as *doorway state resonances* [Block and Feshbach (63)], to emphasize that they serve as the first stage beyond the entrance channel in the development of the complex compound nuclear state; that is, the system would have to pass through the doorway state before the full complexity of the compound nuclear state could be generated. This is illustrated in Fig. 4.2. The doorway state is a relatively simple state, not as complex as the compound state or as simple as the entrance channel state paralleling the inequality (4.1). The hypothesis that such simple states exist and that they are the only states that couple strongly to the entrance channel will be referred to as the *doorway state hypothesis*.

A simple, although somewhat idealized example will help to make the doorway state hypothesis more concrete. Suppose that the incident projectile is a nucleon. Suppose, moreover, that its energy is such that no reactions are possible, so that only elastic scattering can occur. The entrance channel wave function, $\chi_i^{(+)}$, then describes the motion of the incident nucleon in the field of the target nucleus. This nucleon–nuclear interaction is specified by a model Hamiltonian that is appropriate for this energy range. The remainder of the

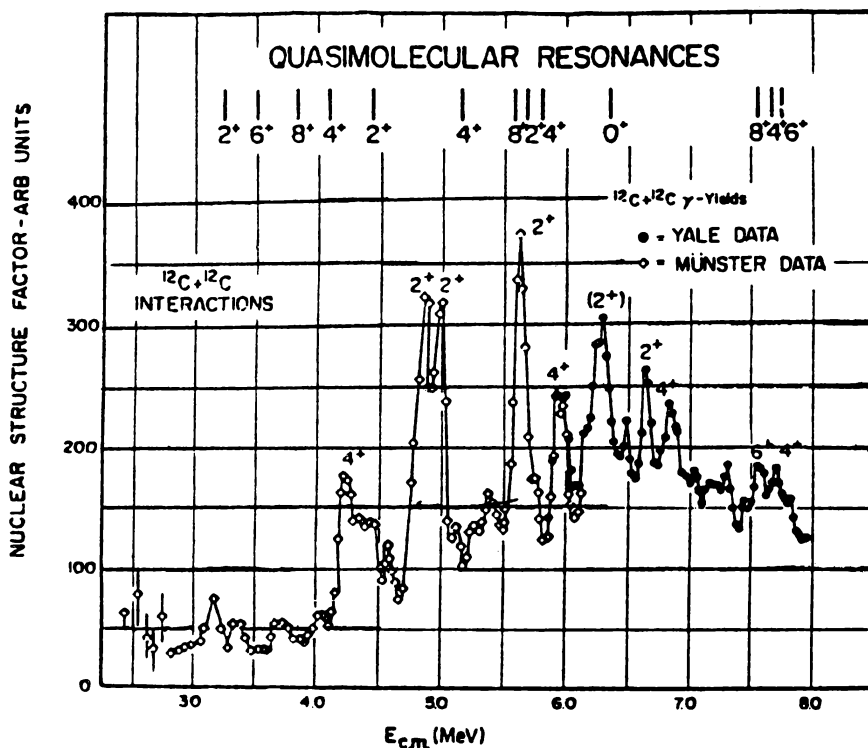


FIG. 4.1. Nuclear structure factors derived from the total γ -radiation yields of the $^{12}\text{C} + ^{12}\text{C}$ interaction. [From Erb and Bromley (84).]

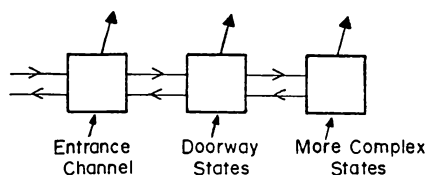


FIG. 4.2

wave function is generated by the residual Hamiltonian given by the difference between the exact and model Hamiltonians. As an example, suppose that we idealize this residual interaction by assuming that it consists of a sum of two-body interactions. Furthermore, as an example, suppose that the target nucleus has a closed shell or subshell so that the appropriate entrance channel Hamiltonian is the shell model Hamiltonian. The entrance channel is then a one-particle state in shell model terminology. The residual interaction acting on $\chi_i^{(+)}$ will excite a particle-hole pair, the incident nucleon changing its state, generating a two-particle/one-hole state (2p-1h). The states produced in this fashion, or a linear combination of them, are doorway states since they are the

only ones that are coupled by the residual interaction to the entrance channel. All the states of this complexity (i.e., of the 2p–1h structure form the doorway state space, \mathcal{D}). Since the particle–hole interaction can build up collective states with preferred spin and isospin (e.g., the dipole $J=1^-$, $T=1$ state), a doorway state may often be more simply described as a particle plus vibration state. More generally, a doorway state can be a particle plus a collective state, and then it may be more convenient to employ collective variables in describing the residual interaction.

The above is simply an example; the doorway concept is not limited to the case of a nucleon incident on a shell model target nucleus. The examples of intermediate structure listed earlier include the case of an incident photon (E1), an incident α -particle, or the collision of two ^{12}C nuclei. What is required is that upon the first collision [Weisskopf (60)] the residual interaction produces a relatively simple configuration, analogous to the 2p–1h states discussed above. In the case of the giant dipole resonance, that simple state is well known to be a linear combination of particle–hole excitations [see deShalit and Feshbach (74, p. 491)].

As discussed in the introduction to this chapter, a resonance occurs whenever there is an approximate state of the system that is bound and whose energy equals the total energy of the system. The important point is that in this state the energy has been redistributed and a sufficient fraction of the incident kinetic energy has become internal energy. A doorway state has just this property, namely that some of the system's energy has been used for excitation rather than remaining as kinetic energy. In the example quoted above, this energy is used to excite a particle–hole pair. If, in addition, the total energy of the doorway state equals the incident kinetic energy, a doorway state resonance will occur, producing as a consequence intermediate structure in the cross section.

The resonant doorway state wave function will generally be composed not only of the states generated directly by the residual interaction acting on the entrance channel wave function but will also include additional components of the same complexity. These are contained within doorway space \mathcal{D} . In our example, after the initial formation of 2p–1h states, the nuclear Hamiltonian acting on them will produce others (as well as states of different complexity) which are not directly coupled to the entrance channel. The resonant doorway state, being an approximate eigenstate, will generally involve these components as well as the directly coupled ones.

The resonant doorway state is not an exact stationary eigenstate of the nuclear Hamiltonian. It will decay with time and thus has a width. In addition to the *escape width* Γ_d^\uparrow , caused by transitions to various exit channels and common to all types of resonances, there is the width, which is a consequence of the possible transition to states of higher complexity, roughly speaking to the fine structure states (see Fig. 4.2). This width, Γ_d^\downarrow , is referred to as the *spreading width*, Γ_d^\downarrow . The total doorway state width, Γ_d , is the sum of these two:

$$\Gamma_d = \Gamma_d^\downarrow + \Gamma_d^\uparrow \quad (4.2)$$

The visibility of the doorway state resonance depends critically upon Γ_d . If Γ_d is too large, intermediate structure will not be seen.

To see this, let us turn to the expression for the $l=0$ elastic scattering cross section, which applies to this case [compare (2.20)].

$$\sigma = \frac{4\pi}{k^2} \left| \sin \delta - e^{i\delta} \frac{\Gamma_d^\dagger/2}{(E - E_d) + (i/2)(\Gamma_d^\dagger + \Gamma_d^\dagger)} \right|^2$$

where $\hbar^2 k^2/2m$ is the energy and δ is a phase shift. We see that Γ_d^\dagger acts as an additional absorption. The maximum magnitude of the resonant doorway term, the second one, occurs at $E = E_d$ and is equal to $\Gamma_d^\dagger/\Gamma_d$, proving the point made in the preceding paragraph.

Stating this result in another way, if the coupling between the resonant doorway state and the compound nuclear states, whose energies differ appreciably from E_d , is substantial, the spreading width Γ_d^\dagger will be large and the resonant cross section will be reduced appreciably. Moreover, if as a consequence of this coupling, Γ_d is on the order of or greater than D_d , the energy spacing between doorway resonances, these will overlap. The doorway resonance will not be isolated and an energy average of the fine structure will consequently average over more than one doorway state, preventing direct observation of the character of each individual doorway resonance.

We turn to the quantitative description of doorway state phenomena. The Hilbert space will now be partitioned into three parts, $\mathcal{P} + \mathcal{D} + \mathcal{D}'$, where \mathcal{P} will contain the prompt channels, \mathcal{D} , the doorway states, and \mathcal{D}' the more complex states, as indicated by Fig. 4.2. Comparing with (2.1), we have

$$\mathcal{D} = \mathcal{D} + \mathcal{D}' \quad (4.3)$$

It is, however, more convenient, for the derivations given below, to group the doorway states with the prompt channels. Let the projection operators that project onto the \mathcal{P} , \mathcal{D} , and \mathcal{D}' subspaces be P , D , and Q' , respectively. Orthogonality of the spaces is presumed, so that

$$\begin{aligned} P^2 &= P & PD &= 0 & PQ' &= 0 & DQ' &= 0 \\ P + D + Q' &= 1 \end{aligned} \quad (4.4a)$$

Finally, let

$$P' \equiv P + D \quad P' + Q' = 1 \quad (4.4b)$$

The analysis of Section 2 applies. One can, for example, immediately write

$$\mathcal{T}_{fi} = \mathcal{T}_{fi}^{(P')} + \left\langle \phi_f^{(-)} \left| H_{P'Q'} \frac{1}{E^{(+)} - H_{Q'Q'} - W_{Q'Q'}} H_{Q'P'} \right| \phi_i^{(+)} \right\rangle \quad (4.5)$$

where

$$(E - H_{P'P'})\phi = 0$$

The functions ϕ can be resolved into prompt and doorway components $P\phi$ and $D\phi$ satisfying the equations

$$(E - H_{PP})P\phi = H_{PD}D\phi \quad (4.6)$$

$$(E - H_{DD})D\phi = H_{DP}P\phi \quad (4.7)$$

$\mathcal{T}_{fi}^{(P')}$ is the transition amplitude generated by this system. Since these equations are identical in form (simply replace Q by D) with (2.3) and (2.4) it is entirely possible, depending of course on H , for this system to exhibit resonances which will be present in $\mathcal{T}_{fi}^{(P')}$ (see Fig. 4.3). The analysis follows exactly that leading to (2.20) or (2.30'). These resonances are the progenitors of the doorway state resonances, for the coupling to \mathcal{Q}' has not yet been included. They will have a width that is roughly the escape width Γ^\dagger . To obtain the full width it is necessary to average over the fine structure, that is, obtain the optical potential for this case.

As we saw earlier, the energy averaged wave function $\langle P'\Psi \rangle$ satisfies

$$(E - H_{\text{opt}})\langle P'\Psi \rangle = 0$$

where

$$H_{\text{opt}} = H_{P'P'} + H_{P'Q'} \frac{1}{\langle 1/e_{Q'Q'} \rangle^{-1} + W_{Q'Q'}} H_{Q'P'} \quad (4.8)$$

We now introduce the critically important assumption, which we shall refer to as the *strong doorway assumption*, namely that \mathcal{P} couples *only* to \mathcal{D} . In other words, \mathcal{Q}' does not couple directly to \mathcal{P} . This assumption leads to the equations

$$H_{PQ'} = 0 \quad H_{P'Q'} = H_{DQ'} \quad (4.9)$$

Therefore,

$$H_{\text{opt}} = H_{P'P'} + H_{DQ'} \frac{1}{\langle 1/e_{Q'Q'} \rangle^{-1} + W_{Q'Q'}} H_{Q'D} \quad (4.10)$$

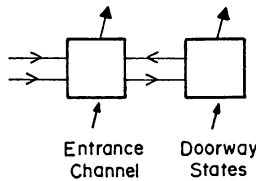


FIG. 4.3

It follows that the equation for $\langle P'\Psi \rangle$ can, by virtue of

$$\langle P'\Psi \rangle = \langle P\Psi \rangle + \langle D\Psi \rangle$$

be written as a pair of coupled equations:

$$(E - H_{PP})\langle P\Psi \rangle = H_{PD}\langle D\Psi \rangle \quad (4.11)$$

$$(E - H_{DD} - \bar{W}_{DD})\langle D\Psi \rangle = H_{DP}\langle P\Psi \rangle \quad (4.12)$$

where

$$\bar{W}_{DD} = H_{DQ'} \frac{1}{\langle 1/e_{Q'Q'} \rangle^{-1} + W_{Q'Q'}} H_{Q'D} \quad (4.13)$$

Comparing with (4.7), we see that the coupling of \mathcal{D} with \mathcal{D}' has produced, upon energy averaging over the fine structure, an additional complex term \bar{W}_{DD} whose imaginary part will give rise to Γ_d^\dagger . One can now immediately obtain the analog of (2.30') by the procedure used to derive that equation. The result is

$$\langle \mathcal{T}_{fi} \rangle = \mathcal{T}_{fi}^{(P)} + \left\langle \chi_f^{(-)} \left| H_{PD} \frac{1}{E - H_{DD} - \bar{W}_{DD} - W_{DD}} H_{DP} \chi_i^{(+)} \right. \right\rangle \quad (4.14)$$

where $\chi_{f,i}^{(\pm)}$ are, as before, solutions of

$$(E - H_{PP})\chi = 0$$

and

$$W_{DD} = H_{DP} \frac{1}{E^{(+)} - H_{PP}} H_{PD} \quad (4.15)$$

W_{DD} describes the coupling of the doorway states to the entrance and exit channels.

If one now makes the single isolated doorway state assumption, (4.14) becomes

$$\langle \mathcal{T}_{fi} \rangle = \mathcal{T}_{fi}^{(P)} + \frac{\langle \chi_f^{(-)} | H_{PD} \psi_d \rangle \langle \psi_d | H_{DP} \chi_i^{(+)} \rangle}{E - E_d + (1/2)i(\Gamma_d^\dagger + \Gamma_d)} \quad (4.16)$$

where

$$\begin{aligned} E_d &= \text{Re} \langle \psi_d | (H_{DD} + W_{DD} + \bar{W}_{DD}) \psi_d \rangle \\ \Gamma_d^\dagger &= -2 \text{Im} \langle \psi_d | W_{DD} \psi_d \rangle = 2\pi \sum_\gamma |\langle \chi_\gamma^{(-)} | H_{PD} \psi_d \rangle|^2 \end{aligned} \quad (4.17)$$

$$\Gamma_d^\downarrow = -2 \operatorname{Im} \langle \psi_d | \bar{W}_{DD} \psi_d \rangle = \frac{4}{\Delta} \sum_q \frac{|\langle \psi_d | H_{DQ} \Phi_q \rangle|^2}{1 + [2(E - \mathcal{E}_q)/\Delta]^2}$$

$$\rightarrow \frac{4}{\Delta} \sum_q |\langle \psi_d | H_{DQ} \Phi_q \rangle|^2$$

Here ψ_d is the doorway state wave function and Φ_q are the wave functions describing the fine structure resonances in \mathcal{Q}' [see (2.9)]. The expression for Γ_d^\downarrow has been obtained by using the Lorentzian average for $\langle 1/e_Q \rangle$. The wave function ψ_d , a solution of

$$(E - H_{DD})\psi_d = 0$$

is a bound-state wave function. The apparent difference between the second and third line of (4.17) is a consequence of the differing normalizations of ψ_d , which is normalized so that the volume integral of $|\psi_d|^2$ is unity, and $\chi_f^{(-)}(E)$, which is normalized so that volume integral of $\chi_f^{(-)*}(E)\chi_f^{(-)}(E')$ is $\delta(E - E')$. As anticipated in the introductory remarks, the magnitude of Γ_d^\downarrow will depend on the magnitude of the residual interaction H_{DQ} , and on the rate with which the series over q converges. If contributions from distant resonances are important, Γ_d^\downarrow will tend to be large and the resonance obscured by the single-step amplitude $\mathcal{T}_{fi}^{(P)}$.

Some further consequences of doorway state resonances can be uncovered by studying the one-channel case. Then the elastic scattering $\langle \mathcal{T} \rangle$ matrix, according to (4.16) and (4.17), is given by

$$\langle \mathcal{T} \rangle = \mathcal{T}^{(P)} + \frac{1}{2\pi} e^{2i\delta} \frac{\Gamma_d^\downarrow}{(E - E_d) + \frac{1}{2}i(\Gamma_d^\downarrow + \Gamma_d^\uparrow)}$$

The average S matrix that follows is

$$\langle S \rangle = e^{2i\delta} \frac{(E - E_d) + \frac{1}{2}i(\Gamma_d^\downarrow - \Gamma_d^\uparrow)}{(E - E_d) + \frac{1}{2}i(\Gamma_d^\downarrow + \Gamma_d^\uparrow)} \quad (4.18)$$

As is obvious, $\langle S \rangle$ is not unitary because of the spreading width, Γ_d^\downarrow , which acts, as stated earlier, as an absorption. The transmission factor (p. 243), T , reflects the presence of absorption since

$$T = 1 - |\langle S \rangle|^2 \quad (4.19)$$

which, in the present case, is

$$T = \frac{\Gamma_d^\downarrow \Gamma_d^\uparrow}{(E - E_d)^2 + \frac{1}{4}\Gamma_d^2} \quad (4.20)$$

Recall that the average absorption cross section is proportional to T . Thus we

obtain the important result that the cross section for absorption into compound nuclear state is enhanced by the presence of doorway state achieving a maximum at $E = E_d$. Obviously, the transmission by the doorway mechanism will be zero if there is no coupling of the entrance channel to the doorway state ($\Gamma_d^\dagger = 0$) or if that state does not couple to the compound nuclear resonances ($\Gamma_d^\dagger = 0$).

The symmetry of T about $E = E_d$ is a consequence of the strong doorway assumption, namely that the entrance channel couples only with the doorway state and not with the more complex states. We now examine the effect of allowing such direct coupling. Upon energy averaging, one obtains, instead of (4.11) and (4.12), the following equations:

$$(E - H_{PP} - \bar{W}_{PP})\langle P\Psi \rangle = (H_{PD} + \bar{W}_{PD})\langle D\Psi \rangle \quad (4.21)$$

$$(E - H_{DD} - \bar{W}_{DD})\langle D\Psi \rangle = (H_{DP} + \bar{W}_{DP})\langle P\Psi \rangle \quad (4.22)$$

where \bar{W}_{DD} is given by (4.13) and

$$\bar{W}_{PD} = H_{PQ'} \frac{1}{\langle 1/e_{Q'Q'} \rangle^{-1} + W_{Q'Q'}} H_{Q'D} \quad (4.23)$$

\bar{W}_{PD} represents the effect of the direct coupling of the subspace \mathcal{P} of the prompt channels and the subspace \mathcal{Q}' on the generation of components contained in subspace \mathcal{D} , while

$$\bar{W}_{PP} = H_{PQ'} \frac{1}{\langle 1/e_{Q'Q'} \rangle^{-1} + W_{Q'Q'}} H_{Q'P} \quad (4.24)$$

represents the effect on the prompt channel of such coupling. All the elements of the \bar{W} matrix are complex. The analysis of (4.21) and (4.22) is identical with that of (4.11) and (4.12).

One effect of the complex \bar{W} matrix is to make the potential scattering \mathcal{T} , absorptive, that is, the phase shift for the single-channel case has a positive imaginary part, while another is that the escape width Γ_d^\dagger given by

$$\Gamma_d^\dagger = 2\pi \langle \chi_f^{(+)} | (H_{PD} + \bar{W}_{PD}) \psi_d \rangle \langle \psi_d | (H_{DP} + \bar{W}_{DP}) \chi_i^{(+)} \rangle \quad (4.25)$$

is complex since \bar{W}_{PD} is not Hermitian; hence

$$\Gamma_d^\dagger = |\Gamma_d^\dagger| e^{i\phi} \quad (4.26)$$

The S -matrix equation (4.18) is replaced by

$$\langle S \rangle = e^{2i\delta} e^{-2\eta} \left[1 - i \frac{|\Gamma_d^\dagger| e^{i\phi}}{(E - E_d) + (i/2)\bar{\Gamma}_d} \right] \quad (4.27)$$

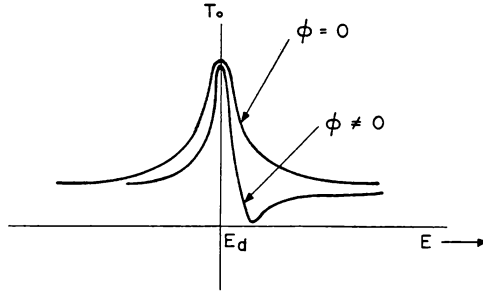


FIG. 4.4

where $\delta + i\eta$ is the potential scattering phase shift and Γ_d is the total width. The transmission T given by (4.19) can readily be evaluated. As long as ϕ is not equal to zero, the resulting T is not symmetric about $E = E_d$. In Fig. 4.4 the T for the symmetric case ($\phi = 0$) is compared with the result obtained when $\phi \neq 0$. The latter is asymmetric and has an interference minimum. Both of these features are a consequence of the relaxation of the strong doorway assumption, $H_{PQ'} = 0$, thereby permitting a direct coupling of \mathcal{P} and \mathcal{Q}' , $H_{PQ'} \neq 0$.

According to the preceding discussion, the wave function for the nuclear system Ψ , can be broken up into three components as follows:

$$\Psi = P\Psi + D\Psi + Q'\Psi$$

The first term, $P\Psi$, describes the prompt channels. In the neighborhood of a compound nuclear resonance, $(D + Q')\Psi = Q'\Psi$ is given by Φ_s and $D\Psi$ is given by the doorway state, ψ_d . Interestingly, the overlap of ψ_d with Φ_s , $\langle \Phi_s | \psi_d \rangle$, is quite small. In other words, ψ_d need not be a major component of Ψ in order to serve as a doorway state. Or, conversely, the doorway state is built up out of small fractions of the compound nuclear resonance wave functions.

The overlap, $\langle \Phi_s | \psi_d \rangle$, can be related to experimentally observable quantities as follows. The compound nuclear state width Γ_s is related to Φ_s according to (2.22) by

$$\Gamma_s = 2\pi |\langle \chi^{(+)} | H_{PQ} \Phi_s \rangle|^2$$

where for simplicity the discussion is restricted to the single-channel case. Expand Φ_s in terms of ψ_d and the states Φ'_s in \mathcal{Q}' . The component of the matrix elements involving Φ'_s is zero because of the strong doorway state assumption. Therefore,

$$\Gamma_s = 2\pi |\langle \Phi_{sd} | \psi_d \rangle|^2 |\langle \chi^{(+)} | H_{PD} \psi_d \rangle|^2$$

or

$$\Gamma_s = \Gamma_d^\dagger |\langle \Phi_{sd} | \psi_d \rangle|^2 \quad (4.28)$$

where the subscript s_d indicates that the compound nuclear resonance is associated with the doorway state ψ_d . The overlap is then

$$|\langle \Phi_{s_d} | \psi_d \rangle|^2 = \frac{\Gamma_s}{\Gamma_d^\dagger} \quad (4.29)$$

Since the doorway state width, Γ_d , encompasses many fine structure resonances and Γ_d and Γ_d^\dagger are usually of the same order of magnitude, $\Gamma_s/\Gamma_d^\dagger$ is found to be much smaller than 1. We thus have demonstrated that the overlap $\langle \Phi_s | \psi_d \rangle$ is small.

Another insight can be obtained from the average value of Γ_s averaged now over an interval ΔE containing not only many compound nuclear resonances, but also many doorway states. This ΔE would be appropriate for the optical model if ΔE satisfies $\Gamma_{sp} \gg \Delta E \gg \Gamma_d$. Thus from (4.28)

$$\frac{1}{\Delta E} \sum_s \Gamma_s = \frac{1}{\Delta E} \sum_d \Gamma_d^\dagger \sum_{s_d} |\langle \Phi_{s_d} | \psi_d \rangle|^2 = \frac{1}{\Delta E} \sum_d \Gamma_d^\dagger$$

or

$$\frac{\langle \Gamma_s \rangle}{D_s} = \frac{\langle \Gamma_d^\dagger \rangle}{D_d} \quad (4.30)$$

where D_s is the energy spacing of the compound nuclear resonances and D_d that of the doorway states. As usual, the angular brackets indicate average quantities. This equation has a simple interpretation. The ratio $\langle \Gamma \rangle / D$, referred to as the *strength function*, represents the fraction of an energy interval occupied by resonances of average width $\langle \Gamma \rangle$. Thus (4.30) states that this fraction of an energy interval is independent of whether one does an extensive average leading directly to the optical model result given on the left-hand side of the equation or performs the average in two steps in which first $\Delta E \ll \Gamma_d$ and therefore reveals the doorway state resonances and then averages over many doorway states.

Problem. Derive (4.30) by equating the optical model average of the single-channel S matrix with the average of $\langle S \rangle$ [given by (4.18)] averaged over many doorway states.

Returning to (4.29) for the overlap probability, we see that it can be rewritten approximately (since the average of a ratio is not the ratio of the average)

$$\langle |\langle \Phi_s | \psi_d \rangle|^2 \rangle \simeq \frac{D_s}{D_d} = \frac{\rho_d}{\rho_s} \quad (4.31)$$

where ρ gives the density of states denoted by the subscripts. Again since the density of compound nuclear levels is of course much greater than the density

of doorway states, the average overlap probability is much smaller than 1, reaffirming the earlier conclusion.

A. Exit Doorways

The discussion has so far emphasized the connection between the entrance channel and the doorway state. Clearly, if in a reaction the final state is well defined experimentally, there is the possibility that a doorway state exists which bears a similar relation to the exit channel. We shall refer to such doorway states as exit doorways, to distinguish from entrance doorways, which are the doorway states discussed above. As one can see from (4.16), the final state $\chi_f^{(-)}$ is connected to ψ_d in precisely the same way as the initial state $\chi_i^{(+)}$. But there is the possibility that the branching ratio, $|\langle \chi_f^{(-)} | H_{PD} \psi_d \rangle|^2 / |\langle \psi_d | H_{DP} \chi_i^{(+)} \rangle|^2$, to the final state is very small, indicating that, in fact, ψ_d is not a doorway state for $\chi_f^{(-)}$. However, there is also the possibility that $\chi_f^{(-)}$ connects strongly to another doorway state $\psi_{d'}$. If these two corresponding resonances overlap, the reaction from $\chi_i^{(+)}$ to $\chi_f^{(-)}$ will be enhanced. This mechanism is important for radiative neutron capture.

One can obtain the transition amplitude for this case starting from the general expression given by (4.14),

$$\langle \mathcal{T}_{fi} \rangle = \mathcal{T}_{fi}^{(P)} + \left\langle \chi_f^{(-)} \left| \left(H_{PD} \frac{1}{E - H_{DD} - \bar{W}_{DD} - W_{DD}} H_{DD} \right) \chi_i^{(+)} \right. \right\rangle \quad (4.32)$$

When there is more than one isolated doorway state it becomes necessary to diagonalize $(H_{DD} + \bar{W}_{DD} + W_{DD})$, a procedure paralleling that described after (2.32). Let the eigenvalues of this operator be $E_d - i/2\Gamma_d$, the corresponding eigenfunction, Ω_d , and those of the adjoint equation $\Omega_d^{(A)}$. Then

$$\langle \mathcal{T}_{fi} \rangle = \mathcal{T}_{fi}^{(P)} + \sum_d \frac{\langle \chi_f^{(-)} | H_{PD} \Omega_d \rangle \langle \Omega_d^{(A)} | H_{DP} \chi_i^{(+)} \rangle}{E - E_d + (i/2)\Gamma_d} \quad (4.33)$$

Sum rules similar to (2.38) can also be derived for this case. In particular,

$$\sum_d \langle \chi_f^{(-)} | H_{PD} \Omega_d \rangle \langle \Omega_d^{(A)} | H_{DP} \chi_i^{(+)} \rangle = \sum_d \langle \chi_f^{(-)} | H_{PD} \psi_d \rangle \langle \psi_d | H_{DP} \chi_i^{(+)} \rangle \quad (4.34)$$

and

$$\frac{1}{2} \sum_d \Gamma_d = -2\pi \sum_d \text{Im} \langle \psi_d | \bar{W}_{DD} + W_{DD} | \psi_d \rangle \quad (4.35)$$

We see that these results are very similar in form to that obtained for overlapping compound nuclear resonances, with the difference that there is an additional absorption measured by $\sum_d \text{Im} \langle \psi_d | \bar{W}_{DD} | \psi_d \rangle$. Note also that Ω_d will

be a linear combination of the various ψ_d states so that even if $\langle \chi_f^{(-)} | H_{PD} \psi_i \rangle$, for example, is small, this is not necessarily the case for $\langle \chi_f^{(-)} | H_{PD} \Omega_i \rangle$. In any event, it is now possible because of interference between two terms, one corresponding to an entrance doorway and another to an exit doorway, to obtain an overlap between entrance and exit doorways.

B. Effect on Fine Structure

We have not yet discussed the impact of the doorway state resonance on the fine-structure resonances or, for that matter, the corresponding effect of direct processes on the doorway state resonance. These will be most clearly seen in the widths of these resonances.

Recall that the width of a fine-structure resonance in \mathcal{Q}' space is, in virtue of the partition,

$$P' + Q' = 1$$

given by (2.22), with P and Q replaced by P' and Q' , and χ by ϕ of (4.5). For the single-channel case to which the discussion will be limited, the width is given by

$$\Gamma_s = 2\pi |\langle \Phi'_s | H_{Q'P'} \phi_i^{(+)} \rangle|^2 \quad (4.36)$$

where Φ'_s satisfies

$$(\mathcal{E}'_s - H_{Q'Q'}) \Phi'_s = 0 \quad (4.37)$$

Because of the doorway state assumption, (4.36) can be replaced by

$$\Gamma_s = 2\pi |\langle \Phi'_s | H_{Q'D} D \phi_i^{(+)} \rangle|^2 \quad (4.38)$$

To obtain $D \phi_i^{(+)}$, we turn to the coupled equations (4.6) and (4.7). Solving the first of these for $P\phi$, and inserting the result in the second yields

$$(E - H_{DD} - W_{DD}) D \phi = H_{DP} \chi_i^{(+)} \quad (4.39)$$

so that

$$D \phi_i^{(+)} = \frac{1}{E - H_{DD} - W_{DD}} H_{DP} \chi_i^{(+)} \quad (4.40)$$

We now make the additional assumption that there is only one doorway state in the energy domain being considered. Then

$$D \phi_i^{(+)} = \frac{1}{E - \mathcal{E}_d + \frac{1}{2} i \Gamma_d^\dagger} \psi_d \langle \psi_d | H_{DP} \chi_i^{(+)} \rangle$$

Substituting in (4.38) yields

$$\Gamma_s = \frac{2\pi |\langle \Phi'_s | H_{Q'D} \psi_d \rangle|^2 |\langle \psi_d | H_{DP} \chi_i^{(+)} \rangle|^2}{(E - \mathcal{E}_d)^2 + \frac{1}{4}(\Gamma_d^\dagger)^2}$$

From (4.17)

$$\Gamma_{di}^\dagger = 2\pi |\langle \psi_d | H_{DP} \chi_i^{(+)} \rangle|^2 \quad (4.41)$$

We also introduce the definition

$$\Gamma_{sd}^\dagger \equiv 2\pi \langle \rho_s \rangle |\langle \Phi'_s | H_{Q'D} \psi_d \rangle|^2 \quad (4.42)$$

where $\langle \rho_s \rangle$ is the average level density of the fine structure levels.

Finally, one obtains

$$\Gamma_s(E) = \frac{\langle D_s \rangle}{2\pi} \frac{\Gamma_{sd}^\dagger \Gamma_{di}^\dagger}{(E - \mathcal{E}_d)^2 + \frac{1}{4}(\Gamma_d^\dagger)^2} \quad (4.43)$$

The energy dependence of the numerator of this expression is slow, being on the scale of the direct prompt processes represented by $\chi_i^{(+)}$. Within the doorway state resonance the main energy dependence is therefore carried by the denominator. We see that $\Gamma_s(E)$ has its maximum value at \mathcal{E}_d , which by the way does not equal the doorway state resonant energy, E_d , because the effect of \bar{W}_{DD} is not included, as it need not be since no averaging has been carried out in obtaining (4.42). (However, if the box average is used, E_d will equal \mathcal{E}_d .) Assuming that the difference $(E_d - \mathcal{E}_d)$ is not large compared to Γ_d^\dagger , one may conclude that for the case of *isolated* fine-structure resonances, those that occur near the center of the doorway state will be broader. These conclusions are modified if the fine-structure resonances are overlapping.

The strong doorway state assumption plays a central role in the foregoing development. If it is relaxed [see the discussion accompanying (4.22)], the general results obtained above would remain, that is, that the widths would be larger when the fine-structure resonance occurs within the doorway state resonance.

This analysis can be adapted for the description of similar relations between the single-particle resonance and both the doorway state and fine-structure resonances. The doorway state case will be considered first.

We divide the space \mathcal{P} into two orthogonal subspaces, \mathcal{M} and \mathcal{N} . The single-particle resonance is taken to be the consequence of a bound state in \mathcal{N} , coupling to the open channel space \mathcal{M} . Moreover, we require that only \mathcal{N} and not \mathcal{M} can couple to \mathcal{D} . It is now possible to set up a one-to-one relationship between the corresponding projection operators M, N , and D with those used

to describe the doorway structure, P, D , and Q' [see (4.4)]:

$$\begin{aligned} M &\leftrightarrow P \\ N &\leftrightarrow D \\ D &\leftrightarrow Q' \end{aligned} \quad (4.44)$$

It follows that the bound single-particle state χ_{SP} with energy E_{SP} satisfies

$$(E_{SP} - H_{NN} - W_{NN})\chi_{SP} = 0 \quad (4.45)$$

where

$$W_{NN} \equiv H_{NM} \frac{1}{E^{(+)} - H_{MM}} H_{MN} \quad (4.46)$$

The analog of $\chi^{(+)}$, the solution of the equation

$$(E - H_{PP})\chi^{(+)} = 0$$

is

$$(E - H_{MM})\tilde{\chi}_i^{(+)} = 0 \quad (4.47)$$

We may now restate (4.43) in terms of M, N , and D , replacing Φ'_s by ψ_d , ψ_d by χ_{SP} , and χ_i by $\tilde{\chi}_i^{(+)}$. One obtains

$$\Gamma_d(E) = \frac{D_d}{2\pi} \frac{\Gamma_{d,SP}^\dagger \Gamma_{SP,i}^\dagger}{(E - \mathcal{E}_{SP})^2 + \frac{1}{4}(\Gamma_{SP}^\dagger)^2} \quad (4.48)$$

where

$$D_d \Gamma_{d,SP}^\dagger = 2\pi |\langle \psi_d | H_{DN} \chi_{SP} \rangle|^2 \quad \text{and} \quad \Gamma_{SP,i}^\dagger = 2\pi |\langle \chi_{SP} | H_{NM} \tilde{\chi}_i^{(+)} \rangle|^2$$

demonstrating that the doorway state width will have a maximum value at \mathcal{E}_{SP} near the single-particle resonance energy.

A second set of relations, similar to (4.48), leads to a formulation of the relationship between the single-particle resonance and an isolated fine-structure resonance, which is close to that obtained by Lane, Thomas, and Wigner (55). The isomorphism used is

$$\begin{aligned} M &\leftrightarrow P \\ N &\leftrightarrow D \\ Q &\leftrightarrow Q' \end{aligned} \quad (4.49)$$

Relation (4.43) now reads

$$\Gamma_s(E) = \frac{\langle D_s \rangle}{2\pi} \frac{\Gamma_{s,SP}^\downarrow \Gamma_{SP,i}^\uparrow}{(E - \mathcal{E}_{SP})^2 + \frac{1}{4}(\Gamma_{SP}^\uparrow)^2} \quad (4.50)$$

where

$$\Gamma_{s,SP}^\downarrow = 2\pi \langle \rho_s \rangle |\langle \Phi_s | H_{QN} \chi_{SP} \rangle|^2$$

so that the fine-structure resonance width will be greater near the single-particle resonance energy, \mathcal{E}_{SP} .

It should be noted that the \mathcal{E}_{SP} and Γ_{SP} of (4.50) are not identical with those of (4.48). Similarly, the fine-structure resonances in space \mathcal{Q}' are not the same as those in space \mathcal{Q} , so that the D_s used in (4.56) is not identical with the D_s in (4.43). However, substantial differences are not expected.

One interesting result that can be obtained from (4.50) yields a direct, albeit approximate, evaluation of $\Gamma_{s,SP}^\downarrow$. We sum both sides of (4.50) over all Γ_s occurring within the single-particle giant resonance:

$$\sum_s \Gamma_s(E_s) \rightarrow \int \frac{dE_s}{\langle D_s \rangle} \Gamma_s(E_s) = \frac{\langle \Gamma_{s,SP}^\downarrow \rangle \langle \Gamma_{SP,i}^\uparrow \rangle}{\langle \Gamma_{SP}^\uparrow \rangle}$$

Assuming a single channel, $\langle \Gamma_{SP}^\uparrow \rangle = \langle \Gamma_{SP,i}^\uparrow \rangle$, leads to

$$\sum_s \Gamma_s(E_s) \simeq \langle \Gamma_{s,SP}^\downarrow \rangle \quad (4.51)$$

Hence the effect of the fine-structure resonances is to increase the width of the single-particle resonance by the sum of the fine-structure widths. This follows from the expression for the transmission factor, (4.20), which for the present application is given by

$$T = \frac{\langle \Gamma_{s,SP}^\downarrow \rangle \langle \Gamma_{SP,i}^\uparrow \rangle}{(E - \mathcal{E}_{SP})^2 + \frac{1}{4}[\langle \Gamma_{s,SP}^\downarrow \rangle + \langle \Gamma_{SP,i}^\uparrow \rangle]^2} \quad (4.52)$$

Thus a coherent hierarchical picture emerges. Because of the single-particle resonance the widths of the fine-structure resonances are enhanced [Eq. (4.50)]. Because of the doorway state resonance there is a substructure within the single-particle resonance (4.43), the enhancement of the fine-structure resonances being greater in the neighborhood of the doorway state energy. Upon averaging over the fine structure, using an averaging energy interval small compared with Γ_d but large compared to Γ_s , the doorway state broadens (the effect of \bar{W}_{dd}). If that broadening is too large, the doorway state resonance may not be visible. This in fact happens frequently to the single-particle resonance; that is, on averaging over an interval small compared to Γ_{SP} but large compared to Γ_d

and Γ_s , the width of the single-particle resonance becomes sufficiently broad as not to be visible in the optical model cross sections.

5. PROJECTION OPERATORS AND ANTISYMMETRIZATION

So far it has not been necessary to specify the projection operators P , Q , and so on, used in the preceding sections. Only their existence has been assumed. This fact points to the great generality of the results obtained. They apply to any system, not only the nuclear one, which exhibits both prompt and time-delayed reaction phenomena. The choice of these operators can be made so as to take into account the physics of the situation under discussion, thereby tailoring the reaction formalism to the phenomena to be understood. On the other hand, by making specific choices, one can obtain a variety of less general reaction formalisms.

The Pauli principle must, of course, be taken properly into account. The wave functions for the projectile and for the target nucleus are always assumed to be separately antisymmetrized. The exit particle and the residual nucleus wave functions are similarly treated. However, a problem arises whenever both the projectile (exit particle) and the target (residual) nucleus contain the same kinds of particles. The situation is simple if the incident particle is an electron and the process is electron elastic or inelastic scattering. In that case it is only necessary to use antisymmetric target and residual wavefunctions. But when the incident particle is a nucleon or a heavy ion, the Pauli principle must be applied to the entire system consisting of $(A_T + A_p)$ nucleons, where A_T is the target mass number and A_p that of the projectile. The Pauli principle does introduce complications, which are physically important, and therefore cannot be ignored, tempting as that may be.

The principal method to be used in this volume is chosen so that it permits a simple and simultaneous treatment of both the direct and resonance processes. As an example, consider scattering processes, both elastic and inelastic, so that the target nucleus can remain in its ground state ψ_0 or may be excited to any of a number of excited states, $\psi_1, \psi_2, \dots, \psi_N$ with excitation energies $\varepsilon_1, \varepsilon_2, \dots$. We consider first the case where the projectile is not composed of nucleons. Then the wavefunction of the system can be written asymptotically as

$$\Psi \rightarrow \sum_0^N u_v(\mathbf{r}_0) \psi_v(\mathbf{r}_1, \mathbf{r}_2, \dots, \mathbf{r}_A) \quad (5.1)$$

where \mathbf{r}_0 is the coordinate of the incident particle with respect to the center of mass of the target nucleus. We shall not explicitly indicate the spin and isospin coordinates so that \mathbf{r}_i contains these as well as the spatial coordinates.

The simplest prompt channel projection operator is given by

$$P\Psi = \sum_0^N u_v(\mathbf{r}_0) \psi_v(\mathbf{r}_1, \dots, \mathbf{r}_A) \quad (5.2)$$

so that

$$P = \sum_0^N \psi_v(\mathbf{r}_1 \cdots \mathbf{r}_A) \langle \psi_v(\mathbf{r}'_1 \cdots \mathbf{r}'_A) \rangle \quad (5.3)$$

where the ψ_v 's are normalized. The dependence on \mathbf{r}_0 and \mathbf{r}'_0 is not given since it is the unit operator that spatially would be $\delta(\mathbf{r}_0 - \mathbf{r}'_0)$. Comparing (5.3) and (5.2) we see that

$$u_v(\mathbf{r}_0) = \langle \psi_v(\mathbf{r}_1 \cdots \mathbf{r}_A) | \Psi(\mathbf{r}_0, \mathbf{r}_1, \dots, \mathbf{r}_A) \rangle \quad (5.4)$$

Asymptotically for $v \neq 0$, $u_v \rightarrow 0(e^{ik_v r_0}/r_0)$, where $k_v = \sqrt{(2m/\hbar^2)(E - \varepsilon_v)}$ where ε_v is the excitation energy of the v th excited state of the target nucleus. When $\varepsilon_v > E$, the wave function u_v decreases exponentially with increasing r_0 for large r_0 . It is not necessary to limit the sums in (5.2) and (5.3) to the open channels. If there is evidence that there are other channels of importance for the prompt processes, as might be the case for the multistep processes, these can readily included by extending the sum.

Using the P above, the equation for the prompt processes

$$(E - H_{PP})(P\Psi) = 0$$

becomes a set of coupled equations for u_v :

$$(E - H_{vv})u_v = \sum_{v' \neq v} H_{vv'}u_{v'} \quad (5.5)$$

where

$$H_{vv'} = \langle \psi_v | H | \psi_{v'} \rangle \quad (5.6)$$

The effect of averaging over the fine-structure resonances is to replace H_{PP} by the optical model H so that H_{vv} is no longer real and $H_{vv'}$ no longer Hermitian. Equations (5.5) are the equations for the coupled-channel method. These are clearly appropriate if the incident projectile is an electron, a muon, or a pion, for example.

If the incident projectile is a nucleon or an ion, two additional features must be considered. The first is the Pauli principle; the second is the possibility of transfer reactions either as open channels or as an intermediate state in a multi-step process. For the present we shall, for simplicity, not include transfer processes. The discussion of the projection operator needed for those cases will be deferred to Chapter VII.

Assume, then, that the incident particle is a nucleon and that asymptotically

$$\Psi \rightarrow \sum_0^N u_v(\mathbf{r}_0) \psi_v(\mathbf{r}_1, \dots, \mathbf{r}_A) \quad (5.7)$$

where \mathcal{A} is the antisymmetrization operator. It is still possible to use

$$P\Psi = \sum_0^N u_v(\mathbf{r}_0)\psi_v(\mathbf{r}_1, \dots, \mathbf{r}_A) \quad (5.2)$$

but then the sum must be extended to highly excited states (N very large), for the following reason. Even though (5.2) is not properly antisymmetrized, it is still possible to obtain a correct result by antisymmetrizing after solving the many-body Schrödinger equation. That is, it is possible to assume that the incident nucleon is distinguishable from the nucleons in the target, solve that problem exactly, and then antisymmetrize. However, that solution must contain the open channel in which the incident nucleon and a target nucleon exchange, a process referred to as *exchange scattering*. In other words, as one lets, for example, r_1 approach infinity, Ψ will contain an outgoing wave in this variable. This can only occur if the sum, (5.2), includes the continuum components of the set of target nuclear wave functions; that is, (5.2) would need to be written

$$\sum u_v\psi_v + \int u(v)\psi(v) dv$$

Moreover, $u(v)$ must be a singular function of v in order that a finite amplitude exist when r_1, r_2, \dots approaches infinity.

Antisymmetrization is most essential if a finite and minimal number of coupled channels is to be used. To see how antisymmetrization helps, consider the case of elastic scattering. Let the scattering without exchange be described by $u_0(\mathbf{r}_0)\psi_0(\mathbf{r}_1, \mathbf{r}_2, \dots, \mathbf{r}_A)$ and the exchange scattering, in which \mathbf{r}_i and \mathbf{r}_0 , are exchanged given by $v_i(\mathbf{r}_i)\psi_0(\mathbf{r}_1, \mathbf{r}_2, \dots, \mathbf{r}_{i-1}, \mathbf{r}_0, \mathbf{r}_{i+1}, \dots, \mathbf{r}_A)$, so that the antisymmetrized Ψ is given asymptotically by

$$\Psi \rightarrow \mathcal{A} \left[u_0(\mathbf{r}_0)\psi_0(\mathbf{r}_1 \cdots \mathbf{r}_A) + \sum_i v_i(\mathbf{r}_i)\psi_0(\mathbf{r}_1, \dots, \mathbf{r}_{i-1}, \mathbf{r}_0, \mathbf{r}_{i+1}, \dots, \mathbf{r}_A) \right]$$

Using the properties of the antisymmetrization operator this expression can be written as follows:

$$\Psi \rightarrow \mathcal{A} \left\{ \left[u_0(\mathbf{r}_0) - \sum_i v_i(\mathbf{r}_i) \right] \psi_0(\mathbf{r}_1 \cdots \mathbf{r}_A) \right\}$$

Thus the term in the antisymmetrized Ψ , which is proportional to ψ_0 , contains both the direct and the exchange amplitude. Importantly, it is not necessary to include in the sum being antisymmetrized contributions from the continuum target wavefunctions to obtain the correct scattering. In other words, the amplitude of the continuum wave functions need not be singular. Of course, if either method is used, antisymmetrization after solving the Schrödinger or

antisymmetrization of the wave function before solution, the same result will be obtained. However, if approximations are to be used, particularly by truncating the system of coupled-channel equations, a better approximation will be obtained if the approximate wave function is antisymmetrized before attempting a solution.

We therefore assume that

$$P\Psi = \mathcal{A} \left[\sum_{v=1}^N u_v(\mathbf{r}_0) \psi_v(\mathbf{r}_1 \cdots \mathbf{r}_A) \right] \quad (5.8)$$

where again N may be larger than the number of open channels. Our problem will be to determine P and thereby Q from this equation.

The form of the wave function given by (5.8) is used by many authors in discussing prompt reactions. However, as pointed out by Bell (62) and Villars (77), the set $\{u_v \psi_v\}$ is overcomplete because of the antisymmetrization required by the Pauli exclusion principle. To see this, consider Fig. 5.1, which shows two possible states of the system, the incident particle being indicated by an open circle, some of the target nucleons by the filled ones. The target wave function corresponding to Fig. 5.1a, say ψ_a , obviously differs from that for Fig. 5.1b, say ψ_b , so that each would give rise to separate terms, $u_a \psi_a$ and $u_b \psi_b$, in expansion equation (5.8). However, because of the identity of the particles, there is no difference between the states of the total system illustrated in Fig. 5.1. In other words, $\mathcal{A}[u_a \psi_a]$ and $\mathcal{A}[u_b \psi_b]$ are not independent. There must be a linear combination of the two which is identically zero.

More generally, there will be functions u'_v that satisfy the equation

$$\mathcal{A} \sum_v [u'_v(\mathbf{r}_0) \psi_v(\mathbf{r}_1 \cdots \mathbf{r}_A)] = 0 \quad (5.9)$$

The functions u'_v satisfying (5.9) will be referred to as *superfluous*. As pointed out by the example given above, one can always add to the series in (5.8) terms coming from exchange scattering without changing $P\Psi$. To demonstrate another example of the solution of (5.9), note that if ψ_v is a Slater determinant made up of single-particle wave functions, (5.9) is satisfied if u'_v is any one of these



FIG. 5.1

wavefunctions. The existence of solutions to (5.9) demonstrates that (5.8) does not provide a complete definition of P . Additional conditions are required.

Elimination of the superfluous solutions is essential for correct treatment of the Pauli exclusion principle. Serious errors can result if such a procedure is not carried out and (5.8) is used, assuming that all the u_v are independent. Friedman (67) has carried out a sample calculation, the scattering of neutrons on ^{16}O , and has shown that neglect of the fact that $\{u_v\}$ forms a dependent set, leads to gross errors in the energies and widths of the resonances, and the prediction of spurious resonances, which are not present in the results obtained with the exact calculation (see Table 5.1).

The needed condition that will eventually permit the determination of P is suggested by the discussion preceding (5.8): namely, that the remainder of the wave function

$$Q\Psi = (1 - P)\Psi$$

does not contain any dependence on the set $\{\psi_v\}$ present in (5.9). This is guaranteed[‡] if

$$\langle \psi_v(\mathbf{r}_1, \mathbf{r}_2, \dots, \mathbf{r}_A) | (1 - P)\Psi(\mathbf{r}_0, \mathbf{r}_1, \dots, \mathbf{r}_A) \rangle = 0 \quad 0 \leq v \leq N \quad (5.10)$$

for all \mathbf{r}_0 . Inserting $P\Psi$ from (5.8), (5.10) becomes

$$U_v(\mathbf{r}_0) = u_v(\mathbf{r}_0) - \sum_{v'=0}^N \langle K_{vv'}(\mathbf{r}, \mathbf{r}_0) | u_{v'}(\mathbf{r}) \rangle \quad (5.11)$$

where

$$U_v(\mathbf{r}_0) \equiv \langle \psi_v(\mathbf{r}_1, \mathbf{r}_2, \dots, \mathbf{r}_A) | \Psi(\mathbf{r}_0, \mathbf{r}_1, \dots, \mathbf{r}_A) \rangle \quad (5.12)$$

and

$$K_{vv'}(\mathbf{r}, \mathbf{r}_0) \equiv A \langle \psi_v(\mathbf{r}, \mathbf{r}_2, \dots, \mathbf{r}_A) | \psi_{v'}(\mathbf{r}_0, \mathbf{r}_2, \dots, \mathbf{r}_A) \rangle \quad (5.13)$$

Note[§] that K is just the one-body density matrix of (I.4.4) in deShalit and Feshbach (74) and of (I.11.11).

[‡]In (5.10) and below, integration is performed over the variables common to the bra and ket of the matrix element.

[§]Kerman (67) points out that K represents the lack of orthogonality between $\mathcal{A}(u_v\psi_v)$ and $\mathcal{A}(u_{v'}\psi_{v'})$ although ψ_v is orthogonal to $\psi_{v'}$. Indeed,

$$\frac{1}{A+1} \langle \mathcal{A}u_v\psi_v | \mathcal{A}u_{v'}\psi_{v'} \rangle = \langle u_v\psi_v | \mathcal{A}u_{v'}\psi_{v'} \rangle = \langle u_v | (\delta_{vv'} - K_{vv'}) u_{v'} \rangle$$

Hence orthogonality will only occur if $K_{vv'} = \delta_{vv'}$, that is, if K is diagonal with eigenvalues of unity.

TABLE 5.1^a Scattering of Neutrons by ¹⁶O

Primary Calculation		Control Calculation	
Energy E_r	Half-Width $\Gamma/2$	Energy E_r	Half-Width $\Gamma/2$
$j = \frac{5}{2}$			
(MeV)	(keV)	(MeV)	(keV)
10.86	0.01	9.67	0.34
10.98	2.5	10.00	4.9
11.01	8.5	10.02	0.22
12.90	0.58	10.55	0.24
13.36	1.7	10.67	0.09
14.48	0.73	11.05	8.3
14.92	10	12.93	0.53
15.52	2.2	13.37	1.6
		14.50	0.83
		14.93	11
		15.52	2.1
$j = \frac{7}{2}$			
(MeV)	(keV)	(MeV)	(keV)
5.94	120	5.24	38
6.97	57	6.72	21
7.88	7.0	7.77	0.009
9.19	42	8.01	39
10.07	1.0	9.03	35
11.21	0.12	9.80	1.1
11.47	0.10	10.16	28
12.54	22	10.92	0.002
13.79	36	11.27	0.01
15.15	15	12.57	18
		13.79	35
		15.15	15
$j = \frac{9}{2}$			
(MeV)	(eV $\times 10^{-3}$)	(MeV)	(eV $\times 10^{-2}$)
5.53	0.53	5.92	1.3
7.33	0.03	7.15	0.36
10.58	190	9.13	0.18
10.75	1.4	10.13	0.009
14.18	54	10.00	190
		14.19	59
$j = \frac{11}{2}$			
(MeV)	(eV)	(MeV)	(eV)
6.75	0.25	5.33	0.48
		8.97	0.54

Source: Friedman (67).

^aResonance parameters for the "exact" case, the primary calculation, and a case in which the projectile was given some properties which distinguished it, the control calculation thus checking the effect of the Pauli principle.

It is convenient to define the matrices

$$u \equiv \begin{pmatrix} u_0 \\ u_1 \\ \vdots \\ u_N \end{pmatrix} \quad U \equiv \begin{pmatrix} U_0 \\ U_1 \\ \vdots \\ U_N \end{pmatrix} \quad K = \int \begin{pmatrix} K_{00} & K_{0N} \\ \vdots & \vdots \\ K_{N0} & K_{NN} \end{pmatrix} \quad (5.14)$$

so that (5.11) becomes

$$U = (1 - K)u \quad (5.15)$$

where

$$1 \equiv \int \delta(\mathbf{r} - \mathbf{r}') \delta_{vv'}$$

Note that

$$\left\langle \psi_v(\mathbf{r}_1 \cdots \mathbf{r}_A) \left| \mathcal{A} \sum_{v'} u_{v'}(\mathbf{r}_0) \psi_{v'}(\mathbf{r}_1 \cdots \mathbf{r}_A) \right. \right\rangle = [(1 - K)u]_v \quad (5.16)$$

We now consider the properties of K . We observe that K is *Hermitian*, that is,

$$K_{vv'}(\mathbf{r}, \mathbf{r}_0) = K_{v'v}^*(\mathbf{r}_0, \mathbf{r})$$

Therefore, K can be diagonalized and its eigenvalues are real:

$$K\omega_\alpha = \kappa_\alpha \omega_\alpha \quad \langle \omega_\alpha, \omega_\beta \rangle = \delta_{\alpha\beta} \quad (5.16')$$

Second $(1 - K)$ is positive definite. For any u [see (5.16)]

$$\langle u | (1 - K)u \rangle = \left\langle \sum_v u_v(\mathbf{r}_0) \psi_v(\mathbf{r}_1 \cdots \mathbf{r}_A) \left| \mathcal{A} \left\langle \sum_{v'} u_{v'}(\mathbf{r}_0) \psi_{v'}(\mathbf{r}_1 \cdots \mathbf{r}_A) \right. \right. \right\rangle$$

Since the ket is antisymmetric, one can rewrite this equation as

$$\langle u | (1 - K)u \rangle = \frac{1}{A+1} \langle \mathcal{A} \sum_v u_v \psi_u | \mathcal{A} \sum_{v'} u_{v'} \psi_{v'} \rangle \quad (5.17a)$$

$$\geq 0 \quad (5.17)$$

concluding the proof.

From these results one can immediately conclude that the eigenvalues of K ,

κ_α , are less than or equal to 1:

$$\kappa_\alpha \leq 1. \quad (5.18)$$

Problem. Show that K_{vv} is positive definite. Therefore, if $P\Psi$ contains only the elastic channel, so that $K = K_{00}$,

$$1 \geq \kappa_\alpha \geq 0$$

Starting from (5.17a), one can derive a further bound on κ_α . Expand $\mathcal{A} \sum_v u_v \psi_v$ in a complete set of target functions $\psi_t(\mathbf{r}_1 \cdots \mathbf{r}_A)$. It is very important to bear in mind that it would extend beyond N , the truncation value given by (5.8). Then from (5.17a),

$$\begin{aligned} \langle u | (1 - K) u \rangle &= \frac{1}{A+1} \sum_{t,t'=0}^{\infty} \left\langle \sum_v u_v (1 - K)_{vt} \psi_t \left| \sum_{v'} u_{v'} (1 - K)_{v't'} \psi_{t'} \right. \right\rangle \\ &= \frac{1}{A+1} \sum_t \left\langle \sum_v u_v (1 - K)_{vt} \psi_t \left| \sum_{v'} u_{v'} (1 - K)_{v't} \psi_t \right. \right\rangle \end{aligned}$$

If we drop the terms for both t and $t' > N$ we drop a positive quantity, so that

$$\langle u | (1 - K) u \rangle \geq \frac{1}{A+1} \sum_{t,t'=0}^N \left\langle \sum_v u_v (1 - K)_{vt} \psi_t \left| \sum_{v'} u_{v'} (1 - K)_{v't'} \psi_{t'} \right. \right\rangle$$

Now insert for u an eigenfunction of K , ω_α , with eigenvalue κ_α . One obtains

$$(1 - \kappa_\alpha) \geq \frac{1}{A+1} (1 - \kappa_\alpha)^2$$

so that

$$\kappa_\alpha \geq -A \quad (5.18')$$

which, together with (5.18), bounds κ_α between $-A$ and 1.

Problem. Prove that

$$\text{tr } K = A(N+1) \quad (5.19)$$

where the trace of a matrix K with elements $K_{vv}(\mathbf{r}, \mathbf{r}_0)$ is defined as

$$\text{tr } K = \sum_v \int d\mathbf{r} K_{vv}(\mathbf{r}, \mathbf{r}) \quad (5.20)$$

Problem. Prove that

$$\text{tr } K^2 \leq (\text{tr } K)^2 = A^2(N+1)^2$$

The properties of K for elastic and inelastic scattering have been discussed extensively by Friedman (67):

One example of K will prove instructive. Suppose that $N=0$; that is, the prompt channel deals only with elastic scattering. K has only one element, K_{00} :

$$K_{00} = A \langle \psi_0(\mathbf{r}, \mathbf{r}_2, \dots, \mathbf{r}_A) | \psi_0(\mathbf{r}_0, \mathbf{r}_2, \dots, \mathbf{r}_A) \rangle \quad (5.21)$$

where ψ_0 is the ground-state wave function. Suppose that this wave function is a Slater determinant constructed of A single-particle wave functions, w_i ; then it is easy to show that

$$K_{00} = \sum_1^A w_\alpha^*(\mathbf{r}) w_\alpha(\mathbf{r}_0) \quad (5.22)$$

For this K the eigenfunctions satisfying

$$K\omega_\alpha = \kappa_\alpha \omega_\alpha$$

are

$$\omega_\alpha(\mathbf{r}) = w_\alpha(\mathbf{r})$$

and

$$\kappa_\alpha = 1 \quad (5.23)$$

Note that, as should have been apparent from the discussion, the eigenfunctions of K do not form a complete set. For this case, however, $\mathcal{A}u_v\psi_v$ and $\mathcal{A}u_{v'}\psi_{v'}$ are orthogonal.

Problem. Consider a two-particle ψ_v . Each ψ_v is a Slater determinant made up of two single-particle wave functions taken from the set w_0, w_1, w_2 : the ground state ψ_0 involving w_0 and w_1 , ψ_1 just w_1 and w_2 and ψ_2 , w_0 and w_2 . Show that the K matrix in this example is

$K =$

$$\begin{bmatrix} w_0^*(\mathbf{r})w_0(\mathbf{r}_0) + w_1^*(\mathbf{r})w_1(\mathbf{r}_0) & \omega_0^*(\mathbf{r})w_2(\mathbf{r}_0) & w_1^*(\mathbf{r})w_2(\mathbf{r}_0) \\ w_2^*(\mathbf{r})w_0(\mathbf{r}_0) & w_1^*(\mathbf{r})w_1(\mathbf{r}_0) + w_2^*(\mathbf{r})w_2(\mathbf{r}_0) & -w_1^*(\mathbf{r})w_0(\mathbf{r}_0) \\ w_2^*(\mathbf{r})w_1(\mathbf{r}_0) & -w_0^*(\mathbf{r})w_1(\mathbf{r}_0) & w_0^*(\mathbf{r})w_0(\mathbf{r}_0) + w_2^*(\mathbf{r})w_2(\mathbf{r}_0) \end{bmatrix}$$

Show that eigenvalues of K are 1 with one exception, for which the eigenvalue is -2 .

Returning to (5.15) it is obvious that any inversion of that equation must treat eigenstates of K with eigenvalues of 1 with care. The corresponding eigenfunctions are denoted $\omega_\alpha^{(1)}$. These solutions are just the *superfluous* solutions mentioned below (5.9). To prove this, consider

$$\langle \psi_v | \mathcal{A} \sum_{v'} \omega_{\alpha v'}^{(1)} \psi_{v'} \rangle = \omega_{\alpha v}^{(1)} - \sum_{v'} \langle K_{vv'} | \omega_{\alpha v'}^{(1)} \rangle$$

But the right-hand side equals zero because $\omega_\alpha^{(1)}$ is an eigenstate of K with eigenvalue of 1, so that

$$\left\langle \psi_v(\mathbf{r}_1 \cdots \mathbf{r}_A) \left| \mathcal{A} \sum_{v'} \omega_{\alpha v'}^{(1)}(\mathbf{r}_0) \psi_{v'} \right. \right\rangle = 0$$

It thus follows that

$$\left\langle \mathcal{A} \sum_v \omega_{\alpha v}^{(1)}(\mathbf{r}_0) \psi_v \left| \mathcal{A} \sum_{v'} \omega_{\alpha v'}^{(1)}(\mathbf{r}_0) \psi_{v'} \right. \right\rangle = 0$$

and therefore

$$\mathcal{A} \sum_v \omega_{\alpha v}^{(1)} \psi_v = 0 \quad (5.9)$$

the condition for the superfluous solution. Moreover, and this is an important point, the final expression for P need not contain any dependence on $\omega_\alpha^{(1)}$, since these terms will not contribute to

$$P\Psi = \mathcal{A} \sum_v u_v \psi_v$$

Hence the use of the term *superfluous*. This fact manifests itself in a property of U defined by (5.12) and (5.14), namely

$$\langle \omega_\alpha^{(1)} | U \rangle = \sum \langle \omega_{\alpha v}^{(1)} | U_v \rangle = 0 \quad (5.24)$$

To prove this, insert (5.15) for U , yielding

$$\langle \omega_\alpha^{(1)} | U \rangle = \langle \omega_\alpha^{(1)} | (1 - K)u \rangle$$

Because of the hermiticity of K ,

$$\langle \omega_\alpha^{(1)} | U \rangle = \langle (1 - K)\omega_\alpha^{(1)} | U \rangle = 0$$

Thus the superfluous solutions are orthogonal to U .

We now return to (5.15):

$$U = (1 - K)u$$

The general solution of this equation is

$$u = \sum_{\kappa_\alpha \neq 1} \omega_\alpha \frac{\langle \omega_\alpha | U \rangle}{1 - \kappa_\alpha} + \text{terms in } \omega_\alpha^{(1)}$$

In accordance with the discussion just concluded, the terms in $\omega_\alpha^{(1)}$ are dropped, so that

$$\langle \omega_\alpha^{(1)} | u \rangle = 0 \quad (5.25)$$

and

$$u = \sum_{\kappa_\alpha \neq 1} \omega_\alpha \frac{\langle \omega_\alpha | U \rangle}{1 - \kappa_\alpha} \equiv \frac{1}{1 - K'} U \quad (5.26)$$

where the operator $1/1 - K'$ is defined by

$$\frac{1}{1 - K'} = \sum_{\kappa_\alpha \neq 1} \frac{\omega_\alpha \rangle \langle \omega_\alpha}{1 - \kappa_\alpha} \quad (5.27)$$

It is convenient to rewrite (5.26) as follows:

$$u = U + \sum_{\kappa_\alpha \neq 1} \omega_\alpha \langle \omega_\alpha | U \rangle \left(\frac{1}{1 - \kappa_\alpha} - 1 \right)$$

where we have made use of (5.24). Finally,

$$u = U + \sum_{\kappa_\alpha \neq 1} \omega_\alpha \langle \omega_\alpha | U \rangle \frac{\kappa_\alpha}{1 - \kappa_\alpha} \quad (5.28)$$

In terms of K' ,

$$u = \frac{1}{1 - K'} U = U + \frac{K'}{1 - K'} U \quad (5.29)$$

Recalling that $U_v \equiv \langle \psi_v | \Psi \rangle$, one obtains

$$P\Psi = \mathcal{A} \sum_v u_v \psi_v = \mathcal{A} \sum_v \left[U_v + \sum_{\kappa_\alpha \neq 1} \omega_{\alpha v} \langle \omega_\alpha | U \rangle \frac{\kappa_\alpha}{1 - \kappa_\alpha} \right] \psi_v$$

In terms of K' ,

$$P = \mathcal{A} \left[\sum_r \psi_v \right] \left\langle \psi_v + \sum_{v,v'} \psi_v \right\rangle \left(\frac{K'}{1-K'} \right)_{vv'} \langle \psi_{v'} \rangle = \mathcal{A} \left[\sum_{vv'} \psi_v \right] \left(\frac{1}{1-K'} \right)_{vv'} \langle \psi_{v'} \rangle \quad (5.30)$$

This is the projection operator which, when applied to Ψ , yields $\mathcal{A} \sum u_v \psi_v$, with the requirement that none of the ψ_v which appear in this sum are present in $Q\Psi$. This requirement must be satisfied if $P\Psi$ is to involve a finite number of ψ_v . Equation (5.30) reduces to the simple form $\sum_v \psi_v \langle \psi_v \rangle$ when all the κ_a are either zero or 1.

With P determined, it now becomes possible to develop an explicit statement for the Schrödinger equation (2.3) and (2.4) or (2.7). Let us use the last form,

$$[E - (H_{\text{eff}})_{PP}]P\Psi = 0 \quad (5.31)$$

To reduce this equation to a set of coupled equations in one variable, namely the distance between the projectile and the center of mass of the target, premultiply (5.31) successively by ψ_v and integrate over all the coordinates of the target nucleons. Note from (5.10) and (5.12) that

$$U_v = \langle \psi_v | \Psi \rangle = \langle \psi_v | P\Psi \rangle \quad (5.32)$$

Since Ψ is an arbitrary antisymmetric function of $(A+1)$ variables, the second pair of equations holds for any such function. Equation (5.31) becomes the set of coupled equations

$$EU_v = \sum_{v',v''} \left\langle \psi_v \left| H_{\text{eff}} \mathcal{A} \sum_{v',v''} \psi_{v'} \left(\frac{1}{1-K'} \right)_{v'v''} U_{v''} \right. \right\rangle \quad (5.33)$$

In this equation, the effect of the projection appears explicitly in the Hamiltonian term. If we now introduce the function u_v , (5.33) becomes

$$E \sum_{v'} (1-K')_{vv'} u_{v'} = \left\langle \psi_v \left| H_{\text{eff}} \mathcal{A} \sum_{v'} \psi_{v'} u_{v'} \right. \right\rangle \quad (5.34)$$

The term on the right involves both direct and exchange terms. The term on the left is modified by the inclusion of normalization corrections. Note, however, the explicit omission of the eigenfunctions of K with unit eigenvalue. Since $K'_{vv'}$ can be written as a finite sum of factorable terms its inclusion does not present any special difficulties. If all the eigenvalues of K are 1 or zero, $K' = 0$, with the result that one need only include the exchange terms in the effective Hamiltonian to take account of antisymmetrization.

An alternative form for (5.34) is obtained by reintroducing the operator K :

$$E \sum_{v'} (1 - K_{vv'}) u_{v'} + E \sum_{\alpha v'} \omega_{\alpha v}^{(1)} \langle \omega_{\alpha v}^{(1)} | u_{v'} \rangle = \left\langle \psi_v \left| H_{\text{eff}} \mathcal{A} \sum_{v'} u_{v'} \psi_{v'} \right. \right\rangle \quad (5.35)$$

Or because of the orthogonality between $\omega_{\alpha}^{(1)}$ and u ,

$$\begin{aligned} E \left\langle \psi_v \left| \mathcal{A} \sum_{v'} u_{v'} \psi_{v'} \right. \right\rangle &= \left\langle \psi_v \left| \mathcal{H}_{\text{eff}} \mathcal{A} \sum_{v'} u_{v'} \psi_{v'} \right. \right\rangle \\ \langle \omega_{\alpha}^{(1)} | u \rangle &= 0 \end{aligned} \quad (5.36)$$

In other words, one can use the naive wave function $\mathcal{A} \sum u_v \psi_v$ in the Schrödinger equation as long as u is orthogonal to all the eigenstates $\omega_{\alpha}^{(1)}$ of K with eigenvalue 1. Which form, (5.34) or (5.36), is used is a matter of convenience. If the $\omega_{\alpha}^{(1)}$ are known a priori, it might be more convenient to use (5.36). On the other hand, if all the eigenvalues of K are zero or 1, (5.34) might prove more useful, especially since the orthogonality of $\omega_{\alpha}^{(1)}$ to u is an automatic consequence of (5.34).

Orthogonality of $\omega_{\alpha}^{(1)}$ can be enforced by projection:

$$\bar{u} = u - \sum_{\alpha} \omega_{\alpha}^{(1)} \langle \omega_{\alpha}^{(1)} | u \rangle$$

The resulting $\mathcal{A} \sum \bar{u}_v \psi_v$ remains a solution of (5.36) since

$$\mathcal{A} \sum_{\alpha} \omega_{\alpha v}^{(1)} \psi_v$$

is identically zero for all α [Saito (69)].

Another method that is particularly useful when asymptotic conditions need to be satisfied explicitly is used by Auerbach, Gal et al (72). For example, rewrite (5.34) [or (5.35)] making the orthogonality of $\omega_{\alpha}^{(1)}$ explicit by introducing the projection operator q_1 and p_1

$$q_1 \equiv 1 - \sum_{\alpha} \omega_{\alpha}^{(1)} \langle \omega_{\alpha}^{(1)} | = 1 - p_1 \quad (5.37)$$

Then both equations can be written in the form

$$q_1 E \rho u = q_1 h u \quad (5.38)$$

If (5.34) is used, ρ is just $1 - K'$. The identical result is obtained if (5.35) is used.

Writing $q_1 = 1 - p_1$, (5.38) becomes

$$(E \rho - h) u = p_1 (E \rho - h) u$$

Let

$$(E\rho - h)u^{(0)} = 0$$

and

$$(E\rho - h)\mathcal{G}^{(+)} = 1$$

Then

$$\begin{aligned} u &= u^{(0)} + \mathcal{G}^{(+)}p_1(E\rho - h)u \\ &= u^{(0)} + \sum_{\alpha} \mathcal{G}^{(+)}\omega_{\alpha}^{(1)} \langle \omega_{\alpha}^{(1)} | (E\rho - h)u \rangle \end{aligned}$$

The orthogonality requirement becomes

$$\langle \omega_{\beta}^{(1)} | u \rangle = \langle \omega_{\beta}^{(1)} | u^{(0)} \rangle + \sum_{\alpha} \langle \omega_{\beta}^{(1)} | \mathcal{G}^{(+)}\omega_{\alpha}^{(1)} \rangle \langle \omega_{\alpha}^{(1)} | (E\rho - h)u \rangle = 0$$

Defining the matrix \hat{g} by

$$g_{\beta\alpha} = \langle \omega_{\beta}^{(1)} | \mathcal{G}^{(+)}\omega_{\alpha}^{(1)} \rangle$$

these equations can be solved for $\langle \omega_{\alpha}^{(1)} | (E\rho - h)u \rangle$:

$$\langle \omega_{\alpha}^{(1)} | (E\rho - h)u \rangle = - \sum_{\beta} (\hat{g}^{-1})_{\alpha\beta} \langle \omega_{\beta}^{(1)} | u^{(0)} \rangle$$

Finally,

$$u = u^{(0)} - \sum_{\alpha} \mathcal{G}^{(+)}\omega_{\alpha}^{(1)} (\hat{g}^{-1})_{\alpha\beta} \langle \omega_{\beta}^{(1)} | u_0 \rangle \quad (5.39)$$

Problem. In (5.34) introduce the wave functions

$$\Omega_v = \sum_{v'} (\sqrt{1 - K'})_{vv'} u_{v'}$$

and derive the coupled equations for Ω_v . Show that the effective Hamiltonian for this equation is Hermitian.

It is perhaps unnecessary to add that H_{eff} in (5.34) or (5.36) can be replaced by H_{opt} and thus provide a description of the prompt processes after averaging over the fine structure. The supplementary condition in (5.36) must, of course, still be satisfied.

In summary, to take into account the Pauli exclusion principle and simultaneously limit the space \mathcal{P} , one first evaluates K . This matrix depends only on the ground state, ψ_0 , of the target nucleus and a finite number of its

excited states, ψ_v . Once K is obtained, and its eigenstates ω_α determined, one can proceed to solve (5.34) using only those ω_α whose eigenvalues differ from zero or 1. Or using only those with eigenvalues of unity, one can solve (5.36), including the supplementary condition. Determining the eigenstates of K is not a formidable task, as K is bounded and Hermitian and depends on one coordinate. However, the target wave functions should include center-of-mass effects, which does introduce some complication.

If determinantal wave functions are used for ψ_v , one avoids calculating K altogether, since then it is known that all the eigenvalues of K are 1 and that the eigenfunctions of K are just the single-particle wave functions making up the determinant. However, the center-of-mass problem remains.

The discussion above is restricted to scattering, elastic and inelastic. The effects of the Pauli principle for particle transfer reactions are discussed in later chapters.

6. ALTERNATIVE REACTION FORMALISMS

Such a wide variety of reaction formalisms have been proposed that it is not possible to present an adequate review of each in this volume. We have, therefore, chosen to describe a few of the more familiar examples. To the extent that each one is exact, they should give identical answers to a specific problem. The advantages of a given approach depend more on the ease with which it can be applied to a given physical situation. One should especially ask: Is it in a form that permits a direct physical interpretation of the experimental results, and similarly, does it have predictive capability? Can it make good use of what is known about the nuclear structure of the colliding systems, of the compound system, and of the produced particles? Can its parameters, in principle, if not immediately, be derived from fundamental nuclear theory, that is from the underlying nucleon–nucleon force, or less ambitiously from a model Hamiltonian plus a residual interaction?

Fortunately for the comparison with experimental data, the *form* of the results for the transition amplitudes and cross sections is the same for all these formalisms. This might be referred to as a *formalism invariance*. An important reason for this similarity lies in the requirements of unitarity. Unitarity, when applied to a *single-channel* process, requires that the S matrix satisfy

$$|S|^2 = 1 \quad \text{or} \quad S = e^{2i\delta}, \quad \delta \text{ real} \quad (6.1)$$

This condition is satisfied by the following form [see (2.44)]:

$$S = e^{2i\phi_P} \frac{1 - i\pi\mathcal{K}}{1 + i\pi\mathcal{K}} \quad (6.2)$$

where ϕ_P is a smoothly varying function of the energy and \mathcal{K} is a real function

which contains that part of S which varies rapidly with energy. The function ϕ_P gives the potential scattering phase shift so that the potential scattering S matrix, S_P , is

$$S_P = e^{2i\phi_P}$$

and (6.2) can be written

$$S = S_P S_R \quad (6.3)$$

where

$$S_R = \frac{1 - i\pi\mathcal{K}}{1 + i\pi\mathcal{K}} \quad (6.4)$$

The words *smoothly* and *rapidly* are not quantitatively defined, so that the factorization equation (6.3) is not completely specified, and indeed, different reaction theories will use differing S_P .

The transition matrix $\mathcal{T} [(1 - S)/2\pi i]$ is

$$\mathcal{T} = \mathcal{T}_P + S_P \mathcal{T}_R \quad (6.5)$$

where

$$\mathcal{T}_P = \frac{1 - S_P}{2\pi i} = -\frac{1}{\pi} e^{i\phi_P} \sin \phi_P$$

and

$$\mathcal{T}_R = \frac{\mathcal{K}}{1 + i\pi\mathcal{K}} \quad (6.6)$$

Equation (6.5) has the same form as (2.47) in the single-channel context. Moreover, the resonance representation of \mathcal{K} can in general be given by

$$\mathcal{K} = \frac{1}{2\pi} \sum \frac{\gamma_s^2}{E - e_s} \quad (6.7)$$

where γ_s^2 and e_s are real. In the case of a single isolated resonance, at say e_0 , \mathcal{T} becomes

$$\mathcal{T} = -\frac{1}{\pi} e^{i\phi_P} \sin \phi_P + e^{2i\phi_P} \frac{(1/2\pi)[\gamma_0^2/(E - e_0)]}{1 + (i/2)[\gamma_0^2/(E - e_0)]}$$

or

$$\mathcal{T} = -\frac{1}{\pi} e^{i\phi_P} \left[\sin \phi_P - e^{i\phi_P} \frac{\gamma_0^2/2}{E - e_0 + (i/2)\gamma_0^2} \right] \quad (6.8)$$

which is just the single-channel resonance formula, showing both a potential scattering term and a resonant term. Equation (6.8) is a consequence of unitarity plus the statement that the two kinds of amplitudes are involved: When there are many terms in the series for \mathcal{K} , \mathcal{T} is not as simple. However, it should be possible to expand \mathcal{T} in terms of the poles of the S matrix, E_μ , such as that given by (2.33):

$$\mathcal{T} = \mathcal{T}_P + e^{2i\phi_P} \sum_{\mu} \frac{\mathcal{A}_{\mu}}{E - E_{\mu}} \quad (6.9)$$

so that

$$\mathcal{T}_R = \sum_{\mu=1}^n \frac{\mathcal{A}_{\mu}}{E - E_{\mu}} = \frac{(1/2\pi) \sum_1^n [\gamma_s^2 / (E - e_s)]}{1 + (i/2) \sum_1^n [\gamma_s^2 / (E - e_s)]} \quad (6.10)$$

Recall that both \mathcal{A}_{μ} and E_{μ} are complex numbers, so that the number of parameters in the middle expression is $4n$ if the number on the right side is $2n$, implying that there are $2n$ relations between $\{\mathcal{A}_{\mu}\}$ and $\{E_{\mu}\}$. These relations can be obtained from (6.10). First expand both sides of (6.10) in a power series in inverse powers of E . The left-hand side gives

$$\mathcal{T}_R = \frac{1}{E} \sum \mathcal{A}_{\mu} + \frac{1}{E^2} \sum \mathcal{A}_{\mu} E_{\mu} + \dots$$

and the right-hand side gives

$$\mathcal{T}_R = \frac{1}{2\pi} \left[\frac{1}{E} \sum \gamma_s^2 + \frac{1}{E^2} \left\{ \sum \gamma_s^2 e_s - \frac{i}{2} (\sum \gamma_s^2)^2 \right\} + \dots \right]$$

so that

$$\begin{aligned} \sum \mathcal{A}_{\mu} &= \frac{1}{2\pi} \sum \gamma_s^2 \\ \sum \mathcal{A}_{\mu} E_{\mu} &= \frac{1}{2\pi} \left[\sum \gamma_s^2 e_s - \frac{i}{2} (\sum \gamma_s^2)^2 \right] \end{aligned}$$

Since $\{\gamma_s^2\}$ is real,

$$\sum \text{Im } \mathcal{A}_{\mu} = 0 \quad (6.11)$$

$$\sum \text{Re } \mathcal{A}_{\mu} = \frac{1}{2\pi} \sum \gamma_s^2 \quad (6.12)$$

An alternative but not independent requirement states that the poles of the

right-hand side of (6.10) occur at E_μ . These poles are the roots of

$$\prod_{s=1}^n (E - e_s) + \frac{i}{2} \sum \gamma_s^2 \prod_{t \neq s} (E - e_t) = 0$$

The sum of the roots equals the coefficient of $-E^{(n-1)}$, so that

$$\sum E_\mu = \sum \left(e_s - \frac{i}{2} \gamma_s^2 \right)$$

implying that

$$\operatorname{Re} \sum E_\mu = \sum e_s \quad (6.13)$$

and

$$\operatorname{Im} \sum E_\mu = -\frac{1}{2} \sum \gamma_s^2 = -\pi \sum \operatorname{Re} \mathcal{A}_\mu \quad (6.14)$$

One can verify from (6.8) that (6.11) and (6.14) hold for an isolated resonance:

$$\operatorname{Im} \mathcal{A}_\mu = 0$$

$$\operatorname{Re} \mathcal{A}_\mu = -\frac{1}{\pi} \operatorname{Im} E_\mu$$

Equations (6.11) and (6.14) state that these equations hold on the average for overlapping resonances. One can readily continue this process. The next order yields

$$2\pi \sum_{\mu > \nu} (\operatorname{Re} \mathcal{A}_\mu)(\operatorname{Re} E_\nu) = \operatorname{Im} \sum_{\mu > \nu} E_\mu E_\nu$$

However, these additional relationships are not informative. The major point, to be gained from the discussion following (6.10), is that the parameters \mathcal{A}_μ and E_μ are not independent, if S is to be unitary.

The sequence of equations (6.5), (6.6), (6.7), and (6.9) present an expansion of \mathcal{T}_R in terms of the poles of the reactance matrix \mathcal{K} , which automatically satisfies unitarity or an expansion in poles of the S matrix, where, however, unitarity is not obvious but is secured through relations such as (6.11) and (6.14). The form of these results is independent of a particular reaction formalism. The difference among the formalisms lies in their statement regarding the potential scattering amplitude \mathcal{T}_P and the consequent differences in the interpretation of the parameters γ_μ^2 , e_μ , \mathcal{A}_μ , and E_μ .

As an example, consider the potential scattering amplitude \mathcal{T}_P . In an early version of the \mathcal{R} -matrix theory (to be described below), \mathcal{T}_P is taken to be hard-sphere scattering for which the phase shift for the zero angular momentum $l=0$ partial wave (and for large energies for all l) is $-kR$, where R is the radius

of the sphere. In the formalism of Section 2 it is the scattering caused by the Hamiltonian \bar{H}_{pp} . How can these give the same total amplitude? Clearly, hard-sphere scattering cannot be correct since it presumes an infinite potential energy. It must therefore be compensated by taking many terms in the series for \mathcal{H} . Summing up the effect of distant resonances, whose energy dependence over a small interval in energy is weak, modifies the hard-sphere shift, presumably into one whose energy dependence is more in accord with scattering caused by a potential. Moreover, we see that these distant resonances are not physically meaningful. Choosing the potential scattering does affect the values for the widths [see, e.g., (2.22)] and the resonance energies. Consistency requires that the same description of potential scattering is used in calculating or developing the energy dependence of the width and resonance energy.

The analysis of experimental data exhibits a similar problem. In fitting a cross section to either (6.6) and (6.7) or to (6.9), it is necessary to determine the parameters ϕ_p as well as say γ_μ and e_μ , and to decide how many terms in the series over μ to use. Changing that number will modify the empirical values of γ_μ , e_μ , and ϕ_p . The pragmatic response to this issue is to include the number of terms as one of the parameters in obtaining a fit. In other words, one looks for a number of terms such that the inclusion of an additional one in the sum over μ does not affect the χ^2 for the fit and does not modify the values of the parameters obtained from the data. One must also require that the potential phase shift does not vary rapidly with energy. It is clear that in presenting an analysis of data, the method used in obtaining the parameters should be carefully stated. Of course, these problems do not arise if the resonance is isolated.

Problem. Write the S matrix in the presence of doorway states is

$$S = S_p S_D S_r$$

where S_p is the S matrix for potential scattering, S_D for doorway state resonances, and S_r for fine-structure resonances. Show that

$$\mathcal{T} = \mathcal{T}_p + S_p \mathcal{T}_D + S_p S_D \mathcal{T}_r \quad (6.15)$$

We turn now to some examples of reaction formalisms. Our general aim will be to relate them to the general discussion given in Sections 2 to 6 of this chapter.

A. The Theory of Kapur and Peierls[†]

This theory sets a boundary condition at each channel radius R_c . In the single-channel case, the boundary condition to be satisfied by the resonant

[†]Kapur and Peierls (38).

state is

$$\frac{\partial X_\mu}{\partial r} = ikX_\mu \quad \text{at } r = R \quad (6.16)$$

The radius R is any distance beyond which the nuclear interactions vanish. The consequence is a resonance series for the S matrix [see (2.46)] of the form given by (2.33). The parameters, the widths and resonance energies, are real but energy dependent. Equation (6.16) simply states that X_μ at R is an outgoing wave with wave number k . The generalization of (6.16) to several channels requires that

$$\frac{\partial X_{\mu c}}{\partial r} = ik_c X_{\mu c} \quad \text{at } r = R_c \quad (6.17)$$

where the subscript c denotes the channel and k_c is the corresponding wave number.

The theory described in Section 2 of this chapter provides a generalization of the theory of Kapur and Peierls free of the use of a boundary condition radius or separation into partial waves. To demonstrate this point, consider the eigenfunctions Ω_μ of the operator $H_{QQ} + W_{QQ}$ discussed in the material following (2.31). They satisfy

$$(E_\mu - H_{QQ} - W_{QQ})\Omega_\mu = 0 \quad (6.18)$$

where

$$W_{QQ} = H_{QP} \frac{1}{E^{(+)} - H_{PP}} H_{PQ}$$

Note the parametric dependence of Ω_μ and E_μ on E , the energy of the system. Equation (6.18) is equivalent to the coupled equations

$$(E - H_{PP})\chi_\mu = H_{PQ}\Omega_\mu \quad (6.19a)$$

$$(E - H_{QQ})\Omega_\mu = H_{QP}\chi_\mu \quad (6.19b)$$

where χ_μ are the open-channel wave functions associated with the resonant state Ω_μ . Equation (6.18) is obtained if the solution of (6.19a) is taken to be

$$\chi_\mu = \frac{1}{E^{(+)} - H_{PP}} H_{PQ}\Omega_\mu \quad (6.19c)$$

The χ_μ , then, satisfy outgoing wave boundary conditions which are the natural generalization of (6.17), concluding the argument. As in the case of the Kapur–Peierls theory, the resonance widths and energies are functions of E .

This dependence is weak; its strength determined by the energy variation of the open-channel wave functions, that is, of the prompt amplitudes. Indeed, this energy dependence is desirable. It takes into account the effect of the energy dependence of the prompt amplitudes upon the resonance parameters. This dependence could be significant if the resonance is wide, or if many resonances in a substantial energy domain, ΔE , are being considered.

B. \mathcal{R} -Matrix Formalism[†]

This method can be considered to be a special case of the formalism, described in this chapter, in which the projection operator P is geometric. Conceptually, the simplest operator, which projects out of the exact solution Ψ , a part that has the same asymptotic behavior as Ψ , is one that is unity outside the region in which the nuclear interaction takes place and zero inside; that is, $P = 1$ as long as $|\mathbf{R}_a - \mathbf{r}_a| > R_c$, where \mathbf{r}_a is the coordinate of the a th nucleon, \mathbf{R}_a the center of mass of the rest of the system, and R_c is the interaction radius appropriate for a channel c . The operator Q then projects into the interaction region. The problems raised by the Pauli principle are thus encountered only in \mathcal{Q} space. In \mathcal{P} space the form used in (5.8) suffices. This assumes that the problems raised by the long-range Coulomb forces are not important.

However, the use of a spatially discontinuous projection operator does give rise to problems that must be carefully treated. It is necessary, for example, to ensure the continuity of total Ψ ; that is, the two discontinuous functions $P\Psi$ and $Q\Psi$ must join smoothly at the surface of the interaction region, $|\mathbf{R}_a - \mathbf{r}_a| = R_c$ for all a . The kinetic energy operators must be suitably defined. Since $P\Psi$ is discontinuous, $\nabla_a^2(P\Psi)$ will be singular on the surface of the interaction. Similar remarks apply to $Q\Psi$. But $\Psi = P\Psi + Q\Psi$ will have no singularities at this surface. Identical problems of this kind occur in the theory of boundary perturbations and Green's functions [Morse and Feshbach (53)] and can be resolved in the same way. The value on the surface of the interaction region of $\nabla_a^2(P\Psi)$ is taken to be its value as one approaches the surface from the field-free region, that is, as $|\mathbf{R}_a - \mathbf{r}_a| \rightarrow R_c^{(+)}$. Similarly, $\nabla_a^2(Q\Psi)$ at this surface is defined in the limit $|\mathbf{R}_a - \mathbf{r}_a| \rightarrow R_c^{(-)}$, that is, as the surface is approached from the interaction region. Continuity for Ψ is ensured, as in the Green's function case, through the use of a singular surface interaction. In the case of the Green's function for the Laplace equation, this procedure is equivalent to assuming the presence of compensating monopole and dipole layers. In the present context, we introduce a surface interaction, \mathcal{B} , which is present in both the field-free and interaction regions. \mathcal{B} is defined by

$$\mathcal{B} = \frac{1}{A+1} \sum_a \mathcal{B}_a, \quad \mathcal{B}_a = b_c \delta(R_c - \rho_a) \left(B_c + \frac{\partial}{\partial \rho_a} \right) \quad (6.20)$$

[†]Wigner and Eisenbud (47).

where

$$\rho_\alpha \equiv |\mathbf{R}_\alpha - \mathbf{r}_\alpha|$$

and $\partial/\partial\rho_\alpha$ is the normal derivative to the surface, $\rho_\alpha = R_c$. B_c is an arbitrary constant. The constant b_c can be determined from the single-channel case to be $\hbar^2/2\mu_c$, where μ_c is the reduced mass for the channel. The interaction region has been assumed to be spherical. It is a simple matter to generalize (6.20) to the case of a deformed shape. The coupled equations (2.3) and (2.4) are replaced by

$$(E - H_{PP} - \mathcal{B})P\Psi = -\mathcal{B}(Q\Psi) \quad (6.21)$$

$$(E - H_{QQ} - \mathcal{B})Q\Psi = -\mathcal{B}(P\Psi) \quad (6.22)$$

We see that the requirements of continuity provide the coupling between $P\Psi$ and $Q\Psi$. Continuity is assured by these equations since the singularities on both sides must match. Note that by defining $\nabla_a^2(P\Psi)$ [and $\nabla_a^2(Q\Psi)$] as indicated above, H_{PP} and H_{QQ} will not be singular at $\rho_a = R$.

The functions Φ_s of (2.9) are solutions of the homogeneous form of (6.22). We shall call these functions X_λ . They satisfy

$$(E_\lambda - H_{QQ} - \mathcal{B})X_\lambda = 0 \quad (6.23)$$

Integrating over a small interval in ρ_α containing R , we find that X_λ satisfies the boundary condition

$$\frac{\partial X_\lambda}{\partial \rho_\alpha} + B_c X_\lambda = 0 \quad \text{at } \rho_\alpha = R_c \quad (6.24)$$

This condition, together with

$$(E_\lambda - H_{QQ})X_\lambda = 0 \quad (6.25)$$

are equivalent to (6.23). Since we are dealing with an “interior problem,” the spectrum of E_λ will be discrete; moreover, because of the nature of H_{QQ} , it will be unbounded from above. The X_λ form an orthonormal complete set. The potential scattering wave functions $\chi^{(\pm)}$ are, similarly, solutions of

$$(E - H_{PP})\chi^{(\pm)} = 0 \quad (6.25')$$

In addition to satisfying the boundary conditions at infinity indicated by their superscripts, they must join continuously with the internal wave functions, H_{PP} consists only of the kinetic energy operator and the long-range electromagnetic interactions.

These results are already sufficient to establish the connection with the

Wigner–Eisenbud \mathcal{R} -matrix theory. However, we can go one step further and derive the relation between the wave function and its derivative needed to obtain the transition amplitude in the \mathcal{R} -matrix theory. By eliminating $Q\Psi$ from (6.22), we obtain the familiar equation for $P\Psi$:

$$\left[E - H_{PP} - \mathcal{B} - \mathcal{B} \frac{1}{E - H_{QQ} - \mathcal{B}} \mathcal{B} \right] P\Psi = 0 \quad (6.26)$$

By requiring that the coefficient of the δ function singularity in the \mathcal{B} -dependent potential be zero, then integrating over a small interval in ρ_α including R , yields the result, after expansion in eigenfunctions X_λ , that

$$\Psi(R; \alpha) = \sum \frac{X_\lambda(R; \alpha) \langle X_\lambda | \mathcal{B} \Psi \rangle}{E_\lambda - E} \quad (6.27)$$

where $\Psi(R; \alpha)$ is the wave function Ψ evaluated with the α th particle on the interaction surface, that is, with $\rho_\alpha = R$. Because of the symmetry of X_λ and Ψ ,

$$\langle X_\lambda | \mathcal{B} \Psi \rangle = \left\langle X_\lambda \left| \delta(R - \rho_\alpha) \left(B - \frac{\partial}{\partial \rho_\alpha} \right) \Psi \right. \right\rangle \quad (6.28)$$

To obtain the Wigner–Eisenbud result it is necessary to introduce a complete and orthonormal set of *surface* wave functions $\Xi_c^{(\alpha)}$ ($1, 2, \dots, \alpha - 1, \alpha + 1, \dots, A + 1; R\hat{\Omega}_\alpha$). The superscript α indicates that the α th particle is on the interaction surface; the remaining coordinates are for the other particles that are located within the interaction region. The subscript c indicates the channel. The orthonormality condition is

$$\int \Xi_c^{(\alpha)*} \Xi_{c'}^{(\alpha)} dS_\alpha = \delta_{cc'} \quad (6.29)$$

where the integration is over the surface $\rho_\alpha = R$ and over the interior volume for the remaining particles. Expanding $\Psi(R; \alpha)$ in terms of these wave functions yields

$$a_c = \sum_{c', \lambda} \frac{\gamma_{\lambda c} \gamma_{\lambda c'}}{E_\lambda - E} (B a_{c'} + b_{c'}) \quad (6.30)$$

where

$$a_c = \langle \Xi_c^{(\alpha)} | \Psi \rangle$$

and

$$b_c = \left\langle \Xi_c^{(\alpha)} \left| \frac{\partial \Psi}{\partial \rho_\alpha} \right. \right\rangle \quad (6.31)$$

are independent of α because of the symmetry of the wave functions. The subscript on B has been dropped to avoid confusion. The quantities $\gamma_{\lambda c}$ are

$$\gamma_{\lambda c} = \langle X_{\lambda} | \Xi_c^{(\alpha)} \rangle \quad (6.32)$$

Equation (6.30) is the primary \mathcal{R} -matrix result as given by Teichmann and Wigner (52). (There are some differences in notation.) The \mathcal{R} matrix is given by

$$\mathcal{R}_{cc'} = \sum_{\lambda} \frac{\gamma_{\lambda c} \gamma_{\lambda c'}}{E_{\lambda} - E} \quad (6.33)$$

The $\gamma_{\lambda c}$ are *independent* of the energy so that the energy dependence of \mathcal{R} is completely explicit. We see that when $B = 0$, roughly speaking, \mathcal{R} gives the relation between the magnitude of Ψ on the surface and its radial derivative.

We shall not carry this development any further. To obtain the reaction amplitudes, we need only note that the external wave functions can also be written in terms of the surface wave functions multiplied by radial wave functions which need to be adjusted so as to satisfy the joining conditions at the channel radius $\rho_{\alpha} = R$ given by (6.30) and the usual combination of an incident wave and an outgoing wave at $\rho_{\alpha} \rightarrow \infty$.

This formalism contains two arbitrary parameters, R and B , for each channel. The predictions are independent of their value. But the question can be asked if there is a best value of each, so that accurate approximations can be readily made. For example, it would be desirable if the series, (6.33), were limited to a few terms. However, there are also some important requirements that must be met which act to increase the number of terms. It would at first seem reasonable to propose the nuclear radius for R . But the intrinsic nuclear wave functions do not fall precipitously to zero at R , nor is the range of nuclear forces equal to zero. Therefore, the region beyond R is in fact not nuclear force free. One could attempt to take this into account by including these terms in H_{pp} , but then the effects of the Pauli principle would have to be explicitly considered. An alternative procedure would be to take a larger value of R , that is, one larger than the nuclear radius. But then the density of the levels E_{λ} increases and the number of terms in the series for $\mathcal{R}_{cc'}$ which would need to be considered, increases correspondingly. The method adopted limits the series to a few terms in the region of energy of interest and considers the remaining terms as an empirical parameter with a weak energy dependence. The effect of this procedure is to modify the potential scattering from that given by (6.25'), in other words, to introduce a potential term in the external region. For further discussions of this problem, the reader is referred to Teichmann and Wigner (52), Thomas (55), and Lane and Thomas (50).

The use of the boundary condition operator was introduced into the theory of nuclear reactions by Bloch (57) and elaborated by Lane and Robson (66, 67). The description above is taken from Feshbach (62). It permits the direct use of

the formalism in Sections 2 to 5 to evaluate the consequence of the \mathcal{R} -matrix assumptions.

C. S-Matrix Formalism[†]

The Kapur–Peierls expansion employs the eigenvalues of the operator $H_{QQ} + W_{QQ}$, where the dependence on the energy E of W_{QQ} is regarded as parametric, so that the eigenvalue E_μ and eigen function Ω_μ are both functions of E :

$$[E_\mu(E) - H_{QQ} - W_{QQ}(E)]\Omega(E) = 0 \quad (6.34)$$

This is an excellent approximation as long as $W_{QQ}(E)$ varies slowly with E . If we have been careful in selecting the prompt channels forming \mathcal{P} , this will be generally true unless the resonance width is an appreciable fraction of the single-particle width. However, this condition is not always satisfied, particularly when the target nucleus is light. It therefore becomes necessary to improve on this approximation by solving

$$[\mathcal{E}_\mu - H_{QQ} - W_{QQ}(\mathcal{E}_\mu)]\Lambda_\mu = 0 \quad (6.35)$$

This is the procedure that was adopted by Lemmer and Shakin (64). From Λ_μ [compare with (6.19c)] one can obtain the prompt wave function:

$$(P\Psi)_\mu = \frac{1}{\mathcal{E}_\mu^{(+)} - H_{PP}} H_{PQ} \Lambda_\mu \quad (6.36)$$

For a given channel α , this wave function satisfies the boundary condition

$$\frac{\partial(P\Psi)_\mu}{\partial\rho_\alpha} \rightarrow ik_\alpha(P\Psi)_\mu \quad (6.37)$$

where

$$k_\alpha^2 = \frac{2\mu}{\hbar^2}(\mathcal{E}_\mu - \varepsilon_\alpha) \quad (6.38)$$

The quantity ε_α is the excitation energy of the residual nucleus. Since \mathcal{E}_μ has a negative imaginary part, $P\Psi_\mu$ will grow exponentially with increasing ρ_α . This exponential increase can be interpreted [Humblet and Rosenfeld (61)] as a consequence of the fact that one finds at ρ_α those particles that were emitted by the system at a time $(t - \rho_\alpha/v)$, where v is an average velocity. Since the time

[†]Siegert (39); Rosenfeld and Humblet (61).

dependence of the state Ψ_μ is

$$e^{-i\mathcal{E}_\mu t/\hbar}$$

this emission occurred when the amplitude of Ψ_μ was larger by the factor $\exp[(\text{Im } \mathcal{E}_\mu)\rho_a/v\hbar]$. This behavior is the familiar one; solutions satisfying boundary condition (6.37) are often referred to as the *Gamow solutions*, used by Gamow and Condon and Gurney in their theory of α -decay.

The expansion of the S matrix in terms of its poles was initially carried out by Siegert (39) for the elastic scattering case and was further developed by Humblet and Rosenfeld (61) to take account of reactions generally. However, because of the exponentially diverging nature of the wave functions associated with the poles of the S matrix, the traditional methods of expansion in terms of an orthonormal set are not possible and these authors had recourse to exploiting the analytic properties of the S matrix on the complex energy plane. [For a resolution of the expansion difficulty, see Feshbach (79).]

This problem is avoided, in the formalism presented in this chapter, if \mathcal{Q} contains only *closed* channels. Lemmer and Shakin (64), for example, simply solved the secular equation (2.36), which is just a form of (6.35). The solutions, Λ_μ , are expanded in terms of the closed-channel wave functions so that there is no normalization problem. The Λ_μ 's and their adjoint functions $\Lambda_\mu^{(A)}$ form a biorthogonal set:

$$\langle \Lambda_\mu^{(A)} | \Lambda_\nu \rangle = \delta_{\mu\nu} \quad (6.39)$$

We may therefore expand the propagator in (2.30') to obtain

$$\mathcal{T}_{fi} = \mathcal{T}_{fi}^{(P)} + \sum_\mu \frac{\langle \chi_f^{(-)} | H_{PQ} \Lambda_\mu \rangle \langle \Lambda_\mu^{(A)} | H_{QP} \chi_i^{(+)} \rangle}{E - \mathcal{E}_\mu} \quad (6.40)$$

where \mathcal{E}_μ and Λ_μ do not depend on the energy E .

This is not an expansion in terms of *all* the S -matrix poles. Referring to (6.3),

$$S = S_P S_R$$

the expansion has been made in terms of poles S_R only, the number being given by the size of the \mathcal{Q} space. The advantages of this procedure are quite manifest. Not only can one obtain an expansion in terms of physically significant matrix elements and energies, but one can also select the energy range over which the expansion is made by selecting the set Φ_s , and one can avoid unimportant poles. It is worthwhile to recall that in single-channel potential scattering, the S_P matrix for a attractive square well has an infinite number of poles. The disadvantage of expansion equation (6.40) is the lack of independence of the various matrix elements and energies \mathcal{E}_μ because of conditions imposed by unitarity.

D. Microscopic Theory

In a microscopic theory of nuclear reactions, the various quantities, such as the widths and the resonance energies and the matrix elements entering the coupled equations (5.33), (5.34), or (5.35), are all evaluated from “first” principles, namely using a nuclear force and a model of the target and residual nuclei. The analysis of this chapter has been employed in this way by Lemmer and Shakin (64), and Friedman (67) for light nuclear targets. These authors use a shell model or deformed shell model description of the target. Bloch (66) proposed a generalization of the shell model for reaction problems which has been developed by Mahaux and Weidenmüller (69) who have written a treatise entitled *Shell Model Approach to Nuclear Reactions*. We briefly discuss some of these attempts below.

It will be convenient to employ the second quantization formalism of Chapter VII in deShalit and Feshbach (74). We briefly review some of the results we shall need in the present context. In the second quantization formalism, the Hamiltonian is expressed in terms of creation and destruction operators, $\hat{\psi}^\dagger(\mathbf{r})$ and $\hat{\psi}(\mathbf{r})$, respectively, where \mathbf{r} , as usual, includes not only spatial but also spin and isospin variables. These operators satisfy the anticommutation relations

$$\{\hat{\psi}(\mathbf{r}), \hat{\psi}^\dagger(\mathbf{r}')\} = \delta(\mathbf{r} - \mathbf{r}'); \quad \{\hat{\psi}^\dagger(\mathbf{r}), \hat{\psi}(\mathbf{r}')\} = \{\hat{\psi}(\mathbf{r}), \hat{\psi}(\mathbf{r}')\} = 0 \quad (6.41)$$

In terms of these operators the number operator, \hat{N} , is given by

$$\hat{N} = \int \hat{\psi}^\dagger(\mathbf{r}) \hat{\psi}(\mathbf{r}) d\mathbf{r} \quad (6.42)$$

An A -particle state is given by

$$|\mathbf{r}_1, \mathbf{r}_2, \dots, \mathbf{r}_A\rangle = \frac{1}{(A!)^{1/2}} \hat{\psi}^\dagger(\mathbf{r}_A) \hat{\psi}^\dagger(\mathbf{r}_{A-1}) \cdots \hat{\psi}^\dagger(\mathbf{r}_2) \hat{\psi}^\dagger(\mathbf{r}_1) |0\rangle \quad (6.43)$$

where the vacuum state $|0\rangle$ satisfies

$$\hat{\psi}(\mathbf{r}) |0\rangle = 0$$

The Fock space wave function, with a definite energy E , is given by $\langle E | \mathbf{r}_1 \cdots \mathbf{r}_A \rangle$. An $(A+1)$ -particle state is given by

$$\frac{1}{\sqrt{A+1}} \hat{\psi}^\dagger(\mathbf{r}_0) |\mathbf{r}_1 \cdots \mathbf{r}_A\rangle$$

The normalization of the state given by (6.43) is

$$\langle \mathbf{r}'_1 \cdots \mathbf{r}'_A | \mathbf{r}_1 \cdots \mathbf{r}_A \rangle = -\frac{1}{A!} \det \delta(\mathbf{r}'_\alpha - \mathbf{r}_\beta) \quad (6.44)$$

In problems dealing with the shell model it will be convenient to expand the operators $\hat{\psi}$ and $\hat{\psi}^\dagger$ in terms of single-particle wave function φ_k , forming a complete orthonormal set of eigenfunctions defined by

$$(T + U)\varphi_k = \varepsilon_k \varphi_k \quad (6.45)$$

where T is the kinetic energy and U is the shell model potential. Let

$$\hat{\psi}(\mathbf{r}) = \sum a(\mathbf{k})\varphi_k \quad a(\mathbf{k}) = \langle \varphi_k | \hat{\psi}(\mathbf{r}) \rangle \quad (6.46)$$

Then the coefficients satisfy

$$\begin{aligned} \{a(\mathbf{k}), a^\dagger(\mathbf{k}')\} &= \delta(\mathbf{k}, \mathbf{k}'), & \{a^\dagger(\mathbf{k}), a^\dagger(\mathbf{k}')\} &= \{a(\mathbf{k}), a(\mathbf{k}')\} = 0 \\ a(\mathbf{k})|0\rangle &= 0 & \langle 0|a^\dagger(\mathbf{k}) &= 0 \\ \hat{N} &= \sum_k a^\dagger(\mathbf{k})a(\mathbf{k}) \end{aligned} \quad (6.47)$$

The operator $K_{vv'}(\mathbf{r}, \mathbf{r}_0)$ can be expressed in terms of the operators $\hat{\psi}$. Note that

$$\begin{aligned} K_{vv'}(\mathbf{r}, \mathbf{r}_0) &\equiv A \int \psi_v^*(\mathbf{r}, \mathbf{r}_2, \dots, \mathbf{r}_A) \psi_{v'}(\mathbf{r}_0, \mathbf{r}_2, \dots, \mathbf{r}_A) d\mathbf{r}_2 \cdots d\mathbf{r}_A \\ &= A \int \langle v | \mathbf{r}, \mathbf{r}_2, \dots, \mathbf{r}_A \rangle \langle \mathbf{r}_0, \mathbf{r}_2, \dots, \mathbf{r}_A | v' \rangle d\mathbf{r}_2 \cdots d\mathbf{r}_A \end{aligned}$$

Using (6.43) as follows:

$$|\mathbf{r}, \mathbf{r}_2, \dots, \mathbf{r}_A\rangle = \frac{1}{\sqrt{A}} \hat{\psi}^\dagger(\mathbf{r}) |\mathbf{r}_2 \cdots \mathbf{r}_A\rangle$$

it follows immediately that

$$K_{vv'}(\mathbf{r}, \mathbf{r}_0) = \langle v | \hat{\psi}^\dagger(\mathbf{r}) \hat{\psi}(\mathbf{r}_0) | v' \rangle \quad (6.48)$$

Inserting expansion (6.46) gives

$$K_{vv'}(\mathbf{r}, \mathbf{r}_0) = \sum \varphi_k^*(\mathbf{r}) \varphi_k(\mathbf{r}_0) \langle kv | K | v' k' \rangle$$

where

$$\langle kv | K | v' k' \rangle = \langle v | a^\dagger(\mathbf{k}') a(\mathbf{k}) | v' \rangle \quad (6.49)$$

The eigenvalue problem for the K operator can now be written as follows:

$$\sum_{v', k'} \langle v | a^\dagger(\mathbf{k}') a(\mathbf{k}) | v' \rangle W_{v' k'}^{(\alpha)} = \kappa_\alpha W_{vk}^{(\alpha)} \quad (6.50)$$

Equation (6.49) demonstrates again that the set $a_k^\dagger|v\rangle$ is not orthogonal, since the overlap between two such states is given by

$$\langle v|a(\mathbf{k})a^\dagger(\mathbf{k}')|v'\rangle = \delta_{vv'}\delta_{kk'} - \langle \mathbf{k}, v|K|\mathbf{k}', v'\rangle$$

Diagonalizing $1 - K$ is a method for restoring orthogonality, and consequently, removing overcompleteness.

With the use of (6.49) it is a relatively simple matter to determine the matrix, K , for a set of Slater determinants for states v . Friedman (67) provides several examples:

Example 1. The states $|v\rangle$ are single-hole states, N in number, so that

$$|v\rangle = a(\mathbf{k}_i)|\Omega\rangle$$

where Ω is an $(A + 1)$ -particle state. Then the $N^2 \times N^2$ matrix for K is

$$\begin{aligned}\langle v|a^\dagger(\mathbf{k}_{j'})a(\mathbf{k}_j)|v'\rangle &= \langle \Omega|a^\dagger(\mathbf{k}_i)a^\dagger(\mathbf{k}_{j'})a(\mathbf{k}_j)a(\mathbf{k}_i)|\Omega\rangle \\ &= \delta(i, i')\delta(j, j') - \delta(i, j)\delta(i', j')\end{aligned}\quad (6.51)$$

This matrix can readily be diagonalized. The eigenvalues κ_α are found to be unity with a multiplicity $N^2 - 1$, and $1 - N$.

Example 2. The states $|v\rangle$ are single-particle states, N in number, so that

$$|v\rangle = a^\dagger(\mathbf{k}_i)|\Omega\rangle \quad i = 1, \dots, N$$

Then

$$\begin{aligned}\langle v|a^\dagger(\mathbf{k}_{j'})a(\mathbf{k}_j)|v'\rangle &= \langle \Omega|a(\mathbf{k}_i)a^\dagger(\mathbf{k}_{j'})a(\mathbf{k}_j)a^\dagger(\mathbf{k}_i)|\Omega\rangle \\ &= \delta(j, j')\delta(i, i')\end{aligned}\quad (6.52)$$

In this case $\kappa_\alpha = 1$ $N(N + 1)/2$ times, and $\kappa_\alpha = -1$, $N(N - 1)/2$ times.

The problem following (5.23) deals with a simple case of three two-particle states with eight eigenvalues $\kappa_\alpha = 1$ and one equal to -2 . Although these results are obtained using Slater determinant wave functions for ψ_v , they can be generalized to a linear combination of the determinants, since such a combination of the determinants is generated by a unitary transformation. As a consequence, the eigenvalues spectrum, κ_α , remains unchanged although the corresponding eigenfunctions of K will be transformed. This is an important remark since it permits the application of the foregoing analysis to more accurate descriptions of the states of the target nuclei, including contributions from unbound orbitals, preserving orthogonality and satisfying the Pauli exclusion principle.

With the eigenfunctions and eigenvalues of K determined, one may now solve the scattering problem using the most convenient of its formulations, (5.33), (5.34), or (5.36). The procedure discussed by Bloch, Mahaux, and Weidenmüller makes two approximations. In the first place it limits the number of nucleons in the continuum of the shell model potential to one, thus restricting the application to scattering (including charge exchange) reactions and not permitting the treatment of particle exchange reactions. This is an approximation even for scattering processes since states with two or more particles in the continuum may be of importance, indeed are, for accurate descriptions of the target wave functions, as mentioned above. The second approximation, not completely independent of the first, limits the description of the target (A particle) states and those of the $(A + 1)$ compound system to linear combinations of Slater determinants formed from bound single-particle wave functions only.

A set of states for the full $(A + 1)$ -particle system is constructed. The "bound" states Φ_i are shell model states, which like the target states consist of linear combinations of Slater determinants constructed from $A + 1$ bound single-particle levels. These are finite in number. The energy of these states can be above the threshold for particle emission so that they will generate resonances as described in the introduction to this chapter. The scattering states of the $(A + 1)$ system, $\chi_c(E)$, are constructed by antisymmetrizing the product of the wave function for a particle in the continuum and a target wave function. Because of the special construction of all the states from single-particle wave functions which are eigenfunctions of a common energy-independent single-particle Hamiltonian, these scattering states, together with the bound states, form an orthogonal set which we will assume is appropriately normalized. We shall refer to them as the *shell model states*. Thus by making the assumptions listed above, the Pauli principle and problems of overcompleteness are avoided.

The formalism developed by Mahaux and Weidenmüller (69) can be expressed in terms of projection operators. These are explicitly constructed from the $(A + 1)$ -particle shell model states. The operator Q projects on to the set Φ_n , while P projects on to the shell model scattering states χ_c .

$$P = \sum_{c'} \int dE' \chi_c(E') \langle \chi_c(E') \rangle \quad (6.53)$$

$$Q = \sum_n \Phi_n \langle \Phi_n \rangle \quad (6.54)$$

These are of course not identical with the P and Q used in Section 5. However, the general analysis of Section 2 is applicable. Equations (2.3) and (2.4) become

$$[E - (H_0)_{PP} - V_{PP}]P\Psi = V_{PQ}Q\Psi \quad (6.55)$$

$$[E - (H_0)_{QQ} - V_{QQ}]Q\Psi = V_{QP}P\Psi \quad (6.56)$$

where the full Hamiltonian H is

$$H = H_0 + V$$

and H_0 is the shell model Hamiltonian.

For further discussion of this model the reader is referred to Mahaux and Weidenmüller's book (69). It is clear that its limitation to one particle in the continuum precludes a realistic description of a compound nuclear resonance and *a fortiori* of transfer reactions. It can be used to describe doorway states, particularly those which are constructed from 1p–1h states excited, for example, by photon absorption [Bloch and Gillet (65)]. This becomes a valid description if V is complex, to allow for energy averaging over compound nuclear resonances. The model is very useful as well in providing a description of the structure of the S matrix, which as we discussed earlier, is insensitive to dynamical details.

7. SUMMARY

In this chapter a formal theory of nuclear reactions is developed, based on a separation of the channels of the system into prompt and time-delaying states. This is accomplished formally through the use of projection operators P and Q . Without specifying any but general properties of these operators, a theory in which direct reactions and compound nuclear resonances appear simultaneously and on equal footing is developed in Section 2. Both the case of an isolated resonance and that of overlapping resonances are treated. Still maintaining the generality of P and Q , the energy average of the transition amplitude is discussed in Section 3 and a derivation of the optical model exhibited. It should be remembered that this optical model is not necessarily the single-channel optical model but can include many channels, so that it provides not only a description of elastic scattering but also one of inelastic scattering and direct processes generally. The theory of the doorway state and its relationship to intermediate structure in the cross section is the subject of Section 4. Exit as well as entrance doorways are treated, as well as the effect of a doorway resonance on the fine structure resonances. In Section 5 we consider a more specific P together with the problems of overcompleteness, the Pauli principle, and the lack of orthogonality which occur if the prompt wave function is expanded as a finite series in the wave functions of the target nucleus, as is appropriate for the discussion of elastic and inelastic scattering. These problems, as encountered more seriously in transfer reactions, will be discussed in a later chapter. Finally, in the last section the general methods (Section 2 particularly) developed in this chapter are compared with other formalisms, including that of Kapur–Peierls, Wigner and Eisenbud, and Bloch, Mahaux, and Weidenmüller. Many contributions to our understanding of nuclear reactions that are appropriate to this chapter have not been discussed. There

is the work of Macdonald, Tobocman and his collaborators, Danos and Greiner, Thaler, Shakin, and many others. Of course, no attempt has been made to provide a historical perspective.

Reactions induced (or produced) by γ -rays can readily be included without modification of the general development. As expected, the width of a resonance, Γ , will now contain a component, Γ_γ , because of the possible radiative decay of a resonance. In addition, direct γ -ray as well as doorway state processes are automatically described by the theory, which is discussed by Estrada [Estrada and Feshbach (63)].

APPENDIX. THE BOUNDARY CONDITION MODEL FOR NUCLEAR REACTIONS[†]

In the boundary condition model, configuration space is divided into two regions, one in which the strong nuclear interactions prevail, $r < R$, and one in which the potential is zero (for neutrons) or Coulombic (for charged particles). R is, roughly speaking, the nuclear radius. No such sharp boundary exists in nature. But the model is useful because it isolates the major physical effects, the corresponding parameters, and qualitative and quantitative estimates of their numerical values. The model was developed in a simple form by Feshbach, Peaslee, and Weisskopf (47) and in a more complete and sophisticated form by Wigner and Eisenbud (47). It has been used by Lomon and Feshbach (68) to study the nucleon-nucleon interaction, by Lomon (89) and by Jaffe and Low (79) for elementary particle reactions.

In this section we use the simpler description of Feshbach et al. (47). Spin is neglected. A partial wave expansion is assumed. The radial wave function for the l th partial wave, corresponding to an orbital angular momentum of $l\hbar$, is given by $(1/r)\psi_l$. The boundary condition to be met by the external wave function ($r > R$) at $r = R$ is

$$f_l = R \left[\frac{d\psi_l/dr}{\psi_l} \right]_{r=R} \quad (\text{A.1})$$

where f_l can be a complex function of the energy. The resultant S matrix is

$$S_l \equiv e^{2i\delta_l} = \frac{w_l^{(-)} f_l/kR - w_l^{(-)'} / w_l}{w_l^{(+)} f_l/kR - w_l^{(+)' } / w_l} \quad (\text{A.2})$$

where $w_l^{(\pm)}$ are solutions of the Schrödinger equation for $r > R$ evaluated at $r = R$. The prime denotes derivative. The functions $w_l^{(\pm)}$ for uncharged particles

[†]Feshbach, Peaslee, and Weisskopf (47).

have the following asymptotic dependence:

$$\begin{aligned} w_l^{(+)}(\zeta) &\xrightarrow[\zeta \rightarrow \infty]{} e^{i(\zeta - l\pi/2)} \\ w_l^{(-)}(\zeta) &\xrightarrow[\zeta \rightarrow \infty]{} e^{-i(\zeta - l\pi/2)} \\ \zeta &= kr \end{aligned} \quad (\text{A.3})$$

Let

$$w_l^{(+)} = |w_l| e^{-i\sigma_l} w_l^{(+)\prime} = |w_l'| e^{-i\tau_l} \quad (\text{A.4})$$

Then

$$|w_l| |w_l'| \sin(\sigma_l - \tau_l) = 1 \quad (\text{A.5})$$

Let

$$\frac{w_l^{(+)\prime}}{w_l^{(+)}} \equiv \Delta_l + is_l \quad (\text{A.6})$$

Then

$$\Delta_l = \frac{|w_l'|}{|w_l|} \cos(\sigma_l - \tau_l) \quad (\text{A.7})$$

$$s_l = \frac{1}{|w_l|^2} \quad (\text{A.8})$$

The scattering matrix can then be written

$$S_l = e^{2i\sigma_l} \frac{(f_l/kR) - \Delta_l + is_l}{(f_l/kR) - \Delta_l - is_l} \quad (\text{A.9})$$

The transmission factor T_l is given by

$$T_l = 1 - |S_l|^2 = -4 \frac{\text{Im } f_l(kRs_l)}{(\text{Re } f_l - kR\Delta_l)^2 + (kRs_l - \text{Im } f_l)^2} \quad (\text{A.10})$$

Note that

$$T_l \geq 0 \quad \text{and} \quad \text{Im } f_l \leq 0 \quad (\text{A.11})$$

Resonance Formula

Consider first $l = 0$, for which $\Delta_0 = 0$. Let E_0 be the value for which $\text{Re } f_0 = 0$. Then in the neighborhood of $E = E_0$,

$$T_0 = \frac{\Gamma_i \Gamma_0}{(E - E_0)^2 + \Gamma^2/4} \quad (\text{A.12})$$

and

$$S_0 - 1 = (e^{2i\sigma_0} - 1) - e^{2i\sigma_0} \frac{i\Gamma_0}{(E - E_0) + i\Gamma/2} \quad (\text{A.13})$$

where

$$\Gamma = \Gamma_0 + \Gamma_i \quad (\text{A.14})$$

$$\Gamma_i = \frac{2|\text{Im } f_0|}{|\partial \text{Re } f_0 / \partial E|_{E=E_0}} \quad (\text{A.15})$$

$$\Gamma_0 = \frac{2kR}{|\partial \text{Re } f_0 / \partial E|_{E=E_0}} \quad (\text{A.16})$$

If the interaction region is a square well,

$$V = -V_0 - iW_0 \quad r \leq R$$

then at resonance

$$\left(\frac{\partial \text{Re } f_0}{\partial E} \right)_{E=E_0} = -\frac{\mu R^2}{\hbar^2}$$

$$\text{Im } f_0 = -\frac{\mu R^2}{\hbar^2} W_0$$

and

$$T_0 = \frac{4W_0(\hbar^2/\mu R^2)kR}{(E - E_0)^2 + [W_0 + (\hbar^2/\mu R^2)kR]^2} \quad (\text{A.17})$$

These results are easily generalized for $l \neq 0$. We find that

$$T_l = \frac{\Gamma_i^{(l)} \Gamma_0^{(l)}}{(E - E_0)^2 + \frac{1}{4}(\Gamma_l)^2} \quad (\text{A.18})$$

where E_0 is the energy at which $\text{Re } f_l - kR\Delta_l = 0$, and

$$\Gamma_l = \Gamma_i^{(l)} + \Gamma_0^{(l)} \quad (\text{A.19})$$

$$\Gamma_i^{(l)} = \frac{2|\text{Im } f_l|}{|\partial(\text{Re } f_l - kRs_l)/\partial E|_{E=E_0}} \quad (\text{A.20})$$

$$\Gamma_0^{(l)} = \frac{2kRs_l}{|\partial(\text{Re } f_l - kRs_l)/\partial E|_{E=E_0}} \quad (\text{A.21})$$

The penetrability P_l is defined to be

$$P_l = kR s_l = \frac{kR}{|w_l|^2} \quad (\text{A.22})$$

\mathcal{R} Matrix ($l=0$)

Let X_λ be the solutions for the interior ($r < R$) problem satisfying

$$X'_\lambda(R) \equiv \left(\frac{\partial X_\lambda}{\partial r} \right)_{r=R} = 0$$

The eigenvalues will form a discrete spectrum. The energy accompanying the eigenfunction X_λ is E_λ . We now expand the exact solution ψ in terms of X_λ in the region $r < R$. We assume that on the surface $r = R$:

$$\psi = \sum_c \chi_c(s) \phi_c(r)$$

where $\chi_c(s)$ forms an orthonormal set on the surface $s, r = R$. It then follows that

$$\phi_c(R) = -\frac{\hbar^2}{2\mu} \sum_{c'} \phi'_{c'}(R) \sum_\lambda \frac{1}{E - E_\lambda} \left[\int ds X_\lambda \chi_c(s) \right] \left[\int ds X_\lambda \chi_{c'}^*(s) \right]$$

The \mathcal{R} matrix is therefore

$$\mathcal{R}_{cc'} = \sum_\lambda \frac{1}{E_\lambda - E} \gamma_{\lambda c}^* \gamma_{\lambda c'} \quad (\text{A.23})$$

where

$$\gamma_{\lambda c} = \sqrt{\frac{\hbar^2}{2\mu}} \int X_\lambda \chi_c dS \quad (\text{A.24})$$

so that

$$\phi_c(R) = \sum_{c'} R_{cc'} \phi'_{c'}(R) \quad (\text{A.25})$$

For the single-channel case, $R_{cc'} = R_{cc} \delta_{cc'}$,

$$\phi_c(R) = R_{cc} \phi'_c(R)$$

so that the f of (A.1) is

$$f_0 = \frac{R}{\mathcal{R}} \quad (\text{A.26})$$

Properties of s_l and Δ_l

$$s_l(\zeta) \xrightarrow{\zeta \rightarrow 0} \left(\frac{\zeta^l}{(2l-1)!!} \right)^2 \quad \Delta_l \xrightarrow{\zeta \rightarrow 0} -\frac{l}{\zeta} \quad (\text{A.27})$$

$$\xrightarrow{\zeta \rightarrow \infty} 1 \quad \xrightarrow{\zeta \rightarrow \infty} O\left(\frac{1}{\zeta^3}\right)$$

$$s_0 = 1 \quad \Delta_0 = 0$$

$$s_1 = \frac{\zeta^2}{(1 + \zeta^2)} \quad \zeta \Delta_1 = -\frac{1}{(1 + \zeta^2)} \quad (\text{A.28})$$

$$s_2 = \frac{\zeta^4}{(9 + 3\zeta^2 + \zeta^4)} \quad \zeta \Delta_2 = -\frac{3(6 + \zeta^2)}{9 + 3\zeta^2 + \zeta^4}$$

For charged particles,

$$w_l^{(+)} = G_l + iF_l \quad (\text{A.29})$$

The properties of F_l and G_l are given by (A.70)–(A.74) in Appendix A at the end of the book.

CHAPTER IV

RESONANCES AND THE STATISTICAL THEORY OF NUCLEAR REACTIONS

1. INTRODUCTION[‡]

This is the first in a series of chapters in which the formalism of Chapter III will be applied to various types of reaction phenomena that are observed experimentally. Extensions of the formal theory will suggest themselves and be developed.

We begin the chapter with the isolated resonance, the dependence of its width upon projectile energy, and the interference of the resonance amplitude with that for the prompt reactions not only for elastic scattering but for other reactions as well. Threshold phenomena, the existence of cusps in the cross section, are naturally considered at this point. These are followed by a discussion of the case of many overlapping resonances. The very important impact of the details of the empirical analysis of the data upon theoretical considerations is stressed. It is now a quick step to the statistical theory of nuclear reactions since analysis of the resonance data provides us with distribution functions for the widths, spacing of resonance energies, and fluctuations in the cross section. Correlations among these various quantities, either self-correlations or cross-correlations of fluctuations in different channels, are important statistical measures that can indicate the existence of significant phenomena. The simple statistical theory for the average reaction cross section can be formulated and compared with experiment, suggesting the need, in some cases, for a more detailed statistical description of a reaction.

[‡]Hodgson (87); Mahaux and Weidmüller (79).

Channels; Angular Distributions. The description of the angular distribution of reaction products differs according to the scheme adopted for labeling the open channels. One common method is to couple the projectile spin \mathbf{i} and the target spin \mathbf{I} to form a channel spin \mathbf{s} , as indicated by the equation

$$\mathbf{I} + \mathbf{i} = \mathbf{s} \quad (1.1)$$

The vector notation is shorthand for $|I - i| < s < I + i$. The spin is then coupled to the orbital angular momentum \mathbf{l} to obtain the total angular momentum of the system, \mathbf{J} :

$$\mathbf{J} = \mathbf{s} + \mathbf{l} = \mathbf{I} + \mathbf{i} + \mathbf{l} \quad (1.2)$$

This procedure is referred to as the *channel coupling scheme*. It is also possible to couple the projectile spin and the orbital angular momentum as would be appropriate if spin-orbit effects were overriding:

$$\mathbf{i} + \mathbf{l} = \mathbf{j} \quad (1.3)$$

To form J , \mathbf{j} would be coupled to \mathbf{I} :

$$\mathbf{j} + \mathbf{I} = \mathbf{J} \quad (1.4)$$

This coupling scheme is referred to as the *spin-orbit coupling scheme*. Finally, the *helicity coupling scheme* of Jacob and Wick (59) has often been used [see Chapter VIII of deShalit and Feshbach (74)], particularly for relativistic phenomena. In this scheme the projections of the projectile and target spin along the direction of motion, λ_a and λ_x , respectively, similar quantities for the reaction products, λ_b and λ_y , together with the total angular momentum J (and its projection M) are used.

Of course, in addition to the angular momenta, one must also include the parity of the channel, the energies of the system in the center-of-mass frame, and the excitation energies of any of the complex particles in the initial or final states of the system. For the sake of definiteness we shall use the channel coupling scheme in this chapter. Then the angular distribution of the reaction products for a two-body final state in which both products are in well-defined quantum states of a given energy is

$$\begin{aligned} \frac{d\sigma(\alpha, \alpha')}{d\Omega} = & \frac{1}{k^2} \sum \frac{1}{(2I+1)(2i+1)} (l_1, s, J_1 \| \sqrt{4\pi} Y_L \| l_2, s, J_2) \\ & \times (l'_1, s', J_1 \| \sqrt{4\pi} Y_L \| l'_2, s', J_2) \operatorname{Re} \pi^2 \mathcal{T}_{\alpha\alpha'}(l'_1 s'; l_1 s; J, \Pi_1) \\ & \times \mathcal{T}_{\alpha\alpha'}^*(l'_2 s'; l_2 s; J_2 \Pi_2) P_L(\cos \Theta) \end{aligned} \quad (1.5)$$

The sum is taken over all angular momentum and parity quantum numbers

with the exception of l, i , and of course α and α' . The final states are normalized per unit energy that is $\langle \chi_c(E) | \chi_c(E') \rangle = 4\pi\delta(E - E')$.

As a consequence, $\mathcal{T}_{\alpha\alpha'}$, the transition matrix, is dimensionless[†]. The integrated cross section is

$$\sigma(\alpha', \alpha) = \frac{4\pi}{k^2} \sum \frac{2J+1}{(2I+1)(2i+1)} |\pi \mathcal{T}_{\alpha\alpha'}(l's'; ls; J\Pi)|^2 \quad (1.6)$$

The reduced matrix elements $(l_1 s J_1 \| \sqrt{4\pi} Y_L \| l_2 s J_2)$ in (1.5) are kinematical in the sense that they do not depend on the nuclear interaction. The angular momenta l_1, l_2 are two possible values in the decomposition of the incident wave into partial waves; s is a possible value of the channel spin. The primed quantities describe the situation for the final state. In addition to (1.2), the reduced matrix elements yield

$$\mathbf{J}_1 + \mathbf{J}_2 = \mathbf{L} \quad (1.7)$$

which together with (1.2) yields

$$\mathbf{l}_1 + \mathbf{l}_2 = \mathbf{L} \quad \text{and} \quad \mathbf{l}'_1 + \mathbf{l}'_2 = \mathbf{L} \quad (1.8)$$

These results can also be obtained from the explicit expression

$$(l_1 s J_1 \| \sqrt{4\pi} Y_L \| l_2 s J_2) = (-)^{s+L+J_2} [(2l_1+1)(2l_2+1)(2J_2+1)(2J_1+1)(2L+1)]^{1/2} \\ \times \begin{pmatrix} l_1 & L & l_2 \\ 0 & 0 & 0 \end{pmatrix} \begin{Bmatrix} l_1 & J_1 & s \\ J_2 & l_2 & L \end{Bmatrix} \quad (1.9)$$

Note the requirements that both $l_1 + l_2 + L$ and $l'_1 + l'_2 + L$ must be even, thus guaranteeing parity conservation. We immediately see from (1.7) and (1.8) that

$$L_{\max} = \min(2l, 2l', 2J) \quad (1.10)$$

where l is the maximum incident angular momentum, l' the maximum emergent, and J the maximum value of the total angular momentum. Equation (1.10) is a precise statement of the complexity theorem [Yang (48)] described in Chapter I.

The \mathcal{T} matrix in (1.5) depends on the nuclear interaction. We see that in the channel spin coupling scheme it describes a transition between two channels c and c' defined by the quantum numbers

$$c \equiv \{\alpha ls; J\Pi\} \\ c' \equiv \{\alpha' l' s'; J\Pi\} \quad (1.11)$$

[†]For spinless particles, $\mathcal{T}_l = -(1/\pi) \sin \delta_l e^{i\delta_l}$, where δ_l is the phase shift.

We shall often, for notational compactness, replace

$$\mathcal{T}_{\alpha'\alpha}(l's'; ls; J\Pi)$$

by

$$\mathcal{T}_{c'c}(J\Pi) \quad (1.12)$$

\mathcal{T} is a symmetric function of c' and c :

$$\mathcal{T}_{c'c} = \mathcal{T}_{cc'}$$

Therefore, from (1.6) it follows that

$$\sigma(\alpha', \alpha) = \frac{k'^2(2I' + 1)(2i' + 1)}{k^2(2I + 1)(2i + 1)} \sigma(\alpha, \alpha') \quad (1.13)$$

This reciprocity relation interchanging initial and final states. $I \rightarrow I'$, $i \rightarrow i'$, and so on, has been used to determine a spin when three of the four I , i , I' , i' are known. For example, the spin of the π meson can be obtained by comparing $p + p \rightarrow \pi^+ + D$ and $\pi^+ + D \rightarrow p + p$ [Marshak (51); Cheston (51)].

2. ISOLATED RESONANCES; INTERFERENCE WITH THE PROMPT AMPLITUDE

The transition $\mathcal{T}_{c'c}(J\Pi)$ can, according to (III.2.25), be written as a sum of two terms, the prompt and the resonant amplitude:

$$\mathcal{T}_{c'c} = \mathcal{T}_{c'c}^{(P)} + \mathcal{T}_{c'c}^{(R)} \quad (2.1)$$

Therefore, the differential cross section (1.5) can be broken up into three parts:

$$\frac{d\sigma(\alpha', \alpha)}{d\Omega} = \frac{d\sigma^{(P)}(\alpha', \alpha)}{d\Omega} + \frac{d\sigma^{(R)}(\alpha', \alpha)}{d\Omega} + \frac{d\sigma^{(I)}(\alpha', \alpha)}{d\Omega} \quad (2.2)$$

The first term on the right side of this equation gives the angular distribution of the reaction products as generated by the prompt processes as indicated by the superscript P . The second, with superscript R , the angular distribution originating in the resonance, while the third, with superscript I , is the angular distribution developed by the interference between the two, the prompt and the resonance process. A similar decomposition is possible for the integrated cross section. From (1.6)

$$\sigma(\alpha', \alpha) = \sigma^{(P)}(\alpha', \alpha) + \sigma^{(R)}(\alpha', \alpha) + \sigma^{(I)}(\alpha', \alpha) \quad (2.3)$$

For example, inserting (2.1) into (1.6) yields

$$\sigma^{(P)}(\alpha', \alpha) = \frac{4\pi}{k^2} \sum \frac{2J+1}{(2I+1)(2i+1)} |\pi \mathcal{T}_{c'c}^{(P)}|^2 = \sum \sigma_{c'c}^{(P)} \quad (2.4)$$

$$\sigma^{(R)}(\alpha', \alpha) = \frac{4\pi}{k^2} \sum \frac{2J+1}{(2I+1)(2i+1)} |\pi \mathcal{T}_{c'c}^{(R)}|^2 = \sum \sigma_{c'c}^{(R)} \quad (2.5)$$

$$\sigma^{(I)}(\alpha', \alpha) = \frac{4\pi}{k^2} \sum \frac{2J+1}{(2I+1)(2i+1)} [\pi^2 \mathcal{T}_{c'c}^{(R)} \mathcal{T}_{c'c}^{(P)*} + \pi^2 \mathcal{T}_{c'c}^{(R)*} \mathcal{T}_{c'c}^{(P)}] \quad (2.6)$$

We consider the case of a single isolated resonance which is designated (just as in the case of bound states) by a specific J and Π . Thus

$$\begin{aligned} \frac{d\sigma^{(R)}(\alpha', \alpha)}{d\Omega} &= \frac{\pi^2}{k^2} \sum \frac{1}{(2I+1)(2i+1)} (l_1 s J \| \sqrt{4\pi} Y_L \| l_2 s J) (l'_1 s' J \| \sqrt{4\pi} Y_L \| l'_2 s' J) \\ &\quad \times \text{Re}(\mathcal{T}_{c'c}^{(R)} \mathcal{T}_{c'c}^{(R)*}) P_L \end{aligned} \quad (2.7)$$

To excite a resonant state of a given parity, $l_1 + l_2$ and $l'_1 + l'_2$ must be even; that is, l_1 and l_2 must have the same parity and similarly for l'_1 and l'_2 . Since [see (1.9)]

$$(l_1 s J \| Y_L \| l_2 s J) \sim \begin{pmatrix} l_1 & L & l_2 \\ 0 & 0 & 0 \end{pmatrix}$$

it follows that L is even. Hence the resonant angular distribution (2.7) is symmetric about 90° .

Problem. Prove directly from (1.9) that if both the projectile and target have zero spin, and if the reaction products have zero spin, then

$$\frac{d\sigma^{(R)}}{d\Omega} \sim [P_J(\cos \vartheta)]^2$$

This result is applicable to resonance reactions such as $^{12}\text{C} + ^{12}\text{C} \rightarrow ^{20}\text{Ne} + \alpha$, $^{12}\text{C} + ^{16}\text{O} \rightarrow ^{24}\text{Mg} + \alpha$, and so on, when the residual nucleus and emergent particles are in spin-zero states.

Before the effect of interference can be discussed, it is necessary to provide explicit expressions for $\mathcal{T}_{c'c}^{(R)}$ and $\mathcal{T}_{c'c}^{(P)}$. The former is given by (III.2.25) as follows:

$$\pi \mathcal{T}_{c'c}^{(R)} = \frac{1}{2} e^{i(\delta_{c'} + \delta_c)} \frac{g_{c'\lambda}(J\Pi) g_{c\lambda}(J\Pi)}{E - E_\lambda + (i/2)\Gamma_\lambda} \quad (2.8)$$

In this last expression the g 's are real numbers and the δ 's give the phases of the distorted waves generated by the potential scattering [Eq. (III.2.24)]:

$$\chi_c = e^{i\delta_c} |\chi_c| \quad (\text{III.2.24})$$

and from (III.2.23),

$$\Gamma_{\lambda c} = g_{\lambda c}^2 \quad (\text{III.2.23})$$

and from (III.2.22),

$$\Gamma_{\lambda} = \sum_c \Gamma_{\lambda c} \quad (\text{III.2.22})$$

Each channel c with an l and s that can combine to give the $J\Pi$ of the resonant state will contribute to (1.5).

The prompt transition amplitude is constructed out of the solutions of

$$(E - H_{PP})\chi^{(\pm)} = 0 \quad (2.9)$$

where generally this is a set of coupled equations connecting the different channels. The DWA (distorted wave amplitude) is constructed by treating the coupling perturbatively. More explicitly, the relevant equations are of the form

$$(E - H_{cc})\chi_c = H_{cc'}\chi_{c'} \quad (2.10)$$

$$(E - H_{c'c'})\chi_{c'} = H_{c'c}\chi_c$$

so that[†]

$$\mathcal{T}_{c'c} = \langle \chi_{c'0}^{(-)} | H_{c'c} | \chi_{c0}^{(+)} \rangle \quad (2.11)$$

where $\chi_{c0}^{(+)}$ and $\chi_{c0}^{(-)}$ are solutions of the uncoupled equation (2.10) that is with $H_{cc'} = H_{c'c} = 0$.

In the discussion that follows we shall employ the DWA approximation for the χ_c and $\chi_{c'}$ appearing in the definition of $\Gamma_{\lambda c}$:

$$\Gamma_{\lambda c} = 2\pi |\langle \Phi_{\lambda} | H_{QP} \chi_c^{(+)} \rangle|^2 \quad (2.13)$$

[†]One can improve upon (2.11) by obtaining a better χ_c by eliminating $\chi_{c'}$, so that

$$\left[E - H_{cc} - H_{cc'} \frac{1}{E - H_{c'c'}} H_{c'c} \right] \chi_c = 0 \quad (2.12)$$

Then the exact $\mathcal{T}_{cc'}^{(P)}$ is given by $\langle \chi_{c'0}^{(-)} | H_{c'c} | \chi_c^{(+)} \rangle$, where $\chi_c^{(+)}$ is a solution of (2.12) [Lamarsh and Feshbach (65)]. Since the wave functions are usually obtained using an empirically determined H_{cc} , it is possible that the DWA is a more accurate approximation than would at first appear.

and the amplitude given by (2.11) for the prompt amplitude. This is a reasonably accurate procedure when the prompt process is a single step and in any event will serve to illustrate the effects of interference between the direct and the resonant amplitude.

From (2.11) it then follows that

$$\pi\mathcal{T}_{c'c}^{(P)} = -e^{i(\delta_{c'} + \delta_c)} A_{c'c}(J\Pi) \quad (2.14)$$

where A is a real amplitude.

To illustrate the effect of interference we consider a simplified situation. Let us first restrict the discussion to elastic scattering. Second, let us assume that the *target nucleus has zero spin*, so that $s' = s$, and in addition assume that the energy is so low that only one angular momentum, the lowest possible value of l , contributes significantly to the formation of the compound nucleus. Suppose that the resonance occurs therefore for a particular combination of $(l, s, J, \Pi) = C$. Then from (1.6) and (2.4),

$$\sigma(\alpha, \alpha) = \sum' \sigma_{c'c}^{(P)} + \sigma_C \quad (2.15)$$

where the prime indicates the omission of the terms $c' = c = C$. The cross section σ_C is

$$\sigma_C = \frac{4\pi}{k^2} \frac{2J+1}{2i+1} |\pi\mathcal{T}(l_i; l_i; J\Pi)|^2 \quad (2.16)$$

For this term the potential scattering amplitude is

$$\pi\mathcal{T}_C^{(\text{pot})} = -e^{-i\delta_C} \sin \delta_C \quad (2.17)$$

Combining (2.17) and (2.8), σ_C is

$$\sigma_C = \frac{4\pi}{k^2} \frac{2J+1}{2i+1} \left| e^{i\delta_C} \sin \delta_C - e^{2i\delta_C} \frac{\Gamma_{\lambda C}/2}{E - E_\lambda + (i/2)\Gamma_\lambda} \right|^2 \quad (2.18)$$

Introducing the resonant phase angle γ_λ ,

$$\tan \gamma_\lambda \equiv \frac{\Gamma_\lambda}{2(E - E_\lambda)}$$

(2.18) becomes

$$\sigma_C = \frac{4\pi}{k^2} \frac{2J+1}{2i+1} \left| e^{2i\delta_C} \left(\sin \delta_C e^{-i\delta_C} - \frac{\Gamma_{\lambda C}}{\Gamma_\lambda} \sin \gamma_\lambda e^{-i\gamma_\lambda} \right) \right|^2 \quad (2.19)$$

The simplest situation occurs when only the elastic channel is open. This,

together with the initial assumptions, has the consequences $\Gamma_{\lambda C} = \Gamma_\lambda$ and δ_C real. Then (2.19) becomes

$$\sigma_C = \frac{4\pi}{k^2} \frac{2J+1}{2i+1} |\sin \delta_C e^{-i\delta_C} - \sin \gamma_\lambda e^{-i\gamma_\lambda}|^2 \quad (2.20)$$

It is immediately clear that completely destructive interference occurs when

$$\gamma_\lambda = \delta_C \quad \sigma_C(\alpha, \alpha) = 0$$

On the other hand, a maximum occurs when

$$\gamma_\lambda = \frac{\pi}{2} + \delta_C$$

with a maximum cross section

$$[\sigma_C(\alpha, \alpha)]_{\max} = \frac{4\pi}{k^2} \frac{2J+1}{2i+1} \quad (2.21)$$

In terms of the energy E we have

$$E = E_\lambda + \frac{\Gamma_\lambda}{2} \cot \delta_C \quad \text{for the minimum value of } \sigma_C(\alpha, \alpha) = 0$$

and

$$E = E_\lambda - \frac{\Gamma_\lambda}{2} \tan \delta_C \quad \text{for the maximum value of } \sigma_C(\alpha, \alpha)$$

We see that the effect of the interference is to shift the maximum and introduce a minimum, with the scale of these shifts given by Γ_λ . For no potential scattering term, that is, no interference, $\delta_C = 0$, the maximum is not shifted while the minimum is at infinity. For δ_C small, the maximum is shifted to a lower (larger) energy for δ_C positive (negative) while the minimum appears on the other side of E_λ . On the other hand, when δ_C approaches $\pi/2$, that is, when the potential scattering resonates, the maximum disappears (i.e., moves off to infinite energy). The resonance now manifests itself by a minimum (in this case a zero) at $E = E_\lambda$. Figure 2.1 gives an example of a resonance with an interference minimum and Fig. 2.2 shows a resonance in which the potential scattering is very small, so that no interference phenomena occur.

If more than one channel is open, $\Gamma_{\lambda C} < \Gamma_\lambda$ and δ_C can be complex since there will be absorption from the elastic scattering channel denoted by C into reaction channels[†]. Under these circumstances the cross section at the interference

[†]By using the eigenphases for the prompt channels similar to the σ_μ of (III.2.45'), one can avoid complex phase shifts.

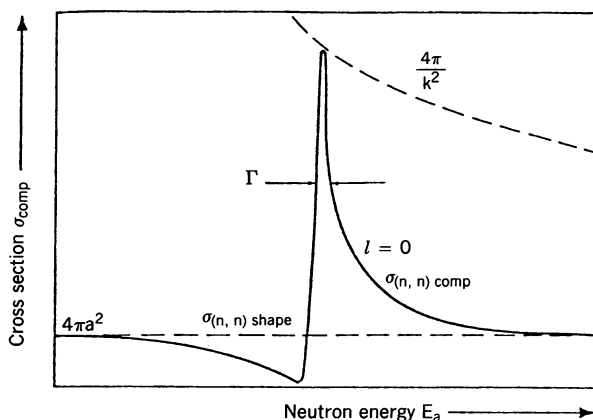


FIG. 2.1. Elastic scattering cross sections for S -wave neutrons near a resonance in the compound nucleus. The figure shows the relationship between the shape-elastic and the compound-elastic cross sections for a spinless target nucleus. [From Marmier and Sheldon (70).]

minimum will no longer be zero and the maximum will no longer be as large as that given by (2.20). The full formulas are given by Feshbach (60). As an example, we quote here the result for δ_c real:

$$\sigma_{\min}^{\max}(\alpha, \alpha) = \frac{\pi}{k^2} \frac{2J+1}{2i+1} \left\{ \left[1 + \left(1 - \frac{\Gamma_{\lambda c}}{\Gamma_{\lambda}} \right)^2 - 2 \left(1 - \frac{\Gamma_{\lambda c}}{\Gamma_{\lambda}} \right) \cos 2\delta_c \right]^{1/2} \pm \frac{\Gamma_{\lambda c}}{\Gamma_{\lambda}} \right\}^2 \quad (2.23)$$

The visibility of a resonance is reduced as $\Gamma_{\lambda c}$ becomes a smaller fraction of Γ_{λ} .

Note also that the elastic scattering resonance contributes only to the partial waves having a fixed J and Π . The cross section will contain the contributions for other values of J that generally will not resonate at E near E_{λ} [as assumed by (2.15)]. It will certainly be considerably easier to observe a resonance when the number of partial waves involved is few, as the nonresonant background tends to obscure the resonance structure.

As this discussion emphasizes, it is more difficult to observe resonance structure in the integrated cross section, particularly as the energy increases. To remove the effects of the nonresonant background and thus make the resonance more visible, it would be obviously helpful for the experiment to be designed so as to be more selective. Choosing a particular channel, for example, would be best. One common and important method looks at the reaction products, which because of selection rules and specificities originating in barrier penetration factors may have many fewer nonresonant background terms. An example is given in Fig. 2.3; the $^{12}\text{C} + ^{12}\text{C}$ reaction shows many resonances detected by examining the γ -ray spectrum generated by reactions leading to the

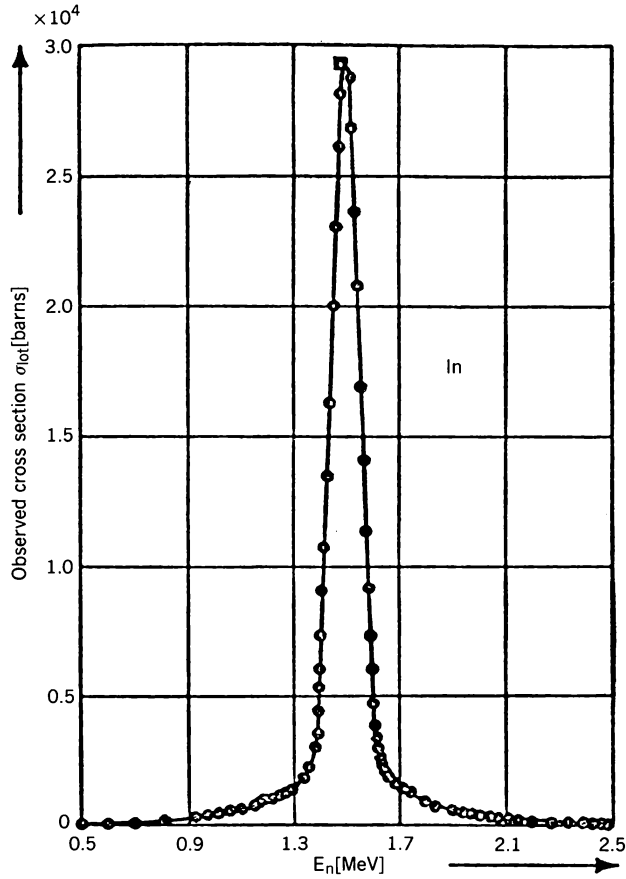


FIG. 2.2. Neutron total cross section for In. [Marmier and Sheldon (1969), taken from Landon and Sailor (55).]

states in ^{20}Ne and ^{23}Na . These resonances are well below the barrier and thus are not as readily detected in, say, elastic scattering, to cite an extreme example.

The angular distribution is much more sensitive than the integrated cross section to the presence of an isolated resonance. To demonstrate this, we take the simple case of an $s = 0$ initial system and an $s = 0$ final system. An example is the elastic scattering of α -particles (or pions or kaons) by a spin-zero nucleus. Then, as one can verify directly from (1.9),

$$l_1 = l'_1 = J_1 \quad l_2 = l'_2 = J_2 \quad (2.24)$$

As one can directly show from (1.5) using (1.9) and, from deShalit and Feshbach (74), (A.2.96) and (A.2.35) deShalit and Feshbach (74)

$$\frac{d\sigma(\alpha', \alpha)}{d\Omega} = \frac{\pi^2}{k^2} \left| \sum (2l+1) P_l(\cos \vartheta) \mathcal{T}_{\alpha'\alpha}(l) \right|^2 \quad (2.25)$$

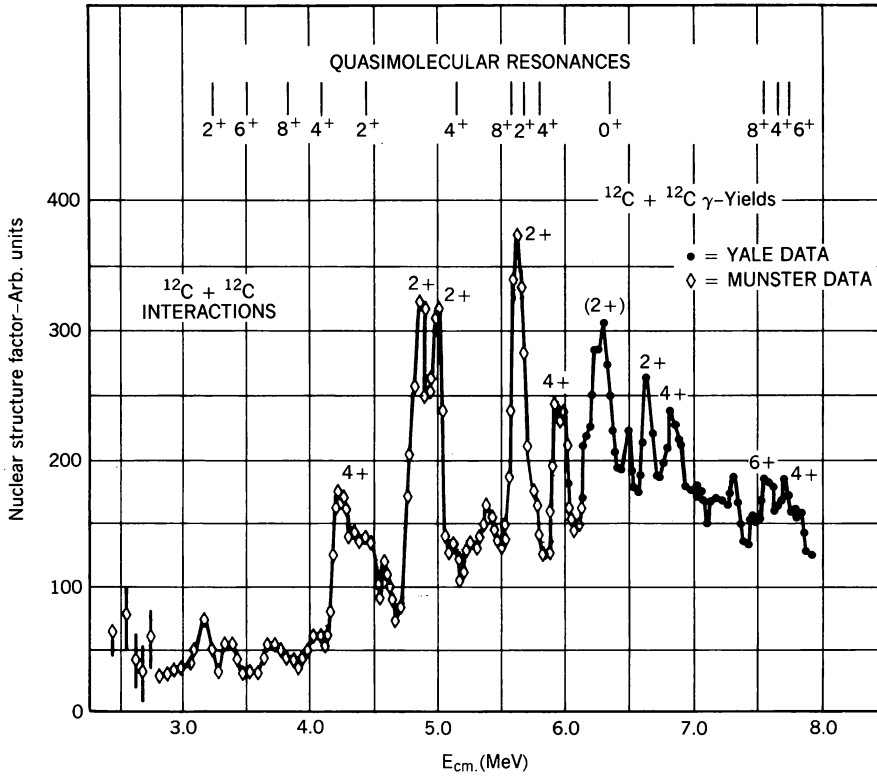


FIG. 2.3. Resonances in the $^{12}\text{C} + ^{12}\text{C}$ reaction [From Erb and Bromley (85).]

where we have abbreviated $\mathcal{T}_{\alpha'\alpha}(l_0; l_0; l\Pi)$ by $\mathcal{T}_{\alpha'\alpha}(l)$. Of course, one can derive this result directly rather than as a special case of (1.5). Let the resonance occur for $l = J$. Then

$$\frac{d\sigma(\alpha', \alpha)}{d\Omega} = \frac{\pi^2}{k^2} |\mathcal{T}_{\alpha'\alpha}^{(P)} + (2J+1)P_J(\cos \vartheta)\mathcal{T}_{\alpha'\alpha}^{(R)}(J)|^2 \quad (2.26)$$

The first term is just the prompt term ("potential" scattering in the elastic case), the second the resonance term. We see that the interference occurs now between the full potential scattering amplitude and the resonant amplitude. This combination will have an interference minimum and a maximum whose positions will vary with angle. It is often the case, particularly at the higher energies, that the prompt amplitude is very small at back angles. In that event, the resonant term will be very prominent in this angular region and the angular distribution will vary like $(P_J)^2$. More generally, an analysis of the angular distribution into partial waves will reveal the resonance. When the channel spins are not zero, extracting the resonance amplitude from the angular distribution might again prove difficult. However, in these cases one can turn

to the polarizations and their angular distributions (if the data are available!) for the needed additional information.

Interference, constructive and destructive, as a consequence of the existence of both a prompt amplitude, (2.14), and a resonating reaction amplitude, (2.8), can occur in reactions as well as elastic scattering. Its strength depends on the relative magnitude of each of the contributing terms, that is, on $g_{c'\lambda}g_{c\lambda}/\Gamma_\lambda$ of (2.8) and on $A_{c'c}(JII)$ of (2.14). Again because of the general tendency of the prompt amplitude eventually to decrease sharply as the angle increases, resonance structure should be more visible at back angles, while interference phenomena should be significant in the intermediate angular region lying between the forward angular region, where the dominant contribution to the differential cross section is from the prompt amplitude and the backward angular region dominated by the resonance reaction.

One should note that because the interference depends on the strengths of the prompt and resonant amplitudes and because these vary with the exit channel, the locations in energy of the interference maximum and minimum will generally vary with channel. The maximum will not be at E_λ ; it may differ from that value by the order of Γ_λ and in extreme cases by more. The customary procedure for the identification of a resonance by observing its presence in each channel must take this possibility into account.

3. PROPERTIES OF THE WIDTHS; THRESHOLD BEHAVIOR OF CROSS SECTIONS; CUSPS

The width of a resonance is given [see (III.2.13)] by

$$\Gamma_{\lambda c} = 2\pi |\langle \Phi_\lambda | H_{QP} \chi_c^{(+)} \rangle|^2 \quad (\text{III.2.13})$$

The value of $\Gamma_{\lambda c}$ depends on the overlap of the channel wave function $\chi_c^{(+)}$ with Φ_λ and H_{QP} . Roughly speaking, this is increased if $\chi_c^{(+)}$ has an appreciable amplitude within the nucleus, that is, within the nuclear volume or on the nuclear surface, according to the nature of the reaction. In other words, the size of $\Gamma_{\lambda c}$ will depend on the probability that the incident wave will penetrate into the nucleus or, equivalently, the probability that the prompt reaction wave can emerge. The barriers that can reduce these probabilities are the angular momentum and Coulomb barriers referred to in Chapter I. The effect of these barriers is largely independent of the nuclear interaction and depends critically on the system's energy, size and the charge of the projectile and target. The angular momentum barrier is important near the threshold for the reaction. The reduction that the Coulomb barrier produces is important for energies near to and below the height of the barrier. Both of these effects can produce a rapid energy dependence of $\Gamma_{\lambda c}$. It would thus be useful to factor these effects out of $\Gamma_{\lambda c}$ so that the remainder will more truly reflect nuclear properties. This factorization cannot be unique.

In this volume we adopt the transmission factor in the channel c , T_c , as a measure of these effects:

$$\Gamma_{\lambda c} \sim T_c \quad (3.1)$$

where T_c is defined by

$$T_c = 1 - \sum_{c'} |\langle S_{cc'} \rangle|^2 \quad (3.2)$$

$S_{cc'}$ is the S matrix, c and c' denoting open channels, while $\langle S_{cc'} \rangle$ is its energy average. The motivation for this choice can be seen most easily by considering the single-channel case, that is, when χ_c is a single-channel wave function. The averaged S can be obtained from the corresponding optical model wave function $\langle \chi_c \rangle$. In Chapter V (p. 367) we show that

$$T_c = 4k \int \langle \chi_c^* \rangle \left(\frac{-2\mu}{\hbar^2} W \right) \langle \chi_c \rangle r^2 dr \quad (3.3)$$

where W is the imaginary part of the complex optical potential. In (3.3) $\langle \chi_c \rangle$ is normalized to have unit amplitude at infinity. Since the angular momentum and Coulomb barriers enter in an identical way for the equations satisfied by χ_c and $\langle \chi_c \rangle$, the behavior of T_c and $\Gamma_{\lambda c}$ should be similar. Obviously, T_c cannot reproduce the dependence of $\Gamma_{\lambda c}$ on λ . However, since W represents the absorptive effects of the reactions as well as the reduction in channel c because of coupling to other channels, T_c provides in a rough fashion a measure of the magnitude of $\Gamma_{\lambda c}$. This relationship is, in fact, demonstrated by (III.3.22'), where the absorption computed from the optical model, which is proportional to T_c , is found in first order to be proportional to the energy average, $\langle \Gamma_{\lambda c} \rangle$. For the present purposes it will suffice to record the approximate result,

$$T_c \simeq 2\pi \langle \omega_\lambda \rangle \langle \Gamma_{\lambda c} \rangle \quad (3.4)$$

where ω_λ is the density of levels of the λ type.

The properties of the transmission factor are listed in the Appendix to Chapter III. Drawing on these results, we find that

$$T_c(E) \sim k^{2l+1} C_l^2(\eta) \quad \text{as } k \rightarrow 0 \quad (3.5)$$

where E is the energy of the relative motion of the two-particle system in channel c , k the wave number is the corresponding momentum divided by \hbar , and lh is the relative angular momentum of the two particles. The quantity η is the Coulomb parameter

$$\eta = \frac{zZe^2}{\hbar v} = \frac{zZ}{137\beta} \quad (3.6)$$

$$\beta = \frac{v}{c} = \frac{1}{21.7} \sqrt{\frac{E(\text{MeV})}{\mu}} \quad (3.7)$$

where v is the relative velocity corresponding to wave number k and μ is the reduced mass in channel c in units of the proton mass. The Coulomb factor C_l^2 is given by (I.8.6), which we repeat here:

$$C_l^2 = \frac{2^{2l}}{[(2l)!]^2} (l^2 + \eta^2) [(l-1)^2 + \eta^2] \cdots (1 + \eta^2) C_0^2(\eta)$$

where

$$C_0^2(\eta) = \frac{2\pi\eta}{e^{2\pi\eta} - 1} \quad (3.8)$$

A short table of C_0^2 is given in (Table I.8.2).

Because of the close relationship between T_c as given by (3.3) and $\Gamma_{\lambda c}$ as expressed by (3.1), it follows that the threshold behavior of $\Gamma_{\lambda c}$ is also given by (3.5), that is,

$$\Gamma_{\lambda c} \sim k^{2l+1} C_l^2(\eta) \quad (3.9)$$

From the analysis of Section 4 in Chapter III, an expression for T near a single-particle resonance [Eq. (III.4.52)] is available:

$$T_c = \frac{\Gamma_{SP}^\uparrow \Gamma_{SP}^\downarrow}{(E - \mathcal{E}_{SP})^2 + \frac{1}{4} \Gamma_{SP}^2} \quad \Gamma_{SP} = \Gamma_{SP}^\uparrow + \Gamma_{SP}^\downarrow \quad (3.10)$$

Γ_{SP}^\uparrow , the escape width from the resonance, is usually referred to in the literature as the single-particle width. It is the single-particle width in the absence of an interaction of the single channel with the compound nuclear channels. An estimate of the order of magnitude of T can be obtained from the results given in the Appendix to Chapter III for T in the resonance region for a square-well optical potential whose imaginary part is W_0 . Then when the relative angular momentum is $l\hbar$, one finds that

$$\Gamma_{SP}^\downarrow \simeq 2W_0 \quad (3.11)$$

$$\Gamma_{SP}^\uparrow = \frac{2\hbar^2}{\mu R^2} k R s_l(kR) \quad (3.12)$$

where R is the radius of the potential and μ is the reduced mass. The function $s_l(kR)$ is given by

$$s_l(x) = \frac{1}{|w_l^{(+)}(x)|^2} \quad (3.13)$$

where $w_l^{(+)}$ is the outgoing wave solution of

$$\frac{d^2 w_l}{dx^2} + \left[1 - \frac{l(l+1)}{x^2} - \frac{2\eta}{x} \right] w_l = 0 \quad (3.14)$$

For uncharged particles ($\eta = 0$)

$$\begin{aligned} s_0 &= 1 \\ s_1 &= \frac{x^2}{1+x^2} \\ s_2 &= \frac{x^4}{9+3x^2+x^4} \\ s_3 &= \frac{x^6}{225+45x^2+6x^4+x^6} \end{aligned} \quad (3.15)$$

The barrier effects given by (3.5) are in (3.10) carried by the factor Γ_{sp}^\dagger , as can readily be demonstrated using (3.12).

The various expressions for T_c are not needed for its numerical evaluation, as this can be easily obtained from the numerical integration of the optical model differential equation for the channel. They serve here to furnish some insight into the properties of T_c , which in turn gives the gross properties of the widths according to (3.1). We shall often write

$$\Gamma_{\lambda c} = \gamma_{\lambda c}^2 T_c \quad (3.16)$$

where $\gamma_{\lambda c}^2$ will carry the deviation of the dependence of $\Gamma_{\lambda c}$ from normal.

The threshold behavior, (3.5), is obviously of importance for channel C . It can also sharply influence the behavior in other channels. For example, consider the scattering in channel C given by (2.18):

$$\sigma_C = \frac{4\pi}{k^2} \left| e^{-i\delta_C} \sin \delta_C - \frac{\frac{1}{2}\Gamma_{C\lambda}}{E - E_\lambda + (i/2)\Gamma_\lambda} \right|^2 \quad (3.17)$$

in the case where two channels C and D can be opened, so that

$$\Gamma_\lambda = \Gamma_{C\lambda} + \Gamma_{D\lambda} \quad (3.18)$$

Suppose that channel D is closed below E_T , and for the sake of the example suppose that the value of l for channel D is zero, so that above threshold

$$\Gamma_\lambda = \Gamma_{C\lambda} + \sqrt{E - E_T} A_{D\lambda} \quad (3.19)$$

where $A_{D\lambda}$ is a finite constant at $E = E_T$. Below E_T

$$\Gamma_\lambda = \Gamma_{c\lambda} \quad (3.20)$$

It is now a simple exercise to verify that

$$\left(\frac{\partial \sigma_c}{\partial E} \right) \rightarrow \infty \quad E \rightarrow E_T^{(+)}$$

while

$$\left(\frac{\partial \sigma_c}{\partial E} \right) \rightarrow \text{const} \quad E \rightarrow E_T^{(-)} \quad (3.21)$$

Hence σ will have a cusp in its dependence on the energy, as illustrated in Fig. 3.1. For larger values of l , singularities in σ_c will appear for higher derivatives (e.g., in the second derivative for $l = 1$), but these effects are much more difficult to discern.

Note. The effects of the angular momentum and Coulomb barrier are not restricted to resonance reactions but hold more generally. The matrix, $\mathcal{T}_{c'c}$, is given by

$$\mathcal{T}_{c'c} = \langle \Psi_{c'}^{(-)} | V | \chi_c \rangle \quad (3.22)$$

so that the dependency of $|\mathcal{T}_{c'c}|^2$ on χ_c is similar to that of $\Gamma_{\lambda c}$. Hence

$$|\mathcal{T}_{c'c}|^2 \sim T_c \sim k^{2l+1} C_l^2(\eta) \quad k \rightarrow 0 \quad (3.23)$$

where l is the orbital angular momentum in the c channel. From (1.6) it follows that

$$\sigma_{c'c} \sim k^{2l-1} C_l^2(\eta) \quad k \rightarrow 0 \quad (3.24)$$

revealing the $1/v$ law for reactions induced by a neutral particle ($\eta = 0$) valid when $l = 0$.

The cusp described by (3.21) is also more general, not being restricted to resonance reactions. This fact may be made evident through the use of one of

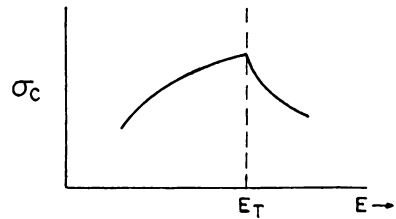


FIG. 3.1. Formation of a cusp in σ_c because of a threshold in another channel.

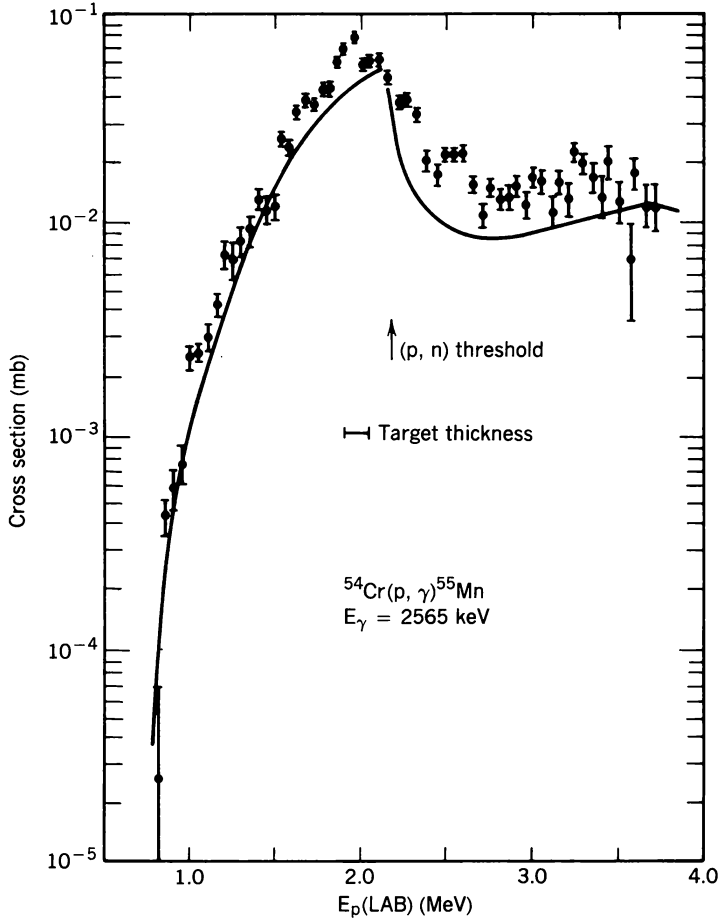


FIG. 3.2. Reaction showing cusp [From Zyskind, Davidson et al. (78).]

the conditions that follow from the unitarity of the S matrix:

$$\sum_d S_{cd}^* S_{cd} = 1 \quad (3.25)$$

Suppose, for example, that there are three channels c , c' , c'' , which must be considered, and moreover, suppose that there is an $l=0$ threshold in the c'' channel. We now look for the effect of this threshold on the c' channel, that is, on $|S_{cc'}|^2$, which is proportional to the cross section for the reaction $c \rightarrow c'$. From (3.25)

$$|S_{cc'}|^2 = 1 - |S_{cc}|^2 - |S_{cc''}|^2$$

The $l = 0$ threshold dependence of $|S_{cc''}|^2$ is given by the factor $\sqrt{E - E_T}$ for E greater than E_T , and by zero for E less than E_T . Therefore, $\partial|S_{cc''}|^2/\partial E$ will have an infinite discontinuity at $E = E_T$ because of the $l = 0$ threshold in the c'' channel. Just such a cusp is shown in Fig. 3.2. The cusp in the $^{54}\text{Cr}(p, \gamma)^{55}\text{Mn}$ reaction is generated by the threshold in the $^{54}\text{Cr}(p, n)$ reaction (Zyskind, Davidson et al. (78)).

4. OVERLAPPING RESONANCES

The analysis of a cross section in terms of a prompt amplitude plus a resonant one can be readily extended to the case of several isolated (i.e., nonoverlapping), resonances. However, it should be noted that the results are not unique in the sense that they depend on the choice for H_{pp} , which in turn determines the prompt term. As was illustrated by several examples in Chapter III, H_{pp} is not unique, so that the prompt term can be the scattering from a hard sphere as in the Wigner–Eisenbud theory, or in another example it can be the amplitude deduced from an optical model potential. Consequently, the value of the widths Γ will vary with the choice of H_{pp} , although the reduced width of (3.16) will generally be less sensitive. This ambiguity reflects the latitude in the definition of what will be considered prompt and what will be considered delayed. It is essential that the presentation of an analysis of experimental results clearly state the choice made for the description of the prompt amplitude, that is, the choice of H_{pp} .

A related question asks how many resonance terms one should add on to the prompt term. Indeed, in some formalisms the number of terms is infinite. There is in some no prompt term initially. That term is recovered by summing over the “distant” resonances. This is, in fact, appropriate since the distant resonances are not resonances at all if by resonances we mean delay times, which are long compared to some appropriate characteristic time.

A simple illustration will clarify this remark. In potential scattering the characteristic time is a/v , where a is the range of the potential and v is the velocity of the incident particle inside the potential. Suppose that a pole of the S matrix occurs at $E - i\Gamma/2$. The delay time is then \hbar/Γ . If that delay time is less than a/v , the time required for the particle to cross the region in which the potential acts, the contribution of the pole term to the scattering amplitude is physically not a resonance. It is physically more correct to consider it as a contribution to the prompt amplitude. To complete this illustration, note that the poles of the S matrix for an attractive square-well potential, no matter how shallow, are infinite in number. In that case, it is mathematically possible to represent the scattering amplitude as a sum of contributions from each of these poles, but of course the resultant total amplitude shows no resonant structure if the well is sufficiently shallow.

These caveats have even more validity when the resonances are overlapping. Analysis of such data can and have been made using (III.2.23) or (III.2.47). In

the first of these, the transition matrix is written as follows:

$$\mathcal{T}_{fi} = \mathcal{T}_{fi}^{(P)} + \sum_{\mu} \frac{A_{fi}^{(\mu)}}{E - E_{\mu}} \quad (\text{III.2.33})$$

As indicated by the earlier discussion the sum over μ contains a finite number of terms, say N . Because of the requirements of unitarity, the parameters $A_{fi}^{(\mu)}$ and E_{μ} , which are slowly varying functions of E , are not independent. To make one such relationship explicit, let

$$A_{fi}^{(\mu)} = \frac{1}{2\pi} e^{i(\delta_f + \delta_i)} e^{i\phi_{\mu}} g_{\mu f}(J\Pi) g_{\mu i}(J\Pi) \quad (4.1)$$

and define

$$\Gamma_{\mu} \equiv \sum_k \Gamma_{\mu k} \quad (4.2)$$

where

$$\Gamma_{\mu k} \equiv g_{\mu k}^2 \quad (4.3)$$

The reader should compare these definitions with (III.2.22)–(III.2.24) given in Section 2 of chapter III. With these definitions (III.2.33) becomes

$$\mathcal{T}_{fi} = \mathcal{T}_{fi}^{(P)} + \frac{1}{2\pi} e^{i(\delta_f + \delta_i)} \sum_{\mu} \frac{e^{i\phi_{\mu}} g_{\mu f}(J\Pi) g_{\mu i}(J\Pi)}{E - \mathcal{E}_{\mu} + (i/2)\Gamma_{\mu} + (i/2)\Gamma'_{\mu}} \quad (4.4)$$

where \mathcal{E}_{μ} is the real part of E_{μ} . The condition relating $A_{fi}^{(\mu)}$ and $\text{Im } E_{\mu}$ given in the single-channel case by (III.2.37) becomes

$$\sum_{\mu} \Gamma'_{\mu} = 0 \quad (4.5)$$

so that the imaginary part of E_{μ} fluctuates about the isolated resonance value of (4.2).

Equation (4.5) is not the only relationship implied by unitarity. Despite the awkwardness of applying these conditions, (III.2.33) is often used in fitting experimental data.

Another procedure that automatically satisfies unitarity uses (III.2.47). In the single-channel case

$$\mathcal{T}_{fi} = \mathcal{T}_{fi}^{(P)} + S_{fi}^{(P)} \frac{\kappa}{1 + i\pi\kappa} \quad (\text{III.2.48''})$$

where κ is given by the series

$$\kappa = \frac{1}{2\pi} \sum_s \frac{\gamma_s^2}{E - e_s} \quad (4.6)$$

The often used *R matrix* fit to resonance data is an example of the use of (III.2.48"). The parameters are γ_s and e_s .

In both methods there are two additional parameters which are not always explicitly mentioned. These are the range, δE , over which a fit is to be made, and the number of terms, N , in the series (4.4) or (4.6). These parameters are not independent. They should be determined by the usual statistical measure of the quality of a fit such as the χ^2 value. In particular, they should be chosen in such a way that the values of γ_s and e_s , for example, are stable against small changes in δE or N .

As the energy of the system increases, the spacing in energy of the resonances becomes smaller, the width of the resonance increases with the consequence that the resonances overlap more and more, and rather soon it becomes impossible to distinguish the individual resonances. Nevertheless, the structure in the energy dependences of the cross section does not immediately disappear. With sufficient energy resolution one observes rapid fluctuations in the energy dependence of the cross section. These are referred to as Ericson-fluctuations [Ericson (60c, 63); Brink and Stephen (63); Brink, Stephen, and Tanner (64)]. They have been observed in a wide variety of reactions.

Statistical measures are used to describe the Ericson-fluctuations. The simplest of these is the energy averaged cross section $\langle \sigma \rangle$, where the average of an energy-dependent quantity $F(E)$ is defined by

$$\langle F(E) \rangle = \int \rho(E, E_0) F(E_0) dE_0 \quad (4.7)$$

where

$$\int \rho(E, E_0) dE_0 = 1 \quad (4.8)$$

To proceed further it is useful to choose H_{pp} to be the optical potential [Kerman, Kwai, and McVoy (73)], for then, from the definition of the optical potential, it follows that in the decomposition of the \mathcal{T} matrix into a prompt and fluctuating part (see Section 8 for further discussion)

$$\mathcal{T} = \mathcal{T}^{(P)} + \mathcal{T}^{(FL)} \quad (4.9)$$

$\mathcal{T}^{(FL)}$ satisfies

$$\langle \mathcal{T}^{(FL)} \rangle = 0 \quad (4.10)$$

It follows that the average cross section can be written as

$$\langle \sigma \rangle = \langle \sigma^{(P)} \rangle + \langle \sigma^{(FL)} \rangle = \sigma^{(P)} + \langle \sigma^{(FL)} \rangle \quad (4.11)$$

The second term does not vanish despite (4.10), since

$$\sigma^{(FL)} \sim |\mathcal{T}^{(FL)}|^2$$

The distribution of $\mathcal{T}^{(FL)}$ and $\sigma^{(FL)}$ about their mean values provides more detailed statistical information. For the distribution of $\mathcal{T}^{(FL)}$, the practice has been to appeal to the central limit theorem of the theory of probability [Feller (68)]. It will be recalled that this theorem states that if a quantity, call it x , is the sum of a large number of random contributions, then the probability $P(x)dx$ that x falls between x and $x + dx$ is given by

$$P(x) = \frac{1}{\sqrt{2\pi\langle x^2 \rangle}} e^{-(1/2)(x^2/\langle x^2 \rangle)} \quad (4.12)$$

where the average value of x , $\langle x \rangle$, is taken to be zero, and $\langle x^2 \rangle$, the average value of x^2 , is defined by

$$\langle x^2 \rangle = \int_{-\infty}^{\infty} P(x)x^2 dx \quad (4.13)$$

Following Ericson (63), we assume that both the real and imaginary parts of \mathcal{T} are such random variables. If

$$\mathcal{T}^{(FL)} = \alpha + i\beta \quad (4.14)$$

then

$$P(\alpha) = \frac{1}{\sqrt{2\pi\langle \alpha^2 \rangle}} e^{-(1/2)(\alpha^2/\langle \alpha^2 \rangle)}$$

If, in addition, one assumes that

$$\langle \alpha^2 \rangle = \langle \beta^2 \rangle = a^2$$

one can write the joint probability $P(\alpha, \beta)$ as

$$P(\alpha, \beta) = \frac{1}{2\pi a^2} e^{-(1/2)(\alpha^2 + \beta^2)/a^2} \quad (4.15)$$

It is now a simple matter to obtain the probability distribution for $\sigma^{(FL)}$ from the relation $\sigma^{(FL)} \sim (\alpha^2 + \beta^2)$. From (4.15),

$$P(\sigma^{(FL)}) = \frac{1}{\sqrt{\langle \sigma^{(FL)} \rangle}} e^{-\sigma^{(FL)}/\langle \sigma^{(FL)} \rangle} \quad (4.16)$$

where

$$\langle \sigma \rangle = \int P(\sigma) \sigma d\sigma \quad (4.17)$$

An experimental test of (4.16) is possible under the assumption that each observed value of $\sigma^{(FL)}$ is a member of the ensemble making up the distribution given by (4.16). In other words, by varying the energy, members of the ensemble are produced. Thus an energy average becomes identical with the ensemble average, a form of the ergodic theorem. An example of an experimental distribution constructed in this way is shown in Fig. 4.1. It will be seen that the probability distribution agrees with the simple result (4.16) rather well. The variance given by

$$\text{var} \equiv \frac{\langle \sigma^2 \rangle - \langle \sigma \rangle^2}{\langle \sigma \rangle^2}$$

equals unity for distribution equation (4.16). We note that the distribution given in Fig. 4.1 has a smaller variance. This can be consequence of the finite experimental energy resolution, which obviously will smooth the data by the rate of $(\Gamma/\Delta E)^2$, where ΔE is the resolution and Γ is the width of the fluctuation.

The ergodic hypothesis made above is not in fact correct, as is demonstrated by the existence of correlations in the fluctuations of the cross section and for that matter of the transition matrix, \mathcal{T} . At a particular angle θ at which the reaction product is observed, an autocorrelation function $C(\epsilon, \theta)$ measuring the

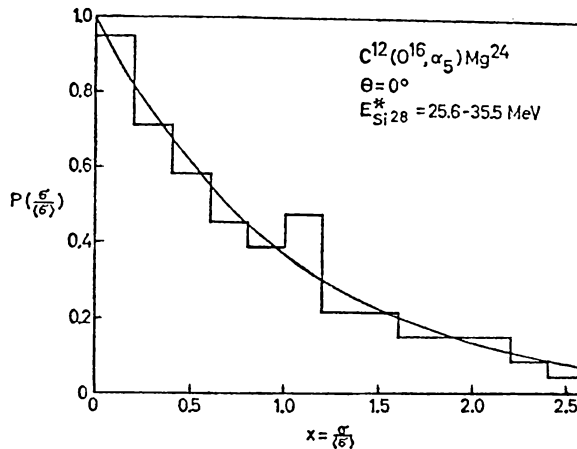


FIG. 4.1. Probability distribution of the differential cross section for $^{12}\text{C}(^{16}\text{O}, \alpha_5)^{24}\text{Mg}$ for the α_5 group leading to the 6.00-MeV excited state in ^{24}Mg . The excitation energy in the compound nucleus ^{28}Si is about 30 MeV [Halbert, Durham, Moak, and Zucker (64).] [From Ericson and Mayer-Kuckuk (66).]

correlations as a function of energy can be defined as follows:

$$C(\varepsilon, \theta) = \frac{\langle \sigma(E + \varepsilon) \sigma(E) \rangle - \langle \sigma \rangle^2}{\langle \sigma \rangle^2} \quad (4.18)$$

where σ is the differential cross section giving the angular distribution. Similarly, an amplitude correlation function, $c(\varepsilon, \theta)$, is given by

$$c(\varepsilon, \theta) = \frac{\langle f(E + \varepsilon) f^*(E) \rangle - |\langle f \rangle|^2}{\langle \sigma \rangle} \quad (4.19)$$

where

$$\sigma = |f|^2$$

It is generally assumed[†] that

$$\langle \sigma(E + \varepsilon) \rangle = \sigma(E)$$

$$\langle f(E + \varepsilon) \rangle = f(E)$$

If $\sigma(E + \varepsilon)$ and $\sigma(E)$ are uncorrelated, $\langle \sigma(E + \varepsilon) \sigma(E) \rangle$ will equal $\langle \sigma(E + \varepsilon) \rangle \langle \sigma(E) \rangle$ and $C(\varepsilon, \theta)$ will vanish. Deviations from zero indicate the presence of correlations.

We shall now write $C(\varepsilon, \theta)$ in terms of the prompt direct cross section and the fluctuating part as given by (4.11). From the assumption that $\sigma^{(P)}$ does not fluctuate, we have

$$\langle (\sigma^{(P)})^2 \rangle = \langle \sigma^{(P)} \rangle^2 \quad (4.20)$$

Using this equation $C(\varepsilon, \theta)$ becomes

$$C(\varepsilon, \theta) = C(0, \theta) C^{(\text{FL})}(\varepsilon, \theta) \quad (4.21)$$

where

$$C(0, \theta) = \frac{\langle (\sigma^{(\text{FL})})^2 \rangle - \langle \sigma^{(\text{FL})} \rangle^2}{[\sigma^{(P)} + \langle \sigma^{(\text{FL})} \rangle]^2} \quad (4.22)$$

and

$$C^{(\text{FL})}(\varepsilon, \theta) = \frac{\langle \sigma^{(\text{FL})}(E + \varepsilon) \sigma^{(\text{FL})}(E) \rangle - \langle \sigma^{(\text{FL})} \rangle^2}{\langle (\sigma^{(\text{FL})})^2 \rangle - \langle \sigma^{(\text{FL})} \rangle^2} \quad (4.23)$$

[†]This assumption is not necessary. One need only redefine $C(\varepsilon, \theta)$ as follows:

$$C(\varepsilon, \theta) = \frac{\langle \sigma(E + \varepsilon) \sigma(E) \rangle - \langle \sigma(E + \varepsilon) \rangle \langle \sigma(E) \rangle}{\langle \sigma(E + \varepsilon) \rangle \langle \sigma(E) \rangle}$$

$C^{(\text{FL})}$ equals unity for $\varepsilon = 0$, and as ε becomes very large one can expect $\sigma^{(\text{FL})}(E + \varepsilon)$ and $\sigma^{(\text{FL})}(E)$ to be uncorrelated, so that $C^{(\text{FL})}(\varepsilon, \theta)$ will approach zero for large values of ε .

Similar expressions can be obtained for $c(\varepsilon, \theta)$ with some simplification since according to (4.10),

$$\langle f \rangle = 0$$

In particular,

$$c(\varepsilon, \theta) = \frac{\langle f^{(\text{FL})}(E + \varepsilon) f^{(\text{FL})*}(E) \rangle}{\langle \sigma \rangle} \quad (4.24a)$$

Note that

$$c(0, \theta) = \frac{\langle \sigma^{(\text{FL})} \rangle}{\sigma^{(P)} + \langle \sigma^{(\text{FL})} \rangle} = 1 - y \quad (4.24b)$$

where

$$y \equiv \frac{\sigma^{(P)}}{\langle \sigma \rangle}$$

In general, $C(\varepsilon, \theta)$ and $c(\varepsilon, \theta)$ are independent. However, under a sufficiently drastic approximation they can be related. Toward this end note that

$$\langle \sigma^{(\text{FL})}(E + \varepsilon) \sigma^{(\text{FL})}(E) \rangle = \langle f^{(\text{FL})}(E + \varepsilon) f^{(\text{FL})*}(E + \varepsilon) f^{(\text{FL})}(E) f^{(\text{FL})*}(E) \rangle \quad (4.25)$$

We now assume that only pair correlations are required to describe the right-hand side, so that

$$\begin{aligned} & \langle f^{(\text{FL})}(E + \varepsilon) f^{(\text{FL})*}(E + \varepsilon) f^{(\text{FL})}(E) f^{(\text{FL})*}(E) \rangle \\ & \simeq \langle f^{(\text{FL})}(E + \varepsilon) f^{(\text{FL})*}(E + \varepsilon) \rangle \langle f^{(\text{FL})}(E) f^{(\text{FL})*}(E) \rangle \\ & \quad + \langle f^{(\text{FL})}(E + \varepsilon) f^{(\text{FL})*}(E) \rangle \langle f^{(\text{FL})*}(E + \varepsilon) f^{(\text{FL})}(E) \rangle \\ & = \langle \sigma^2 \rangle [1 + |c(\varepsilon, \theta)|^2] \end{aligned} \quad (4.26)$$

It should be noted that third-order terms such as $\langle f^{(\text{FL})}(E + \varepsilon) f^{(\text{FL})*}(E + \varepsilon) f^{(\text{FL})}(E) \rangle \langle f^{(\text{FL})*}(E) \rangle$ vanish in any event in virtue of (4.10). In deriving (4.26) we have also assumed that $\langle f^{(\text{FL})}(E + \varepsilon) f^{(\text{FL})}(E) \rangle$ is zero. This follows from (4.10) if that equation is valid because of the random phases of the components of $f^{(\text{FL})}$. It is thus indicated that the major error in the derivation of (4.26) is the possible presence of a quadrilinear correlation which cannot be expressed, as in (4.26), in terms of lower-order correlations.

It immediately follows from (4.26) that

$$C(\varepsilon, \theta) = |c(\varepsilon, \theta)|^2 \quad (4.27)$$

Although $c(\varepsilon, \theta)$ can and has been measured directly [Feshbach and Yennie (62)], it is considerably simpler experimentally to measure $C(\varepsilon, \theta)$.

Before we look at some of the experimental data, it is useful to present a theoretical estimate of $c(\varepsilon, \theta)$. Toward this end we use expression (III.2.33) quoted earlier:

$$\mathcal{T}^{(\text{FL})}(E) = \sum_{\mu} \frac{A^{(\mu)}}{E - \mathcal{E}_{\mu} + (i/2)\Gamma} \quad (4.28)$$

We have dropped the subscripts f and i , which are to be understood, and the simplifying approximation that the imaginary part of the poles, E_{μ} , is independent of μ and equal to $\Gamma/2$ has been made. We now wish to evaluate

$$\langle \mathcal{T}^{(\text{FL})}(E + \varepsilon) \mathcal{T}^{(\text{FL})*}(E) \rangle = \sum_{\mu, \nu} \left\langle \frac{A_{\mu} A_{\nu}^*}{[E + \varepsilon - \mathcal{E}_{\mu} + (i/2)\Gamma][E - \mathcal{E}_{\nu} - (i/2)\Gamma]} \right\rangle \quad (4.29)$$

We make the assumption that the important contributions to the sum occur when $\mu = \nu$. The other terms are small because they will generally have phases which if there are enough terms in the sum will take on all possible values. The net effect is a considerable cancellation. In the limit that we take here that the cancellation is complete, this assumption is known as the random phase assumption[†]. Under this assumption

$$\langle \mathcal{T}^{(\text{FL})}(E + \varepsilon) \mathcal{T}^{(\text{FL})*}(E) \rangle = \sum_{\mu} \left\langle \frac{|A_{\mu}|^2}{[E + \varepsilon - \mathcal{E}_{\mu} + (i/2)\Gamma][E - \mathcal{E}_{\mu} - (i/2)\Gamma]} \right\rangle$$

Neglecting the energy dependence of A_{μ} and \mathcal{E}_{μ} , the energy average of this quantity can be readily computed[§] with the result that

$$c(\varepsilon, \theta) = c(0, \theta) \frac{i\Gamma}{\varepsilon + i\Gamma} \quad (4.30)$$

[†]More explicitly if ϕ_{μ} is the phase of A_{μ} , the right-hand side of (4.28) can be written

$$\sum_{\mu, \nu} e^{i(\phi_{\mu} - \phi_{\nu})} \frac{|A_{\mu} A_{\nu}^*|}{[E + \varepsilon - \mathcal{E}_{\mu} + (i/2)\Gamma][E - \mathcal{E}_{\nu} - (i/2)\Gamma]}$$

If we now assume that ϕ_{μ} and ϕ_{ν} are chosen from an ensemble of random numbers, the ensemble average of this quantity will contain only the $\phi_{\mu} = \phi_{\nu}$ terms, the remaining vanishing. Finally, one assumes that the ensemble and energy averages (i.e., the ergodic theorem) are identical.

[§]The calculation proceeds as follows:

$$\left\langle \frac{1}{[E + \varepsilon - \mathcal{E}_{\mu} + (i/2)\Gamma][E - \mathcal{E}_{\mu} - (i/2)\Gamma]} \right\rangle = \frac{1}{2\Delta} \int_{E_0 - \Delta}^{E_0 + \Delta} \frac{dE}{[E + \varepsilon - \mathcal{E}_{\mu} + (i/2)\Gamma][E - \mathcal{E}_{\mu} - (i/2)\Gamma]} \quad (\text{Continued})$$

and

$$C(\varepsilon, \theta) = C(0, \theta) \frac{\Gamma^2}{\varepsilon^2 + \Gamma^2} \quad (4.31)$$

The width, Γ , scales the rate at which $C(\varepsilon, \theta)$ goes to zero with increasing ε . The value of \hbar/Γ measures the time during which the compound nuclear system, formed by the projectile and target nucleus, lives. In contrast to the compound nuclear resonance, for which \hbar/Γ gives the lifetime of a well-defined state, there is no well-defined state with a width Γ . Rather, because the resonances overlap, the system moves from resonance to resonance before finally breaking up into the final observed products. The quantity \hbar/Γ measures the time for this process, and thus it would be most appropriate to refer to it as the *interaction time*. The quantity Γ is called the *coherence energy*.

The special nature of the form used for $\mathcal{T}^{(FL)}$ should be remarked upon. In the first place, the correlations between the coefficients $A^{(\mu)}$, the widths Γ , and the energies \mathcal{E}_μ because of unitarity have been neglected. More important, perhaps, is the neglect of effects of intermediate structure signaling the presence of doorway states. These will introduce another scale in addition to Γ , of the order of Γ_d , the average width of doorway states. Pappalardo (64) has suggested that one could search for doorway states by looking for this second scale factor in the autocorrelation function, as indicated in Fig. 4.2, which presents a highly idealized situation. As indicated in the figure, the small ε behavior (dashed line) is dominated by Γ and the large ε dependence is governed by Γ_d .

The existence of these fluctuation effects was predicted by Ericson (60c). It was first demonstrated by Colli, Facchini, and their collaborators (59). Some experimental results obtained by von Witsch, von Brentano, Meyer-Kuckuk, and Richter (66) using the $^{37}\text{Cl}(p, \alpha)^{34}\text{S}$ are shown in Figs. 4.3 and 4.4. In Fig. 4.3 we see the excitation functions for this reaction at 12 scattering angles taken with an energy resolution of $\Delta E \lesssim 5$ keV. The presence of fluctuations is clearly indicated. In Fig. 4.4 the autocorrelation function is plotted for three separate

where $\Delta \gg \varepsilon$. Let $x = (2/\Gamma)E$. Then the integral becomes

$$\frac{\Gamma}{\Delta} \int_{x_0 - (2/\Gamma)\Delta}^{x_0 + (2/\Gamma)\Delta} dx \frac{1}{(x + (2\varepsilon/\Gamma) - x_\mu + i)(x - x_\mu - i)}$$

If now it is assumed that the averaging interval 2Δ is much larger than Γ , the limits of the integral can be approximated by $\pm \infty$ and the integral evaluated by the calculus of residues, for example, to give

$$\frac{\pi i \Gamma}{\Delta} \frac{1}{i + \varepsilon/\Gamma}$$

from which (4.30) follows.

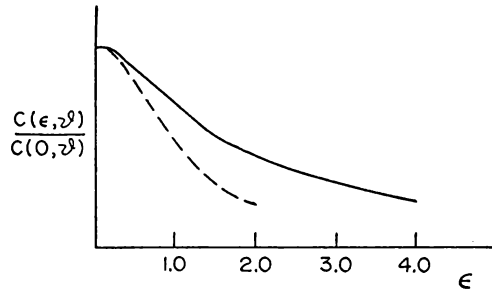


FIG. 4.2. Autocorrelation function in the presence of a doorway state.

angles. It will be observed that after an initial decrease as predicted by (4.31), $C(\epsilon, \theta)$ fluctuate about the zero value. These fluctuations are referred to as *finite range deviations* (FRDs) and arise from the fact that a finite energy range was used in making the averages and correlations. The requisite corrections have been developed by Böhning (66). Fitting the small ϵ part of the results in Fig. 4.4 gives a mean value of Γ of about 18 keV.

On examining Fig. 4.3, it is quite clear that there is considerable angular correlation. For example, the peak at about 11.5 MeV proton energy at the laboratory angle $\theta = 175^\circ$ also appears at 170° , 162° , and 157° . Angular correlations are to be expected simply from the complexity theorem mentioned in Chapter I and by (1.10). This states that if there are maximum values of the orbital angular momentum in either the entrance or exit channel, there is a

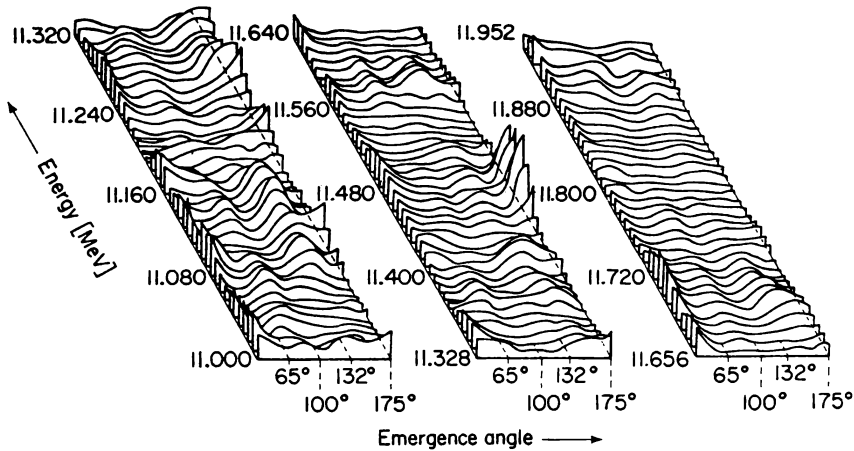


FIG. 4.3. Three-dimensional representation of the variation of the angular distribution of the α -particles emerging from the reaction $^{37}\text{Cl}(p, \alpha)^{34}\text{S}$ and proceeding to the ground state of ^{34}S , shown as a function of energy between 11.000 and 11.952 MeV in steps of 0.008 MeV [von Witsch, von Brentano et al. (66)]. [From Marmier and Sheldon (70).]

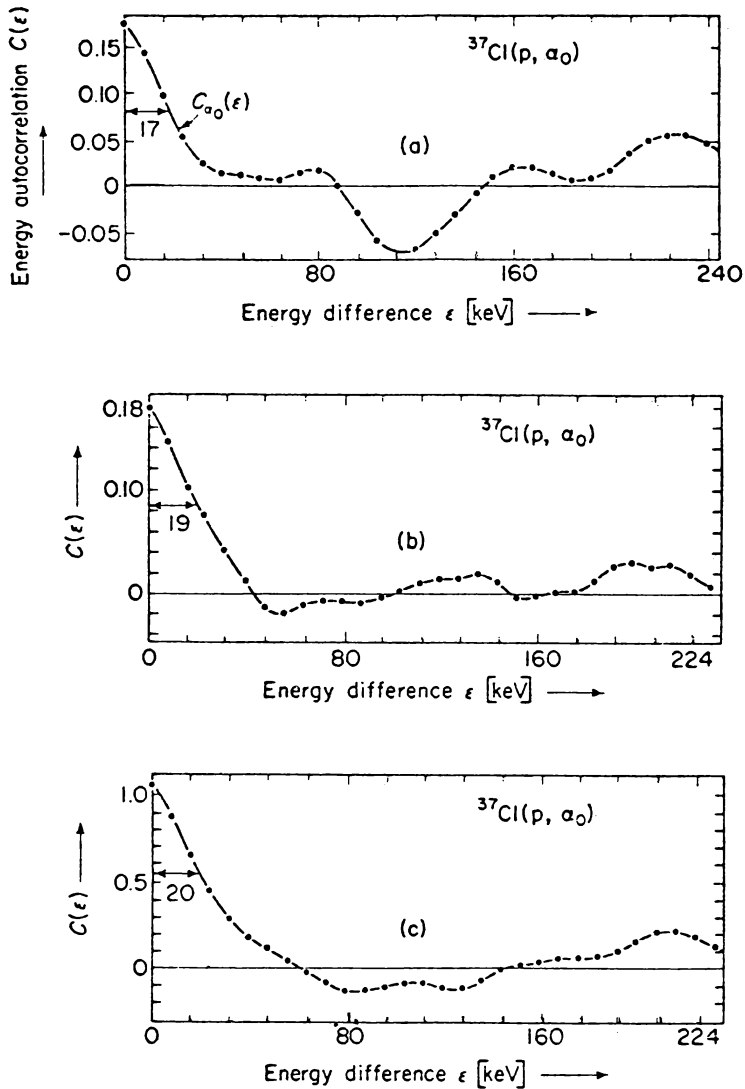


FIG. 4.4. Energy autocorrelation functions $C(\epsilon)$ plotted as a function of the energy difference ϵ for (a) $\theta = 33^\circ$, (b) $\theta = 80^\circ$, (c) $\theta = 175^\circ$ (CM) in the case of the $^{37}\text{Cl}(p, \alpha_0)^{34}\text{S}$ reaction proceeding to the ground state of ^{34}S . The coherence energy Γ can be derived from the width at half-height of the first peak; the results indicate that $\Gamma = 18$ keV, which corresponds to a mean lifetime for the compound nucleus $^{38}\text{Ar}^*$ of $\tau = \hbar/\bar{\Gamma} = 3.7 \times 10^{-20}$ s [von Witsch, von Brentano, et al (66)]. [From Marmier and Sheldon (70).]

maximum value of the order, L , of the Legendre polynomial P_L required to describe the angular distribution of the reaction. Well above the Coulomb barrier, these maxima values are set by the angular momentum barrier. If the momentum change is q , then

$$\frac{qR}{\hbar} \simeq l_{\max} \theta \approx 1 \quad (4.32)$$

Experimental verification of the validity of this remark has been given by Dearnley, Gibbs, Leachman, and Rogers (65).

We observe that there are two causes of angular fluctuations. One, just discussed, is a consequence of the finite size of the nuclear system. The second, which originates in the energy fluctuations, affects the differential cross section $d\sigma/d\Omega$. The appropriate correlation function is defined as follows:

$$C(\theta, \theta') = \frac{\langle (d\sigma^{(\text{FL})}/d\Omega)(d\sigma^{(\text{FL})}/d\Omega') \rangle - \langle d\sigma^{(\text{FL})}/d\Omega \rangle \langle d\sigma^{(\text{FL})}/d\Omega' \rangle}{\langle d\sigma/d\Omega \rangle \langle d\sigma/d\Omega' \rangle} \quad (4.33)$$

The averages in (4.33) are energy averages. This correlation function can be evaluated using the expression for the \mathcal{T} matrix, (1.5). We shall not carry that calculation out but will leave it as an exercise for the reader who may be helped by the following derivation of $\langle d\sigma/d\Omega \rangle$. According to (1.5),

$$\begin{aligned} \langle d\sigma^{(\text{FL})}/d\Omega \rangle &= \frac{4\pi^3}{k^2} \frac{1}{(2i+1)(2I+1)} \sum (l_1 s J_1 \| Y_L \| l_2 s J_2) (l'_1 s' J_1 \| Y_L \| l'_2 s'_2 J_2) \\ &\quad \times \langle \text{Re}[\mathcal{T}^{(\text{FL})}(l'_1, s'; l_1 s; J, \Pi_1) \mathcal{T}^{(\text{FL})*}(l'_2, s'; l_2 s; J_2 \Pi_2)] \rangle P_L(\cos \theta) \end{aligned} \quad (4.34)$$

To evaluate the average we make use of the random-phase approximation, which in the present context takes the form

$$\begin{aligned} \langle \text{Re}(\mathcal{T}^{(\text{FL})} \mathcal{T}^{(\text{FL})*}) \rangle &= \delta(l'_1, l'_2) \delta(l_1, l_2) \delta(J_1, J_2) \delta(\Pi_1, \Pi_2) \langle |\mathcal{T}^{(\text{FL})}(l'_1 s'; l_1 s; J_1 \Pi_1)|^2 \rangle \\ \left\langle \frac{d\sigma^{(\text{FL})}}{d\Omega} \right\rangle &= \frac{4\pi^3}{k^2} \frac{1}{(2I+1)(2i+1)} \sum (l s J \| Y_L \| l s J) (l' s' J \| Y_L \| l' s' J) \\ &\quad \times \langle |\mathcal{T}^{(\text{FL})}(l' s'; l s; J \Pi)|^2 \rangle P_L(\cos \theta) \end{aligned} \quad (4.35)$$

From the properties of the reduced matrix elements of Y_L , it follows that L is even, so that $\langle d\sigma^{(\text{FL})}/d\Omega \rangle$ is symmetric about 90° . Later in this chapter we describe how to evaluate $\langle |\mathcal{T}^{(\text{FL})}|^2 \rangle$ using the statistical theory of nuclear reactions.

5. LEVEL DENSITY[†]

In considering reactions that lead to highly excited states of residual nuclei, it is usually neither practical nor desirable to observe the cross sections for the excitation of a particular state. Generally, the experimental energy resolution, ΔE , is not sufficiently small to permit the selection of a given final state or to go on to define its properties such as spin, parity, moments, and so on. Under these circumstances the summation in the expression for the cross section

$$\sigma = \frac{4\pi^3}{k^2} \sum_f |\mathcal{T}_{fi}|^2 \quad (5.1)$$

where f designates the final states of the system contained in the energy interval ΔE , is replaced by an integral as follows:

$$\sigma = \frac{4\pi^3}{k^2} \int dE_f \omega(E_f) |\mathcal{T}_{fi}|^2 \quad (5.2)$$

Here $\omega(E_f)$ is the level density of the residual nucleus. The quantity $\omega(E)dE$ gives the number of levels between E and $E + dE$. It is, of course, possible to partition the density further by asking, for example, for the density of levels with a given quantum number, such as the spin, J , or with a given set of quantum numbers, J, Π, T , and so on.

We shall also be interested in the density of levels at a particular energy of excitation of the compound nucleus. Except for a relatively small energy range, in which the resonances can be individually observed, it is generally not possible to determine the properties of the individual resonances, and a more global approach in which the occurrence of resonances is given by a level density is preferred.

In both cases, density of levels in the compound or in the residual nucleus, the energy spectrum is taken to be discrete. This certainly can be the case for the residual nucleus. For the compound nucleus, the levels are taken to be the levels of the states of the system in what was designated in Chapter III as the \mathcal{Q} space. This Hilbert space is defined as containing those states in which no part of the system is in the continuum, so that \mathcal{Q} is the closed-channel subspace. Because of this restriction, the energies of the \mathcal{Q} space form a discrete spectrum even though the energy of the system is positive. The levels in \mathcal{Q} space become observable resonances with finite widths, when one includes the effect of the coupling to the open-channel subspace designated by \mathcal{P} .

For a discrete energy spectrum with energies ε_j , the level density $\omega(E)$ is given exactly by

$$\omega(E) = \sum_j \delta(E - \varepsilon_j) \quad (5.3)$$

[†]Ericson (60c); Bloch (69, 72); Huizenga and Moretto (72); Huizenga (72).

where

$$\int_{E_2}^{E_1} \omega(E) dE = N(E_1) - N(E_2) \quad (5.4)$$

$N(E)$ gives the total number of levels with energies less than E .

Equation (5.3) is exact. Using an integral representation of ω which follows from (5.3), it will be possible in the limit of large E to obtain a continuous approximation to the series of delta functions. Toward this end introduce the Fourier representation of $\delta(E - \varepsilon_j)$:

$$\delta(E - \varepsilon_j) = \frac{1}{2\pi} \int_{-\infty}^{\infty} e^{-i\kappa(E - \varepsilon_j)} d\kappa$$

so that

$$\omega(E) = \frac{1}{2\pi} \int_{-\infty}^{\infty} e^{-i\kappa E} \left(\sum_j e^{i\kappa \varepsilon_j} \right) d\kappa$$

Letting $\kappa = i\beta$,

$$\omega(E) = \frac{1}{2\pi i} \int_{-i\infty}^{i\infty} e^{\beta E} Z(\beta) d\beta \quad (5.5)$$

where $Z(\beta)$ is the partition sum:

$$Z(\beta) = \sum_j e^{-\beta \varepsilon_j} = \text{tr}(e^{-\beta H}) \quad (5.6)$$

the trace is restricted to the states in \mathcal{Q} . The partition sum is a familiar object in statistical mechanics and one is tempted to relate the integration variable, β , with the inverse of the temperature. That would be the case if the system were in contact with a heat bath and if one could describe the excited nucleus as an equilibrated system.

In the limit of large E , the method of steepest descents [Morse and Feshbach ((53), 437 et seq.)] can be used to obtain an approximate evaluation of the integral in (5.5). Rewriting the integrand as $\exp[\beta E + \ln Z(\beta)]$, we expand the bracketed expression around the saddle point, β_0 , defined to be a point at which the derivative of $\beta E + \ln Z(\beta)$ with respect to β is zero.

$$E + \frac{d \ln Z(\beta)}{d\beta} = 0 \quad \text{at } \beta = \beta_0$$

The integral for $\omega(E)$ is then approximately given by

$$\omega(E) = \frac{1}{2\pi} e^{\beta_0 E} Z(\beta_0) \int_{-\infty}^{\infty} \exp \left[-\frac{1}{2} \left| \frac{d^2 \ln Z}{d\beta^2} \right| (\beta - \beta_0)^2 \right] d\beta$$

where we have assumed it to be possible to deform the path of integration from the pure imaginary axis to the real one in the neighborhood of $\beta = \beta_0$. Hence

$$\omega \simeq \left[\frac{1}{2\pi |d^2 \ln Z / d\beta_0^2|} \right]^{1/2} e^{\beta_0 E} Z(\beta_0) = \left[\frac{1}{2\pi |dE/d\beta_0|} \right]^{1/2} e^{\beta_0 E} Z(\beta_0) \quad (5.7)$$

This result, providing a continuous function approximating the ω that is given in (5.3) by a series of δ functions, can be valid only for sufficiently large energy E . The energy interval around E over which expression (5.3) has been effectively averaged to obtain (5.7) should contain a sufficiently large number of levels.

Problem. Show that

$$E = \frac{\sum \varepsilon_j e^{-\beta_0 \varepsilon_j}}{\sum e^{-\beta_0 \varepsilon_j}} \equiv \langle \varepsilon_j(\beta_0) \rangle \quad (5.8)$$

and

$$\frac{d^2 \ln Z}{d\beta_0^2} = \langle \varepsilon_j^2 \rangle - \langle \varepsilon_j \rangle^2 \quad (5.9)$$

where

$$\langle \varepsilon_j^2 \rangle = \frac{\sum \varepsilon_j^2 e^{-\beta_0 \varepsilon_j}}{\sum e^{-\beta_0 \varepsilon_j}} \quad (5.10)$$

Equation (5.7) for ω does not explicitly take into account constraints that can be imposed on the system because of conservation conditions. For example, one might ask for the level density for a system consisting of a given number, N , of nucleons, or for a system whose angular momentum is J , and so on. In what follows we generalize the discussion leading to (5.7) asking for the density $\omega(E, N)$.

The density $\omega(E, N)$ is given by

$$\omega(E, N) = \sum_{j, \gamma} \delta(v - N) \delta(E - \varepsilon_j(v)) \quad (5.11)$$

where, as indicated, ε_j is a function of the number of nucleons. Introducing the Fourier integral representation of the δ functions, one is immediately led to the analog of (5.5):

$$\omega(E, N) = \frac{1}{(2\pi i)^2} \int_{-i\infty}^{i\infty} d\beta_1 \int_{-i\infty}^{i\infty} d\beta_2 Z(\beta_1, \beta_2) e^{\beta_1 E - \beta_2 N} \quad (5.12)$$

where

$$Z(\beta_1, \beta_2) = \sum_{j,v} e^{\beta_2 \epsilon_j - \beta_1 \epsilon_j(v)} \quad (5.13)$$

The method of steepest descents applied to the integral in (5.12) yields

$$\omega(E, N) = \frac{1}{2\pi |\det L|^{1/2}} Z(\beta_1^{(0)}, \beta_2^{(0)}) e^{\beta_1^{(0)} E - \beta_2^{(0)} N} \quad (5.14)$$

where the saddle-point values of β_1 and β_2 , $\beta_1^{(0)}$ and $\beta_2^{(0)}$, respectively, are determined by the equations

$$E + \frac{\partial}{\partial \beta_1} \ln Z(\beta_1^{(0)}, \beta_2^{(0)}) = 0 \quad (5.15)$$

$$N - \frac{\partial}{\partial \beta_2} \ln Z(\beta_1^{(0)}, \beta_2^{(0)}) = 0 \quad (5.16)$$

and

$$L_{ij} = \frac{\partial^2 \ln Z(\beta_1, \beta_2)}{\partial \beta_i \partial \beta_j} \quad (5.17)$$

A. The Level Density for the Independent Particle Model

Let us suppose that N nucleons move independently in an average one-body potential [see Chapter V) in deShalit and Feshbach (74)]. Suppose, moreover, that the one-body energy levels in this potential are given by $\epsilon_1, \epsilon_2, \dots$. Because of the Pauli exclusion principle, the number of nucleons in each level is either zero or 1, where we are using the m -representation [deShalit and Feshbach (74, p. 221)]. Then

$$\sum n_s = N \quad (5.18)$$

$$\sum n_s \epsilon_s = E \quad (5.19)$$

The partition sum, (5.13), is

$$Z(\beta_1, \beta_2) = \sum_{\text{all } n_s} \exp[\beta_2 \sum n_s - \beta_1 \sum n_s \epsilon_s] = \sum_{\text{all } n_s} \exp \left[\sum_s (\beta_2 - \beta_1 \epsilon_s) n_s \right] \quad (5.20)$$

or

$$Z(\beta_1, \beta_2) = \prod_s (1 + e^{(\beta_2 - \beta_1 \epsilon_s)}) \quad (5.21)$$

Further development requires assumptions regarding ϵ_s . We shall assume that

the spectrum ε_s can be replaced by a smoothly varying continuous spectrum as indicated by the Fermi-gas model [see Chapter II in deShalit and Feshbach (74)]. Then

$$\ln Z(\beta_1, \beta_2) = \sum_s \ln(1 + e^{(\beta_2 - \beta_1 \varepsilon_s)}) \rightarrow \int_{\varepsilon_0}^{\infty} \omega(\varepsilon) \ln(1 + e^{(\beta_2 - \beta_1 \varepsilon)}) d\varepsilon \quad (5.22)$$

where ε_0 is the smallest value of ε_s . This integral will be evaluated for large β_2 and β_1 . The validity of this assumption will be justified *a posteriori*. Under these circumstances the exponential, $\exp(\beta_2 - \beta_1 \varepsilon)$, will for small or negative values of ε , be much larger than unity, so that the logarithm in (5.22) is approximately equal to $\beta_2 - \beta_1 \varepsilon$. For large values of ε , the exponential will be negligible and the logarithm will tend to zero. The drop to zero occurs precipitously for large values of β_2 and β_1 , at

$$\varepsilon_F \equiv \frac{\beta_2}{\beta_1} \quad (5.23)$$

As the notation indicates, for the saddle-point values of β_2 and β_1 , the ratio equals the Fermi energy.

In this limit

$$\ln Z \xrightarrow{\beta_2, \beta_1 \gg 1} F^{(\infty)} \equiv \int_{\varepsilon_0}^{\varepsilon_F} \omega(\varepsilon)(\beta_2 - \beta_1 \varepsilon) d\varepsilon$$

or

$$F^{(\infty)} = \beta_2 N(\varepsilon_F) - \beta_1 W(\varepsilon_F) \quad (5.24)$$

where

$$N(\varepsilon_F) \equiv \int_{\varepsilon_0}^{\varepsilon_F} \omega(\varepsilon) d\varepsilon \quad (5.25a)$$

gives the number of single-particle states up to ε_F , while

$$W(\varepsilon_F) \equiv \int_{\varepsilon_0}^{\varepsilon_F} \varepsilon \omega(\varepsilon) d\varepsilon \quad (5.25b)$$

gives the total energy of these states.

The next order is obtained by evaluating

$$\ln Z - F^{(\infty)} = \int_{\varepsilon_F}^{\infty} \omega(\varepsilon) \ln(1 + e^{\beta_2 - \beta_1 \varepsilon}) d\varepsilon + \int_{\varepsilon_0}^{\varepsilon_F} \omega(\varepsilon) \ln(1 + e^{-\beta_2 + \beta_1 \varepsilon}) d\varepsilon$$

In the first integral let $\beta_1 \varepsilon - \beta_2 = x$ and in the second $\beta_2 - \beta_1 \varepsilon = x$. Then

$$\begin{aligned} \ln Z - F^{(\infty)} &= \frac{1}{\beta_1} \int_0^\infty \omega\left(\frac{x}{\beta_1} + \varepsilon_F\right) \ln(1 + e^{-x}) dx \\ &\quad + \frac{1}{\beta_1} \int_0^{\beta_2 - \beta_1 \varepsilon_0} \omega\left(-\frac{x}{\beta_1} + \varepsilon_F\right) \ln(1 + e^{-x}) dx \end{aligned}$$

As β_1 increases, taking ε_0 to be negative, to $O(1/\beta_1)$, one obtains

$$\ln Z - F^{(\infty)} \simeq \frac{2\omega(\varepsilon_F)}{\beta_1} \int_0^\infty \ln(1 + e^{-x}) dx = \frac{(\pi^2/6)\omega(\varepsilon_F)}{\beta_1}$$

Combining this with (5.24) for $F^{(\infty)}$ yields

$$\ln Z \simeq \beta_2 N(\varepsilon_F) - \beta_1 W(\varepsilon_F) + \frac{(\pi^2/6)\omega(\varepsilon_F)}{\beta_1} \quad \varepsilon_F \equiv \frac{\beta_2}{\beta_1} \quad (5.26)$$

This result can now be substituted in (5.15) and (5.16), determining the saddle-point values of $\beta_1^{(0)}$ and $\beta_2^{(0)}$. Take, for example, (5.1):

$$N = \frac{\partial \ln Z}{\partial \beta_2} \simeq N(\varepsilon_F) + \frac{\pi^2}{6\beta_1^2} \omega'(\varepsilon_F)$$

For large values of β_1 and smooth single-level density ω ,

$$N \simeq N(\varepsilon_F) \quad (5.27)$$

so that indeed ε_F is, to this approximation, the Fermi energy. In the same approximation, (5.16),

$$E = W(\varepsilon_F) + \frac{\pi^2}{6} \frac{\omega(\varepsilon_F)}{\beta_1^2} + \text{terms in } \omega'(\varepsilon_F) + \dots \quad (5.28)$$

Since $W(\varepsilon_F)$ is the energy of the Fermi gas in its ground state, the excitation energy U is given by

$$U = \frac{\pi^2}{6} \frac{\omega(\varepsilon_F)}{\beta_1^2} \quad (5.29)$$

The two equations $\beta_2/\beta_1 = \varepsilon_F$ and (5.29) then determine both β_2 and β_1 .

We also need to compute the determinant L , whose elements are given by (5.17). The second derivatives are readily calculated in the limit of β_1 and β_2

large from (5.26) bearing in mind that $\varepsilon_F = \beta_2/\beta_1$. One obtains

$$\begin{aligned}\frac{\partial^2 \ln Z}{\partial \beta_1^2} &= \frac{\omega(\varepsilon_F)}{\beta_1} & \frac{\partial^2 \ln Z}{\partial \beta_1^2} &= \left(\frac{\pi^2}{3} + \beta_2^2 \right) \frac{\omega(\varepsilon_F)}{\beta_1^3} \\ \frac{\partial^2 \ln Z}{\partial \beta_1 \partial \beta_2} &= -\frac{\beta_2}{\beta_1^2} \omega(\varepsilon_F)\end{aligned}$$

so that

$$\det L = \frac{\pi^2}{3} \left(\frac{\omega(\varepsilon_F)}{\beta_1^2} \right)^2$$

It is now possible to evaluate the right-hand side of (5.14) to obtain $\omega(E, N)$. The result[†] is [Bethe (37)]

$$\omega(U, N) \simeq \frac{1}{\sqrt{48}U} \exp\left(\frac{\pi^2 \omega}{3\beta_1}\right)^{1/2} = \frac{1}{\sqrt{48}U} \exp\left[2\sqrt{\frac{\pi^2 \omega(\varepsilon_F)U}{6}}\right] \quad (5.30)$$

where for convenience we have changed the independent variable from E to U . This form is commonly used in the semiempirical description of the density of levels to be discussed. The constant $1/\beta_1$ plays the role of a temperature, t , so that (5.29) relates the temperature and the excitation energy[‡]:

$$U = at^2 \quad (5.31)$$

where the Fermi-gas model gives

$$a = \frac{\pi^2 \omega(\varepsilon_F)}{6}$$

[†]Morrison (53) has compared this result and that obtained by Hardy and Ramanujan (18) for the different ways, $p(n)$, to form a given number n by any of the possible sums of smaller integers. For large n they find that

$$p(n) = \frac{1}{\sqrt{48n}} \exp\left[2\left(\frac{\pi^2}{6}n\right)^{1/2}\right]$$

The reader is invited to consider the relationship of this result and (5.30).

[‡]A statistical-mechanical definition of temperature T is

$$T^{-1} = \frac{1}{\omega} \frac{\partial \omega}{\partial E} = -\frac{1}{U} + \sqrt{\frac{c}{U}}$$

or approximately,

$$U = c\left(T - \frac{1}{c}\right)^2$$

or

$$t = \left[\frac{6U}{\pi^2 \omega(\varepsilon_F)} \right]^{1/2}$$

Problem. Using (5.21) and $N = \partial \ln Z / \partial \beta_2$, show that

$$N = \sum \frac{1}{1 + e^{\beta_1(\varepsilon_s - \varepsilon_F)}} = \sum \bar{n}(\varepsilon_s)$$

where $\bar{n}(\varepsilon_s)$ is the average occupation number of the one-body state with energy ε_s . Using the continuous approximation for the spectrum of ε_s [see (5.22)], this becomes

$$N = \int_0^\infty \frac{d\varepsilon \omega(\varepsilon)}{1 + e^{\beta_1(\varepsilon - \varepsilon_F)}} = \int_{\varepsilon_0}^\infty d\varepsilon \omega(\varepsilon) \bar{n}(\varepsilon)$$

See Fig. 5.1 for a plot of $\bar{n}(\varepsilon)$. Using the approximation developed following (5.22), show that $N = N(\varepsilon_F)$. Show that the number of particles excited above ε_F is

$$\frac{(\ln 2)\omega}{\beta_1}$$

Thus the average number of degrees of freedom (particles plus holes) excited when the excitation energy is U is given by

$$n_s = \frac{(2 \ln 2)\omega}{\beta_1}$$

or

$$n_{\text{exc}} = 2 \ln 2 \sqrt{\frac{6U\omega(\varepsilon_F)}{\pi^2}} \quad (5.32)$$

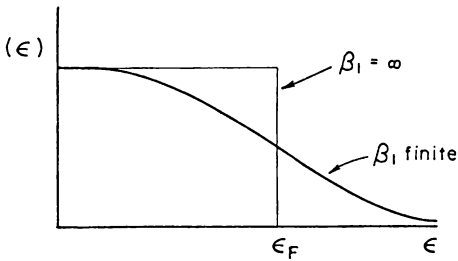


FIG. 5.1. Average occupation number, $\bar{n}(\varepsilon)$ of a one-body state with energy ε for two values of β_1 .

If we write the exponent in (5.30) as $2\sqrt{aU}$,

$$n_{\text{exc}} = \frac{12 \ln 2}{\pi^2} \sqrt{aU} = 0.84 \sqrt{aU} \simeq 0.3 \sqrt{AU_{\text{MeV}}}$$

where we have used the empirical $a = A/8$.

It is, of course, clear that (5.30) is incorrect near U equal to zero, that is, when the excitation energy goes to zero, and is applicable only for sufficiently large values of U and N . A comparison of (5.30) with an exact calculation of the density of levels when the single-particle levels are equidistantly spaced is shown on Fig. 5.2. Except at small values of the excitation energy, the agreement is excellent.

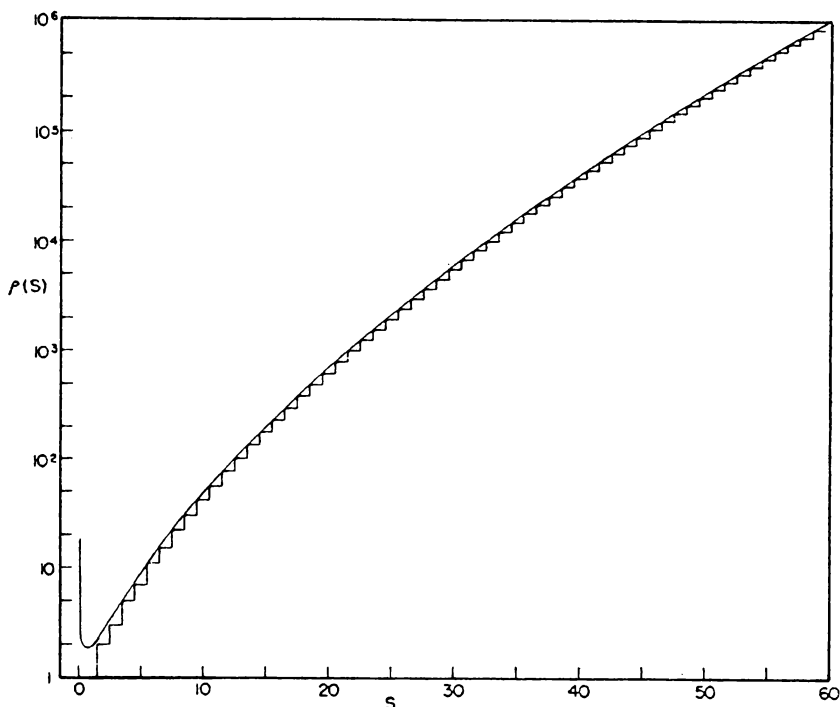


FIG. 5.2. Exact level density per unit single particle spacing for a Fermi system of one kind of particles with equidistant single-particle levels versus excitation energy s in units of this spacing. The solid smooth curve is the approximate solution, (5.30). [From Ericson (60).]

Fluctuations. If these results gave an exact evaluation of the expression (5.11) for $\omega(E, N)$ the value of $(\bar{N})^2$ and of \bar{N}^2 would be equal, where

$$\bar{N}\omega(E, N) = \sum_{j,v} v \delta(v - N) \delta(E - \varepsilon_j(v))$$

and

$$\bar{N}^2\omega(E, N) = \sum_{j,v} v^2 \delta(v - N) \delta(E - \varepsilon_j(v))$$

A measure of the accuracy of these calculations is then furnished by the fluctuation defined by

$$\left[\frac{\bar{N}^2 - \bar{N}^2}{(\bar{N})^2} \right]^{1/2} = \left[\frac{(N - \bar{N})^2}{\bar{N}^2} \right]^{1/2} \equiv \frac{\Delta N}{\bar{N}}$$

From (5.12) and (5.13) we see that

$$\bar{N} = \frac{\int d\beta_1 \int d\beta_2 [\partial Z(\beta_1, \beta_2) / \partial \beta_2] e^{\beta_1 E - \beta_2 N}}{\int d\beta_1 \int d\beta_2 Z(\beta_1, \beta_2) e^{\beta_1 E - \beta_2 N}}$$

Evaluating Z and $\partial Z / \partial \beta_2$ at the saddle point gives the result

$$\bar{N} \simeq \frac{\partial \ln Z(\beta_1, \beta_2)}{\partial \beta_2} \quad \text{at } \beta_1 = \beta_1^{(0)}, \beta_2 = \beta_2^{(0)}$$

in agreement with (5.16).

The value of \bar{N}^2 is similarly given by

$$\bar{N}^2 = \frac{\partial^2 Z(\beta_1, \beta_2) / \partial \beta_2^2}{Z(\beta_1, \beta_2)}$$

so that

$$\bar{N}^2 - \bar{N}^2 = \frac{\partial^2 \ln Z(\beta_1, \beta_2)}{\partial \beta_2^2}$$

The independent particle model [see below (5.29)] gives

$$\bar{N}^2 - \bar{N}^2 = (\Delta N)^2 = \frac{\omega(\varepsilon_F)}{\beta_1}$$

or using (5.29),

$$(\Delta N)^2 = \left[\frac{6U\omega(\varepsilon_F)}{\pi^2} \right]^{1/2}$$

Inserting the Fermi-gas model value for ω ,

$$\omega = \frac{3N}{2\varepsilon_F}$$

one obtains

$$(\Delta N)^2 = \left(\frac{9UN}{\pi^2 \varepsilon_F} \right)^{1/2}$$

Introducing u , the excitation energy per nucleon (and replacing $9/\pi^2$ by 1)

$$u = \frac{U}{N}$$

one finally obtains

$$\frac{\Delta N}{N} \simeq N^{-1/2} \left(\frac{u}{\varepsilon_F} \right)^{1/4}$$

indicating the error is least for heavier nuclei and smaller excitation energies. For a further discussion, see Feshbach (88).

B. Angular Momentum Distribution

The level density, $\omega(E, N)$, (5.30), derived just above, takes account of all states regardless of their angular momentum. Because of the important role played by angular momentum barriers as discussed briefly in Section 4, we shall find knowledge of the level density for levels with energy E and with angular momentum J , $\omega(E, N, J)$, essential for the interpretation of nuclear reactions.

In the procedure developed by Bloch (54), one adds to the constraints that the total number of particles be N and that the total energy be E , the constraint that the projection of the total angular momentum along an axis be M ; that is, in addition to the conditions given by (5.18) and (5.19), we add

$$M = \sum n_s m_s$$

The resulting level density is $\omega(E, N, M)$. The density we seek $\omega(E, N, J)$ is then given by

$$\begin{aligned} \omega(E, N, J) &= \omega(E, N, M = J) - \omega(E, N, M = J + 1) \\ &\simeq - \left(\frac{\partial \omega(E, N, M)}{\partial M} \right)_{M = J + 1/2} \end{aligned} \quad (5.33)$$

We begin by forming the partition function Z , which will now depend on

three parameters $\beta_1, \beta_2, \beta_3$:

$$Z(\beta_1, \beta_2, \beta_3) = \sum \exp(\beta_2 v + \beta_3 M_s(v) - \beta_1 \varepsilon_s(v))$$

Applying the method of steepest descents [see (5.12)] yields

$$\omega(E, N, M) = \frac{1}{(2\pi)^{3/2} |\det L|^{1/2}} Z(\beta_1^{(0)}, \beta_2^{(0)}, \beta_3^{(0)}) e^{\beta_1^{(0)} E - \beta_2^{(0)} N - \beta_3^{(0)} M} \quad (5.34)$$

where $\beta_i^{(0)}$, the saddle-point values of β_i , satisfy (5.15) through (5.17) and the additional equation

$$\frac{\partial \ln Z}{\partial \beta_3} = M \quad (5.35)$$

The generalization of (5.22) becomes

$$\ln Z = \sum_m \int \omega(\varepsilon, m) \ln(1 + e^{\beta_3 m + \beta_2 - \beta_1 \varepsilon}) d\varepsilon \quad (5.36)$$

where $\omega(\varepsilon, m)$ is the single-particle level density for particles of energy ε and projected angular momentum m . The evaluation of the integral in (5.36) proceeds according to method described above following (5.23). One obtains

$$\ln Z = \sum_m \left\{ (\beta_2 + \beta_3 m) N_m(\varepsilon_F(m)) - \beta_1 W_m(\varepsilon_F(m)) + \frac{\pi^2}{6} \frac{\omega(\varepsilon_F(m), m)}{\beta_1} \right\} \quad (5.37)$$

where

$$N_m(\varepsilon_F(m)) = \int_{\varepsilon_0}^{\varepsilon_F(m)} \omega(\varepsilon, m) d\varepsilon \quad (5.38a)$$

$$W_m(\varepsilon_F(m)) = \int_{\varepsilon_0}^{\varepsilon_F(m)} \varepsilon \omega(\varepsilon, m) d\varepsilon \quad (5.38b)$$

where the Fermi energy $\varepsilon_F(m)$ is defined by

$$\varepsilon_F(m) \equiv \frac{\beta_2 + \beta_3 m}{\beta_1} \quad (5.39)$$

We now define a Fermi energy independent of m , ε_F , by averaging $\varepsilon_F(m)$ over m :

$$\varepsilon_F \equiv \frac{\beta_2 + \beta_3 \bar{m}}{\beta_1} \quad (5.40)$$

where

$$\bar{m} = \frac{\sum m \omega(\varepsilon_F(m), m)}{\sum \omega(\varepsilon_F(m), m)}$$

or using

$$\omega(\varepsilon_F) = \sum_m \omega(\varepsilon_F(m), m) \quad (5.41)$$

$$\bar{m} = \frac{\sum m \omega(\varepsilon_F(m), m)}{\omega(\varepsilon_F)} \quad (5.42)$$

Similarly,

$$\overline{m^2} = \frac{\sum m^2 \omega(\varepsilon_F(m), m)}{\omega(\varepsilon_F)} \quad (5.43)$$

Finally, the functions N and W of the preceding section are given by

$$N(\varepsilon_F) = \sum_m N_m(\varepsilon_F) \quad (5.44)$$

and

$$W(\varepsilon_F) = \sum_m W_m(\varepsilon_F) \quad (5.45)$$

Inserting these relations into (5.37) yields

$$\ln Z = \beta_2 N(\varepsilon_F) + \beta_3 M(\varepsilon_F) - \beta_1 W(\varepsilon_F) + \frac{1}{2\beta_1} \omega(\varepsilon_F) \left[\frac{\pi^2}{3} + \beta_3^2 (\overline{m^2} - \bar{m}^2) \right] \quad (5.46)$$

where a Taylor expansion of $N_m(\varepsilon_F(m))$ to first order and $W_m(\varepsilon_F(m))$ to second order has been used:

$$N_m(\varepsilon_F(m)) = N_m \left(\frac{\beta_3 m + \beta_2}{\beta_1} \right) \simeq N_m(\varepsilon_F) + \frac{\beta_3}{\beta_1} (m - \bar{m}) \omega(\varepsilon_F(m), m)$$

Terms up to $\omega(\varepsilon_F(m), m)$, but not including its derivatives, have been taken into account.

Using the conditions (5.15), (5.16), and (5.35), one obtains

$$\begin{aligned} E &= W(\varepsilon_F) + \frac{\omega(\varepsilon_F)}{2\beta_1^2} \left[\frac{\pi^2}{3} + \beta_3^2 (\overline{m^2} - \bar{m}^2) \right] \\ N &= N(\varepsilon_F) \\ M &= M(\varepsilon_F) + \frac{\beta_3 \omega(\varepsilon_F)}{\beta_1} (\overline{m^2} - \bar{m}^2) \end{aligned} \quad (5.47)$$

The last equation can be solved for β_3 and the result introduced into (5.46) as follows:

$$\beta_3 = \frac{\beta_1 \Delta M}{\omega(\varepsilon_F)(\overline{m^2} - \bar{m}^2)}$$

$$\Delta M \equiv M - M(\varepsilon_F)$$

and

$$U = E - W(\varepsilon_F) = \frac{\pi^2}{6\beta_1^2} \omega(\varepsilon_F) + \frac{\frac{1}{2}(\Delta M)^2}{\mathcal{I}} \quad (5.48)$$

$$\mathcal{I} \equiv \omega(\varepsilon_F)(\overline{m^2} - \bar{m}^2) \quad (5.49)$$

The second term in (5.48) can be interpreted as the rotation kinetic energy of excitation, where \mathcal{I} is the moment of inertia about the axis upon which the angular momentum is projected, an identification that requires justification.

Problem. Prove that \mathcal{I} approximately equals the rigid moment of inertia for a spherical nucleus. Use

$$\omega(\varepsilon_F) = \frac{3}{2} \frac{A}{\varepsilon_F} \quad (5.50)$$

and

$$\overline{m^2} \simeq \overline{(xp_y - yp_x)^2}$$

It is now a straightforward calculation to obtain the level density by using the results above in (5.34). We find that

$$\omega(E, N, M) = \frac{1}{(2\pi)^{3/2} [(\pi^2/3)(\omega(\varepsilon_F)/\beta_1^2)(\mathcal{I}/\beta_1)]^{1/2}} \exp \left[\frac{\pi^2}{3} \frac{\omega(\varepsilon_F)}{\beta_1} \right] \quad (5.51)$$

Inserting the value of β_1 from (5.48) and differentiating the result according to (5.33) to obtain $\omega(E, N, J)$, one obtains

$$\omega(U, N, J) = \frac{2J+1}{2} \frac{\omega(U - \mathcal{R}, N)}{[2\pi\mathcal{I}^3((6/\pi^2)\omega(\varepsilon_F))(U - \mathcal{R})^{3/2}]^{1/2}} \quad (5.52)$$

where again the independent variable E has been replaced by U . In this equation, $\omega(U, N)$ is given by (5.30), and

$$\mathcal{R} = \frac{(J + \frac{1}{2})^2}{2\mathcal{I}} \quad (5.53)$$

is the rotational energy. In obtaining (5.52), $M(\epsilon_F)$ has been placed equal to zero, as would be the case when the ground-state spin is zero. Note again that this expression fails when U equals \mathcal{R} , that is, on the Yrast line.[†]

When \mathcal{R} is small compared to U , that is, away from the Yrast line, we can expand (5.52) about $\mathcal{R} = 0$ to obtain

$$\omega(U, N, J) = \frac{2J+1}{\sqrt{8\pi\sigma^3}} \omega(U, N) e^{-[J+(1/2)]^2/2\sigma^2} \quad (5.54)$$

where [see below (5.32)]

$$\sigma^2 \equiv \mathcal{J} \left(\frac{6U}{\pi^2 \omega(\epsilon_F)} \right)^{1/2} = \mathcal{J} \left(\frac{U}{a} \right)^{1/2} \quad (5.55)$$

Problem. Prove that

$$\sum_J (2J+1) \omega(E, N, J) \rightarrow \int_0^\infty dJ (2J+1) \omega(U, N, J) = \omega(U, N)$$

Problem. Show from (5.51) that

$$\omega(U, N, M) = \frac{1}{\sqrt{2\pi}} \frac{\omega(U - \frac{1}{2}(\Delta M^2/\mathcal{J}), N)}{[\mathcal{J}((6/\pi^2)\omega(\epsilon_F))(U - \frac{1}{2}(\Delta M^2/\mathcal{J}))^{1/2}]^{1/2}}$$

In the limit of $\frac{1}{2}(\Delta M)^2/\mathcal{J} \ll U$,

$$\omega(U, N, M) = \frac{1}{\sqrt{2\pi\sigma}} \omega(U, N) e^{-(\Delta M)^2/2\sigma^2} \quad (5.54')$$

Thus in this approximation the angular momentum distribution is a Gaussian with a root-mean-square derivation, σ , given by (5.55), which increases with increasing excitation energy. One can expect [see (3.4)] that the absorption cross section will decrease when J exceeds σ . This is simply the statement that it will be much less probable for the angular momenta of the individual nucleons to line up to obtain a given J as J increases. However, the probability improves if the excitation energy increases since a greater variation in the values of the angular momenta for the individual nucleons occurs.

[†]The Yrast line is defined as the curve in the (U, J) plane giving the lowest possible value of J for a given value of U .

C. Rotational Nuclei

In addition to the total angular momentum I , the state of rotational nuclei are characterized by the quantum number K [see (VI.3.30) in deShalit and Feshbach (74)], the projection of I on the body-fixed axis of symmetry, assuming axially symmetric nuclear deformation. We can now ask for the density of levels with a given I and K .

Since K is a projection, approximation (5.54) can be used:

$$\omega(U, N, K) = \frac{1}{\sigma_K \sqrt{2\pi}} \omega(U, N) \exp\left(-\frac{K^2}{2\sigma_K^2}\right) \quad (5.56)$$

where σ_K is given by (5.55), employing for \mathcal{J} the moment of inertia about the symmetry axis. The density of levels for a given value of I is then obtained by summing:

$$\omega(U, N, I) = \frac{1}{2} \sum_{K=-I}^I \omega(U - \mathcal{R}(K, I), N, K) \quad (5.57)$$

where \mathcal{R} is the rotational energy associated with rotation about the axes perpendicular to the symmetry axis [see (VI.2.12) in deShalit and Feshbach (74)]:

$$\mathcal{R} = \frac{1}{2\mathcal{J}_\perp} [(I)(I+1) - K^2]$$

and \mathcal{J}_\perp is the appropriate moment of inertia. The factor of $\frac{1}{2}$ takes into account the fact that the sum includes both K and $-K$. Inserting this value for \mathcal{R} and using the approximation $\mathcal{R} \ll U$ yields

$$\omega(U, N, I) = \frac{1}{\sqrt{8K\sigma_K}} \omega(U, N) \sum_{K=-I}^I e^{-(1/2\sigma_K^2)(I)(I+1) - (1/2)(1/\sigma_K^2 - 1/\sigma_\perp^2)K^2} \quad (5.58)$$

where σ_\perp^2 is given by (5.55) with \mathcal{J} replaced by \mathcal{J}_\perp . The factor multiplying K^2 in the exponent depends on the difference $(1/\mathcal{J}_K - 1/\mathcal{J}_\perp)$. In a rigid body in the shape of a prolate spheroid,

$$\mathcal{J}_K = \mathcal{J}_{\text{sph}}(1 - \frac{2}{3}\delta) \quad \mathcal{J}_\perp = \mathcal{J}_{\text{sph}}(1 + \frac{1}{3}\delta) \quad (5.59)$$

where δ is the eccentricity parameter [see deShalit and Feshbach (74, p. 416)] and \mathcal{J}_{sph} is the moment of inertia of a rigid sphere of radius R_0 where R_0 is the mean radius [see deShalit and Feshbach (74, p. 415)]. Then

$$\frac{1}{\mathcal{J}_K} - \frac{1}{\mathcal{J}_\perp} = \frac{1}{\mathcal{J}_{\text{sph}}} \frac{\delta}{(1 - \frac{2}{3}\delta)(1 + \frac{1}{3}\delta)}$$

A contribution to the energy of rotation coming from rotation about the symmetry axis is possible only at excitations sufficiently great that pairing effects are reduced. Under these circumstances, the superfluidity [see deShalit and Feshbach (74, p. 568)] thought to be responsible for condition equation (VI.4.1) in deShalit and Feshbach will be correspondingly less and this moment of inertia, \mathcal{J}_K , will approach the rigid value, (5.59). More explicitly, if the average number of unpaired particles is ν and the average value of K^2 for one particle is K_1^2 , then

$$\sigma_K^2 = \nu K_1^2 = \mathcal{J}_K \left[\frac{6U}{\pi^2 \omega(\epsilon_F)} \right]^{1/2}$$

At low energies the number of unpaired particles goes rapidly to zero, so that \mathcal{J}_K is reduced from its rigid value, which applies at sufficiently large excitation energies.

The angular distribution of fission fragments depends on the K dependence of $\omega(U, N, I)$, permitting a determination of \mathcal{J}_K from experiment. [See Reising, Bate, and Huizenga (66) and Bohr and Mottelson (75, p. 619); see also Huizenga, Behkamu, et al. (74) and Døssing and Jensen (74).]

D. Isospin Distribution

The results obtained for the angular momentum distribution, in particular (5.54'), can be quickly adapted to this problem. The level density $\omega(U, N, T_3)$, giving the density of levels at an excitation energy U , number of particles N , and isospin component T_3 [$\equiv \frac{1}{2}(Z - N)$], is

$$\omega(U, N, T_3) = \frac{1}{\sigma_\tau \sqrt{2\pi}} \omega(U, N) \exp\left(-\frac{T_3^2}{2\sigma_\tau^2}\right) \quad (5.60)$$

where

$$\sigma_\tau^2 = (\overline{m_\tau^2} - \bar{m}_\tau^2) \left[\frac{6\omega(\epsilon_F)U}{\pi^2} \right]^{1/2}$$

Of course, $\bar{m}_\tau^2 = \frac{1}{4}$. Near the Fermi energy,

$$\bar{m}_\tau = \frac{1}{2} \frac{\omega_P(\epsilon_F) - \omega_N(\epsilon_F)}{\omega_P(\epsilon_F) + \omega_N(\epsilon_F)}$$

where ω_P and ω_N are the single-particle level density for protons and neutrons, respectively. Hence

$$\sigma_\tau^2 = \left[\frac{6\omega(\epsilon_F)U}{\pi^2} \right]^{1/2} \frac{\omega_N(\epsilon_F)\omega_P(\epsilon_F)}{[\omega_N(\epsilon_F) + \omega_P(\epsilon_F)]^2} \quad (5.61)$$

where

$$\omega(\varepsilon_F) = \omega_N(\varepsilon_F) + \omega_P(\varepsilon_F)$$

Equation (5.60) becomes

$$\begin{aligned} \omega(U, N, T_3) = & \frac{6^{1/4}}{12} \omega(\varepsilon_F) \left[\frac{\omega^2(\varepsilon_F)}{\omega_N(\varepsilon_F) \omega_P(\varepsilon_F)} \right]^{1/2} [\omega(\varepsilon_F) U]^{-5/4} \\ & \times \exp \left[2 \sqrt{\frac{\pi^2}{6} \omega(\varepsilon_F) U - \frac{T_3^2}{2\sigma_\tau^2}} \right] \end{aligned} \quad (5.60')$$

All the considerations above are based on the independent particle model of the model; that is, the Hamiltonian is assumed to be given by

$$H = \sum_s a_s^\dagger a_s \varepsilon_s \quad (5.62)$$

where a_s^\dagger and a_s are the Fermion creation and destruction operators associated with a single-particle level of energy ε_s . In addition, it is assumed that single-particle level density is a smooth function of the single-particle energy. Under these circumstances the level density for the nucleus depends primarily on $\omega(\varepsilon_F)$, the single-particle density evaluated at the Fermi energy.[†]

Improvements can be obtained by using a more realistic nuclear Hamiltonian and single-particle level density. For example, the single-particle levels of the independent particle shell model are bunched and the possibility of degeneracy is substantially different when a shell is, for example, half filled than when it is completely filled. The assumption of a smooth single particle density is not a good approximation under these conditions. Rosenzweig (57) has, for example, calculated the nuclear level density using a simple model that exhibits both the bunching and variation of degeneracy, characteristic of the shell model. In another, obvious improvement the interactions are taken into account. For example, Hartree–Fock single-particle levels can be inserted in (5.62). Proceeding further, the quasi-particle description of Chapter VII of deShalit and Feshbach (74), which should be especially advantageous in view of the strong dependence of $\omega(U)$ on $\omega(\varepsilon_F)$, can be used. H will now include both the single-particle energies and the pairing Hamiltonian [Moretto (72a, 72b)]. Finally, more sophisticated methods based on the Goldstone linked cluster expansion [Section VII.14 in deShalit and Feshbach (74)] could in principle be adapted for the calculation of nuclear level densities.

[†]The saddle-point evaluation of the density of levels is an approximation to the exact density. The latter can be obtained for noninteracting nucleons by using the combinatorial method. This method amounts to finding the number of ways in which the nucleons can be distributed among the single-particle levels for a given energy of the nucleus. A systematic approach to this enumeration has been given by Hillman and Grover (69).

The results of these calculations are not readily summarized by an analytical expression. However, some features that can be readily understood qualitatively emerge. These have formed the basis of a semiempirical description of the nuclear level density.

The major effects of the residual interaction on the nuclear levels of the independent particle shell model include the lifting of degeneracies of that model and the motion of the energy levels to different values of the energy. Of particular importance for our discussion is the substantial descent of some levels, these thereby becoming either the ground state or lying much closer to the ground state. On the other hand, at relatively high excitation energies the motion of the levels does not result in any substantial change in the level density from that predicted by the independent particle model. The two spectra before and after the residual interaction is “turned on” are illustrated in Fig. 5.3. It is clear from the figure that one can use the independent particle model result for $\omega(U)$ for the spectrum of Fig. 5.3b for sufficiently large U if U is replaced by $U - \Delta$. In other words, one shifts the ground-state energy from which U is calculated to the value it has before the residual interaction is turned on. This is, of course, not an exact statement, since the differences in the spectra can hardly be expressed by means of only one parameter. However, by choosing an empirical value for Δ , one might expect to be able to match the spectrum of (b) at sufficiently large U . If $\omega_0(U)$ is the level density for the independent particle model, then for sufficiently large U , $\omega_0(U - \Delta)$ is the level density when interactions are taken into account.

This concept of a reference level, differing from the ground state, for the calculation of the effective excitation energy [Hurwitz and Bethe (51)] has been incorporated into (5.52) with Δ as well as a and σ as empirical parameters to be determined from experiment [Huizenga (72)]. The effect of pairing energy on level density can be included in this way. Recall from (II.3.1) in deShalit and Feshbach (74) that the pairing energy is taken to be zero for odd–even nuclei and is given by a positive function of Δ , $\delta(A)$, for odd–odd nuclei and by $-\delta(A)$ for even–even nuclei. Taking the same reference level, that is, the odd–even nucleus, Δ is given by $-\delta(A)$ for odd–odd nuclei and by $\delta(A)$ for even–even nuclei [Ericson (59)].

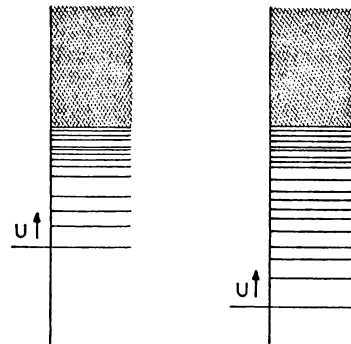


FIG. 5.3. Effect of the residual interactions on the distribution of the nuclear energy levels.

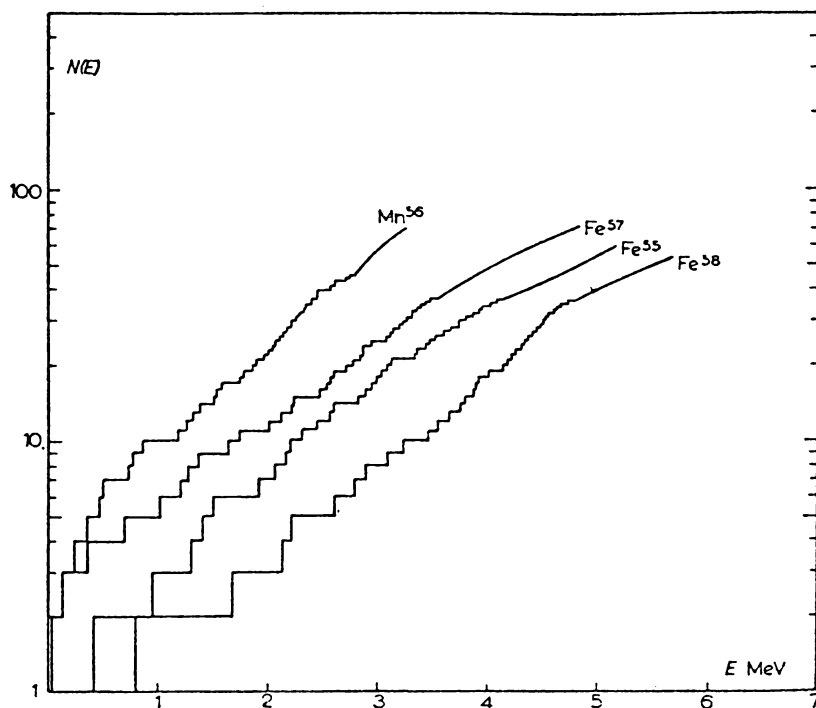


FIG. 5.4. Total number of states up to the excitation energy E for Mn^{56} , Fe^{55} , Fe^{57} , and Fe^{58} versus E . The resolution is somewhat higher in the case of Mn^{56} than for the rest. The figure compares the total numbers of states for even, odd, and odd-mass nuclei. [From Ericson (59).]

The odd-even effect is illustrated in Fig. 5.4, which gives the total number of states up to an excitation energy U for four nuclei: ^{56}Mn (odd, odd), ^{57}Fe (even, odd), ^{55}Fe (even, odd), and ^{58}Fe (even, even). As expected, the odd-odd nucleus has the greatest number of states, the even-even the fewest, while the even-odd nuclei fall in between. The shell model provides a reason that the number of states of ^{57}Fe is greater than that for ^{55}Fe for a given excitation energy; namely, ^{55}Fe has only one neutron outside the closed neutron shell at $N = 28$, while ^{57}Fe has three such neutrons. There is, therefore, a larger number of states that can be formed in ^{57}Fe than in ^{55}Fe .

More quantitatively, one might hope to use the experimental determinations of the level density to obtain the parameters a , σ , and Δ . The systematics of their dependence upon excitation energy, and the mass, Δ , and atomic number, Z , of the nucleus might then provide insights into the properties of excited nuclei. For the most part such systematic studies have not been carried out. Unfortunately, it is often the case that different expressions are used for ω so that the values of a and σ obtained are not immediately comparable.

A compilation [Facchini and Saetta-Memchella (68); Baba (70)] of the values

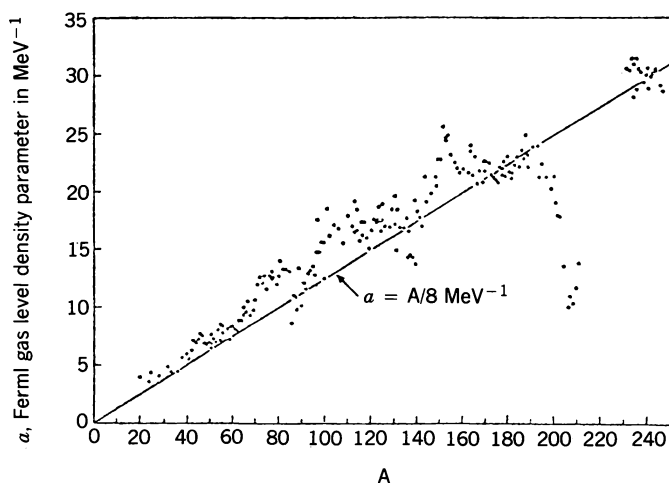


FIG. 5.5. Level density parameter a as a function of atomic mass A [Baba (70)]. [From Huizenga and Moretto (72).]

for a are shown in Fig. 5.5. To obtain these, σ , the spin-cut off parameter, was calculated from (5.55) using the rigid moments of inertia, and Δ was taken to be equal to the pairing energy values given by Gilbert and Cameron (65). We observe that these values of a are marked by substantial deviations from the expected linear dependence on A , (5.50), deviations that are especially large for nuclei near the closed shells. This can be related to the fact that the density of single-particle levels near the Fermi energy is markedly smaller for closed-shell nuclei. The correctness of this analysis is indicated by theoretical level density calculations using the single-particle levels provided by the Nilsson model [see Chapter VI in deShalit and Feshbach (74)] for nuclei close to the doubly magic nucleus ^{208}Pb . The results are shown in Fig. 5.6. As expected, ^{208}Pb has the smallest level density. The level densities for neighboring nuclei increase with increasing distance of the nuclei from ^{208}Pb .

The values of σ that are extracted from those experiments, particularly those sensitive to the value of the maximum angular momentum which can contribute to the reaction cross section, are shown in Fig. 5.7. The excitation energy, U , is approximately 8 MeV. The solid line that gives the value of σ computed using the rigid moment of inertia [Chang (70); Coceva, Corvi, Giacobbe, and Stefansson (72)] is in substantial agreement with the experimental results for $A \leq 110$. It is not possible to draw any conclusions for larger values of A in view of the little information available.

Theoretical values of the spin cutoff parameter, σ , have also been obtained using the Nilsson model. The results are shown in Fig. 5.8. The nuclei involved do not overlap with those experimentally observed in Fig. 5.7, but the comparison would suggest that the theoretical values will be too large.

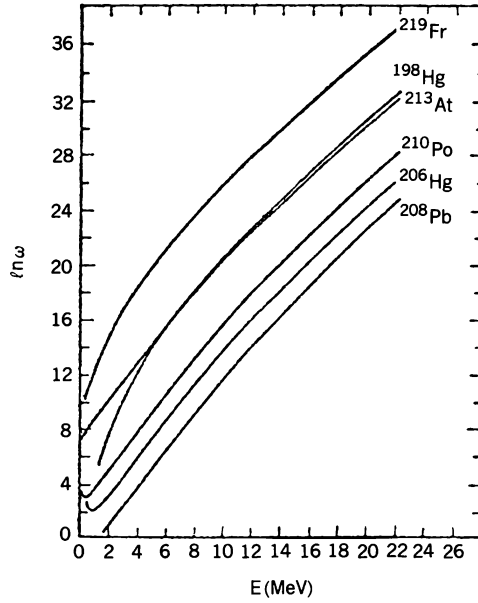


FIG. 5.6. Theoretical level densities as a function of excitation energy for nuclei in the neighborhood of the ^{295}Pb doubly closed shell. The Nilsson shell model has been used to obtain the spherical set of single particle levels [Moretto, Stella, and Carmella-Crespi (70).] [From Huizenga and Moretto (72).]

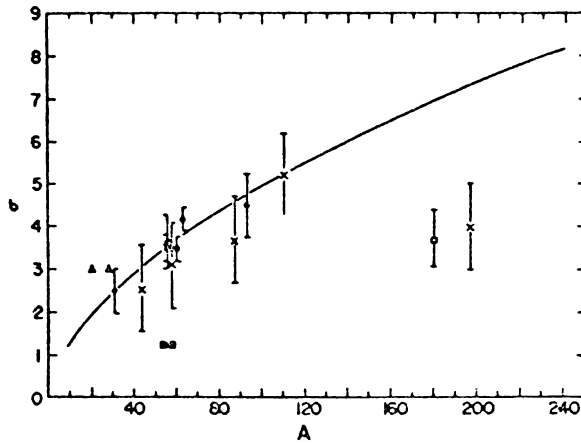


FIG. 5.7. Computation of values of σ . [From Huizenga (72).]

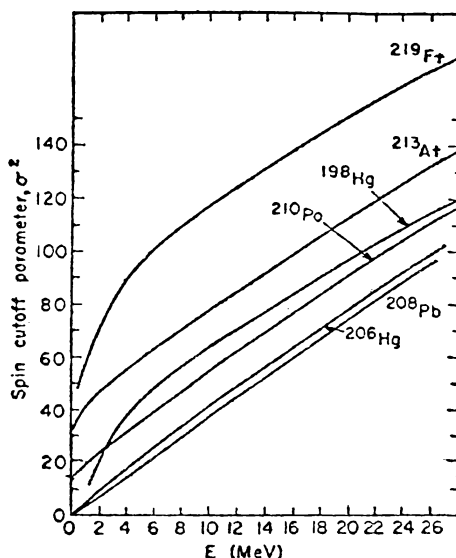


FIG. 5.8. Theoretical spin cutoff parameters σ^2 as a function of excitation energy for nuclei in the ^{205}Pb region. The calculations have been performed on the basis of the Nilsson diagram [Moretto, Stella, and Caramella-Crespi (70).] [From Huizenga and Moretto (72).]

The experimental results that form the basis of the foregoing comparisons with the theory are obtained from a variety of sources. The most obvious involves simply counting of the levels, which is possible only if they are isolated, as can be the case for low-energy neutron resonances. However, this procedure rapidly becomes impossible as the excitation energy increases. The primary method then exploits the dependence of reaction cross sections, total as well as differential, on the nuclear level density, as will be made evident in later sections of this chapter (see Section 7). For the present we illustrate the results that can be obtained by Fig. 5.9 for the case of ^{60}Ni .

French and his collaborators have developed a statistical method for determining the nuclear level density which is appropriate for the interacting shell model. In this model the wave functions for the system are assumed to be expressible in terms of the shell model single-particle wave functions. Moreover, a finite number of shells are assumed to be mixed by the residual interaction forming the shell model space. Thus the effective Hamiltonian is given by the finite matrix $\langle \Phi_j | H | \Phi_i \rangle$, in that shell model space where the set $\{\Phi_i\}$ are the independent-particle (i.e., noninteracting shell model), wave functions. The theory attempts to compensate for the effect of omission of the states outside the model space by using an adjusted ("renormalized") residual interaction. This procedure is in obvious difficulty when the actual interaction brings down into the energy domain of interest, states that have appreciable components not

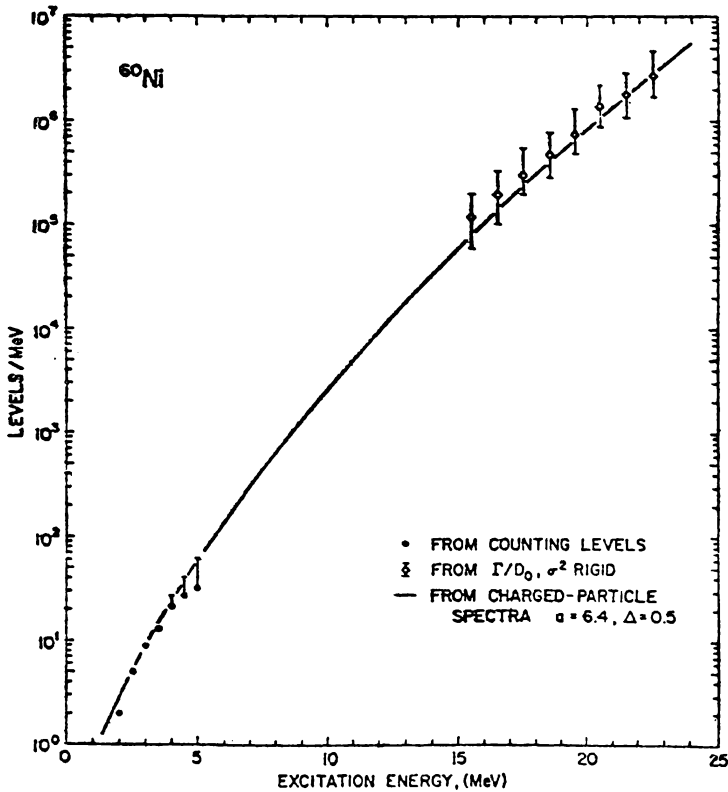


FIG. 5.9. Plot of the experimental level density of ^{60}Ni as a function of excitation energy [Lu, Vag, and Huizenga (72).] [From Huizenga and Moretto (72).]

included in the model space. These are referred to as *intruder* states. It should also be noted that even when the unrenormalized residual interaction is two-body, the renormalized interaction will generally contain many-body interactions as components. The energies of the system are given by the eigenvalues of the Hamiltonian $\langle \Phi_j | H | \Phi_i \rangle$. Generally, the diagonalization of such a matrix is a formidable numerical task. For instance, the $J = 3$, $T = 1$ matrix in the shell with 12 particles has the dimension of 6706, so that there are 2.25×10^6 different matrix elements and 6706 eigenvalues. If, however, the residual interaction is two-body, as is usually assumed [see Chapter V in deShalit and Feshbach (74)], the number of independent matrix elements is only 63. The two-body assumption is not generally correct, as the omission of states outside the model space rigorously requires the introduction of many-body forces, so that the number of independent matrix elements will be larger than 63. There is an upper bound to this number when the number of active particles is m , since then the many-body force is at most an m -body force.

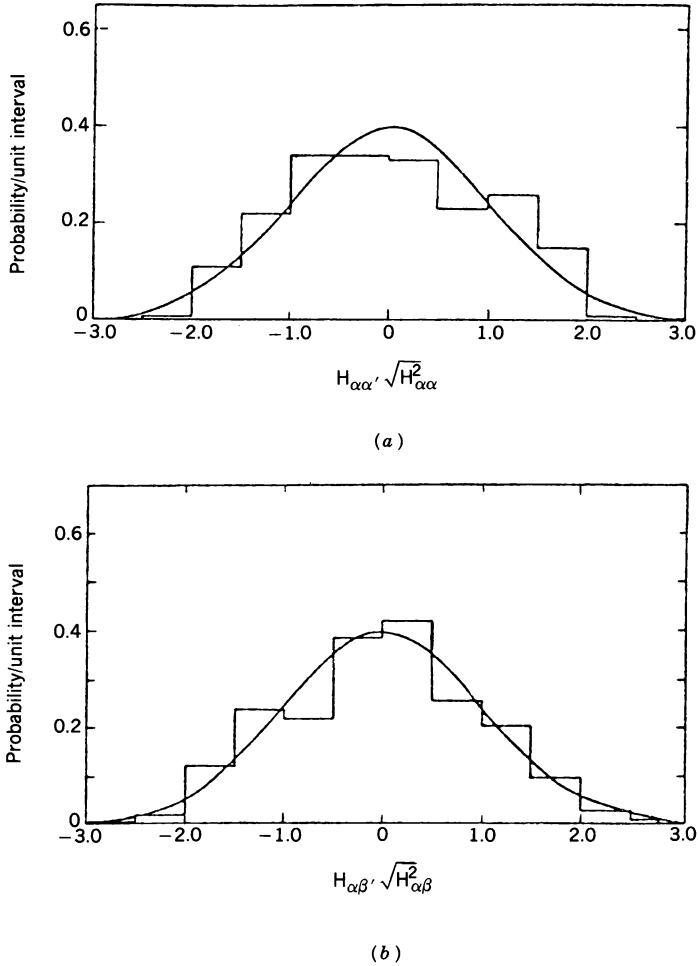


FIG. 5.10. (a) Plot of the distribution of 196 diagonal nuclear shell model matrix elements from the work of D. Kurath. The solid curve is a simple normal distribution $(2\pi)^{-1/2} \exp(-H_{\alpha\alpha}^2/2\overline{H_{\alpha\alpha}^2})$ in which $H_{\alpha\alpha}$ is the diagonal element minus the mean diagonal element for each matrix. (b) Plot of the distribution of 675 off-diagonal matrix elements obtained in the work of D. Kurath. The solid curve is a simple normal distribution $(2\pi)^{-1/2} \exp(-H_{\alpha\beta}^2/2\overline{H_{\alpha\beta}^2})$ in which $H_{\alpha\beta}$ is the off-diagonal element; the mean value of the off-diagonal elements is very close to zero. [From Porter and Rosenzweig (60).]

The statistical method adopted by French and Wong (70) and Bohigas and Flores (71) makes use of the empirical result (see Fig. 5.10) that the matrix elements of a short-range residual interaction are random. By this we mean that the distribution of values of the matrix elements when the excitation energy or the mass number of the nucleus is varied is Gaussian. A justification of this

result is indicated by the following plausible but hardly rigorous argument. In terms of $\phi_n(\mathbf{r})$, the single-particle shell model wave function, the matrix element of a two-body potential $v(\mathbf{r}, \mathbf{r}')$ is

$$\langle \phi_k \phi_l | v \phi_m \phi_n \rangle = \int \phi_k^*(\mathbf{r}) \phi_l^*(\mathbf{r}') v(\mathbf{r}, \mathbf{r}') \phi_m(\mathbf{r}) \phi_n(\mathbf{r}') d\mathbf{r} d\mathbf{r}' \quad (5.63)$$

For large quantum numbers (i.e., for reasonably high excitation energies) the ϕ_n 's will have a large number of nodes. The overlap of these wave functions as they occur in (5.63) will generally yield a very irregular and complex dependence on \mathbf{r} and \mathbf{r}' . Since v is short range, the matrix element of (5.63) is a sum of contributions that come from the regions in which the overlap is constructive. To the extent that these contributions are effectively random, the central limit theorem may be applied and the distribution of the matrix elements is Gaussian.

This empirical result suggests the following procedure. One can construct an ensemble of possible Hamiltonians with model shell space by choosing each of the independent matrix elements randomly (i.e., from a Gaussian distribution), and then solving the resulting secular equation for the energy eigenvalues of the system. By this means it would then be possible to develop an energy eigenvalue distribution. The fundamental assumption is then made that this distribution is identical with that which would be obtained from the energies of the levels in a given nucleus or from a variety of nuclei. This hypothesis is referred to as the ergodic hypothesis and is reminiscent of the hypothesis made in statistical mechanics, in which the time behavior of a system is related statistically to the properties of an ensemble of trajectories generated by random initial conditions.

An important simplification in the calculation of the distribution of energies can be obtained if one assumes that the distribution is Gaussian.

$$\omega(E) = \frac{1}{\sqrt{2\pi\lambda^2}} \exp\left[-\frac{(E - \varepsilon)^2}{2\lambda^2}\right] \quad (5.64)$$

where the average energy \bar{E} is given by ε and the mean-square deviation $\overline{E^2} - \bar{E}^2$ by λ^2 . The validity of (5.64) has been shown by numerical calculations as well as through an application of the central limit theorem [Mello (78)] when the number of particles is larger than two, when the interaction is two-body, or larger than k , when the interaction is k -body.

It is thus no longer necessary to diagonalize the Hamiltonian. One need only compute the mean energy and the dispersion using the expressions

$$\varepsilon = \frac{1}{d} \sum_i \langle \Phi_i | H \Phi_i \rangle$$

and

$$\lambda^2 = \frac{1}{d} \sum_i \langle \Phi_i | (\varepsilon - H)^2 \Phi_i \rangle = \frac{1}{d} \sum_i \langle \Phi_i | H^2 \Phi_i \rangle - \varepsilon^2 \quad (5.65)$$

or

$$\lambda^2 = \frac{1}{d} \sum_{i,j} |\langle \Phi_i | H \Phi_j \rangle|^2 - \varepsilon^2 \quad (5.66)$$

In these expressions d is the dimension of the space, while the matrix elements are linear combinations of randomly chosen quantities. Such a procedure was used by Ayik and Ginocchio (74) to compute the level densities for light nuclei. The orbital single-particle, wave functions of the $2s$, $1d$, and $f_{7/2}$ shell were used.

Some comment should be made with regard to the Gaussian form, (5.64). It differs sharply from the expression (5.30) obtained earlier, which showed an ever-increasing density of levels. The reduction in the level density at large E is a consequence of the use of a finite shell model space and is simply an expression of the fact that the energy eigenvalues in such a space will be bounded from above. The Gaussian, 5.64, is therefore meaningful only in the low-energy region, $E < \varepsilon$. The resulting form in this domain is not identical with (5.30). However, Ayik and Ginocchio's calculations take interactions and shell model effects into account.

6. SPACING OF ENERGY LEVELS; WIDTH DISTRIBUTIONS[†]

The preceding discussion provides an overall broad view of the distribution of nuclear energy levels. We turn next to the description of local properties of the energy spectrum as posed by the question: What is the probability that the separation between two neighboring energy levels is s ? Further specifications would include the probability that two levels are separated by an interval s containing n levels. We shall consider only the simplest case, $n = 0$.

Let $\omega(s)ds$ be the probability of finding a level at a distance between s and $s + ds$ from a given level. The probability we seek is given by $\omega(s)$ multiplied by the probability that there is no level in the interval s . This last factor can be calculated as follows. Divide the interval between 0 and s into elements of size Δs_n . The probability that there is no level in the interval Δs_n is given by $1 - \omega(s_n)\Delta s_n$. The the probability of finding no level in the interval 0 to s is given by

$$\begin{aligned} \prod_n [1 - \omega(s_n)\Delta s_n] &= \exp \sum_n \log(1 - \omega(s_n)\Delta s_n) = \exp[-\sum \omega(s_n)\Delta s_n] \\ &\rightarrow \exp \left[- \int_0^s \omega(s) ds \right] \end{aligned}$$

[†]Brody, Flores et al. (81); Porter (65); Bohigas and Weidenmüller (88), Bloch (68).

Finally, the probability $p(s)ds$ of finding a level between s and $s + ds$ from a given level with no level in between is

$$p(s) = C\omega(s) \exp \left[- \int_0^s \omega(s) ds \right] \quad (6.1)$$

where C is a normalizing constant. If $\omega(s)$ is a constant, one obtains the Poisson distribution

$$p(s) = \frac{1}{D} e^{-s/D}, \quad \frac{\int_0^\infty p(s)s ds}{\int_0^\infty p(s) ds} = D \quad (6.2)$$

where D is the average spacing.

However, as we show shortly, levels with the *same quantum numbers* do not cross (for nonsingular perturbations); that is, as the residual interaction is changed, two levels may approach each other but will eventually repel each other. Under these circumstances one might use, as suggested by Wigner, $\omega(s) \sim s$, so that

$$p(s) = \frac{\pi}{2} \frac{s}{D^2} e^{-(\pi/4)(s/D)^2} \quad (6.3)$$

the Wigner distribution law for spacings. Note that the probability for small spacings is substantially smaller for this distribution compared with the Poisson.

The agreement of the Wigner distribution with experiment as shown in Fig. 6.1 is remarkable in view of the simplicity of the argument. The reduction for small s is clearly seen.[†] Interestingly the Wigner distribution also gives a good fit to the spacing between the two lowest levels in nuclear having the same J and π as shown in Fig. 6.2.

To obtain additional insight into the spacing distribution has required the introduction of a model. We shall briefly[§] mention two statistical models, the Gaussian orthogonal ensemble (GOE) and the two body random Hamiltonian ensemble (TBRE), described at the end of Section 5. The former, although it is not realistic, as it assumes many-body forces equal in rank to the number of particles making up the system, has the advantage of being analytically tractable. For the most part, the properties of the TBRE require numerical determination. This model is also not completely realistic because it restricts the interaction to two-body forces, an assumption that is not correct because of its use of a finite-dimensional shell model space.

[†]One should note that the Wigner distribution is found to be valid for atomic spectra [Porter and Rosenzweig (60)] as well as for the spacing of the first two levels with the same J and Π in each nucleus.

[§]The reader should be aware of the "unitary ensemble" introduced by Dyson (62).

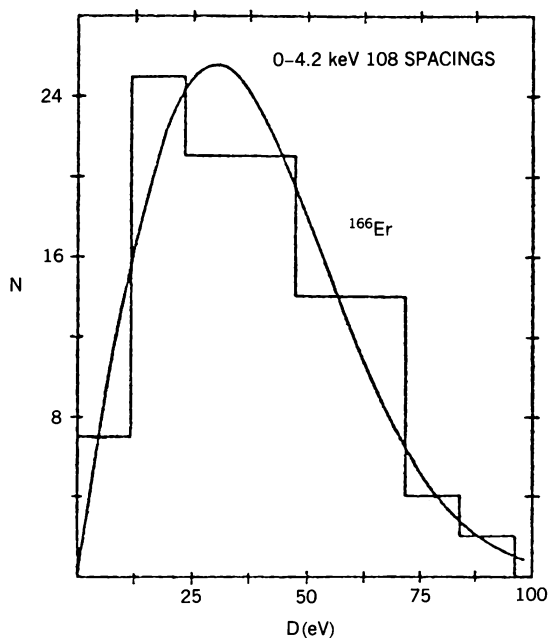


FIG. 6.1. Histogram for nearest-neighbor spacings for ^{166}Er , compared with Wigner's surmise [Liou, Camarda, et al. (72).] [From Mello (78).]

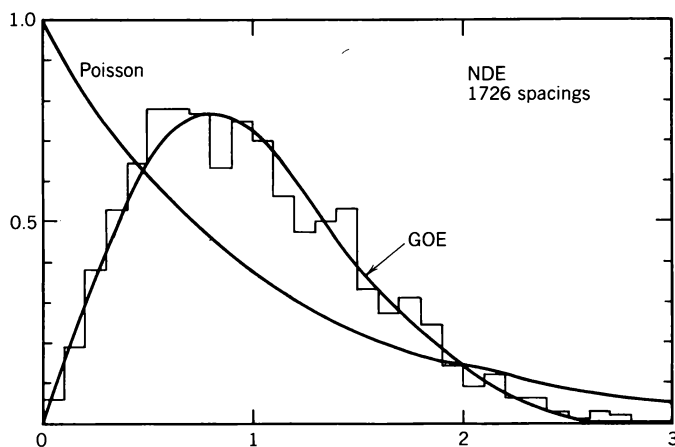


FIG. 6.2. Histogram for the nearest neighbor spacing distribution for the nuclear data ensemble plotted versus the level spacing in units of its mean volume [Bohigas, Hag and Pandey (83)]. [From Bohigas and Weidenmüller (88).]

The GOE assumes that the distributions of the individual matrix elements of the Hamiltonian are independent. This is unphysical because for residual two-body (or at most, few-body) forces usually envisaged the matrix elements are strongly correlated. The second assumption is that the joint distribution of all the matrix elements are invariant under a change of representation. This assumption is not justifiable even if the representations involved are complete. There may be, indeed are expected to be, representations which because of dynamical reasons are more appropriate for the application of the statistical hypothesis; that is, the representations conform more closely to the physics of the system under study.

With this “caveat emptor” in mind, consider a two-dimensional infinitesimal rotation which transforms only the eigenfunctions Φ_1 and Φ_2 , that is,

$$\Phi'_1 = \Phi_1 + \varepsilon \Phi_2$$

$$\Phi'_2 = \Phi_2 - \varepsilon \Phi_1$$

assuming that H is Hermitian and that Φ_1 and Φ_2 are real, the matrix elements of H transform as follows:

$$H'_{11} = \langle \Phi'_1 | H \Phi'_1 \rangle = H_{11} + 2\varepsilon H_{12}$$

$$H'_{22} = \langle \Phi'_2 | H \Phi'_2 \rangle = H_{22} - 2\varepsilon H_{12}$$

$$H'_{12} = H_{12} + \varepsilon(H_{22} - H_{11})$$

$$\left. \begin{aligned} H'_{1\mu} &= H_{1\mu} + \varepsilon H_{2\mu} \\ H'_{2\mu} &= H_{2\mu} - \varepsilon H_{1\mu} \end{aligned} \right\} \quad \mu > 2$$

The distribution function $P(H_{11}, H_{12}, H_{22}, H_{1\mu}, H_{2\mu}, \dots)$ transforms as follows:

$$\begin{aligned} \frac{\partial P}{\partial \varepsilon} &= 2H_{12} \frac{\partial P}{\partial H_{11}} + (H_{22} - H_{11}) \frac{\partial P}{\partial H_{12}} - 2H_{12} \frac{\partial P}{\partial H_{22}} \\ &+ \sum_{\mu > 2} \left(H_{2\mu} \frac{\partial P}{\partial H_{1\mu}} - H_{1\mu} \frac{\partial P}{\partial H_{2\mu}} \right) \end{aligned}$$

The invariance condition requires that $\partial P / \partial \varepsilon = 0$, which will be the case if

$$\frac{\partial P}{\partial H_{11}} = -\alpha H_{11} P \quad \frac{\partial P}{\partial H_{12}} = -2\alpha H_{12} P \quad \frac{\partial P}{\partial H_{22}} = -\alpha H_{22} P \quad (6.4)$$

$$\frac{\partial P}{\partial H_{1\mu}} = -2\alpha H_{1\mu} P \quad \frac{\partial P}{\partial H_{2\mu}} = -2\alpha H_{2\mu} P \quad (6.5)$$

It is left as an exercise for the reader to prove by extensions of the argument

leading to (6.4) that the constant α in (6.5) is identical with the α in (6.4). Integrating (6.4) yields

$$P = Ce^{-\alpha \sum_{i,j} H^2_{ij}} = Ce^{-\alpha \text{tr} H^2} \quad (6.6)$$

where C is a normalization constant. The invariance condition is thus extremely restrictive. Note that the distribution function for the diagonal elements, $\exp(-\alpha H^2_{ii})$, has a wider spread than that for the nondiagonal elements, $\exp(-2\alpha H^2_{ij})$. The fact that P can be expressed as a trace demonstrates explicitly the independence of P with regard to representation.

As an example of the application of this result for P , we use it to calculate the spacing distribution for the case of a two-dimensional space involving therefore only H_{11} , H_{12} , and H_{22} . For this case the energy eigenvalues, E_+ and E_- , are given by

$$E_{\pm} = \frac{1}{2}[H_{11} + H_{22} \pm \sqrt{(H_{11} - H_{22})^2 + 4H_{12}^2}] \quad (6.7)$$

The spacing

$$s = \sqrt{(H_{11} - H_{22})^2 + 4H_{12}^2} \quad (6.8)$$

is a positive-definite quantity, a result from which the absence of level crossing, alluded to earlier in this section, can be deduced. It is a result that is not restricted to the two-dimensional case.

From (6.6) and (6.8), the probability distribution for the spacing is given by

$$P(s) = C \int dH_{11} \int dH_{12} \int dH_{22} e^{-\alpha(H_{11}^2 + 2H_{12}^2 + H_{22}^2)} \delta(s - \sqrt{(H_{11} - H_{22})^2 + 4H_{12}^2}) \quad (6.9)$$

The integration is straightforward so we leave it to the reader to carry it out. The result is the Wigner distribution (6.3). However, this coincidence occurs only for the two-dimensional case. Agreement with the Wigner distribution is achieved again when the dimensionality becomes very large. The comparison with an exact calculation of Gaudin (61) is shown in Table 6.1.

Remarkably, it is actually possible to obtain the probability distribution for the eigenvalues of the GOE in closed form. Toward this end, note that the Hamiltonian matrix of dimensionality N has $N(N+1)/2$ independent matrix elements. Upon diagonalization the new variables are the N energy eigenvalues E_a and $N(N-1)/2$ parameters α_i describing the transformation to the diagonal basis. These parameters do not appear explicitly in (6.6) for P since

$$\text{tr} H^2 = \sum E_a^2$$

Finally, it is necessary to transform from the volume element $dH_{11}dH_{12}dH_{22}$

TABLE 6.1 Comparison between the Wigner Two Level Distribution (p_w) and the Exact Calculation (p) of Gaudin

S/D	p	p_w
0	0	0
0.064	0.104	0.0996
0.127	0.207	0.1974
0.191	0.303	0.2915
0.255	0.395	0.3801
0.318	0.477	0.4617
0.382	0.549	0.5350
0.446	0.6117	0.5989
0.509	0.6630	0.6525
0.573	0.7032	0.6954
0.637	0.7308	0.7273
0.764	0.7547	0.7587
0.891	0.7396	0.7502
1.018	0.6933	0.7083
1.146	0.6255	0.6417
1.273	0.5445	0.5598
1.400	0.4587	0.4713
1.528	0.3750	0.3836
1.655	0.2978	0.3023
1.782	0.2301	0.2308
1.910	0.1730	0.1709
2.037	0.1267	0.1229
2.164	0.0906	0.0837
2.292	0.0631	0.0581
2.419	0.0429	0.0383
2.546	0.0286	0.0245
2.674	0.0185	0.0153
2.801	0.0117	0.0092
2.928	0.0062	0.0054
3.055	0.0030	0.0031
3.183	0.002	0.0017

Source: Gaudin (61).

$dH_{13}dH_{23}dH_{33}\cdots$ to $dE_1dE_2\cdots dE_Nd\alpha_1\cdots d\alpha_{(N)(N-1)/2}$; that is, we need to compute the Jacobian of the transformation. Toward this end, note that the matrix element is linear in the energy eigenvalues E_a :

$$H_{ij} = \langle \Phi_i | H \Phi_j \rangle = \langle \sum_a \alpha_{ia} \chi_a | H \sum_b \alpha_{jb} \chi_b \rangle = \sum_a \alpha_{ia}^* E_a \alpha_{ja}$$

where the parameters α_i are selected from the set α_{ia} and $\chi_{a,b}$ are eigenfunctions of H . Therefore, the element in the Jacobian, $\partial H_{ij} / \partial E_a$, is independent of E ,

while the remaining $(N)(N-1)/2$ elements $\partial H_{ij}/\partial \alpha_{ja}$ will be linear in E_a . Hence the Jacobian is a multinomial of degree $N(N-1)/2$ in the eigenvalues E_a . Finally, note that if any pair of eigenvalues are equal (i.e., if there is a degeneracy), the transformation from $\{E_a, \alpha_a\}$ space to H_{ij} space is singular. Hence the Jacobian must go to zero whenever two eigenvalues E_a and E_b are equal. Thus as far as the dependence upon E_a and E_b is concerned, the Jacobian is proportional to

$$\prod_{a < b=1}^N |E_a - E_b|$$

and P becomes[†]

$$P(E_1, \dots, E_N) \sim \prod_{a > b=1}^N |E_a - E_b| e^{-\alpha \sum_a E_a^2} \quad (6.10)$$

where we have integrated over the dependence on the parameters α_i . This result is referred to as the *Wishart distribution*. Evaluating the constant of proportionality in (6.10) and determining the distribution for the spacing and other measures of distribution requires elegant and ingenious mathematical arguments which we shall not describe here. It is from these results that one deduces that for large dimensionality, N , the Wigner result is recovered. Indeed, it seems that the Wigner result is approximately correct for large N even for the two-body (TBRE) case. This is illustrated by Fig. 6.3. These exact calculations also exhibit a long-range anticorrelation, which is presumably a consequence of the repulsion of energy levels.[§] It has been observed experimentally.

We turn finally to the distribution function for one of the amplitudes of the eigenvectors of the random Hamiltonian. If these are denoted by $a_1, a_2 \dots a_N$, the joint distribution function is

$$P(a_1, a_2, \dots, a_N) = \frac{2}{\Omega_N} \delta\left(1 - \sum_1^N a_i^2\right) \quad (6.11)$$

since the amplitudes must remain normalized under an orthogonal transformation. The quantity Ω_N is the total solid angle subtended by an

[†]It has been pointed out by Dyson that this expression can be thought of as the configurational part of the partition function for a two-dimensional Coulomb gas with each particle held in a one-particle oscillator potential.

[§]The correlation function is evaluated by Dyson and Mehta (63). However, they did not deal with the GOE but rather with the "orthogonal ensemble" of unitary matrices, whose eigenvalues are of the form $e^{i\theta_i}$. Porter therefore refers to the ensemble as the COE, the circular orthogonal ensemble. One can consider the Dyson ensemble to be a theory of random S matrices, while Wigner, Porter, and Rosenzweig consider random Hamiltonian matrices with real matrix elements, assuming time-reversal invariance. The violation of time reversal led [Dyson [62]] to the consideration of "unitary ensembles." It leads to substantial differences for the spacing distribution from that which follows from the circular orthogonal ensemble.

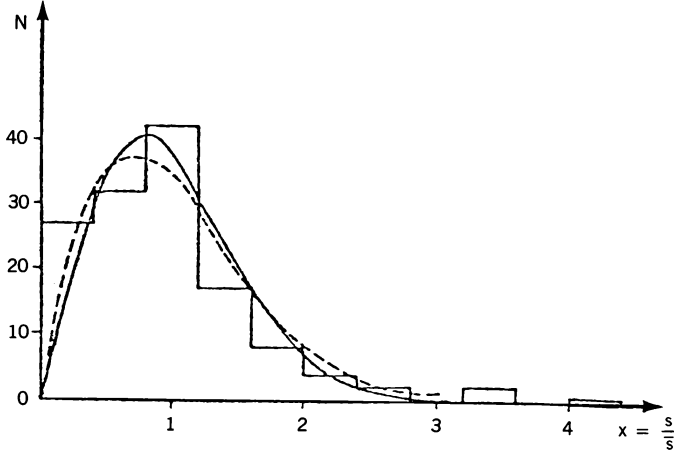


FIG. 6.3. Histogram obtained collecting the lowest energy difference between states with the same J and Π in the nuclear table. The solid line represents Wigner's distribution $p_w(x)$ and the dashed line shows the prediction of the TBRE in the ground-state region taken from Cota, Flores, Mello, and Yipez (74). The number of spacings is 135 and the probability of χ^2 is 3% when the histogram is compared with $p_w(x)$ and 13% when compared with the $\rho(0; x)$ of the TBRE. [From Mello (78).]

N -dimensional sphere. To show this, introduce N -dimensional spherical coordinates:

$$\begin{aligned}
 A^2 &= \sum a_i^2 \\
 a_1 &= A \cos \vartheta_1 \\
 a_2 &= A \sin \vartheta_1 \cos \vartheta_2 \\
 &\vdots \\
 a_N &= A \sin \vartheta_1 \sin \vartheta_2 \cdots \sin \vartheta_{N-1}
 \end{aligned} \tag{6.12}$$

The volume element is given by

$$A^{N-1} dA d\Omega_N$$

so that

$$\begin{aligned}
 \int P(a_1, a_2, \dots, a_N) da_1 \cdots da_N &= \frac{2}{\Omega_N} \int \delta(1 - A^2) A^{N-1} dA d\Omega_N \\
 &= 2 \int \delta(1 - A^2) A^{N-1} dA = 1
 \end{aligned}$$

as desired.

The distribution for a_1 is given by

$$\begin{aligned} P(a) &= \int P(a_1, \dots, a_N) \delta(a_1 - a) da_1 \cdots da_N \\ &= \int P(a_1 \cdots a_N) \delta(a_1 - a) A^{N-1} dA \sin^{N-2} \vartheta_1 d\vartheta_1 d\Omega_{N-1} \end{aligned} \quad (6.13)$$

where we have used

$$\begin{aligned} d\Omega_N &= \sin^{N-2} \vartheta_1 \sin^{N-3} \vartheta_2 \cdots \sin \vartheta_{N-3} d\vartheta_1 \cdots d\vartheta_{N-1} \\ &= \sin^{N-2} \vartheta_1 d\Omega_{N-1} \end{aligned} \quad (6.14)$$

Note that $0 < \vartheta_\alpha < \pi$, $\alpha \neq N-1$, while $-\pi < \vartheta_{N-1} < \pi$. Hence

$$\begin{aligned} P(a) &= \frac{\Omega_{N-1}}{\Omega_N} \int \delta(a - \cos \vartheta_1) \sin^{N-2} \vartheta_1 d\vartheta_1 \\ &= \frac{\Omega_{N-1}}{\Omega_N} (1 - a^2)^{(N-3)/2} \end{aligned} \quad (6.15)$$

One can readily show by integrating the first line of (6.14) that

$$\Omega_N = \frac{2\pi^{N/2}}{\Gamma(N/2)}$$

Assuming that $a^2 \ll 1$ and $N \gg 1$, (6.15) becomes

$$P(a) da = \left(\frac{N}{2\pi} \right)^{1/2} e^{-Na^2/2} da \quad (6.16)$$

Since the single particle width, Γ , is proportional to a^2 , its distribution can be obtained directly from (6.16). Let

$$\frac{\Gamma}{\langle \Gamma \rangle} = Na^2$$

we then obtain the Porter–Thomas (56) distribution for the widths:

$$P(\Gamma) d\Gamma = \frac{1}{\sqrt{2\pi}} \left(\frac{\langle \Gamma \rangle}{\Gamma} \right)^{1/2} e^{-(1/2)(\Gamma/\langle \Gamma \rangle)} \frac{d\Gamma}{\langle \Gamma \rangle} \quad (6.17)$$

where $\langle \Gamma \rangle$ is the average of Γ .

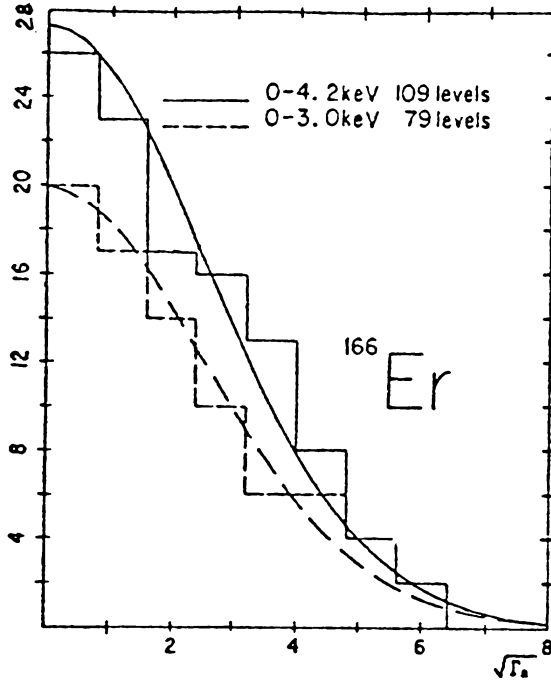


FIG. 6.4. Plot of the distribution of amplitudes for ^{166}Er from 0 to 3 and from 0 to 4.2 keV. The porter–Thomas curves are shown for comparison. [From Mello (78).]

The Porter–Thomas distribution has been amply verified experimentally as illustrated by Fig. 6.4. If ν channels contribute to the width, one can calculate the result by folding the Porter–Thomas distribution for single channels:

$$P_{\nu}(\Gamma) = \int P(\Gamma_1)P(\Gamma_2) \cdots P(\Gamma_{\nu}) \delta\left(\Gamma - \sum_1^{\nu} \Gamma_i\right) d\Gamma_1 \cdots d\Gamma_{\nu} \quad (6.18)$$

This calculation can be carried easily by using the representation of the δ function

$$\delta(\Gamma - \sum \Gamma_i) = \frac{1}{2\pi} \int \exp[ik(\Gamma - \sum \Gamma_i)] dk$$

Inserting this result into (6.18) yields

$$P_{\nu}(\Gamma) = \frac{1}{2\pi} \int dk e^{ik\Gamma} \left[\prod_1^{\nu} \int P(\Gamma_i) e^{-ik\Gamma_i} d\Gamma_i \right]$$

This integral can be carried out to obtain a single closed form when the average

widths for each channel are equal:

$$\langle \Gamma_i \rangle = \frac{\langle \Gamma \rangle}{\nu}$$

The one obtains the “ χ^2 distribution for ν degrees of freedom”:

$$P_\nu(\Gamma) d\Gamma = \left(\frac{\nu \Gamma}{2\langle \Gamma \rangle} \right)^{\nu/2} \frac{1}{\Gamma(\nu/2)} \exp\left(\frac{-\nu \Gamma}{2\langle \Gamma \rangle} \right) \frac{d\Gamma}{\Gamma} \quad (6.19)$$

One can readily show that

$$\langle \Gamma^2 \rangle - \langle \Gamma \rangle^2 = \frac{2}{\nu} \langle \Gamma \rangle^2 \quad (6.20)$$

showing that as the number of channels increase the variance decreases. For a large number of contributing channels it is good approximation to neglect fluctuations, so that

$$\langle f(\Gamma) \rangle \rightarrow f(\langle \Gamma \rangle) \quad \nu \text{ large} \quad (6.21)$$

7. STATISTICAL THEORY OF NUCLEAR REACTIONS[‡]

As can be seen from Fig. 5.6, the level densities in the heavy nuclei quickly approach astronomical values with increasing excitation energy. For the lighter nuclei, the level density does not reach as large values for the same excitation energy, but the numbers are still substantial as illustrated by Figs 7.1 and 7.2. To obtain either theoretically or experimentally the cross section for the excitation of each of these levels is generally not possible or worthwhile. There are exceptions. At very low excitation energies, the level density is sufficiently small, so that the individual compound nuclear resonances can be observed. At higher excitation energies special structures such as the doorway state resonances (isobar analog resonances, the giant multipole resonances, etc.), which in fact involve averages over many levels, are of great importance. In the discussion that follows we assume that such unusual structures are not present in the energy domain being considered. Excluding these exceptions, the large level density precludes the study of the individual levels. Under these circumstances a statistical approach becomes unavoidable.

The justification of a statistical theory of nuclear reactions is similar in content to that used to justify statistical mechanics. Indeed, the statistical theory of nuclear reactions may be considered to be an example of nonequilibrium

[‡]Blatt and Weisskopf (52); Hauser and Feshbach (52).

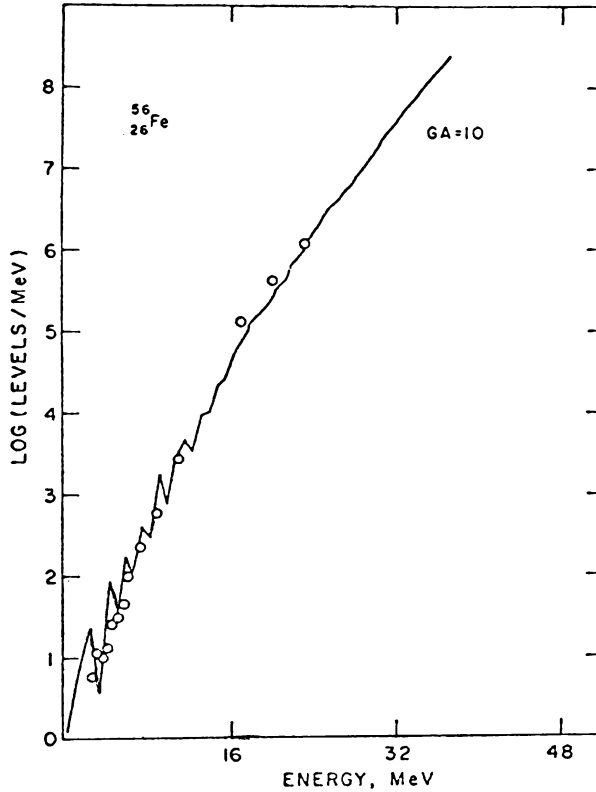


FIG. 7.1. Comparison of Hillman-Grover level density with experimental values for ^{56}Fe . Circles are experimental points. [From Lefort (76).]

statistical mechanics. At a sufficiently high excitation energy when the level density is large, it is reasonable to assume that the states are complicated linear combinations of simple states. As an example, consider a nucleon incident upon a nucleus for which a shell model description is adequate. The nucleon will excite the target by exciting one of the nucleons so that the system may be considered to be in a $2p-1h$ state. A second encounter with a target nucleon may lead to a $3p-2h$ state. Successive interaction will eventually generate $4p-3h$ components, $5p-4h$ components, and so on (see Fig. 7.3). The wave functions of the compound nuclear system will consist of a linear combination of the incident state and states belonging to these various excitation categories: $2p-1h$, and so on. In terms of this shell model representation, the number of terms in the linear combination forming the wave function will be very large, on the order of the number of levels in an interval of a few MeV. Under these circumstances, it is not surprising that the transition amplitudes $\mathcal{T}_{cc'}$, which depend on the overlap between the initial wave function and the complex nuclear wave function, will be a complex random variable. That is, the value of $\mathcal{T}_{cc'}$,

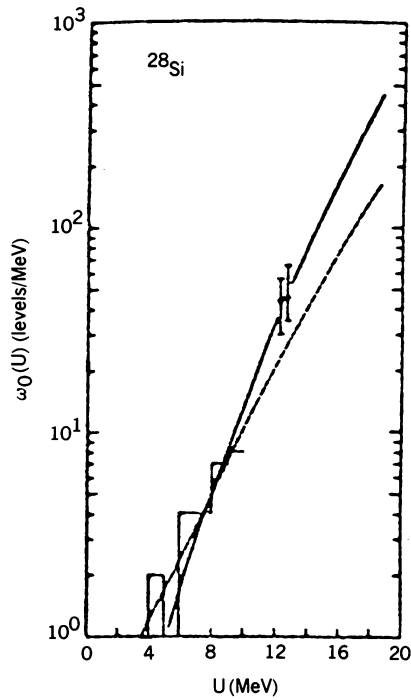


FIG. 7.2. Level density. [From Huizenga (72).]

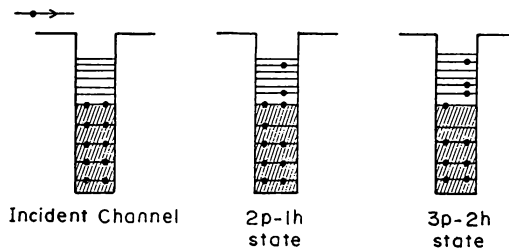


FIG. 7.3. Multistep nuclear excitation.

because of the complexity of the nuclear wave function, will depend on relatively accidental features of the latter. The value of $\mathcal{T}_{cc'}$ will fluctuate rapidly as the energy changes, giving rise to the Ericson-fluctuations discussed earlier in this chapter. The values of $\mathcal{T}_{cc'}$ obtained from a sufficiently large energy range form an ensemble with respect to which average properties of the system can be calculated. It is assumed, and this is a form of an ergodic theorem, that the ensemble average and the average with respect to an energy interval are equal.

Perhaps the most essential hypothesis made in the development of the statistical theory is the *random-phase* hypothesis. This hypothesis is the most direct application of the insight that the complexity of the nuclear wave function

will lead to effective randomness. We first provide a general statement of the random-phase hypothesis, as there will be many applications in differing contexts. Suppose that an amplitude u can be written as a sum as follows:

$$u = \sum_n u_n$$

We shall, moreover, assume that the average values of u and u_n , the nature of the average depending on the problem under consideration, are zero:

$$\langle u \rangle = 0 \quad \langle u_n \rangle = 0 \quad (7.1)$$

The question is asked as to the average value of $|u|^2$, which generally will differ from zero:

$$\langle |u|^2 \rangle = \sum_{n,m} \langle u_n^* u_m \rangle \quad (7.2)$$

The random-phase assumption states that the phases of u_n are random, from which (7.1) follows immediately. To see this, let

$$u_n = e^{i\phi_n} |u_n|$$

The various possible values of ϕ_n ranging from 0 to 2π are assumed to be equally probable, so that the average is given by

$$\langle u_n \rangle = \frac{1}{2\pi} \int_0^{2\pi} u_n d\phi_n = 0$$

The same analysis applied to (7.2) yields

$$\langle u_n^* u_m \rangle = \delta_{nm} |u_n|^2 \quad (7.3)$$

so that

$$\langle |u|^2 \rangle = \sum_n |u_n|^2 \quad (7.4)$$

The dependence of this result on the representation used to obtain the expansion of u should be noted. The physics of the system under consideration dictates the selection of the representation to be used. It is through this choice that a physics content is given to the random phase hypothesis. We shall see many examples.

As a first application of the random phase assumption, we make use of the result of Kawai, Kerman, and McVoy (73) to be described later in this chapter. It states that it is possible to break up the transition matrix \mathcal{T} into two parts:

a prompt (or direct) term, $\mathcal{T}^{(P)}$, the channel indices are suppressed for the time being, and a fluctuation (or resonance) term, $\mathcal{T}^{(FL)}$

$$\mathcal{T} = \mathcal{T}^{(P)} + \mathcal{T}^{(FL)} \quad (7.5)$$

so that upon taking averages

$$\begin{aligned} \langle \mathcal{T} \rangle &= \langle \mathcal{T}^{(P)} \rangle \\ \langle \mathcal{T}^{(FL)} \rangle &= 0 \end{aligned} \quad (7.6)$$

The cross section is proportional to $|\mathcal{T}|^2$. Taking the average assuming that a random relative phase exists between $\mathcal{T}^{(P)}$ and $\mathcal{T}^{(FL)}$ one obtains

$$\langle |\mathcal{T}|^2 \rangle = \langle |\mathcal{T}^{(P)}|^2 \rangle + \langle |\mathcal{T}^{(FL)}|^2 \rangle \quad (7.7)$$

or in terms of the cross section, the cross section can be given a corresponding decomposition

$$\langle \sigma \rangle = \sigma^{(P)} + \sigma^{(FL)} \quad (7.8)$$

The above results apply to the entire cross section. But they apply as well as the partial wave cross sections so that

$$\langle |\mathcal{T}(J\Pi)|^2 \rangle = \langle |\mathcal{T}^{(P)}(J\Pi)|^2 \rangle + \langle |\mathcal{T}^{(FL)}(J\Pi)|^2 \rangle \quad (7.9)$$

As a second example consider the application of the random phase hypothesis to the angular distribution (1.5). We then need to average $\mathcal{T}_{c_1 c_1}^{(FL)} \mathcal{T}_{c_2 c_2}^{(FL)*}$, where c stands for the quantum numbers $\alpha, l, s; J\Pi$ so that

$$\mathcal{T}_{c_1, c_1}^{(FL)} \equiv \mathcal{T}_{\alpha', \alpha}^{(FL)}(l' s'_1; l s; J, \Pi)$$

Using the random-phase hypothesis,

$$\langle \mathcal{T}_{c_1, c_1}^{(FL)} \mathcal{T}_{c_2 c_2}^{(FL)*} \rangle = \delta_{c_1, c_2} \delta_{c_1, c_2} |\mathcal{T}_{c_1, c_1}^{(FL)}|^2 \quad (7.10)$$

We then obtain for the angular distribution

$$\begin{aligned} \left\langle \frac{d\sigma^{(FL)}(\alpha', \alpha)}{d\Omega} \right\rangle &= \frac{1}{k^2} \sum \frac{1}{(2I+1)(2i+1)} (lsJ \| \sqrt{4\pi} Y_L \| lsJ) (l' s' J \| \sqrt{4\pi} Y_L \| l' s' J) \\ &\times \langle |\pi^2 \mathcal{T}_{\alpha' \alpha}^{(FL)}(l' s'; l s; J\Pi)|^2 \rangle P_L(\cos \vartheta) \end{aligned} \quad (7.11)$$

Since [see (1.9)]

$$(lsJ \| \sqrt{4\pi} Y_L \| lsJ) \sim \begin{pmatrix} l & L & l \\ 0 & 0 & 0 \end{pmatrix}$$

only even values of L will occur in the sum in (7.11), with the consequence that the angular distribution is symmetric about 90° . This result follows directly from the fact that according to (7.10), the random-phase hypothesis permits interference only between states of the same parity. We shall leave it as an exercise for the reader to show that, in view of the fact that the polarization is an interference phenomenon, it will vanish under the random-phase hypothesis. Of course, this result applies only to the fluctuation term. Other polarization parameters such as D , the “depolarization,” do not vanish.

The limiting form of isotropy follows from the general expression (7.11) only if additional assumptions are made. The assumption is made that the transition matrix $\mathcal{T}_{c',c}$ does not depend on the channel spin s' . Second, it is assumed that the density of states with a given spin s' is $(2s' + 1)$. This differs from (5.54) in that the cutoff is not included. As a consequence, the implicit assumption is made that the principal contributions come from sufficiently low s' . Turning to (1.9), the s' dependent factors in the sum over s' of (7.11) are

$$\begin{aligned} \sum_{s'} (-)^{s'+L+J} (2s' + 1) \begin{Bmatrix} l' & J & s' \\ J & l' & L \end{Bmatrix} &= \sum_{s'} (-)^{s'+L+J} (2s' + 1) \begin{Bmatrix} J & J & L \\ l' & l' & s' \end{Bmatrix} \\ &= (-)^{L+l'+2J} \sqrt{(2J+1)(2l'+1)} \delta_{L0} \end{aligned}$$

Since only the $L=0$ term survives, the angular distribution in this limit is isotropic. Isotropy is a consequence of the evaporation models of Weisskopf (31) and Frenkel (36).

The symmetry about 90° has been verified experimentally, and indeed deviations from it are taken to indicate the presence of prompt processes. An example of a symmetric angular distribution as it occurs in the reaction $^{58}\text{Ni}(\alpha, p)^{61}\text{Cu}$ is given in Fig. 7.4. An example from heavy-ion physics is shown in Fig. 7.5, where the colliding nuclei are ^{40}Ar and ^{77}Sc .

We turn next to the evaluation of $\langle |\mathcal{T}_{cc'}^{(\text{FL})}|^2 \rangle$. Our goal will be to replace this term by an expression that can be evaluated through the use of the semiempirical optical model. The expression for $\mathcal{T}_{cc'}^{(\text{FL})}$ is given by (4.4):

$$2\pi\mathcal{T}_{c'c}^{(\text{FL})} = e^{i(\delta_f + \delta_i)} \sum_{\lambda} e^{i\phi_{\lambda}(c',c)} \frac{g_{\lambda}(c')g_{\lambda}(c)}{E - E_{\lambda} + (i/2)(\Gamma_{\lambda} + \Gamma'_{\lambda})} \quad (7.12)$$

where $g_{\lambda}(c)$, a real quantity, is the magnitude of the matrix element $\langle \Phi_{\lambda} | H_{QP} | \psi_c^{(+)} \rangle$ connecting a channel c with wave function $\psi_c^{(+)}$ with the state for the compound system Φ_{λ} . The partial width $\Gamma_{\lambda c}$ is given by

$$\Gamma_{\lambda c} = g_{\lambda}^2(c) \quad (7.13)$$

and Γ_{λ} by

$$\Gamma_{\lambda} = \sum_c \Gamma_{\lambda c} \quad (7.14)$$

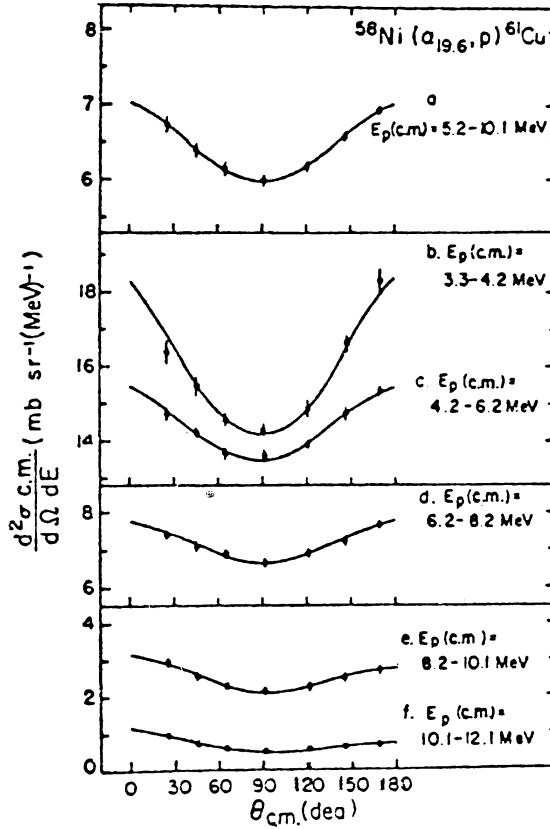


FIG. 7.4. Angular distribution for protons emitted by ^{62}Zn compound nuclei for several kinetic energy ranges in $^{58}\text{Ni}(\alpha, p)^{61}\text{Cu}$ -induced reactions at 19.67 MeV [Barker and Sarantites (74).] [From Lefort (76).]

The quantity Γ'_λ differs from zero when the levels overlap. However, it has the property [see (4.5)] that

$$\sum_\lambda \Gamma'_\lambda = 0 \quad (7.15)$$

so that Γ'_λ is not a positive-definite quantity such as Γ_λ .

In the preceding section it was shown that the distribution of the widths for the single-channel case is given by the Porter-Thomas distribution, (6.17), when the Hamiltonian is random. Equivalently, this means that the distribution of the amplitudes g is Gaussian.

$$P(g) dg = \frac{1}{\sqrt{2\pi\langle g^2 \rangle}} \exp\left(\frac{-\frac{1}{2}g^2}{\langle g^2 \rangle}\right) \quad (7.16)$$

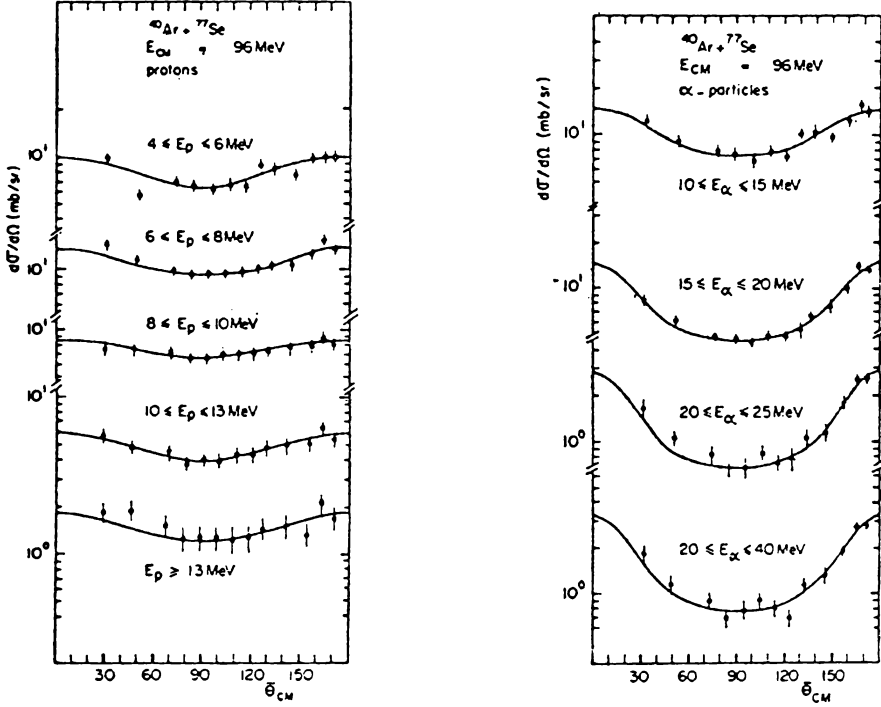


FIG. 7.5. Angular distributions for protons and α -particles emitted from ^{117}Te compound nuclei in several kinetic energy ranges [Galin, Gatty, et al. (74).] [From Lefort (76).]

where $\langle g^2 \rangle$ is the average value of g^2 taken with respect to this distribution:

$$\langle g^2 \rangle = \int_{-\infty}^{\infty} P(g) g^2 dg \quad (7.17)$$

The important point here is not the existence of a “derivation” but rather that it has been verified experimentally (see Fig. 6.4.). Since the distribution given by (7.16) is, according to the central limit theorem (see p. 251), that of a quantity composed of a sum of random quantities, g itself can be considered as random with

$$\langle g \rangle = 0 \quad (7.18)$$

Assuming the phase ϕ_λ to be random as well, (7.6), $\langle \mathcal{F}_{cc'}^{(\text{FL})} \rangle = 0$, can be verified directly.

Of course, $\langle |\mathcal{F}^{(\text{FL})}|^2 \rangle$ and therefore the partial cross section $\langle \sigma^{(\text{FL})}(J\Pi) \rangle$ are

not zero. We proceed now to evaluate $\langle \sigma^{(\text{FL})} \rangle$ where

$$\begin{aligned} \sigma^{(\text{FL})}(J\Pi) &= 4\pi^3 \lambda^2 |\mathcal{T}^{(\text{FL})}(J\Pi)|^2 \\ &= \pi \lambda^2 \sum_{\lambda\mu} e^{i(\phi_\lambda - \phi_\mu)} \frac{g_{\lambda f} g_{\mu f} g_{\lambda i} g_{\mu i}}{[E - E_\lambda + (i/2)(\Gamma_\lambda + \Gamma'_\lambda)][E - E_\mu - (i/2)(\Gamma_\mu + \Gamma'_\mu)]} \end{aligned} \quad (7.19)$$

Note that E_λ , Γ_λ , and Γ'_λ are independent of the specific nature of the incident or final channel. The random-phase hypothesis yields

$$\langle \sigma^{(\text{FL})}(J\Pi) \rangle = \pi \lambda^2 \sum_{\lambda} \left\langle \frac{\Gamma_{\lambda f} \Gamma_{\lambda i}}{(E - E_\lambda)^2 + \frac{1}{4}(\Gamma_\lambda + \Gamma'_\lambda)^2} \right\rangle \quad (7.20)$$

We evaluate the right-hand side in several limits:

1. There are a large number of exit channels. Under these circumstances the variance in $\Gamma_\lambda + \Gamma'_\lambda$ is reduced substantially [see (6.20)]. It is therefore a good approximation to rewrite

$$\left\langle \sum_{\lambda} \frac{\Gamma_{\lambda f} \Gamma_{\lambda i}}{(E - E_\lambda)^2 + \frac{1}{4}(\Gamma_\lambda + \Gamma'_\lambda)^2} \right\rangle \rightarrow \sum_{\lambda} \frac{\langle \Gamma_{\lambda f} \Gamma_{\lambda i} \rangle}{(E - E_\lambda)^2 + \frac{1}{4}(\Gamma_\lambda + \Gamma'_\lambda)^2}$$

A second assumption asserts that $\Gamma_{\lambda f}$ and $\Gamma_{\lambda i}$ are, for $i \neq f$, uncorrelated. Hence

$$\langle \Gamma_{\lambda f} \Gamma_{\lambda i} \rangle = \langle \Gamma_{\lambda f} \rangle \langle \Gamma_{\lambda i} \rangle \quad (7.21)$$

Since the ensemble over which the averages are made consist for each case of the widths $\Gamma_{\lambda f}$ and $\Gamma_{\lambda i}$ themselves, both $\langle \Gamma_{\lambda f} \rangle$ and $\langle \Gamma_{\lambda i} \rangle$ will be independent of λ . They will be designated by $\langle \Gamma_f \rangle$ and $\langle \Gamma_i \rangle$, respectively, where Γ_i is the average width for forming the compound nucleus in the energy region covered by the sum and Γ_f is the average width for decay into the final state.

We may therefore replace (7.20) by

$$\langle \sigma_{fi}^{(\text{FL})}(J\Pi) \rangle = \pi \lambda^2 \langle \Gamma_f \rangle \langle \Gamma_i \rangle \sum \quad (7.22)$$

where

$$\sum = \sum_{\lambda} \frac{1}{(E - E_\lambda)^2 + \frac{1}{4}(\Gamma_\lambda + \Gamma'_\lambda)^2} \quad (7.23)$$

The factorization explicitly shown in (7.22) can be used to obtain an interesting result. If $\langle \sigma_{fi}^{(\text{FL})} \rangle$ is summed over all possible final states, one obtains the

cross section for the forming of the compound nucleus[†]

$$\sum_f \sigma_{fi}^{(\text{FL})} = \sigma_i^{(c)} = \pi \lambda^2 \langle \Gamma \rangle \langle \Gamma_i \rangle \sum \quad (7.24)$$

We can now eliminate the \sum factor between (7.22) and (7.24), obtaining

$$\sigma_{fi}^{(\text{FL})} = \sigma_i^{(c)} \frac{\langle \Gamma_f \rangle}{\langle \Gamma \rangle} \quad (7.25)$$

and

$$\frac{\sigma_{fi}^{(\text{FL})}}{\sigma_{gi}^{(\text{FL})}} = \frac{\langle \Gamma_f \rangle}{\langle \Gamma_g \rangle} \quad (7.26)$$

Thus the probability of decay of the compound system in a final channel is given by the branching ratio $\langle \Gamma_f \rangle / \langle \Gamma \rangle$, which is independent of the incident channel i and therefore of the manner in which the compound system was formed. This is referred to as the *Bohr independence hypothesis*.

Verification of the Bohr independence hypothesis in either form (7.25) and (7.26) is difficult since it holds individually for each partial wave with given values of J and Π but not for the sum of such terms; that is, although each term in the sum factors, the sum itself will generally not. However, if a compound system can be formed by two different methods (i.e., by using differing projectiles and targets), if the energy domain of the compound system is the same for the two, if the distribution of the J 's and parities are the same, and so on, the ratio of the cross sections for identical products should be constant over their energy spectrum. Meeting all these conditions is not simple unless the reaction picks out a unique final J and Π . Examples of a comparison between two such reactions is given in Figs 7.6 and 7.7 [see the discussion by J.M. Miller (72)].

To make further progress, the relationship to the optical model of the quantities we have been using will be exploited. This procedure is advantageous since the parameters of the optical model potential can be determined empirically by fitting the elastic scattering (and polarization if available) and the total cross section.

The optical model has been derived in Chapter III and will be discussed in greater detail in Chapter V. We briefly review some salient features here. It states that the energy average of the wave function $\langle \psi \rangle$ is the solution of a Schrödinger equation with a complex potential. In the many-channel case, the Schrödinger equation reduces to a set of coupled equations for the open-channel wave functions. In the present context the relevant quantities is the transmission

[†]This is not exact since (7.21) and therefore (7.22) are not correct for the elastic term $i = f$. In writing (7.24) we are assuming that the elastic scattering width is small, as should be the case when many channels are open.

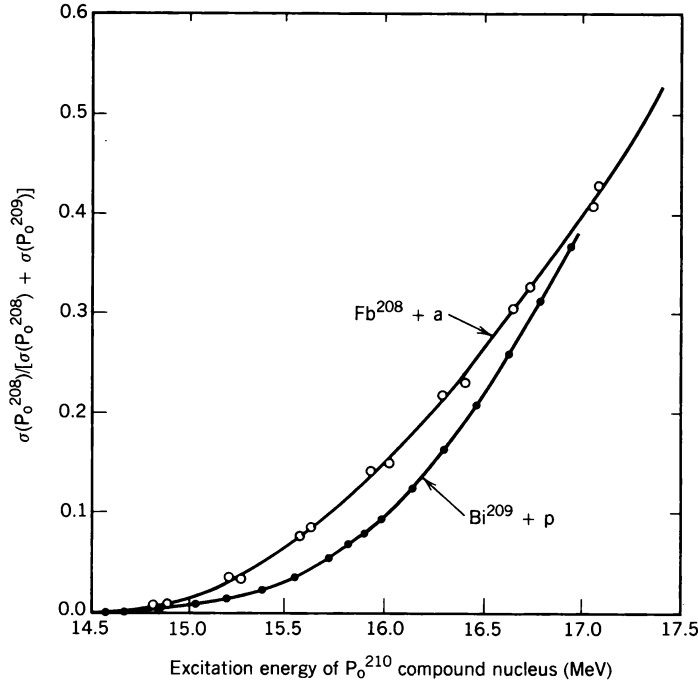


FIG. 7.6. Experimentally measured values of $\sigma(\text{Po}^{208})/[\sigma(\text{Po}^{208}) + \sigma(\text{Po}^{209})]$ as a function of the excitation energy of the Po^{210} compound nucleus prepared in two ways: $p + \text{Bi}^{209}$ and $\alpha + \text{Pb}^{206}$ [Grover and Nagle (64)]. [From Miller (72).]

coefficient T_c . We employ the generalization $T_{cc'}$ (where the subscript denotes the open channels) defined by Satchler (63) as follows:

$$T_{cc'}^{(\text{opt})} = \delta_{cc'} - \sum_{c''} S_{cc''}^{(\text{opt})} S_{c'c''}^{(\text{opt})*} \quad (7.27)$$

where $S^{(\text{opt})}$ is the energy-averaged S matrix, which can be obtained from the energy-averaged wave function $\langle \psi \rangle$ of the optical model. If the optical model conserved flux (which it does not because of the process of energy averaging), $S^{(\text{opt})}$ would be unitary and $T^{(\text{opt})}$ would be zero. The transmission coefficient T_c is the diagonal element of the matrix $T^{(\text{opt})}$:

$$T_c \equiv T_{cc}^{(\text{opt})} = 1 - \sum_{c''} |S_{cc''}^{(\text{opt})}|^2 \quad (7.28)$$

If we write the total S matrix as

$$S = S^{(\text{opt})} + S^{(\text{FL})} \quad (7.29)$$

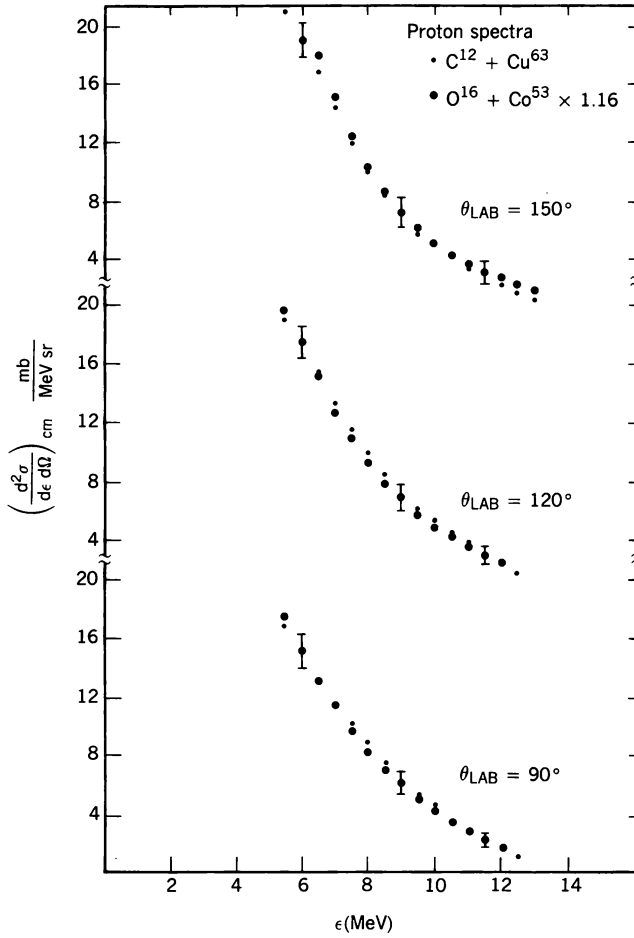


FIG. 7.7. Energy spectra of emitted protons. Cross sections from $O^{16} + Co^{59}$ multiplied by 1.16 [D'Auria, Fluss, et al. (68)]. [From Miller (72).]

where

$$\langle S^{(FL)} \rangle = 0 \quad (7.30)$$

we see that

$$T_c = \left\langle \sum_{c''} |S_{cc''}^{(FL)}|^2 \right\rangle \quad (7.31)$$

Note. To prove this, use the unitarity condition $SS^\dagger = 1$, replace S by (7.29).

Then average using (7.30). One then finds that

$$T_{cc'} = \left\langle \sum_{c''} S_{cc''}^{(\text{FL})} S_{c'c''}^{(\text{FL})*} \right\rangle \quad (7.32)$$

Using $S^{(\text{FL})} = -2\pi i \mathcal{T}^{(\text{FL})}$ and expression (7.12), we have

$$S_{cc'}^{(\text{FL})} = -ie^{i(\delta_c + \delta_{c'})} \sum_{\lambda} \frac{e^{i\phi_{\lambda}} g_{\lambda c} g_{\lambda c'}}{(E - E_{\lambda}) + (i/2)(\Gamma_{\lambda} + \Gamma'_{\lambda})} \quad (7.33)$$

Substituting in (7.31) and using the random-phase approximation,

$$T_c = \left\langle \sum_{\lambda, c''} \frac{|g_{\lambda c}|^2 |g_{\lambda c''}|^2}{(E - E_{\lambda})^2 + \frac{1}{4}(\Gamma_{\lambda} + \Gamma'_{\lambda})^2} \right\rangle \quad (7.34)$$

In the limit of a large number of channels, so that $(\Gamma_{\lambda} + \Gamma'_{\lambda})$ is a constant equal to $\langle \Gamma \rangle$, and assuming independence of $\Gamma_{\lambda c} = |g_{\lambda c}|^2$ and $\Gamma_{\lambda c''}$, (7.34) becomes

$$T_c = \langle \Gamma_c \rangle \langle \Gamma \rangle \sum \quad (7.35)$$

where \sum is given by (7.23). Substituting this relationship into (7.22) yields the familiar result

$$\sigma_{fi}^{(\text{FL})}(J\Pi) = \pi \lambda_i^2 \frac{T_i T_f}{\sum_a T_a} \quad (7.36)$$

Note that in the derivation it was not necessary to evaluate \sum , so that the question of the distribution of E_{λ} , the end point effects, the size of $\langle \Gamma \rangle$ relative to D , the method of averaging did not arise. Moreover, it has *not* been necessary to assume that $T_c \ll 1$, which is a required and heavily criticized feature of many of the derivations of (7.36).

The angular distribution, (7.11), is given by

$$\begin{aligned} & \left\langle \frac{d\sigma_{fi}^{(\text{FL})}}{d\Omega} \right\rangle \\ &= \sum \frac{1}{(2I+1)(2i+1)} (lsJ \parallel Y_L \parallel lsJ)(l's'J \parallel Y_L \parallel l's'J) \sigma_{fi}^{(\text{FL})}(l's'; ls; J\Pi) P_L(\cos \Theta) \end{aligned} \quad (7.37)$$

where we have used (7.19). Similarly, the total fluctuation cross section according to (1.6) is given by

$$\langle \sigma_{fi}^{(\text{FL})} \rangle = \sum \frac{2J+1}{(2I+1)(2i+1)} \sigma_{fi}^{(\text{FL})}(l's'; ls; J\Pi) \quad (7.38)$$

where one uses (7.36) for $\sigma_{fi}^{(\text{FL})}$.

The cross sections given by (7.36) and (7.38) describe the excitation of a particular final state in the residual nucleus. However, for all except the rather low-lying states, it is more appropriate to regard the spectrum of the residual nucleus forming a continuum with a level density given by $\omega_f(U, J)$. Then the angle integrated spectrum (for example) is given by

$$\left\langle \frac{d\sigma_{fi}^{(FL)}}{dU} \right\rangle = \pi \lambda^2 \sum \omega_f(U, J) \frac{2J+1}{2I+1} \frac{T_f(J\Pi) T_i(J\Pi)}{\sum_c [T_c + \int T_c(J\Pi) \omega_c(U_c, J)]} \quad (7.39)$$

where both a sum and an integral are included in the denominator in order to take account of both the discrete and continuum level spectrum.

Equations (7.36)–(7.39) (to be suitably modified by the width fluctuation factor whose importance has been emphasized by Moldauer) referred to as the Hauser–Feshbach (52) theory are the fundamental results of the statistical theory of nuclear reactions. Their application is discussed in Section 9. For the present, note that one only needs the optical model transmission coefficients. In applying (7.36) one would need to know as well the energies, spins, and so on, of the levels to be excited as well as of those which are competitive (i.e., contribute to the denominator). To apply (7.39), one needs to know, in addition to the transmission coefficients, the density of levels of the residual nucleus.

It will be useful (but not essential) to evaluate the sum, \sum , of (7.23). A few comments are in order. Qualitatively, the sum over λ will contain those levels with energies E_λ that fall within the averaging interval in energy, ΔE . The energy E is at the midpoint of the interval ΔE so as to avoid end effects. Thus as E moves, ΔE moves with it. When the width (in a single channel) is very large, it is not always possible to avoid end effects since in that case the requirements of unitarity would require a very tight correlation among the levels [Mello and Feshbach (72)]. One of the consequences would be an instability of the averages to the interval size ΔE . Experimentally, this would manifest itself as an instability with respect to the energy resolution and could be so identified. The analysis that follows assumes the absence of end effects.

In calculating \sum we shall also assume that new channels do not become open in the interval ΔE ; that is, there are no thresholds in the interval. This is generally not the case, particularly as the excitation energy increases. As Kerman and Sevgen (76) point out, one consequence of this assumption is that unitarity need no longer be satisfied exactly.

Finally, some attention should be paid to the size of ΔE . For the present discussion it is to be of such a size that fine structure (Ericson–Brink fluctuations) and doorway state resonances but not the single-particle structure are averaged. Therefore, ΔE satisfies the inequalities

$$\Gamma_{SP} \gg \Delta E \gg \Gamma_d, \Gamma_\lambda, D \quad (7.40)$$

where Γ_{SP} is the single-particle width, Γ_d , the doorway state width, Γ_λ the width of the fine-structure resonances, and D is the distance in energy between them (D^{-1} = density of levels).

With these various caveats in mind, we proceed to evaluate Σ , replacing the sum by an integral

$$\Sigma = \frac{1}{D} \int_{E-(1/2)\Delta E}^{E+(1/2)\Delta E} \frac{dE_\lambda}{(E - E_\lambda)^2 + \frac{1}{4}(\Gamma_\lambda + \Gamma'_\lambda)^2} \quad (7.41)$$

Replacing Γ_λ and Γ'_λ by their average values over the interval, $\langle \Gamma \rangle$ and $\langle \Gamma' \rangle = 0$, respectively, Σ becomes

$$\Sigma = \frac{2}{D(\Gamma + \Gamma')} \int_{x_-}^{x_+} \frac{dx}{1 + x^2}$$

where $x_\pm = (2/\langle \Gamma + \Gamma' \rangle)(E \pm \frac{1}{2}\Delta E)$. If $\Delta E \gg \langle \Gamma + \Gamma' \rangle$ as assumed and in the absence of important end effects, as assumed, the limits of the integral can be taken to be $\pm \infty$, so that

$$\Sigma = \frac{2\pi}{D\langle \Gamma \rangle} \quad (7.42)$$

Equation (7.22) now reads

$$\sigma_{fi}^{(FL)} = \pi \lambda^2 \frac{2\pi \langle \Gamma_i \rangle \langle \Gamma_f \rangle}{D \langle \Gamma \rangle} \quad (7.43)$$

Moreover, the value of T_c given in (7.35) becomes

$$T_c = \frac{2\pi}{D} \langle \Gamma_c \rangle \quad (7.44)$$

a result to which we have referred in Section 2 of this chapter. Finally, from (7.24) one obtains

$$\sigma_i^{(c)} = \pi \lambda_i^2 T_i \quad (7.45)$$

We remind the reader that the value of Σ , (7.42), is not needed to obtain the fundamental equations (7.36)–(7.39).

2. We consider next the case when the exit channels are so few in number that fluctuations in the total widths Γ_λ must be considered. We return to (7.20):

$$\langle \sigma^{(FL)}(J\Pi) \rangle = \pi \lambda^2 \sum_\lambda \left\langle \frac{\Gamma_{\lambda f} \Gamma_{\lambda i}}{(E - E_\lambda)^2 + \frac{1}{4}(\Gamma_\lambda + \Gamma'_\lambda)^2} \right\rangle \quad (7.20)$$

It is more convenient in this situation to evaluate the energy average directly:

$$\langle \sigma^{(\text{FL})}(J\Pi) \rangle = \pi \hat{\kappa}^2 \frac{1}{\Delta E} \int_{E_0 - (1/2)\Delta E}^{E_0 + (1/2)\Delta E} dE \sum_{\lambda} \frac{\Gamma_{\lambda f} \Gamma_{\lambda i}}{(E - E_{\lambda})^2 + \frac{1}{4}(\Gamma_{\lambda} + \Gamma'_{\lambda})^2} \quad (7.46)$$

It is possible to choose ΔE to be large compared to $\Gamma_{\lambda} + \Gamma'_{\lambda}$, yet small enough so that their energy variation as well as that of E_{λ} is negligible. This possibility exists because the scale over which these quantities change is on the order of the single-particle width, Γ_{SP} , that is, of the order of several MeV, whereas Γ_{λ} , the width of the fine structure, must of course be much smaller than Γ_{SP} . Neglecting end effects (we remind the reader that the observer will always choose ΔE so as to minimize these effects), the integral can readily be evaluated:

$$\langle \sigma_{fi}^{(\text{FL})} \rangle = \frac{\pi \hat{\kappa}^2}{\Delta E} \sum_{\lambda} \frac{2\pi \Gamma_{\lambda f} \Gamma_{\lambda i}}{\Gamma_{\lambda} + \Gamma'_{\lambda}}$$

or

$$\langle \sigma_{fi}^{(\text{FL})} \rangle = \pi \hat{\kappa}^2 \frac{2\pi}{D} \left\langle \frac{\Gamma(f)\Gamma(i)}{\Gamma + \Gamma'} \right\rangle \quad (7.47)$$

If we assume that Γ and Γ' do not fluctuate, (7.47) reduces to (7.43). It is convenient to introduce a correction factor expressing the difference:

$$W \equiv \left\langle \frac{[\Gamma(f)/\langle \Gamma(f) \rangle][\Gamma(i)/\langle \Gamma(i) \rangle]}{(\Gamma + \Gamma')/\langle \Gamma \rangle} \right\rangle \quad (7.48)$$

W is referred to as the *width fluctuation* correction factor [Dresner (57); Moldauer (64)]. This correction factor should be most important when the number of exit channels are few, as would be the case near the threshold for the excitation of the first inelastic level. In any event, one would expect that under these circumstances the levels E_{λ} are well separated, so that Γ' vanishes approximately. Assuming that each Γ satisfies the Porter–Thomas distribution, it is relatively easy to evaluate W . To illustrate, suppose that there are only two channels, Γ_1 and Γ_2 , so that

$$\begin{aligned} W_2 &= \frac{\langle \Gamma_1 \rangle + \langle \Gamma_2 \rangle}{\langle \Gamma_1 \rangle \langle \Gamma_2 \rangle} \left\langle \frac{\Gamma_1 \Gamma_2}{\Gamma_1 + \Gamma_2} \right\rangle \\ &= [\langle \Gamma_1 \rangle + \langle \Gamma_2 \rangle] \frac{1}{2\pi} \int_0^{\infty} dx_1 \int_0^{\infty} dx_2 \frac{e^{-(1/2)x_1}}{\sqrt{x_1}} \frac{e^{-(1/2)x_2}}{\sqrt{x_2}} \frac{x_1 x_2}{x_1 \langle \Gamma_1 \rangle + x_2 \langle \Gamma_2 \rangle} \end{aligned}$$

where $x_a = \Gamma_a / \langle \Gamma_a \rangle$. The integration can be performed after an integral

representation of the denominator is introduced:

$$W_2 = [\langle \Gamma_1 \rangle + \langle \Gamma_2 \rangle] \frac{1}{2\pi} \int_0^\infty d\alpha \int_0^\infty dx_1 \sqrt{x_1} e^{-[(1/2) + \alpha \langle \Gamma_1 \rangle]x_1} \\ \times \int_0^\infty dx_2 \sqrt{x_2} e^{-[(1/2) + \alpha \langle \Gamma_2 \rangle]x_2}$$

or

$$W_2 = [\langle \Gamma_1 \rangle + \langle \Gamma_2 \rangle] \int_0^\infty \frac{d\alpha}{(1 + 2\alpha \langle \Gamma_1 \rangle)^{3/2} (1 + 2\alpha \langle \Gamma_2 \rangle)^{3/2}} \quad (7.49)$$

This integral can be performed exactly with the result for W that follows:

$$W_2 = \frac{\langle \Gamma_1 \rangle + \langle \Gamma_2 \rangle}{(\sqrt{\langle \Gamma_1 \rangle} + \sqrt{\langle \Gamma_2 \rangle})^2} \quad (7.50)$$

A plot of W_2 as a function of $\langle \Gamma_2 \rangle / \langle \Gamma_1 \rangle$ is shown in Fig. 7.8. Since it is a symmetric function of $\langle \Gamma_1 \rangle$ and $\langle \Gamma_2 \rangle$, only the values of W_2 from $\langle \Gamma_2 \rangle / \langle \Gamma_1 \rangle$ equal to zero to 1 are shown. We see that W_2 is generally considerably less than 1 approaching $\frac{1}{2}$ for $\langle \Gamma_2 \rangle / \langle \Gamma_1 \rangle = 1$. The effect of this correction is therefore to reduce the cross section from the value given by (7.36).

It is easy to generalize this result to the case in which there are more than two open channels. A review has been presented by Gruppelaar and Ruffo (77). An interesting case occurs when there are many such channels, for then one

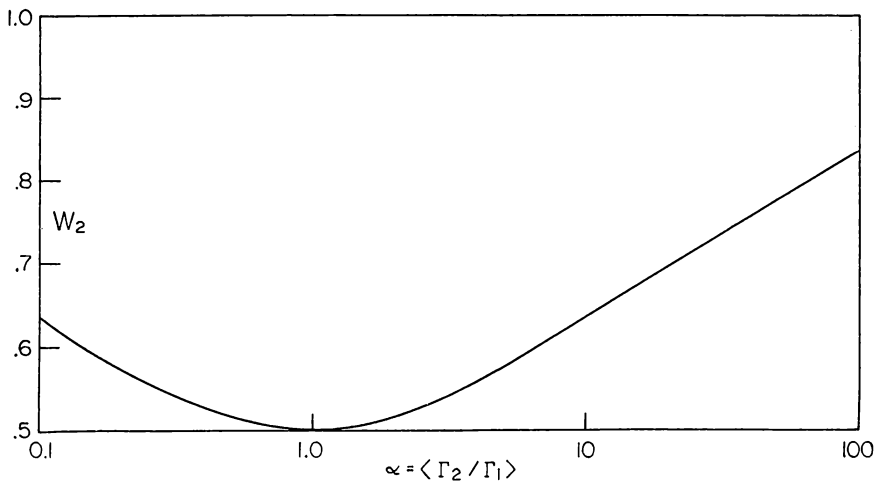


FIG. 7.8. Width fluctuation factor [see (7.50)].

can establish a connection with the discussion in Section 6. Consider

$$W_N = \frac{\langle \Gamma \rangle}{\langle \Gamma_1 \rangle + \langle \Gamma_2 \rangle} \left\langle \frac{\Gamma_1 \Gamma_2}{\sum \Gamma_i} \right\rangle, \quad \langle \sum \Gamma_i \rangle = \langle \Gamma \rangle$$

Then it can readily be shown in the limit of a large number, N , of open channels that

$$W_N \simeq \left[1 + 3 \frac{\langle \Gamma_1 \rangle + \langle \Gamma_2 \rangle}{\langle \Gamma \rangle} \right]^{-1} \quad (7.51)$$

showing that neglecting the fluctuations in the total width, Γ is a good approximation only if that width is large compared to Γ_1 and Γ_2 , even if the number of channels is large.

This treatment fails in the difficult intermediate regime when the levels overlap, at which point it is necessary to take account of the fluctuations in Γ' . Very little information is available regarding these fluctuations. One possibility is to assume that they are independent of the other parameters of the problem and that their distribution is given by a Gaussian:

$$P(\Gamma') d\Gamma' = \frac{1}{\sqrt{2\pi\langle\Gamma'^2\rangle}} \exp\left(-\frac{\frac{1}{2}\Gamma'^2}{\langle\Gamma'^2\rangle}\right) d\Gamma'$$

With this assumption (7.50) for W_2 would be replaced by

$$W_2 = \frac{\langle \Gamma_1 \rangle + \langle \Gamma_2 \rangle}{\sqrt{2\pi\langle\Gamma'^2\rangle}} \int_0^\infty d\alpha \frac{\exp[-\alpha\Gamma' - \frac{1}{2}\Gamma'^2/\langle\Gamma'^2\rangle]}{(1 + 2\alpha\langle\Gamma_1\rangle)^{3/2}(1 + 2\alpha\langle\Gamma_2\rangle)^{3/2}} \quad (7.52)$$

so that in principle by studying the width fluctuation correction factor, one would be able to determine $\langle\Gamma'^2\rangle$. However, there are many other corrections (discussed in Section 8), which makes this possibility illusory.

Fluctuation scattering can also contribute to elastic scattering. This process is referred to as *compound elastic scattering*. In that case $\Gamma_{\lambda f}$ and $\Gamma_{\lambda i}$ are no longer independent and (7.22) is not valid. We must instead calculate $\langle\Gamma_1^2\rangle$. Using the Porter-Thomas distribution, one finds that

$$\langle\Gamma_1^2\rangle = 3\langle\Gamma_1\rangle^2 \quad (7.53)$$

so that the width fluctuation correction for compound elastic scattering has the value of 3 in this limit. Introducing the fluctuations in Γ due to Γ_1 will reduce this value; the leading term is $1/[(1 + 5\langle\Gamma_1\rangle/\langle\Gamma\rangle)]$. In the limit of a single channel W reduces to unity, so that for compound elastic scattering W can have a rather broad range of values.

8. EFFECT OF THE DIRECT REACTIONS ON THE STATISTICAL THEORY

The discussion of Section 7 is based on the assumption that the partial widths $\Gamma_{\lambda c}$ are uncorrelated, and not correlated to the energies E_λ . It is assumed that an energy average can be replaced by an ensemble average in which the $\Gamma_{\lambda c}$ are random following a Porter–Thomas distribution. For large values of Γ involving many contributions for which the width fluctuation correction, W , is unimportant, one obtains the Bohr independence hypothesis, that is, factorization of the partial cross sections. The relation of these factors to the transmission factor, T_c , (7.35), is established using the same assumptions. This derivation of (7.36) does not require the evaluation of Σ , about which there has been some debate; it makes no assumption regarding the size of T_c , nor is it necessary to introduce $\sigma^{(c)}$, the cross section for the formation of the compound nucleus or to make use of (7.44) connecting T_c with Γ_c/D .

The statistical assumptions with regard to $\Gamma_{\lambda c}$ and E_λ have been the subject of a spirited debate extending for nearly two decades. Correlations do exist because of the existence of direct (prompt) reactions which can contribute to the cross section and importantly, modify the wave functions which are to be inserted into the defining matrix elements.

Moldauer (75a, 75b) particularly, and more recently Weidenmüller and his collaborators [Engelbrecht and Weidenmüller (73); Tepel, Hofman, and Weidenmüller (74); Tepel (75); Hofman, Richert, Tepel, and Weidenmüller (75); and Hofman, Richert, and Tepel (75)], have emphasized the importance of the correlations imposed by unitarity. Unitarity requires that

$$SS^\dagger = 1$$

or

$$\sum_b S_{ab} S_{cb}^* = \delta_{ac} \quad (8.1)$$

We see that the elements of S (or \mathcal{T} , which is linearly related to S) must satisfy a number of nonlinear relations, which in turn impose relations between the sets of quantities ϕ_λ , $g_{\lambda a}$, and E_λ [see (III.2.37), the discussion of the reactance matrix K , and (III.6.11) and the ensuing discussion]. The result, $\sum \Gamma'_\lambda = 0$, which we have used repeatedly, can be considered to be a consequence of unitarity. The unitarity condition can be very restrictive when the average of the partial widths $\langle \Gamma_{c\lambda} \rangle$ are large compared to the spacing in energy $\langle D_\lambda \rangle$. In that case [see Mello and Feshbach (72)] the individual values of $\Gamma_{c\lambda}$ are very large, so that very strong correlations must then exist between the various $\Gamma_{\lambda c}$ in order to satisfy unitarity. Under these circumstances, the results obtained both theoretically and experimentally become very sensitive to the manner in which averages are carried out and to the size of the averaging interval ΔE . It is noteworthy that such sensitivities have not been observed, indicating that their

occurrence is either rare or more likely that the analysis of the experimental data naturally selects out such large widths and regards them as nonstatistical.

Before attempting to perform the difficult task of taking the effects of unitarity into account, one should first understand if it is essential to do so in order to provide a statistical interpretation of nuclear reactions. We need to be particularly concerned with real situations and the manner in which data are analyzed.

Kerman and Sevgen (76) point out that unitarity need not be satisfied exactly since, in the energy domain under discussion, $\Gamma \gg D$, there is a high probability for new channels to become open in the averaging energy interval ΔE . Unless the effect of these is included in the statistical treatment, and that is generally not done in the many open-channel situations we are considering, there will be a loss of flux to the new channels, with a consequent failure of unitarity. Taking this effect into account quantitatively requires the introduction of new parameters, as discussed by Kerman and Sevgen.

A second point is that unitarity is not the only condition to be placed upon the transition amplitudes since they all are deduced from a common Schrödinger equation using the nuclear Hamiltonian, which is of course not random. These correlations cannot be stated as explicitly as the unitarity conditions, but they are certainly as real. One must ask which of these many restrictions are to be applied and which are to be neglected.

The point is that the statistical theory is an approximation; it cannot be exact. Statistics enters when the matrix elements of the Hamiltonian involve such complicated wave functions that the value of these matrix elements can be considered to be random, following Gaussian probability distributions. It should be noted that the distribution does not tell us when the particular value of the matrix element occurs. It can only provide the frequency with which it does. Thus statistical description can and does fail if inappropriately applied. It will fail, for example, if the wave functions are not sufficiently complicated. As we shall discuss in Chapter VI, only after the system has gone through a number of interactions will the necessary complication be developed. If the reaction product is produced at an early stage, the statistical theory will of course fail. The nature of the physical phenomena is the important issue.

Moreover, it may be argued that it is not useful to regard a pole term in the S matrix with a large partial width as a statistical fluctuation. As pointed out earlier, a consequence of a large average width is a close correlation among the properties of all the levels in the averaging interval as well as a marked sensitivity to the size of the averaging interval. This situation can hardly be described as statistical. And indeed, in an analysis of such data one would label such structures as nonstatistical and would consider them worthy of further study.

The reader is referred to the review by Mahaux and Weidenmüller (79) for a detailed discussion of the impact of unitarity and a summary of the present understanding.[‡] The present understanding depends very heavily on numerical

[‡]References to the pioneering work of Moldauer and other will be found there.

studies. Weidenmüller and his associates have employed the representation of the \mathcal{T} matrix in terms of the reactance matrix, \mathcal{K} [see (III.2.44) and the material following], using a pole expansion of \mathcal{K} [see (III.6.7)], which can be obtained from (III.2.43). Unitarity is thereby guaranteed. The pole parameters are assumed to be random. Moldauer (75a) has also performed a number of calculations with similar results. We mention two of these. First, one obtains a verification of the random-phase hypothesis for the S matrix in the case where the number of terms Λ in the pole expansion of K is large, and Λ is large compared to the number of open channels. The result is that $\langle S_{ab}^{(FL)} S_{cd}^{(FL)} \rangle$ vanishes unless two pairs of indices coincide. The second result, discovered by Moldauer (75a), is referred to as *M cancellation*. Briefly, he finds that the various correlation corrections cancel leading to (7.36), including the width fluctuation correction (7.48) multiplicatively. This result holds for nonelastic cross sections. The situation for elastic scattering will be discussed below following the methods of Kawai, Kerman, and McVoy (73). This paper addresses two questions of importance in the present context. The first to be discussed asks for a formulation of the problem of reactions that explicitly separate the \mathcal{T} matrix into two components, the direct and fluctuation, that is, into $\mathcal{T}^{(DI)}$ and $\mathcal{T}^{(FL)}$, with the energy average of $\mathcal{T}^{(FL)}$ equal to zero. We have made repeated use of this separation in this chapter. The second deals with the width correlations, which are induced by the presence of the direct reactions.

The essence of the solution of the first question lies in the fact that the optical model does provide calculation of the energy averaged amplitude. It will be recalled [(Eq. (III.3.16))] that the averaged many-channel amplitude satisfies the equation

$$(E - H^{(opt)}) \langle P\Psi \rangle = 0 \quad (8.2)$$

with

$$H^{(opt)} = H_{PP} + H_{PQ} \frac{1}{E - H_{QQ} + iI} H_{QP} \quad (8.3)$$

This is to be compared with the exact equation satisfied by $P\Psi$ [Eq. (III.2.7)]:

$$\left(E - H_{PP} - H_{PQ} \frac{1}{E - H_{QQ}} H_{QP} \right) (P\Psi) = 0 \quad (8.4)$$

Equation (8.3) is obtained using the Lorentzian averaging function, with I the energy averaging interval. The comparison suggests rewriting (8.4) as follows:

$$\left[E - H^{(opt)} - H_{PQ} \left(\frac{1}{E - H_{QQ}} - \frac{1}{E - H_{QQ} + iI} \right) H_{QP} \right] (P\Psi) = 0$$

This equation can be restored to the canonical form (8.4):

$$\left[E - H^{(\text{opt})} - V_{PQ} \frac{1}{E - H_{QQ}} V_{QP} \right] (P\Psi) = 0 \quad (8.5)$$

where

$$V_{PQ} = H_{PQ} \sqrt{\frac{iI}{E - H_{QQ} + iI}} \quad (8.6)$$

Equation (8.5) is equivalent to the coupled equations:

$$\begin{aligned} (E - H^{(\text{opt})})(P\Psi) &= V_{PQ}(Q\Psi) \\ (E - H_{QQ})(Q\Psi) &= V_{QP}(P\Psi) \end{aligned} \quad (8.7)$$

The \mathcal{T} matrix for this system is [Eq. (III.2.30')]

$$\mathcal{T}_{fi} = \mathcal{T}_{fi}^{(\text{opt})} + \left\langle \psi_f^{(-)} \left| V_{PQ} \frac{1}{E - H_{QQ} - W_{QQ}} V_{QP} \psi_i^{(+)} \right. \right\rangle \quad (8.8)$$

where $\psi_{f,i}$ are the distorted wave solutions of

$$(E - H^{(\text{opt})})\psi_{f,i} = 0$$

with appropriate boundary conditions, while

$$W_{QQ} \equiv V_{QP} \frac{1}{E^{(+)} - H^{(\text{opt})}} V_{PQ} \quad (8.9)$$

Since by definition

$$\langle \mathcal{T} \rangle = \mathcal{T}^{(\text{opt})}$$

it follows that the second term of (8.8) is $\mathcal{T}^{(\text{FL})}$, so that

$$\begin{aligned} \mathcal{T}_{fi}^{(\text{FL})} &= \left\langle \psi_f^{(-)} \left| V_{PQ} \frac{1}{E - H_{QQ} - W_{QQ}} V_{QP} \psi_i^{(+)} \right. \right\rangle \\ \langle \mathcal{T}_{fi}^{(\text{FL})} \rangle &= 0 \end{aligned} \quad (8.10)$$

thus achieving the desired decomposition.

As a beneficial dividend, the coupling potential V acquires a desirable dependence on H_{QQ} . As one can see from (8.6), the contributions to V from the eigenfunctions of H_{QQ} whose energy differs substantially from E is correspon-

dingly reduced so that the problems of convergence raised, for example, by Simonius (74) are resolved. This has a sound physical basis since the contributions of these distant “resonances” should be included in the optical model. It is achieved at the cost of an energy dependence which is, however, relatively weak, such as that of the optical potential itself. Note that the formalism of Chapter III can be used without any formal change in view of (8.7).

Because of (8.10), the cross section can be written

$$\sigma_{fi}(J\Pi) = \sigma_{fi}^{(\text{opt})} + \sigma_{fi}^{(\text{FL})}$$

where [see (7.12)]

$$\langle \sigma_{fi}^{(\text{FL})} \rangle = 4\pi^3 \lambda_i^2 \langle |\mathcal{T}_{fi}^{(\text{FL})}|^2 \rangle = \pi \lambda_i^2 \left\langle \left| \sum_{\lambda} \frac{e^{i\phi_{\lambda}(f,i)} g_{\lambda}(f) g_{\lambda}(i)}{E - E_{\lambda} + (i/2)(\Gamma_{\lambda} + \Gamma'_{\lambda})} \right|^2 \right\rangle$$

Using the random-phase approximation this reduces to

$$\begin{aligned} \langle \sigma_{fi}^{(\text{FL})} \rangle &= \pi \lambda_i^2 \left\langle \sum_{\lambda} \frac{g_{\lambda}^2(f) g_{\lambda}^2(i)}{(E - E_{\lambda})^2 + \frac{1}{4}(\Gamma_{\lambda} + \Gamma'_{\lambda})^2} \right\rangle \\ &\simeq \pi \lambda_i^2 \langle g_{\lambda}^2(f) g_{\lambda}^2(i) \rangle \sum \end{aligned} \quad (8.11)$$

where in (8.11) we have retained the assumption that one can neglect the correlations between the numerator and denominator of the pole expansion because of the assumed large number of participating open channels. If now one neglects the correlations among the g 's, the results of Section 13.7 follow.[‡]

We now include the correlations but make the approximation (or assumption) that only pairwise correlations are important:

$$\langle g_{\lambda}^2(f) g_{\lambda}^2(i) \rangle = \langle g_{\lambda}^2(f) \rangle \langle g_{\lambda}^2(i) \rangle + \langle g_{\lambda}(f) g_{\lambda}(i) \rangle \langle g_{\lambda}(i) g_{\lambda}(f) \rangle \quad (8.11')$$

Defining the matrix

$$\langle g_{\lambda}(f) g_{\lambda}(i) \rangle = X_{fi}$$

the cross section equation (8.11) becomes

$$\sigma_{fi}^{(\text{FL})} \simeq \pi \lambda_i^2 \sum [X_{ff} X_{ii} + X_{fi} X_{if}] \quad (8.12)$$

The second term in brackets represents a significant change from the discussion of Section 7. The Bohr independence hypothesis, for example, is not valid if this term is significant.

[‡]This derivation differs from that given by Kawai, Kerman, and McVoy (73) in that the sum, \sum , is not evaluated explicitly.

We now must relate the optical model transmission factor $T_{fi}^{(\text{opt})}$ and the matrix X . From (7.27), (7.30), and the unitarity condition one can immediately show that [see (7.32)]

$$T_{fi} = \left\langle \sum_c S_{fc}^{(\text{FL})} S_{ic}^{(\text{FL})*} \right\rangle \quad (8.13)$$

Inserting (7.36') and using the random-phase approximation,

$$T_{fi} = (\sum) \sum_c \langle g_\lambda(f) g_\lambda(c) g_\lambda(i) g_\lambda(c) \rangle$$

Again making the pair correlation assumption, one finds that

$$T_{fi} = (\sum) \sum_c [\langle g_\lambda(f) g_\lambda(i) \rangle \langle g_\lambda(c) g_\lambda(c) \rangle + \langle g_\lambda(f) g_\lambda(c) \rangle \langle g_\lambda(c) g_\lambda(i) \rangle]$$

In terms of X ,

$$T_{fi} = \sum [X_{fi} \text{tr } X + (X^2)_{fi}] \quad (8.14)$$

or equivalently

$$T = \sum (X \text{tr } X + X^2) \quad (8.15)$$

The problem of expressing $\sigma_{fi}^{(\text{FL})}$ in terms of T_{fi} is reduced to solving this equation for X . The principal limitation on this development arises from the pair correlation assumption, which will fail if Γ is too large, for then many level correlations will become important. Equation (8.14) is in agreement with a conjecture of Vager (71).

The simple result (7.36) follows if the second term in (8.15) is neglected. Then

$$T = \sum X \text{tr } X \quad (8.16')$$

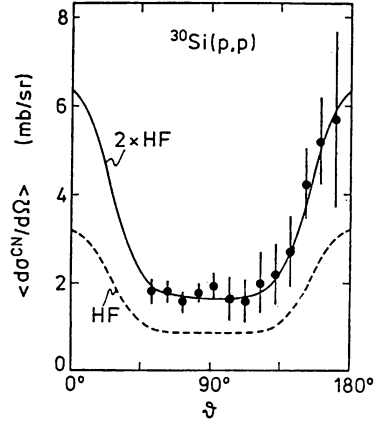
Taking the trace of both sides one can solve for $\text{tr } X$ and finally for X :

$$X \simeq \frac{T}{(\sum \text{tr } T)^{1/2}} \quad (8.16)$$

We recover (7.36) if this result is substituted for the first term of (8.12). Note again that \sum drops out and needs not to be evaluated. If both terms in (8.12) are included,

$$\sigma_{fi}^{(\text{FL})} \simeq \frac{\pi \hat{\lambda}_i^2 (T_{ff} T_{ii} + T_{fi}^2)}{\sum_c T_{cc}} \quad (8.17)$$

FIG. 8.1. Angular distribution of the average CN cross section for the elastic scattering $^{30}\text{Si}(p,p)$ for $8.5 \text{ MeV} < E_p < 10.7 \text{ MeV}$. The filled circles are the measured values; the direct elastic contribution has been determined from the analyzing power and has been subtracted. The dashed curve is calculated from the Hauser-Feshbach formula; the full curve is twice this value [Kretschmer and Wangler (78)]. [From Mahaux and Weidenmüller (79).]



Factorization and the Bohr hypothesis are no longer exactly valid. In the case of the compound elastic scattering ($f = i$),

$$\sigma_{\text{el}}^{(\text{FL})} = \frac{2\pi\chi_i^2 T_{ii}}{\sum T_{aa}} \quad (8.18)$$

We see in this case the appearance of a factor of 2, compared to simpler results that would be obtained if (7.39) were used for this case. Experimental verification of the factor of 2 is shown in Fig. 8.1.[†]

To go beyond (8.16), we solve (8.15) for X in terms of T and

$$X = \frac{1}{2} \left(-\text{tr } X + \sqrt{(\text{tr } X)^2 + \frac{4T}{\Sigma}} \right) \quad (8.19)$$

In principle one can take the trace of both sides and so obtain an equation for

[†]It will be recalled that the width fluctuation correction calculated in Section (7) is 3 rather than 2. The reason for the difference can be seen from (8.11'), which states that for $f = i$,

$$\langle g_\lambda^2(i) g_\lambda^2(i) \rangle = 2 \langle g_\lambda^2 \rangle^2$$

But the left-hand side equals $\langle g_\lambda^4(i) \rangle$. If the Gaussian distribution is used for g_λ [or the Porter-Thomas for $\Gamma_\lambda(i)$], one obtains

$$\langle g_\lambda^4(i) \rangle = 3 \langle g_\lambda^2 \rangle^2 \quad (\text{Porter-Thomas})$$

We see that the pair correlation assumption is not consistent with the Porter-Thomas distribution. The factor of 2 corresponds to an exponential distribution for Γ_λ . This is in agreement with the numerical calculations of Moldauer (75a) in the limit of large $\text{tr } T$.

$\text{tr } X$:

$$(N + \frac{1}{2}) \text{tr } X = \frac{1}{2} \sum_c \sqrt{(\text{tr } X)^2 + \frac{4T_{cc}}{\Sigma}} \quad (8.20)$$

This equation for $\text{tr } X$ is not solvable analytically and one must resort to numerical methods. Tepel, Hoffman, and Weidenmüller (74) provide a simple approximate solution. Here we shall be content with obtaining the first-order correction to (8.16') and solving for $\text{tr } X$. This is accomplished by expanding the square root in (8.19) to second-order. We find that

$$\text{tr } X = \frac{1}{(\sum \text{tr } T)^{1/2}} [(\text{tr } T)^2 - (\text{tr } T^2)]^{1/2} \quad (8.21)$$

Equation (8.16) is obtained if $\text{tr}(T^2)$ is dropped compared to $(\text{tr } T)^2$. Since the former is proportional to N and the latter to N^2 , this appears to be a good approximation. If we now examine the result for X ,

$$X = \left[\frac{\text{tr } T}{\sum [(\text{tr } T)^2 - \text{tr } T^2]} \right]^{1/2} \left(T - \frac{T^2}{\text{tr } T} \right) \sim \frac{1}{[\text{tr } T \Sigma]^{1/2}} \left(T - \frac{T^2}{\text{tr } T} \right) \quad (8.22)$$

(8.16) will be recovered in the limit where $\text{tr } T$ is large. To summarize, the conditions for the validity of (8.16),

$$(\text{tr } T)^2 \gg \text{tr } T^2 \quad (8.23a)$$

and

$$T_{fi} \text{tr } T \gg (T^2)_{fi} \quad (8.23b)$$

Inequality (8.23a) is a necessary condition. It should be borne in mind that the values of the matrix elements of T can be obtained from the multichannel optical model so that inequalities (8.23) can be verified, the matrix elements of X can be obtained approximately from (8.22) or numerically from (8.20) and (8.19), and finally, $\sigma_{fi}^{(FL)}$ from (8.12).

Further discussion will be found in the review by Mahaux and Weidenmüller (79). We have not included the connection of the results above with the understanding of the "precompound" reactions. These are discussed in Chapter VI.

9. APPLICATIONS OF THE STATISTICAL THEORY

The statistical theory of nuclear reactions is applicable when the level density of the residual nucleus is large, that is, when its excitation is sufficiently high, corresponding to the low-energy portion of the spectrum of the emitted particle.

It applies as well at sufficiently low projectile (generally, neutron) energies for which the direct reactions do not make a significant contribution. For high-energy projectiles, the direct reactions dominate. However, the residual nucleus may be left in a highly excited state. Its subsequent decay may be calculated using statistical theory.

A. Angular Distributions

As a consequence of the random-phase hypothesis, the angular distributions are symmetric about 90° . When the residual nucleus is excited to an energy for which all possible orientations of its spin over the surface of a sphere occur with equal probability, the angular distribution is isotropic. An example of isotropy is furnished by an early experiment by Rosen and Stewart (55) from the low-energy portion of the neutron spectrum produced by the inelastic scattering of 14.1-MeV neutrons by Bi (Fig. 9.1). Inelastic scattering to particular levels in ^{209}Bi by 2.5-MeV neutrons [Cranberg, Oliphant, Levin, and Zafaratos (67)] demonstrate the symmetry about 90° (Fig. 9.2). Similar results are shown for ^{206}Pb , with the addition of a small contribution from the direct reaction process. Examples for heavy ions ($^{40}\text{Ar} + ^{77}\text{Sc} \rightarrow \alpha + \text{X}$) and for $^{58}\text{Ni}(\alpha, p)$ were given earlier in Figs. 7.5 and 7.4. The collision of light ions also furnish examples as illustrated in Fig. 9.3.

The success of this prediction, symmetry about 90° , has led to its use to identify reactions that are dominated by statistical processes. As we shall see in Chapter VI, this is not entirely correct, as symmetry about 90° is also a

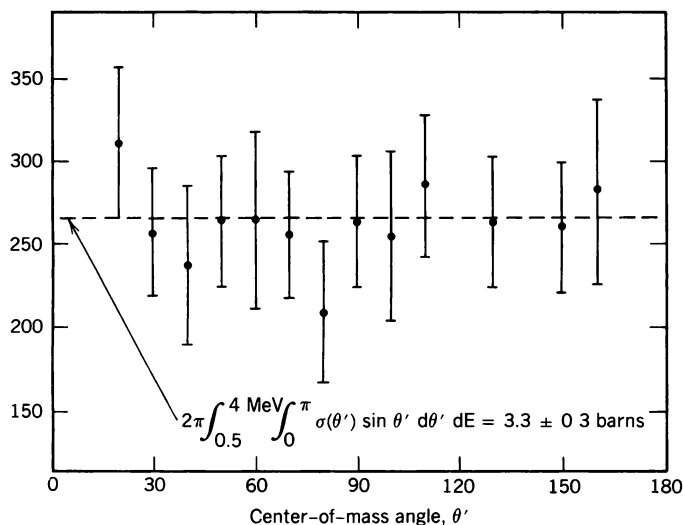


FIG. 9.1. Angular distribution of inelastically scattered 14.1-MeV neutrons from bismuth [Rosen and Stewart (55)]. [From Ribe (63).]

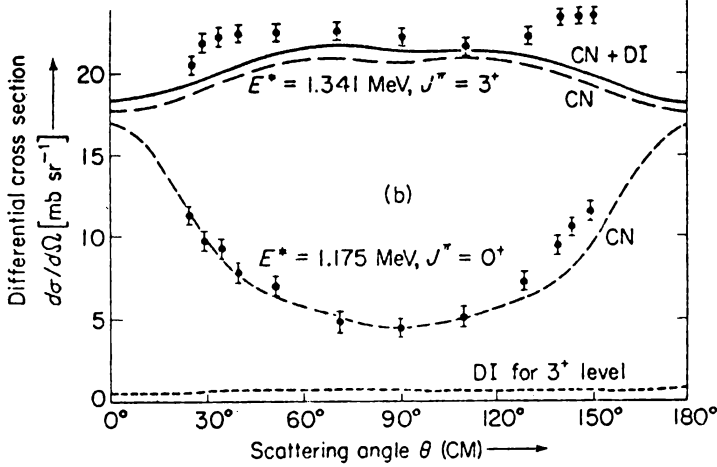


FIG. 9.2. Fits to the measured angular distributions of 2.5-MeV neutrons inelastically scattered to two levels in ^{206}Pb . In the calculation of the compound nucleus cross section (CN) the width fluctuation factor was taken into account. The direct interaction contribution is labeled DI [Cranberg, Oliphant, Levin, and Zafaratos (67)]. [From Marmier and Sheldon (70).]

feature of the statistical multistep compound process of which the statistical theory described in this chapter is a limiting case.

B. Energy Spectrum

We next consider the energy spectrum of the emitted particle, considering the case in which the excitation energy of the residual nucleus is sufficiently high that the residual nucleus levels effectively form a continuum with level density $\omega_f(U)$. The angle integrated cross section in the statistical theory is given by (7.39) multiplied by the width fluctuation correction if needed:

$$\left\langle \frac{d\sigma_{fi}^{(\text{FL})}}{dU} \right\rangle = \pi \lambda_i^2 \sum_f \omega_f(U, J) \frac{2J+1}{(2I+1)(2i+1)} \frac{T_f(J\Pi)T_i(J\Pi)}{\sum_c [T_c + \int dU_c T_c \omega_c(U, J)]} \quad (9.1)$$

where the complete parametric dependence of T_f is $T_f(l's'; J\Pi)$, where we recall that l' is the orbital angular momentum of the emitted particle, and s' is the channel spin. These combine vectorially to form J :

$$l' + s' = J$$

T_i depends similarly on the entrance channel l and s . The level density $\omega_s(U)$ takes into account the spin of the emitted particle i' as well as the spin of the residual nucleus, I' . The denominator sums over all ways in which the compound

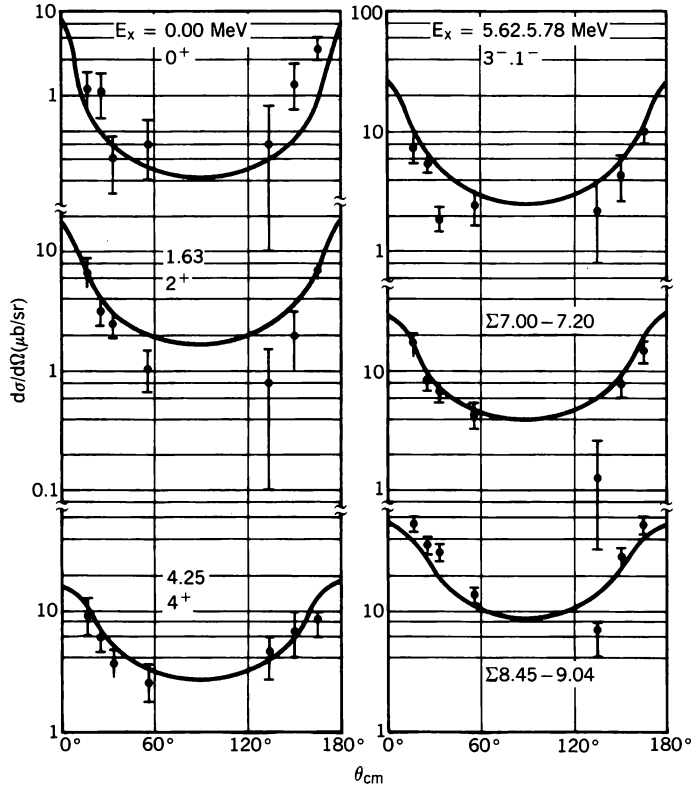


FIG. 9.3. Angular distribution for the reaction $^{12}\text{C}(^{14}\text{N}, ^6\text{Li})^{20}\text{Ne}$, $E_{\text{cm}} = 36$ MeV compared with the predictions of the statistical model (HF) [Belote, Anyas-Weiss, et al. (73)]. [From Stokstad (85).]

system can decay, including different modes of decay symbolized by the subscript c . The decay can occur to discrete levels as well as to the continuum part of the spectrum of the residual nuclei. To obtain the Weisskopf formula, (I.4.5), a number of approximations to (9.1) need to be made. It is assumed that T_f and T_i depend only on the orbital angular momenta l' and l , respectively. Second, we assume, as was done in the derivation of the isotropic angular distribution (see p. 301), that

$$\omega_f(U, J) \simeq (2s' + 1)(2l' + 1)\omega_0(U) \quad (9.2)$$

Finally, the discrete sum in (9.1) is dropped and in fact it is assumed that the residual nucleus for all the exit channels is the same. Inclusion of the effect of other types of exit channels is straightforward and left for the reader to derive.

With these approximations (9.1) becomes

$$\left\langle \frac{d\sigma_{fi}^{(FL)}}{dU} \right\rangle = \pi \lambda_i^2 \omega_0(U) \frac{\sum_{l'} (2l' + 1) T_f(l') \sum_l (2l + 1) T_i(l)}{\sum_{c, l_c} \int dU_c T_c(l_c) (2l_c + 1) \omega_0(U_c)} \quad (9.3)$$

Defining

$$\sigma_a^{(c)} \equiv \pi \lambda_a^2 \sum_l (2l + 1) T_a(l) \quad (9.4)$$

[that this agrees exactly with (7.4)], we obtain the Weisskopf result:

$$\left\langle \frac{d\sigma_{fi}^{(FL)}}{dU_f} \right\rangle = \sigma_i^{(c)}(E) \frac{\mu_F E' \sigma_f^{(c)}(E') \omega_0(U_F)}{\sum_a \int dU_a E'' \sigma_a^{(c)}(E'') \omega_0(U_a) \mu_a} \quad (9.5)$$

where μ_a is the reduced mass of the particle emitted in channel a .

Note that in this derivation no use was made of the law of detailed balance, as is the case for the traditional derivation given in Chapter I. Detailed balance cannot, in fact, be used without further justification since the cross section in (9.5) is energy and state averaged, and detailed balance holds between particular states with well-defined energies. Recall that for a given initial state

$$U_a = E - E' + Q_a$$

where E is the initial kinetic energy in the center-of-mass coordinate system, E' is the final kinetic energy of the emitted particle, and Q_a is the “ Q ” for the reaction. Casting ω_0 into an exponential form,

$$\omega_0 = \exp[S(U)]$$

and expanding $S(E + Q - E')$ about $E + Q$,

$$S(U) = S(E + Q - E') = S(E + Q) - E' \left(\frac{\partial S}{\partial U} \right)_{E+Q=U}$$

one obtains

$$\omega_0 = e^{S(E+Q)} e^{-E'/T} \quad (9.6)$$

where

$$\frac{1}{T} \equiv \left(\frac{\partial S}{\partial U} \right)_{E+Q=U} \quad (9.7)$$

T is referred to as the nuclear temperature. Substituting (9.6) into (9.4) yields

the Weisskopf–Frenkel evaporation formula. When S equals $2\sqrt{a(U - \Delta)}$ (see p. 278),

$$T = \left[\frac{1}{a}(E + Q - \Delta) \right]^{1/2} \quad (9.8)$$

Inserting (9.6) into (9.4), we observe that

$$\frac{1}{E' \sigma_f^{(c)}(E')} \left\langle \frac{d\sigma_{fi}^{(FL)}}{dU} \right\rangle \sim e^{-E'/T} \quad (9.9)$$

where we have omitted multiplicative factors that do not depend on E' . Thus the logarithm of the left-hand side of (9.9) should be a straight-line function of E' with a negative slope equal to $(1/T)$.

Another and somewhat more general result states that for a given E , the left-hand side of (9.9) depends only upon U_f , and in principle one should therefore be able to determine ω_0 . The branching ratio, that is, the ratio of the differential cross sections for two differing reactions initiated by the same

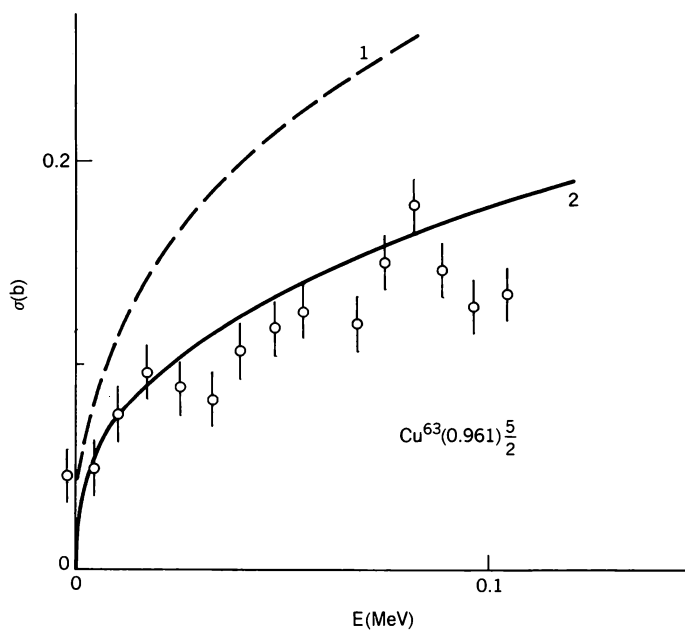


FIG. 9.4. Inelastic neutron scattering exciting the 0.961-MeV level in ^{63}Cu . The curve labeled (1) does not include the width fluctuation factor; curve (2) does. [From Tucker, Wells, and Meyerhoff (65).]

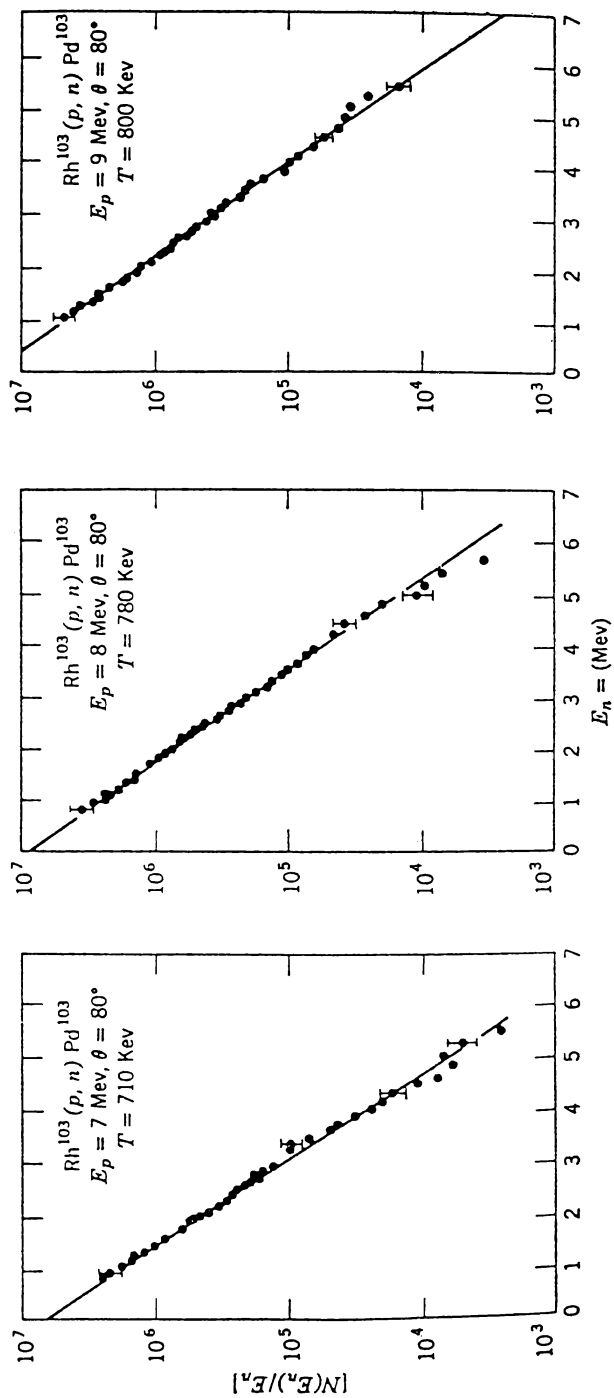


FIG. 9.5. Spectrum of neutrons from the $\text{Rh}(p, n)$ reaction at a neutron emission angle of 80° .
[From Holbrow and Barschall (63).]

projectile, is

$$\frac{\langle d\sigma_{ai}^{(FL)}/dU_a \rangle}{\langle d\sigma_{bi}^{(FL)}/dU_b \rangle} = \frac{\mu_a E_a \sigma_a^{(c)}(E_a) \omega_0(U_a)}{\mu_b E_b \sigma_b^{(c)}(E_b) \omega_0(U_b)} \quad (9.10)$$

The dominant factors in the ratio (if one is well above the thresholds) is given by the ratio of the level densities at the appropriate excitation energies.

We conclude this section with some experimental results that provide examples of the application of these results. We begin with the simplest case, that in which the spin and energies of the levels of the residual nuclei are known up to a sufficiently high energy. Then the cross section is given by (7.38) corrected

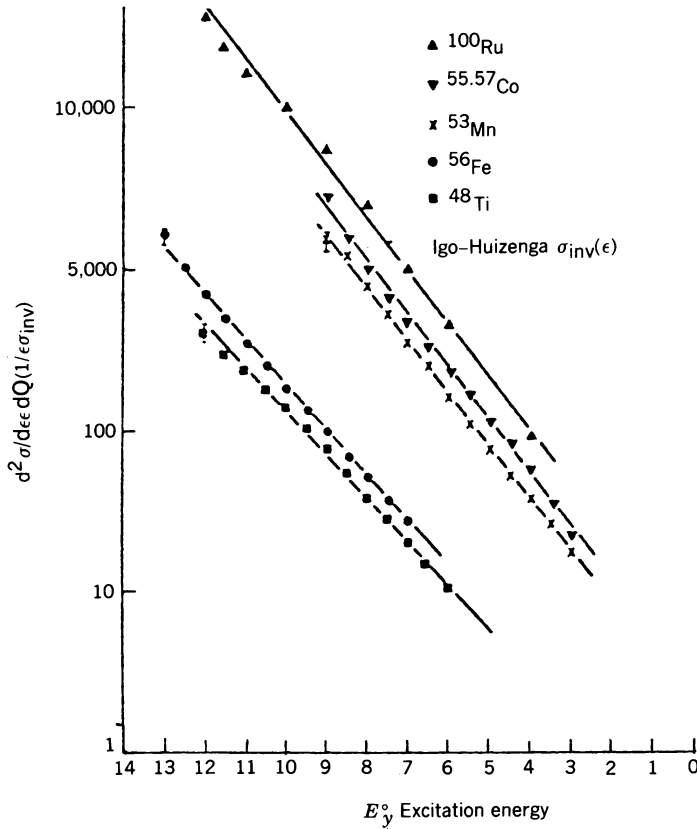


FIG. 9.6. Energy spectra of α -particles plotted as $d^2 \sigma / d\epsilon dQ (1/\epsilon \sigma_{inv})$ versus excitation energy. The inverse cross section σ_{inv} is calculated from an optical model by Igo and Huizenga [Sherr and Brady (61)]. [From Lefort (76).]

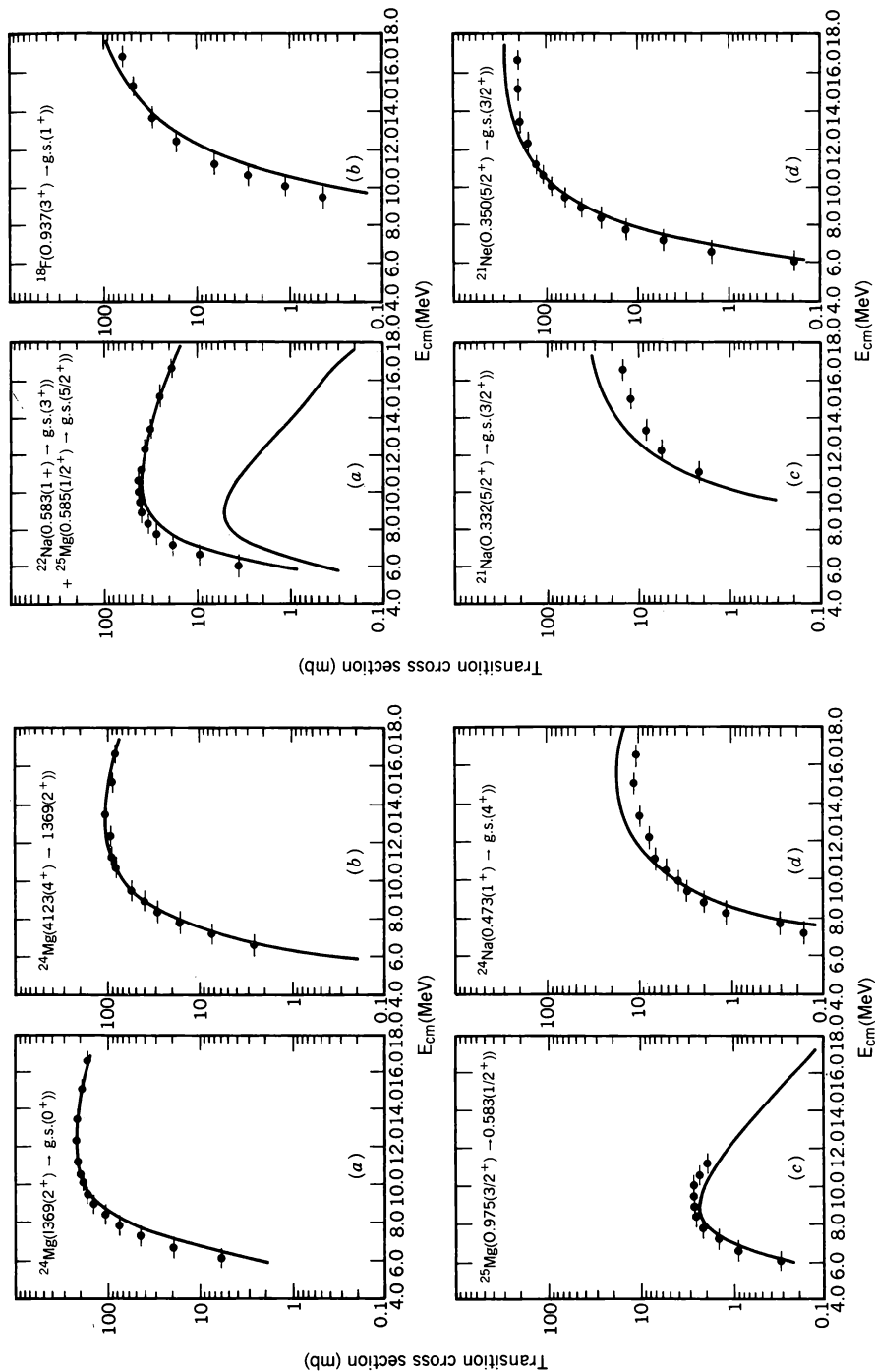


FIG. 9.7. Absolute γ -ray yields from $^{12}\text{C} + ^{14}\text{N}$ -induced reactions. The full curves are absolute Hauser-Feshbach predictions [Erb, Olmer, et al. (73)]. [From Stokstad (85).]

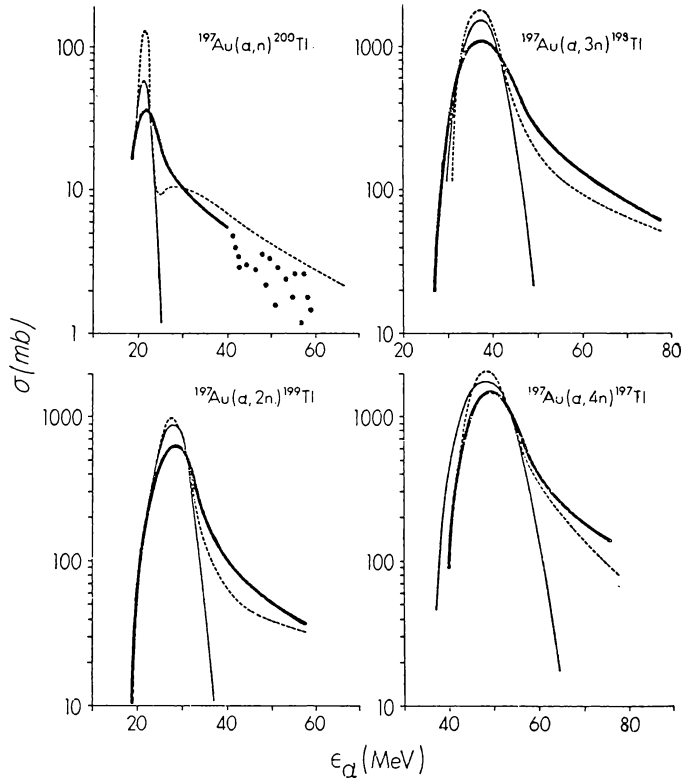


FIG. 9.8. Calculated and experimental excitation functions for the reactions $^{197}\text{Au}(\alpha, xn)$. The heavy solid curves represent experimental yields. The thin solid curves represent equilibrium statistical model calculations. [From Blann (72).]

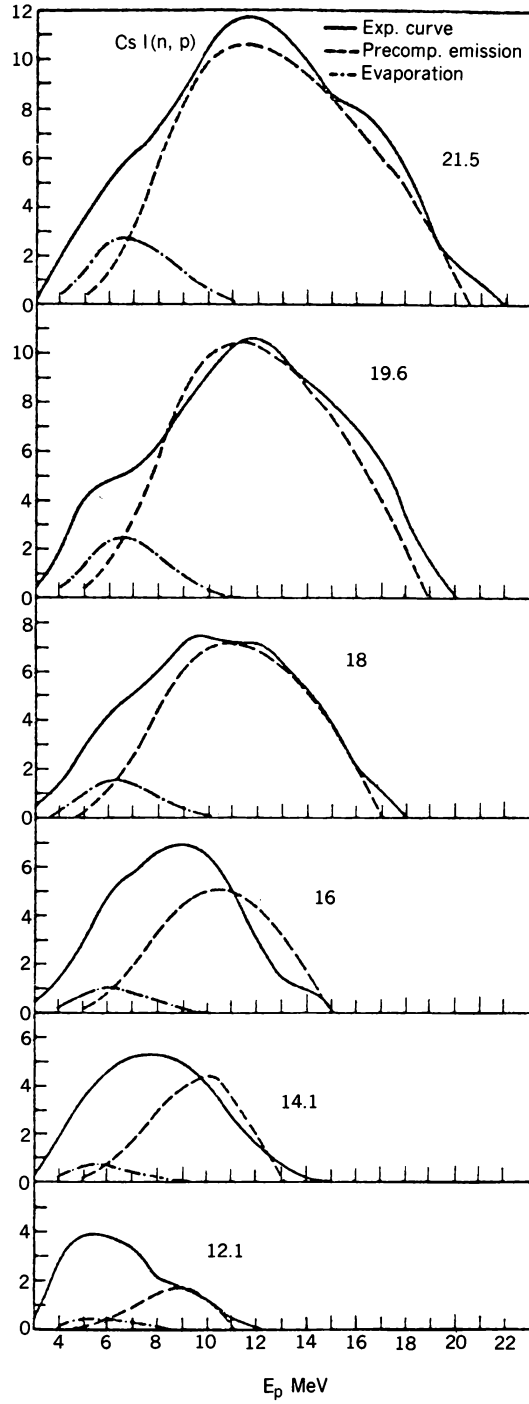
by the width fluctuation correction W_J :

$$\langle \sigma^{(\text{FL})} \rangle = \sum \frac{2J+1}{(2I+1)(2i+1)} \frac{T_f(l', s'; J\Pi) T_i(l, s; J\Pi)}{\sum T_a(l_a, s_a; J\Pi)} W_J \quad (9.11)$$

An example of the application of this formula in which it is assumed that all values of J of the compound system which are allowed by angular momentum and parity conservation are included in the sum is shown in Fig. 9.4. We see the important effect of the width correction factor in some cases.

In Fig. 9.5 we present some of the results of Holbrow and Barschall (63), who considered the $\text{Rh}(p, n)$ reaction. The straight line on the semilog plot is

FIG. 9.9. Comparison between the experimental spectrum for protons emitted in $\text{CsI}(n, p)$ reaction (full line) at various energies and the calculated evaporate (—) and preequilibrium (---) contributions. [From Gadioli and Milazzo-Colli (73).]



in agreement with (9.9) [assuming that $\sigma_f^{(c)}(E')$ is a constant equal to πR^2 , where R is the nuclear radius]. The derivation from the straight line occurs at low neutron energy near the threshold for the $(p, 2n)$ reaction. Another example is given in Fig. 9.6, in which α -particle spectra produced in a (p, α) reaction involving a variety of target nuclei are given. As a final example, the prediction of γ -ray yields in light-ion reactions are shown in Fig. 9.7. Note that no adjustable parameters are used in this case.

The examples given in the section above show, in view of the crudeness of the statistical model, a surprisingly excellent agreement with experiment. This agreement indicates that once entrance and exit channel effects are included through the transmission coefficients, the remaining features of the reactions do not depend on the details of the nuclear Hamiltonian. From the theoretical development of the fundamental equations (7.39) and (9.11), a necessary condition for their validity appears to be that the wave functions involved be sufficiently complicated so that the matrix element of the residual potential with respect to these wave functions is a random number. However, the wave function does have simple components, and if the reaction is dominated by these, statistical considerations will fail. The condition for the validity of the statistical theory is not only that the wave function be complicated but also that the complicated components dominate. A rephrasing of these considerations using time-dependent language is instructive. In the early phase of the reaction, only simple states can be developed, the complicated states requiring a relatively long period of time involving the residual interaction acting many times. If the reaction terminates at an early stage, the statistical theory will fail. Indeed, a direct reaction may be involved, and then the angular distribution will be asymmetric, peaked toward the forward direction. The statistical theory will be valid only if the reaction terminates at a sufficiently late stage. In Chapter VI we discuss a formalism that includes both the early and late stages. That theory will provide criteria for which the statistical theory is a limiting result. For example, at sufficiently low energies, one requires that emission by the system is much less probable than proceeding to the next stage of complication, so that most of the reaction will involve emission from very complicated states.

For the present it will suffice to point to some examples of the failure of the statistical theory. In Fig. 9.8 we present a comparison between the cross section for the production of neutrons as indicated by the collision of α -particles striking ^{197}Au . The failure of the statistical model as the α -particle energy increases is evident. Another example is shown in Fig. 9.9, where the proton spectrum when neutrons of the indicated energies are incident on CsI . Neither the shape nor the magnitude of the evaporation contributions resemble the experimental results. Will the discrepancy be made up by the single step direct process? We shall provide some examples in Chapter VI to show that generally it will not suffice.

CHAPTER V

ELASTIC AND INELASTIC SCATTERING

1. INTRODUCTION

Chapter IV is devoted to the study of reactions involving a relatively long interaction time as exemplified by compound nuclear resonances and by these reactions to which the statistical theory applies. The latter is appropriate when the excitation energy, U , of the residual nucleus is sufficiently large and the energy of the emitted particles are sufficiently small. The angular distribution is symmetrical about 90° and the energy variation of the cross section (assuming sufficiently good resolution) is rapid. In this chapter we consider the direct reaction, that is, prompt reactions (a term that we prefer to use if one could revise history!). In this case the interaction time is relatively short, on the order of the time it would take the projectile to traverse the nucleus. The angular distribution is asymmetric, thereby revealing the direction of the incident projectile. The variation of the cross section with energy is slow, as one would expect to follow from the short interaction time.

According to Chapter III, the governing description for prompt reactions is given by the multichannel optical model. The open channels are the ones usually included but on occasion, particularly near thresholds, it may be important to include closed channels as well. The phrase *optical model* refers to the fact the prompt reactions can be selected by considering the energy-averaged wave function, $\langle P\Psi \rangle$, which satisfies the equation

$$\left[E - H_{PP} - H_{PQ} \frac{1}{E - H_{QQ} + iI/2} H_{QP} \right] \Psi^{(\text{opt})} = 0 \quad (1.1)$$

where

$$\Psi^{(\text{opt})} = \langle P\Psi \rangle \quad (1.2)$$

In this equation, I is the energy interval over which the average is taken. It clearly has the function of smoothing the dependence of the propagator $(E - H_{QQ} + iI/2)^{-1}$ upon the energy. It is this term that takes into account the effect of the closed channels upon the optical model wave function. The function $\Psi^{(\text{opt})}$ is a multicomponent wave function of dimension equal to the number of channels included in \mathcal{P} space. If (1.1) is written in terms of the channel wave functions, it becomes a set of coupled Schrödinger equations.

In the approximate treatment of these coupled equations, the elastic channel plays a central role. We project it out by introducing the projection operator p and its orthogonal complement R . Defining $H^{(\text{opt})}$ by

$$H^{(\text{opt})} \equiv H_{pp} + H_{pQ} \frac{1}{E - H_{QQ} + iI/2} H_{Qp} \quad (1.3)$$

(1.1) can be rewritten as follows:

$$\begin{aligned} (E - H_{pp}^{(\text{opt})})\psi_{el} &= H_{pR}^{(\text{opt})}\psi_R \\ (E - H_{RR}^{(\text{opt})})\psi_R &= H_{Rp}^{(\text{opt})}\psi_{el} \end{aligned} \quad (1.4)$$

using the notation

$$H_{pR}^{(\text{opt})} = pH^{(\text{opt})}R, \quad \text{etc.}$$

The wave function ψ_R is a multicomponent wave function containing all the reaction channels with the exception of the elastic channel, whose wave function is given by ψ_{el} . We can solve for ψ_R bearing in mind that the channels involved are open:

$$\psi_R = \frac{1}{E^{(+)} - H_{RR}^{(\text{opt})}} H_{Rp}^{(\text{opt})} \psi_{el} \quad (1.5)$$

Therefore, ψ_{el} satisfies

$$\left[E - H_{pp}^{(\text{opt})} - H_{pR}^{(\text{opt})} \frac{1}{E^{(+)} - H_{RR}^{(\text{opt})}} H_{Rp}^{(\text{opt})} \right] \psi_{el} = 0 \quad (1.6)$$

Note that

$$H_{pp}^{(\text{opt})} = H_{pp} + H_{pQ} \frac{1}{E - H_{QQ} + iI/2} H_{Qp} \quad (1.7)$$

We see that the elastic channel wave function satisfies a Schrödinger equation with a complex and, therefore, absorptive interaction. The absorption has two sources. One is loss of flux from the incident channel, is produced by the prompt reactions that can occur. This is described by the third term, involving the subscript R , in brackets in (1.6). The other source stems from the fact that $\Psi^{(\text{opt})}$, and therefore, ψ_{el} , are the results of an energy average of $P\Psi$. Following Friedman and Weisskopf (55), it can be argued that taking the energy average is equivalent to selecting the prompt component of $P\Psi$. In terms of the development under discussion here, this conclusion follows from the fact that $H^{(\text{opt})}$ is a smooth function of E . The function $\Psi^{(\text{opt})}$, and therefore ψ_{el} , will exhibit an absorption because they do not contain the delayed component of $P\Psi$. In more picturesque terms, the wave packet formed by taking the energy average is attenuated on passing through the nucleus, because some of its flux is left behind to form the compound nucleus. This flux will be emitted later. It is this process that is described by the second term in brackets in (1.6). This effect is present even when only elastic scattering is possible, that is, for energies below the threshold for nonelastic reactions.

In principle, (1.6) can be used to determine the averaged elastic scattering amplitude. To determine the reaction amplitude leading to a particular channel c , we project out that channel with an operator c so that (1.4) becomes

$$(E - H_{pp}^{(\text{opt})})\psi_{\text{el}} = H_{pc}^{(\text{opt})}\psi_c + H_{pr}^{(\text{opt})}\psi_r \quad (1.8a)$$

$$(E - H_{cc}^{(\text{opt})})\psi_c = H_{cp}^{(\text{opt})}\psi_{\text{el}} + H_{cr}^{(\text{opt})}\psi_r \quad (1.8b)$$

$$(E - H_{rr}^{(\text{opt})})\psi_r = H_{rp}^{(\text{opt})}\psi_{\text{el}} + H_{rc}^{(\text{opt})}\psi_c \quad (1.8c)$$

where

$$R = c + r \quad \text{and} \quad cr = 0$$

Note that if ψ_r and ψ_c are eliminated, the resulting equation for ψ_{el} must be identical to (1.6). If ψ_r is eliminated, one obtains a pair of coupled equations for ψ_{el} and ψ_c . The inclusion of the effect of the other open channels

Problem. Show that these coupled equations for ψ_{el} and ψ_c are

$$\begin{aligned} (E - \mathcal{H}_{pp})\psi_{\text{el}} &= \mathcal{H}_{pc}\psi_c \\ (E - \mathcal{H}_{cc})\psi_c &= \mathcal{H}_{cp}\psi_{\text{el}} \end{aligned} \quad (1.9)$$

where

$$\begin{aligned} \mathcal{H} &= H^{(\text{opt})} + W \\ W_{ab} &= H_{ar}^{(\text{opt})} \frac{1}{E^{(+)} - H_{rr}^{(\text{opt})}} H_{rb}^{(\text{opt})} \end{aligned} \quad (1.10)$$

Show that the transition matrix for the excitation of c is

$$\langle \mathcal{T}_{ci} \rangle = \langle \phi_c^{(-)} | \mathcal{H}_{cp} \psi_{ei}^{(+)} \rangle \quad (1.11)$$

where

$$(E - \mathcal{H}_{cc})\phi_c^{(-)} = 0 \quad (1.12)$$

which are projected by r is required if multistep processes are important. If it is assumed that only a single-step process is important, the DWA (distorted wave approximation) is used. In this approximation [Lamarsh and Feshbach (65)] the exact equation for ψ_{ei} , (1.6), is used and (1.8b) is replaced by

$$(E - H_{cc}^{(\text{opt})})\psi_c \simeq H_{cp}^{(\text{opt})}\psi_{ei} \quad (1.13)$$

so that

$$\langle \mathcal{T}_{ci} \rangle = \mathcal{T}_{ci}^{(\text{dir})} \simeq \langle \chi_c^{(-)} | H_{cp}^{(\text{opt})} \psi_{ei}^{(+)} \rangle \quad (1.14)$$

where

$$(E - H_{cc}^{(\text{opt})})\chi_c^{(-)} = 0 \quad (1.15)$$

Comparing with the exact expression (1.11) we see that $\mathcal{H}_{pc}^\dagger \phi_c^{(-)}$ has been approximated by $H_{pc}^\dagger \chi_c^{(-)}$. The coupling of the channel c to the open channels r has been neglected in both H_{pc}^\dagger and $\chi_c^{(-)}$. The waves $\chi_c^{(-)}$ and ψ_{ei} are distorted (i.e., are not plane waves) because of the potential terms present in $H_{cc}^{(\text{opt})}$ and in the effective Hamiltonian for the single-channel wave function ψ_{ei} as given by (1.6). The approximate equation (1.14) for the transition amplitude is referred to as the *distorted wave born approximation* (DWA). Using the DWA requires the determination of the single-channel wave functions $\psi_{ei}^{(+)}$ and $\chi_c^{(-)}$, as well as the coupling Hamiltonian H_{cp} . We discuss the first of these issues in the next section.

Note. In many applications of the DWA, the interaction Hamiltonian used in the calculation, (1.14), is empirically determined using parameter choices that produce best fits to the data. As a consequence, many of the effects of the omitted open channels are included to the extent that this is permitted by the forms used for the Hamiltonian. However, when these effects are too severe, it may be necessary to recognize their importance through the use of a system of coupled-channel Schrödinger equations, taking explicitly into account those channels that have the major impact.

2. THE SINGLE-CHANNEL OPTICAL MODEL

The empirical optical model is used to develop the single-channel wave functions required by the DWA. The model was developed originally to provide an

understanding of the low-energy neutron–nucleus interaction as observed by Barschall and his collaborators [Barschall (52)]. Although it was derived in the sense that it was shown that the model wave function and model scattering amplitude were energy averages of the exact wave function and exact scattering amplitude, the optical model has been used since semiempirically. An *a priori* form is chosen for the optical model potential, that is, for the Hamiltonian of (1.6). Its parameters are then adjusted so as to yield agreement with the data, such as the total cross section σ_T ; the elastic angular distributions $d\sigma_{el}/d\Omega$; the polarization of the emergent particles, if available; and so on. Smooth behavior of the parameters with respect to changes in projectile energy and target are desired for physical significance. Substantial discontinuities may imply the presence of a phenomenon for which the single-channel optical model is inadequate, requiring, perhaps, the use of a multichannel optical model.

A. Average Cross Sections

Since in the optical model the scattering amplitude is energy averaged, the optical model cross section $\langle\sigma\rangle$ cannot, except for one situation, be compared directly with the energy-averaged cross sections, $\bar{\sigma}$, since cross sections are quadratic functions of the scattering amplitude. The one exception is the total cross section σ_T , since it is a linear function of the amplitude in virtue of the optical theorem:

$$\sigma_T = \frac{4\pi}{k} \text{Im } f(0^\circ) \quad (2.1)$$

Energy averaging[†] both sides then gives the result

$$\langle\sigma_T\rangle = \bar{\sigma}_T \quad (2.2)$$

that is, the optical model total cross section equals the energy-averaged total cross section. This is not the case for the angular distribution or other observables. In those cases we have from (IV.7.7)

$$|\mathcal{F}_{fi}|^2 = |\mathcal{F}_{fi}^{(\text{opt})}|^2 + |\mathcal{F}_{fi}^{(\text{FL})}|^2$$

Averaging, one obtains

$$\bar{\sigma}_{el} = \langle\sigma_{el}\rangle + \bar{\sigma}_{el}^{(\text{FL})} \quad (2.3)$$

Before the optical model can be compared with experiment, the fluctuation cross section, $\bar{\sigma}^{(\text{FL})}$, must be added to optical model cross section $\langle\sigma_{el}\rangle$.

[†]Angular brackets are used to indicate model quantities and a bar indicates energy-averaged quantities.

The optical model also predicts an absorption cross section $\langle \sigma_r \rangle$, which is related to $\langle \sigma_T \rangle$ as follows:

$$\langle \sigma_r \rangle = \langle \sigma_T \rangle - \langle \sigma_{el} \rangle \quad (2.4)$$

A similar quantity can be defined for the energy-averaged cross sections

$$\bar{\sigma}_r = \bar{\sigma}_T - \bar{\sigma}_{el} \quad (2.5)$$

The relationship between $\bar{\sigma}_r$ and $\langle \sigma_r \rangle$ follows from (2.2) and (2.3):

$$\langle \sigma_r \rangle = \bar{\sigma}_r + \bar{\sigma}_{el}^{(FL)} \quad (2.6)$$

The first term, $\bar{\sigma}_r$, is a consequence of real inelastic processes, while $\bar{\sigma}_{el}^{(FL)}$ represents the contribution of the delayed processes. We have discussed the presence of these two contributions in Section 1 [see (1.6) and the ensuing discussion].

The cross section $\bar{\sigma}_{el}^{(FL)}$, is just the compound elastic scattering that was discussed in Chapter IV. Its calculation in terms of transmission factors is given there. One expects processes competitive with compound elastic scattering would become so significant as the projectile energy increases that $\bar{\sigma}_{el}^{(FL)}$ would tend to zero as that energy increases. In other words, the fraction of the flux that is delayed and reemitted into the elastic channel eventually decreases with energy. Most of the delayed flux will contribute to reactions. In the limit, then,

$$\begin{aligned} \langle \sigma_r \rangle &\rightarrow \bar{\sigma}_r \\ \langle \sigma_{el} \rangle &\rightarrow \bar{\sigma}_{el} \end{aligned} \quad (2.7)$$

The cross section $\langle \sigma_r \rangle$ is directly related to the transmission coefficients T_c [see (IV.7.28)]. From this last equation and for the single-channel case, each partial wave yields

$$T_c = 1 - |\langle S_{cc} \rangle|^2$$

The corresponding partial reaction cross section is

$$\langle \sigma_r^{(c)} \rangle = \pi \lambda^2 T_c$$

which must be multiplied by the appropriate weighting factor for each partial wave. For a spin-independent optical model potential the partial wave series is a series in the orbital angular momentum, l . In that case the weighting factor is $2l + 1$. Comparing with (IV.7.45), one finds that this cross section is identical with the $\sigma^{(c)}$, the cross section for the formation of the compound nucleus, so that

$$\langle \sigma_r \rangle = \sigma^{(c)} \quad (2.8)$$

B. Nonlocal Potentials

It is immediately obvious from the general expression (1.1) for the multichannel optical model, and *a fortiori* for the single-channel projection, (1.7), that the optical model Hamiltonian is energy dependent and nonlocal. The energy dependence is explicitly visible [see (1.1)] in the propagator $(E - H_{QQ} + iI/2)^{-1}$. The nonlocality originates in this term since it describes the process in which the system leaves the incident channel, going to \mathcal{Q} space, propagates in \mathcal{Q} space and then returns to the incident channel. In coordinate space this operator would be a function of two variables, the point at which the interaction, H_{QP} , induces the transition to \mathcal{Q} space and the point at which the interaction, H_{PQ} , induces the return to \mathcal{P} space.[‡]

Such a nonlocal energy-dependent operator can also be thought of as an energy- and momentum-dependent operator. To see this, let the nonlocal potential \mathcal{V} (assumed spin independent, for simplicity) have the general form

$$\mathcal{V}\psi = \int v_E(\mathbf{r}, \mathbf{r}' - \mathbf{r})\psi(\mathbf{r}') d\mathbf{r}' \quad (2.9)$$

where the subscript E reminds us that v is energy dependent. This reduces to a local operator if

$$v_E(\mathbf{r}, \mathbf{r}' - \mathbf{r}) = \delta(\mathbf{r}' - \mathbf{r})v_E(\mathbf{r}) \quad (2.10)$$

since substituting in (2.9) yields

$$\mathcal{V}\psi = v_E(\mathbf{r})\psi(\mathbf{r})$$

Upon making the substitution

$$\mathbf{r}' - \mathbf{r} = \boldsymbol{\rho}$$

in (2.9), one obtains

$$\mathcal{V}\psi = \int v_E(\mathbf{r}, \boldsymbol{\rho})\psi(\mathbf{r} + \boldsymbol{\rho}) d\boldsymbol{\rho}$$

or using the identity

$$e^{i\hbar\boldsymbol{\rho}\cdot\mathbf{p}}\psi(\mathbf{r}) = \psi(\mathbf{r} + \boldsymbol{\rho})$$

[‡]One should combine this dynamic nonlocality, with the contribution of the nonlocality of the nucleon-nucleon forces, a consequence of the composite structure of the nucleon. From the existence of the excited state of the nucleon, the Δ at 1236 MeV, one estimates the size of the nucleon to be $\hbar/(m_\Delta - M_N)c \sim 0.7$ fm.

where

$$\mathbf{p} = \frac{\hbar}{i} \nabla_r \quad (2.11)$$

one obtains

$$\mathcal{V}\psi = \left(\int v_E(\mathbf{r}, \boldsymbol{\rho}) e^{i/\hbar \boldsymbol{\rho} \cdot \mathbf{p}} d\boldsymbol{\rho} \right) \psi(\mathbf{r})$$

Thus the nonlocal potential acting on ψ given by (2.9) can be written as an energy- and momentum-dependent potential

$$\mathcal{V} = V_E(\mathbf{r}, \mathbf{p}) \equiv \int v_E(\mathbf{r}, \boldsymbol{\rho}) e^{i/\hbar \boldsymbol{\rho} \cdot \mathbf{p}} d\boldsymbol{\rho} \quad (2.12)$$

Clearly, the \mathbf{p} in the exponent operates on ψ and not on v_E .

For the most general operator $v_E(\mathbf{r}, \boldsymbol{\rho})$ V_E will contain all powers of the momentum operator \mathbf{p} . Two approximations that are commonly used are instructive. In the first, most appropriate at high energy [Perey and Saxon (64)] the momentum operator, \mathbf{p} , is replaced by the projectile momentum (in the center of mass) \mathbf{p}_0 , so that

$$\mathcal{V} \simeq V_E(\mathbf{r}, \mathbf{p}_0) = \int v_E(\mathbf{r}, \boldsymbol{\rho}) e^{i/\hbar \boldsymbol{\rho} \cdot \mathbf{p}_0} d\boldsymbol{\rho} \quad (2.13)$$

With this approximation, \mathcal{V} becomes just a function of E , the energy, and of \mathbf{r} . We note one important consequence of (2.13). Assuming that the dependence of v_E on $\boldsymbol{\rho}$ is smooth, that is, significant changes occurring over a range, a , then V_E will decrease with increasing momentum p_0 , once $p_0 \geq \hbar/a$. Such a decrease would be modulated by the explicit energy dependence.[†] Indeed, as we shall discuss later, such a decrease does occur, the real part of the optical model potential going through a zero near a projectile energy of 200 MeV. In the present context, this could be considered to be the consequences of an averaging that occurs once the wave length (\hbar/p_0) of the projectile is much smaller than the scale of the nonlocality.

The Perey–Saxon momentum approximation can be improved by using the momentum inside the interaction region [Frahn (65)] rather than that of the incident projectile. In this local momentum approximation one expands $V_E(\mathbf{r}, \mathbf{p})$

[†]An empirical analysis omitting explicit E dependence yields ~ 1 fm, or a p_0 very close to the Fermi momentum p_F . As can be seen from the high-energy multiple scattering approximation for the optical potential (Chapter II), the nonlocal term is in part a consequence of correlations. The empirical scale, p_F , could be taken to indicate that the Pauli correlations generated by the exclusion principle is the one of significance.

about $p^2 = P^2$, that is,

$$V_E(\mathbf{r}, \mathbf{p}) \equiv \bar{V}_E(\mathbf{r}, p^2) \simeq \bar{V}_E(\mathbf{r}, P^2) + \left[\frac{\partial \bar{V}_E(\mathbf{r}, p^2)}{\partial p^2} \right]_{p^2=P^2} (p^2 - P^2) \quad (2.14)$$

where we have made explicit use of the assumption that V_E depends only on p^2 . Inserting (2.14), replacing \mathbf{p} by $(\hbar/i)\nabla$, into the Schrödinger equation yields

$$\left\{ E + \frac{\hbar^2}{2m} \nabla^2 - \bar{V}_E(\mathbf{r}, P^2) - V_L(\mathbf{r}) - 2m \left[\frac{\partial \bar{V}_E(\mathbf{r}, p^2)}{\partial p^2} \right]_{p^2=P^2} \left[\left(\frac{\hbar^2}{2m} \nabla^2 + \frac{P^2}{2m} \right) \right] \right\} \psi = 0$$

where $V_L(\mathbf{r})$ is the local part of the optical model potential, H_{pp} of (1.1). If we now chose $P^2(\mathbf{r})$ to satisfy

$$\frac{1}{2m} P^2(\mathbf{r}) = E - \bar{V}_E(\mathbf{r}, P^2(\mathbf{r})) - V_L(\mathbf{r}) \quad (2.15)$$

this Schrödinger equation reduces to

$$\left[\frac{\hbar^2}{2M} \nabla^2 + (E - \bar{V}_E(\mathbf{r}, P^2(\mathbf{r})) - V_L(\mathbf{r})) \right] \psi = 0 \quad (2.16)$$

Equation (2.15) reduces to the choice $P = p_0$ when $V_L + \bar{V}_E \ll E$, that is, at high energies. It is otherwise an equation determining $P^2(\mathbf{r})$ and therefore the effective potential in (2.16).

Problem. Consider $v_E(\mathbf{r}, \mathbf{p}) = U(\mathbf{r})[1/(\pi^{1/2}a)^3]e^{-\rho^2/a^2}$. Solve (2.15) graphically, discussing the behavior of $\bar{V}_E(\mathbf{r}, P^2(\mathbf{r}))$ as a function of E . Discuss the validity of the expansion equation (2.14). If a is on the order of 1 fm, beyond what energy can this nonlocal potential be treated as a small perturbation?

When the wave length of the incident projectile is long, an expansion of the exponential operator in (2.12) is appropriate:

$$V_E(\mathbf{r}, \mathbf{p}) = \int v_E(\mathbf{r}, \boldsymbol{\rho}) d\boldsymbol{\rho} + \frac{1}{\hbar} \int v_E(\mathbf{r}, \boldsymbol{\rho}) \boldsymbol{\rho} \cdot \mathbf{p} d\boldsymbol{\rho} + \frac{1}{2} \left(\frac{i}{\hbar} \right)^2 \int v_E(\mathbf{r}, \boldsymbol{\rho}) (\boldsymbol{\rho} \cdot \mathbf{p})^2 d\boldsymbol{\rho} + \dots$$

The first term yields a local energy-dependent potential,

$$v_E(\mathbf{r}) \equiv \int v_E(\mathbf{r}, \boldsymbol{\rho}) d\boldsymbol{\rho}$$

The second term vanishes if we assume that the dependence of $v_E(\mathbf{r}, \boldsymbol{\rho})$ on $\boldsymbol{\rho}$ is spherical, that is, depends only on ρ^2 . (This may not be the case for deformed

nuclei or if the spin degree of freedom is taken into account). Under the same assumption the third term becomes

$$\frac{\partial V_E}{\partial p^2} = -\frac{p^2}{6\hbar^2} \int v_E(\mathbf{r}, \mathbf{p}) \rho^2 d\mathbf{p}$$

so that with $k = p/\hbar$,

$$V_E(\mathbf{r}, \mathbf{p}) \simeq v_E(\mathbf{r}) + \left(\frac{\partial V_E}{\partial k^2} \right) k^2 = v_E(\mathbf{r}) - \left(\frac{1}{2k} \frac{\partial V_E}{\partial k} \right) \nabla^2 \quad (2.17)$$

demonstrating explicitly the momentum dependence of the nonlocal $V_E(\mathbf{r}, \mathbf{p})$. The partial derivatives are evaluated at $k=0$. This momentum- and energy-dependent potential can be written as an energy-dependent potential as follows. The optical model Schrödinger equation following from (2.17) is

$$\left[\frac{\hbar}{2m} \nabla^2 + E - V_L - v_E(r) + \frac{1}{2k} \frac{\partial V_E}{\partial k} \nabla^2 \right] \psi = 0 \quad (2.18a)$$

or

$$\left\{ \nabla^2 + \frac{2m}{\hbar^2} \left[E - V_L - v_E - \frac{(m/\hbar^2 k)(\partial V_E/\partial k)}{1 + (m/\hbar^2 k)(\partial V_E/\partial k)} (E - V_L - v_E) \right] \right\} \psi = 0 \quad (2.18b)$$

In discussing this equation one should bear in mind that v_E and $\partial V_E/\partial k$ may both be complex.

On the other hand, one could replace the energy dependence of the nonlocal potential by momentum dependence. Toward this end, expand v_E as follows:

$$v_E = v_0 + E \left(\frac{\partial v_E}{\partial E} \right)_0 + \dots$$

In this equation we now replace E by

$$E \rightarrow -\frac{\hbar^2}{2m} \nabla^2 + V_L + v_0$$

where we have dropped the term in $\partial V/\partial k^2$ as being of higher order when multiplied by $\partial v_E/\partial E$. The Schrödinger equation, (2.18a), becomes to this order

$$\left\{ \left[\frac{\hbar^2}{2m} + \frac{1}{2k} \frac{\partial V_E}{\partial k} + \frac{\hbar^2}{2m} \left(\frac{\partial v_E}{\partial E} \right)_0 \right] \nabla^2 + E - (V_L + v_0) \left(1 + \frac{\partial v_E}{\partial E} \right)_0 \right\} \psi = 0 \quad (2.19)$$

The brackets multiplying ∇^2 can be related to a space-dependent complex effective mass, m_c^*

$$\frac{\hbar^2}{2m_c^*} = \frac{\hbar^2}{2m} + \frac{1}{2k} \frac{\partial V_E}{\partial k} + \frac{\hbar^2}{2m} \left(\frac{\partial v_E}{\partial E} \right)_0$$

or

$$\frac{m_c^*}{m} = \frac{1}{1 + (m/\hbar^2 k)(\partial V_E/\partial k) + (\partial v_E/\partial E)_0}$$

Define m_{Ec} and m_{kc} by

$$\frac{m_{Ec}}{m} \equiv 1 - \left(\frac{\partial v_E}{\partial E} \right)_0 \quad (2.20a)$$

$$\frac{m_{kc}}{m} \equiv \frac{1}{1 + (m/\hbar^2 k)(\partial V_E/\partial k)} \quad (2.20b)$$

where m_{Ec} depends on the change in mass arising from energy dependence and m_{kc} depends on the change due to momentum dependence. Then to first order,

$$\frac{m_c^*}{m} = \frac{m_{Ec}}{m} \frac{m_{kc}}{m} \quad (2.21)$$

This equation is satisfied exactly in the case of infinite nuclear matter [Migdal (61); Brown (72); the case m_{kc}/m is given in Feshbach (58b)]. No attempt has been made to separate out the imaginary components of m_c^* , m_{Ec} , and m_{kc} . If real values are desired, we define

$$\frac{m_E}{m} \equiv 1 - \operatorname{Re} \left(\frac{\partial v^{(0)}}{\partial E} \right)_0 \quad \frac{m_k}{m} = \frac{1}{1 + (m/\hbar^2 k) \operatorname{Re}(\partial V_E/\partial k)} \quad (2.22a)$$

with

$$\frac{m^*}{m} = \frac{m_k}{m} \frac{m_E}{m} \quad (2.22b)$$

We note that for finite nuclei these quantities are functions of \mathbf{r} ; in the case of infinite nuclear matter they are constants.

Evaluations of these quantities have been made for infinite nuclear matter using the Brueckner–Hartree–Fock approximation, similar to that described in Chapter VII of de Shalit and Feshbach (74) [Jeukenne, Lejeune, and Mahaux (76, 77); Mahaux (78)]. Brueckner–Hartree–Fock determinations of the optical potential have also been made by Brieva and Rook (77, 78) and Brieva, Geramb, and Rook (78). We shall not discuss these relatively complex calculations but

will use the results of the Liege group to illustrate the behavior of these effective masses with momentum in infinite nuclear matter. Usually the results obtained with a first-order calculation indicated by the subscript 1 will be presented. Higher-order calculations have been made. There are quantitative changes, but the qualitative picture is not modified. In Figs. 2.1 and 2.2 we show the behavior of m_{E1} as a function of k for two nucleon densities, $k_F = 1.35 \text{ fm}^{-1}$ and $k_F = 1.10 \text{ fm}^{-1}$. Two features should be noted. First, m_{E1}/m is greater than unity for $k < 1.5k_F$, and second, it has a sharp peak just above $k = k_F$. This last result depends critically on the choice of the reference spectrum (see Chapter VII of deShalit and Feshbach (74). If a sizable gap is introduced, the sharp energy dependence seen in Figs. 2.2 and 2.3 disappears. The calculated m_{k1}/m are shown in Fig. 2.3. This quantity increases smoothly as the momentum increases. Its value is less than unity, compensating to some extent for m_{E1}/m being greater than unity, in the calculation of the product, (2.23). The values for m_1^*/m are shown in Figs. 2.4 and 2.5.

The strong variation with k in m_{k1}/m persists in the values of m_1^*/m . From each of these sets of curves, Figs. 2.1 to 2.5, it is clear that in the momentum range $k \leq 2k_F$, the deviation of the effective mass from unity is substantial and

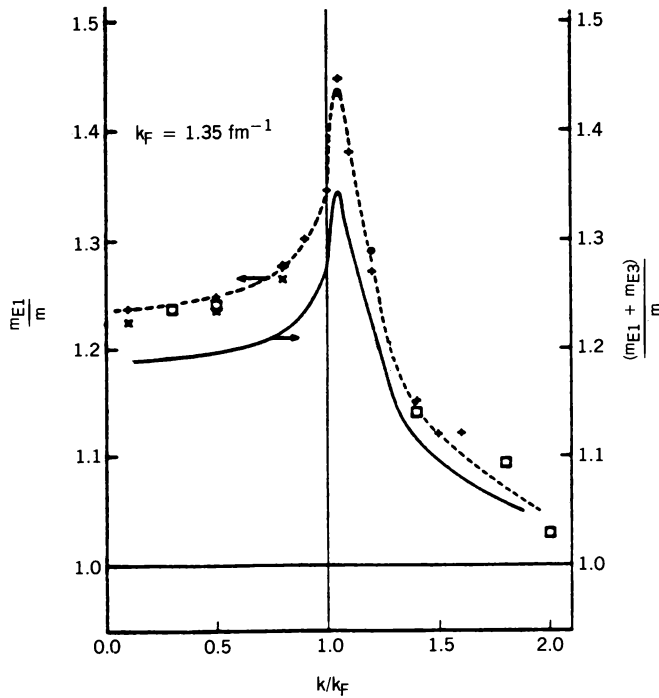


FIG. 2.1. Effective mass m_{E1}/m (dashed curve) and $(m_{E1} + m_{E3})/m$ (solid line) as a function of k for $k_F = 1.35 \text{ fm}^{-1}$. [From Jeukenne, Lejeune, and Mahaux (76).]

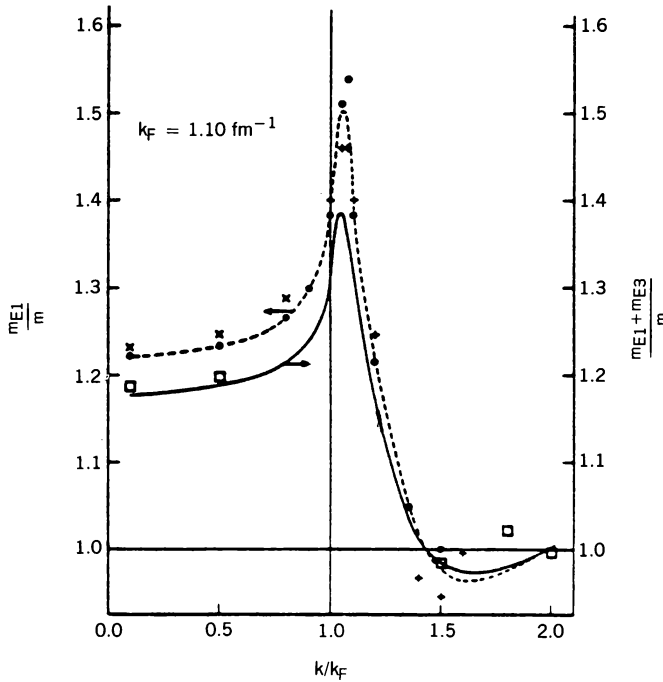


FIG. 2.2. Effective mass m_{E1}/m (dashed curve) and $(m_{E1} + m_{E3})/m$ (solid line) as a function of k for $k_F = 1.10 \text{ fm}^{-1}$. [From Jeukenne, Lejeune, and Mahaux (76).]

that there are appreciable effects arising from the nonlocal nature and energy dependence of the optical potential.

There are two consequences of nonlocality and energy dependence that are of special importance for applications. It follows directly from (2.9) (i.e., from nonlocality) that current conservation is not satisfied locally. This result holds also in the effective mass approximation. Using standard procedures (and taking m^* to be real in order to isolate the effect of interest; current conservation is, of course, not valid in the presence of absorption), it follows from (2.19) that

$$\frac{\partial \rho}{\partial t} + \text{div } \mathbf{j} = \left(1 - \frac{m}{m^*(r)}\right) \text{div } \mathbf{j} \quad (2.23)$$

where \mathbf{j} , the current density, and ρ , the particle density, are given by

$$\mathbf{j} = \frac{\hbar}{2mi} [\psi^* \nabla \psi - \psi \nabla \psi^*] \quad \rho = \psi^* \psi$$

From this current-conservation equation we see that in addition to the decrease in particle density because of current flow, there is a loss ($m^* < m$) because of

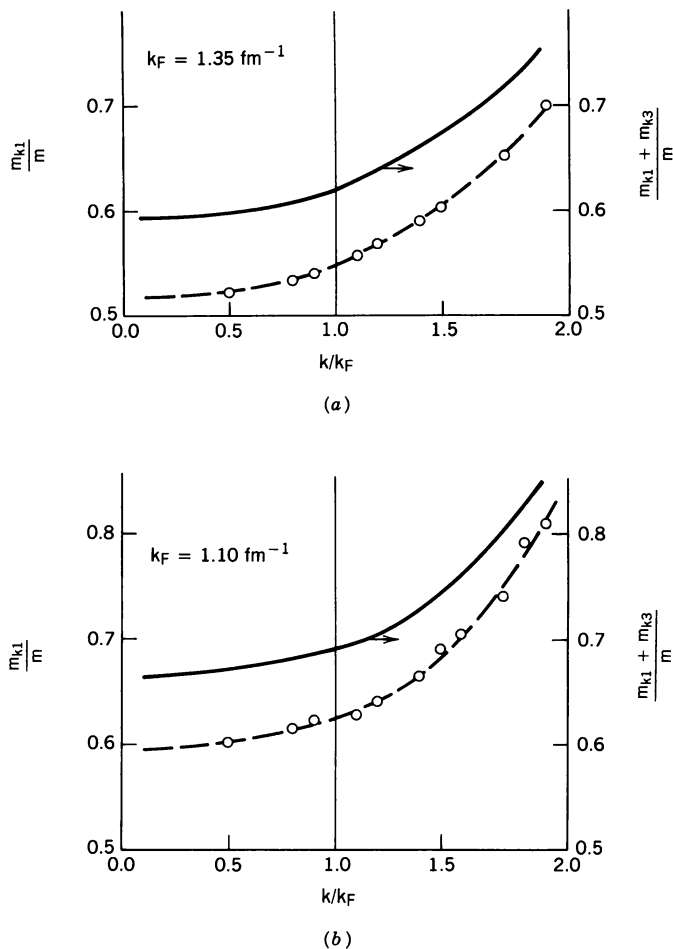


FIG. 2.3. Effective mass m_{k1}/m (dashed curve) and $(m_{k1} + m_{k3})/m$ (solid line) as a function of k_{for} (a) $k_F = 1.35 \text{ fm}^{-1}$ and (b) $k_F = 1.10 \text{ fm}^{-1}$. [From Jeukenne, Lejeune, and Mahaux (76).]

nonlocality and energy dependence. As a consequence, the actual value of ρ in the interaction region where ($m^* < m$) will be less than that which would be computed using current conservation, as is done when a semiempirical optical model wave function is used. This is known as the *Perey effect* [Perey (63)]. When m^* is a constant independent of r , the empirical particle density should be multiplied by m^*/m , and the corresponding empirical wave function by $(m^*/m)^{1/2}$ in the interaction region.

The second consequence of energy dependence of the optical model potential is the nonorthogonality of wave functions corresponding to different energies. This is a real effect. The exact many-body wave functions are of course

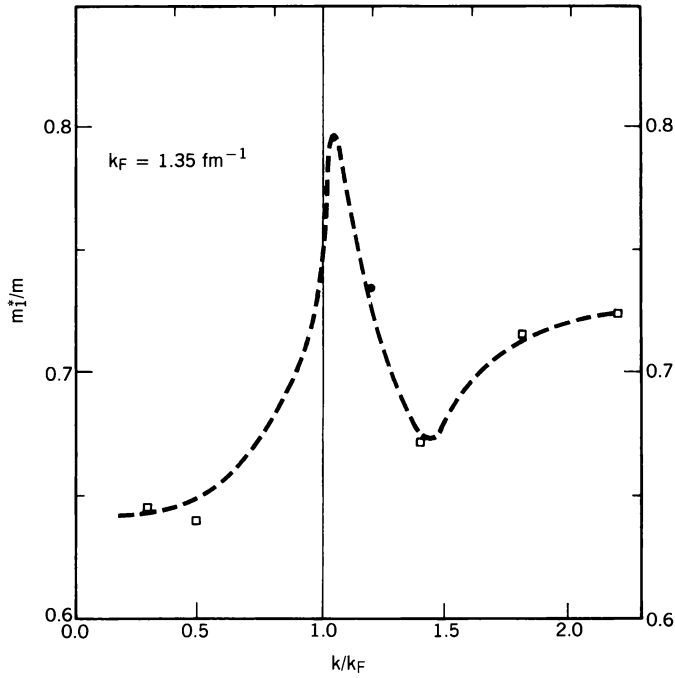


FIG. 2.4. Effective mass m_1^*/m as a function of k for $k_F = 1.35 \text{ fm}^{-1}$. [From Jeukenne, Lejeune, and Mahaux (76).]

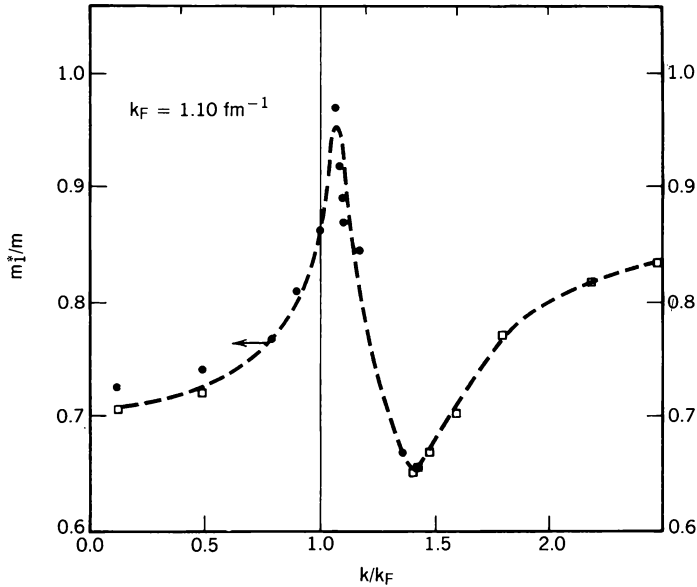


FIG. 2.5. Effective mass m_1^*/m as a function of k for $k_F = 1.10 \text{ fm}^{-1}$ [From Jeukenne, Lejeune, and Mahaux (76).]

orthogonal. But their projections onto the open channels—in this case, to the elastic channel—are not. The physics lies in the fact that the coupling of the open channels to the closed ones (and to each other) is energy dependent, as is immediately obvious from (1.1). Even though the energy has been eliminated, the departure from orthogonality remains in the effective mass approximation, (2.19). The usual orthogonality there is replaced by the new condition

$$\int \tilde{\psi}_E^{(+)*} \psi_{E'}^{(+)} m^*(\mathbf{r}) d\mathbf{r} = 0 \quad E \neq E' \quad (2.24)$$

where clearly the dependence of m^* on \mathbf{r} is important.

C. The Infinite Medium

Before considering in some detail results obtained from semiempirical analysis, it is desirable to present a global qualitative view of features of the optical model potential for nucleons. Great theoretical simplifications occur if we limit the discussion to the infinite nuclear medium. In that case the nonlocal potential of (2.9) is constrained by the condition that translational invariance be maintained as follows:

$$v_E(\mathbf{r}, \mathbf{r} - \mathbf{r}') \rightarrow v_E(\mathbf{r} - \mathbf{r}')$$

Equation (2.12) becomes

$$\mathcal{V} = \int v_E(\mathbf{p}) e^{i\mathbf{p} \cdot \mathbf{k}} d\mathbf{p} = \mathcal{V}(E, \mathbf{k})$$

The local potential V_L must be constant but can depend upon E . Finally, we note that the solutions of the Schrödinger equation in the infinite medium are plane waves. For a wave of momentum $\hbar\mathbf{k}$, the Schrödinger equation reduces to

$$\begin{aligned} E &= \frac{\hbar^2}{2m} k^2 + V(E, \mathbf{k}) \\ V &= V_L(E) + \mathcal{V}(E, \mathbf{k}) \end{aligned} \quad (2.25)$$

an equation determining the relation $E(k)$ or $k(E)$. The nuclear medium is dispersive, the group velocity being given by $(1/\hbar)(dE/dk)$. From (2.25) one can write $V = V(E, k(E))$, where now the potential is local.

Problem. Prove that the group velocity is given by $\hbar k/m^*$.

We shall also make use of the dispersion relation connecting $\text{Re } V$ and $\text{Im } V$. Such a relationship is given in (III.2.13). It is useful because even with modest

information on $\text{Im } V$ obtained, both theoretically and experimentally, it permits calculating a component of $\text{Re } V$ from $\text{Im } V$.

There are some penalties to be paid in going to the infinite nuclear matter. The spin-orbit potential no longer appears. We shall be concerned only with the central potential. The empirical values of the central potential are obtained through the analysis of collisions of nucleons with finite nuclei in which the surface plays a significant role. Two extrapolations are used. In the first, the value of the local optical model potential (which has spatial and energy dependence, as we shall see in Section 2.E), $V_{\text{OPT}}(E, r)$ at $r = 0$, $V_{\text{OPT}}(E, 0)$, is used as the empirical value of $V(E, k(E))$. The thought is that the conditions which exist at the center of the nucleus approximate those of the infinite medium. As a function of mass number, there will be substantial fluctuations because of nuclear structure effects. There are also ambiguities, particularly with regard to $\text{Im } V(E, 0)$, because different models of the optical potential will weight the surface and volume differently. More recently, rather than using $V_{\text{OPT}}(E, 0)$, the volume integral per nucleon of the potential

$$J = \frac{1}{A} \int V_{\text{OPT}}(E, \mathbf{r}) dv$$

is found to be less sensitive to these ambiguities.

It is also necessary to rephrase dispersion relation (III.2.13) since in the nuclear matter limit the sum over bound states is replaced by an integral as these states form a continuum below the Fermi energy ε_F . It is easy to “guess” the form of the answer, namely to extend the limits in the principal value integral to $-\infty$. The formal development proceeds by using the symmetric particle-hole representation of Chapter VII in deShalit and Feshbach (74, p. 554). Recalling that discussion, we define the creation operator α_k^\dagger as follows:

$$\alpha_k^\dagger = \begin{cases} a_k^\dagger & \varepsilon(k) > \varepsilon_F \\ -a_{-k} & \varepsilon(k) < \varepsilon_F \end{cases}$$

so that α_k^\dagger either creates a particle with energy $\varepsilon(k)$ greater than the Fermi energy or a hole if $\varepsilon(k) < \varepsilon_F$ in the Fermi sea. It is then possible to write

$$P\Psi = \int d\mathbf{k} \alpha_k^\dagger u_k |0\rangle$$

where $|0\rangle$ is the “vacuum”, equal in this case to a Fermi sea filled to the Fermi energy ε_F , and u_k is the amplitude of the excitation $\alpha_k^\dagger |0\rangle$.

With this definition it is possible to carry out the derivation leading to

(III.2.13). One obtains

$$\operatorname{Re} V_{\text{eff}}(E, k) = V_{PP} - \frac{1}{\pi} \mathcal{P} \int_{-\infty}^{\infty} \frac{\operatorname{Im} V_{\text{eff}}(\mathcal{E}, k)}{E - \mathcal{E}} d\mathcal{E} \quad (2.26)$$

One subtraction is performed.

$$\operatorname{Re} V_{\text{eff}}(E, k) = \operatorname{Re} V_{\text{eff}}(\varepsilon_F, k) + \frac{E - \varepsilon_F}{\pi} \mathcal{P} \int_{-\infty}^{\infty} \frac{\operatorname{Im} V_{\text{eff}}(\mathcal{E}, k)}{(\varepsilon_F - \mathcal{E})(E - \mathcal{E})} d\mathcal{E} \quad (2.27)$$

This relation agrees with that used by Mahaux and Ngô (81) if one replaces the E in their (10) by $E + i\varepsilon$, $\varepsilon \rightarrow 0^+$.

The momentum \mathbf{k} appears as a parameter, that is, the dispersion relation must hold for each \mathbf{k} . The empirical results for V_{eff} are usually given as functions of the energy only. This reduction can be obtained in principle by replacing k by solving (2.25). In the high-energy limit, the Perey–Saxon result can be used. Or one can average both sides of (2.27) over a k domain. Or one can evaluate at a particular value of k . For example, $V_{\text{eff}}(E, k=0)$ gives the volume integral of $V_{\text{eff}}(E, \mathbf{p})$, which should be simply related to J . Mahaux and Ngô (81) assume that $\operatorname{Im} V_{\text{eff}}(E, k)$ varies slowly with respect to k for $k < 2.5 \text{ fm}^{-1}$. One cannot be that cavalier with $\operatorname{Re} V_{\text{eff}}(E_F, k)$ since the nonlocalities arising from the Pauli principle must be taken into account. Mahaux and Ngô expand that term around k_F and use the effective mass approximation. Only m_k enters. The first term, $\operatorname{Re} V_{\text{eff}}(\varepsilon_F, k_F)$, is given empirically by -53.3 MeV . With these approximations it is possible to proceed with the exploitation of dispersion relations (2.27).

However, we need an estimate of the magnitude of $\operatorname{Im} V_{\text{eff}}(E)$. The method of Lane and Wandel (55) and Clementel and Villi (56), which makes explicit the role of the Pauli principle, provides a first look. The method used is that developed by Goldberger (48). It is based essentially on kinetic theory, from which we learn that the mean free path, L , for a nucleon traveling through a medium, in this case nuclear matter, composed in this case of nucleons, is given by

$$L = \frac{1}{\rho\sigma} \quad (2.28)$$

where ρ is the density of nuclear matter and σ is the nucleon–nucleon cross section. The mean free path L may be related to the imaginary part of the potential as follows. In an infinite medium, a plane wave, $e^{i(k_0 + ik_I)Z}$, is a solution of the Schrödinger equation. It follows immediately that

$$L = \frac{1}{2k_I} \quad k_I = \frac{\rho\sigma}{2} \quad (2.29)$$

Substituting in Schrödinger equation (2.25) gives for weak absorption

$$\begin{aligned} -\operatorname{Im} V &= \hbar v k_I \\ &= \frac{\hbar \rho v \sigma}{2} \end{aligned} \quad (2.30)$$

where v is the velocity, $\hbar k_0/m$.

The medium consists of a Fermi gas of nucleons with levels filled to an energy ε_F and momentum k_F . It is therefore necessary to average σv over the Fermi sea:

$$\langle \sigma \rangle \equiv \frac{\langle v \sigma \rangle}{v} = \frac{3}{4\pi p_F^3} \int \frac{|\mathbf{p} - \mathbf{k}|}{p} d\mathbf{k} \int \sigma(q, \mathbf{q} \cdot \mathbf{q}') d\Omega' \quad q = q'$$

where $\sigma(q, \mathbf{q} \cdot \mathbf{q}')$ is the differential cross section, \mathbf{p} is the incident nucleon momentum, \mathbf{k} is the initial target nucleon momentum, and \mathbf{q} and \mathbf{q}' are the relative initial and final momenta [e.g., $\mathbf{q} = \frac{1}{2}(\mathbf{p} - \mathbf{k})$]. Assuming isotropy [no dependence on $(\mathbf{q} \cdot \mathbf{q})$, so that $\sigma(\mathbf{q}, \mathbf{q} \cdot \mathbf{q}')$ becomes $\sigma(q)/4\pi$, one obtains

$$\langle \sigma \rangle = \frac{3}{4\pi p_F^3 p} \int \frac{p^2 + k^2 - 2p_F^2}{|\mathbf{p} + \mathbf{k}|} \sigma(q) d\mathbf{k}$$

The integration over the Fermi sphere can be readily performed when $\sigma(q)$ is a constant σ_0 . Then

$$\begin{aligned} \langle \sigma \rangle &= \sigma_0 \left(1 - \frac{7}{5} \left(\frac{p_F}{p} \right)^2 \right) \quad p^2 > 2p_F^2 \\ &= \sigma_0 \left\{ 1 - \frac{7}{5} \left(\frac{p_F}{p} \right)^2 + \frac{2}{5} \left(\frac{p_F}{p} \right)^2 \left(2 - \left(\frac{p}{p_F} \right)^2 \right)^{5/2} \right\} \quad p^2 \leq p_F^2 \\ &\rightarrow \frac{3}{4} \sigma_0 \left(1 - \frac{p_F^2}{p^2} \right)^2 \quad p \rightarrow p_F \end{aligned} \quad (2.31)$$

The result is to be inserted into (2.30) to obtain an estimate of $\operatorname{Im} V$.

We note that as p goes to p_F , $\operatorname{Im} V$ will go to zero. This is a consequence of the Pauli principle since it forbids all collisions in which either nucleon ends with an energy less than ε_F . As the incident nucleon energy approaches ε_F , the amount of phase space available for the collision goes to zero. The Pauli effect goes to zero and $\langle \sigma \rangle$ approaches σ_0 as p grows. Of course, the assumptions, such as a constant σ_0 , are much too crude for comparison with experiment. Nevertheless, the correct order of magnitude of $\operatorname{Im} V$ is obtained with (2.30).

Passatore (67, 68) who pioneered the use of dispersion calculation of $\operatorname{Re} V_{\text{eff}}$,

showed that if $\text{Im } V$ is constant at large energies, $\text{Re } V$ at large energies decreases in magnitude, eventually becoming repulsive. As one can see when (2.31) is inserted into (2.27), initially the real part of the potential depends linearly on the energy but eventually develops a logarithmic dependence. Both of these results have been confirmed experimentally. See, for example, the results obtained by Nadasen et al. (81), described in Section V.2.

Mahaux and Ngô (81) quote results obtained using the results of nuclear matter calculations carried out by Mahaux and his collaborators, and compare them to the empirical results. This comparison is shown in Fig. 2.6. The values of $W = -\text{Im } V$ for $E < \varepsilon_F$ are obtained from the spreading width of one-hole states $\Gamma^{1/2} = W$. Up to $|E - \varepsilon_F| \sim 50 \text{ MeV}$, the theoretical results are in reasonable agreement with experiment. There is, of course, a great deal of scatter in the empirical data, presumably a consequence of structure effects, which nuclear matter calculations cannot include explicitly. According to Mahaux and Ngô, the results for $\text{Re } V$ are not sensitive to the values of W above $|E - \varepsilon_F| = 50 \text{ MeV}$. Their results for the $\text{Re } V$ are shown in Fig. 2.7 for $|E - \varepsilon_F| < 50 \text{ MeV}$. The agreement with the empirical depths is good, as the

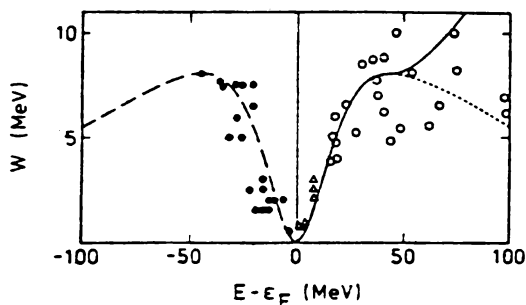


FIG. 2.6. Energy dependence of the imaginary part of the single-particle potential for medium-light nuclei. [From Mahaux and Ngô (81).]

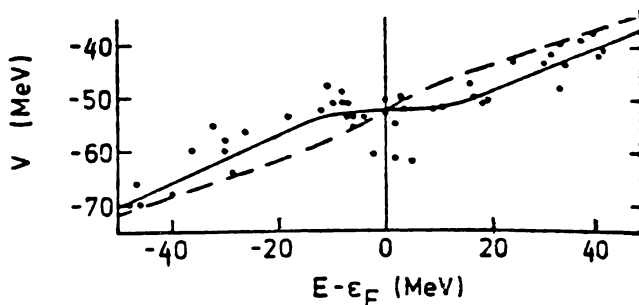


FIG. 2.7. Single-particle potential. The dashed curve gives the Hartree-Fock field and the solid curve the full shell model potential. The dots are the empirical depths. [From Mahaux and Ngô (81).]

theory describes correctly the magnitude, the overall energy dependence, and the plateau at $E = \varepsilon_F$. The plateau is a consequence of the peaking of m^*/m near ε_F .

We conclude this section with a description of the important influence of nonlocality on the imaginary part of the optical potential. To make the latter explicit, rewrite (2.25a) as follows:

$$E = \frac{\hbar^2}{2m} k^2 + V_R(E, \mathbf{k}) - iW(E, \mathbf{k}) \quad (2.32)$$

In the effective mass approximation, and assuming that W varies slowly with k , V can be expanded about a value of k , say k_0 . Then

$$E \simeq \frac{\hbar^2 k^2}{2m} + V_R(E, k_0) - iW(E, k_0) + (k^2 - k_0^2) \frac{\partial V_R(E, k_0)}{\partial k_0^2} \quad (2.33)$$

If one now puts

$$k = k_R + ik_I \quad L = \frac{1}{2k_I}$$

and chooses k_0 as the solution of

$$E = \frac{\hbar^2}{2m} k_0^2 + V_R(E, k_0) \quad (2.34)$$

one obtains from (2.32) to first order in k_I :

$$\begin{aligned} E &= \frac{\hbar^2}{2m} k_R^2 + V_R(E, k_0) + (k_R^2 - k_0^2) \frac{\partial V_R}{\partial k_0^2} \\ 0 &= \frac{\hbar^2}{m} k_I k_R - W(E, k_0) + 2k_I k_R \frac{\partial V_R}{\partial k_0^2} \end{aligned}$$

From the first of these equations and (2.34), $k_R = k_0$. From the second

$$k_I = \frac{mW(E, k_0)}{\hbar^2 k_0 [1 + (m/\hbar^2 k_0)(\partial V/\partial k_0)]}$$

so that

$$k_I = \frac{m_k W(E, k_0)}{\hbar^2 k_0} \quad L = \frac{\hbar^2 k_0}{2m_k W(E, k_0)} \quad (2.35)$$

This result has important implications. As noted earlier, k can be eliminated from the potential term in (2.32) so that only the potential energy terms depend only on E :

$$E = \frac{\hbar^2}{2m} k^2 + \bar{V}_R(E) - i\bar{W}(E) \quad (2.36)$$

where

$$\bar{V}_R(E) \equiv V_R(E, k(E)), \quad \bar{W} \equiv W(E, k(E))$$

If one once more picks $k = k_0 + ik_I$ and uses (2.34) and (2.35), one finds that

$$\bar{W} = \frac{m_k}{m} W(E, k_0) \quad L = \frac{\hbar^2 k_0}{2m_k \bar{W}(E)} \quad (2.37)$$

The last of these equations demonstrates the large effect of non-locality on the imaginary part of the optical potential [Negele and Yazaki (81); Fantoni, Frimen, and Pandhariponde (81); Bernard and Van Glai (78)]. When the nonlocal energy-dependent optical potential is approximated by a local energy-dependent potential through the Perey–Saxon approximation, $k \rightarrow k_0$, the imaginary part of the potential must be multiplied by m_k/m to take the effect of nonlocality into account. This effect must also be contained in the effective potential method of Frahn as outlined in the discussion following (2.14).

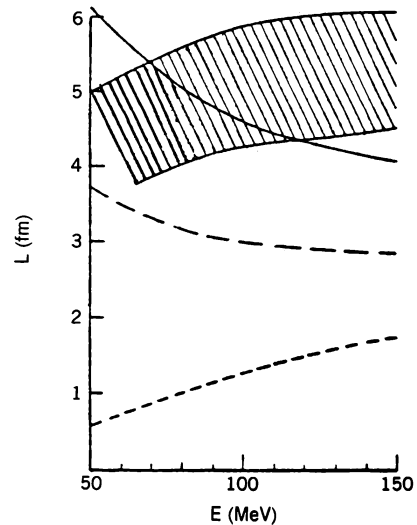


FIG. 2.8. Comparison of three approximations to the mean free path with the range of values compatible with the reaction cross sections for Ca, Zr, or Pb (shaded band). The short dashed curve is given by $(1/\sigma p)$; the long dashed curve is obtained from (2.37) neglecting the factor m_k/m . The solid line is the correct nonlocal expression in (2.37). [From Negele and Yazaki (81).]

An immediate application of these considerations is to the mean free path. Negele and Yazaki (81) calculated the mean free path using the results of Jeukenne Lejeune, and Mahaux (76) (see Fig. 2.8). Agreement with experiment, which provides only rough estimates, showed that the effective mass correction given by (2.37) is essential. It has the effect of increasing the mean free path by as much as 1.7. Negele and Yazaki make the point that the effect of nonlocality is important for an understanding of the large mean free path of a nucleon in nuclear matter, a result of importance for the understanding of the foundation of the mean field (shell model, optical model, etc.) approximation in nuclei.

D. Angular-Momentum-Dependent Potentials

Optical model potentials, which are functions of L^2 ($L = \mathbf{r} \times \mathbf{p}$), the square angular momentum operator, have been proposed by Kobos and MacIntosh (79). This particular kind of momentum dependence could be a consequence of a particular sort of nonlocality in which the kernel $v_E(\mathbf{r}, \mathbf{r}' - \mathbf{r})$ in (2.9) involves only those \mathbf{r}' that can be obtained from \mathbf{r} by a rotation. Such a special connection, \mathbf{r} and \mathbf{r}' , could occur for interactions limited to the surface region of the nuclear system. The underlying physical mechanism could be surface waves propagating from \mathbf{r}' to \mathbf{r} . If the system is deformed, these would correspond to excitation of rotational levels and their deexcitation. More generally, potentials that are L dependent can be obtained directly from (2.9) by expansion of v_E in a series of Legendre polynomials that are functions of $\mathbf{r} \cdot \mathbf{r}'$. Such an expansion is entirely equivalent to the Taylor series of (2.17).

E. Empirical Optical Model Potentials: Nucleon Projectile

In the empirical determination of the optical model potentials, one initially assumes the functional form of the potential involving a number of unspecified parameters. This is followed by a determination of these parameters which are chosen so as to obtain a best fit the experimental data. As the data have become more accurate and as more aspects of the nucleon–nucleus interaction have been studied, the forms used have become more elaborate. A commonly used form, the ‘*standard form*’, is given by Perey (63), and Perey and Perey (74):

$$V_{\text{opt}} = \mathcal{V}_c + \boldsymbol{\sigma} \cdot \mathbf{L} \mathcal{V}_{so}$$

$$\mathcal{V}_c \equiv V_{\text{Coul}} - Vf(x_0) - i \left[Wf(x_w) - 4W_D \frac{d}{dx_D} f(x_D) \right] \quad (2.38a)$$

$$\mathcal{V}_{so} = \left(\frac{\hbar}{m_\pi c} \right)^2 V_{s0} \frac{1}{r} \frac{d}{dr} f(x_{s0}) \quad (2.38b)$$

and where $\hbar \mathbf{L}$ is the angular momentum operator and V , W , W_D , V_{s0} are constants. V_{Coul} is the Coulomb interaction with a uniformly charged sphere of

radius R_c :

$$V_{\text{Coul}} = \begin{cases} \frac{zZe^2}{r} & r \geq R_c \\ \frac{zZe^2}{2R_c} \left(3 - \frac{r^2}{R_c^2} \right) & r \leq R_c \end{cases} \quad (2.39)$$

where ze is the charge of the projectile and Ze that of the target nucleus. The function $f(x)$ is usually taken to be in the Woods–Saxon (54) form:

$$f(x_i) = \frac{1}{1 + e^{x_i}} \quad x_i = \frac{r - r_i A^{1/3}}{a_i} \quad R_i = r_i A^{1/3} \quad (2.40)$$

The Woods–Saxon form (see Fig. 2.9) characteristically is roughly constant within the nucleus, decaying exponentially at large distances at a rate governed by the value of a_i . The radius parameters, R_i , is the value of r at which $f(x_i)$ is one-half of its value at $r = 0$. The function $-4f'(x)$ has its largest values in the surface region, $r = R \pm 1.5a$. Thus V_{opt} has a real term that has its largest value for $r < R_0$ and is therefore referred to as a volume term. The imaginary component has a volume term $f(x_W)$ and a surface term $(-4f'(x_D))$. In addition, there is a spin-orbit term that is concentrated at the surface. Qualitatively, these components are intuitively satisfactory. The real potential should be a reasonable continuation of the shell model potential into positive energies; the absorption should have a strong surface component, particularly at the lower energies, where the excitation of surface collective models should dominate; and the spin-orbit term should be surface dominated since it vanishes in the infinite nucleus limit.[†] However, it must not be forgotten that the Woods–Saxon form has no other validating support, and indeed many other forms have been used [see Marmier and Sheldon (70, p. 1102) and Feshbach (58)] that have similar properties. As we shall see at intermediate energies (see Section 2.F), it must be replaced by a nonmonotonic form with a repulsive central region and an attractive surface component.

The parameters, V , W , W_D , V_{so} , R_c , R_i , and a_i are adjusted to fit all the available data. Moreover, they are required to “track,” that is, to vary smoothly with the nucleon energy and with atomic and mass number. By a fine tuning of the values of the parameters, one can generally obtain a nearly perfect fit of the data for each target nucleus and for each energy. Such precise fits are often necessary for the calculation of reaction processes. However, in this volume we

[†]The comparison with the shell model potential is not straightforward. Both it and the optical model are single-channel potentials in which the effect of other channels or configurations are included approximately. It is not clear to what extent the approximations in the two cases are consistent. However, in the limit in which the mean field approximation (e.g., as obtained from the Brueckner–Hartree–Fock method) is accurate, the comparison is valid.

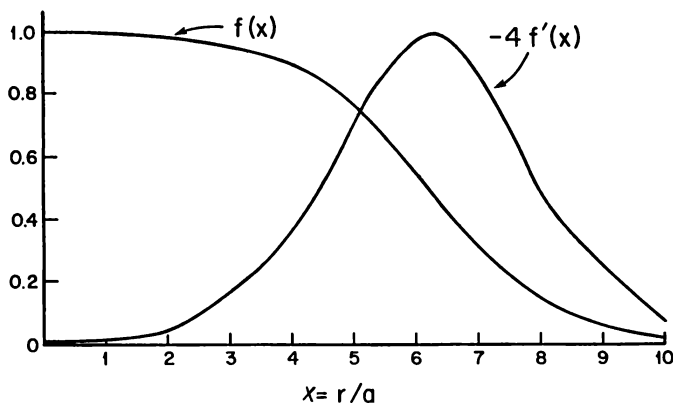


FIG. 2.9. Woods-Saxon potential and its derivative.

are concerned more with the global properties of these parameters to see the trends as a function of energy and target. Strong fluctuations away from the average for a given nucleus of class of nuclei could indicate the presence of nuclear structure effects. We shall discuss these in some detail later. For the present it will suffice to remark that strong fluctuations may be removed if the coupling of the elastic channel to other channels is explicitly considered through the use of the coupled-channel optical model in place of the single-channel description. Generally, this coupling gives rise to smooth behavior in the elastic channel, so that a single-channel optical model suffices. However, in the presence of special effects, as exemplified by coupling to vibrational or rotational states or generally to doorway state resonances, a single channel is inadequate and the results physically not meaningful.

Form equation (2.38) exhausts the possible spatial invariants only if the target nucleus has zero spin. If it has a spin I , with corresponding spin operator \mathbf{I} , many other invariants can be formed [Feshbach (58)]. A few of the many possibilities are

$$\boldsymbol{\sigma} \cdot \mathbf{I}, \quad \mathbf{L} \cdot \mathbf{I}, \quad (\boldsymbol{\sigma} \cdot \mathbf{r})(\mathbf{I} \cdot \mathbf{r}), \quad (\boldsymbol{\sigma} \cdot \mathbf{I})(\mathbf{L} \cdot \mathbf{I}), \quad \text{etc.} \quad (2.41)$$

The evidence for the presence of these terms is rather meager, indicating that they are relatively weak, on the order of a fraction of an MeV [see Hodgson (80); Batty (71)].

Phase-Shift Analysis: Elastic Scattering. Restricting our considerations to potential equation (2.38), that is, either to spin-zero target nuclei or neglecting terms dependent on the spin of the target I , such as those given in (2.41), the scattering amplitude can be written as follows (see Appendix B):

$$f = A(k, \theta) + B(k, \theta) \boldsymbol{\sigma} \cdot \mathbf{n} \quad (2.42)$$

where \mathbf{n} is a unit vector perpendicular to the scattering plane:

$$\mathbf{n} = \frac{\mathbf{k}_i \times \mathbf{k}_f}{|\mathbf{k}_i \times \mathbf{k}_f|} \quad (2.43)$$

where $\hbar\mathbf{k}_i$ is the incident momentum, $\hbar\mathbf{k}_f$ the final momentum, and θ is the angle between them:

$$\mathbf{k}_i \cdot \mathbf{k}_f = k^2 \cos \theta, \quad |\mathbf{k}_i \times \mathbf{k}_f| = k^2 \sin \theta$$

The quantities A and B can be expanded in a partial wave series:

$$A(k, \theta) = \frac{1}{2ik} \sum_0^{\infty} [(l+1)(e^{2i\delta_l^{(+)}} - 1) + l(e^{2i\delta_l^{(-)}} - 1)] P_l(\cos \theta) \quad (2.44a)$$

$$B(k, \theta) = \frac{1}{2k} \sum_1^{\infty} (e^{2i\delta_l^{(+)}} - e^{2i\delta_l^{(-)}}) P_l^{(1)}(\cos \theta) \quad (2.44b)$$

where

$$P_l^{(1)} = \sin \theta \frac{d}{d(\cos \theta)} P_l(\cos \theta)$$

The phase shifts $\delta_l^{(\pm)}$ are obtained from the asymptotic form of the solutions to the radial Schrödinger equations

$$\frac{d^2 \psi(j = l + \frac{1}{2}, r)}{dr^2} + \left[k^2 - \frac{l(l+1)}{r^2} - \mathcal{V}_c - l\mathcal{V}_{so} \right] \psi(j = l + \frac{1}{2}, r) = 0$$

$$\frac{d^2 \psi(j = l - \frac{1}{2}, r)}{dr^2} + \left[k^2 - \frac{l(l+1)}{r^2} - \mathcal{V}_c + (l+1)\mathcal{V}_{so} \right] \psi(j = l - \frac{1}{2}, r) = 0$$

In obtaining these equations, we have made use of the results

$$(\boldsymbol{\sigma} \cdot \mathbf{L})\psi(j = l + \frac{1}{2}, r) = l\psi(j = l + \frac{1}{2}, r)$$

$$(\boldsymbol{\sigma} \cdot \mathbf{L})\psi(j = l - \frac{1}{2}, r) = -(l+1)\psi(j = l - \frac{1}{2}, r)$$

Asymptotically,

$$\psi(j = l \pm \frac{1}{2}, r) \rightarrow \sin \left(kr - \frac{l\pi}{2} + \delta_l^{(\pm)} \right) \quad (2.45)$$

The differential cross section for the elastic scattering of an unpolarized beam is

$$\left\langle \frac{d\sigma}{d\Omega} \right\rangle_{\text{unpol}} = |A|^2 + |B|^2 \quad (2.46)$$

while the total elastic cross section is

$$\langle \sigma_{\text{tot}}^{\text{el}} \rangle = \frac{\pi}{k^2} \sum_{l=0}^{\infty} \{ |(l+1)(e^{2i\delta_l^{(+)}} - 1) + l(e^{2i\delta_l^{(-)}} - 1)|^2 + [l(l+1)] |e^{2i\delta_l^{(+)}} - e^{2i\delta_l^{(-)}}|^2 \}$$

or

$$\langle \sigma_{\text{tot}}^{\text{el}} \rangle = \frac{\pi}{k^2} \sum_{l=0}^{\infty} [(l+1)|e^{2i\delta_l^{(+)}} - 1|^2 + l|e^{2i\delta_l^{(-)}} - 1|^2] \quad (2.47)$$

The total cross section is given by the optical theorem:

$$\langle \sigma_{\text{tot}} \rangle = \frac{2\pi}{k^2} \sum_{l=0}^{\infty} [(l+1)(1 - \text{Re } e^{2i\delta_l^{(+)}}) + l(1 - \text{Re } e^{2i\delta_l^{(-)}})] \quad (2.48)$$

The optical model reaction cross section is the difference, (2.4):

$$\langle \sigma_r \rangle = \langle \sigma_{\text{tot}} \rangle - \langle \sigma_{\text{tot}}^{\text{el}} \rangle = \frac{\pi}{k^2} \sum_{l=0}^{\infty} [(2l+1) - (l+1)|e^{2i\delta_l^{(+)}}|^2 - l|e^{2i\delta_l^{(-)}}|^2] \quad (2.49)$$

These expressions, (2.46), (2.47) (2.48), and (2.49), in the absence of the spin-orbit potential so that $\delta_l^{(+)} = \delta_l^{(-)}$, reduce to the spin-zero results. These are:

$$f(\theta) = \frac{1}{2ik} \sum_0^{\infty} (2l+1)(e^{2i\delta_l} - 1)P_l(\cos \theta) \quad \text{---(2.44a')} \quad (2.49')$$

$$\langle \sigma_{\text{tot}}^{\text{el}} \rangle = \frac{\pi}{k^2} \sum_0^{\infty} (2l+1)|e^{2i\delta_l} - 1|^2 = \frac{4\pi}{k^2} \sum_0^{\infty} (2l+1)[\sin^2 \xi_l e^{-2\eta_l} + \frac{1}{4}(1 - e^{-2\eta_l})^2] \quad (2.47')$$

inserting $\delta = \xi + i\eta$. Finally,

$$\langle \sigma_{\text{tot}} \rangle = \frac{4\pi}{k^2} \sum_0^{\infty} (2l+1)[\sin^2 \xi_l e^{-2\eta_l} + \frac{1}{2}(1 - e^{-2\eta_l})] \quad (2.48')$$

$$\langle \sigma_r \rangle = \frac{\pi}{k^2} \sum_0^{\infty} (2l+1)(1 - e^{-4\eta_l}) \quad (2.49')$$

and the transmission factor [see (IV.3.2)]

$$T_l = 1 - e^{-4\eta_l} \quad (2.49'')$$

The polarization (= analyzing power if time-reversal invariance is satisfied) generated in the elastic scattering of an unpolarized beam is transverse to the

scattering plane:

$$\mathbf{P} = \frac{\text{tr } f^+ \boldsymbol{\sigma} f}{\text{tr } f^+ f} = 2 \frac{\text{Re } AB^*}{|A|^2 + |B|^2} \mathbf{n} = 2P\mathbf{n} \quad (2.50)$$

If the incident beam is polarized, the angular distribution becomes

$$\left\langle \frac{d\sigma}{d\Omega} \right\rangle_{\text{pol}} = \left\langle \frac{d\sigma}{d\Omega} \right\rangle_{\text{unpol}} (1 + P_p P \mathbf{n}_p \cdot \mathbf{n}) \quad (2.51)$$

where P_p gives the beam polarization and \mathbf{n}_p its polarization direction. By measuring the asymmetry, that is, the difference in $d\sigma/d\Omega$ with respect to the scattering plane, one can determine P . Measurements of the angular distribution after a second scattering, that is, by analyzer, permit the determination of $\text{Im } AB^*$ (and $|B|^2$) and finally, of A and B separately (to within a phase) if $\langle d\sigma/d\Omega \rangle_{\text{pol}}$ is measured as well.

The following parametrization for AB^* is often used:

$$\frac{2AB^*}{(|A|^2 + |B|^2)} = P(\theta) + iQ(\theta) \quad (2.52)$$

where Q is referred as the spin rotation function, so that

$$Q = \frac{2 \text{Im } AB^*}{(|A|^2 + |B|^2)}$$

Q is related to the Wolfenstein parameters $R(\theta)$ and $A(\theta)$ (see Appendix B) by

$$Q = R(\theta) \sin \theta + A(\theta) \cos \theta \quad (2.53)$$

Note that if σ , P , and Q are measured, the amplitude f is determined to within a phase.

Low-Energy Scattering. At sufficiently low projectile energy only the $s, l=0$ term in the partial wave analysis will be significant. The angular distribution is spherical,

$$A(k, \theta) \rightarrow \frac{1}{2ik} (e^{2i\delta} - 1) \quad (2.54)$$

$$B(k, \theta) \rightarrow 0$$

At these low energies only neutral projectiles, in particular neutrons, are useful. Writing

$$\delta_0 = \xi_0 + i\eta_0 \quad \eta_0 \geq 0 \quad (2.55)$$

since the potentials involved are complex and absorptive, we obtain for the scattering amplitude equation (2.42):

$$\langle f \rangle = \frac{i}{2k} (1 - e^{-2\eta_0} e^{2i\xi_0}) \quad (2.56)$$

The various cross sections are

$$\langle \sigma_{\text{tot}}^{(\text{el})} \rangle = \frac{4\pi}{k^2} \left[e^{-2\eta_0} \sin^2 \xi_0 + \left(\frac{1 - e^{-2\eta_0}}{2} \right)^2 \right] \quad (2.57a)$$

$$\langle \sigma_{\text{tot}} \rangle = \frac{4\pi}{k^2} \left[\left(e^{-2\eta_0} \sin^2 \xi_0 + \frac{1 - e^{-2\eta_0}}{2} \right) \right] \quad (2.57b)$$

$$\langle \sigma_r \rangle = \frac{\pi}{k^2} (1 - e^{-4\eta_0}) \quad (2.57c)$$

Note that according to (2.49'), the optical model transmission factor $1 - |e^{2i\delta_0}|^2$ equals

$$\langle T_0 \rangle = 1 - e^{-4\eta_0} \quad (2.57d)$$

At zero energy both ξ_0 and η_0 approach zero. Define these limits by

$$\xi_0 \rightarrow -ka \quad \eta_0 \rightarrow kb \quad (2.58)$$

so that

$$kA \rightarrow \delta_0 \rightarrow -k(a - ib) \quad (2.59)$$

where $a - ib$ is a *complex scattering length*. The total elastic cross section is

$$\begin{aligned} \langle \sigma_{\text{tot}}^{(\text{el})} \rangle &\rightarrow 4\pi(a^2 + b^2) \\ \langle \sigma_r \rangle &\rightarrow 4\pi \left(\frac{b}{k} - 2b^2 \right) \end{aligned} \quad (2.60)$$

so that

$$\langle \sigma_{\text{tot}} \rangle \rightarrow 4\pi \left(a^2 - b^2 + \frac{b}{k} \right) \quad (2.61)$$

where the assumption that follows from the effective range relation has been made:

$$\eta_0 \rightarrow kb + O(k^3)$$

The reaction and total cross section both grow like $1/k$ as k approaches zero. This is the familiar $(1/v)$ absorption law. The elastic cross section $\langle \sigma_{\text{tot}}^{(\text{el})} \rangle$ is used to define an effective radius, \bar{R} :

$$\langle \sigma_{\text{tot}}^{(\text{el})} \rangle = 4\pi \bar{R}^2$$

where

$$\bar{R}^2 = a^2 + b^2 \quad (2.62)$$

For reference we give the low-energy limit for the case of a target nucleus with spin I . The two possible values for the total J are $I \pm \frac{1}{2}$. Since the weighting factor for each value of J is

$$g = \frac{2J+1}{2(2I+1)}$$

(2.47) is replaced by

$$\langle \sigma_{\text{tot}} \rangle \rightarrow 4\pi \left[g_+(a_+^2 - b_+^2) + \frac{b_+}{k} \right] + 4\pi \left[g_-(a_-^2 - b_-^2) + \frac{b_-}{k} \right] \quad (2.63)$$

where $a_+ - ib_+$ is the scattering length for $J = I + \frac{1}{2}$, $a_- - ib_-$ for $J = I - \frac{1}{2}$. The weights g_+ and g_- are given by

$$g_+ = \frac{I+1}{2I+1} \quad (2.64)$$

$$g_- = \frac{I}{2I+1}$$

Finally, we shall relate the parameter b with the strength function $\langle \Gamma/D \rangle$. To that end we write the exact elastic amplitude as the sum of a potential scattering term plus a sum of resonance terms. Moreover, at these very low energies, the width for inelastic processes (radiative capture) can be neglected compared to the elastic width. Hence [see (IV.2.18)]

$$f = \frac{1}{k} \left[e^{i\delta} \sin \delta - e^{2i\delta} \sum_{\lambda} \frac{\Gamma_{\lambda}/2}{E - E_{\lambda} + (i/2)\Gamma_{\lambda}} \right]$$

where δ , the potential scattering phase shift, is real. This formula assumes that the resonances in the sum over λ are not overlapping. Using the "box" averaging (it is assumed that δ , k , Γ_{λ} , or E_{λ} do not vary appreciably over ΔE),

$$\langle f \rangle = \frac{1}{k} \left[e^{i\delta} \sin \delta - e^{2i\delta} \sum_{\lambda} \frac{1}{\Delta E} \int_{E_{\lambda}-\Delta E/2}^{E_{\lambda}+\Delta E/2} \frac{(\Gamma_{\lambda}/2)dE}{E - E_{\lambda} + i(\Gamma_{\lambda}/2)} \right]$$

The integral is easily evaluated. Assuming that $\Delta E/\Gamma_\lambda \gg 1$, one obtains

$$\langle f \rangle = \frac{1}{k} \left(e^{i\delta} \sin \delta + \frac{i\pi e^{2i\delta}}{2} \sum_\lambda \frac{\Gamma_\lambda}{\Delta E} \right)$$

Noting that

$$\frac{\sum \Gamma_\lambda}{\Delta E} = \frac{\langle \Gamma \rangle}{D}$$

where D is the average distance between levels λ , we rewrite $\langle f \rangle$ in a form that makes comparisons with (2.56) easy:

$$\langle f \rangle = \frac{i}{2k} \left(1 - e^{2i\delta} + \frac{\pi \langle \Gamma \rangle}{D} e^{2i\delta} \right)$$

This yields

$$e^{-2\eta_0 + 2i\xi_0} = e^{2i\delta} \left(1 - \frac{\pi \langle \Gamma \rangle}{D} \right)$$

For $\langle \Gamma \rangle/D < 1$, it follows that

$$\begin{aligned} \xi_0 &= \delta \\ e^{-2\eta_0} &= 1 - \pi \frac{\langle \Gamma \rangle}{D} \end{aligned} \quad (2.65a)$$

so that

$$\langle \sigma_r \rangle = \frac{4\pi}{k^2} \frac{\pi \langle \Gamma \rangle}{2D} \left(1 - \frac{\pi \langle \Gamma \rangle}{2D} \right) = \frac{\pi}{k^2} \langle T_0 \rangle \quad (2.65b)$$

$$\langle \sigma_{\text{tot}} \rangle = \frac{4\pi}{k^2} \left[\left(1 - \frac{\pi \langle \Gamma \rangle}{D} \right) \sin^2 \xi_0 + \frac{\pi}{2} \frac{\langle \Gamma \rangle}{D} \right] \quad (2.65c)$$

Comparing (2.65a) with (2.60), we find that

$$b = \frac{1}{k} \frac{\pi \langle \Gamma \rangle}{2D} \left(1 + \frac{\pi \langle \Gamma \rangle}{2D} \right) \quad (2.66)$$

The relevant experimental data are generally summarized in two figures. In one the strength function S_0 (the subscript refers to the l value)

$$S_0 = \frac{\langle \Gamma \rangle}{D} \left(\frac{E_0}{E} \right)^{1/2}$$

where E_0 is an arbitrary energy, usually taken to be 1 eV, is plotted. In the other, the length

$$R' \equiv \left(1 - \frac{\pi \langle \Gamma \rangle}{D}\right)^{1/2} a$$

Figure 2.10 gives the strength function $(E_0/E)^{1/2} S_0$ with $E_0 = 1$ eV. The experimental points are obtained by direct measurement of the width of individual neutron s -wave resonances, summing the widths in an interval ΔE and dividing the sum by ΔE . The solid line gives the results of an optical model calculation which includes the effect of deformation, while the dashed line is obtained from a spherical optical model. The peaks represent values of A , or more precisely, values of the nuclear radius R for which the overlap of the square magnitude of the wave function inside the nucleus $|\chi_0|^2$ [see (2.68)] with the imaginary potential is a maximum. Using the rough formula

$$\sqrt{\frac{2mV_0}{\hbar^2}} R = (n + \frac{1}{2})\pi$$

which gives the values of n for which the s radial wave function has a maximum at R , one can readily show that the maxima Fig 2.10 are due to the $3s(n=2)$ and $4s(n=3)$ resonances. Deformations split the large peak at $A \sim 152$ into two peaks with maxima near $A \sim 148$ and $A \sim 185$, in substantial agreement with

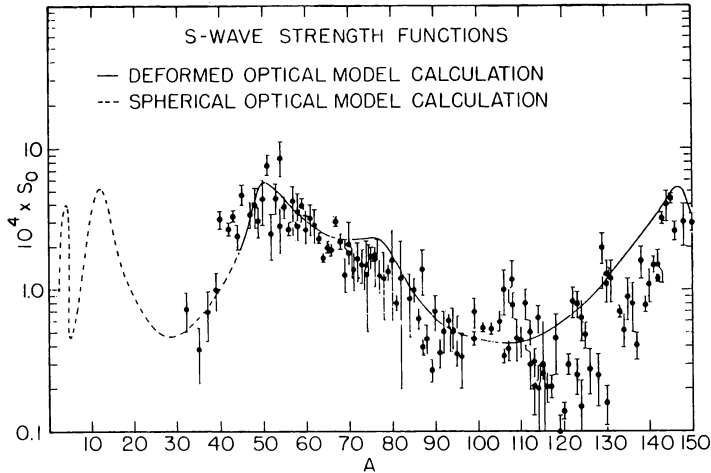


FIG. 2.10. Comparison of theoretical with experimental values of the s -wave neutron strength function. The solid curve represents deformed optical model calculations, and the dashed curve is based on spherical optical model calculations [Mughabghab, Divadeenam, and Holden (84)].

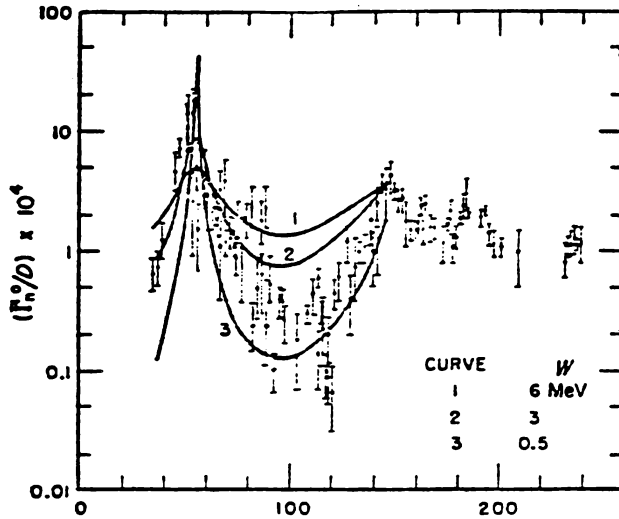


FIG. 2.11. S-wave strength function comparison of experiment with three strengths for the volume absorption potential. [From Moldauer (63).]

much of the data. A splitting that is much less pronounced occurs near the $A \sim 60$ peak. However, anomalies remain. The most pronounced is the large group of very low values of S_0 in the region extending from $A \sim 80$ to $A \sim 130$. This can be summarized by stating that the value of the imaginary potential W is anomalously low in this region (Fig. 2.11).

One physical explanation has been suggested by Block and Feshbach (63), in which it is proposed that the density of the two particle-one hole doorway states, through which the formation of the compound nucleus proceeds, is low in this region. The comparison between experiment and theory is shown in Fig. 2.12. More recently, Kirouac (75) has considered, on essentially this basis, the strength function $\langle S_0 \rangle$ for $143 < A < 158$, where, as he has shown, there is a strong odd-even effect, as illustrated in Fig. 2.13. The theoretical results are in good agreement with the data (Fig. 2.14). The Block mechanism, based on nuclear structure considerations, thus provides an explanation for the fluctuations as well as the average behavior.

On the other hand, a fit to the average behavior has been obtained by Moldauer (63) by using "surface" absorption optical potential concentrated somewhat outside the surface region. The maximum of this potential is 0.5 fm greater than the radius parameters of the Woods-Saxon form used for the volume potentials, $Vf(x_0)$ of (2.26) (see Fig. 2.15).

These two approaches exemplify one of the tactical problems that arise in making optical model fits. Should one adjust the parameters of the potential to obtain a fit, or should one search for the explanation of an anomaly in nuclear structure properties? The first procedure is of importance for

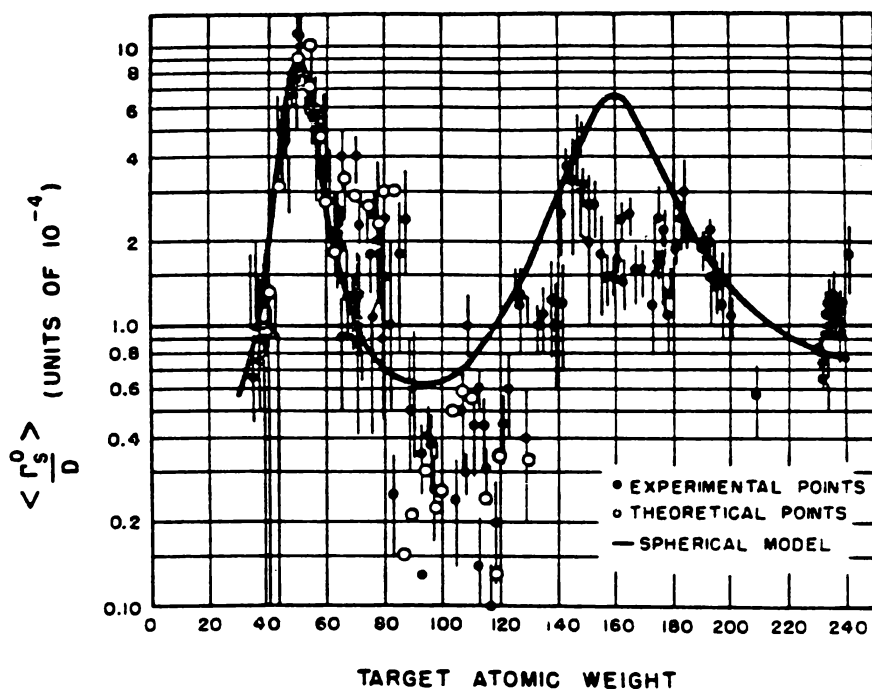


FIG. 2.12. *S*-wave strength function. [From Block and Feshbach (63).]

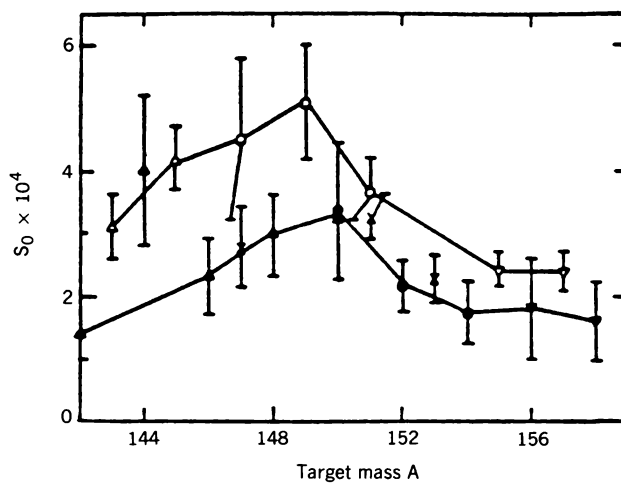


FIG. 2.13. *S*-wave neutron strength functions of even *Z*-odd *N* nuclei (open symbols) and even *Z*-even *N* nuclei (closed symbols) in the first peak of the 4*S* resonance. Three odd-*Z* isotopes (×) are also shown. [From Kirouac (75).]

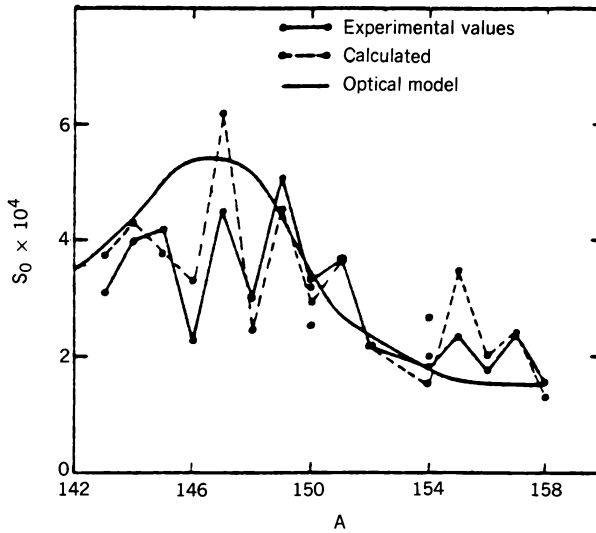


FIG. 2.14. Calculated fluctuations in s -wave neutron strength functions $143 < A < 158$. [From Kirouac (75).]

applications. But differences in the various potentials will be difficult to interpret, being sensitive to the choice of the forms used for the optical model potential. The second is, in the long run, more fundamental, but its meaning will be clarified completely only with the development of a quantitative understanding of the optical model potential.

Problem. Starting with the equation

$$\frac{1}{r^2} \frac{d}{dr} r^2 \frac{d\chi_l}{dr} + \left[k^2 - \frac{l(l+1)}{r^2} - \frac{2\mu}{\hbar^2} (V + iW) \right] \chi_l = 0$$

derive (IV.3.3)

$$\langle T_l \rangle = 4k \int \chi_l^* \left(-\frac{2\mu}{\hbar^2} W \right) \chi_l r^2 dr$$

Using the approximate relation [see (2.65b) and (2.57d)], valid for $\Gamma_0/D \ll 1$,

$$\langle T_0 \rangle = 2\pi \frac{\langle \Gamma_0 \rangle}{D} \quad (2.67)$$

show that

$$\frac{\langle \Gamma_0 \rangle}{D} = \frac{2k}{\pi} \int \chi_0^* \left(-\frac{2\mu}{\hbar^2} W \right) \chi_0 r^2 dr \quad (2.68)$$

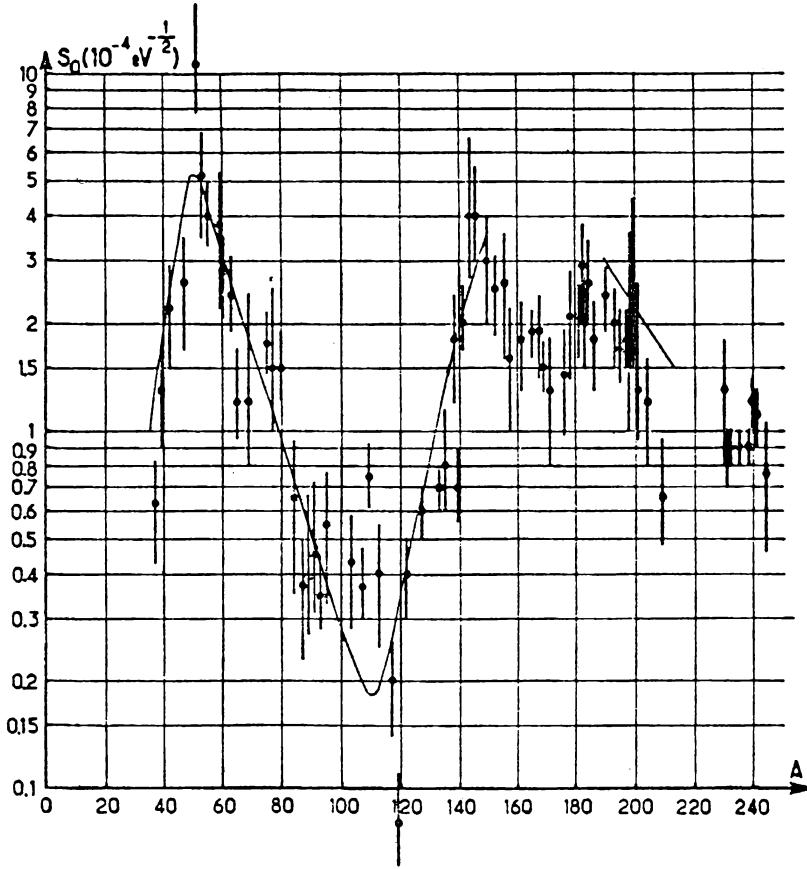


FIG. 2.15. Strength-function S_0 calculated using the potential of Moldauer (63), a Woods-Saxon potential with surface absorption:

$$V(r) = U_0 \left[1 + \exp\left(\frac{r-R}{d}\right) \right]^{-1} + iW_0 \exp\left(-\frac{r-R-c}{f}\right)^2 \\ + U_{s0} \left(\frac{\hbar}{m_\pi c}\right)^2 \boldsymbol{\sigma} \cdot \mathbf{l} \frac{1}{r} \frac{d}{dr} \left[1 + \exp\left(\frac{r-R}{d}\right) \right]^{-1}$$

where $R = r_0 A^{1/3} + r_1$; $U_0 = -46$ MeV; $W_0 = -14$ MeV; $U_{s0} = 7$ MeV; $r_0 = 1.16$ fm; $r_1 = 0.6$ fm; $d = 0.62$ fm; $f = 0.5$ fm; $c = 0.5$ fm. [From Morgenstern, Alves, Julien, and Samour (69).]

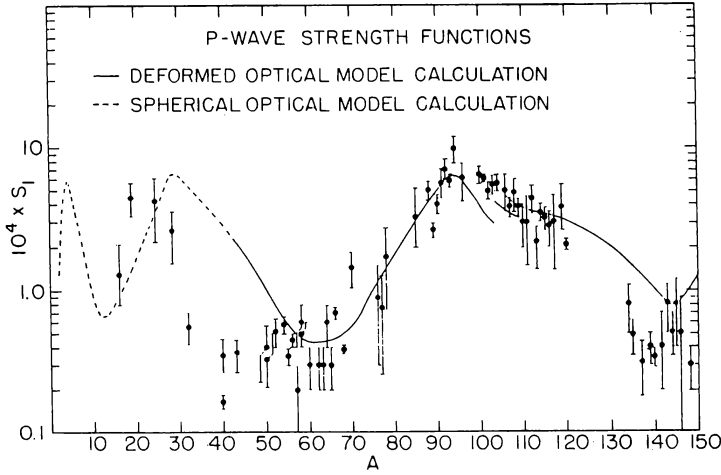


FIG. 2.16. Comparison of theoretical with experimental values of the p -wave neutron strength function. The solid curve represents deformed optical model calculations, and the dashed curve is based on spherical optical model calculations of Mughabghab, Divadeenam, and Holden (84).

Discuss the sensitivity of the calculated $\langle \Gamma \rangle / D$ to χ_0 when W is sharply peaked at the surface. Note particularly the effect of a node of χ_0 at the nuclear surface. Relate to the Moldauer potential.

It is considerably more difficult to measure the strength function for $l = 1$ and $l = 2$ neutrons. The measured values are given in Figs. 2.16 and 2.17. These strength functions S_1 and S_2 are defined by

$$\frac{\langle \Gamma_l \rangle}{D} \equiv s_l(kR) S_l \quad (2.69)$$

where an average over the possible spins $j = l \pm \frac{1}{2}$ with the weights $(2j + 1/2)$ has been performed in obtaining Γ_l/D . The functions s_l are given in (IV.3.15). Obviously, in any study of S_l one should ascertain the value of R and E_0 that were used in extracting S_l . Quite good agreement with optical model calculations is obtained once the effects of deformation are included. However, there are substantial deviations from the optical model predictions, indicating the presence of structure effects.

The values of a are given in Fig. 2.18 together with the calculations of Perey and Buck (62). Substantial agreement has been obtained. The s -wave strength functions for protons should be similar to those of neutrons at energies at which the protons are moving with nearly zero energy, that is,

$$E_p \rightarrow E_n + \text{C.B.}$$

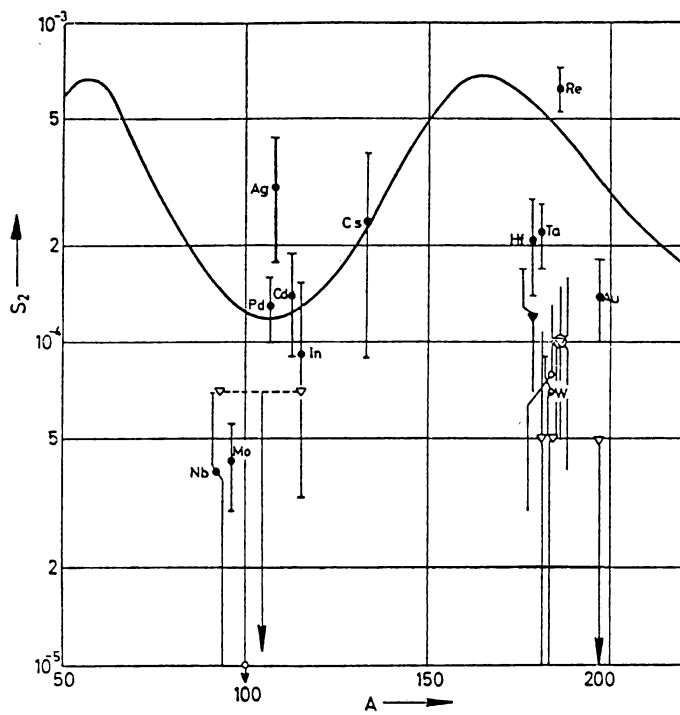


FIG. 2.17. *D*-wave strength function. [From Wilmore and Hodgson (1975).]

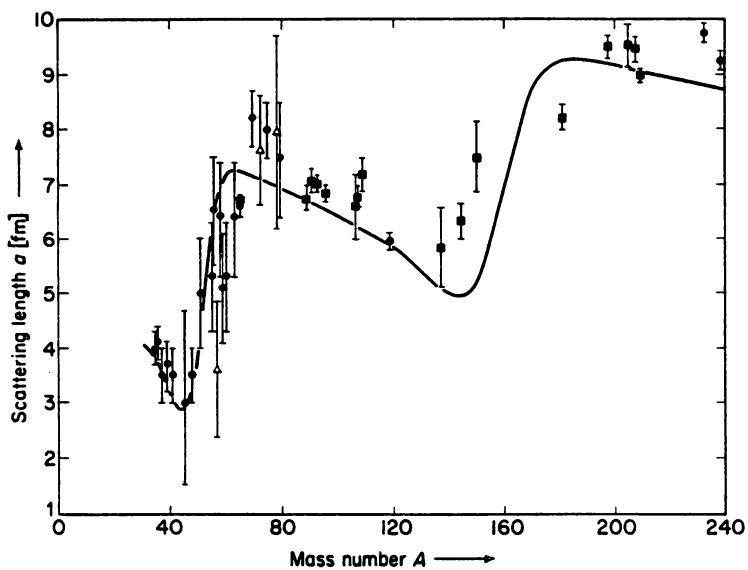


FIG. 2.18. Comparison of measured values (■:BNL; ●:Duke; △:ORNL) of the scattering length a for a range of nuclei with the predictions of the Perey-Buck nonlocal optical potential. [From Marmier and Sheldon (70)].

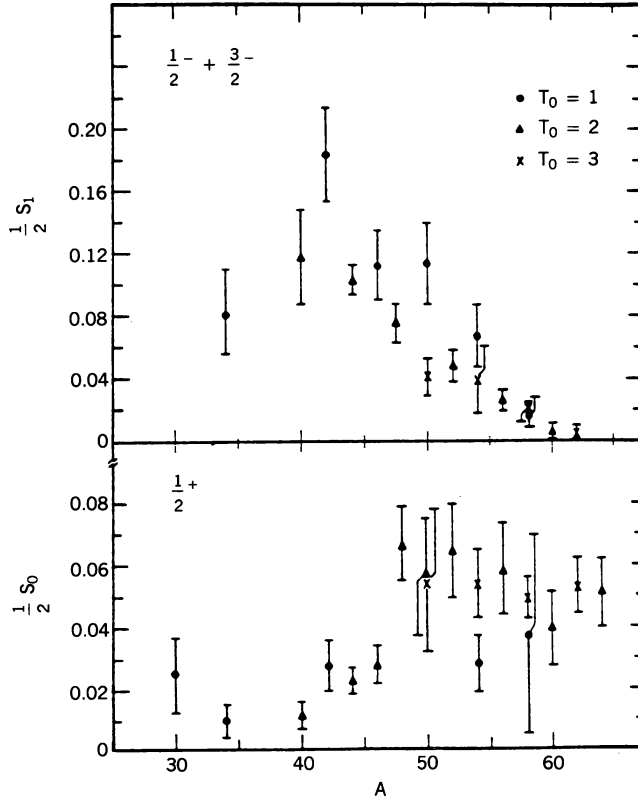


FIG. 2.19. Proton strength function for P - and S -wave resonances. [From Mitchell (80).]

where C.B. is the Coulomb barrier energy [Margolis and Weisskopf (57); Johnson, Galonsky, and Ulrich (58)]. For experimental examples, see Schiffer and Lee (57, 58); Johnson, Galonsky, and Ulrich, Schiffer (64); Elwyn, Marinov, and Schiffer (66); Johnson and Kernell (69, 70). These are for the most part based on the (p, n) reaction.

Developments in experimental methods, particularly by the Duke group, have made it possible to measure the widths of isolated resonances in proton resonance reactions [Bilpuch, Lane, Mitchell, and Moses (76)]. The resulting strength functions are shown in Fig. 2.19, where the Coulomb penetrabilities have been factored out; that is, in (2.69) the Coulomb wave functions have been to evaluate s_l . For the case of the $l=1$ strength function, a maximum corresponding to a $2p$ resonance at about $A = 40$ is observed.

Intermediate Energies ($E < 100$ MeV). The form (2.38) for the optical model potential contains parameters: the radius parameters r_c , r_0 , r_w , r_D , and r_{s0} ; the surface parameters a_0 , a_w , a_D , and a_{s0} ; and the parameters giving the strength

of the potential, V , W , W_D , and V_{so} . Perey and Perey (74) tabulate a list of values of these parameters for individual target nuclei and various projectiles. For our purposes the global parameters they give are of more interest. These are given in Table 2.1 together with those obtained by Rosen, Beery, Goldhaber, and Auerbach (65) after a full study of polarization. The Wilmore–Hodgson potential is the local equivalent of the Perey–Buck potential (62):

$$V\psi = -\left(\frac{\hbar}{m_\pi c}\right)^2 \frac{1}{ar} \frac{e^{(r-R_{so})/a_{so}}}{(1 + e^{(r-R_{so})/a_{so}})^2} V_{so} \left(\frac{\boldsymbol{\sigma} \cdot \mathbf{L}}{2}\right) \psi + \int V(\mathbf{r}, \mathbf{r}') \psi(\mathbf{r}') d\mathbf{r}' \quad (2.70)$$

where

$$V(\mathbf{r}, \mathbf{r}') = U\left(\frac{1}{2}|\mathbf{r} + \mathbf{r}'|\right) T\left(\frac{|\mathbf{r} - \mathbf{r}'|}{\rho}\right) \quad (2.71)$$

Nonlocality follows when T deviates from a delta function; the quantity ρ parameterizes the range of the nonlocality. Perey and Buck take

$$T(r) = \left(\frac{1}{\sqrt{\pi\rho}}\right)^3 e^{-r^2/\rho^2} \quad (2.72)$$

and

$$U(r) = V_0 f(x_0) + 4iW_D \frac{d}{dx_d} f(x_D) \quad (2.73)$$

Their fit to neutron data yields $V_0 = 71$ MeV, $W_D = 15$ MeV, $r_{so} = r_0 = r_D = 1.22$ fm, $a_{so} = a_0 = 0.65$ fm, $a_D = 0.47$ fm, $\rho = 0.85$ fm, and $V_{so} = 7.2$ MeV.

Turning to Table 2.1, we note that the leading term of the central potential, V , as well as the radius parameter, r_0 , which are independent of energy, N and Z dependence are in agreement, reflecting the diffraction structure of the differential cross section. The imaginary term is dominated by the surface term W_D , the value of W_D , a_D , and r_D being sensitive to the reaction cross section. Some volume absorption improves the fit. Including it results in a value of r_D that is considerably larger than the real potential, in qualitative agreement with Moldauer's (63) suggestion. The spin-orbit terms, needed to explain the polarization data [Rosen, Beery, Goldhaber, and Auerbach (65)], are in reasonable agreement with each other. The energy dependence in several of the parameters reflects the nonlocality and energy dependence of the nonlocal potential (e.g., that of Perey and Buck). The term $0.4Z/A^{1/3}$ is an estimate of the change of the Coulomb potential because of the nonlocality using the effective mass approximation. It needs to be identified before the symmetry term in $(N-Z)/A$ can be extracted empirically. Unfortunately, it is not easy to separate the $(N-Z)/A$ term from the $Z/A^{1/3}$ term. Some removal of this ambiguity can be obtained by including the charge exchange (p, n) interaction. This is discussed in Section 3.

TABLE 2.1

	V (MeV)	r_o (fm)	a_o (fm)	W (MeV)	r_w (fm)	a_w (fm)	W_D (MeV)	r_D (fm)	a_D (fm)	V_{so} (MeV)	r_{so} (fm)	a_{so} (fm)	r_c
<i>Protons</i>													
Becchetti and Greenless (69); $A > 40$, $E < 50$ MeV	$54.0 - 0.32E$ $+ 24 \frac{N-Z}{A}$ $+ 0.4 Z/A^{1/3}$	1.17	0.75	$0.22E - 2.7$ if > 0 0 otherwise	1.32	$0.51 + 0.7$ $\times \frac{N-Z}{A}$	$11.8 - 0.25E$ $+ 12 \frac{N-Z}{A}$ if > 0 0 otherwise	1.32	0.51 $+ 0.7 \frac{N-Z}{A}$	6.2	1.01	0.75	1.149 $+ 1.788A^{-2/3}$ $- 1.163A^{-4/3}$
Menet et al. (71); $E < 60$ MeV	$49.9 - 0.22E$ $+ 26.4 \frac{N-Z}{A}$ $+ 0.4 Z/A^{1/3}$	1.16	0.75	$1.2 + 0.09E$	1.37	$0.74 - 0.008E$ $+ 1.0 \frac{N-Z}{A}$	$4.2 - 0.05E$ $+ 15.5 \frac{N-Z}{A}$	1.37	$0.74 - 0.008E$ $+ 1.0 \frac{N-Z}{A}$	6.04	1.064	0.78	1.25
Rosen et al. (65)	$53.8 - 0.33E$	1.25	0.65				7.5	1.25	0.7	5.5	1.25	0.65	
<i>Neutrons</i>													
Becchetti and Greenless (69); $A > 70$, $5 < E < 24$ MeV	$56.3 - 0.32E$ $- 24 \frac{N-Z}{A}$	1.17	0.75	$0.22E - 1.56$ if > 0 0 otherwise	1.26	0.58	$13 - 0.25E$ $- 12 \frac{N-Z}{A}$ if > 0 0 otherwise	1.26	0.58	6.2	1.1	0.75	
Wilmore and Hodgson (64)	$47.01 - 0.267E$ $- 0.018E^2$	$1.32 - 0.76$ $\times (10^{-3}A)$ $+ 4(10^{-3}A)^2$ $- 8(10^{-3}A)^3$	0.66				$9.42 - 0.053E$	1.266 $- 0.37(10^{-3}A)$ $+ 2(10^{-3}A)^2$ $- 4(10^{-3}A)^3$	0.48				
Rosen et al. (65)	$49.3 - 0.33E$	1.25	0.65				5.75	1.25	0.7	5.5	1.25	0.65	

level, which is analogous to the fragmentation of a single-particle resonance into fine structure resonances as described in Chapter III [see (III.4.49)].

Bear and Hodgson (78) have therefore restricted their study to the single-particle energies of nuclei, nearly closed shells, where level fragmentation is minimal. The form of the potential they use is that given by (2.38) with $W = W_D = 0$. They take $r_0 = 1.236$ fm, $a = 0.62$ fm, and $a_{so} = 0.65$ for the spin-orbit case. Moreover, V_{so} is chosen to be 7 MeV, leaving only V to be determined. The results are shown in Fig. 2.20 and can be fitted as indicated by

$$V = \begin{cases} V_0 \pm V_1 \frac{N-Z}{A} & \text{for } E > -15 \text{ MeV} \\ V_0 \pm V_1 \frac{N-Z}{A} + \beta(E + 15) & \text{for } E < -15 \text{ MeV} \end{cases} \quad (2.74)$$

where E is measured from the Fermi energy E_F . The empirical values of V_0 , V_1 , and β are given in Table 2.2.

Folding Model: Empirical. Satchler (67), Slanina and McManus (68), and Greenless, Pyle, and Tang (68) have suggested an alternative form for the optical model potential, to be used in place of that given by (2.38). This development is suggested by the high-energy multiple scattering theory, which in first order yields the potential of the form

$$V(\mathbf{r}) = \int \rho(\mathbf{r}_1) t(\mathbf{r} - \mathbf{r}_1) d\mathbf{r}_1$$

where t is the two-nucleon free-space transition matrix. This expression is not correct as the nucleon energy is lowered. There are already substantial errors, presumably arising because of the influence of the medium in which the two interacting nucleons find themselves at proton energies of 500 MeV [Ray (83)].

A similar result is obtained if one drops the second term in the effective

TABLE 2.2

Nucleus	V_0 (MeV)	V_1 (MeV)	β
^{12}C	56.7		
^{16}O	56.0		
^{40}Ca	56.0		
^{48}Ca	54.9	38.1	0.32
^{58}Ni	57.4	40.0	0.64
^{90}Zr	54.4	42.8	0.47
^{208}Pb	54.5	36.2	

Hamiltonian of Chapter III:

$$H_{\text{eff}} = H_{PP} + H_{PQ} \frac{1}{E^{(+)} - H_{QQ}} H_{QP} \quad (2.75)$$

keeping only H_{PP} . Recall that when P projects only on the elastic channel,

$$P\Psi = \mathcal{A}u_0\phi_0$$

where ϕ_0 is the ground-state wave function of the target nucleus. As a consequence,

$$V_{PP}(P\Psi) = \left\langle \phi_0 \left| \sum_i v_{0i} \right| \mathcal{A}u_0\phi_0 \right\rangle$$

where v_{0i} is the interaction between the i th target nucleon and the incident projectile. Evaluating the matrix element on the right (the integrations are only over the target nucleon coordinates), one obtains

$$V_{PP}(P\Psi) = \left[\int \rho(\mathbf{r}_1) v_{01}(\mathbf{r}_0, \mathbf{r}_1) d\mathbf{r}_1 \right] u_0(\mathbf{r}_0) - \int \rho(\mathbf{r}_1, \mathbf{r}_0) v_{01}(\mathbf{r}_0, \mathbf{r}_1) u_0(\mathbf{r}_1) d\mathbf{r}_1 \quad (2.76)$$

The errors in this approach come mainly from the neglect of the second term in (2.75), which contains the effects that can be described as involving excitation of the target nucleus, such as core polarization and correlations.

The empirical folding potential takes account of these limitations by replacing the two-nucleon interaction v_{01} by an effective two-body potential, so that (2.76) is replaced by

$$V\chi_{\text{opt}} = \left[\int \rho(\mathbf{r}_1) g_{pt}(\mathbf{r}_p, \mathbf{r}_1) d\mathbf{r}_1 \right] \chi_{\text{opt}}(\mathbf{r}_p) - \int \rho(\mathbf{r}_1, \mathbf{r}_p) g_{pt}(\mathbf{r}_p, \mathbf{r}_1) \chi_{\text{opt}}(\mathbf{r}_1) d\mathbf{r}_1 \quad (2.77)$$

The quantity $g_{pt}(\mathbf{r}_p, \mathbf{r}_1)$ is the effective two-body interaction in the nucleus, where \mathbf{r}_p represents all the projectile coordinates (spatial, spin, isospin) and \mathbf{r}_1 those of a target nucleon. The subscripts p and t refer to projectile and target, respectively. Note that the single-channel wave function u_0 of (2.76) has been replaced by the optical model wave function χ_{opt} . This can be justified using the partition proposed by Kawai, Kerman, and McVoy (75) given by (III.8.5). Note that this form reduces to that developed by first-order multiple scattering (which neglects the effects of the Pauli principle) theory as noted above, with g_{pt} replacing the two-body transition matrix $t(\mathbf{r}_p - \mathbf{r}_1)$.

The linear dependence of V_{opt} on the density is illusory, as the effective interaction g_{pt} depends on the nuclear medium, and thus on the density and other parameters describing the nuclear system. The hope is that g_{pt} will depend

slowly on these variables and thus can be replaced by an average value over a substantial range of target nuclei and energy.

Note. A microscopic theory of the effective interaction can be developed. Clearly, the Bethe–Goldstone equation (now with one nucleon in the continuum) will yield information. The papers of Mahaux and his school and of Brieva and Rook discussed earlier employ the Bruecker–Hartree–Fock method to calculate the effective single-body potential in nuclear matter. In the course of this calculation the effective two-body interaction in nuclear matter is obtained. One can then apply a local density approximation to obtain an effective two-body interaction appropriate for two nucleons in a finite nucleus. This procedure is a generalization of the G -matrix method described in Chapter VII of deShalit and Feshbach (74). The g_{pt} obtained in this manner is density dependent. Moreover, if such a calculation were to be done directly for a finite nucleus rather than by applying the local density approximation, g_{pt} would show nuclear structure effects arising from core polarization and correlation effects.

Returning to (2.77), let us define and/or describe $\rho(\mathbf{r}_1)$, $\rho(\mathbf{r}_1, \mathbf{r}_p)$ more completely. The quantity $\rho(\mathbf{r}_1)$ is the one-particle target ground state density *normalized to A* :

$$\rho(\mathbf{r}_1) = A \int |\Psi_0(\mathbf{r}_1, \mathbf{r}_2, \mathbf{r}_3, \dots)|^2 d\mathbf{r}_2 \dots \quad (2.78)$$

The quantity $\rho(\mathbf{r}, \mathbf{r}')$ is the ground-state density matrix discussed in Chapter II of deShalit and Feshbach (74). It is defined by

$$\rho(\mathbf{r}, \mathbf{r}') = A \int \Psi_0^*(\mathbf{r}, \mathbf{r}_2, \dots) \Psi_0(\mathbf{r}', \mathbf{r}_2, \dots) d\mathbf{r}_2 \dots \quad (2.79)$$

Note that the density $\rho(\mathbf{r})$ is just the diagonal element of $\rho(\mathbf{r}, \mathbf{r}')$:

$$\rho(\mathbf{r}) = \rho(\mathbf{r}, \mathbf{r}) \quad (2.80)$$

Problem. Prove

$$\rho(\mathbf{r}) = \left\langle \Psi_0 \left| \sum_i \delta(\mathbf{r} - \mathbf{r}_i) \right| \Psi_0 \right\rangle \quad (2.81)$$

and

$$\rho(\mathbf{r}, \mathbf{r}') = \frac{1}{A-1} \left\langle \Psi_0(\mathbf{r}_1, \mathbf{r}_2, \dots) \left| \sum_{i \neq j} \delta(\mathbf{r} - \mathbf{r}_i) \delta(\mathbf{r}' - \mathbf{r}_j) \right| \Psi_0(\mathbf{r}'_1, \mathbf{r}'_2, \dots) \right\rangle \quad (2.82)$$

Note in (2.82) that the factor $\delta(\mathbf{r}-\mathbf{r}_i)\delta(\mathbf{r}'-\mathbf{r}'_i)$ is understood to be multiplied by the unit operator in the other coordinates, $\delta(\mathbf{r}_1-\mathbf{r}'_1)\delta(\mathbf{r}_2-\mathbf{r}'_2)\cdots$.

The factor $g_{pt}(\mathbf{r}_p, \mathbf{r}_1)$ is the effective projectile nucleon–target nucleon interaction inside the target nucleus. It depends not only on \mathbf{r}_p and \mathbf{r}_1 but on the spin and isospin variables (i.e., on $\boldsymbol{\sigma}_1$, $\boldsymbol{\sigma}_p$, \mathbf{r}_1 , and \mathbf{r}_p) as well.

Note. For reasons of simplicity in presentation, the spin/isospin dependence of g_{pt} , $\rho(\mathbf{r})$ and $\rho(\mathbf{r}, \mathbf{r}')$ have been suppressed. The effective interaction g_{pt} can be written as a linear combination

$$g_{pt} = \sum_{S,T} g_{pt}^{ST} P^{ST} \quad (2.83)$$

where P^{ST} are projection operators in spin and isospin space:

$$P^{ST} = P^S P^T \quad (2.84)$$

where S and T can have the values zero (singlet) or 1 (triplet). The corresponding operators are

$$P^{(0)} = \frac{1 - \boldsymbol{\sigma}_p \cdot \boldsymbol{\sigma}_1}{4} \quad P^{(1)} = \frac{3 + \boldsymbol{\sigma}_p \cdot \boldsymbol{\sigma}_1}{4}$$

Note that expansion (2.83) is valid in the presence of spin-orbit $(\boldsymbol{\sigma}_p + \boldsymbol{\sigma}_1) \cdot \mathbf{l}_{p1}$, and tensor $(3\boldsymbol{\sigma}_p \cdot \hat{\mathbf{r}}_p \boldsymbol{\sigma}_1 \cdot \hat{\mathbf{r}}_1 - \boldsymbol{\sigma}_p \cdot \boldsymbol{\sigma}_1)$ interaction terms, since these vanish in the singlet spin state.

Under these circumstances $\rho(\mathbf{r}_1)g_{pt}$ of (2.77) becomes

$$\rho(\mathbf{r}_0)g_{pt} \rightarrow \sum_{S,T} \rho^{ST}(\mathbf{r}_0)g_{pt}^{ST}$$

where, for example,

$$\rho^{10}(\mathbf{r}_0) = \left\langle \Psi_0 \left| \sum_i \delta(\mathbf{r}_0 - \mathbf{r}_i) \left(\frac{3 + \boldsymbol{\sigma}_0 \cdot \boldsymbol{\sigma}_i}{4} \right) \left(\frac{1 - \boldsymbol{\tau}_0 \cdot \boldsymbol{\tau}_i}{4} \right) \right| \Psi_0 \right\rangle$$

In an empirical analysis the form of g_{pt} is assumed. Its parameters are then adjusted to fit the data under investigation.

The first term in (2.66) for the folded potential V_{opt} is referred to as the *direct term*, $V_{\text{opt}}^{(D)}$.

$$V_{\text{opt}}^{(D)} \equiv \int \rho(\mathbf{r}_1)g_{pt}(\mathbf{r}_p, \mathbf{r}_1) d\mathbf{r}_1 \quad (2.85)$$

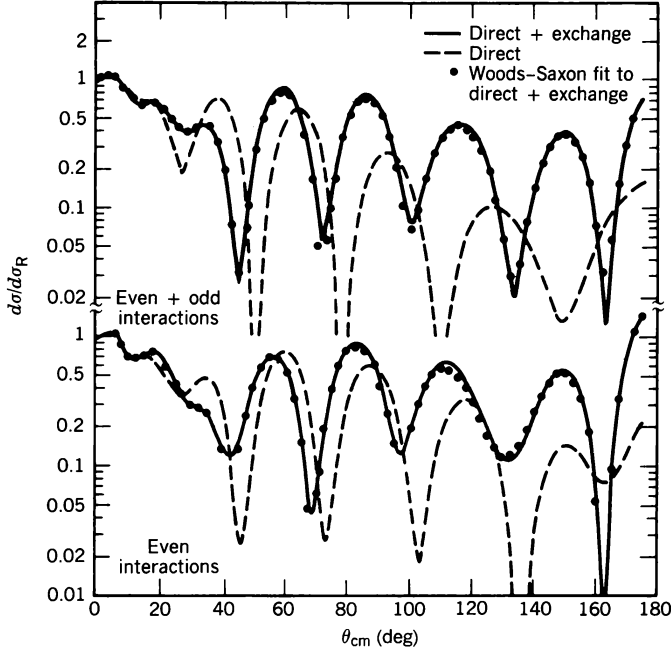


FIG. 2.21. Differential cross sections for 30-MeV protons on ^{120}Sn . [From Owen and Satchler (70).]

and the second is referred to as the *exchange term*. In the earliest formulations of the folding potential model this term was omitted. However, as Owen and Satchler (70) soon demonstrated, this exchange contribution cannot be neglected (see Fig. 2.21). The exchange term is nonlocal. Because of its origin, one can expect it to have a range of the order of $1/k_F$. In calculations it is often replaced by a local equivalent potential using one of the methods described earlier in this section (see Sec. 2B this chapter).

The effective nucleon–nucleon potential to be inserted for g_{pt} in (2.77) has the general form [Greenlees, Pyle, and Tang (68); Petrovitch and Love (80)]

$$\begin{aligned} \mathcal{V}_{\text{eff}} = & v_{00}^C + v_{01}^C \boldsymbol{\tau}_0 \cdot \boldsymbol{\tau}_i + v_{10}^C \boldsymbol{\sigma}_0 \cdot \boldsymbol{\sigma}_i + v_{11}^C \boldsymbol{\sigma}_0 \cdot \boldsymbol{\sigma}_i \boldsymbol{\tau}_0 \cdot \boldsymbol{\tau}_i \\ & + [v_0^T + v_1^T \boldsymbol{\tau}_0 \cdot \boldsymbol{\tau}_i] S_{0i} + [v_0^{LS} + v_1^{LS} \boldsymbol{\tau}_0 \cdot \boldsymbol{\tau}_i] \mathbf{L}_{0i} \cdot (\boldsymbol{\sigma}_0 + \boldsymbol{\sigma}_i) \end{aligned} \quad (2.86)$$

In this expression, the coefficients v_{ab} , v_a^T , and v_a^{LS} are functions of the distance, $|\mathbf{r}_0 - \mathbf{r}_i|$, between the incident projectile \mathbf{r}_0 and the target nucleus nucleon \mathbf{r}_i . The subscripts a and b refer to the spin and isospin character of the interaction. The superscripts C for central, T for tensor, and LS for spin-orbit refer to the spatial symmetry. The tensor operator S_{0i} is defined by

$$S_{0i} = 3\boldsymbol{\sigma}_0 \cdot \hat{\mathbf{r}}_0 \boldsymbol{\sigma}_i \cdot \hat{\mathbf{r}}_i - \boldsymbol{\sigma}_0 \cdot \boldsymbol{\sigma}_i \quad (2.87)$$

where $\hat{\mathbf{r}}_0$ is the unit vector in the \mathbf{r}_0 direction, while

$$\mathbf{L}_{0i} = \frac{1}{\hbar} (\mathbf{r}_0 - \mathbf{r}_i) \times (\mathbf{p}_0 - \mathbf{p}_i) \quad (2.88)$$

It is useful to break up the interaction, (2.86), according to the spin and isospin of the interacting pair, using the projection operators P^{ST} of (2.84).

Noting that both the tensor and spin-orbit potentials vanish when operating as a single spin state ($\sigma_0 = -\sigma_i$), we obtain

$$g_{pt} \equiv v_{\text{eff}} \equiv P^{(11)}V_i^{(11)} + P^{(01)}V_i^{(01)} + P^{(10)}V_i^{(10)} + P^{(00)}V_i^{(00)} \quad (2.89)$$

where

$$V_i^{(11)} = v_{00}^C + v_{01}^C + v_{10}^C + v_{11}^C + (v_0^T + v_1^T)S_{0i} + (v_0^{LS} + v_1^{LS})\mathbf{L}_{0i} \cdot (\boldsymbol{\sigma}_0 + \boldsymbol{\sigma}_i)$$

$$V_i^{(01)} = v_{00}^C + v_{01}^C - 3v_{10}^C - 3v_{11}^C$$

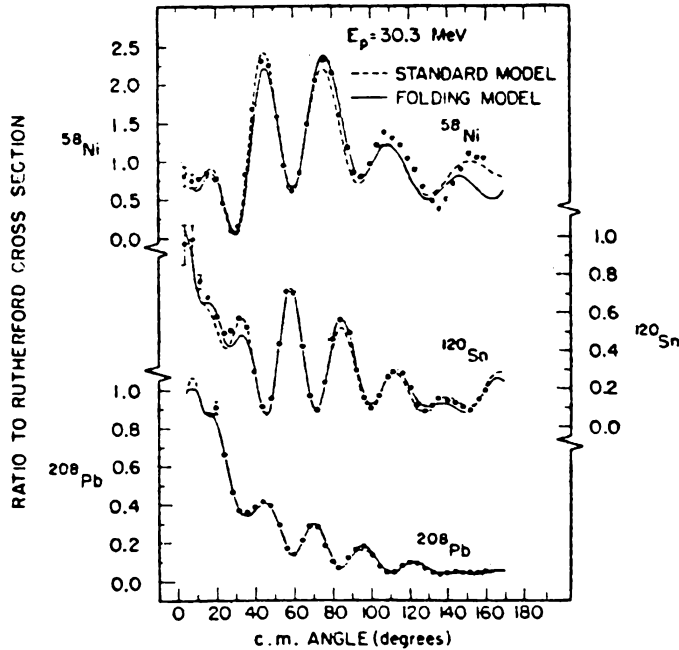


FIG. 2.22. Experimental differential cross-section data points, with errors, for the elastic scattering of 30.3-MeV protons together with predictions. (From Greenlees, Hnizdo, et al. (70).]

$$\begin{aligned}
V_i^{(10)} &= v_{00}^C - 3v_{01}^C + v_{10}^C - 3v_{11}^C + (v_0^T - 3v_1^T)S_{0i} + (v_0^{LS} - 3v_1^{LS})\mathbf{L}_{0i} \cdot (\boldsymbol{\sigma}_0 + \boldsymbol{\sigma}_i) \\
V_i^{(00)} &= v_{00}^C - 3v_{01}^C - 3v_{10}^C + 9v_{11}^C
\end{aligned} \tag{2.90}$$

The Pauli principle requires that $V_i^{(11)}$ and $V_i^{(00)}$ act only when the relative orbital angular momenta of the two interacting nucleons are odd. The often-used Serber force puts both of these equal to zero so that v_{eff} acts only on even relative orbital states. Applications of interaction equation (2.89) to elastic scattering of protons (energies extending up to 40 MeV) have been made by Greenless and his collaborators [Greenless, Pyle, and Tang (68); Greenless, Makofake, and Pyle (70)]. Only the first term in (2.77), the direct term, was used. The exchange term containing effects of the Pauli principle was neglected. Presumably some of its effects are included in the empirical $g(\mathbf{r}_1, \mathbf{r}_p)$. The targets were all even-even nuclei, with the consequence that only v_{00}^C, v_{01}^C and $(v_0^{LS} + v_1^{LS})$ contribute to V_{opt} . These interactions were taken to be real. It was, therefore, necessary to add imaginary potentials of the surface and volume variety, familiar from (2.38), to the V_{opt} of (2.77). The reader is referred to the original papers for the details of the calculation. Comparison of the calculation (eight empirical parameters) with data is shown in Figs 2.22 and 2.23. This subject is discussed further in Section 5.

Intermediate Energies 100 MeV < E < 200 MeV [Nadasen, Schwandt, et al. (81); Schwandt (83)]. The analysis based on the standard model, (2.38), has been continued to higher energies as these have become available. The overall situation has been reviewed by Schwandt (83). We shall make use of that review as well as the paper by Nadasen, Schwandt, et al. (81). In that paper, an optical model analysis using the standard model is developed for the observed angular distribution and polarization for protons with energies ranging up to about 180 MeV elastically scattered from a wide variety of nuclei. The results are given in Table 2.3. The symbols used are those of (2.38). E_p is the proton energy in MeV. $E_p^>$ in the expression for W signifies that the expression $(E_p^> - 135)$ differs from zero only for $E_p > 135$ MeV.

Note that the linear energy dependence of the depth of real part of the central potential as given in Table 2.1, valid at lower energies, is replaced by a logarithmic energy dependence, in agreement with Passatore's earlier prediction. Second, the imaginary term has no surface term and grows rapidly with energy above 135 MeV, presumably as a consequence of pion production. Note, again in contrast with Table 2.1, that the geometrical factors r_0, a_0, r_w , and a_w are energy dependent. Finally, we see that the spin-orbit depth is complex.

The experimental reason for the latter lies in the dominance of the contributions of the spin channel component $\sigma^{(+)}$ corresponding to $\boldsymbol{\sigma} \cdot \mathbf{n} = 1(\mathbf{n} = \hat{k}_{\text{in}} \times \hat{k}_{\text{out}})$ over the contribution from the $\boldsymbol{\sigma} \cdot \mathbf{n} = -1(\sigma^{(-)})$ component, as demonstrated in Fig. 2.24. From the point of view of the optical model this result is a consequence of the complex spin-orbit potential, which enhances the $j = l + \frac{1}{2}$ partial wave with respect to the $j = l - \frac{1}{2}$ component.

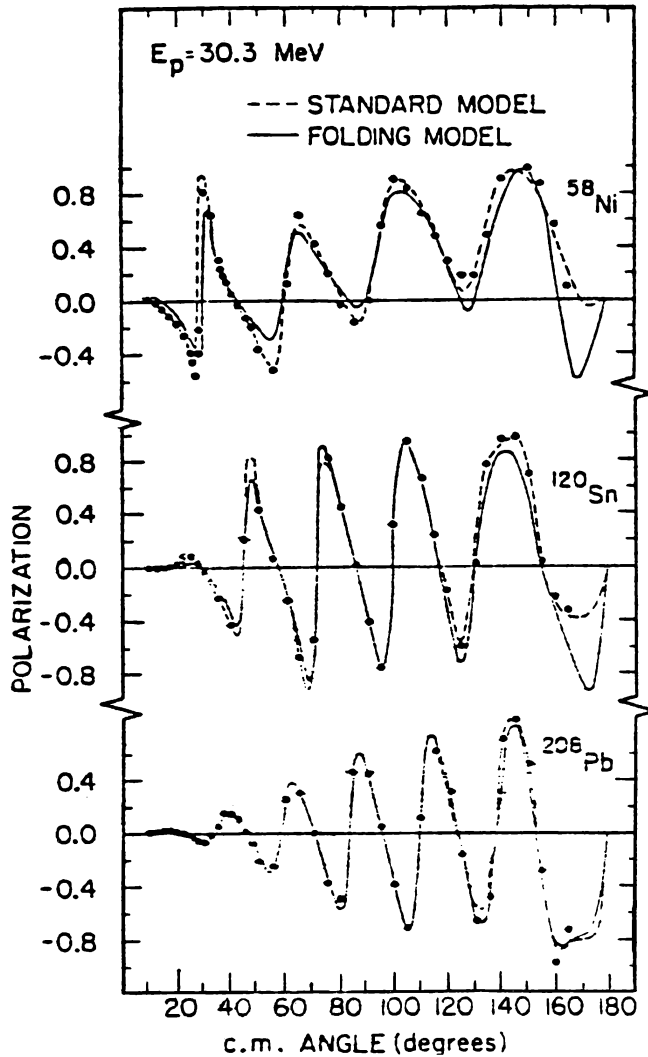


FIG. 2.23. Experimental polarization data points for the elastic scattering 30.3-MeV polarized protons, together with predictions. [From Greenlees, Hnizdo, et al. (70).]

An indication of the energy and isospin dependence of the parameters in Table 2.3 can be obtained from Fig. 2.25. The energy dependence of these optical model parameters seems to indicate the need for modification of the standard equation (2.38) model.

Intermediate Energies > 200 MeV. The difficulties that are suggested by the comparatively rapid energy dependence of the optical model parameters become

TABLE 2.3

$V = \left(92.5 + 64 \frac{N-Z}{A}\right) (1 - 0.155 \ln E_p)$	MeV
$r_0 = 1.18 + \left(0.34 + \frac{6.5}{A}\right) 10^{-3} E_p$	fm
$a_0 = 0.77 - (1.2 \times 10^{-4}) A^{0.4} (180 - E_p)$	
$W = 3.8 + 3 \frac{N}{Z} + (1.23 \times 10^{-3}) (E_p - 135)^2$	MeV, $W_D = 0$
$r_W = 1.16 + \beta \ln(185 - E_p), \quad \beta = \begin{cases} 0.065 & \text{Ca} \\ 0.053 & \text{Zr} \\ 0.058 & \text{Pb} \end{cases}$	fm
$a_W = 0.37 + (1.8 \times 10^{-3}) E_p$	fm
The V_{so} of (2.38b) is replaced by $V_{so} + iW_{so}$.	
$V_{so} = 16.5(1 - \eta \ln E_p)$	MeV, $\eta = 0.160 + 0.06 \frac{N-Z}{A}$
$W_{so} \simeq 5.2(1 - 0.262 \ln E_p)$	MeV
$r_{so} \simeq 1.015 + 5 \times 10^{-4} A$	fm
$a_{so} \simeq 0.60$	fm

explicit in this energy region. For example, the standard Woods–Saxon model fails to provide a good fit to the angular distribution and analyzing power observed in the elastic scattering of 400-MeV protons by ^{40}Ca (see Fig. 2.26). As Meyer, Schwandt et al. (81) have shown, this failure is a consequence of the restriction of the radial behavior of the components of the potential to the Woods–Saxon form. If, for example, the real central potential $-Vf_{ws}(x_0)$ is modified by the addition of a repulsive term:

$$-Vf_{ws}(x_0) \rightarrow -V[f_{ws}(x_0) + \eta f_{ws}^2(x_0)] \quad (2.91)$$

and similarly for other terms, agreement with experiment is vastly improved (see Fig. 2.27). The corresponding central potentials, real and imaginary, are shown in Fig. 2.28. We see the presence of a repulsive central region in the real part of the central potential, together with a substantial increase in the absorptive term. The need for a repulsive central region together with an attractive potential at large r was first suggested by Elton (66).

A qualitative explanation of this important result is provided by the local density approximation using the infinite matter calculation of the real potential, V . As can be seen from Fig. 2.29, the variation of V with energy depends strongly on the density. It decreases more rapidly with energy with the larger density ρ_0 than for the density $\rho_0/2$. The first, in fact, becomes repulsive at roughly 250 MeV, while close to 200 MeV the second already exceeds the first. In the local density approximation one can thus expect a nonmonotonic form for the

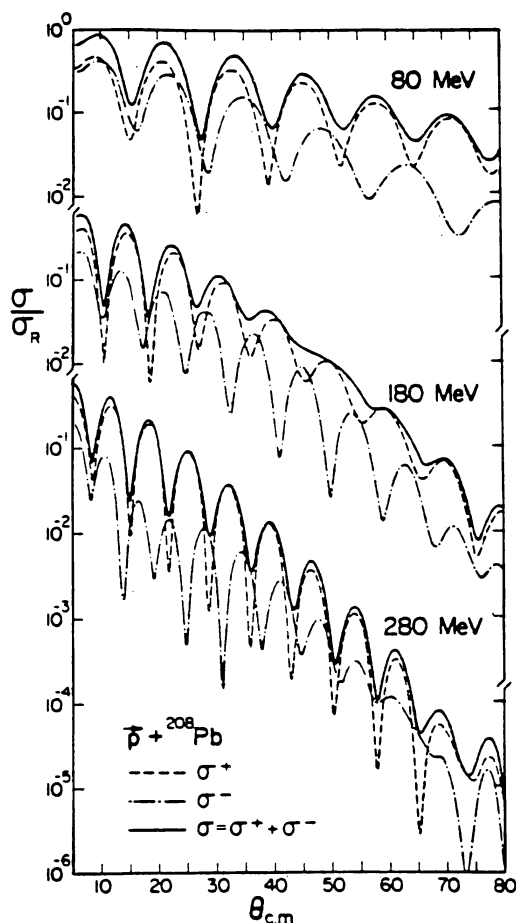


FIG. 2.24. Calculated differential cross-section angular distributions (solid curves) plotted as ratio-to-Rutherford for 80-, 180-, and 280-MeV proton elastic scattering from ^{208}Pb . The partial spin-channel decomposition of the cross sections ("spin up" dashed curves; "spin-down" dot-dashed curves) is also plotted, illustrating the origin of the damping of the oscillatory structure observed around 180 MeV. [From Nadasen, Schwandt, et al (81).]

central potential. In the small r region the potential will become repulsive, while for larger r in the surface region where the density is reduced, the potential will remain attractive, although eventually it, too, will become repulsive at sufficiently large energies in agreement with high-energy (~ 1 GeV) analysis.

Quantitatively good agreement with the 400-MeV data is obtained using the local density approximation and the infinite nuclear matter real potential obtained by Geramb and Nakano (83) based on the Paris nucleon-nucleon potential. A direct comparison is shown in Fig. 2.30 for 400-MeV proton

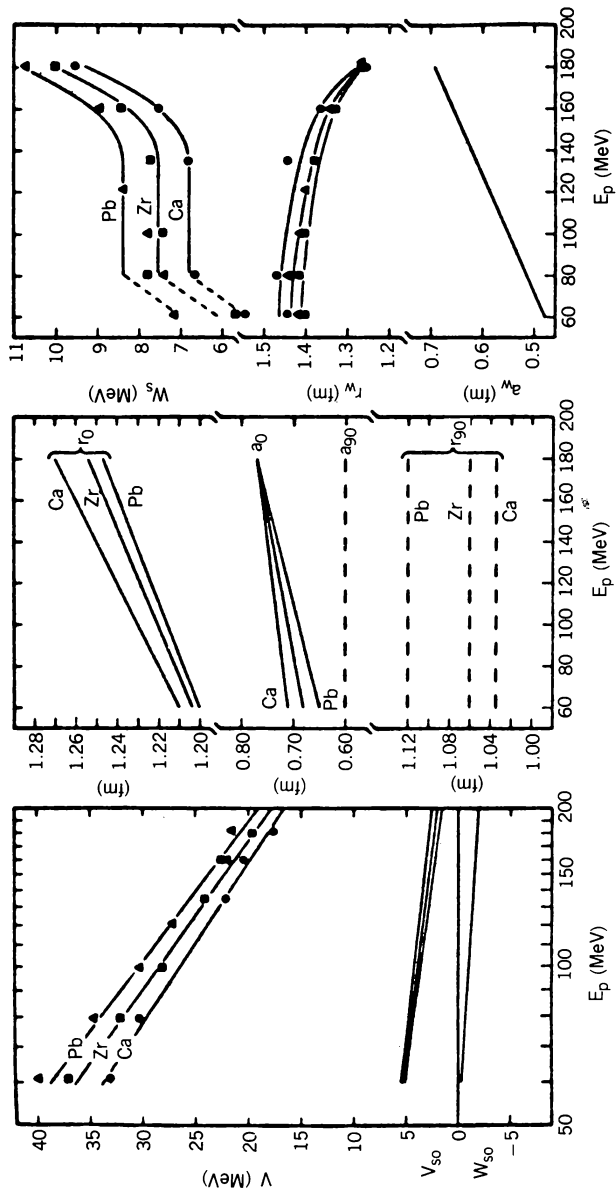


FIG. 2.25. Energy dependence of the complex central and spin-orbit potential parameters obtained in the fixed-spin-orbit fits to the cross-section data. Note the logarithmic energy scale in the left-hand panel. [From Nadasen, Schwandt, et al. (81).]

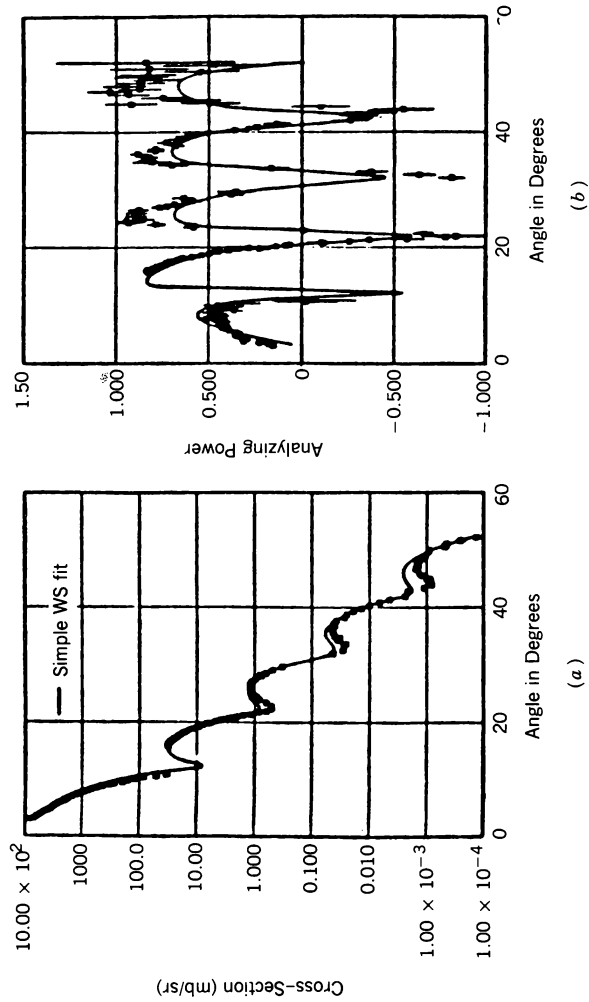


FIG. 2.26. Angular distribution (a) and analyzing power (b) compared to the Woods-Saxon fit. [From Schwandt (8.3).]

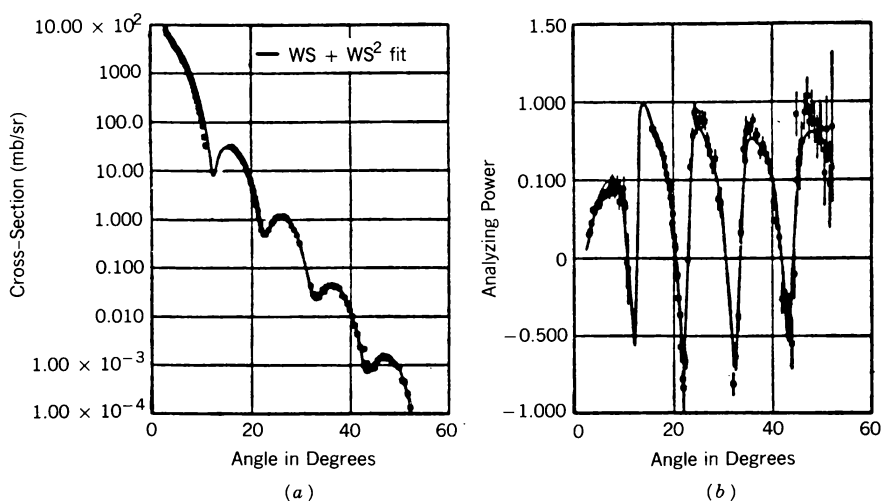


FIG. 2.27. Angular distribution (a) and analyzing power (b) compared to a Woods-Saxon plus (Woods-Saxon)² fit. [From Schwandt (83).]

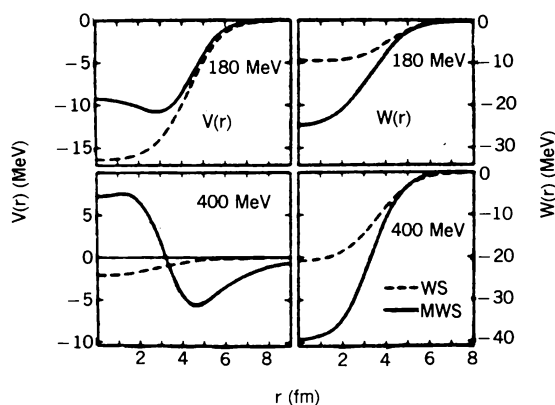


FIG. 2.28. Radial dependence of the real and imaginary parts of the central potential at 180 and 400- MeV. The solid lines give the modified Woods-Saxon fit (see Fig.2.27). [From Schwandt (83).]

scattering by ^{208}Pb . These microscopic calculations remain viable below 200 MeV, as Fig. 2.31 indicates from a comparison of the cross section for 135-MeV protons scattered by ^{16}O with theory. Of course, in this energy region the standard model provides a good fit, as discussed earlier.

The Relativistic Optical Model: Dirac Phenomenology [Clark, Hama, and Mercer (83)]. In this analysis the Schrödinger wave equation is replaced by

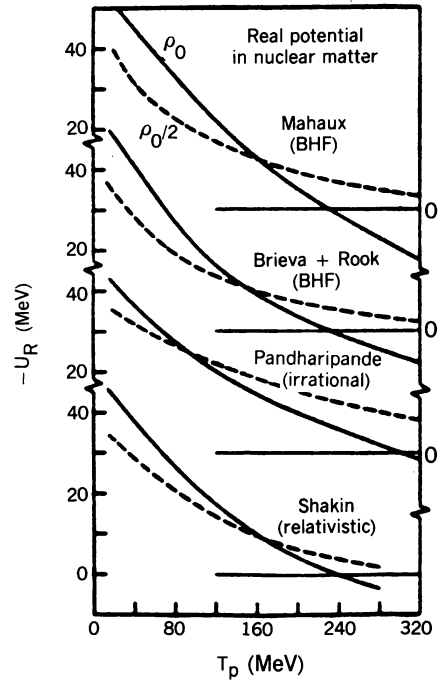


FIG. 2.29. Dependence of the real potential in nuclear matter for normal nuclear density ρ_0 and for $\rho_0/2$ for several models. [From Schwandt (83).]

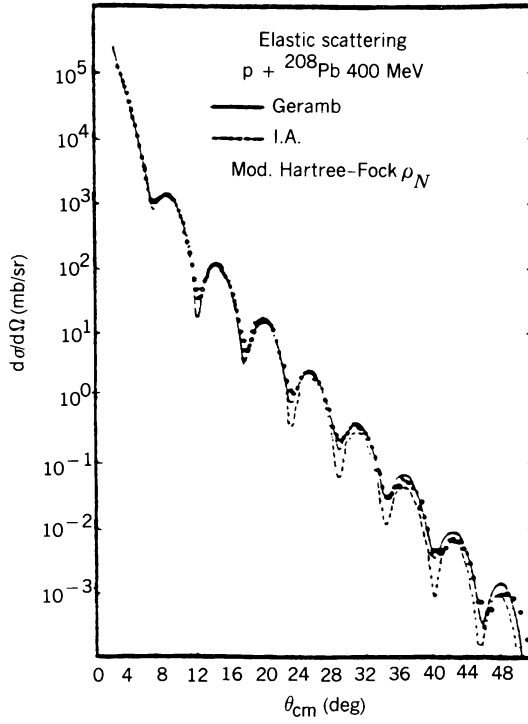
the Dirac equation as if the incident nucleon were a relativistic spin- $\frac{1}{2}$ particle moving in the field of an infinite mass nucleus. This single-channel formulation omits any explicit calculation of recoil associated with the target. The results are in surprisingly good agreement with experiment. When the Dirac equation is reduced to an equivalent Schrödinger equation, the repulsive addition [see. (2.91)], energy dependence, and correct spin-order coupling are obtained. Inasmuch as the physical origins of, for example, the energy dependence in the relativistic model differ so sharply from the physics of the nonrelativistic model of, say, Jeukenne, Lejeune, and Mahaux (76), one remains tentative in evaluating the success of the relativistic model.

The Dirac equation in Hamiltonian form[†] is

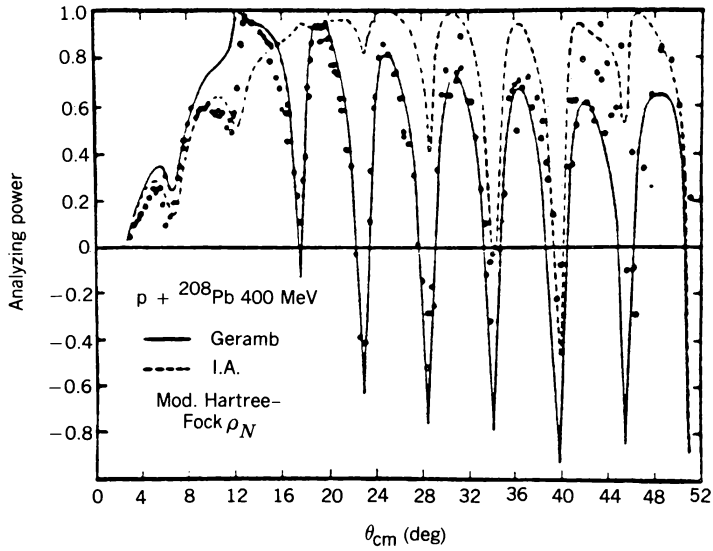
$$[c\boldsymbol{\alpha} \cdot \mathbf{p} + \beta(mc^2 + U_s) + U_0]\psi = E\psi \quad (2.92)$$

[†]For notation, see appendix to ChIX, deShalit and Feshbach (1974) and ChIX.

FIG. 2.30. Angular distribution (a) and analyzing power (b) for 400-MeV protons scattered by ^{208}Pb compared with the calculations using the effective interactions derived by von Geramb and Nakano (83) and with the second-order multiple scattering using a modified Hartree-Fock nucleon density. [From Ray (83).]



(a)



(b)

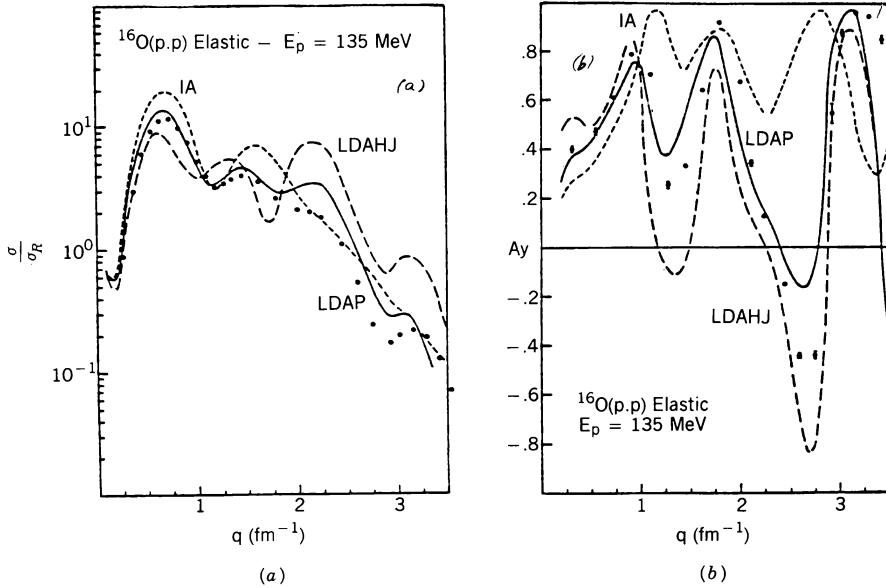


FIG. 2.31. Angular distribution (a) and asymmetry (b) for 135-MeV protons scattered by ^{16}O compared with the impulse approximation (IA), with the local density approximation using the Paris potential (LDAP) or using the Hamada–Johnston potential (LDAHJ). The quantity q is the momentum transfer. [From Kelly (83).]

Other invariants can be added to the β term, but it has sufficed for the empirical treatment to employ only the combination of a scalar potential U_s and the fourth component of a four-vector, U_0 . To obtain a comparison with the Schrödinger optical model equation, one first introduces

$$\psi = \begin{pmatrix} \psi_L \\ \psi_S \end{pmatrix} \quad (2.93)$$

and obtains

$$(\boldsymbol{\sigma} \cdot \mathbf{p})\psi_S = [(E - U_0) - (mc^2 + U_s)]\psi_L \quad (2.94a)$$

$$(\boldsymbol{\sigma} \cdot \mathbf{p})\psi_L = [(E - U_0) + (mc^2 + U_s)]\psi_S \quad (2.94b)$$

Solving the second of these equations for ψ_S and introducing the result into (2.94a) yields

$$\begin{aligned} & [(E - U_0)^2 - (mc^2 + U_s)^2] \psi_L \\ &= \left[(E - U_0) + (mc^2 + U_s) c \boldsymbol{\sigma} \cdot \mathbf{p} \frac{1}{E - U_0 + mc^2 + U_s} c \boldsymbol{\sigma} \cdot \mathbf{p} \right] \psi_L \end{aligned}$$

Evaluating the quantity on the right under the assumption that U_0 and U_s are functions of r yields only

$$[(E - U_0)^2 - (mc^2 + U_s)^2] \psi_L = c^2 p^2 \psi_L + \left[i \frac{c^2}{rA} \frac{\partial A}{\partial r} \boldsymbol{\sigma} \cdot \mathbf{L} - c^2 \frac{1}{rA} \frac{\partial A}{\partial r} (\mathbf{r} \cdot \mathbf{p}) \right] \psi_L$$

where

$$A \equiv \frac{(E - U_0) + (mc^2 + U_s)}{E + mc^2} \quad (2.95)$$

To remove the linear term in \mathbf{p} we replace ψ_L by

$$\psi_L = A^{1/2} \phi \quad (2.96)$$

with the result

$$\begin{aligned} & \left[\frac{1}{c^2} (E - U_0)^2 - \frac{1}{c^2} (mc^2 + U_s)^2 - p^2 \right] \phi \\ &+ \left[-\frac{3}{4} \frac{1}{A^2} \left(\frac{\partial A}{\partial r} \right)^2 + \frac{1}{2r^2 A} \frac{\partial}{\partial r} \left(r^2 \frac{\partial A}{\partial r} \right) + \frac{1}{rA} \frac{\partial A}{\partial r} \boldsymbol{\sigma} \cdot \mathbf{L} \right] \phi = 0 \end{aligned}$$

or placing

$$E^2 - m^2 c^4 \equiv c^2 k^2$$

one obtains the Schrödinger equation:

$$\left(\frac{k^2}{2m} - \frac{p^2}{2m} - V_{\text{eff}} \right) \phi = 0 \quad (2.97)$$

$$\begin{aligned} V_{\text{eff}} \equiv & \frac{E}{mc^2} U_0 + U_s + \frac{1}{2mc^2} (U_s^2 - U_0^2) + \frac{3}{8m} \frac{1}{A^2} \left(\frac{\partial A}{\partial r} \right)^2 \\ & - \frac{1}{4mr^2 A} \frac{\partial}{\partial r} r^2 \frac{\partial A}{\partial r} - \frac{1}{2mrA} \frac{\partial A}{\partial r} \boldsymbol{\sigma} \cdot \mathbf{L} \end{aligned} \quad (2.98)$$

In V_{eff} , note the energy dependence of the U_0 term as well as the presence of the square terms, which by suitable choice of U_s and U_0 can produce a repulsive

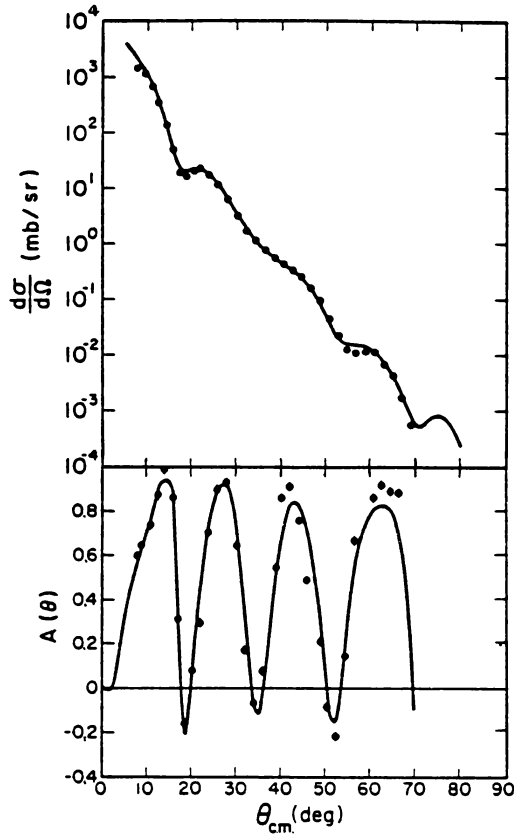


FIG. 2.32. Elastic p - ^{40}Ca cross sections and analyzing powers at 181 MeV. The smooth curves are the results of the relativistic optical model analysis described in the text. [From Arnold, Clark, Mercer, and Schwandt (81).]

term as required by (2.91). These three terms would appear naturally in any single-body relativistic formulation, as they originate from $[(E - U_0)^2 - (mc^2 + U_S)^2]$. In the above, the Coulomb term is included in U_0 . The spin-orbit term and the preceding two terms (also making repulsion contribution) are consequences of the special character of the Dirac equation. To obtain the energy dependence observed, $\text{Re } U_0$ must be repulsive (positive) and $\text{Re } U_S$ attractive (negative). Note that U_0 and U_S are complex. The effect of an attractive U_S is to reduce the nucleon mass inside the interaction region considerably (~ 0.5 m), thereby, amplifying the relativistic effects.

In using the Dirac optical model, (2.92), to fit experimental data [see Clark, Hama, and Mercer (83) for a summary], U_S and U_0 are chosen as follows:

$$U_0 = V_0 f_0(r) + iW_0 g_0(r)$$

$$U_S = V_s f_s(r) + iW_s g_s(r)$$

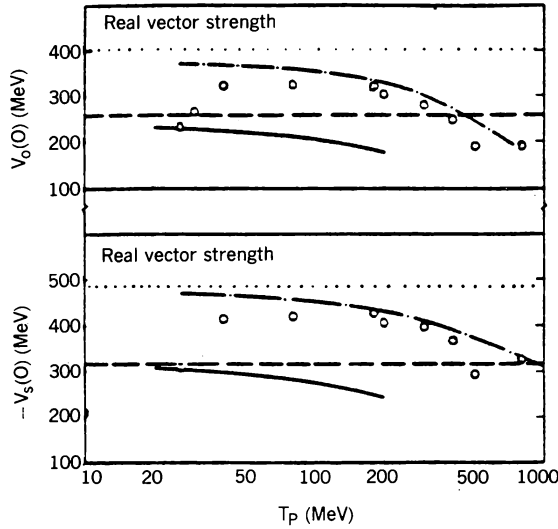


FIG. 2.33. Values of the real scalar V_s and V_0 potentials at $r=0$ determined from the 12-parameter analysis of p - ^{40}Ca data. The upper dotted lines are the values from the relativistic mean field calculation of Arnold, Clark, Mercer, and Schwandt (81). The dashed lines are from Boguta (81); the curved lines are from the relativistic Brueckner Hartree-Fock calculations of Shakin (83); the dashed-dotted curves are from Arnold et al. (82). [From Clark, Hama, and Mercer (83).]

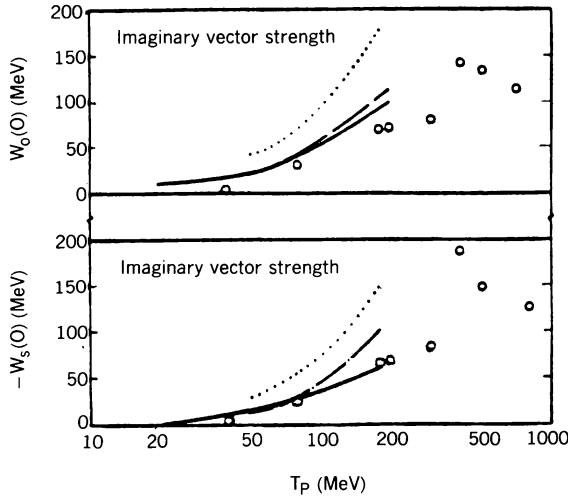


FIG. 2.34. Values of the imaginary scalar W_s and vector W_0 potentials at $r=0$ determined from the 12-parameter analysis of p - ^{40}Ca data described in the text. The dotted lines are the calculations of Jaminon (83); the dashed lines of Horowitz (82), the smooth curves, of Shakin (83). [From Clark, Hama, and Mercer (83).]

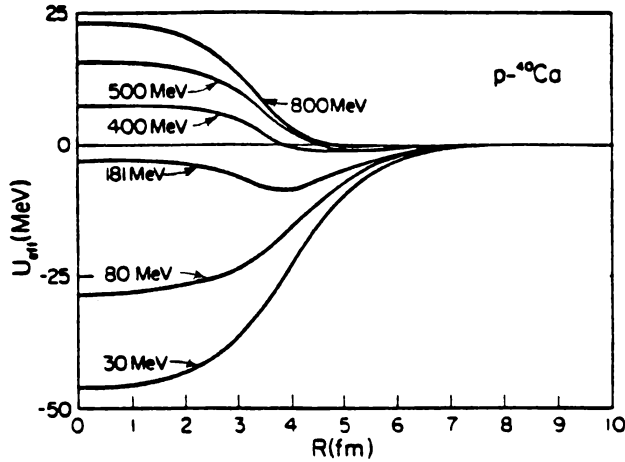


FIG. 2.35. Real part of the Schrödinger equivalent central potential U_{eff} , determined from the Dirac equation based analysis of $p\text{-}^{40}\text{Ca}$ elastic scattering experiments. The Darwin term is omitted. [From Arnold et al. (82).]

where f_0 , f_s , g_0 , and g_s are in the Woods–Saxon form:

$$\frac{1}{1 + e^{(r-R)/a}}$$

The geometrical parameters for f_0 and f_s are obtained by comparison with the results of the Walecka relativistic model (74) obtained by Horowitz and Serot (81). For the case of 181-MeV protons incident on ^{40}Ca , the parameters are as follows:

$$R_0 = 3.474 \text{ fm}$$

$$R_s = 3.453 \text{ fm}$$

$$a_0 = 0.668 \text{ fm}$$

$$a_s = 0.692 \text{ fm}$$

The methods used to obtain these results are described in Arnold, Clark, Mercer, and Schwandt (81). In that paper the geometrical parameters for the imaginary components of U_0 and U_s were chosen identical with those of $\text{Re } U_s$. These, together with the depths $V_{0,s}$ and $W_{0,s}$, were varied in order to obtain a fit of the experimental data, making a six-parameter fit in all. The standard model uses 12 parameters. The fits to the 181-MeV proton data are shown in Fig. 2.32.

The values of the parameters to be combined with those given above are $\text{Re } U_0 = 334 \text{ MeV}$, $\text{Re } U_s = -437 \text{ MeV}$, $\text{Im } U_0 = -107 \text{ MeV}$, and $\text{Im } U_s =$

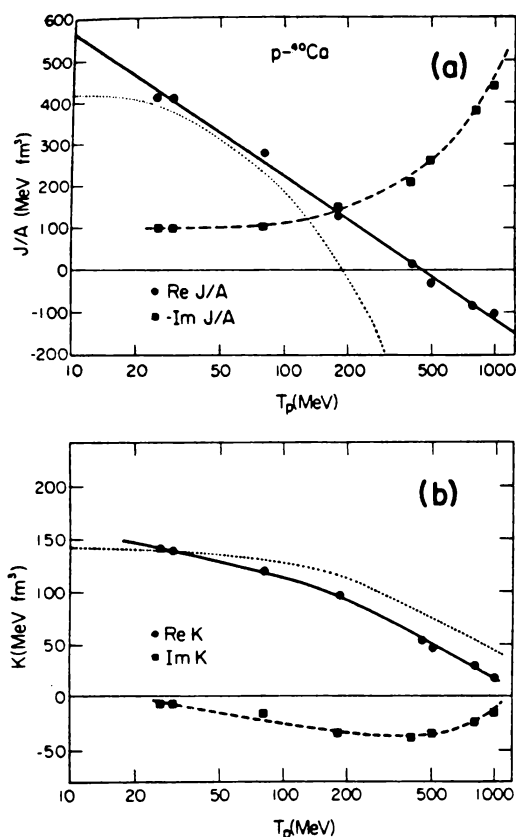


FIG. 2.36. (a) Values of the volume integrals of the real and imaginary parts of the Schrödinger equivalent central potential for ^{40}Ca . The smooth line is a linear fit. The dashed line is to guide the eye. The dotted line gives the Dirac-Hartree values. (b) Values of the volume integrals of the real and imaginary parts of the Schrödinger equivalent spin-orbit potential for ^{40}Ca . The smooth and dashed lines are to guide the eye. The dotted line gives the Dirac-Hartree values. [From Arnold et al. (82).]

109 MeV, where the geometrical parameters for $\text{Im } U_0$ are $R = 3.487 \text{ fm}$ and $a = 0.716 \text{ fm}$. The energy dependence of the potential depths is shown in Figs 2.33 and 2.34.

The real part of the effective potential, (2.98), is shown in Fig. 2.35. The characteristic intermediate wine bottle shape is seen at 181 MeV. The potential is mainly repulsive at 400 MeV and above, with a small attractive tail that diminishes in amplitude as the energy increases. The radial dependence of the effective spin-orbit potential is shown in Fig. 2.36. The excellent agreement at 181 MeV and 400 MeV is repeated at 497 MeV. A new feature at this energy is the measurement of the spin rotation function $Q(\theta)$ shown in Fig. 2.37. The

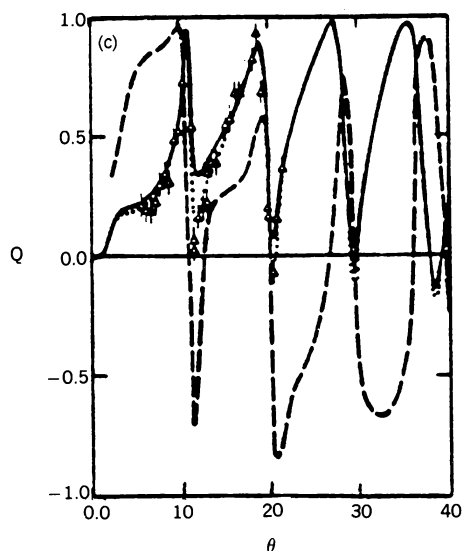


FIG. 2.37. Spin rotation function Q .
(From Schwandt (83).]

relativistic model agrees very well indeed, whereas the standard model result given by the dashed line is in strong disagreement with experiment.

The excellent agreement obtained with the relativistic theory over a wide range of energies is a strong incentive for further study, especially those involving reactions, which will serve as tests of the theory. The one-boson exchange picture used by Walecka (74) and Shakin (83) involving a scalar (σ) and a vector boson (ρ) is not easily made consistent with the quark picture of a nucleon with a root-mean-square radius of 0.8 fm. Thus at the time this is being written, much remains to be done.

3. CHARGE EXCHANGE REACTIONS: OPTICAL MODEL DESCRIPTION[†]

Because of the near identity of the neutron and proton, the charge exchange reactions (p, n) or (n, p) should be closely related to the elastic (p, p) and (n, n) elastic scattering. However, these connections are not simple because of the presence of interactions, such as the Coulomb interaction, which do not conserve isospin. To make this issue more concrete, consider the final state in a (p, n) reaction, in which the target nucleus (Z, N, A) is converted into the nucleus ($Z + 1, N - 1, A$). The target nucleus is in the ground state. The energy-level spectra of the two nuclei, the target and residual are compared in Fig. 3.1. We see that the level in the nucleus ($Z + 1, N - 1$), corresponding to the ground state in the target nucleus (Z, N), is not its ground state, but rather one lifted by an energy approximately equal to the Coulomb energy, which is

[†]Satchler (69), Robson (69), Auerbach, Gal, Hüfner, and Kerman (72).

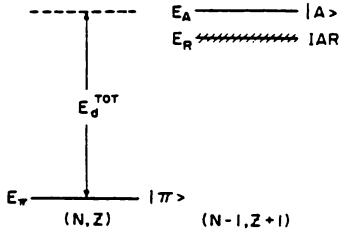


FIG. 3.1. Schematic representation of the relation of the displacement energy $E_d^{(\text{tot})} = E_A - E_w$ and the observed energy of the isobaric analog resonance, E_R . [From Auerbach, Gal, Hüfner, and Kerman (72).]

the dominant isospin symmetry-breaking term. This state in the $(Z + 1, N - 1)$ nucleus is referred to as the *analog* of the ground state of the (Z, N) nucleus. To the extent that T , the isospin, is a good quantum number, it is the ground state (i.e., the lowest state) of the $T = (N - Z)/2$ states in the $(Z + 1, N - 1)$ nucleus. The value of T_z for the ground state of the (Z, N) nucleus is $-T$, while for the analog, $T_z = -T + 1$. It is clear that the channel which should be considered along with the proton, plus the ground state of the (Z, N) nucleus channel, in discussing elastic scattering is the neutron plus analog state of the $(Z + 1, N - 1)$ nucleus. In other words, we consider elastic scattering in the $T = (N - Z)/2$ channel, which, because of the Coulomb shift, should better be referred to as *quasi-elastic scattering*.

One should question the use of isospin quantum numbers for the target and residual nuclei in the presence of a symmetry-breaking Coulomb force, which, particularly for heavy nuclei, must be regarded as strong. The saving grace is that this force is long range, that is, varies slowly over the nuclear volume. Thus its nondiagonal matrix elements between nuclear states are relatively small. As a consequence, the principal effect of this long-range symmetry-breaking force will be to shift the position of the energy levels but not to change substantially the wave functions inside the nuclear volume. In this respect, it therefore makes good sense to continue the use of isospin concepts and nomenclature even for the heavier nuclei, although it should be kept in mind that the states under consideration are not pure. This argument breaks down at sufficiently high excitation energies, for then the smallness of the nondiagonal matrix elements will be compensated by the high density of states with differing isospins that couple to a state with a specific isospin via the isospin symmetry-breaking interaction. Isospin impurity will therefore grow with increasing excitation energy.

We turn now to a consideration of the isospin extension of the optical model. First, we collect some simple results regarding the states involved. The state of the target nucleus will be designated by $|\pi\rangle$ for “parent” and the state of the proton plus target by $|p\pi\rangle$. The analog state, $|A\rangle$, is obtained by converting a neutron in the target to a proton[†]

$$|A\rangle \equiv \alpha T_+ |\pi\rangle \quad (3.1)$$

[†]Recall that in these volumes $\tau_+ |p\rangle = 0$, $\tau_+ |n\rangle = |p\rangle$, $\tau_- |p\rangle = |n\rangle$, $\tau_- |n\rangle = 0$, $\mathbf{t} = \boldsymbol{\tau}/2$.

where α is a normalization factor. We determine α by calculating $\langle A|A \rangle$ and choosing α so that $\langle A|A \rangle$ is unity:

$$\langle A|A \rangle = \alpha^2 \langle \pi | T_- T_+ | \pi \rangle = \alpha^2 [T(T+1) - T_z^2 - T_z]$$

where it has been assumed that $|\pi \rangle$ is a state with a well-defined isospin T with the projection

$$T_z |\pi \rangle = -\frac{1}{2}(N-Z) |\pi \rangle$$

With $T = (N-Z)/2$ we find that

$$\frac{1}{\alpha} = (N-Z)^{1/2} = (2T)^{1/2}$$

so that

$$|A \rangle = \frac{1}{\sqrt{N-Z}} T_+ |\pi \rangle = \frac{1}{\sqrt{2T}} T_+ |\pi \rangle \quad (3.2a)$$

Note that

$$T_- |\pi \rangle = 0 \quad (3.2b)$$

Note. The corrections to (3.2) because of the isospin impurity are discussed by Auerbach, Gal, Hüfner, and Kerman (72).

The states $|p\pi \rangle$ and $|nA \rangle$ can be written as linear combinations of states with isospin $T_> (= T + \frac{1}{2})$ and $T_< (= T - \frac{1}{2})$ using Clebsch–Gordan coefficients:

$$\begin{aligned} |p\pi \rangle \equiv |\tfrac{1}{2}, T, T_z \rangle &= \langle T + \tfrac{1}{2}, T_z + \tfrac{1}{2} | \tfrac{1}{2}, T, T_z \rangle |T_>, T_z + \tfrac{1}{2} \rangle \\ &+ \langle T - \tfrac{1}{2}, T_z + \tfrac{1}{2} | \tfrac{1}{2}, T, T_z \rangle |T_<, T_z + \tfrac{1}{2} \rangle \end{aligned}$$

Taking $T_z = -T$, we obtain [see deShalit and Feshbach (74, p. 927)]

$$|p\pi \rangle \equiv |\tfrac{1}{2}, T, -T \rangle = \frac{1}{\sqrt{2T+1}} [|T_> \rangle + \sqrt{2T} |T_< \rangle] \quad (3.3a)$$

Similarly,

$$|nA \rangle \equiv |\tfrac{1}{2}, -\tfrac{1}{2}, T, -T+1 \rangle = \frac{1}{\sqrt{2T+1}} [\sqrt{2T} |T_> \rangle - |T_< \rangle] \quad (3.3b)$$

Inverting yields

$$|T_> \rangle = \frac{1}{\sqrt{2T+1}} [|p\pi \rangle + \sqrt{2T} |nA \rangle] \quad (3.4a)$$

$$|T_< \rangle = \frac{1}{\sqrt{2T+1}} [\sqrt{2T} |p\pi \rangle - |nA \rangle] \quad (3.4b)$$

The isospin operators that will enter into our discussion include t_3 ($\equiv \frac{1}{2}\tau_3$) operating on the nucleon projectile and $\mathbf{t} \cdot \mathbf{T}$ ($\mathbf{t} \equiv \frac{1}{2}\boldsymbol{\tau}$), where \mathbf{t} operates on the nucleon and \mathbf{T} on the nuclear (π or A) coordinates. The matrix elements of t_3 in the two representations (3.3) and (3.4) are

$$\begin{aligned} \langle p\pi | t_3 | p\pi \rangle &= \frac{1}{2} & \langle p\pi | t_3 | nA \rangle &= 0 = \langle nA | t_3 | p\pi \rangle \\ \langle nA | t_3 | nA \rangle &= -\frac{1}{2} \end{aligned} \quad (3.5)$$

$$\begin{aligned} \langle T_> | t_3 | T_> \rangle &= -\frac{1}{2} \frac{2T-1}{2T+1} = -\langle T_< | t_3 | T_< \rangle \\ \langle T_> | t_3 | T_< \rangle &= \langle T_< | t_3 | T_> \rangle = \frac{\sqrt{2T}}{2T+1} \end{aligned} \quad (3.6)$$

The matrix elements of $\mathbf{t} \cdot \mathbf{T}$ operator are most easily obtained in the representation given by (3.4) since

$$\mathbf{T} \cdot \mathbf{t} = \frac{(\mathbf{T} + \mathbf{t})^2 - T^2 - t^2}{2}$$

One obtains

$$\begin{aligned} \langle T_> | \mathbf{T} \cdot \mathbf{t} | T_> \rangle &= \frac{1}{2}T \\ \langle T_< | \mathbf{T} \cdot \mathbf{t} | T_< \rangle &= -\frac{1}{2}(T+1) \\ \langle T_> | \mathbf{T} \cdot \mathbf{t} | T_< \rangle &= 0 = \langle T_< | \mathbf{T} \cdot \mathbf{t} | T_> \rangle \end{aligned} \quad (3.7)$$

In representation (3.3),

$$\begin{aligned} \langle p\pi | \mathbf{T} \cdot \mathbf{t} | p\pi \rangle &= -\frac{T}{2} \\ \langle nA | \mathbf{T} \cdot \mathbf{t} | nA \rangle &= \frac{1}{2}(T-1) \\ \langle nA | \mathbf{T} \cdot \mathbf{t} | p\pi \rangle &= \langle p\pi | \mathbf{T} \cdot \mathbf{t} | nA \rangle = \frac{1}{2}\sqrt{2T} \end{aligned} \quad (3.8)$$

Note that the operator $\mathbf{T} \cdot \mathbf{t}$ induces the charge exchange reaction $p\pi \leftrightarrow nA$.

With these results in hand it will be possible to discuss the extension to the optical model in isospin space proposed by Lane (62), namely,

$$V = V_0 + 4V_1 \frac{\mathbf{t} \cdot \mathbf{T}}{A} \quad (3.9)$$

These are the only invariants on isospin spin space since the isospin operator for the projectile \mathbf{t} can at most appear linearly. If we were dealing with other projectiles (e.g., heavy ions, pions) whose isospin is greater than unity, other

invariants are possible [Satchler (69)]. In the original Lane model, V_0 and V_1 were assumed to be central potentials, but obviously this can be extended to include spin-orbit terms or other spin-dependent terms, so that generally V_0 and V_1 can have the general form given in (2.38). The spin-dependent term can have a profound effect. For the present we shall assume that V_0 and V_1 depend only on the radial coordinate.

The potential equation (3.9) is not complete since, for example, it does not include the symmetry-breaking interaction between the incident proton and the target nucleus. The principal component of this interaction is the Coulomb force, which in (2.38) is taken to be the interaction of the proton with a spherical distribution of charge of radius R_c and charge Ze . This is an approximation to the sum of Coulomb interactions between the incident protons and the protons in the nucleus. There are additional electromagnetic terms, including magnetic terms, describing the interaction of the magnetic moment and orbital current of the proton with the currents and magnetic moments of the nucleons inside the target nucleus. It should be noted that the Coulomb interaction is modified by vacuum polarization. These effects, which should be added on to Coulomb potential, are discussed in considerable detail by Auerbach, Gal, Hüfner, and Kerman (72). They will not be included in the empirical analysis discussed below.

In the $|nA\rangle$ channel the electromagnetic symmetry-breaking interaction of the neutron with the nucleus A is a consequence of the interaction of its magnetic moment with the currents and fields inside the nucleus. These are similar to those discussed in the preceding paragraph and will be neglected in the empirical analysis.[†]

The optical model Hamiltonian is thus

$$H = H_0 + T_0 + V_0 + 4V_1 \frac{\mathbf{t} \cdot \mathbf{T}}{A} + V_c(\frac{1}{2} + t_3) \quad (3.10)$$

The last term is present only in the $|p\pi\rangle$ channel vanishing in the $|nA\rangle$ channel. The operator H_0 is the Hamiltonian for the target nuclear system of A nucleons; T_0 is the kinetic energy of the nucleon relative to the nucleus. The state vector $|\pi\rangle$ is an eigenstate of H_0 with the energy scale chosen so that the eigenvalue is zero.

With this Hamiltonian, the Schrödinger equation

$$H\Psi = E\Psi$$

can be reduced to a pair of coupled-channel equations by using either

[†]However, the small-angle scattering induced by the interaction of the neutron moment with the electric field of the nucleus can be used to produce polarized neutrons, as pointed out by Schwinger and referred to as *Schwinger polarization scattering* [Schwinger (48)].

representation

$$\Psi = \psi_p(\mathbf{r})|p\pi\rangle + \psi_n(\mathbf{r})|nA\rangle \quad (3.11a)$$

or

$$\Psi = \psi_>(\mathbf{r})|T_>\rangle + \psi_<(\mathbf{r})|T_<\rangle \quad (3.11b)$$

Inserting (3.11a) into the Schrödinger equation and using (3.5)–(3.7), one obtains

$$\left[E - T_0 - V_0 + \frac{2TV_1}{A} - V_C \right] \psi_p = 2\sqrt{2T} \frac{V_1}{A} \psi_n \quad (3.12a)$$

$$\left[E - T_0 - \Delta_C - V_0 - \frac{2(T-1)V_1}{A} \right] \psi_n = 2\sqrt{2T} \frac{V_1}{A} \psi_p \quad (3.12b)$$

with the asymptotic boundary condition that ψ_p approach the incident plane wave plus outgoing scattered wave, while ψ_n yield only an outgoing wave if the total energy in the neutron channel is positive; if negative, an exponentially decaying wave would be required. From (3.12b) one sees that the energy in the neutron channel is $E - \Delta_C$ with

$$\Delta_C = \langle A|H_0|A\rangle - \langle \pi|H_0|\pi\rangle \quad (3.13)$$

If isospin were conserved, Δ_C would be zero. But in virtue of the isospin symmetry-breaking potential, the Coulomb potential, Δ_C , is not zero but rather gives the additional Coulomb energy possessed by the analog nucleus because of the replacement of a neutron in the parent nucleus by a proton. To demonstrate this more closely, we introduce (3.1) expressing $|A\rangle$ in terms of $|\pi\rangle$. One obtains

$$\Delta_C = \frac{1}{2T} \langle \pi|T_-[H_0, T_+]| \pi \rangle \simeq \frac{1}{2T} \langle \pi|[T_-, [H_0, T_+]]| \pi \rangle \quad (3.14)$$

Only if H_0 contains a term that does not conserve isospin and therefore leads to a nonzero value of the commutator $[H_0, T_+]$ will Δ_C differ from zero.

Problem. Assume that the only isospin symmetry-breaking term in H_0 is the Coulomb energy [see (II.6.6) in deShalit and Feshbach (74)]. Express it in terms of isospin spin operators and A ($\equiv N + Z$) and evaluate the double commutator in (3.14).

The value of Δ_C using the Fermi-gas model turns out to be

$$\Delta_C \simeq \frac{3e^2}{5R} [(2Z + 1) - 1.02Z^{1/3}] \quad (3.15)$$

[see Spencer and Kerman (72)], where R is the nuclear radius. For ^{88}Sr , Δ_c is about 11.5 MeV.

For a sufficiently low E , the available energy for the neutron analog channel, (3.12b), is negative, so that the wave function decays exponentially. Moreover, the homogeneous form of (3.12b) obtained by placing the right-hand side equal to zero will admit bound-state solutions. As we know from the example introducing Chapter III, this has the consequence that the proton channel will exhibit a resonance at an energy close to the energies of these bound states. These are the elastic isobar analog resonances.

Before discussing these, one more feature must be added to (3.12a). The imaginary component of the potential, V_0 , is not necessarily the same for the proton and neutron channel since the coupling of these channels to other channels and to more complex excitations differ. In other words, additional isospin dependence needs to be added. The issues involved are clearer if we make use of the $T_> (= T + \frac{1}{2})$ and $T_< (= T - \frac{1}{2})$ representations. Inserting (3.11b) into the Schrödinger equation yields

$$\begin{aligned} & \left[E - T_0 - V_0 - \frac{2TV_1}{A} - \Delta_c + \frac{1}{2T+1}(\Delta_c - V_c) \right] \psi_> \\ &= -\frac{1}{2T+1} \sqrt{2T}(\Delta_c - V_c) \psi_< \end{aligned} \quad (3.16a)$$

$$\begin{aligned} & \left[E - T_0 - V_0 + \frac{2(T+1)}{A} V_1 - V_c - \frac{1}{2T+1}(\Delta_c - V_c) \right] \psi_< \\ &= -\frac{1}{2T+1} \sqrt{2T}(\Delta_c - V_c) \psi_> \end{aligned} \quad (3.16b)$$

As is clear from (3.4), the major component of $\psi_>$ is the neutron channel. As originally emphasized by Robson (65), we also note that the coupling between the $T_>$ and $T_<$ channel occurs “outside” the nucleus. In the nuclear interior Δ_c and V_c will cancel approximately. Thus the mixing between the two states is referred to as *external*.

It is anticipated that the coupling of the $T_>$ channel to channels and states that have not been included in (3.16) will be small since the density of $T_>$ states is relatively small, whereas the density of $T_<$ states will be normal. We therefore add an imaginary term to (3.16b) only, that is, replace V_0 by $V_0 + iW_0$ in that equation. In isospin language this is described by

$$V_0 \rightarrow V_0 + iW_0 \frac{(T + \frac{1}{2})(T + \frac{3}{2}) - (\mathbf{T} + \mathbf{t})^2}{2T+1} \quad (3.17)$$

Equations (3.12) are modified as a consequence. They now become

$$\left[E - T_0 - V_0 + \frac{2TV_1}{A} - V_c - \frac{2T}{2T+1}iW_0 \right] \psi_p = \left(\frac{2V_1}{A} - \frac{iW_0}{2T+1} \right) \sqrt{2T} \psi_n \quad (3.18a)$$

$$\left[E - \Delta_c - T_0 - V_0 - \frac{2(T-1)V_1}{A} - \frac{iW_0}{2T+1} \right] \psi_n = \left(\frac{2V_1}{A} - \frac{iW_0}{2T+1} \right) \sqrt{2T} \psi_p \quad (3.18b)$$

These equations can now be used to study the isobar analog resonances using the optical model forms of Perey and Buck (62) or Rosen, Beery, Goldhaber, and Auerbach (65), taking V_1 to have the same form as W_0 . An example of a fit to the observed resonances in the reaction ($p + {}^{88}\text{Sr}$) is shown in Fig. 3.2. Note that the proton energy employed is always considerably less than the value of Δ_c , which is taken to be 11.45 MeV. Writing

$$V_1 = v_1 f_W(x)$$

where $f_W(x)$ is given by (2.28), $4v_1/A$ has the value of 2.2 MeV and v_1 the value 48.4 MeV.

When the target nucleus has a spin, as, for example, ${}^{89}\text{Y}$ with a spin of $\frac{1}{2}$, the analog resonance can have two spin values ($j \pm \frac{1}{2}, j \neq 0$) according to the value of the spin of the neutron in the neutron channel [see (3.18b)]. To obtain a fit, it is necessary to add a spin-dependent term to the optical model Hamiltonian of the form $\sigma \cdot \mathbf{I}$, a possibility mentioned earlier in this chapter [see

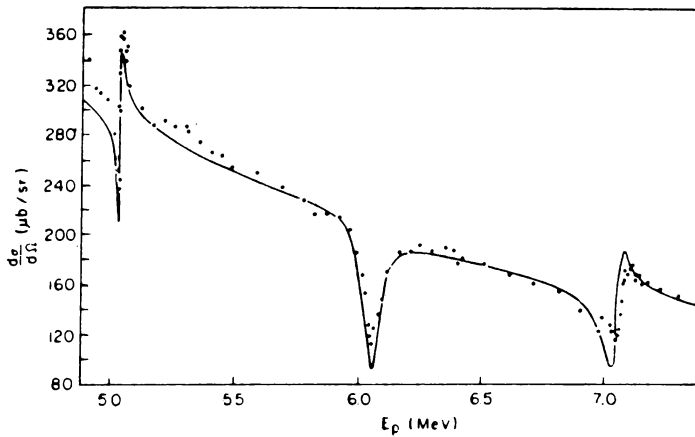


FIG. 3.2. Calculated differential cross sections at 90° for $p + {}^{88}\text{Sr}$. [From Auerbach and Dover (66).]

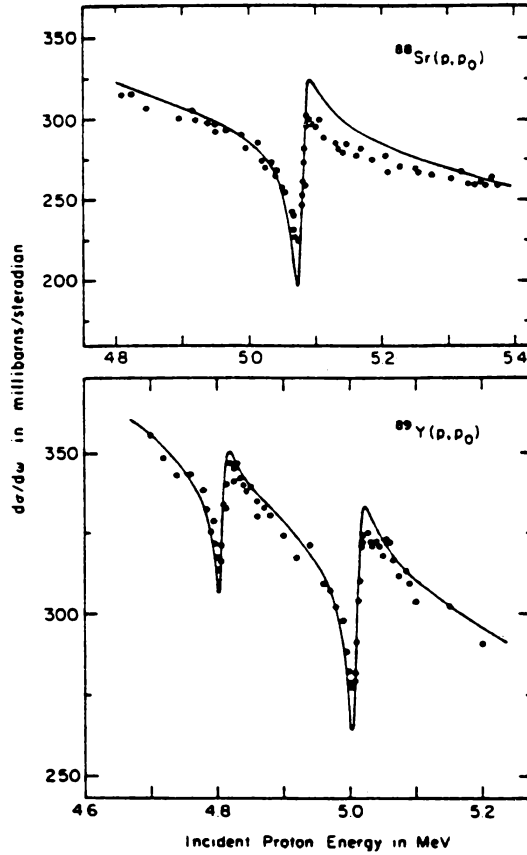


FIG. 3.3. Comparison of the calculated energy dependence of the cross-sections at 90° for ^{88}Sr and ^{89}Y with experiment. [From Spencer and Kerman (72).]

(2.41)]. Taking this additional term as

$$\frac{V_2}{A} f_W(x)$$

Spencer and Kerman (72) find V_2/A to equal to 0.7 MeV. Their results are shown in Fig. 3.3.

We now turn to a discussion of the global analysis of the (p, p) , (n, n) , and (p, n) reaction, where the last goes to the isobar analog state, developed by Patterson, Doering, and Galonsky (76). These authors use (3.12), employing the DWA for the (p, n) reaction. In this application of the DWA, the homogeneous

forms of (3.12) are used to describe the proton and neutron scattering:

$$\left[E - T_0 - V_0 + \frac{2TV_1}{A} - V_C \right] \psi_p \simeq 0 \quad (3.19a)$$

$$\left[E - \Delta_C - T_0 - V_0 - \frac{2(T-1)V_1}{A} \right] \psi_n \simeq 0 \quad (3.19b)$$

while the (p, n) transition amplitude is given approximately by

$$\mathcal{T}_{pn}^{\text{IAS}} \simeq \left\langle \psi_n^{(-)} \left| 2\sqrt{2T} \frac{V_1}{A} \right| \psi_p^{(+)} \right\rangle \quad (3.20)$$

The potential (3.9) is written

$$V = -\mathcal{V}_0(r, E) + \mathcal{V}_{so}(r) + 4\mathcal{V}_1(r, E) \frac{\mathbf{t} \cdot \mathbf{T}}{A} \quad (3.21)$$

where

$$\begin{aligned} \mathcal{V}_k(r, E) = & (V_{kC} + EV_{kE})f(r, R_R, a_R) + i(W_{kC} + EW_{kE})f(r, R_I, a_I) \\ & - ia_I(WS_{kC} + EWS_{kC}) \frac{d}{dr} f(r, R_I, a_I) \quad k = 0, 1 \end{aligned} \quad (3.22)$$

and where

$$f(r, R, a) = \left[1 + \exp\left(\frac{r-R}{a}\right) \right]^{-1} \quad R_p = r_p A^{1/3} \quad (3.23)$$

The spin-orbit potential is

$$\mathcal{V}_{so}(r) = V_{so} \left(\frac{\hbar}{m_\pi c} \right)^2 \boldsymbol{\sigma} \cdot \mathbf{l} \frac{1}{r} \frac{d}{dr} f(r, R_{so}, a_{so}) \quad (3.24)$$

They also take V_C in the form given by (2.27) with

$$R_C = 1.149A^{1/3} + 1.788A^{-1/3} - \frac{1.163}{A}$$

Patterson, Doering, and Galonsky (76) find (for details, see their paper)

$$\begin{aligned} \text{Re} \left(-\mathcal{V}_0 \pm \frac{2T\mathcal{V}_1}{A} \right) = & \left(55.8 - 0.32E \pm 17.7 \frac{N-Z}{A} \text{ MeV} \right) f(r, R_R, a_R) \\ r_R = & 1.17 \text{ fm} \quad a_R = 0.75 \text{ fm} \end{aligned} \quad (3.25)$$

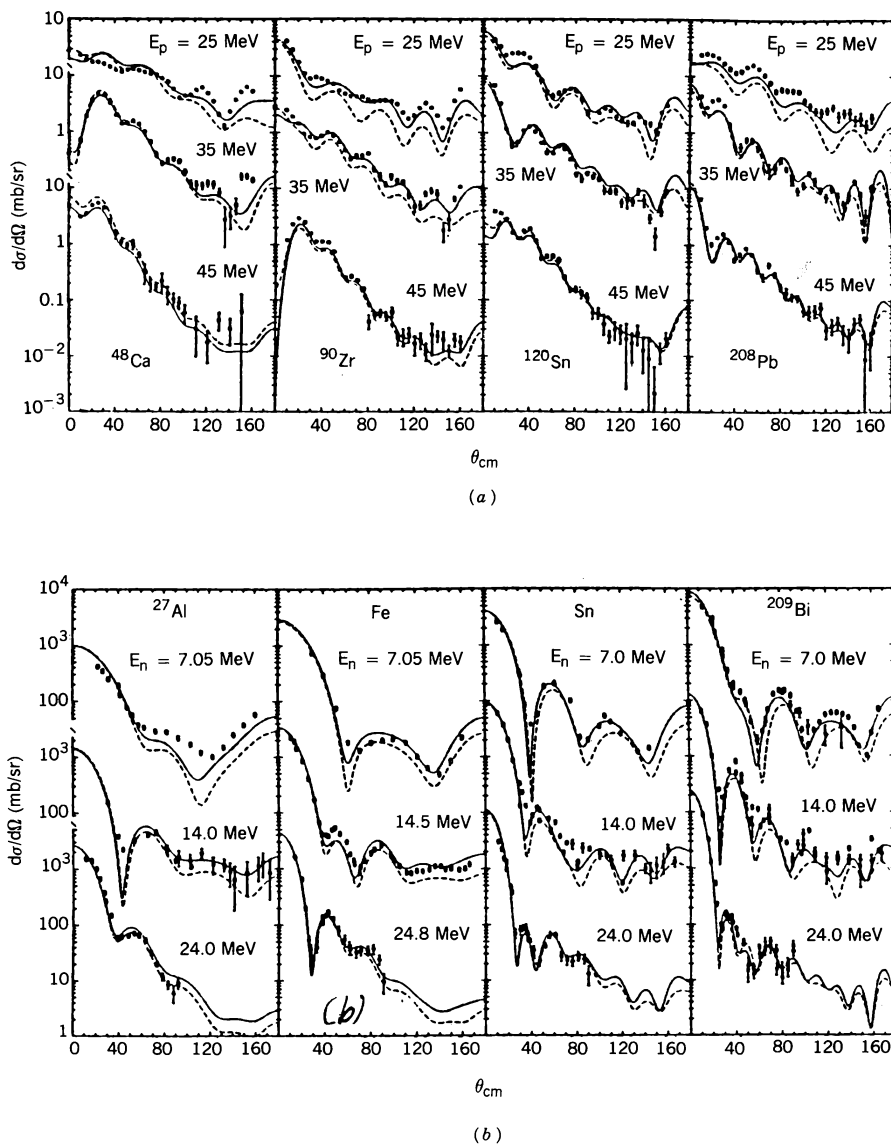


FIG. 3.4. (a) Comparison of DWA calculations with (p,n) isobar analog differential cross-section data; (b) comparison of optical model calculations with (n,n) elastic differential cross-section data. [From Patterson, Doering, and Galonsky (76).]

$$\begin{aligned}
\text{Im}\left(-\mathcal{V}_0 \pm \frac{2TV_1}{A}\right) &= (-1.4 + 0.22E) \text{ MeV } f(r, R_I, a_I) \\
&\quad - a_I \left(9.6 - 0.22E \pm (18.1 - 0.31E) \frac{N-Z}{A}\right) \frac{d}{dr} f(r, R_I, a_I) \\
r_I &= 1.32 \text{ fm} \quad a_I = 0.51 + 0.7 \frac{N-Z}{A}
\end{aligned} \tag{3.26}$$

The spin-orbit strength

$$V_{so} = 6.2 \text{ MeV} \tag{3.27}$$

with

$$r_{so} = 1.01 \text{ fm} \quad a_{so} = 0.75 \text{ fm}$$

The plus sign in the results above refers to the proton channel, the negative to the neutron channel. In (3.19), $T-1$ has been replaced by T . The coupling term in (3.20) is

$$-\frac{2\sqrt{N-Z}}{A} [17.7 \text{ MeV } f(r, R_R, a_R) + i(18.1 - 0.31E)f(r, R_I, a_I)] \tag{3.28}$$

Comparisons with the fit to (p, p) elastic scattering data ($E_p = 25, 35, 45 \text{ MeV}$) by Becchetti and Greenlees (69), with (p, n) cross sections for the same energies and the same target nuclei, ^{48}Ca , ^{90}Zr , ^{120}Sn , and ^{208}Pb , are made. Predictions of neutron elastic scattering at E_n of about 7, 14, and 24 MeV for target nuclei ^{27}Al , Fe , Sn , and ^{209}Bi are compared with experiment. The results are satisfactory. A representative sample is shown in Fig. 3.4.

4. INELASTIC SCATTERING

In this section we consider the inelastic scattering reaction, in which an incident projectile excites the target nucleus:

$$a + A \rightarrow A^* + a' \tag{4.1}$$

We assume that the process is a prompt one; that is, it is the result of a direct interaction. As a consequence, we expect the angular distribution of nucleon a' in the center-of-mass system to be asymmetric, peaked in the forward cone. The energy variation of the cross section will be relatively slow, while the angular distribution will exhibit characteristic diffraction oscillations, a consequence of the relatively well-defined nuclear radius.

At low and intermediate energies, the surface region of the target plays the important dynamic role. A qualitative discussion of surface reactions is given

in Chapter I. We repeat some of the arguments here. Let the incident and final momentum of the projectile be \mathbf{p}_i and \mathbf{p}_f , respectively. Since we are dealing with a surface reaction, the incident and final orbital angular momenta are $\mathbf{p}_i R$, and $\mathbf{p}_f R$, respectively, where R is the nuclear radius. The net resulting change in angular momentum $\hbar \Delta J$ is thus

$$\hbar \Delta J = |\mathbf{p}_i - \mathbf{p}_f| R \equiv \hbar q R \quad (4.2)$$

implying a maximum in the angular distribution at an angle θ_M given by

$$\sin^2 \frac{\theta_M}{2} = \frac{1}{4p_i p_f} \left[\left(\frac{\hbar \Delta J}{R} \right)^2 - (p_i - p_f)^2 \right] \quad (4.3)$$

When $p_i \approx p_f$, as often occurs,

$$\theta_M \simeq \frac{\hbar \Delta J}{p_i R} \quad (4.4)$$

We note that θ_M increases with increasing ΔJ . It also follows from (4.3) that the cross section will vanish for $\theta < \theta_M$ since in this region, $\hbar \Delta J < |\mathbf{p}_i - \mathbf{p}_f| R$. This is a classical result, of course. Quantum mechanically, the cross section will diminish rapidly as θ decreases from θ_M , so that θ_M is the first maximum in the angular distribution. In Chapter I this simple result is compared with the measured angular distributions for inelastic α -scattering by ^{58}Ni and is shown to give good results, especially when a Coulomb correction is made. The oscillations in the cross section have an angular separation $\Delta\theta$ predicted by the uncertainty principle to be

$$\Delta\theta \simeq \frac{1}{\Delta J} = \frac{1}{qR}$$

Some further insight into the inelastic scattering process can be obtained if one makes use of the high-energy approximation to the optical model wave function in (1.14):

$$\mathcal{F}_{fi}^{(\text{dir})} = \langle \chi_f^{(-)} | H_{fi}^{(\text{opt})} \psi_i^{(+)} \rangle \quad (4.5)$$

We assume that $\psi_i^{(+)}$ and $\chi_f^{(-)}$ can be written as a product of the projectile wave function and the target nuclear wave function Ψ_i and Ψ_f for the ground and excited states, respectively. Thus

$$\psi_i^{(+)} = \phi_i^{(+)} \Psi_i$$

and

$$\chi_f^{(-)} = \phi_f^{(-)} \Psi_f \quad (4.6)$$

For didactic simplicity we have neglected the antisymmetrization that is required when the projectile consists of one or more nucleons (the effect of antisymmetrization is discussed on p. 195). The transition Hamiltonian $H_{fi}^{(\text{opt})}$ is taken to be a sum of two particle interactions between the incident nucleon and the nucleons of the target, and, again for simplicity, we assume these residual interactions to be central and complex:

$$H_{fi}^{(\text{opt})} = \sum_i v(\mathbf{r}_0, \mathbf{r}_i) \quad (4.7)$$

where \mathbf{r}_i is the coordinate of the target nucleus and \mathbf{r}_0 that of the incident projectile. With these assumptions, (4.5) becomes

$$\mathcal{T}_{fi}^{(\text{dir})} = \langle \phi_f^{(-)}(\mathbf{r}_0) | \mathcal{V}_{fi}(\mathbf{r}_0) \phi_i^{(+)}(\mathbf{r}_0) \rangle \quad (4.8)$$

where

$$\mathcal{V}_{fi}(\mathbf{r}_0) \equiv \langle \Psi_f | \sum_j v(\mathbf{r}_0, \mathbf{r}_j) \Psi_i \rangle \quad (4.9)$$

The high-energy approximation[†] assuming a spin-independent central optical potential to $\phi_i^{(+)}$ is [see (II.5.7)]

$$\phi_i^{(+)} \sim \exp \left\{ i \left[\mathbf{k}_i \cdot \mathbf{r}_0 - \frac{\mu}{\hbar^2 k_i} \int_{-\infty}^{z_0} V_{\text{opt}}(\mathbf{b}_0, z) dz \right] \right\} \quad (4.10)$$

The z direction is given by \mathbf{k}_i , and \mathbf{b}_0 is the coordinate vector (x_0, y_0) perpendicular to \mathbf{k}_i . The magnitude, b_0 , is the *impact parameter*. Similarly,

$$\phi_f^{(-)*} \sim \exp i \left\{ \left[-\mathbf{k}_f \cdot \mathbf{r}_0 + \frac{\mu}{\hbar^2 k_f} \int_{\infty}^{z'_0} V_{\text{opt}}(\mathbf{b}'_0, z) dz \right] \right\} \quad (4.11)$$

where z'_0 is the direction of \mathbf{k}_f . In combining (4.10) and (4.11) we shall, for the second term in the exponential of (4.11), make the approximation $k_i \approx k_f$, valid when the excitation energy is small compared to the projectile energy, and the approximation that the directions of z'_0, \mathbf{b}'_0 are the same[§] as that of z_0 and \mathbf{b}_0 , implying small-angle scattering. Under these circumstances, the product $\phi_f^{(-)*} \phi_i^{(+)}$ is given by the simple expression

$$\phi_f^{(-)*} \phi_i^{(+)} \simeq \exp \{ i [(\mathbf{k}_i - \mathbf{k}_f) \cdot \mathbf{r}_0] \} \exp \left[-i \frac{\mu}{\hbar^2 k_i} \int_{-\infty}^{\infty} V_{\text{opt}}(\mathbf{b}_0, z) dz \right]$$

[†]This is accurate at sufficiently high energy, $E > 100$ MeV [Bassichis, Feshbach, and Reading (71)], but the results obtained will be useful, as they are qualitatively correct below that energy.

[§]Some improvement in the last of these approximations can be made if the mutual directions of z_0 and z'_0 is taken to that of $\frac{1}{2}(\mathbf{k}_i + \mathbf{k}_f)$.

The first exponential is that which appears in the Born approximation. The second is an approximation to the effect of the distortion caused by the optical potential. We note that it depends only on the impact parameter b_0 ; there is no z dependence. Since V_{opt} has a negative imaginary component ($\equiv -iW$), to take absorption into account, the magnitude of the second factor is less than 1 and is given by

$$\exp\left[-\frac{\mu}{\hbar^2 k_i} \int_{-\infty}^{\infty} W(\mathbf{b}_0, z) dz\right] \quad (4.12)$$

The integral is the total absorption along a path parallel to the z axis (i.e., in the incident direction) at a distance b_0 away from that axis. The maximum attenuation for the optical potentials commonly used will occur for a ray through the center of the nucleus. The attenuation will decrease as b_0 increases, since the path length is shorter and the absorption generally weaker. Once $b > R$, $W \rightarrow 0$ and the attenuation will go to zero. The factor, (4.12), therefore emphasizes the contribution of the nuclear surface to the direct reaction amplitude.

To complete the calculation, we need to evaluate $\mathcal{V}_{fi}(\mathbf{r}_0)$, defined by (4.9), and then perform the integral over \mathbf{r}_0 indicated by (4.8) to obtain $\mathcal{T}_{fi}^{(\text{dir})}$. The problem is simplified somewhat if we let v be a delta function of strength g , so that

$$\begin{aligned} \mathcal{V}_{fi} &= g \langle \Psi_f | \sum_i \delta(\mathbf{r}_0 - \mathbf{r}_i) \Psi_i \rangle \\ &= Ag \langle \Psi_f | \delta(\mathbf{r}_0 - \mathbf{r}_1) \Psi_i \rangle \\ &= Ag \int \Psi_f^*(\mathbf{r}_0, \mathbf{r}_2, \dots) \Psi_i(\mathbf{r}_0, \mathbf{r}_2, \dots) d\mathbf{r}_2 \dots \end{aligned} \quad (4.13)$$

$$= Ag \rho_{fi}(\mathbf{r}_0) \quad (4.14)$$

where ρ_{fi} is the density matrix measuring the overlap of the initial and final nuclear wave functions. The density matrix can be expanded in spherical harmonics (in the absence of spin),

$$\rho_{fi}(\mathbf{r}_0) = \sum \rho_{fi,lm}(r_0) Y_{lm}(\Omega_0) \quad (4.15)$$

where

$$|J_i - J_f| \leq l \leq (J_i + J_f) \quad (4.16)$$

The quantity, l is then the transferred angular momentum.

With these approximations, (4.8) for $\mathcal{T}_{fi}^{(\text{dir})}$ has the form

$$\mathcal{T}_{fi}^{(\text{dir})}(lm) \sim \int d\mathbf{r}_0 e^{i\mathbf{q} \cdot \mathbf{r}_0} e^{i\chi(\mathbf{b}_0)} \rho_{fi,lm}(r_0) Y_{lm}(\Omega_0) \quad (4.17)$$

where various constants of proportionality have been omitted and one of the Y_{lm} 's has been selected. The function $\chi(\mathbf{b}_0)$ is

$$\chi(\mathbf{b}_0) = -\frac{\mu}{\hbar^2 k_i} \int_{-\infty}^{\infty} V_{\text{opt}}(\mathbf{b}_0, z) dz \quad (4.18)$$

The vector $\mathbf{q} \equiv (\mathbf{k}_i - \mathbf{k}_f)$ has the components

$$q_z = k_i - k_f \cos \theta \quad q_x = -k_f \sin \theta \quad q_y = 0$$

so that

$$\mathbf{q} \cdot \mathbf{r}_0 = (k_i - k_f \cos \theta) z_0 - k_f b_0 \sin \theta \cos \varphi_0$$

The angle θ is the scattering angle, the angle between \mathbf{k}_f and \mathbf{k}_i .

It is natural to use cylindrical coordinates, (z_0, b_0, φ_0) in evaluating integral equation (4.17). Recalling that $Y_{lm}(\Omega) \sim e^{im\varphi_0} P_{lm}(\cos \theta_0)$, the φ_0 integral can be performed immediately to yield $2\pi \cdot i^m J_m(k_f b_0 \sin \theta)$. The z_0 integration requires the calculation of a Fourier transform of the z_0 dependence of $\rho_{fi,lm}(r_0) P_{lm}(\cos \theta)$. To obtain a rough value, we assume that the longitudinal momentum transfer $(k_i - k_f \cos \theta)R$ is small and that the overlap, $\rho_{fi,lm}(r_0)$, has its maximum at the nuclear radius. The first of these assumptions holds if the scattering angle is small and if the energy loss is small compared to the incident energy. The second specifies the interaction to favor a surface reaction. Combined with the attenuation originating in $\chi(\mathbf{b}_0)$, these assumptions lead to the result that the contribution to the z_0 integral comes primarily from the $z_0 = 0$ region. Thus the active region in the target nucleus for inelastic scattering in the forward direction and with small energy loss is the neighborhood of the perimeter of the great circle (for a spherical nucleus) perpendicular to the incident direction. With $z_0 = 0$ one may replace $P_{lm}(\cos \theta)$ by $P_{lm}(0)$ (i.e., $\theta_0 = \pi/2$). This function differs from zero only when $l + m$ is even.

Returning to k_0 , (4.17), one finds that

$$\mathcal{T}_{fi}^{(\text{dir})}(lm) \sim P_{lm}(0) \int db_0 b_0 e^{i\chi(b_0)} J_m(k_f b_0 \sin \theta) \int \rho_{fi,lm} e^{i(k_i - k_f \cos \theta)z_0} dz_0 \quad (4.19)$$

The angular dependence originating in the z_0 integral is relatively weak by assumption. In the strong absorption model the magnitude of e^{ix_0} is zero for small b_0 and rises sharply to unity at the nuclear radius R . The l, m component density matrix $\rho_{fi,lm}$, on the other hand, drop off rapidly beyond this value of b_0 , so that the b_0 integrand peaks at R and one can approximate $\mathcal{T}_{fi}^{(\text{dir})}(lm)$ by

$$\mathcal{T}_{fi}^{(\text{dir})}(lm) \sim P_{lm}(0) J_m(k_f R \sin \theta) \quad (4.20)$$

Thus, for a given angular momentum transfer l , $\mathcal{T}_{fi}^{(\text{dir})}(l)$ will be a linear combination of J_0, J_2, \dots, J_l if l is even and J_1, J_3, \dots, J_l if l is odd. For large

values of $k_f R \sin \theta$,

$$\begin{aligned}
 J_m(k_f R \sin \theta) &\rightarrow \sqrt{\frac{2}{\pi k_f R \sin \theta}} \cos\left(k_f R \sin \theta - \frac{\pi}{4} - \frac{m\pi}{2}\right) \\
 &\rightarrow \sqrt{\frac{2}{\pi k_f R \sin \theta}} (-)^{m/2} \cos\left(k_f R \sin \theta - \frac{\pi}{4}\right) \quad m \text{ even} \\
 &\rightarrow \sqrt{\frac{2}{\pi k_f R \sin \theta}} (-)^{(m-1)/2} \sin\left(k_f R \sin \theta - \frac{\pi}{4}\right) \quad m \text{ odd}
 \end{aligned}$$

Hence, away from the forward direction, the even l angular momentum transfer reaction angular distribution will be 180° out of phase with the angular distribution for the odd- l case. In the same approximation [see (II.5.25a)] the elastic scattering angular distribution is proportional to $J_1(kR \sin \theta)/\sin \theta$, in phase with the l -odd inelastic angular distribution. This set of phase relations are known as *Blair's phase rule*. The agreement of this with appropriate experiments is excellent, as can be seen from Fig. 4.1. However, as one can also see, the theoretical curves fall much less sharply than experiment.

The result is sensitive to the sharp-cutoff, strong absorption model leading to (4.20), as can be seen if we use a specific model for $\rho_{fi,lm}$. Let

$$\rho_{fi,lm} \sim r^{2\bar{l}} e^{-\mu r^2}$$

where

$$\bar{l} = \frac{1}{2}(l_f + l_i)$$

Moreover,[†] let e^{ix} be

$$e^{ix} = 1 - e^{-\gamma b_0^2} \quad (4.21)$$

Inserting these forms into (4.19), taking $m=0$, and considering only the b_0 integration yields the following integral for consideration:

$$I_0 = \int_0^\infty db_0 b_0^{2\bar{l}+1} (1 - e^{-\gamma b_0^2}) e^{-\mu b_0^2} J_0(k_f b_0 \sin \theta)$$

This integral can be evaluated in closed form when \bar{l} is an integer:

$$I_0 = \frac{1}{2} \Gamma(\bar{l}+1) \left[\frac{e^{-k_f^2 \sin^2 \theta / 4\mu}}{\mu^{\bar{l}+1}} p_{\bar{l}+1} \left(\frac{k_f^2 \sin^2 \theta}{4\mu} \right) - \frac{e^{-k_f^2 \sin^2 \theta / 4(\mu+\gamma)}}{(\mu+\gamma)^{\bar{l}+1}} p_{\bar{l}+1} \left(\frac{k_f^2 \sin^2 \theta}{4(\mu+\gamma)} \right) \right] \quad (4.22)$$

[†]This is a simplified version of the form used by Lee and McManus (67).

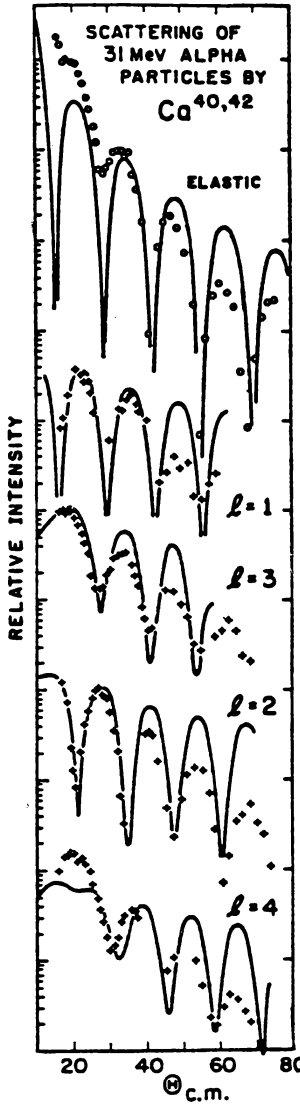


FIG. 4.1. Comparison of the Blair theory with experimental data for the elastic and inelastic scattering of 31-MeV α -particles by $^{40,42}\text{Ca}$. The elastic and $l = 1$ data for ^{40}Ca , all others are for ^{42}Ca . [From Austern (70).]

where $p_{\bar{l}+1}$ is a polynomial of order $\bar{l} + 1$ in the variable indicated. Compared to (4.20), the new feature is the exponential decrease $[\times (k_f^2 \sin \theta / 4\mu)^{\bar{l}+1}]$ with increasing scattering angle, as required by the experimental data. Comparison with the data indicates that the experimental situation lies between assumption (4.21) and that leading to (4.20).

At sufficiently small angles,

$$\mathcal{F}_{fi}^{(\text{dir})}(lm) \sim \sin^{|m|} \theta \quad (4.23)$$

so that for even l , the dominant term is the J_0 one, whereas for odd l , it is J_1 . Thus the angular momentum transferred is approximately perpendicular to the scattering plane.

A. Diffraction

The oscillating angular distributions are very similar to those that prevail in the diffractive scattering of short-wavelength sound and electromagnetic waves by absorbing obstacles. In these classical cases, it can be shown [see Morse and Feshbach (53, p. 1552)] that the scattering in the forward direction is given by the radiation from the shadowed surface of the obstacle. The illumination on that side is taken to be zero, $\psi = 0$, so that the scattered wave $\psi_s = \psi - \psi_i$ on the surface is just equal and opposite to the incident wave, ψ_i , evaluated in the surface. This classical case is developed for elastic scattering. In the discussion that follows we extend the diffractive analysis to quantum-mechanical inelastic scattering.

This development focuses on the projectile wave functions. The dependence on the target nuclear coordinates is carried along. The final expression is then an operator whose matrix element with respect to the initial Ψ_i and final Ψ_f , the target nuclear wave functions, yields the transition matrix for direct inelastic scattering. The full Hamiltonian is used:

$$(E - T_0 - H_N - V^{\text{opt}})\phi = 0 \quad (4.24)$$

where H_N is the Hamiltonian for the target nucleus, T_0 the projectile kinetic energy operator, and V^{opt} the full many-channel optical potential. The target nuclear variables in both H_N and V^{opt} , and therefore in ϕ , are temporarily to be regarded as constants. We shall replace H_N by E_i for $\phi = \phi_i$ and similarly for ϕ_f . This is known as the *adiabatic approximation*. The equation for $\mathcal{T}_{fi}^{(\text{dir})}$ can then be written as

$$\mathcal{T}_{fi}^{(\text{dir})} = \langle \Psi_f | \phi_f^{(-)} V^{\text{opt}} \phi_i^{(+)} | \Psi_i \rangle \quad (4.25)$$

Substituting for $V^{\text{opt}} \phi_i^{(+)}$ from (4.24) leads to

$$\mathcal{T}_{fi}^{(\text{dir})} = \langle \Psi_f | \phi_f^{(-)*} (E - E_i - T_0) \phi_i^{(+)} | \Psi_i \rangle$$

But $\phi_f^{(-)} \Psi_f$ satisfies (4.24) in the absence of V^{opt} , so that

$$(E - T_0 - H_N) \phi_f^{(-)} = (E - T_0 - E_f) \phi_f^{(-)} = 0$$

that is, $\phi_f^{(-)}$ is a plane wave. Replacing E , then, by $T_0 + E_f$ yields

$$\mathcal{T}_{fi}^{(\text{dir})} = \langle \Psi_f | (T_0 \phi_f^*) \phi_i^{(+)} - \phi_f^* (T_0 \phi_i^{(+)}) + (E_f - E_i) \phi_f^* \phi_i^{(+)} | \Psi_i \rangle$$

The last term vanishes because of orthogonality, so that

$$\mathcal{T}_{fi}^{(\text{dir})} = \langle \Psi_f | M | \Psi_i \rangle \quad (4.26)$$

where

$$M \equiv -\frac{\hbar^2}{2\mu} \int d\mathbf{r}_0 [\varphi_f^* \nabla_0^2 \phi_i^{(+)} - (\nabla_0^2 \varphi_f^*) \phi_i^{(+)}] \quad (4.27)$$

M is an operator in target nuclear space because of the dependence of ϕ_i on target nuclear variables such as the radius. Assuming that ρ_{fi} falls off sharply beyond the “nuclear radius”, R , the integral in (4.27) should be evaluated within the nuclear volume. Writing first

$$\phi_i^{(+)} = e^{i\mathbf{k}_i \cdot \mathbf{r}} + \phi_{\text{scatt}}$$

so that for $k_f \approx k_i$

$$M = -\frac{\hbar^2}{2\mu} \int d\mathbf{r}_0 [\varphi_f^* \nabla_0^2 \phi_{\text{scatt}} - (\nabla_0^2 \varphi_f^*) \phi_{\text{scatt}}]$$

and using Green’s theorem yields

$$M = -\frac{\hbar^2}{2\mu} \int dS \mathbf{n}_0 \cdot [\varphi_f^* \nabla_0 \phi_{\text{scatt}} - (\nabla_0 \varphi_f^*) \phi_{\text{scatt}}]$$

where \mathbf{n}_0 is the outward-pointing normal to the surface. We can break up this surface integral into two parts; the front half of the nuclear volume in the shadow and the back illuminated portion. The front half leads to the diffraction scattering. On that front surface, ϕ_{scatt} scattering equals $-e^{i\mathbf{k}_i \cdot \mathbf{r}}$, so that the total ϕ is zero. Hence

$$M_{\text{diff}} = -\frac{\hbar^2}{2\mu} \int_{\text{front}} dS_0 \mathbf{n}_0 \cdot [e^{-i\mathbf{k}_f \cdot \mathbf{r}_0} \nabla_0 e^{i\mathbf{k}_i \cdot \mathbf{r}_0} - \nabla_0 (e^{-i\mathbf{k}_f \cdot \mathbf{r}_0}) e^{i\mathbf{k}_i \cdot \mathbf{r}_0}]$$

It can be shown[†] [Morse and Feshbach (53, p. 1552)] that the surface integral can be reduced to a line integral on the edge of the shadowed surface. (If the scatterer is spherical, this argument is not necessary, as the surface integration over the spherical surface can be readily performed.) As a consequence, any

[†]The transformation is known as the Maggi transformation (Copson). A Simple proof [Morse and Feshbach (53, p. 1552)] notes that the quantity in brackets is divergenceless if $k_f \approx k_i$, already assumed. It may then be written as the curl of a vector and by Stokes’ theorem reduced to a line integral.

surface will do. We shall use a disk bounded by the surface edge, assuming that the edge is a circle perpendicular to the incident projectile direction. In that event

$$\begin{aligned} M_{\text{diff}} &= -i(k_i + k_f \cos \theta) \frac{\hbar^2}{2\mu} \int_0^{2\pi} d\phi \int_0^B b db e^{-ik_f b \sin \theta \cos \phi} \\ &= -\frac{ik\hbar^2}{\mu} \int_0^\pi d\phi \int_0^B b db e^{-ik_f b \sin \theta \cos \phi} \end{aligned} \quad (4.28)$$

Note. It is possible to improve on this result by using the high-energy approximation for ϕ_{sc} . From (4.11),

$$\phi_{\text{sc}}^* = e^{-ik_f r_0} \left[e^{-i(\mu/\hbar^2 k_f) \int_{z_0}^\infty V_{\text{opt}}(\mathbf{b}_0, z) dz} - 1 \right]$$

to be evaluated on the shadowed surface, that is, at $z_0 = (R^2 - b^2)^{1/2}$. For strong absorption the first term is negligible.

To illustrate the use of this formula, consider the case for which the disk radius B is given by

$$B = R + \sum \xi_{lm} Y_{lm}^* \left(\frac{\pi}{2}, \phi \right) \quad (4.29)$$

where ξ_{lm} are operators in the target nuclear space. Such an expansion is employed in the Bohr–Mottelson picture when the target is a spherical vibrator [see Chapter VI] in deShalit and Feshbach (74). The disk of integration is circular, passing through the center of the nucleus. Hence θ in Y_{lm} is $\pi/2$. Then to first order in ξ_{lm} ,

$$\begin{aligned} M_{\text{diff}} &= \frac{-ik\hbar^2}{\mu} \int_0^{2\pi} d\phi \left\{ \int_0^R e^{-ik_f b \sin \theta \cos \phi} b db + R \sum \xi_{lm} (-)^m \left[\frac{2l+1}{4\pi} \frac{(l-|m|)!}{l+|m|!} \right]^{1/2} \right. \\ &\quad \times P_{lm}(0) e^{im\phi} e^{-ik_f R \sin \theta \cos \phi} \left. \right\} \\ &= -\frac{2\pi i k \hbar^2}{\mu} \left[\int_0^R J_0(k_f b \sin \theta) b db + R \sum_{lm} \xi_{lm} \left[\frac{2l+1}{4\pi} \frac{(l-|m|)!}{(l+|m|)!} \right]^{1/2} \right. \\ &\quad \times P_{lm}(0) (-)^{1/2(l-m)} J_m(k_f R \sin \theta) \left. \right] \end{aligned} \quad (4.30)$$

Matrix elements of M_{diff} must now be taken between initial and final nuclear states. The first term in (4.30), under the assumption that the target nuclear density is constant over the nuclear volume, yields the elastic scattering

amplitude

$$M_{\text{diff}}^{(\text{el})} = -\frac{2\pi i \hbar^2 R}{\mu \sin \theta} J_1(k_f R \sin \theta)$$

and the differential elastic cross section quoted earlier,

$$\left(\frac{d\sigma}{d\Omega}\right)_{\text{diff}}^{(\text{el})} = R^2 \frac{|J_1(k_f R \sin \theta)|^2}{\sin^2 \theta} \quad (4.31)$$

The inelastic cross section is given by

$$\left(\frac{d\sigma}{d\Omega}\right)_{\text{diff}}^{(\text{inel})} = (k^2 R^2) \sum_{lm} |\langle \Psi_f | \xi_{lm} | \Psi_i \rangle|^2 \left[\frac{2l+1}{4\pi} \frac{(l-|m|)!}{(l+|m|)!} (P_{lm}(0))^2 \right] |J_m(k_f R \sin \theta)|^2 \quad (4.32)$$

One can verify that the Blair phase rule is a consequence of (4.32) since $P_{lm}(0)$ differs from zero only for $l+m$ even.

To finish the calculation we need to specify the properties of the target nucleus as described by Ψ_f and Ψ_i and the quantities ξ_{lm} that follows from the dynamics upon which (4.29) is based. The nuclear model that can readily be inserted into this theory is the model of Bohr and Mottelson (62). We consider two situations:

Vibrational Nuclei [see deShalit and Feshbach (74, p. 471 et seq.)]. In this case the target nucleus is a vibrator with sets of equally spaced levels. The spacing of each is given by $\hbar w_l$, where w_l can be expressed in terms of a mass parameter B_l and a force constant C_l :

$$w_l = \sqrt{\frac{C_l}{B_l}}$$

The excited states can conveniently be thought of as consisting of the ground state plus a number of phonons. Each of the phonons carries an energy $\hbar w_l$, and angular momentum l_1 with a z component of m . In terms of this model [see deShalit and Feshbach (74, p. 473)]

$$\xi_{lm} = \left(\frac{\hbar}{2B_l w_l} \right)^{1/2} b_{lm}^\dagger \quad (4.33)$$

where b_{lm}^\dagger is a boson creation operator, creating a phonon of the lm type. If the final state involves a one-phonon excitation,

$$\Psi_f = b_{lm}^\dagger \Psi_i$$

so that

$$|\langle \Psi_f | \xi_{lm} | \Psi_i \rangle|^2 = \frac{\hbar}{2B_l w_l} = \frac{\hbar w_l}{2C_l} \quad (4.34)$$

independent of m . Therefore,

$$\left(\frac{d\sigma}{d\Omega} \right)_{\text{diff}}^{(\text{inel})} = k^2 R^2 \sum_l \frac{\hbar w_l}{2C_l} \cdot \frac{2l+1}{4\pi} \left\{ \sum_m \frac{(l-|m|)!}{(l+|m|)!} [P_{lm}(0)]^2 |J_m(k_f R \sin \theta)|^2 \right\} \quad (4.35)$$

From its derivation it is clear that $\hbar w_l/2C_l$ is a measure of the amplitude of oscillation away from the spherical equilibrium shape.

The analysis above can readily be extended to multiphonon states by including higher-order terms in the evaluation of M_{diff} of (4.30). The Blair phase rule in its simplest form will not be valid if both single phonon and multiphonon excitation are equally important. Note that the effects of the Coulomb interaction, which can be of great importance, have been omitted in this discussion.

Deformed Nuclei. We begin with the more complex expression for the deformation given on page 471 of deShalit and Feshbach (74), which we rewrite as

$$\delta R = \sum_{lm'} \alpha_{lm'} Y_{lm'}^*(\theta' \phi') \quad (4.36)$$

The volume-conserving term has been omitted in (4.36), as it will not play a role in the excitations discussed below. The angles, (θ', ϕ') , are in the body-fixed system, so that the expression in (4.36) needs to be transformed to the scattering frame [see (A.2.26) in the Appendix of deShalit and Feshbach (74)] as follows:

$$\delta R = \sum_{lm'} \alpha_{lm'} D_{mm'}^{(l)*}(\theta_k) Y_{lm'}^*(\theta, \phi) \quad (4.37)$$

where θ_k are the collective coordinates. Therefore,

$$\xi_{lm} = \sum_{m'} \alpha_{lm'} D_{mm'}^{(l)}(\theta_k)$$

The matrix element in (4.32) becomes

$$\langle \Psi_f | \xi_{lm} | \Psi_i \rangle = \sum_{m'} \langle \Psi_f | D_{mm'}^{(l)*}(\theta_k) \alpha_{lm'} | \Psi_i \rangle$$

where the nuclear wave functions are given by (VI.4.9) in deShalit and Feshbach (74). The value of this matrix element is given by (VI.6.9) in deShalit and Feshbach (74):

$$\begin{aligned}
& \langle I_f K_f M_f | \alpha_{lm'} D_{m'm}^{(l)*} | I_i K_i M_i \rangle \\
&= (-)^{M-K} \sqrt{(2I_i+1)(2I_f+1)} \begin{pmatrix} I_f & l & I_i \\ -M_f & m & M_i \end{pmatrix} \\
&\times \left[\begin{pmatrix} I_f & l & I_i \\ -K_f & m' & K_i \end{pmatrix} \langle K_f | \alpha_{lm'} | K_i \rangle + (-)^{I_i} \right. \\
&\times \left. \begin{pmatrix} I_f & l & I_i \\ -K_f & m' & -K_i \end{pmatrix} \langle K_f | \alpha_{lm'} | -K_i \rangle \right] \quad (4.38)
\end{aligned}$$

where the quantum numbers I_i , K_i and M_i specify the initial rotational state of the target nucleus, I_f , and so on, specify the final state. The matrix elements of α_{lm} are taken with respect to the intrinsic wave functions describing the rotational nucleus.

To obtain the cross section we must take the square of the magnitude of $\langle \Psi_f | \xi_{lm} | \Psi_i \rangle$, sum over M_f , and average over M_i . We need consider only the factors outside the brackets in (4.38), since they contain the entire m dependence. We recall that

$$\frac{1}{2I_i+1} \sum_{M_i, M_f} (2I_i+1)(2I_f+1) \begin{pmatrix} I_f & l & I_i \\ -M_f & m & M_i \end{pmatrix}^2 = \frac{2I_f+1}{2l+1} \quad (4.39)$$

Note the important result that any dependence on M disappears upon summing over final states and averaging over initial states. As a consequence, in (4.32) one can remove the matrix element of ξ_{lm} from the sum on m :

$$\left(\frac{d\sigma}{d\Omega} \right)_{\text{diff}}^{(\text{inel})} = k^2 R^2 \sum_l \frac{2l+1}{4\pi} |\langle \Psi_f | \xi_l | \Psi_i \rangle|^2 \left\{ \sum_m \frac{(l-|m|)!}{(l+|m|)!} |P_{lm}(0)|^2 |J_m(k_f R \sin \theta)|^2 \right\} \quad (4.40)$$

We see that the excitation of rotational level leads to same angular distribution as the excitation of a vibrational level for each multiple given by the expression within the braces in (4.40) and (4.35). The weighting of each multipole will differ. For the rotational case [see (VI.7.1) in deShalit and Feshbach (74)],

$$|\langle \Psi_f | \xi_l | \Psi_i \rangle| \approx \beta_l R$$

A more detailed microscopic theory would need the more detailed statement for (4.38).

B. Adiabatic Approximation and Elastic Scattering

The calculations described in Section 4.A are examples of the use of the adiabatic approximation in which the scattering of the projectile is determined in terms

of properties of the target nucleus that are considered to remain fixed during the encounter. This is a reasonable description if the passage time for the projectile is small compared to the periods of the characteristic modes of motion of the nucleus. The passage time τ_p is approximately given by

$$\tau_p \sim \frac{R}{v} \sim \frac{r_0 A^{1/3}}{c} \left[\frac{mc^2}{2(V+E)} \right]^{1/2}$$

where V is a measure of the interaction energy given by the real part of the depth of the central components of the optical potential. It can readily be shown that the characteristic times associated with rotation and vibration are much longer than the passage time. However, τ_p is much shorter than the characteristic times associated with single-particle motion only if the energy E is sufficiently high.

When the adiabatic approximation is valid, one can consider the projectile scattering to occur in the presence of a fixed configuration of nucleons of the nucleus. The resulting projectile transition matrix, \mathcal{T}_p , is then a function of the target nucleon coordinates. Its matrix element with respect to the initial and final nuclear states gives an approximation for the transition matrix for the process.

To be more specific, the many-body Schrödinger equation describing the projectile–target interaction is

$$(E - H_t - V_{tp} - T_p)\Phi = 0 \quad (4.41)$$

where H_t is the target nuclear Hamiltonian, V_{tp} the interaction of the projectile with the target nucleons, and T_p the projectile kinetic energy. Centre-of-mass frame variables are assumed. If we now consider the target nucleons to be fixed, (4.41) becomes a single-channel equation whose transition matrix is $\mathcal{T}_p(\mathbf{r}_1, \mathbf{r}_2, \dots; \mathbf{k}_f, \mathbf{k}_i)$, where \mathbf{r}_i are the coordinates of the target nucleons and \mathbf{k}_f and \mathbf{k}_i are the final and initial momenta, respectively. Only when the scattering is elastic will $k_f = k_i$. The transition matrix for the nuclear transition $\Psi_i \rightarrow \Psi_f$ in this approximation is given by

$$\mathcal{T}_{fi} = \langle \Psi_f | \mathcal{T}_p(\mathbf{r}_1, \mathbf{r}_2, \dots) | \Psi_i \rangle \quad (4.42)$$

This adiabatic approximation is an essential part of the multiple scattering formalism of Chapter II. We now wish to discuss its use when collective coordinates are the primary nuclear dynamical variables involved in the collision. In that case we go to the energy averaged optical model as described in Chapter III, with the consequence that (4.41) is replaced by

$$(E - T_p - V_{\text{opt}})\chi = 0 \quad (4.43)$$

where the collective coordinates such as the nuclear radius appear as a parameter

in V_{opt} . The transition matrix corresponding to (4.43) will then be a function of the collective coordinates, which we shall symbolize by R , so that

$$\mathcal{T}_p = \mathcal{T}_p(R; \mathbf{k}_f, \mathbf{k}_i)$$

The transition matrix element for the transition is given by

$$\mathcal{T}_{fi} = \langle \Psi_f | \mathcal{T}_p(R; \mathbf{k}_f, \mathbf{k}_i) | \Psi_i \rangle \quad (4.44)$$

The Austern–Blair result [Austern (70, pp. 278–280)] is a perturbation result in which R is assumed to be close to a fixed value R_0 . When the perturbation involves the projectile coordinates, it is convenient to write \mathcal{T}_p as follows:

$$\mathcal{T}_p(R; \mathbf{k}_f, \mathbf{k}_i) = \iint e^{-i\mathbf{k}_f \cdot \mathbf{r}} \mathcal{T}_p(R; \mathbf{r}, \mathbf{r}_0) e^{i\mathbf{k}_i \cdot \mathbf{r}_0} d\mathbf{r} d\mathbf{r}_0 \quad (4.45)$$

Perturbatively, R is given by

$$R = R_0 + \delta R$$

so that

$$\mathcal{T}_p(R; \mathbf{k}_f, \mathbf{k}_i) = \mathcal{T}_p(R_0; \mathbf{k}_f, \mathbf{k}_i) + \delta \mathcal{T}_p$$

where

$$\begin{aligned} \delta \mathcal{T}_p &= \frac{\partial}{\partial R_0} \iint e^{-i\mathbf{k}_f \cdot \mathbf{r}} \mathcal{T}_p(R_0; \mathbf{r}, \mathbf{r}_0) \delta R e^{i\mathbf{k}_i \cdot \mathbf{r}_0} d\mathbf{r} d\mathbf{r}_0 \\ &= \frac{\partial}{\partial R_0} \int e^{-i\mathbf{k}_f \cdot \mathbf{r}} \delta R V(\mathbf{r}, R_0) \psi_i^{(+)}(\mathbf{k}_i, \mathbf{r}; R_0) d\mathbf{r} \end{aligned} \quad (4.46)$$

Austern and Blair proceed by expanding $\psi_i^{(+)}$ in a partial wave series and evaluating the integrals term by term. This is left as a problem for the reader.

In the case that we are dealing with, surface reactions, it is possible to develop expression (4.46) further without resorting to a partial wave expansion. Let us then assume that

$$\delta R = \delta R(\xi; r, \theta, \phi)$$

where, as before, ξ represents a set of operators operating on the nuclear wave functions $\Psi_{f,i}$. Then (4.46) becomes

$$\delta \mathcal{T}_p = \frac{\partial}{\partial R_0} \int d\mathbf{r} e^{-i\mathbf{k}_f \cdot \mathbf{r}} \delta R(\xi; r, \theta, \phi) V(r, R_0) \psi_i^{(+)}$$

We now make use of the fact that δR can be written as a function of $\cos \theta$ and

$e^{\pm i\phi}$ and these can be expressed as differential operators as follows:

$$\cos \theta e^{-i\mathbf{k}_f \cdot \mathbf{r}} = i \frac{\mathbf{k}_i}{k_i r} \cdot \nabla_{\mathbf{k}_f} e^{-i\mathbf{k}_f \cdot \mathbf{r}}$$

where the z direction has been chosen along \mathbf{k}_i . (It is, of course, possible to make a choice that will result in a more symmetric final expression.) Second,

$$e^{i\phi} e^{-i\mathbf{k}_f \cdot \mathbf{r}} = \frac{i}{r} \left(\frac{\partial}{\partial k_{f_x}} + i \frac{\partial}{\partial k_{f_y}} \right) e^{-i\mathbf{k}_f \cdot \mathbf{r}}$$

Hence

$$\delta \mathcal{T}_p = \frac{\partial}{\partial R_0} \left\{ \delta R \left[\xi; R_0, \frac{i\mathbf{k}_i \cdot \nabla_{\mathbf{k}_f}}{k_i R_0}, \frac{i}{R_0} \left(\frac{\partial}{\partial k_{f_x}} + i \frac{\partial}{\partial k_{f_y}} \right) \right] \mathcal{T}_p(R_0; \mathbf{k}_f, \mathbf{k}_i) \right\} \quad (4.47)$$

where r has been replaced by R_0 because of the surface reaction assumptions and $\delta R[\cdot]$ is defined by

$$\delta R[\xi; \cos \theta, e^{i\phi}] \equiv \delta R(\xi; \theta, \phi)$$

The net transition matrix given by (4.44) is obtained from (4.47). The quantity $\mathcal{T}_p(R_0; \mathbf{k}_f, \mathbf{k}_i)$ is not the elastic scattering amplitude since $k_f \neq k_i$. At sufficiently small angles (where in any event the DWA is most reliable) and for sufficiently small energy losses, E_f and E_i , and therefore k_f and k_i , can be replaced by some average value. Another approximation suggested by Hahne (67, 68) [see also Austern (70, p. 280)] is appropriate when the Austern–Blair partial wave analysis is used. For the formulation above we have only the Schwarz inequality result,

$$|\mathcal{T}_p(R_0; \mathbf{k}_f, \mathbf{k}_i)| \leq |\mathcal{T}_p(R_0, \mathbf{k}_f, \mathbf{k}_f) \mathcal{T}_p(R_0, \mathbf{k}_i, \mathbf{k}_i)|^{1/2} \quad (4.48)$$

This implies that the geometric mean may be adequate but useful at best only for a low order of differentiation in (4.47).

C. Formal DWA

The numerical evaluation of the direct transition matrix element given by (4.8) and (4.9) for a given model of the nuclear structure has been studied extensively, and a number of computer codes for this purpose have been developed and widely used. In this section we carry out the kinematic reductions to the point where numerical methods must be invoked. To illustrate the methods involved, we consider the somewhat simplified case for which the optical potential defining the distorted wave functions $\phi_{f,i}$ is spin and isospin independent, as is appropriate when the exciting projectile is an α -particle.

Consider the form factor $\mathcal{V}_{fi}(\mathbf{r}_0)$ defined by (4.9). Because of the antisymmetry of the wave functions $\Psi_{f,i}$, (4.9) can be rewritten as

$$\mathcal{V}_{fi}(\mathbf{r}_0) = A \langle J_f M_f | v(\mathbf{r}_0, \mathbf{r}_1) | J_i M_i \rangle \quad (4.49)$$

where A is the mass number of the target nucleus and $J_{f,i}$ and $M_{f,i}$ are the angular momentum quantum numbers for the nuclear states involved. Recall that \mathbf{r}_0 is the projectile coordinate. The interaction can be expanded in a *multipole series*:

$$v(\mathbf{r}_0, \mathbf{r}_1) = \sum_{l,\mu} v_l(r_0, r_1) (-)^l T_{-\mu}^{(l)}(0) T_{\mu}^{(l)}(1)$$

where $T^{(l)}$ is a spherical tensor that depends on spherical angular coordinates and spin.[†] Taking the matrix element in (4.49) and using the Wigner–Eckart theorem, one obtains

$$\mathcal{V}_{fi} = A \sum_{l\mu} (-)^{J_f - M_f} \begin{pmatrix} J_f & l & J_i \\ -M_f & \mu & M_i \end{pmatrix} (J_f \| v_l(r_0, r_1) T^{(l)}(1) \| J_i) (-)^l T_{\mu}^{(l)} \quad (4.50)$$

where the reduced matrix element involves an integration over \mathbf{r}_1 .

From the properties of the $3-j$ symbol it follows that the angular momentum transferred equals l :

$$\mathbf{J}_f = \mathbf{J}_i + \mathbf{l}$$

If v is spin independent, so that $T_{\mu}^{(l)} \sim Y_{l\mu}$, the transferred parity is $(-)^l$. If $J_i = 0^+$, a spin independent v_l will excite only states of *natural parity*, that is, states with spin l and parity $(-)^l$, such as 0^+ , 1^- , 2^+ , and so on. When spin dependence is included, $T_{\mu}^{(l)}$ can include as well

$$[i^k Y_k \otimes \boldsymbol{\sigma}]_m^{(l)} = \sum_{\kappa_1 \kappa_2} (k \kappa_1, 1 \kappa_2 | lm) (i^k Y_{k\kappa_1}) \sigma_{\kappa_2} \quad (4.51)$$

To indicate the composite character of such a term, the notation $T_m^{(k\sigma)l}$ is often used. We shall for the most part not use this more detailed notation in this section. The presence of such terms as well as spin-dependent terms will permit transitions in which for $J_i = 0^+$, states of unnatural purity can be excited.

The reduced matrix element in (4.50) is directly dependent on the nondiagonal

[†]If there is no spin dependence,

$$v(\mathbf{r}_0, \mathbf{r}_1) = \sum_{l,m} v_l(r_0, r_1) \frac{4\pi}{2l+1} (i^l Y_{lm}(\hat{\mathbf{r}}_0))^* (i^l Y_{lm}(\hat{\mathbf{r}}_1))$$

density matrix, ρ_{fi} . The matrix element can be determined from

$$\begin{aligned}
 & \begin{pmatrix} J_f & l & J_i \\ -J_f & m & J_i \end{pmatrix} (J_f \| v_l(r_0, r_1) T_m^{(l)} \| J_i) \\
 &= \int \Psi_f^*(J_f, M_f = J_f; \mathbf{r}_1, \mathbf{r}_2, \dots) v_l(r_0, r_1) T_m^{(l)}(\hat{\mathbf{r}}_1) \Psi_i(J_i, M_i = J_i; \mathbf{r}_1, \mathbf{r}_2, \dots) d\mathbf{r}_1 d\mathbf{r}_2 \dots \\
 &= \int \rho_{fi}(\mathbf{r}_1) v_l(r_0, r_1) T_m^{(l)}(\hat{\mathbf{r}}_1) d\mathbf{r}_1 \quad (4.52)
 \end{aligned}$$

where

$$\rho_{fi} \equiv \int \Psi_f^*(J_f, M_f = J_f; \mathbf{r}_1, \mathbf{r}_2, \dots) \Psi_i(J_i, M_i = J_i; \mathbf{r}_1, \mathbf{r}_2, \dots) d\mathbf{r}_2 \dots$$

As a probe of nuclear structure, inelastic scattering thus provides information on ρ_{fi} . Other probes (e.g., inelastic electron and pion scattering) act similarly, however weighting ρ_{fi} in different ways, depending on the excitation interaction responsible. That is, the operator, $v_l(r_0, r_1)$ in (4.26) depends on the probe involved, but ρ_{fi} does not change. By using a variety of probes it is possible to determine the space-symmetry structure of both ρ_{fi} and the interactions involved. It should be emphasized that this conclusion relies on the validity of the DWA.

We now insert multipole series (4.50) into the expression for the transition matrix \mathcal{T}_{fi} :

$$\mathcal{T}_{fi} = \langle \phi_f^{(-)} | \mathcal{V}_{fi} | \phi_i^{(+)} \rangle \quad (4.53)$$

where $\phi_i^{(+,-)}$ are solutions of the optical model Schrödinger equation with indicated outgoing and incoming boundary conditions. Expanding these in a partial wave series (the assumption of spin independence for reason of simplicity is made at this point) yields

$$\begin{aligned}
 \phi_i^{(+)} &= \sum (2l_i + 1) i^{l_i} P_{l_i}(\hat{\mathbf{k}}_i \cdot \hat{\mathbf{r}}) e^{i\delta_{l_i}} \frac{u_{l_i}(r)}{k_i r} \\
 &= \sum \sqrt{4\pi(2l_i + 1)} \mathcal{Y}_{l_i 0}(\hat{\mathbf{k}}_i \cdot \hat{\mathbf{r}}) e^{i\delta_{l_i}} \frac{u_{l_i}(r)}{k_i r} \quad (4.54)
 \end{aligned}$$

The complex conjugate $\phi_f^{(-)*}$ is

$$\phi_f^{(-)*} = \sum (2l_f + 1) i^{l_f} P_{l_f}(-\hat{\mathbf{k}}_f \cdot \hat{\mathbf{r}}) e^{i\delta_{l_f}} \frac{u_{l_f}(r)}{k_f r}$$

Using the properties of P_{l_f} , such as the addition theorem, we obtain

$$\phi_f^{(-)*} = 4\pi \sum \mathcal{Y}_{l_f, m_f}^*(\hat{\mathbf{k}}_i \cdot \hat{\mathbf{r}}) Y_{l_f, m_f}(\hat{\mathbf{k}}_i \cdot \hat{\mathbf{k}}_f) e^{i\delta_{l_f}} \frac{u_{l_f}(r)}{k_f r} \quad (4.55)$$

Combining these results with (4.50) it is an easy matter to obtain \mathcal{T}_{fi} :

$$\begin{aligned} \mathcal{T}_{fi} = & (4\pi)^{3/2} \sum (-)^{J_f - M_f + m + l_f - m_f} \begin{pmatrix} J_f & l & J_i \\ -M_f & m & M_i \end{pmatrix} \begin{pmatrix} l_f & l & l_i \\ -m_f & -m & 0 \end{pmatrix} \sqrt{2l_i + 1} \\ & \times I^{(l)}(l_f J_f; l_i J_i) e^{i(\delta_{l_i} + \delta_{l_f})} Y_{l_f, m_f}(\hat{\mathbf{k}}_i \cdot \hat{\mathbf{k}}_f) \end{aligned} \quad (4.56)$$

where $I^{(l)}$ is given by

$$I^{(l)}(l_f J_f; l_i J_i) = \frac{4\pi A}{k_f k_i} (J_f l_f \| T^{(l)}(0) v_l(r_0, r_1) T^{(l)}(1) \| J_i l_i) \quad (4.57)$$

We now must average the square magnitude of \mathcal{T}_{fi} over M_i and sum over M_f . One obtains, using the 3-j normalization [(A.2.70) in the Appendix of deShalit and Feshbach (74)],

$$\begin{aligned} \frac{1}{2J_i + 1} \sum_{M_i, M_f} |\mathcal{T}_{fi}|^2 = & (4\pi)^3 \sum \frac{\sqrt{(2l_i + 1)(2l'_i + 1)}}{(2l + 1)(2J_i + 1)} (-)^{l_f + l'_f - m_f - m'_f} \\ & \times \begin{pmatrix} l_f & l & l_i \\ -m_f & -m & 0 \end{pmatrix} \begin{pmatrix} l'_f & l & l'_i \\ -m'_f & -m & 0 \end{pmatrix} Y_{l_f, m_f} Y_{l'_f, m'_f}^* \\ & \times e^{i(\delta_{l_i} + \delta_{l_f} - \delta_{l'_i}^* - \delta_{l'_f}^*)} I^{(l)}(l_f J_f; l_i J_i) I^{(l)*}(l'_f J_f; l'_i J_i) \end{aligned} \quad (4.58)$$

This can be written as a sum over multipole order as follows:

$$\begin{aligned} \frac{1}{2J_i + 1} \sum_{M_i, M_f} |\mathcal{T}_{fi}|^2 = & (4\pi)^3 \sum_{l, m} \frac{1}{(2l + 1)(2J_i + 1)} \left| \sum_{l_f, l_i, m_f} (-)^{l_f - m_f} \sqrt{2l_i + 1} \right. \\ & \times \begin{pmatrix} l_f & l & l_i \\ -m_f & -m & 0 \end{pmatrix} Y_{l_f, m_f} I^{(l)}(l_f J_f; l_i J_i) e^{i(\delta_{l_i} + \delta_{l_f})} \left. \right|^2 \end{aligned} \quad (4.59)$$

a result that is often the most convenient one to use. However, it is possible to carry (4.58) further by expanding the product of the Y 's in (A.2.35) of deShalit and Feshbach (74):

$$\begin{aligned} Y_{l'_f, m'_f}^* Y_{l_f, m_f} = & (-)^{m'_f} \sum_{\lambda \mu} \sqrt{\frac{(2l'_f + 1)(2l_f + 1)(2\lambda + 1)}{4\pi}} \\ & \times \begin{pmatrix} l'_f & l_f & \lambda \\ 0 & 0 & 0 \end{pmatrix} \begin{pmatrix} l'_f & l_f & \lambda \\ -m'_f & m_f & \mu \end{pmatrix} Y_{\lambda \mu} \end{aligned}$$

The resultant product of $3-j$ symbols can be summed to a $6-j$ symbol using (A.2.93) of deShalit and Feshbach (74). Finally, relating the result to the reduced matrix element of Y_λ gives

$$\begin{aligned} \frac{1}{2J_i + 1} \sum |\mathcal{T}_{fi}|^2 = \sum \frac{(-)^{l_f}(2\lambda + 1)}{(2J_i + 1)(2l + 1)} \begin{pmatrix} l_f & l_f & \lambda \\ 0 & 0 & 0 \end{pmatrix} (l_i l_f \| \sqrt{4\pi} Y_\lambda \| l_i l_f) \\ \times e^{i(\delta_{l_f} + \delta_{l_i} - \delta_{l_f}^* - \delta_{l_i}^*)} I^{(l)}(l_f J_f; l_i J_i) I^{(l)*}(l_f J_f; l_i J_i) P_\lambda(\hat{\mathbf{k}}_f \cdot \hat{\mathbf{k}}_i) \end{aligned} \quad (4.60)$$

The cross section is obtained by multiplying this result by $(\mu/2\pi\hbar^2)^2(k_f/k_i)$. The total inelastic cross section $\sigma_T^{(\text{inel})}$ is given by

$$\sigma_T^{(\text{inel})} = \left(\frac{\mu}{2\pi\hbar^2} \right)^2 k_f \sum \frac{1}{(2J_i + 1)(2l + 1)} |I^{(l)}(l_f J_f; l_i J_i)|^2 e^{-2\text{Im}(\delta_{l_f} + \delta_{l_i})} \quad (4.61)$$

The properties of the reduced matrix element of Y_λ in (4.60) provide most of the kinematic properties of the reaction. It vanishes unless

$$\begin{aligned} l_i + l &= l_f \\ l_i' + l &= l_f' \end{aligned} \quad (4.62a)$$

$$\begin{aligned} l_i + \lambda &= l_i' \\ l_f + \lambda &= l_f' \end{aligned} \quad (4.62b)$$

$$\begin{aligned} l_i' + l_i + \lambda &= \text{even number} \\ l_f' + l_f + \lambda &= \text{even number} \end{aligned} \quad (4.62c)$$

where the last equation is a property of the $3-j$ symbol multiplying the reduced matrix element of Y_L . Relations (4.62a) show that l is the angular momentum transfer. Equation (4.62b) yields the C.N. Yang result on the complexity of the angular distribution, namely that $\lambda < \min(2l_i, 2l_f)$. Other properties are present in the $I^{(l)}$ factors that contain the reduced matrix elements of $T^{(l)}$. These will be proportional to [see (A.2.48) in deShalit and Feshbach (74)]

$$(a) \quad \begin{pmatrix} J_f & l & J_i \\ 0 & 0 & 0 \end{pmatrix} \quad \text{and} \quad (b) \quad \begin{pmatrix} l_f & l & l_i \\ 0 & 0 & 0 \end{pmatrix} \quad (4.63)$$

The first of these combined with the results (4.59a) yields conservation of angular momentum for the reaction

$$\begin{aligned} \mathbf{J}_i + \mathbf{l} &= \mathbf{J}_f \\ l_i + l &= l_f \end{aligned}$$

while the evenness of $J_f + l + J_i$ and $l_f + l + l_i$ yields conservation of parity. The dynamics of the reaction is contained in the $I^{(l)}$ factors, as these involve integrations over $v_i(r_0, r_1)$. Note also the exponential factors in (4.60) and (4.61), which explicitly demonstrate the effects of absorption in both the initial and final optical model channels.

Some further insight into the kinematic factors can be obtained for strong absorption in the limit $l_{i,f} \gg 1$. In the case of strong absorption, the contribution to (4.60) comes from a narrow range of l_i and of l_f , so that $l_i \approx l'_i$ and $l_f \approx l'_f$. It therefore becomes a good approximation for the expression appearing in (4.60):

$$\begin{aligned} & \begin{pmatrix} l_f & l'_f & \lambda \\ 0 & 0 & 0 \end{pmatrix} (l_i l_f \parallel \sqrt{4\pi} Y_\lambda \parallel l'_i l'_f) \\ &= (-)^{l+\lambda+l_f} \sqrt{(2l_i+1)(2l'_i+1)(2l_f+1)(2l'_f+1)(2\lambda+1)} \\ & \times \begin{pmatrix} l_f & l'_f & \lambda \\ 0 & 0 & 0 \end{pmatrix} \begin{pmatrix} l_i & l'_i & \lambda \\ 0 & 0 & 0 \end{pmatrix} \left\{ \begin{matrix} l_i & l_f & l \\ l'_f & l'_i & \lambda \end{matrix} \right\} \end{aligned} \quad (4.64)$$

to replace l_i and l'_i by an average value, \bar{l}_i , and similarly, l_f and l'_f by \bar{l}_f . Then, using the result valid for large $\bar{l}_{i,f}$ [Brusaard and Tolhoek (57); Biedenharn (53); Racah (51)], we have

$$\begin{aligned} & \left\{ \begin{matrix} \bar{l}_i & \bar{l}_f & l \\ \bar{l}_f & \bar{l}_i & \lambda \end{matrix} \right\} \simeq \frac{(-)^{l+\bar{l}_i+\bar{l}_f}}{\sqrt{2\bar{l}_i+1}(2\bar{l}_f+1)} P_\lambda(\cos l(\bar{\mathbf{l}}_i \cdot \bar{\mathbf{l}}_f)) \\ & \cos(l(\bar{\mathbf{l}}_i \cdot \bar{\mathbf{l}}_f)) \equiv \frac{l(l+1) - \bar{l}_i(\bar{l}_i+1) - \bar{l}_f(\bar{l}_f+1)}{2\bar{l}_i\bar{l}_f} \end{aligned}$$

so that

$$\begin{aligned} & \begin{pmatrix} l_f & l'_f & \lambda \\ 0 & 0 & 0 \end{pmatrix} (l_i l_f \parallel \sqrt{4\pi} Y_\lambda \parallel l'_i l'_f) \simeq (-)^{\bar{l}_i} \sqrt{(2\bar{l}_i+1)(2\bar{l}_f+1)(2\lambda+1)} \\ & \times \begin{pmatrix} l_f & l'_f & \lambda \\ 0 & 0 & 0 \end{pmatrix} \begin{pmatrix} l_i & l'_i & \lambda \\ 0 & 0 & 0 \end{pmatrix} P_\lambda(\cos l(\bar{\mathbf{l}}_i \cdot \bar{\mathbf{l}}_f)) \end{aligned} \quad (4.65)$$

From the expression for $\cos(\bar{\mathbf{l}}_i \cdot \bar{\mathbf{l}}_f)$, we see that $|P_\lambda|$ achieves a maximum value close to unity when $l = \bar{l}_i \pm \bar{l}_f$, for then the cosine is close to ± 1 . The two vectors, the incident angular momentum \mathbf{l}_i and the final \mathbf{l}_f , tend to line up, to be parallel or antiparallel, the net sum being equal to the multipole order l . If the multipole order is large (e.g., $J_f \gg 1$, $J_f \gg J_i$), then either \bar{l}_f or \bar{l}_i or both are large. As we shall see, the matching condition that maximizes the integrals $I^{(l)}$ when the energy of the incident beam is much larger than the excitation energy

yields $l_i \approx l_f$. Under these conditions $l_i \approx l_f \approx l/2$, so that the maximum value of λ will be l , the multipole order. At sufficiently high energy and large multipole order, the angular distribution (4.60) will reflect the multipole order quite directly. This consequence has clearly been verified by inelastic proton scattering experiments for energies in the range above 100 MeV. Here it has been possible to determine, as we shall discuss, the nature of the coupling potential $v(\mathbf{r}_0, \mathbf{r}_1)$.

To go further it is necessary to examine the integrals $I^{(l)}$. We take the simple case, the excitation of a single nucleon creating a residual nucleus in a particle-hole state. Consider the excitation of a nucleon in an orbital (j_i, Λ_i, m_i) , to another orbital (j_f, Λ_f, m_f) , where j is the total nuclear spin, m its z projection, and Λ the orbital angular momentum. The corresponding wave function is

$$|jm\Lambda s\rangle = \sum_{m_\Lambda} \langle jm|\Lambda m_{\Lambda} \frac{1}{2} m_s\rangle \mathcal{Y}_{\Lambda, m_\Lambda} \chi_{s, m_s} \frac{R_\Lambda}{r_0}$$

Additionally, to keep the discussion as simple as possible, let the interaction $v(\mathbf{r}_0, \mathbf{r}_1)$ be spin independent, so that

$$T_m^{(l)} \rightarrow \mathcal{Y}_{lm}$$

It immediately follows that

$$I^{(l)}(l_f j_f; l_i j_i) = \frac{4\pi}{k_f k_i} (l_f \| \mathcal{Y}_l \| l_i) (j_f \Lambda_f \frac{1}{2} \| \mathcal{Y}_l \| j_i \Lambda_i \frac{1}{2}) \mathcal{J}^{(l)}(l_f j_f; l_i j_i) \quad (4.66)$$

where

$$\mathcal{J}^{(l)}(l_f j_f; l_i j_i) = \iint u_{l_f}(r_0) R_{\Lambda_f}^*(r_1) v_l(r_0, r_1) u_{l_i}(r_0) R_{\Lambda_i}(r_0) dr_0 dr_1 \quad (4.67)$$

The reduced matrix elements are given in (A.2.48) and (A.2.49) of deShalit and Feshbach (74):

$$\begin{aligned} (l_f \| \sqrt{4\pi} \mathcal{Y}_l \| l_i) &= i^{l_f + l + l_i} (2l_f + 1)^{1/2} (2l_i + 1)^{1/2} (2l + 1)^{1/2} \begin{pmatrix} l & l_i & l_f \\ 0 & 0 & 0 \end{pmatrix} \\ (j_f \Lambda_f \frac{1}{2} \| \sqrt{4\pi} \mathcal{Y}_l \| j_i \Lambda_i \frac{1}{2}) &= (i)^{2j_f + l - \frac{1}{2}} [1 + (-)^{\Lambda_f + l + \Lambda_i}] \begin{pmatrix} j_f & l & j_i \\ -\frac{1}{2} & 0 & \frac{1}{2} \end{pmatrix} (2j_f + 1)^{1/2} \\ &\quad \times (2j_i + 1)^{1/2} (2l + 1)^{1/2} \end{aligned}$$

We note parity conditions

$$\begin{aligned} l + l_i + l_f &= \text{even number} \\ \Lambda_f + \Lambda_i + l &= \text{even number} \end{aligned}$$

so that the parity change in the projectile wave function is compensated by the parity change in the nuclear transition.

The double radial integral depends on the transition densities, $\rho_{fi}^{(N)} \equiv R_{\Lambda f}^* R_{\Lambda i}$ and $\rho_{fi}^{(P)} \equiv u_{lf} u_{li}$. The Coulomb repulsion plays an important role. Obviously, a strong repulsion will reduce the value of $\rho_{fi}^{(P)}$. The density $\rho_{fi}^{(P)}$ will also be reduced in the nuclear interior if the effective absorption in the projectile channels is large. Under these circumstances, Coulomb repulsion and/or strong absorption, surface reactions will be favored. The cross section will be greatest, then, for nuclear densities $\rho_{fi}^{(N)}$ which peak at the surface, an effect that is strengthened if $v_l(r_0, r_1)$ is largest on the surface or short ranged. Maximum overlap at the surface occurs for l_f^0 and l_i^0 such that

$$\frac{l_f^0}{k_f} \approx \frac{l_i^0}{k_1} \approx R$$

For l_i and l_f greater than l_i^0 and l_f^0 , respectively, the angular momentum barrier will further reduce the amplitude of u_{lf} and u_{li} , so that $\mathcal{J}^{(l)}$ will be small for these values of $l_{i,f}$. Thus the major contributions to the angular distribution comes from a narrow range in l_i and l_f , a result that has been employed above and in agreement with results obtained using the WKB approach leading to (4.20).

D. Exchange Effects

The effect of antisymmetry with respect to the incident nucleon has not been explicitly considered. In the “naive” approach the incident-state (and similarly for the final-state) wave function used above is antisymmetrized:

$$\phi_i^{(+)}(0)\psi_i(1, 2, \dots) \rightarrow \mathcal{A}[\phi_i^{(+)}(0)\psi_i(1, 2, \dots)] = \left(1 - \sum_{\mu} P_{0\mu}\right) \phi_i^{(+)}\psi_i(1, 2, \dots) \quad (4.68)$$

where $P_{0\mu}$ is the permutation operator, for example,

$$P_{01}\phi_i^{(+)}(0)\psi_i(1, 2, \dots) = \phi_i^{(+)}(1)\psi_i(0, 2, \dots)$$

However, this procedure is incorrect since the resulting initial- and final-state wave functions are not orthogonal. In fact (see Section III.5),

$$\frac{1}{A+1} \langle \mathcal{A}\phi_f^{(-)}(0)\psi_f(1, 2, \dots) | \mathcal{A}\phi_i^{(+)}(0)\psi_i(1, 2, \dots) \rangle = \langle \phi_f^{(-)} | \delta_{fi} - K_{fi} | \phi_i^{(+)} \rangle$$

where

$$K_{fi}(\mathbf{r}, \mathbf{r}_0) = A \langle \psi_f(\mathbf{r}, \mathbf{r}_2, \dots) | \psi_i(\mathbf{r}_0, \mathbf{r}_2, \dots) \rangle \quad (4.69)$$

The resolution of this problem is indicated by the discussion of the impact of the Pauli principle upon the theory of reactions in Section III.5. We recall [Eq. (III.5.33)] that

$$EU_v = \sum_{v'} \langle \psi_v | H_{\text{eff}} \mathcal{A} \psi_{v'} u_{v'} \rangle \quad (4.70)$$

$$= \sum_{v'} \left\langle \psi_v | H_{\text{eff}} \mathcal{A} \psi_{v'} \left(\frac{1}{1 - K'} \right)_{v'v''} U_{v''} \right\rangle \quad (4.71)$$

which are simply the coupled channel Schrödinger equations in which the target wave functions range through a finite set $\{\psi_v\}$, $v = 1, \dots, n$. U_v is the projection of the Schrödinger wave function on ψ_v :

$$U_v(0) = \langle \psi_v(1, 2, \dots) | \Psi \rangle \quad (4.72)$$

The function u_v is given by [see (III.5.15)]

$$U_v = u_v - \sum K'_{vv'} u_{v'} = (1 - K')_{vv'} u_{v'} \quad (4.73)$$

where all eigenstates $\omega_{\alpha}^{(1)}$ of $K_{vv'}$ with eigenvalues 1 have been removed, as indicated by the prime on K . These are the superfluous solutions of Section III.5 satisfying the condition (III.5.9)

$$\mathcal{A} \sum_v \omega_{\alpha v}^{(1)} \psi_v = 0 \quad (4.74)$$

Hence

$$K'_{vv'} = K_{vv'} - \sum_{\alpha} \omega_{\alpha v}^{(1)} \langle \omega_{\alpha v'}^{(1)} \rangle \quad (4.75)$$

From (4.71) the DWA amplitude with Pauli principle included is

$$\mathcal{T}_{fi}^{(\text{dir})} = \left\langle U_f^{(-)} \psi_f \left| \sum_i v(\mathbf{r}_0, \mathbf{r}_i) \right| \mathcal{A} \sum_{v'} \psi_{v'} u_{v'}^{(+)} \right\rangle \quad (4.76)$$

$$u_{v'} = \sum \left(\frac{1}{1 - K'} \right)_{v'v''} U_{v''} = \left(\frac{1}{1 - K'} \right)_{v'i} U_i$$

where the last of these equations is a consequence of the initial condition on $U_{v''}$. Equation (4.75) implies orthogonality of $U_f \psi_f$ with $\mathcal{A} \sum \psi_{v'} u_{v'}$. Orthogonality does indeed follow:

$$\begin{aligned}
\langle U_f \psi_f | \mathcal{A} \psi_v u_v \rangle &= \sum_{v'} \langle U_f^{(-)} | (1 - K')_{fv'} | u_v^{(+)} \rangle \\
&= \sum_{v'} \langle U_f^{(-)} | (1 - K')_{fv'} \left(\frac{1}{1 - K'} \right)_{v'i} | U_i^{(+)} \rangle \\
&= \langle U_f^{(-)} | \delta_{fi} | U_i^{(+)} \rangle = 0
\end{aligned}$$

since $i \neq f$.

Evaluation of (4.76) requires the determination not only of U_f and U_i but also of the eigenvalues and eigenfunctions of K , those for which the eigenvalues are neither 1 or zero. The problem of determining K for the shell model description has been solved by Friedman (67) [Some of his results are given in Section III.5 (see (III.6.51) and (III.6.52)]. In the case where the eigenvalues of K are 0 and 1, u_i equals U_i . This simplest case occurs if the wave functions ψ_v are Slater determinants made up of mutually orthogonal single-particle wave functions.

Returning to (4.76), one obtains

$$\begin{aligned}
\mathcal{F}_{fi}^{(\text{dir})} &= \left\langle U_f^{(-)}(\mathbf{r}_0) \psi_f(\mathbf{r}_1, \mathbf{r}_2, \dots) \left| \sum_j v(\mathbf{r}_0, \mathbf{r}_j) \right| \sum \psi_v(\mathbf{r}_1, \mathbf{r}_2, \dots) u_v^{(+)}(\mathbf{r}_0) \right\rangle \\
&\quad - A \left\langle U_f^{(-)}(\mathbf{r}_0) \psi_f(\mathbf{r}_1, \mathbf{r}_2, \dots) \left| \sum_j v(\mathbf{r}_0, \mathbf{r}_j) \right| \sum \psi_v(\mathbf{r}_0, \mathbf{r}_2, \dots) u_v^{(+)}(\mathbf{r}_1) \right\rangle
\end{aligned}$$

or

$$\begin{aligned}
\mathcal{F}_{fi}^{(\text{dir})} &= A \left\langle U_f^{(-)}(\mathbf{r}_0) \psi_f(\mathbf{r}_1, \mathbf{r}_0, \dots) \left| v(\mathbf{r}_0, \mathbf{r}_1) (1 - P_{01}) \right| \sum \psi_v(\mathbf{r}_1, \mathbf{r}_2, \dots) u_v^{(+)}(\mathbf{r}_0) \right\rangle \\
&\quad - A \left\langle U_f^{(-)}(\mathbf{r}_0) \psi_f(\mathbf{r}_1, \mathbf{r}_2, \dots) \left| \sum_2^A v(\mathbf{r}_0, \mathbf{r}_j) \right| \sum_v \psi_v(\mathbf{r}_0, \mathbf{r}_2, \dots) u_v^{(+)}(\mathbf{r}_1) \right\rangle \quad (4.77)
\end{aligned}$$

Thus $\mathcal{F}_{fi}^{(\text{dir})}$ consists of a direct term [the first term in (4.77)], an exchange term referred to as the *knock-on term* [the second term in (4.77)], and finally, the *heavy-particle stripping term* [the third and last term in (4.77)]. The knock-on term is just what would be expected if one is dealing with a two-body interaction in which the rest of the target (the core) does not participate in the reaction, that is, acts as spectator. In the heavy-particle stripping term the particle labeled \mathbf{r}_0 becomes unbound while the particle labeled \mathbf{r}_1 becomes bound, under the influence of interactions, $v_{02} + v_{03} \dots$. This is most unlikely, being proportional to the "amount" of $u_v^{(+)}(\mathbf{r}_1)$ present in $\psi_f(\mathbf{r} \dots)$, going to zero if $u_i^{(+)}$ and ψ_f are orthogonal. This, indeed, would be the case if ψ_f is a Slater determinant of bound orthogonal orbitals and $u_i^{(+)}$ is a continuum wave function that is orthogonal to all bound single-particle wave functions. It is the virtue of anti-

symmetrization and the elimination of the superfluous states that one is not required to include, in the sum over v in (4.26) and (4.77), terms in which any of the target nucleons are in continuum orbitals. It appears, therefore, to be a good approximation to drop the last term in (4.77), that is, to use models in which the u_v are orthogonal to ψ_f .

Finally, one makes the approximation of dropping all but ψ_i in the sum over v in the leading terms of (4.77), so that

$$\mathcal{T}_{fi}^{(\text{dir})} \simeq A \langle U_f^{(-)}(\mathbf{r}_0) \psi_f(\mathbf{r}_1, \mathbf{r}_2, \dots) | v(\mathbf{r}_0, \mathbf{r}_1) (1 - P_{01}) | \psi_i(\mathbf{r}_1, \mathbf{r}_2, \dots) u_i^{(+)}(\mathbf{r}_0) \rangle \quad (4.78)$$

This result is also obtained in the high-energy limit where first-order multipole scattering theory applies. The impulse approximation, in which the incident projectile interacts only with one of the nucleons in the nucleus, is applicable and only the two-body Pauli principle, as in (4.78), is involved. Comparing (4.78) with (4.76), we see that this approximation is valid only when the eigenvalues of the K matrix are either 1 (the Slater determinant case) or zero. When this is not the case [Friedman (67) provides important examples; see Chapter III], the orthogonality between the initial and final states is destroyed in this approximation and one must keep the sum over v in (4.77).

The importance of the errors induced by the approximations is not clear. The initial wave functions and the interactions v_{01} used in (4.78) are determined empirically, for example, from elastic scattering. Then some of the required attributes of the wave functions used in (4.78) may be implicitly contained. However, that these sufficiently reduce the error remains, at the present time, a speculation.

The operator P_{01} equals the product of the space exchange P_{01}^x , spin exchange P_{01}^σ , and the isospin exchange operators P_{01}^τ :

$$P_{01} = P_{01}^x P_{01}^\sigma P_{01}^\tau$$

Introducing the projection operators P^{ST} of (2.84), where S and T are the spin and isospin quantum numbers of the two nucleon system, respectively, one obtains

$$\begin{aligned} P_{01} &= P_{01}^x (P_{01}^{11} - P_{01}^{01} - P_{01}^{10} + P_{01}^{00}) \\ &= P_{01}^x \sum (-)^{S+T} P_{01}^{(ST)} \end{aligned}$$

Therefore, using (2.89) yields

$$\begin{aligned} v_{01}(1 - P_{01}) &= \sum_{ST} v_{01}^{(ST)} P_{01}^{(ST)} (1 - P_{01}) \\ &= \sum_{ST} v_{01}^{(ST)} P_{01}^{(ST)} [1 - (-)^{S+T} P_{01}^x] \end{aligned} \quad (4.79)$$

When $S + T$ is odd (i.e., in states in which the relative wave function is even),

the direct and exchange terms add, whereas when $S + T$ is even, they have opposite signs.

Inserting (4.79) into the expression for the transition matrix (4.78) yields

$$\mathcal{T}_{fi} = A \sum_{ST} \langle U_f^{(-)}(\mathbf{r}_0) \psi_f(\mathbf{r}_1, s^f, t^f) | v_{01}^{(ST)} P_{01}^{(ST)} (1 - (-)^{S+T} P_{01}^x) | \psi_i(\mathbf{r}_1, s^i, t^i, \dots) u_i^{(+)}(\mathbf{r}_0) \rangle$$

where the spin and isospin coordinates are explicitly given. Then

$$\begin{aligned} \mathcal{T}_{fi} = A \sum_{ST} [& \langle U_f^{(-)}(\mathbf{r}_0, s_0^f, t_0^f) | \rho_{fi}^{(ST)}(\mathbf{r}_1, \boldsymbol{\sigma}_0, \mathbf{t}_0) v_{01}^{ST} u_i^{(+)}(\mathbf{r}_0, s_0, t_0) \rangle \\ & - (-)^{S+T} \langle U_f^{(-)}(\mathbf{r}_0, s_0^f, t_0^f) | K_{fi}^{(ST)}(\mathbf{r}_1; \mathbf{r}_0 \boldsymbol{\sigma}_0 \mathbf{t}_0) v_{01}^{ST} u_i^{(+)}(\mathbf{r}_1, s_0^i, t_0^i) \rangle] \quad (4.80) \end{aligned}$$

where

$$\rho_{fi}^{(ST)}(\mathbf{r}_1, \boldsymbol{\sigma}_0 \mathbf{t}_0) = \langle \psi_f(\mathbf{r}_1 \dots) | P_{01}^{(ST)} | \psi_i(\mathbf{r}_1 \dots) \rangle \quad (4.81)$$

and

$$K_{fi}^{(ST)}(\mathbf{r}_1; \mathbf{r}_0, \boldsymbol{\sigma}_0 \mathbf{t}) = \langle \psi_f(\mathbf{r}_1, s_1, t_1; \dots) | P_{01}^{(ST)} | \psi_i(\mathbf{r}_0, s_1, t_1; \dots) \rangle \quad (4.82)$$

The transition densities $\rho_{fi}^{(ST)}$ are a generalization of the one-body densities discussed earlier [see the note following (2.82)]. They occur in the Born approximation (distorted or plane wave) treatment of the inelastic scattering from ψ_i to ψ_f produced by a collision with a nucleon, pion, electron, and so on. Generally, then, these densities can be deduced by considering the data obtained with all of these projectiles. The data obtained with electrons play a central role since in that case the interaction is best known, although exchange current effects do introduce some uncertainties.

The mixed density $K_{fi}^{(ST)}(\mathbf{r}_1, \mathbf{r}_0)$ is present only for the nucleon projectile case because it is only then that the Pauli principle acts. It does, however, occur when second-order (multi-step) processes are considered and then is intimately related to the correlation function [see Feshbach (81)].

$$C_{fi}(\mathbf{r}_1, \mathbf{r}_2) = \rho_{fi}(\mathbf{r}_1, \mathbf{r}_2) - \rho_{fi}(\mathbf{r}_1) \rho_{ii}(\mathbf{r}_2) - \rho_{ff}(\mathbf{r}_1) \rho_{fi}(\mathbf{r}_2)$$

However, up to now it has proven difficult to extract this quantity from experiment.

In a complete DWA theory one will need to diagonalize $K_{fi}^{(ST)}(\mathbf{r}_1, \mathbf{r}_0)$ to most readily obtain orthogonality as discussed earlier in this section, and that diagonalization can be used in this context as well. We write (dropping the superscripts S and T for notational simplicity)

$$K_{fi}(\mathbf{r}_1, \mathbf{r}_0) = \sum w_a^{(f)}(\mathbf{r}_1) \langle w_a^{(i)}(\mathbf{r}_0)$$

where w_a are the eigenfunctions of K and $w_a^{(f)}$ is its component in the final state channel in (see the discussion in Section III.5). These are single-particle wave

functions. They are finite in number and permit a relatively simple evaluation of the exchange term in (4.80), which involves the matrix elements

$$\sum_a \langle U_f^{(-)}(\mathbf{r}_0) w_a^{(f)}(\mathbf{r}_1) | v_{01} | w_a^{(i)}(\mathbf{r}_0) u_i^{(+)}(\mathbf{r}_1) \rangle$$

The local approximation is generally used in evaluating the exchange term in (4.80). The technique is identical with that used in the discussion following (2.9). Consider (suppressing spin variables)

$$V_{\text{exch}}(\mathbf{r}_0) u_i^{(+)}(\mathbf{r}_0) = \int K_{fi}(\mathbf{r}_1, \mathbf{r}_0) v(\mathbf{r}_1 - \mathbf{r}_0) u_i^{(+)}(\mathbf{r}_1) d\mathbf{r}_1 \quad (4.83)$$

Introducing $\mathbf{p} = \mathbf{r}_1 - \mathbf{r}_0$, we obtain

$$\begin{aligned} V_{\text{exch}}(\mathbf{r}_0) u_i^{(+)}(\mathbf{r}_0) &= \int K_{fi}(\mathbf{p} + \mathbf{r}_0, \mathbf{r}_0) v(\mathbf{p}) u_i^{(+)}(\mathbf{r}_0 + \mathbf{p}) d\mathbf{p} \\ &= \int v(\mathbf{p}) K_{fi}(\mathbf{p} + \mathbf{r}_0, \mathbf{r}_0) e^{i[(\mathbf{p} \cdot \hat{\mathbf{p}})/\hbar]} d\mathbf{p} u_i^{(+)}(\mathbf{r}_0) \end{aligned} \quad (4.83')$$

where the operator $i\hat{\mathbf{p}}/\hbar = \nabla$ operates only the \mathbf{r}_0 variable, so that

$$V_{\text{exch}}(\mathbf{r}_0) = \int v(\mathbf{p}) K_{fi}(\mathbf{p} + \mathbf{r}_0, \mathbf{r}_0) e^{i[(\mathbf{p} \cdot \hat{\mathbf{p}})/\hbar]} d\mathbf{p} \quad (4.84)$$

The Perey–Saxon approximation consists in replacing operator $\hat{\mathbf{p}}/\hbar$ by the incident momentum $\mathbf{p}_i/\hbar = \mathbf{k}_i$. A somewhat more elaborate approximation takes the variation of the index of refraction inside the interaction region into account:

$$\frac{\hat{\mathbf{p}}}{\hbar} \rightarrow \left[\frac{2\mu}{\hbar^2} (E - V_{\text{opt}}(r_0)) \right]^{1/2} \quad (4.85)$$

With this replacement of $\hat{\mathbf{p}}$, $V_{\text{exch}}(\mathbf{r}_0)$ becomes a local operator. A further approximation is made by Petrovich, McManus et al. (69, 79) and Love (79a). When \mathbf{k}_i is very large, that is, for sufficiently large energies, the value of $V_{\text{exch}}(\mathbf{r}_0)$ comes mostly from small values of \mathbf{p} , so that in that limit

$$\begin{aligned} V_{\text{exch}}(\mathbf{r}_0) &\rightarrow \rho_{fi}(\mathbf{r}_0) \int e^{i\mathbf{k}_i \cdot \mathbf{p}} v(\mathbf{p}) d\mathbf{p} \\ &\rightarrow \rho_{fi}(\mathbf{r}_0) \tilde{v}(\mathbf{k}_i) \end{aligned} \quad (4.86)$$

where \tilde{v} is the Fourier transform of v .

With the local approximation, (4.80) becomes

$$\mathcal{T}_{fi} = A \sum_{ST} \langle U_f^{(-)}(\mathbf{r}_0) [V_{\text{direct}}^{(ST)} - (-)^{S+T} V_{\text{exch}}^{(ST)}] u^{(+)}(\mathbf{r}_0) \rangle \quad (4.87)$$

where

$$V_{\text{direct}}^{(ST)} = \int d\mathbf{r}_1 \rho_{fi}^{(ST)}(\mathbf{r}_1) v^{ST}(\mathbf{r}_1) \quad (4.88)$$

We note that in this approximation only the single-particle transition density $\rho_{fi}^{(ST)}$ enters in both (4.86) and (4.88). This represents a great reduction in the complexity of the calculation, and as noted earlier, permits the use of empirical information on $\rho_{fi}^{(ST)}(\mathbf{r})$ available for example from electron scattering.

The analysis leading to (4.87) requires modification for the spin-orbit and tensor interactions present for the spin triplet state of the projectile nucleon and target nucleon. For example, consider the case of the spin-orbit interaction, (2.90), appearing in components of $V^{(ST)}$, V^{10} , and V^{11} , in the form

$$v^{LS}(\boldsymbol{\rho}) \frac{1}{2}(\boldsymbol{\sigma}_0 + \boldsymbol{\sigma}_1) \cdot [(\mathbf{r}_1 - \mathbf{r}_0) \times (\mathbf{p}_1 - \mathbf{p}_0)] = v^{LS}(\boldsymbol{\rho})(\boldsymbol{\sigma}_0 + \boldsymbol{\sigma}_1) \cdot (\boldsymbol{\rho} \times \mathbf{p}_\rho) \quad (4.89)$$

In evaluating $V_{\text{exch}}^{(SL)}$, using the procedures described above, one needs explicitly to include the result that $V_{\text{exch}}^{(SL)}$ vanishes when K_{fi} is independent of \mathbf{r}_1 , which we shall now demonstrate. Under this condition

$$V_{\text{exch}}^{(SL)} \sim \int v^{LS}(\boldsymbol{\rho})(\boldsymbol{\rho} \times \nabla_\rho) u(\mathbf{r}_1) d\boldsymbol{\rho}$$

Integrating by parts gives

$$V_{\text{exch}}^{(SL)} \sim \int [(\boldsymbol{\rho} \times \nabla_\rho v^{LS}(\boldsymbol{\rho})) u(\mathbf{r}_1)] d\boldsymbol{\rho} = 0 \quad K_{fi} \text{ constant}$$

In the analysis that follows we take this result into account by replacing $K_{fi}(\mathbf{r}_1, \mathbf{r}_0)$ by ΔK_{fi} :

$$\Delta K_{fi} = K_{fi}(\mathbf{r}_0 + \boldsymbol{\rho}, \mathbf{r}_0) - K_{fi}(\mathbf{r}_0, \mathbf{r}_0)$$

The $\boldsymbol{\sigma}_0$ term will be considered in detail. Because $\boldsymbol{\sigma}_0 + \boldsymbol{\sigma}_1$ automatically selects triplet ($S=1$) states, one can drop the operator P^{ST} in (4.79). Inserting (4.89) into (4.84) yields

$$\begin{aligned} V_{\text{exch}}^{(LS)}(\mathbf{r}_0) &\equiv \boldsymbol{\sigma}_0 \cdot \int d\boldsymbol{\rho} \Delta K_{fi}(\mathbf{r}_0 + \boldsymbol{\rho}, \mathbf{r}_0) v^{LS}(\boldsymbol{\rho}) [\boldsymbol{\rho} \times \mathbf{p}_\rho] e^{i\ell(\boldsymbol{\rho} \cdot \mathbf{p}_0)/\hbar} \\ &= \boldsymbol{\sigma}_0 \cdot \int d\boldsymbol{\rho} \Delta K_{fi}(\mathbf{r}_0 + \boldsymbol{\rho}, \mathbf{r}_0) v^{LS}(\boldsymbol{\rho}) [\boldsymbol{\rho} \times \mathbf{p}_0] e^{i\ell(\boldsymbol{\rho} \cdot \mathbf{p}_0)/\hbar} \\ &= \boldsymbol{\sigma}_0 \cdot \int d\boldsymbol{\rho} \Delta K_{fi}(\mathbf{r}_0 + \boldsymbol{\rho}, \mathbf{r}_0) v^{LS}(\boldsymbol{\rho}) [\hbar i \nabla_{\mathbf{p}_0} \times \mathbf{p}_0] e^{i\ell(\boldsymbol{\rho} \cdot \mathbf{p}_0)/\hbar} \end{aligned} \quad (4.90)$$

or using $\hbar i \nabla_{\mathbf{p}_0} = \mathbf{r}_0$, and making the Perey–Saxon approximation $\mathbf{p}_0 \rightarrow \hbar \mathbf{k}_i$ in the exponent, one finally has

$$V_{\text{exch}}^{(LS)}(\mathbf{r}_0) = \int d\boldsymbol{\rho} \Delta K_{fi}(\mathbf{r}_0 + \boldsymbol{\rho}, \mathbf{r}_0) v^{LS}(\boldsymbol{\rho}) e^{i\mathbf{k}_i \cdot \boldsymbol{\rho}} \boldsymbol{\sigma}_0 \cdot \mathbf{L}_0$$

$$\mathbf{L}_0 = \mathbf{r}_0 \times \mathbf{p}_0 \quad (4.91)$$

Problem. Verify (4.90) using Fourier transforms to momentum space of $u(\mathbf{r}_1)$, and so on.

In the high momentum limit,

$$V_{\text{exch}}^{LS}(\mathbf{r}_0) = \frac{1}{ik_i} \mathbf{k}_i \cdot \nabla_1 K_{fi}(\mathbf{r}_1, \mathbf{r}_0)_{1 \rightarrow 0} \frac{\partial \tilde{v}^{LS}(k_i)}{\partial k_i} \boldsymbol{\sigma}_0 \cdot \mathbf{L}_0 \quad (4.92)$$

where

$$\nabla_1 K_{fi}(\mathbf{r}_1, \mathbf{r}_0)_{1 \rightarrow 0} = \lim_{\mathbf{r}_1 \rightarrow \mathbf{r}_0} \nabla_{\mathbf{r}_1} K_{fi}(\mathbf{r}_1, \mathbf{r}_0)$$

A local approximation can also be derived for the $\boldsymbol{\sigma}_1$ term in (4.89). However, $K_{fi}(\mathbf{r}_1, \mathbf{r}_0)$ must be replaced by a vector \mathbf{K}_{fi}^σ in spin space:

$$\mathbf{K}_{fi}^\sigma(\mathbf{r}_1; \mathbf{r}_0) = \langle \psi_f(\mathbf{r}_1 s_1 t_1, \dots) | \boldsymbol{\sigma}_1 | \psi_1(\mathbf{r}_0, s_1, t_1; \dots) \rangle \quad (4.93)$$

a term that is important if the transition involves a spin-flip of a target nucleon.

5. THE INTERACTION POTENTIALS

In this section we discuss the interaction potentials, v_{0i} , to be inserted into the expression for the direct process inelastic \mathcal{T} matrix. For the present, our attention will be focused on their derivation from the nucleon–nucleon force. Comparison with experiment is deferred to Section 6. Prediction of experimental results depends on both v_{0i} and the properties of the incident and final wave functions as contained in the transition density matrix.

Bertsch, Borysowicz, McManus, and Love (77) [see also Love, Scott, et al. (78) and earlier work of Slanina and McManus (68)] proceed by fitting the potentials v_{0i} so as to have the same matrix elements, in an oscillator basis, as the elements of the G matrix determined, for example, from the application of the G -matrix method to semiempirical nucleon–nucleon forces. The central and spin-orbit potentials are taken to be the sum of three terms, each of the Yukawa form, with the ranges 1.4, 0.7 and 0.4 fm. The first of these is the range of the one-pion exchange potential; the other two are phenomenological, corresponding to intermediate and short-range potentials. The final recommended interaction ($M3Y$) is based primarily on the Reid nucleon–nucleon potential [Reid

(68)]. This interaction potential is real and independent of density. It is applicable for the energy range $E \lesssim 60$ MeV. The resulting potentials are given in Fig. 5.1.

Petrovich, Stanley, and Bevelacqua (77) point out that the $M3Y$ interaction does not lead to saturation. They add a density-dependent term proportional to the density to achieve saturation. On the other hand, Geramb, Brieva, and Rook (79) use the more recently developed "Paris" nucleon-nucleon potential [Lacombe, Loiseau, et al. (80)]. The local density approximation [see Vol. deShalit and Feshbach (74)] is used, employing plane wave matrix elements. These are matched for each value of the density and energy by the plane wave

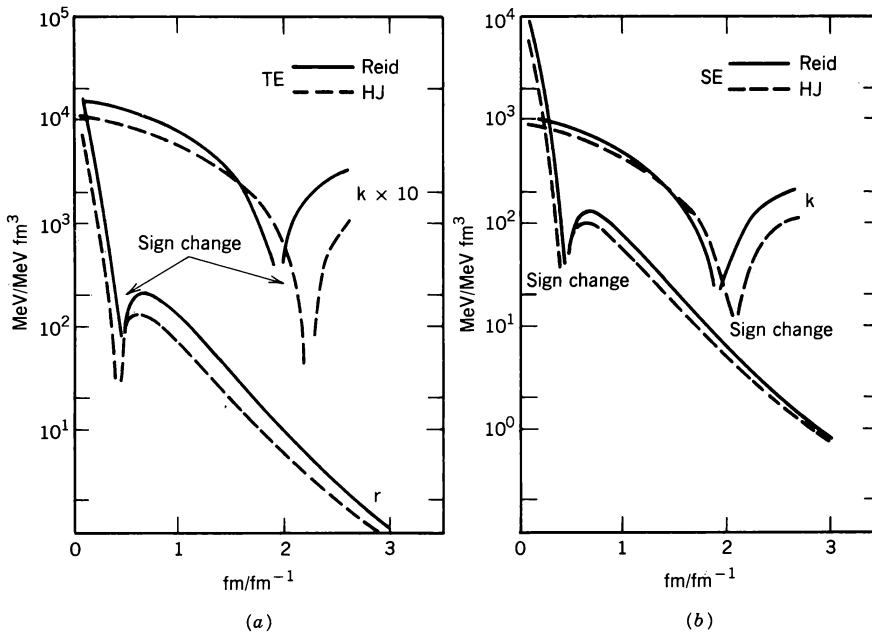


FIG. 5.1. (a) TE component of the interaction as fitted to three Yukawas is shown in configuration space (V in MeV versus r in fm and labeled by r) and in momentum space (V in $\text{MeV} \cdot \text{fm}^3$ versus k in fm^{-1} and labeled by k). The change in sign of the interaction near the origin is shown in the figure. TE = Central triplet ($S = 1$) even ($T = 0$) [see (2.86).] (b) SE component of the interaction same convention as (a). SE = singlet ($S = 0$) even ($T = 0$) [see (2.86)]. (c) TNE component of the interaction. The solid and dashed curves correspond to r^2 Yukawa-type fits. The solid circles correspond to ROPEP fit (same convention (a)). TNE = tensor even ($T = 0$). (d) TNO component of the interaction [same convention as (a)]. TNO = tensor odd ($T = 1$). (e) LSE and LSO components of the interaction [conventions as in (a) except \bar{V} is in $\text{MeV} \cdot \text{fm}^5$]. LSE = spin orbit, $T = 0$, LSO = spinorbit $T = 1$. (f) SO and TO components of the interaction from Elliott matrix elements (same convention as in (a)). SO = singlet central, $T = 1$. TO = triplet central, $T = 1$. [From Bertsch, Borysowicz, McManus, and Love (77).]

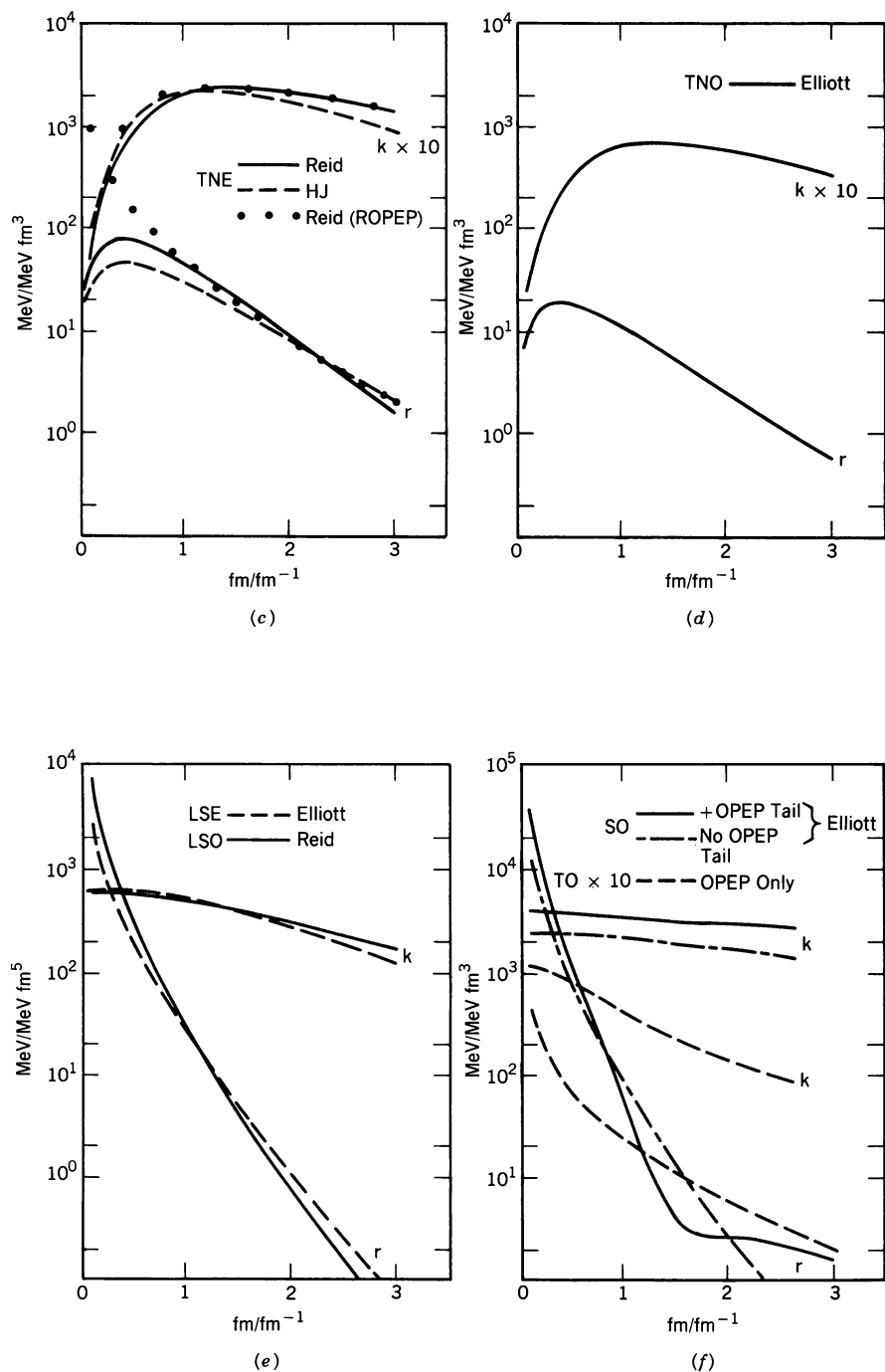


FIG. 5.1. (Continued)

matrix elements of a sum of four Yukawa potentials. Several averages are performed (over the Fermi sphere for the target nucleons, over angular momenta) to finally obtain a local potential. The details are given in the original paper [see also Geramb (83)]. The resulting interactions are complex and are density and energy dependent. They do not appear, however, to include the effective mass correction of Equation (2.21). Neither do Petrovich and Love (81) and Love and Franey (81), who advocate the use of the $M3Y$ at low energies (< 100 MeV) and the free-space nucleon–nucleon transition matrix as derived as the first term of the multiple scattering approximation (see Chapter II) for higher energies. The plane wave matrix elements are matched by the matrix elements of a sum of Yukawa potentials. The resulting interactions are complex and energy dependent. They are not density dependent.

Typical results following from the Brieva, Rook, and Geramb approach are shown in Fig. 5.2, in which the real and imaginary parts of \tilde{v}_{00}^C , the isoscalar central, are shown as a function of q , the momentum transfer, where

$$\tilde{v}_{00}^C(\mathbf{q}) \equiv \int e^{i\mathbf{q}\cdot\mathbf{r}} v_{00}^C(r) d\mathbf{r}$$

and of the density, which is related to the parameter k_F by

$$k_F = (\frac{3}{2}\pi^2\rho)^{1/3}$$

Recall that $k_F \sim 1.36 \text{ fm}^{-1}$ corresponds to normal nuclear density. Note the change in sign of $\text{Re } \tilde{v}_{00}^C$ and $\text{Im } \tilde{v}_{00}^C$. These provide the input required to construct the local density approximation to $v_{00}^C(|\mathbf{r}_0 - \mathbf{r}_i|)$, the density employed, and therefore the choice of the various curves shown in Fig. 5.2, being evaluated at the average position of the two points \mathbf{r}_0 and \mathbf{r}_1 [i.e., at $\frac{1}{2}(\mathbf{r}_0 + \mathbf{r}_1)$].

Figure 5.2 also contains the results obtained by Love and collaborators [Love and Franey (81)]. It is clear that at this energy (140 MeV) there is a substantial difference, so that the effect of the nuclear medium is significant and cannot be disregarded. Nevertheless, *qualitatively* the Brieva et al. curves are similar to the Love–Franey free-space results, so that within an overall reduction factor, one can obtain qualitatively useful results using the Love–Franey interaction. However, it cannot be expected to be quantitatively valid.

It is therefore appropriate to examine the results obtained by Love and Franey (81) given in Fig. 5.3, in which the magnitudes of the effective interactions are plotted as a function of the momentum transfer, q , for energy ranging from 100 to 800 MeV. As the energy increases, these effective interactions should become increasingly accurate. At the lower energies, the omitted medium effects become significant. In discussing these results, note that the relevant components of v [for normal parity transition from spin-zero target ground states is $\Delta\pi = (-)^J$, where J is the spin of the excited state] are the central interactions, v_{00} and v_{01} , and the spin-orbit terms, v^{LS} , while the abnormal parity transitions [$\Delta\pi = (-)^{J+1}$] are dominated by the spin-orbit, tensor and spin-dependent

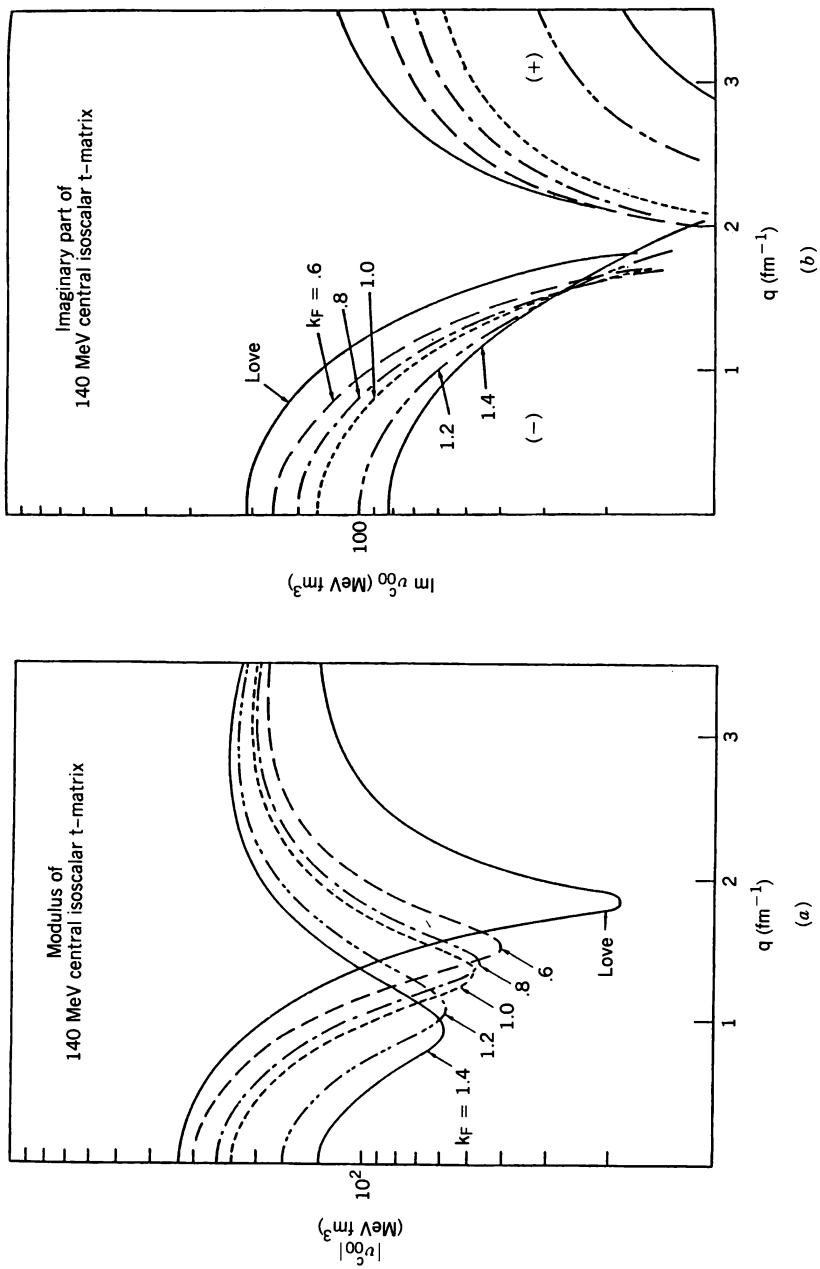


FIG. 5.2. Comparison of the isoscalar central potentials, (2.), computed from the calculation of von Geramb, Brieva, and Rook (79) for various values of k_F and those obtained by Love, Scott, et al. (78). q is the momentum transfer [From Kelly (81).]

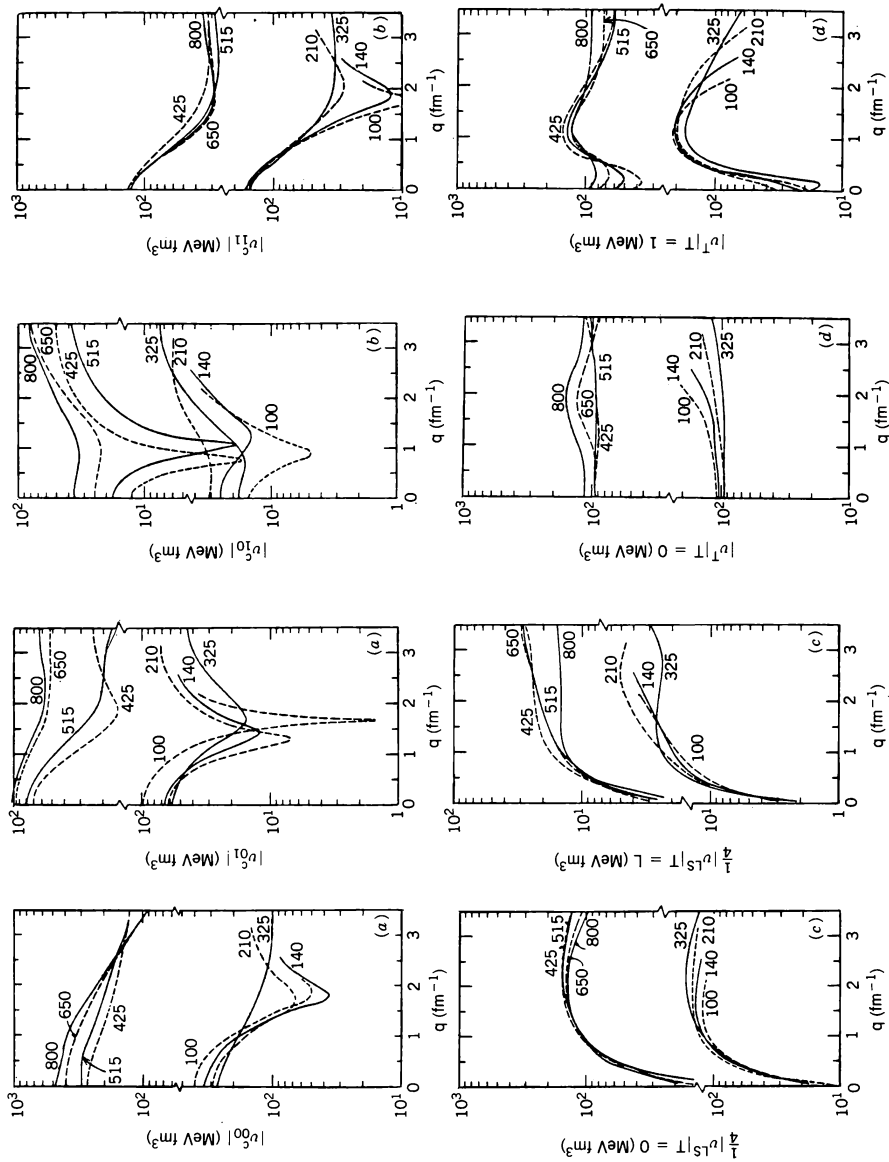


FIG. 5.3. Magnitudes of the effective nucleon-nucleon potential, (2.86), as a function of momentum transfer, q and bombarding energy (number on curve in MeV). [From Love and Franey (81).]

parts of the central terms, v_{10} and v_{11} . The parity change is accompanied by a spin flip of the target nucleon.

Problem. Prove this last statement.

We first discuss the normal parity transitions. In both v_{00} and v_{01} , note the strong minima in the range $100 \text{ MeV} < E < 210 \text{ MeV}$ for $q \sim 1.6 \text{ fm}^{-1}$. In this domain, the spin-orbit contributions, especially $v^{LS}(T=0)$, will dominate. At low q , the dominant contribution will come from scalar-isoscalar v_{00} . The latter is illustrated by Fig 5.4, which shows $v_{00} \gg v_{01}, v_{10}, v_{11}$.

Turning next to the unnatural parity excitations, the $T=1$ contribution is dominated at small q by v_{11} . At larger q and for the lower group of energies a minimum is present in v_{11} , and $v^T(T=1)$ should dominate. For $T=0$, the tensor term $v^T(T=0)$ is strongest at low q . At larger q , v_{10} , $v^{LS}(T=0)$ and $v^T(T=0)$ will all be important. Note that the last two are relatively constant for large q and slowly varying with energy.

We note the important result that the corresponding components of the density matrix will be measurable. For example, low- q normal parity transitions will be sensitive to the scalar density ρ^{00} . While for abnormal parity transition, the spin components ρ^{11} and ρ^{10} will be important. If, on the other hand, the nuclear structure is well known, the interactions can be extracted from experiment.

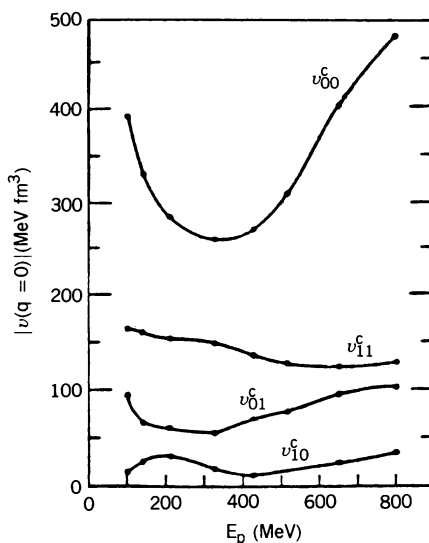


FIG. 5.4. Energy dependence of the magnitude of the central parts of the N - N t matrix as described in Fig. 5.3. [From Love and Franey (81).]

G-Matrix Method [Mahaux (79); Brieva and Rook (78)]. In this section we briefly outline the G -matrix method used in the lower-energy range to obtain the effective two-body interaction. The procedure used is called the Brueckner–Hartree–Fock method. [We refer the reader to deShalit and Feshbach (74), (VII.18.13) and (VII.18.14).] The first of these is the equation for the G matrix,

$$G(\varepsilon) = v + v \frac{Q_F}{\varepsilon - H_0} G(\varepsilon) \quad (5.1)$$

where v is the nucleon–nucleon potential, Q_F is the Pauli operator that projects on to unfilled states, and H_0 is the unperturbed Hamiltonian:

$$H_0 = \sum h_i$$

$$h_i = \frac{k^2}{2m} + U_i \quad (5.2)$$

where U_i is a one-body potential chosen so as to minimize higher-order effects in the evaluation of the energy:

$$E = \sum_i \langle i | T | i \rangle + \frac{1}{2} \sum \langle ij | G(\varepsilon_i + \varepsilon_j) | ij \rangle \quad (5.3)$$

In the positive energy domain the Bethe–Goldstone equation (5.1) is replaced, using lower case g , by

$$g(E) = v + v \frac{Q_F}{E^{(+)} - H_0} g(E) \quad (5.4)$$

The resulting nucleon–nucleus interaction is then given by an extension of the second term of (5.3) as

$$V_{\text{eff}}(k, E) = \sum_{j < k_F} \langle k, j | g(E + e(j)) | k, j \rangle \quad (5.5)$$

This is the Brueckner–Hartree–Fock approximation for V_{eff} for positive energies E . It contains the effects of particle–hole excitations but not, for example, excitations involving two or more holes. It is thus the first term in an expansion in the number of hole lines. Evidently, g is the effective two-nucleon interaction inside the nucleus.

There remains the problem of choosing U_i in (5.2). Jeukenne, Lejeune, and Mahaux (76) use a self-consistent procedure as follows. Take

$$U(k) = \text{Re } V_{\text{eff}}(k, E(k))$$

where

$$E(k) = \frac{k^2}{2m} + \text{Re } V_{\text{eff}}(k, E(k))$$

[Compare with (2.32).] Since H_0 depends on U , an iterative procedure is used, determining g , U , and V_{eff} simultaneously.

Jeukenne, Lejeune, and Mahaux (76) [see also Mahaux (78) and Brieva and Rook (77, 78)] have applied this method to the case of infinite nuclear matter, thereby deriving values of g and V_{eff} for various values of the density. Several differing approximations are made by each group which we will not pursue here. Using the local density approximation permits the approximate extension to finite nuclei. The results, as we have indicated earlier, are surprisingly good and as also shown by the comparison of the theoretical and empirical volume integrals of the potential shown in Fig. 5.5. One must bear in mind the omission,

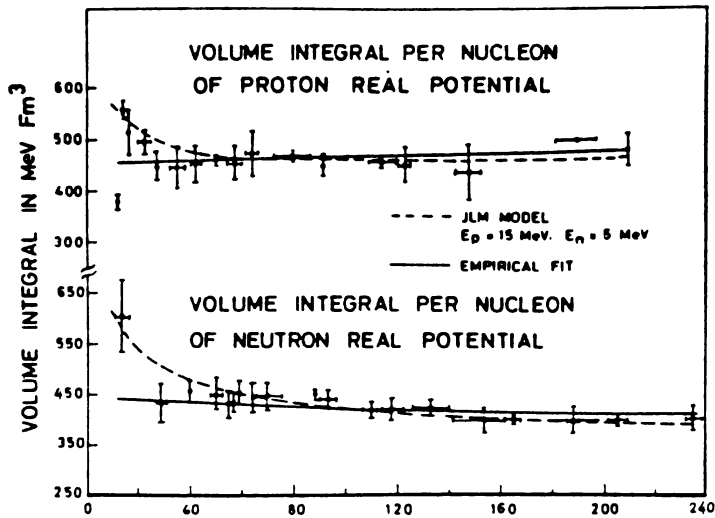


FIG. 5.5. (a) Compilation of empirical volume integrals per nucleon for $10 < E < 20$ MeV protons (upper part) and for $1 < E < 8$ MeV neutrons (lower part). The dashed curves are the theoretical values, computed for $E_p = 15$ MeV and $E_n = 5$ MeV [Jeukenne, Lejeune, and Mahaux.]

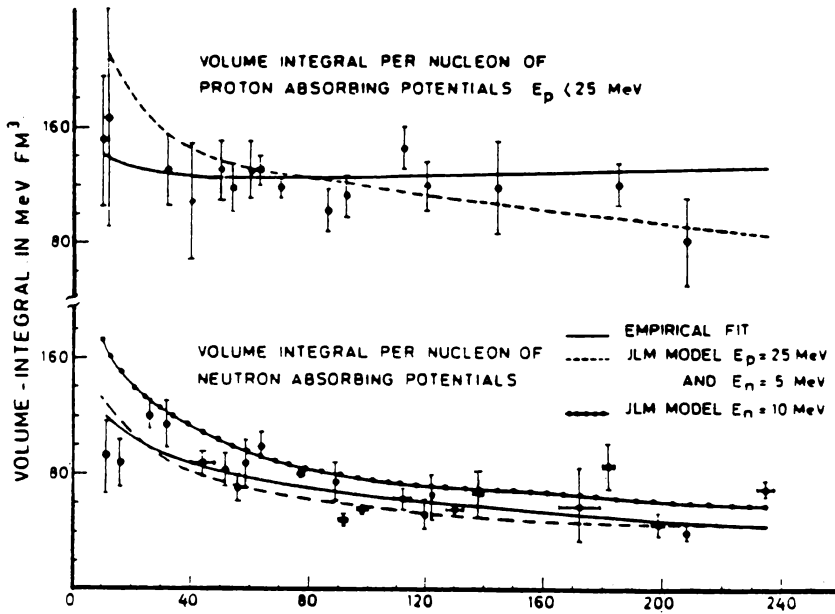


FIG. 5.5. (b) Dependence on A of the volume integral per nucleon of the imaginary part of the optical model potential. The dots are obtained from a compilation of empirical values for $17 (\pm 8)$ MeV protons and for $5 (\pm 3)$ MeV neutrons. The theoretical curves refer to $E_p = 25$ MeV and $E_n = 5$ MeV (short dashes) and $E_n = 10$ MeV (full curve with dots) [Jeukenne, Lejeune, and Mahaux (76)]. [From Mahaux (79).]

at least explicitly, of surface effects which in finite nuclei contribute importantly to the absorptive potential. Of equal, if not greater concern is the failure of the Brueckner–Hartree–Fock method [see Chapter VII in deShalit and Feshbach (74)], without some additional phenomenological devices, to predict the nuclear matter binding energy/nucleon as well as the properties of the bound states of finite nuclei.

6. COMPARISON WITH EXPERIMENT

We select a few examples from the immense literature on this subject. In comparing the direct interaction theory of inelastic scattering with experiment, one should bear in mind its major conceptual approximation. The assumption (see Sections 1 and 4) is made that the process can be described by a single step; that is, reaction paths in which the system passes through the intermediate states are not important. As we discuss in a later chapter, this is not the case for nucleon projectile energies in the range 25 to 65 MeV, where the multistep

contributions have been calculated [Bonetti, Colli-Milazzo Doda and P. E. Hodgson (82)]. At the endpoints of this interval the single-step direct process contributes 82% and 70%, falling to 50% in between, respectively, indicating that the multistep process becomes unimportant for energies somewhat below 25 MeV and above 65 MeV. These multistep contributions become more important as the scattering angle and/or the energy loss increases. Thus, at and below ~ 65 MeV, one can expect agreement of the DWA with experiment only at forward angles and small energy loss. In addition, because simple wave functions are used to describe the initial and final nuclear states, a normalization factor must be introduced to obtain the correct order of magnitude of the cross section. That factor is generally much smaller than unity, indicating that the model wave function used is a small component of the exact wave function. Above ~ 65 MeV, the nucleus is sufficiently transparent so that one-step processes dominate.

In addition to the coupling potentials of Section 4.D, to obtain a theoretical prediction to compare with experiment, one needs the distorted incident and outgoing nucleon wave function as well as the density matrices describing the nuclear transition [see (4.81)]. In principle, the distorted wave functions should be obtained as solutions of the Schrödinger equation using the folding optical potential obtained from the same “two-body” interactions used in deriving the interaction potentials for inelastic scattering. This procedure is not always used; rather, the empirical optical model, adjusted to fit the elastic scattering data, is used. This inconsistency is faced if the folding potential optical does not give a good fit to the elastic scattering. Generally, also, the orthogonality requirements on the initial and final wave functions [see the discussion following (4.68)] are not rigorously satisfied. With regard to derivations of the interaction potentials from the empirical nucleon–nucleon forces, it should be mentioned that the effects of effective nuclear mass [see (2.37)] are not taken into account.

Using the representation of the effective two-body potential given by (2.86), one sees that the density matrices that are needed include isoscalar and isovector components of ρ :

$$\begin{aligned}\rho_{fi}^0 &= \langle \psi_f | \sum \delta(\mathbf{r} - \mathbf{r}_i) | \psi_i \rangle \\ \rho_{fi}^\sigma &= \left\langle \psi_f(\mathbf{r}_1 \cdots) \left| \sum_i \delta(\mathbf{r} - \mathbf{r}_i) \boldsymbol{\sigma}_i \right| \psi_i \right\rangle \\ \rho_{fi}^T &= \left\langle \psi_f(\mathbf{r}_1 \cdots) \left| \sum_i \delta(\mathbf{r} - \mathbf{r}_i) \boldsymbol{\sigma}_i \mathbf{r}_i \right| \psi_i \right\rangle \\ \rho_{fi}^L &= \left\langle \psi_f(\mathbf{r}_1 \cdots) \left| \sum_i \delta(\mathbf{r} - \mathbf{r}_i) \mathbf{L}_i \right| \psi_i \right\rangle \\ \rho_{fi}^{so} &= \left\langle \psi_f(\mathbf{r}_1 \cdots) \left| \sum_i \delta(\mathbf{r} - \mathbf{r}_i) \boldsymbol{\sigma}_i \cdot \mathbf{L}_i \right| \psi_i \right\rangle\end{aligned}$$

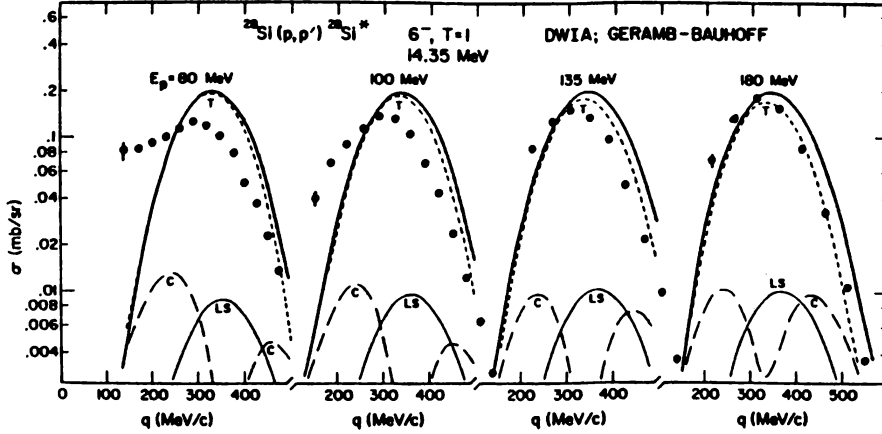


FIG. 6.1. Momentum transfer dependence of the cross sections for proton inelastic excitation of the 6^- , $T = 1$ state at 14.35 MeV in ^{28}Si . The curves are DWIA calculations (multiplied by 0.25) using the Geramb–Bauhoff effective interaction and optical potentials appropriate for the various incident energies. [From Olmer (83).]

Electron scattering from nuclei can provide information on these density matrices, but, of course, for a particular isovector and isoscalar combination, since the electron interacts primarily with the nuclear protons.[‡]

We shall give two examples of the applications of this analysis in the multi-hundred-MeV range. In the first, reported by Olmer (83), inelastic proton scattering from ^{28}Si to its 6^- , $T = 0$, $T = 1$ states[§] is compared to several theoretical interaction potentials, v_{ij} . We shall compare with the Geramb–Bauhoff interaction (80) based on the Paris potential Lecombe et al. (80). The ground state of ^{28}Si contains six $d_{5/2}$ orbital neutrons and six $d_{5/2}$ protons. The excitation lifts one of these to the $f_{7/2}$ forming the particle–hole configuration ($f_{7/2}d_{5/2}^{-1}$). These states are referred to as “stretched” since they correspond to the maximum possible spin for this configuration. Harmonic oscillation wave functions derived from inelastic electron scattering from the same nuclei are used for these orbitals. The “unnatural parity” of the resultant 6^- states requires the action of parity-changing parts of the interaction; that is, the spin–spin, spin–orbit, and tensor terms should be dominant.

The comparison between theory and experiment is shown in Fig. 6.1 for the excitation of the $T = 1$ state. As one can see, these transitions are dominated

[‡]The use of other probes, such as pions, kaons, and so on, can provide additional information. Elastic scattering by positive kaons would, in fact, be most effective in this regard.

[§]Olmer reports on excitations of the 5^+ state, as well.

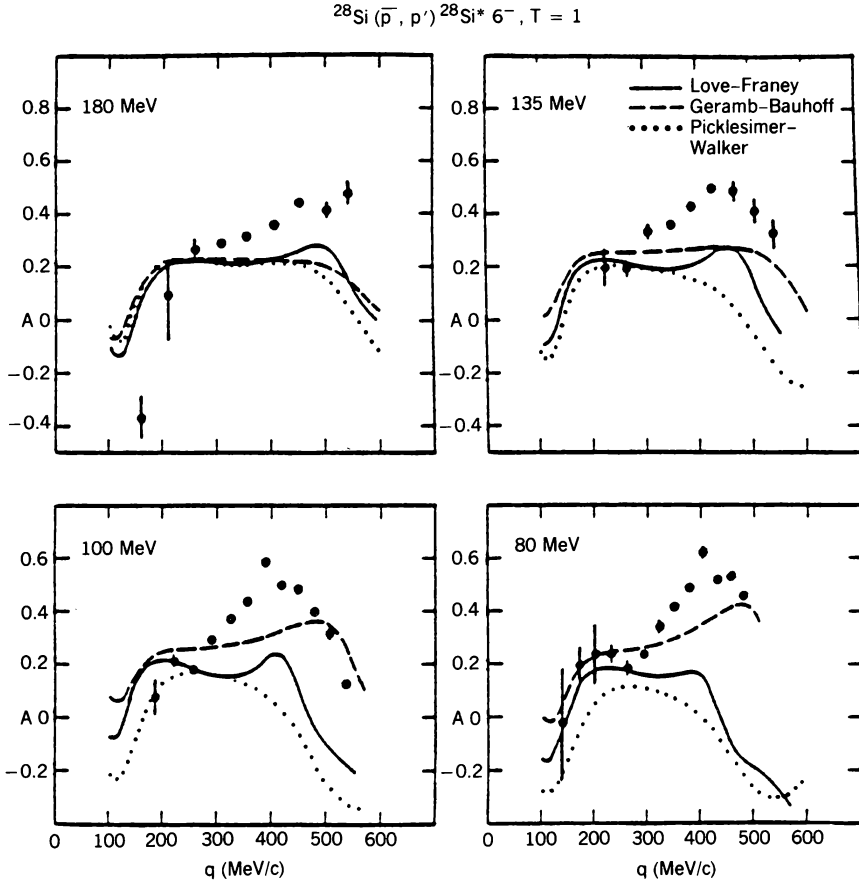


FIG. 6.2. Momentum transfer dependence of the analyzing powers for proton inelastic excitation of the $6^-, T = 1$ state at 14.35 MeV in ^{28}Si . [From Olmer (83).]

by the tensor terms in qualitative agreement with the discussion presented in the preceding section. Agreement is not good for low momentum transfer, q , and lower E . Note that these are semilog plots of the cross section. Moreover, an overall reduction of the theoretical prediction by $\frac{1}{4}$ is required to obtain the correct magnitude. In Fig. 6.2 the analyzing powers, A , are shown. Although the magnitude of A is correctly predicted, the shapes, as a function of q , are not. The cross section for the excitation of the $T=0, 6^-$ state is shown in Fig. 6.3. This time, the predicted magnitudes must be multiplied by a factor of 0.15. And again, there is a problem with the comparison at low q , and E . Note that the tensor and LS components dominate, in disagreement with the qualitative remarks of the preceding section. Obviously, much remains to be done!

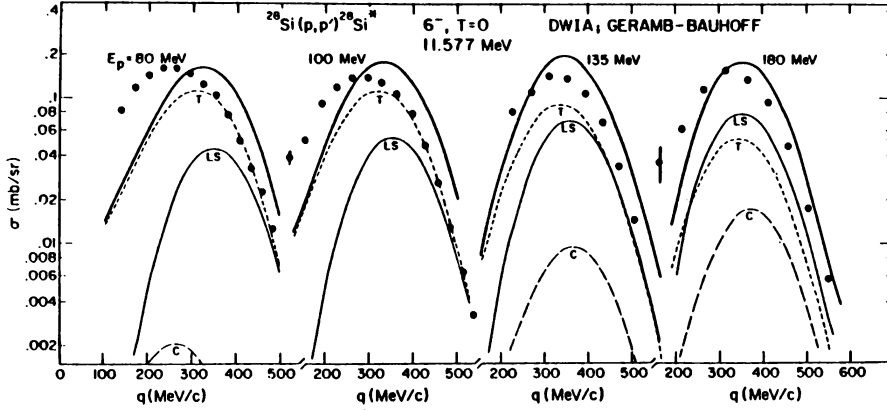


FIG. 6.3. Momentum transfer dependence of the cross sections (for proton inelastic excitation of the 6^- , $T=0$ state at 11.58 MeV in ^{28}Si). The curves are DWIA calculations (multiplied by 0.15) using the Geramb–Bauhoff effective interaction and optical potentials appropriate for the various incident energies. [From Olmer (83).]

A more satisfactory picture is presented by Kelly (83) for the elastic scattering of 135-MeV protons by ^{16}O . The Paris potential is used, as developed by Brieva, Geramb, and Rook (78). Figure 6.4 compares the experimental elastic scattering and the analyzing power with the resultant theoretical predictions. The agreement is by no means perfect, but it must be remembered that there are no adjustable parameters! The inelastic scattering to the “normal” 1^- and 3^- state in ^{16}O is shown in Fig. 6.5. The agreement is very good, indeed. This indicates that the isoscalar spin-independent central component is given correctly by the microscopic theory of Brieva et al. Most important, the Love–Franey interactions, in which there are no medium corrections, fail to reproduce the inelastic cross section. We see from these data (the same can be inferred from Olmer’s result) that the effective two-nucleon interaction is density dependent.

A few examples of comparisons at lower energies employing the $M3Y$ interaction in the folding model will now be discussed. The paper of Bertsch, Barysowicz, McManus, and Love (77) in which this interaction was introduced contains a number of comparisons. As is generally the case in this energy range, an empirical optical model is used to describe the projectile wave functions. Figure 6.6 presents a comparison between experimental and theory for the excitation of states of normal parity 3^- , 5^- in ^{208}Pb by inelastic proton scattering.

The theory does provide reasonable agreement with the shapes of these angular distributions. The dominant role of the central component of the interaction is evident. On the other hand, the prediction of the cross section for the excitation of unnatural parity levels in ^{40}Ca is less successful (see Fig. 6.7). The central part of the interaction alone is inadequate, as expected,

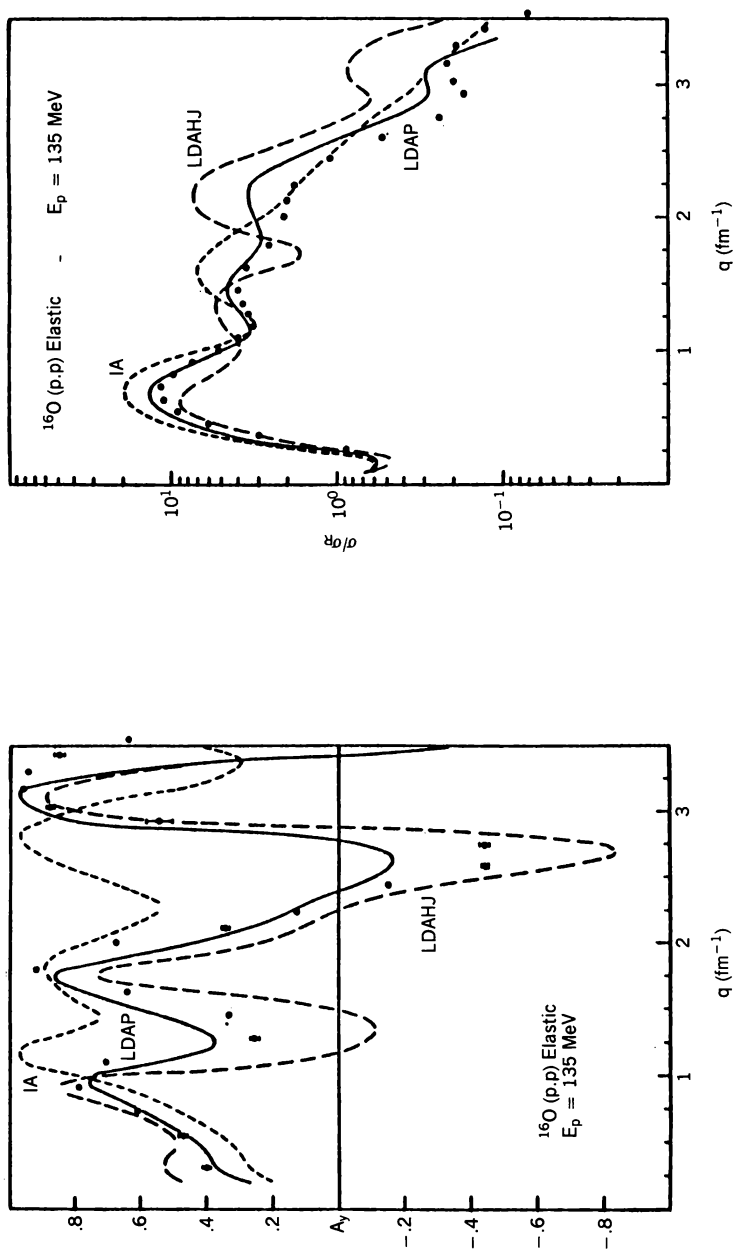


FIG. 6.4. Elastic Scattering of 135-MeV protons by ^{16}O . LDAP = local density approximation using the Paris potential; LDAHJ = local density approximation using the Hamada-Johnston potential. [From Kelly (83).]

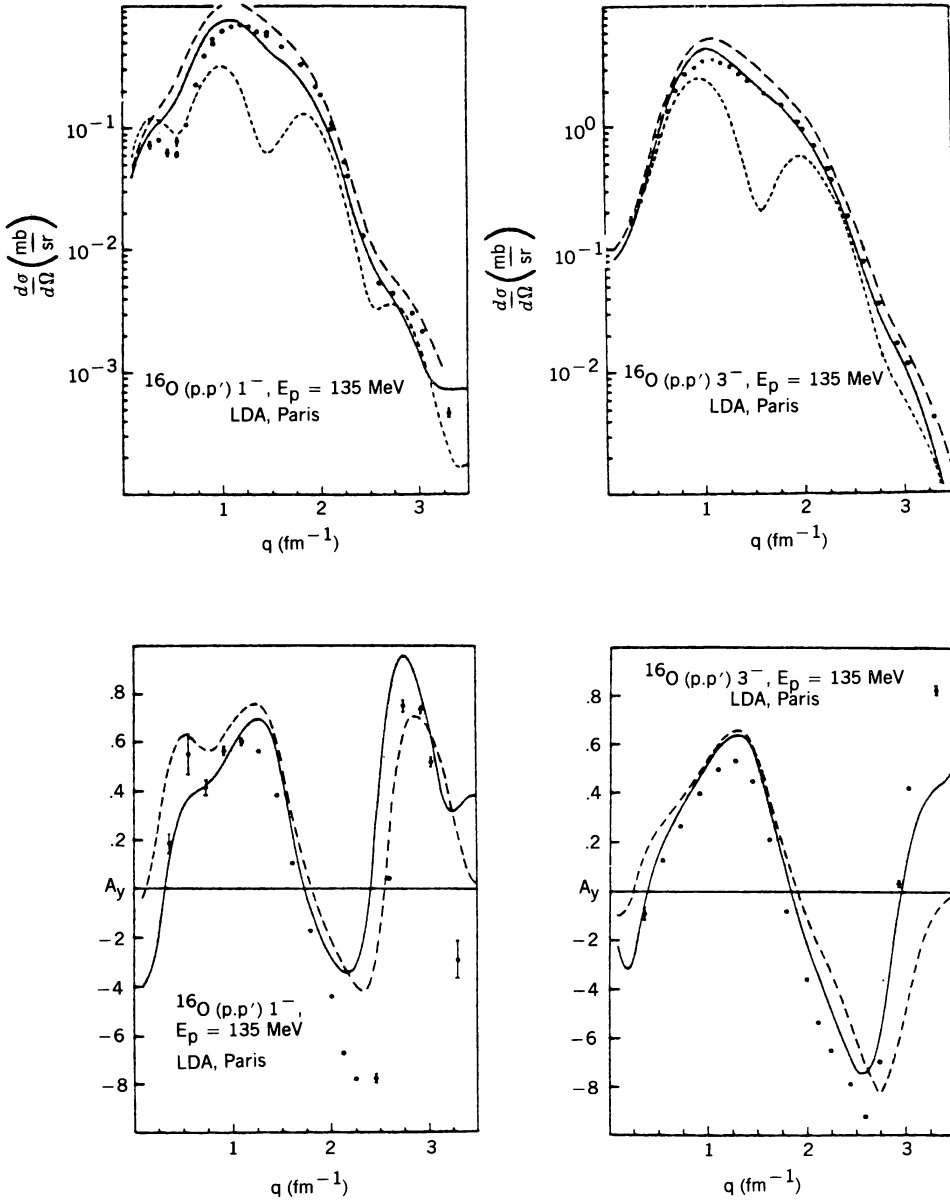


FIG. 6.5. Differential cross section and asymmetry for the inelastic scattering of protons by ^{16}O to the 1^- and 3^- levels compared with the LDA using the Paris potential. [From Kelly (83).]

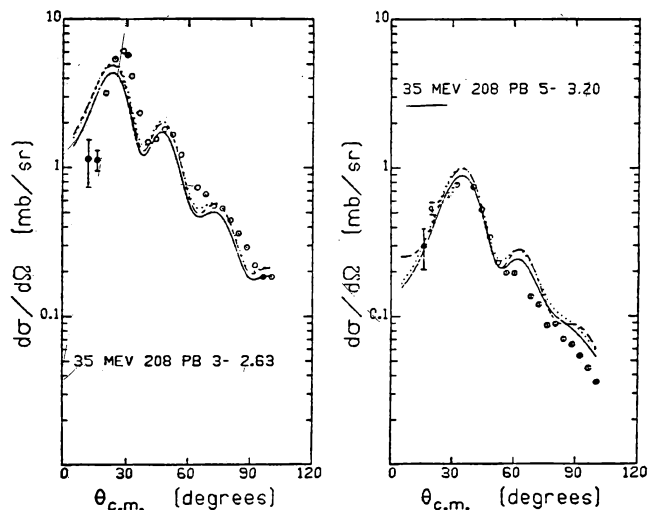


FIG. 6.6. Excitation of lowest 3^- and 5^- states in ^{206}Pb by 35-MeV protons. The solid lines are theory the dotted line is with the central odd interaction removed, and the dashed line is with the central even interaction only. [From Bertsch, Borysowicz, McManus, and Love (77).]

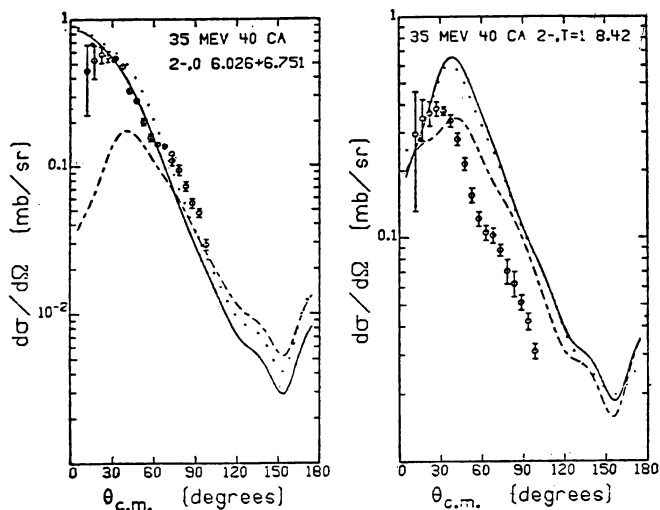


FIG. 6.7. Excitation of 2^- , $T=0$ and 1 states in ^{40}Ca by 35-MeV protons. Conventions are as in Fig. 6.6. [From Bertsch, Borysowicz, McManus, and Love (77).]

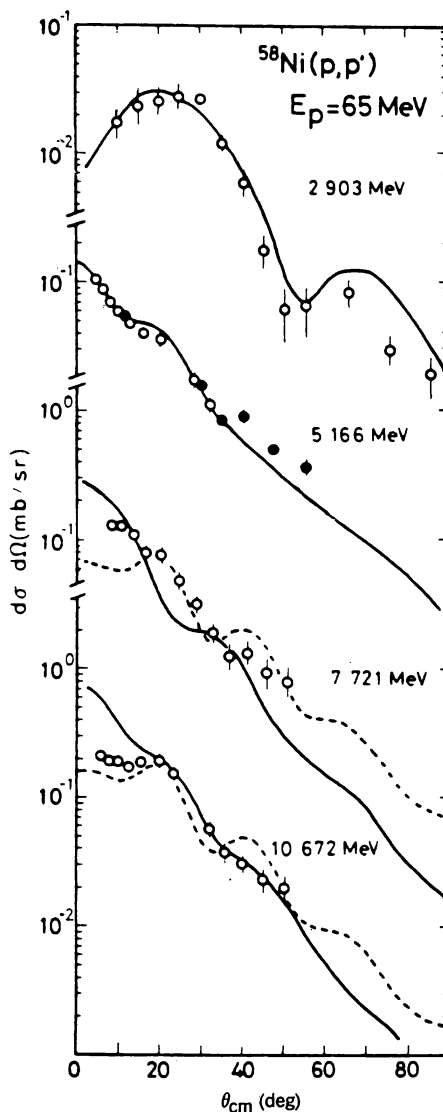


FIG. 6.8. Differential cross sections for the peaks corresponding to the 2.903⁻, 5.166⁻, 7.721⁻, and 10.672 MeV states in ^{58}Ni . The solid curves are the microscopic DWA predictions calculated with the M3Y interaction [Bertsch, Borysowicz, McManus, and Love (77).] The results of the collective $L=2$ DWA calculations are shown for comparison by the dashed curves. [From Fujiwara, Fujita, et al. (83).]

indicating the importance of spin-dependent terms. The disagreement becomes more severe when the excitation energy increases, as Bertsch et al. demonstrate for the $4^-(T=0$ and $T=1)$ levels in ^{40}Ca .

In a more recent comparison, Fujiwara et al. (83) study the excitation of the 1^+ levels in ^{58}Ni by 65-MeV protons. Their results are shown in Fig. 6.8. We

observe the excellent agreement for the excitation of the 2.903- and 5.166-MeV levels, aside for normalization factors of 0.31 and 0.24, respectively. The different shapes are in large part a reflection of the differing structure of the final states. The quality of the agreement decreases and the normalization factors become rather small with increasing excitation energy. The magnitude of the apparent disagreement in the forward direction is sensitive to the optical model parameters, as the authors points out.

CHAPTER VI

TRANSFER REACTIONS

1. INTRODUCTION

Transfer reactions have been of critical importance for the study of nuclear structure. The results obtained from the study of the stripping (d, p) and pickup (p, d) reactions involving single-neutron transfer helped to validate the nuclear shell model by identifying the single-particle states, since to a large extent the (d, p) reaction can be understood as one in which the neutron in the deuteron is transferred to a single-particle state of the final nucleus. In the pickup reaction, a neutron in a single-particle state is picked up by the incident proton to form the deuteron. Reactions in which a proton is transferred, such as the ($^3\text{He}, d$) and ($d, ^3\text{He}$), provide similar information regarding the proton single-particle states. The reactions (t, p) and (p, t) involve the transfer of two neutrons. These reactions are most useful for study of the *superconducting* nuclei, such as the tin isotopes. In these cases, the (t, p) reaction has a relatively large cross section for the transfer of two neutrons in the 1S_0 state, as predicted, for the formation of the final nucleus in a superconducting state.

In the course of these transfer reactions, energy, momentum, and angular momentum are exchanged by the projectile and target nucleus, as in the case for inelastic scattering. But in addition, in the transfer reaction there is a transfer of mass that produces a fundamental change in the description of the reaction from that used for inelastic scattering.

The strong specificity of these reactions at modest projectile energies follows from their surface character, a consequence of the limited penetration of the deuteron into the nuclear interior. If \mathbf{p}_D is the incident deuteron momentum and \mathbf{p}_f the momentum of the emerging proton, the momentum \mathbf{p}_t transferred

to the target nucleus by the transfer of the neutron to the nucleus is given by conservation of momentum:

$$\mathbf{p}_t = \mathbf{p}_D - \mathbf{p}_f \quad (1.1)$$

From this equation one can immediately determine the magnitude of \mathbf{p}_t :

$$p_t^2 = p_D^2 + p_f^2 - 2p_D p_f \cos \vartheta \quad (1.2)$$

where ϑ is the angle between the direction of the final proton and the direction of the incident deuteron. The angular momentum transferred, $\hbar l_t$, must be less than $p_t R$, where R is the projectile-target separation at which the reaction occurs. Hence

$$\hbar^2(l_t + \frac{1}{2})^2 \leq p_t^2 R^2$$

or

$$(l_t + \frac{1}{2})^2 \leq (k_D^2 + k_f^2 - 2k_D k_f \cos \vartheta) R^2$$

so that

$$\cos \vartheta \leq \frac{(k_D R)^2 + (k_f R)^2 - (l_t + \frac{1}{2})^2}{2(k_D R)(k_f R)} \quad (1.3)$$

where $\hbar k$ as usual equals p , and the WKB value of \hat{l}^2 , $(l + \frac{1}{2})^2$, has been used. Classically, then, one expects that the reaction will be forbidden for angles smaller than ϑ_m , the angle at which the equality of (1.3) is satisfied. Quantum mechanically, there will be some penetration into the classically forbidden region, so that the cross section should show a rise from $\vartheta = 0$ with a maximum at ϑ_m . One can employ that result to obtain an estimate of the value of l_t . R is treated as an empirical parameter, which, however, must be the same for all values of l_t .

For example, consider the $^{90}\text{Zr}(d, p)^{91}\text{Zr}$ reaction whose cross sections to various levels in ^{91}Zr are given in Fig. 1.1. The similarity of the curves labeled $l = 2$ in the left-hand panel, of those labeled $l = 4$, and those labeled $l = 0$ is striking. If one assumes that the angle at the first peak equals ϑ_m , one can identify the l_t as well as R by requiring that R have a reasonable value. For example, the $l = 2$, $Q = 1.33\text{-MeV}$ cross section gives $R = 5.4\text{ fm}$ for $l_t = 2$, $R = 3.1\text{ fm}$ for $l_t = 1$, and $R = 7.6\text{ fm}$ for $l_t = 3$. When one takes into account the result obtained from quantitative studies that (1.3) underestimates the value of R at which the reaction occurs, the most reasonable value of R is 5.4 fm and the l_t transferred is 2. Using the same value of R , one can determine l_t for the three curves labeled $l = 4$ to be $l_t = 4$. The curves marked $l = 0$ have their first maxima at $\vartheta = 0$, which is presumed to be $l_t = 0$ transfer reaction.

The values $l_t = 0, 2, 4$ correspond very nicely to shell model expectations. The nucleus, ^{90}Zr , is a closed-shell nucleus [see Fig. IV.8.1 in deShalit and Feshbach

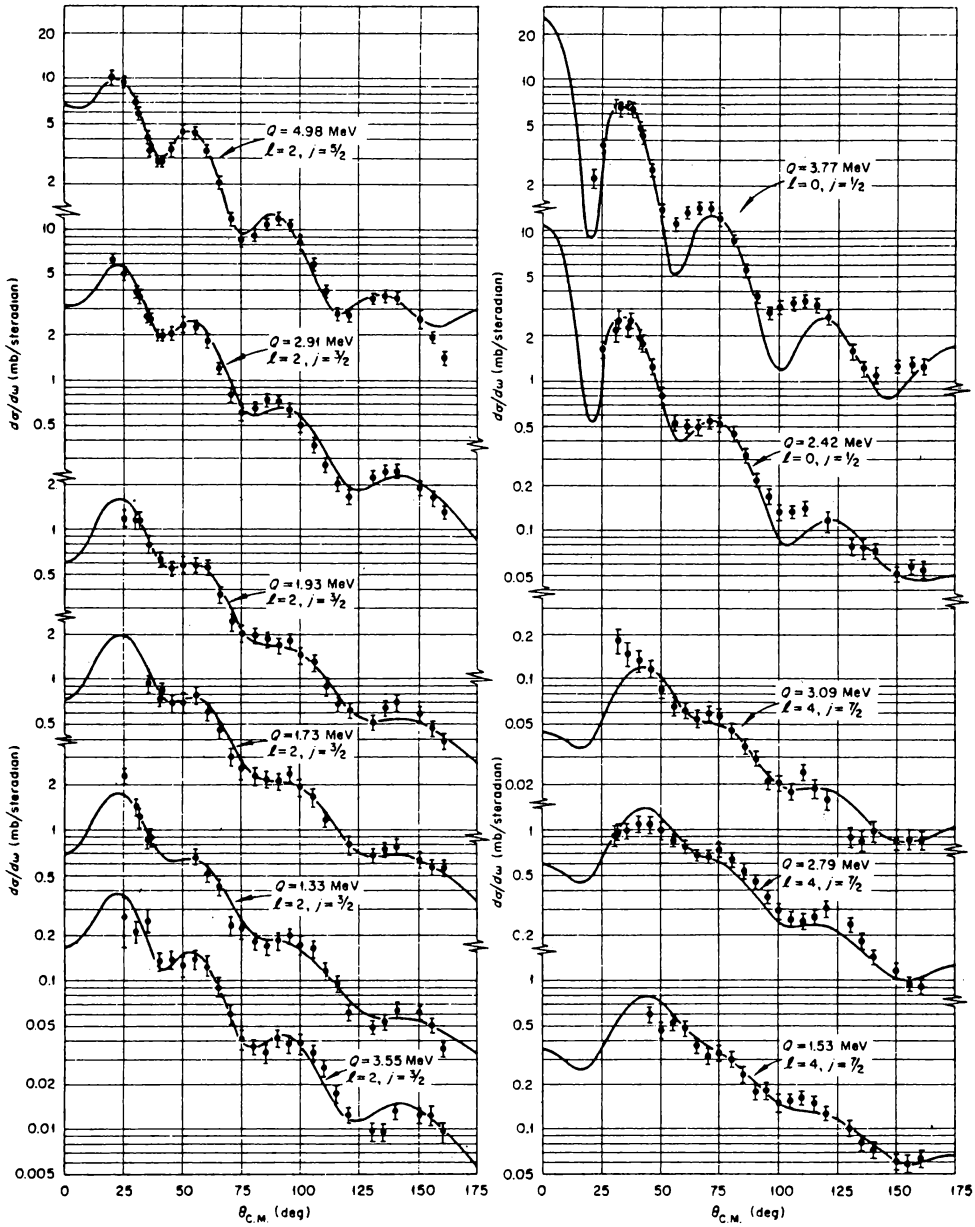


FIG. 1.1. Comparison between measurements and cross sections calculated using the distorted-waves method for the $^{90}\text{Zr}(d,p)^{91}\text{Zr}$ reaction with 12-MeV deuterons. Transitions with $l=0, 2$, and 4 are shown. [Dickens, Perey et al. (67)]. [From Satchler (83).]

(74)]. The neutron added in the (d, p) reaction would thus go into the shell, $50 \leq N \leq 82$ composed of $1g, 2d, 3s$ orbitals (i.e., $l = 4, 2, 0$), corresponding precisely to the values obtained for l_i .

The $^{90}\text{Zr}(d, p)$ example illustrates the extraordinary specificity of the (d, p) reaction that occurs at sufficiently low energies. By examining the angular distribution, one can deduce the orbital angular momentum transferred along with the captured neutron to the largest nucleus. Of course, a quantitative understanding of the angular distribution is essential before one can rely on this conclusion. The results of such a calculation, whose theoretical basis will be discussed later, are shown by the solid lines in Fig. 1.1. In this calculation it is assumed that the transferred neutron occupies a single-particle orbital of the target nucleus. The agreement with experiment is excellent (note the logarithmic scale for the cross sections)—an agreement with experiment that is repeated when targets throughout the periodic table are used, thus validating the single-step character of the transfer reaction mechanism.

The angular distribution is not sensitive[†] to the value of the total angular momentum, j , transferred; that is, it does not distinguish between the two possible values, $j = l \pm \frac{1}{2}$. That sensitivity can be obtained in the (d, p) reaction using polarized deuterons and measuring the asymmetry of the produced protons. An example is shown in Fig. 1.2.

A qualitative understanding of the origin of the polarization of the proton emitted in (d, p) reaction (or equivalently, of the asymmetry of the emitted proton that occurs if the incident deuteron is polarized) has been given by Huby, Refai, and Satchler (58). For the production of nucleon polarization, it is essential that an asymmetry of the transition amplitude with respect to the normal to the scattering plane exist. The absence of such an asymmetry would make the production of a nucleon with a spin oriented in the “up” direction (i.e., in the direction of the normal to the scattering plane) indistinguishable from the production of a nucleon whose spin is in the opposite direction. An asymmetry will be present in the stripping amplitude for a given direction of the emergent proton if the amplitude differs according to which side of the target nucleus the stripping occurs. The origin of the asymmetry in the stripping amplitude lies classically in the differing paths, involving, for example, a different probability of absorption, taken by the proton and deuteron according to the side of the nucleus the deuteron strikes. Quantum mechanically, the asymmetry is a consequence of the distortion of the incident and emergent waves by the nuclear field. If the favored value of the projection, m , of the captured neutron is $(+l)$, and the spin of the final neutron single-particle state, j , is $l + \frac{1}{2}$, the neutron spin must be up. Since the incident spin of the deuteron is one, the spins of the neutron and proton are parallel, the emergent protons will be polarized with their spins up.

The determination of the spin-quantum numbers as well as of the energies

[†]There does seem to be some dependence at back angles which is marked for $l = 1$, but less so for larger values of l [see Satchler (83, p. 706)].

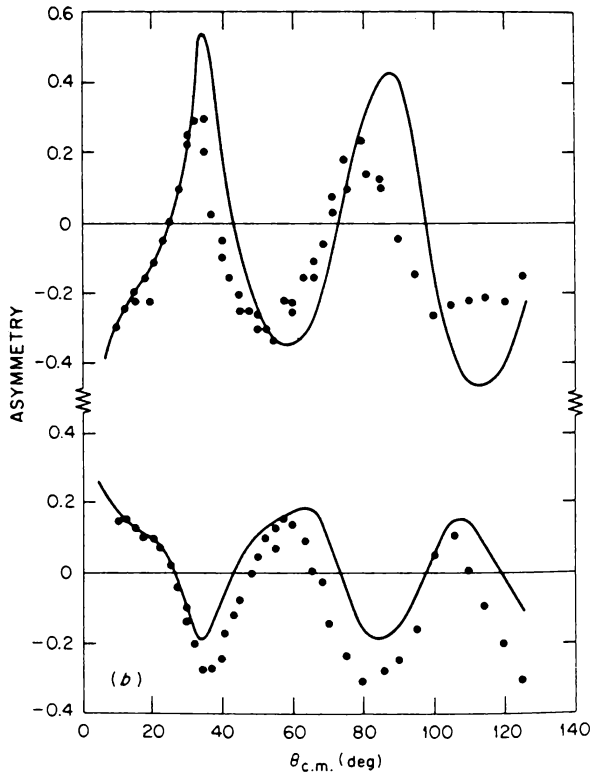


FIG. 1.2. Analyzing powers for $p_{1/2}$ (upper) and $p_{3/2}$ (lower) transfers in $^{52}\text{Cr}(\text{d}, \text{p})$ reactions at 10 MeV. The curves are from DWA calculations [Kocher and Haberli (72)]. [From Satchler (1983).]

of the single-particle orbits provides obviously important spectroscopic information. But one can go beyond this to obtain information on the structure of the nuclear wave function. The single-particle orbit for the neutron provides only one component of the total wave function, which will, for example, include as well excitations of the target nucleus plus the neutron in other orbits. From the magnitude of the (d, p) cross section one can in principle determine the strength of the single-particle state generated by the (d, p) reaction. More precisely, the single-particle component of the final-state wave function has the form

$$\frac{1}{\sqrt{A+1}} \mathcal{A}[\Psi_T(1, 2, \dots, A)\phi_{jm}(A+1)] \quad (1.4)$$

where \mathcal{A} is the antisymmetry operator, Ψ_T the target nucleus wave function, and ϕ_{jm} the single-particle wave function. The quantity $\mathcal{S}(j)$, referred to as the

spectroscopic factor, measures the strength of the single-particle component in the final-state wave function, so that

$$\mathcal{S}^{1/2}(j) = \frac{1}{\sqrt{A+1}} \langle \mathcal{A}[\Psi_T(1, 2, \dots, A)\phi_{jm}(A+1)] | \Psi_f(1, 2, \dots, A, A+1) \rangle \quad (1.5)$$

and

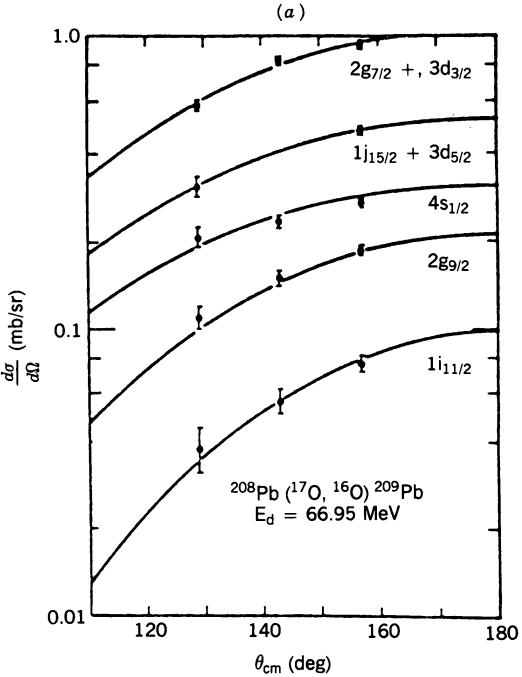
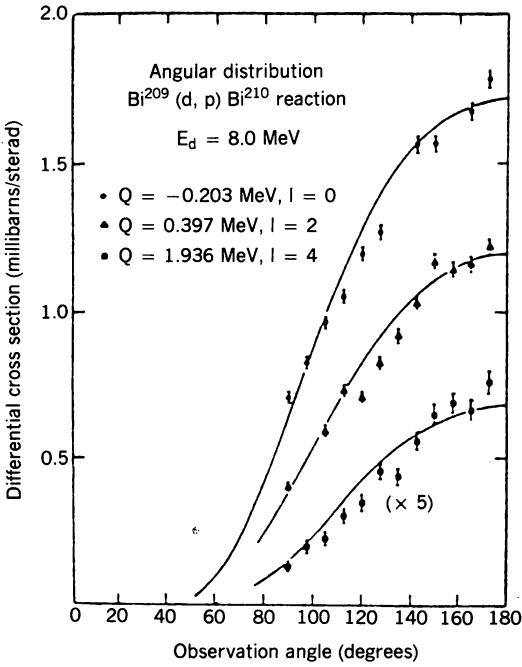
$$\Psi_f = \frac{\mathcal{S}^{1/2}}{\sqrt{A+1}} \mathcal{A}(\Psi_T \phi_{jm}) + \dots$$

$\mathcal{S}(j)$ is unity only in the limit of the noninteracting independent particle shell model for closed-shell target nuclei. This result holds not only for (d, p) reactions but also for (p, d) reaction. In the later, instead of adding a particle to the closed-shell target, one creates a “hole” in a filled shell. This is made completely clear in a formalism in which particle and hole formation are treated symmetrically, as described in (VII.9.11) in deShalit and Feshbach (74). However, in the interacting shell model any state of the $A+1$ system will consist of a linear combination of one-particle states and two-particle/one-hole states, three-particle/two-hole states, and so on. In that case \mathcal{S}_j will be less than 1; the deviation from one describing the probability that the system is not in a single-particle state given by (1.4).

Can the spectroscopic factor be determined experimentally? The answer is that any such determination is model dependent. To be sure, the cross section is proportional to \mathcal{S}_j . But the other factors depend on the models used for describing the initial and final wave functions as well as upon the interactions of the proton and neutron with the target nucleus as well as their mutual interaction. Only if these are well known can \mathcal{S}_j be determined from the magnitude of the cross section. Within a given framework, that is, a particular nuclear model and fixed interactions, the relative value of \mathcal{S}_j are meaningful, especially if a consistent picture of the reaction over a range of nuclei can be established.

Consistency must also be established with respect to other models of populating single-particle states. One obvious example is the (n, γ) reaction, in which the neutron after γ emission ends up in the same state produced in the (d, p) reaction. Another example is the isobar analog resonance. For example, through the resonant elastic scattering of protons on an (N, Z) nucleus, one obtains information on the analog states in the $(N+1, Z)$ nucleus [see deShalit

FIG. 1.3. Angular distributions for nucleon transfer at sub-Coulomb energies for different l transfers. The curves are the results of DWA calculations: (a) (d, p) at 8.0 MeV [Erskine, Buechner and Enge et al. (62)]; (b) $(^{17}\text{O}, ^{16}\text{O})$ reaction at 67 MeV [Franeý Lilley and Phillips et al. (79)]. [From Satchler (83).]



and Feshbach (74, p. 102)], which again can be compared with the (d, p) reaction on the target (N, Z) nucleus.

The striking correlation between the (d, p) angular distribution and nuclear structure is present only in a limited energy range. At very low energies, below the Coulomb barrier, the process is dominated by the Coulomb interaction and the angular distributions are rather featureless (Fig. 1.3). At high energies, the

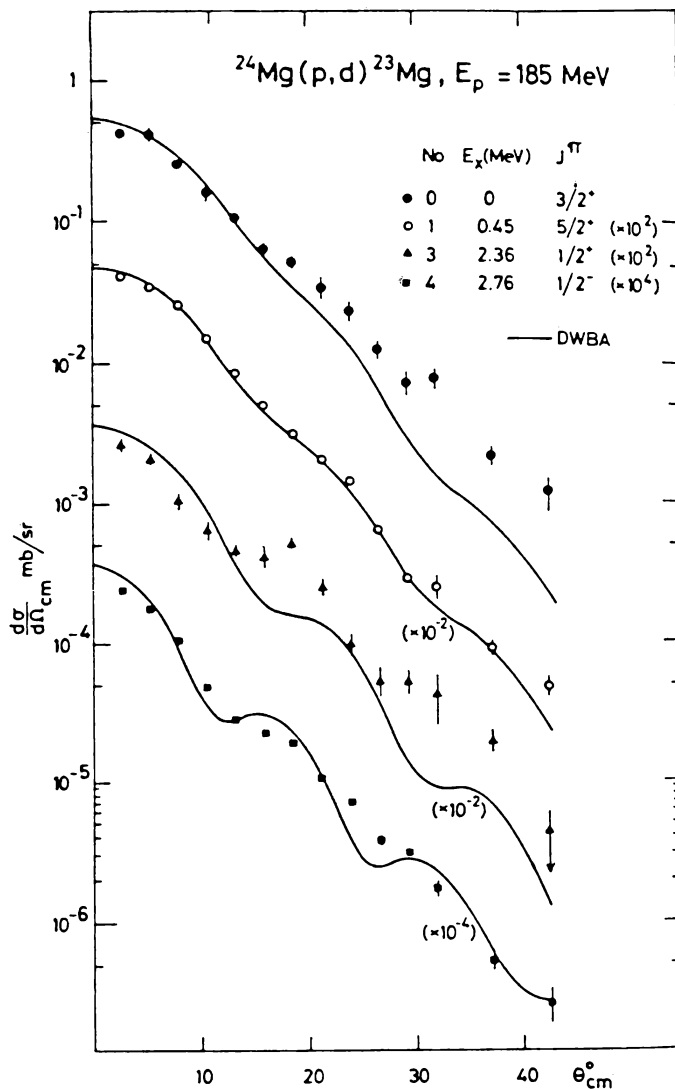


FIG. 1.4. Angular distributions for medium-energy (p, d) reactions. The curves are from DWA calculations [Kallne and Fagerstrom (79)]. [From Satchler (83).]

deuteron penetrates into the nuclear interior, and again the angular distribution does not as directly provide nuclear structure information (Fig. 1.4). It is the intermediate energy region throughout which the deuteron can penetrate to the nuclear surface, but not much beyond, that (d, p) experiments manifest their specificity most clearly. The reaction in this energy domain is peripheral and it is this condition that underlies the interpretation of the resulting structured angular distribution.

2. THE DWA AMPLITUDE

For the most part, the analysis of the (d, p) and (p, d) reactions has been based on the distorted wave approximation (DWA). Its derivation is, however, not as straightforward as the DWA for inelastic scattering given in Chapter V. In that case the DWA amplitude is an approximation to the solution of a pair of coupled equations obtained by projecting out the incident and inelastic channels. The effect of the remaining channels was included through an energy averaging that introduced imaginary components into both the diagonal and coupling potentials. An important element in this procedure is the orthogonality of the ground state and the excited state of the target nucleus. To be sure, when the incident particle is a nucleon or composed of nucleons, this advantage is diluted by the nonorthogonality introduced by the Pauli principle, but we have learned how to take account of that feature by the method developed in Section III.5.

Extension to the case of particle transfer is possible, but there is a characteristic problem that must first be resolved. To be concrete, let us consider the $^{16}\text{O}(d, p)^{17}\text{O}$ stripping reaction. In that case one must consider at least the two partitions [Satchler (83)] $d + ^{16}\text{O}$ and $p + ^{17}\text{O}$ of the 18-particle system. The natural spatial coordinates of the first partition include the relative distance between the neutron and proton of the deuteron and the distance between the center of mass of the deuteron and the center of mass of the ^{16}O nucleus, and finally, the (3×15) independent internal coordinates of the nucleons making up the ^{16}O nucleus. The total number of coordinates should be (3×17) . However, these coordinates are not convenient for the description of the final system, which involves the distance between the proton and the center of mass of the ^{17}O nucleus and the (3×16) independent internal coordinates for the ^{17}O nucleus. It is possible to introduce a complete set of the $d + ^{16}\text{O}$ wave functions that would need to include the continuum states of the deuteron, in which the neutron and proton are no longer bound in order to include a description of the final state, $p + ^{17}\text{O}$.

Diagrammatically (Fig. 2.1), the deuteron breaks up at vertex 1, the proton moving ahead while the released neutron is captured by the ^{16}O nucleus to form ^{17}O . Diagrams of this sort and their corresponding analytic transition amplitudes are very helpful for forming an intuitional understanding and have provided the base for theories developed by Shapiro (67) and Schnitzer (64).

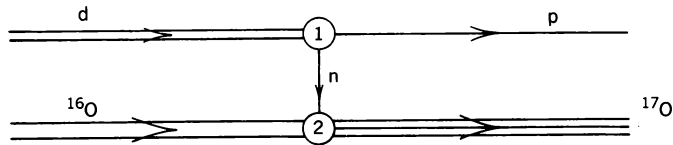


FIG. 2.1. Stripping reaction.

However, they have not for the most part been adopted as the preferred method for analyzing particle transfer reactions.

The method, which is most commonly used and which by suitable manipulations leads to the DWA, employs a mixed representation. In the initial channel, this might include the deuteron and ^{16}O in their ground state plus excited states of ^{16}O . In the final channel one would include the proton plus various states of ^{17}O according to the reaction involved. The total wave function would then contain contributions from both of these sets of wave functions. The remainder will be energy averaged with the consequent introduction of complex potentials. Such a wave function would permit the calculation of not only the one-step process but also for the multistep process, of which the two-step is illustrated in Fig. 2.2. The wave function corresponding to that figure would include the ^{16}O and ^{17}O ground and first excited states.

A traditional approach to the *single-step process* [say, (d, p)] has been to truncate the wave function Ψ of the system as follows:

$$\Psi = \mathcal{A}[u\phi + v\chi\psi] + \dots \quad (2.1)$$

where ϕ is the residual nucleus wave function (^{17}O), χ the internal deuteron wave function, and ψ the initial nucleus wave function. The functions u (proton) and v (deuteron) to be determined depend on the distance between the proton and center of mass of ^{17}O , the residual nucleus, and between the center of mass of the deuteron and ^{16}O , the initial nucleus, respectively. \mathcal{A} is the antisymmetrization operator. The indicated truncation does have a serious drawback. The omitted terms in the series would contain components such as excited

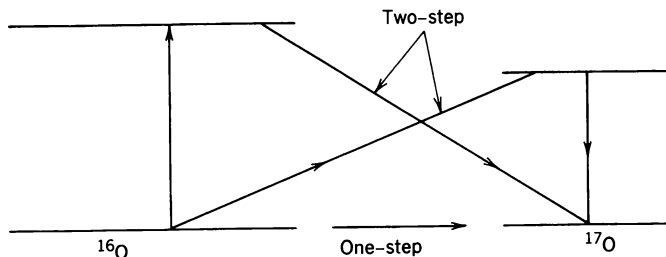


FIG. 2.2. One- and two-step contributions to a pickup reaction.

states of ^{17}O , which together with the proton wave function would have a substantial overlap with the deuteron channel wave function $\chi\psi$. It therefore should be included in (2.1) in order to obtain the total asymptotic reaction amplitude. Similarly, excited continuum states of the deuteron combined with the ^{16}O wave function (ground and excited states) would combine to form $^{17}\text{O} + p$ states. These difficulties are very similar to that of exchange scattering discussed in Section III.5 and are resolved in exactly the same way. We write

$$\Psi = P\Psi + Q\Psi \quad (2.2)$$

where as usual P and Q are projection operators and $Q = 1 - P$. $P\Psi$ is

$$P\Psi = \mathcal{A}[u\phi + v\chi\psi] \quad (2.3)$$

Because

$$\langle P\Psi | Q\Psi \rangle = 0 \quad (2.4)$$

and the related constraints

$$\langle \phi | Q\Psi \rangle = 0 \quad (2.5)$$

$$\langle \chi\psi | Q\Psi \rangle = 0 \quad (2.6)$$

$Q\Psi$ will not contain any components that can contribute to $u\phi$ or $v\chi\psi$. The function $P\Psi$ contains all the information required for the determination of the reaction amplitude. Conditions (2.5) and (2.6) also solve the problems raised by the identity of the particles involved. The reasoning is identical with that given in Section III.5 and need not be repeated.

Before proceeding to a consideration of (2.5) and (2.6), it is useful to point to another problem associated with ansatz [see (2.1)]. This can be seen if one substitutes $u\phi + v\chi\psi$ for Ψ in the Schrödinger equation

$$H\Psi = E\Psi \quad (2.7)$$

We drop the antisymmetrization operator, \mathcal{A} , to simplify the argument. Including \mathcal{A} will not change the substance of the discussion. Multiplying (2.7) from the left by ϕ and integrating over all the coordinates contained in ϕ yields an equation for u coupled to v . A second equation is obtained by multiplying by $\chi\phi$ and integrating. These equations are

$$\langle \phi | Hu\phi \rangle - Eu = E\langle \phi | v\chi\psi \rangle - \langle \phi | Hv\chi\psi \rangle \quad (2.8a)$$

$$\langle \chi\psi | Hv\chi\psi \rangle - Ev = E\langle \chi\psi | u\phi \rangle - \langle \chi\psi | Uu\phi \rangle \quad (2.8b)$$

We observe the presence of a coupling term on the right-hand side of each of these equations, proportional to the energy. These are present because ϕ is not

orthogonal to $\chi\psi$. The range of this coupling term is given roughly by the radius of the deuteron, which is relatively large. Some study of this situation has been made. [See Satchler (83), Section 3.32, for further discussion; see also Ohmura, Imanishi, Schimura, and Kawai (70); Imanishi et al (74); Cotanch (75); and Cotanch and Vincent (76).] Satchler summarizes by noting that in the cases discussed by these authors “the effects [of these terms] appears to be small, not always negligible on the absolute sense, but with the uncertainties that one might subjectively associate with the models being used.” In the standard DWA applications, these overlap terms are generally ignored. As we shall show, terms of this type (proportional to the energy E) need not appear in the coupled equations for u and v when the representation (2.2)–(2.6) is used.

These equations are exact. However, the choice for $P\Psi$, and the eventual replacement of $Q\Psi$ by an energy average introducing thereby an optical potential into the equation for $P\Psi$, involve some implicit assumptions. The possibilities not explicitly included in (2.3), such as multistep processes as well as the polarization of the deuteron under the combined influence of electrostatic and nuclear fields, are assumed either to be of little importance or to have effects that vary slowly with the experimental parameters. Under the latter set of circumstances it may be expected that a correspondingly slow variation in the optical model parameters determined empirically will suffice to take these effects into account.

We turn now to (2.2)–(2.6). A complete analysis of these equations has been given by Döhnert (68, 71) [see also Mittelman (64), and Horiuchi (77)]. Formally, the results are quite simple. However, Döhnert’s calculations are quite complicated, although with the computational aids developed since that paper appeared they should be much less formidable. In the present context, Döhnert’s results are important since they demonstrate the existence of the projection operator P and therefore of coupled equations for u and v from which the DWA can be extracted. Note that the results to be obtained below apply, after suitable but trivial generalizations, to the collision of a heavy ion with a nucleus.

Equations (2.5) and (2.6) reduce to two equations for u and v in terms of U and V defined by

$$U \equiv \langle \phi | \Psi \rangle \quad V \equiv \langle \chi\psi | \Psi \rangle \quad (2.9)$$

where the integrations are carried out only over the variables in ϕ and $\chi\psi$, respectively. Consider first (2.5):

$$0 = \langle \phi | Q\Psi \rangle = \langle \phi | \Psi \rangle - \langle \phi | P\Psi \rangle \quad (2.10)$$

We immediately obtain

$$U = \langle \phi | P\Psi \rangle \quad (2.11)$$

and similarly,

$$V = \langle \chi\psi | P\Psi \rangle \quad (2.12)$$

Substituting (2.3) in (2.10), one obtains

$$U = \langle \phi | \mathcal{A}(u\phi) \rangle + \langle \phi | \mathcal{A}(v\chi\psi) \rangle$$

Defining the operators K_{uu} and K_{uv} by

$$(1 - K_{uu})u \equiv \langle \phi | \mathcal{A}(u\phi) \rangle \quad K_{uv}v \equiv -\langle \phi | \mathcal{A}(v\chi\psi) \rangle \quad (2.13)$$

the equation for U becomes

$$U = (1 - K_{uu})u - K_{uv}v \quad (2.14)$$

Note that operator K_{uu} [identical with K of (III.5.13)] is Hermitian. This can be seen formally since the operator

$$1 - K_{uu} \equiv \langle \phi | \mathcal{A} \phi \rangle = \langle \mathcal{A} \phi | \phi \rangle \quad (2.15)$$

A similar analysis of (2.6) yields

$$V = (1 - K_{vv})v - K_{vu}^\dagger u \quad (2.16)$$

where K_{vv} is Hermitian since

$$1 - K_{vv} = \langle \chi\psi | \mathcal{A} \chi\psi \rangle = \langle \mathcal{A} \chi\psi | \chi\psi \rangle$$

The operator K_{uu} and K_{uv} contain the effects of antisymmetry while the nondiagonal K_{uv} includes the antisymmetry and overlap effects. Defining

$$W \equiv \begin{pmatrix} U \\ V \end{pmatrix} \quad w \equiv \begin{pmatrix} u \\ v \end{pmatrix} \quad \hat{K} \equiv \begin{pmatrix} K_{uu} & K_{uv} \\ K_{vu}^\dagger & K_{vv} \end{pmatrix} \quad (2.17)$$

Equations (2.13) and (2.16) can be summarized as follows:

$$W = (1 - \hat{K})w \quad (2.18)$$

where \hat{K} is Hermitian. This equation is identical in form with (III.5.15) and its analysis is completely parallel to that following this equation.

Since \hat{K} is Hermitian its eigenvalues κ_α are real and its eigenfunctions w_α forms an orthonormal set. Moreover, $(1 - \hat{K})$ is positive definite. To prove this, note that

$$\langle w | (1 - \hat{K}) w \rangle = \langle u\phi + v\chi\psi | \mathcal{A}(u\phi + v\chi\psi) \rangle \quad (2.19)$$

Because of the antisymmetry of the ket, this can be written as

$$\langle \mathcal{A}(u\phi + v\chi\psi) | \mathcal{A}(u\phi + v\chi\psi) \rangle \geq 0 \quad (2.20)$$

We can additionally conclude that the eigenvalues of \hat{K} , κ_α , are less than 1:

$$\kappa_\alpha \leq 1 \quad (2.21)$$

Since the operators in \hat{K} involve only square-integrable functions [see (2.13) and (2.15)], \hat{K} is bounded. The trace of \hat{K} , $\text{tr } \hat{K}$, involves the trace of K_{uu} and K_{vv} only. These traces have been shown to be bounded in the discussion dealing with elastic scattering, so that $\text{tr } \hat{K}$ is bounded. We can therefore conclude that the eigenvalue spectrum of \hat{K} is discrete.

Special attention needs to be paid to $w_\alpha^{(1)} = \begin{pmatrix} u_\alpha^{(1)} \\ v_\alpha^{(1)} \end{pmatrix}$, eigenfunctions of \hat{K} whose eigenvalue κ_α is unity $\hat{K} w_\alpha^{(1)} = w_\alpha^{(1)}$. We shall show that

$$\mathcal{A}(u_\alpha^{(1)}\phi + v_\alpha^{(1)}\chi\psi) \equiv 0 \quad (2.22)$$

To prove this, note that

$$\langle \mathcal{A}(u\phi + v\chi\psi) | \mathcal{A}(u\phi + v\chi\psi) \rangle = \langle (1 - \hat{K})w | (1 - \hat{K})w \rangle$$

Inserting $w_\alpha^{(1)}$ for w in this last equation, we obtain

$$\langle \mathcal{A}(u_\alpha^{(1)}\phi + v_\alpha^{(1)}\chi\psi) | \mathcal{A}(u_\alpha^{(1)}\psi + v_\alpha^{(1)}\chi\psi) \rangle = \langle (1 - \hat{K})w_\alpha^{(1)} | (1 - \hat{K})w_\alpha^{(1)} \rangle = 0$$

Equation (2.22) follows from this result. These solutions, $w_\alpha^{(1)}$, are referred to as *superfluous solutions* [see (III.5.19)]. These solutions do not contribute to $P\Psi$, as follows from (2.22).

These results are for the most part similar to the results obtained for elastic and inelastic scattering with one notable difference. In elastic and inelastic scattering the appearance of K and the associated superfluous solutions are formally a consequence of the nonorthogonality introduced by antisymmetrization. In the particle transfer case, \hat{K} and the associated superfluous solutions arise not only because of antisymmetrization but also because of the overlap between the cluster wave functions ϕ and $\chi\psi$.

We are now able to invert (2.18):

$$w = \frac{1}{1 - \hat{K}'} W \quad (2.23)$$

where the prime superscript on \hat{K}' indicates that in the spectral expansion of \hat{K}' ,

$$\hat{K}' = \sum_{\kappa_\alpha \neq 1} \kappa_\alpha w_\alpha \rangle \langle w_\alpha \quad (2.24)$$

all eigenfunctions of \hat{K} with unit eigenvalue are to be omitted. Hence

$$w = \sum_{\kappa_\alpha \neq 1} \frac{1}{1 - \kappa_\alpha} w_\alpha \rangle \langle w_\alpha | W \rangle = W + \sum_{\kappa_\alpha \neq 1} \frac{\kappa_\alpha}{1 - \kappa_\alpha} w_\alpha \rangle \langle w_\alpha | W \rangle$$

An explicit expression for the projection operator P of (2.3) can be obtained. Define matrices $\Phi\rangle$ and $\langle\Phi$ as follows:

$$\Phi\rangle \equiv \begin{pmatrix} \phi \\ \chi\psi \end{pmatrix} \quad \langle\Phi \equiv (\phi, \chi\psi) \quad (2.25)$$

Equation (2.3) can then be written

$$P\Psi = \mathcal{A}(\Phi, w) = \mathcal{A}(\phi, \chi\psi) \begin{pmatrix} u \\ v \end{pmatrix} = \mathcal{A}(u\phi + v\chi\psi)$$

Inserting (2.23) and noting that the matrix W is

$$W = \begin{pmatrix} \langle\phi|\Psi\rangle \\ \langle\chi\psi|\Psi\rangle \end{pmatrix} = \langle\Phi|\Psi\rangle \quad (2.26)$$

we have

$$P = \mathcal{A}\Phi\rangle \frac{1}{1 - \hat{K}'} \langle\Phi \quad (2.27)$$

Employing the spectral series for $1/(1 - \hat{K}')$ with

$$w_\alpha = \begin{pmatrix} u_\alpha \\ v_\alpha \end{pmatrix}$$

one obtains

$$P = \sum_{\kappa_\alpha \neq 1} \mathcal{A} \left[u_\alpha \phi + v_\alpha \chi\psi \right] \frac{1}{1 - \kappa_\alpha} \langle u_\alpha \phi + v_\alpha \chi\psi \rceil$$

Once P is known it becomes possible to obtain the Schrödinger equation for $P\Psi$ and the coupled system for u and v . The constraints on u and v are now carried by the operator $(1/1 - \hat{K}')$. The equation for $P\Psi$, (III.2.7), is

$$\left(E - H_{PP} - H_{PQ} \frac{1}{E - H_{QQ}} H_{QP} \right) P\Psi = 0 \quad (\text{III.2.7})$$

Upon energy averaging, the last two terms can be combined into a complex (i.e., non-Hermitian) optical model Hamiltonian, $PH_{\text{eff}}P$:

$$(E - PH_{\text{eff}}P)P\Psi = 0 \quad (2.28)$$

Multiplying from the left by Φ and integrating, one obtains

$$EW = \langle \Phi | PH_{\text{eff}} P \Psi \rangle = \langle \Phi | H_{\text{eff}} P \Psi \rangle \quad (2.29)$$

and from (2.27),

$$\begin{aligned} EW &= \left\langle \Phi | H_{\text{eff}} \mathcal{A} \Phi \frac{1}{1 - \hat{K}'} W \right\rangle \\ &= \langle \Phi | H_{\text{eff}} \mathcal{A} \Phi W \rangle = \langle \Phi | H_{\text{eff}} \mathcal{A} (u\phi + v\chi\psi) \rangle \end{aligned} \quad (2.30)$$

an equation determining W [see (2.17) and (2.26)]. Note that the operator $\langle \Phi | \mathcal{A} \Phi (1/1 - \hat{K}') \rangle$ is just the unit operator since $\langle \Phi | \mathcal{A} \Phi \rangle$ equals $(1 - \hat{K})$. Therefore, (2.29) can also be written

$$\left\langle \Phi | (E - H_{\text{eff}}) \mathcal{A} \Phi \frac{1}{1 - \hat{K}'} W \right\rangle = 0 \quad (2.31)$$

This is a pair of coupled equations for U and V :

$$\begin{aligned} EU &- \left\langle \phi | H_{\text{eff}} \mathcal{A} \left\{ \phi \left[\frac{1}{1 - \hat{K}'} \right]_{uu} + \chi\psi \left[\frac{1}{1 - \hat{K}'} \right]_{vu} \right\} U \right\rangle \\ &= - \left\langle \phi | (E - H_{\text{eff}}) \mathcal{A} \left\{ \phi \left[\frac{1}{1 - \hat{K}'} \right]_{uv} + \chi\psi \left[\frac{1}{1 - \hat{K}'} \right]_{vv} \right\} V \right\rangle \end{aligned} \quad (2.32a)$$

$$\begin{aligned} EV &- \left\langle \chi\psi | H_{\text{eff}} \mathcal{A} \left\{ \phi \left[\frac{1}{1 - \hat{K}'} \right]_{uv} + \chi\psi \left[\frac{1}{1 - \hat{K}'} \right]_{vv} \right\} V \right\rangle \\ &= - \left\langle \chi\psi | (E - H_{\text{eff}}) \mathcal{A} \left\{ \phi \left[\frac{1}{1 - \hat{K}'} \right]_{uu} + \chi\psi \left[\frac{1}{1 - \hat{K}'} \right]_{vu} \right\} U \right\rangle \end{aligned} \quad (2.32b)$$

One can immediately obtain the transition amplitude for the (d, p) reaction from (2.32a):

$$\mathcal{T}_{dp} = - \left\langle U_{0,f}^{(-)} \phi | (E - H_{\text{eff}}) \mathcal{A} \left\{ \left(\phi \left[\frac{1}{1 - \hat{K}'} \right]_{uv} + \chi\psi \left[\frac{1}{1 - \hat{K}'} \right]_{vv} \right) V_i^{(+)} \right\} \right\rangle \quad (2.33)$$

where $U_{0,f}$ satisfies the homogeneous equation (2.32a):

$$EU_0 = \left\langle \phi | H_{\text{eff}} \mathcal{A} \left\{ \phi \left[\frac{1}{1 - \hat{K}'} \right]_{uu} + \chi\psi \left[\frac{1}{1 - \hat{K}'} \right]_{vu} \right\} U_0 \right\rangle \quad (2.34)$$

The quantity $U_{0,f}\phi$ describes the elastic channel proton-residual nucleus wave function, taking into account the orthogonality to the deuteron-target nucleus channel but omitting the coupling to that channel, that is, to V . It therefore satisfies a Schrödinger equation involving just the Hamiltonian, H_f , describing the effective interaction in the elastic final-state channel:

$$H_f(U_{0,f}\phi) = E(U_{0,f}\phi) \quad (2.35)$$

The residual interaction giving the coupling to the deuteron channel is

$$\mathcal{V}^{(f)} \equiv H_{\text{eff}} - H_f \quad (2.36)$$

Therefore,

$$\mathcal{T}_{dp} = \left\langle U_{0,f}^{(-)}\phi \left| \mathcal{V}^{(f)} \mathcal{A} \left\{ \phi \left[\frac{1}{1 - \hat{K}'} \right]_{uv} + \chi \psi \left[\frac{1}{1 - \hat{K}'} \right]_{vv} \right\} V_i^{(+)} \right\rangle \quad (2.37)$$

With this equation we obtain a complete formal solution of the particle transfer problem, including the effects of nonorthogonality and antisymmetry. Its derivation is sufficiently general so that it can be applied to any transfer reaction (e.g., those induced by heavy ions) for which (2.3) is appropriate and can readily be generalized to other cases, since the structure given by (2.18) of the relation between W and w and the Schrödinger equation for $P\Psi$, (III.5.26) remains unchanged.

Problem. Define

$$\bar{W} \equiv \frac{1}{\sqrt{1 - \hat{K}'}} W \quad (2.38)$$

Show that

$$E\bar{W} = \left\langle \Phi \left| \frac{1}{\sqrt{1 - \hat{K}'}} H_{\text{eff}} \mathcal{A} \Phi \frac{1}{\sqrt{1 - \hat{K}'}} \bar{W} \right\rangle \quad (2.39)$$

In this equation, the operator acting on W on the right-hand side is symmetric, implying time-reversal invariance.

A number of approximations are commonly applied to (2.37). Many authors neglect the nonorthogonality kernels K_{uv} and K_{uv}^+ [Eq. (2.13)]. \hat{K} is then diagonal, with the consequence that only the effects of antisymmetry in the initial and final channels are taken into account. For example, (2.34) for U_0 becomes

$$EU_0 \simeq \left\langle \phi \left| H_{\text{eff}} \left(\frac{1}{1 - K'_{uu}} \right) U_0 \right\rangle \quad (2.40)$$

which is just the equation satisfied by the wave function for proton scattering by the residual nucleus. Since H_{eff} is determined empirically, some of the coupling and orthogonality effects are included. Similarly, (2.32) for U simplifies to

$$EU - \left\langle \phi | H_{\text{eff}} \mathcal{A} \left\{ \phi \frac{1}{1 - K'_{uu}} U \right\} \right\rangle = - \left\langle \phi | (E - H_{\text{eff}}) \mathcal{A} \left\{ \chi \psi \frac{1}{1 - K'_{vv}} V \right\} \right\rangle$$

or

$$EU - \langle \phi | H_{\text{eff}} \mathcal{A}(\phi u) \rangle = - \langle \phi | (E - H_{\text{eff}}) \mathcal{A}(v \chi \psi) \rangle \quad (2.41)$$

The equation for V becomes

$$EV - \left\langle \chi \psi | H_{\text{eff}} \mathcal{A} \left\{ \chi \psi \frac{1}{1 - K'_{vv}} V \right\} \right\rangle = - \left\langle \chi \psi | (E - H_{\text{eff}}) \mathcal{A} \left\{ \phi \frac{1}{1 - K'_{uu}} U \right\} \right\rangle$$

or

$$EV - \langle \chi \psi | H_{\text{eff}} \mathcal{A}(v \chi \psi) \rangle = - \langle \chi \psi | (E - H_{\text{eff}}) \mathcal{A}(u \phi) \rangle \quad (2.42)$$

The transition matrix equation (2.37) reduces to

$$\mathcal{T}_{dp} \simeq \left\langle U_{0,f}^{(-)} \phi | \mathcal{V}^{(f)} \mathcal{A} \left\{ \chi \psi \left(\frac{1}{1 - \hat{K}'} \right) V_i^{(+)} \right\} \right\rangle \quad (2.43)$$

$$= \langle U_{0,f}^{(-)} \phi | \mathcal{V}^{(f)} \mathcal{A}(v_i^{(+)} \chi \psi) \rangle \quad (2.44)$$

where U_0 now satisfies (2.40). Finally, the approximation in which $V_i^{(+)}$ in (2.43) is replaced by the "unperturbed" $V_{0,i}^{(+)}$, which satisfies

$$EV_0 - \left\langle \chi \psi | H_{\text{eff}} \mathcal{A} \left\{ \chi \psi \frac{1}{1 - K'_{vv}} V_0 \right\} \right\rangle = 0 \quad (2.45)$$

is made. One obtains

$$\mathcal{T}_{dp}^{(\text{DWA})} = \left\langle U_{0,f}^{(-)} \phi | \mathcal{V}^{(f)} \mathcal{A} \left\{ \left(\frac{1}{1 - K'_{vv}} \right)_v V_{0,i}^{(+)} \right\} \right\rangle \quad (2.46)$$

or the more familiar form

$$\mathcal{T}_{dp}^{(\text{DWA})} = \langle U_{0,f}^{(-)} \phi | \mathcal{V}^{(f)} \mathcal{A}(v_{0,i}^{(+)} \chi \psi) \rangle \quad (2.46)$$

As has been pointed out earlier, much of the error of the last approximation may be reduced because of the use of an empirical interaction for $\mathcal{V}^{(f)}$. In

principle, one could eliminate V from (2.41) by first solving (2.42) for V in terms of W and substituting in (2.41). The effects of antisymmetrization as required in (2.46) or (2.43) can be carried out by direct evaluation of the eigenfunctions and eigenvalues of the operator \tilde{K}_{vv} . These can be used to provide a representation of $1/(1 - K'_{vv})$. Another procedure requires finding only the eigenfunction of the operator K_{vv} , $V^{(1)}_\alpha$, with eigenvalue of unity and then insisting that $v_{0,i}$ be orthogonal to all the $v^{(1)}_\alpha$ [Saito (68, 69)]. For a review of recently developed procedures, see Arima (78) and Horiuchi (77). A recent example is in the paper by Kato, Okabe, and Abe (85). Of course, there may be circumstances in which the non-orthogonality operator K_{uv} cannot be neglected (much here depends on the choice for ϕ and $\chi\psi$). In that event one must return to the exact \mathcal{T}_{dp} of (2.37). The DWA result would then be obtained by replacing $V^{(+)}_i$ by $V^{(+)}_{0,i}$ in that equation.

In principle, the application of (2.46) is straightforward. One must first obtain the elastic channel wave functions for the deuteron–target nucleus and the proton–residual nucleus systems with appropriate attention to the requirements of antisymmetry. These wave functions are solutions of a Schrödinger-type equation [see (2.45) and (2.40)]. Since we are considering a prompt process, H_{eff} is taken to be an optical model complex Hamiltonian, while H_f is the diagonal part of H_{eff} in the (p -nucleus) channels, and $\mathcal{V}^{(f)}$ is the nondiagonal part. Note that one must be careful to maintain the permutation symmetry of the underlying Hamiltonian in choosing $\mathcal{V}^{(f)}$. A simple procedure is to antisymmetrize $U^{(-)}_{0,f}$ before inserting $\mathcal{V}^{(f)}$ and multiply by $1/A + 1$, where $A + 1$ is the total number of nucleons.

In actual practice, the elastic channel wave function is obtained as a solution of the single-channel optical model Hamiltonian which has been adjusted so that the resulting elastic scattering cross sections agree with experiment. Usually, these wave functions do not satisfy the Pauli exclusion principle so that its effect must in some fashion and to some extent be contained in the empirical potential used. This is more explicit when the potential is a folded one, as antisymmetry gives rise to an exchange term. One is in serious danger of overcounting if one simply orthogonalizes the empirical wave functions with respect to $\chi\psi v^{(1)}_\alpha$ [Fleissbach and Mang (76); Fleissbach (78)]. One should obviously return to the original elastic scattering problem and readjust the optical potential so that orthogonality with respect to the superfluous solutions and agreement with the experimental data are obtained simultaneously.

Post-prior Representations. Equation (2.33) for \mathcal{T} can be condensed by staying with the Φ, W formalism [see (2.26)]. It becomes

$$\begin{aligned}\hat{\mathcal{T}}_{fi} &= \langle W^{(-)}_{0,f} \Phi | (E - H_{\text{eff}}) \mathcal{A} (\Phi W^{(+)}_i) \rangle \\ &= - \left\langle W^{(-)}_{0,f} \Phi | (E - H_{\text{eff}}) \mathcal{A} \left\{ \Phi \left(\frac{1}{1 - \hat{K}'} \right) W^{(+)}_i \right\} \right\rangle\end{aligned}\quad (2.47)$$

and the alternative expression

$$\begin{aligned}\hat{\mathcal{T}}_{fi} &= -\langle \mathcal{A}(\Phi W_f^{(-)}) | (E - H_{\text{eff}}) W_{0,i}^{(+)} \Phi \rangle \\ &= -\left\langle \mathcal{A} \left(\frac{1}{1 - \hat{K}'} W_f^{(-)} \right) \right| (E - H_{\text{eff}}) W_{0,i}^{(+)} \Phi \rangle\end{aligned}\quad (2.48)$$

The circumflex on $\hat{\mathcal{T}}$ is a reminder that $\hat{\mathcal{T}}$ is a matrix and that one must specify the initial and final states. For the stripping (d, p) reaction, $W_{0,f}^{(-)}\Phi$ in (2.47) is, according to (2.33), the proton–nucleus unperturbed final-state wave function $U_{0,f}^{(-)}\phi$. The function $W_i^{(+)}\Phi$ is the exact initial channel deuteron nucleus wave function $\chi\psi v_i^{(+)}$. With these substitutes, (2.47) and (2.33) become identical. One can then obtain (2.37) for \mathcal{T}_{dp} . This result is referred to as the *postrepresentation* of the transition amplitude, since it involves the residual interaction in the final channel, $\mathcal{V}^{(f)}$.

In using (2.48) to obtain an expression for the stripping transition amplitude, the unperturbed initial state is given by $\chi\psi V_{0,i}^{(+)}$; the final-state component of interest is $\phi u_f^{(-)}$. Thus one obtains

$$\mathcal{T}_{dp} = -\left\langle \mathcal{A} \left\{ \left(\phi \left(\frac{1}{1 - \hat{K}'} \right)_{uu} + \chi\psi \left(\frac{1}{1 - \hat{K}'} \right)_{vu} \right) U_f^{(-)} \right\} \right| (E - H_{\text{eff}}) \chi\psi V_{0,i}^{(+)} \right\rangle\quad (2.49)$$

We now introduce the Hamiltonian H_i for the initial channel

$$H_i(\chi\psi V_{0,i}^{(+)}) = E(\chi\psi V_{0,i}^{(+)})\quad (2.50)$$

and the residual potential in the initial channel, $\mathcal{V}^{(i)}$:

$$\mathcal{V}^{(i)} \equiv H_{\text{eff}} - H_i\quad (2.51)$$

Equation (2.49) then becomes

$$\mathcal{T}_{dp} = \left\langle \mathcal{A} \left\{ \left(\phi \left(\frac{1}{1 - \hat{K}'} \right)_{uu} + \chi\psi \left(\frac{1}{1 - \hat{K}'} \right)_{vu} \right) U_f^{(-)} \right\} \right| \mathcal{V}^{(i)}(\chi\psi V_{0,i}^{(+)}) \right\rangle\quad (2.52)$$

which should be compared with (2.37). This is known as the *priori* representation, since it involves the residual interaction in the initial channel. The analog of the (2.46') becomes, upon neglecting K_{uv} ,

$$\mathcal{T}_{dp}^{(\text{DWA})} = \langle \mathcal{A} u_{0,f}^{(-)} \phi | \mathcal{V}^{(i)} v_{0,i}^{(+)} \chi\psi \rangle\quad (2.53)$$

The two expressions (2.52) and (2.33) are equal numerically if no further approximations are made. Which one is used is a matter of convenience, as approximations in their evaluation may be made with greater validity when

one rather than the other is used, as we shall see. We emphasize once more that the use of the operator \hat{K}' is essential if antisymmetry, overlap, and continuum effects are to be properly included.

3. APPLICATIONS

This section is concerned with the implementation of the discussion of the preceding section to the process of stripping. The starting point is the post-transition (or the corresponding prior transition) matrix element given by (2.37) and the DWA form (2.46), in which overlap and the perturbation of the deuteron-target nucleus wave function arising from the possibility of the transition to the proton-nucleus system are neglected. (The error resulting from this last approximation is reduced considerably by the use of a semiempirical potential between the deuteron and the target nucleus, which to some extent must include the effects of the two-step processes, in which, for example, the neutron is stripped from the deuteron by the target nucleus and then in the second step is picked up by the proton to reform the deuteron.) Elements entering into the calculation consist of the initial and final wave functions and the residual interactions $\mathcal{V}^{(f)}$ or $\mathcal{V}^{(i)}$.

According to (2.36),

$$\mathcal{V}^{(f)} = H_{\text{eff}} - H_f$$

The Hamiltonian H_{eff} is generally chosen to be of the form

$$H_{\text{eff}} = H_A + T_0 + T_1 + w_{0,A} + w_{1,A} + w(0,1) \quad (3.1)$$

where H_A is the Hamiltonian for the target nucleus, T_1 and T_0 the kinetic energy operators for the neutron and proton, $w_{0,A}$ is the interaction of the proton with the target nucleus, $w_{1,A}$ that of the neutron, and $w(0,1)$ the neutron-proton interaction. The final Hamiltonian is given by

$$H_f = H_A + T_1 + w_{1,A} + T_0 + w \quad (3.2a)$$

$$= H_{A+1} + T_0 + w \quad (3.2b)$$

Here w is a mean, generally complex potential representing the interaction between the proton and the residual $(A+1)$ nucleus. Taking the difference between (3.2) and (3.1) yields

$$\begin{aligned} \mathcal{V}^{(f)} &= w_{0,A} + w(0,1) - w \\ &= \sum_{i=1}^{A+1} w(0,i) - w \end{aligned} \quad (3.3)$$

The mean potential w cannot induce any transitions, so that its (d, p) matrix element vanishes. Hence, from (2.46'),

$$\mathcal{T}_{dp}^{(\text{DWA})} = \left\langle U_{0,f}^{(-)} \phi \left| \sum_{i=1}^{A+1} w(0, i) \mathcal{A}(v_{0,i}^{(+)} \chi \psi) \right. \right\rangle \quad (3.4)$$

One now makes the *spectator* approximation. Qualitatively it is assumed that the proton does not participate in the reaction. More precisely, one assumes that the only terms in the sum over $w(0, i)$ that contribute significantly to \mathcal{T}_{dp} are those for which the nucleons denoted by i are neutrons. Moreover, since the wave function ϕ , as well as the indicated initial state, are antisymmetric in the neutron coordinates, one obtains

$$\mathcal{T}_{dp}^{(\text{DWA})} \simeq (N_A + 1) \langle U_{0,f}^{(-)} \phi | w(0, 1) \mathcal{A}(v_{0,i}^{(+)} \chi \psi) \rangle \quad (3.5)$$

where N_A is the number of neutrons in the target nucleus. Finally, if the exchange integrals in this equation are small, as is often the case, one obtains the simple result

$$\mathcal{T}_{dp}^{(\text{DWA})} \simeq (N_A + 1) \langle U_{0,f}^{(-)} \phi | w(0, 1) v_{0,i}^{(+)} \chi \psi \rangle \quad (3.6)$$

Forms (3.5) and (3.6) are most convenient because $w(0, 1)$ has a short range, so that domains in which the neutron-proton separation is large do not contribute to \mathcal{T}_{dp} . Exploiting this feature leads to a considerable simplification, as we shall now show.

We need to make explicit the spatial arguments of the functions occurring in (3.5). The function χ as well as $w(0, 1)$ depends on $\mathbf{r}_1 - \mathbf{r}_0$, where \mathbf{r}_0 is the proton coordinate and \mathbf{r}_1 the neutron. The function v depends on the separation of the deuteron center of mass from the center of mass, \mathbf{r}_A , of the target nucleus: that is,

$$\mathbf{r}_D \equiv \mathbf{r}_A - \frac{1}{2}(\mathbf{r}_1 + \mathbf{r}_0) = \mathbf{r}_A - \mathbf{r}_1 + \frac{\mathbf{r}_1 - \mathbf{r}_0}{2} \quad (3.7)$$

The function U depends on the separation of the proton from the center of mass of the target nucleus and the neutron:

$$\mathbf{r}_p = \frac{A\mathbf{r}_A + \mathbf{r}_1}{A+1} - \mathbf{r}_0 = \frac{A}{A+1}(\mathbf{r}_A - \mathbf{r}_1) + \mathbf{r}_1 - \mathbf{r}_0 \quad (3.8)$$

Equation (3.6) becomes

$$\begin{aligned} \mathcal{T}_{dp}^{(\text{DWA})} = & \int d\mathbf{r}_p \int d\mathbf{r}_D \int d\mathbf{r}_2 \cdots U_{0,f}^{(-)*}(\mathbf{r}_p) \phi_f^*(\mathbf{r}_1 - \mathbf{r}_A, \mathbf{r}_2 - \mathbf{r}_A, \dots) \\ & \times w(\mathbf{r}_1 - \mathbf{r}_0) v_{0,i}^{(+)}(\mathbf{r}_D) \chi(\mathbf{r}_1 - \mathbf{r}_0) \psi_i(\mathbf{r}_2 - \mathbf{r}_A, \mathbf{r}_3 - \mathbf{r}_A, \dots) \end{aligned}$$

Performing the integration over $\mathbf{r}_2, \mathbf{r}_3, \dots$ yields

$$\langle \phi_f(\mathbf{r}_1 - \mathbf{r}_A, \mathbf{r}_2 - \mathbf{r}_A, \dots) | \psi_i(\mathbf{r}_2 - \mathbf{r}_A, \mathbf{r}_3 - \mathbf{r}_A, \dots) \rangle = f_{fi}^*(\mathbf{r}_1 - \mathbf{r}_A) \quad (3.9)$$

so that

$$\mathcal{T}_{dp}^{(\text{DWA})} = (N_A + 1) \int d\mathbf{r}_p \int d\mathbf{r}_D U_{0,f}^{(-)*}(\mathbf{r}_p) f_{fi}^*(\mathbf{r}_1 - \mathbf{r}_A) w(\mathbf{r}_1 - \mathbf{r}_0) \chi(\mathbf{r}_1 - \mathbf{r}_0) v_{0,i}^{(+)}(\mathbf{r}_D) \quad (3.10)$$

We now evaluate $w\chi$ in the limit of zero range of the neutron-proton potential. Neglecting the tensor force between neutron and proton, the Schrödinger equation satisfied by χ is

$$\nabla^2 \chi + \left(-\gamma^2 - \frac{m}{\hbar^2} w \right) \chi = 0 \quad (3.11)$$

where the dependent variable is $\mathbf{r}_1 - \mathbf{r}_0$. The eigenvalue γ^2 is related to the binding energy B of the deuteron by

$$\gamma^2 = \frac{\hbar^2}{m} B$$

Solving (3.11) for $w\chi$ yields

$$w\chi = \frac{\hbar^2}{m} (\nabla^2 - \gamma^2) \chi \quad (3.12)$$

For zero range w ,

$$\chi = N e^{-\gamma r} / r \equiv N \frac{u}{r} \quad (3.13)$$

where N is the normalization. N can be expressed in terms of the effective range ρ_t ,

$$\rho_t \equiv 2 \int_0^\infty (e^{-2\gamma r} - u^2) dr$$

It follows that

$$\int_0^\infty u^2 dr = \frac{1 - \gamma \rho_t}{2\gamma}$$

But

$$\int_0^\infty \chi^2 d\mathbf{r} = 1 = 4\pi N^2 \int_0^\infty u^2 dr = 4\pi N^2 \frac{1 - \gamma\rho_t}{2\gamma}$$

Solving for N yields

$$N = \frac{1}{\sqrt{4\pi}} \left(\frac{2\gamma}{1 - \gamma\rho_t} \right)^{1/2} \quad (3.14)$$

The current value of ρ_t is 1.767 fm.

Inserting (3.13) into (3.12) yields

$$w\chi = \sqrt{4\pi} \left(\frac{2\gamma}{1 - \gamma\rho_t} \right)^{1/2} \frac{\hbar^2}{m} \delta(\mathbf{r}) \quad (3.15)$$

We can now return to (3.10) and replace the integration variables \mathbf{r}_p and \mathbf{r}_0 by $\mathbf{r}_A - \mathbf{r}_1 \equiv \mathbf{R}$ and $\mathbf{r} \equiv \mathbf{r}_1 - \mathbf{r}_0$. Integrating over \mathbf{r} , one obtains, including the Jacobian of the transformation,

$$\begin{aligned} \mathcal{T}_{dp}^{(\text{DWA})} &= \sqrt{4\pi} \frac{\hbar^2}{m} \left(\frac{2\gamma}{1 - \gamma\rho_t} \right)^{1/2} \frac{A+2}{2(A+1)} (N_A + 1) \\ &\times \int d\mathbf{R} U_{0,f}^{(-)*} \left(\frac{A}{A+1} \mathbf{R} \right) f_{fi}^*(-\mathbf{R}) v_{0,i}^{(+)}(\mathbf{R}) \end{aligned} \quad (3.16)$$

The zero range approximation reduced the six-dimensional integral, (3.10), to a three-dimensional one. The latter is readily evaluated by expanding $U^{(-)}$ and $v^{(+)}$ in a partial wave series, so that (3.16) becomes, after making the relatively simple angular integration and evaluating spin matrix elements, a sum of one-dimensional integrals. The function $U_{0,f}^{(-)}$ is generally taken from the optical model analyses of the proton–nucleus interaction described in Chapter V. A similar optical model analysis has been made of the deuteron–nucleus interaction. However, it should be remembered that an understanding of the latter is based on a much smaller data pool than that available from the proton–nucleus interaction. A table of optical model parameters for the deuteron projectile is given in Section 4.

The overlap function $f_{fi}(\mathbf{R})$ is, in the independent-particle description of the nucleus, proportional to a single-particle wave function. As we discussed earlier, the residual interactions will add multiparticle components to the nuclear wavefunctions. However, these cannot contribute to f_{fi} and to $\mathcal{T}_{dp}^{(\text{DWA})}$. Thus the effect of the residual interaction is to reduce the strength of the single-particle component since the total nuclear wave function is normalized to unity. This

is taken into account by the introduction of the *spectroscopic factor* \mathcal{S} [see (1.5)]:

$$f_{fi}(\mathbf{R}) = \frac{\mathcal{S}^{1/2}(\alpha, j)\phi_j(\mathbf{R})}{\sqrt{N_A + 1}} \quad (3.17)$$

Putting the arguments of $\mathcal{S}^{1/2}$ equal only to the angular momentum j of the neutron single-particle orbital ϕ_j is an assumption, since in principle f_{fi} could depend on other properties of the initial and final nuclei. The function ϕ_j is assumed to be orthogonal to ψ . We remind the reader that in the limit of the independent-particle model, when the target is a closed-shell nucleus, \mathcal{S} , with the normalization above, is unity. This completes the description of the various factors entering into (3.16) for the transition matrix \mathcal{T}_{dp} .

Some qualitative conclusions that follow from (3.16) for the transition matrix $\mathcal{T}_{dp}^{(\text{DWA})}$ can now be drawn. Since both the $U^{(-)}$ and $v^{(+)}$ are wave functions describing the motion of particles in an absorptive potential, their magnitudes will be reduced in the nuclear interior. As a consequence, those partial waves of $U^{(-)}$ and $v^{(+)}$ that are large at the nuclear surface will make the most important contribution to the transition matrix. Roughly, this will occur for those partial waves l_i and l_f of $v^{(+)}$ and $U^{(-)}$, respectively, satisfying the conditions

$$k_p R \sim l_i \quad (3.18)$$

$$\frac{Ak_p}{A+1} R \sim l_f \quad (3.19)$$

Hence the orbital angular momentum L of the single-particle nuclear wave function ϕ of (3.17) which will be most strongly populated will satisfy the condition

$$\mathbf{L} = \mathbf{l}_i - \mathbf{l}_f \quad (3.20)$$

Under these circumstances (large absorption) the (d, p) reaction is a surface reaction,

These conclusions can easily be deduced from the overlap integral in (3.16) by making a partial wave series for $U^{(-)}$ and $u^{(+)}$. For this purpose it is not necessary to take spin into account, so that

$$v_{0,i}^{(+)} = \sum_{l_i} (2l_i + 1) i^{l_i} P_{l_i}(\hat{\mathbf{k}}_i \cdot \hat{\mathbf{r}}) e^{i\delta_{l_i}} \phi_{l_i}(r) = \sqrt{4\pi} \sum_{l_i} \sqrt{2l_i + 1} i^{l_i} Y_{l_i,0} e^{i\delta_{l_i}} \phi_{l_i}(r) \quad (3.21)$$

and

$$\begin{aligned} U_{0,f}^{(-)*} &= \sum_{l_f} (2l_f + 1) i^{-l_f} P_{l_f}(\hat{\mathbf{k}}_f \cdot \hat{\mathbf{r}}) e^{i\delta_{l_f}} \psi_{l_f}(r) \\ &= 4\pi \sum_{l_f, m_f} i^{-l_f} e^{i\delta_{l_f}} Y_{l_f, m_f}(\hat{\mathbf{k}}_i \cdot \hat{\mathbf{k}}_f) Y_{l_f, m_f}^*(\hat{\mathbf{k}}_i \cdot \hat{\mathbf{r}}) \psi_{l_f}(r) \end{aligned} \quad (3.22)$$

Finally, let

$$\phi_j(\mathbf{r}) = \chi_L(r) Y_{LM}(\hat{\mathbf{k}}_i \cdot \hat{\mathbf{r}})$$

The transition matrix becomes

$$\begin{aligned} \mathcal{T}_{dp}^{(\text{DWA})} &= (4\pi)^2 \frac{\hbar^2}{m} \left(\frac{2\gamma}{1 - \gamma\rho_t} \right)^{1/2} \mathcal{S}^{1/2}(\alpha, L) \sqrt{N_A + 1} \frac{A + 2}{2(A + 1)} \\ &\times \sum_{l_i, l_f} \sqrt{2l_i + 1} i^{l_i - l_f} e^{i(\delta_{l_i} + \delta_{l_f})} I(l_i, l_f, L) Y_{l_f, m_f}(\hat{\mathbf{k}}_i \cdot \hat{\mathbf{k}}_f) \\ &\times \int d\Omega Y_{l_i, 0} Y_{l_f, m_f}^* Y_{LM}^* \end{aligned}$$

where

$$I(l_i, l_f, L) = \int \psi_{L_f} \varphi_{l_i} \chi_L r^2 dr \quad (3.23)$$

The angular integral can be performed using (A.2.35) from the Appendix in deShalit and Feshbach (74):

$$\begin{aligned} \int d\Omega Y_{l_i, 0} Y_{l_f, m_f}^* Y_{LM}^* &= \left[\frac{(2l_i + 1)(2l_f + 1)(2L + 1)}{4\pi} \right]^{1/2} \\ &\times \begin{pmatrix} l_i & L & l_f \\ 0 & M & m_f \end{pmatrix} \begin{pmatrix} l_i & L & l_f \\ 0 & 0 & 0 \end{pmatrix} \end{aligned}$$

so that

$$\begin{aligned} \mathcal{T}_{dp}^{(\text{DWA})} &= (4\pi)^{3/2} \frac{\hbar^2}{m} \left(\frac{2\gamma}{1 - \gamma\rho_t} \right)^{1/2} \mathcal{S}^{1/2}(\alpha, L) \sqrt{N_A + 1} \frac{A + 2}{2(A + 1)} \\ &\times \sum_{l_i, l_f} \sqrt{2l_i + 1} i^{l_i - l_f} e^{i(\delta_{l_i} + \delta_{l_f})} I(l_i, l_f, L) Y_{l_f, m_f}(\hat{\mathbf{k}}_i \cdot \hat{\mathbf{k}}_f) \\ &\times [(2l_i + 1)(2l_f + 1)(2L + 1)]^{1/2} \begin{pmatrix} l_i & L & l_f \\ 0 & M & m_f \end{pmatrix} \begin{pmatrix} l_i & L & l_f \\ 0 & 0 & 0 \end{pmatrix} \quad (3.24) \end{aligned}$$

The 3- j coefficients yield not only the angular momentum conservation condition of (3.20) but parity conservation as well, since $l_i + L + l_f$ must be even. The magnitude of the factor $\exp[i(\delta_{l_i} + \delta_{l_f})]$, is, for absorption optical potentials, much less than unity for small l 's rising sharply to unity at the grazing values of l_i and l_f given approximately by (3.18) and (3.19). The integral I will tend to zero as l_i and l_f exceed these grazing values since the corresponding angular

momentum barriers become important beyond the nuclear radius. The integral I will be small for these values of l_i and l_f for which the absorption is large, that is, for l_i and l_f considerably smaller than the grazing values. As Austern (61) pointed out, this is a consequence of destructive interference between the optical model deuteron and proton wave functions. As the reader should verify, the radial wave functions for each of these waves inside the nuclear interior will for the most part be of the form $\exp(-iKr)/r$, where K is the internal

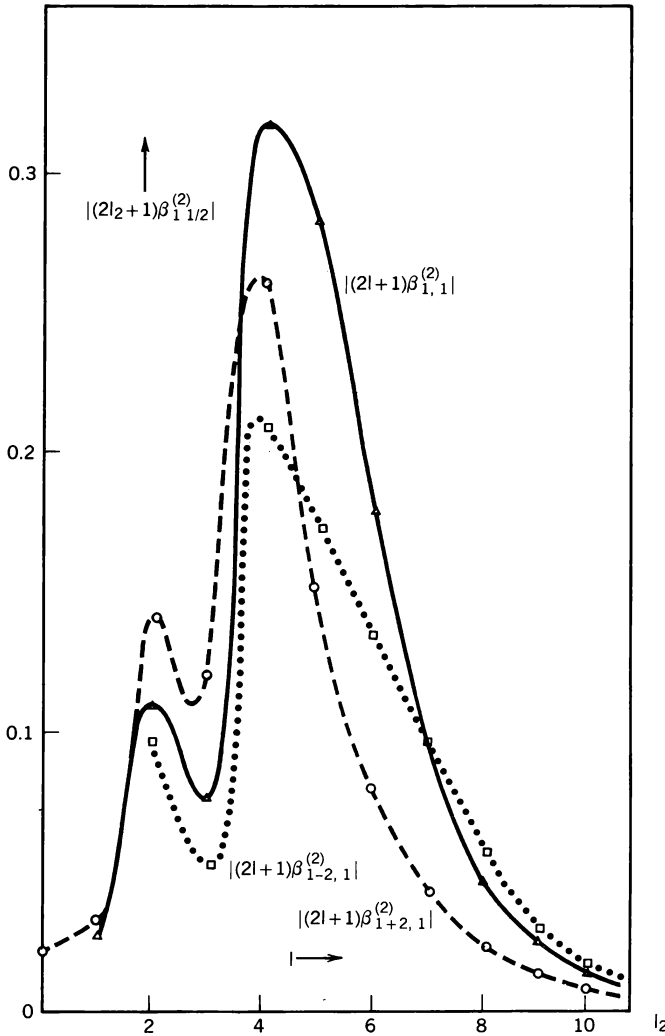


FIG. 3.1. The l window. The modulus of the stripping integrals contributing to an $\Delta l = 2$ transfer reaction $^{24}\text{Mg}(d,p)^{25}\text{Mg}$, ground state at $E_d = 10.1$ MeV plotted against $l_2 = l_f$. [From Hooper (66).]

momentum appropriate for each particle. This is not correct near $r = 0$, but in that region the magnitude of the deuteron wave function is small as a consequence of the absorption. Elsewhere the product in the integral of I will fluctuate strongly and I will be small.

These arguments demonstrate the existence of an l window—that there is a range in l_f and l_i , respectively, for which $\exp(\delta_{l_i} + \delta_{l_f})I$ is appreciable. It is negligible if l_i or l_f fall outside these ranges. This is illustrated in Fig. 3.1.

The impact of the l window on the angular distribution can be seen from (3.24). The angular distribution will be oscillatory with a frequency that will lie between $\pi/2l_{\max}$ and $\pi/2l_{\min}$, where l_{\max} and l_{\min} are the maximum and minimum values of l_f or l_i .

Examination of the integral I yields another qualitative result that could have been anticipated—that the momentum transfer is bounded by the “momentum” of the captured neutron. That is,

$$\left| \frac{A}{A+1} k_f - k_i \right| < \sqrt{\frac{2m}{\hbar^2}} |\varepsilon| \quad (3.25)$$

where $|\varepsilon|$, the binding energy of the captured neutron, is given by the Q of the reaction plus the binding energy of the deuteron, 2.246 MeV. As k_f and k_i increase, this inequality implies that the reaction proceeds when k_f is about equal to k_i , this is, for good *momentum matching*. “Good momentum matching gives slow radial oscillations and large overlaps only in the nuclear surface region where the distorted wave functions are not yet affected by absorption” [Austern, Iseri et al (87)]. Since when multiplied by the nuclear radius, the left-hand side of this inequality gives the maximum angular momentum transfer L , we see that for a given (d, p) reaction, L is generally limited to fairly small values.

The discussion above does not take the spin variable into account. For a given L of the captured neutron, two values of j , its total angular momentum, $L \pm \frac{1}{2}$, are possible. These correspond to two different single-particle states and therefore to two different radial wave functions χ_L , so that I is spin dependent. The spin dependence of the proton and deuteron optical potential as well as the deuteron D state will give \mathcal{T} additional spin dependence. However, the net effect is quite small, although it may be observable, as indicated by Fig. 3.2. A deep minimum at the back angles is seen for the $l = 1$ transfer for $p_{1/2}$ and not for $p_{3/2}$. The spin dependence is much more dramatically revealed in experiments that measure the polarization of the proton, or if the deuteron beam is polarized, the vector analyzing power, as illustrated in Fig. 3.3. (Polarization is discussed in Appendix C.)

When spin is included in the discussion, the angular momentum balance must be reconsidered. If \mathbf{J}_i is the spin of the target nucleus, \mathbf{s}_p that of the deuteron, \mathbf{J}_f that of the final nucleus, and \mathbf{s}_p the spin of the proton, conservation of angular momentum requires that

$$\mathbf{J}_i + \mathbf{s}_D + \mathbf{l}_i = \mathbf{J}_f + \mathbf{s}_p + \mathbf{l}_f \quad (3.26)$$

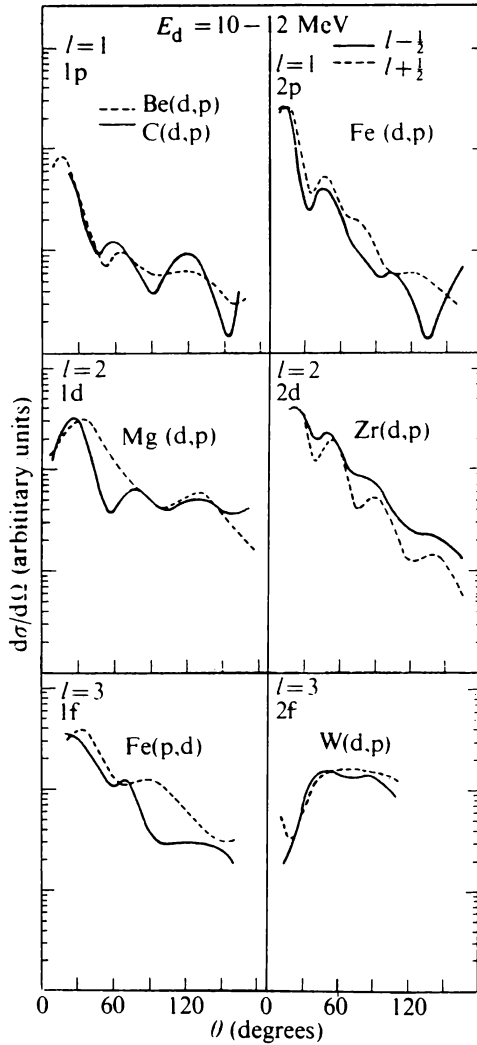


FIG. 3.2. Summary of j -dependent effects in (d, p) reactions. The curves represent the trend of the experimental data for different j values [Schiffer (68)]. [From Barrett and Jackson (77).]

The assumption that the transferred neutron is in a single-particle state leads to the requirement

$$\mathbf{J}_f = \mathbf{J}_i + \mathbf{j}_n = \mathbf{J}_i + \mathbf{L} + \mathbf{s}_n \quad (3.27)$$

where \mathbf{L} and \mathbf{s}_n are the angular momentum and spin of the neutron. Substituting (3.27) into (3.26) yields

$$\mathbf{s}_d + \mathbf{l}_i = \mathbf{L} + \mathbf{l}_f + \mathbf{s}_n + \mathbf{s}_p$$

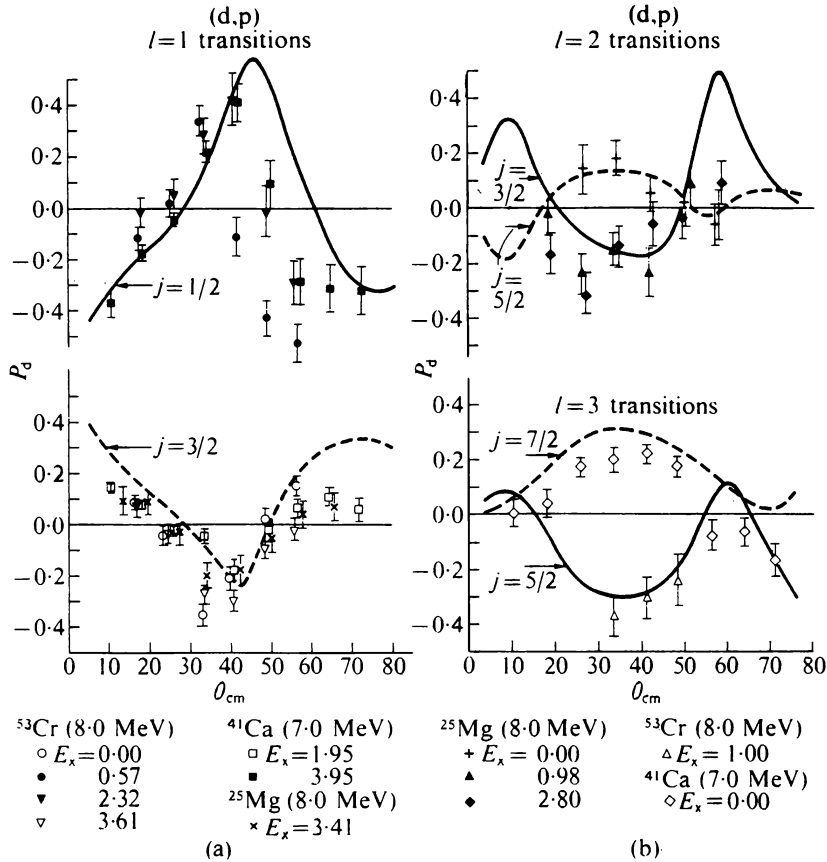


FIG. 3.3. Vector analyzing power for various (d,p) reactions [Glashauser and Thirion (69)]. [From Barrett and Jackson (77).]

Presuming the absence of spin-dependent terms in the optical potentials of the proton and deuteron and in the neutron-proton potential yields (3.20). Hence the equation above reduces to the obvious result

$$\mathbf{s}_d = \mathbf{s}_n + \mathbf{s}_p$$

Since the deuteron is in a spin-1 state, the captured neutron and the emerging proton must also be in a spin-1 state. If the deuteron spin is parallel or antiparallel to the normal to the scattering plane, the bound neutron and the emergent proton spins will be parallel. If the spin of the deuteron lies in the plane, the neutron and proton spins will be antiparallel. If the incident deuteron beam is unpolarized, the three deuteron spin states will have equal populations.

Therefore, the neutron and the proton spin will be parallel on the average. Hence by observing the emerging proton spin, one determines the captured neutron spin and therefore the total angular momentum, $L \pm \frac{1}{2}$, of the neutron state. We shall leave the verification of the discussion above as an exercise for the reader.

The cross section is obtained by squaring \mathcal{T} , given by (3.24), summing over m_f , averaging over the deuteron spin, and multiplying by the ratio of the emitted current to the incident current. The latter contains the factor $(N_A + 1)$. One obtains

$$\begin{aligned} \frac{d\sigma_{d,p}}{d\Omega} = & \frac{1}{3} \left(\frac{A+2}{A+1} \right)^2 \frac{k_f}{k_i} \frac{\mu_i \mu_f}{m^2} \left(\frac{2\gamma}{1-\gamma\rho_t} \right) \mathcal{S}(\alpha, L)(2L+1) \sum_{\substack{l_i l'_i \\ l_f l'_f \\ l}} (-)^l (2l+1)(2l_i+1)(2l'_i+1) \\ & \times (2l_f+1)(2l'_f+1) e^{i(\delta_{l_i} + \delta_{l_f} - \delta_{l'_i}^* - \delta_{l'_f}^*)} \begin{pmatrix} l_i & L & l_f \\ 0 & 0 & 0 \end{pmatrix} \begin{pmatrix} l'_i & L & l'_f \\ 0 & 0 & 0 \end{pmatrix} \\ & \times \begin{pmatrix} l_f & l'_f & l \\ 0 & 0 & 0 \end{pmatrix} \begin{pmatrix} l_i & l'_i & l \\ 0 & 0 & 0 \end{pmatrix} \left\{ \begin{matrix} l_i & l'_i & l \\ l'_f & l_f & l \end{matrix} \right\} I(l_i l_f L) I^*(l'_i l'_f L) P_l(\cos \vartheta) \quad (3.28) \end{aligned}$$

This formula is less formidable than it looks because the sums on $l_i l'_i$, l_f , and l'_f are over a limited range because of the l window discussed earlier.[‡] The sum over l is limited as a consequence. We also see that the maximum value of l is the least of the maximum values of $2l_i$ and $2l_f$.

The derivation of (3.28) makes a number of approximation that we shall now review. We have mentioned the neglect of spin-dependent terms in the proton and deuteron optical potentials as well as the D component of the deuteron wave function. Because these terms are comparatively small, a perturbation treatment is useful [see Satchler (83, p. 384)]. The inclusion of spin-orbit coupling in the optical potentials will not modify the angular distributions greatly. However, the overall magnitude and therefore the spectroscopic factors extracted from the data can be changed substantially [Lee, Schiffer, et al. (64); Seth, Biggerstaff, Miller, and Satchler (67)]. There are special effects. For example, as we noted above, a systematic effect for $l = 1$ transfer is observable. The spin-orbit coupling in the optical potentials is responsible [Lee, Schiffer, et al. (64)]. A similar effect is seen for $l = 2$ and $l = 3$ transfers. In this case both the spin-orbit coupling in the optical potentials and the D state of the deuteron are sources of the effect [Delic and Robson (74)].

We turn next to the zero range approximation, (3.13) and (3.15). To obtain

[‡]Highly developed computer codes make comparison of experiment with stripping theory correspondingly straightforward.

the next order, return to (3.10) and insert the variables given by (3.7) and (3.8):

$$\mathcal{T}_{dp}^{(\text{DWA})} = \frac{A+2}{2(A+1)} (N_A+1) \int d\mathbf{r} \int d\mathbf{R} U_{0,f}^{(-)*} \left(\frac{A}{A+1} \mathbf{R} + \mathbf{r} \right) \times f_{fi}^*(-\mathbf{R}) w(\mathbf{r}) \chi(\mathbf{r}) v_{0,i}^{(+)}(\mathbf{R} + \frac{1}{2}\mathbf{r}) \quad (3.29)$$

The next step is to expand $U_{0,f}^{(-)}$ and $v_{0,i}^{(+)}$ in a Taylor series in \mathbf{r} and perform the \mathbf{r} integration assuming that $w(\mathbf{r})\chi(\mathbf{r})$ is spherically symmetrical. One then obtains after some simple manipulations

$$\mathcal{T}_{dp}^{(\text{DWA})} = \frac{A+2}{2(A+1)} (N_A+1) B \int d\mathbf{R} U_{0,f}^{(-)} \left(\frac{A}{A+1} \mathbf{R} \right) f_{fi}^*(-\mathbf{R}) v_{0,i}^{(+)}(\mathbf{R}) \times \left\{ 1 + \frac{1}{6}\rho \left(\frac{m}{\hbar^2} \right) \left[\mathcal{V}_n(\mathbf{R}) + \mathcal{V}_p \left(\frac{A}{A+1} \mathbf{R} \right) - \mathcal{V}_D(\mathbf{R}) + B \right] \right\} \quad (3.30)$$

where

$$B \equiv \int d\mathbf{r} w\chi \quad (3.31a)$$

$$\rho B = \int d\mathbf{r} r^2 w\chi \quad (3.31b)$$

The potentials \mathcal{V}_n , \mathcal{V}_p , and \mathcal{V}_D are, respectively, the binding potential of the neutron, the optical potential for the proton, and the optical potential for the deuteron. B is given by $(E_D + |E_n| - E_p)$, where $|E_n|$ is the binding energy of the neutron. In deriving (3.30) the limit of $A \rightarrow \infty$ was taken except for the argument of \mathcal{V}_p .

As one can immediately verify, when (3.15) is used, the first term, independent of ρ , of (3.30) agrees with (3.16). The use of (3.31a) provides some flexibility, however, since it makes possible the use of a more realistic expression for $w\chi$. The term proportional to ρ can readily be included in the calculations. The effect of the ρ term is to reduce the contributions from the interaction region. A comparison with the exact calculation is shown in Fig. 3.4. See Dickens, Drisco, Perey, and Satchler (65), Stock, Bock, et al. (67), and Santos (73) for further discussion.

In passing, note that the Perey effect (effective mass) will also reduce the amplitude of the proton and deuteron wave functions in the interaction region. The Perey effect is a consequence of the nonlocality and energy dependence of the optical potential.

Part of that nonlocality is generated by the Pauli principle, which tends to reduce the amplitude of the proton and neutron wave functions when they overlap the target and the residual nuclei. Antisymmetry can be included to

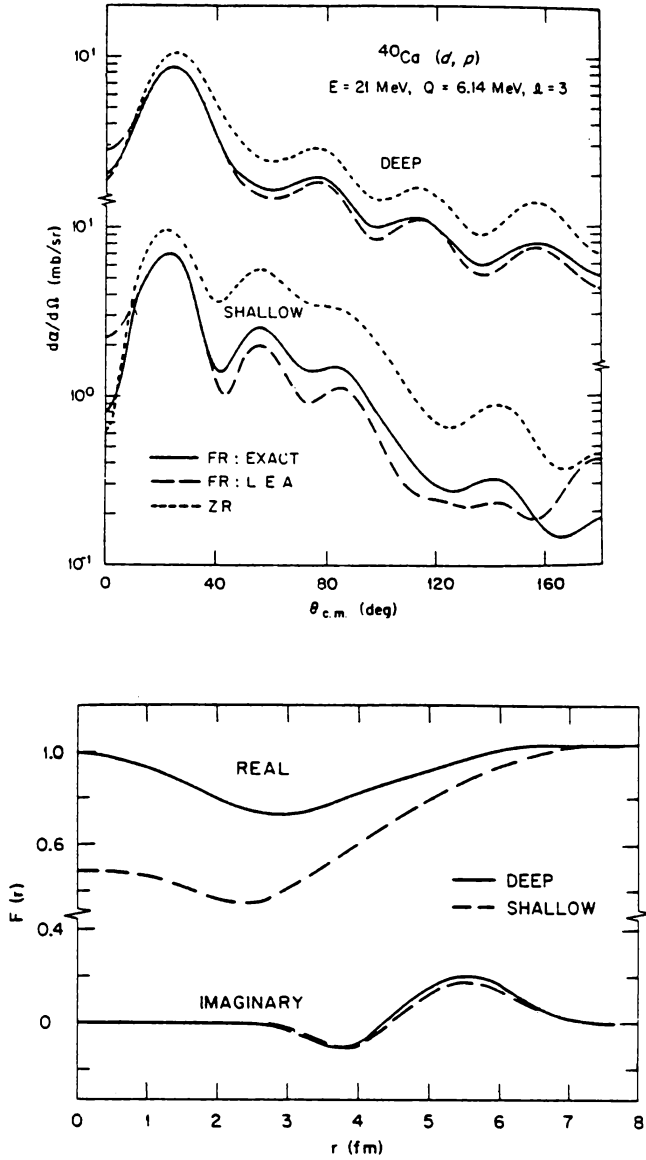


FIG. 3.4. Finite range effects. The dashed line is obtained using (3.30). $F(r)$ equals the expression within the braces in (3.30). The dotted line results from the use of the zero range approximation. The labels “shallow” and “deep” refer to the depth of the deuteron optical potential used ($V = 67$ MeV and 112 MeV, respectively). [From Satchler (83).]

some extent by adding in the exchange integral to (3.10). More accurately, the analysis of Section 2 should be used, including both the antisymmetry and nonorthogonality effects. That this is possible is demonstrated by the calculations of Döhnert (71) and those of several Japanese physicists, for example, Horiuchi (77). For an approximate treatment of antisymmetry that permits continued use of (3.1), see Johnson, Austern, and Hopes (82). The substantial agreement between DWA theory and experiment, particularly in the critical forward angle region, indicates that these effects, at least as far as the angular distribution is concerned, are small.

4. THE DEUTERON–NUCLEUS INTERACTION

The DWA amplitude depends strongly on the distorted deuteron wave function and therefore on the deuteron optical model. The deuteron has a comparatively large structure (diameter ~ 4.4 fm) and is very loosely bound (B.E. = 2.246 MeV). It can therefore readily “break up” when subjected to external forces provided by the target nucleus, a process that is aided by the Pauli exclusion principle. Deformation of the deuteron without breakup can also occur, but breakup is more likely. As a consequence, one finds strong deuteron absorption when the deuteron penetrates the nuclear interior. It is this strong absorption that is the most important factor in producing the l window of Section 3.

As in the nucleon case, one approach to the deuteron optical model potential has been empirical; that is, the parameters of an optical potential of an assumed form are adjusted so as to fit the observed deuteron–nucleus elastic scattering. A second approach attempts to relate the deuteron optical model with the underlying nucleon–nucleon forces. At a simple level, the folding model is used. It suffers from the obvious omission of the breakup channels and thus leads to a serious underestimate of the absorption component. A more complete treatment based on the general analysis developed in Chapter III and used in Section 2 of this chapter has been carried out by Döhnert (71). Döhnert includes the effects of antisymmetry, which involves the possible exchange of one or both of the deuteron nucleons with those in the target nucleus. The effects of breakup (as well as multistep processes) on stripping are included as well. This is ensured by the orthogonality conditions (2.5) and (2.6). However, the Döhnert procedure does not permit a calculation of the breakup that occurs in a deuteron–nucleus collision. A correct description of the nonlocality induced by the Pauli principle as well as the contribution coming from the finite size of the deuteron is thus obtained. One can at this point insert the nucleon–nucleon potentials as well as the wave functions for the target nucleus to obtain the deuteron optical model potential, recognizing from the beginning that only the elastic amplitude can be described by such a potential. Such a calculation does not seem to have been carried out for the deuteron [see Döhnert (71)], although Horiuchi (77) has performed the equivalent calculation for α -particle nucleus interaction. A less ambitious program employs the form derived by Dohnert for the empirical

analyses of the elastic scattering of the deuteron by the target nucleus, thereby avoiding the difficulties associated with the microscopic approach.

However, most of the analyses reported in the literature use directly a simple empirical form for the deuteron optical potential, similar to that employed for the nucleon optical potential described in Chapter V. The hope, underlying this convenient approach, is that the potential so obtained will yield wave functions that mimic the exact ones faithfully and so include effects such as antisymmetry and nonlocality implicitly. This can be the case only if the assumed form for the potential is sufficiently flexible so as to be capable of including the effects arising from nonlocality, such as the Perey effect (see p. 346).

The local form commonly used is [see (V.2.38)]

$$V_{\text{opt}}^{(D)} = \mathcal{V}_c + \mathbf{S} \cdot \mathbf{L} \mathcal{V}_{s0} \quad (4.1)$$

where

$$\begin{aligned} \mathcal{V}_c &= V_{\text{Coul}} - Vf(x_0) - i \left[WF(x_w) - 4W_D \frac{d}{dx_D} f(x_D) \right] \\ \mathcal{V}_{s0} &= \left(\frac{\hbar}{m_\pi c} \right)^2 V_{s0} \frac{1}{r} \frac{d}{dr} f(x_{s0}) \end{aligned}$$

and

$$f(x) = \frac{1}{1 + e^x} \quad x = \frac{r - r_i A^{1/3}}{a_i}$$

V , W , W_D , V_{s0} are constants, while r_i and a_i may have differing values for x_c , x_w , x_d , and x_{s0} . V_{Coul} is identical with that used in (V.2.38). \mathbf{S} is the spin operator for the deuteron, normalized so that $S^2 = 2$.

A thorough analysis has been made of the data available at the time to obtain a global optical model for deuteron energies ranging from 12 to 90 MeV by Daehnick, Childs, and Vrcelj (DCV) (80) and for nuclei with mass between ^{37}Al and ^{238}Th . Their results are given in Table 4.1. Note that the DCV form assumes that $x_w = x_D$. As in the nucleon case, the central potential depth V decreases with increasing E , while the diffusivity grows with E . The volume absorption W is less important than the surface absorption W_D at the lower energies but is of equal importance at the highest energy. The diffusivity of the absorption potential, a_w , exhibits a dependence on neutron shell closure. The spin-orbit coupling decreases with increasing energy. Daehnick et al. (80) have also considered a complex spin-orbit coupling and have included in their table values of the parameters for nonrelativistic dynamics.

Examples of the quality of the fits obtained are given in Figs 4.1 to 4.4. The fits on the whole are quite good, although there are some deviations of significant size, but these are not systematic. Note that the ordinate scale is logarithmic. The authors believe that in part these may be a consequence of structure effects

TABLE 4.1 Recommended Global Parameter Prescriptions That Fit a Wide Range of Deuteron Scattering Data^a

$V = 88.5 - 0.26E + 0.88ZA^{-1/3}$	MeV
$r_0 = 1.17$	fm
$a_0 = 0.709 + 0.0017E$	fm
$W = (12.2 + 0.0626E) \times (1 - e^\beta)$	MeV
$W_D = (12.2 + 0.026E)e^\beta$	MeV
$r_W = 1.325$	fm
$a_W = 0.53 + 0.07A^{1/3} - 0.04 \sum_i e^{-\mu_i}$	fm
$r_c = 1.30$	fm
$V_{s0} = 7.33 - 0.029E$	MeV
$r_{s0} = 1.07$	fm
$a_{s0} = 0.66$	fm

^aPotential name: 79 DCV *L* (nonrelativistic kinematics only). *A*, mass number; *Z*, proton number; $\beta = -(E/100)^2$; $\mu_i = [(M_i - N)/2]^2$, where M_i = magic numbers (8, 20, 28, 50, 82, 126); *N*, neutron number; *E*, deuteron laboratory energy (MeV).

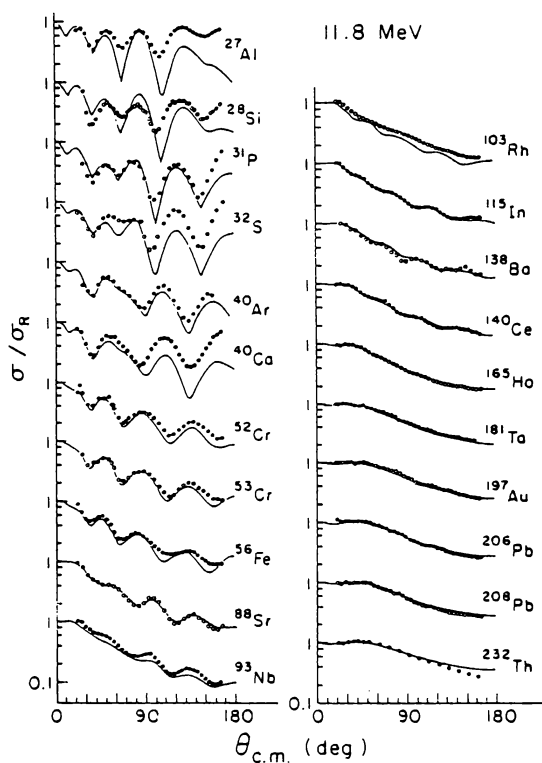


FIG. 4.1. Comparison of 11.8-MeV data with predictions of potential *L* (Table 4.1). [From Daehnick, Childs, and Vrcelj (80).]

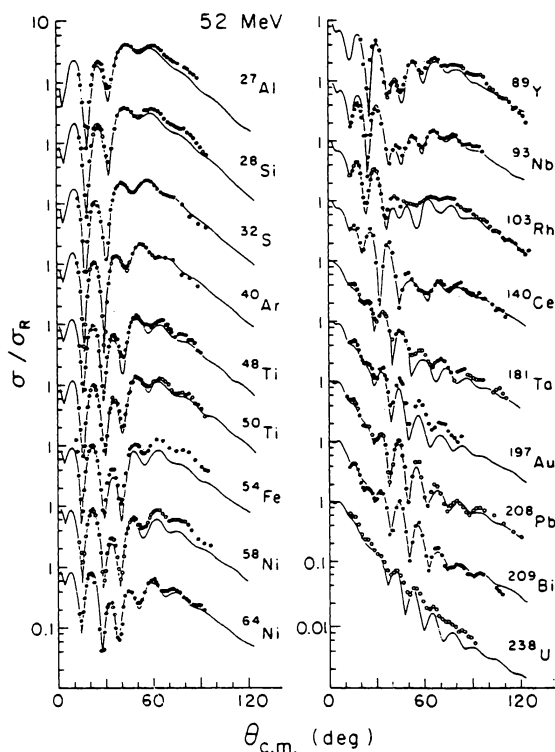


FIG. 4.2. Comparison of 52-MeV data with predictions of potential L (Table 4.1). [From Daehnick, Childs, and Vrcelj (80).]

and, at low energies, of contributions of compound elastic scattering. Resolution limitations are important for deformed nuclei targets when these have low-lying excited states. Reaction cross sections obtained from the optical model are systematically higher than the experimental values, indicating perhaps a need to modify the Woods-Saxon shape used in (4.1).

It is interesting to compare these phenomenological results with those obtained for the neutron-nucleus (n -nucleus) and proton-nucleus (p -nucleus interactions) (see Table V.2.1). We see that the real central (d -nucleus) potential is much greater than the corresponding nucleon potentials. Moreover, it differs substantially from the sum of the (p -nucleus) and n -nucleus real central interactions. However, the diffusivity a_0 is not very different. Both the imaginary central volume and surface terms, W and W_D , of the (d -nucleus) potential are very much larger than the corresponding nucleon-nucleus cases. The spin-orbit terms are not very different. Qualitatively, the difference in the real central deuteron potential from the sums of the nucleon potentials can be understood as a consequence of the finite size of the deuteron, while greater absorption

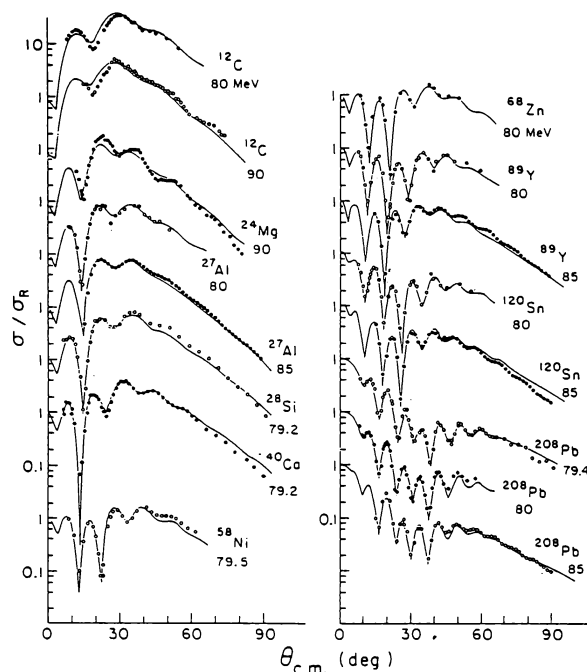


FIG. 4.3. Comparison of 80- to 90-MeV data with predictions of potential L , (Table 4.1). [From Daehnick, Childs, and Vrcelj (80).]

occurs because the penetrating deuteron breaks up readily in view of its small binding energy.

It has been pointed out that a two-step process involving breakup could be of some importance for stripping. The first step involves the breakup of the deuteron (i.e., a transition to the n - p continuum state) because of the interaction with the target nucleus followed by the capture of the neutron by the nucleus. In principle, this effect could be estimated using perturbation theory or the Dohnert procedure. Instead, the strategy in which the deuteron optical potential has been modified has been used. This has the convenience that the standard DWA formula whose evaluation by computer is a thoroughly tested and available procedure can be used. We discuss this approach in Section 6.

5. OVERLAP WAVE FUNCTION

The overlap wave function $f_{fi}(\mathbf{r})$ is defined as

$$f_{fi}(\mathbf{r}) = \langle \psi_i(\mathbf{r}_2, \mathbf{r}_3, \dots) | \phi_f(\mathbf{r}, \mathbf{r}_2, \dots) \rangle \quad (3.9)$$

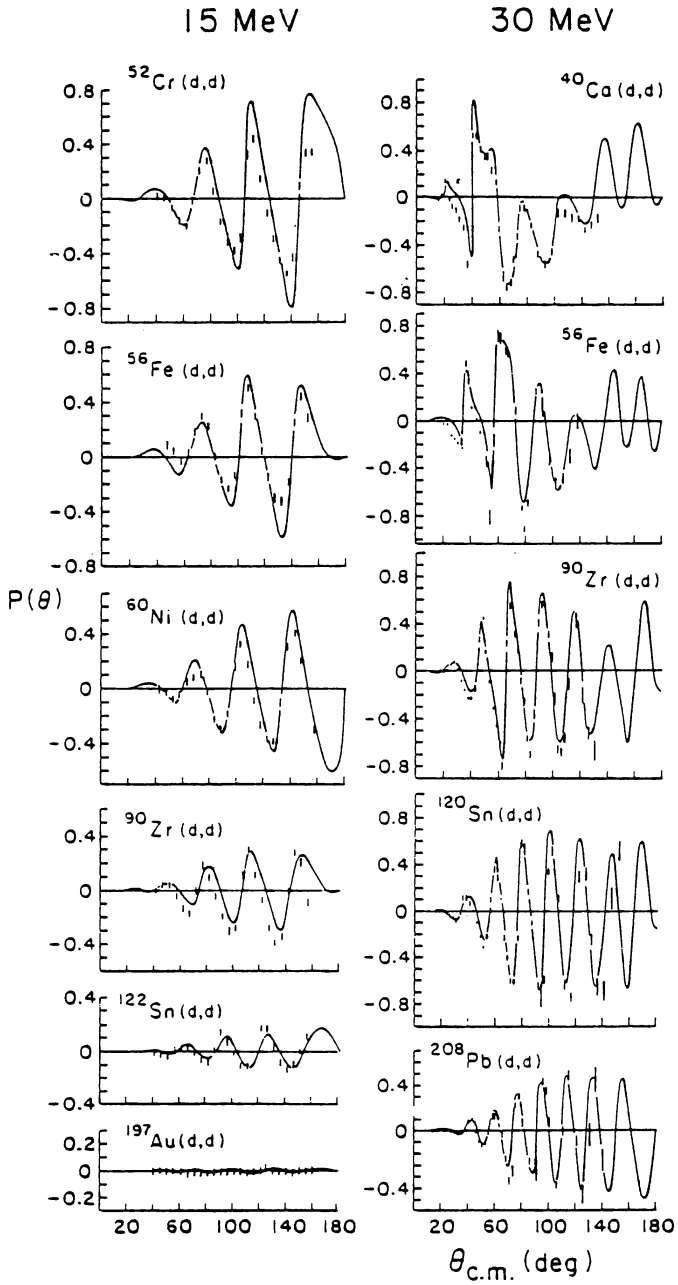


FIG. 4.4. Comparison of the predictions of the potential (Table 4.1) with vector polarization data. [From Daehnick, Childs, and Vrcelj (80).]

where integration over the coordinates common to ψ and ϕ_f is assumed. The functions ψ_i and ϕ_f are the wave functions describing the target and residual nuclei. From the Schrödinger equations satisfied by ψ_i and ϕ_f , one immediately obtains

$$f_{fi}(\mathbf{r}) \xrightarrow{r \rightarrow \infty} e^{-\kappa r}/r \quad (5.1)$$

where

$$\frac{2m}{\hbar^2}(E_i - E_f) = \kappa^2 \quad (5.2)$$

The energy $(E_i - E_f)$ equals the energy required to break up the final nucleus into the initial nucleus plus a zero-energy neutron.

The overlap wave function generally used in a stripping DWA calculation is obtained by solving the Schrödinger equation for a neutron moving in the mean field of the target nucleus. The latter is taken to be an empirical potential such as the Woods–Saxon potential [see Bear and Hodgson (78)] whose parameters are appropriate for the target nucleus and the neutron single-particle state under study, and of course satisfy (5.1) and (5.2). This last condition is important to the extent that the reaction occurs at the surface. Harmonic oscillator wave functions are not adequate because they do not satisfy (5.1) and (5.2). Obviously, the more realistic the models used in terms of the experimental evidence that they can explain, the more meaningful is the understanding of nuclear structure that can be extracted from the one-particle transfer reactions.

The overlap wave function is significantly modified when the target and/or the residual nuclei are deformed, since the effects of deformation are most important on the surface region. The deformed potential is obtained from a spherical one that has been found suitable for spherical nuclei in a nearby range of the periodic table. One can, for example, expand the radius parameter R in a multipole series. [See Rost (67) and Bang and Vaagen (80) for details.]

6. THREE-BODY MODEL[‡]

The three bodies in this model are the neutron, the proton, and the target nucleus. The neutron–nucleus and proton–nucleus interactions are taken to be the optical model potentials, while the neutron–proton interaction usually is a simplified version of the nucleon–nucleon interaction, allowing of course for the formation of the deuteron. The optical model potentials include the effects of the excitation of the target nucleus on the elastic scattering of the neutron and proton by the nucleus. Otherwise, the nucleus is inert, so that inelastic and fragmentation processes are not included in this model.

[‡]Austern, Iseri, et al. (87).

The focus of the study of this system is on the effect of breakup on the wave function and on the elastic scattering of the deuteron. The approximations used eliminate the stripping channel. Stripping is calculated in the next order of approximation by using the three-body model wave function in the DWA transition amplitude. The implied assumption is that the stripping channel does not induce a substantial change in the wave function.

The simplest Schrödinger equation for the three-body model has the following form:

$$[E - T_p - T_n - V_{pn} - (V_p + iW_p) - (V_n + iW_n)]\psi(\mathbf{r}_p, \mathbf{r}_n) = 0 \quad (6.1)$$

The quantities T_p and T_n are the kinetic energy operator for the proton and neutron respectively, V_{pn} is the neutron-proton interaction, and $V_p + iW_p$ and $V_n + iW_n$ are optical model potentials. The energy dependence of the empirical optical model parameters present a problem in that the energy at which these parameters should be used is not clear. The practice has been to evaluate them at an energy equal to $E/2$ on the supposition that the neutron and proton share the energy equally, as is approximately the case for the incident deuteron. There is in addition a threshold effect; the absorption potential W_n must go to zero when the proton energy exceeds E , since then the neutron is bound. To take this effect into account, W_n in (6.1) is replaced by

$$W_n \rightarrow W\left(\mathbf{r}, \frac{E}{2}\right)\theta(E - h_p) \quad (6.2)$$

where θ is the unit function and h_p is the proton Hamiltonian

$$h_p = T_p + V_p \quad (6.3)$$

A similar modification is suggested for W_p .

One should also take antisymmetry into account. The wave functions of the neutron and proton must be orthogonal to the wave functions of the nucleons in the target nucleus.

In most of the calculations that have been performed, the threshold effect and the antisymmetry are neglected. Estimates of the latter are discussed by Austern. We then return to the Schrödinger equation, (6.1).

We discuss three procedures that have been used to obtain approximate solutions to (6.1). In all of these approximations, the variables

$$\mathbf{r} = \mathbf{r}_p - \mathbf{r}_n \quad \mathbf{R} = \frac{\mathbf{r}_p + \mathbf{r}_n}{2} \quad (6.4)$$

are used. Letting

$$U \equiv V + iW$$

the potential in (6.1) becomes

$$U_p\left(\mathbf{R} + \frac{\mathbf{r}}{2}\right) + U_n\left(\mathbf{R} - \frac{\mathbf{r}}{2}\right) + V_{np}(\mathbf{r}) \quad (6.5)$$

A Coulomb term $U_C(\mathbf{R})$, dependent on \mathbf{R} only, is added to (6.5). Since the dependence of the Coulomb potential on \mathbf{r} is neglected, this term will have no effect on break up.

A. Watanabe Potential[†]

This is obtained by taking the expectation value of (6.1) with respect to the internal deuteron wave function $\phi_d(\mathbf{r})$, omitting the 3D_1 state component of ϕ_d . This yields the equation

$$[E + |\varepsilon_d| - T_R - U_C(R) - U_{wat}(R)]\psi(\mathbf{R}) = 0 \quad (6.6)$$

where T_R is the kinetic energy of the center of mass of the neutron-proton system,

$$U_{wat} \equiv \int d\mathbf{r} |\phi_d(\mathbf{r})|^2 \left[U_p\left(\mathbf{R} + \frac{\mathbf{r}}{2}\right) + U_n\left(\mathbf{R} - \frac{\mathbf{r}}{2}\right) \right] \quad (6.7)$$

and

$$\psi(\mathbf{r}_p, \mathbf{r}_n) \equiv \Psi(\mathbf{r}, \mathbf{R}) \quad (6.8)$$

has been approximated by

$$\Psi(\mathbf{r}, \mathbf{R}) \simeq \phi_d(\mathbf{r})\Psi(\mathbf{R}) \quad (6.9)$$

The Watanabe potential is just an example of the folding potential [see (V.2.76)]. In view of (6.9), the breakup channel is not included.

B. The Adiabatic Approximation[‡]

We first rewrite (6.1) in the neutron-proton relative and center-of-mass coordinates, \mathbf{r} and \mathbf{R} , respectively:

$$(E - h_{np} - T_R - U(\mathbf{r}, \mathbf{R}))\psi(\mathbf{r}, \mathbf{R}) = 0 \quad (6.10)$$

[†]Watanabe (58).

[‡]Johnson and Soper (70).

where

$$U(\mathbf{r}, \mathbf{R}) \equiv U_p + U_n + U_c$$

and h_{np} is the neutron-proton Hamiltonian

$$h_{np} = T_r + V_{np} \quad (6.11)$$

T_r is the kinetic energy of the relative motion of the neutron and proton. The adiabatic approximation is obtained by replacing h_{np} by $-|\varepsilon_d|$, where ε_d is the binding energy of the deuteron, with the result

$$(E + |\varepsilon_d| - T_R - U(\mathbf{r}, \mathbf{R}))\psi^{AD}(\mathbf{r}, \mathbf{R}) = 0 \quad (6.12)$$

This equation is solved as a scattering problem in the variable \mathbf{R} ; the variable \mathbf{r} is taken to be a parameter, so that solutions are calculated for each value of \mathbf{r} . The incident wave is taken to be $\phi_d(\mathbf{r})e^{i\mathbf{K}\cdot\mathbf{R}}$. Deuteron elastic scattering is obtained by taking the expectation value of the outgoing component of ψ^{AD} with respect to the deuteron wave function $\phi_d(\mathbf{r})$. Breakup is obtained by taking the expectation value with respect to the neutron-proton continuum wave functions, $\phi(\mathbf{k}, \mathbf{r})$.

C. Coupled Equations[†]

The Watanabe wave function, (6.9), is the first term in a more complete expansion of $\Psi(\mathbf{R}, \mathbf{r})$ in terms of the bound state (the deuteron) and the continuum states of two nuclear system. Austern, Iseri, et al. (86) write

$$\begin{aligned} \Psi(\mathbf{r}, \mathbf{R}) &= \sum_{JM} a_{JM} \frac{1}{R} \psi_{JM}(\mathbf{r}, \mathbf{R}) \\ \psi_{JM}(\mathbf{r}, \mathbf{R}) &= \phi_D(\mathbf{r}) f^J(R) Y_{JM}(\hat{R}) \\ &\quad + \sum_l \sum_{L=|J-l|}^{J+l} \int_0^\infty dk \phi_l(k, r) g_{lL}^J(\lambda, R) [Y_l(\hat{\mathbf{r}}), Y_L(\hat{\mathbf{R}})]_{JM} \end{aligned} \quad (6.13)$$

In this equation $f^J(R)$ and $g_{lL}^J(\lambda, R)$ are unknown functions to be determined by the coupled equations obtained when (6.13) is substituted for the wave function in the Schrödinger equation. The continuum wave function $\phi_l(k, r) Y_{lm}$ satisfies the neutron-proton equation:

$$\begin{aligned} [\varepsilon(k) - T_r - V_{pn}(r)] \phi_l(k, r) Y_{lm}(\hat{\mathbf{r}}) &= 0 \\ \varepsilon(k) &= \frac{\hbar^2 k^2}{M} \end{aligned} \quad (6.14)$$

[†]Austern, Iseri, et al. (89).

The parameter λ gives the center-of-mass momentum of the neutron-proton system, so that

$$E = \varepsilon(k) + \frac{\hbar^2 \lambda^2(k)}{4M} \quad (6.15)$$

Finally, $[Y_l(\hat{\mathbf{r}}), Y_L(\hat{\mathbf{R}})]_{JM}$ is given by

$$[Y_l(\hat{\mathbf{r}}), Y_L(\hat{\mathbf{R}})]_{JM} = \sum_{m,\mu} \langle JM | lm, L\mu \rangle Y_{lm}(\hat{\mathbf{r}}) Y_{L\mu}(\hat{\mathbf{R}}) \quad (6.16)$$

The first term of (6.13) describes elastic deuteron scattering, and the second term describes the breakup component. The expansion in l permits the description of the effects connected with the orientation of the deuteron.

Inserting (6.13) into the three-body Schrödinger equation leads to an infinite set of coupled differential-integral equations. Some method of truncation is needed. The dynamical origin of the coupling is in the potential U :

$$U = U_p \left(\mathbf{R} + \frac{\mathbf{r}}{2} \right) + U_n \left(\mathbf{R} - \frac{\mathbf{r}}{2} \right) + U_c \quad (6.17)$$

This can be expanded in a *multipole* series:

$$U = \sum_l U_l(r, R) P_l(\hat{\mathbf{r}} \cdot \hat{\mathbf{R}}) \quad (6.18)$$

If $U_p \approx U_n$, which is nearly true, the sum goes over the even l 's only. *Truncation of this series at $l = l_{\max}$* is reasonable physically. A *posteriori* verification can be obtained, and in fact l_{\max} equals 2; that is, only two terms in (6.18) are needed.

This is demonstrated by Table 6.1, which gives the partial cross sections as l_{\max} is increased beyond 2 for $J = 17$, the dominant wave in the example discussed by Austern, Iseri, et al. (87). The $l = 1$ contribution is found to be unimportant.

TABLE 6.1 Partial Cross Section $\sigma_l^{(J)}$ for $J = 17$

l_{\max}	2	4	6	0
$\sigma_0^{(17)}$	4.067	3.930	3.989	10.273
$\sigma_2^{(17)}$	12.596	11.651	11.351	
$\sigma_4^{(17)}$		1.830	1.684	
$\sigma_6^{(17)}$			0.202	
$\sum_l \sigma_l^{(J)}$	16.663	17.411	17.226	10.275
$\sigma_{\text{el}}^{(J)}$	74.230	73.502	73.568	90.106
$\sigma_{\text{react}}^{(J)}$	99.444	100.32	100.33	93.429

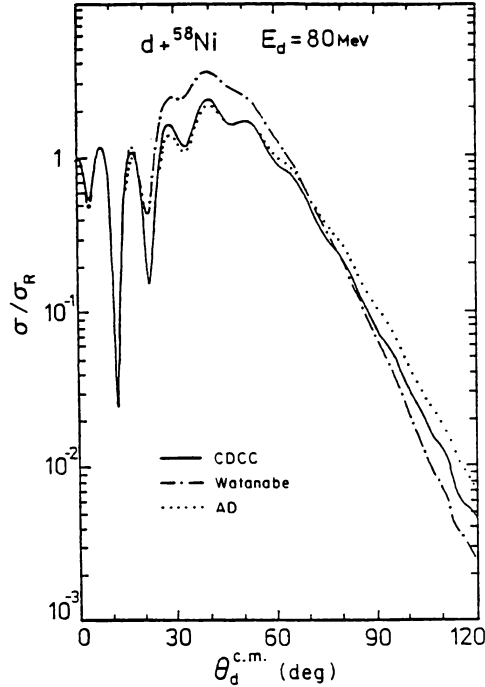


FIG. 6.1. Elastic scattering cross-sections for $d + {}^{58}\text{Ni}$. Comparisons are made between the Watanabe model, the adiabatic approximation, and the coupled-channel (CDCC) calculations [Yahiro (85)]. [From Austern, Iseri, et al. (87).]

We also see that the Watanabe ($l=0$) term is not usable. To be consistent, one must similarly cut off the expansion over l in (6.13) at $l = l_{\text{max}}$. The Schrödinger equation for $\psi(\mathbf{r}, \mathbf{R})$ now becomes a finite set of coupled integrodifferential equations. These must be solved numerically. In making this truncation, the stripping channel asymptotic amplitude vanishes faster than $1/r$, so that this formulation can yield a finite stripping amplitude only in the next approximation, described below.

The Watanabe potential is obtained if only the first term in (6.13) is retained. The adiabatic approximation can be obtained from (6.13) if $\varepsilon(k)$ is appropriately replaced by $-|\varepsilon_d|$, or as is sometimes done, by a constant that can be used as a parameter. Of the three approaches, the coupled-equation description should thus be regarded as the most precise.

The elastic scattering and breakup cross sections calculated using these three approximations are shown in Figs 6.1 and 6.2. From Fig. 6.1 we note that the Watanabe cross section is in substantial disagreement with the coupled-equation results beyond about 30° . The adiabatic cross section is in much better agreement departing from the coupled-equation results at about 90° . On the other hand,

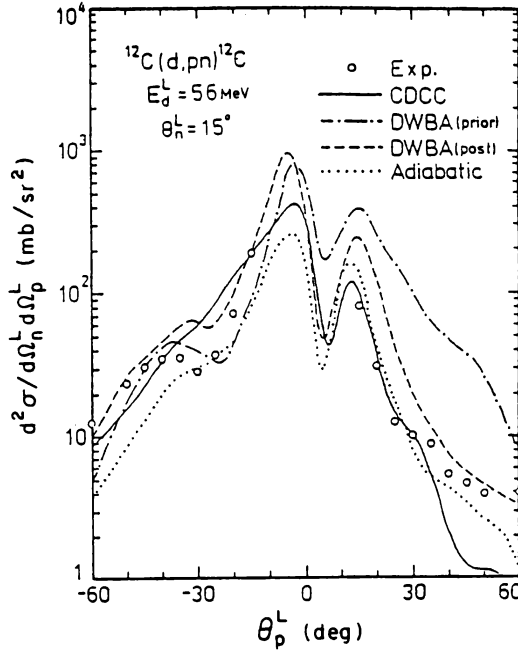


FIG. 6.2. Comparison of breakup cross sections of 56-MeV deuterons by ^{12}C with calculations by CDCC, DWBA, and the adiabatic models. In this experiment the neutron detector is fixed at $\theta_n^L = 15^\circ$ [Yahiro, Iseri, Kamimura, and Makano (84); Yahiro 85)]. (From Austern, Iseri, et al. (87).]

the adiabatic breakup cross section (Fig. 6.2) has a slope similar to that obtained with the coupled equations but fails when the proton angle θ_p^L deviates substantially from the neutron angle θ_n^L .

The importance of the $l=2$ term for the elastic scattering, which gives rise to the deviation from the Watanabe results, can also be seen when an optical model potential is fitted to the coupled-equation elastic scattering. The Watanabe potential has a very diffuse surface. But according to Austern, Iseri, et al. (87), when the effect of the $l=2$ multipole is included, the diffusiveness of the optical model potential is reduced to a value equal to that of the nucleon optical model potential. This is in good agreement with the empirical results of Section 4. A similar behavior is found when the adiabatic model is used.

Stripping can be calculated on the basis of the three-body model using the \mathcal{T} -matrix element

$$\mathcal{T}_{dp} = \langle \chi_p^{(-)}(\mathbf{k}_p, \mathbf{r}_p) \psi_n(\mathbf{r}_n) V_{pn} \psi^{(+)}(\mathbf{r}_p, \mathbf{r}_n) \rangle \quad (6.19)$$

where the outgoing nucleon is a proton and $\psi^{(+)}(\mathbf{r}_p, \mathbf{r}_n)$ is chosen to be the three-body model eigenfunction corresponding to an incident deuteron. In the

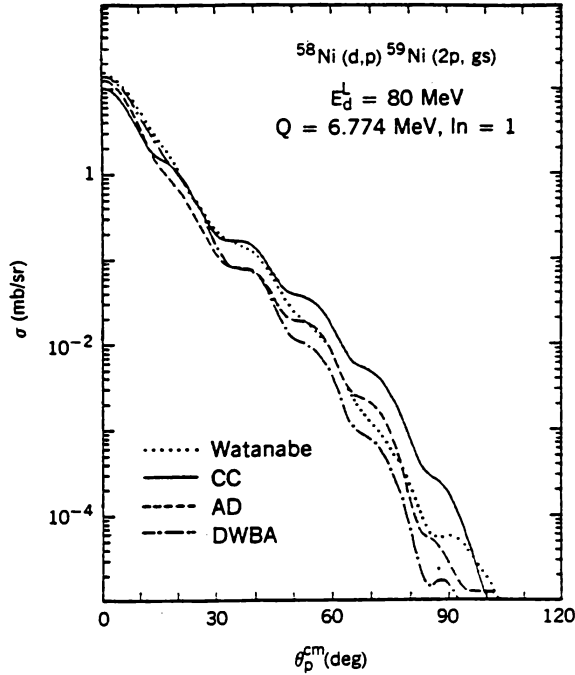


FIG. 6.3. Cross sections for $^{58}\text{Ni}(d,p)^{59}\text{Ni}(3p, \text{g.s.})$ at $E_d = 80$ MeV obtained from CDCC, AD, Watanabe, and DWA Calculations [Iseri (85)]. [From Austern, Iseri, et al. (87).]

zero range approximation,

$$(\mathcal{T}_{dp})_{ZR} = \int d\mathbf{R} \chi_p^{(-)*}(\mathbf{R}) \psi_n^*(\mathbf{R}) \phi^{(+)}(\mathbf{k}_d, \mathbf{R}) \quad (6.20)$$

with

$$\phi^{(+)}(\mathbf{k}_d, \mathbf{R}) = 8 \int d\mathbf{r} V_{pn}(\mathbf{r}) \Psi^{(+)}(\mathbf{r}, \mathbf{R}) \quad (6.21)$$

Roughly, $\phi^{(+)} \sim \Psi^{(+)}(0, \mathbf{R})$.

We now look for the effects on stripping of the break up channels. These are two in number. First the presence of the breakup channels will draw flux, so that the contribution of the $\phi_D f^J(r)$ term in (6.13), to be referred to as the *elastic* contribution, will be reduced. Second, in the event of poor momentum matching, thereby reducing the elastic contribution (see p. 482), the breakup contribution may become important since there will be a range in k in the breakup component of (6.13) which permits good momentum matching.

These effects are illustrated in Figs 6.3 to 6.5. In Fig. 6.3 we compare the calculations using the deuteron wave function provided by the Watanabe

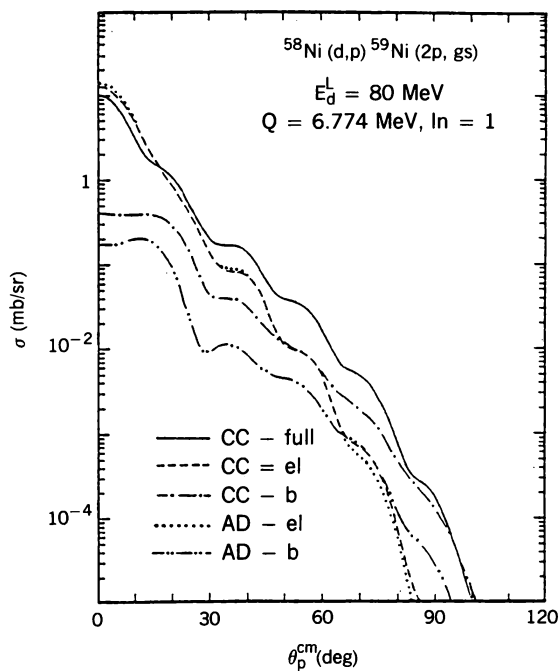


FIG. 6.4

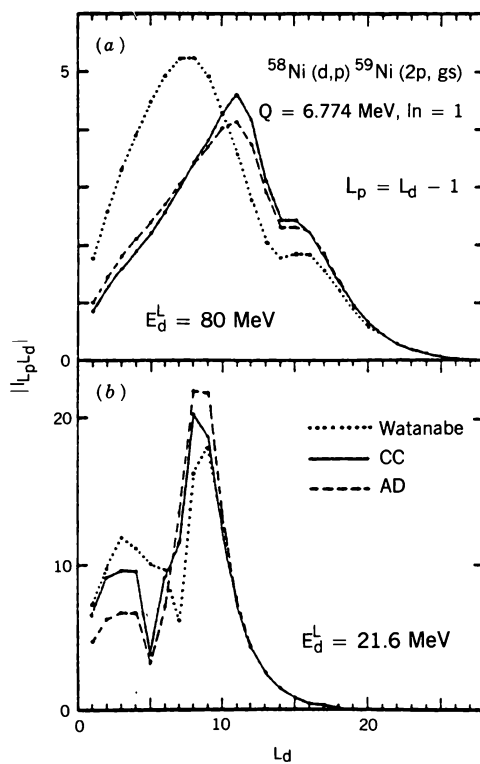


FIG. 6.5

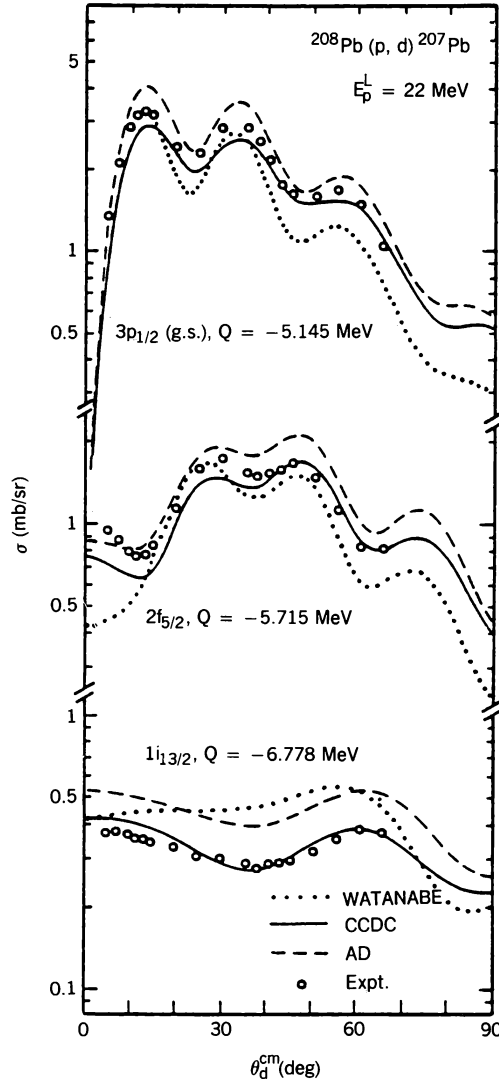


FIG. 6.6. Cross section for the reaction $^{208}\text{Pb}(p, d)$ at $E_p = 22$ MeV. The incident protons are polarized [Iseri (85)]. [From Austern Iseri, et al. (87).]

FIG. 6.4. Decomposed cross sections for $^{58}\text{Ni}(d, p)$ $^{59}\text{Ni}(2p, \text{g.s.})$ at $E_d = 80$ MeV for the CCDC and AD calculations showing the contributions for the elastic and breakup processes [Iseri (85)]. [From Austern, Iseri, et al. (87).]

FIG. 6.5. Modulus of the overlap integral I for $^{58}\text{Ni}(d, p)$ $^{59}\text{Ni}(2p, \text{g.s.})$ at $E_d = 80$ and 21.6 MeV. The angular momentum L_p is taken to equal $L_d - 1$ [Iseri (85)]. [From Austern, Iseri, et al. (87).]

potential, the adiabatic approximation, the coupled-equation procedure, and the DWA. In the last case, a deuteron potential that yields a coupled-equation elastic cross section. Comparison of the coupled equation with the Watanabe result demonstrates the importance of breakup, especially at the larger angle. The adiabatic cross section and the DWA also disagree with the coupled-equation results. In the former case, which includes breakup, the deviation from the coupled equation results is presumably due to the inaccuracy in the breakup amplitude because of the adiabatic assumption. Phase relations are extremely important in this situation. But in addition, the adiabatic approximation includes only the $l=0$ breakup contribution not the $l=2$. This effect is important at lower energies.

Further insight is obtained from Fig. 6.4 in which are plotted the elastic and breakup contributions to the stripping cross sections for both the adiabatic and coupled-equation approximations. In the coupled-equation case, note that the breakup contribution dominates beyond proton angles of 50° . In the adiabatic case this crossover does not occur. In fact, the breakup cross section is much smaller than the elastic cross section over the entire angular range. Figure 6.5 demonstrates that breakup reduces the contribution to stripping made by the smaller deuteron angular momenta in the Watanabe calculation. Breakup thereby emphasizes the surface character of stripping.

In Fig. 6.6 the three methods are compared with experimental data. We see that in these cases, by far the best results are achieved with coupled equations. The adiabatic approximation is a considerable improvement over the Watanabe recipe, especially at large angles.

In conclusion, the single-step DWA approximation of Section 3 can be considered to be valid only in the forward angular range. Employing the adiabatic model will result in a substantial improvement. But the use of the more exact coupled-equation method is computationally laborious, limiting its utilization for the analysis of data.

CHAPTER VII

MULTISTEP REACTIONS

1. INTRODUCTION

The DWA as used in Chapter V and Section VI.3 describes a single-step reaction as exhibited by the explicit appearance of the responsible interaction only once in the transition matrix element [see (V.4.8) and (VI.2.26')]. More picturesquely, one visualizes the incident projectile passing near the target and exciting the latter or transferring a particle to it and then departing without further exchange of energy or mass. Clearly, it is possible that more than one interaction can occur before the final state is achieved. For example, in the case of a particle transfer reaction to the ground state of the residual nucleus, the particle may be transferred to form an excited state of the residual nucleus, which upon a second interaction makes a transition to its ground state. Or in the case of elastic scattering of a deuteron, one step might involve the transfer of the deuteron's neutron to the target, followed by the second step, in which the neutron is emitted and combines with the proton to reform the deuteron. Both of these examples are *two-step reactions*. The reader can devise other examples of two-step reactions or indeed, reactions involving many steps. One refers to this class as *multistep (direct) reactions*. In this chapter we develop the theoretical framework in which these reactions can be studied.

When will the multistep process be important? Certainly, when the single-step reaction cross section is abnormally reduced, as occurs for production at large angles, for large energy loss, and for large angular and linear momentum transfers. It may occur because of poor overlap between the initial and final wave functions (because of poor momentum matching) for deformed nuclei if a considerable change in shape were to occur. On the other hand, there may be specially favored transitions to intermediate states that can serve as doorway

states en route to the final state. Two reactions we refer to later in this chapter may serve as examples. The excitation of the 4_1^+ state of a vibrational nucleus can be accomplished by either a single step induced by a fourth-order multipole or by two quadrupole steps proceeding therefore through a 2_1^+ intermediate state. The amplitude for these steps are comparable. In the transfer (p, t) reaction, the ground state-to-ground state reaction is favored in superconducting nuclei. In considering the excitation of the 2^+ level by this reaction, one must include not only the single-step but also the two-step reaction, in which the first step is ground state-to-ground state transition, followed by an inelastic excitation. Or the inelastic excitation can occur in the target nucleus and the transfer to the excited state of the final nucleus follows.

As the change from the initial nuclear structure increases, more steps may become important. However, the number of steps is limited since the probability for an individual step is less than unity. At higher energies, the probability for any single step is much reduced, with the consequence that at sufficiently high energy the single-step approximation suffices.

On the other hand, at sufficiently low energies the incident projectile may lose so much energy to the target nucleus that it becomes trapped and eventually fuses with the target to form a compound nucleus. Reemission of the projectile or other particles now occurs through an evaporation-like process, as described in Chapter IV. Of course, if the energy is high enough, the system may emit before the compound nucleus is formed; this process is referred to as *pre-compound reaction*. After a number of steps, precompound emission becomes improbable and the compound nucleus is formed. In this book we use the term *statistical multistep compound reaction* to describe both the precompound emission and the formation of the compound nucleus.

Of course, in a given reaction, all of the reaction types discussed above can occur; that is, the reaction can be single-step and multi-step direct. It can lead to the formation of a compound nucleus, or it can terminate before the compound nucleus is formed, as in the multistep compound reaction just discussed. These possibilities are reflected in the spectrum of a given reaction product at a given emission angle. A typical spectrum for a (p, n) reaction is illustrated in Fig. 1.1, where the double differential cross section for the production of a neutron at an energy E_n and at angle ϑ_0 is plotted as a function of neutron energy. The incident proton has an energy of some tens of MeV. As indicated in the figure, each of the processes discussed above dominates a particular spectral region. This is a qualitative rather than a quantitative association. But by and large, the excitation of individual low-lying energy levels in the residual nucleus proceeds via the single-step direct process. On the other hand, the low-energy slow neutrons are for the most part produced after the target nucleus and incident proton combine to form a compound nucleus. As one goes away from the extremes, the multistep processes become dominant. On the low-energy end, emission before the compound nucleus is fully developed takes place, while at the high-energy end, the increased energy loss to the target is more readily obtained in several steps than in one. In the intermediate region

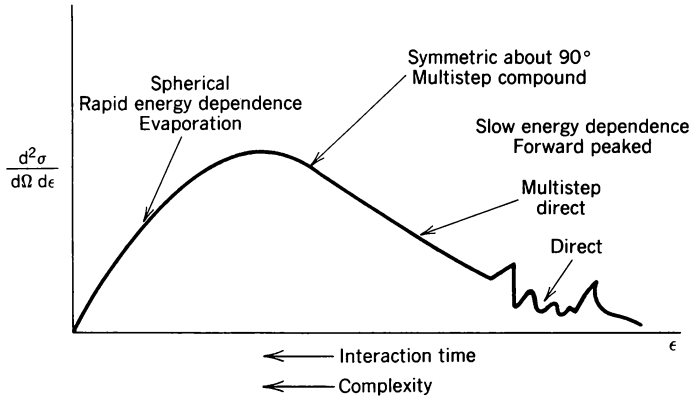


FIG. 1.1. Neutron energy (E) spectrum of an angle $\vartheta = \vartheta_0$.

far from the extremes, both the multistep direct and compound reactions play equally important roles.

With a change in the angle ϑ_0 , the relative emphasis on the various processes changes. At forward angles the single direct process will dominate and there will be relatively little cross section in the low-energy part of the spectrum. At large angles, the multistep direct process will be important for relatively high neutron energies, while the evaporation and multistep compound reactions will dominate the low-energy end of the spectrum.

At low energies of the incident projectile, one can expect that the compound and multistep compound reactions will dominate since it will be relatively easy for the projectile and target to fuse after relatively few steps. However, as the projectile energy increases, the direct processes become increasingly important and eventually make the major contribution to the cross section.

Increasing E_n in Fig. 1.1 maps qualitatively into decreasing interaction time. For large E_n , the angular distribution is forward peaked, while variation of the cross section with projectile energy is slow. Both features are characteristic of a short interaction time (i.e., the time during which the projectile and target interact). The slow energy dependence, using the Heisenberg uncertainty relation, directly indicates short interaction times. The forward peaking corroborates this result since the information indicating the incident direction is preserved. For small E_n the angular distribution in the evaporation region is spherical, indicating complete loss of information regarding the incident direction and therefore a long interaction time. As one moves into the multistep compound domain, the angular distribution is symmetric about 90° but is definitely anisotropic. The variation in cross section with energy is rapid (see the discussion of Ericson fluctuations in Chapter IV), demonstrating that the interaction time is relatively long.

One anticipates that a longer interaction time indicates a greater number of steps. Moreover, an increasing number of steps correlates with increasing complexity of the wave function. These correlations are indicated in Fig. 1.1.

This sketch of the emitted spectrum omits the influence of special features such as giant resonances. This depends critically on the nature of the interference between the resonant and nonresonant amplitudes. If the excitation energy is sufficiently high, so that many levels in the residual nucleus can be excited, it is anticipated that on averaging over these levels, the interference term will average to zero. Then the cross section will be a sum of the cross sections for the resonant and for nonresonant processes.

The formal treatment of multistep direct processes can proceed by evaluating the transition matrix to n th order in the coupling potential v , where n is the number of steps. For example, for a three-step process,

$$\begin{aligned} \mathcal{T}_{fi} = & \langle \phi_f^{(-)} v \phi_i^{(+)} \rangle + \left\langle \phi_f^{(-)} v \frac{1}{E^{(+)} - H} v \phi_i^{(+)} \right\rangle \\ & + \left\langle \phi_f^{(-)} v \frac{1}{E^{(+)} - H} v \frac{1}{E^{+} - H} v \phi_i^{(+)} \right\rangle + \dots \end{aligned} \quad (1.1)$$

where $\phi_i^{(+)}$ and $\phi_f^{(-)}$ are the initial and final wave functions, $1/(E^{(+)} - H)$ is the intermediate-state propagator, and H is the intermediate-state Hamiltonian. The spectral decomposition of $1/(E^{(+)} - H)$ provides various possibilities for intermediate states. The first term in (1.1) is the single-step, the second term the two-step, and the last term the three-step amplitude. We discuss later how these terms might be evaluated.

Equation (1.1) is adequate if v is relatively weak but fails if the coupling is strong. This is, in fact, the case when the low-lying collective states are involved, for then a particular multipole moment (e.g., the quadrupole) of the coupling potential can produce, with substantial probability, a particular member of the band of collective states. As a consequence, iterations of the coupling can be appreciable. Moreover, because of the close relation of the collective states to each other, there can be phase relations among the various multistep amplitudes that will lead to significant interference effects. An expansion like (1.1) is not useful under these circumstances.

Instead, one must put all of these excitations and the ground state on a more-or-less equal footing. Toward this end, one employs the *multichannel* optical model described in Chapter V [Eqs. (8.5), (8.6), and (8.7)], which takes the form

$$(E - H_{\text{eff}})P\Psi = 0 \quad (1.2)$$

where P projects on to all the channels of interest. H_{eff} contains the effects of the omitted channels, usually energy averaged, so that H_{eff} is an optical model Hamiltonian. One must be careful to distinguish if from the *single-channel*

optical model of Chapter V. In the first place, H_{eff} involves explicitly more than one channel, whereas the single-channel optical model deals only with the elastic channel; the effects of all the other channels are contained in the single-channel optical model Hamiltonian. As a consequence, the magnitude of the absorptive component of the single-channel optical Hamiltonian will be larger (often, substantially) than the absorptive component of H_{eff} .

Upon expressing $P\Psi$ in terms of the channels included in P , (1.1) becomes a set of coupled Schrödinger equations. The steps of which we spoke earlier are generated by the coupling between the channels. In principle, one can proceed by solving these equations exactly, a procedure that is practical only if the number of these equations is not too large. On the other hand, when the number of coupled channels is large, statistical methods can be employed. The resulting process is referred to as the *statistical multistep direct reaction*. There are in-between situations in which the coupling among some special channels has to be treated exactly, while statistical methods will suffice for the remainder.

In summary, the multistep direct reactions can be treated using (1) higher-order DWA, (2) through the use of coupled channels, and finally (3) when the number of channels becomes large by using the statistical multistep direct theory. As remarked earlier, a discussion of the formation of the compound nucleus, including the precompound emission, will lead to the theory described as the statistical multistep compound reaction.

2. COUPLED CHANNELS AND HIGHER-ORDER DWA[‡]

It is convenient to combine the discussion of the coupled-channel method and the higher-order DWA, which is a particular approximation to the results obtained using the coupled-channel method. Moreover, at the start, for reasons of simplicity, we shall be concerned only with inelastic scattering, in which the target nucleus is excited by the incident projectile. It will be again assumed, for simplicity that the multistep process involves only excited states of the target. The Pauli principle required if the projectile is composed of nucleons will also be disregarded in this discussion. (See Section III.5, for a rigorous treatment.)

To obtain the coupled-channel equations, expand $P\Psi$ of (1.2) into the finite series

$$P\Psi = \sum_i \phi_i(0) \psi_i(1, 2, \dots) \quad (2.1)$$

where ψ_i are the wave functions describing the ground and excited states of the target, while ϕ_i depends on the coordinates of the projectile relative to the center of mass of the target nucleus. The optical model Hamiltonian H_{eff} is the sum of the target Hamiltonian H_t , the kinetic energy operator T giving the

[‡]Tamura (65, 74); Satchler (83).

relative motion of the projectile–target nucleus system and the interaction $V^{(pt)}$ between the projectile and the target:

$$H_{\text{eff}} = H_t + T + V^{(pt)} \quad (2.2)$$

The wave functions ψ_i satisfy the equations

$$\begin{aligned} H_i \psi_i &= \varepsilon_i \psi_i \\ \langle \psi_i | \psi_j \rangle &= \delta_{ij} \end{aligned} \quad (2.3)$$

Inserting (2.1) into (1.2), one obtains

$$[E - \varepsilon_i - T - \langle \psi_i | V^{(pt)} | \psi_i \rangle] \phi_i = \sum_{j \neq i} \langle \psi_i | V^{(pt)} | \psi_j \rangle \phi_j \quad (2.4)$$

These equations are to be solved subject to the boundary conditions at infinity. These are (1) that except for the incident channel (target nucleus in the ground state), all the ϕ_i behave as $e^{ik_i r_0}/r_0$ where $k_i = [(2\mu/\hbar^2)(E - \varepsilon_i)]^{1/2}$ as $r_0 \rightarrow \infty$; (2) the incident channel wave function consists of a plane wave plus an outgoing wave in the same limit.

The first-order DWA for the excitation of the state ψ_a is obtained if one assumes that ϕ_a couples only to the incident channel ϕ_0 , whose coupling to ϕ_a is neglected:

$$\begin{aligned} (E - \varepsilon_0 - T - V_{00})\phi_0 &= 0 \\ (E - \varepsilon_a - T - V_{aa})\phi_a &= V_{a0}\phi_0 \end{aligned} \quad (2.5)$$

where we have adopted the notation

$$V_{ab} \equiv \langle \phi_a | V^{(pt)} | \phi_b \rangle$$

The second-order DWA is obtained if one assumes that ϕ_a couples to the other states ϕ_b , which, however, couple only to the incident channel:

$$\begin{aligned} (E - \varepsilon_0 - T - V_{00})\phi_0 &= 0 \\ (E - \varepsilon_b - T - V_{bb})\phi_b &= V_{b0}\phi_0 \end{aligned} \quad (2.6a)$$

or

$$\phi_b = \frac{1}{E^{(+)} - \varepsilon_b - T - V_{bb}} V_{b0}\phi_0 \quad (2.6b)$$

The equation for ϕ_a is

$$(E - \varepsilon_a - T - V_{aa})\phi_a = V_{a0}\phi_0 + \sum_{b \neq a} V_{ab}\phi_b \quad (2.7)$$

Substituting for ϕ_b from (2.6), one obtains

$$(E - \varepsilon_a - T - V_{aa})\phi_a = V_{a0}\phi_0 + \sum_{b \neq a} V_{ab} \frac{1}{E^{(+)} - \varepsilon_b - T - V_{bb}} V_{b0}\phi_0 \quad (2.8)$$

The transition matrix is then

$$\mathcal{T}_{a0} \simeq \langle \phi_{a,0}^{(-)} | V_{a0} \phi_0^{(+)} \rangle + \sum_{b \neq a} \left\langle \phi_{a,0}^{(-)} \left| \left[V_{ab} \frac{1}{E^{(+)} - \varepsilon_b - T - V_{bb}} V_{b0} \right] \phi_0^{(+)} \right. \right\rangle \quad (2.9)$$

where

$$(E - \varepsilon_a - T - V_{aa})\phi_{a,0}^{(-)} = 0$$

The first term is the first-order DWA, while the second is the second-order DWA and is in the form given by (1.1). One can evaluate the second-order DWA directly from (2.9), but in practice it is simpler to numerically integrate the equation for ϕ_0 , then solve (2.6a) for ϕ_b . Substituting these results in (2.7), one then solves for ϕ_a directly.

When the coupling is strong, one must resort to the complete coupled equations, (2.4), and integrate them numerically. One procedure, which we shall now develop, reduces the coupled equations to coupled radial linear differential equations by eliminating all the angle and spin dependence. Assume that the potential V^{pt} is a scalar, so that the total angular \mathbf{J} of the interacting system is conserved. We may therefore restrict the discussion to partial waves with a given J . The angular momentum of the system consists of the spins of the target and projectile j_t and j_p , respectively, added to their relative angular momentum \mathbf{l} :

$$\mathbf{J} = \mathbf{j}_t + \mathbf{j}_p + \mathbf{l} \quad (2.10)$$

Two coupling schemes that lead to the spin-angle functions with J and M_J quantum numbers have been used. The *channel spin coupling* scheme proceeds in two steps, first coupling the spins,

$$\mathbf{j}_t + \mathbf{j}_p = \mathbf{S} \quad (2.11)$$

and then coupling \mathbf{S} and \mathbf{l} to form \mathbf{J} :

$$\mathbf{S} + \mathbf{l} = \mathbf{J} \quad (2.12)$$

The spin-orbit coupling scheme first couples \mathbf{j}_p and \mathbf{l} to form \mathbf{J}_p and then couples \mathbf{J}_p to \mathbf{j}_t to form \mathbf{J} :

$$\begin{aligned} \mathbf{j}_p + \mathbf{l} &= \mathbf{J}_p \\ \mathbf{J}_p + \mathbf{j}_t &= \mathbf{J} \end{aligned} \quad (2.13)$$

The wave functions corresponding to these two coupling schemes are connected by the $6-j$ symbol [see Appendix A, Eq. (2.85), in deShalit and Feshbach (74)]. Which coupling scheme is more convenient to use depends on the physics of the problem: Spin-orbit coupling would be appropriate when the spin-orbit interaction is strong.

We shall provide an explicit discussion of the coupled channel for channel spin coupling only since the algebra is simplest for that case. In order to separate the geometric factors as completely as possible, the dependence on l of $\phi_i(0)$ in (2.1) will be factored out, leaving only the radial dependence. For a given total angular momentum of the system J , z component M , we couple

$$\mathcal{Y}_{lm} = i^l Y_{lm}(\hat{\mathbf{r}}_0)$$

with the channel spin wave function $\psi_\alpha(Sm_s; \mathbf{r})$ to form a wave function with J and M :

$$\Phi_\alpha(JM; S, l) = \sum_{m, m_s} (lm Sm_s | JM) \mathcal{Y}_{lm}(\hat{\mathbf{r}}_0) \psi_\alpha(Sm_s; \mathbf{r}) \quad (2.14)$$

The subscript α orders the possible wave functions whose spin is given by J . The variable \mathbf{r} represents all the target nuclear coordinates. The functions Φ_α satisfy

$$\langle \Phi_\alpha(J'M'; S, l') | \Phi_\beta(JM; S', l) \rangle = \delta_{JJ'} \delta_{MM'} \delta_{ll'} \delta_{SS'} \delta_{\alpha\beta} \quad (2.15)$$

The integrations are carried out over \mathbf{r} , the internal coordinates, and Ω_0 , the angular coordinates for the relative motion. The channel spin wave function $\psi(S, m_s)$ is obtained by coupling the target nucleus wave function $\psi(j_t m_t)$ and the spin wavefunction $\chi(j_p m_p)$ of the projectile:

$$\begin{aligned} \psi_\alpha(Sm_s; \mathbf{r}) &= \psi_\alpha((j_p j_t) S(m_s; \mathbf{r})) \\ &= \sum_{m_p, m_t} (j_p m_p j_t m_t | Sm_s) \psi_\alpha(j_t, m_t) \chi(j_p, m_p) \end{aligned} \quad (2.16)$$

One now expands $P\Psi$ in terms of $\Phi_\alpha(JM; Sl)$, in that way providing the dependence of $P\Psi$ on \mathbf{r} and $\hat{\mathbf{r}}_0$. The coefficients of the expansion will then depend only upon r_0 . Therefore,

$$P\Psi = \frac{1}{r_0} \sum_{\alpha} u_\alpha(J(Sl); r_0) \Phi_\alpha(JM; Sl) A(JM; S; l_i) \quad (2.17)$$

The coefficient $A(JM; S; l_i)$ is chosen so that the incident channel associated with the ground state of the target and denoted by $S; l_i$ contains the only incoming wave. We shall determine this coefficient later. Introducing (2.17) yields sets of

coupled differential equations for u_α . Only those u_α with the same J and M will couple. For a given J , these equations are

$$\begin{aligned} & \left\{ E - \varepsilon_\alpha + \frac{\hbar^2}{2\mu} \left[\frac{d^2}{dr_0^2} - \frac{l(l+1)}{r_0^2} \right] - (J(Sl) \| V^{(pt)} \| J(Sl)) \right\} u_\alpha(J(Sl); r_0) \\ &= \sum_{\substack{\alpha \neq \alpha' \\ S', l'}} (J(Sl) \| V^{(pt)} \| J(S'l') u_{\alpha'}(J(S'l'); r_0) \end{aligned} \quad (2.18)$$

The next step is to evaluate the reduced matrix elements of $V^{(pt)}$. For this purpose, we expand $V^{(pt)}$ in a multipole series:

$$V^{(pt)} = \sum \mathbf{Q}_\lambda(\mathbf{r}) \cdot \mathbf{Y}_\lambda(\Omega_0) v_\lambda(r_0) \quad (2.19)$$

Note that this expansion assumes a term-by-term factorization of the dependence \mathbf{r} and r_0 , which we will justify later. Evaluating the matrix elements can be accomplished by using (A.2.54) of deShalit and Feshbach (74). One obtains

$$\begin{aligned} (J(Sl) \| V^{(pt)} \| J(S'l')) &= \sum_\lambda (-)^{l+J+S'} \sqrt{2J+1} \begin{Bmatrix} S & l & J \\ l' & S' & \lambda \end{Bmatrix} \\ &\times (S \| Q_\lambda \| S') (l \| Y_\lambda \| l') v_\lambda(r_0) \end{aligned}$$

Inserting (A.2.48) of deShalit and Feshbach (74) for $(l \| Y_\lambda \| l')$, one finally has

$$\begin{aligned} (J(Sl) \| V^{(pt)} \| J(S'l')) &= \sum_\lambda (-)^{J+S+(l'-l)/2} \sqrt{\frac{(2l+1)(2l'+1)(2\lambda+1)(2J+1)}{4\pi}} \\ &\times \begin{Bmatrix} S & l & J \\ l' & S' & \lambda \end{Bmatrix} \begin{pmatrix} l & \lambda & l' \\ 0 & 0 & 0 \end{pmatrix} (S \| Q_\lambda \| S') v_\lambda(r_0) \end{aligned} \quad (2.20)$$

A further reduction is possible since $\mathbf{S} = \mathbf{j}_i + \mathbf{j}_p$, and Q_λ depends only on \mathbf{r} . Equation (A.2.55) of deShalit and Feshbach (74) would be used for this purpose. The complete formula is given by Tamura (65). From (2.20) we see that

$$\begin{aligned} \mathbf{S} + \mathbf{l} &= \mathbf{J} \quad (a) & \mathbf{l}' + \mathbf{l} &= \lambda \quad (c) \\ \mathbf{S}' + \mathbf{l}' &= \mathbf{J} \quad (b) & \mathbf{S}' + \mathbf{S} &= \lambda \quad (d) \end{aligned} \quad (2.21)$$

and

$$l + \lambda + l' = \text{even number} \quad (2.22)$$

Equations (2.21a) and (2.21b) express the conservation of angular momentum in the process. Equations (2.21c) and (2.21d) give the changes in l and S induced by the interaction. From (2.22) one obtains the conservation of parity. Note

that in (2.20) the other properties of the target nucleus are contained in the reduced matrix elements ($S \parallel Q_\lambda \parallel S'$). In principle, these can be determined from experimental data and compared with the predictions of the theory of the target nucleus.

As long as S' and l' satisfy (2.21b), $u(J(S'l'))$ will be coupled to $u(J(Sl))$. The number of coupled equations increases as the number of excited states are included in the calculation. It increases as the energy increases. To illustrate, suppose that the projectile is an α -particle (intrinsic spin 0), so that S equals the angular momentum of the nuclear levels. Suppose these are 0, 2, 4, where the spin of the ground state is 0, and suppose that λ is even. The value of J for the l th particle wave is l . For $S = 2$, $|J - S| < l' < J + S$, so that for $J (= l) > S$, l' can be $l - 2$, l , or $l + 2$. Similarly, for $S = 4$ if $J \geq 4$, l' can be $l - 4$, $l - 2$, l , $l + 2$, $l + 4$. If $J < 4$, l' can equal $l + 4$, $l + 2$, l , and as on, breaking off at $l' = 4 - J = 4 - l$. Thus if $J \geq 4$, the number of coupled equations is nine. The number of J 's is given approximately by $J = l_{\max}$, where $l_{\max} \simeq k_i R$, where k_i is the incident value of k and R is the nuclear radius.

Returning to the coupled equations, (2.18), one particular (S, l) will correspond to incident channel. For that channel

$$u_i(J(Sl))_{r_0 \rightarrow \infty} e^{-i(k_i r_0 - l\pi/2)} - S_{Jl}(S_i l_i, S_i l_i) e^{i(k_i r_0 - l\pi/2)} \quad (2.23a)$$

For other channels with the same value of J ,

$$u_\alpha(J(S'l'))_{r_0 \rightarrow \infty} - S_{J\alpha}(S_i l_i, S' l') e^{i(k_\alpha r_0 - l'\pi/2)} \quad (2.23b)$$

$S_{J\beta}(Sl; S'l')$ is the S matrix in terms of which the amplitude for elastic and inelastic scattering can be expressed.

Using (2.23) it is now possible to calculate the reaction amplitudes in terms of S_J . One first needs the expansion for the incident wave function, $\Psi_{JM}^{(i)}$, where

$$\begin{aligned} \Psi^{(i)} &= e^{i\mathbf{k}_i \cdot \mathbf{r}_0} \psi_i(S_i m_{si}; \mathbf{r}) \\ &= 4\pi \sum_{lm} j_l(k_i r_0) Y_{lm}^*(\hat{\mathbf{k}}_i) l^l Y_{lm}(\hat{\mathbf{r}}_0) \psi_i(S_i m_{si}; \mathbf{r}) \\ &= 4\pi \sum_{lm} j_l(k_i r_0) Y_{lm}^*(\hat{\mathbf{k}}_i) \sum_{JM} \Phi(JM; S_i l) (lm S_i m_{si} | JM) \end{aligned}$$

Therefore,

$$\Psi_{JM}^{(i)} = 4\pi \sum_{lm} j_l(k_i r_0) Y_{lm}^*(\hat{\mathbf{k}}_i) \Phi(JM; S_i l) (lm S_i m_{si} | JM) \quad (2.24)$$

Asymptotically,

$$\Psi_{JM}^{(i)} \rightarrow \frac{2\pi i}{k_i r_0} \sum (e^{-i[k_i r_0 - (\pi/2)l]} - e^{i[k_i r_0 - (\pi/2)l]}) Y_{lm}^*(\hat{\mathbf{k}}_i) \Phi(JM; S_i l) (lm S_i m_{si} | JM)$$

Because of the interaction, $\Psi_{JM}^{(i)}$ becomes Ψ_{JM} :

$$\begin{aligned} \Psi_{JM} \rightarrow \frac{2\pi i}{k_i r_0} \sum_{lm}^{lm} (\delta_{S'S} e^{-i[k(S') - (\pi/2)l]} - S_J(S_i l, S' l') e^{i[k(S') r_0 - (\pi/2)l]} \\ \times Y_{lm}^*(\hat{\mathbf{k}}_i) \Phi(JM; S' l') (lm S_i m_{si} | JM) \end{aligned}$$

Expanding $\Phi(JM; S' l')$ according to (2.14), and taking the z direction to be along \mathbf{k}_i so that

$$Y_{lm}^*(\hat{\mathbf{k}}_i) = \sqrt{\frac{2l+1}{4\pi}} \delta_{m0}$$

one finally obtains the reaction amplitude:

$$\begin{aligned} f_{JM}(S_i, m_{si} \rightarrow S', m'_s) = \frac{\sqrt{\pi}}{k_i} \sum_{l'l'm'_s}^{l'l'S'} i^{l'} \sqrt{2l+1} (l0 S_i m_{si} | JM) (l' m' S' m'_s | JM) \\ \times [\delta_{S'S_i} - S_J(S_i l, S' l')] Y_{l'm'}(\hat{\mathbf{r}}_0) \end{aligned} \quad (2.25)$$

The cross section is given by

$$\sigma(S_i \rightarrow S') = \frac{k(S')}{k_i} \frac{1}{2S_i + 1} \sum_{m_{si}, m'_s} |f_{JM}(S_i m_{si} \rightarrow S' m'_s)|^2 \quad (2.26)$$

Although the sums over the m 's can be performed analytically, one gains little advantage over inserting (2.25) in (2.26) and summing numerically.

The results obtained for other coupling schemes and the methods used for integrating the differential equations (2.18) are discussed in detail by Satchler (83) in Chapter 5 of his book. With these formalisms, one can discuss inelastic and elastic scattering, including as many possible steps as needed and practicable, extracting from the data the S matrix and finally the target nuclear parameters ($S \parallel Q_\lambda \parallel S'$).

For the case of the deformed rotor of Bohr and Mottelson (62), the procedure described above is generally replaced by the adiabatic approximation. In this approximation, the problem is solved, keeping the five macroscopic variables, the three Euler angles giving the orientation of the body-fixed axes with respect to a frame fixed in space, and the two variables β and γ giving the vibrational degrees of freedom about the average deformation β_0 and γ_0 . It is assumed that the variation of these five variables during the course of the interaction will be small, a condition that is well satisfied above a rather low projectile energy.

Under these assumptions, we solve for the *elastic* scattering in the *body*-fixed frame, obtaining an amplitude that is a function of β and γ . Transforming to the space-fixed frame, one obtains an amplitude that is a function of β , γ , and

the Eulerian angles. The amplitudes for inelastic or elastic scattering are obtained by taking matrix elements between the initial ground state of the target and the final state.

Let the interaction between the projectile and the target in the body-fixed frame be

$$V_\lambda = \sum_{\lambda} V_\lambda(r, \alpha, \beta) [i^\lambda Y_{\lambda 0}(\hat{\mathbf{r}})]^* \quad (2.27)$$

where we have assumed axial symmetry, as indicated by the zero projection of λ along the symmetry axis. Differing orbital angular momenta will be coupled so that the coupled equations for adiabatic elastic scattering take on the form

$$\left[\frac{d^2}{dr^2} + k^2 - \frac{l'(l' + 1)}{r^2} - \frac{2m}{\hbar^2} \langle l' \mu | V | l' \mu \rangle \right] u_{l'l}^{(\mu)}(r) = \frac{2m}{\hbar^2} \sum_{l''} \langle l' \mu | V | l'' \mu \rangle u_{l''l}^{(\mu)}(r) \quad (2.28)$$

where μ is the projection of \mathbf{l} along the symmetry axis and m is the reduced mass. Note that μ does not change because of the zero projection of $Y_{\lambda 0}$ in the interaction, (2.27). The indicated matrix elements are readily evaluated using (A.2.25) of deShalit and Feshbach (74). One obtains

$$\begin{aligned} \langle l' \mu | V | l \mu \rangle &= \sum_{\lambda} V_\lambda(r, \alpha, \beta) i^{l-l'-\lambda} (-)^{\mu} \\ &\times \left[\frac{(2l' + 1)(2\lambda + 1)}{4\pi} 2l + 1 \right]^{1/2} \begin{pmatrix} l' & \lambda & l \\ \mu & 0 & -\mu \end{pmatrix} \begin{pmatrix} l' & \lambda & l \\ 0 & 0 & 0 \end{pmatrix} \end{aligned} \quad (2.29)$$

Using the boundary conditions given in (2.23) suitably modified, one obtains the adiabatic elastic scattering amplitude in the body-fixed frame:

$$f(\mathbf{k}_i \rightarrow \mathbf{k}) = \frac{2\pi}{k_i} \sum_{l, l', \mu} [\delta_{l'l} - S_{l'l}^{(\mu)}] Y_{l\mu}^*(\hat{\mathbf{k}}_i) Y_{l'\mu}(\hat{\mathbf{k}}) \quad (2.30)$$

where $\hat{\mathbf{k}}$ is taken in the direction of \mathbf{r}_0 . We now refer $Y_{l\mu}^*$ and $Y_{l'\mu}$ to the space-fixed frame using (A.2.26) of deShalit and Feshbach (74):

$$Y_{l\mu}^*(\hat{\mathbf{k}}_i) Y_{l'\mu}(\hat{\mathbf{k}}) = \sum_{\mu'', \mu'''} (-)^{\mu} Y_{l, \mu''} D_{\mu''', -\mu}^{(l)} Y_{l', \mu'} D_{\mu', \mu}^{(l')}$$

The product of the two D functions can be expressed in terms of a single D using (A.2.75) of deShalit and Feshbach (74) with the result

$$\begin{aligned} Y_{l\mu}^*(\hat{\mathbf{k}}_i) Y_{l'\mu}(\hat{\mathbf{k}}) &= \sum_{\mu'', \mu''', L} (-)^{\mu} (2L + 1) Y_{l\mu''}(\hat{\mathbf{k}}_i) Y_{l'\mu'}(\hat{\mathbf{k}}) \\ &\times \begin{pmatrix} l & l' & L \\ \mu'' & \mu' & M \end{pmatrix} \begin{pmatrix} l & l' & L \\ -\mu & \mu & 0 \end{pmatrix} D_{M0}^{(L)*} \end{aligned}$$

But the sums over μ' and μ'' give just the tensor product

$$[Y_l \otimes Y_{l'}]_{L, -M} [(-)^{l-l'+M} / \sqrt{2L+1}],$$

so that

$$f_{L, -M}(k_i \rightarrow k) = \frac{2\pi i}{k_i} \sum_{l, l', \mu, L} (-)^{\mu+L} \sqrt{2L+1} [\delta_{l'l} - S_{l'l}^{(\mu)}] [Y_l \otimes Y_{l'}]_{L, M} \times \begin{pmatrix} l & L & l' \\ -\mu & 0 & \mu \end{pmatrix} D_{M0}^{(L)} \quad (2.31)$$

The amplitude for a transition from the ground state S_i to an excited state S' is given by $\langle S' | f_{L, -M}(\mathbf{k}_i \rightarrow \mathbf{k}) | S_i \rangle$. In this context, $f_{L, -M}$ is a tensor of rank L , component M , and will allow the same transitions as an L multipole with the condition $S' = S_i + L$.

From a practical point of view, the usefulness of this approach is limited by the number of coupled differential equations in (2.28). This is determined for a given l by the condition $l' = l + \lambda$ and the parity condition $(l + l' + \lambda)$ even. For a small λ , the number of coupled equation will thus be acceptable, although solutions must be obtained for each μ and for all relevant l 's.

3. APPLICATIONS

The coupled-channel formalism developed in Section 2 has been applied to elastic and inelastic scattering of a variety of projectiles, nucleons, light and heavy ions, pions by a variety of target nuclei, and over a wide range in energy. Usually, this method of analysis is applied to direct reactions when the DWA approximation or the spherical optical model of Chapter V fails. A rough indication of the importance of a given step ($a \rightarrow b$) where an energy-conserving excitation of b is possible is given by the parameter $(1/2\pi)(\mu k_b/\hbar^2) J_{ba}$, where J_{ba} is the volume integral of the coupling potential, k_b the wave number of the projectile after excitation of b , and μ the reduced mass. For example, the strength of a two-step transition $a \rightarrow b \rightarrow c$ compared to a one-step transition $a \rightarrow c$ is given by

$$\frac{1}{2\pi} \frac{\mu k_b}{\hbar^2} \frac{J_{cb} J_{ba}}{J_{ca}}$$

If this quantity is small, it is unlikely that the two-step transition will be of importance. It should be noted that there will always be additional contributions from compound nuclear formation. These can be particularly important at low energies and back angles.

A situation most likely to require the use of the coupled-channel equations occurs when the target nuclear energy levels are collective. In that case, the wave functions of these levels are simply connected, for example, by the application of a raising and lowering operator \hat{O} , enhancing the possibility of

relatively strong and coherent coupling between the levels. This will generally take place if a significant component of the projectile–nucleus interaction is proportional to $\hat{0}$. Moreover, because of the simple connection, there will be well-defined phase relations among the various multistep reaction amplitudes, including the single step. Under these circumstances, constructive interference can occur, leading to a strong enhancement of the amplitude; or of course, the interference could be destructive, with a consequent anomalous decrease in cross section. Moreover, the associated angular distributions will, because of the interference, oscillate irregularly.

Not surprisingly, inelastic scattering from deformed and vibrational nuclei furnishes an excellent example of the use of a coupled-channel analysis. The procedure used was proposed by Glendenning Hendrie, and Jarvis (68) for inelastic scattering of 50-MeV α -particles. A spherical optical model potential is adjusted so as to fit the experimental data (angular distribution, total cross section, polarization, etc.) for elastic scattering by spherical nuclei in the neighborhood of the collective target nuclei to be studied and in the projectile energy range of interest. In the case of neutron scattering to be discussed later, this analysis is quite extensive, going to the lowest energies, including the strength functions (Chapter IV), as well as the zero energy scattering length. This potential, (V.2.38), will depend parametrically on radius parameters R_0 , R_W , R_D , and R_{s0} , where R_0 enters into the central potential. R_W is the volume absorbing radius, R_D is the surface absorbing radius, and R_{s0} is the spin orbit radius. In most cases the “standard” form (V.2.38) has been used, the radial dependence given by the Woods–Saxon form, $(1 + e^{(r-R)/a})^{-1}$, and its derivative. To include the effects of deformation, one replaces R (where R can equal R_0 , R_W , R_D , or R_{s0}) by (VI.13.1) of deShalit and Feshbach (74):

$$R = R_0(1 + \sum \alpha_{\lambda\mu} Y_{\lambda\mu}(\theta, \phi)) \quad (3.1)$$

for a vibrational nucleus. The coefficients $\alpha_{\lambda\mu}$ are operators. For a deformed nucleus, as we have seen in the preceding section, the calculations are best performed in the body-fixed system, so that one write

$$R = R_0 \left(1 + \sum_{\lambda} \beta_{\lambda} Y_{\lambda 0}(\theta', 0) \right) \quad (3.2)$$

where θ' is the spherical angle in the body-fixed case. The coefficients β_{λ} are not operators. The next step is to express the resulting potential in the forms given by (2.19) and (2.27). For the case of the vibrating nucleus [see (3.1)], this is accomplished by expanding the potential in a power series in $\sum \alpha_{\lambda\mu} Y_{\lambda\mu}$. The matrix elements of Q_{λ} [(2.19) and (2.20)] will be proportional to the matrix elements of $\alpha_{\lambda\mu}$ between various vibrational states. For the deformed nucleus according to Tamura (65), the power series in $\sum \beta_{\lambda} Y_{\lambda 0}$ will not be adequate for large deformations, so that one must collect all the contributions to the coefficient of $Y_{\lambda 0}$ from higher powers of $\sum \beta_{\lambda} Y_{\lambda 0}$.

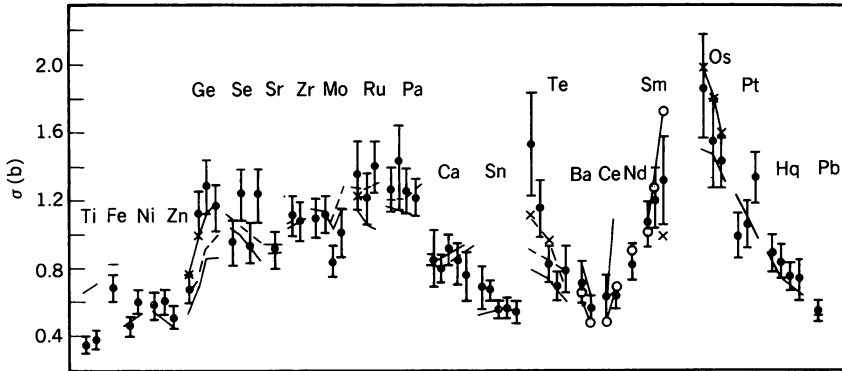


FIG. 3.1. Neutron inelastic scattering cross sections for scattering to first 2^+ levels at incident energies 300 keV above the excitation threshold. [Konobeevskii, Musaelyan, Popov, and Surkova (82)]. [From McEllistrem (85).]

Let us now turn to one example of the use of coupled equations: namely, the study of nuclear reactions induced by neutrons incident on vibrational and deformed target nuclei [McEllistrem (85)]. The strong deformation effects on inelastic neutron scattering are demonstrated by the strong peak in the Sm, Os, and Pt region shown in Fig. 3.1 [Konobeevskii, Musaelyan, Popov, and Surkova (82)]. A similar result is reported by Glasgow and Foster (71), who found that the spherical optical model adjusted to fit the neutron total cross section for a wide range of target nuclei failed for the deformed nuclei. Resolution of this difficulty required the coupled-channel analysis of the preceding section. In Fig. 3.2 a comparison is made between the experimental data for neutron scattering by ^{76}Se and ^{80}Se and two models, the spherical vibrator and the deformed potential model, in which the matrix elements are taken from Coulomb excitation. In Fig. 3.3 neutron scattering by ^{194}Pt is compared with the predictions of asymmetric rigid rotor model (ARM) of Davydov and Filippov [see deShalit and Feshbach (74, p. 484)] and the dynamic deformation models (PPQ) of Kumar (69, 85) or the interacting boson model (IBM) model of Arima and Iachello (75, 76, 78, 79) as given for this nucleus by Bijker, Dieprink, Scholten, and Spanhoff (80). A careful treatment of the contribution of the compound nuclear contribution was necessary because of the low neutron energy. In both examples, the central real potential and the surface absorbing potential were deformed. The spin-orbit potential was not deformed. A volume absorbing term was not included. To obtain the most accurate results, it was found necessary to include several of the levels that can couple to the state whose excitation is under study.

In both of these examples we note that one obtains good agreement with the data for both magnitude and angular distributions. Second, it is possible to distinguish among various models. In the case of Fig. 3.2 one can conclude that

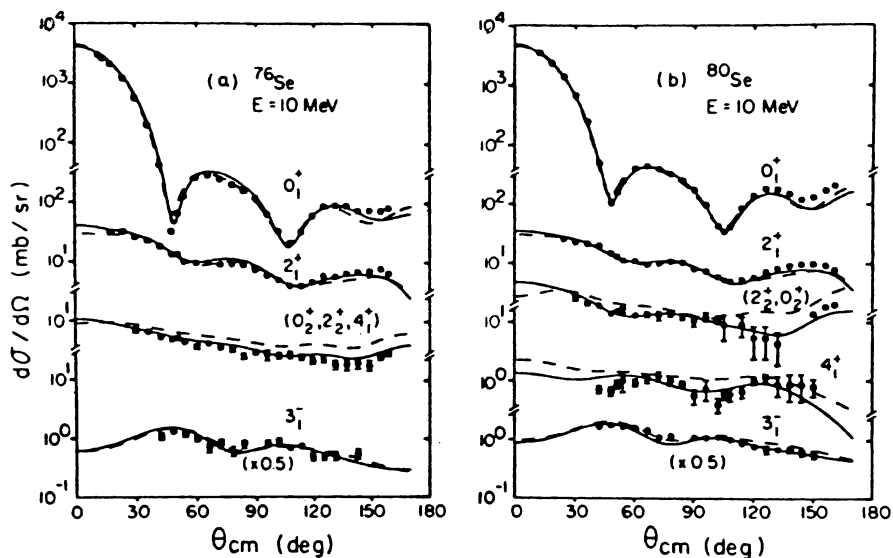
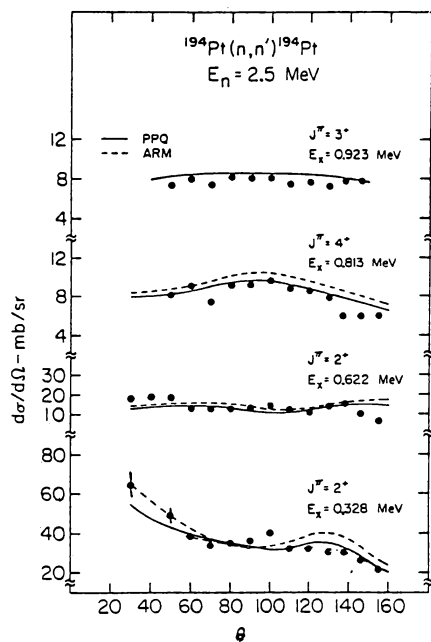
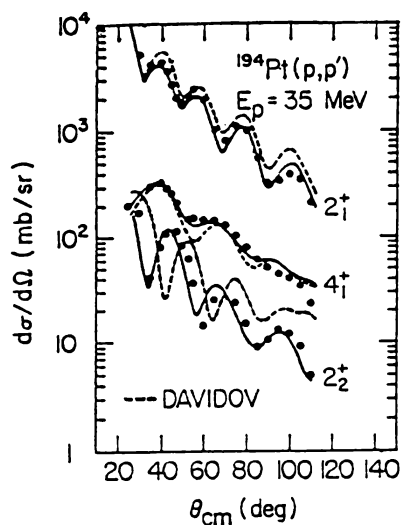


FIG. 3.2. Scattering cross sections for two Se isotopes. Dashed curves are for spherical vibrator calculations. Solid curves result from use of matrix elements deduced from Coulomb excitation measurements. (From McEllistrem (85).]



(a)



(b)

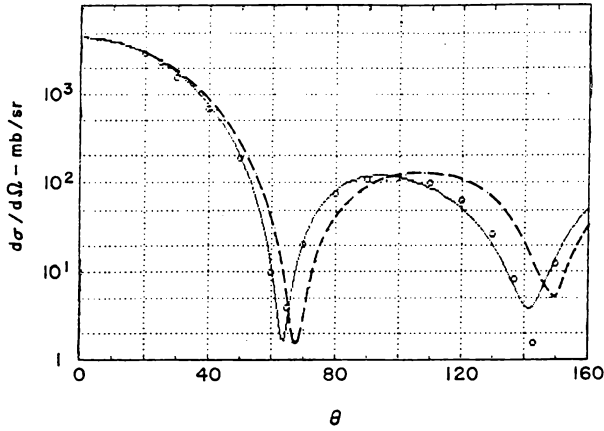


FIG. 3.4. Shape elastic scattering cross sections at 2.5 MeV for neutron scattering by ^{192}Os . Curves are for spherical one-channel (dashed) and for coupled-channel models fitted to the total cross section. [From McEllistrem (85).]

the spherical vibrator model does not describe the Se nuclei. In the Pt case (Fig. 3.3) one sees that the asymmetric rigid-rotor model is inferior to the dynamic deformation or the IBM model. (Note that the ordinates in these figures are the logarithm of the cross section indicated.) The latter models yield a γ soft description of ^{194}Pt for the energy levels, transition probabilities, and inelastic neutron scattering which the *rigid* rotor of the ARM model cannot match. Another conclusion that can be drawn from Fig. 3.2 and other investigations is that within a few percent the quadrupole moment for the *charge* distribution and for the *matter* distribution are equal. More generally, values of the deformation parameters β_λ obtained from neutron scattering are in agreement with values obtained with other probes.

The effects of deformation are also visible in the elastic scattering. Both the spherical potential and the coupled-channel potentials are adjusted so as to yield good agreement with the total cross section for neutrons, with energies between 0.25 and 4 MeV incident on ^{192}Os . The angular distributions calculated with these two options are substantially different (see Fig. 3.4)—with agreement with the data being obtained with the coupled-channel analysis.

FIG. 3.3. (a) Measured and calculated inelastic cross sections for the first four excited levels. PPQ is the model of Kumar (69). ARM is the asymmetric rotator model of Davydov and Filippov (58). (b) Inelastic scattering cross sections for lowest three excited levels. The solid curves are for the IBA model. [From McEllistrem (85).]

4. COUPLED-CHANNEL BORN APPROXIMATION (CCBA) AND TRANSFER REACTIONS

The examples of Section 3 demonstrate the strong coupling that a band of collective states exhibits in elastic and inelastic scattering, requiring the use of coupled channels. In a transfer reaction, one must take that coupling into account, as the transition between the target nucleus and the residual nucleus may be preceded by inelastic scattering to various members of the target nucleus band, and/or may be followed by inelastic scattering to members of residual nucleus collective band states.

The DWA was based on a two-channel *ansatz* for stripping given by (VI.2.3):

$$P\Psi = \mathcal{A}[u\phi + v\chi\psi] \quad (\text{VI.2.3})$$

In this equation, ϕ is the wave function of the residual nucleus, χ the internal deuteron wave function, ψ the ground-state wave function of the target nucleus, and u and v the channel wave functions for the proton and deuteron, respectively. The resultant DWA matrix element is given by (VI.2.46'):

$$\mathcal{T}_{dp}^{(\text{DWA})} = \langle U_{0,f}^{(-)}\phi | \mathcal{V}^{(f)} \mathcal{A}(v_{0,i}^{(+)}\chi\psi) \rangle \quad (\text{VI.2.46}')$$

where $v_{0,i}$ is usually taken to be the deuteron optical single-channel wave function. (For the definition of the other symbols, see Section VI.2.) To take the excited states of the target nucleus into account (we shall deal with this case only; the reader should be able to discuss the effect of including the excited states of the residual nucleus), one replaces (VI.2.3) as follows:

$$P\Psi = \mathcal{A}[u\phi + (\sum v_{\alpha}\psi_{\alpha})\chi] \quad (4.1)$$

The wave functions for the states of the target nucleus are given by ψ_{α} . The corresponding deuteron-nucleus channel wave functions are given by v_{α} . The analysis given in Section VI.2 beginning with (VI.2.3) is readily generalized. The major change is in the K matrix, which instead of being a 2×2 matrix is now an $(n+1) \times (n+1)$ matrix, where n equals the number of states of the target nucleus included in the sum in (4.1). The equations of Section VI.2 can be taken over completely if one replaces the v and V of that section by a semicolumnar matrix with elements v_{α} and V_{α} . The DWA approximation, now renamed CCBA, is obtained by neglecting the overlap integrals and the coupling to the proton channel. The result, replacing (VI.2.46'), is

$$\mathcal{T}_{dp}^{(\text{CCBA})} = \sum_{\alpha} \langle U_{0,f}^{(-)}\phi | \mathcal{V}^{(f)} \mathcal{A}(v_{0,\alpha}^{(i)}\psi_{\alpha}\chi) \rangle \quad (4.2)$$

where $v_{0,\alpha}^{(i)}$ are solutions of the many-channel optical model Schrödinger equation describing elastic and inelastic scattering of the deuteron by the target nucleus.

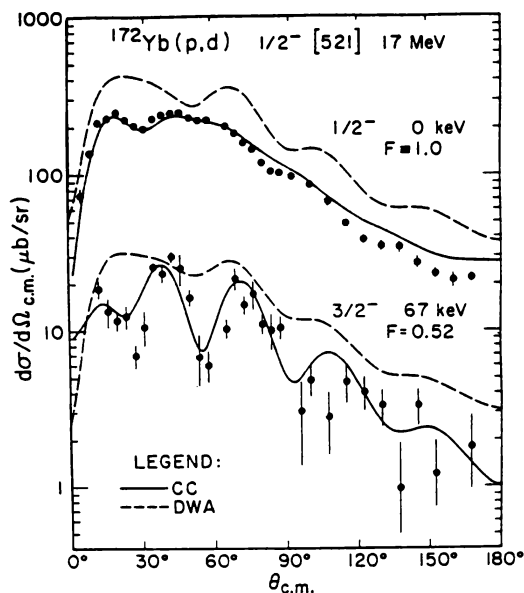


FIG. 4.1. Data and calculations for $^{172}\text{Yb}(p,d)^{171}\text{Yb}$ leading to the first two members of the ground band. The cross-section scale is the experimental one. The probable error for the absolute cross-section normalization is $\sim 30\%$. The coupled-channel calculations have been normalized individually for each state to the data. [From Ascuitto, King, McVay, and Sørensen (74).]

These are just the coupled-channel equations of Section 2 of this chapter. A particular procedure for determining the reaction amplitude, known as the *source term method* has been developed by Ascuitto and Glendenning (69). For a review, see Ascuitto and Seglie (84).

As may be expected, it is important to use the CCBA when the nuclei involved are deformed or vibrational. An example is given in Fig. 4.1, in which the DWA and CCBA predictions for pickup reaction $^{172}\text{Yb}(p,d)$ are compared with each other and with experiment. The improvement obtained using the CCBA is striking.

The analysis sketched above, taking the effect of inelastic channels into account, can readily be extended to include a more general set of channels. The K matrix can be generalized as that the resulting coupled-channel equations would then take both antisymmetry and overlap into account. Neglecting the latter will then yield a CCBA approximation in the form given by (4.2). The nontrivial problem that remains is one of physics. What are the important channels? Or stated in terms of the multistep concept, what are the important intermediate states that need to be taken to account?

5. STATISTICAL DIRECT AND COMPOUND MULTISTEP REACTIONS[†]

When the number of possible intermediate states becomes large, the solution of the resulting couple-channel equations becomes impractical and uninformative. If the intermediate states do not have the strong interconnections, exhibited for example by the collective states, the detailed analysis provided by coupled-channel equations should be unnecessary. Under each or both of these circumstances, a method that will provide reasonably accurate predictions of the gross (macro) structure of the experimental cross section but will not be able to reproduce the finer details, the microstructure, is suggested. The development of such a formalism is the main subject of this section. A statistical method similar to one used in Section IV.7 will be employed. It will yield expressions for the average cross sections. Such an analysis will necessarily omit the cross sections arising out of special circumstances, such as those associated with isolated doorway states. In most cases these are to be added to the statistical ones we shall be concerned with now.[‡]

In this theory, the number of steps can be as large as is necessary. Under these circumstances, the genesis of the formation of the compound nucleus will be developed automatically. The theory provides a step-by-step description of this process and will thus include the possibility that it may be interrupted before the compound state is achieved, leading to the statistical multistep compound reaction.

We begin by recalling the discussion in the introduction to this chapter, where it was shown that the various reaction types are closely correlated with the interaction time, which in turn is roughly measured by the number of steps involved. The greater the number of steps, the greater the complexity of the wave functions. The wave function associated with the single-step direct reaction is the simplest and that describing the compound nucleus is the most complex. The multistep direct reaction may involve several steps. The multistep compound reaction will also involve several steps. For each of these, the process may be terminated by emission to the final state. The flux that survives goes on to form the compound nucleus. Thus the wave function for the multistep compound reaction has components from the steps leading to the compound nucleus plus the compound nuclear component.

This discussion suggests that it would be advantageous to classify the states of the system in increasing order of complexity. An example employing the shell model is illustrated in Fig. 5.1. The incident channel consists of a nuclear projectile and a target nucleus represented schematically by nucleons in a potential well. As a result of the interaction between the incident nucleon and the target nucleus, one of the nucleons in the nucleus will gain energy while the projectile will lose energy. Two situations can occur: one set of states, in which none of the nucleons are in the continuum, is labeled Q space, and another

[†]Feshbach, Kerman, and Koonin (80); Feshbach (73); Bonetti, Chadwick, Hodgson, Carlson and Hussein (91).

[‡]See, however, Bonetti et al. (91) Sec. 6.

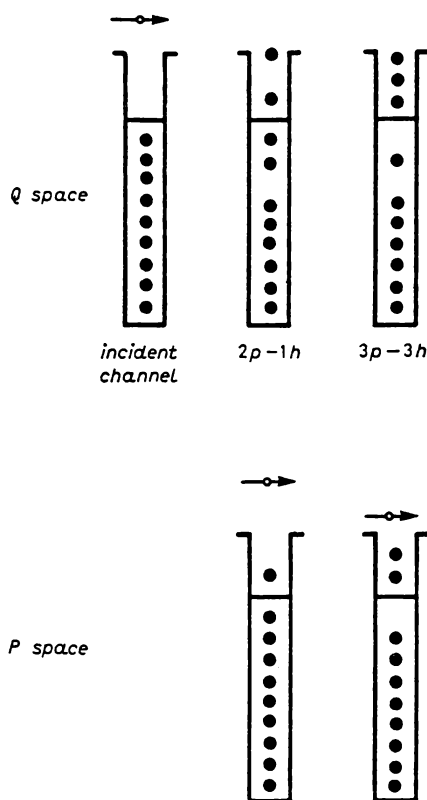


FIG. 5.1. Schematic shell model example of increasing complexity.

set, in which at least one nucleon is in the continuum is labeled P space. In Q space the interaction results in the formation of a two-particle/one-hole ($2p-1h$) state. Further interactions can result in $3p-2h$ states; $4p-3h$ states, and so on. These (the $1p$, $2p-1h$, $3p-2h$, etc.) are a series of states of increasing complexity. In the case of the P space, the target nucleus, on interacting with the projectile, can be excited to a $1p-1h$ state, and on further interactions with the projectile, be excited to a $1p-1h$ state, a $2p-2h$ state, and so on, again a series of states of increasing complexity.

More generally, the Hilbert space of the problem can be broken up into orthogonal subspaces, each of which contains all the states of a given complexity. This partition is illustrated in Fig. 5.2. In terms of the example, the "box" P_0 contains the incident nucleon plus the unexcited target nucleus. The P_1 box contains all the $1p-1h$ excitations and one nucleon in the continuum. The P_2 box contains all the $2p-2h$ excitations, and so on. On the other hand, the Q_1 box contains all the $2p-1h$ excitations, the Q_2 the $3p-2h$ excitations, and so on. The chain ends at Q_r . The r th stage is defined to be the one at which the

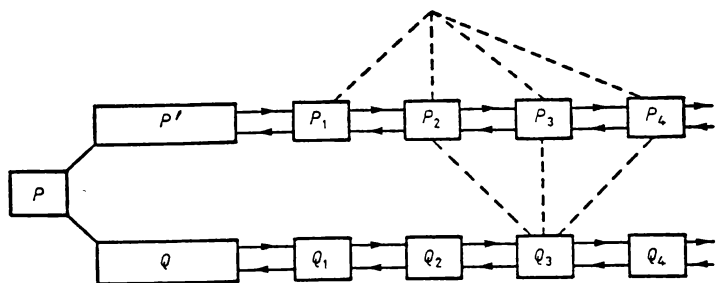


FIG. 5.2. Partition of Hilbert space into subspace of increasing complexity indicated by the subscript.

system is “trapped” as described in the introduction to Section 5; that is, the ratio of probability of emission compared to the probability of developing more complex configurations is small. This component of the wave function therefore, lives, a relatively long time and “equilibrium” is established. It should be referred to as the compound nuclear component, while *precompound* or *preequilibrium* refers to the preceding $(r - 1)$ stages. At low energies, one may expect that r will be small; that is, the compound nucleus is established after just a few interactions.

To progress further, two principal assumptions are made. The first is the *chaining hypothesis*. It assumes that the interaction can change the complexity of the wave function by at most one unit. Thus the interaction can move the system from box P_3 to boxes P_4 and P_2 but not to one labeled P_5 . An identical condition holds for the boxes Q_n and for transitions from Q space to P' space.

One can distinguish two differing processes corresponding to the two chains, P' and Q . In one, referred to as the *statistical multistep compound reaction*, the system is confined to the Q -space chain. A transition to the final state can occur at any stage along the chain in Q space by a transition to P space as indicated in Fig. 5.2 and then to the final state. Because of the chaining hypothesis, three stages in P space, $P_n, P_{n \pm 1}$, will be involved as the emission from a given stage. The final wave function is composed of contributions from all stages, as indicated in Fig. 5.2. At each stage there is a probability that the reaction terminates and a probability that it continues on to the next stage. When the latter probability is unity, complete equilibrium will develop and the compound nuclear evaporation process will dominate. The chaining hypothesis is exact if the residual interaction acting in each chain is composed of two-body potentials. Note that the chaining hypothesis is the generalization of the doorway state hypothesis of Chapter III. That hypothesis asserted that there was a state or states through which the system had to pass before the compound nucleus is formed. As can be seen from Fig. 5.2, such states are contained in subspace Q . But now wave functions in subspace Q_2 act as doorways for the rest of the

chain. A statistical theory involving the primary doorways, those in Q_1 , is, in retrospect, contained in the paper by Block and Feshbach (63).

The second process, indicated in Fig. 5.2, is one in which the system is confined to P' space and is referred to as the *statistical multistep direct process*. The equations describing that reaction type are just the coupled equations, all of them, which was the main subject of the preceding sections of this chapter.

The second principal assumption is the random phase approximation. This was discussed in Section IV.7. The principal result is as follows: Let

$$u = \sum_n u_n \quad (5.1)$$

Moreover, let the phase average [see Section IV.7, the equation below (IV.7.2)] of u and u_n be zero:

$$\langle u \rangle = 0 \quad \langle u_n \rangle = 0 \quad (5.2)$$

(If these conditions are not satisfied, consider $u - \langle u \rangle$ and $u_n - \langle u_n \rangle$). Then the random phase approximation yields

$$\langle |u|^2 \rangle = \sum_n |u_n|^2 \quad (5.3)$$

In applying the random phase approximation, one assumes that the phases of the components, u_n , are random, and that each value of the phase occurs with equal probability. Therefore, the phase-averaged values yield the expectation value of u and $|u|^2$. We recall the physics underlying the random phase hypothesis. It is that the wave functions are so complex that the matrix elements of the short-range interaction involving them are to a good approximation random variables. The consequence, according to (5.3), is the absence of any interference terms.

This is, of course, not the case when the states involved are members of a collective band, a situation we described earlier in this chapter. In that event, for example, when the nuclei are deformed, one must expand the P subspace of Fig. 5.2 to include the solutions of the coupled equations as described in Section 2. The initial wave function for subspace P is then given by (2.17) or the adiabatic "elastic" wave function involving the $u_l^{(\mu)}(r)$ in (2.28).

The random-phase approximation has an immediate consequence for the Q chain. Since all the states involved are bound, the appropriate quantum numbers are angular momentum and parity. The sum over n becomes a sum over these quantum numbers. Equation (5.3) tells us that terms with differing parity do not interfere. If the u_n are transition matrix elements, $|u|^2$ will be proportional to the differential cross section and one can immediately draw the conclusion that the angular distribution for the statistical multistep compound reaction will be symmetric around 90° , an important result. [For a more detailed discussion, see the discussion following (IV.7.9).]

In the case of the statistical multistep direct reaction, the quantum numbers involved include not only by the angular momentum and parity of the residual nucleus but also the momentum \mathbf{k} of the system in the continuum state. The angular distribution is, as we shall see, quite similar to that of the single-step direct reaction, that is, peaked in the forward hemisphere. It will differ from the single-step angular distribution in not decreasing as rapidly as the single step as the backward hemisphere is approached. The substantially different behavior of the Q -chain and P -chain wave functions requires partitioning of the Hilbert space into the Q and P sectors.

A. Statistical Multistep Direct Reactions

We begin with

$$(E - H_{\text{eff}})P\Psi = 0 \quad (1.2)$$

where H_{eff} is the multichannel optical model Hamiltonian. This equation was the starting point for the coupled-channel analysis discussed in Section 2. As in that case, one decomposes H_{eff} with a diagonal part, $H^{(D)}$, and a coupling interaction v with respect to an appropriate set of wave functions:

$$H_{\text{eff}} = H^{(D)} + v \quad (5.4)$$

In the example of inelastic scattering discussed in Section 2, that set is made up of the wave functions ψ_α for the states of the target nucleus, so that

$$\begin{aligned} H^{(D)} &= \sum_\alpha \psi_\alpha \langle \psi_\alpha | H_{\text{eff}} | \psi_\alpha \rangle \langle \psi_\alpha | \equiv \sum_\alpha \psi_\alpha \langle \psi_\alpha | H_\alpha \langle \psi_\alpha | \\ v &= \sum_{\alpha \neq \beta} \psi_\alpha \langle \psi_\alpha | H_{\text{eff}} | \psi_\beta \rangle \langle \psi_\beta | \end{aligned} \quad (5.5)$$

In terms of $H^{(D)}$ and v , (1.2) can be rewritten as follows:

$$P\Psi_i^{(+)} = \phi_i^{(+)} + \frac{1}{E^{(+)} - H_{\text{eff}}} v \phi_i^{(+)} \quad (5.6)$$

where $\phi_i^{(+)}$ the incident wave satisfies

$$(E - H^{(D)})\phi_i = 0 \quad (5.7)$$

The \mathcal{T} matrix for transitions induced by v following from (5.6) is

$$\mathcal{T}_{fi} \equiv \langle \phi_f^{(-)} | v P \Psi_i^{(+)} \rangle = v_{fi} + \left\langle \phi_f^{(-)} | v \frac{1}{E^{(+)} - H_{\text{eff}}} v \phi_i^{(+)} \right\rangle \quad (5.8)$$

where $\phi_f^{(-)}$ is a solution of (5.7) describing the final state and v_{fi} is defined by

$$v_{fi} \equiv \langle \phi_f^{(-)} v \phi_i^{(+)} \rangle \quad (5.9)$$

The first term in (5.8) is the single-step amplitude. The multistep (more than one) is given by the second term. We shall refer to it as $\mathcal{T}_{fi}^{(\text{msd})}$, where (msd) symbolizes multistep direct. Explicitly,

$$\mathcal{T}_{fi}^{(\text{msd})} = \sum_{\mu} \mathcal{T}_{fi}^{(\mu)} \quad (5.10)$$

where

$$\mathcal{T}_{fi}^{(\mu)} = \left\langle \phi_f^{(-)} P_f v_{f\mu} P_{\mu} \frac{1}{E^{(+)} - H_{\text{eff}}} P_1 v_{1i} P_i \phi_i^{(+)} \right\rangle \quad (5.11)$$

In this equation P_{μ} is a projection operator that projects onto the subspace P_{μ} of Fig. 5.2. These operators satisfy the orthogonality condition,

$$P_{\mu} P_{\nu} = P_{\mu} \delta_{\mu\nu} \quad (5.12)$$

In terms of these operators

$$v = \sum v_{\mu\lambda} \quad v_{\mu\lambda} = P_{\mu} v P_{\lambda} \quad (5.13)$$

Equation (5.11) makes use of this expansion as well as the chaining hypothesis,[†] which asserts that the interaction takes the system from its initial state to the subspace P_1 . The amplitude $\mathcal{T}_{fi}^{(\mu)}$ describes passage of the system from the initial state to the first-stage subspace projected by P_1 , followed by propagation until the μ th stage is reached. At this point the transition to the final state occurs.

The chaining hypothesis is now employed to factorize $P_{\nu}(E^{(+)} - H_{\text{eff}})^{-1}P_1$. In the appendix to this chapter it is shown that

$$P_{\mu} \frac{1}{E^{(+)} - H_{\text{eff}}} P_1 = G_{\mu} v_{\mu,\mu-1} P_{\nu-1} \frac{1}{E^{(+)} - H_{\text{eff}}} P_1 \quad (5.14)$$

Hence

$$P_{\mu} \frac{1}{E^{(+)} - H_{\text{eff}}} P_1 = G_{\mu} v_{\mu,\mu-1} G_{\mu-1} v_{\mu-1,\mu-2} \cdots G_2 v_{21} G_1 \quad (5.15)$$

[†]There is no implied limitation since one can always define the subspace P_1 as containing those wave functions generated from ϕ_i by the action of v and orthogonalized with respect to v [see Feshbach, Kerman, and Koonin (80)].

In these equations G_μ satisfies the recurrence relation

$$G_\mu = \frac{1}{E - H_\mu^{(D)} - v_{\mu,\mu+1} G_{\mu+1} v_{\mu+1,\mu}} \quad (5.16)$$

and

$$G_M = \frac{1}{E - H_M^{(D)}} \quad (5.17)$$

M is chosen to be so large ($M \rightarrow \infty$) that G_{M+1} can be taken to be zero. This corresponds to the cutoff used in the coupled-channels analysis of Section 2 to obtain a finite number of equations. Here, however, no limit is placed on M .

Inserting (5.15) into the expression (5.11) for $\mathcal{T}_{fi}^{(\mu)}$ yields

$$\mathcal{T}_{fi}^{(\mu)} = \langle \phi_f^{(-)} | v_{f\mu} G_\mu v_{\mu,\mu-1} G_{\mu-1} v_{\mu-1,\mu-2} \cdots v_{2,1} G_1 v_{1i} \phi_i^{(+)} \rangle \quad (5.18)$$

Thus the system enters subspace P_1 via the interaction v_{1i} , propagates in this space according to G_1 , makes a transition to subspace P_2 , and so on, eventually arriving at the P_μ subspace and after propagation in that space makes a transition to the final state.

The multistep cross section is proportional to

$$\sum_{\mu\nu} \mathcal{T}_{fi}^{(\mu)*} \mathcal{T}_{fi}^{(\nu)}$$

In virtue of the random-phase hypothesis, only the $\mu = \nu$ terms survive. Hence

$$\begin{aligned} \langle \sum \mathcal{T}_{fi}^{(\mu)*} \mathcal{T}_{fi}^{(\nu)} \rangle &= \sum \mathcal{T}_{fi}^{(\mu)*} \mathcal{T}_{fi}^\mu \\ &= \sum_\mu \langle \phi_f^{(-)} | v_{f\mu} G_\mu v_{\mu,\mu-1} \cdots v_{2,1} G_1 v_{1i} v_{i1}^* G_1^* v_{12}^* \cdots v_{\mu-1,\mu}^* G_\mu^* v_{\mu f}^* | \phi_f^{(-)} \rangle \end{aligned} \quad (5.19)$$

To proceed further, we make a spectral decomposition of G_μ using the eigenfunctions of G_μ^{-1} defined by

$$(H_\mu^{(D)} + v_{\mu,\mu+1} G_{\mu+1} v_{\mu+1,\mu}) \psi_{\mu,\alpha} = \left(\varepsilon_{\mu\alpha} + \frac{\hbar^2}{2m} k_\mu^2 \right) \psi_{\mu,\alpha} \quad (5.20)$$

where $\varepsilon_{\mu\alpha}$ and $\hbar^2/2mk_\mu^2$ are the energies of the residual nucleus and the particle in the continuum, respectively. Then

$$G_\sigma = \sum_\alpha \int \frac{d\mathbf{k}_\sigma}{(2\pi)^3} \frac{\psi_{\sigma\alpha}^{(+)} \langle \tilde{\psi}_{\sigma\alpha}^{(+)} }{E^{(+)} - (\hbar^2/2m)k_\sigma^2 - \varepsilon_{\sigma\alpha}} \quad (5.21)$$

where[†]

$$\langle \tilde{\psi}_{\alpha,\beta}^{(+)}, \psi_{\sigma\alpha}^{(+)} \rangle = \delta_{\alpha\beta}$$

As Austern and Vincent (74) pointed out, the terms in this expansion will fluctuate strongly. Their phase must be carefully taken into account to obtain a correct result. Since G_σ is well behaved, there must be considerable interference, resulting in substantial cancellations. The use of the random phase approximation under such circumstances would therefore lead to serious errors. Resolution of this difficulty [Feshbach (85, 86)] exploits the fact that G_σ is well behaved. Therefore, one can energy-average G_σ without affecting its value appreciably. The result of the averaging yields the following replacements:

$$\tilde{\psi}_{\sigma\alpha}^{(+)} \rightarrow \chi_{\sigma\alpha}^{(-)} \quad \psi_{\sigma\alpha}^{(+)} \rightarrow \chi_{\sigma\alpha}^{(+)} \quad (5.22)$$

to be made *within the interaction region*. The functions $\chi^{(\pm)}$ are eigenfunctions of a new Hamiltonian \bar{H}_{eff} . The change from H_{eff} is a consequence of the energy average. This energy is noted at this point because it emphasizes the character of G_σ . However, it should be noted that an energy average is required in any event by the developments that follow.

We now substitute (5.21) into (5.19), making the replacements given by (5.22) in the matrix elements. To illustrate the resulting calculation, consider the terms in (5.19), which deal with G_1 and couples to states in P_2 :

$$\begin{aligned} v_{21} G_1 v_{1i} v_{i1}^* G_1^* v_{12}^* &= \int \frac{d\mathbf{k}_1}{(2\pi)^3} \int \frac{d\mathbf{k}'_1}{(2\pi)^3} \sum_{\alpha,\beta} \bar{v}_{\gamma\alpha}(\mathbf{k}_2, \mathbf{k}_1) \\ &\times \frac{1}{E - (\hbar^2/2m)k_1^2 - \varepsilon_{1\alpha} + i\eta} \bar{v}_{\alpha i}(\mathbf{k}_1, \mathbf{k}_i) \\ &\times \bar{v}_{i\beta}^*(\mathbf{k}_i, \mathbf{k}'_1) \frac{1}{E - (\hbar^2/2m)k'^2_1 - \varepsilon_{1\beta} - i\eta} \bar{v}_{\beta\gamma'}^*(\mathbf{k}'_1, \mathbf{k}'_2) \end{aligned} \quad (5.23)$$

where

$$\bar{v}_{\gamma\alpha}(\mathbf{k}_2, \mathbf{k}_1) \equiv \langle \chi_{2\gamma}^{(-)}(\mathbf{k}_2) | v \chi_{1\alpha}^{(+)}(\mathbf{k}_1) \rangle \quad (5.24)$$

One now makes use of the random phase approximation, which asserts that

[†]Let $H_{\text{eff}} = H_0 + v$. Let $\phi_{0\alpha}$ be an eigenfunction of H_0 . Then

$$\psi_{\sigma\alpha}^{(+)} = \phi_{\sigma\alpha} + \frac{1}{E^{(+)} - H_{\text{eff}}} V \phi_{\sigma\alpha}$$

and

$$\tilde{\psi}_{\sigma\alpha}^{(+)} = \phi_{\sigma\alpha} + \frac{1}{E^{(+)} - H_{\text{eff}}^\dagger} V^\dagger \phi_{\sigma\alpha}$$

the only surviving contribution to the sum over α and β comes from the $\alpha = \beta$ terms. We note again that this assumes that the matrix elements of v appearing in (5.23) and (5.19) are random variables with an average value of zero. The resulting sum over α involves an energy integral over $\varepsilon_{1\alpha}$. This integral can be done presuming that the major contributions come from the singularities in the propagators. Then one may replace the matrix elements in (5.23) by energy averages taken in the neighborhood of the singularity. The integral over $\varepsilon_{1\alpha}$ becomes

$$I = \int \frac{M(\varepsilon_{1\alpha}, \mathbf{k}_1, \mathbf{k}'_1)}{[E - (\hbar^2/2m)k_1^2 - \varepsilon_{1\alpha} + i\eta][E - (\hbar^2/2m)k_1'^2 - \varepsilon_{1\alpha} - i\eta]} \rho_1(\varepsilon_{1\alpha}) d\varepsilon_{1\alpha}$$

where ρ_1 is the density of states, χ_α . M is a product of the matrix elements $\bar{v}_{\gamma\alpha}\bar{v}_{\alpha i}\bar{v}_{i\alpha}^*\bar{v}_{\alpha\gamma}^*$, which we replace by a constant with respect to $\varepsilon_{1\alpha}$, obtained by suitably energy averaging about the singularities in the denominator. One then obtains

$$I \simeq \rho_1 \left(E - \frac{\hbar^2}{2m} k_1^2 \right) M \left(E - \frac{\hbar^2}{2m} k_1'^2, \mathbf{k}_1, \mathbf{k}'_1 \right) \frac{2\pi i}{(\hbar^2/2m)(k_1^2 - k_1'^2) + 2i\eta} \quad (5.25)$$

The last factor can be written as the sum of a principal values and δ -function. Equation (5.25) is now inserted into (5.23) and the integration over \mathbf{k}_1 and \mathbf{k}'_1 performed. Assuming a slow variation of M with respect to k_1' near k_1 , the principal-value part of the integral over k_1' vanishes. When k_1' differs appreciably from k_1 , the integrand is zero as a consequence of the random phase approximation as applied to the sum over α . Hence

$$I \simeq \frac{4\pi m}{\hbar^2} \rho_1 \left(E - \frac{\hbar^2}{2m} k_1^2 \right) M \left(E - \frac{\hbar^2}{2m} k_1^2, \mathbf{k}_1, \mathbf{k}_1 \right) \delta(k_1^2 - k_1'^2)$$

Thus

$$\begin{aligned} v_{21} G_1 v_{i1}^* G_1^* v_{12}^* &= \int \frac{d\mathbf{k}_1}{(2\pi)^3} \int \frac{d\boldsymbol{\Omega}'_1}{4\pi} \frac{mk_1}{\hbar^2} \rho_1(U_1) \sum_{\alpha} \bar{v}_{\gamma\alpha}(\mathbf{k}_2, \mathbf{k}_1) \bar{v}_{\alpha i}(\mathbf{k}_1, \mathbf{k}_i) \\ &\quad \times \bar{v}_{i\alpha}^*(\mathbf{k}_i, k_1 \boldsymbol{\Omega}'_1) \bar{v}_{\alpha\gamma'}^*(k_1 \boldsymbol{\Omega}'_1, \mathbf{k}'_2) \end{aligned} \quad (5.26)$$

where

$$U_1 = E - \frac{\hbar^2}{2m} k_1^2 \quad (5.27)$$

and the prime on the sum over α indicates that only those configurations in the subspace P_1 whose energy equals U_1 are to be included in the sum. The final step is to apply the random phase approximation to the sum:

$$\sum_{\alpha} \bar{v}_{\gamma\alpha}(\mathbf{k}_2, \mathbf{k}_1) \bar{v}_{\alpha i}(\mathbf{k}_1, \mathbf{k}_i) v_{i\alpha}^*(\mathbf{k}_i, k_1 \Omega'_1) v_{\alpha\gamma'}(k_1 \Omega'_1, \mathbf{k}'_2) \\ = \delta(\Omega_1 - \Omega'_1) \langle \bar{v}_{\gamma 1}(\mathbf{k}_2, \mathbf{k}_1) | \bar{v}_{1i}(\mathbf{k}_1, \mathbf{k}_i) |^2 \bar{v}_{1\gamma'}^*(\mathbf{k}_1, \mathbf{k}'_2) \rangle \quad (5.28)$$

The bracketed expression is defined by this equation. The replacement of α by the numerical subscript serves to indicate that an average of the matrix element over the states in subspace P_1 must be taken.

Substituting (5.28) into (5.26) yields

$$v_{21} G_1 v_{1i} v_{i1}^* G_1^* v_{12}^* = \int \frac{d\mathbf{k}_1}{(2\pi)^3} \frac{mk_1}{4\pi\hbar^2} \rho_1(U_1) \langle \bar{v}_{\gamma 1}(\mathbf{k}_2, \mathbf{k}_1) | \bar{v}_{1i}(\mathbf{k}_1, \mathbf{k}_i) |^2 \bar{v}_{1\gamma'}^*(\mathbf{k}_1, \mathbf{k}'_2) \rangle$$

This result can be substituted in (5.19) and the analysis repeated with respect to the variables γ, γ', k'_2 , and so on, until one comes to the μ th contribution, which connects to the final state.

There is still one more averaging to be performed. The final state $\phi_f^{(-)}$ is a linear combination of contributions from each subspace. Experimentally, it is not generally possible to isolate a particular final state; rather, the energy average is measured. We must therefore take an energy average of the results obtained from (5.19), that is, over $\phi_f^{(-)}$. If one again assumes that the contribution from each subspace is random, and therefore employs the random phase approximation, the cross section becomes an incoherent sum of contributions from the subspaces connected to the μ th by the interaction v . Because of the chaining hypothesis, this will include contributions from $P_{\mu+1}$ and $P_{\mu-1}$. The average multistep differential cross section following from (5.19) can now be obtained. *The single-step cross section must be added to the multistep contribution to obtain the complete answer.*

The multistep contribution denoted by the subscript msd is

$$\left[\frac{d^2\sigma(\mathbf{k}_f, \mathbf{k}_i)}{d\Omega_f dU_f} \right]_{\text{msd}} = \sum_{m=\mu \pm 1} \int \frac{d\mathbf{k}_1}{(2\pi)^3} \dots \int \frac{d\mathbf{k}_\mu}{(2\pi)^3} \left[\frac{d^2 w_{m,\mu}(\mathbf{k}_f, \mathbf{k}_\mu)}{d\Omega_f dU_f} \right] \\ \times \left[\frac{d^2 w_{\mu,\mu-1}(\mathbf{k}_\mu, \mathbf{k}_{\mu-1})}{d\Omega_\mu dU_\mu} \right] \dots \left[\frac{d^2 w_{2,1}(\mathbf{k}_2, \mathbf{k}_1)}{d\Omega_2 dU_2} \right] \left[\frac{d^2 \sigma_{1i}(\mathbf{k}_1, \mathbf{k}_i)}{d\Omega_1 dU_1} \right] \quad (5.29)$$

where

$$\frac{d^2 w_{v,v-1}(\mathbf{k}_v, \mathbf{k}_{v-1})}{dU_v d\Omega_v} = 2\pi^2 \rho(k_v) \rho_v(U_v) |\bar{v}(\mathbf{k}_v, \mathbf{k}_{v-1})|_{\text{av}}^2 \quad (5.30)$$

measures the probability that the system passes from the $(v-1)$ st stage to the

vth with the continuum particle momentum changing from \mathbf{k}_{v-1} to \mathbf{k}_v . The density of states of the continuum particle and the residual nucleus are given by $\rho(k_v)$ and $\rho_v(U_v)$, respectively, where

$$E = U_v + \frac{\hbar^2}{2m} k_v^2 \quad (5.31)$$

Finally, $d\sigma_{1i}/d\Omega_1 dU_1$ is the average cross section for forming the first stage. It is given by

$$\frac{d\sigma_{1i}}{dU_1 d\Omega_1} = \frac{2\pi m}{\hbar^2 k_i} \rho(k_1) \rho_1(U_1) |\bar{v}_{1i}(\mathbf{k}_1, \mathbf{k}_i)|_{av}^2 \quad (5.32)$$

Note that in these formulas the distorted wave for the continuum particle has been normalized to a plane wave of unit amplitude at infinity.

The statistical multistep direct cross section, (5.29), for μ steps is expressed as a convolution of the probabilities for each step to occur. Quantum mechanics enters only in the calculation of these probabilities, which involves a DWA-type matrix element \bar{v} , whose magnitude squared is to be averaged over the possibly excited configuration. Energy is conserved at each step.

Since each factor in (5.29) is forward peaked, one may expect the multistep angular distribution to be forward peaked but generally broader than that of the single step, reflecting the number of stages contributing significantly.

Problem. Assume that each factor in (5.29) is a function of the momentum transfer, $\mathbf{k}_v - \mathbf{k}_{v-1}$, occurring at step. Evaluate the integral in (5.29), showing that it has the form

$$\int e^{i\gamma_f \cdot (\mathbf{k}_f - \mathbf{k}_i)} \prod_1^\mu f_v(\gamma_f) d\gamma_f$$

where

$$\frac{d^2 w(\mathbf{k}_v, \mathbf{k}_{v-1})}{d\Omega_v dU_v} = \int e^{i\gamma_v \cdot (\mathbf{k}_v - \mathbf{k}_{v-1})} f_v(\gamma_v) d\gamma_v$$

Show from this result that the integral in (5.29) will have a broader angular distribution than that given by the individual step.

B. Statistical Multistep Compound Reactions

The separation of the \mathcal{T} matrix into a direct term and a fluctuating one with vanishing average value using the results of Kawai, Kerman, and McVoy (73) has been discussed in Section IV.8. The direct reactions described by the direct term have been the subject of the discussion in the chapter up to this point.

We turn now to a consideration of the fluctuating term, which has its origin in the Q -subspace chain of Fig. 5.2. Equation (IV.8.8) gives the \mathcal{T} matrix for that case:

$$\mathcal{T}_{fi}^{(\text{msc})} = \left\langle \phi_f^{(-)} V_{PQ} \frac{1}{E - h_{QQ}} V_{QP} \phi_i^{(+)} \right\rangle \quad (5.33)$$

where

$$h_{QQ} = H_{QQ} + V_{QP} \frac{1}{E^{(+)} - H_{\text{opt}}} V_{PQ} \quad (5.34)$$

V_{PQ} is defined by (IV.8.6), H_{QQ} equals QH_Q , and H_{opt} is the multichannel optical model Hamiltonian. We see that the effect of the P subspace is included in h_{QQ} through its dependence on H_{opt} .

The analysis of $\mathcal{T}_{fi}^{(\text{msc})}$ given by (5.33) parallels completely that of $\mathcal{T}_{fi}^{(\text{msd})}$ following (5.11). First one can write $\mathcal{T}_{fi}^{(\text{msc})}$ as a linear combination of amplitudes coming from each stage:

$$\mathcal{T}_{fi}^{(\text{msc})} = \sum_1^r \mathcal{T}_{fi}^{(m)} \quad (5.35)$$

where

$$\mathcal{T}_{fi}^{(m)} = \left\langle \phi_f^{(-)} V_{PQ_m} \frac{1}{E - h_{QQ}} V_{Q_1P} \phi_i^{(+)} \right\rangle \quad (5.36)$$

where

$$V_{PQ_m} \equiv PVQ_m$$

and Q_m is the projection operator for subspace Q_m . As in (5.14),

$$Q_k \frac{1}{E - h_{QQ}} Q_1 = G_k V_{k,k-1} G_{k-1} \frac{1}{E - h_{QQ}} Q_1 \quad (5.37)$$

where

$$V_{k,k-1} \equiv Q_k V Q_{k-1}$$

and

$$G_k = \frac{1}{E - h_{kk} - V_{k,k+1} G_{k+1} V_{k+1,k}} \quad (5.38)$$

[see (5.16)].

Note that the sum over m in (5.35) terminates at $m = r$, so that $G_r = (E - h_{rr})^{-1}$.

Equation (5.37) is now to be inserted in (5.36). One obtains

$$\mathcal{T}_{fi}^{(m)} = \langle \phi_f^{(-)} V_{Pm} G_m V_{m,m-1} G_{m-1} \cdots V_{21} G_1 V_{1P} \phi_i^{(+)} \rangle \quad (5.39)$$

[Compare with (5.11)]. Recall that

$$Q_k \Psi_i^{(+)} = Q_k \frac{1}{E - h_{QQ}} V_{1P} \phi_i^{(+)}$$

where the left-hand side gives the component in space Q_k of the exact solution of the Schrödinger equation for the system. Using (5.37) yields

$$Q_k \Psi_i^{(+)} = G_k V_{k,k-1} Q_{k-1} \Psi_1^{(+)} \quad (5.40)$$

so that (5.39) can be written as follows:

$$\mathcal{T}_{fi}^{(m)} = \langle \phi_f^{(-)} V_{Pm} G_m V_{m,m-1} Q_{m-1} \Psi_i^{(+)} \rangle \quad (5.41)$$

We need to calculate the energy average of $|\mathcal{T}_{fi}^{(m)}|^2$. Rapid variations in the energy dependence of $\mathcal{T}_{fi}^{(m)}$ is assumed to originate in the propagators G_k . From (5.38) we see that an implicit source of energy dependence is given by the term $V_{k,k+1} G_{k+1} V_{k+1,k}$. We shall now describe one set of circumstances (verifiable in a detailed calculation) under which the energy dependence of this term can be neglected. The inverse of G_{k+1} will have eigenfunctions and eigenvalues given by

$$G_{k+1}^{-1} \psi_{k+1,\alpha} = \varepsilon_{k+1,\alpha} \psi_{k+1,\alpha} \quad (5.42)$$

and

$$(G_{k+1}^{-1})^\dagger \tilde{\psi}_{k+1,\alpha} = \varepsilon_{k+1,\alpha}^* \tilde{\psi}_{k+1,\alpha} \quad (5.43)$$

Since G_{k+1} is not generally Hermitian, the eigenvalue $\varepsilon_{k+1,\alpha}$ will be complex:

$$\varepsilon_{k+1,\alpha} = E_{k+1,\alpha} - i \frac{\Gamma_{k+1,\alpha}}{2} \quad (5.44)$$

In terms of these eigenfunctions,

$$w_{kk} \equiv V_{k,k+1} G_{k+1} V_{k+1,k} = \sum_{\alpha} V_{k,k+1} \psi_{k+1,\alpha} \frac{1}{E - \varepsilon_{k+1,\alpha}} \langle \tilde{\psi}_{k+1,\alpha}$$

We see that the energy dependence of w_{kk} will be smooth over the energy variation given by $\Gamma_{k+1,\alpha}$. For the purpose of energy averaging and employing the random phase approximation, it is necessary that many states $\psi_{k,\beta}$ be continued in that interval, leading to the condition

$$\rho_k \Gamma_{k+1} \gg 1 \quad \text{or} \quad \Gamma_{k+1} \gg D_k \quad (5.45)$$

where ρ_k is the density of levels in k th subspace, D_k the energy spacing, and

Γ_{k+1} the average value of $\Gamma_{k+1,\alpha}$. Under this condition, *self-averaging* takes place. The condition is equivalent to the statement that the Poincaré time for the k th stage is large compared to the lifetime of the states in the $(k+1)$ st stage. Condition (5.45) can be checked by direct calculation. In the examples to be described, the condition is well satisfied.

Assuming (5.45), it becomes possible to expand G_m in (5.41) in a spectral series so that

$$\mathcal{T}_{fi}^{(m)} = \sum \langle \phi_f^{(-)} V_{Pm} \psi_{m,\alpha} \rangle \frac{1}{E - \varepsilon_{m\alpha}} \langle \tilde{\psi}_{m,\alpha} V_{m,m-1} Q_{m-1} \Psi_i^{(+)} \rangle \quad (5.46)$$

when $\varepsilon_{m\alpha}$ varies slowly with energy.

Problem. Prove that the energy average of $\mathcal{T}_{fi}^{(m)}$ is zero.

To obtain the cross section we need to compute the energy average of $|\mathcal{T}_{fi}^{(\text{mse})}|^2$:

$$|\mathcal{T}_{fi}^{(\text{mse})}|^2 = \sum_{mm'} (\mathcal{T}_{fi}^{(m')})^* (\mathcal{T}_{fi}^{(m)}) \rightarrow \sum_m |\mathcal{T}_{fi}^{(m)}|^2$$

where the random-phase approximation is used to obtain the last expression. Using (5.46) yields

$$\begin{aligned} |\mathcal{T}_{fi}^{(m)}|^2 &= \sum_{\alpha\beta} \langle \phi_f^{(-)} V_{Pm} \psi_{m,\alpha} \rangle \frac{1}{E - \varepsilon_{m\alpha}} \langle \tilde{\psi}_{m,\alpha} V_{m,m-1} Q_{m-1} \Psi_i^{(+)} \rangle \\ &\quad \times \langle \phi_f^{(-)} V_{Pm} \psi_{m,\beta} \rangle^* \frac{1}{E - \varepsilon_{m\beta}^*} \langle \tilde{\psi}_{m,\beta} V_{m,m-1} Q_{m-1} \Psi_i^{(+)} \rangle \end{aligned}$$

Again because of the random-phase approximation the double sum can be collapsed to a single sum since only the $\alpha = \beta$ terms survive. Therefore,

$$|\mathcal{T}_{fi}^{(m)}|^2 = \sum_{\alpha} |\langle \phi_f^{(-)} V_{Pm} \psi_{m\alpha} \rangle|^2 \frac{1}{|E - \varepsilon_{m\alpha}|^2} |\langle \tilde{\psi}_{m,\alpha} V_{m,m-1} Q_{m-1} \Psi_i^{(+)} \rangle|^2$$

The energy average is taken assuming that only the variation of the energy denominator is important and that the energy variation of the matrix elements is slow, so that their magnitude squared can be replaced by an average value over the set $\psi_{m\alpha}$. The result is

$$\langle |\mathcal{T}_{fi}^{(m)}|^2 \rangle = \frac{\Gamma_m^{(f)}}{\Gamma_m} \frac{\langle |\langle \tilde{\psi}_{m,\alpha} V_{m,m-1} Q_{m-1} \Psi_i^{(+)} \rangle|^2 \rangle}{D_m} \quad (5.47)$$

Where

$$\Gamma_m^{(f)} \equiv 2\pi \langle |\phi_f^{(-)} V_{Pm} \psi_{m\alpha} \rangle|^2 \rangle \quad (5.48)$$

is referred to as the escape width. One now uses (5.40) again on the remaining factor in (5.47), to obtain

$$\langle |\mathcal{T}_{fi}^{(m)}|^2 \rangle = \frac{\Gamma_m^{(f)} \Gamma_{m-1}^\downarrow}{\Gamma_m \Gamma_{m-1}} \frac{\langle |\langle \tilde{\psi}_{m-1,\alpha} V_{m-1,m-2} Q_{m-2} \Psi_i^{(+)} \rangle|^2 \rangle}{D_{m-1}}$$

where

$$\Gamma_{m-1}^\downarrow = \frac{2\pi}{D_m} \langle |\langle \tilde{\psi}_{m,\alpha} V_{m,m-1} \psi_{m-1,\beta} \rangle|^2 \rangle \quad (5.49)$$

is referred to as the *spreading width*. The averages are over the states in the m th and $(m-1)$ st subspaces. Iterating, one obtains

$$\langle |\mathcal{T}_{fi}^{(m)}|^2 \rangle = \frac{1}{(2\pi)^2} \frac{\Gamma_m^{(f)}}{\Gamma_m} \prod_{k=1}^{m-1} \frac{\Gamma_k^\downarrow}{\Gamma_k} \frac{2\pi\Gamma_1^{(i)}}{D_1} \quad (5.50)$$

where

$$\Gamma_1^{(i)} = 2\pi \langle |\langle \psi_{1\alpha} V_{1P} \phi_i^{(+)} \rangle|^2 \rangle \quad (5.51)$$

Therefore

$$\langle |\mathcal{T}_i^{(\text{msc})}|^2 \rangle = \frac{1}{(2\pi)^2} \sum_{m=1}^r \frac{\Gamma_m^{(f)}}{\Gamma_m} \left[\prod_{k=1}^{m-1} \frac{\Gamma_k^\downarrow}{\Gamma_k} \right] \frac{2\pi\Gamma_1^{(i)}}{D_1} \quad (5.52)$$

It is convenient to normalize $\phi_i^{(+)}$ and $\phi_f^{(-)}$ so that the widths have the dimension of an energy and \mathcal{T} is dimensionless. This is the case if the normalization is per unit energy. The cross section for a given channel with quantum numbers designated by γ is given by

$$\sigma_{fi}^{(\text{msc})} = \frac{\pi}{k^2} \sum_{m=1}^r \frac{\Gamma_m^{(f)}}{\Gamma_m} \left[\prod_{k=1}^{m-1} \frac{\Gamma_k^\downarrow}{\Gamma_k} \right] \frac{2\pi\Gamma_1^{(i)}}{D_1} \quad (5.53)$$

while the expression for the angular distribution is given by (5.55').

Equation (5.52) can be described as a product of factors with relatively simple meaning. The first $(2\pi\Gamma_1^{(i)}/D_1)$ is the strength function measuring the probability of the system making the transition from the incident channel to the first subspace Q_1 . This is followed by a product that measures the attenuation because of emission en route to the m th channel and finally, the branching ratio for emission from the m th subspace. the total widths Γ_k are generally not the sum of the escape and spreading widths [see Feshbach, Kerman, and Koonin (80)] except in the case of weak coupling between the P and Q spaces.

Finally, it is necessary to average $d\sigma_\gamma^{(\text{msc})}/dU$ over the final states since experimentally it is not possible to distinguish among them. The final wave function $\phi_f^{(-)}$ in (5.48) for $\Gamma_m^{(f)}$ is composed of contributions from all stages, P_μ . However, because of the chaining hypothesis, the states in subspace Q_m can

make transitions only to P_m , P_{m-1} , and P_{m+1} . Assuming that the coupling among the various P_μ spaces is strong, the wave function $\phi_f^{(-)}$ will be "well mixed", so that to a good approximation the probability of the component of $\phi_f^{(-)}$ being in subspace of P_μ is given by $\rho_\mu^{(\gamma)}(U)/\rho^{(\gamma)}(U)$ when $\rho_\mu^{(\gamma)}$ is the density of the states in subspace P_μ with channel quantum numbers symbolized by γ , and $\rho^{(\gamma)}(U)$ is the total density of channels of the type γ at the excitation energy U :

$$\rho^{(\gamma)}(U) = \sum_{\mu} \rho_{\mu}^{(\gamma)}(U)$$

With this assumption

$$\Gamma_m^{(\gamma)} = \sum_{\mu=m-1}^{m+1} \frac{\rho_{\mu}^{(\gamma)}(U)}{\rho^{(\gamma)}(U)} \Gamma_{m\mu}^{(\gamma)}(U) \quad (5.54)$$

where $\Gamma_{m\mu}^{(\gamma)}$ is given by

$$\Gamma_{m\mu}^{(\gamma)} = 2\pi \langle |\chi_{\mu\beta}^{(-)} V_{Pm} \psi_{m\alpha}|^2 \rangle$$

where $\chi^{(-)}$ is given by (5.22). The average is taken over the indices β and α .

We can now average $\sigma_f^{(\text{mse})}$ over a small energy interval dU , where U is the excitation energy of the residual nucleus. The right-hand side of (5.53) is multiplied by $\rho^{(\gamma)}(U)dU$ and $\Gamma_m^{(\gamma)}$ is replaced by its average value, $\rho_\mu^{(\gamma)}(U)\Gamma_{m\mu}^{(\gamma)}(U)/\rho^{(\gamma)}(U)$. We thus finally obtain

$$\frac{d\langle \sigma_{\gamma}^{(\text{mse})} \rangle}{dU} = \frac{\pi}{k^2} \sum_{m=1}^r \sum_{\mu=m-1}^{m+1} \frac{\langle \rho_{\mu}^{(\gamma)}(U) \Gamma_{m\mu}^{(\gamma)}(U) \rangle}{\Gamma_m} \left[\sum_1^{m-1} \frac{\Gamma_k^{\downarrow}}{\Gamma_k} \right] \frac{2\pi \Gamma_1^{(i)}}{D_1} \quad (5.55)$$

The channel parameters γ are, for example, those used in Section 2: namely, channel spin S , critical angular momentum l , and total angular momentum J . The angular distribution is obtained in the standard way, with the result.

$$\frac{d^2 \sigma}{d\Omega dU} = \sum \frac{(-)^{S-S'}}{(2I+1)(2i+1)} \bar{Z}(lJlJ; SL) \bar{Z}(l'Jl'J; S'L) P_L(\cos \vartheta) \frac{d\sigma_{\gamma}^{(\text{mse})}}{dU} \quad (5.55')$$

where

$$\begin{aligned} \bar{Z}(lJlJ; SL) &= (-)^{S+J+L} (lSj \| Y_L \| lSJ) \\ &= 0 \quad \text{unless } L \text{ is even} \end{aligned}$$

Formula (5.55) appears to be similar to that used in the preequilibrium theories reviewed, for example, by Blann (72). It is not identical, as the latter refer to the angle integrated cross section and do not predict angular distributions. Because of the random-phase approximation, the statistical

multistep compound reaction cross section is symmetric about 90° . Note finally that (5.55) automatically contains the compound nuclear contribution to the cross section given by the r th term in (5.55).

Because of the preliminary stages through which the system has to pass before arriving at the statistical compound state, the Bohr independence hypothesis and its consequence the statistical reaction theory (Hauser–Feshbach) must be modified. This is seen most readily if we return to (5.55) and examine just the compound nuclear term, the r th term:

$$\sigma_{fi,r}^{(\text{msc})} = \frac{\pi}{k^2} \frac{\Gamma_r^{(f)}}{\Gamma_r} \prod_1^{r-1} \frac{\Gamma_k^\downarrow}{\Gamma_k} \cdot \frac{2\pi\Gamma_1^{(i)}}{D_1} \quad (5.56)$$

Since the Q_r subspace is the last subspace in the chain, Γ_r is equal to the escape width:

$$\Gamma_r = \Gamma_r^\dagger = \sum_c \Gamma_r^{(c)} \quad (5.57)$$

where the sum is over all possible final states. Let the transmission factor T_c be given by

$$T_c \equiv \frac{2\pi\Gamma_r^{(c)}}{D_r}$$

Then

$$\sigma_{fi,r}^{(\text{msc})} = \frac{\pi}{k^2} \frac{T_f T_i}{\sum_c T_c} \quad (5.58)$$

The factor T_i is

$$T_i \equiv 2\pi \frac{\Gamma_1^{(i)}}{D_1} \prod_{k=1}^{r-1} \frac{\Gamma_k^\downarrow}{\Gamma_k} \quad (5.59)$$

Although (5.58) is similar to the Hauser–Feshbach expression, it can differ substantially because of the presence of the depletion factor, that is,

$$\sigma_{fi,r}^{(\text{msc})} = \sigma_{\text{HF}} \prod_{k=1}^r \frac{\Gamma_k^\downarrow}{\Gamma_k} \quad (5.60)$$

Here σ_{HF} is the Hauser–Feshbach expression. Moreover, since the depletion factor depends on the nature of the entrance channel, which determines the quantification of complexity and therefore the partition of Hilbert space in P and Q and of Q into Q_μ , the Bohr independence hypothesis is violated.

One interesting sum rule can be obtained from (5.53). Sum this cross section over all possible final states to obtain the total reaction cross section, σ :

$$\sigma = \sum_f \sigma_{fi}^{(msc)} = \frac{\pi}{k^2} \sum_{m=1}^r \frac{\Gamma_m^\dagger}{\Gamma_m} \left[\prod \frac{\Gamma_k^\dagger}{D_1} \right] \frac{2\pi\Gamma_1^{(i)}}{D_1} \quad (5.61)$$

If now one makes the weak PQ coupling approximation

$$\Gamma_\mu = \Gamma_\mu^\dagger + \Gamma_\mu^\downarrow$$

(5.61) reduces to

$$\sigma = \frac{\pi}{k^2} \frac{2\pi\Gamma_1^{(i)}}{D_1} \quad (5.62)$$

Thus the total reaction cross section is proportional to the strength function for the formation of doorway states in subspace Q_1 .

6. APPLICATIONS

The results of Section 5 [Eqs. (5.29) and (5.55)] have been applied to the analysis of experiments in which the incident and emerging particles are nucleons, such as (p, p') , (n, n') , (p, n) , (n, p) , and (\mathbf{p}, n) . Projectile energies range from 14 to 65 MeV, while a variety of target nuclei, including medium heavy as well as heavy nuclei, were used. There have been a few calculations carried out for ^3He - and ^4He -induced reactions [Bonetti, Colli-Milazzo, and Melanotte (81)]. Generalizations have been developed (and explained) which are appropriate for the study of reactions with multiparticle final states [Feshbach (79); Ciangaru, Chang, et al. (84); Field, Bonetti, and Hodgson (85)].

The calculations for nucleon induced reactions have been carried out by Colli-Milazzo, Bonetti, Hodgson, and their colleagues in more than a dozen papers [de Rosa, Inglis, et al. (78); Bonetti, Caninasio, Colli-Milazzo, and Hodgson (81); Bonetti, Colli-Milazzo, and Melanotte (81a, 81b, 83); Bonetti, Colli-Milazzo, et al. (80, 82a, 82b); Bonetti and Columbo (83); Avaldi et al. (80); Austin et al. (80), Field et al. (86) Holler et al. (85)]. It is not possible to describe the details involved in these many analyses. We shall give some examples of the results obtained, together with the principal conclusions.

The elements that enter into the calculation include the residual potential responsible for the transition between stages, the bound-state wave functions, and the wave functions for the particle in a continuum state. The choice is guided by the standard DWA results. In the more precise calculations, the residual interaction is taken to be a Yukawa potential. Distorted waves for the continuum and the bound-state wave function are obtained using a Woods-Saxon potential selected in accord with elastic scattering and single-step

DWA results available in the energy range and for the target of interest. Overall good agreement with experiment, illustrated below, was obtained with *identical* residual interactions employed in all cases: target nuclei, excitation energy and angle, and for both statistical multistep direct and compound reactions. That strength between unlike nucleons is taken to be 27 MeV with a range of 1 fm [Bonetti and Columbo (83), Bonetti, Colli-Milazzo, and Melanotte (81a)]. Rough calculations have also been made for the statistical multistep compound reaction with δ function residual potential and constant bound-state wave functions. It turns out that the effect of these approximations on the energy spectra and angular distributions is small.

In each situation it is necessary to choose a path in reaction space; that is, what are the stages in which the system can be found? For example, in the (p, n) statistical multistep direct case [Bonetti, Colli-Milazzo, and Melanotte (81a)], the first stage is generated by a charge exchange scattering with the formation of a proton-particle-neutron-hole in the target nucleus plus a neutron in the continuum. The more complex states, P_n , involve $np-nh$ states with a neutron in the continuum. Clearly, there are many other possibilities. For example, the charge exchange scattering could be postponed to a later stage.

The sensitivity of the results to the various paths in reaction space has not been studied systematically. However, Bonetti, Colli-Milazzo, and Melanotte (81a) found that for their several cases they need not distinguish between the neutrons and protons provided that an averaged interaction strength is used and except for the initial and final step. Chao, Hachenberg, and Hüfner (82) have emphasized the importance of the first step and suggest a relative insensitivity to the nature of the succeeding stages.

The density of particle-hole states required in both SMC and SMD processes is given by the Ericson (60c) expression. We give a simple derivation of the result. One assumes a constant density g of single-particle states; that is, the probability that a particle has an energy between x and $x + dx$ is $g dx$. Then the probability that p particles and h holes ($N = p + h = \text{exciton number}$) have an excitation energy E is

$$\rho_{\text{ph}}(E) = \frac{1}{p! h!} \int_0^\infty dx_1 \cdots dx_p \int_0^\infty dy_1 \cdots dy_h g^{p+h} \delta\left(E - \sum_1^p x_i - \sum_1^h y_i\right) \quad (6.1)$$

where we have assumed that g is a constant, an assumption which can be easily modified. Replacing the δ function by its integral representation

$$\delta\left(E - \sum_1^p x_i - \sum_1^h y_i\right) = \frac{1}{2\pi} \int_{-\infty}^\infty dk e^{ik(E - \sum x_i - \sum y_i)}$$

Equation (6.1) becomes

$$\rho_{\text{ph}}^{(N)}(E) = \frac{1}{2\pi} \frac{g^N}{p! h!} \int_{-\infty}^\infty dk e^{ikE} \left(\int_0^\infty dx e^{-ikx} \right)^p \left(\int_0^\infty dy e^{-iky} \right)^h$$

For the x and y integrals to be convergent, the path of the k integration must lie in the lower half of the complex k plane. One obtains

$$\rho_{\text{ph}}^{(N)}(E) = \frac{1}{2\pi} \frac{g^N}{p! h!} \int_{-\infty}^{\infty} dk \frac{e^{ikE}}{(ik)^N}$$

Using the Cauchy integral formula yields the Ericson result,

$$\rho_{\text{ph}}^{(N)}(E) = \frac{g(gE)^{N-1}}{p! h! (N-1)!} \quad (6.2)$$

To obtain the density of particle-hole states formed from single-particle states of a given J , one must multiply (6.2) by spin distribution function (IV.5.54), yielding

$$\rho_{\text{ph}}^{(N)}(E, J) = \rho_{\text{ph}}^{(N)}(E) R_N = \frac{g(gE)^{N-1}}{p! h! (N-1)!} \frac{2J+1}{\sqrt{8\pi\sigma^3} N^{3/2}} e^{-(J+1/2)^2/2N\sigma^2} \quad (6.3)$$

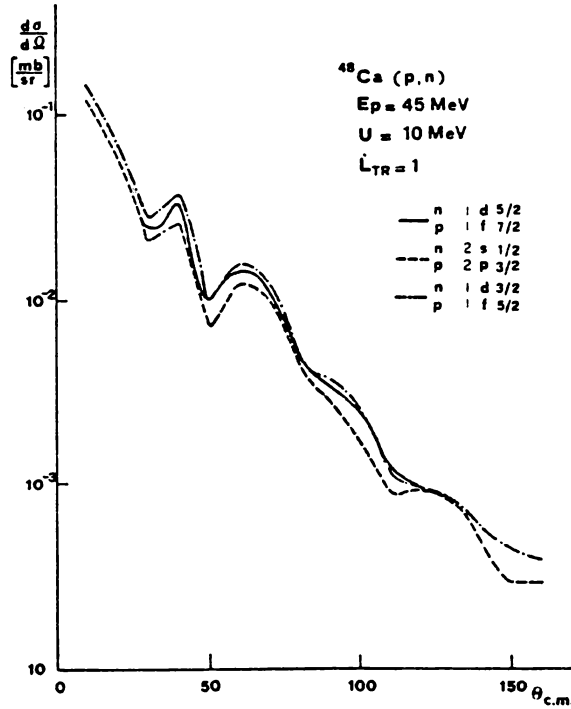


FIG. 6.1. Calculated differential cross sections for some typical transitions in ^{48}Ca at 45 MeV between shell model states corresponding to $\Delta L = 1$, showing their overall similarity. [From Bonetti, Camnasio et al. (81).]

In the shell-model basis, the states in stage $n + 1$ differ from those in stage n by a particle-hole excitation; that is, $N = 2$, $p = 1$, and $h = 1$.

The average of the square matrix elements is given by

$$\langle |\bar{v}(\mathbf{k}_i, \mathbf{k}_f)|^2 \rangle = \sum_L (2L + 1) \langle |\bar{v}(\mathbf{k}_i, \mathbf{k}_f, L)|^2 \rangle R_2(L)$$

and

$$\left\langle \left[\frac{d^2 \sigma(\mathbf{k}_i, \mathbf{k}_f)}{dU d\Omega} \right]_{\text{single step}} \right\rangle = \sum_L (2L + 1) \rho^{(2)}(E) R_2(L) \left\langle \left(\frac{d\sigma}{d\Omega} \right)_L \right\rangle$$

in the case that the spin of the target is zero and if the spin of the nucleons is neglected (then $J = L$). The average over $(d\sigma/d\Omega)_L$ for various possible values of the particle-hole angular momenta is readily accomplished because of the similarity of the results for each of the possibilities. This is illustrated by Fig. 6.1.

Some results that illustrate the degree of agreement with experiment will now be presented. Note that in all cases the log of the cross section is plotted. Figures 6.2 to 6.5 compare the results of a multistep direct calculation of the

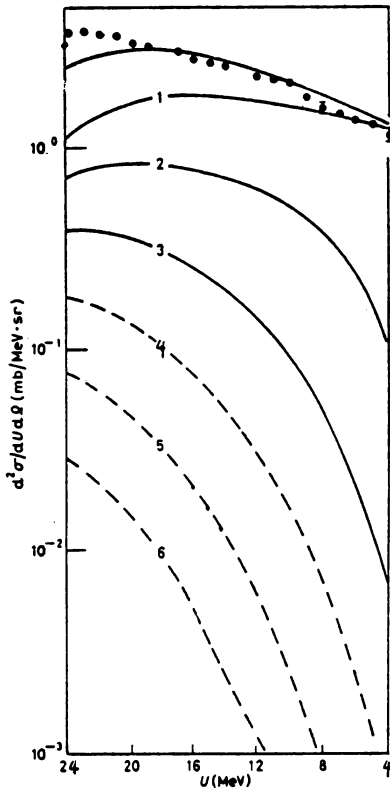


FIG. 6.2. Neutron energy spectrum for the reaction $^{120}\text{Sn}(p, n)$, $E_p = 45 \text{ MeV}$, $\theta_{\text{cm}} = 30^\circ$. The black dots are the experimental points; the solid line the calculated results. The numerical labels correspond to the number of steps. [From Avaldi, Bonetti, and Colli-Milazzo (80).]

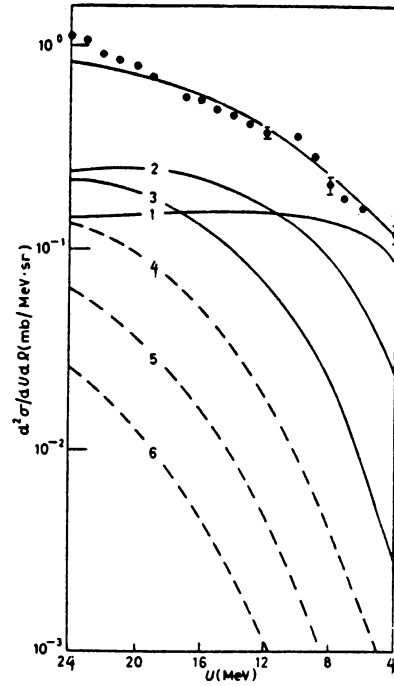


FIG. 6.3. Neutron energy spectrum for the reaction $^{120}\text{Sn}(p, n)$, $E_p = 45 \text{ MeV}$, $\theta_{\text{cm}} = 90^\circ$ (see legend for Fig. 6.2). [From Avaldi, Bonetti, and Colli-Milazzo (80).]

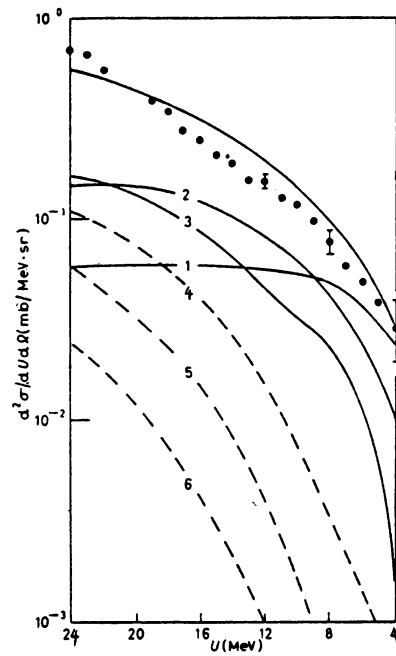


FIG. 6.4. Neutron energy spectrum for the reaction $^{120}\text{Sn}(p, n)$, $E_p = 45 \text{ MeV}$, $\theta_{\text{cm}} = 120^\circ$ (see legend for Fig. 6.2). [From Avaldi, Bonetti, and Colli-Milazzo (80).]

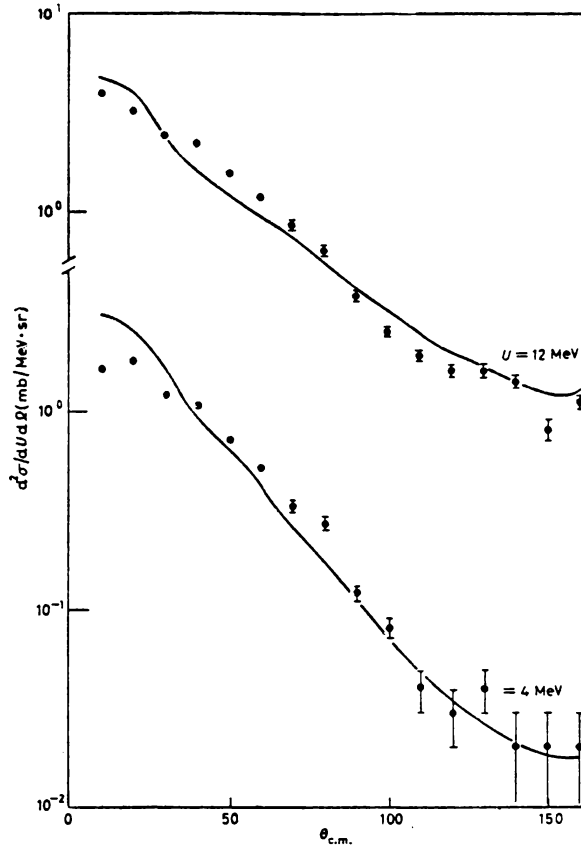


FIG. 6.5. Neutron angular distribution for the reaction $^{120}\text{Sn}(p, n)$, $E_p = 45$ MeV. The solid lines are calculated results. [From Avaldi, Bonetti, and Colli-Milazzo (80).]

$\text{Sn}(p, n)$ cross sections for 45-MeV protons [Avaldi, Bonetti, and Colli-Milazzo (80)]. Good agreement is obtained. There is some deviation at low neutron energies, where there is a contribution from the multistep compound process not included in the calculation. We note that the single-step process gives accurate results only with a low excitation energy of the residual nucleus and in the forward direction. But as the excitation energy increases and/or the emission angle increases, the contribution of the two-step and then the three-step process becomes important. No more than three steps are required in the angular range beyond 150° . The calculated angular distribution shown in Fig. 6.5 matches experiment throughout the angular range. Similar calculations have been performed for a (p, n) reaction, proton energy 45 MeV, for a number of nuclei [Bonetti, Colli-Milazzo, and Melanotte (81a)] with similar success. The need to include contributions from the SMC process as the proton energy decreases is shown in Fig. 6.6.

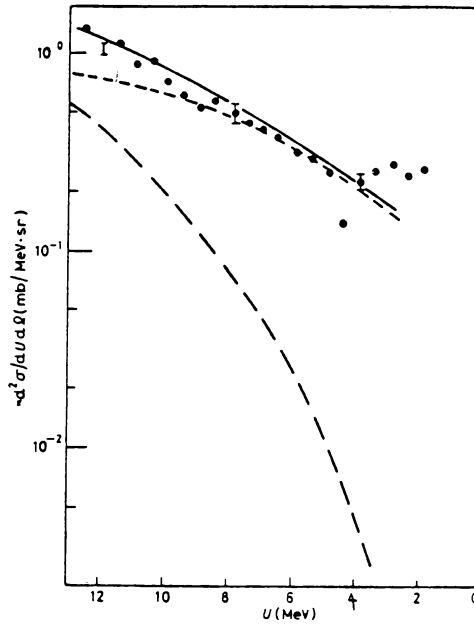


FIG. 6.6. Neutron energy spectrum for the reaction $^{120}\text{Sn}[p, n]$ $E_p = 25$ MeV, $\theta_{\text{cm}} = 110^\circ$; ———, total; ———, multi step direct, ———, multistep compound. [From Colli-Milazzo private communication quoted in Feshbach (86).]

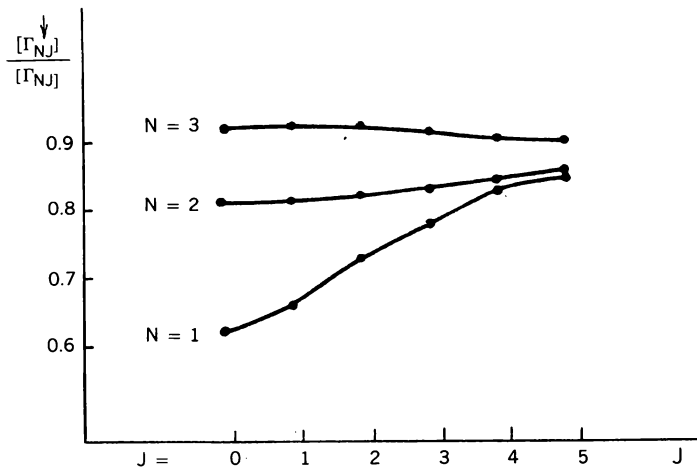


FIG. 6.7. Transmission probability $\langle \Gamma_{NJ}^1 \rangle / \langle \Gamma_{NJ} \rangle$ as function of J in the case of $^{40}\text{Ca}(n, p)$ [From Bonetti, Colli-Milazzo, and Melanotte (83).]

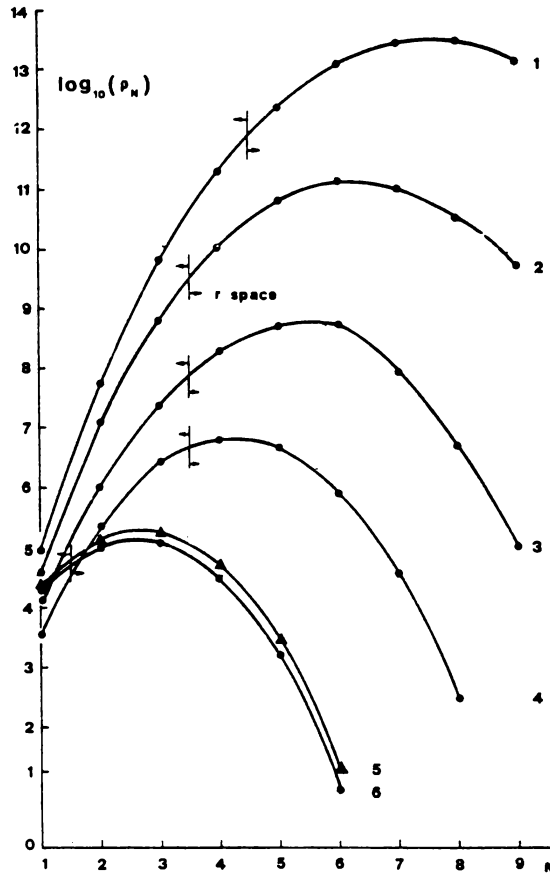


FIG. 6.8. Level density of the various composite nuclei as a function of the stage N of the precompound chain: (1) ^{104}Pd , (2) ^{90}Zr , (3) ^{60}Ni , (4) ^{41}Ca , (5) ^{30}P , and (6) ^{28}Si . [From Bonetti, Colli-Milazzo, and Melanotte (83).]

We turn next to some examples of the statistical multistep compound (SMC) reactions. “Equilibrium” sets in at about the fourth step, as indicated by Fig. 6.7, where we see that by the third step the branching ratio to the fourth step is approximately 0.9. Note that the level density at the fourth stage is on the order of 10 times that at the third stage (see Fig. 6.8), so that the self-averaging condition of Tang Xuetian (81) is well satisfied. It is important in the SMC calculations to include only bound orbits, as emphasized by Bonetti, Colli-Milazzo, and Melanotte (83). Two examples are shown. In Fig. 6.9 a comparison is made between experiment and theory for the $^{51}\text{V}(p,n)^{51}\text{Cr}$ reaction, for a proton energy of 22 MeV. We see the striking failure of the evaporation model and the good agreement that is obtained when the SMC theory, which takes into account the emission that occurs before the equilibra-

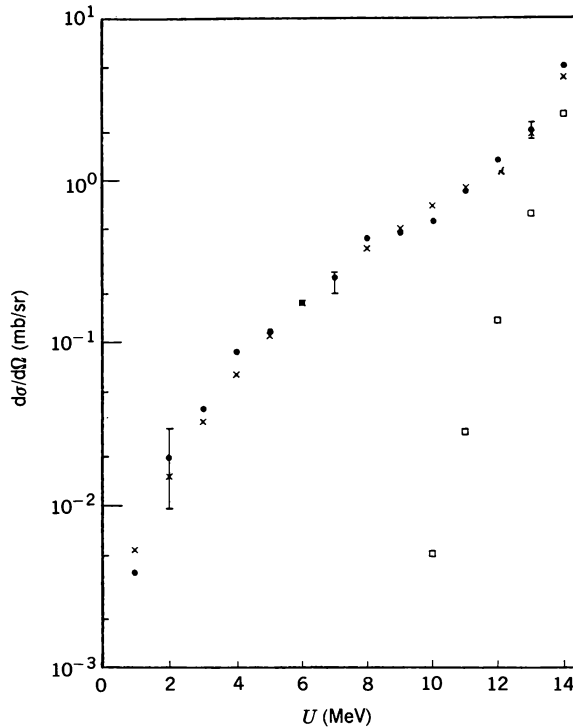


FIG. 6.9. Double differential spectrum for the reaction $^{51}\text{V}(p, n)^{51}\text{Cr}$, $E_p = 22 \text{ MeV}$, $\theta = 144^\circ$. Experimental points from Grimes, Anderson, et al. (71) are given by circles, the calculated evaporation spectrum by the squares, and the total statistical multistep compound by the crosses. [From Feshbach, Kerman, and Koonin (80).]

tion (r th) stage, is reached. In Fig. 6.10 a comparison is made for the case of 14-MeV neutrons incident on ^{93}Nb , including the (n, n') , $(n, 2n)$, and (n, pn) contributions. The dashed line gives the contribution from the r th stage (the evaporation component) for (n, n') , the dotted line for the $(n, 2n)$ and (n, pn) .

The behavior of parameters of the SMD theory is shown in Table 6.1. In this table σ is the spin cutoff parameter, $6a/\pi^2$ gives single-particle density g , V_0 is the strength of the Yukawa potential with a range of 1 fm [used for the residual $(p - n)$ potential], \bar{V}_0 is the strength averaged over the $p - n$ and $n - n$ interaction strengths, and finally, the ratio of the single-step cross section to the total is shown. Bonetti and Columbo (83) show that the strength of the potentials used in the SMC is consistent with that given by the table.

The statistical multistep direct theory has also been employed to predict the inelastic scattering of 65-MeV polarized protons by ^{58}Ni [Bonetti, Colli-Milazzo, et al. (82b)]. Comparisons with the measurements of Sakai, Hosono, et al. (80) show excellent agreement with the angular distributions and

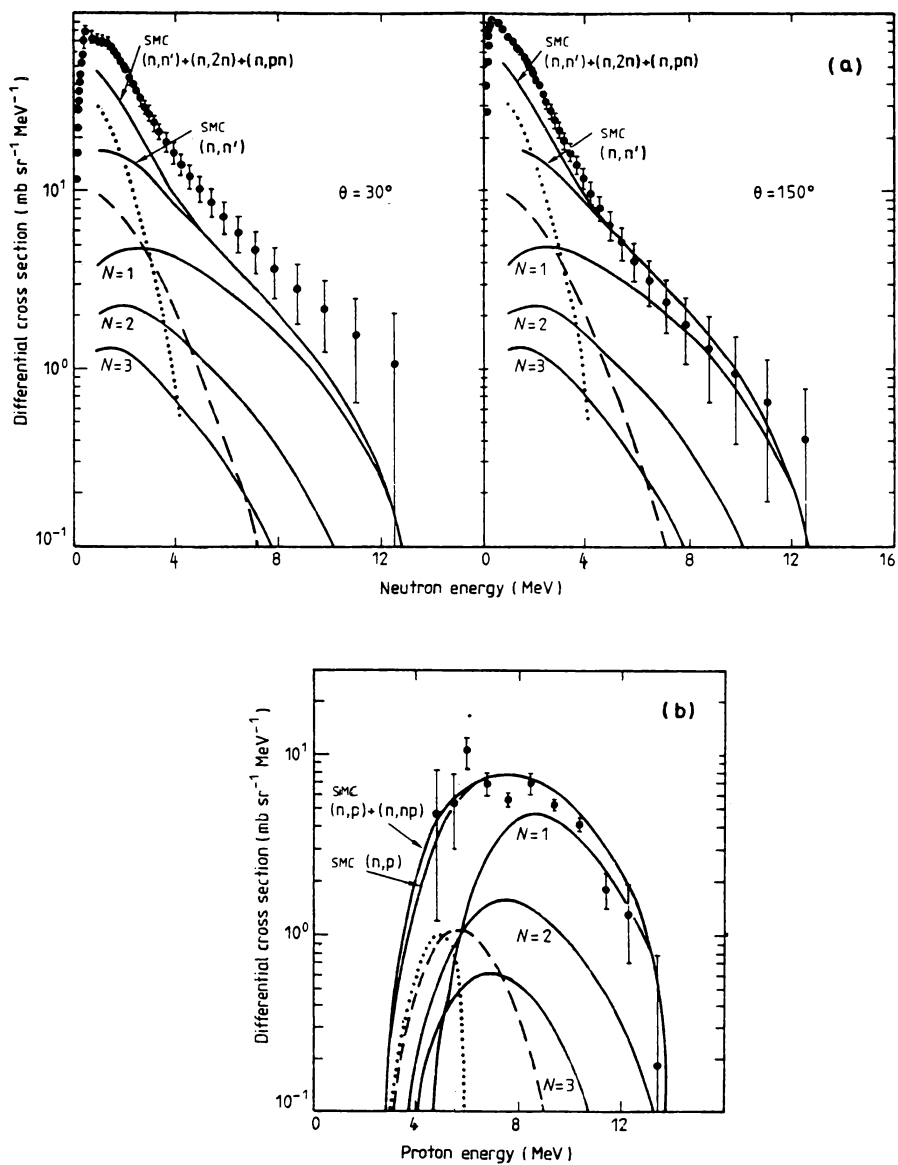


FIG. 6.10. (a) Energy spectrum of neutrons emitted at 30° and 150° from ^{93}Nb at an incident neutron energy of 14 MeV. The experimental data of Salnikov, Lovchikova et al. (70, 71) are compared with the statistical multistep compound calculations. (b) Energy spectrum of protons emitted at 150° from ^{93}Nb at an incident neutron energy of 14 MeV. The experimental data of Grimes, Anderson, et al. (78) are compared to statistical multi step compound calculations. For both (a) and (b) the curves labeled with N show the contributions of the N -step process. The dashed and dotted lines give the contributions of r stage processes which for case (a) are (n,n') and $(n,2n) + (n,pn)$, respectively; for (b) they are (n,p) and (n,np) , respectively. [From Field, Bonetti, and Hodgson (86).]

TABLE 6.1

Target	σ	$a(=\pi^2/6g)(\text{MeV}^{-1})$	$V_0(\text{MeV})$	$\bar{V}_0(\text{MeV})$	$\sigma_1/\sigma_{\text{tot}}$
$^{48}\text{Ca}(E_p=45 \text{ MeV})$	1	7.4	27.5	15.5	0.55
$^{90}\text{Zr}(E_p=45 \text{ MeV})$	1.4	10	27.5	17	0.55
$^{120}\text{Sn}(E_p=25 \text{ MeV})$	1.8	16	27.5	16	0.82
$^{129}\text{Sn}(E_p=35 \text{ MeV})$	1.8	16	27.5	16	0.72
$^{208}\text{Pb}(E_p=45 \text{ MeV})$	2.4	13	27	15	0.47

Source: Bonetti and Colambo (83).

analyzing power. Agreement with the latter is good only for relatively low excitation, $U = 10$ and 14 MeV but fails in the intermediate angular range $45^\circ < \theta < 110^\circ$ for $U = 18$ and 22 MeV . Presumably, the inclusion of the MSC process is needed for these large excitation energies.

A number of conclusions can be drawn from this analysis: The division of the statistical reaction process into multistep direct and multistep compound components appears to be useful and important. The multistep direct process dominates at the higher projectile energies, while the multistep compound is important for large excitation energies of the residual nucleus as well as for lower projectile energies. At sufficiently low energies the system is “trapped” on the first step so that there is no precompound emission. Therefore, at low energies, compound nucleus formation dominates. As the energy increases, the precompound emission (as given by the SMC theory) must be included, as the evaporation theory fails by orders of magnitude. At still higher projectile energies, the SMD process begins to be important and eventually is dominant, with the exception of cases in which the residual nucleus is highly excited and the emerging particle has a low energy. For these reactions the SMC process must be taken into account. Moreover one learns that the single-step direct process (DWA) is inadequate for proton energies lying between 25 and 65 MeV . It provides only 55% of the cross section for $E_p = 45 \text{ MeV}$.

7. SUMMARY

In this chapter we have discussed the influence of multistep processes on nuclear reactions. In Sections 2 and 3 we considered examples in which relatively few levels of the target and/or residual nucleus could be involved as intermediate steps in a multistep process. For these cases a coupled-channel description was employed. In Section 4 the influence of inelastic multistep processes on particle transfer reactions was considered. Here the coupled-channel Born approximation (CCBA) was used, in which the coupled-channel description was used to describe the mutual and final states and the transfer reaction was calculated as a single-step process. It was found that multi-step processes were important when

the states of the nuclei involved are collective (e.g., vibrational or rotational). When the number of states involved is large, we suggest the statistical theory developed in Section 5, with applications in Section 6. Many of the concepts used were developed by an earlier semiclassical theory based on pioneering papers by Griffin (66,67) and Weisskopf (60). This analysis is reviewed by Blann (75). For a comparison between the SMC theory and the semiclassical theory, see Holler, Kaminsky, et al. (85). Other theories of the MSC process are given by Agassi and Weidenmüller (75), Mantzouranis (76), and Friedman, McVoy, Hussein, and Mello (81). The latter authors develop formalisms that do not require the use of the chaining hypothesis but are more difficult to apply. Other theories for the SMD reaction have been proposed by Tamura, Udagawa, and Lenske (82), Agassi, Mantzouranis and Weidenmüller (75), and Mantzouranis (76). The first of these is limited to two-step processes, while the latter uses the Pauli master equation, involving, however, some ad hoc assumptions regarding the underlying nucleon–nucleon interaction.

The theory presented in Section 5 has a wide range of applicability, far wider than as described in the applications described in Section 6. In particular, the application to heavy ion reactions has not yet been developed except for the light helium ions (see, however, Section VIII.6). It would also be useful in determining the nature of the background in giant resonance reactions, permitting a more accurate determination of the widths of the resonances.

APPENDIX

The propagator $\mathcal{G} = (E^{(+)} - H^{(D)})^{-1}$ is defined by

$$(E^{(+)} - H^{(D)})\mathcal{G} = 1 \quad (\text{A.1})$$

The quantity of interest is \mathcal{G}_μ :

$$\mathcal{G}_\mu = P_\mu \mathcal{G} P_1 \quad (\text{A.2})$$

Multiplying (A.1) from the left by P_μ and from the right by P_1 leads to a set of coupled equations for \mathcal{G}_μ :

$$(E - H_\mu^{(D)})\mathcal{G}_\mu = v_{\mu,\mu-1}\mathcal{G}_{\mu-1} + v_{\mu,\mu+1}\mathcal{G}_{\mu+1} \quad (\text{A.3})$$

When $\mu = M$,

$$(E - H_M^{(D)})\mathcal{G}_M = v_{M,M-1}\mathcal{G}_{M-1}$$

or

$$\mathcal{G}_M = G_M v_{M,M-1}\mathcal{G}_{M-1} \quad (\text{A.4})$$

where

$$G_M = (E^{(+)} - H_M^{(D)})^{-1}$$

Turn next to (A.3) with $\mu = M - 1$:

$$(E - H_{M-1}^{(D)})\mathcal{G}_{M-1} = v_{M-1,M-2}\mathcal{G}_{M-2} + v_{M-1,M}\mathcal{G}_M$$

Substituting from (A.4) yields

$$(E - H_{M-1}^{(D)} - v_{M-1,M}G_M v_{M,M-1})\mathcal{G}_{M-1} = v_{M-1,M-2}\mathcal{G}_{M-2}$$

Therefore, using recurrence relation (5.16) yields

$$\mathcal{G}_{M-1} = G_{M-1}v_{M-1,M-2}\mathcal{G}_{M-2} \quad (\text{A.5})$$

One can now proceed stepwise to consider the equation satisfied by \mathcal{G}_{M-2} . The solution will have the same form as (A.5):

$$\mathcal{G}_{M-2} = G_{M-2}v_{M-2,M-3}\mathcal{G}_{M-3} \quad (\text{A.6})$$

One can now use mathematical induction to establish (5.14):

$$\mathcal{G}_\mu = G_\mu v_{\mu,\mu-1}\mathcal{G}_{\mu-1} \quad (5.14)$$

CHAPTER VIII

HEAVY IONS

1. INTRODUCTION[‡]

Heavy-ion physics is concerned with the reactions induced by nuclear projectiles whose mass number A is greater than or equal to 4. Nuclei ranging in mass number from the α -particle to the uranium nucleus have been accelerated to energies varying from a few MeV per nucleon (MeV/ A) to many GeV/ A . As this is being written, an accelerator at CERN is producing beams of ^{16}O nuclei with an energy[†] of 200 GeV/ A ; at Brookhaven, beams of nuclei up to ^{32}S with energies of approximately 15 GeV/ A have become available. Experiments at the Bevelac at Berkeley have been performed with beams of mass number extending up to uranium and with energies extending up to 2.1 GeV/ A . The capability of lower-energy machines is shown in Fig. 1.1. Of course, to make the story complete one would need to specify, as well, the currents that are available for each ion species and energy. It is not appropriate here to describe the various stratagems employed to obtain these beams. Usually, they involve the use of several accelerators (two or three) operating in tandem. The plan in each case involves stripping the heavy-ion projectile of some or all of its atomic electrons by passing the heavy-ion beam through a stripper, generally a foil. The process increases in effectiveness with increasing beam energy. The resulting heavy ion will then have a large net charge, which permits its acceleration to very high energies using electromagnetic fields. The extraordinarily rich set of phenomena produced when a heavy ion collides with a nucleus has three fundamental

[‡]Bromley (84).

[†]The energy of a 200 GeV/ A ion equals 0.32 ergs/ A !

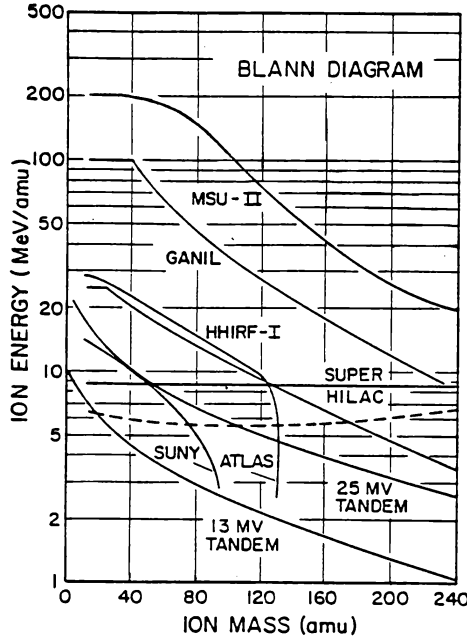


FIG. 1.1. Ion energy in MeV/nucleon as a function of the ion mass for a variety of facilities as of 1984. [From Bromley (84).]

sources: the strong electric field of the heavy ion, its large mass, and its compositeness.

The magnitude of the electric field at the surface of a nuclei is given by

$$|E| = \frac{Ze}{R^2} \simeq \frac{Z}{A^{2/3}} \frac{MV}{\text{fm}} = \frac{Z}{A^{2/3}} 10^{19} \text{ V/cm} \quad (1.1)$$

a very strong field that decreases like $1/r^2$ with increasing distance R from the nuclear surface. The energy stored in the field outside of the nuclear surface is

$$E = \frac{Z^2 e^2}{R} = 1.2 \frac{Z^2}{A^{1/3}} \text{ MeV} \quad (1.2)$$

which yields an energy of 67.6 MeV for ^{27}Al and 1362 MeV for ^{208}Pb .

As a consequence of the strong, long-range electric field, it becomes possible for the incident heavy ion to excite the target nucleus electromagnetically. This phenomenon, referred to as *Coulomb excitation*, has been most important in the determination of the energy spectrum of deformed nuclei, permitting excitations to very high spin values. An example is given in Fig. 1.2, obtained by 1165-MeV ^{232}Th projectile incident upon Pb nuclei.

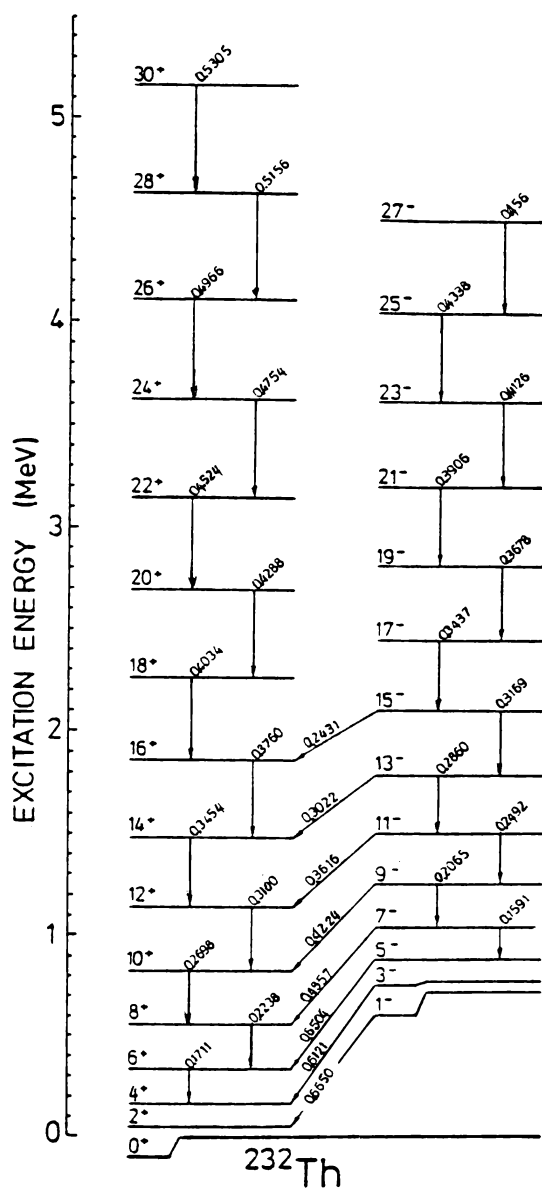


FIG. 1.2. Partial level scheme of ^{232}Th with the transitions seen in the Coulomb excitation by ^{208}Pb . [From deBoer (84).]

The strong electric field can, in fact, disintegrate the target nucleus. At the high energies available at the Bevelac, one can approximately replace the incident projectile by a beam of photons (Weizsäcker–Williams method) with the spectrum

$$N(\omega)d\omega \simeq \frac{2}{\pi} \frac{Z^2 e^2}{\hbar c} \left(\frac{c}{v}\right)^2 \frac{d\omega}{\omega} \quad (1.3)$$

where the photon energy is $\hbar\omega$. The photon can be absorbed by the target ejecting one or in some cases two nucleons. The cross section for the process is given by

$$\sigma = \frac{2}{\pi} \frac{Z^2 e^2}{\hbar c} \left(\frac{c}{v}\right)^2 \int \frac{\sigma_\gamma(\omega) d\omega}{\omega} \quad (1.4)$$

where σ_γ is the photoelectric cross section. Note that σ is proportional to Z^2 . The experimental evidence for this process is illustrated in Fig. 1.3. Here the ratio of the cross section to that of ${}^9\text{Be}$ is plotted for ${}^{18}\text{O}$ beams with 1.7 GeV/ A energy incident on a variety of nuclei up to uranium. Disintegration of the ${}^{18}\text{O}$ beams is observed. The solid line gives the cross section generated by nonelectromagnetic interaction. [For this separation, see Friedlander and Heckman (85).] The deviation from the solid line increases approximately as

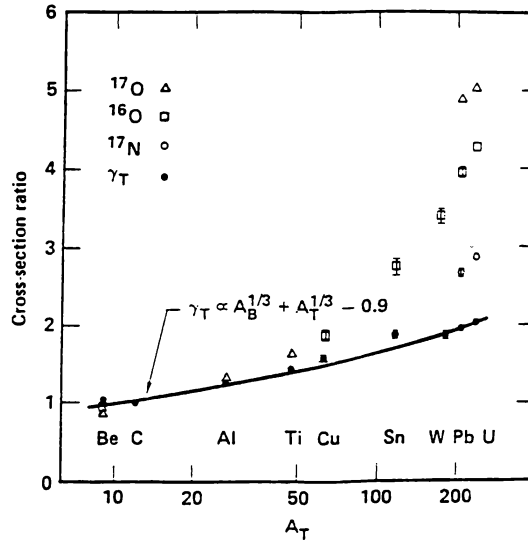


FIG. 1.3. Beam-rapidity fragment production cross-section ratios (normalized to the ${}^9\text{Be}$ cross section for ${}^{18}\text{O}$ at 1.7A GeV plotted versus mass number of the target. [From Friedlander and Heckman (84).]

Z^2 , in agreement with (1.4). There is some dependence on Z in σ_γ . Detailed calculations using an improved Weizsäcker–Williams photon spectrum yield quite good agreement with experiment.

Because of the intense electric fields, it is possible for pair production to occur in the collision of heavy ions. The observed position energy spectrum is shown in Fig. 1.4 for several pairs of heavy ions for the indicated projectile energies. The narrow peak at 300 keV has continued to escaped explanation.

Because of its large mass, the angular momentum of a heavy ion with respect to the center of mass of the target nucleus can be very large. The angular momentum in units of \hbar is classically given by

$$kR = 0.22 \sqrt{\frac{A_p A_t}{A_p + A_t} E_{\text{MeV}}} R_{\text{fm}} \quad (1.5)$$

where A_p and A_t are the projectile and target mass number, E the projectile energy in the center-of-mass system in MeV [$= (A_t/A_t + A_p) E_{\text{lab}}$], and R the sum of the target and projectile radii in fermis. If, for example, $A_p \sim {}^{48}\text{Ca}$, the target is ${}^{108}\text{Pd}$, and $E_{\text{lab}} = 205$ MeV, then $kR = 153$. Thus if these nuclei were to fuse, the resulting compound system could have a very large angular momentum. A proton at the same energy per nucleon would have a kR value of 2.6.

When a compound system of high spin is produced, the spin is, from the discussion above, approximately perpendicular to the scattering plane. Neutrons will generally be evaporated, but being isotropic, these will not carry off angular momentum. The isotopes formed in this way may also decay by γ emission. For example, in the reaction ${}^{48}\text{Ca} ({}^{108}\text{Pd}, 4n) {}^{152}\text{Dy}$, an isotope of Dysprosium is formed. Its γ -decay has been measured. Figure 1.5 shows the gamma spectrum of the highest spin band. The number marking each line is the spin of the level in ${}^{152}\text{Dy}$ emitting the γ -ray. This band is based on a prolate “superdeformation” described by Bohr and Mottelson (62). [See also the calculations of Dudek and Nazarewicz (85).] These authors showed that nucleons moving in an axially symmetric deformed oscillator well would have a *closed shell* for nucleon number 86 when the ratio of ω_x , the harmonic frequency transverse to the symmetry axis, is twice ω_z , the harmonic frequency along that axis. The corresponding deformation δ [see (VI.10.14) in deShalit and Feshbach (74)] is $\frac{1}{2}$.

Because of the large mass, the projectile has a very short wavelength. Using

$$\chi_{\text{fm}} = \frac{1}{k} = 4.55 \sqrt{\frac{A_p + A_t}{A_p A_t} \frac{1}{E_{\text{MeV}}}} \quad (1.6)$$

the χ for ${}^{48}\text{Ca}$ is 0.067 fm with $E_{\text{lab}} = 205$ MeV. As a consequence, one can use the methods of physical optics, that is, one can use the trajectories, obtained by solving Newton’s equations of motion, as describing the path taken by the wavefront rays. By calculating the change in phase of each ray, one can construct

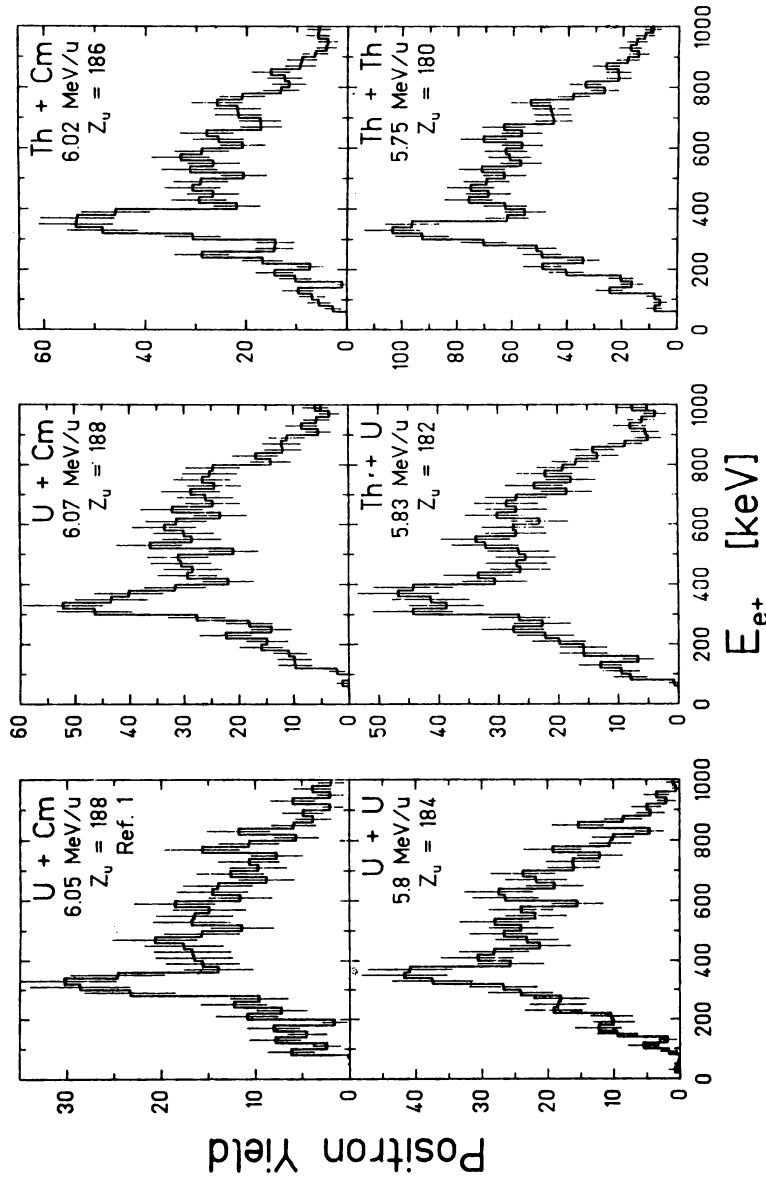


FIG. 1.4. Positron energy spectra for the five collision systems and bombarding energies indicated. [From Cowan et al. (85).]

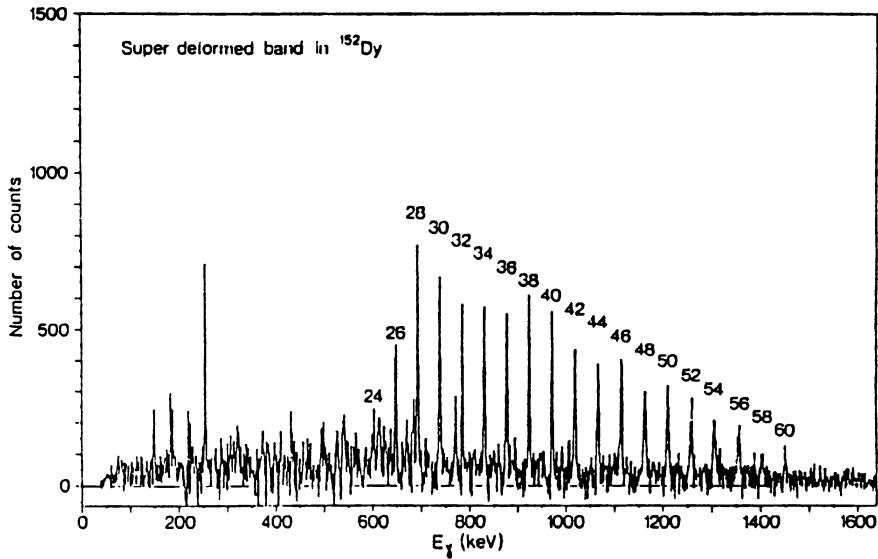


FIG. 1.5. Gamma-ray spectrum in the superdeformed band in ^{152}Dy following the $^{108}\text{Pd}(^{48}\text{Ca}, 4n)^{152}\text{Dy}$ reaction at 205 MeV. [From Twin et al. (86).]

the new equiphase wavefront, thus taking the effect of the interaction into account (see p. 103).

The Newtonian trajectory of the projectile in the Coulomb field of force exerted by the target nucleus is of obvious importance below and in the neighborhood of the Coulomb barrier energy. That trajectory is a hyperbola in the scattering plane given by

$$\frac{1}{r} = -\frac{k}{\eta} \tan^2 \frac{\vartheta}{2} \left[1 - \csc \frac{\vartheta}{2} \sin \left(\theta - \frac{\vartheta}{2} \right) \right] \quad (1.7)$$

where r is the distance from the center of charge of the target nucleus and θ measures the angle made by the vector from the scatterer to a point on the trajectory with respect to the incident direction, as illustrated in Fig. 1.6. The

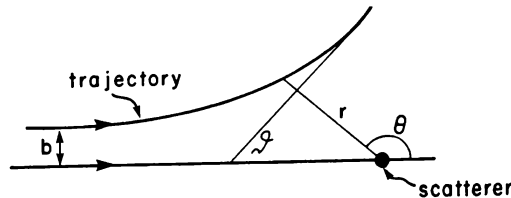


FIG. 1.6. Coulomb trajectory.

angle ϑ is the scattering angle and η is the Sommerfeld parameter:

$$\eta = \frac{Z_t Z_p e^2}{\hbar v} \quad (1.8)$$

Note that $r \rightarrow \infty$ when $\theta = \vartheta$ and also at $\theta = \pi$. The distance of closest approach, d , is obtained by placing $dr/d\theta = 0$. This yields $\theta = \pi/2 + \vartheta/2$. Therefore,

$$d = \frac{\eta}{k} \left(1 + \csc \frac{\vartheta}{2} \right) \quad (1.9)$$

while the impact parameter, b , is given by

$$b = \frac{\eta}{k} \cot \frac{\vartheta}{2} \quad (1.10)$$

Note that $\eta/k = Z_t Z_p e^2 / \hbar v k = Z_t Z_p (e^2 / \hbar c) (\hbar c / 2E)$. Numerically, $\eta/k = Z_t Z_p / 1.37E$, where E is in MeV and η/k is in fermis. The straight-line asymptote to the hyperbolic trajectory is given by

$$y \cos \vartheta = x \sin \vartheta + b \quad (1.11)$$

where x is the incident direction and y is perpendicular to x . Finally, the classical differential cross section is

$$\frac{d\sigma}{d\Omega} = \frac{b}{\sin \vartheta} \left| \frac{db}{d\vartheta} \right| \quad (1.12)$$

Using (1.10), one obtains the Rutherford cross section:

$$\frac{d\sigma}{d\Omega} = \left(\frac{\eta}{2k} \right)^2 \frac{1}{\sin^4(\vartheta/2)} = \left(\frac{Z_t Z_p}{2\mu v^2} \right)^2 \frac{1}{\sin^4(\vartheta/2)} \quad (1.13)$$

where μ is the reduced mass. The cross section drops rapidly with angle and can be quite large. For example, for 205-MeV ^{48}Ca incident on ^{208}Pb , $d\sigma/d\Omega$ equals $56 \csc^4 \frac{1}{2}\vartheta \text{ (fm)}^2$, which at $\vartheta = 30^\circ$ becomes 0.896 barn. The grazing angle ϑ_{gr} , which will play an important role in many of the discussions in this chapter, is given according to (1.9) by

$$R = \frac{\eta}{k} (1 + \csc \frac{1}{2}\vartheta_{\text{gr}}) \quad (1.14)$$

where R is the sum of the radius of the projectile R_p and the radius of the target R_t . The trajectory corresponding to the scattering angle ϑ_{gr} just touches the surface of the target nucleus.

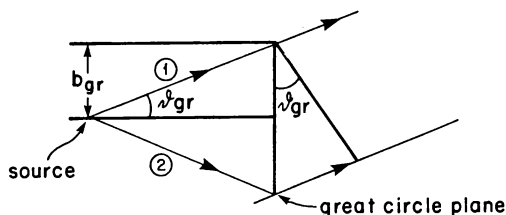


FIG. 1.7. Properties of the grazing trajectory.

As is clear from Fig. 1.6, the Coulomb field has an effect similar to that of a diverging lens [Frahn (66)]. The effective source for a point Coulomb field is a line source. However, when the nucleus is black, completely absorbing, which as we shall discuss later, is the case for most of the energy range of interest and for a wide variety of target and projectile nuclei, the grazing trajectory and the corresponding source point ($x = -b_{gr} \csc \vartheta_{gr}$) are of special importance. This is because (see discussion on p. 414) the intensity beyond the target nucleus in the forward direction can be calculated as if the perimeter of the great circle perpendicular to the incident direction acts as a source. If the path difference between the grazing trajectory labeled (1) in Fig. 1.7 and the trajectory passing through the opposite side labeled (2) equals the wavelength λ , the intensity pattern will be of the Fresnel type. If it is much less than λ the intensity pattern is of the Fraunhofer type. We obtain the conditions

$$p \gg 1 \quad \text{Fresnel}, \quad p < 1 \quad \text{Fraunhofer} \quad (1.15)$$

where

$$p = kb_{gr} \sin \vartheta_{gr} = 2\eta \cos^2 \frac{\vartheta_{gr}}{2} \quad (1.16)$$

Thus when the Sommerfeld parameter η is large, the angular distribution will be of the Fresnel type. This will be the case if the nuclei involved are reasonably heavy. [Note: Frahn's p is $\frac{1}{2}$ that given in (1.16).] The angular distribution in the geometric optics limit is illustrated in Fig. 1.8. In the physical optics limit, diffraction oscillations will be present for $\vartheta \lesssim \vartheta_{gr}$, while for larger angles, the shadow region, $\vartheta > \vartheta_{gr}$, the cross section will decrease rapidly.

An example of Fresnel scattering is shown in Fig. 1.9. The value of p for this case is 28. The angular region with the smooth and sharp decrease corresponds

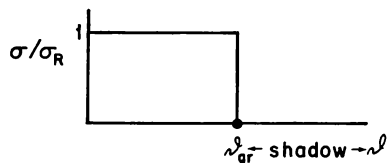


FIG. 1.8. Angular distribution in the geometric optics limit.

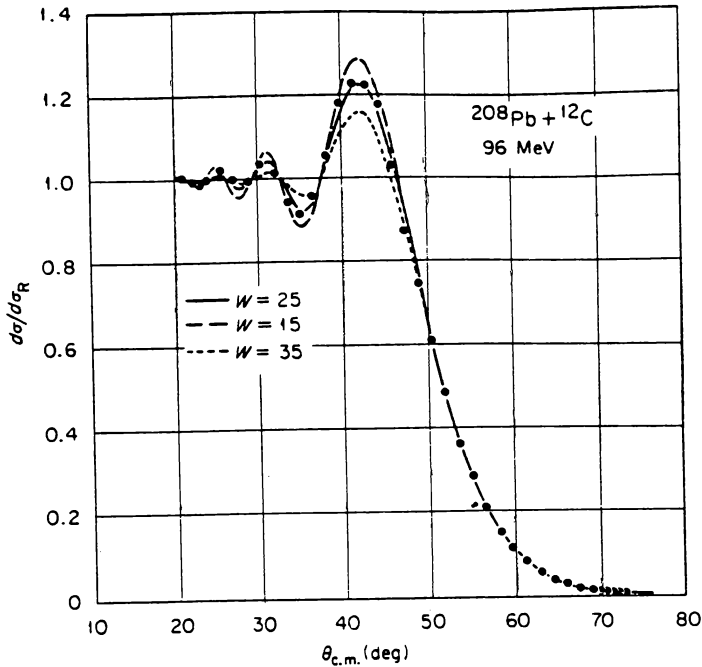


FIG. 1.9. Showing the sensitivity of the structure in the illuminated region of Fresnel scattering to the ratio of the strengths of the real (V) and imaginary (W) parts of the optical potential. In each case $V = 40$ MeV. [From Satchler (75).]

to the shadow cast by the target. Large-angle scattering corresponds to small values of the impact parameter. For these values the incident trajectory would strike the target and be absorbed. An example of Fraunhofer scattering is shown in Fig. 1.10. The value of p for this case is 3.

When the nuclear interaction is taken into account, another interference phenomena becomes important. In Fig. 1.11 we show the trajectories in the presence of a real Woods–Saxon nuclear potential acting between the heavy ions in addition to the Coulomb interaction [Glendenning (75)]. Trajectory g is the grazing trajectory. Trajectory 1 is a Coulomb trajectory, and trajectory 3 shows the effect of the nuclear interaction. The scattering angle for trajectories 1 and 3 are identical. If the interaction surface is free of absorption, one can expect fluctuations in the angular distribution. Figure 1.12, which gives the angular distribution for the reaction $^{60}\text{Ni}(^{18}\text{O}, ^{16}\text{O})^{62}\text{Ni}(\text{g.s.})$, shows very large oscillations. Because this reaction involves the transfer of two neutrons, one can be certain that the nuclear interaction is involved. Baltz, Bond, Garrett, and Kahana (75) conclude that the absorption component of the optical potential consists of two parts. One is the interior volume potential, which drops off very sharply at the nuclear surface. The second is a surface derivative of a

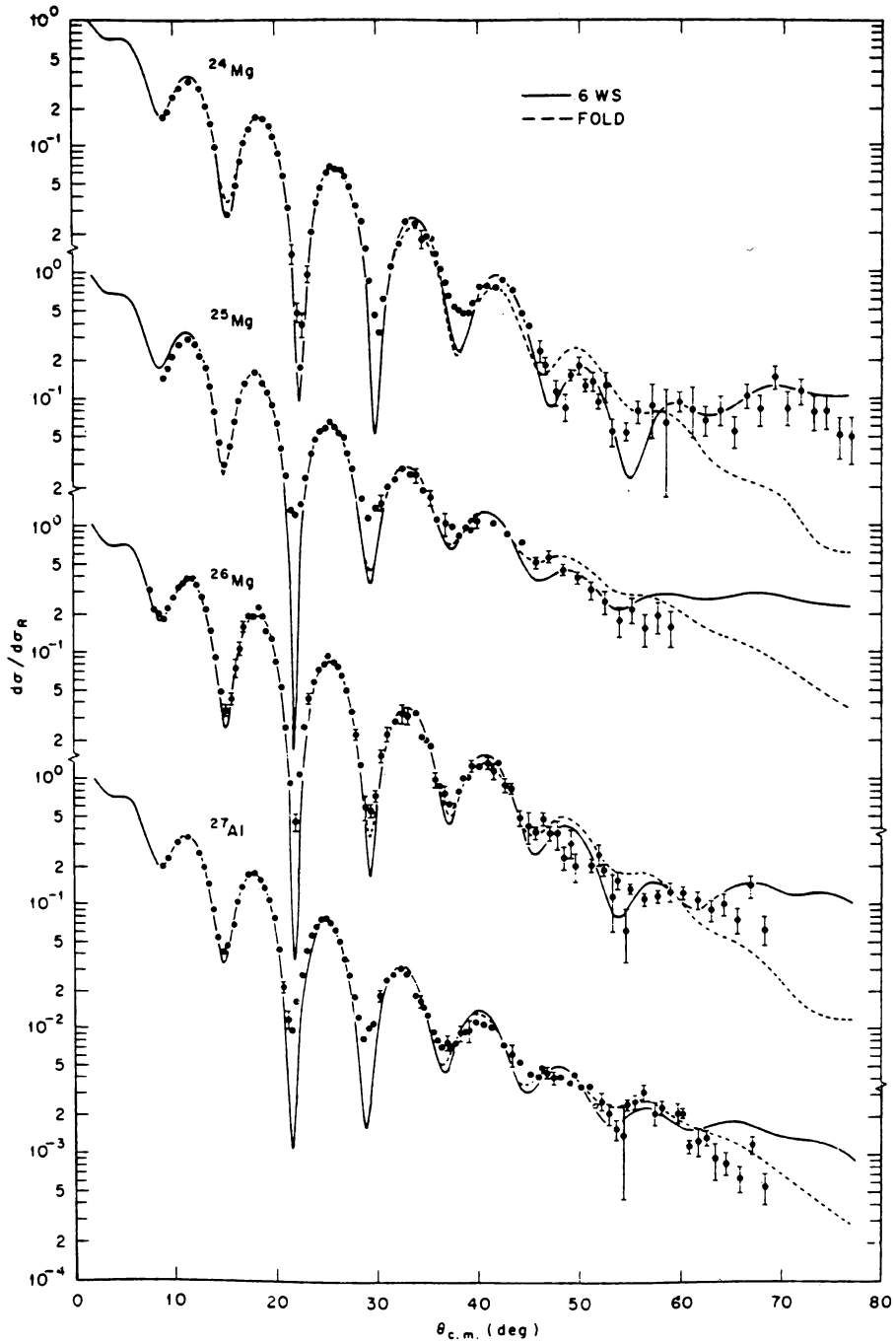


FIG. 1.10. Appearance of Fraunhofer-type patterns in the elastic scattering of ${}^6\text{Li}$ at 88 MeV. Optical-model fits using both Woods-Saxon and folded real potentials are shown. [From Fulmer, Satchler, et al. (81).]

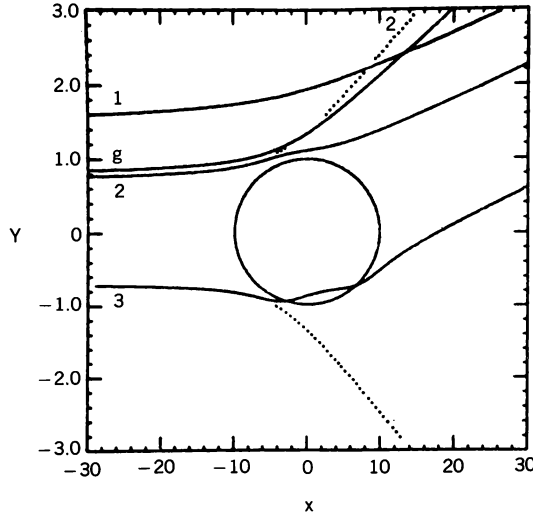


FIG. 1.11. Four classical orbits described in the text [Glendenning (75).]

Woods–Saxon potential, which is much weaker in the nuclear surface region but stronger in the nuclear interior. The stronger absorption in the nuclear interior attenuates its contribution to the reaction, which therefore originates in the surface. The interference phenomena described above occurs because of the near transparency of the surface region.

The classical deflection angle Θ plays an important role in qualitative discussions. Its relation to the potential acting between the two nuclei can be obtained from the WKB expression for the phase shift δ_λ [see Morse and Feshbach (53, p. 1102)].

$$\delta_\lambda = \int_{r_0}^{\infty} \sqrt{k^2 - U - \frac{\lambda^2}{r^2}} dr - \int_{r_1}^{\infty} \sqrt{k^2 - \frac{\lambda^2}{r^2}} dr \quad (1.17)$$

where $k^2 = 2\mu/\hbar^2 E$, $U = 2\mu/\hbar^2 V$, and $\lambda = l + \frac{1}{2}$. The turning points r_0 and r_1 are zeros of the respective integrands. Differentiating with respect to λ yields

$$\frac{\partial \delta_\lambda}{\partial \lambda} = -\lambda \int_{r_0}^{\infty} \frac{dr}{r^2 \sqrt{k^2 - U - \lambda^2/r^2}} + \lambda \int_{r_1}^{\infty} \frac{dr}{r^2 \sqrt{k^2 - \lambda^2/r^2}} \quad (1.18)$$

Since

$$k^2 - U - \frac{\lambda^2}{r^2} = \frac{\mu^2}{\hbar^2} \dot{r}^2 \quad \left(\dot{r} = \frac{dr}{dt} \right)$$

the first term in (1.18) is

$$-\frac{\lambda\hbar}{\mu} \int_{r_0}^{\infty} dr \left(\frac{1}{r^2 \dot{r}} \right)$$

But the angular momentum $\lambda\hbar$ can be related to the deflection angle Θ :

$$\lambda\hbar = \mu r^2 \dot{\Theta}$$

so the integral becomes $\int_{r_0}^{\infty} d\Theta$. A similar result is obtained for the second term in (1.18). The net result is then $\frac{1}{2}\Theta_t$, where Θ_t is the *total* deflection angle, including the incoming and outgoing trajectories. Equation (1.18) becomes (the second integral yields just $\pi/2$)

$$\frac{\partial \delta_\lambda}{\partial \lambda} = \frac{1}{2} \Theta_t = \frac{\pi}{2} - \lambda \int_{r_0}^{\infty} \frac{dr}{r^2 \sqrt{k^2 - U - \lambda^2/r^2}} \quad (1.19)$$

The scattering angles ϑ and Θ are not identical, as is illustrated by the three trajectories in Fig. 1.12, with identical values of ϑ . Bearing in mind that the sense of rotation is defined with respect to $(\mathbf{r} \times \mathbf{k})$, the value of Θ equals ϑ for case (a) equals $-\vartheta$ for case (b), and equals $(\vartheta - 2\pi)$ for case (c). Case (a) corresponds to a repulsive potential; case (b) and case (c), increasingly stronger attractive potentials acting along the trajectories.

Finally, we consider collisions in which the complex structure of the projectile and target enter in an essential fashion. The extraordinarily rich phenomena that are a consequence have been only partially explored and understood. In peripheral collisions ($d \gtrsim R$), elastic scattering, Coulomb excitation, inelastic scattering, and transfer reactions are the dominant phenomena. There are sometimes referred to as *elastic* and *quasi-elastic scattering*. As the impact parameter decreases ($d < R$), *deep inelastic scattering*, in which much of the kinetic energy of the incident projectile is converted into internal energy occurs

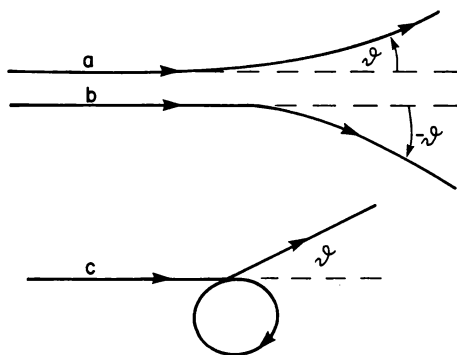


FIG. 1.12. Scattering angle ϑ for different trajectories.

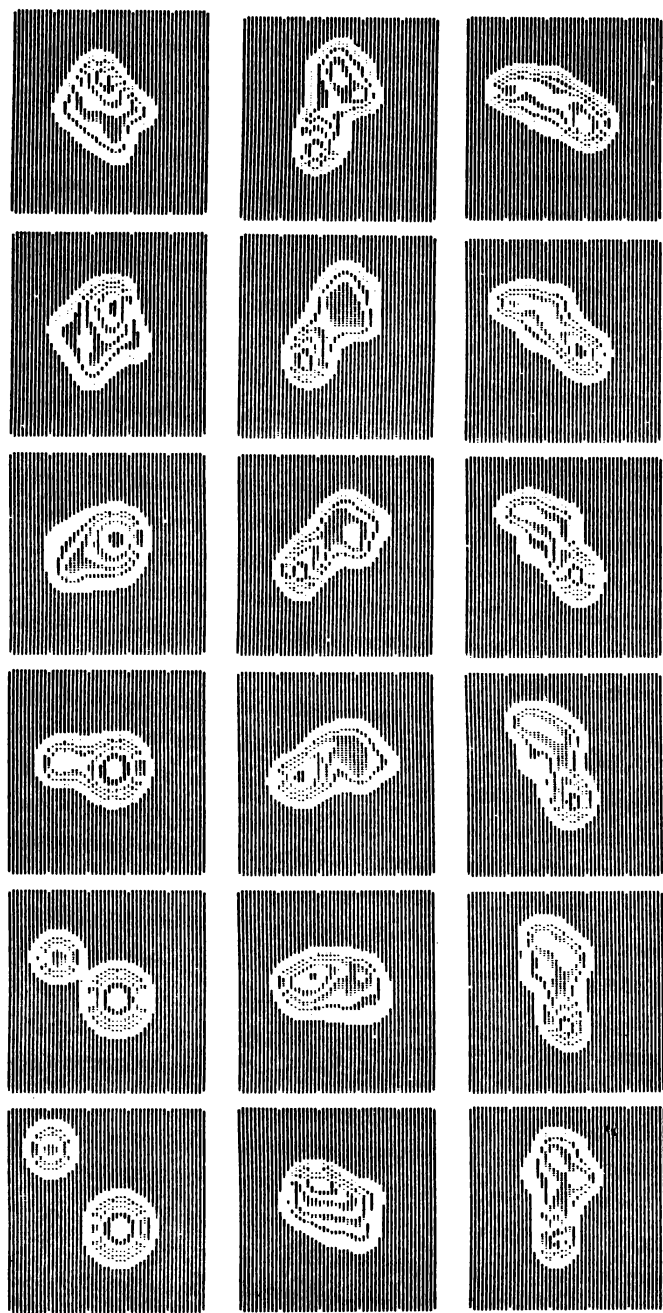


FIG. 1.13. Contour plots at sequential times of the density in the center of mass integrated over the normal to the reaction plane for $^{16}\text{O} + ^{40}\text{Ca}$ collision at the laboratory energy of 315 MeV. The initial angular momentum is $60\hbar$. [From Negele (82).]

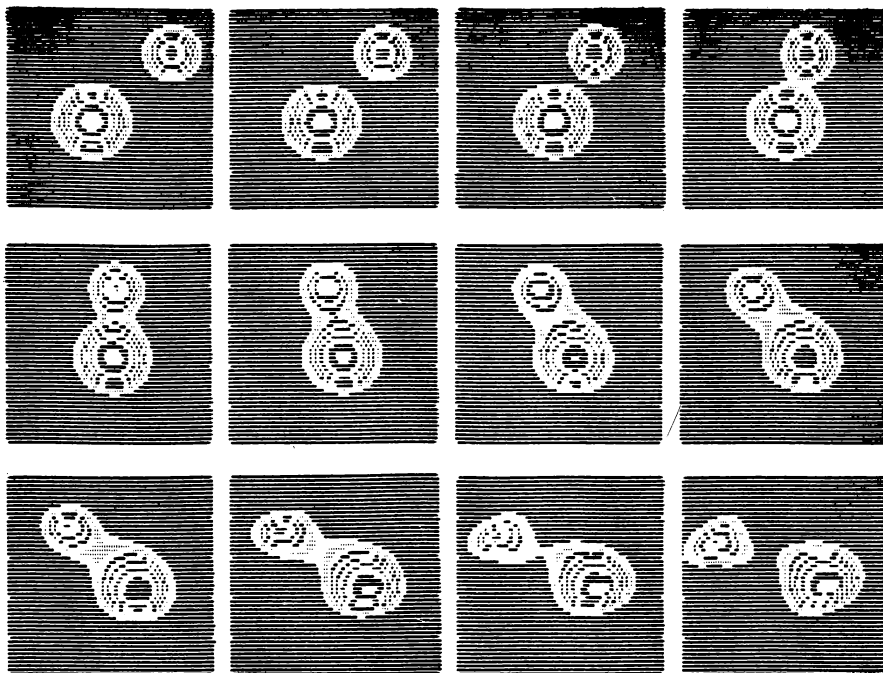


FIG. 1.14. Contour plots at sequential times of the density in the center of mass integrated over the normal to the reaction plane for $^{16}\text{O} + ^{40}\text{Ca}$ Collision at the laboratory energy of 315 MeV. The initial angular momentum is $80\hbar$. [From Negele (82).]

so that the kinetic energy of the final nuclei derives mostly from the Coulomb repulsion. In this class of phenomena, which occurs for the most part with the heavier nuclei, the nuclei may undergo small changes in A and Z as several nucleons are interchanged while the angular distribution is strongly anisotropic. Finally, under suitable conditions the projectile can penetrate and a compound system is formed. This reaction is referred to as *fusion* reaction. If the compound system lives long enough to randomize completely, a compound nucleus in an excited state is the result. These two classes of reactions, deep inelastic and fusion, are illustrated in Figs 1.13 and 1.14, obtained by using the time-dependent Hartree–Fock method (to be discussed later). The first illustrates fusion. We see that the two nuclei join forming a very elongated nucleus, which then proceeds in three complete rotations being reduced in size as it does so. The second illustrates deep inelastic scattering. Again the elongated nucleus is formed. But after rotating through roughly 90° , it breaks apart. An intermediate situation in which complete rotations occur but the system does not fuse is referred to as *fast fission*.

These qualitative considerations are summarized in Fig. 1.15, in which the range in angular momentum l (or impact parameter b) for which the various

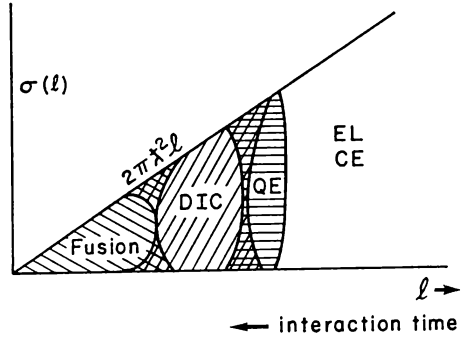


FIG. 1.15. Various reaction types as a function of the angular momentum, l .

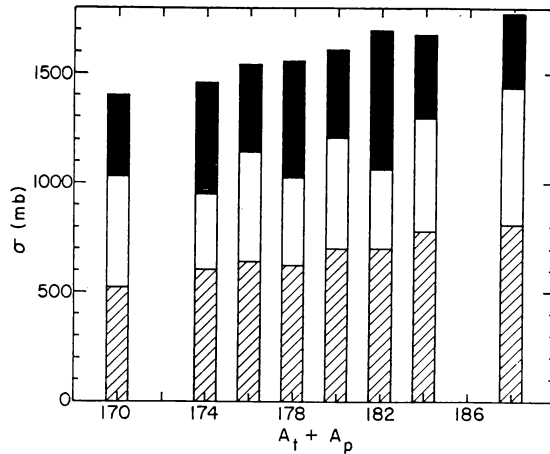


FIG. 1.16. Decomposition of the reaction cross sections as a function of the total mass number $A_t + A_p$ for the Ni-induced reactions on the even- A Sn isotopes around $E_{\text{cm}} = 220$ MeV. Shaded bars indicate values for the total fusion cross sections; fully shaded bars give the values for the total quasi-elastic transfer cross sections. [From van den Berg, Henning, et al. (88).]

processes discussed above are dominant is indicated. The crosshatched areas involve a mix of the two neighboring types. The possible value of the partial cross section $\sigma(l)$ is bounded by the geometrical cross section $2\pi k^2 l$. For the low angular momenta, compound nucleus formation and more generally fusion dominate, to be succeeded at higher angular momenta by deep inelastic scattering. This is followed by quasi-elastic scattering, that is, peripheral (one-step) reactions, and finally, for impact parameters greater than the interaction radius by elastic scattering and Coulomb excitation. Of course, these divisions are not sharp. Indeed, according to Rehm, Van denBerg, et al. (85), their experimental results indicate that the quasi-elastic processes gradually make

the transition to deep inelastic as single-particle transfers are replaced by multistep processes.

It is possible to establish a connection with the concepts employed in the discussion of the statistical multistep reactions discussed in Chapter VII (see Section 5 and Fig. 1.1). Note that the interaction time increases, as indicated, from large to small l values, the formation of the compound nucleus involving the longest interaction time. The quasi-elastic processes are identical with the single-step direct reaction, the deep inelastic has all the properties expected of the statistical multistep direct reaction, while fusion generally is an example of the statistical multistep compound reaction.

Of course, all values of l will contribute in a given reaction. In Fig. 1.16 we give an example of the relative magnitudes of each contribution for the reactions induced by $^{58,64}\text{Ni}$ incident on the various Sn isotones. The energy of the ^{58}Ni beam is 330 MeV, while the ^{64}Ni beam has energies 341 and 380 MeV. These energies correspond to center-of-mass energies roughly 30 MeV greater than the barrier energy. The proportions of each contribution will vary with the experimental situation.

2. FUSION

Let us now consider each of these regions in more detail. We begin with fusion. The discussion will be made in terms of macroscopic variables. The microscopic description is the subject of Sections 6 to 8. The macroscopic variables describe the relatively slow motions of the system. The microscopic description is concerned with the motion of the individual nucleons, which is relatively rapid. One obvious macroscopic variable is the distance R between the centers of mass of the colliding nuclei. Another variable that measures the deformation will be defined later. Models using only the R variable are referred to as one-dimensional models. The potential energy of the colliding nuclei illustrated in Fig. 2.1 is taken as a linear combination of a central Woods–Saxon potential, the Coulomb potential, and the centrifugal potential. Note the minimum or “pocket,” which decreases in depth as the orbital angular momentum l (and therefore the impact parameter) increases, until finally at $l = l_b$ the minimum disappears. The depth of the pocket as well as l_b decreases as the product $Z_1 Z_2$ for the interacting nuclei increases. For an impact parameter below l_b/k and a given energy, there will be a finite probability that the system will be trapped in the minimum for a time sufficiently long for the two nuclei to fuse completely and form a compound nucleus. That probability increases with the depth and width of minimum. In detail this is accomplished through mutual excitation, particle and cluster transfer, and by interpenetration.[‡] These processes occur not only in the pocket but more generally as the nuclei approach each other, with the result that some of the kinetic energy of the system is converted into

[‡]Interpretation and transfer of large clusters are not distinguishable.

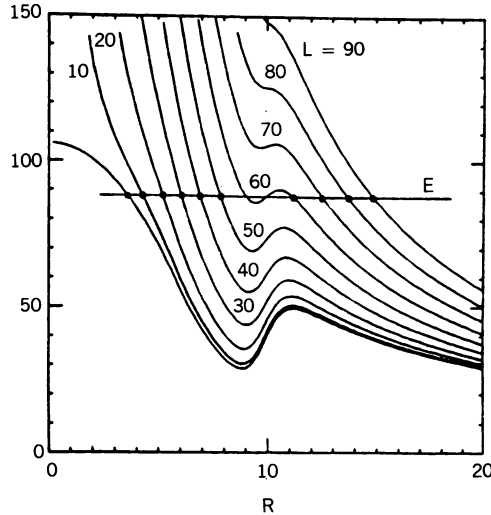


FIG. 2.1. For the system $^{18}\text{O} + ^{120}\text{Sn}$, the sum of the nuclear, Coulomb, and centrifugal potentials are shown for the indicated values of the angular momentum l . The horizontal line marks $E_{\text{cm}} = 87$ MeV. The turning points for various l 's are indicated by dots. [From Glendenning (75).]

internal energy. Thus by the time the barrier region is reached, the kinetic energy may already be reduced, facilitating the formation of the compound nucleus even when the initial orbital angular momentum exceeds l_b . The conversion of kinetic into internal energy with the consequent slowing of the nuclei can be described classically and macroscopically in terms of the action of a frictional force. Friction is invoked in classical models of the nucleus–nucleus collision.

Instead of the transfer of clusters from one nucleus to the other occurring in the potential minimum, it is clearly possible for them to be emitted before the compound nucleus is formed. The mass number of the final compound nucleus will then be less than the sum of mass numbers of the two colliding nuclei. Moreover, its momentum will be less than the momentum of the incident projectile, since some momentum is carried off by the emitted cluster, which can, for example, be an α -particle or heavier nuclear system. This process is referred to as *incomplete fusion*. This process is an example of a precompound or the multistep compound reaction discussed in Chapter VII, in which the road to complete fusion is interrupted by the emission of a cluster. It differs from the discussion in Chapter VII in that the remaining fragment can still go on to fuse.

The clusters carry off angular momentum. This is important because the compound nucleus may not be able to support the large angular momentum acquired in its formation. One such bound is provided by the Yrast line [see

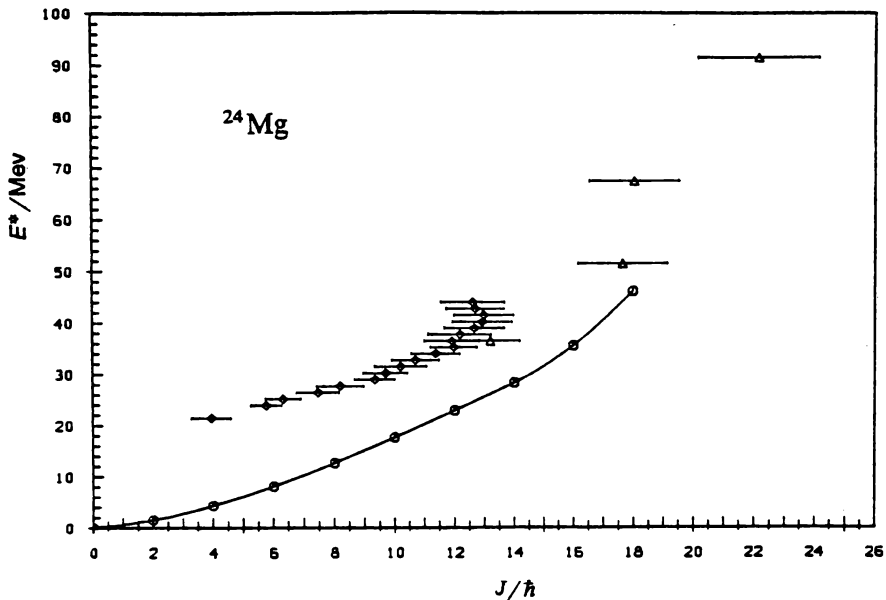


FIG. 2.2. Fusion data from $^{12}\text{C} + ^{12}\text{C} \rightarrow ^{24}\text{Mg}$ as obtained by Kovar, Gessamen, et al. (79) (diamonds) and Namboodiri, Chulick, and Natowitz (76) (triangles). The solid line and circles are a result of an Yrast line calculation for ^{24}Mg by Mülhans, Müller, Neegård, and Mosel (81) [From Mosel (84).]

Fig. 2.2 and Vandenbosch and Lazzarini (81)]. If the excitation energy and angular momentum fall to the right of the Yrast line, a compound nucleus will not be formed. If the angular momentum and energy carried by the emitted cluster or clusters are sufficient to move the original values of E and J to the left of the Yrast line, a compound nucleus can be formed. A second limitation has been discussed by Cohen, Plasil, and Swiatecki (74). The issue is the stability of a charged rotating nonviscous liquid drop. A rigid moment of inertia is assumed and the energy calculated for a variety of shapes. Their results are shown in Fig. 2.3. According to these calculations, the limiting angular momentum is about $100\hbar$ for a nucleus with $A \approx 130$. However, for both lighter and heavier nuclei, the limiting values are considerably less. Again we see that the precompound emission of clusters may be required if a compound nucleus is to be formed.

A particular example of a precompound process is referred to as *fast fission*. Of course, the compound nucleus formed by fusion may fission. Fast fission occurs *before* that compound nucleus is formed. In terms of the behavior shown in Figs 1.13 and 1.14 in fast fission, complete rotations do occur, but instead of fusing, the system breaks apart. According to Gregoire, Ngô, et al. (82), during the rotation and as a consequence of the exchange of energy, momentum and

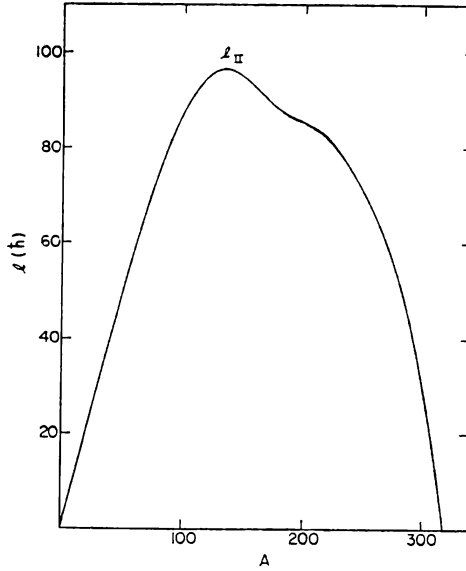


FIG. 2.3. The curve l_{II} is the angular momentum at which the fission barrier of a beta-stable nucleus with mass number A is predicted to vanish. [From Cohen, Plasil, and Swiatecki (74).]

mass, the system equilibrates and a different radial dependence of the potential $V(R)$ develops. If this potential does not have a sufficiently deep minimum, fusion will not occur; fission will. The various possible situations according to Gregoire, Ngô et al. (82) are illustrated in Fig. 2.4.

This last discussion brings the importance of time scales to our attention. The relaxation time τ_n for the motion of the nucleons to be randomized and equilibrium established is generally much smaller (except at small excitation energies) than the relaxation time for collective motion to disappear. The third time, τ_{app} , of significance is the time it takes the system to penetrate to the potential minimum. If τ_{app} is shorter than τ_n , the system will arrive in the potential minimum before equilibrium is established. The compound nucleus will then be formed as described earlier. However, if $\tau_{app} > \tau_n$, equilibrium will develop before the potential minimum is attained. As a consequence, a new interaction $V(R)$ will operate. Fast fission or deep inelastic scattering may then occur.

The simple one-dimensional interaction, $V(R)$, does not take into account the role of deformation. From the point of view of the compound nucleus, the two nuclei, at their point of contact, for example, form a highly deformed system. The passage from that situation to the deformation characteristic of the compound nucleus follows from the nature of the dependence of the potential energy upon the deformation as well as upon R . This is shown in Fig. 2.5. Nix and Sierk (77) [see also Möller and Nix (76) and Krappe, Nix, and Sierk (79)]

	$l < l_{Bf}$	$l > l_{Bf}$	$Z_1 Z_2 \sim 2000 - 2500$	$Z_1 Z_2 \geq 2500 - 3000$
SUDDEN POTENTIAL				
ADIABATIC POTENTIAL				
	COMPOUND NUCLEUS FORMATION	FAST FISSION	FAST FISSION	NO COMPOUND NUCLEUS FORMATION NOR FAST FISSION

FIG. 2.4. Conditions for fast fission and compound nucleus formation. The quantity l_{Bf} is the value of the angular momentum at which the fission barrier vanishes. [From Gregoire, Ngô, et al. (82).]

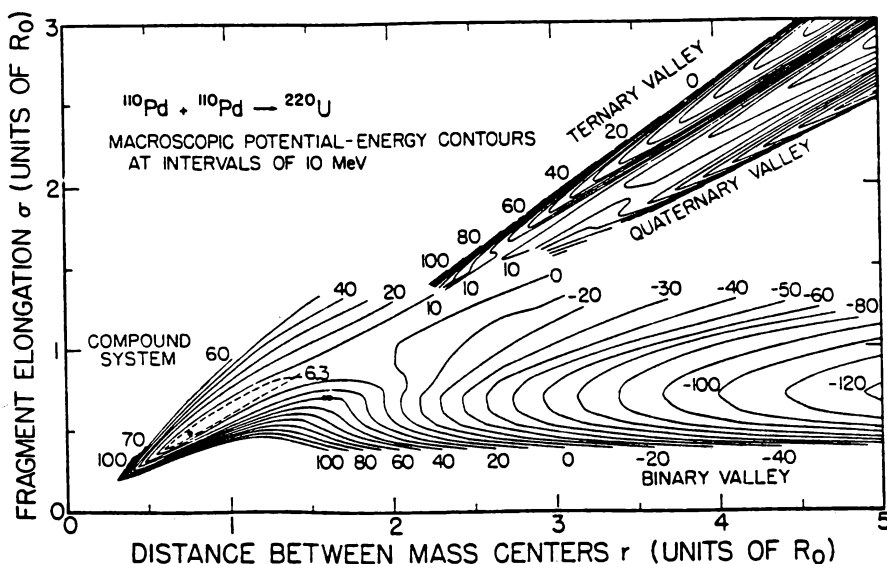


FIG. 2.5. Potential energy surface for ^{220}U as a function of two shape parameters, r and σ . Whereas r directly describe the distances between the centers of mass of the two interacting nuclei, σ is a measure for the deformation of the two. The ground state of ^{220}U is normalized to zero energy; the numbers at the contours give the energies relative to it in MeV. The contact point of two spherical touching ^{110}Pd nuclei lies at $r \approx 1.6$, $\sigma \approx 0.71$. [From Nix and Sierk (77).]

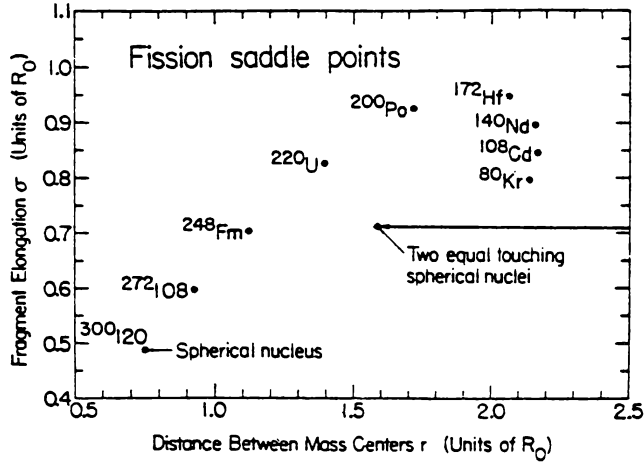


FIG. 2.6. Locations of the binary macroscopic zero angular-momentum fission saddle points in the r - σ plane for selected nuclear systems. These systems can be formed in symmetric collisions of two neutron-rich β -stable nuclei. [From Nix and Sierk (77).]

calculate the Coulomb and nuclear energy for a variety of shapes of the interacting nuclei. The diffusivity of the nuclear surface, as well as the finite range of the nuclear force (central only), is taken into account. No single-particle effects are included. Dissipation is neglected. The collision is head on, that is, $l = 0$. The colliding nuclei are identical. The deformation is measured by the elongation, σ , defined as $2[\langle Z^2 \rangle - \langle Z \rangle^2]$, where Z is along the symmetry axis. The factor of 2 takes the elongation of both nuclei into account. Two points in Fig. 2.5 are important. One is the value of σ and R at which the two nuclei are in contact. The other is the fission saddle point. As one deforms the spherical compound nucleus, the potential energy increases arriving eventually at a maximum, the fission saddle point. If the nucleus has enough energy to pass over or penetrate the barrier, fission will occur. If the contact point occurs to the left of the fission saddle point, compound nucleus formation will occur. This is generally the case for light nuclei. If, on the other hand, it occurs to the right, it must have enough energy to pass over the barrier to form a compound nucleus, as will be required for the heavier nuclei. The extra amount of energy beyond the barrier is known as *extra push* [see also Swiatecki (82)]. The $l = 0$ situation for a variety of identical colliding nuclei is shown in Fig. 2.6. Clearly, systems whose total mass number beyond about $A = 220$ will have a low probability of forming a spherical compound nucleus since the fission saddle point for heavier compound nuclei lies far to the left of the contact point. The effect of angular momentum (collisions with a finite value of the impact parameter) and of the energy of the colliding systems is shown in Fig. 2.7, where again the interacting nuclei are both ^{110}Pd but the energy is now 20 MeV above the barrier energy for $l = 0$. The fission saddle points for each value of l are

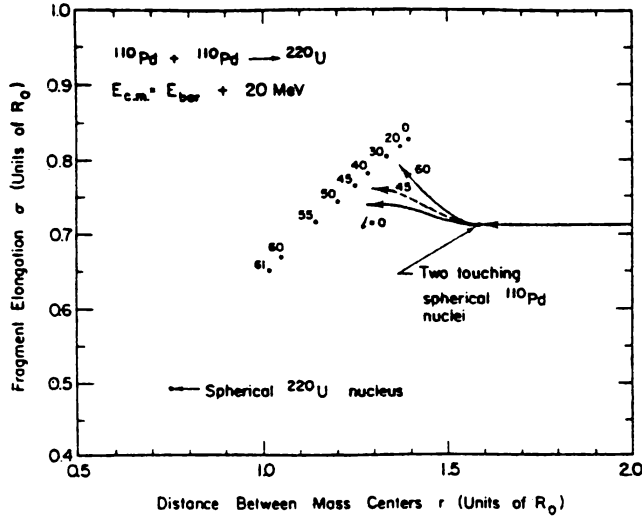


FIG. 2.7. Dynamical trajectories in the r - σ plane for the reaction $^{110}\text{Pd} + ^{110}\text{Pd} \rightarrow ^{220}\text{U}$ at a bombarding energy in the center-of-mass system that is 20 MeV above the maximum in the one-dimensional zero-angular-momentum interaction barrier. The dashed curve gives the trajectory for the critical angular momentum $l_{\text{crit}} = 45$. [From Nix and Sierk (77).]

indicated by the solid dots. The various lines leading from the contact point indicate the paths of the system on the R - σ plane. For all $l \leq 45$, the fission saddle points lie to the right of the trajectory, so that it becomes possible to form the compound nucleus. On the other hand, for $l > 45$, an *extra push* beyond 20 MeV will be necessary.

Swiatecki (82) has derived a simple algebraic expression for the extra push energy E_x . The final expression, including adjustment of constants through comparison with experiment, is given by Bjornholm (82) as

$$E_x = 200(x_e - 0.7)^2 \text{ MeV}$$

where

$$x_e \equiv \left(\frac{Z^2}{A} \right)_{\text{eff}} \left(\frac{Z^2}{A} \right)_{\text{crit}}$$

where

$$\left(\frac{Z^2}{A} \right)_{\text{eff}} = \frac{4Z_1Z_2}{(A_1A_2)^{1/3}(A_1^{1/3} + A_2^{1/3})} + \left(\frac{fl}{l_{\text{ch}}} \right)^2$$

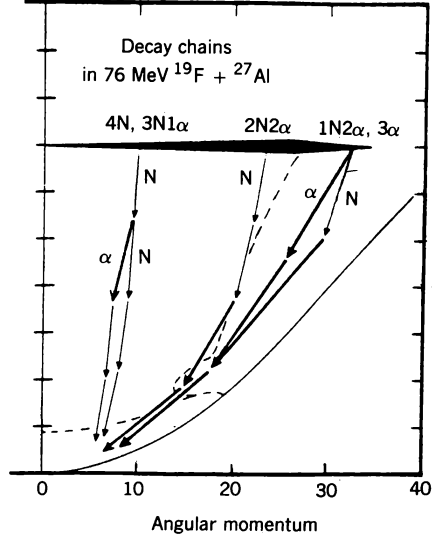


FIG. 2.8. The most likely chains in the reaction $76 \text{ MeV } ^{19}\text{F} + ^{27}\text{Al}$ are shown for differing angular momenta of the compound nucleus ^{46}Ti . Heavy arrows are for α -particle emission, thin ones are for nucleon emission. [From Stokstad (85).]

$$\left(\frac{Z^2}{A}\right)_{\text{crit}} = 50.9 \left[1 - 1.78 \left(\frac{N_1 + N_2 - Z_1 - Z_2}{A_1 + A_2} \right) \right]^2$$

$$I_{\text{ch}}^2 = 0.0105 \frac{(A_1 A_2)^{4/3} (A_1^{1/3} + A_2^{1/3})^2}{A_1 + A_2} \quad (2.1)$$

and

$$f = 0.75 \pm 0.05$$

Fusion cross sections are determined by observing the products of the decay of the compound nucleus formed by the reaction. Usually, the compound nucleus will be highly excited and generally will therefore decay before they are detected. For light nuclei, nucleon and α -particle emission is compete. For high angular momentum states, α -particle emission is favored (see Fig. 2.8). γ -Ray emission becomes important near and below the threshold for particle emission. Fission is not significant for the light nuclei. For medium-weight nuclei, fission will compete with neutron emission, especially for high-angular-momentum states, while charged particle decay will be less important because of the Coulomb barrier. For heavy nuclei only fission and neutron emission compete. A statistical model calculation showing the competition between neutron and γ -ray deexcitation for ^{164}Er formed by a beam of ^{40}Ar incident on ^{124}Sn is illustrated in Fig. 2.9. We see that the emission of four neutrons followed by γ -ray emission is the most probable decay chain. By observing the residues, one can verify the assumption behind the calculation leading to Fig. 2.9.

A considerable help in this endeavor is obtained by observing the multiplicity $\langle M_\gamma \rangle$ of the emitted γ -rays. These are related to the average nuclear angular

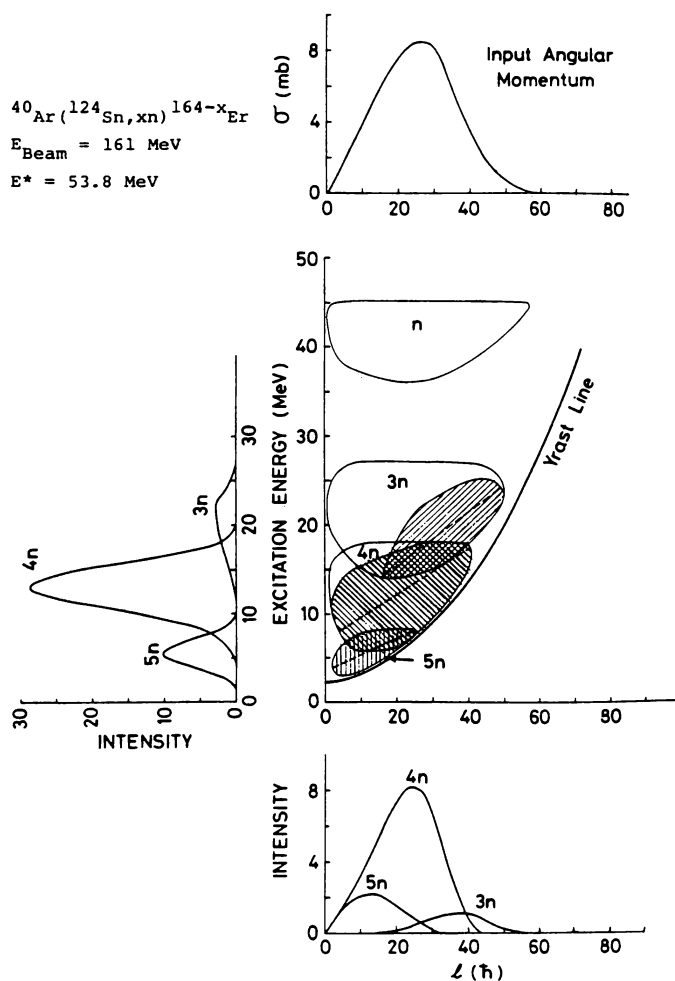


FIG. 2.9. Statistical model predictions for the decay of the ^{164}Er compound system formed at an excitation energy of 54 MeV with 147-MeV ^{40}Ar ions incident on ^{124}Sn . The assumed population of the ^{164}Er compound system is given as a function of angular momentum in the top portion of the figure. The calculated populations $\sigma(l, E^*)$ are indicated as a function of the excitation energy and angular momentum for the system after the emission of 1–5 neutrons. The shaded region of $3n$ – $5n$ population shows the portion in which gamma-ray emission competes. The entry populations for the $3n$ – $5n$ evaporation residues are indicated as a function of angular momentum and excitation energy at the bottom and to the left side of the figure. The predicted entry line is shown for each γ -ray emitting region [Tjønn, Espe, et al. (79)]. [From Stokstad (85).]

momentum l by the *empirical* formula

$$l = 2(M_\gamma - 4) \quad (2.2)$$

As is evident from this last discussion, the statistical theory of nuclear reactions (Section IV.7) plays an important role in the analysis of heavy ion reactions. This is especially the case when one measures the number of nuclei of a given type produced in the reaction. For fusion reactions, since each such nucleus is a consequence of the reaction, one obtains a direct determination of the number of reactions that have occurred. One must add to this cross section, referred to as σ_{ER} (ER \equiv evaporation residues), the cross section that results in fission, σ_{FI} , to obtain the total cross section. However, both the deep inelastic and quasi-elastic can contribute to the observed results, especially for the light, nearly symmetric, colliding nuclei. Statistical theory may be used to separate the fusion and fission contributions. For heavier nuclei and higher energies, incomplete fusion may contribute particularly for the larger angular momenta. One would then find that the statistical theory would underestimate the number of α -particles, for example, produced. In the case of fissioning nuclei it is possible to determine the total momentum carried off by the fission fragments. Compared to the critical momentum, one can determine the missing momentum carried off before the system fissioned. Note that neutron emission from the compound nucleus will generally be spherical and therefore not contribute to the linear momentum balance.

The characteristic symmetry about 90° of reactions involving the formation of the compound nucleus (see Section IV.7) can be used to separate fusion from quasi-elastic and deep inelastic reactions. Applying directly the results of the statistical theory leads to comparisons with experiment that are quite good. Figure 2.10, which gives the experimental and statistical angular distributions in the reaction $^{12}\text{C} (^{14}\text{N}, ^6\text{Li})^{20}\text{Ne}$, is a typical example. A simple classical consideration [Ericson (60a); Ericson and Strutinski (58)] shows that under circumstances to be described below the angular distribution obeys a $1/\sin \vartheta$ law. One assumes that the spin of the residual nucleus and emitted particle are small with the consequence that the orbital angular momentum of the emitted particle that is perpendicular to the final momentum must align itself with the angular momentum of the compound nucleus (Fig. 2.11). Moreover, assume that the spin of the compound nucleus, I , acquired from the collision is also orbital and therefore in a plane perpendicular to the original direction. The angular distribution is then proportional to the Dirac delta function $\delta(\hat{\mathbf{k}}_f \cdot \mathbf{I})$. To obtain the observed angular distribution, we must average over the possible orientations \mathbf{I} :

$$\frac{d\sigma}{d\Omega} \sim \frac{1}{2\pi} \int_0^{2\pi} \delta(\hat{\mathbf{k}}_f \cdot \mathbf{I}) d\phi = \frac{1}{2\pi} \int_0^{2\pi} \delta(I \sin \vartheta \cos \phi) d\phi = \frac{1}{2\pi I \sin \vartheta} \quad (2.3)$$

completing the proof. Of course, this result fails near $\vartheta = 0$ and π . The critical

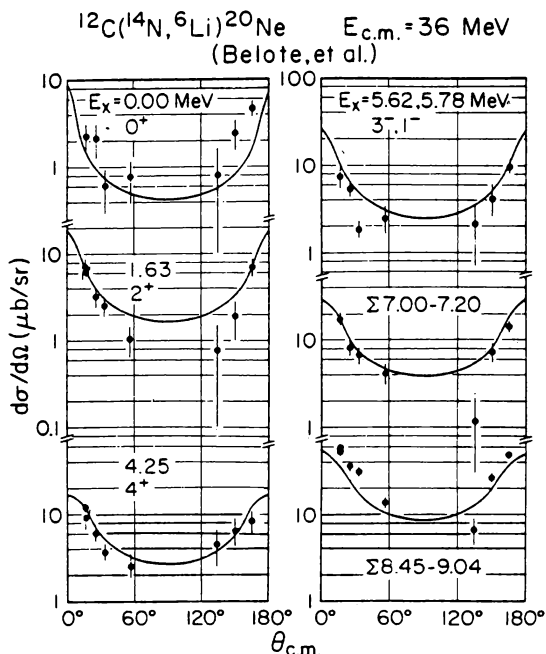


FIG. 2.10. Absolute Hauser-Feshbach statistical model calculations compared with experimental angular distributions for low-lying states in ^{20}Ne populated by the $^{12}\text{C}(^{14}\text{N}, ^6\text{Li})^{20}\text{Ne}$ reaction at $E_{\text{cm}} = 36 \text{ MeV}$ (Hanson, Stokstad, et al. (74)). [From Stokstad (85).]

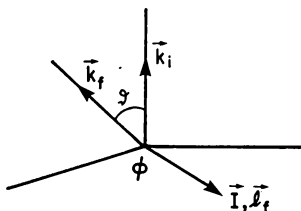


FIG. 2.11. Diagram for classical calculation of the angular distribution.

angle according to Ericson is j_f/J , where j_f is the spin of the emitted particle. Examples of the fit to this distribution are shown in Figs 2.12 and 2.13. Generally, comparison with experiment shows that the $1/\sin \theta$ distribution provides a good fit near 90° , but fails as one approaches the forward and backward directions.

In summary, the statistical theory of nuclear reactions can be used to (1) distinguish fusion from other reaction modes, (2) determine the spin of the compound nucleus formed, and (3) describe the decay of the compound nucleus, giving the yield of the particles emitted and their multiplicities. Fusion yields are also correctly given provided that one takes the density of final states to

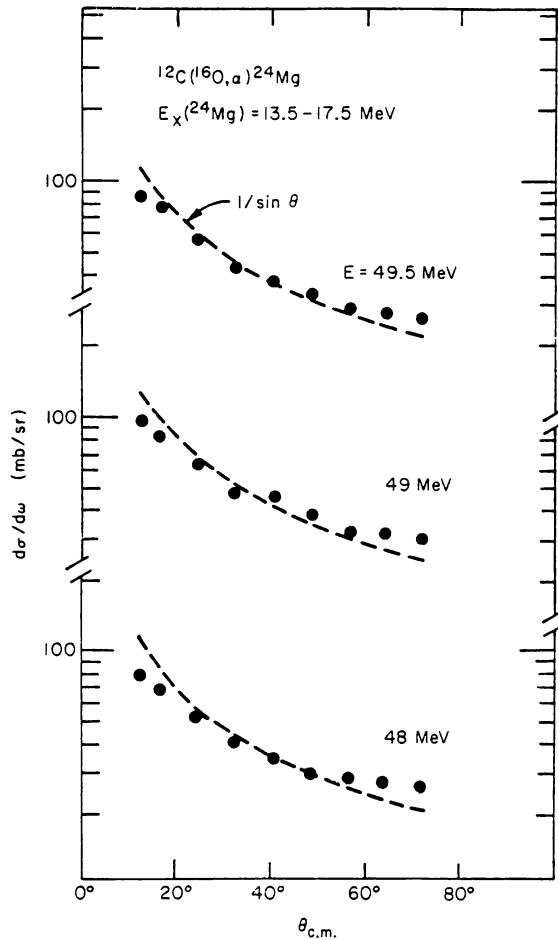


FIG. 2.12. Total α -particle angular distributions for $E_x = 13.5 - 17.5 \text{ MeV}$ in ^{24}Mg for incident energies of 48, 49, and 49.5 MeV. The dashed lines are least-squares fits to the function $1/\sin \theta$ [Greenwood, Katori, et al. (72)]. [From Stokstad (85).]

be the density of states of the compound nucleus at the fission saddle point [see Stokstad (85, pp. 115, 121, et seq.)]. In most cases the number of possible reaction paths is not small and even the statistical theory calculations become quite complex. As a consequence, several statistical model computer codes have been developed. These are listed to Stokstad (85, p. 125). Their use is discussed in the accompanying text. An important simplification has been recently obtained by Friedman and Lynch (83), who consider the time evolution of the evaporating systems. Their procedure should prove to be very useful.

Typical complete fusion cross sections are shown in Fig. 2.14. We note that in each of these cases the cross section falls on two straight lines. For low

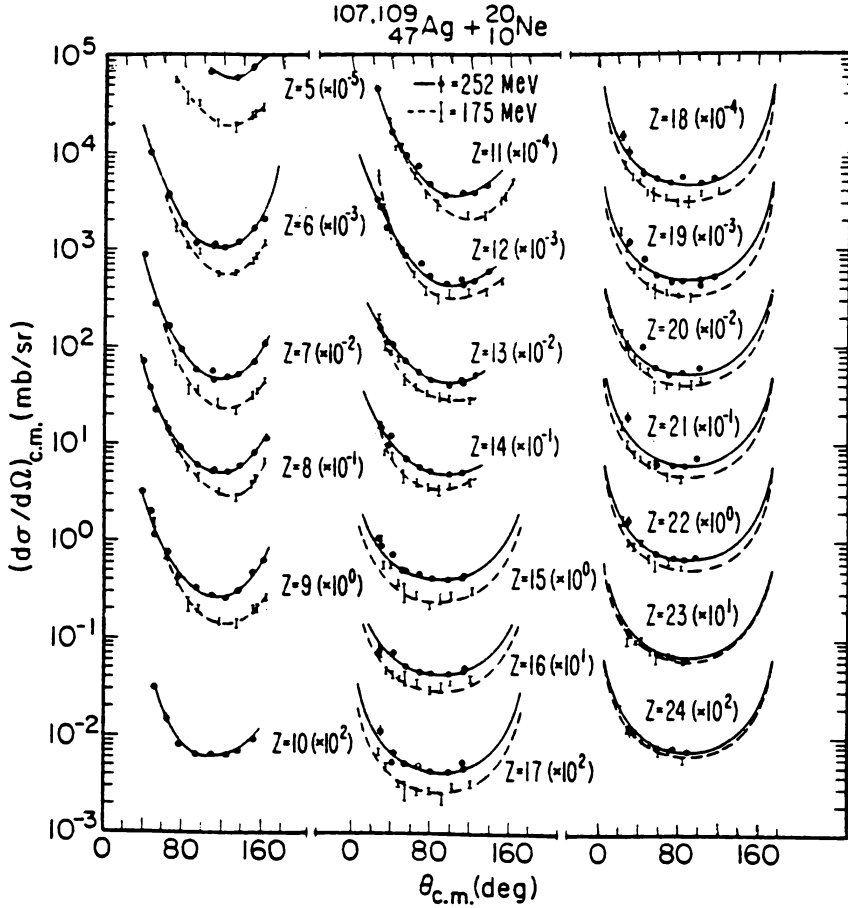


FIG. 2.13. The center-of-mass angular distributions of fragments from the reaction $^{107,109}\text{Ag} + ^{20}\text{Ne}$ at $E_{\text{lab}} = 175$ and 252 MeV. For fragment atomic numbers of $Z > 15$ curves drawn through the data correspond to $d\sigma/d\Omega \sim (\sin\theta_{\text{cm}})^{-1}$. [From Babinet, Moretto, et al. (76).]

energies, below the intersection of the two lines, referred to as region I, the fusion cross section σ_{CF} equals the reaction cross section σ_{R} , while for larger energies, region II $\sigma_{\text{CF}} \ll \sigma_{\text{R}}$. The one-dimensional radial model provides a simple explanation. In the low-energy region domain, the reaction, and therefore the fusion cross section, is given by

$$\sigma_{\text{R}} = \sigma_{\text{CF}} = \frac{\pi}{k^2} \sum_{l=0} (2l+1) T_l$$

where T_l are the transmission coefficients. One can calculate these from the

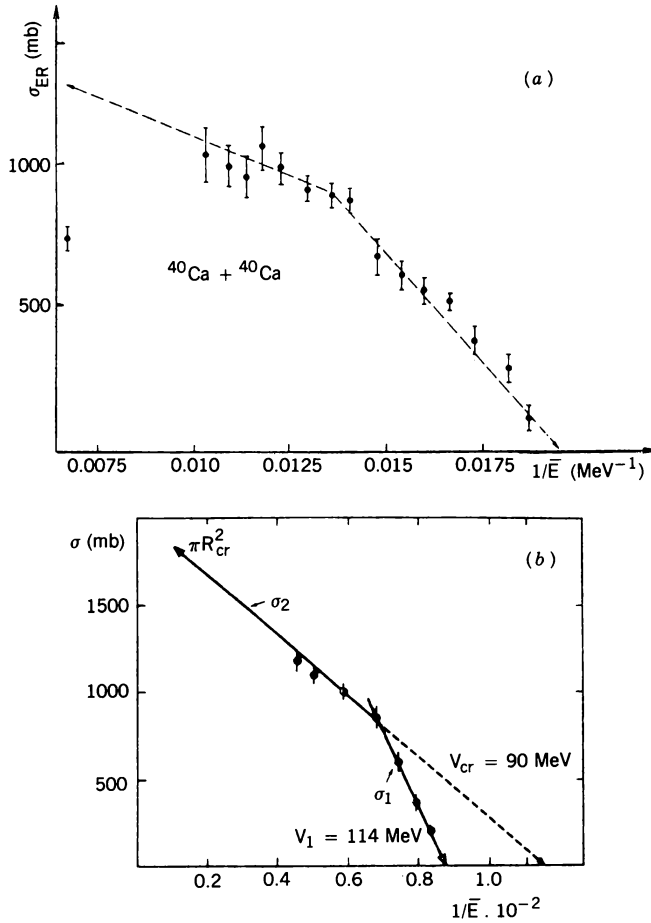


FIG. 2.14. Experimental fusion cross sections as a function of $(1/E)$: (a) medium-mass system $^{40}\text{Ca} + ^{40}\text{Ca}$; (b) heavy system $^{40}\text{Ar} + ^{121}\text{Sb}$. [From Lefort and Ngô (78).] (c) Fusion cross sections for $^{16}\text{O} + ^{27}\text{Al}$ compared with the formula of Glas and Mosel. [From Hodgson (78).]

optical model. A rough analytic approximation is obtained using the *sharp cutoff model*, in which

$$T_l = \begin{cases} 1 & \text{for } l \leq L \\ 0 & \text{for } l > L \end{cases} \quad (2.4)$$

Then

$$\sigma_{\text{CF}} = \frac{\pi}{k^2} \sum_0^L (2l+1) = \frac{\pi}{k^2} (L+1)^2 \simeq \frac{\pi}{k^2} L^2 \quad (2.5)$$

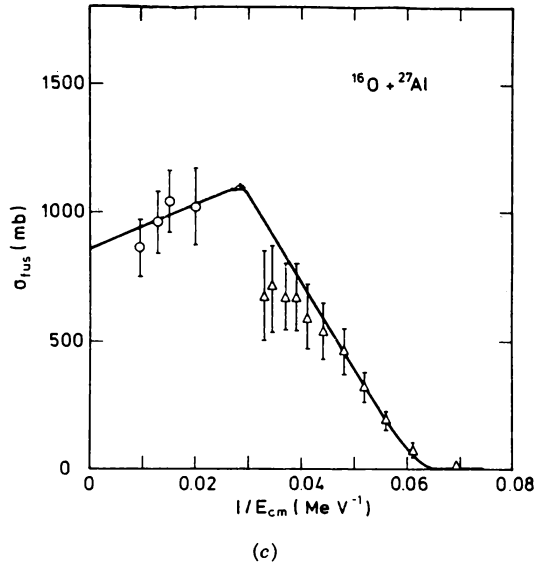


FIG. 2.14. (Continued)

Equation (2.4) corresponds to the assumption that for all l 's less than or equal to L , a minimum in the potential $V(R)$ exists which is of sufficient strength to trap the system for a long enough time for the interacting nuclei to fuse. For $R > L$, this is no longer possible. The value of L is given approximately by the effective wave number k_B at R_B multiplied by R_B , where $V(R)$ has its maximum. This recipe is verified by an optical model calculation. Thus

$$L = k_B R_B = k R_B \left(1 - \frac{V_B}{E} \right)^{1/2} \quad (2.6)$$

so that

$$\sigma_{CF} = \pi R_B^2 \left(1 - \frac{V_B}{E} \right) \quad (2.7)$$

in agreement with experiment. By comparing with experiment, one can determine R_B and V_B .

In region II, that is, at greater energies, the collision does not necessarily lead to fusion. The potential does not have a minimum of sufficient strength to trap the system. However, fusion can occur some fraction of the time if a sufficient interchange of mass and energy between the two nuclei has occurred: macroscopically, if friction has slowed the system down enough. This slowing-down process is more effective as R decreases, and for a sufficiently small R , R_C , will lead to fusion. One can calculate the probability of this occurring by assuming that for $r \geq R_C$, the wave function for the system

consisting of the colliding nuclei in this ground state is zero because of the probability of excitation and mass transfer. Using the WKB method for penetration through a parabolic barrier [Glas and Mosel (74, 75); Wong (72, 73), one obtains

$$\sigma_{\text{CF}} = \frac{\hbar\omega}{2E} R_B^2 \ln \frac{1 + e^{2\pi(E - V_B)/\hbar\omega}}{1 + e^{2\pi[E - V_B - (R_C/R_B)^2(E - V_B)]/\hbar\omega}} \quad (2.8)$$

where $\hbar\omega$ measures the width of the barrier and V_C is the potential at R_C . For high energies,

$$E \left[1 - \left(\frac{R_C}{R_B} \right)^2 \right] \gg V_B - \left(\frac{R_C}{R_B} \right)^2 V_C$$

one obtains

$$\sigma_{\text{CF}} = \pi R_C^2 \left(1 - \frac{V_C}{E} \right) \quad (2.9)$$

in agreement with experiment. At low energies,

$$\sigma_{\text{CF}} = \frac{\hbar\omega}{2E} R_B^2 \ln [1 + e^{2\pi(E - V_B)/\hbar\omega}] \rightarrow \pi R_B^2 \left(1 - \frac{V_B}{E} \right)$$

in agreement with (2.7). The quantity V_C is negative for Fig. 2.14a, while for Fig. 2.14b and c, V_C is positive. Empirically,

$$R_C = r_c (A_1^{1/3} + A_2^{1/3}) \quad r_c = 1 \pm 0.07 \text{ fm} \quad (2.10)$$

where A_1 and A_2 are the mass numbers of the interacting nuclei. Of course, one can compute σ_{CF} directly from the optical model with appropriate boundary conditions at R_C .

There are substantial disagreements of (2.8) with experiment which are exhibited when the cross sections for heavy-ion fusion reactions leading to the same compound nucleus are compared. One would not expect the fusion cross sections $^{14}\text{N} + ^{12}\text{C}$ and $^{16}\text{O} + ^{10}\text{B}$ to differ greatly, but they do. It is also surprising that the cross section for reaction $^{14}\text{N} + ^{12}\text{C}$ differs substantially from that of reaction $^{15}\text{N} + ^{12}\text{C}$. This has led to the development of an alternative explanation of the cross sections for region II based on Yrast line considerations discussed above [Harar (78); Matsuse, Arima and Lee (82)]. The critical value, L , is now given by the maximum value L , which is permitted by the Yrast line. For larger values of L , states of the compound nucleus do not exist. The value of L is given by the equation

$$E + Q = \hbar^2 \frac{L(L+1)}{2\mathcal{I}} + \Delta Q \quad (2.11)$$

where \mathcal{I} is the Yrast moment of inertia. ΔQ is the band head energy [Harar (78)]. Substituting in (2.5), one obtains

$$\sigma_{\text{CF}} = \frac{\pi \mathcal{I}}{\mu} \left(1 + \frac{Q - \Delta Q}{E} \right) \quad (2.12)$$

where μ is reduced mass. An example of the efficacy of this equation is provided by the comparison of the two reactions $^{14}\text{N} + ^{12}\text{C}$ and $^{16}\text{O} + ^{19}\text{B}$, which lead to the same compound nucleus ^{16}Al . These two reactions give very different cross sections. However, the relation between $E^* = E + Q$ and L determined empirically for these two reactions is identical. One can go further and compare the theoretical and empirical \mathcal{I} . One finds that the empirical values of L are consistently smaller than the values predicted by calculations of the Yrast line. Vandenbosch (79) and Vandenbosch and Lazzarini (81) make the reasonable suggestion that the compound nucleus formation will occur only if there is a sufficient density of levels, which would move the predicted value of L away from the Yrast line to smaller values of L . According to Mosel (84), the question of whether it is the density of compound nuclear levels or the density of doorway states leading to compound nucleus formation has not been resolved.

Investigation of the fusion cross section at higher energies reveal another straight-line dependence on $1/E$, as illustrated in Fig. 2.15. This is referred to as region III. Matsuse, Arima, and Lee (82) propose a description in which the cross section for region I is given by (2.7), region II by the Yrast limit, (2.12), and region III by (2.9), where we recall that r_C is the distance at which the two colliding nuclei lose their identity and become the compound nucleus. This distance can be determined according to Matsuse et al. from the equation giving the mean-square radius of the compound nucleus mass number A in terms of

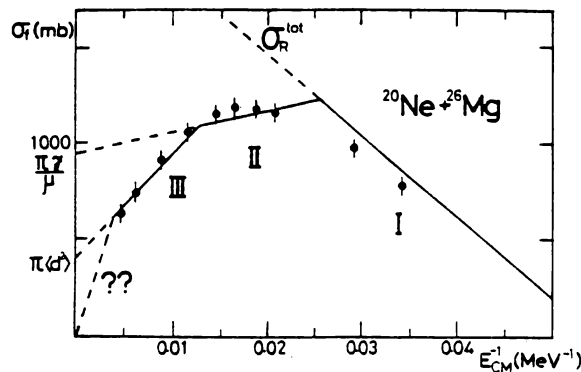


FIG. 2.15. Fusion cross-section excitation function Experiment (ϕ) compared with theory of Matsuse et al. [From Matsuse, Arima, and Lee (82).]

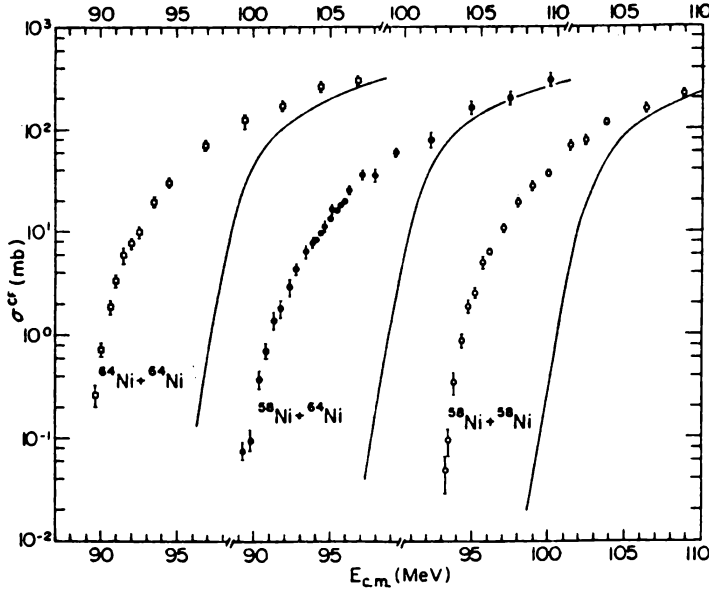


FIG. 2.16. Excitation functions for complete fusion of $^{58}\text{Ni} + ^{58}\text{Ni}$, $^{58}\text{Ni} + ^{64}\text{Ni}$, and $^{64}\text{Ni} + ^{64}\text{Ni}$. Smooth curves give WKB predictions. [From Beckerman (85).]

the mean-square radii of the colliding nuclei, A_1 and A_2 .

$$A\langle r^2 \rangle_A = A_1\langle r^2 \rangle_{A_1} + A_2\langle r^2 \rangle_{A_2} + \frac{A_1 A_2}{A} \langle r_c^2 \rangle$$

For further details the reader is referred to their paper.

We conclude this section on fusion with a brief mention of the recently discovered phenomenon of *subbarrier fusion* [Steadman (85)], which is illustrated by Fig. 2.16. The center-of-mass energies are far below the Coulomb barrier energy for two touching spherical nuclei. One would there expect that the Coulomb interaction would dominate this reaction and that therefore one should be able to calculate the cross section with some confidence. However, calculations made with the one-dimensional radial model given approximately by the solid lines fall far below the experimental values. Nearly all the various explanations for these major discrepancies can be understood as examples of coupled-channel calculations, which take into account the vibration of the nuclear surfaces. As one may expect, the coupling to low-lying collective states is of major importance. This is illustrated by Fig. 2.17.

Henning, Wolfs et al. (87) have emphasized the importance of nuclear transfer for the observed fusion enhancement. This is based on experiments using $^{16,18}\text{O}$ and ^{58}Ni beams incident on Sn isotopes in which a strong correlation between the transfer cross section and fusion enhancement is seen. They suggest that

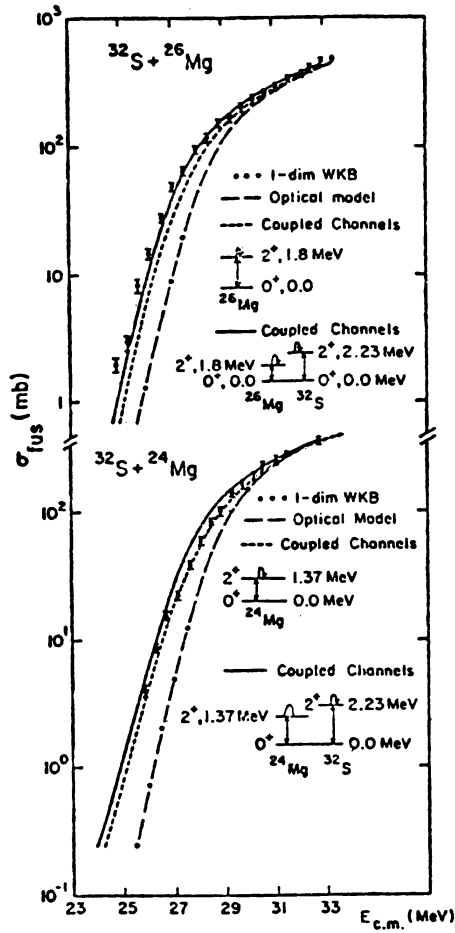


FIG. 2.17. Calculation of fusion cross section for the reactions $^{32}\text{S} + ^{26}\text{Mg}$ and $^{32}\text{S} + ^{24}\text{Mg}$. The dotted and long-dashed line are for the two equivalent one-dimensional calculations. The other curves show the effect of coupling in various low-lying states in ^{32}S and/or $^{24,26}\text{Mg}$. [From Rhoades-Brown, Braun-Munzinger, Prakash, and Sen (85).]

the neutron transfer opens a doorway through which the system can proceed to fusion. These reactions are of great importance in astrophysics, where they play an important role in energy production and element formation [Barnes (85)].

3. DEEP INELASTIC SCATTERING[†]

As has been illustrated in Fig. 1.15, in deep inelastic collisions, the two interacting nuclei are thought to be in contact for a relatively long time, during which the combined system rotates through a finite fraction of a complete revolution

[†]Schröder and Huizenga (84); Lefort and Ngô (78).

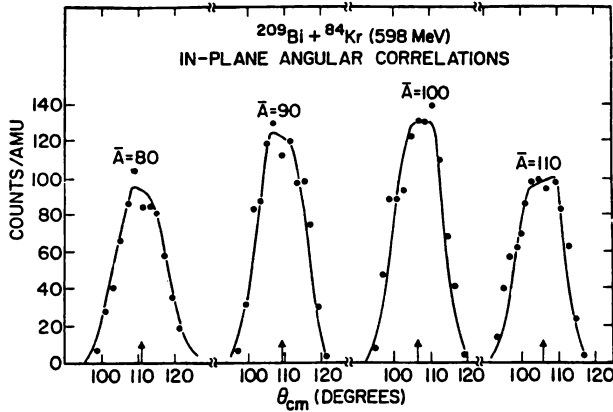


FIG. 3.1. In-plane angular correlation of fragments from the reaction $^{209}\text{Bi} + ^{84}\text{Kr}$ at 600 MeV, where the light fragment of mass A was measured at $\theta_L = 48.5^\circ$. The average emission angles expected from two-body kinematics are indicated by arrows. The curves represent an evaporation calculation [Wolf and Roche (76).] [From Schröder and Huizenga (84).]

before separating into two final fragments. The fact that the reaction is essentially binary is demonstrated by Fig. 3.1, where the angular correlation of the fragments is shown for differing values of the mass number of the lighter fragments. The average emission angles of the heavier fragment, calculated by assuming two-body kinematics, is indicated by arrows. The agreement with the maxima of the correlation distributions is excellent. The distributions are a consequence of evaporation of the fragments, so that the original values of A must be determined from statistical reaction theory. On the average, the evaporated particles are emitted isotropically, so that the average provides a good measure of the direction of the fragment upon separation from the lighter fragment. The binary character of deep inelastic scattering helps to distinguish the deep inelastic collision from a fusion reaction that is followed by fission. The latter is generally symmetric (i.e., the fusion leads to two nearly identical fragments). If the collision under consideration is between two nuclei with significantly differing atomic and mass numbers, the deep inelastic process will lead most probably to two final nuclei with substantially the same value of A and Z and not to two nearly identical nuclei.

In general, fusion is improbable for heavier elements (see Fig. 3.2). For these elements the strength of the Coulomb potential is so great that even with the addition of an attractive nuclear potential, no "pocket" in the total potential is formed. Hence no fusion. For this reason, we shall choose the illustrations of various phenomena associated with deep inelastic scattering to be discussed below, from collision between nuclei the product of whose charges ($Z_1 Z_2$) is greater than roughly 3000.

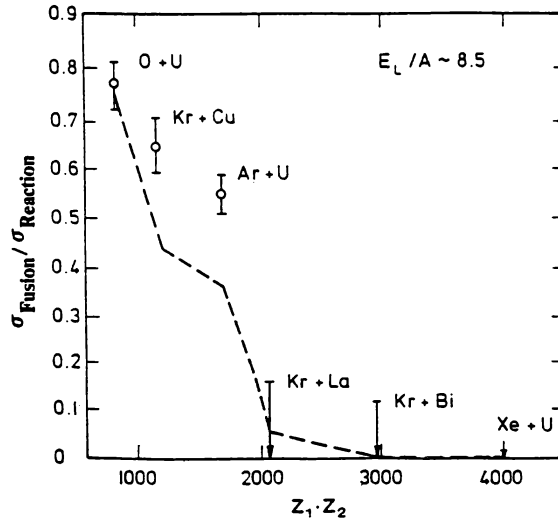


FIG. 3.2. Ratio of reaction to fusion cross section for several reactions involving heavy targets. [Vandenbosch (79); From Mosel (84).]

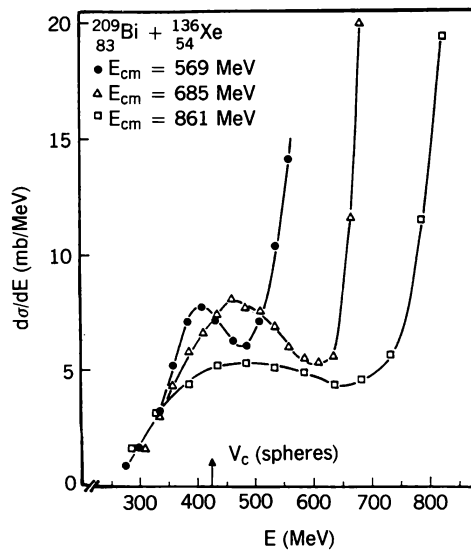


FIG. 3.3. Total kinetic energy distribution $d\sigma/dE$ of final fragments produced in the reaction $^{209}\text{Bi} + ^{136}\text{Xe}$ at three bombarding energies. The energies were calculated from the measured projectile-like fragments assuming two-body kinematics. The energy spectra are integrated over all fragments and reaction angles. The arrow (V_c) indicates the entrance channel Coulomb interaction energy at the strong-absorption radius. [From Huizenga and Birkelund (82).]

Another characteristic of deep inelastic collision is the wide range of energies that can be lost from the kinetic energy of relative motion to internal degrees of freedom. This feature distinguishes it from the quasi-elastic scattering, in which the binary final state is retained but the loss of energy is relatively small. In Fig. 3.3 the cross section for a final kinetic energy E produced by the collision of $^{209}_{83}\text{Pb}$ with $^{136}_{54}\text{Xe}$ is shown for three differing initial kinetic energies. These cross sections are obtained after integration over all angles and summing over all fragments. Near the initial energy we see a strong quasi-elastic peak. At a lower final energy there is a broad maximum in the distribution corresponding to an energy loss ranging from 170 MeV for the lowest initial energy to 370 MeV for the greatest critical energy. The distributions are very broad. Energy losses as high as 600 MeV for an incident energy of 861 MeV have been recorded.

The dependence of the total kinetic energy cross sections on the atomic number of the lighter fragment is shown in Fig. 3.4. Quasi-elastic peaks are seen for the Z of the fragment equal to the atomic number of the projectile $^{136}_{54}\text{Xe}$ and nearby $\langle Z \rangle = 57$. However, the quasi-elastic peak disappears quite rapidly as $\langle Z \rangle$ differs from 54. In these cases the energy distribution follows a bell-shaped curve. The widths of the distribution as well as the maximum value of the cross section decreases with increasing $\langle Z \rangle$ beyond $\langle Z \rangle = 54$.

Two differing types of angular distributions can be seen in deep inelastic collisions. The strong focusing distribution that prevails in the collisions of the very heavy nuclei after integration over energy and fragmentation type is

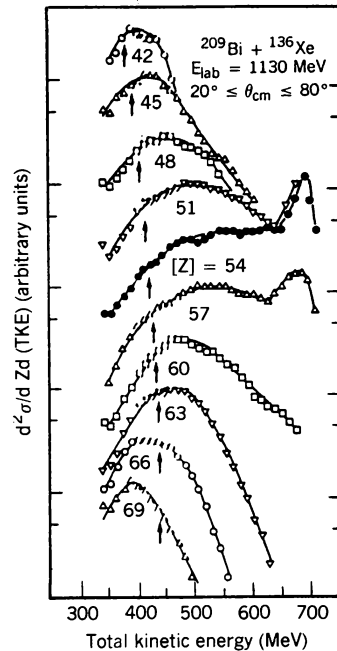


FIG. 3.4. Double-differential cross section $d^2\sigma/dZ dE$ for the reaction $^{209}\text{Bi} + ^{136}\text{Xe}$ at $E_{\text{lab}} = 1130 \text{ MeV}$ integrated over $20^\circ \leq \theta_{\text{cm}} \leq 80^\circ$ [Schröder, Birkelund, et al. (78)]. [From Schröder and Huizenga (84).]

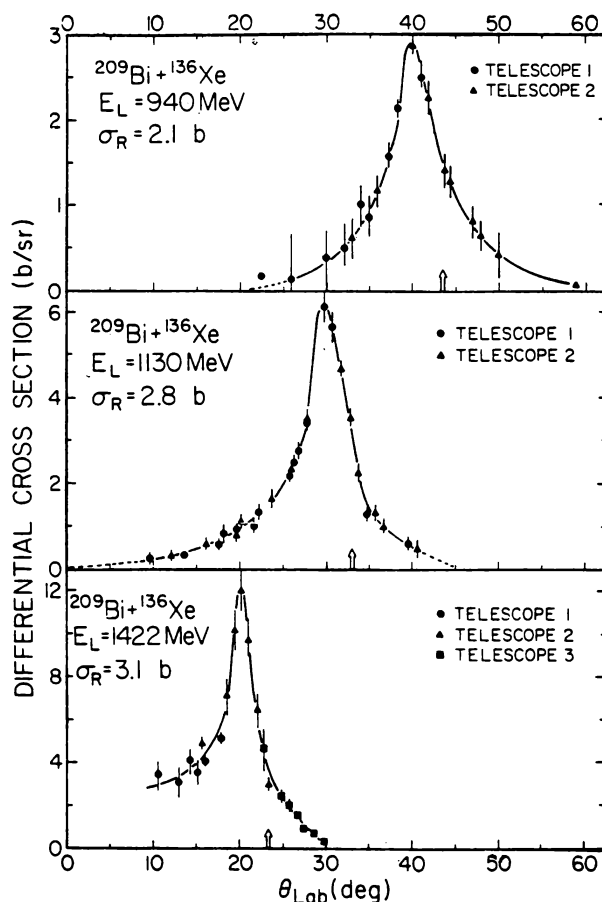


FIG. 3.5. Laboratory angular distributions for the $^{209}\text{Bi} + ^{136}\text{Xe}$ reaction at three energies. The centre-of-mass energies above the Coulomb barrier are 1.75, 3.14, and 5.29 MeV/nucleon, respectively. [From Schröder and Huizenga (84).]

illustrated in Fig. 3.5. The reaction products fall within a narrow angle peaked roughly at the grazing angle. The strong focusing is also exhibited by the Wilczyński plot of Fig. 3.6, where a contour plot of $d^2\sigma/d\Omega d(\text{TKE})$ in the $\text{TKE}-\vartheta_{\text{cm}}$ plane is shown (TKE = total kinetic energy). The ridge of the maximum cross section stays at a constant angle with increasing kinetic energy loss, but eventually as in the orbiting case, the rate of energy loss with angle slows down appreciably. The width of the angular distribution increases as the energy loss increases.

The angular distribution for each fragment integrated over the final fragment energies is shown in Fig. 3.7. The strong focusing effect at the grazing angle is visible for the fragments whose atomic number is near that of the projectile

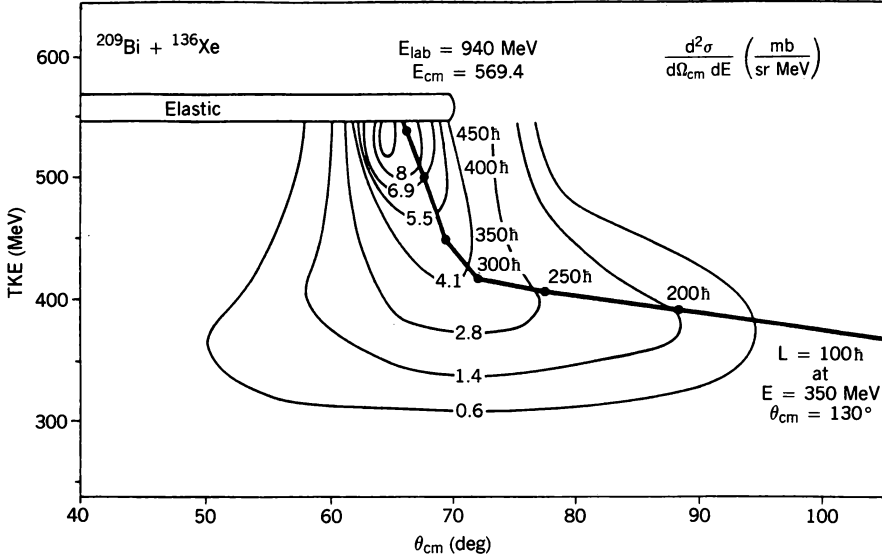


FIG. 3.6. Wilczyński plot for $^{137}\text{Xe} + ^{209}\text{Bi}$ at $E_{\text{lab}} = 9 \text{ MeV}$. [From Negele (82).]

$Z = 54$. For changes from 54 of six units or larger the angular distributions broaden considerably.

The second type of angular distribution is a consequence of the *orbiting* process. It occurs for the lighter systems and higher energies. A typical Wilczyński plot for the orbiting process is shown in Fig. 3.8. The colliding nuclei are ^{18}Ar and ^{232}Th . Along the maximum cross-section ridge, the angle at first decreases rapidly, as the energy loss increases, approaching zero, and then increases quite slowly for further losses in energy. This last branch has been interpreted by Wilczyński (73) as negative angle reactions. His reasoning is illustrated by Fig. 3.9. Deep inelastic collisions are supposed to occur for those values of l (or impact parameters) that lie between l_{crit} and l_g . For $l < l_{\text{crit}}$, fusion dominates, while for $l > l_g$, quasi-elastic processes are the principal reaction channels. The trajectories near l_g will be Coulomb dominated, but as one moves away from l_g , the nuclear interaction will become more important, there will be an energy loss as a consequence, and the trajectory will be bent toward zero degrees and eventually beyond it to negative angles. Detectors do not distinguish between negative and positive angles, so that as the reaction angle passes zero, the cross sections as shown in the Wilczyński plot will be recorded as positive. We also see that the negative angle branch is closely associated with large energy loss.

The two types of angular distribution, orbital and angular focusing, are examples of extreme situations, angular focusing dominating for collisions between heavy nuclear and lower energies. The transition from one type to

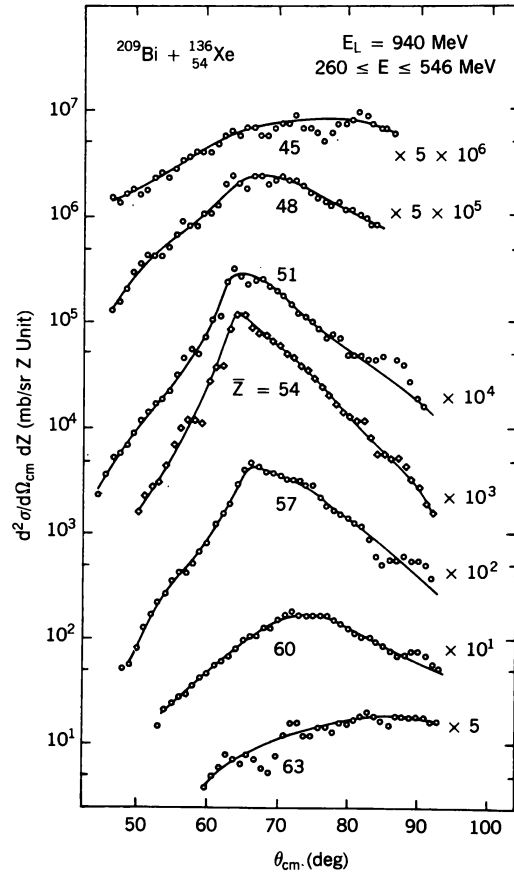


FIG. 3.7

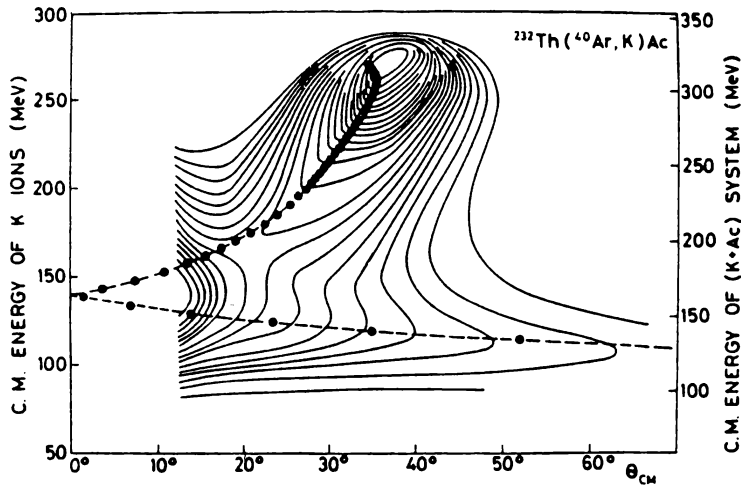


FIG. 3.8

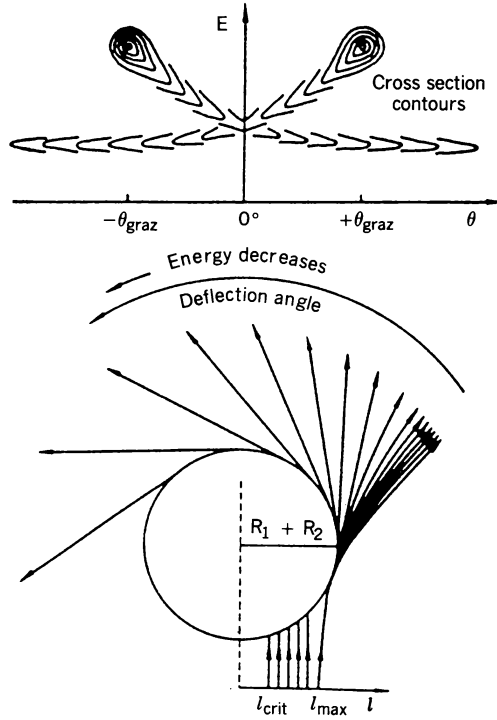


FIG. 3.9. Illustration of the orbiting phenomenon in damped nuclear reactions. Trajectories for a band of l waves between l_{max} and the critical angular momentum l_{crit} for fusion are depicted at the bottom. The associated cross section pattern is displayed at the top as a contour diagram plotted vs. final fragment energy E and deflection angle θ . Negative reaction angles correspond to rotation of the intermediate system through the beam direction ($\theta = 0^\circ$). [From J. Wilczyński (73).]

another has been found to depend empirically [Galín (76); Moretto and Schmitt (76)] on the Sommerfeld parameter evaluated at the Coulomb barrier:

$$\eta' = \frac{e^2 Z_p Z_t}{\hbar} \left[\frac{\mu}{2(E_{\text{cm}} - V_{\text{Coul}})} \right]^{1/2} \quad (3.1)$$

FIG. 3.7. Center-of-mass angular distributions of the light fragments from the damped reaction $^{209}\text{Bi} + ^{136}\text{Xe}$ at $E_{\text{lab}} = 940$ MeV as a function of Z . The experimental double-differential cross sections are multiplied by the factors listed on the right before plotting. [From Wilcke, Birkelund, et al. (80).]

FIG. 3.8. Contour diagram of $d^2\sigma/dE d\theta$ for the reaction $^{232}\text{Th}(^{40}\text{Ar}, \text{K})$ at $E_{\text{lab}} = 388$ MeV. The circles indicate the predicted correlation between scattering angle and final energy for different values of the angular momentum ranging from $l = 180$ to 250. [From Lefort and Ngô (78).]

Empirically, orbiting dominates for $\eta' \lesssim 150$, while angular focusing dominates in the range $250 \lesssim \eta' \lesssim 400$. For $\eta' \gtrsim 500$ angular focusing is accompanied by a noticeable tail at larger angles.

As we shall see, correlations among many of the observables are observed. Some insight into these can be obtained from the dependence of observables on the interaction time, τ , that is, the time during which the colliding nuclei interact before separating. One expects that τ will be smallest for the largest values of the impact parameter (or l) and will increase as l decreases. This suggests two characteristic times, corresponding to two different dynamical situations. One time, τ_a , is the time required to achieve a approximate saturation value of the energy loss, achieved in this case for $l = 300$. For larger interaction times corresponding to smaller values of l , the energy loss increases very slowly with decreasing l . In the first phase, the conversion of kinetic into internal energy is generated by the flow of matter, nucleons, or clusters of nucleons from one nucleus to the other and/or the excitation of giant resonances as the surface regions of each interact.

A rough estimate of the time involved can be deduced from experiment by the following argument. In the laboratory frame, assume that the target nucleus is excited by the flow of nucleons from the projectile while the projectile is slowed down by the flow of nucleons from the target. The energy carried by each nucleon entering the target is E/A_p , where E is the incident energy of the projectile. A rough estimate of the total energy transferred to the target is obtained by assuming thermal equilibrium between the projectile and target. That energy is $(A_t/A_p + A_t)\Delta E$, where ΔE is the total energy loss. Thus the number of nucleons transferred to the target is

$$n = \frac{A_t A_p}{A_p + A_t} \frac{\Delta E}{E}$$

The time it takes each nucleon to transfer is given approximately by the distance traversed, on the order of the surface thickness s divided by the Fermi velocity. Thus the time τ_1 for the first phase is

$$\tau_1 = \frac{ns}{v_F} = \frac{A_t A_p}{A_p + A_t} \frac{s}{v_F} \frac{\Delta E}{E}$$

Turning to our example, for $l = 300$, $\Delta E = 169$ MeV, $E = 940$ MeV, $s \sim 2$ fm, and $v_F/c \sim 0.27$, we obtain 3.6×10^{-22} s and $n \sim 15$. This crude result appears to be of the correct order of magnitude as obtained from calculations using macroscopic and microscopic models.

The second phase must involve low-lying modes of excitation. The models suggest that their major effect is the slowing down of the rotational motion. The mechanism is analogous to the slowing-down action of the tides. The rotational states are thus the modes excited. The time involved is given by the

uncertainty principle by

$$\tau_2 = \frac{\hbar}{\Delta E}$$

where ΔE is of the order of 160 keV, so that $\tau_2 \sim 10^{-20}$ s, a much longer time than that occupied by the first phase.

The results above are characteristic of very heavy systems. For lighter ones the second phase is replaced by fusion, which does not occur for the heavier systems, as discussed earlier.

These considerations become explicit and quantitative in the macroscopic friction model of Gross and Kalinowski (78). Two variables are used, the distance r between the centers and φ the angle made by \mathbf{r} with the incident direction. The Newtonian equations of motion are then

$$\frac{d}{dt}(\mu \dot{r}) - \mu r \dot{\varphi}^2 + \frac{dV}{dr} + K_r \dot{r} = 0 \quad (3.2)$$

and

$$\frac{d}{dt}(\mu r^2 \dot{\varphi}) + K_\varphi r^2 \dot{\varphi} = 0 \quad (3.3)$$

The quantity μ is the reduced mass, while K_r , the radial friction coefficient, and K_φ , the tangential one, are both functions of r . The function V , the potential, nuclear plus Coulomb, is taken to be a function of r only. These are the most general parity-conserving equations with friction forces linearly dependent on \dot{r} and $\dot{\varphi}$. Gross and Kalinowski take point Coulomb potentials and the folding potential,

$$V_{12}(r) = \int V_1(|\mathbf{r} - \mathbf{r}'|) \rho_2(\mathbf{r}') d\mathbf{r}'$$

where V_1 is a real Woods–Saxon potential describing the interaction of a nucleon in nucleus designated by the subscript 2, with the nucleus designated by the subscript 1 integrated over nucleus 2. The function V in (3.2) is $V_N + Z_1 Z_2 e^2/r$, where $V_N = \frac{1}{2}(V_{12} + V_{21})$. The function ρ_2 is taken from electron scattering. Thus Gross and Kalinowski (78) use

$$\begin{aligned} \rho(r) &= \frac{\rho_0}{1 + e^{(r-R_D)/a_D}} & V_1 &= \frac{V_0}{1 + e^{(r-R_p)/a_p}} \\ \rho_0 &= 0.17 \text{ fm}^{-3} & V_0 &= -50 \text{ MeV} \\ R_D &= 1.12 - 0.86 A^{-1/3} \text{ fm} & R_p &= 1.25 A^{1/3} \\ a_D &= 0.54 \text{ fm} & a_p &= 0.65 \text{ fm} \end{aligned} \quad (3.4)$$

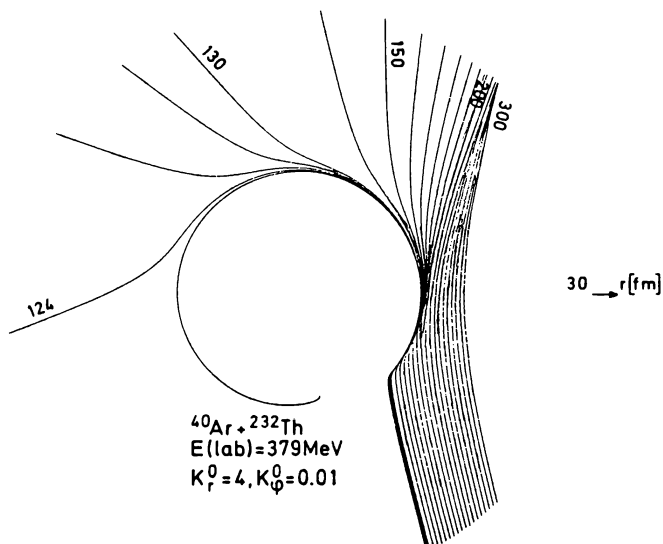


FIG. 3.10. Trajectories given by the friction model for various values of l . The last contribution to the fusion cross section is $l = 122$; the first to the deep inelastic cross section is $l = 124$.) [From Gross and Kalinowski (78).]

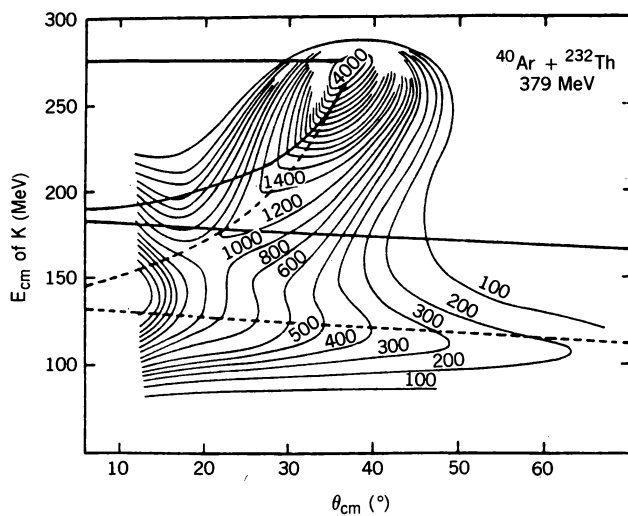


FIG. 3.11. Contour diagram of $df/ds d\theta$ ($\mu\text{b}/\text{MeV} \cdot \text{rad}$) versus scattering angle θ_{cm} and E_{cm} of K ions. The dashed line contains the effects of deformation. [From Gross and Kalinowski (78).]

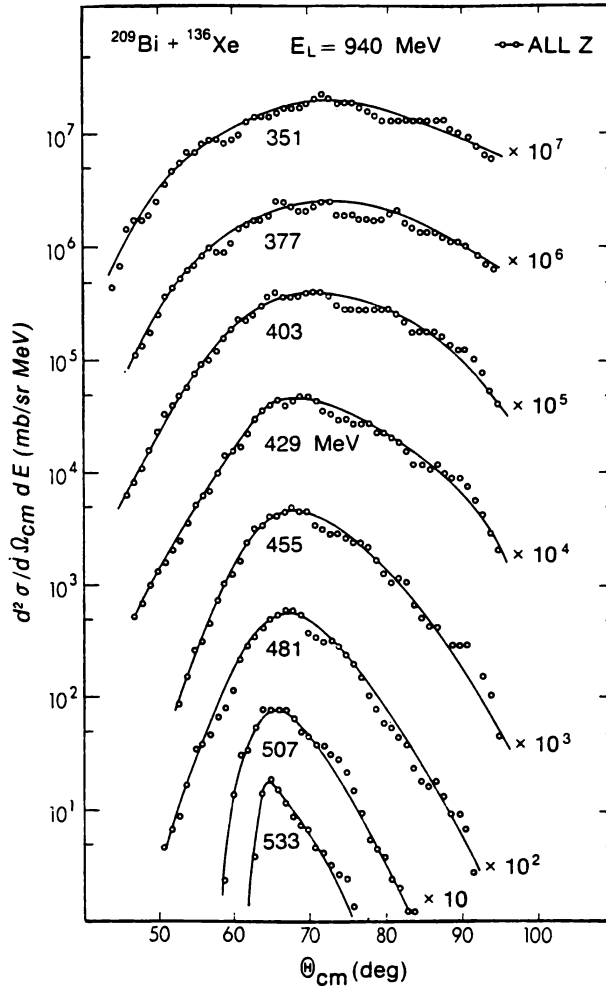


FIG. 3.12. Angular distribution as a function of total kinetic energy for the $^{209}\text{Bi} + ^{136}\text{Xe}$ reaction at $E_{\text{lab}} = 940$ MeV. Each energy bin is 26 MeV wide and is integrated over Z of the light fragments. The centroid energy of each bin is given at each curve. The solid lines are drawn through the data points. [From Wilcke, Birkelund, et al. (80).]

For the friction coefficients, these authors use the following:

$$K_r = K_r^0 (\nabla V_N)^2 \quad K_\phi = K_\phi^0 (\nabla V_N)^2 \quad (3.5)$$

These friction coefficients are most important in the surface region. The constants K_r^0 and K_ϕ^0 are taken from fits to experiment to be 4×10^{-23} and 10^{-25} s/MeV, respectively. The tangential friction is therefore much weaker than the radial one as might expect.

The time constant for the decay of the tangential motion as obtained from (3.3) is of the order of μ/\bar{K}_ϕ , where \bar{K}_ϕ is the ratio of the averages $\langle K_\phi r^2 \rangle$ and $\langle r^2 \rangle$. Estimating ∇V as $|V_0|/4a$, where $a \simeq a_D + a_p = 1.19$ fm, one obtains

$$\tau \sim 2 \times 10^{-22} \text{ s}$$

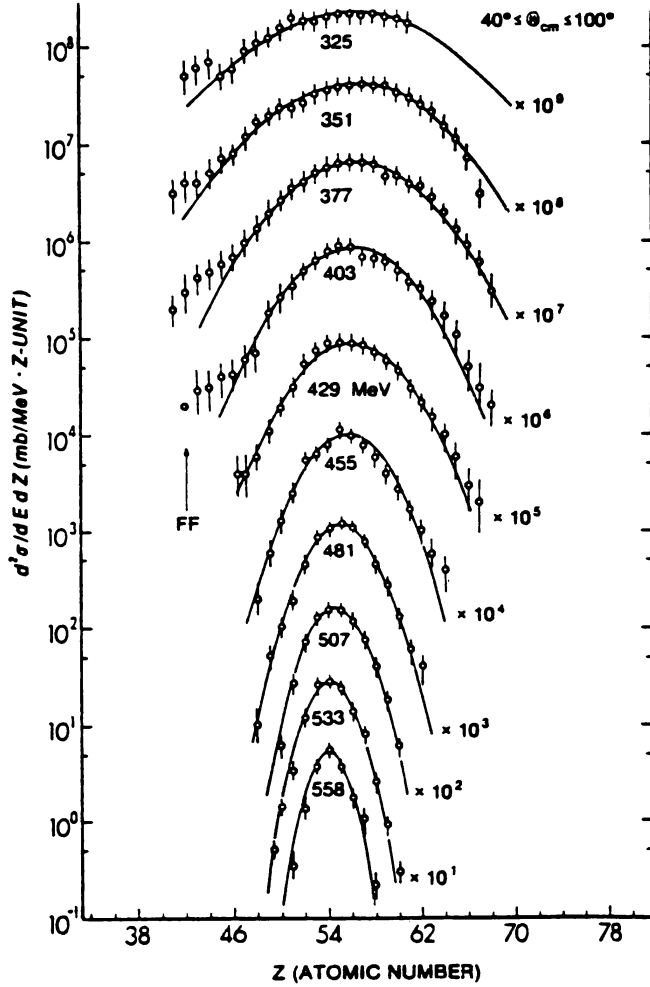


FIG. 3.13. Z distributions of fragments from the reaction $^{209}\text{Bi} + ^{136}\text{Xe}$ at $E_{\text{lab}} = 940$ MeV are plotted as a function of final total kinetic energy indicated at the curves. Energy bins are MeV wide. Solid curves represent Gaussian fits to the data (open circles). The distribution 558 MeV corresponds to elastically scattered Xe ions and illustrates the experimental resolution. The arrow (FF) indicates contamination of the data by events from sequential fission of target-like reaction fragments. [From Wilcke, Birkelund, et al. (80).]

which is close to the estimate made above. Gross and Kalinowski have given some results using (3.2), (3.3), and (3.10) which do (with one further adjustment!) reproduce the observed data to the extent that their model permits. In Fig. 3.10, the trajectories for the reaction $^{40}\text{Ar} + ^{232}\text{Th}$, laboratory energy of 379 MeV, are shown. The trajectories for angular momentum $l \geq 124$ contribute to the deep inelastic cross section, which those for $l \leq 122$ to the fusion cross section. The process pictured is then of the orbiting type. The resulting path (the solid line) on the Wilczyński plot is shown in Fig. 3.11. This theory thus does not give the full details of the Wilczyński plot but only the path followed by the ridge. The solid line gives a qualitative match to the data. It does not yield enough energy loss. These authors surmise that this may be caused by an additional energy loss because of an additional degree of freedom (deformation?) not taken into account by (3.4) and (3.5). Be that as it may, they effectively increase the energy loss by increasing the magnitude of the nuclear potential from the distance of closest approach outward, that is, during the final half of the collision [see Siwek-Wilczyński and Wilczyński (76)]. Under this assumption one obtains the dashed line, now giving an excellent fit. Using the same constants, scaling the nuclear radii as $A^{1/3}$, a good fit is obtained by Gross and Kalinowski for several cases.

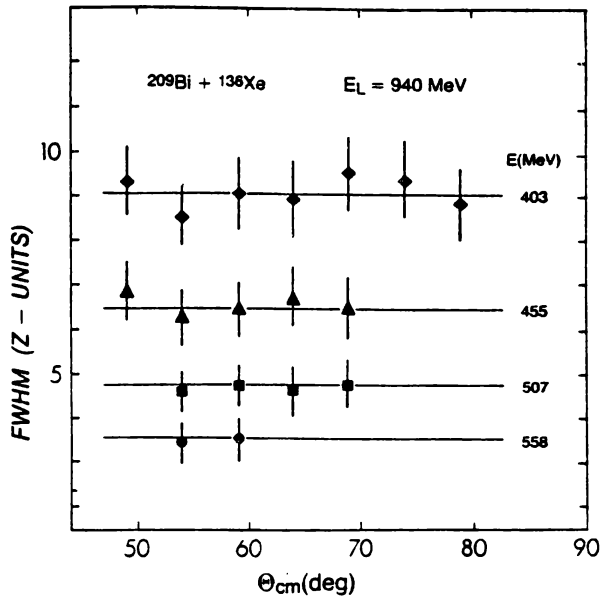


FIG. 3.14. The FWHM of Z distributions $d^3\sigma/d\Omega dE dZ$ for the indicated final kinetic energies is plotted versus center-of-mass reaction angle, for projectile-like fragments from the reaction $^{209}\text{Bi} + ^{136}\text{Xe}$ at $E_{\text{lab}} = 940$ MeV. The horizontal lines represent the fits to the angle-integrated Z distributions $d^2\sigma/dZ dE$. [From Wilcke, Birkelund, et al. (80).]

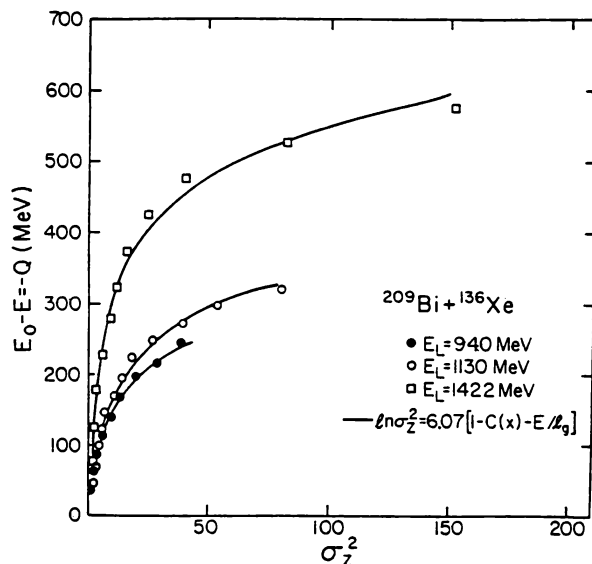


FIG. 3.15. Correlation between variance σ_Z^2 of the Z distribution and total kinetic energy loss $E_{\text{loss}} = -Q$ for projectile-like fragments from the reaction $^{209}\text{Bi} + ^{136}\text{Xe}$ at three laboratory bombarding energies E_L . The curves drawn through the data points are fits. [From Huizenga and Birkelund (82).]

We learn from this discussion that particularly during the first phase of the reaction, kinetic energy loss increases as the interaction time increases. Therefore, one may use kinetic energy loss as a measure of interaction time. This permits the understanding of the direct experimental measures of various correlations. For example, we see from Fig. 3.12 the broadening of the angular distribution as the kinetic energy loss and therefore time increases. Similarly, one can expect a broadening of the distribution in atomic number Z of the nuclear reaction products as given in Fig. 3.13. The full width at half-maximum of the distributions on Z is independent of the reaction angle but does increase significantly as the kinetic energy loss increases, as shown by Fig. 3.14. These widths increase more rapidly with energy loss for increasing laboratory energy (see Fig. 3.15).

4. QUASI-ELASTIC SCATTERING[†]

We turn next to quasi-elastic scattering, which prevails for large values of the orbital angular momentum, l , according to Fig. 1.15. In this regime, the interaction time is relatively small, and direct processes that occur in the surface

[†]Arima and Kubono (84).

region dominate. These include inelastic excitation of each or both nuclei, as well as particle transfer. The processes involved are quite similar to that described for light ions in Chapter VII. Both are surface reactions but probe different parts of nuclear surface. There is one significant difference, in that heavy ions upon collision can exchange large amounts of mass, linear, and angular momentum. This exchange may be accomplished in one step, a cluster being transferred as a whole. Or in the other limit, the mass may be transferred sequentially, that is, one nucleon at a time. The sequential process involves a longer interaction time and is thus a precursor of deep inelastic scattering. Generally, these large mass and momentum transfers will excite multiparticle-hole states with high spin.

Conservation rules limit the allowable changes in linear and angular momentum of each nucleus. Brink (72), (77) has derived approximate classical conditions expressing these limitations. Brink assumes that the nucleus A_1 is moving with velocity v past the target nucleus A_2 . The cluster of mass M to be transferred from A_1 to A_2 has an internal energy in A_1 and in A_2 , equal to ε_1 and ε_2 , respectively. The interaction time is therefore given by $\hbar/(\varepsilon_1 + \frac{1}{2}Mv^2 - \varepsilon_2)$. The corresponding length is $\hbar v/(\varepsilon_1 + \frac{1}{2}Mv^2 - \varepsilon_2)$ and thus the momentum of the cluster leaving A_i is

$$\hbar k_1 = \frac{1}{v}(\varepsilon_1 + \frac{1}{2}Mv^2 - \varepsilon_2)$$

The momentum of the cluster in A_2 can be obtained by symmetry, that is, by going to the coordinate system in which A_2 is moving and A_1 is at rest. Then the momentum of the cluster in A_2 is

$$\hbar k_2 = -\frac{1}{v}(\varepsilon_2 + \frac{1}{2}Mv^2 - \varepsilon_1)$$

The minus sign in front of the expression on the right-hand side is needed since we wish to compute the momentum of the cluster entering rather than leaving A_2 . The reaction proceeds most effectively if the angular momentum leaving A_1 matches the angular momentum of the cluster $\hbar\lambda_1$ at the surface of A_1 , that is,

$$\lambda_1 = k_1 R_1 = \frac{R_1}{\hbar v}(\frac{1}{2}Mv^2 + Q) \quad (4.1)$$

where

$$Q = \varepsilon_1 - \varepsilon_2$$

Similarly, the momentum and the angular momentum $\hbar\lambda_2$ at the surface of A_2 should agree:

$$\lambda_2 = -k_2 R_2 = \frac{R_2}{\hbar v}(\frac{1}{2}Mv^2 - Q). \quad (4.2)$$

The minus sign($-k_2R_2$) takes account of the fact that the rotation in A_2 is opposite to that in A_1 .

Eliminating Q between (4.1) and (4.2) yields

$$\frac{\lambda_1}{R_1} + \frac{\lambda_2}{R_2} = \frac{Mv}{\hbar} \quad (4.3)$$

Taking the difference, one obtains

$$\lambda_1 - \lambda_2 = \frac{1}{\hbar v} (R_1 + R_2)Q + \frac{1}{2} (R_1 - R_2) \frac{Mv}{\hbar} \quad (4.4)$$

Equations (4.3) and (4.4) are the Brink (72, 77) kinematic conditions as usually quoted in the literature. Equation (4.3) expresses the conservation of linear momentum, while the conservation of angular momentum yields (4.4). These results hold for the transfer of neutral clusters. If the cluster is charged, one must include the change in the Coulomb energies in calculating $\varepsilon_1 - \varepsilon_2$. The net effect is to replace Q in (4.4) by Q_{eff} :

$$Q_{\text{eff}} \equiv Q - \frac{(Z_{1f}Z_{2f} - Z_{1i}Z_{2i})e^2}{d} \quad (4.5)$$

where Z_1 and Z_2 are the atomic numbers of the two nuclei, the subscripts i and f referring to their initial and final states, respectively, and d is the distance of closest approach. For other derivations, see Kahana and Baltz (77) and Ichimura, Takoda, Tamaya, and Nagatami (81); see also Bertsch and Schaeffer (77).

For a given initial spin λ_1 one can determine the optimum value, l_{opt} , of $l \equiv |\lambda_1 - \lambda_2|$ and the optimum value of Q , Q_{opt} , from (4.3) and (4.4) or (4.1) and (4.2). The cross section is largest when l and Q equal or are close to l_{opt} and Q_{opt} . The range in l and Q around l_{opt} and Q_{opt} over which the cross section will be appreciable is referred to as the l window and the Q window. The width of these windows, more precisely the windows associated with (4.1) and (4.2), is given according to Brink (77) by $(\gamma_1 R_1)^{1/2}$ for (4.1) and $(\gamma_2 R_2)^{1/2}$ for (4.2), where $\gamma_i^2 = (2M/\hbar^2)|\varepsilon_i|$. Thus the larger the separation energies $|\varepsilon_i|$, the wider the l window corresponding to a more localized interaction region, while a narrow l window corresponds to a less localized interaction region.

The angular distribution of the reaction products reflect the width of the l window. When the l window is large, the angular range in which the reaction products are found is characteristically narrow. The angular distribution is then "bell shaped" around the grazing angle, as illustrated by Fig. 4.1.

On the other hand, when the l window is narrow, the angular distribution shows a diffraction pattern as illustrated by Fig. 4.2. As the figure shows, the diffraction distribution appears as the energy of the projectile is raised. This

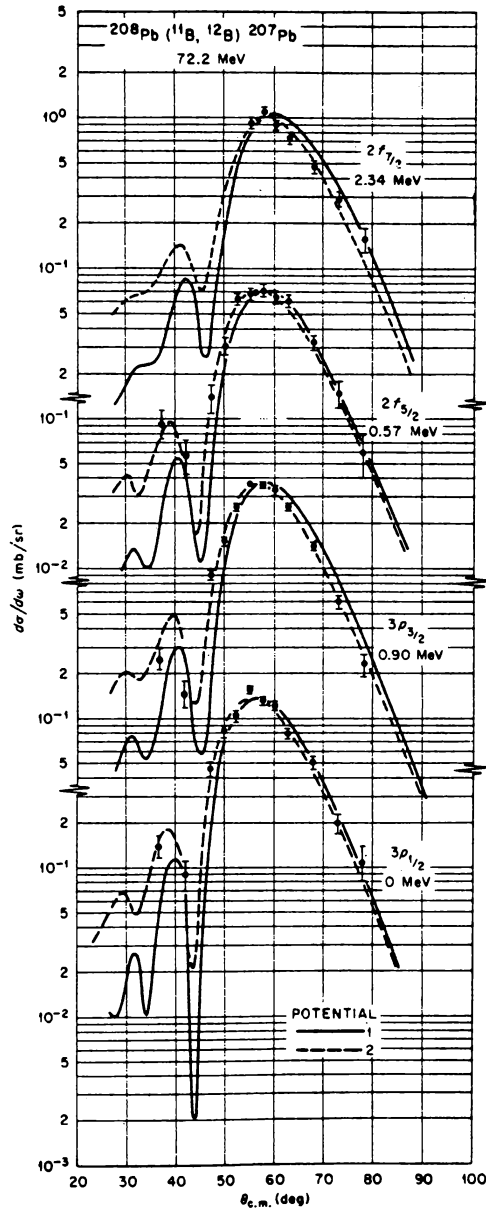


FIG. 4.1. Typical bell-shaped distributions for transfer reactions with heavy ions at energies close to the Coulomb barrier. The curves are from DWA calculations with two different optical potentials. The transitions are labeled by the hole state excited in ^{207}Pb . [From Ford, Toch, et al. (74).]

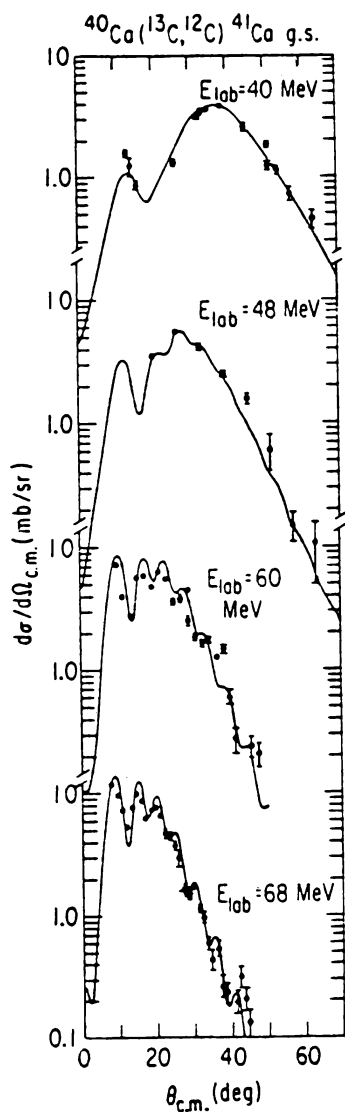


FIG. 4.2. Example of the evolution from a bell-shaped distribution to the appearance of diffraction structure as the energy is raised. [From Kahana and Baltz (77).]

behavior is expected since the penetration of the projectile increases with increasing energy so that the spatial region over which the interaction occurs increases.

In the case of a multiparticle transfer, M will be generally be large and the final state ε_2 will be highly excited so that Q will be negative. It thus becomes favorable for λ_1 to be small and λ_2 to be large according to (4.1) and (4.2). Transfer of large mass clusters will therefore predominately populate high-spin states.

In analogy with the use of stripping and pickup reactions to gain information with regard to single-particle states, one might hope to use cluster transfer reactions to explore the state of clusters within nuclei; or stated more precisely, the nature of n -particle correlations, where n is the number of particles in the cluster. Such a hope is not universally realized, since the cluster transfer must be observed in the presence of competing (and interfering!) mechanisms such as sequential transfer reactions, in which the n particles are transferred one by one. This is demonstrated by Fig. 4.3, where one can compare the importance of the single-step transfer of the two neutrons (DWA) with their transfer one neutron at a time.

However, when there is a good match between the correlations that exist in the final state of the residual nucleus and those of the transferred cluster, the spectroscopic factor and the cross section will be relatively large. This is the case for the (t, p) reaction on the tin isotopes. The cluster transferred consists of two neutrons in the 1S_0 state, the dominant component of the two-neutron amplitude in ^3H . But this is exactly the nature of the neutron correlations in the superconducting ground state of the tin isotopes enforced in that case by the pairing interaction. These form a superfluid band analogous to the rotational band in deformed nuclei. The ground state-to-ground state transition therefore has a favorable probability. [See Broglia, Hansen, and Riedel (73) for a review of this process.] It is found [Scott, Harvey, et al. (77)] that in that case the cross section for cluster transfer is more than an order of magnitude larger than the sequential transfer. A similar phenomenon may be expected for the appropriate reaction with heavy ions. One example is $^{120}\text{Sn}(^{18}\text{O}, ^{16}\text{O})\text{Sn}$, illustrated in Fig. 4.4.

The experimental and theoretical understanding of one-to-many particle transfers in heavy-ion reactions is summarized by Arima and Kubono (84), to which the reader is referred. For this volume it will suffice to present some salient features. As in the case of light-ion-induced reactions, the angular distributions, particularly the position of the first peak, depends on the orbital angular momentum, l , transferred. This is illustrated in Fig. 4.5 for the case of an α -cluster transfer, $^{54}\text{Fe}(^6\text{Li}, d)^{58}\text{Ni}$ and $^{58}\text{Ni}(^6\text{Li}, d)^{62}\text{Zn}$. In contrast to the (d, p) reaction, the (p, α) and (α, p) reactions are markedly sensitive to the total angular momentum transferred (see Fig. 4.6). The important effect of the finite size of the projectile is illustrated by Fig. 4.7. For a thorough study of the finite-size effect in the (t, p) reaction, see Bayman (70, 71). In that case Bayman shows that a substantial increase, often more than an order of magnitude, of the absolute value of the cross section results. In his case he found that the finite range effects do not change the angular distributions from that obtained from zero-range DWA. This conclusion is important because generally the zero-range DWA yields a cross section that is far smaller than the experimental one. There are other effects that go in the same direction. Because the theoretical results depend on the values of the wave functions involved in the surface region, there is a great sensitivity to the accuracy of these wave functions in that narrow region. The harmonic oscillator wave functions often used are grossly inadequate

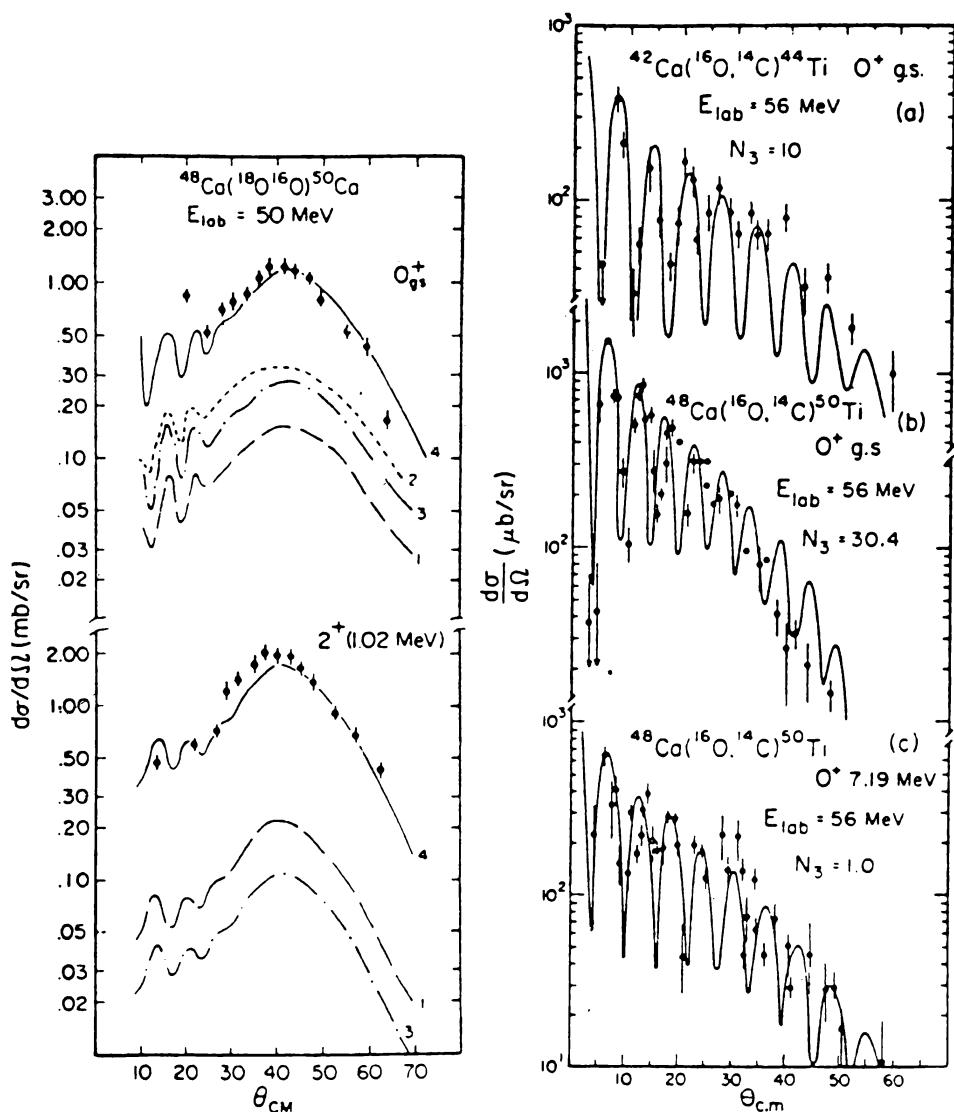


FIG. 4.3. Analysis of two-nucleon transfer reactions, including simultaneous and sequential transfer and using realistic overlap functions in exact finite-range DWA calculations. (a) Two-neutron transfer. Curves 1 and 2 are for simultaneous transfer using simple and realistic nuclear wave functions, respectively, while curve 3 is the sequential transfer. Curve 4 is for the coherent sum of the two processes. The theoretical curves have not been renormalized to fit the data. (b) Two-proton transfer. Also calculated with realistic wave functions and including simultaneous plus sequential transfer. Although the angular distributions are the same as the measured ones, only the magnitude of the transition to the excited ^{50}Ti state is in agreement. The calculated cross sections for the ground-state transitions are too small by factors of $N_3 = 10$ (^{44}Ti) and 30.4 (^{50}Ti). [From Feng, Udagawa, et al, (76).]

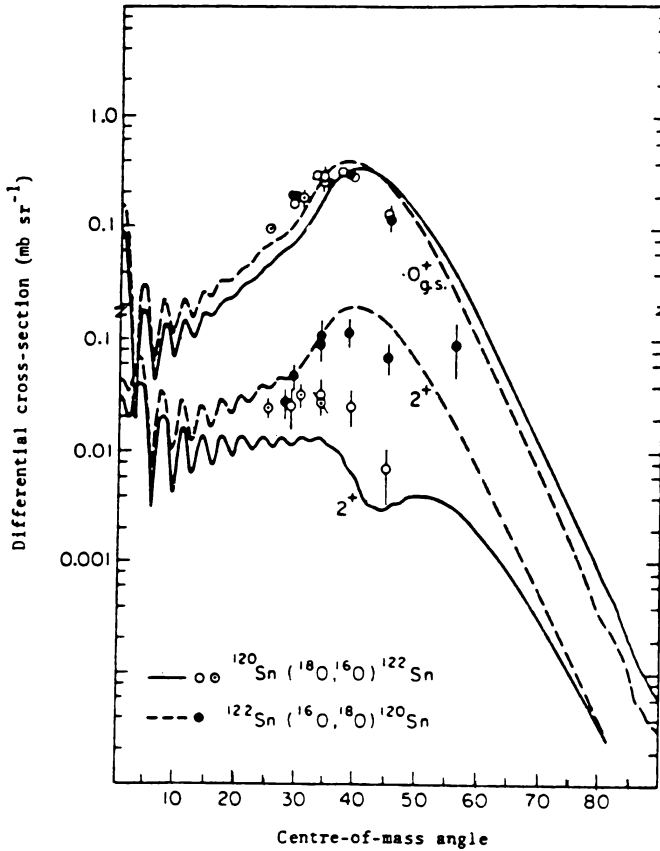


FIG. 4.4. Contrasting the direct-indirect interferences for pickup and stripping of two neutrons in a heavy-ion reaction at about 100 MeV, exciting the 2^+ vibrational states of the residual nuclei. Except for a small change in energy, the ground-state transitions are the inverses of each other, but the 2^+ states are in different nuclei. [From Scott, Harvey, et al. (75).]

since their decrease in the surface region is Gaussian rather than exponential. To obtain better agreement, it then becomes necessary to take linear combinations of many harmonic oscillator wave functions, as Tonozuka and Arima (79) found. The inadequacy of these wave functions is more severe in the case of heavy-ion compared to light-ion projectiles because the cross section is more sensitive to the wave functions for *larger* values of the radial variable.

The examples discussed above consider the excitation of discrete levels close to and including the ground state of the residual nucleus. The excitation levels in the continuum has also been observed, for example, $^{40}\text{Ca}(^{20}\text{Ne},^{16}\text{O})^{44}\text{Ti}$ [Frölich, Shimoda, et al. (79)], in which the ^{16}O spectrum is observed. Interestingly, the direct α -cluster transfer process is generally accompanied by

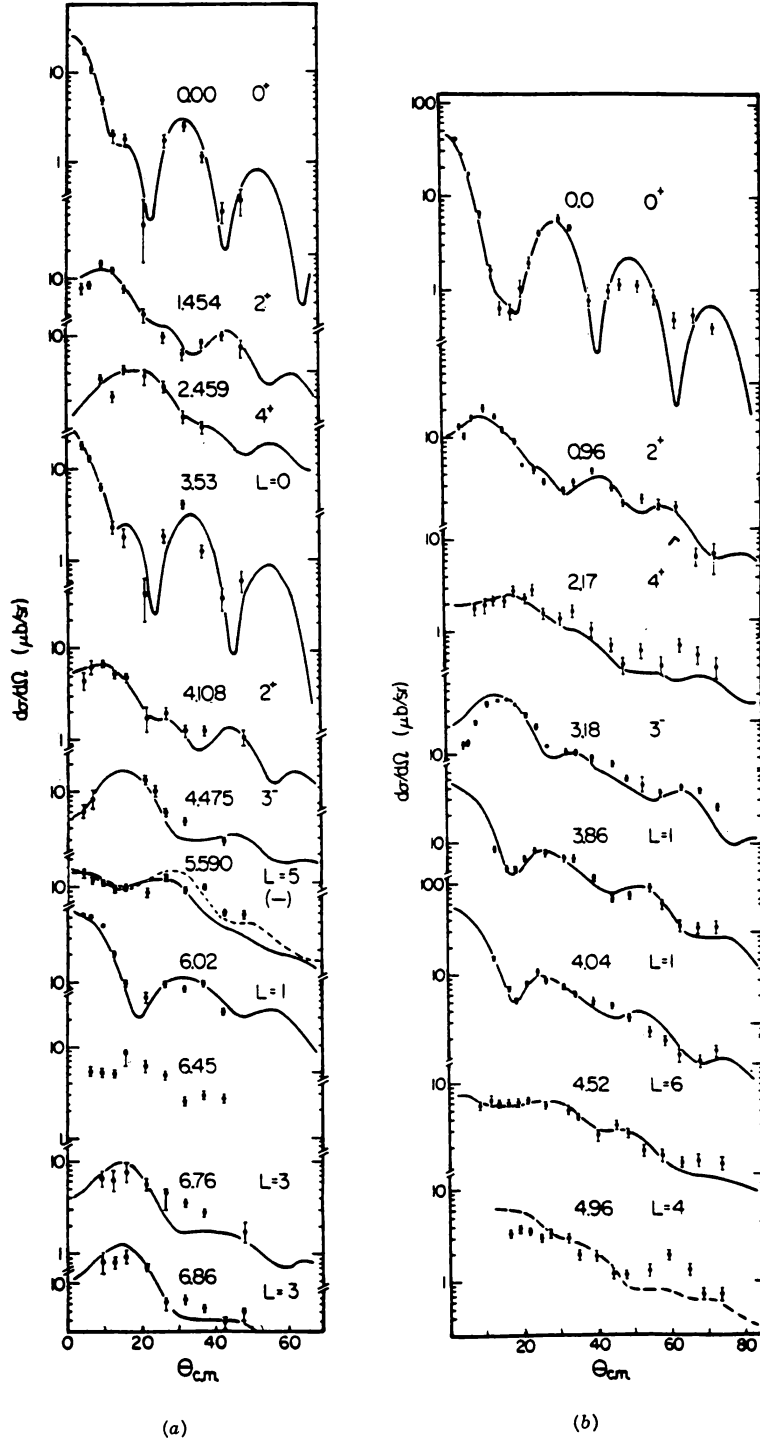


FIG. 4.5. Angular distributions of (a) the $^{54}\text{Fe}(^6\text{Li}, d)^{58}\text{Ni}$ reaction and (b) the $^{58}\text{Ni}(^6\text{Li}, d)^{62}\text{Zn}$ reaction of several transferred angular momenta at 28 MeV. The lines are the DWA calculations. [From Fulbright, Strohhusch, et al. (75).]

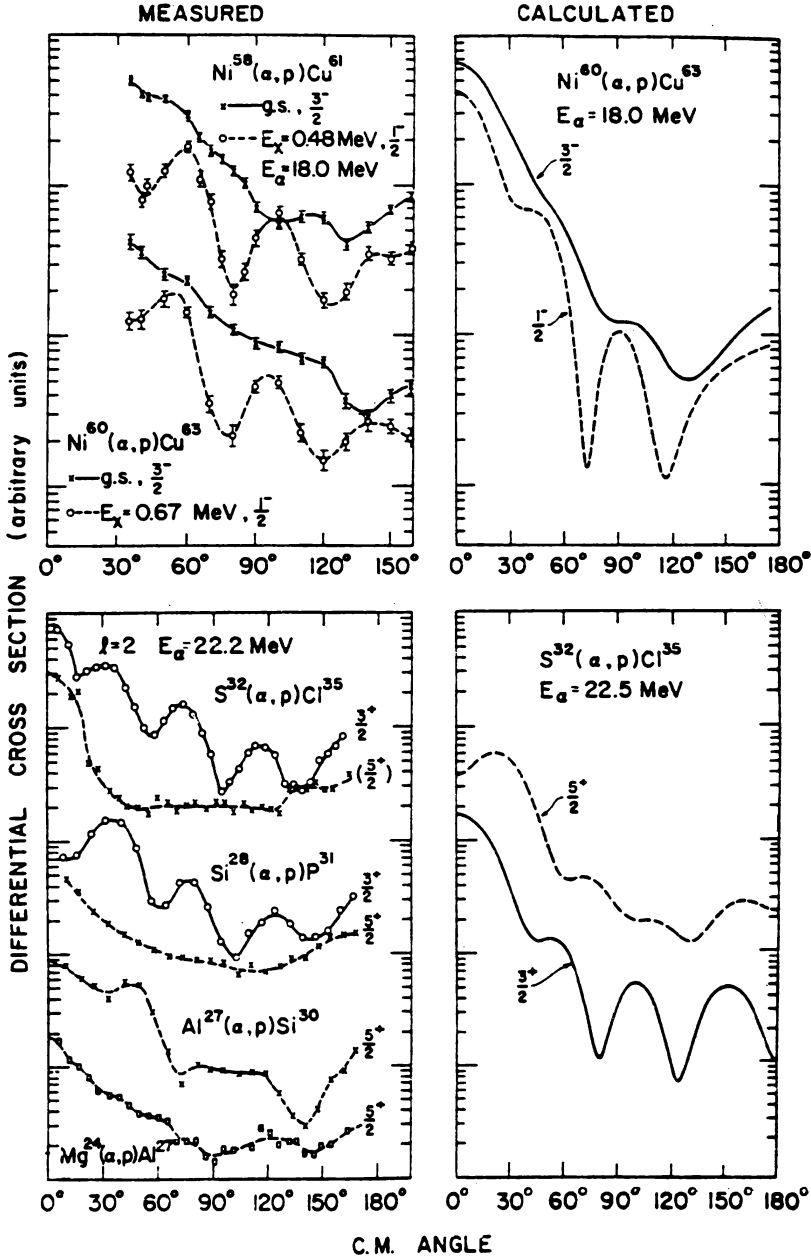


FIG. 4.6. The j -dependence of the (α, p) reactions in some l -transfer processes. The left-hand side is the experimental data and the right-hand side is the DWBA calculations with spin-orbit potentials. [From Yamazaki, Kondo, and Yamato (63); Lee, Marinov, et al. (65).]

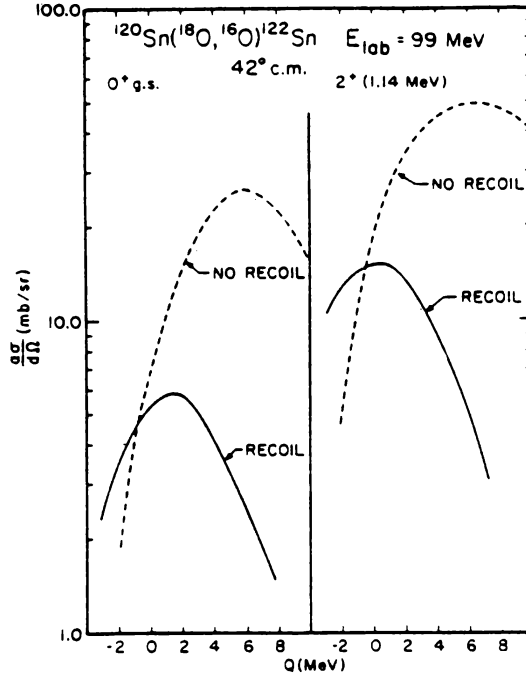


FIG. 4.7. Distortion of the Q window for a two-nucleon transfer when the no-recoil approximation is made. Calculated peak cross sections at 42° for $l = 0$ and 2 transactions as a function of Q . [From Feng, Udagawa, et al. (76).]

the fragmentation of the incident projectile ^{20}Ne . The reader should recall that essentially the same process is responsible for incomplete fusion. The excitation of continuum levels involves large energy transfers from the incident kinetic energy to internal energy. In fact, one can regard the quasi-elastic domain as one in which the elementary transfer processes, which are in part responsible for fusion and deep inelastic scattering, are revealed. Because of the long interaction time for the latter reaction types, it is possible to repeat the elementary transfers several times, leading one way or another to large mass and energy transfers [see Rehm, vanden Berg, et al. (78)]. Truly massive transfers are often involved, but sequential transfers one particle or cluster at a time are equally important. At energies near the Coulomb barrier, the single neutron transfer is found to be a major part of the reaction cross section. For example, in the collision of ^{58}Ni with ^{58}Ni and ^{64}Ni and $E_{\text{cm}} \sim 100$ MeV, one finds [Rehm, Wolfs, et al. (85)] that the cross section of one and two neutron transfers is one-third of the reaction cross section and is larger than the fusion cross section.

The DWA approximation, in this heavy-ion context, does not differ conceptually from that discussed in Chapter VI on the (d, p) and (p, d) reaction.

Of course, it is far more complicated both geometrically and numerically, so that the use of modern computers is essential. Improvements on the DWA can be obtained with simple generations of the methods described in Chapter VI. The inclusion of the effects of the Pauli principle, of overlap and the reduction to coupled channels, are accomplished by exploiting the properties of a generalized K matrix. That matrix, described by (VI. 2.17), has a rank equal to the number of channels explicitly included. In the (d, p) case it was two, corresponding to the deuteron and proton channels. In the case of heavy ions one may need to include a greater number of exit channels. This is certainly the case when sequential transfer is important. Once the K matrix is determined, the next step is to determine its eigenvalues, especially those whose value is 1. One must eliminate the corresponding eigenstates, by projection or by the use of the orthogonality condition method of Saito. In any event, one then obtains the coupled-channel equations, which include rigorously the Pauli principle and overlap effects. For more details, see the paper by H. Horiuchi (77).

An alternative approach makes the semiclassical time-dependent approximation for the motion of the heavy ions. At each position in the orbit there is a transition probability that a reaction will occur. This is calculated quantum mechanically. This method was used very successfully by Alder, Bohr, et al. (56) in calculating the electromagnetic excitation of nuclei by charged particles. Its adaptation to the nuclear excitation in heavy-ion collisions has been developed by Broglia and Winther (72) and Broglia, Landowne, et al. (74). A similar procedure was developed by Bertsch and Schaeffer (77).

5. HEAVY-ION RESONANCES[†]

Resonances in the collision of heavy ions were first observed by Almqvist, Bromley and Kuehner, and (60). The heavy ions involved were ^{12}C and the center-of-mass energy was about 6 MeV, very close to the Coulomb barrier energy. The observations included scattering and reaction channels. Since that time, further resonances have been discovered in the $^{12}\text{C} + ^{12}\text{C}$ system, as well as in the $^{12}\text{C} + ^{16}\text{O}$ system, and more recently in the $^{28}\text{Si} + ^{28}\text{Si}$ system [Betts et al. (81)]. However, no such structure was observed for $^{40}\text{Ca} + ^{40}\text{Ca}$. Some examples are given in the following figures. Figure 5.1 gives the total γ -radiation yields (divided by the Coulomb transmission factor, which removes most of the energy dependence). Note the large number of peaks and the fact that spin and parity have been assigned to many. Figure 5.2 shows resonances in the $^{12}\text{C} + ^{16}\text{O}$ system, which appear in the inelastic scattering. Another example is provided by the radiative capture of ^{12}C by ^{16}O shown in Fig. 5.3. In Fig. 5.4 the 90° elastic $^{28}\text{Si} + ^{28}\text{Si}$ scattering is shown, while in Fig. 5.5 a high-resolution study of the scattering is recorded. The data exhibit two kinds of structure. There are

[†]Erb and Bromley (84).

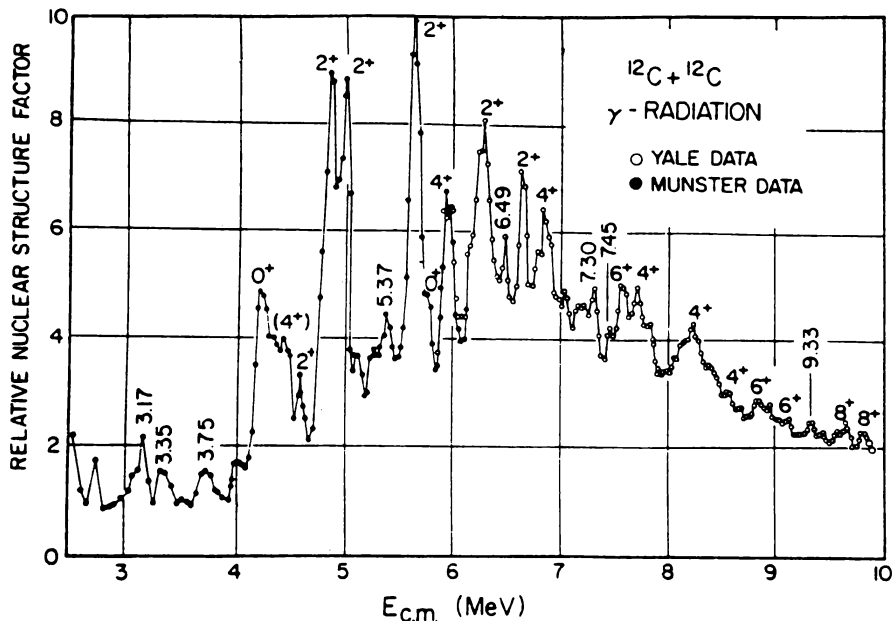


FIG. 5.1. Nuclear structure factors derived from the total γ -radiation yields of the $^{12}\text{C} + ^{12}\text{C}$ interaction. The nuclear structure factor is defined by

$$T_L = \frac{E\sigma(E)}{\sum_{L=0}^{10} (2L+1)T_L} = \frac{KR}{F_L^2(KR) + G_L^2(KR)}$$

where $R = 1.4(12^{1/3} + 12^{1/3})$ and F_L and G_L are the regular and irregular Coulomb wave functions, respectively. [From Erb and Bromley (84).]

broad envelopes with a width on the order of 150 keV and an energy separation of the order of a few hundred keV.

Most systems do not resonate. Or stated more carefully, the resonance amplitudes, if they exist, are not sufficiently strong to be observable. As an example, see Fig. 5.6, giving the total γ -radiation in the neighborhood of the Coulomb barrier of $^{16}\text{O} + ^{16}\text{O}$. One sees very little structure, which hardly compares with violent fluctuations, which appear in Fig. 5.1 for $^{12}\text{C} + ^{12}\text{C}$.

In analyzing the experimental data, two problems must be solved. In one, the issue is distinguishing the resonance peaks from the Ericson random fluctuations. In the other, how can the spin and parity of the resonances be determined? Turning to the first of these, one can obtain an estimate of the magnitude of the Ericson fluctuations using the statistical theory of nuclear reactions. If the peak under study has a width much larger than predicted by the statistical theory and/or if its magnitude is much greater, it is probably a resonance. Another indication is obtained by comparing reactions involving

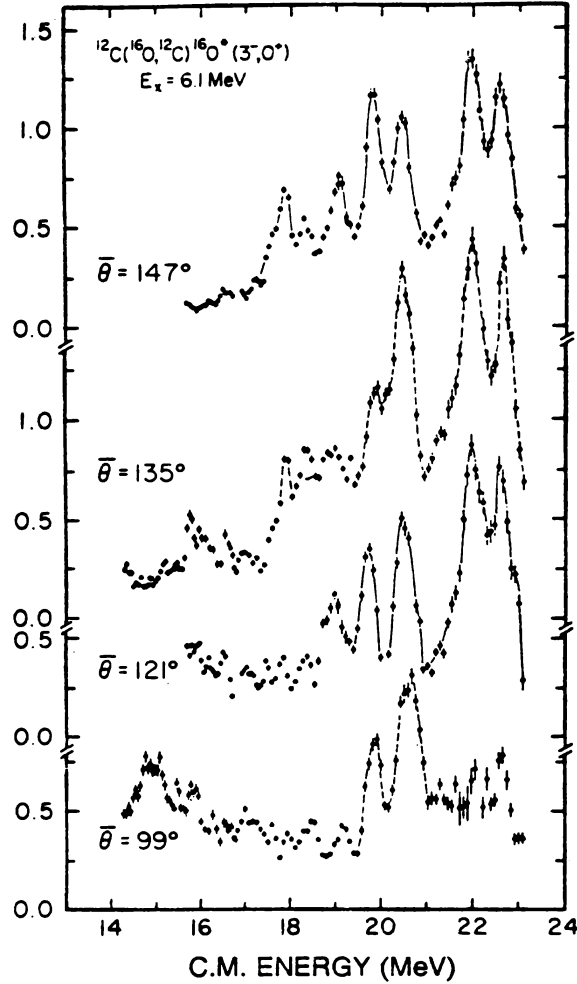


FIG. 5.2. $^{16}\text{O}(3^-)$ in elastic yields. [From Malmin, Harris, and Paul (78).]

the same compound nucleus. If peaks appear in one channel and not in the other, one is certainly not dealing with Ericson fluctuations. As an example, see the comparison of $^{12}\text{C}(^{16}\text{O}, \alpha)^{24}\text{Mg}$ and $^{14}\text{N}(^{14}\text{N}, \alpha)^{24}\text{Mg}$ in Fig. 5.7. The cross section for the first reaction has structure, the second does not. Second, if one sums the cross sections for differing channels, the statistical fluctuations will tend to average out so that peaks in the summed cross section are probably resonances. Finally, if one can establish a correlation among the peaks in the various channel cross sections, a resonance of the system is indicated. One must be careful since the energy of a peak may shift from one channel to the next by the order of a width because of interference with a nonresonant amplitude.

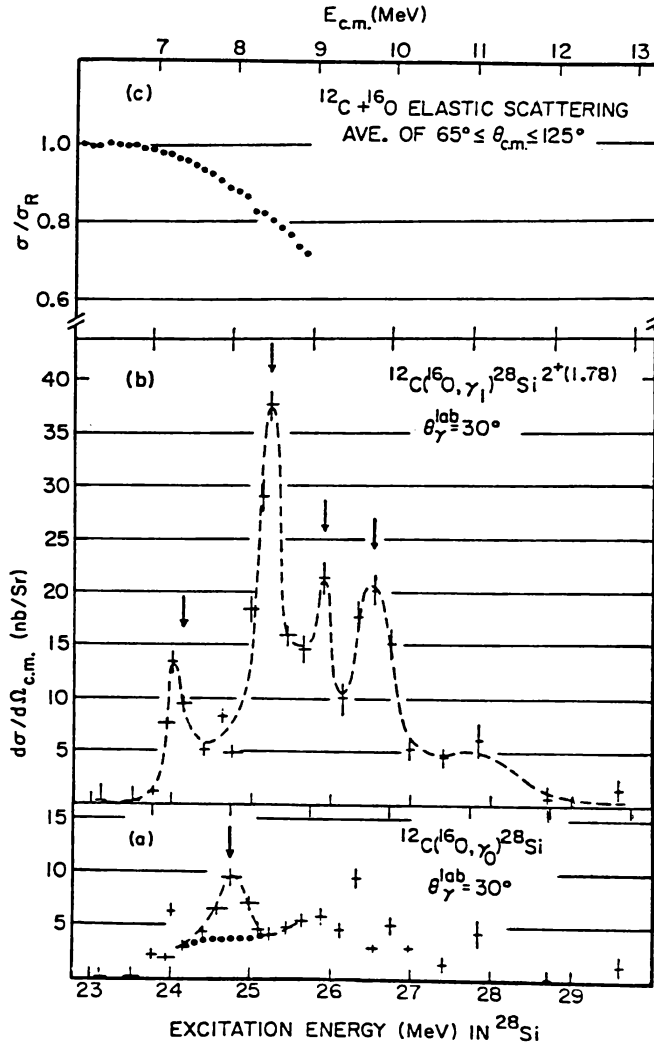


FIG. 5.3. Excitation functions for the radiative capture of ^{12}C by ^{16}O . The elastic scattering data are from Spinka and Winkler (74). The dashed lines are drawn to guide the eye. [From Collins and Sandorfi (82).]

An example of this analysis is shown in Figs. 5.8 and 5.9. In Fig. 5.8 the cross sections to different levels of ^{20}Ne formed by the reaction $^{12}\text{C}(^{12}\text{C}, \alpha)^{20}\text{Ne}$ are plotted together with their sum. The shown shows several peaks. The anomalies at 7.71, 9.84, and 10.59 MeV are studied [Erb et al. (77)]. The widths of the 7.71- and 9.84-MeV peaks are one to two orders of magnitude greater than that given by a Hauser-Feshbach calculation. The 10.59-MeV peak turns out

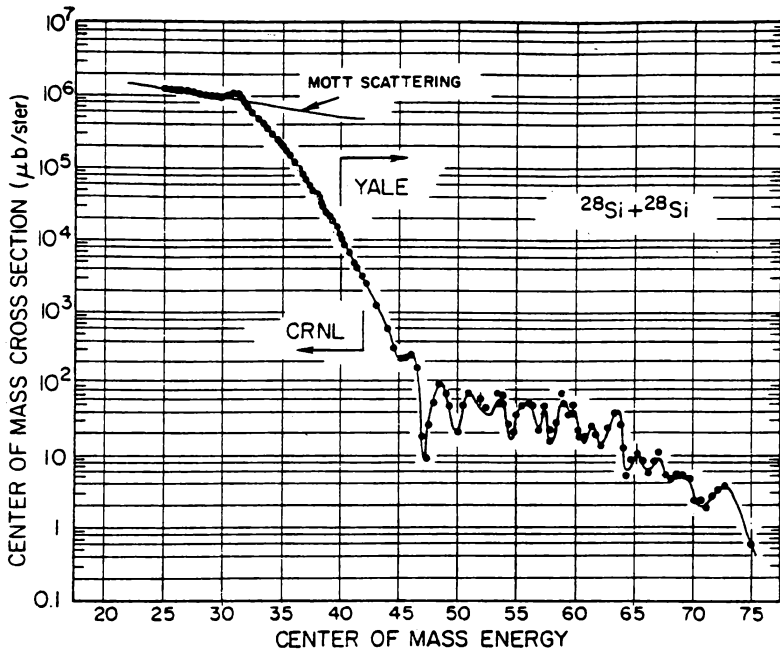


FIG. 5.4. Excitation function for $^{28}\text{Si} + ^{28}\text{Si}$ elastic scattering at $\theta_{\text{cm}} = 90^\circ$. [From Erb and Bromley (84).]

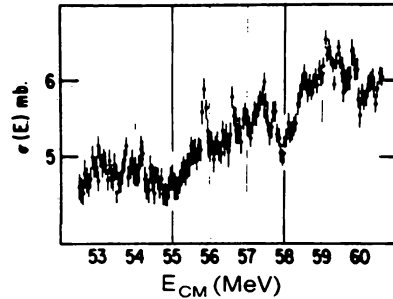


FIG. 5.5. High-resolution cross-section of the summed elastic and inelastic excitation function for the $^{28}\text{Si} + ^{28}\text{Si}$ system. [From Betts, Diczienzo, and Peterson (81).]

not to have an unusual strength, so that it is probably a fluctuation and not a resonance. Figure 5.9 gives the angular distribution of the α -particles for the 7.71- and 9.84-MeV peaks. We see that these beautifully follow $|P_4(\cos \vartheta)|^2$ and $|P_8(\cos \vartheta)|^2$ distributions suggesting the spin of 4 in the 7.71-MeV resonance and 8 for the 9.84 resonance.

This description provides one method for determining the spin of a resonance. It is by itself not enough but should be augmented by a study of the energy dependence of the angular distribution. This is illustrated by Fig. 5.10, where

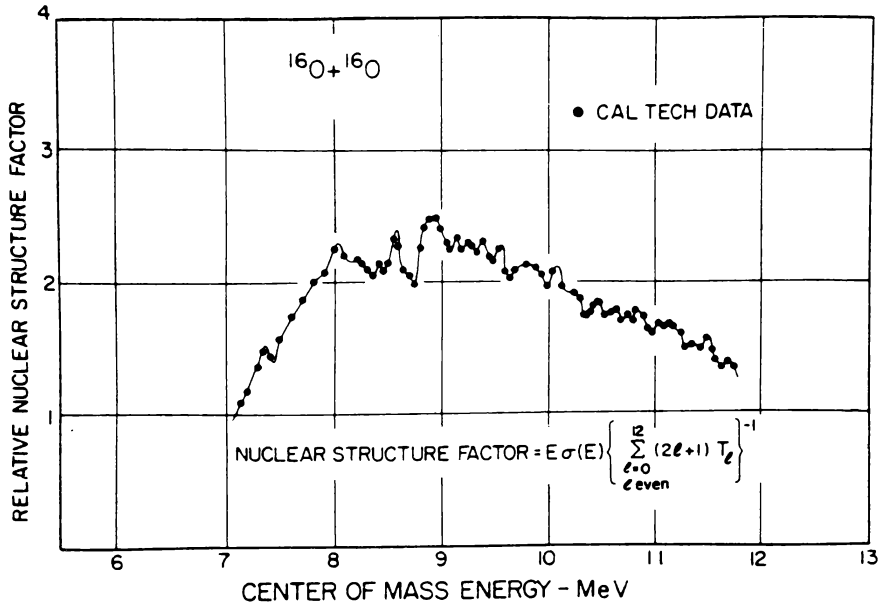


FIG. 5.6. Nuclear structure factors for the $^{16}\text{O} + ^{16}\text{O}$ interaction (see Fig. 5.1). [From Erb and Bromley (84).]

one sees the comparatively featureless angular distributions interrupted by strong oscillatory behavior at, for example, energies 7.71 and 9.84 MeV.

Another general procedure is to attempt a phase shift analysis of the elastic scattering. As long as the number of nuclear partial waves is low, this is a practical method. A closely related method involves fitting the energy-averaged cross section by an optical model. To obtain the intermediate structure, one adds Breit-Wigner contributions to the optical model phase shifts. An example of the first of these two methods is given in Fig. 5.11. Note that the magnitude of the S matrix, η_L , has deep minima at the resonant energies of 6.65 MeV in the $L = 2$ partial wave and 6.85 MeV in the $L = 4$ partial wave, thus identifying the spin of these resonances. Similar analyses have been made at higher energies by Cosman et al. (82). From the Breit-Wigner fit one can get an estimate of the ratio Γ_{el}/Γ . For the $L = 2$ case this turns out to be 0.29, while for the $L = 4$ case it is 0.09. Both values are much larger than the statistical estimates of these partial width ratios.

These analyses provide a list of isolated resonant states. Overlapping states have been discussed, but disentangling these has not proved practical, especially for states of high spin. Our first question is: What are the nature of these resonant states? Our second is: What is the mechanism that produces these resonances? And as a corollary: What conditions need to be met?

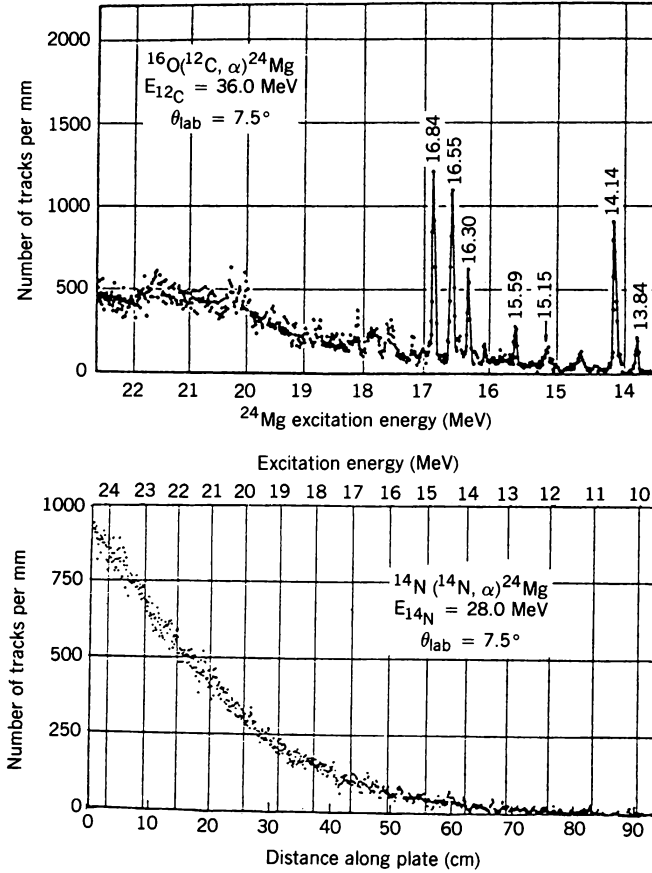


FIG. 5.7. Alpha particle spectra from the $^{16}\text{O}(^{12}\text{C}, \alpha)^{24}\text{Mg}$ and $^{14}\text{N}(^{14}\text{N}, \alpha)^{24}\text{Mg}$ reactions. [From Bromley (78).]

With regard to the first question, it is clear that these states are doorway states. Their widths (~ 100 keV) are much smaller than the width of structures (e.g., shape resonances) generated by an optical model on the order of 2.5 MeV. On the other hand, these widths are too large to be compound nuclear widths. Indeed, if very high resolution measurements are made [Bromley (78)], one finds the Ericson fluctuation structure (see also Fig. 5.5).

We can refer to Section III.4 for a discussion of doorway states. The expression for the transition amplitude for a reaction proceeding through an isolated doorway resonance, (III.4.16), is appropriate here. It is

$$\langle \mathcal{T}_{fi} \rangle = \mathcal{T}_{fi}^P + \frac{\langle \chi_f^{(-)} | H_{PD} \psi_d \rangle \langle \psi_d | H_{DP} \chi_i^{(+)} \rangle}{E - E_d + i/2(\Gamma_d^\dagger + \Gamma_d)} \quad (\text{III.4.16})$$

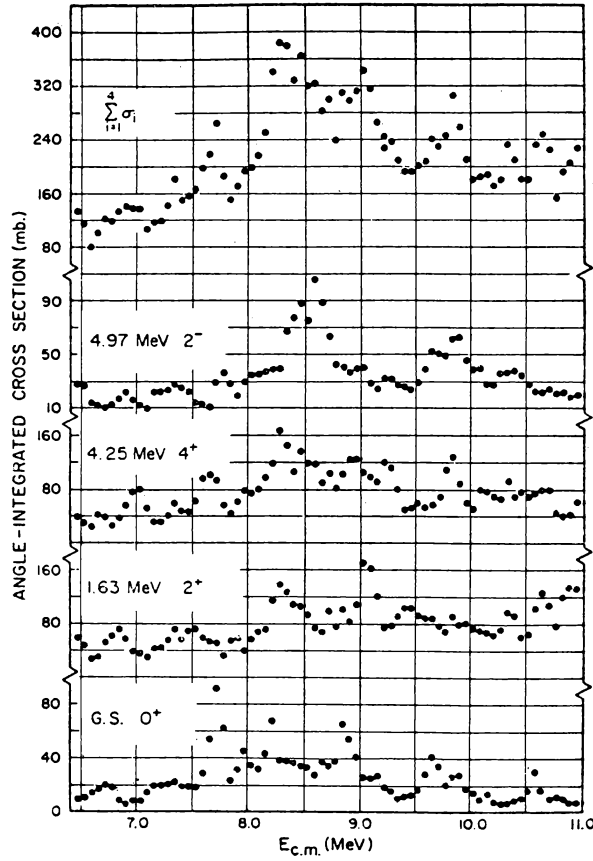


FIG. 5.8. Angle integrated cross sections as functions of the energy for the $^{12}\text{C}(^{12}\text{C}, \alpha)^{20}\text{Ne}^*$ reaction populating low-lying levels of ^{20}Ne . [From Erb et al. (77).]

The average is over the fine structure. H_{DP} and H_{PD} are the operators connecting the entrance channel or exit channel wave functions $\chi_i^{(+)}$ and $\chi_f^{(-)}$ with the doorway wave function ψ_d . \mathcal{T}^P is the transition for the prompt, nonresonant amplitude, while Γ_d^\dagger is the escape width:

$$\Gamma_d^\dagger = 2\pi \sum_\gamma |\langle \chi_\gamma^{(-)} | H_{PD} \psi_d \rangle|^2$$

which gives the probability that the doorway state will decay into an exit channel, $\chi_\gamma^{(-)}$. The spreading width, Γ_d^\downarrow , gives the probability that the doorway state will decay into the more complex states. For elastic scattering and a particular partial wave, the S matrix $\langle S_{el} \rangle$ can be obtained directly from

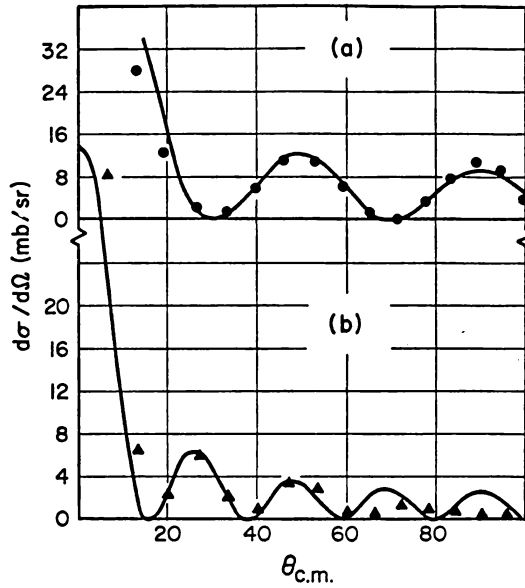


FIG. 5.9. The $^{12}\text{C}(^{12}\text{C}, \alpha)^{20}\text{Ne}$ angular distribution compared to the Legendre functions $|P_L(\cos \theta)|^2$, not normalized: (a) $E_{cm} = 7.71$ MeV ($L = 4$); (b) $E_{cm} = 9.84$ MeV ($L = 8$). [From Erb et al. (77).]

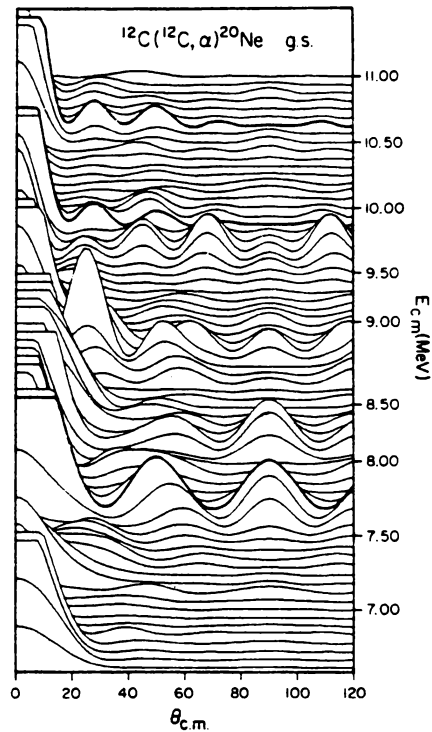


FIG. 5.10. Evolution of the ^{20}Ne ground-state angular distributions as a function of bombarding energy. The heavy curves signify angular distributions at energies of maxima in the total yields that are particularly well fitted by pure $|P_L(\cos \theta)|^2$ shapes. [From Erb and Bromley (84).]

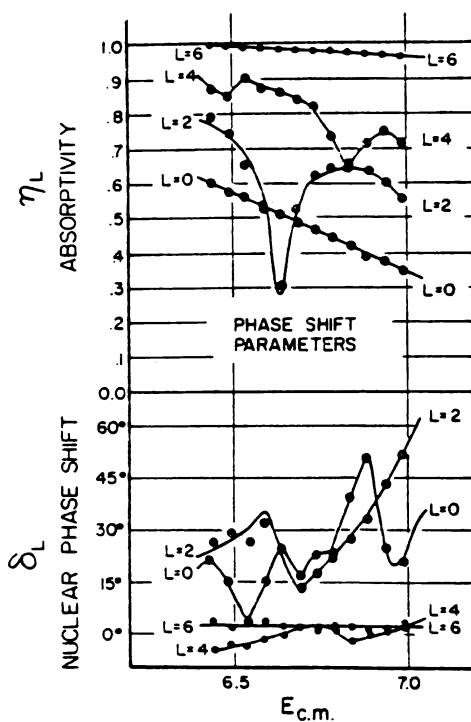


FIG. 5.11. Phase-shift parameters $S = \eta_L e^{i\delta_L}$ deduced from the phase-shift analysis of $^{12}\text{C} + ^{12}\text{C}$ elastic scattering. [From Korotky, Erb, Willett, and Bromley (79).]

(III.4.16). One obtains

$$\langle S_{el} \rangle = e^{2i\delta} \frac{(E - E_d) + \frac{1}{2}i(\Gamma_d^\downarrow - \Gamma_d^\uparrow)}{(E - E_d) + \frac{1}{2}i(\Gamma_d^\downarrow + \Gamma_d^\uparrow)} \quad (\text{III.4.18})$$

where δ is the phase associated with the prompt (potential) scattering. Note that the magnitude of $\langle S_{el} \rangle$ squared is

$$e^{-4\eta} = \frac{(E - E_d)^2 + \frac{1}{4}(\Gamma_d^\uparrow - \Gamma_d^\downarrow)^2}{(E - E_d)^2 + \frac{1}{4}(\Gamma_d^\uparrow + \Gamma_d^\downarrow)^2}$$

We see that this magnitude has a minimum at $E = E_d$ as observed (see Fig. 5.11).

We turn now to the second question, the nature of the doorway states and the mechanism that generates them. In the $^{12}\text{C} + ^{12}\text{C}$ case, it is possible to establish a qualitative understanding. Toward that end, examine Fig. 5.12, where we have plotted the energy of the observed resonance versus $J(J + 1)$ [Feshbach (76, 77)]. Look also at a plot of the excitation energy centroids of the levels of

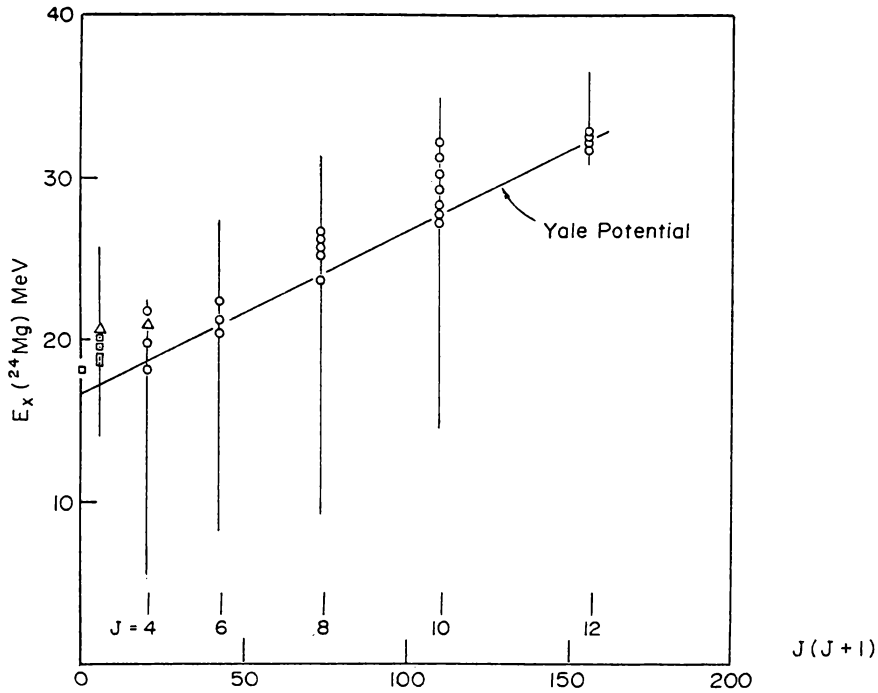


FIG. 5.12. Excitation energy of $^{12}\text{C} + ^{12}\text{C}$ resonances as a function of $J(J+1)$, J = spin of the resonance. The line marked "Yale potential" is the locus of the values of J and E_x corresponding to grazing [Feshbach (77,78).]

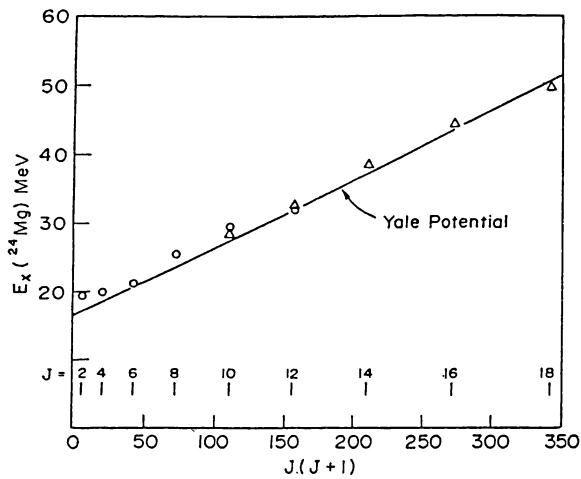


FIG. 5.13. Average energy of levels in ^{24}Mg excited in the $^{12}\text{C} + ^{12}\text{C}$ versus $J(J+1)$. [From Feshbach (78).]

a given J given in Fig. 5.13. The line labeled the “Yale potential” is obtained by Arima et al. (72) by determining the values of the orbital angular momentum L and energies at which the potential devised by Reilly et al. (73) to fit the elastic $^{12}\text{C} + ^{12}\text{C}$ scattering generates a pole in the S matrix. These values of L will not differ especially from the grazing L . That potential is a central potential composed of Woods–Saxon forms for both the real and imaginary parts (see Chapter V). The parameters are $V = 14$ MeV, $R = 6.18$ fm, $a = 0.35$ fm, $W = 0.4 + 0.1 E$, $R_I = 6.41$ fm, and $a_I = 0.35$ fm. The shallow depth, and especially the weak imaginary terms, are required to obtain the rather large oscillations of the observed angular distributions (see Fig. 5.14).

The experimental fact that the centroids are a linear function of $J(J + 1)$ is noteworthy (see Fig. 5.13). The fact that this straight line follows from the Yale potential suggests the following model [Feshbach (76)]. At special values of the energy there will be an optical model resonance (a peak would be sufficient) in a given partial wave, say L . The energy width of these peaks is on the order of a few MeV, and a corresponding lifetime of a few times 10^{-22} s. During this time, the system will couple with other partitions of the $^{12}\text{C} + ^{12}\text{C}$ system. This could include inelastic excitations of either or both ^{12}C to such levels as the 2^+ , 4.43-MeV level or the 0^+ , 7.63-MeV level. It could include such reaction channels as $^{20}\text{Ne} + \alpha$ or $^8\text{Be} + ^{16}\text{O}$, involving various excited states of these nuclei. This coupling will convert some of the initial kinetic energy of the system into internal energy of excitation, making possible the formation of quasi-bound states. Generally, the coupling will tend to fragment the optical model resonance (or shape maximum) into a number of resonances of a smaller width as observed [Fletcher, Foy, et al. (76)]. These are the doorway states, which couple to even more complex states. Interestingly, the sum of the widths for the doorway state resonance of a given L is on the order of the width of the optical potential resonance. This qualitative description leaves problems for the theorists and experimentalists. For the latter it requires experiments that will determine which of the various excitations are involved and with what amplitudes. Theoretically, it is necessary to solve the coupled Schrödinger equations implied by the description above and to find the conditions under which isolated doorway state resonances will be developed.

However, some qualitative conditions follow from (III.4.16). Obviously, Γ^\downarrow , that is, the probability of coupling to more complex modes, cannot be too large, for then the resonant amplitude will be much reduced. This width depends multiplicatively on the density of the more complex states and the coupling matrix element. Table 5.1 gives the level density in the compound nucleus relative to $^{12}\text{C} + ^{12}\text{C}$ at the Coulomb barrier energy [Hanson, Stokstad, et al. (74)].

We have only tabulated those cases with the lowest relative level density, except for the $^{14}\text{N} + ^{14}\text{N}$ case, which shows the large effect of the entrance channel. The condition of low relative level density is not a sufficient condition, as the absence of resonances in the $^9\text{Be} + ^{12}\text{C}$ reaction suggests. It is proposed as a necessary condition. It is, in addition, necessary that the matrix elements coupling the doorway state to more complex states also be small. In the

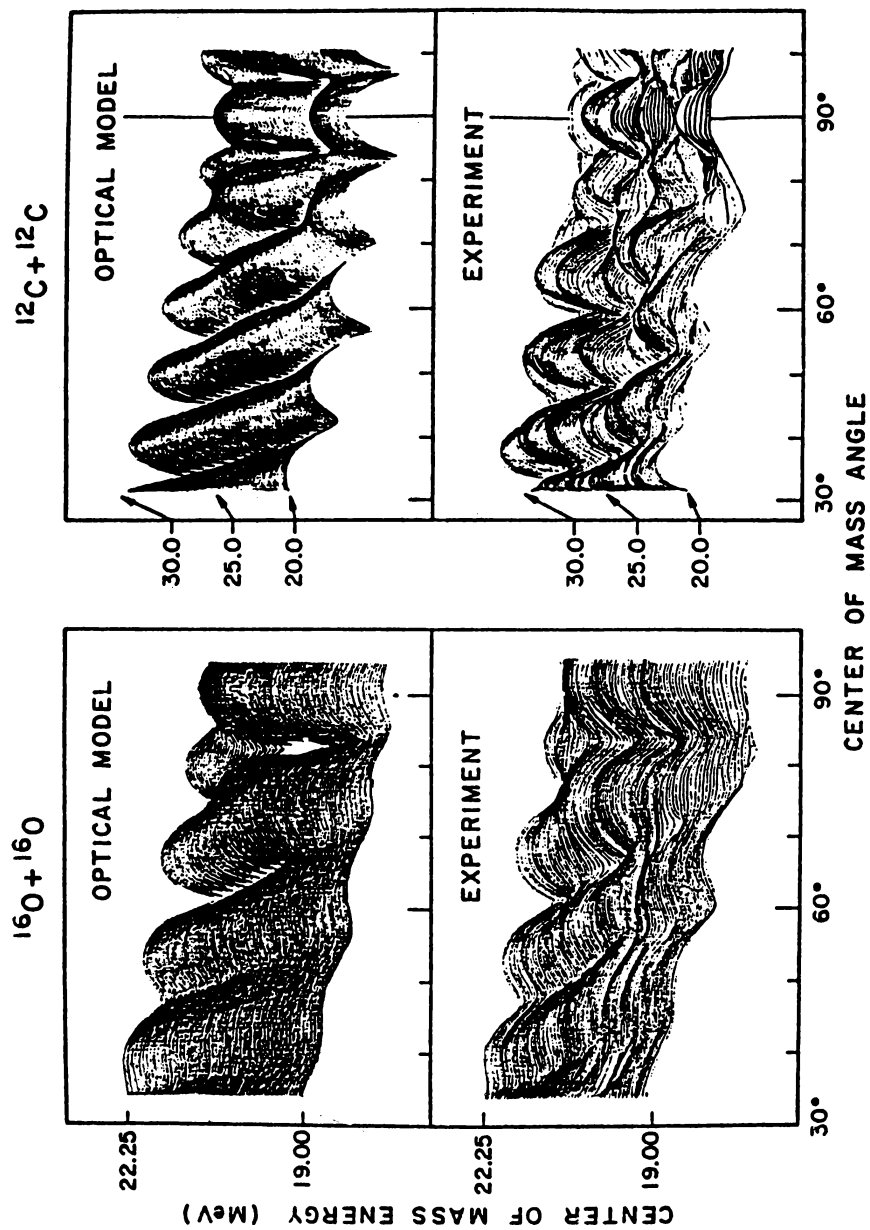


FIG. 5.14. Comparison of the experimental angle-energy cross-section surfaces with the corresponding optical model for the $^{16}\text{O} + ^{16}\text{O}$ and $^{12}\text{C} + ^{12}\text{C}$ systems. [From Gobbi, Wieland, et al. (73).]

TABLE 5.1

Reaction	Compound System	E_x Coulomb Barrier, (MeV)	Relative Level Density
$^{12}\text{C} + ^{12}\text{C}$	^{24}Mg	20.6	1
$^9\text{Be} + ^{12}\text{C}$	^{21}Ne	21.7	3.3
$^{12}\text{C} + ^{16}\text{O}$	^{28}Si	25.2	3.8
$^{14}\text{N} + ^{14}\text{N}$	^{28}Si	35.8	110
$^{12}\text{C} + ^{13}\text{C}$	^{25}Mg	22.9	7.1
$^{11}\text{B} + ^{12}\text{C}$	^{23}Na	23.8	11
$^{12}\text{C} + ^{14}\text{C}$	^{26}Mg	25.7	13
$^{10}\text{B} + ^{12}\text{C}$	^{22}Na	23.0	15

$^{12}\text{C} + ^{12}\text{C}$ case this is likely, since both nuclei are deformed, so that the combined system may not have good overlap with many of the ^{24}Mg levels present at 20.6 MeV, an example of shape isomerism. This leads to the prediction that resonances are more likely to be observable when the colliding nuclei are deformed. In the case of $^9\text{Be} + ^{12}\text{C}$, the relatively easy polarizability of ^9Be because of the valence neutron makes it likely that the coupling matrix elements will be relatively large as will be Γ^\downarrow .

Another condition requires that the resonant energy E_d fall within the width of the shape resonance. The shape resonance maximizes the value of the matrix element $\langle \phi_i | H_{DP} \chi_i^{(+)} \rangle$ since $\chi_i^{(+)}$ has its maximum value in the interaction region. When the coupling between the entrance channel wave function and the intermediate channels is strong, there may very well be a correspondingly strong energy shift, which may move E_d outside the range in energies in which $\chi_i^{(+)}$ is large. One should also note that the transition matrix element to the final state $\langle \chi_f^{(-)} | H_{PD} \psi_d \rangle$ must be sufficiently large so that the particular final state show the resonance. As a corollary, the cross section to not all final states will have an observable resonance.

Finally, note that an important parameter is the angular momentum range over which the incident channel wave function is relatively large. In the case of $^{12}\text{C} + ^{12}\text{C}$ this angular momentum window is narrow. This may not be the case for other systems. If so, one may well find resonances with differing values of L within a given energy interval. This is the case for the $^{12}\text{C} + ^{16}\text{O}$ system, where the angular momentum window is on the order of 3 to 4 units. See Fletcher and Frawley (81) and Braun-Munzinger (81).

It appears that $^{12}\text{C} + ^{12}\text{C}$ is a unique system in that the conditions discussed above for isolated resonances to be observable seem to be satisfied. The $^{12}\text{C} + ^{16}\text{O}$ system is not as clear cut, as there is much controversy with regard to spin assignments.

The relatively large $^{12}\text{C} + ^{12}\text{C}$ elastic widths reported above imply that the $^{12}\text{C} + ^{12}\text{C}$ amplitude, in which both ^{12}C 's are in their ground states, is a significant part of the entire wave function; or in other words, the probability

Harvey (75) has given an intuitive and instructive demonstration of the importance of the Pauli principle, and at the same time has shown that the intermediate state is deformed. It is in fact “superdeformed.” As illustrated in Fig. 5.15, the nucleus C in its ground state, according to the harmonic oscillator model, consists of four nucleons on the 1s shell and eight on the 1p shell. The figure shows the nucleon configuration for the two colliding ^{12}C nuclei. Assuming that the nuclei approach along the z axis with their axes of symmetry perpendicular to that axis, only the value of n_z is presumed to change. For example, four of the nucleons in the 1s state in the incident carbons will go into 1s state in $^{24}\text{Mg}^*$, which precludes its being filled by nucleons in the (001) state in ^{12}C . These must go to the (002) and (003) state. There is no way of

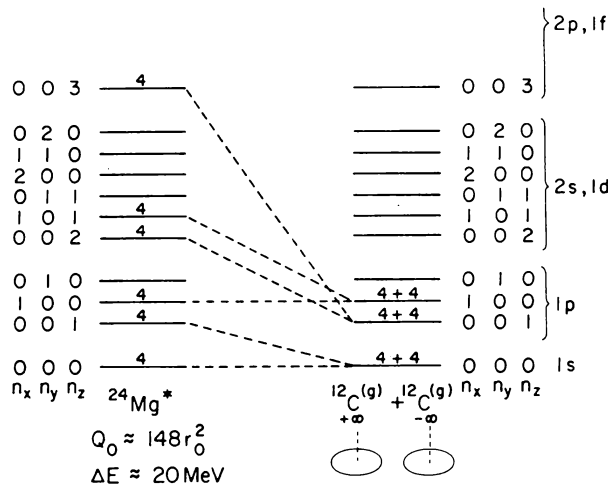


FIG. 5.15. Formation of excited states of ^{24}Mg by $^{12}\text{C} + ^{12}\text{C}$ collision. Symmetry axes are parallel. [From Harvey (75); Rae (87).]

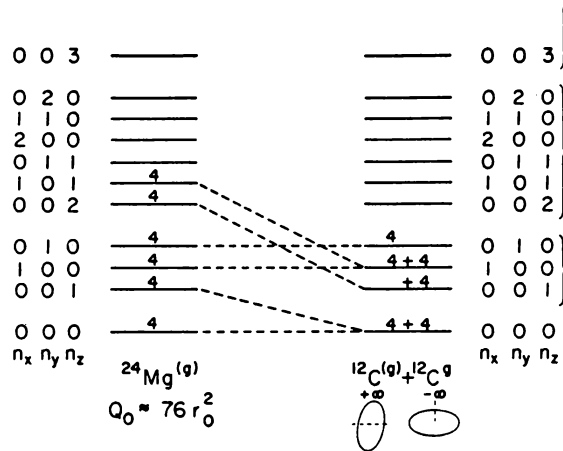


FIG. 5.16. Formation of excited states of ^{24}Mg by $^{12}\text{C} + ^{12}\text{C}$ collision. Symmetry axes are orthogonal. [From Harvey (75).]

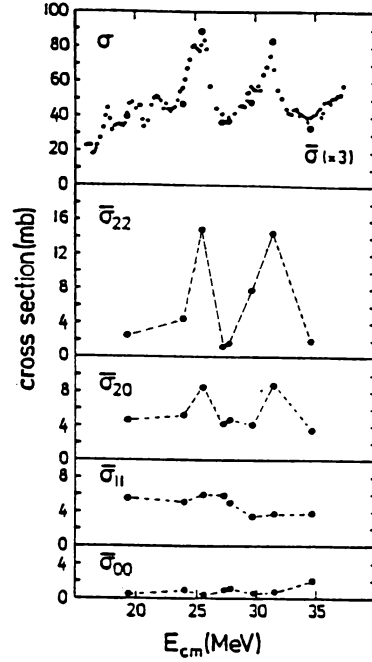
filling the (010) state in ^{24}Mg . The result is a four particle–four-hole state, substantially deformed.

On the other hand, if the axes of the two carbon nuclei are orthogonal as in Fig. 5.16, then as shown in the figure the ground state of ^{24}Mg can be populated. A collision with this orientation of the symmetry axes cannot produce the resonant states we have been discussing but rather, would produce the states of the ground-state band.

Remarkably, this picture has been verified by experiment [Konnerth, Dürnweber et al. (85)]. These authors studied the spin orientations in the reaction $^{12}\text{C} + ^{12}\text{C} \rightarrow ^{12}\text{C}(2^+) + ^{12}\text{C}(2^+)$ by measuring the directions of both 4.439-MeV γ -ray emitted by each $^{12}\text{C}(2^+)$ in coincidence with each mutually inelastic scattering event. Taking the axis of quantization perpendicular to the scattering plane and integrating over the azimuth, it becomes possible to decompose the cross section for the reaction into components $\bar{\sigma}_{|m_1||m_2|}$. Here m_i is the projection of the spin of the quadrupole radiation and therefore of the spin of the emitting $^{12}\text{C}^*$ on the quantization axis. The results are shown in Fig. 5.17. The resonance examined are two of those observed by Cormier, Applegate et al. (77) and Cormier, Jackenski, et al. (78) at $E_{\text{cm}} = 25.6$ and 31.5 MeV. We see very strong maxima in the $\bar{\sigma}_{22}$ cross section, implying that, for the most part, the spins of the two emitting nuclei are parallel while they rotate about each other with the appropriate angular momentum. This result confirms Harvey's picture presented in Figs. 5.15 and 5.16.

It is necessary to go beyond Harvey's considerations, to obtain a more quantitative and clearer understanding. Several models have been studied. Leander and Larsson (75) and Larsson et al. (76) calculated the potential energy surface for $N = Z$ nuclei using essentially the Nilsson–Strutinsky procedure.

FIG. 5.17. Decomposition of the cross section for mutually inelastic $^{12}\text{C} + ^{12}\text{C}$ scattering into the contributions from different m -substate combinations. The particle-inclusive cross section $\bar{\sigma}$ (scaled up by a factor of 3 in the upper panel, large dots) and the contributions $\bar{\sigma}|m_1||m_2|$ (the sum of which yields $\bar{\sigma}$) are integrated over the angular range $45^\circ < \theta_{\text{cm}} < 90^\circ$. The total integrated cross section σ (small dots, upper panel) is taken from Cormier, Applegate, et al. (77). The target thickness corresponds to an average over $E_{\text{cm}} = 100$ to 170 KeV. [From Konnerth, Dünnweber, et al. (85).]



Chandra and Mosel (78) used the two-center model, while Rae (87) and Rae and Marsh (85) employ the cranked-cluster model. The results are quite consistent.

Leander and Larsson's results are summarized in Table 5.2 and an example of (^{24}Mg) of the potential energy surface is shown in Fig. 5.18. The table lists the minima together with the ratios of the harmonic oscillator parameters ω_x : ω_y : ω_z . For many of the minima these are ratios of whole numbers and would be expected to give rise to superdeformed bands. The ground state of ^{24}Mg and the next minimum ($\varepsilon = 1.0$, $\gamma = 0$, $\varepsilon_3 = 0.3$) correspond to prolate spheroid shapes; the next three are oblate ($\varepsilon = 1.23$, $\gamma = 6^\circ$), triaxial ($\varepsilon = 1.26$, $\gamma = 42^\circ$), and "chain" ($\varepsilon = 1.25$, $\gamma = 0$). The corresponding density contours as obtained by Rae and Marsh [Rae (87)] are shown in Fig. 5.19. We see that the chain consists of 6α clusters in a row; the oblate is given by (d) while the triaxial (g) appears to be two-carbon nuclei aligned perpendicular to the line joining their centers. The prolate configuration (e) appears to be of the α - ^{16}O - α form. The triaxial minimum corresponds, then, to the resonances observed by Cormier, Applegate, et al. (77) and Cormier, Jackenski, et al. (78). With respect to the resonances at lower energies there is some debate. Rae (87) believes these to be generated by the prolate configuration, while Cosman (81) and Ledoux, Ordonez, et al. (84) assign all the resonances to the triaxial minimum. According to Rae, the Cormier resonances have spins of 16, 18, and 20, starting a new band,

TABLE 5.2 Properties of the Minima in the Potential Energy Surfaces for the Doubly Even $N-Z$ Nuclei^a

Nucleus	ε	ε_3	ε_4	γ (deg)	Configuration	$\omega_x:\omega_y:\omega_z$	Energy (MeV)	
							Min.	Barr.
¹² C	0.83	0	0.20	60	(1) ⁻⁴	2:1:1	0	
	1.11	0	0.24	0	(1) ⁻⁸ (2) ⁴	3:3:1	1	14
¹⁶ O	0.00	0	0.00	0		1:1:1	0	
	1.04	0	0.24	43	(1) ⁻⁴ (2) ⁴	4:2:1	9	16
²⁰ Ne	1.2	0	0.24	0	(1) ⁻⁸ (2) ⁴ (3) ⁴	4:4:1	9	20
	0.40	0	-0.10	0	(2) ⁴	2:2:1	0	
	1.17	0	0.24	50	(1) ⁻⁴ (2) ⁸	8:3:2	9	14
	1.25	0	0.24	0	(1) ⁻⁸ (2) ⁴ (3) ⁴ (4) ⁴	5:5:1	13	21
²⁴ Mg	0.45	0	0.08	20	(2) ⁸	4:3:2	0	
	1.0	0.3	0.20	0	(2) ⁴ (3) ⁴		(6)	12.5
	1.23	0 ^b	0.24	60	(1) ⁻⁴ (2) ¹²	3:1:1	8	14.5
	1.26	0	0.24	42	(1) ⁻⁴ (2) ⁸ (3) ⁴	5:2:1	10	14.5
	1.25	0	0.08	0	(1) ⁻⁸ (2) ⁴ (3) ⁴ (4) ⁴ (5) ⁴	6:6:1	20	25
²⁸ Si	0.49	0	-0.06	60	(2) ¹²	2:1:1	0	
	0.45	0	0.16	0	(2) ¹²	3:3:2	1	3.5
	1.0	0.3	0.20	0	(2) ⁴ (3) ⁴ (4) ⁴		13	15.5
	1.35	0	0.24	60	(1) ⁻⁴ (2) ¹² (3) ⁴		13	17.5
	1.32	0	0.24	35	(1) ⁻⁴ (2) ⁸ (3) ⁴ (4) ⁴	6:3:1	19	20
³² S	0.21	0	0.08	20	(2) ⁻⁸	5:4:3	0	
	0.68	0	0.08	0	(2) ⁻¹² (3) ⁴	2:2:1	0.1	4.5
	1.42	0	0.24	54	(1) ⁻⁴ (2) ⁻¹² (3) ⁸	10:3:2	16	18
	1.0	0.3	0.20	0	(2) ⁸ (3) ⁴ (4) ⁴		16	17
³⁶ Ar	1.30	0	0.24	30	(1) ⁻⁴ (2) ⁸ (3) ⁸ (4) ⁴		21	23
	0.29	0	0.16	60	(2) ⁻⁴	3:2:2	0	
	0.74	0	0.16	7	(2) ⁻¹² (3) ⁸		9	11
	1.45	0	0.24	55	(1) ⁻⁴ (2) ⁻¹² (3) ¹²		27	27.5
⁴⁰ Ca	1.33	0	0.24	47	(1) ⁻⁴ (2) ⁻¹² (3) ⁸ (4) ⁴		27	27.5
	0.00	0	0.00	0		1:1:1	0	
	0.45	0	0.16	50	(2) ⁻⁴ (3) ⁴	7:5:4	9	10.5
	0.84	0	0.08	5	(2) ⁻¹² (3) ⁸ (4) ⁴		17	18
⁴⁴ Ti	1.50	0	0.24	60	(1) ⁻⁴ (2) ⁻¹² (3) ¹⁶		34	36.5
	0.18	0	0.00	0	(3) ⁴	3:3:2	0	
	0.52	0	0.16	38	(2) ⁻⁴ (3) ⁸		3	5.5
	0.86	0	0.16	0	(2) ⁻¹² (3) ¹² (4) ⁴		11	15
	1.50	0	0.24	60	(1) ⁻⁴ (2) ⁻¹² (3) ¹⁶ (4) ⁴		29	31.5

^aThe deformation parameters ε , ε_3 , ε_4 , γ are defined in the legend to Fig. 5.18. The last two columns contain the energy and minimum barrier height relative to the ground-state minimum.

^b $\varepsilon_{33} = 0.05$.

Source: Leander and Larsson (75).

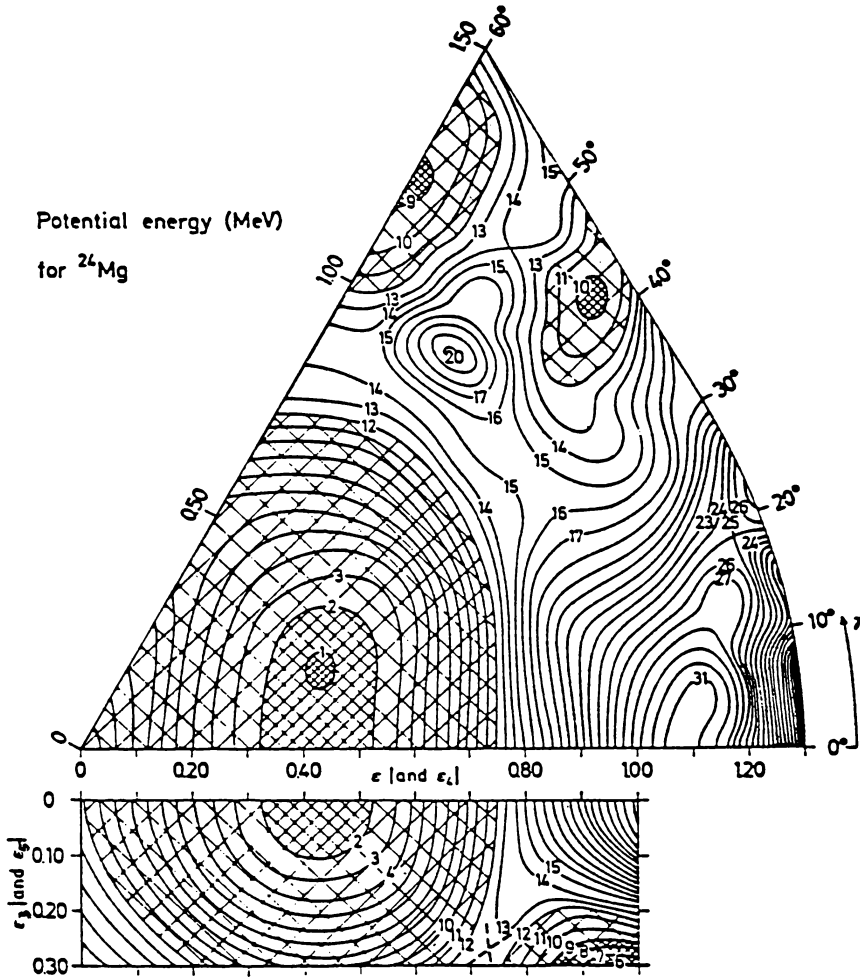


FIG. 5.18. Potential energy surface for ^{24}Mg . The deformation parameters are defined by the deformed nuclear potential:

$$\begin{aligned}
 V = & \frac{1}{2} \hbar \omega_0 \rho^2 \left[1 + 2\varepsilon_1 P_1(\cos \theta_l) - \frac{2}{3} \varepsilon \cos \gamma P_2(\cos \theta_l) \right. \\
 & + \frac{1}{3} \varepsilon \sin \gamma \sqrt{\frac{8}{5}} \pi (Y_{22}(\theta_l, \phi_l) + Y_{2-2}(\theta_l, \phi_l)) \\
 & + 2\varepsilon_3 P_3(\cos \theta_l) + 2\varepsilon_{33} \sqrt{\frac{4}{7}} \pi (Y_{33}(\theta_l, \phi_l) - Y_{3-3}(\theta_l, \phi_l)) \\
 & \left. + 2\varepsilon_4 P_4(\cos \theta_l) + 2\varepsilon_5 P_5(\cos \theta_l) \right] \\
 & - \kappa \hbar \omega_0 [2l_t \cdot s + \mu(l_t^2 - \langle l_t^2 \rangle)].
 \end{aligned}$$

The potential energy in the (ε, γ) plane, including the macroscopic energy, was calculated for each value of (ε, γ) and then minimized with respect to ε_4 . For the $(\varepsilon, \varepsilon_3)$ plane $\gamma=0$. For definitions of ρ, θ_l , and ϕ_l , see the original reference. [From Leander and Larsson (75).]

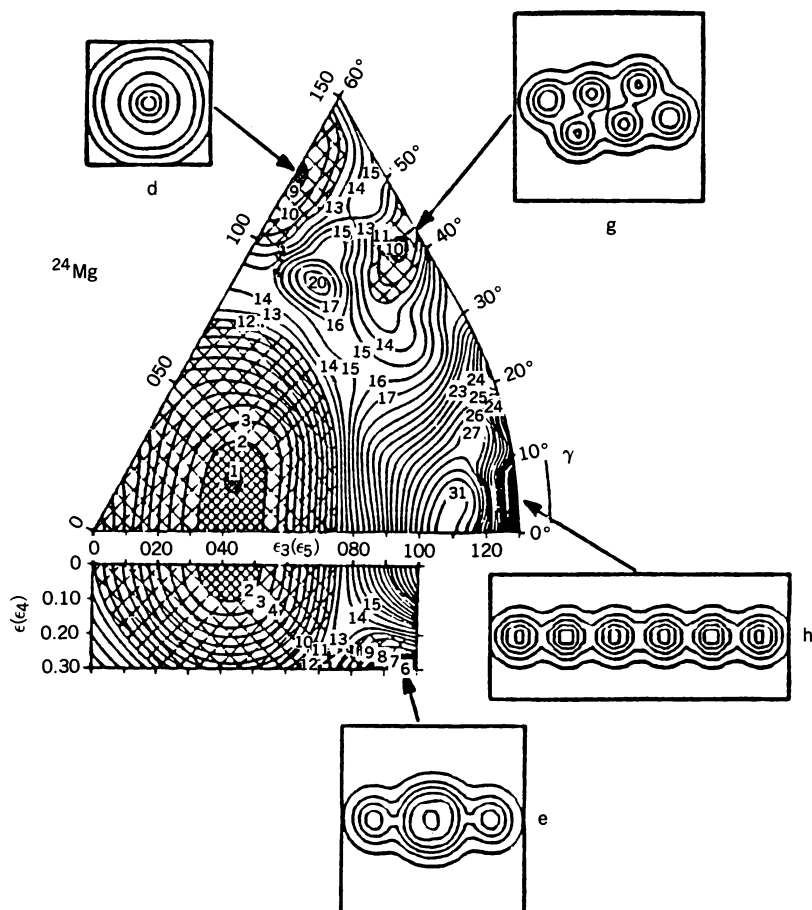


FIG. 5.19. Potential energy surface for ^{24}Mg (see Fig. 5.19) together with density contours for the stable cluster configurations. [From Rae and Marsh as described by Rae (87).]

while Cosman and Ledoux et al. would have spins of 14, 16, and 18, joining in with the lower-energy band.

In any event it is evident that deformation must be taken explicitly into account before the $^{12}\text{C} + ^{12}\text{C}$ resonances will be understood. However, at the present time a calculation of the reaction cross sections for the excitation of the resonances taking deformation into account has not been made.

The various theoretical approaches to the problem of heavy-ion resonances, particularly in the $^{12}\text{C} + ^{12}\text{C}$ and $^{12}\text{C} + ^{16}\text{O}$ cases, fit the rubric described earlier. The intermediate states that couple to the incident channel is taken to be $^{12}\text{C}(\text{g.s.}) + ^{12}\text{C}(2^+)$ by Imanishi (68,69). Konda, Abe, and Matsuse (79) include the excitation of both ^{12}C 's to the 2^+ state. Similar studies have been

made by Schied, Greiner, and Lemmer (70) and their colleagues [Greiner and Scheid (71); Fink et al. (72); Park et al. (74)]. The α -particle model of Michaud and Vogt (69, 72) can be considered as equivalent to involving intermediate states, in which the ^{12}C nuclei are excited to the 7.67-MeV 0^+ level. The calculations made are of the coupled-channel variety. A simplified version has been presented by Abe (78). However, these calculations do not take into account the deformation effects alluded to above.

Other models have been proposed by Cindro (78a), Cindro and Greiner (83), and Iachello (81). Cindro assumes that the resonance energies are given by the spectrum of the rotational and vibrational excitations of a quadrupole. Iachello assumes that the spectrum is that of a three-dimensional vibrator. His four-parameter expression for the resonances fits the observed spectrum quite clearly [Erb and Bromley, (81)], but an underlying microscopic justification is still lacking. The prolate spheroidal configuration (e) of the cluster model according to Rae and Marsh (85), would provide such a justification. Additional supporting evidence is provided by time-dependent Hartree–Fock (TDHF) calculations [Strayer, Cusson, et al. (84); Umar, Strayer, et al. (85); Umar and Strayer (86)]. See also Satpathy et al. (86) and critical remarks by Kato and Abe (87).

6. DIFFUSION THEORY

The remaining sections of this chapter are devoted to theory, with emphasis on the deep inelastic process. It is not possible to review here all of the many theoretical models that have been proposed for the description of this process. In this regard not even the Bromley volumes are complete. The semiclassical method is the subject of a book by Broglia and Winther (1981). The master equation, which has been used, for example, by Agassi, Ko, and Wiedenmüller (77, 79), is reviewed by Dietrich (85). The hydrodynamic model, advanced by W. Greiner and his colleagues, is discussed by Maruhn (85) in the same set of lectures. A transport theory that takes into account the coupling between the collective and intrinsic degrees of freedom because of two-body collisions has been developed by Nörenberg (85) [see also Ayik and Nörenberg (82) and Cassing and Nörenberg (83)]. He refers to this description as “dissipative adiabatic dynamics.” Hofmann and Siemens (76, 77) have investigated a linear response theory. The internuclear cascade has been exploited by Fraenkel and his colleagues [Chen et al. (68); Yariv and Fraenkel (79, 81)] and by Cugnon (82). This procedure is briefly discussed in Chapter IX. There are many others, other names to be associated with the above as well as other approaches. In this chapter we discuss the application of the classical transport equation of Uehling and Uhlenbeck, by Aichelin and Bertsch [(85)], Aichelin [(86)] as well as the time-dependent Hartree–Fock (TDHF) methods [Negele (82)], but not the adiabatic time-dependent Hartree–Fock method of Villars (77) and Moya de Guerra and Villars (77). This choice is idiosyncratic, based in part on a prejudice

for theories that do not assume thermal equilibrium, based in part on the availability of examples of quantitative applications.

All of these theories require extensive numerical calculations, making it difficult to establish an intuitional understanding of the dynamics for a wide set of parameters. For that reason we first establish some qualitative features making use of the theory of multistep direct reactions described in Chapter VII, which is appropriate for the study of deep inelastic processes. Note that the application of that theory uses the cross section for the single-step process, which is obtained from the understanding of the quasi-elastic cross sections. The double differential cross section for the statistical multistep direct process is given by (VII.5.29) and repeated below:

$$\left[\frac{d^2\sigma(\mathbf{k}_f, \mathbf{k}_i)}{d\Omega_f dU_f} \right]_{msd} = \sum_{\substack{\alpha, m \\ m=\alpha \pm 1}} \int \frac{d\mathbf{k}_1}{(2\pi)^3} \dots \int \frac{d\mathbf{k}_\alpha}{(2\pi)^3} \left[\frac{d^2w_{m,\alpha}(\mathbf{k}_f, \mathbf{k}_\alpha)}{d\Omega_f dU_f} \right] \left[\frac{d^2w_{\alpha,\alpha-1}(\mathbf{k}_\alpha, \mathbf{k}_{\alpha-1})}{d\Omega_\alpha dU_\alpha} \right] \dots \left[\frac{dw_{2,1}(\mathbf{k}_2, \mathbf{k}_1)}{d\Omega_2 dU_2} \right] \left[\frac{d^2\sigma_{1i}(\mathbf{k}_1, \mathbf{k}_i)}{d\Omega_1 dU_1} \right] \quad (6.1)$$

The cross section for a single-step process is to added. The sum is over α which indicates the number of steps that is followed by transition to the final states designated by $\alpha \pm 1$ and \mathbf{k}_f . The momenta $\hbar\mathbf{k}_\alpha$ are the relative momenta of the two interacting nuclei, while the subscript α includes the internal quantum numbers and energies of the states of the two nuclei. Note that the deep inelastic process is a two-body reaction, so that \mathbf{k}_f refers to the relative momentum of the two final nuclei. U_f is then the total excitation energy given by

$$U_f = E - \frac{\hbar^2}{2\mu} k_f^2 \quad (6.2)$$

where μ is the reduced mass. It is necessary to include the independent variables describing the exchange of charge and mass. Following Greiner these are taken to be

$$\eta^{(A)} \equiv \frac{A_t - A_p}{A_t + A_p} \quad \eta^{(Z)} \equiv \frac{Z_t - Z_p}{Z_t + Z_p} \quad (6.3)$$

where the subscripts t and p refer to the target and projectile, respectively. The one-step transition probabilities are dependent on the variables $\eta_\alpha^{(A)}$ and $\eta_\alpha^{(Z)}$ and $\eta_{\alpha-2}^{(A)}$ and $\eta_{\alpha-1}^{(Z)}$ where the subscript α denotes the stage. The differential transition probability is given by (VII.5.30)

$$\frac{d^2w_{\alpha,\alpha-1}(\mathbf{k}_\alpha, \eta_\alpha; \mathbf{k}_{\alpha-1}, \eta_{\alpha-1})}{dU_\alpha d\Omega_\alpha} = 2\pi^2 \rho(\mathbf{k}_\alpha) \rho(U_\alpha) |\bar{v}(\mathbf{k}_\alpha, \eta_\alpha; \mathbf{k}_{\alpha-1}, \eta_{\alpha-1})|^2$$

where the dependence on $\eta_\alpha^{(A)}$ and $\eta_\alpha^{(Z)}$ is indicated by η_α . Finally, changes in

deformation of each of the nuclei in the transition from stage to stage may occur so that deformation parameters should also be included as independent variables in (6.4).

Equation (6.1) provides a framework for the calculation of the cross section. The physics has yet to be inserted, namely the nature of each of the intermediate stages. There are many possibilities for a heavy-ion reaction and a method for a rapid exploration has not been developed; presumably, some simulation using a Monte Carlo evaluation could be used. One therefore turns to an approximate method that will yield an expression whose form can be compared with experiment, yielding some overall information on the intermediate stages involved.

For reasons of clarity we shall suppress, for the time being, the dependence on $\eta^{(A)}$ and $\eta^{(Z)}$. Define the transfer function $Y_\alpha(\mathbf{k}_\alpha)$ as follows:

$$Y_\alpha(\mathbf{k}_\alpha) \equiv \int \frac{d\mathbf{k}_1}{(2\pi)^3} \dots \int \frac{d\mathbf{k}_{\alpha-1}}{(2\pi)^3} \frac{d^2 w_{\alpha,\alpha-1}}{d\Omega_\alpha dU_\alpha} \dots \frac{d^2 w_{2,1}}{d\Omega_2 dU_2} \frac{d^2 w_{1i}}{d\Omega_1 dU_1} \quad (6.4)$$

The cross section is then given by

$$\begin{aligned} \left[\frac{d^2 \sigma(\mathbf{k}_f, \mathbf{k}_i)}{d\Omega_f dU_f} \right]_{\text{msd}} &= \frac{2\pi\mu}{\hbar^2 k_{i,m,v}} \int \frac{d\mathbf{k}_v}{(2\pi)^3} \frac{d^2 w_{m,v}}{dU_f d\Omega_f} Y_v(\mathbf{k}_v) \\ &= \sum_v \int \frac{d\mathbf{k}_v}{(2\pi)^3} \left[\frac{d^2 \sigma(\mathbf{k}_{v+1}, \mathbf{k}_v)}{d\Omega_f dU_f} \Big|_{\mathbf{k}_{v+1} \rightarrow \mathbf{k}_f} + \frac{d^2 \sigma(\mathbf{k}_{v-1}, \mathbf{k}_v)}{d\Omega_f dU_f} \Big|_{\mathbf{k}_{v-1} \rightarrow \mathbf{k}_f} \right] \quad (6.4') \end{aligned}$$

The transfer function Y_v satisfies the equation

$$Y_v(\mathbf{k}_v) = \int \frac{d\mathbf{k}_{v-1}}{(2\pi)^3} \frac{d^2 w_{v,v-1}(\mathbf{k}_v, \mathbf{k}_{v-1})}{d\Omega_v dU_v} Y_{v-1}(\mathbf{k}_{v-1}). \quad (6.5)$$

The assumption is now made that the change in momentum in the transition from stage $v-1$ to stage v is small. One may therefore expand $Y_{v-1}(\mathbf{k}_{v-1})$ in terms of $Y_{v-1}(\mathbf{k}_v)$ as follows:

$$Y_{v-1}(\mathbf{k}_{v-1}) = Y_{v-1}(\mathbf{k}_v) + (\mathbf{k}_{v-1} - \mathbf{k}_v) \cdot \nabla Y_{v-1} + \frac{1}{2} [(\mathbf{k}_{v-1} - \mathbf{k}_v) \cdot \nabla]^2 Y_{v-1} \dots$$

Inserting this equation in (6.5) yields

$$Y_v(\mathbf{k}_v) = W_v^{(0)}(\mathbf{k}_v) Y_{v-1}(\mathbf{k}_v) + \mathbf{W}_v^{(1)}(\mathbf{k}_v) \cdot \nabla Y_{v-1}(\mathbf{k}_v) + \frac{1}{2} \sum_{a,b} W_{ab} \nabla_a \nabla_b Y_{v-1}(\mathbf{k}_v) \quad (6.6)$$

where

$$W_v^{(0)} = \int \frac{d\mathbf{k}_{v-1}}{(2\pi)^3} \frac{d^2 w_{v,v-1}(\mathbf{k}_v, \mathbf{k}_{v-1})}{d\Omega_v dU_v} \quad (6.7a)$$

$$\mathbf{W}_v^{(1)} = \int \frac{d\mathbf{k}_{v-1}}{(2\pi)^3} (\mathbf{k}_{v-1} - \mathbf{k}_v) \frac{d^2 w_{v,v-1}(\mathbf{k}_v, \mathbf{k}_{v-1})}{d\Omega_v dU_v} \quad (6.7b)$$

and

$$W_{ab} = \int \frac{d\mathbf{k}_{v-1}}{(2\pi)^3} (\mathbf{k}_{v-1} - \mathbf{k}_v)_a (\mathbf{k}_{v-1} - \mathbf{k}_v)_b \frac{d^2 w_{v,v-1}(\mathbf{k}_v, \mathbf{k}_{v-1})}{d\Omega_v dU_v} \quad (6.7c)$$

The subscripts a and b refer to Cartesian components. We simplify (6.6) by introducing the quantity

$$f_v \equiv \prod_1^v W_\alpha^0(\mathbf{k}_\alpha) \quad W_v^0 = \frac{f_v}{f_{v-1}} \quad v \geq 1, \quad f_0 = 1 \quad (6.8)$$

and the new dependent variable Z_v

$$Z_v \equiv \frac{Y_v}{f_v} \quad (6.9)$$

Equation (6.6) becomes

$$W_v^0(Z_v - Z_{v-1}) = \frac{1}{f_{v-1}} [\mathbf{W}_v^{(1)} \cdot \nabla(f_{v-1} Z_{v-1})] + \frac{1}{2f_{v-1}} \sum_{ab} W_{ab} \nabla_a \nabla_b (f_{v-1} Z_{v-1}) \quad (6.10)$$

We replace the discrete variable v by continuous variables τ such that $\Delta\tau = 1/W_v^0$. Then the left-hand side of (6.10) is given by $\Delta Z/\Delta\tau$, which is approximated by $\partial Z/\partial\tau$. Note that

$$\tau = \sum_{\alpha=1}^v \frac{1}{W_\alpha^0} \quad (6.11)$$

It is clearly a variable that measures the number of stages and can be conveniently thought of as the interaction time.[†] It is a function of v and \mathbf{k}_v among other variables. One eliminates v on the right side of (6.10) by solving (6.11) for v in terms of τ and \mathbf{k} . The equation for Z becomes

$$\frac{\partial Z}{\partial\tau} = \frac{1}{f(\tau, \mathbf{k})} [\mathbf{w}_1 \cdot \nabla(fZ) + \frac{1}{2} \sum w_{ab} \nabla_a \nabla_b (fZ)] \quad (6.12)$$

[†]If W_α^0 is independent of α , $\tau = v/W_0$. If as is more realistic, $W_\alpha^0 = e^{-\alpha\gamma} W$, $W\tau = (e^{\gamma(v+1)} - 1)/e^\gamma - 1$. Solving for v , $v = 1/\gamma \ln [(1 - W\tau)e^{-\gamma} + W\tau]$, which approaches $v = 1/\gamma \ln W\tau$ for large γ and $W\tau - 1$ for small γ .

where

$$\mathbf{w}_1(\tau, \mathbf{k}) = W_v^{(1)}(\mathbf{k}_v) \quad \text{etc.} \quad (6.13)$$

We have thus obtained a momentum Fokker–Planck diffusion equation for Z in a very general form. To make further progress, assume that

$$w_{ab} = \delta_{ab} w$$

and that f depends only on τ . This is accomplished by replacing \mathbf{k} in f by \mathbf{k}_τ . See (6.15). Then (6.12) becomes

$$\frac{\partial Z}{\partial \tau} = \mathbf{w}_1 \cdot \nabla Z + \frac{1}{2} w \nabla^2 Z. \quad (6.14)$$

Further simplification is obtained by assuming that w is independent of k . Equation (6.14) can be solved in a closed form when \mathbf{w}_1 is a constant vector or proportional to a unit vector tangent to the unit sphere in \mathbf{k} space. We shall follow an approximate procedure that reproduces correctly the solutions for the above assumptions for \mathbf{w}_1 , but is capable of dealing with a more general form for this vector.

We assume that

$$Z(\mathbf{k}, \tau) = \left(\frac{1}{2\pi w \tau} \right)^{3/2} e^{-(1/2\tau w)(\mathbf{k} - \mathbf{k}_\tau)^2} \quad (6.15)$$

where \mathbf{k}_τ is a function of τ reducing to \mathbf{k}_0 at $\tau = 0$. Note that $Z(k, \tau) \rightarrow \delta(\mathbf{k} - \mathbf{k}_0)$ as $\tau \rightarrow 0$. Here \mathbf{k}_0 is taken to be \mathbf{k}_i the incident \mathbf{k} for the collision of light nuclei. For heavy nuclei when the collision is Coulomb dominated, \mathbf{k}_0 is taken to be equal in magnitude to k_i but with the direction given by the grazing Coulomb orbit at the point of grazing. To determine \mathbf{k}_τ we calculate

$$\langle \mathbf{k} \rangle \equiv \int \mathbf{k} Z(\mathbf{k}, \tau) d\mathbf{k} \quad (6.16)$$

Equation (6.14) will then yield a differential equation for \mathbf{k}_τ .

We assume the following form for \mathbf{w}_1 linear in \mathbf{k}

$$\mathbf{w}_1 = \mathbf{w}_C + w_R(\hat{\mathbf{k}}_0 \times \mathbf{k}) + \frac{1}{4} w_D \mathbf{k} \quad (6.17)$$

where \mathbf{w}_C is a constant vector independent of \mathbf{k} . Multiplying (6.14) by \mathbf{k} and integrating yields

$$\frac{d\mathbf{k}_\tau}{d\tau} = -[\mathbf{w}_C + (\hat{\mathbf{k}}_0 \times \mathbf{k}_\tau)w_R + w_D \mathbf{k}_\tau] \quad (6.18)$$

These equations can be integrated subject to the condition $\mathbf{k}_\tau(0) = \mathbf{k}_0$. Let the direction along \mathbf{k}_0 to be designated by the 0 subscript. One obtains

$$(\mathbf{k}_\tau)_0 = \mathbf{k}_0 e^{-w_D \tau} - \frac{(\mathbf{w}_C)_0}{w_D} (1 - e^{-w_D \tau}) \quad (6.19)$$

and

$$\begin{aligned} (\mathbf{k}_\tau)_\perp = \frac{1}{w_D^2 + w_R^2} \{ & \hat{\mathbf{k}}_0 \times (\hat{\mathbf{k}}_0 \times \mathbf{w}_C) [w_D(1 - \cos \omega_R \tau e^{-w_D \tau}) + \omega_R \sin \omega_R \tau e^{-w_D \tau}] \\ & + (\hat{\mathbf{k}}_0 \times \mathbf{w}_C) [w_R(1 - \cos \omega_R \tau e^{-w_D \tau}) - w_D \sin \omega_R \tau e^{-w_D \tau}] \} \end{aligned} \quad (6.19a)$$

Here $(\mathbf{k}_\tau)_\perp$ is the component of \mathbf{k}_τ in the plane perpendicular to \mathbf{k}_0 . The sinusoidal terms describe a damped rotation in the $(k_\tau)_\perp$ plane with a radius given by $w_{C\perp}/\sqrt{w_D^2 + w_R^2}$. For large τ

$$(k_\tau)_\perp \xrightarrow{\tau \rightarrow \infty} \frac{1}{w_D^2 + w_R^2} [(\hat{\mathbf{k}}_0 \times (\hat{\mathbf{k}}_0 \times \mathbf{w}_C))w_D + (\hat{\mathbf{k}}_0 \times \mathbf{w}_C)w_R] \quad (6.20)$$

The component of \mathbf{k}_τ in the \mathbf{k}_0 direction decreases because of the damping of the \mathbf{k}_0 term. It is also affected by the 0 component of \mathbf{w}_C , subtracting or adding according to whether w_{C0} is positive or negative; w_D is a magnitude and therefore positive. Asymptotically

$$(k_\tau)_0 \rightarrow -\frac{(\mathbf{w}_C)_0}{w_D} \quad (6.21)$$

The value of k_τ^2 , which is proportional to the average kinetic energy is given by the sum $(k_\tau)_\perp^2 + (k_\tau)_0^2$, where

$$\begin{aligned} (k_\tau)_\perp^2 &= \frac{w_{C\perp}^2}{w_D^2 + w_R^2} (1 - 2 \cos \omega_R \tau e^{-w_D \tau} + e^{-2w_D \tau}) \xrightarrow{\tau \rightarrow \infty} \frac{w_{C\perp}^2}{w_D^2 + w_R^2} \\ (k_\tau)_0^2 &= \left[\mathbf{k}_0 e^{-w_D \tau} - \frac{(\mathbf{w}_C)_0}{w_D} (1 - e^{-w_D \tau}) \right]^2 \xrightarrow{\tau \rightarrow \infty} \frac{w_{C0}^2}{w_D^2} \end{aligned} \quad (6.22)$$

Returning to (6.15) for $Z(\mathbf{k}, \tau)$ we see that as τ increases, Z broadens while its center moves from the direction \mathbf{k}_0 to \mathbf{k}_τ given by (6.19). For the motion of \mathbf{k}_τ one can “predict” the solid center lines in Fig. 3.6 (if \mathbf{w}_C , w_R and w_D are known or fitted, if not) where E would be obtained from (6.22) and the deviation from the original \mathbf{k}_0 direction from the equation

$$\tan(\vartheta - \theta_0) = \frac{(k_\tau)_\perp}{(k_\tau)_0} \quad (6.23)$$

where θ_0 is the direction of \mathbf{k}_0 . Note that \mathbf{k}_t and the energy approach constant asymptotic values, as indicated by Fig. 3.6. Subsequently the energy loss is dominated by excitation of low-lying modes which are described on page 596 as a process that involves long interaction times and a smaller rate of energy loss. This would require a different set of values of w_C , w_R , and w_D as obtained for example from (6.7).

The function $Y(\mathbf{k}, \tau)$ is now obtained from (6.9). Making the reasonable approximation that W_α^0 is independent of α (we have already assumed that it is independent of \mathbf{k}), f_v is given by $(W_0)^v$. Converting from v to τ dependence, we parametrize f_v by

$$f_v = f_0 e^{-\gamma\tau} \quad (6.24)$$

since τ is proportional to v . With $Y(\mathbf{k}, \tau)$ known, the cross section can be obtained by summing over v according to (6.4). The sum over v is replaced by an integration over τ :

$$\sum_v \rightarrow W_0 \int d\tau$$

Hence

$$\begin{aligned} \left[\frac{d^2\sigma}{d\Omega_f dU_f} \right]_{\text{msd}} &= \frac{4\pi\mu}{\hbar^2 k_i} W_0 \int Y d\tau = W_0 \int (s_{v+1} + s_{v-1}) Y_1(\mathbf{k}_f, \tau) d\tau \\ &\simeq 2W_0 \bar{s} \int Y(\mathbf{k}_f, \tau) d\tau \end{aligned} \quad (6.25a)$$

where we have assumed that

$$\left. \frac{k_v}{k_i} \frac{d^2\sigma(\mathbf{k}_{v+1}, \mathbf{k}_v)}{d\Omega_f dU_f} \right|_{\mathbf{k}_{v+1}=\mathbf{k}_f} \simeq (2\pi)^3 \delta(\mathbf{k}_f - \mathbf{k}_v) s_{v+1} \quad (6.25b)$$

To obtain these equations we have assumed that the angular distribution is sharply pointed in the direction of \mathbf{k}_v and that the energy is not substantially changed. Finally, it is assumed that s_v varies slowly with v and can be replaced by an average \bar{s} .

We now consider the integral.

$$I = \int Y d\tau = f_0 \int_0^\infty \frac{d\tau}{(2\pi\omega\tau)^{3/2}} e^{-\gamma\tau - (1/2\tau w)(\mathbf{k} - \mathbf{k}_t)^2} \quad (6.26)$$

As an example of the results which follow from this analysis we taken $w_R = 0$. Then

$$\mathbf{k}_t = \mathbf{k}_0 - \left(\frac{w_C}{w_D} + \mathbf{k}_0 \right) (1 - e^{-w_D\tau}) \quad w_R = 0 \quad (6.27)$$

Furthermore, assume that $w_D\tau < 1$. The conditions under which this inequality will hold will be determined in what follows. Then

$$\begin{aligned}\mathbf{k}_\tau &\simeq \mathbf{k}_0 + \mathbf{k}_1\tau \\ \mathbf{k}_1 &= -(\mathbf{w}_C + \mathbf{k}_0 w_D)\end{aligned}\tag{6.28}$$

With this approximation, the integral can be done exactly. However, to identify the important value of τ and so be able to assess the range of validity of the result, we shall use the method of steepest descents. Toward that end one places the derivative of the exponent in (6.26) equal to zero. Solving for τ , one finds that

$$\tau^2 = \frac{(\mathbf{k}_0 - \mathbf{k})^2}{k_1^2 + 2\gamma w}\tag{6.29}$$

We thus see that $w_D\tau$ will be small if $|\mathbf{k}_0 - \mathbf{k}|$ is sufficiently small. For small w_C the condition is

$$w_D\tau \sim \frac{|\mathbf{k}_0 - \mathbf{k}|}{k_0} \ll 1\tag{6.30}$$

This condition restricts the region of applicability to the forward quadrant but does not strongly restrict the difference between k_0 and k .

The steepest descent result for the integral, (6.26) yields

$$I(\mathbf{k}) = \frac{f_0}{\sqrt{2(2\pi w)}} \frac{1}{|\mathbf{k}_0 - \mathbf{k}|} \exp - \frac{1}{w} [K_1 |\mathbf{k}_0 - \mathbf{k}| + \mathbf{k}_1 \cdot (\mathbf{k}_0 - \mathbf{k})]\tag{6.31}$$

where $K_1^2 \equiv k_1^2 + 2\gamma w$. The cross section is from (6.25)

$$\left[\frac{d^2\sigma}{d\Omega_f dU_f} \right]_{\text{msd}} = 2W_0 \bar{S}I(\mathbf{k}_f).\tag{6.32}$$

The peak of the angular distribution will occur at the minimum of the bracketed expression in (6.31). Let ϑ be the angle between \mathbf{k}_0 and \mathbf{k} and let the minimum occur at $\bar{\vartheta}$. Assuming $\bar{\vartheta}$ to be small, one finds that

$$\sin \bar{\vartheta} = \frac{k_1 |k_0 - k| \sin \psi}{k_0 k_1 + k_1 |k_0 - k| \cos \psi}\tag{6.33}$$

where ψ is the angle between \mathbf{k}_0 and the component of \mathbf{k}_1 in the $(\mathbf{k}, \mathbf{k}_0)$ plane. For ϑ near $\bar{\vartheta}$ the angular distribution is Gaussian.

The energy spectrum at each angle can also be determined from (6.31). Generally, one finds that as the angle increases the rate of exponential decrease

of the cross section increases. [One can always obtain an exponential decay with E for any function $e^{-f(E)}$ for small $E_0 - E$ as long as $f'(E_0)$ is positive as it is in this case.] This is identical to the exponential decrease obtained in the statistical theory [see (1.4.5) to (1.4.7)]. One thus finds the statement in the experimental literature that the “temperature” decreases with increasing angle. However, as we see from the calculation one cannot conclude that the system has approached a thermal equilibrium. For that conclusion to be correct the angular distribution must be spherical corresponding to an angle-independent temperature.

There are other variables, besides the momentum \mathbf{k} , such as mass and charge asymmetry [see (6.3)], and deformation parameters, which can change with each stage of the multistep process. The discussion given above presumes a known path in reaction space or an averaging over the various possibilities. However, this is not adequate when, for example, we wish to calculate the charge and mass distributions of the final fragment. In the analysis to be presented below, we develop a Fokker–Planck equation which explicitly contains the effects of the mass asymmetry $\eta^{(A)}$. Analogous equations can readily be obtained for variations in charge asymmetry or other parameters.

One must first make explicit the dependence of $d^2w/d\Omega dU$ on η as follows:

$$\frac{d^2w(\mathbf{k}_\alpha, \mathbf{k}_{\alpha-1})}{dU_\alpha d\Omega_\alpha} d\mathbf{k}_{\alpha-1} \rightarrow \frac{d^3w(\mathbf{k}_\alpha, \eta_\alpha^{(A)}, \mathbf{k}_{\alpha-1}, \eta_{\alpha-1}^{(A)})}{dU_\alpha d\Omega_\alpha d\eta_\alpha^{(A)}} d\mathbf{k}_{\alpha-1} d\eta_{\alpha-1}^{(A)} \quad (6.34)$$

giving the probability that the system will undergo a transition from a momentum between $\mathbf{k}_{\alpha-1}$ and $\mathbf{k}_{\alpha-1} + d\mathbf{k}_{\alpha-1}$ and a mass parameter between $\eta_{\alpha-1}^{(A)}$ and $\eta_{\alpha-1}^{(A)} + d\eta_{\alpha-1}^{(A)}$ to \mathbf{k}_α and $\eta_\alpha^{(A)}$, respectively. Equation (6.1) is replaced by

$$\begin{aligned} \frac{d^3\sigma(\mathbf{k}_f, \eta_f^{(A)}, \mathbf{k}_i, \eta_i^{(A)})}{d\Omega_f dU_f d\eta_f^{(A)}} = & \sum_{\alpha, m} \int \frac{d\mathbf{k}_1}{(2\pi)^3} d\eta_1 \dots \int \frac{d\mathbf{k}_\alpha}{(2\pi)^3} d\eta_\alpha^{(A)} \left[\frac{d^3w_{m,\alpha}(\mathbf{k}_f, \eta_f^{(A)}, \mathbf{k}_\alpha, \eta_\alpha^{(A)})}{d\Omega_f dU_f d\eta_f^{(A)}} \right] \\ & \times \left[\frac{d^3w_{\alpha,\alpha-1}(\mathbf{k}_\alpha, \eta_\alpha^{(A)}, \mathbf{k}_{\alpha-1}, \eta_{\alpha-1}^{(A)})}{d\Omega_\alpha dU_\alpha d\eta_\alpha^{(A)}} \right] \dots \left[\frac{d^3w_{2,1}(\mathbf{k}_2, \eta_2^{(A)}, \mathbf{k}_1, \eta_1^{(A)})}{d\Omega_2 dU_2 d\eta_1^{(A)}} \right] \\ & \times \left[\frac{d^2\sigma_{1i}(\mathbf{k}_1, \eta_1^{(A)}, \mathbf{k}_i, \eta_i^{(A)})}{d\Omega_1 dU_1 d\eta_1^{(A)}} \right] \end{aligned} \quad (6.35)$$

One now introduces the function $Y_\alpha(\mathbf{k}_\alpha, \eta_\alpha^{(A)})$ [see (6.4)]:

$$\begin{aligned} Y_\alpha(\mathbf{k}_\alpha, \eta_\alpha^{(A)}) = & \int \frac{d\mathbf{k}_1}{(2\pi)^3} d\eta_1 \dots \int \frac{d\mathbf{k}_{\alpha-1}}{(2\pi)^3} d\eta_{\alpha-1} \frac{d^3w_{\alpha,\alpha-1}}{d\Omega_\alpha dU_\alpha d\eta_\alpha^{(A)}} \\ & \dots \frac{d^3w_{2,1}}{d\Omega_2 dU_2 d\eta_2^{(A)}} \frac{d^3w_{1i}}{d\Omega_1 dU_1 d\eta_1^{(A)}} \end{aligned} \quad (6.36)$$

The differential cross section in terms of Y_α is

$$\frac{d^3\sigma(\mathbf{k}_f, \eta_f^{(A)}, \mathbf{k}_i, \eta_i^{(A)})}{d\Omega_f dU_f d\eta_f^{(A)}} = \frac{2\pi\mu}{\hbar^2 k_{i,m,v}} \sum \int \frac{d\mathbf{k}_v}{(2\pi)^3} d\eta_v^{(A)} \frac{d^3 w_{m,v}}{dU_f d\Omega_f d\eta_f^{(A)}} \quad (6.37)$$

The function Y_v satisfies the equation

$$Y_v(\mathbf{k}_v, \eta_v^{(A)}) = \int \frac{d\mathbf{k}_{v-1}}{(2\pi)^3} d\eta_{v-1} \frac{d^3 w_{v,v-1}(\mathbf{k}_v, \eta_v^{(A)}, \mathbf{k}_{v-1}, \eta_{v-1}^{(A)})}{dU_v d\Omega_v d\eta_v^{(A)}} Y_{v-1}(\mathbf{k}_{v-1}, \eta_{v-1}^{(A)}) \quad (6.38)$$

The assumption is made that the change in momentum and $\eta^{(A)}$ in the transition from stage $v-1$ to stage v is small. One may therefore expand $Y_{v-1}(\mathbf{k}_{v-1}, \eta_{v-1}^{(A)})$ in terms of $Y_{v-1}(\mathbf{k}_v, \eta_v^{(A)})$ as follows:

$$\begin{aligned} Y_v(\mathbf{k}_{v-1}, \eta_{v-1}^{(A)}) &= Y_{v-1}(\mathbf{k}_v, \eta_v^{(A)}) + (\mathbf{k}_{v-1} - \mathbf{k}_v) \cdot \nabla Y_{v-1} + (\eta_{v-1}^{(A)} - \eta_v^{(A)}) \frac{\partial Y_{v-1}}{\partial \eta_v^{(A)}} \\ &\quad + \frac{1}{2} \left[(\mathbf{k}_{v-1} - \mathbf{k}_v) \cdot \nabla + (\eta_{v-1}^{(A)} - \eta_v^{(A)}) \frac{\partial}{\partial \eta_v^{(A)}} \right]^2 Y_{v-1} \end{aligned}$$

Inserting this equation into (6.38) yields

$$\begin{aligned} Y_v(\mathbf{k}_v, \eta_v^{(A)}) &= W_v^{(00)} Y_{v-1}(\mathbf{k}_{v-1}, \eta_{v-1}^{(A)}) \\ &\quad + \left[\mathbf{W}_v^{(10)} \cdot \nabla Y_{v-1}(\mathbf{k}_v, \eta_v^{(A)}) + W_v^{(01)} \frac{\partial Y_{v-1}(\mathbf{k}_v, \eta_v^{(A)})}{\partial \eta_v^{(A)}} \right] \\ &\quad + \frac{1}{2} \sum_{a,b} W_{ab}^{(20)} \nabla_a \nabla_b Y_{v-1}(\mathbf{k}_v, \eta_v^{(A)}) \\ &\quad + \mathbf{W}_v^{(11)} \cdot \nabla \left(\frac{\partial Y_{v-1}}{\partial \eta_v^{(A)}} \right) + \frac{1}{2} W_v^{(02)} \frac{\partial^2 Y_{v-1}}{\partial \eta_v^{(A)2}} \end{aligned} \quad (6.39)$$

where the coefficients W are generalizations of (6.7). Reducing this equation follows the procedure described after (6.7). The function Z_v is introduced as before by

$$Z = \frac{Y_v}{f_v} \quad f_v = \prod_1^v W_\alpha^{(00)}(\mathbf{k}_\alpha, \eta_\alpha^{(A)})$$

Finally, the interaction time variable τ by

$$\tau = \sum_1^v \frac{1}{W_\alpha^{(00)}}$$

One finally obtains

$$\begin{aligned} \frac{\partial Z}{\partial \tau} = \frac{1}{f(\tau, \mathbf{k}, \eta^{(A)})} & \left[\mathbf{w}^{(10)} \cdot \nabla (fZ) + w^{(01)} \frac{\partial (fZ)}{\partial \eta^{(A)}} + \frac{1}{2} \sum_{ab} w_{ab}^{(20)} \nabla_a \nabla_b (fZ) \right. \\ & \left. + \mathbf{w}^{(11)} \cdot \nabla \frac{\partial (fZ)}{\partial \eta^{(A)}} + \frac{1}{2} w^{(02)} \frac{\partial^2 (fZ)}{\partial \eta^2} \right] \end{aligned} \quad (6.40)$$

We again make the assumption that f is independent of \mathbf{k} and η^A so that (6.40) becomes

$$\begin{aligned} \frac{\partial Z}{\partial \tau} = \mathbf{w}^{(10)} \cdot \nabla Z + w^{(01)} \frac{\partial Z}{\partial \eta^{(A)}} + \frac{1}{2} \sum_{ab} w_{ab}^{(20)} \nabla_a \nabla_b Z \\ + \mathbf{w}^{(11)} \cdot \nabla \frac{\partial Z}{\partial \eta^{(A)}} + \frac{1}{2} w^{(02)} \frac{\partial^2 Z}{\partial \eta^{(A)^2}} \end{aligned} \quad (6.41)$$

One can now follow the procedure described after (6.13). We shall leave the discussion to the reader, the coupling between the \mathbf{k} and $\eta^{(A)}$ dependence being the new feature of interest.

We shall content ourselves with integrating both sides of (6.41) with respect to \mathbf{k} . Assuming that all the coefficients are independent of \mathbf{k} [compare with (6.17)], let

$$\zeta(\eta^{(A)}) \equiv \int Z d\mathbf{k} \quad (6.42)$$

Then

$$\frac{\partial \zeta}{\partial \tau} = w^{(01)} \frac{\partial \zeta}{\partial \eta^{(A)}} + \frac{1}{2} w^{(02)} \frac{\partial^2 \zeta}{\partial^2 \eta^{(A)}} \quad (6.43)$$

This equation can be integrated. Let

$$\eta' = \eta^{(A)} + w^{(01)} \tau \quad \tau' = \tau$$

Then

$$\frac{\partial \zeta}{\partial \tau'} + \frac{\partial \zeta}{\partial \eta'} w^{(01)} = w^{(01)} \frac{\partial \zeta}{\partial \eta'} + \frac{1}{2} w^{(02)} \frac{\partial^2 \zeta}{\partial^2 \eta'}$$

or

$$\frac{\partial \zeta}{\partial \tau'} = \frac{1}{2} w^{(02)} \frac{\partial^2 \zeta}{\partial^2 \eta'}$$

The solution has the one-dimensional form [see (6.15)]

$$\zeta(\eta^{(A)}, \tau) = \left(\frac{1}{2\pi w^{(02)}\tau} \right)^{1/2} e^{-[1/2\tau w^{(02)}](\eta^{(A)} + w^{(01)}\tau - \eta^{(A)}(0))^2} \quad (6.44)$$

where $\eta^{(A)}(0)$ is the initial value of $\eta^{(A)}$. The mass asymmetry is in this approximation a Gaussian whose center changes linearly with τ and whose width changes like $\tau^{1/2}$.

Returning to (6.37) for the cross section, and once again utilizing (6.24) and (6.25a), one obtains

$$\int d\mathbf{k}_f \frac{d^3\sigma(\mathbf{k}_f, \eta_f^{(A)}, \mathbf{k}_i, \eta_i^{(A)})}{d\Omega_f d\Omega_f d\eta_f^{(A)}} = \frac{4\pi\mu f_0 \bar{s} W^{(00)}}{\hbar^2 k_i'} \int_0^\infty \frac{d\tau e^{-\gamma\tau - [1/2\tau w^{(02)}](\eta_f^{(A)} + w^{(01)}\tau - \eta_f^{(A)})^2}}{(2\pi w^{(02)}\tau)^{3/2}}$$

The integral can be performed, yielding

$$\begin{aligned} \int d\mathbf{k}_f \frac{d^3\sigma(\mathbf{k}_f, \eta_f, \mathbf{k}_i, \eta_i)}{d\Omega_f dU_f d\eta_f^{(A)}} &= \frac{4\sqrt{2}\pi\mu f_0}{\hbar^2 k_1} \frac{\bar{s} W^{(00)}}{|\eta - \eta_0|} \\ &\times e^{-1/w^{(02)}[\sqrt{2\gamma w^{(02)} + (w^{(01)})^2}|\eta_f^{(A)} - \eta_f^{(A)}(0)| + w^{(01)}(\eta_f^{(A)} - \eta_f^{(A)}(0))]} \end{aligned} \quad (6.45)$$

The distribution is no longer symmetric about $\eta_f^{(A)} = \eta_0^{(A)}$, falling off less rapidly for $\eta_f^{(A)} < \eta_f^{(A)}(0)$ when $w^{(01)}$ is positive, and vice versa when it is negative.

7. THE LORENTZ, BOLTZMANN, UHLENBECK, AND UEHLING (LBUU) METHOD[‡]

This method for treating heavy-ion collisions is based on a classical (nonquantum) method, describing the motion of A particles, employed in kinetic theory [Huang (87)]. The Hamiltonian determining the many-body motion is taken to be

$$H = \sum_{i=1}^A \left[\frac{\mathbf{p}_i^2}{2m} + V(r_i) \right] + \sum_{i < j} v(|\mathbf{r}_i - \mathbf{r}_j|) \quad (7.1)$$

The potential V is the mean potential and v is the residual two-body potential.

One asks for the distribution function $f(\mathbf{r}_1, \mathbf{r}_2, \dots, \mathbf{r}_A; \mathbf{p}_1, \mathbf{p}_2, \dots, \mathbf{p}_A, t)$, the number density for finding particle 1 at \mathbf{r}_1 with a momentum \mathbf{p}_1 , particle 2 at \mathbf{r}_2 with momentum \mathbf{p}_2 , and so on, at a time t . The one-particle distribution $f_1(\mathbf{r}_1; \mathbf{p}_1)$ defined as the number density at a time t for finding a particle at \mathbf{r}_1

[‡]Huang (87).

with momentum \mathbf{p}_1 is given by

$$f_1(\mathbf{r}_1; \mathbf{p}_1 t) = \int d\mathbf{r}_2 d\mathbf{p}_2 d\mathbf{r}_3 d\mathbf{p}_3 \cdots f(\mathbf{r}_1, \mathbf{r}_2, \mathbf{r}_3, \dots, \mathbf{r}_A; \mathbf{p}_1, \mathbf{p}_2, \mathbf{p}_3, \dots, \mathbf{p}_A; t) \quad (7.2)$$

The number density at a time for finding s particles at $\mathbf{r}_1, \mathbf{r}_2, \dots, \mathbf{r}_s$ with momenta $\mathbf{p}_1, \mathbf{p}_2, \dots, \mathbf{p}_s$ is

$$f_s(\mathbf{r}_1 \cdots \mathbf{r}_s; \mathbf{p}_1 \cdots \mathbf{p}_s; t) = \frac{(A-s)!}{(A-1)!} \int d\mathbf{r}_{s+1} \cdots d\mathbf{r}_A d\mathbf{p}_{s+1} \cdots d\mathbf{p}_A f(\mathbf{r}_1 \cdots \mathbf{r}_A; \mathbf{p}_1 \cdots \mathbf{p}_A; t) \quad (7.3)$$

The normalization of f is given by

$$\int d\mathbf{r}_1 \cdots d\mathbf{r}_A d\mathbf{p}_1 \cdots d\mathbf{p}_A f(\mathbf{r}_1 \cdots \mathbf{r}_A; \mathbf{p}_1 \cdots \mathbf{p}_A; t) = \int d\mathbf{r}_1 d\mathbf{p}_1 f_1(\mathbf{r}_1; \mathbf{p}_1; t) = A \quad (7.4)$$

The probability density ρ is obtained from the number density by division by A :

$$\rho(\mathbf{r}_1 \cdots \mathbf{r}_A; \mathbf{p}_1 \cdots \mathbf{p}_A; t) = \frac{1}{A} f(\mathbf{r}_1 \cdots \mathbf{r}_A; \mathbf{p}_1 \cdots \mathbf{p}_A; t) \quad (7.5)$$

The space defined by the vectors $\mathbf{r}_1 \cdots \mathbf{r}_A; \mathbf{p}_1 \cdots \mathbf{p}_A$ is referred to as *phase space*. Its dimension is $6A$. We will denote a vector with components $\mathbf{r}_1 \cdots \mathbf{p}_A$ by ζ , so that (7.4) reads

$$\int d\zeta f(\zeta, t) = A$$

Since ρ is a probability density, the average value of any function $O(\zeta)$ in phase space is given by

$$\langle O(\zeta) \rangle = \int d\zeta \rho(\zeta) O(\zeta)$$

Because the number of particles is conserved as a function of time, the density must satisfy the equation of continuity:

$$\frac{\partial \rho}{\partial t} + \text{div}(\rho \mathbf{v}_\zeta) = 0 \quad (7.6)$$

where \mathbf{v}_ζ is the velocity in phase space with components $\dot{\mathbf{r}}_1, \dot{\mathbf{r}}_2, \dots, \dot{\mathbf{p}}_A$. The divergence is taken in the $6A$ -dimensional space. Using this equation and

Hamilton's equation, *Liouville's theorem*,

$$\frac{d\rho}{dt} = 0 \quad (7.7)$$

can be obtained. The proof follows. First note that

$$\frac{d\rho}{dt} = \frac{\partial \rho}{\partial t} + \nabla \rho \cdot \mathbf{v}_\zeta$$

From (7.6) we have

$$-\frac{\partial \rho}{\partial t} = \nabla \rho \cdot \mathbf{v}_\zeta + \rho \operatorname{div} \mathbf{v}_\zeta \quad (7.8)$$

where

$$\operatorname{div} \mathbf{v}_\zeta = \sum_i [(\nabla_r)_i \cdot \dot{\mathbf{r}}_i + (\nabla_p)_i \cdot \dot{\mathbf{p}}_i]$$

But

$$\dot{\mathbf{r}}_i = (\nabla_p)_i H \quad \dot{\mathbf{p}}_i = -(\nabla_r)_i H$$

so that

$$\operatorname{div} \mathbf{v}_\zeta = 0 \quad (7.9)$$

The flow in phase space is like that of an incompressible fluid. Inserting this equation into (7.8) and the result in the equation for $d\rho/dt$ yields (7.7).

The Liouville theorem is the fundamental equation of kinetic theory. We shall return to it later. For the present we shall consider directly the equation satisfied by f_1 . Recall that $f_1(\mathbf{r}, \mathbf{p}) d\mathbf{r} d\mathbf{p}$ is the number of particles in $d\mathbf{r} d\mathbf{p}$ at \mathbf{r} and \mathbf{p} . The function f_1 changes with time because (1) as a consequence of their velocity, particles leave the volume $d\mathbf{r}$; (2) the particles are acted on by the mean field forces $(-\nabla V_i)$ changing their momenta; and (3) particles collide with each other as induced by $\Sigma(v|\mathbf{r}_i - \mathbf{r}_j|)$.

If there are no collisions, the points in a volume element $d\mathbf{p} d\mathbf{r}$ will simply move into another volume element located at $\mathbf{r} + \mathbf{v} dt$ and $\mathbf{p} - (\nabla_r V) dt$. The change in f_1 in a time dt will be written $(\partial f_1 / \partial t)_{\text{coll}}$. Therefore,

$$f_1(\mathbf{r} + \mathbf{v} dt, \mathbf{p} - (\nabla_r V) dt, t + dt) = f_1(\mathbf{r}, \mathbf{p}, t) + \left(\frac{\partial f_1}{\partial t} \right)_{\text{coll}} dt$$

or

$$\frac{\partial f_1}{\partial t} + \mathbf{v} \cdot \nabla_r f_1 - \nabla_r V \cdot \nabla_p f_1 = \left(\frac{\partial f_1}{\partial t} \right)_{\text{coll}} \quad (7.10)$$

We assume that only binary collisions are important. The effects of a collision will depend on the number of pairs in a volume element $d\mathbf{r}$ with momenta \mathbf{p}_1 and \mathbf{p}_2 in the volume $d\mathbf{p}_1 d\mathbf{p}_2$. Let this be $F(\mathbf{r}, \mathbf{p}_1, \mathbf{p}_2, t) d\mathbf{r} d\mathbf{p}_1 d\mathbf{p}_2$. The number of particles leaving $d\mathbf{r} d\mathbf{p}_1$ per unit time because of collisions is

$$d\mathbf{r} d\mathbf{p}_1 \iint F(\mathbf{r}, \mathbf{p}_1, \mathbf{p}_2, t) dw(\mathbf{p}'_1, \mathbf{p}'_2; \mathbf{p}_1, \mathbf{p}_2) d\mathbf{p}_2 d\mathbf{p}'_2 \quad (7.11)$$

Here dw is the probability per unit time that a pair of particles with momenta \mathbf{p}_1 and \mathbf{p}_2 will, upon collision, acquire momenta \mathbf{p}'_1 and \mathbf{p}'_2 . Since we are interested only in the total number of particles leaving $d\mathbf{r} d\mathbf{p}_1$, we integrate over \mathbf{p}_2 and \mathbf{p}'_2 . The value of \mathbf{p}'_1 is given by energy and momentum conservation. The value of dw is

$$dw(\mathbf{p}'_1, \mathbf{p}'_2; \mathbf{p}_1, \mathbf{p}_2) = \frac{2\pi}{\hbar} j_i \rho(E') |\mathcal{T}(\mathbf{p}_1 \rightarrow \mathbf{p}'_1, \mathbf{p}_2 \rightarrow \mathbf{p}'_2)|^2 d\Omega' \quad (7.12)$$

where j_i is the magnitude of the incident current density, $|\mathbf{v}_1 - \mathbf{v}_2|$ and \mathcal{T} is the transition matrix. Inserting (7.12) into (7.11) yields

$$d\mathbf{r} d\mathbf{p}_1 \iint F(\mathbf{r}, \mathbf{p}_1, \mathbf{p}_2, t) |\mathbf{v}_1 - \mathbf{v}_2| \frac{d\sigma}{d\Omega'} (\mathbf{p}_1 \rightarrow \mathbf{p}'_1, \mathbf{p}_2 \rightarrow \mathbf{p}'_2) d\mathbf{p}_2 d\Omega' \quad (7.13a)$$

Similarly, the number entering volume element $d\mathbf{r} d\mathbf{p}_1$ because of collisions is

$$d\mathbf{r} d\mathbf{p}_1 \iint F(\mathbf{r}, \mathbf{p}'_1, \mathbf{p}'_2, t) |\mathbf{v}'_1 - \mathbf{v}'_2| \frac{d\sigma}{d\Omega} (\mathbf{p}'_1 \rightarrow \mathbf{p}_1, \mathbf{p}'_2 \rightarrow \mathbf{p}_2) d\mathbf{p}'_2 d\Omega \quad (7.13b)$$

Using detailed balance gives

$$|\mathcal{T}(\mathbf{p}_1 \rightarrow \mathbf{p}'_1, \mathbf{p}_2 \rightarrow \mathbf{p}'_2)|^2 = |\mathcal{T}(\mathbf{p}'_1 \rightarrow \mathbf{p}_1, \mathbf{p}'_2 \rightarrow \mathbf{p}_2)|^2$$

One may rewrite (7.13b) as follows:

$$d\mathbf{r} d\mathbf{p}_1 \iint F(\mathbf{r}, \mathbf{p}'_1, \mathbf{p}'_2, t) |\mathbf{v}_1 - \mathbf{v}_2| \frac{d\sigma}{d\Omega'} d\mathbf{p}_2 d\Omega' \quad (7.14)$$

Combining (7.13a) and (7.13b) yields

$$\left(\frac{\partial f_1}{\partial t} \right)_{\text{coll}} = \iint d\mathbf{p}_2 d\Omega' |\mathbf{v}_1 - \mathbf{v}_2| \frac{d\sigma}{d\Omega'} [F(\mathbf{r}, \mathbf{p}'_1, \mathbf{p}'_2, t) - F(\mathbf{r}, \mathbf{p}_1, \mathbf{p}_2, t)] \quad (7.15)$$

To obtain the Lorentz–Boltzmann equation, one further approximation is made.

It is assumed that the probability of particle 1 being at \mathbf{r} with momentum \mathbf{p} does not depend on the position or momentum of particle 2. Hence

$$F(\mathbf{r}, \mathbf{p}_1, \mathbf{p}_2, t) \approx f_1(\mathbf{r}, \mathbf{p}_1, t) f_1(\mathbf{r}, \mathbf{p}_2, t) \quad (7.15')$$

Introducing this assumption into (7.15), one can now complete (7.10). One finds that

$$\frac{\partial f_1}{\partial t} + \mathbf{v} \cdot \nabla_{\mathbf{r}} f_1 - \nabla_{\mathbf{r}} V \cdot \nabla_{\mathbf{p}_1} f_1 = \int d\mathbf{p}_2 d\Omega' |\mathbf{v}_1 - \mathbf{v}_2| \frac{d\sigma}{d\Omega'} [f'_1 f'_2 - f_1 f_2] \quad (7.16)$$

where f'_2 is $f_1(\mathbf{r}, \mathbf{p}'_2, t)$, and so on. The values of \mathbf{p}_1 and \mathbf{p}'_2 on the right side of this equation are given by conservation of energy and momentum applied to the binary collision. Equation (7.16) is referred to as the *Lorentz-Boltzmann equation*. Because of assumption (7.15'), one expects it to be most useful for dilute systems. To improve upon (7.16) it is necessary to consider correlations, and therefore f_2 of (7.3), $s=2$ for correlations, and more generally, f_s for higher-order correlations. As we shall show, f_s coupled only to f_{s+1} , that is, f_1 to f_2 , f_2 to f_3 . This is a consequence of the assumption that the particle interaction potentials [see (7.1)] are two-body. This system of equations is called the BBGKY (Bogoliubov, Born, Green, Kirkwood, Yvon) hierarchy. We shall follow Huang (87) in developing these equations.

One begins with the Liouville theorem, (7.7):

$$\frac{\partial \rho}{\partial t} + \mathbf{v}_\zeta \cdot \nabla_\rho = 0 \quad (7.7)$$

In component form,

$$\begin{aligned} \mathbf{v}_\zeta \cdot \nabla_\rho &= \sum_i [\dot{\mathbf{r}}_i \cdot \nabla_{\mathbf{r}_i} \rho + \dot{\mathbf{p}}_i \cdot \nabla_{\mathbf{p}_i} \rho] \\ &= \sum_i [(\nabla_{\mathbf{p}_i} H) \cdot \nabla_{\mathbf{r}_i} - (\nabla_{\mathbf{r}_i} H) \cdot \nabla_{\mathbf{p}_i}] \rho \end{aligned}$$

Introducing H as given by (7.1), one obtains

$$\frac{\partial \rho}{\partial t} + \hat{h}_A \rho = 0 \quad (7.17)$$

where

$$\begin{aligned} \hat{h}_A &= \sum_i \left[\frac{\mathbf{p}_i}{m} \cdot \nabla_{\mathbf{r}_i} + \left\{ \mathbf{F}_i - \sum_{i \neq j} \nabla_{\mathbf{r}_i} v(|\mathbf{r}_i - \mathbf{r}_j|) \right\} \cdot \nabla_{\mathbf{p}_i} \right] \\ &\equiv \sum_i \hat{S}_i + \frac{1}{2} \sum_{i \neq j} \hat{P}_{ij} \end{aligned} \quad (7.18)$$

Here

$$\hat{S}_i \equiv \frac{\mathbf{p}_i}{m} \cdot \nabla_{\mathbf{r}_i} + \mathbf{F}_i \quad \mathbf{F}_i = -\nabla_{\mathbf{r}_i} V \quad (7.19)$$

and

$$\hat{P}_{ij} = \mathbf{K}_{ij} \cdot \nabla_{\mathbf{p}_i} + \mathbf{K}_{ji} \cdot \nabla_{\mathbf{p}_j} \quad \mathbf{K}_{ij} = -\nabla_{\mathbf{r}_i} v(|\mathbf{r}_i - \mathbf{r}_j|) \quad (7.20)$$

The distribution function f_s then satisfies

$$\frac{\partial f_s}{\partial t} = \frac{A!}{(A-s)!} \int d\zeta_{s+1} \frac{\partial \rho}{\partial t} = -\frac{A!}{(A-s)!} \int d\zeta_{s+1} \hat{h}_A \rho \quad (7.21)$$

where

$$d\zeta_{s+1} = d\mathbf{r}_{s+1} d\mathbf{r}_{s+2} \cdots d\mathbf{r}_A d\mathbf{p}_{s+1} d\mathbf{p}_{s+2} \cdots d\mathbf{p}_A$$

We now break up \hat{h}_A into terms that depend on ζ_1 to ζ_s and those that depend on ζ_{s+1} to ζ_A :

$$\hat{h}_A = \sum_{i=1} \hat{S}_i + \frac{1}{2} \sum_{i \neq j} \hat{P}_{ij} + \sum_{i=s+1}^A \hat{S}_i + \frac{1}{2} \sum_{i,j=s+1}^A \hat{P}_{ij} + \sum_{i=1}^s \sum_{j=s+1}^A \hat{P}_{ij}$$

This can be rewritten as

$$\hat{h}_A = \hat{h}_s + \hat{h}_{A-s} + \sum_{i=1}^s \sum_{j=s+1}^A \hat{P}_{ij} \quad (7.22)$$

Note that

$$\int d\zeta_{s+1} \hat{h}_{A-s} \rho = 0 \quad (7.23)$$

since \hat{h} involves momentum-dependent gradient operators linearly while K_{ij} depends only on spatial coordinates. Equation (7.22) would not be correct if the two-body potential were velocity dependent.

Inserting (7.22) into (7.21) yields

$$\begin{aligned} \frac{\partial f_s}{\partial t} + \hat{h}_s f_s &= -\frac{A!}{(A-s)!} \int d\zeta_{s+1} \sum_{i=1}^s \sum_{j=s+1}^A \hat{P}_{ij} \rho \\ &= -\sum_{i=1}^s \int \int d\mathbf{r}_{s+1} d\mathbf{p}_{s+1} \frac{A!}{(A-s-1)!} \hat{P}_{i,s+1} \int d\zeta_{s+2} \rho \\ &= -\int \int d\mathbf{r}_{s+1} d\mathbf{p}_{s+1} \left(\sum_{i=1}^s \hat{P}_{i,s+1} \right) f_{s+1} \end{aligned} \quad (7.24)$$

Substituting for $\hat{P}_{i,s+1}$ from (7.20), one finally obtains the BBGKY hierarchy:

$$\frac{\partial f_s}{\partial t} + \hat{h}_s f_s = -\int \int d\mathbf{r}_{s+1} d\mathbf{p}_{s+1} \left(\sum_{i=1}^s \mathbf{K}_{i,s+1} \cdot \nabla_{\mathbf{p}_i} f_{s+1} \right) \quad (7.25)$$

For example,

$$\frac{\partial f_1}{\partial t} + \hat{h}_1 f_1 = - \int \int d\mathbf{r}_2 d\mathbf{p}_2 \mathbf{K}_{12} \cdot \nabla_{\mathbf{p}_1} f_2 \quad (7.26a)$$

$$\frac{\partial f_2}{\partial t} + \hat{h}_2 f_2 = - \int \int d\mathbf{r}_3 d\mathbf{p}_3 (\mathbf{K}_{13} \cdot \nabla_{\mathbf{p}_{+1}} + \mathbf{K}_{23} \cdot \nabla_{\mathbf{p}_2}) f_3 \quad (7.26b)$$

To obtain the Lorentz–Boltzmann equation (7.16), one truncates (7.25) by placing f_3 and $\partial f_2 / \partial t = 0$. Finally, one assumes that $f_2(\mathbf{r}_1, \mathbf{p}_1, \mathbf{r}_2, \mathbf{p}_2)$ can be written as $f_1(\mathbf{r}_1, \mathbf{p}_1) f_2(\mathbf{r}_2, \mathbf{p}_2)$ thereby dropping two-body correlations.

The solutions of the Lorentz–Boltzmann satisfy conditions that follow from conservation laws such as conservation of mass, momentum, and energy satisfied in the two-body collision. Following Huang, let $\chi(\mathbf{r}, p)$ be such a conserved quantity, that is,

$$\chi(\mathbf{r}, \mathbf{p}_1) + \chi(\mathbf{r}, \mathbf{p}_2) = \chi(\mathbf{r}, \mathbf{p}'_1) + \chi(\mathbf{r}, \mathbf{p}'_2) \quad (7.27)$$

We can now show that

$$J = \int \left(\frac{\partial f_1}{\partial t} \right)_{\text{coll}} \chi(\mathbf{r}, \mathbf{p}) d\mathbf{p} = 0 \quad (7.28)$$

We use expression (7.11), bearing in mind the symmetries satisfied by F and dw .

Equation (7.28), including now explicitly the conservation of energy and momentum, is

$$\begin{aligned} J = & \int d\mathbf{p}_1 d\mathbf{p}_2 d\mathbf{p}'_1 d\mathbf{p}'_2 \delta(E_1 + E_2 - E'_1 - E'_2) \delta(\mathbf{p}_1 + \mathbf{p}_2 - \mathbf{p}'_1 - \mathbf{p}'_2) \\ & \times w(\mathbf{p}'_1, \mathbf{p}'_2, \mathbf{p}_1, \mathbf{p}_2) [F(\mathbf{r}, \mathbf{p}'_1, \mathbf{p}'_2, t) - F(\mathbf{r}, \mathbf{p}_1, \mathbf{p}_2, t)] \chi(\mathbf{r}, \mathbf{p}_1) \end{aligned}$$

Now we note that J is unchanged if under the integral spin we exchange \mathbf{p}_1 and \mathbf{p}_2 or \mathbf{p}_1 and \mathbf{p}'_1 together with the exchange of \mathbf{p}_2 and \mathbf{p}'_2 or if one exchanges \mathbf{p}_1 and \mathbf{p}'_2 together with \mathbf{p}_2 and \mathbf{p}'_1 . This result is a consequence of the symmetry of both w and F . Performing the exchanges and adding the results yields

$$\begin{aligned} J = & \int d\mathbf{p}_1 d\mathbf{p}_2 d\mathbf{p}'_1 d\mathbf{p}'_2 \delta(E_1 + E_2 - E'_1 - E'_2) \delta(\mathbf{p}_1 + \mathbf{p}_2 - \mathbf{p}'_1 - \mathbf{p}'_2) \\ & \times w(\mathbf{p}'_1, \mathbf{p}'_2, \mathbf{p}_1, \mathbf{p}_2) [F(\mathbf{r}, \mathbf{p}'_1, \mathbf{p}'_2, t) - F(\mathbf{r}, \mathbf{p}_1, \mathbf{p}_2, t)] \\ & \times [\chi(\mathbf{r}, \mathbf{p}_1) + \chi(\mathbf{r}, \mathbf{p}_2) - \chi(\mathbf{r}, \mathbf{p}'_1) - \chi(\mathbf{r}, \mathbf{p}'_2)] \end{aligned}$$

Hence because of conservation condition (7.27), $J = 0$, proving (7.28).

As a consequence of this equation, one obtains from the Lorentz–Boltzmann equation the equation

$$\int d\mathbf{p} \chi(\mathbf{r}, \mathbf{p}) \left[\frac{\partial f_1}{\partial t} + \sum_i \frac{\mathbf{p}_i}{m} \frac{\partial f_1}{\partial x_i} + F_i \frac{\partial f_1}{\partial p_i} \right] = 0 \quad (7.29)$$

where

$$F_i \equiv -\nabla_r U$$

We now rewrite this equation so that no derivatives act on f_1 under the integral sign. Thus

$$\begin{aligned} 0 = & \frac{\partial}{\partial t} \int d\mathbf{p} \chi f_1 + \sum_i \frac{\partial}{\partial x_i} \int d\mathbf{p} \frac{\mathbf{p}_i}{m} \chi f_1 - \sum_i \int d\mathbf{p} \left(\frac{\mathbf{p}_i}{m} \frac{\partial \chi}{\partial x_i} \right) f_1 \\ & + \sum F_i \int d\mathbf{p} \frac{\partial (\chi f_1)}{\partial p_i} - \sum_i F_i \int d\mathbf{p} \left(\frac{\partial \chi}{\partial p_i} \right) f_1 \end{aligned} \quad (7.30)$$

Integrating the fourth term on the right yields zero. We introduce the definitions

$$\begin{aligned} \langle A \rangle & \equiv \frac{\int d\mathbf{p} A f_1}{\int d\mathbf{p} f_1} = \frac{1}{n} \int d\mathbf{p} A f_1 \\ \mathbf{v} & = \frac{1}{m} \mathbf{p} \end{aligned}$$

Note that n , the number of particle density, is a function of \mathbf{r} and t . Equation (7.30) becomes

$$0 = \frac{\partial}{\partial t} \langle n\chi \rangle + \nabla_r \cdot \langle n\mathbf{v}\chi \rangle = \langle n\mathbf{v} \cdot \nabla_r \chi \rangle - \left\langle \frac{n}{m} \mathbf{F} \cdot \nabla_v \chi \right\rangle \quad (7.31)$$

The functions n and \mathbf{F} can be removed from inside the brackets since they do not depend on \mathbf{p} .

For conservation of mass, $\chi = m$, (7.31) becomes the equation of continuity:

$$\frac{\partial n}{\partial t} + \nabla_r \cdot (n\mathbf{u}) = 0 \quad (7.32)$$

where

$$\mathbf{u} = \langle \mathbf{v} \rangle \quad (7.33)$$

For conservation of momentum, $\chi = m\mathbf{v}$,

$$0 = \frac{\partial}{\partial t} (n\mathbf{v}) + \nabla_r \cdot n \langle \mathbf{v}\mathbf{v} \rangle - \frac{1}{m} n \mathbf{F} \quad (7.34)$$

where the *dot product in the second term is with the \mathbf{v} that immediately follows the dot*. We now replace $\langle \mathbf{v}\mathbf{v} \rangle$ as follows:

$$\langle \mathbf{v}\mathbf{v} \rangle = \langle (\mathbf{v} - \mathbf{u})(\mathbf{v} - \mathbf{u}) \rangle + \mathbf{u}\mathbf{u}$$

Substituting in (7.26) and using (7.24), one obtains

$$n \left[\frac{\partial \mathbf{u}}{\partial t} + (\mathbf{u} \cdot \nabla) \mathbf{u} \right] = \frac{1}{m} n \mathbf{F} + \nabla \cdot n \langle (\mathbf{v} - \mathbf{u})(\mathbf{v} - \mathbf{u}) \rangle \quad (7.35)$$

The *pressure tensor* P_{ij} is defined by

$$P_{ij} \equiv mn \langle (\mathbf{v}_i - \mathbf{u}_i)(\mathbf{v}_j - \mathbf{u}_j) \rangle \quad (7.36)$$

so that

$$n \left[\frac{\partial \mathbf{u}}{\partial t} + (\mathbf{u} \cdot \nabla) \mathbf{u} \right] = \frac{1}{m} n \mathbf{F} + \frac{1}{m} \nabla \cdot \vec{P} \quad (7.37)$$

where

$$\nabla \cdot \vec{P} = \sum \frac{\partial P_{ij}}{\partial x_i}$$

Problem. Prove that this quantity is conserved in a two-body collision.

Finally, we exploit the conservation of energy by letting $\chi = \frac{1}{2}|\mathbf{v} - \mathbf{u}|^2$. The analysis is straightforward. The result is

$$n \frac{\partial T}{\partial t} + n \mathbf{u} \cdot \nabla_r T + \frac{2}{3} \nabla_r \cdot \mathbf{q} = -\frac{2}{3} \vec{P} \cdot \vec{\Lambda} \quad (7.38)$$

where

$$\vec{P} \cdot \vec{\Lambda} = \sum_{ij} P_{ij} \Lambda_{ij} \quad (7.39)$$

and

$$\Lambda_{ij} = \frac{1}{2} \left(\frac{\partial u_j}{\partial x_i} + \frac{\partial u_i}{\partial x_j} \right) \quad (7.40)$$

T is the temperature in energy units:

$$T = \frac{1}{3} \langle |\mathbf{v} - \mathbf{u}|^2 \rangle$$

The vector \mathbf{q} measures the heat flux:

$$\mathbf{q} = \frac{1}{2} n \langle (\mathbf{v} - \mathbf{u}) |\mathbf{v} - \mathbf{u}|^2 \rangle \quad (7.41)$$

The exploitation of (7.32), (7.37), and (7.38) requires evaluation of the average values indicated by the bracket and therefore knowledge of f_i . If, for example, one assumes local thermal equilibrium, so that f_1 is given locally by the Maxwell distribution,

$$f_1 \approx \frac{n}{(2\pi mT)^{3/2}} e^{-(m/2T)(\mathbf{v}-\mathbf{u})^2}$$

one obtains the equations describing nonviscous hydrodynamics. If f_1 is improved by a first-order term, one obtains the Navier–Stokes equation for viscous flow [see Huang (87)]. Therefore, the equations of hydrodynamics are an approximation to the Lorentz–Boltzmann equation obtained by averaging that equation over an assumed distribution function.

A. Quantum Transport[‡]

The discussion above is classical so that the question of quantum effects naturally surfaces. Of course, the exact evaluation of the quantum effects requires the solution of the quantum-mechanical many-body problem. What would be useful would be a statement of the quantum problem, which is similar in form to the Lorentz–Boltzmann equation. The analog to the one-particle distribution function is given by one-particle Wigner function (30) defined by

$$f_W(\mathbf{r}, \mathbf{k}, t) = \left(\frac{1}{2\pi}\right)^3 \int d\mathbf{r}_0 e^{-i\mathbf{k}\cdot\mathbf{r}_0} \psi^*(\mathbf{r} - \frac{1}{2}\mathbf{r}_0, t) \psi(\mathbf{r} + \frac{1}{2}\mathbf{r}_0, t) \quad (7.42)$$

or

$$f_W(\mathbf{r}, \mathbf{k}, t) = \left(\frac{1}{2\pi}\right)^3 \int d\mathbf{r}_0 e^{-i\mathbf{k}\cdot\mathbf{r}_0} \rho\left(\mathbf{r} - \frac{1}{2}\mathbf{r}_0, \mathbf{r} + \frac{1}{2}\mathbf{r}_0, t\right) \quad (7.43)$$

Integrating f_W with respect to \mathbf{k} yields

$$\int f_W(\mathbf{r}, \mathbf{k}, t) d\mathbf{k} = \rho(\mathbf{r}, t) \quad (7.44)$$

Taking moments, one finds that

$$\begin{aligned} \int f_W(\mathbf{r}, \mathbf{k}, t) \mathbf{k} d\mathbf{k} &= \left(\frac{1}{2\pi}\right)^3 \int d\mathbf{k} \int d\mathbf{r}_0 i\nabla_0 e^{-i\mathbf{k}\cdot\mathbf{r}_0} \psi^*\left(\mathbf{r} - \frac{\mathbf{r}_0}{2}, t\right) \psi\left(\mathbf{r} + \frac{\mathbf{r}_0}{2}, t\right) \\ &= \left(\frac{1}{2\pi}\right)^3 \int d\mathbf{k} \int d\mathbf{r}_0 e^{-i\mathbf{k}\cdot\mathbf{r}_0} \left(\frac{1}{i} \nabla_0(\psi^* \psi)\right) \end{aligned}$$

[‡]Carruthers and Zachariasen (83); Zachariasen (85).

$$= \left(\frac{1}{2\pi}\right)^3 \int d\mathbf{k} \int d\mathbf{r}_0 e^{-i\mathbf{k}\cdot\mathbf{r}_0} \left[-\frac{1}{2i} \left(\nabla\psi^* \left(\mathbf{r} - \frac{\mathbf{r}_0}{2}, t \right) \psi \left(\mathbf{r} + \frac{\mathbf{r}_0}{2}, t \right) \right) \right. \\ \left. + \frac{1}{2i} \psi^* \left(\mathbf{r} - \frac{\mathbf{r}_0}{2}, t \right) \nabla\psi \left(\mathbf{r} + \frac{\mathbf{r}_0}{2}, t \right) \right]$$

or

$$\int f_W(\mathbf{r}, \mathbf{k}, t) \frac{\mathbf{p}}{m} d\mathbf{k} = \mathbf{j}(\mathbf{r}, t) \quad (7.45)$$

Finally,

$$\int f_W(\mathbf{r}, \mathbf{k}, t) \frac{p^2}{2m} d\mathbf{k} = K(\mathbf{r}, t) \quad (7.46)$$

where $K(\mathbf{r}, t)$ is the kinetic energy density. [The reader should verify (7.46).] These results, (7.44), (7.45), and (7.46), are identical to those that can be obtained using the classical distribution function. But the Wigner distribution is not a probability distribution, as is the case for the classical distribution. This follows because f_W is not positive definite. Because of the close similarity to the Boltzmann distribution function, it is not surprising that f_W satisfies a Lorentz–Boltzmann type of equation. To demonstrate this, evaluate $\partial f_W / \partial t$ using the Schrödinger equation:

$$i\hbar \frac{\partial \psi}{\partial t} = H\psi \quad \text{and} \quad -i\hbar \frac{\partial \psi^*}{\partial t} = H\psi^*$$

assuming H to be Hermitian. One obtains

$$\frac{\partial f_W}{\partial t} = \left(\frac{1}{2\pi}\right)^3 \int d\mathbf{r}_0 e^{-i\mathbf{k}\cdot\mathbf{r}_0} \left[\left(\frac{i}{\hbar} H\psi^* \right) \psi - \frac{i}{\hbar} \psi^* (H\psi) \right]$$

Replace H by $-(\hbar^2/2m)\nabla^2 + V$, where ∇^2 operates on the dependence on the spatial coordinates $\mathbf{r} - \frac{1}{2}\mathbf{r}_0$ and $\mathbf{r} + \frac{1}{2}\mathbf{r}_0$. The result, after some simple algebra, is

$$\frac{\partial f_W}{\partial t} + \frac{\mathbf{p}}{m} \cdot \nabla_r f_W = -\frac{i}{\hbar} \int d\mathbf{r}_0 \psi^* \left[V \left(\mathbf{r} + \frac{\mathbf{r}_0}{2} \right) - V \left(\mathbf{r} - \frac{\mathbf{r}_0}{2} \right) \right] \psi e^{-i\mathbf{k}\cdot\mathbf{r}_0} \quad (7.47)$$

In the limit where V is assumed to be smooth, so that

$$V \left(\mathbf{r} + \frac{\mathbf{r}_0}{2} \right) \simeq V(\mathbf{r}) + \frac{\mathbf{r}_0}{2} \cdot \nabla V$$

(7.47) becomes

$$\frac{\partial f_W}{\partial t} + \frac{\mathbf{p}}{m} \cdot \nabla_r f_W - \nabla V \cdot \nabla_p f_W = 0 \quad (7.48)$$

identical with the Lorentz–Boltzmann equation (7.15) when the collision term $(\partial f / \partial t)_{\text{coll}}$ is zero. Equation (7.48) is known as the *Vlasov equation*.

This treatment can be generalized to the many-body problem, employing an A -particle Wigner distribution function [see Zachariasen (85)]

$$\begin{aligned} f_W^{(N)}(\mathbf{k}_1, \mathbf{r}_1, \mathbf{k}_2, \mathbf{r}_2, \dots, \mathbf{k}_A, \mathbf{r}_A, t) \\ = \left(\frac{1}{2\pi} \right)^{3A} \int d\mathbf{r}'_1 \cdots \int d\mathbf{r}'_A \exp(-i\sum \mathbf{k}_i \cdot \mathbf{r}'_i) \Psi^*(\mathbf{r}_1 - \tfrac{1}{2}\mathbf{r}'_1, \dots, \mathbf{r}_A - \tfrac{1}{2}\mathbf{r}'_A, t) \\ \cdot \Psi(\mathbf{r}_1 + \tfrac{1}{2}\mathbf{r}'_1, \dots, \mathbf{r}_A + \tfrac{1}{2}\mathbf{r}'_A, t) \end{aligned} \quad (7.49)$$

One can, in analogy with the procedure used to derive the BBGKY hierarchy, define reduced distribution functions $f_W^{(s)}$ by

$$f_W^{(s)} = (2\pi)^{3s} \int d\mathbf{r}_{s+1} \cdots \int d\mathbf{r}_A \int d\mathbf{k}_{s+1} \cdots \int d\mathbf{k}_A f_W^{(N)} \quad (7.50)$$

Applying the Schrödinger equation to (7.49), one finds a set of equations in which $f_W^{(s)}$ is coupled to $f_W^{(s+1)}$, the quantum analog of the BBGKY hierarchy. We shall not pursue this discussion further since as far as this author knows, no application of these quantum equations to heavy-ion reactions has been made.

B. Applications

Before it is possible to apply the Lorentz–Boltzmann equation to heavy-ion reactions it is necessary to take the Pauli principle into account. The necessary modification has been derived by Uehling and Uhlenbeck (33). Instead of (7.16), one obtains

$$\begin{aligned} \frac{\partial f_1}{\partial t} + \mathbf{v} \cdot \nabla_{\mathbf{r}} f_1 - \nabla_{\mathbf{r}} V \cdot \nabla_{\mathbf{p}} f_1 \\ = \int d\mathbf{p}_1 d\Omega' |\mathbf{v}_1 - \mathbf{v}_2| \frac{d\sigma}{d\Omega'} \{f'_1 f'_2 (1 - f_1)(1 - f_2) - f_1 f_2 (1 - f'_1)(1 - f'_2)\} \end{aligned} \quad (7.51)$$

The additional factors are intuitively obvious. Scattering out of \mathbf{p}'_1 and \mathbf{p}'_2 in \mathbf{p}_1 and \mathbf{p}_2 is not possible if the states \mathbf{p}_1 and \mathbf{p}_2 are occupied. Equation (7.51) is referred to as the Boltzmann–Uehling–Uhlenbeck equation (BUU).

Aichelen and Bertsch (85); Aichelin (86) [see also Kruse et al. (85) and Stöcker et al. (81)] have applied (7.51) to the study of heavy-ion reactions. [For additional references, see Aichelin (86).] Since the equation is classical, its use is limited to sufficiently high energies. At very high energies the intranuclear cascade model, discussed in Chapter IX, and to which (7.51) reduces, is appropriate. At low energies, where the Pauli blocking reduces the impact of

the collision term, one may use the time-dependent Hartree-Fock (TDHF) method, discussed in Section 8. Equation (7.51) applies when the collision term and/or the mean potential, V (which can be neglected at high energies), are significant. In their studies, Bertsch and Aichelin have investigated $^{12}\text{C} + ^{16}\text{O}$ at 25 MeV/A, $^{12}\text{C} + ^{12}\text{C}$ at 84 MeV/A, $^{16}\text{O} + ^{197}\text{Au}$ at 25 and 250 MeV/A, and $^{12}\text{C} + ^{197}\text{Au}$ at 84 MeV/A. The collisions with ^{197}Au are most important since one can study the progress toward equilibration, the possible presence of hot spots, and other local properties, such as density and local thermal equilibrium. One can also study the validity of the spectator model in which it is assumed that the reaction occurs only in the region where the projectile and target nuclei overlap.

Predictions can be made only for single-particle spectra and angular distribution. For the light nuclei, Coulomb effects are neglected, while for the heavy nuclear targets, Coulomb effects are neglected after the first nucleon-nucleon collision.

These authors find that the course of the reaction is determined by the relative importance of the mean field, the collision term, and the Pauli principle. At the

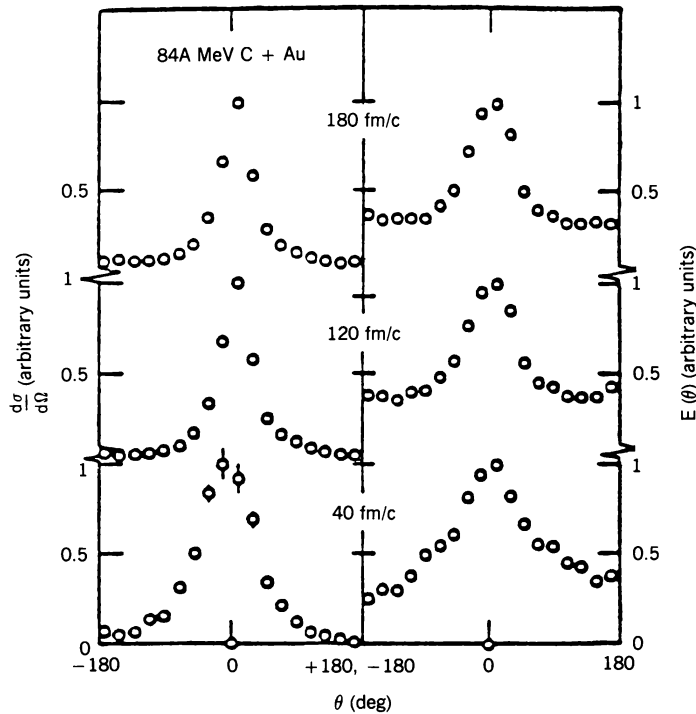


FIG. 7.1. Angular distribution and average kinetic of emitted protons as a function of time. Positive angles correspond to positive values of the x component of the momentum of the emitted particles. [From Aichelin (86).]

lower end of the energies considered, the mean field and the Pauli principle dominate. The nucleons of the incident projectile are more readily trapped by the mean field but have a longer mean free path. Fusion is the endpoint of the reaction. The single-particle spectrum is exponential but with a slope parameter increasing as a function of angle in agreement with the discussion in Section 6, which relies on a Fokker–Planck equation in the momentum space. At higher energies, 84 MeV/A, the multistep direct reaction as well the multistep compound reaction become significant. The reaction thus shows a substantial preequilibrium component which develops during the early stages of the reaction. The mean field does trap some particles, so that the final stages of the multistep compound leads to a final remnant compound nucleus which oscillates radially. The angular distribution consists of roughly two components. The preequilibrium reaction gives rise to a forward peaked anisotropic distribution, while the remnant compound nucleus will emit isotropically in the center of mass. At the highest energy considered, 250 MeV/A, the collision term dominates in the overlap region. However, these authors state that even at this energy a clear-cut separation between participant and spectator nucleons is not possible. The multistep direct reaction with its forward peaked angular

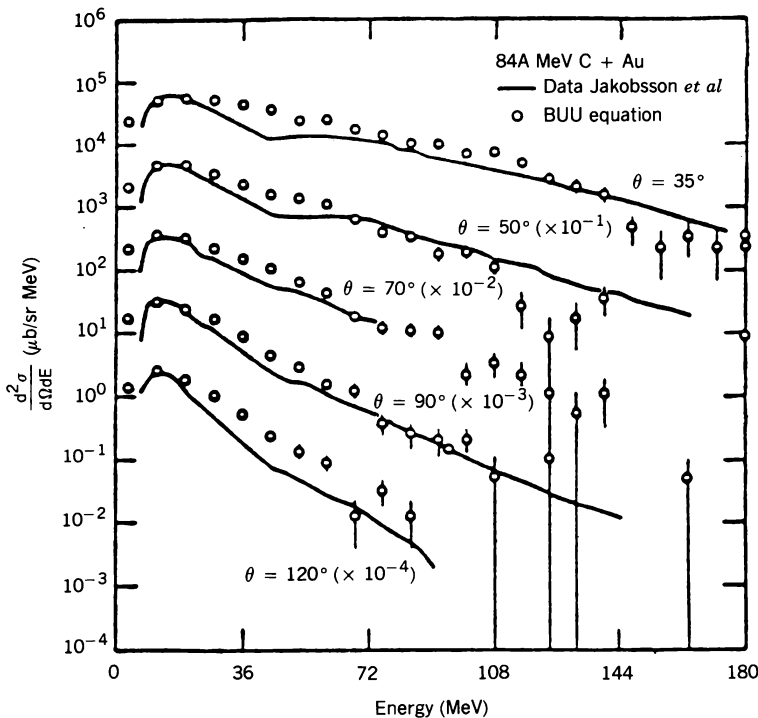


FIG. 7.2. Proton spectrum produced by the reaction $^{12}\text{C} + ^{197}\text{Au}$ at 84 MeV/A compared with the results of Jakobsson et al. (82). [from Aichelin (86).]

distribution is dominant, and even in the overlap region complete equilibrium is not achieved.

The predicted single-particle spectrum is compared with experiment (84 MeV/A) in Fig. 7.1. Substantial agreement (note that this is a semilog plot) is obtained. However, the slope parameter for the high-energy tails increases with angle, in agreement with the momentum space Fokker–Plank equation [see (6.31) et seq.] Correspondingly, the angular distribution is strongly anisotropic, indicating the dominant presence of multistep direct processes (see Fig. 7.2). A similar result prevails at 250 MeV/A. Equilibrium, which requires an isotropic distribution, is not attained. The author concludes that the hydrodynamic approach is not valid at 84 MeV/A, and this writer would add—probably not at 250 MeV/A.

8. TIME-DEPENDENT HARTREE–FOCK METHOD[†]

The Lorentz–Boltzmann approach of Section 7 is not valid in the low-energy domain (energies $\simeq 10$ MeV/A). The Pauli principle and quantum effects must be treated carefully. Because of the Pauli blocking, the effect of collisions of a low-energy nucleon with the nucleons of the nucleus is strongly reduced, increasing the mean free path so that at 10 MeV it is on the order of the diameter of the nucleus. As many fewer nuclear states are involved, quantum effects become significant. However, it is just under this regime that the mean field approximation becomes valid. The nucleon is acted on by an average field generated by all the nucleons in the nucleus whose coordinates essentially disappear from the problem to be replaced by the parameters describing the mean field (e.g., the nuclear radius). The zeroth approximation to the mean field is the Hartree–Fock approximation. To improve upon it, one can use the time-dependent Hartree–Fock (TDHF), described in Section III.3 of deShalit and Feshbach (74). As shown there, for small deviations from the Hartree–Fock approximation, one obtains the RPA approximation [Thouless (61); Kerman and Koonin (76)]. However, in the case of heavy-ion collisions, we are concerned with relatively large deviations. The method to be used was first proposed by Dirac (30), and applied to large-amplitude dynamics and heavy-ion collisions by Kerman and Koonin (76) and Bonche, Koonin, and Negele (76) to a one-dimensional case.

We begin with a variation principle for the time-dependent many-body Schrödinger equation:

$$\delta S = 0 \quad (8.1)$$

[†]Kerman and Koonin (76); Negele (82); Davies, Devi, Koonin, and Strayer (84); Pal (85).

where

$$S = \int dt \int d\mathbf{r}_1 \cdots d\mathbf{r}_n d\mathbf{r}'_1 \cdots d\mathbf{r}'_n \Psi^*(\mathbf{r}_1 \cdots \mathbf{r}_n, t) \cdot \left[i\hbar \frac{\partial}{\partial t} - H(\mathbf{r}_1 \cdots \mathbf{r}_n; \mathbf{r}'_1 \cdots \mathbf{r}'_n) \right] \Psi(\mathbf{r}'_1 \cdots \mathbf{r}'_n, t) \quad (8.2)$$

Varying Ψ^* yields the time-dependent Schrödinger equation for Ψ . The trial function to be used in TDHF is a time-dependent Slater determinant:

$$\psi_{SD} = \frac{1}{\sqrt{n!}} \begin{vmatrix} \psi_1(\mathbf{r}_1, t) & \psi_1(\mathbf{r}_2, t) & \cdots & \psi_1(\mathbf{r}_n, t) \\ \psi_2(\mathbf{r}_1, t) & \psi_2(\mathbf{r}_2, t) & \cdots & \psi_2(\mathbf{r}_n, t) \\ \vdots & \vdots & \ddots & \vdots \\ \psi_n(\mathbf{r}_1, t) & \psi_n(\mathbf{r}_2, t) & \cdots & \psi_n(\mathbf{r}_n, t) \end{vmatrix} \quad (8.3)$$

where the trial single-particle wave functions are orthonormal:

$$\langle \psi_\mu(\mathbf{r}, t) | \psi_\nu(\mathbf{r}, t) \rangle = \delta_{\mu\nu} \quad (8.4)$$

Inserting Ψ_{SD} for Ψ in (8.2) and varying with respect to ψ_ν^* yields the one-body equation for ψ_ν :

$$i\hbar \frac{\partial \psi_\nu}{\partial t} = T\psi_\nu + \sum_\mu \int d\mathbf{r}_2 d\mathbf{r}'_1 d\mathbf{r}'_2 \psi_\mu^*(\mathbf{r}_2, t) \tilde{v}(\mathbf{r}_1, \mathbf{r}_2; \mathbf{r}'_1, \mathbf{r}'_2) \psi_\mu(\mathbf{r}'_2, t) \psi_\nu(\mathbf{r}'_1, t) \\ \equiv (T + V)\psi_\nu \quad (8.5)$$

In this equation, T is the kinetic energy operator. We have assumed that the potential v in H is two-body operator:

$$v(\mathbf{r}_1 \cdots \mathbf{r}_m, \mathbf{r}'_1 \cdots \mathbf{r}'_n) = v(\mathbf{r}_i, \mathbf{r}_j; \mathbf{r}'_i, \mathbf{r}'_j) \delta(\mathbf{r}_1 - \mathbf{r}'_1) \cdots \delta(\mathbf{r}_{i-1} - \mathbf{r}'_{i-1}) \delta(\mathbf{r}_{i+1} - \mathbf{r}'_{i+1}) \cdots \\ \delta(\mathbf{r}_{j-1} - \mathbf{r}'_{j-1}) \delta(\mathbf{r}_{j+1} - \mathbf{r}'_{j+1}) \cdots \delta(\mathbf{r}_n - \mathbf{r}'_n).$$

The quantity \tilde{v} in (8.5) is then

$$\tilde{v}(\mathbf{r}_1, \mathbf{r}_2; \mathbf{r}'_1, \mathbf{r}'_2) \equiv v(\mathbf{r}_1, \mathbf{r}_2; \mathbf{r}'_1, \mathbf{r}'_2) - v(\mathbf{r}_1, \mathbf{r}_2; \mathbf{r}'_2, \mathbf{r}'_1) \quad (8.6)$$

Equation (8.5) yields a set of coupled nonlinear equations whose solutions give the time and spatial dependence of the single-particle wave function $\psi_\nu(\mathbf{r}, t)$. The time-independent Hartree-Fock equations are obtained by assuming that each particle wave function has an exponential dependence on time. Note that when v satisfies translational invariance, that is,

$$v(\mathbf{r}_1, \mathbf{r}_2; \mathbf{r}'_1, \mathbf{r}'_2) = \delta(\mathbf{r}_1 - \mathbf{r}'_1) \delta(\mathbf{r}_2 - \mathbf{r}'_2) v(\mathbf{r}_1 - \mathbf{r}_2)$$

then

$$\tilde{v} = [\delta(\mathbf{r}_1 - \mathbf{r}'_1)\delta(\mathbf{r}_2 - \mathbf{r}'_2) - \delta(\mathbf{r}_1 - \mathbf{r}'_2)\delta(\mathbf{r}_2 - \mathbf{r}'_1)]v(\mathbf{r}_1 - \mathbf{r}_2)$$

Equation (8.5) becomes

$$i\frac{\partial\psi_v}{\partial t} = T\psi_v + \sum_{\mu} \int d\mathbf{r}_2 [\psi_{\mu}^*(\mathbf{r}_2)\psi_{\mu}(\mathbf{r}_2)\psi_v(\mathbf{r}_1) - \psi_{\mu}^*(\mathbf{r}_2)\psi_{\mu}(\mathbf{r}_1)\psi_v(\mathbf{r}_2)]v(\mathbf{r}_1 - \mathbf{r}_2) \quad (8.7)$$

The first term in brackets is the direct or Hartree term, the second term is the exchange or Fock term. The direct term is local, while the exchange term is nonlocal.

The trial function, Ψ_{SD} , will not provide a complete description of the nuclear state no matter how accurately (8.5) is solved, as only the correlations induced by the Pauli exclusion principle are present. The correlations induced by the potential v are not. As a consequence, one can expect that the matrix elements of only single-body operators will be given accurately using Ψ_{SD} . It would not be correct to use Ψ_{SD} to evaluate matrix elements of two- (or more) body operators.

The TDHF equations (8.5) imply a number of conservation laws. One asserts that the orthonormal condition (8.4) holds at all times t . To prove this, consider

$$\frac{d}{dt} \int d\mathbf{r} \psi_v^*(\mathbf{r}, t) \psi_{\mu}(\mathbf{r}, t) = \int d\mathbf{r} \left(\frac{\partial}{\partial t} \psi_v^* \psi_{\mu} + \psi_v^* \frac{\partial \psi_{\mu}}{\partial t} \right)$$

Substituting from (8.5), one obtains

$$\frac{d}{dt} \int d\mathbf{r} \psi_v^*(\mathbf{r}, t) \psi_{\mu}(\mathbf{r}, t) = -\frac{i}{\hbar} \int d\mathbf{r} [\psi_v^*(T + V)^{\dagger} \psi_{\mu} - \psi_v^*(T + V) \psi_{\mu}] = 0$$

The expectation value of any one-body operator that commutes with H is conserved [Koonin (79)]. To prove this, we calculate

$$\frac{d}{dt} \langle \psi_{SD} \hat{O} \psi_{SD} \rangle = \sum_v \int d\mathbf{r} d\mathbf{r}' \left[\frac{\partial \psi_v^*(\mathbf{r}, t)}{\partial t} \hat{O}(\mathbf{r}, \mathbf{r}') \psi_v(\mathbf{r}', t) + \psi_v^*(\mathbf{r}, t) \hat{O}(\mathbf{r}, \mathbf{r}') \frac{\partial \psi_v(\mathbf{r}', t)}{\partial t} \right]$$

Replacing the time derivatives by the right-hand side of (8.5) yields

$$\frac{d}{dt} \langle \Psi_{SD} \hat{O} \Psi_{SD} \rangle = \frac{i}{\hbar} \sum_v \int d\mathbf{r} d\mathbf{r}' [\psi_v^*(\mathbf{r}, t) (\hat{O} \mathcal{H} - \mathcal{H} \hat{O}) \psi_v(\mathbf{r}', t)]$$

where

$$\mathcal{H} \equiv T + V$$

The proof is completed by replacing V by its definition in (8.5). Quantities that are conserved include the expectation value of \mathcal{H} , the TDHF energy, the expectation value of the total momentum, and the total angular momentum.

The time-dependent Hartree-Fock equations can be reexpressed in a representation-independent form using the density matrix $\rho(\mathbf{r}, \mathbf{r}', t)$, where

$$\rho(\mathbf{r}_1, \mathbf{r}'; t) = n \int \Psi^*(\mathbf{r}, \mathbf{r}_2, \dots, t) \Psi(\mathbf{r}', \mathbf{r}_2, \dots, t) d\mathbf{r}_2 \cdots \quad (8.8)$$

The expectation of a one-body operator $\sum_i \hat{O}(\mathbf{r}_i, \mathbf{r}_i)$ is

$$\langle \Psi^* \hat{O} \Psi \rangle = \int \hat{O}(\mathbf{r}', \mathbf{r}) \rho(\mathbf{r}, \mathbf{r}', t) d\mathbf{r} d\mathbf{r}' = \text{tr } \hat{O} \rho \quad (8.9)$$

where the trace is taken with respect to the spatial coordinates. We note another property of ρ using determinantal wave functions, (8.3), for Ψ . In that case

$$\rho(\mathbf{r}, \mathbf{r}'; t) = \sum_{\mu} \psi_{\mu}(\mathbf{r}, t) \psi_{\mu}^*(\mathbf{r}', t) \quad (8.10)$$

and

$$\int \rho(\mathbf{r}, \mathbf{r}'; t) \rho(\mathbf{r}', \mathbf{r}''; t) d\mathbf{r}' = \rho(\mathbf{r}, \mathbf{r}'', t) \quad (8.11)$$

Or in operator language,

$$\hat{\rho}^2 = \hat{\rho} \quad (8.12)$$

In terms of ρ , (8.7) becomes

$$\begin{aligned} i\hbar \frac{\partial \psi_v}{\partial t} &= T \psi_v + \int d\mathbf{r}_2 \rho(\mathbf{r}_2, \mathbf{r}_2; t) v(\mathbf{r}_1 - \mathbf{r}_2) \psi_v(\mathbf{r}_1, t) \\ &\quad - \int d\mathbf{r}_2 \rho(\mathbf{r}_1, \mathbf{r}_2; t) v(\mathbf{r}_1 - \mathbf{r}_2) \psi_v(\mathbf{r}_2) \end{aligned} \quad (8.13)$$

which we abbreviate as follows:

$$i\hbar \frac{\partial \psi_v}{\partial t} = \int h(\mathbf{r}_1, \mathbf{r}_2; t) \psi_v(\mathbf{r}_2) d\mathbf{r}_2 \quad (8.14)$$

It is now possible to derive the equation of motion for ρ using the representation (8.10). One obtains

$$i\hbar \frac{\partial \rho}{\partial t} = \int d\mathbf{r}_2 [h(\mathbf{r}, \mathbf{r}_2, t) \rho(\mathbf{r}_2, \mathbf{r}', t) - \rho(\mathbf{r}, \mathbf{r}_2, t) h(\mathbf{r}_2, \mathbf{r}', t)] \quad (8.15)$$

Equation (8.15) can be written

$$i\hbar \frac{\partial \rho}{\partial t} = [h, \rho] \quad (8.16)$$

The one-body Hamiltonian, h , depends on ρ , so that (8.15) is nonlinear, as is the equation for ψ_v .

Equations (8.12) and (8.16) are the starting points for Baranger and Vereroni's (78) formulation of the adiabatic limit to TDHF. These authors point out that

$$\rho = e^{i\chi} \rho_0 e^{-i\chi} \quad (8.17)$$

satisfies (8.12), where ρ_0 is time even and satisfies $\rho_0^2 = \rho_0$. When χ is sufficiently small, ρ may be expanded in a power series in terms of the odd and even components of ρ . The equations relating them is obtained from (8.16). By constraining ρ_0 to be time even, the odd-time dependence is given by χ .

We return to the TDHF single-particle equation (8.5). To complete the description of this equation, one needs to specify the interaction potential, \tilde{v} , and the initial conditions. Integration of these equations is a very large task, so that one seeks to minimize the labor involved subject to the condition that no essential physics be lost. In this case, one selects a \tilde{v} that leads to local mean field, V , in (8.15). Toward this end one starts with the Skyrme potential [see Eq. (VII.18.24) in deShalit and Feshbach (74)] which leads to (VII.18.29) in the same reference for the single-particle Hamiltonian $H(\mathbf{r})$. Most of the calculations do not keep the spin-orbit terms, while the terms in the gradient of the density are replaced by a Yukawa-type interaction. The exchange properties of the last are chosen so that the resulting potential is local. Finally, one notes that (VII.18.29) of deShalit and Feshbach (74) is correct only for a stationary system such as the ground state. For moving system, (VII.18.29) of the same reference is written in a Galilean invariant form. This means that terms like ρT , where T is the kinetic energy density $\sum |\nabla \psi_v|^2$, are replaced by $\rho T - J^2$ where,

$$\mathbf{J} = \sum_v \text{Im} [\psi_v^* \nabla \psi_v] \quad (8.18)$$

The resulting single-particle Hamiltonian is

$$\begin{aligned} H = \int H(\mathbf{r}) d(\mathbf{r}) = \int d(\mathbf{r}) \left\{ \frac{\hbar^2}{2m} (T_n + T_p) + \frac{1}{2} t_0 [(2 + x_0) \rho_n \rho_p + \frac{1}{2} (1 - x_0) (\rho_n^2 + \rho_p^2)] \right. \\ \left. + \frac{1}{4} (t_1 + t_2) [(\rho_n + \rho_p)(T_n + T_p) - (\mathbf{J}_n + \mathbf{J}_p)^2] \right. \\ \left. + \frac{1}{8} (t_2 - t_1) [\rho_n T_n - J_n^2 + \rho_p T_p - J_p^2] + \frac{1}{4} t_3 (\rho_n \rho_p^2 + \rho_p \rho_n^2) \right\} \\ + \frac{1}{2} v_L [E_y(\rho_n, \rho_n) + E_y(\rho_p, \rho_p)] + v_u E_y(\rho_n, \rho_p) + C(\rho_p, \rho_p) \quad (8.19) \end{aligned}$$

TABLE 8.1 Parameters of the Effective Hamiltonian Density [Eq. (8.19)]

	SK II	SK III	Local
$t_0(\text{MeV}\cdot\text{fm}^3)$	-104.49	-333.47	-497.726
x_0	4.01	1.743	0
$t_1(\text{MeV}\cdot\text{fm}^5)$	585.6	395.6	0
$t_2(\text{MeV}\cdot\text{fm}^5)$	-27.1	-95.0	0
$t_3(\text{MeV}\cdot\text{fm}^6)$	9331.0	14,000.0	17,270.0
$v_L(\text{MeV})$	-444.85	-355.79	-363.044
$v_u(\text{MeV})$	-868.63	-619.60	-363.044
$\mu(\text{fm}^{-1})$	2.175	2.175	2.175
m^*/m	0.58	0.76	1

Source: Negele (82).

The quantities E_y and C are defined as follows:

$$E_y(\rho_a, \rho_b) = \iint d\mathbf{r} d\mathbf{r}' \frac{e^{-\mu|\mathbf{r}-\mathbf{r}'|}}{|\mathbf{r}-\mathbf{r}'|} \rho_a(\mathbf{r}) \rho_b(\mathbf{r}') \quad (8.20)$$

$$C(\rho_p, \rho_p) = \frac{1}{2} e^2 \iint d\mathbf{r} d\mathbf{r}' \frac{\rho_p(\mathbf{r}) \rho_p(\mathbf{r}')}{|\mathbf{r}-\mathbf{r}'|}$$

The parameters of this Hamiltonian are to $t_0, t_1, t_2, t_3, v_L, v_u$, and μ . The parameters [see discussion in deShalit and Feshbach (74, p. 626)] are fixed by the volume, surface, symmetry energies, and the value of the effective mass, m^* . The value of the parameters are listed in Table 8.1 for these variants of the Skyrme potential.

The Hamiltonian governing the evolution of the single-particle wave function will have the form [see (VII.18.33) in deShalit and Feshbach (74)]

$$-\nabla \cdot \frac{\hbar^2}{2m^*} \nabla + U(\mathbf{r}) + \frac{1}{2i} (\nabla \cdot \mathbf{I} + \mathbf{I} \cdot \nabla)$$

where m^* , U , and \mathbf{I} depend on the densities and currents present in (8.19). A list of the calculations done with each of the forces above is given by Negele (82).

We turn next to the initial conditions obtained when the ions are far apart. Each ion is described by a Slater determinant. The single-particle wave functions are given by solutions of the Hartree-Fock equations boosted to the initial velocity of the ion. If the solutions of the Hartree-Fock equations are $\psi_v^0(\mathbf{r})$ with energy ε_v , the boosted initial wave function is

$$\psi_v^{(i)}(\mathbf{r}, t) = e^{-i\hbar(\varepsilon_v + E/A)t} e^{i(\mathbf{K}/A) \cdot \mathbf{r}} \psi_v^{(0)}(\mathbf{r} - \mathbf{v}t) \quad (8.21)$$

where E is the kinetic energy of the ion and $\hbar\mathbf{K}$ is its momentum. The density matrix and potential energy transform as follows:

$$\rho^{(i)}(\mathbf{r}, \mathbf{r}', t) = e^{i\mathbf{K}/A \cdot (\mathbf{r} - \mathbf{r}')} \rho^{(0)}(\mathbf{r} - \mathbf{v}t, \mathbf{r}' - \mathbf{v}t) \quad (8.22a)$$

and

$$V^{(i)}(\mathbf{r}, \mathbf{r}', t) = e^{i\mathbf{K}/A \cdot (\mathbf{r} - \mathbf{r}')} V^{(0)}(\mathbf{r} - \mathbf{v}t, \mathbf{r}' - \mathbf{v}t) \quad (8.22b)$$

The Slater determinant formed using $\psi_v^{(i)}$ cannot be factorized into a wave function, depending only on the center-of-mass coordinate and a wave function, depending only on coordinates relative to the center of mass, \mathbf{R} . The latter wave function will also depend on \mathbf{R} . However, it vanishes when \mathbf{R} is outside the ion. Therefore, one is dealing with a center-of-mass wave packet $2R$ in diameter, where R is the nuclear radius. The corresponding spread in the center-of-mass momentum is

$$\Delta p_{\text{cm}} = \frac{\hbar}{2R}$$

and the spread in energy is

$$\frac{\Delta E}{E} = \frac{\hbar}{R(2mAE)^{1/2}}$$

For an oxygen beam whose energy is 2 MeV/A, $\Delta E/E = 0.07$, suggesting that the results of the TDHF approximation for light projectiles has a limited validity.

A. Collision of Semi-infinite Slabs

The collision of two semi-infinite slabs of finite thickness permits great calculational simplifications. In addition, slab collisions permit a clear-cut study of the behavior of the longitudinal degrees of freedom. This is especially instructive because in the fully three-dimensional collisions the coupling between longitudinal and transverse motion proves to be weak.

The single-particle wave functions are of the form $f(x, y)\phi_n(z, t)\chi_{\tau\sigma}$, where χ is a spin-isospin wave function. When $f(x, y)$ is a plane wave, $\exp(i\mathbf{k}_\perp \cdot \mathbf{r})$, where $\hbar\mathbf{k}_\perp$ is the transverse momentum, the function, $\phi_n(z, t)$ satisfies, as indicated, a one-dimensional time-dependent Schrödinger equation. The interaction potential $v(\mathbf{r}, \mathbf{r}')$ is given by

$$v(\mathbf{r}, \mathbf{r}') = t_0 \delta(\mathbf{r} - \mathbf{r}') + \frac{1}{6} t_3 \delta(\mathbf{r} - \mathbf{r}') \rho(\mathbf{r}) + V_0 \frac{e^{-\mu|\mathbf{r} - \mathbf{r}'|}}{\mu|\mathbf{r} - \mathbf{r}'|} \left(\frac{16}{15} + \frac{4}{15} P_x \right) \quad (8.23)$$

where P_x is the space-exchange operator. The combination $(\frac{16}{15} + \frac{4}{15} P_x)$ is chosen

so that the resulting mean field, $V(z, t)$, is local and has no spin or isospin dependence. Substituting in (8.4) yields

$$V(z, t) = \frac{3}{4}t_0\rho(z, t) + \frac{3}{16}t_3\rho^2(z, t) + 2\pi\frac{V_0}{\mu^3}\int_{-\infty}^{\infty} dz'\rho(z', t)e^{-\mu|z-z'|} \quad (8.24)$$

and

$$i\hbar\frac{\partial\phi_n}{\partial t} = -\frac{\hbar^2}{2m}\frac{\partial^2\phi_n}{\partial z^2} + V(z, t)\phi_n \quad (8.25)$$

Initially ($t = 0$, not boosted), ϕ_n is the self-consistent Hartree-Fock solution of

$$\epsilon_n\phi_n^{(0)} = -\frac{\hbar^2}{2m}\frac{d^2}{dz^2}\phi_n^{(0)} + V(z)\phi_n^{(0)} \quad (8.26)$$

To complete (8.25) and (8.26) an expression for $\rho(z, t)$ in terms of ϕ_n is needed.

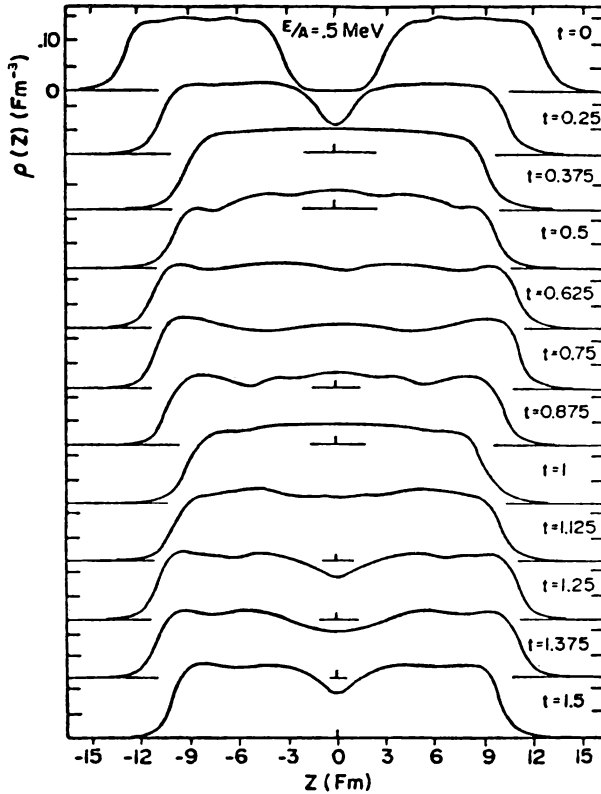


FIG. 8.1. Density distributions for $E/A = 0.5$ MeV [From Negele (78).]

We begin with (8.10). Initially [not boosted; see (8.22)],

$$\rho^{(0)}(z) = \sum_n |\psi_\mu^{(0)}(\mathbf{r}, t)|^2 = 4 \sum_n \int \frac{d\mathbf{k}_\perp}{(2\pi)^3} \rho(\mathbf{k}_\perp) |\phi_n^{(0)}(z)|^2$$

The integration on \mathbf{k}_\perp covers the range from ε_n to ε_F , the Fermi energy, with the result

$$\rho^{(0)}(z) = \sum_n A_n |\phi_n^{(0)}(z)|^2 \quad (8.27)$$

where

$$A_n = \frac{2m}{\pi\hbar^2} (\varepsilon_F - \varepsilon_n) \quad (8.28)$$

Since there is no coupling between the transverse and longitudinal modes, $\rho(z, t)$,

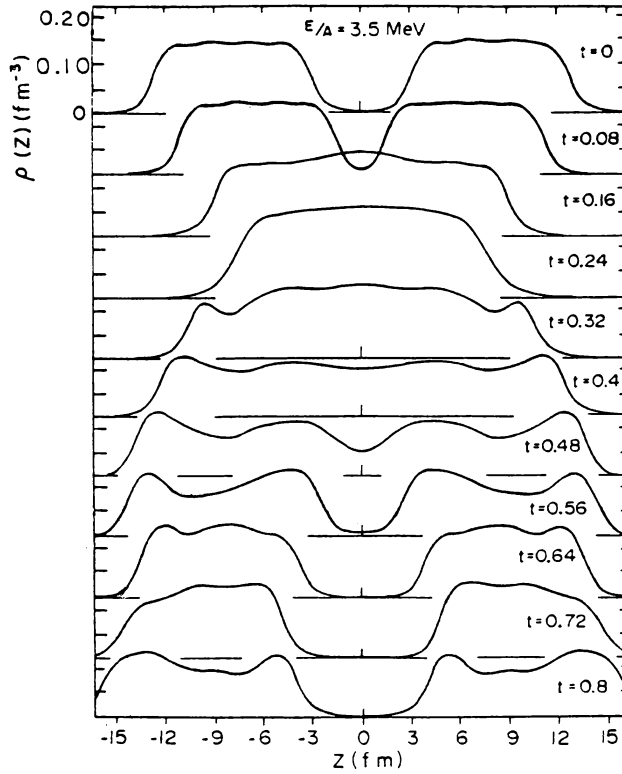


FIG. 8.2. Density profiles $\rho(z, t)$ at sequential times t , specified in units of 10^{-21} s, for a cm energy $E/A = 3.5$ MeV. [From Negele (82).]

as needed for the calculation of $V(z, t)$, (8.24), is

$$\rho(z, t) = \sum A_n |\phi_n(z, t)|^2 \quad (8.29)$$

The initial conditions are obtained by boosting the wave functions appropriately [see (8.21) et seq.]. The solutions are obtained by numerical integration of (8.25) using (8.29). In the calculations to be reported below, the constants used are taken from the “local” column in Table 8.1. These yield a nuclear matter density of 15.77 MeV per particle at $k_F = 1.29 \text{ fm}^{-1}$.

Figures 8.1, 8.2, and 8.3 give the density profiles as a function of time for the incident energies 0.5, 3.5 and 25 MeV/A. In the first (Fig. 8.1), fusion is indicated. In Fig. 8.2 the two slab pass through each other, but the final states of both systems are highly excited. In the high-energy case, fragmentation occurs. A detailed examination of these examples reveals two phenomena: (1) because the collision modifies the relative phases, the original coherence of the single-particle wave functions is destroyed; and (2) strong dissipation occurs. The second is related to the first since the destruction of the coherence characteristic of the ground state leads inevitably to excitation, so that some of the initial kinetic energy is converted into excitation energy. The large loss of kinetic energy is shown in Fig. 8.4. There are some energies, for example, near $E/A = 2 \text{ MeV}$, for which the energy loss is reduced. The loss of coherence occurs because the changing mean field affects each single-particle wave function differently, as can be seen from Fig. 8.5. Importantly, one sees that although two-body collisions are not included, the variety of phenomena, especially the large dissipation observed in heavy-ion collisions, is reproduced by the TDHF.

B. Collision of Realistic Systems

The integration of the time-dependent single-particle equations obtained from (8.19) by varying ψ_v^* is a formidable task. One must keep track of $(A_1 + A_2)$ complex numbers in a $(3 + 1)$ -dimensional space. Simplifications in addition to those already described are essential for a programmatic study of many cases. As we shall see, these involve restricting the functional dependence of the single-particle wave functions, effectively decreasing the number of degrees of freedom of the system. Such constraints will reduce the dissipation and increase the time required to establish equilibrium. With this caveat in mind we shall now proceed to describe two simplifications commonly used. [See Davies, Devi, Koonin, and Strayer (84) and Negele (82) for a more complete discussion of these and other methods.]

One procedure reduces the dimensionality to $2 + 1$ dimensions by assuming axial symmetry. In the “clutching” model [Koonin, Davies, et al. (77)], the single-particle wave functions are taken to be

$$\psi_\mu(\mathbf{r}) = \chi_\mu(r, z) e^{im_\mu \phi} \quad (8.30)$$

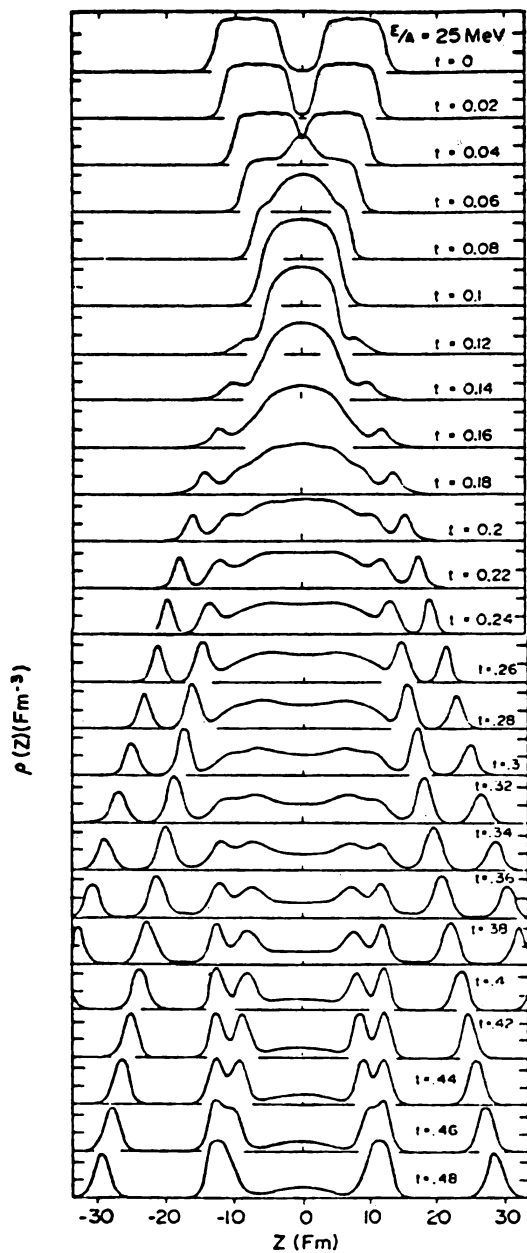


FIG. 8.3. Density profiles as a function of time for center-of-mass energy $E/A = 25 \text{ MeV}$. [From Negele (78).]

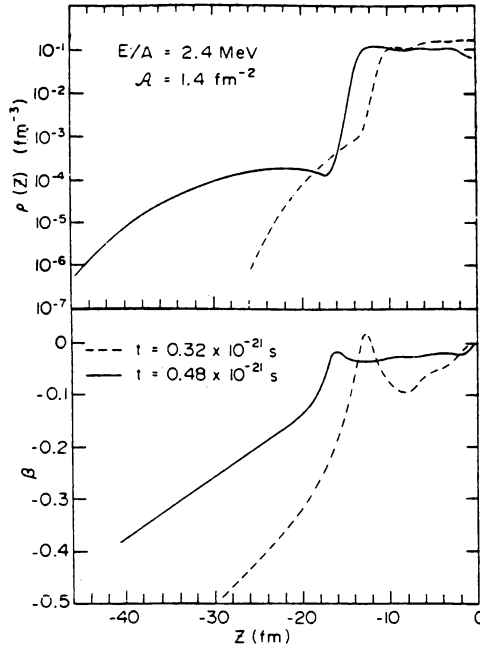


FIG. 8.4. Density profiles and velocity distributions for separating slabs showing particle emission. Only the left-hand plane is shown for this symmetric collision. The velocity is specified by $\beta = v/c$. [From Negele (82).]

In this equation cylindrical coordinates are used, the symmetry axis is along z , and $\hbar m_\mu$ is the angular momentum around the symmetry axis. The single-particle time-dependent equation for ψ_μ now reduces to an equation for χ_μ . The wave functions ψ_μ are regarded as intrinsic wave functions of a rotator as in the Bohr–Mottelson–Nilsson mode. One must add to the Hamiltonian of (8.1) the rotational energy in the form $L^2/2\mathcal{I}(\rho)$, where L is the initial angular momentum, a constant of the motion, and $\mathcal{I}(\rho)$ is the moment of inertia. The rotation is about an axis perpendicular to the reaction plane. The moment of inertia is taken to be that of two point masses a distance R apart when the colliding nuclei are not overlapping:

$$\mathcal{I}_{\text{point}} = m \frac{A_1 A_2}{A_1 + A_2} R^2$$

When the nuclei overlap (taken to be when the overlap density is one-half the saturation density), the rigid moment of inertia is used, that is,

$$\mathcal{I}_{\text{rigid}} = 2\pi \int \int dr dz (z^2 + r^2) \rho(r, z)$$

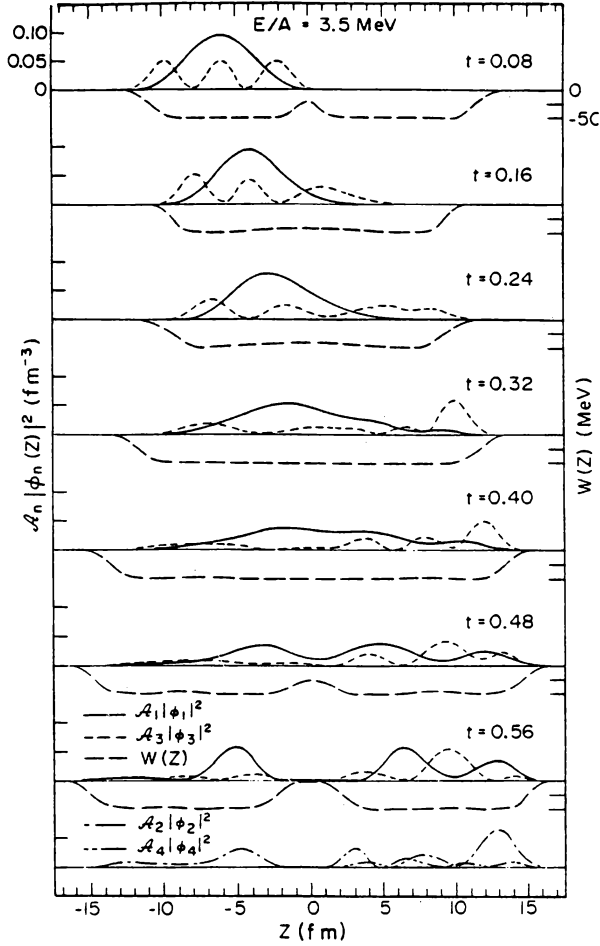


FIG. 8.5. Contributions of individual single-particle wave functions for the collision shown in Fig. 8.2. In the upper graphs, the mean field is denoted by the long-dashed line, with the scale shown to the right. The contributions to the density of the lowest orbital and third orbital originating in the left slab are indicated by the solid and short-dashed lines, respectively. The bottom graph displays the contributions of the second and fourth orbitals at the final time. [From Negele (82).]

In a second procedure referred to as the “2D frozen approximation” [Devi and Strayer (78), Koonin, Flanders, et al. (78)], it is assumed that ψ_μ can be written

$$\psi_\mu(\mathbf{r}, t) = \varphi_\mu(x, y, t) \chi_\mu(z) \quad (8.31)$$

This approximation is based on the presumption that most of the dynamical effects occur in the reaction plane, that is, that there is little change in the z

dependence of ψ_μ with time. This *ansatz* is borne out by the few three-dimensional calculations that have been performed. The function χ_μ is chosen at $t = 0$ to be a harmonic oscillator wave function whose scale is chosen so as to minimize the Hartree-Fock energy for the separated nuclei. This model has an important advantage over the clutching model in that it permits the excitation of nonaxially symmetric modes, thereby permitting more possibilities for energy dissipation and a more rapid approach to fusion and equilibration.

A further approximation, the “filling approximation”, is made with respect to open-shell nuclei whose Hartree-Fock states would show a high degeneracy. For these cases the expression for ρ (at $t = 0$) given by (8.10) is replaced by

$$\rho^{(0)} = \sum_{\mu} n_{\mu} \psi_{\nu}(\mathbf{r}, 0) \psi_{\nu}^*(\mathbf{r}', 0) \quad (8.32)$$

where n_{μ} are the fractional occupation probabilities. This quantity is adjusted so that the resultant mean field is spherically symmetric; that is, $n_{\mu} = 1$ for filled shells and equal to $m/2(2l + 1)$ for a shell of orbital angular momentum l containing m particles. Moreover, these probabilities are assumed to be time dependent.

The TDHF theory provides a microscopic understanding of the macroscopic parameters described in Sections 1 to 5. Good qualitative understanding or agreement is obtained for the most part. There are discrepancies. For example, the experimental values of the widths of the charge and mass distributions are very much larger than the TDHF values. Cross sections cannot be obtained, as that would involve calculating the matrix elements of a many-body operator. The TDHF method is accurate for the matrix elements of one-body operators. In view of the approximation made, more precise methods for evaluating their validity and in estimating the theoretical error on the TDHF calculations are needed. At the present time, tests are made by comparing the results obtained using, for example, the models described above with each other and/or with three-dimensional calculations for various cases, colliding nuclei, energy, and angular momentum.

We consider fusion first. A good example is shown in Fig. 8.6. More generally, a fusion event is defined as “one in which the coalesced one-body density survives through at least one rotation or several oscillations of its rms radius” [Davies, Devi, Koonin, and Strayer (84)]. The fusion cross section is defined by the equation

$$\sigma_{\text{CF}} = \frac{\pi}{\kappa^2} \sum_{l_m}^{l_M} (2l + 1) = \frac{\pi}{\kappa^2} [(l_M + 1)^2 - (l_m + 1)^2] \quad (8.33)$$

Note that this equation differs from (2.5) in that it leaves open the possibility that the orbital angular momenta from $l = 0$ to $l = l_m - 1$ do not contribute to the fusion cross section. For a given reaction, the values of l_M and l_m are determined by interpolating TDHF calculations for various values of l .

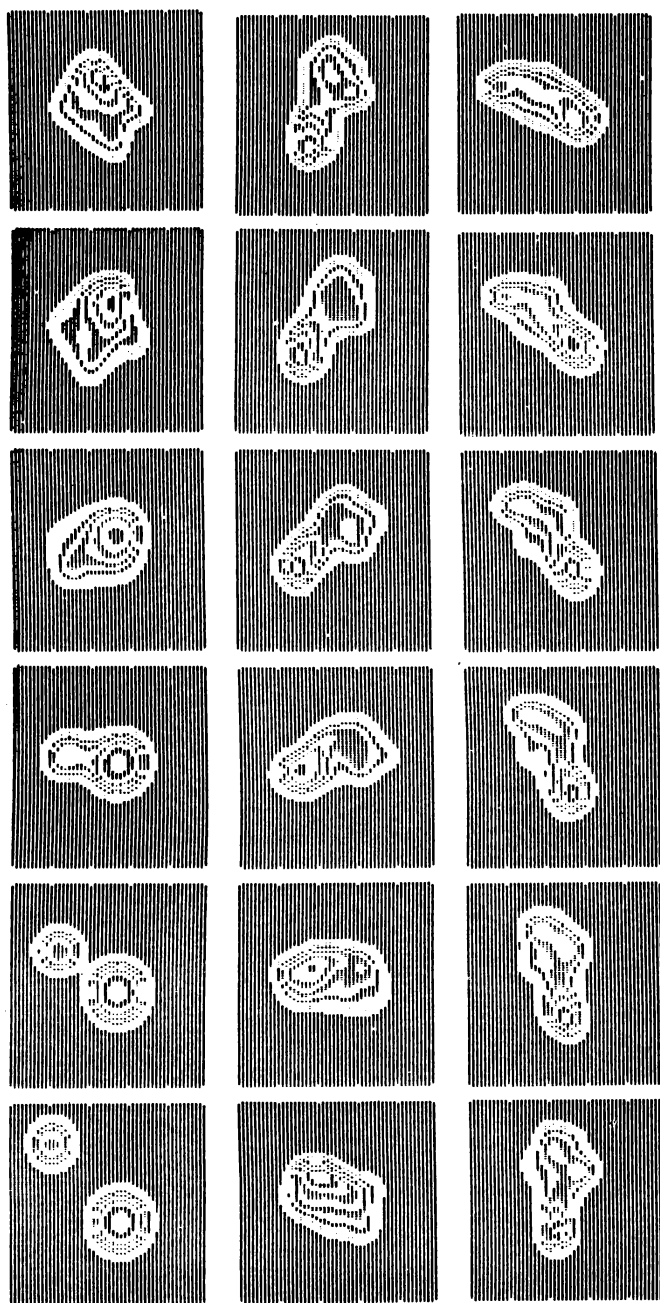


FIG. 8.6. Contour plots at sequential times of the density in the center-of-mass integrated over the normal to the reaction plane for $^{16}\text{O} + ^{40}\text{Ca}$ collision at a laboratory energy of 315 MeV. The initial angular momentum is 60 \hbar . [From Negele (82).]

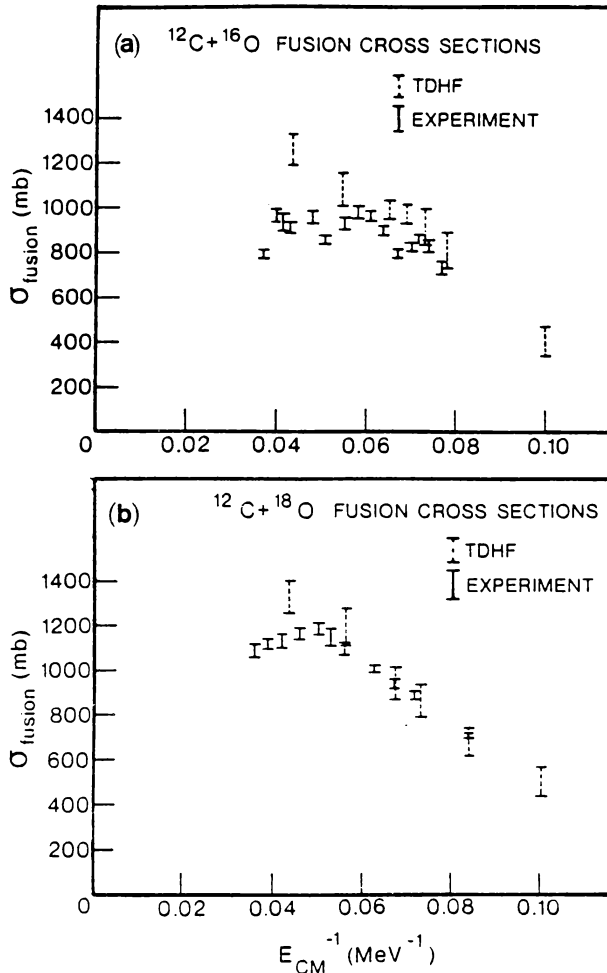


FIG. 8.7. Fusion excitation functions for (a) $^{12}\text{C} + ^{16}\text{O}$ and (b) $^{12}\text{C} + ^{18}\text{O}$ collisions are compared with the experimental data. [From Krieger and Davies (79).]

TABLE 8.2

System	$(l_M)_{\text{max}}$	
	TDHF	Liquid Drop
$^{16}\text{O} + ^{16}\text{O}$	31	32
$^{16}\text{O} + ^{27}\text{Al}$	45	43
$^{16}\text{O} + ^{24}\text{Mg}$	42	42
$^{16}\text{O} + ^{40}\text{Ca}$	62	58
$^{28}\text{Si} + ^{28}\text{Si}$	50	58
$^{40}\text{Ca} + ^{40}\text{Ca}$	≥ 60	67
$^{16}\text{O} + ^{93}\text{Nb}$	≥ 77	86

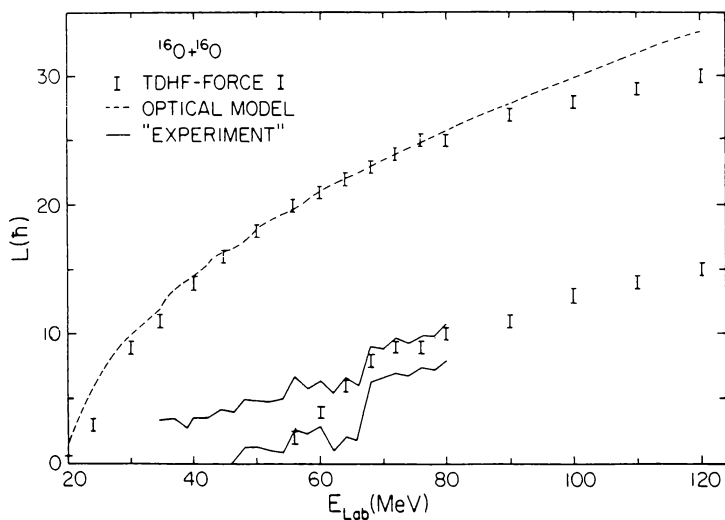


FIG. 8.8. Angular momentum limits to fusion for $^{16}\text{O} + ^{16}\text{O}$ collisions. Also shown in the upper angular momentum limit extracted from the optical model total reaction cross section and the "experimental" lower limit. [From Bonche et al. (78).]

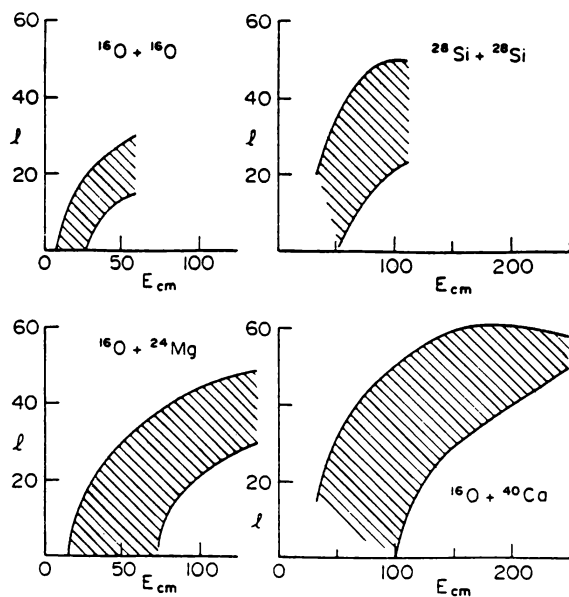


FIG. 8.9. Fusion regions, indicated by shaded areas, specifying the ranges of initial angular momentum l in units of \hbar and center-of-mass energy, E_{cm} , in MeV for which the TDHF initial value problem leads to a final state interpreted as a fused compound system. [From Negele (82).]

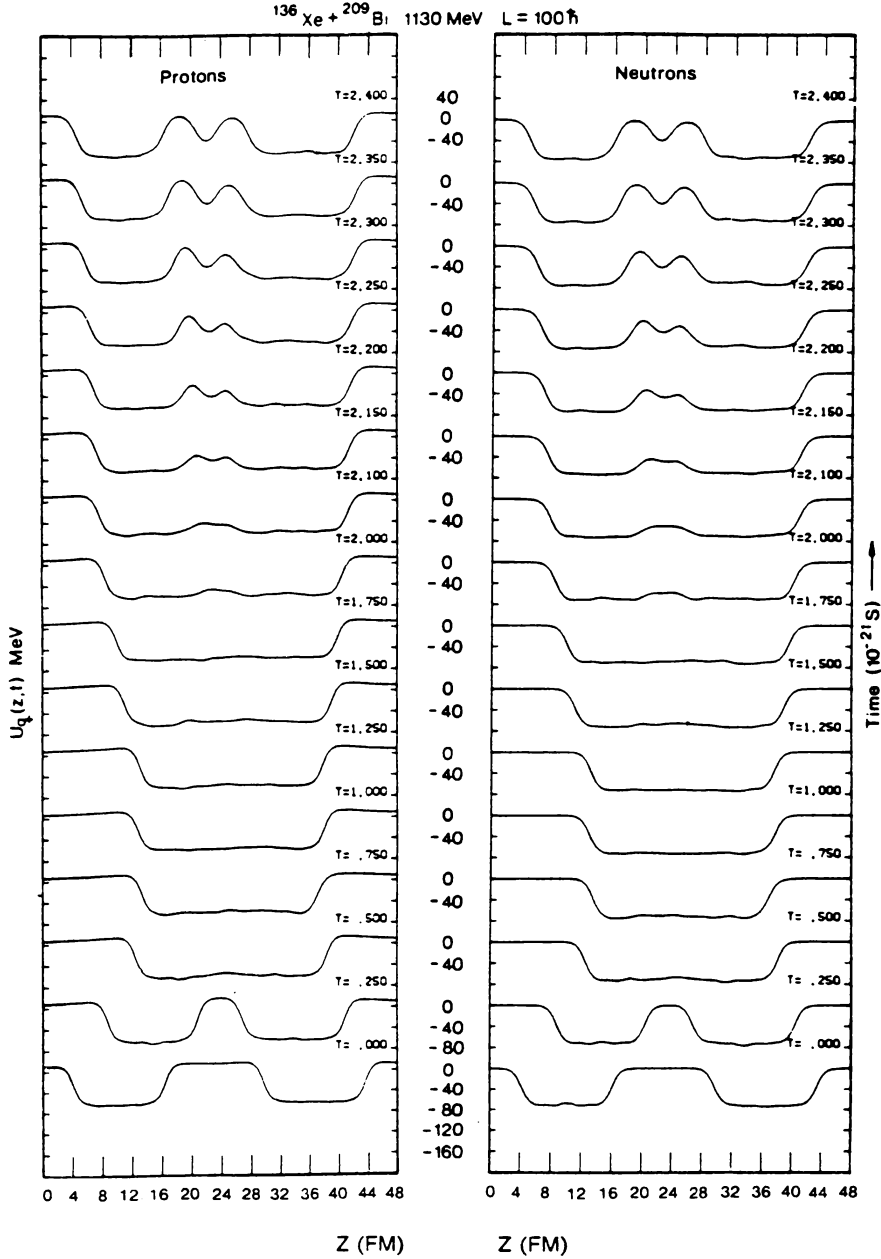


FIG. 8.10. Time evolution of the proton and neutron Hartree-Fock potentials along the symmetry axis for $^{136}\text{Xe} + ^{209}\text{Bi}$ at $E_{\text{lab}} = 1130 \text{ MeV}$ and $l = 100$. [From Dhar, Nelson, Davies, and Koonin (81).]

An example of the agreement of experiment with theory is illustrated in Fig. 8.7. One notes the linear dependence on $1/E$ in agreement with (2.7), permitting a determination of the macroscopic parameters R_B and V_B of that equation. This is shown in more detail in Fig. 8.8, where the value of l_M using (2.6) is plotted against the TDHF results. In Table 8.2 we compare the maximum value of l_M as a function of energy beyond which fusion does not occur (as discussed in Section 2, the compound nucleus cannot sustain higher values of l_M) with the values obtained from the liquid-drop model [Cohen, Plasil and Swiatecki (74)].

One of the surprising results obtained in TDHF calculations is the existence of a minimum value of l , l_m of (8.33) which is greater than zero. This is referred to as the *angular momentum window*. This is illustrated in Fig. 8.9.

We turn next to deep inelastic collisions. We restrict the discussion to heavy nuclei, for in those cases the collision is dominated by the deep inelastic process, as fusion is highly improbable. Consider the collision of ^{136}Xe with ^{209}Bi at a laboratory energy of 1130 MeV (about 8.3 MeV/A). The time evolution of the TDHF proton and neutron potentials along the symmetry axis for $l = 100$ is shown in Fig. 8.10. We see the merging of the two potential wells to form a

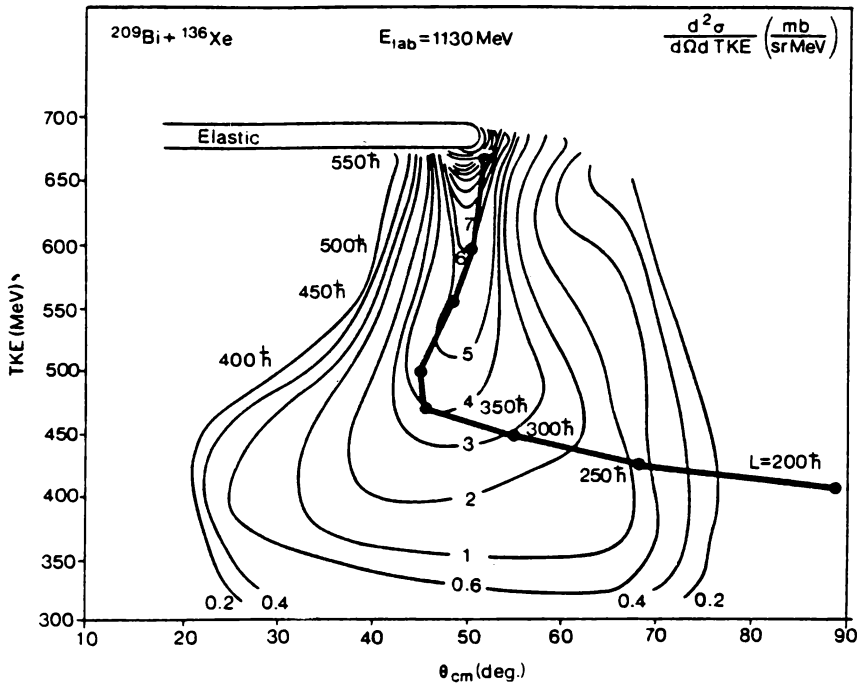


FIG. 8.11. Comparison of calculated points with the experimental Wilczyński plot for $^{136}\text{Xe} + ^{209}\text{Bi}$ at $E_{\text{lab}} = 1130 \text{ MeV}$. The calculated points for various initial orbital angular momenta are connected by a full line. [From Dhar, Nelson, Davies, and Koonin (81).]

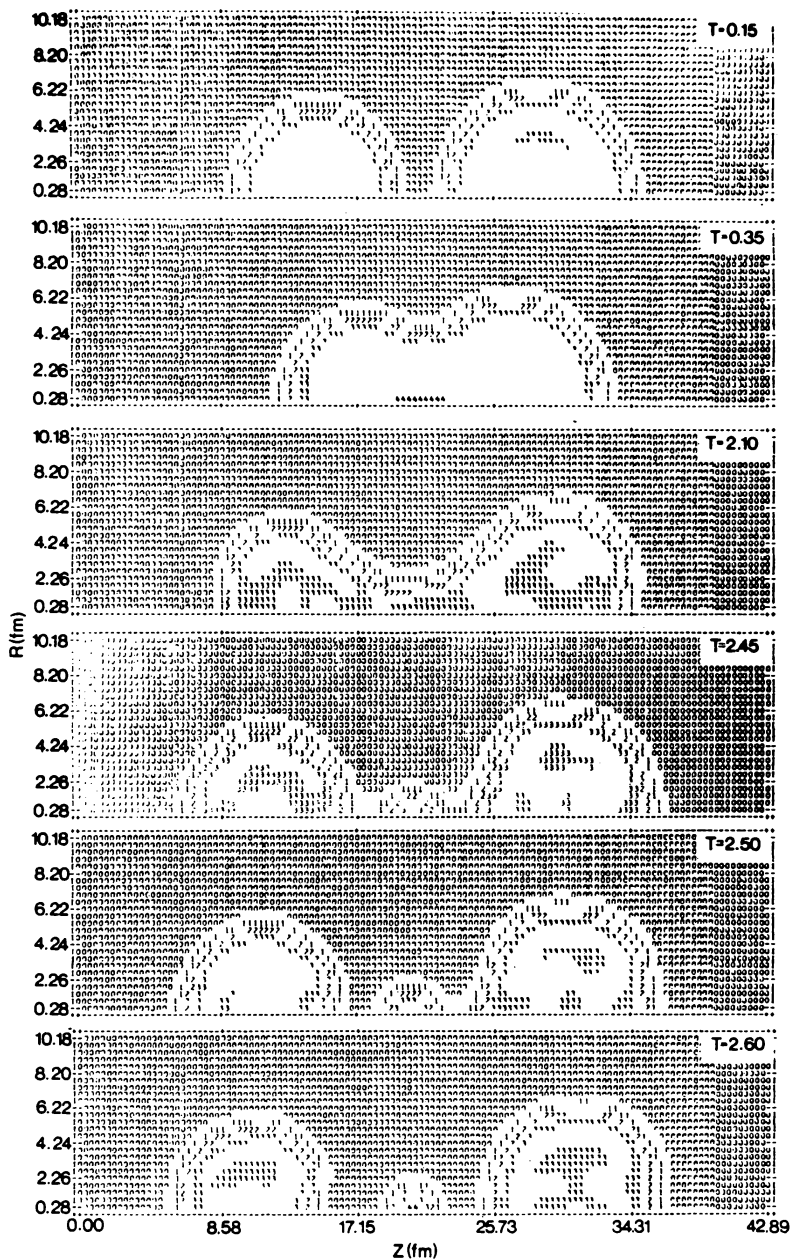


FIG. 8.12. Equidensity contours at various times during a $^{86}\text{Kr} + ^{139}\text{La}$ collision at $E_{\text{lab}} = 710$ MeV and $l = 100$. The symmetry axis lies along the line joining the mass centers of the projectile and target. All times are in units of 10^{-21} s. [From Davies, Sandhya Devi, and Strayer (79).]

common well and then the reformation of the original two wells plus an additional well. More about this later. A popular way of summarizing the experimental data is the Wilczyński plot, in which the cross section contours are plotted in the total kinetic energy, and θ_{cm} plane. Such a plot is shown in Fig. 8.11. The TDHF calculations are given by the connected points, which plot the total kinetic energy versus the scattering angle. Each impact parameter (indicated by l) in a TDHF calculation yields a point on this line. It is presumed that the line will follow the ridge of the cross section contours. We see the characteristic very rapid drop on kinetic energy followed by a slower rate of decrease. We also observe that the TDHF energy loss at “small” l is not as large as the experimental results require. This is a common failure of the TDHF calculation (and the charge and mass distribution mentioned above). However, apart from this problem, the TDHF results are in semiquantitative agreement with experiment. One feature should be noted—namely, that there is a large interchange of target and projectile nucleons. One may also use the calculations to compare with the macroscopic phenomenology of Nix and Sierk discussed in Section 2. These authors introduce the coordinates R , measuring the separation of the ions, and σ , the elongation.

The TDHF calculation predicts the early emission of neutrons in the process. This occurs because the projectile nucleon energy in the common well (see Fig. 8.10) exceeds the Fermi plus binding energy. A more unexpected phenomenon is the production of an α -particle at scission. This is illustrated in Fig. 8.12. Returning to Fig. 8.10, we note the formation of three wells at 2.4×10^{-21} s. The well in the center governs the evolution of the α -particle.

The TDHF method thus provides good insight into the dynamics of the low-energy heavy-ions collisions. Its major failure is that it does not provide a method for the calculation of cross sections.

CHAPTER IX

HIGH-ENERGY NUCLEAR PHENOMENA

1. INTRODUCTION

In this chapter we consider reactions induced by projectiles whose energy per particle is in the GeV or sub-GeV range. The projectiles are, for the most part, electrons and protons, although there will be some discussion of relativistic heavy-ion projectiles. The phenomena discussed includes elastic, inelastic, and quasi-elastic scattering and, in the case of relativistic heavy ions, fragmentation. The production of bosons with various values of hypercharge and their interaction with nuclei will be left to Chapter X. These areas of physics, those in this and the next chapter, are referred to as *medium-energy nuclear physics*.

High energy translates into high momentum and short wavelength. Because of the short wavelength and relatively weak interaction of the electrons, high-energy electron accelerators are effectively electron microscopes, studying the nucleus and, at sufficiently high energy, the structure of the individual nucleons. As we shall describe, through the use of electron scattering, we are able to obtain a detailed understanding of the spatial distribution of charge and current in the target nucleus. It should be emphasized that such results can be obtained only because the properties of the probe, the electron, and its interaction with the electromagnetic field in this case generated by the target nucleus as given by quantum electrodynamics are so very well known.

In more detail, the matrix elements of nuclear charge and current can be directly related to the nuclear multipole moments. These are of two types, the Coulomb and the transverse electric and magnetic. The latter also occur in the description of photon emission [see deShalit and Feshbach (74, p. 689)] with identical selection rules (deShalit and Feshbach (74, p. 670)). The selection rules

associated with the Coulomb multipole moments are the same as those for the transverse electric multipoles. The information obtained from electron scattering is much richer than that which can be extracted from photon-induced transitions. In the latter case, there is only one independent variable, the energy transfer ω in units of \hbar , whereas in electron scattering there are two, the energy transfer and the momentum transfer q in units of \hbar . Of course, momentum transfer does occur in the case of photon reactions. But its magnitude is ω/c . In electron scattering the momentum transfer and the energy transfer are not coupled; q can differ from ω/c by several orders of magnitude. Electron scattering thus yields the q dependence of both the transverse and Coulomb multipole moments, and by Fourier inversion their spatial dependence. One is thus able to map the charge and current distribution experimentally and compare them with the predictions of theoretical models.

In particular, the transverse moments that measure the nuclear current distribution are, according to the shell model, sensitive to the wave functions of the valence neutrons and protons. This follows from the fact that the net current generated by the core is zero. On the other hand, note that the Coulomb moments are sensitive only to the proton distribution. Fortunately, by choosing appropriate kinematic conditions it is possible to measure separately the transverse and Coulomb moments.

These results assume that the nuclear charge and current operators are one-body operators, given by (VII.2.1)–(VII.2.4) in deShalit and Feshbach (74). This is an approximation, as there are two-body terms as well, such as those given by exchange currents and exchange charge [see Section VIII.3 in deShalit and Feshbach (74)]. Before claiming the observation of exchange currents, one must use sufficiently accurate nuclear wave functions in the evaluation of the nuclear matrix elements. For example, the independent particle description must be supplemented by configuration interactions [Chapter V in deShalit and Feshbach (74)] and by correlations (Chapter III and VII of the same reference). In some cases, those in which the spin–isospin ($\sigma\tau$) transitions dominate, the excitation of the nucleons to Δ 's may be important.

Because of the high energy, the electron can excite states in the continuum, such as isobar analog states and the giant resonances. Because of the associated high momentum, one can study multipoles of high order and one can form stretched nuclear states. Because of their high energy the electrons can eject one or more nucleons from the target. The underlying process, quasi-elastic scattering, is the collision between the electron and nucleon in the nucleus. Its cross section peaks at an energy transfer ω for large enough q at $q^2/2m^* + \varepsilon$, where m^* is the nucleon's effective mass and ε is its binding energy. In a Fermi gas model the width of the quasi-elastic peak is $k_F q/m^*$ (see I.3.9). Removing a nucleon in an $(e, e'p)$ or (γ, p) experiment may permit a determination of the momentum distribution of a single-particle state and the lifetime of a deep one-hole state. At still higher energies the electron can excite the individual nucleon, forming the nucleon isobar Δ , which can decay by emitting a pion. Direct pion production without the intermediary of a Δ will also occur. These

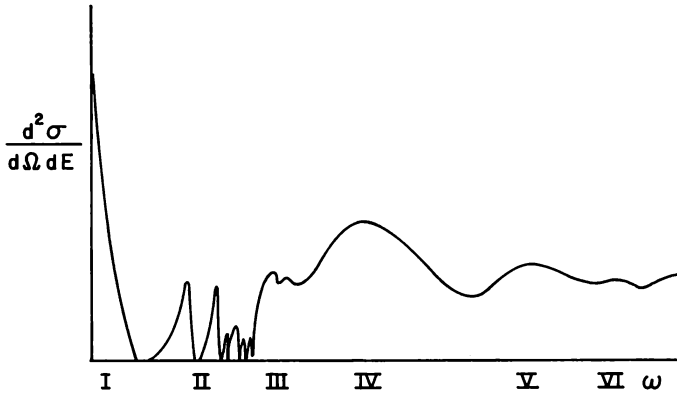


FIG. 1.1. Schematic electron energy loss spectrum. Region I, elastic scattering; II, excitation of discrete levels; III, excitation of giant resonances; IV, quasi-elastic scattering; V, pion production and Δ formation; VI, N^* formation.

various possibilities are shown in Fig. 1.1, which schematically pictures the electron spectrum at a given q .

When an electron is scattered by a nucleus, there is a high probability that it will also emit a photon. As a consequence of this energy loss, the elastic and inelastic scattering cross sections will exhibit a tail on the low-energy side, usually referred to as a radiative tail. The observed cross section will, in addition, depend on the energy resolution, ΔE , of the detector since it will count electrons that have radiated photons whose energy is less than ΔE . These effects can be calculated with great accuracy [Schwinger (49b)] and the experimental cross section unfolded to yield the radiation-free cross section. It is this corrected cross section that is usually quoted in the experimental papers. Figure 1.1 is qualitatively correct only in this sense. Otherwise, the gaps between levels as shown in Fig. 1.1 would be partially filled in. An experimental example is shown in Fig. 1.2. The radiative corrections are thoroughly described by Überall (71).

As this is being written, electron scattering studies are entering a new era in which it is anticipated important advances in our understanding of nuclei will be obtained. Up to recently, the electron accelerators had a low duty cycle. As a consequence, some experiments were difficult. The new CW ($\sim 100\%$ duty cycle) accelerators, some already available and others under construction, will make greatly improved coincidence measurements possible as well as make available tagged and thereby monochromatic γ -ray beams. In addition, there is the prospect of polarized electrons and polarized internal jet nuclear targets. With coincidence experiments one can reduce the radiative tail background enormously (see Fig. 1.3).

With these new tools it becomes possible experimentally to measure the individual multipole moment amplitudes separately. With the low-duty-cycle accelerators, a complicated model-dependent analysis is necessary. It will also

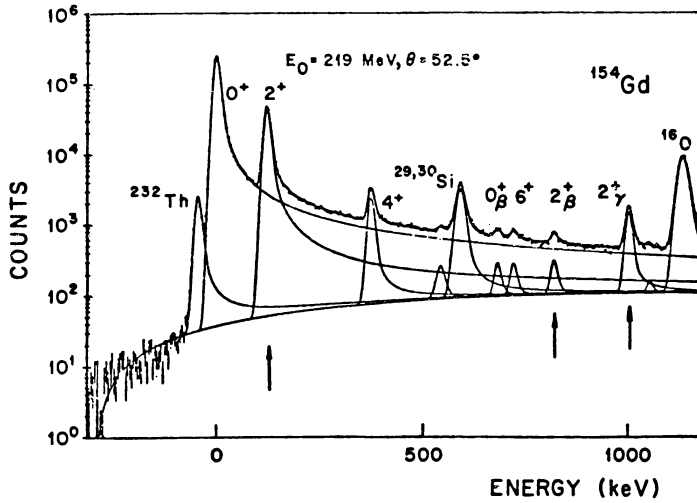


FIG. 1.2. Sample electron excitation spectrum for ^{154}Gd . The incident electron energy is 219 MeV. The scattered electron is observed at 52.5° . [From Bates Linear Accelerator proposal (84).]

become possible to observe the particle emission from giant resonances and make improved measurements on deep one-hole and stretched states.

The experimental studies undertaken with high-energy protons are very similar in character to those described above using electrons. Elastic and inelastic scattering, including excitation of discrete levels, of the giant resonances of one-hole and stretched states, Δ and pion production have been observed. Polarized beams have also been used. There is, of course, one very great difference: namely, the interactions in the proton case are “strong” and not completely known. One must rely on multipole scattering theory (Chapter II), in which proton–nucleus interaction is approximated by an optical potential V . In its simplest first-order form, V in momentum space is given by

$$V(\mathbf{k}, \mathbf{k}') = (A - 1)\hat{\rho}(-\mathbf{q})\hat{t}_E(\mathbf{q}) \quad (1.1)$$

where $\hat{\rho}$ is the nucleon density operator and $\hat{t}_E(\mathbf{q})$ is the transition matrix operator for nucleon–nucleon scattering. The vector \mathbf{q} is the momentum transfer (\mathbf{k} , initial momentum, \mathbf{k}' final momentum). The function t_E is evaluated at the center-of-mass energy of the nucleon–nucleus system with due regard for the transformation from the nucleon–nucleon system (see II.7). The discussion in this chapter will rely on (1.1).

By taking matrix elements of V , the appropriate potentials for various experimental situations can be obtained. For elastic scattering

$$V_{00} \equiv \langle 0 | V | 0 \rangle = (A - 1) \langle 0 | \hat{\rho} \hat{t}_E | 0 \rangle \quad (1.2)$$

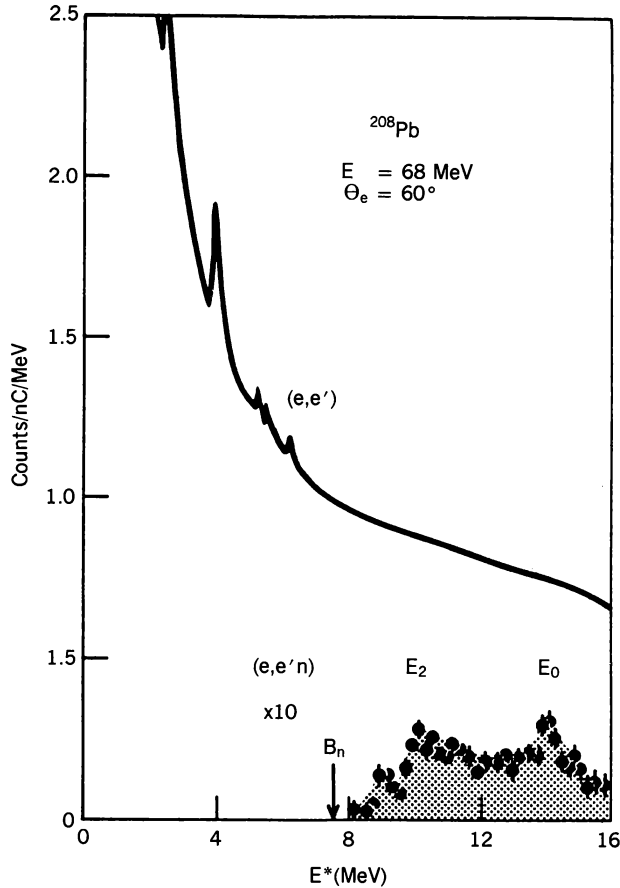


FIG. 1.3. Single arm and coincident $(e, e'n)$ spectra from ^{208}Pb . The coincidence condition removes the radiative tail, revealing the excitation of giant resonances. [From Frois and Papanicolas (87).]

where $|0\rangle$ is the ground-state nuclear wave function. For inelastic scattering to a level $|f\rangle$, the transition potential is

$$V_{f0} = (A - 1) \langle f | \hat{\rho} \hat{t} | 0 \rangle \quad (1.3)$$

Since \hat{t} depends on the spin and isospin operators, V_{00} and V_{f0} will depend on various spin and isospin components of the elastic and transition density, respectively. These combinations differ from the electron case, so that nucleon-nucleus scattering provides information which complements that obtained from electron scattering.

Equation (1.1) is a first approximation to V . Higher-order approximations

involving higher powers of ϑ have been obtained. These depend on correlation functions.

2. ELECTRON SCATTERING

Let us begin with some kinematics. The incident electron with four momentum $k_\mu(\mathbf{k}, E)$ is scattered through an angle ϑ . We shall work in units with $\hbar = c = 1$. Its final momentum is $k'_\mu(\mathbf{k}', E')$. The three momentum transfer is \mathbf{q} :

$$\mathbf{q} = \mathbf{k} - \mathbf{k}'$$

while the energy transfer is ω :

$$\omega = E - E'$$

The magnitude of \mathbf{q} is

$$q^2 = (k^2 - 2kk' \cos \vartheta + k'^2) \xrightarrow{k=k'} 4k^2 \sin^2 \frac{1}{2} \vartheta \quad (2.1)$$

Since the electron energy will be very much greater than its rest mass, $k = E$ and $k' = E'$. In this limit

$$q^2 = \omega^2 + 4EE' \sin^2 \frac{1}{2} \vartheta \quad (2.2a)$$

and

$$q_\mu^2 = q^2 - \omega^2 = 4EE' \sin^2 \frac{1}{2} \vartheta \geq 0 \quad (2.2b)$$

For elastic electron scattering, the target nucleus will recoil with a momentum q , so that

$$\omega = (q^2 + M^2)^{1/2} - M \quad (2.3)$$

where M is the mass of the target (m_A). Transposing M to the left-hand side of this equation and squaring yields

$$\omega = \frac{1}{2M} q_\mu^2 \quad (2.4)$$

In (2.2b) replace E' by $E - \omega = E - (1/2M)q_\mu^2$. Solving for q_μ^2 yields

$$q_\mu^2 = \frac{1}{f_{\text{rec}}} (4E^2 \sin^2 \frac{1}{2} \vartheta) \quad (2.5)$$

where

$$f_{\text{rec}} = 1 + \frac{2E}{M} \sin^2 \frac{1}{2} \vartheta \quad (2.6)$$

From (2.3)

$$q^2 = (2\omega M) \left(1 + \frac{\omega}{2M} \right) \quad (2.7)$$

and finally from (2.4) and (2.6), we obtain

$$E' = \frac{E}{f_{\text{rec}}} \quad (2.8)$$

In the forward direction ($\vartheta = 0$), E' equals E .

A. Elastic Scattering from Spin-Zero Nuclei

The modern era in electron scattering was initiated by R. Hofstadter by his studies of the elastic scattering of electrons by spin-zero nuclei. This is perhaps the most highly studied process involving electrons. Very great accuracy has been achieved. To start with, we assume that the nucleus is describable by a static (time-independent) charge distribution $\rho(\mathbf{r})$. The resulting electrostatic potential, ϕ , is the solution of the Poisson equation:

$$\nabla^2 \phi = -4\pi\rho \quad (2.9)$$

In momentum space

$$\phi = \frac{4\pi\rho(\mathbf{q})}{q^2} \quad (2.10)$$

where

$$\rho(\mathbf{q}) = \int e^{i\mathbf{q}\cdot\mathbf{r}} \rho(\mathbf{r}) d\mathbf{r} \quad (2.11)$$

We shall discuss the Born approximation to the scattering produced by ϕ . It is of course necessary to employ the relativistic Dirac equation:[†]

$$[\gamma_\mu(p_\mu - eA_\mu) - im]\psi = 0 \quad (2.12)$$

[†]In the rest of this chapter \hbar and c will be placed equal to unity. The four-vector p_μ has components (\mathbf{p}, E) , where \mathbf{p} is the momentum and E is the energy. Similarly, \mathbf{A} is the vector potential, $A_4 = i\phi$. Finally

$$\boldsymbol{\gamma} = \rho_2 \boldsymbol{\sigma} \quad \text{where } \rho_2 = \begin{pmatrix} 0 & -i \\ i & 0 \end{pmatrix}$$

The summation convention is used in this equation. For the situation under study, (2.1) becomes

$$(\gamma_\mu p_\mu - im)\psi = ie\gamma_4\phi\psi$$

Multiplying by $(\gamma_\mu p_\mu + im)$, we obtain

$$(p^2 - E^2 + m^2)\psi = ie(\gamma_\mu p_\mu + im)\gamma_4\phi\psi$$

or

$$(\nabla^2 + k^2)\psi = -ie(\gamma_\mu p_\mu + im)\gamma_4\phi\psi \quad (2.12')$$

so that the scattering amplitude operator, \hat{f} , is

$$\hat{f} = \frac{ie}{4\pi} \int e^{-ik'\cdot r} (\gamma_\mu p_\mu + im)\gamma_4\phi\psi_i^{(+)} d\mathbf{r} \quad (2.13)$$

Or integrating by parts, we have

$$\hat{f} = \frac{ie}{4\pi} (\gamma_\mu k'_\mu + im)\gamma_4 \int e^{-ik'\cdot r} \phi\psi_i^{(+)} d\mathbf{r} \quad (2.13')$$

where $k'_4 = iE$. In the Born approximation

$$\psi_i \longrightarrow e^{ik\cdot r} u_i \quad (2.14)$$

so that

$$\gamma = \begin{pmatrix} 0 & -i\sigma \\ i\sigma & 0 \end{pmatrix} \quad \alpha = \begin{pmatrix} 0 & \sigma \\ \sigma & 0 \end{pmatrix}$$

In this last equation σ are the two-row/two-column Pauli spin matrices. The matrix γ_4 is

$$\gamma_4 = \begin{pmatrix} 1 & 0 \\ 0 & -1 \end{pmatrix}$$

The γ 's satisfy

$$\gamma_\mu \gamma_\nu + \gamma_\nu \gamma_\mu = 2\delta_{\mu\nu}$$

The trace of products of the γ 's are [see (IX.11.22) in deShalit and Feshbach (74)]

$$\text{tr} 1 = 4$$

$$\text{tr} \gamma_\mu \gamma_\nu = 4\delta_{\mu\nu}$$

$$\text{tr}(\gamma_\mu \gamma_\nu \gamma_\lambda \gamma_\omega) = 4[\delta_{\mu\nu} \delta_{\lambda\omega} - \delta_{\mu\lambda} \delta_{\nu\omega} + \delta_{\mu\omega} \delta_{\nu\lambda}]$$

The trace of an odd number of γ 's is zero. For more details, see the appendix to Chapter IX and p. 825 et seq. in deShalit and Feshbach (74).

where u_i is a four-element columnar matrix given by (5.8) and (5.9) of the Appendix to Chapter IX in deShalit and Feshbach (74). These are *positive energy* solutions of the field-free Dirac equation with spin up and spin down, respectively. Introducing (2.14) into (2.13'), one obtains

$$\hat{f} = \frac{ie}{4\pi}(\gamma_\mu k'_\mu + im)\gamma_4 u_i \phi(\mathbf{q}) \quad (2.15)$$

Employing (2.10) for $\phi(\mathbf{q})$, \hat{f} becomes

$$\hat{f} = \frac{ie}{q^2}(\gamma_\mu k'_\mu + im)\gamma_4 u_i \rho(\mathbf{q}) \quad (2.16)$$

The amplitude is thus linearly related to the Fourier transform of the charge density. The scattering amplitude to a given final state is

$$f_{fi} = \frac{ie\rho(\mathbf{q})}{q^2} \langle u_f(\gamma_\mu k'_\mu + im)\gamma_4 u_i \rangle$$

To obtain the cross section, one must square the magnitude of f_{fi} , sum over all final spin states, and average over the initial ones:

$$\sigma = \frac{1}{2} \sum_{f,i} |f_{fi}|^2 \quad (2.17)$$

One can reduce the calculation of σ to the evaluation of a trace by using the projection operator P on the positive energy. This operator has been derived in deShalit and Feshbach (74, p. 825, et seq.). It is

$$P = \frac{1}{2iE}(\gamma_\mu k_\mu + im)\gamma_4 \quad (2.18)$$

so that (2.17) becomes

$$\frac{d\sigma}{d\Omega} = \frac{1}{2} \text{tr}(\hat{f}^\dagger P_f \hat{f} P_i) \quad (2.19)$$

where the subscript i , for example, indicates that in (2.18), k_μ equals the incident momentum and energy. Inserting \hat{f} from (2.16), (2.19) becomes

$$\frac{d\sigma}{d\Omega} = -\frac{e^2 |\rho(\mathbf{q})|^2}{q^4 8E^2} \text{tr}[\gamma_4(\gamma_\mu k'_\mu - im)(\gamma_\nu k'_\nu + im)\gamma_4(\gamma_\lambda k'_\lambda + im)\gamma_4(\gamma_\omega k'_\omega + im)\gamma_4] \quad (2.20)$$

The γ_4 's at the beginning and end of this expression cancel. The trace can then

be readily evaluated using the results in the footnote on page 686. One obtains

$$\frac{d\sigma}{d\Omega} = \frac{2e^2 |\rho(\mathbf{q})|^2}{q^4} (\mathbf{k} \cdot \mathbf{k}' + E^2 + m^2) = |e\rho(\mathbf{q})|^2 \frac{1 - \beta^2 \sin^2 \frac{1}{2}\vartheta}{(2\beta^2 E \sin^2 \frac{1}{2}\vartheta)^2} \quad (2.21)$$

where $\beta = v/c$. The charge density ρ_0 of a zero-radius-point nucleus is

$$\rho_0(\mathbf{r}) = Ze\delta(\mathbf{r})$$

so that

$$\rho_0(\mathbf{q}) = Ze$$

The resulting cross section divided by Z^2 is referred to as the *Mott cross section* σ_M :

$$Z^2 \sigma_M = (1 - \beta^2 \sin^2 \frac{1}{2}\vartheta) \frac{(Ze^2)^2}{(2\beta^2 E \sin^2 \frac{1}{2}\vartheta)^2} \quad (2.22)$$

$$\xrightarrow{\beta \rightarrow 1} \frac{(Ze^2)^2 \cos^2 \frac{1}{2}\vartheta}{(2E \sin^2 \frac{1}{2}\vartheta)^2} \quad (2.23)$$

These results hold in the center-of-mass system or if the target mass M is infinite. In the laboratory frame, the recoil of the target must be taken into account. Repeating the calculation above in the laboratory frame leads to (2.21), which, however, must be multiplied by k'/k or ε'/ε in the zero-electron-mass limit. Then using (2.8), one obtains

$$\frac{d\sigma}{d\Omega} = \frac{1}{f_{\text{rec}}} \sigma_M |\rho(\mathbf{q})|^2 \quad (2.24)$$

This Born approximation result is valid at best for light nuclei. By a measurement of elastic electron scattering, one can in principle determine the *charge* density distribution. But there are several corrections. The most obvious is the effect of the nuclear Coulomb field on the electron wave functions. Therefore, the plane wave approximation for the electron wave functions used above is incorrect, especially for the large Z nuclei. Second, the calculation above is incomplete since it includes only the elastic scattering produced by the nuclear charge distribution. Scattering produced by the nuclear currents and magnetization are not accounted for. Finally, there are the effects of virtual inelastic scattering on the elastic scattering. These are referred to as *dispersion corrections*.

B. Coulomb Scattering

The wave functions for an electron moving in the Coulomb field of a point nucleus have been described in deShalit and Feshbach (74, pp. 915–916). As in

that review, let the Dirac wave function ψ be a two-element matrix, each element of which is a spinor

$$\psi = \begin{pmatrix} u \\ v \end{pmatrix} \quad (2.25)$$

The wave functions u and v for the state with a given angular momentum, j , are products of a radial function and a function giving the spin and angle dependence:

$$u(j, l) = \frac{G(r)}{r} \mathcal{Y}_m(j, l) \quad (2.26a)$$

$$v(j, l) = \frac{f(r)}{r} (-i\boldsymbol{\sigma} \cdot \hat{\mathbf{r}}) \mathcal{Y}_m(j, l) \quad (2.26b)$$

where

$$\mathcal{Y}_m(j, l) = \sum (\tfrac{1}{2}m_s, lm_l | jm) \chi_{1/2}(m_s) \mathcal{Y}_{lm_l} \quad (2.27)$$

The spin wave function is $\chi_{1/2}$, while $\mathcal{Y}_{lm_l} = i^l Y_{lm}$, where Y_{lm} is a spherical harmonic.

The equations satisfied by f and G for an arbitrary radial potential $V(r)$ are

$$(E - m - V)G + \frac{df}{dr} - \kappa \frac{f}{r} = 0 \quad (2.28a)$$

$$-(E + m - V)f + \frac{dG}{dr} + \kappa \frac{G}{r} = 0 \quad (2.28b)$$

where

$$\kappa = -[1 + \boldsymbol{\sigma} \cdot \mathbf{L}] = \begin{cases} (j + \frac{1}{2}), & l = j + \frac{1}{2} \\ -(j + \frac{1}{2}), & l = j - \frac{1}{2} \end{cases} \quad \text{or} \quad \kappa = \begin{cases} l \\ -(l + 1) \end{cases}$$

The exact solutions are given in deShalit and Feshbach (74, p. 916) in terms of the confluent hypergeometric function. We quote here only the behavior of G and f as $r \rightarrow 0$ and $r \rightarrow \infty$.

$$G(r \rightarrow 0) \rightarrow (\varepsilon + 1)^{1/2} N_s \cos \phi_s(2kr)^s \quad (2.29a)$$

$$f(r \rightarrow 0) \rightarrow (\varepsilon - 1)^{1/2} N_s \sin \phi_s(2kr)^s \quad (2.29b)$$

$$G(r \rightarrow \infty) \rightarrow (\varepsilon + 1)^{1/2} \cos \left[kr + \eta \log 2kr - \frac{\pi}{2}(l + 1) + \delta_{\kappa}^{(c)} \right] \quad (2.30a)$$

$$f(r \rightarrow \infty) \rightarrow -(\varepsilon - 1)^{1/2} \sin \left[kr + \eta \log 2kr - \frac{\pi}{2}(l + 1) + \delta_{\kappa}^{(e)} \right] \quad (2.30b)$$

where

$$\begin{aligned} s &= \sqrt{(j + \frac{1}{2})^2 - (Ze^2)^2} & \eta &= Ze^2 \frac{E}{k} & \varepsilon &= \frac{E}{m} \\ e^{2i\phi_s} &= -\frac{\kappa - i(Ze^2)m/k}{s + i\eta} & N_s &= \frac{|\Gamma(s + 1 + i\eta)|}{\Gamma(2s + 1)e^{-\eta\pi/2}} \\ e^{2i\delta_{\kappa}^{(e)}} &= -\frac{\kappa + iZe^2m/k}{s - i\eta} \frac{\Gamma(s + 1 - i\eta)}{\Gamma(s + 1 + i\eta)} e^{\pi/2 i(l + 1 - s)} \end{aligned} \quad (2.31)$$

Using these results, Mott (29, 32) expressed the cross section for the scattering of an electron by a nucleus in terms of two conditionally convergent infinite series. To first order in $Ze^2\beta$, these series can be summed [McKinley and Feshbach (48)] to yield:

$$\sigma = \left(\frac{Ze^2}{2\beta^2 E \sin \frac{1}{2}\vartheta} \right)^2 \left[1 - \beta^2 \sin^2 \frac{\vartheta}{2} + \pi Ze^2\beta \sin \frac{\vartheta}{2} \left(1 - \sin \frac{\vartheta}{2} \right) \right] \quad (2.32)$$

To obtain the results for positron scattering, replace Z by $(-Z)$. This result is useful for sufficiently light nuclei. For larger values of Z , numerical methods are required. Tables are given by McKinley and Feshbach (48), Feshbach (52), and Curr (55). Yennie et al. (55) improve the convergence by multiplying the Mott series by $(1 - \cos \vartheta)^3$ and employing the Legendre function recurrence relation to reorder the series.

C. Effect of Finite Size of the Nucleus

The results above are obtained by using $V = -Ze^2/r$ in (2.28). Taking the charge structure of the nucleus into account requires replacing it by the solution of the Poisson equation (2.10). For spin-zero nuclei the resulting V is a function of r only. For $r > R$ (the nuclear radius) V will approach the point Coulomb value. The solutions of (2.28) are obtained in the usual fashion, that is, by joining the solutions of (2.28) to the Coulomb wave functions for $r > R$. Asymptotically, this means replacing $\delta_{\kappa}^{(e)}$ in (2.30) by δ_{κ} . Note also that the singularity exhibited by the Coulomb wave functions at $r = 0$ for $j = \frac{1}{2}$ [see (2.29)] disappears when the finite size of the nucleus is taken into account. The wave function now approaches r^{l+1} . The scattering amplitude is given by Acheson (51):

$$\hat{f} = f(\vartheta) + ig(\vartheta)\boldsymbol{\sigma} \cdot \mathbf{n} \quad (2.33)$$

where

$$\mathbf{n} = \hat{k} \times \hat{k}'$$

and

$$f(\vartheta) = \frac{1}{2ik} \sum_{\kappa > 0} \kappa [e^{2i\delta_\kappa} P_\kappa(\cos \vartheta) + e^{2i\delta_{-\kappa}} P_{\kappa-1}(\cos \vartheta)] \quad (2.34a)$$

and

$$g(\vartheta) = -\frac{1}{2ik} \sum_{\kappa > 0} [e^{2i\delta_\kappa} P_\kappa^{(1)}(\cos \vartheta) - e^{-2i\delta_{-\kappa}} P_{\kappa-1}^{(1)}(\cos \vartheta)] \quad (2.34b)$$

where according to (2.28), κ equals l , and $-\kappa = -(l+1)$. The functions $P_\kappa^{(1)}(\cos \vartheta)$ are the associated Legendre functions

$$P_\kappa^{(1)}(x) = (1-x^2)^{1/2} \frac{d}{dx} P_\kappa(x)$$

The elastic cross section for an unpolarized incident electron beam averaged over the final spin is

$$\sigma = |f|^2 + |g|^2 \quad (2.35)$$

The polarization produced by the scattering of an unpolarized beam is

$$\mathbf{P} = \frac{1}{\sigma} \text{tr} \langle \hat{f}^\dagger \boldsymbol{\sigma} f \rangle = \frac{i(f^* g - g f^*)}{|f|^2 + |g|^2} \mathbf{n} \quad (2.36)$$

so that the polarization of the electrons is perpendicular to the scattering plane.

Simplifications do occur in the limit of $m/E \rightarrow 0$; that is, in the high-energy limit, (2.28) reduces to

$$(E-V)G + f' - \frac{\kappa f}{r} = 0$$

$$(E-V)f - G' - \frac{\kappa G}{r} = 0$$

For $\kappa = -l$,

$$(E-V)G_l + f'_l + \frac{l f_l}{r} = 0$$

$$(E-V)f_l - G'_l + \frac{l G_l}{r} = 0$$

For $\kappa = l$, we have

$$(E-V)G_{-l} + f'_{-l} - \frac{l f_{-l}}{r} = 0$$

$$(E-V)f_{-l} - G'_{-l} - \frac{l G_{-l}}{r} = 0$$

Comparing the (G_l, f_l) equations with those for (G_{-l}, f_{-l}) , we see that these equations become identical if

$$\begin{aligned} G_{-l} &= f_l \\ f_{-l} &= -G_l \end{aligned} \quad (2.37)$$

From the asymptotic forms, (2.30), with $\delta_\kappa^{(c)}$ replaced by δ_κ , it follows that [Feshbach (51)]

$$\begin{aligned} \delta_l &= \delta_{-(l+1)} \\ \text{or} \\ \delta_\kappa &= \delta_{-\kappa} \quad \frac{m}{E} \rightarrow 0 \end{aligned} \quad (2.38)$$

This result holds for the Coulomb phase shift (2.31), from which one finds that

$$e^{2i[\delta_{-\kappa}^{(c)} - \delta_\kappa^{(c)}]} \simeq 1 - \frac{Ze^2m}{k\kappa} \quad (2.39)$$

For the energies of interest ($k \gg m$), the error is indeed small. Equation (2.38) is obviously computationally useful. Inserting (2.38) into (2.34b) and using

$$P'_\kappa - P'_{\kappa-1} = \kappa(P_\kappa + P_{\kappa-1}) \tan \frac{1}{2}\vartheta$$

we obtain

$$g(\vartheta) = (\tan \frac{1}{2}\vartheta) f(\vartheta)$$

so that

$$\sigma = \sec^2 \frac{1}{2}\vartheta |f(\vartheta)|^2 \quad (2.40)$$

and

$$\mathbf{P} \rightarrow 0 \quad (2.41)$$

Therefore, the polarization produced by the scattering tends to zero as the energy increases.

In the high-energy limit it is useful to obtain an eikonal approximation for the wave function. We return to (2.12') to the Schrödinger equation from

$$(\nabla^2 + k^2)\psi = U\psi$$

where

$$U = -ie(\gamma_\mu p_\mu + im)\gamma_4\phi \quad (2.42)$$

The eikonal solution to the Schrödinger equation has been given in Chapter II

[Eq. (II.5.7)]:

$$\psi = \exp \left\{ i \left[kz + \int_{-\infty}^z dz' (\sqrt{k^2 - U} - k) \right] \right\} u$$

or

$$\simeq \left\{ \exp i \left[kz - \frac{1}{2k} \int_{-\infty}^z U dz' \right] \right\} u \quad (2.43)$$

In this equation u is a spinor. Consistent with the eikonal approximation, we drop the m term in (2.42) and replace the operator p_u by k_u . This introduces a new condition for the validity of the results to be obtained below:

$$\frac{\nabla \phi}{k \phi} \ll 1 \quad (2.44)$$

This condition is very well satisfied for an extended nuclear charge density. Note that this last approximation need not be made. The analysis that follows can be carried through with $\gamma_\mu k_\mu \phi$ replaced by $\gamma_\mu k_\mu \phi + (1/i) \boldsymbol{\gamma} \cdot \nabla \phi$. With these approximations, ψ becomes

$$\psi \simeq \left\{ \exp \left[i \left(kz + \frac{ie}{2k} (\gamma_\mu k_\mu) \gamma_4 \int_{-\infty}^z \phi dz \right) \right] \right\} u \quad (2.45)$$

Rewriting $(\gamma_\mu k_\mu) \gamma_4 = i(E + \boldsymbol{\alpha} \cdot \mathbf{k})$, one needs to evaluate

$$e^{i(\boldsymbol{\alpha} \cdot \mathbf{k})A}$$

where A does not involve spinor operators. One finds that

$$e^{i(\boldsymbol{\alpha} \cdot \mathbf{k})A} = \cos kA + i \boldsymbol{\alpha} \cdot \hat{\mathbf{k}} \sin kA$$

This is to operate in u . We assume that because the electron energy is high, u satisfies

$$\boldsymbol{\alpha} \cdot \hat{\mathbf{k}} u = u \quad (2.46)$$

so that

$$e^{i(\boldsymbol{\alpha} \cdot \mathbf{k})A} = e^{ikA}$$

Finally, then

$$\begin{aligned} \psi &\simeq \left\{ \exp \left[i \left(kz - \frac{k+E}{2k} \int_{-\infty}^z e \phi dz' \right) \right] \right\} u \\ &\simeq \left\{ \exp i \left(kz - \int_{-\infty}^z e \phi dz' \right) \right\} u \end{aligned} \quad (2.47)$$

One can now insert this result into the exact equation (2.13) to obtain the scattering amplitude. The discussion from here on follows that of Ch. II [see after (VII.5.7)] and need not be repeated here.

A further approximation to (2.47) is often made. It recognizes the fact that because of the Coulomb attraction, the electron momentum increases as it approaches the nucleus. To estimate this, expand the integral in (2.47) as follows:

$$\int_{-\infty}^z \phi dz' \sim \int_{-\infty}^0 \phi dz' + z\phi(z=0, \mathbf{p}) + \dots$$

Hence, for a given impact parameter ρ , the effective value of k is

$$k_{\text{eff}}(\mathbf{p}) = k \left(1 - \frac{e\phi(0, \mathbf{p})}{k} \right) \quad (2.48)$$

In many applications of this result, a still cruder approximation is used:

$$k'_{\text{eff}} \sim k \left(1 - \frac{e\phi(0, 0)}{k} \right) \quad (2.47')$$

For the case of a homogeneous charge distribution of radius R ,

$$\phi = -\frac{Ze}{R} \left(\frac{3}{2} - \frac{1}{2} \frac{r^2}{R^2} \right), \quad r < R$$

this becomes

$$k'_{\text{eff}} \sim k \left(1 + \frac{3Ze^2}{2kR} \right)$$

We turn next to effects of the structure of the nucleons. The protons have a finite size [see deShalit and Feshbach (74, p. 110)]. As a consequence, we must replace (VIII.2.1) of that reference by the charge density:

$$\hat{\rho}_{\text{ch}}(\mathbf{r}) = \sum_i f(\mathbf{r} - \mathbf{r}_i) \quad (2.49)$$

where the function f replaces the point charge $\delta(\mathbf{r} - \mathbf{r}_i)$. The sum is over the protons only. The charge density then becomes

$$\rho_{\text{ch}}(\mathbf{r}) = \langle \psi | \hat{\rho}(\mathbf{r}) | \psi \rangle = Z \int \rho_N(\mathbf{r}_0) f(\mathbf{r} - \mathbf{r}_0) d\mathbf{r}_0 \quad (2.50)$$

where

$$\rho_N(\mathbf{r}_0) = \int \psi^*(\mathbf{r}_0, \mathbf{r}_1, \dots) \psi(\mathbf{r}_0, \mathbf{r}_1, \dots) d\mathbf{r}_1 d\mathbf{r}_2 \dots$$

The form factor $\rho_{\text{ch}}(\mathbf{q})$ is

$$\rho_{\text{ch}}(\mathbf{q}) = Z \rho_N(\mathbf{q}) F(\mathbf{q}) \quad (2.51)$$

Thus to obtain the nuclear form factor ρ_N , one must divide the form factor determined from experiment $\rho_{\text{ch}}(\mathbf{q})$ by $F(\mathbf{q})$, the form factor of the proton:

$$F(\mathbf{q}) = \int e^{i\mathbf{q}\cdot\mathbf{r}} f(\mathbf{r}) d\mathbf{r}$$

A second effect originates in the interaction of the moving anomalous magnetic moment of a nucleon with an electrostatic field. That such an interaction exists can immediately be understood by transforming to the rest frame of the nucleon. Under such a transformation the electron–nucleon electrostatic field acquires a magnetic field component that will interact with nucleon magnetic moment. An interaction with the electrostatic field can, in this case, be interpreted in terms of an effective charge possessed by the nucleon. This effect was explored by Schwinger (49a) in his discussion of the polarization resulting from the interaction of a neutron with a nucleus. We now discuss its application to electron scattering.

We begin with the matrix element of the current operator for a nucleon [Bjorken and Drell (64)]:

$$\langle \mathbf{p}' \lambda' | \hat{J}_\mu(0) | \mathbf{p} \lambda \rangle = \bar{u}_{\lambda'}(\mathbf{p}') \left(F_1 \gamma_\mu + \frac{\kappa}{2M} F_2 \sigma_{\mu\nu} q_\nu \right) u_\lambda(\mathbf{p}) \quad (2.52)$$

where F_1 and F_2 are form factors that are functions of q^2 , κ is the anomalous magnetic moment, and λ gives the helicity. The spinors $u_\lambda(\mathbf{p})$ are four-element matrices whose helicity is indicated by λ . The derivation of (2.52) follows the procedures employed in deShalit and Feshbach (74, p. 846 et seq). The spinors are given in the Appendix to Chapter IX of that reference, Eqs. (5.8)–(5.10). They can be represented by

$$u_\lambda = \left(\frac{E+M}{2E} \right)^{1/2} \begin{pmatrix} 1 & 0 \\ \frac{\boldsymbol{\sigma} \cdot \mathbf{p}}{E+M} & 0 \end{pmatrix} \chi_\lambda \quad (2.53)$$

where χ_λ is $\begin{pmatrix} \alpha \\ 0 \end{pmatrix}$ or $\begin{pmatrix} 0 \\ \beta \end{pmatrix}$, according to the value of λ . Here M is the nucleon mass. Inserting (2.53) into (2.51) and remembering that $\bar{u} = u^\dagger \gamma_4$, one obtains for the charge operator ($\mu = 4$),

$$\langle \mathbf{p}' \lambda' | \hat{\rho}(0) | \mathbf{p} \lambda \rangle \simeq -i \chi_{\lambda'}^\dagger \left[F_1 - \left(\frac{q^2}{8M} + i \frac{\mathbf{q} \cdot \boldsymbol{\sigma} \times \mathbf{p}}{4M^2} \right) (F_1 + 2\kappa F_2) \right] \chi_\lambda \quad (2.54)$$

where $E(p)$ has been replaced by $M + p^2/2M$ and terms of order up to $1/M^2$ have been retained. The $1/M$ and $1/M^2$ terms are called the Darwin–Foldy and spin-orbit terms, respectively, and contribute to the charge density.

Following Friar and Negele (75), we replace F_1 and F_2 by the Sachs form factors G_E and G_M [see (IX.3.8) et seq. in deShalit and Feshbach (74)]:

$$G_E \equiv F_1 - \frac{\kappa q^2 F_2}{M} \quad (2.55)$$

$$G_M = F_1 + \kappa F_2 \quad (2.56)$$

Therefore,

$$\langle \mathbf{p}' \lambda' | \hat{\rho}(0) | \mathbf{p} \lambda \rangle = -i \chi_{\lambda'}^\dagger \left[\left(1 - \frac{q^2}{8M^2} \right) G_E - i \frac{\mathbf{q} \cdot \boldsymbol{\sigma} \times \mathbf{p}}{4M^2} (2G_M - G_E) \right] \chi_\lambda \quad (2.57)$$

where terms of order higher than $1/M^2$ have been dropped.

The empirical value of the parameters G_E and G_M obtained from $e-p$ and $e-d$ scattering for protons and neutrons are given on page 678 of deShalit and Feshbach (74) [Feld (69)]. They are

$$G_E^{(p)} \simeq \frac{G_M^{(p)}}{\mu_p} \simeq \frac{G_M^{(n)}}{\mu_n} \simeq \frac{4M^2 c^2}{\mu_n q^2} G_E^{(n)} \simeq \left[1 + \frac{q^2}{0.71(\text{GeV}/c)^2} \right]^2$$

where the superscripts p and n refer to protons and neutrons, respectively. The “dipole” form given by the q dependence corresponds to an exponential charge distribution,

$$\rho_p \sim e^{-.843r} \quad (2.58)$$

with an rms radius of 0.82 fm. The units of the constant in the exponential are $\text{GeV}/\hbar c$.

Equation (2.57) gives the nucleon charge density. For a nucleus we have

$$\rho(q^2) = \sum_i \left\langle 0 \left| \hat{e}_i e^{i\mathbf{q} \cdot \mathbf{r}_i} - i\mathbf{q} \cdot \frac{2\hat{\mu}_i - \hat{e}_i}{8M^2} \{ (\boldsymbol{\sigma}_i \times \mathbf{p}_i), e^{i\mathbf{q} \cdot \mathbf{r}_i} \} \right| 0 \right\rangle \quad (2.59)$$

where (again to order q^2/M^2)

$$\hat{e}_i = \frac{1}{\sqrt{1 + q^2/4M^2}} \left(G_E^{(p)} \frac{1 + \tau_3(i)}{2} + G_E^{(n)} \frac{1 - \tau_3(i)}{2} \right) \quad (2.60)$$

$$\hat{\mu}_i = \frac{1}{\sqrt{1 + q^2/4M^2}} \left(G_M^{(p)} \frac{1 + \tau_3(i)}{2} + G_M^{(n)} \frac{1 - \tau_3(i)}{2} \right) \quad (2.61)$$

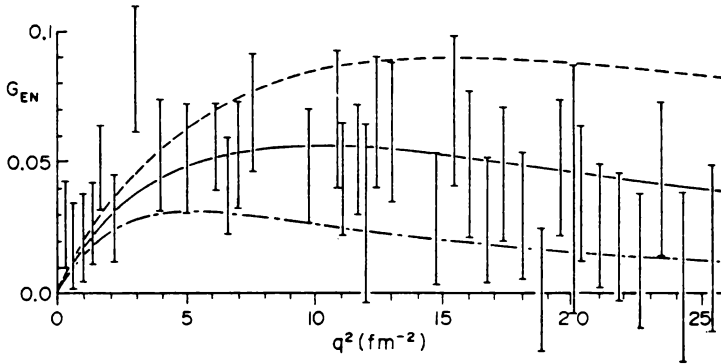


FIG. 2.1. Neutron form factor assuming an exponential neutron charge distribution compared with experimental data extracted with the use of Hamada–Johnston and boundary conditions model deuteron wave functions. Solid, dashed, and dashed–dotted curves correspond to average neutron radii equal to 0.80, 0.63, and 1.07 fm, respectively. [From Bertozzi, Friar, et al. (72).]

As Bertozzi et al. (72) have shown, the neutron charge distribution can have a considerable effect on the electron scattering. The experimental results for $G_E^{(n)}$ are shown in Fig. 2.1. The consequences for elastic scattering by ^{40}Ca and ^{208}Pb are shown in Fig. 2.2. The effects are substantial and especially large at the cross section minima and large momentum transfers.

Two other effects have been subjects of several investigations. The first of these is referred to as a dispersion correction, which arise as the result of the virtual excitation of the target nucleus by the incident electron. The electron excites the target nucleus, and then in a second interaction the nucleus deexcites, returning to its ground state if we are discussing elastic scattering. As we have seen in Chapter II, where the identical process is discussed in a multiple scattering approximation, the cross section for this process depends on the pair correlation function $C(\mathbf{r}_1, \mathbf{r}_2)$. However, calculations indicate that the dispersion effects are small [see Bethe and Molinari (71) and Friar and Rosen (74)] and little information on $C(\mathbf{r}_1, \mathbf{r}_2)$ can be obtained from these experiments.

We finally mention dynamical nuclear recoil corrections. These have been treated using the Breit (29) two-body interaction by Grotch and Yennie (69). These corrections also turn out to be small [see Sick and McCarthy (70)].

D. Model Independence

At a comparatively low energy (but still such that $k \gg m$) (m = electron mass) the product kR can be much less than 1. Under those circumstances only the $l=0$ phase shift, δ_0 is affected by the finite nuclear size. Moreover, as we shall show, that phase shift depends only on the rms nuclear radius and does not depend on other nuclear parameters.

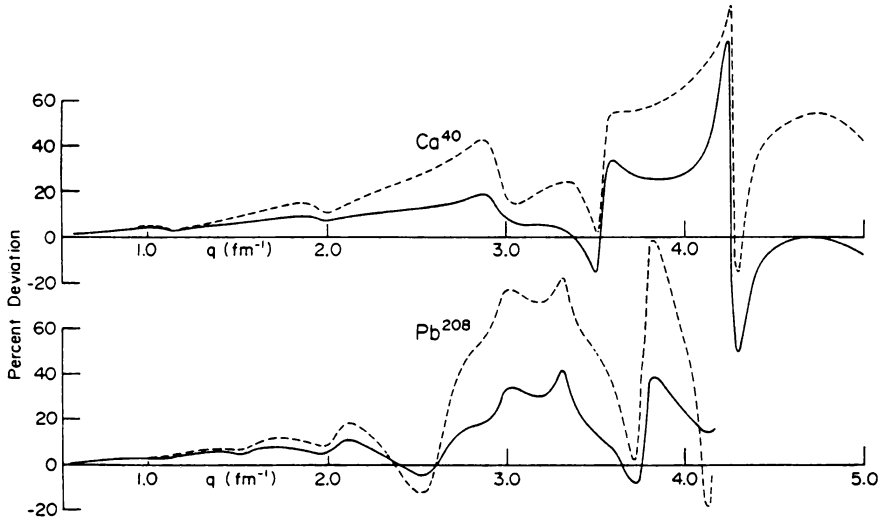


FIG. 2.2. Fractional change in electron scattering cross sections caused by including the charge density arising from the finite spatial charge distribution of the neutron for ^{40}Ca and ^{208}Pb . The dashed and solid curves denote the effect obtained using the maximal and minimal neutron form factors, respectively. [From Bertozzi, Friar, et al. (72).]

Let us compare the results obtained with two differing potentials V_1 and V_2 . The Dirac wave functions satisfy (2.27):

$$\begin{aligned} (E - m - V_1)G_1 + \frac{df_1}{dr} - \frac{\kappa f_1}{r} &= 0 \\ -(E + m - V_1)f_1 + \frac{dG_1}{dr} + \frac{\kappa G_1}{r} &= 0 \end{aligned}$$

We now form

$$\begin{aligned} G_2 \frac{df_1}{dr} - f_2 \frac{dG_1}{dr} + f_1 \frac{dG_2}{dr} - G_1 \frac{df_2}{dr} &= \frac{d}{dr}(f_1 G_2) - \frac{d}{dr}(f_2 G_1) \\ &= (V_1 - V_2)(G_1 G_2 + f_1 f_2) \end{aligned}$$

Integrating both sides from zero to infinity yields

$$f_1 G_2 - f_2 G_1 \Big|_0^\infty = \int_0^\infty (V_1 - V_2)(G_1 G_2 + f_1 f_2) dr$$

Using the asymptotic forms for f and G , the left-hand side equals

$$(\epsilon^2 - 1)^{1/2} \sin(\delta_1 - \delta_2) = - \int_0^\infty (V_1 - V_2)(G_1 G_2 + f_1 f_2) dr \quad (2.62)$$

Note that the difference $(V_1 - V_2)$ does not contain the long-range part of the Coulomb potential. Let

$$V_i \equiv -\frac{Ze^2}{r} + \bar{V}_i \quad (2.63)$$

Then

$$V_1 - V_2 = \bar{V}_1 - \bar{V}_2 \quad (2.64)$$

We see that two descriptions of the finite nuclear size will yield the same phase shift if

$$\int_0^\infty \bar{V}_1(G_1 G_2 + f_1 f_2) dr = \int_0^\infty \bar{V}_2(G_1 G_2 + f_1 f_2) dr$$

In the long-wavelength limit ($kR \ll 1$),

$$G_1 G_2 + f_1 f_2 \sim r^2 \quad kR \ll 1 \quad (2.65)$$

Elastic electron scattering experiments satisfying $kR \ll 1$ therefore determine one parameter,

$$I = \int_0^\infty \bar{V} r^2 dr \quad (2.66)$$

This result was obtained by Feshbach (51) employing a variational method [see also Elton (53) and Bodmer (53)]. Using the Poisson equation, \bar{V} can be expressed in terms of the charge density ρ_{ch} . One can then express I in terms of ρ_{ch} , with the result that when $kR \ll 1$, elastic electron scattering experiments determine the rms radius of the charge in the nucleus:

$$r_{\text{rms}}^2 = \frac{\int r^2 \rho_{\text{ch}} d\mathbf{r}}{\int \rho_{\text{ch}} d\mathbf{r}} \quad (2.67)$$

At higher energies, when $kR \lesssim 1$ the approximation given by (2.65) is no longer valid. The methods for extracting ρ_{ch} from the elastic scattering data then employed is referred to as a *model-independent analysis*. It is, in fact, a method designed to obtain an estimate of the uncertainty in ρ_{ch} so obtained. There are two sources of error. One is, of course, the experimental error. A second has

its origin in the fact that a given experiment determines the elastic scattering up to a maximum momentum transfer, q_{\max} . However, to obtain $\rho(\mathbf{r})$ from $\rho(\mathbf{q})$ from the inverse Fourier transform,

$$\begin{aligned}\rho(\mathbf{r}) &= \left(\frac{1}{2\pi}\right)^3 \int \rho(\mathbf{q}) e^{-i\mathbf{q}\cdot\mathbf{r}} d\mathbf{q} \\ &= \frac{1}{2\pi^2} \int_0^\infty \rho(q) \frac{\sin qr}{r} q dq\end{aligned}$$

requires a knowledge of q beyond q_{\max} .

There are a number of procedures that have been developed. These are reviewed by Friar and Negele (75), who described the work of Friedrich and Lenz (72), Borysowicz and Hetherington (73, 74), Friar and Negele (73, 75), Sick (74), and others. Briefly, one writes the density as follows:

$$\rho = \rho_0(r) + \sum_1^M C_i f_i(r) \quad (2.68)$$

The quantity ρ_0 is a zeroth-order approximation obtained from, for example, a density-dependent Hartree–Fock calculation or more phenomenologically from a fit using the “Fermi” charge density distribution, which in its most elaborate form is

$$\rho_{\text{Fm}} = \frac{\rho_0(1 + wr^2/c^2)}{e^{(r-c)/a_0} + 1} \quad (2.69)$$

where ρ_0 , w , c , and a_0 are parameters that are chosen to give a best fit to experiment. Modern calculations generally use the Hartree–Fock for ρ_0 because among other things these give good descriptions of the surface properties of nuclei. The functions f_i are a complete set, for example [Meyer–Berkhout, K. W. Ford, et al. (59)],

$$f_i = \frac{1}{r} \sin \frac{i\pi r}{R} \Theta(r - \bar{R}) \quad (2.70)$$

where \bar{R} is chosen to be in the region where ρ vanishes. The parameter M is given by

$$M = \frac{R}{\pi} q_{\max} \quad (2.71)$$

since experiment does not provide data beyond q_{\max} . The spatial resolution

obtained from the analysis of experiment is

$$\Delta r \sim \frac{\pi}{q_{\max}}$$

On the other hand, the resolution in momentum space is

$$\Delta q \sim \frac{\pi}{r_{\max}}$$

where r_{\max} is the largest value of r for which ρ is determined. Or the largest value of r , r_{\max} , for which ρ can be accurately known is

$$r_{\max} \sim \frac{\pi}{\Delta q} \quad (2.72)$$

where Δq is now the experimental momentum resolution. As a consequence of this result, one can expect that the large r dependence of ρ will not be well determined by experiment. It is for this reason that the density-dependent Hartree–Fock results have been used for $\rho_0(r)$ in (2.68).

In the procedure used by Friar and Negele, one first obtains the coefficients C_i from experiment using perturbation theory, which gives a linear relation between the cross sections and the density, to obtain a first approximation to the coefficients C_i . The resulting ρ is inserted into the Dirac equation to obtain a more accurate calculation of the cross section. The C_i 's are modified by perturbation theory to take care of the differences from the experimental cross sections and the entire process is repeated. For ^{208}Pb , Friar and Negele found that with 11 terms in the series, three iterations were needed. The quantity M can also be varied. It is found that once M exceeds $(R/\pi)q_{\max}$ [Eq. (2.71)], the χ^2 increases significantly. Over the last decade this method, and others surveyed by Friar and Negele (75), have been fine tuned, and with the great increase in experimental accuracy and extension to larger values of q_{\max} , excellent descriptions of the charge density of spin-zero nuclei has been achieved. The example in Fig. 2.3 shows the percent of deviation from experiment using the analysis just described for both the Mainz data [Rothaas (78)] and the earlier 1970 Stanford and 1972 Amsterdam data.

One should bear in mind that additional important data are provided by μ mesonic atoms and must be included in the analysis. We shall not discuss this aspect here. [See the discussions in Friar and Negele (75) and Barrett and Jackson (77).]

Some of the results for ρ_{ch} obtained with this or related analyses are shown in Figs. 2.4 and 2.5. The thickness of the line indicates the uncertainty in the experimental determination of ρ_{ch} . The dashed line gives the density-dependent Hartree–Fock results and the dotted lines show the effect of going beyond the

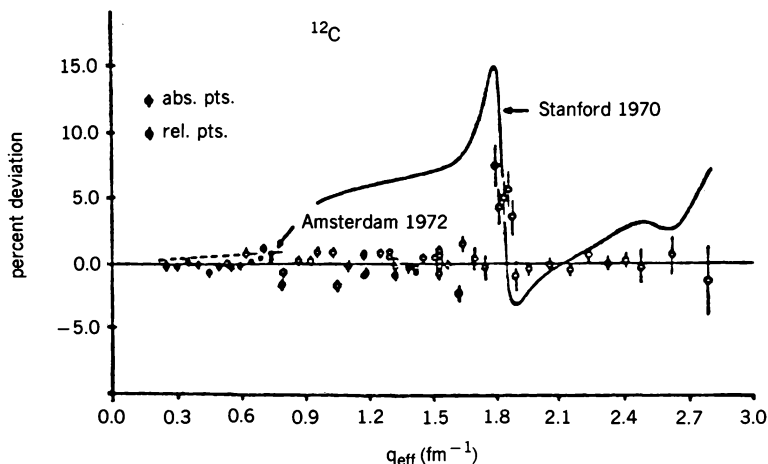


FIG. 2.3. Deviation from model-independent analysis. Solid line, Stanford data, 1970; dashed line, Amsterdam data, 1972; points, Mainz data, 1982. [From Bertozzi (82).]

mean field by using the RPA. We note a significant difference between experiment and theory for the small r . In all cases, even upon including the RPA, the theory predicts too large a density. The RPA correlations do damp the fluctuations in the interior nuclear region. [See Negele and Vautherin (72, 75), Gogny (79), Dechargé and Gogny (68), and Dechargé and Sips (83)]. We are left with the general remark that further correlations and/or two-body components of the correlation need to be included, although it is not clear whether short- or long-range correlations are needed.

An important insight is obtained by comparing the electron scattering by ^{206}Pb and ^{205}Tl [Euteneuer, Friedrich, and Voegler (78); Cavedon et al. (82)]. These two nuclei differ in their single-particle structure by a 3s proton. The impact of this difference is shown in Fig. 2.6, where the ratio of $\sigma(^{205}\text{Tl})$ to $\sigma(^{206}\text{Pb})$ is compared with the mean field prediction. We see a strong characteristic peak at $q = 2$ in both theory and experiment. However, agreement with the peak strength is obtained only if the single particle occupation probability is reduced by 30%. This is demonstrated once again in Fig. 2.7, where one sees the reduction in the charge density from that predicted by mean field theory [Frois et al. (83)]. It is this reduction that we see in Fig. 2.5 for ^{208}Pb . As Zamick, Klemm, and Speth (75) point out, ^{205}Tl is not obtained only by creating a proton hole in the ground state of ^{206}Pb . There are also components coming from a proton-hole in the excited states of ^{206}Pb , such as a $d_{3/2}$ hole and $d_{5/2}$ hole in the 2^+ excited state. The data demonstrating this are provided by the reaction $^{206}\text{Pb} (^3\text{He}, d)$. The correlations in this case are long range.

We conclude this section on charge scattering from spherical nuclei with Table 2.1, which lists rms radii obtained from experiment and theory [DeJager

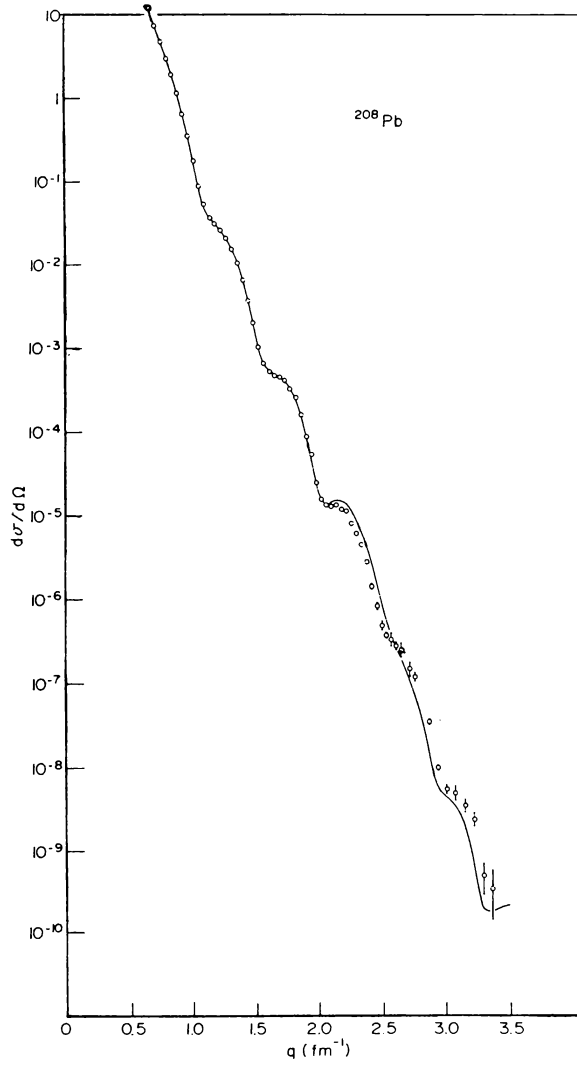


FIG. 2.4. Cross sections for elastic electron scattering from ^{208}Pb at 502 MeV compared with DME mean-field theory prediction (solid line). [From Negele (82).]

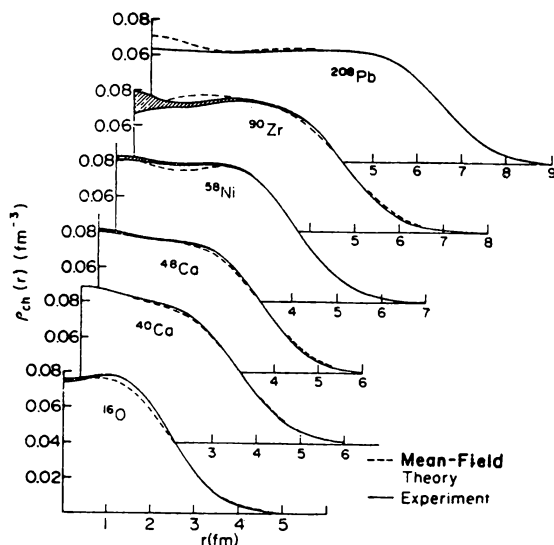


FIG. 2.5. Comparison of DME mean-field theory charge distributions in spherical nuclei (dashed lines) with empirical charge densities. The solid curves and shaded regions represent the error envelope of densities consistent with the measured cross sections and their experimental uncertainties. [From Negele (82).]

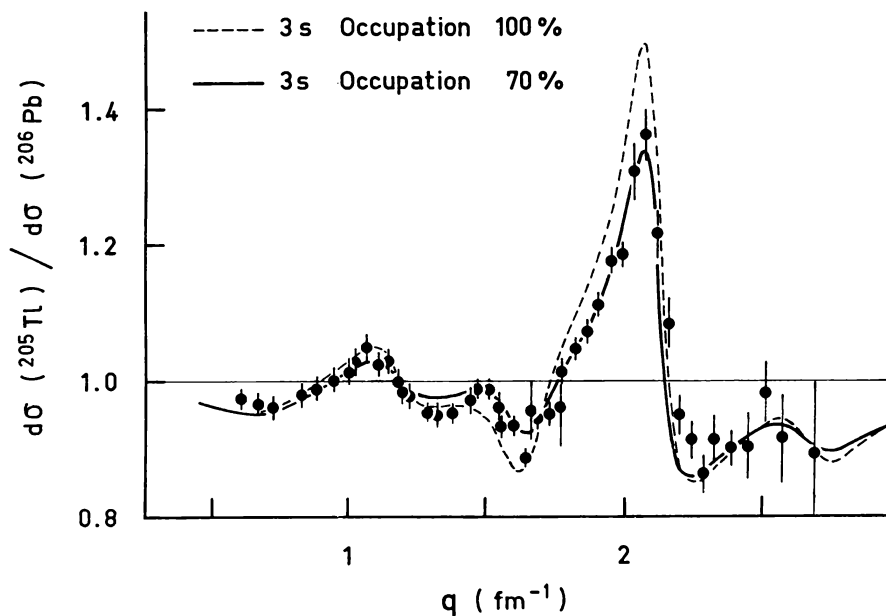


FIG. 2.6. Ratio of elastic cross sections from ^{205}Tl and ^{206}Pb . The peak at $q = 2 \text{ fm}^{-1}$ is the signature of the $3s$ orbit. The curves are mean-field predictions due to X. Campi. [From Frois and Papanicolas (87).]

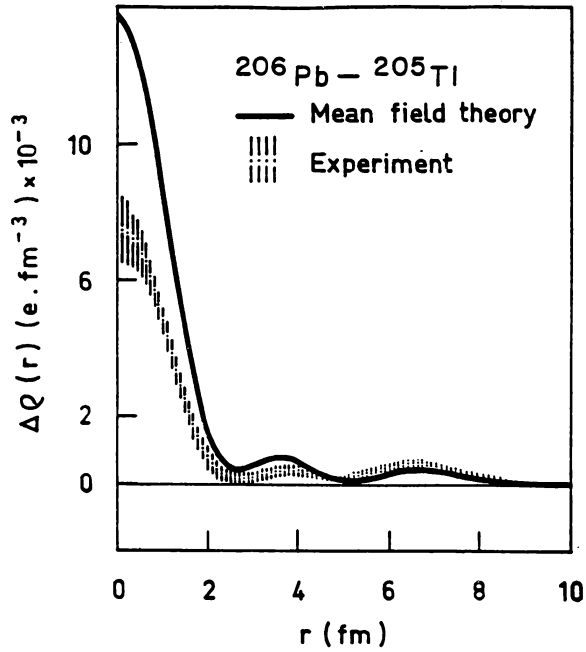


FIG. 2.7. Charge density difference of ^{206}Pb and ^{205}Tl . [From Frois and Papanicolas (87).]

TABLE 2.1

	$\langle r^2 \rangle_{\text{ch}}^{1/2} \text{ (fm)}$	
	Theory	Experiment
^{16}O	2.79	2.71 ± 0.01
^{40}Ca	3.50	3.48
^{48}Ca	3.50	3.47
^{56}Ni	3.80	4.78
^{190}Zr	4.29	4.28 ± 0.02
^{116}Sn	4.63	4.62 ± 0.01
^{200}Pb	5.49	5.50

DeVries, and DeVries (74)]. See also the more extensive table, Table 6.2, in Barrett and Jackson (77).

E. Deformed Nuclei[†]

Elastic and inelastic scattering of electrons by deformed nuclei demonstrate the electron's power as a probe of nucleon structure. As discussed in Chapter VI of deShalit and Feshbach (74), the rotational wave function is given in terms of an intrinsic wave function χ_K and a factor depending on the Euler angles, which transforms the wave function for a body fixed to a space-fixed coordinate system. The wave function is [see (VI.4.9) in deShalit and Feshbach (74)]

$$\psi(IKM) = \sqrt{\frac{2I+1}{16\pi^2}} [D_{MK}^{I*}(\theta_K)\chi_K(\mathbf{r}') + (-)^{I-J} D_{M,-K}^{I*}(\theta_K)\chi_{-K}(\mathbf{r}')] \quad K > 0 \quad (2.73a)$$

while for $K = 0$,

$$\psi(I, K = 0, M) = \frac{1}{\sqrt{2\pi}} Y_{Im}(\theta_K)\chi_{K=0}(\mathbf{r}') \quad (2.73b)$$

As pointed out in that chapter, the ratio of the electromagnetic transition probabilities within a rotational band for a particular multipole [see (VI.6.21) and (VI.6.22) in deShalit and Feshbach (74)] do not depend on the intrinsic wave function, but only on the quantum numbers I_f , I_i , and K . This is a consequence of the fact that the wave function for each member of a rotational band contains the same intrinsic wave function χ_K . The electromagnetic transitions tests this property of the rotational wave functions at $q = 0$. The electron scattering experiments extends that test to finite q , thus checking that $\chi_K(\mathbf{r})$ is the same for each member of the rotational band as a function of \mathbf{r} .

Inelastic scattering will play an important role since we shall compare cross sections for the excitation of different members of usually the ground-state band. The electron-nuclear interaction responsible for the transition can be treated perturbatively, but the plane wave approximation is not valid for the heavier target nuclei. The appropriate formalism is the DWA (see Chapter VI for its use in dealing with inelastic processes) in which in this case the Coulomb interaction is treated exactly, while the transition Hamiltonian is taken into account using perturbation theory.

We shall only outline the DWA for this case. The details are similar to those given in Chapter VI, with some special details because of the required Dirac algebra. The details can be found in Überall's (71) second volume. The Hamiltonian of the system is given by

$$H = H_N + H_D + H_{int} \quad (2.74)$$

[†]Moya de Guerra (86).

where H_N is the Hamiltonian of the nucleus and H_D is the Dirac Hamiltonian,

$$H_D = (\boldsymbol{\alpha} \cdot \mathbf{p}) + \beta m \quad (2.75)$$

and for charge scattering

$$H_{\text{int}} = e\phi \quad (2.76)$$

where ϕ depends on the charge distribution in the nucleus. One then defines the diagonal and transfer part of ϕ with respect to the wave functions of the nucleus as follows:

$$\begin{aligned} \hat{\phi}_D &= I \langle I | \phi | I \rangle \langle I | \\ \hat{\phi}_{\text{tr}} &= \sum_{I'} I \langle I | \phi | I' \rangle \langle I' | + \text{h.c.} \quad I \neq I' \end{aligned} \quad (2.77)$$

By taking the matrix element of the Schrödinger–Dirac equation,

$$H\Psi = E\Psi$$

one obtains a set of coupled equations for the spinor electron wave function ψ_I :

$$[H_D + e\hat{\phi}_D]\psi_I = - \sum \langle I | \hat{\phi}_{\text{tr}} | I' \rangle \psi_{I'}$$

The DWA result for the transition $I \rightarrow I'$ is obtained by solving the approximate equations

$$[H_D + e\hat{\phi}_D]\psi_I = 0 \quad (2.78a)$$

$$[H_D + e\hat{\phi}_D]\psi_{I'} = - \langle I' | \hat{\phi}_{\text{tr}} | I \rangle \psi_I \quad (2.78b)$$

The solution of (2.78a) gives the elastic scattering from the nucleus, while (2.78b) yields the inelastic scattering. The solution of (2.78a) for ψ_I can be obtained in a partial wave series as in the preceding section. That series, substituted in (2.78b), leads to the desired wave function $\psi_{I'}$, also expressed in a partial wave series.

To obtain an insight into what can be learned from this analysis, we return to the Born approximation for the inelastic reaction in which discrete nuclear levels are excited. The cross section in the center-of-mass system is

$$\frac{d\sigma}{d\Omega} = \sigma_M \frac{1}{2J_i + 1} \sum_{M_i M_f} |\langle J_f M_f | \rho(\mathbf{q}) | J_i M_i \rangle|^2 \quad (2.79)$$

where σ_M is the Mott cross section. But $\rho(\mathbf{q})$ can be expanded in a partial wave

series,

$$\begin{aligned}\rho(\mathbf{q}) &= \int e^{i\mathbf{q}\cdot\mathbf{r}} \rho(\mathbf{r}) d\mathbf{r} \\ &= \sum_{JM} 4\pi i^J \int j_J(qr) Y_{JM}(\hat{\mathbf{r}}) Y_{JM}^*(\hat{\mathbf{q}}) \rho(\mathbf{r}) d\mathbf{r}\end{aligned}$$

so that

$$\langle J_f M_f | \rho(\mathbf{r}) | J_i M_i \rangle = 4\pi \sum_{JM} i^J Y_{JM}^*(\hat{\mathbf{q}}) \langle J_f M_f | \hat{M}_{JM}^{(c)}(\mathbf{q}) | J_i M_i \rangle \quad (2.80)$$

In this equation

$$\hat{M}_{JM}^{(c)}(\mathbf{q}) = \int j_J(qr) Y_{JM}(\hat{\mathbf{r}}) \rho(\mathbf{r}) d\mathbf{r} \quad (2.81)$$

so that (2.80) is the multipole expansion of ρ and $\hat{M}_{JM}^{(c)}$ transforms like a tensor operator of order J . Using the Wigner–Eckart theorem, one has

$$\langle J_f M_f | \hat{M}_{JM}^{(c)}(\mathbf{q}) | J_i M_i \rangle = (-)^{J_f - M_f} \begin{pmatrix} J_f & J & J_i \\ -M_f & M & M_i \end{pmatrix} (J_f \| \hat{M}_J^{(c)}(\mathbf{q}) \| J_i) \quad (2.82)$$

Performing the indicated sums, using the sum rules of Appendix A of deShalit and Feshbach (74), one obtains

$$\frac{d\sigma}{d\Omega} = \sigma_M \frac{1}{2J_i + 1} \sum_J |(J_f \| \hat{M}_J^{(c)}(\mathbf{q}) \| J_i)|^2 \quad (2.83)$$

For deformed nuclei, the matrix element of $\hat{M}_{JM}^{(c)}$ has been derived [(VI.6.9) in deShalit and Feshbach (74), where J_i is replaced by I' and J_f by I]. One obtains

$$\begin{aligned}(IK \| \hat{M}_J^{(c)}(\mathbf{q}) \| I'K') &= \sqrt{(2I+1)(2I'+1)} \\ &\times \sum_{\mu} \left\{ \begin{pmatrix} I & J & I' \\ -K & \mu & K' \end{pmatrix} \langle K | \hat{M}_{J\mu}^{(c)}(\mathbf{q}) | K' \rangle \right. \\ &\left. + (-)^{I'} \begin{pmatrix} I & J & I' \\ -K & \mu & -K' \end{pmatrix} \langle K | \hat{M}_{J\mu}^{(c)}(\mathbf{q}) | -K' \rangle \right\} \quad (2.84)\end{aligned}$$

This result holds for K and $K' \neq 0$. When K' is zero,

$$\begin{aligned}(I, K \| \hat{M}_J^{(c)} \| I', K' = 0) &= \sqrt{(2I+1)(2I'+1)} \begin{pmatrix} I & J & I' \\ -K & K & 0 \end{pmatrix} \\ &\times \langle K | \hat{M}_{J0}^{(c)}(\mathbf{q}) | K' = 0 \rangle \begin{cases} \sqrt{2} & K \neq 0 \\ 1 & K = 0 \end{cases} \quad (2.85)\end{aligned}$$

In these equations $\hat{M}_J^{(c)}(\mathbf{q})$ are calculated in the body-fixed coordinate system. The matrix elements $\langle K | \hat{M}_J^{(c)}(\mathbf{q}) | K' \rangle$ involve only the intrinsic wave functions χ_K and are independent of I and I' as long as I and I' are members of the corresponding rotational bands. Thus the electron-induced transitions between members of the two bands (which can be identically) will each involve the matrix elements of \hat{M}_J . These will, of course, vary with J so that differing aspects of χ_K will be probed by the inelastic scattering. Analysis of the data should then yield the \mathbf{q} dependence of the matrix elements. In the case of even-even nuclei transitions from the ground state ($I' = 0 = K'$) to excited states of the same band ($I, K = 0$), only one matrix element $\langle K = 0 | \hat{M}_J^{(c)}(\mathbf{q}) | K' = 0 \rangle$ enters for each J and I .

When the spin of the ground state is not zero, several matrix elements are involved in a given transition. Nevertheless, one can determine each of these as the following example illustrates [Bertozzi (82)]. Suppose that the energy spectrum of a nucleus is given by Fig. 2.8. The multipole matrix elements involved in a given transition are shown. The matrix elements of the multipole operators with respect to the intrinsic wave functions [see (2.8)] are identical for each of the transitions indicated. There are five transitions and four matrix elements, $M0, M2, M4$, and $M6$. One can, for example, determine the matrix elements using four of the transitions and predict the fifth, thereby testing the correctness of the wave function (2.72). Bertozzi (82) gives an example of such a test. The nucleus is ^{175}Lu with a ground state of spin of $7/2^+$. The $7/2, 9/2, 13/2, 15/2$ cross sections are used to predict the $11/2$ cross section. The results are shown in Fig. 2.9. The agreement is good, demonstrating the validity of the rotational model.

The cross section given by (2.83) applies as well to inelastic scattering from spherical nuclei in the Born approximation. It is traditional to use the concept of transition charge density ρ_{tr} in these cases. It is defined as follows:

$$(J_f \| \hat{M}_J^{(c)}(\mathbf{q}) \| J_i) = \int_0^\infty j_J(qr) \rho_{tr}(r) r^2 dr \quad (2.86)$$

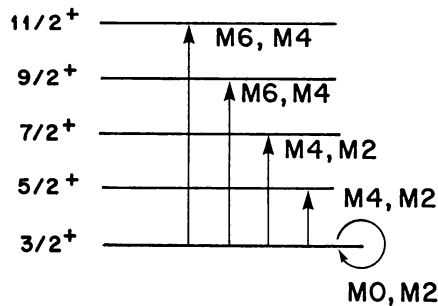


FIG. 2.8. Possible multipole excitations.

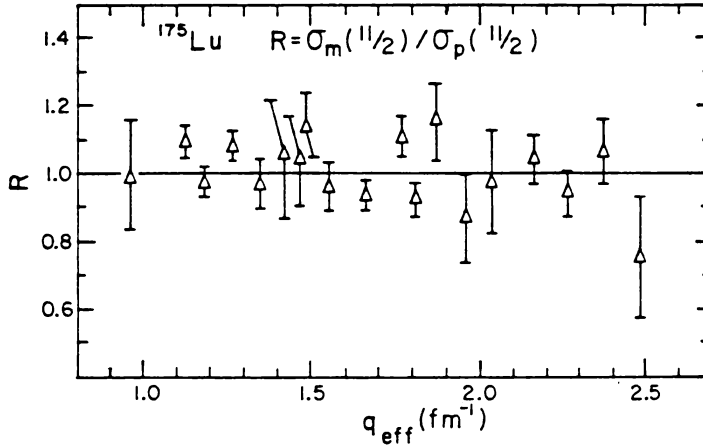


FIG. 2.9. Test of single intrinsic state assumption of the rotational model. The nucleus is ^{175}Lu . R is the ratio of the measured $\frac{11}{2}^+$ cross section to the value predicted from the measured $\frac{7}{2}^+$, $\frac{9}{2}^+$, $\frac{13}{2}^+$, and $\frac{15}{2}^+$ cross sections. [From Bertozzi (82).]

Inserting (2.82) yields

$$\rho_{\text{tr}}(r) = \int d\Omega Y_{JM}(\hat{\mathbf{r}}) \times \left[(2J+1) \sum_{M_i, M_f} (-)^{J_f - M_f} \begin{pmatrix} J_f & J & J_i \\ -M_f & M & M_i \end{pmatrix} \langle J_f M_f | \rho(\mathbf{r}) | J_i M_i \rangle \right] \quad (2.87)$$

Since $(J_f \| \hat{M}_J^{(c)} \| J_i)$ is independent of M , we can choose M . A convenient choice is $M = 0$. For even-even nuclei, $J_i = 0$ and ρ_{tr} equals

$$\rho_{\text{tr}}(r) = (2J+1)^{1/2} \int d\Omega Y_{J0}(\hat{\mathbf{r}}) \langle J0 | \rho(\mathbf{r}) | 00 \rangle \quad (2.87')$$

where we have used

$$\begin{pmatrix} J_f & J & 0 \\ 0 & 0 & 0 \end{pmatrix} = \frac{(-)^J \delta_{J_f, J}}{\sqrt{2J+1}}$$

Obtaining ρ_{tr} involves determining $(J_f \| \hat{M}_J^{(c)}(\mathbf{q}) \| J_i)$ from experiment and then inverting (2.86) with the attendant difficulties discussed earlier in this chapter. A model-independent resolution is available in this case as well.

These levels can also be excited by the interaction of the electron with the nuclear currents. However, it is possible, as we shall see, using suitable kinematics and analysis to extract the charge- and current-induced cross section separately.

The transition densities obtained from inelastic scattering by several magic nuclei to the highly collective 3^- state and by ^{90}Zr to the 2^+ , 4^+ , 6^+ , 8^+ states are shown in Figs. 2.10 and 2.11.

The transition density for both of these cases peaks strongly at the surface. The dashed line in Fig. 2.10 gives the theoretical results obtained using an RPA description of the states involved. The general structure of the prediction does follow experiment. But there are deviations. The peak transition density can differ substantially from experiment, while for the interior the theoretical results

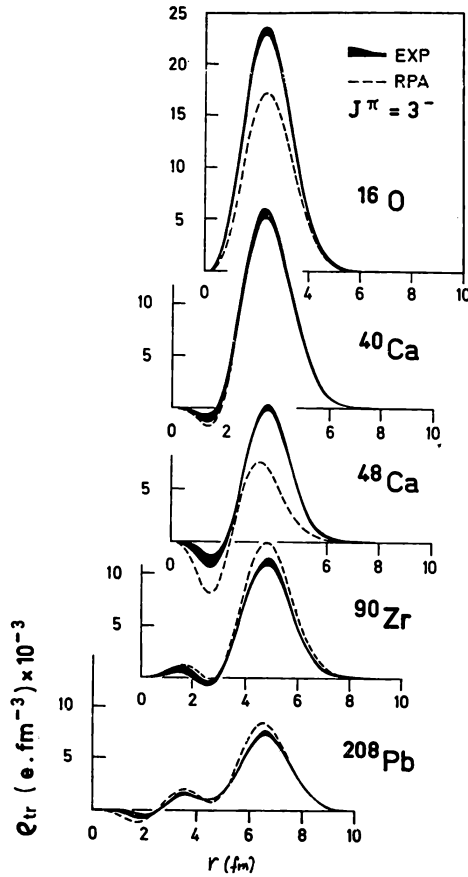


FIG. 2.10. Transition charge densities for the first collective octupole vibrations of doubly closed shell nuclei. Experimental uncertainty is given by the thickness of the solid line. The theoretical predictions are obtained in a self-consistent RPA calculation. [From Frois and Papanicolas (87).]

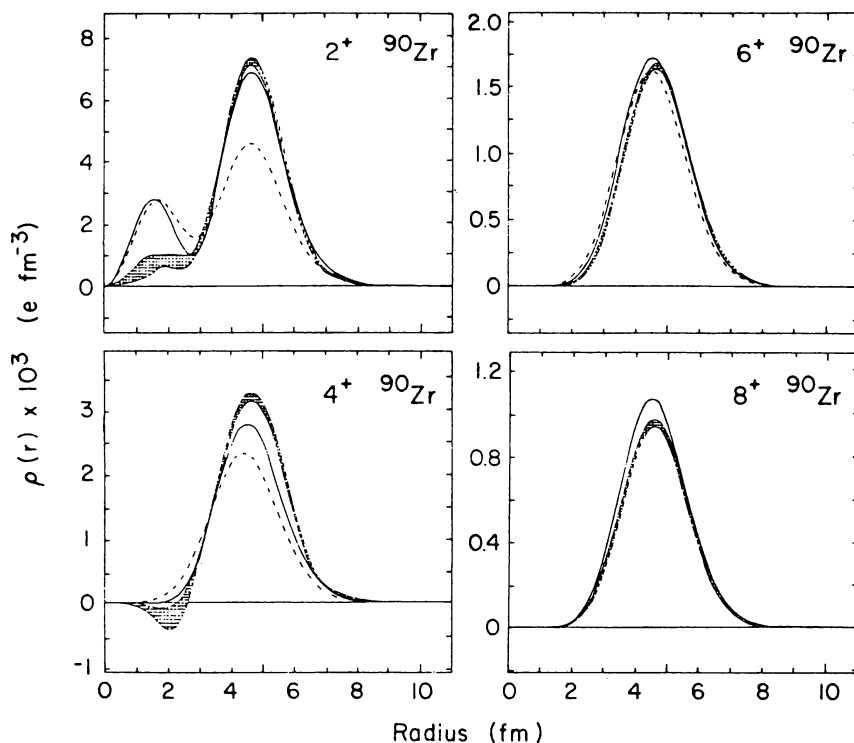


FIG. 2.11. Experimental and calculated transition densities for the 2^+ , 4^+ , 6^+ , and 8^+ multiplet in ^{90}Zr . [From Heisenberg (87).]

oscillate more violently than the data. Figure 2.11 contains a comparison between the experimental and calculated transition charge density. In the single-particle picture, these transitions are to states in which two protons in the filled $1g_{9/2}$ orbitals are recoupled to spin 2^+ , 4^+ , 6^+ , and 8^+ . In the ground state they couple to zero. As Fig. 2.11 shows, the calculations based on this simple assumption fail substantially for the 2^+ and 4^+ but are satisfactory for the 6^+ and 8^+ states. The solid line includes the effect of core polarization (i.e., the inclusion of states in which the core is excited). As we see from the figure, core polarization does have some effect in the 2^+ and 4^+ cases, but that effect is nearly not large enough to reduce the small r fluctuations in the 2^+ case, although it does greatly improve the agreement in the main peak.

Comparing the experimental transfer charge density with theory reveals the same diseases that were seen with spherical nuclei namely the predictions in the interior deviate from experiment. This is illustrated in Fig. 2.12. In Fig. 2.12a the theory predicts too large a charge density in the interior. In Fig. 2.12b the theoretical ρ_{tr} fluctuates more strongly than its experimental values in the interior, although theory and experiment are in good agreement in the surface

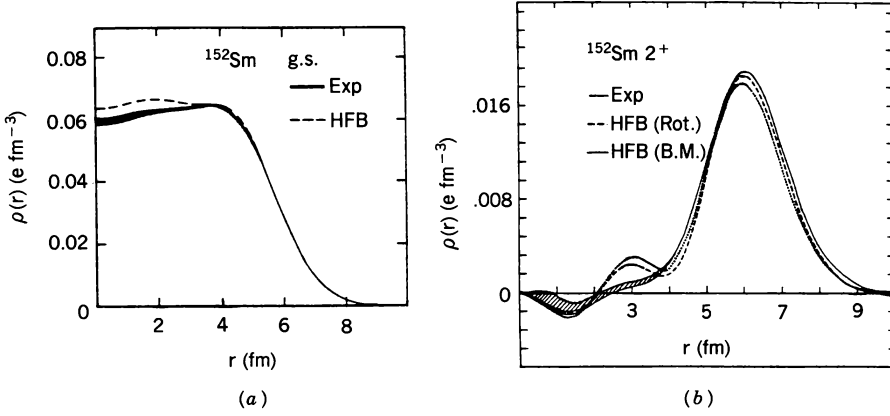


FIG. 2.12. (a) Charge density for ground state of ^{152}Sm ; (b) transition charge density for excitation of the 2^+ level in ^{152}Sm . [From Bertozzi (82).]

region. This substantially good agreement for the $0^+ \rightarrow 2^+$ transition deteriorates somewhat for the $0 \rightarrow 4^+$. This is a general pattern for the rare earth nuclei and for ^{238}U according to Bertozzi.

F. A Remark on the Charge Density

The two-body density matrix $\rho(\mathbf{r}_1, \mathbf{r}_2)$ has been discussed in Ch. III (where it was called K). There it was shown [III.2.88 Feshbach (62)] that it could be written as

$$\rho(\mathbf{r}_1, \mathbf{r}_2) = \sum \kappa_\alpha \omega_\alpha(\mathbf{r}) \omega_\alpha^*(\mathbf{r}_2) \quad (2.88)$$

where

$$\langle \omega_\alpha(r_1) \omega_\beta(r_1) \rangle = \delta_{\alpha\beta} \quad (2.89)$$

and

$$\int \rho(\mathbf{r}_1, \mathbf{r}_2) \omega_\alpha(\mathbf{r}_2) d\mathbf{r}_2 = \kappa_\alpha \omega_\alpha(\mathbf{r}_1) \quad (2.90)$$

The density is

$$\rho(\mathbf{r}_1) = \rho(\mathbf{r}_1, \mathbf{r}_1) = \sum \kappa_\alpha |\omega_\alpha(r_1)|^2 \quad (2.91)$$

In the case of a Slater determinant, $\kappa_\alpha = 1$. But the many-body wave functions are generally not single Slater determinants, so that generally $\kappa_\alpha \neq 1$ but will lie between 0 and 1. One can interpret κ_α as giving the occupation probability of the orbital, ω_α . In fact, the interior deviations observed in nearly all of the

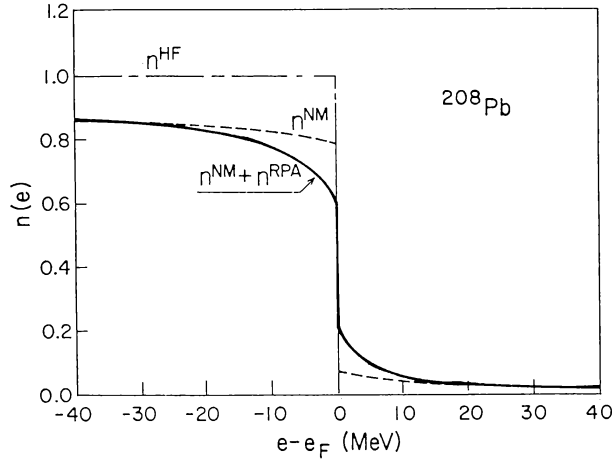


FIG. 2.13. Calculated occupation probabilities in ^{208}Pb . [From Heisenberg (87).]

nuclei, including both the spherical and deformed nuclei can be explained if the occupation probabilities of the single-particle orbitals have been chosen appropriately. Their deviation from unity is an expression of the existence of residual interactions and the consequent correlations. Pandharipande, Papanicolas, and Wambach (84) have calculated the occupation probabilities for ^{208}Pb . The results are shown in Fig. 2.13, where HF refers to Hartree-Fock, and NM to nuclear matter calculations. The overall reduction in n , the occupation number, is qualitatively in accordance with the experimental situation. But experimental uncertainties in the $3s_{1/2}$ occupation probability are, according to Heisenberg (87), too large for a definitive comparison of experiment and theory. (See Heisenberg for a discussion of the E5 transitions in ^{89}Y , ^{90}Zr , and ^{92}Mo .)

G. Current-Induced Scattering

We continue with the Born approximation. We return to Dirac equation (2.12). The vector potential A_μ is a solution of the inhomogeneous wave equation

$$\nabla^2 A_\mu + \omega^2 A_\mu = -4\pi j_\mu \quad (2.92)$$

where simple harmonic time dependence has been assumed. Then in momentum space

$$A_\mu = \frac{4\pi j_\mu}{q^2 - \omega^2} = \frac{4\pi j_\mu}{q_\mu^2} \quad (2.93)$$

$$q_\mu^2 = q^2 - \omega^2 \quad (2.94)$$

Equation (2.12') is replaced by

$$(\nabla^2 + k'^2)\psi = -e(\gamma_\nu p_\nu + im)(\gamma_\mu A_\mu)\psi_i$$

where k' is the electron momentum with the nucleus excited, ψ the corresponding wave function, and ψ_i the elastic scattering (nucleus in the ground state) wave function. In the DWA approximation,

$$\hat{f} = \frac{e}{4\pi} \int e^{-ik'\cdot r} (\gamma_\nu p_\nu + im)(\gamma_\mu A_\mu) \psi_i^{(+)} d\mathbf{r}$$

On introducing (2.93) and making the Born approximation [see (2.14)] we obtain

$$f_{fi} = \frac{e}{q_\mu^2} \langle u_f (\gamma_\nu k'_\nu + im) (\gamma_\mu j_\mu(\mathbf{q})) u_i \rangle \quad (2.95)$$

where

$$j_\mu(\mathbf{q}) = \int e^{iq\cdot r} j_\mu(\mathbf{r}) d\mathbf{r} \quad (2.96)$$

To obtain the cross section for a nuclear transition $J_i \rightarrow J_f$ and electron spins from m_i and m_f , we must calculate

$$\frac{d\sigma}{d\Omega} = \frac{1}{2} \frac{1}{2J_i + 1} \sum_{\substack{M_i, M_f \\ m_i, m_f}} |\langle J_f M_f; m_f | f_{fi} | J_i M_i; m_i \rangle|^2 \quad (2.97)$$

The sum over the electron spin is obtained by using the technique following (2.17). The result is

$$\frac{1}{2} \sum_{m_i, m_f} |\langle J_f M_f; m_f | f_{fi} | J_i M_i; m_i \rangle|^2 = \frac{e^2 k'}{q_\mu^4 k} [k_\nu k'_\sigma - \delta_{\nu\sigma} k_\kappa k'_\kappa + k_\sigma k'_\nu] j_\sigma(\mathbf{q}) j_\nu^*(\mathbf{q}) \quad (2.98)$$

where the summation convention is used. Following DeForest and Walecka (66), one introduces the coordinates

$$Q_\mu = \frac{1}{2}(k_\mu + k'_\mu) \quad (2.99)$$

Replacing then k_μ and k'_μ by Q_μ and q_μ and bearing in mind that $Q_\mu^2 = -\frac{1}{4}q_\mu^2$, one obtains

$$\sigma = \frac{e^2 k'}{q_\mu^4 k} \frac{1}{2J_i + 1} \sum_{M_i, M_f} [2(Q_\nu \bar{j}_\nu^*)(Q_\sigma \bar{j}_\sigma) + \frac{1}{2} q_\sigma^2 \bar{j}_\mu^* \bar{j}_\mu]$$

where

$$\bar{J}_\sigma = \langle J_f M_f | j_\sigma | J_i M_i \rangle \quad (2.100)$$

Further development of this result requires an analysis of j_v . Toward this end we introduce the unit vectors \mathbf{u}_α [see (VII.4.4f), deShalit and Feshbach (74)], whose z axis is taken along the direction of \mathbf{q} :

$$\mathbf{u}_0 = \frac{1}{q} \mathbf{q} \quad (2.101)$$

Then setting up a Cartesian coordinate system with unit vectors \mathbf{u}_x and \mathbf{u}_y , one can define

$$\mathbf{u}_1 = -\frac{1}{\sqrt{2}}(\mathbf{u}_x + i\mathbf{u}_y) \quad (2.102)$$

$$\mathbf{u}_{-1} = \frac{1}{\sqrt{2}}(\mathbf{u}_x - i\mathbf{u}_y) \quad (2.103)$$

The *three-vector* $\mathbf{j}(\mathbf{q})$ can then be written:

$$\mathbf{j} = j_0 \mathbf{u}_0^\dagger + j_1 \mathbf{u}_1^\dagger + j_{-1} \mathbf{u}_{-1}^\dagger$$

The continuity equation for $\mathbf{j}(\mathbf{r})$,

$$\text{div } \mathbf{j} + \frac{\partial \rho}{\partial t} = 0$$

becomes in momentum space

$$q_\mu j_\mu = 0$$

or

$$\mathbf{q} \cdot \mathbf{j} = \rho q_0 = q j_0$$

Therefore,

$$\mathbf{j} = j_1 \mathbf{u}_1^\dagger + j_{-1} \mathbf{u}_{-1}^\dagger + \frac{q_0}{q} \rho(\mathbf{q}) \mathbf{u}_0^\dagger \quad (2.104)$$

The three-current \mathbf{j} is composed of two components orthogonal to \mathbf{q} (the transverse components) and one along \mathbf{q} (the longitudinal component). The magnitude of the last is proportional to $\rho(\mathbf{q})$, which must be combined with the $\gamma_4 j_4$ contribution discussed earlier in this section, giving rise to a change in the kinematic factors only. We therefore focus on the contributions coming from the transverse components. These have been discussed in Chapter VIII of

deShalit and Feshbach (74). Here we shall follow the methods that have become traditional in electron–nuclear physics. One needs the expansion

$$\mathbf{u}_\lambda e^{i\mathbf{q}\cdot\mathbf{r}} = - \sum_{J=1}^{\infty} [2\pi(2J+1)]^{1/2} i^J \left[\lambda j_J(qr) \mathbf{Y}_{JJ}^{(\lambda)} + \frac{1}{q} \text{curl}(j_J(qr) \mathbf{Y}_{JJ}) \right] \quad \lambda = \pm 1 \quad (2.105)$$

In this equation j_J is the spherical Bessel function, and[†]

$$\mathbf{Y}_{Jl}^{(M)} \equiv \sum_{mm'} (lm' | JM) Y_{lm} \mathbf{u}_{m'} \quad (2.106)$$

From (2.104) we have

$$\begin{aligned} j_\lambda(q) &= \mathbf{u}_\lambda \cdot \mathbf{j}(\mathbf{q}) = \int \mathbf{j}(\mathbf{r}) \cdot \mathbf{u}_\lambda e^{i\mathbf{q}\cdot\mathbf{r}} d\mathbf{r} \\ &= - \sum_{J \geq 1} [2\pi(2J+1)]^{1/2} i^J (\lambda T_{J\lambda}^{(\text{mag})} + T_{J\lambda}^{\text{el}}) \end{aligned} \quad (2.107)$$

where

$$T_{J\lambda}^{(\text{mag})} \equiv \int \mathbf{j}(\mathbf{r}) \cdot j_J(qr) \mathbf{Y}_{JJ}^{(\lambda)} d\mathbf{r} \quad (2.108)$$

and

$$T_{J\lambda}^{\text{el}} \equiv \frac{1}{q} \int \mathbf{j}(\mathbf{r}) \cdot \text{curl } j_J(qr) \mathbf{Y}_{JJ}^{(\lambda)} d\mathbf{r} \quad (2.109)$$

These quantities transform like tensors of rank J . Applying the Wigner–Eckart theorem yields

$$\langle J_F M_f | T_{J\lambda}^{(\text{mag})} | J_i M_i \rangle = (-)^{J_f - M_f} \begin{pmatrix} J_f & J & J_i \\ -M_f & \lambda & M_i \end{pmatrix} (J_f \| T_J^{(\text{mag})} \| J_i)$$

It is now possible using (2.107) to compute

$$\begin{aligned} & \frac{1}{2J_i + 1} \sum_{\substack{M_i M_f \\ \lambda, \lambda'}} \langle J_f M_f | j_\lambda | J_i M_i \rangle \langle J_f M_f | j_{\lambda'} | J_i M_i \rangle^* \\ &= \frac{2\pi}{2J_i + 1} \left[\sum_J |(J_f \| T_J^{(\text{mag})} \| J_i)|^2 + |(J_f \| T_J^{\text{el}} \| J_i)|^2 \right] \end{aligned} \quad (2.110)$$

One can now complete the evaluation of (2.97) for the cross section in the

[†]The derivation of (2.105) is straightforward when one realizes that $\mathbf{Y}_{JJ}^{(\lambda)}$ and $(1/q) \text{curl } j_J(qr) \mathbf{Y}_{JJ}^{(\lambda)}$ form mutually orthogonal and normalized sets of vector wave functions on the unit sphere. Thus the coefficient of $\mathbf{Y}_{JJ}^{(\lambda)}$ in expansion (2.105) is given by $\int d\Omega \mathbf{Y}_{JJ}^{(\lambda)\dagger} \cdot \mathbf{u}_\lambda e^{i\mathbf{q}\cdot\mathbf{r}}$. The coefficient of the second term is $1/q \int d\Omega \mathbf{Y}_{JJ}^{(\lambda)\dagger} \cdot \text{curl}(\mathbf{u}_\lambda e^{i\mathbf{q}\cdot\mathbf{r}})$.

center-of-mass frame. After some algebra it can be cast into the following form:

$$\frac{d\sigma}{d\Omega} = \sigma_M \left[\frac{q_\mu^4}{q^4} F_L^2(\mathbf{q}) + \left(\frac{1}{2} \frac{q_\mu^2}{q^2} + \tan^2 \frac{\vartheta}{2} \right) F_T^2(\mathbf{q}) \right] \quad (2.111)$$

where σ_M is the Mott cross section evaluated at the incident energy and

$$F_L^2 = \frac{4\pi}{2J_i + 1} \sum_{J_f=0} |(J_f \| \hat{M}_J^{(CO)}(\mathbf{q}) \| J_i)|^2 \quad (2.112)$$

and

$$F_T^2 = \frac{4\pi}{2J_i + 1} \sum_{J_f=1} \{ |(J_f \| \hat{T}_J^{(el)}(\mathbf{q}) \| J_i)|^2 + |(J_f \| \hat{T}_J^{(mag)}(\mathbf{q}) \| J_i)|^2 \} \quad (2.113)$$

Note that experimentally it is possible separately to determine F_L^2 and F_T^2 as functions of \mathbf{q} by suitably choosing the experimental parameters. For example, if $\vartheta \sim \pi$, the cross section is dominated by $|F_T|^2$. Varying the incident energy will then yield $|F_T(\mathbf{q})|^2$. The matrix elements in (2.112) and (2.113) reduce to those obtained from photon excitation if $q = \omega$ [see Chapter VIII in deShalit and Feshbach (74)]. Inelastic electron scattering gives a much more complete picture by providing the q dependence for $q > \omega$ and, by Fourier inversion, the spatial dependence of the current as well as the charge distribution. The selection rules are identical with those of the photon case, namely

$$\mathbf{J}_f = \mathbf{J}_i + \mathbf{J}$$

with parity changes of $(-)^J$ for $\hat{T}^{(el)}$ and $\hat{M}^{(CO)}$ and $(-)^{J+1}$ for $\hat{T}^{(mag)}$.

The current density \mathbf{j} , to be inserted into (2.108) and (2.109) to obtain $\hat{T}^{(el)}$ and $\hat{T}^{(mag)}$ have been discussed in Chapter VIII of deShalit and Feshbach (74). The point-charge current as given by (VIII.2.3) and (VIII.2.4) in that reference is broken up into two components, a convection spin-independent current \mathbf{j}_c , and a spin-dependent magnetization current, \mathbf{j}_m :

$$\mathbf{j} = \mathbf{j}_c + \mathbf{j}_m$$

$$\mathbf{j}_c = e \sum_i \frac{1}{2} (1 + \tau_3(i)) \frac{1}{2} [\mathbf{v}_i \delta(\mathbf{r} - \mathbf{r}_i) + \delta(\mathbf{r} - \mathbf{r}_i) \mathbf{v}_i] \quad (\text{VIII.2.3})$$

$$\mathbf{j}_m = \frac{e\hbar}{4m} \sum_i \frac{1}{2} [(g_n + g_p) + \tau_3(i)(g_p - g_n)] \text{curl}[\boldsymbol{\sigma}_i \delta(\mathbf{r} - \mathbf{r}_i)] \quad (\text{VIII.2.4})$$

The velocity \mathbf{v}_i is defined by

$$\mathbf{v}_i = \frac{i}{\hbar} [H, \mathbf{r}_i] = \frac{\partial H}{\partial \mathbf{p}_i} \quad (\text{VIII.2.5})$$

where H is the full Hamiltonian, including the electromagnetic terms.

However, nucleons have a finite nonzero size and have a structure. This has two consequences. First the delta functions in (VIII.2.3) and (VIII.2.4) must be replaced by form factors [see (VIII.3.8), deShalit and Feshbach (74)].

Second, the one-body operators of the equations above must be supplemented by two-body and higher-order operators whose physical origin lies in the meson exchange currents (MEC), which were mentioned briefly in Chapter VIII of deShalit and Feshbach (74). Currents are present whenever the nucleons in the nucleus exchange pions and other mesons such as the ρ and ω in the course of generating the nuclear force between the exchanging nucleons. The currents, known as *exchange currents*, will interact with an external electromagnetic field. The various contributions to that interaction are illustrated by Fig. 2.14. In Fig. 2.14a the electromagnetic wave is absorbed by a pion, indicated by a dashed line as the pion is exchanged. In Fig. 2.14b, the electromagnetic wave is absorbed by the nucleon, which may remain a nucleon. Or the γ -ray may make a N, \bar{N} pair, the latter interacting with one of the nucleons to make a pion which is then picked up by the other nucleon. Or the γ -ray may simply excite one of the nucleons, creating a nucleon isobar which then exchanges a pion with the other nucleon, reverting to the nucleon in its ground state. The final two diagrams, Fig. 2.14d and e, involve the heavy mesons designated by M and M' . The results, appropriate for transitions in complex nuclei, are summarized in the review article by Donnelly and Sick (84), to which the reader is referred for details and references. The short-range contributions described by Fig. 2.14d and c are not included. The diagram involving the nucleon intermediate state (Fig. 2.14b) is dropped since this term is automatically included in the convection current term. One is therefore left with contributions from Fig. 2.14c, the antinucleon intermediate state in Fig. 2.14b, and the excited nucleon intermediate state (Fig. 2.14c). The last will include both the Δ and Roper nucleon resonances. Importantly, to order $(1/M)$ (M = nucleon mass), ρ_{exch} is zero. In addition, the leading term is an isovector. Gauge invariance is guaranteed to the extent that wave functions used arise from nucleon-nucleon interactions involving the same diagrams (Fig. 2.14) used in calculating the exchange currents. If the wave functions and exchange currents are not consistent, there can be considerable error since the operators involved are not positive definite and therefore are sensitive to the properties of the wave functions.

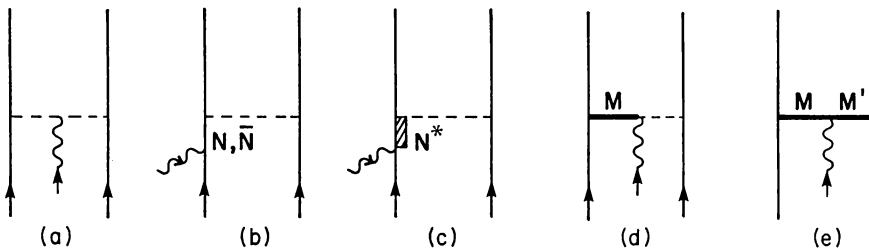


FIG. 2.14. Exchange currents.

H. Magnetic Elastic Electron Scattering

We turn now to the study of elastic magnetic electron scattering by nuclei [Donnelly and Sick (84)], from which $|F_T|^2$ of (2.111) and (2.113) may be determined as a function of the momentum transfer \mathbf{q} and compared to nuclear model predictions. In contrast to the charge scattering, the magnetic scattering is sensitive to the properties of the valence nucleons since the net contribution of the core nucleons is zero in the spherical shell model description. The information on single-particle states obtained from nuclear transfer reactions is complementary since the responsible nuclear interaction differs from the electron interaction. In addition, magnetic elastic scattering is sensitive to neutron and proton distribution, as the equation for \mathbf{j}_m [Eq. (VIII.2.4) in deShalit and Feshbach (74)] demonstrates.

Of course, the independent particle shell model is not correct. The deviations in the case of spherical nuclei are expressed in terms of configuration mixing, in which excited states of the core generated by the interaction with the valence nucleons are components of the total wave function. These interactions draw strength from the single-particle component, so that generally the magnetic elastic scattering crosssection is less than predicted by the extreme valence nucleon model. This fragmentation of the strength is clearly visible for deformed nuclei, where the Nilsson orbitals (which in the limit of zero deformation combine to yield a spherical orbital) play the dominant role. The magnetic elastic scattering by odd- A nuclei is sensitive to coupling of the valence particle with the deformed core. As expected, there is a reduction from the values predicted in the absence of this coupling. Much of the strength available in the spherical limit now goes into the inelastic scattering of the excited states built on the deformed ground state. Finally, in spherical cases for which the convection current \mathbf{j}_c effects are dominant, the exchange current effects may be observable. We shall now illustrate these points with examples drawn from Donnelly's and Sick's (84) review. As we shall see, detailed information on the single-particle wave functions that these experiments yield is quite remarkable.

We first consider elastic magnetic scattering by a target nucleus with a spin J_0 . It is assumed that the scattering caused by a single unpaired valence nucleon whose angular momentum is also J_0 ; the net angular momentum of the remaining nucleus equals zero. Moreover, we select those nuclei for which $J_0 = l + \frac{1}{2}$ (l = orbital angular momentum), that is, a stretched configuration. The largest multipole order is then $2J_0$. For this case the contribution of the convection current vanishes since it will be proportional to the square of the reduced matrix element $(\frac{1}{2}lJ_0 \| Y_{2J_0} \| \frac{1}{2}lJ_0)$. From (A.2.49) and (A.2.81) of deShalit and Feshbach (74) we have

$$(\frac{1}{2}lJ_0 \| Y_{2J_0} \| \frac{1}{2}lJ_0) \sim \begin{Bmatrix} J_0 & J_0 & 2J_0 \\ J_0 - \frac{1}{2} & J_0 - \frac{1}{2} & \frac{1}{2} \end{Bmatrix} \begin{pmatrix} J_0 - \frac{1}{2} & J_0 - \frac{1}{2} & 2J_0 \\ 0 & 0 & 0 \end{pmatrix}$$

The $6-j$ symbol vanishes since $\mathbf{J}_0 - \frac{1}{2} + \mathbf{J}_0 - \frac{1}{2} \neq 2\mathbf{J}_0$. As a consequence, only

the magnetization current, \mathbf{j}_m , contributes to $|F_T|^2$, it is, moreover, easy to show that

$$F_T \sim \int R^2(r) j_{(2J_0-1)}(qr) r^2 dr \quad (2.114)$$

where R is the radial function for the single-particle valence wave function. Inversion to obtain R^2 with the limitations discussed earlier with respect to the determination of the charge density is possible in principle[†]

The discussion above assumes the validity of the single orbital description of the nuclear ground state. There will, of course, be configuration mixing. However, the additions to the single-particle contribution that can contribute to the $2J_0$ multipole moment transition must involve an orbital with $j \geq J_0$. Such an orbital with the correct parity will be available first, two shells above involving an excitation of $2\hbar\omega$. One therefore expects a very small amplitude for such a component in the ground state. Thus the form factor F_T will still be given by (2.114). The only effect on this transition of configuration mixing will be a reduction in the magnitude of F_T which can be related to the spectroscopic factor associated with that state as determined from nucleon inelastic scattering or from a transfer reaction.

For multipole moments of order less than $2J_0$, configuration mixing can have a large effect. This is particularly true when the configuration added is one that would readily be excited in an inelastic collision. Under those circumstances there will be interference between the strong single-particle term and the added configuration. The result will be to reduce the value of F_T , since some of the single-particle strength will be lost to inelastic channels. Obviously, states of the core that can be strongly excited play an important role.

Finally, experimentally the contribution of the very largest possible multipole moment will be very visible in the large q domain. The contribution of the moments of lower order will decrease rapidly for large enough momentum transfer q . However, this domination by the large multipole moment does not persist for a sufficiently large range of q at the low- q side, so that the inversion indicated by (2.114) is not feasible.

Many of these conclusions are exemplified by magnetic elastic scattering from ^{17}O . Because of the close agreement of the magnetic moment of ^{17}O with the single-particle Schmidt value, it has been thought that this was a good example of a valence nucleon (in this case a neutron in a $d_{5/2}$ state) moving in the field of an ^{16}O core. As illustrated in Fig. 2.15, we see that the single-particle

[†]Note: Use the result

$$\text{curl}(j_J \mathbf{Y}_{JJ}) = -i \left(\frac{J}{2J+1} \right)^{1/2} j_{J+1} \mathbf{Y}_{J,J+1} + i \left(\frac{J+1}{2J+1} \right)^{1/2} j_{J-1} \mathbf{Y}_{J,J-1}$$

and (A.2.49) and (A.2.81).

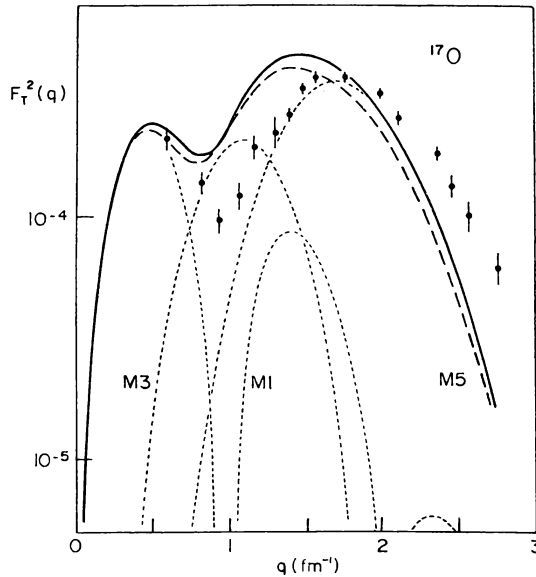


FIG. 2.15. The ^{17}O data of Hynes, Miska, et al. (79) are compared to prediction of the extreme single-particle model calculated using a harmonic oscillator wave function (solid curve). The dashed curve is calculated using a Woods-Saxon radial wave function. [From Hynes, Miska, et al. (79).]

model greatly overestimates $|F_T|^2$ for values of q between about 0.9 and 1.8 fm^{-1} and underestimates $|F_T|^2$ for greater values of q . When configuration mixing is introduced phenomenologically [Burzynski, Baumgartner, et al. (83)], one obtains Fig. 2.16. The contribution of the MEC is estimated theoretically. The M5 and M1 components are very close to the predictions of the single-particle model. This is expected for M5 and the low- q values of M1. However, the M3 component is strongly reduced, indicating the effect of configuration mixing with core excited states. It was pointed out by Zamick (78) and examined in detail by Bohannon, Zamick, and Moya de Guerra (80) that the admixtures induced by an E2 M1 excitation of the nucleus will have a strong overlap through the M3 multipole with the single-particle orbital. This reduced the M3 moment by a factor of 2 [see also Arima, Horikawa, et al. (78)]. This excitation will not affect the M1 or M5 multipole.

Configuration mixing in terms of spherical nuclear wave function is very large for deformed nuclei. The effects described above are present, for example, for magnetic elastic scattering by ^{25}Mg . In Fig. 2.17, the results using a spherical single-particle wave function for the valence neutron are compared with the results obtained using a Nilsson orbital wave function, and with experiment. We observe a general reduction from the spherical case. The shape of the M5 form factor is not much changed, but the M3 form factor is greatly reduced.

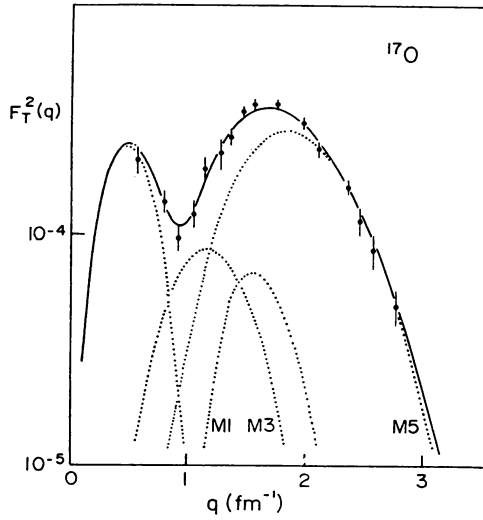


FIG. 2.16. The ^{17}O data of Hynes, Miska, et al. (79) corrected for the contribution of MEC, are compared to the fit of Burzynski, Baumgartner et al. (83) calculated using a Woods–Saxon radial wave function. [From Donnelly and Sick (84).]

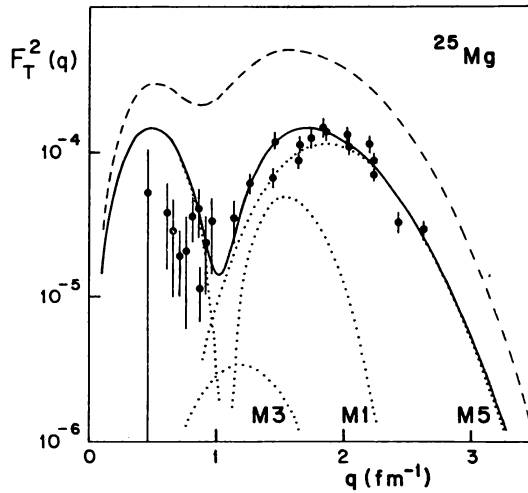


FIG. 2.17. The ^{25}Mg magnetic form factor is shown for the ESPM (dashed curve) and the Nilsson model (solid and dotted curves), all calculated using harmonic oscillator radial wave functions ($b = 1.63 \text{ fm}$). [From Donnelly and Sick (84).]

The major lesson to be learned from these examples is that configuration mixing must be taken into account before a quantitative agreement between theory and experiment is possible. The wave functions are rarely describable by the naive independent-particle model. Once configuration mixing is taken into account and occasionally, the effect of exchange currents included (with a considerable error $\sim 50\%$), agreement with experiment is obtained. (Note that the comparisons with experiment are made on semilog plots.)

Parenthetically, the data on the M1 transition as well as the isoscalar and isovector magnetic moment and the Gamow–Teller matrix element as obtained from β decay and (p, n) reactions have been analyzed for nuclei in the s – d shell by Brown and Wildenthal and their colleagues [Brown (86)]. The wave functions are obtained by treating the two-body residual interaction matrix elements as empirical parameters which are determined by the ground and excited states in the s – d shell. [see Brown (86) for a review.] The resultant wave functions can then be used in the evaluation of the transition matrix elements. Very briefly, it is found possible to fit the data mentioned above by assuming an M1 operator that varies smoothly with A . The free nucleon M1 operator is [see Chapter VIII] is deShalit and Feshbach (74)]

$$M1 = g_s \mathbf{s} + g_l \mathbf{l}$$

To this operator one adds a “correction”

$$g_s[\delta_s \mathbf{s} + \delta_l \mathbf{l} + \delta_p(\sqrt{8\pi}[Y_2 \times \mathbf{s}]^{(1)})]$$

where δ_s , δ_l , and δ_p are parameters. The third term includes configuration mixing of the type suggested by Zamick (78).

The parameters are found empirically to vary smoothly with A .

I. Quasi-Elastic Scattering

In this section the processes in which one or more nucleons are ejected from the nucleus by the incident electron are discussed. The term *quasi-elastic scattering* is used because it is thought that because of the high electron energy, nucleon knockout is the consequence of the elastic collision of the electron, with a nucleon in the nucleus having a momentum $\hbar \mathbf{k}$. As a consequence, it should be possible to determine the nucleon momentum distribution by observing the angular and energy distribution of the final electron. This hope is encouraged by the success of the analogous experiment determining the momentum distribution of the electrons in an atom. However, as we shall see, there are important limitations. It is convenient to mention one of these now. In an inclusive experiment, $(e, e'X)$, in which only the scattered electron is observed, it is possible that more than one nucleon is ejected from the nucleus. Moreover, generally the final nucleus may be left in a highly excited state. In

the multiple scattering picture of Chapter II, the nucleon initially struck by the electron will be scattered by the other nucleons in the nucleus, thereby exciting the residual nucleus and possibly ejecting a second nucleon.

The kinematics implied by the simple single-nucleon knockout has been discussed in Chapter I [see (I.3.9)]. A brief review is in order. An incident electron with momentum $\hbar\mathbf{k}_1$ is scattered by a nuclear nucleon of momentum $\hbar\mathbf{k}$, thus acquiring a momentum $\hbar\mathbf{k}_2$ (see Fig. 2.18). The momentum and energy transfer to the nucleon is $\hbar\mathbf{q} = \hbar(\mathbf{k}_1 - \mathbf{k}_2)$ and $\hbar\omega$, respectively. The emerging nucleon has a momentum $\hbar(\mathbf{k} + \mathbf{q})$. Nonrelativistic conservation of energy requires

$$\frac{\hbar^2}{2m^*}(\mathbf{k} + \mathbf{q})^2 = \frac{\hbar^2 k^2}{2m^*} + \hbar\omega - \varepsilon_b \quad (2.115)$$

where ε_b is the minimum energy needed to remove the nucleon from the nucleus and m^* is the effective mass assumed to be the same for the target and the ejected nucleon. [See, however, the discussion of the effective mass in Chapter V, where we find that the effective mass is a function of momentum and energy.] Solving the equation above for $\hbar\omega$, we obtain

$$\hbar\omega = \varepsilon_b + \frac{\hbar^2}{2m^*}(2\mathbf{k} \cdot \mathbf{q} + q^2) \quad (2.116)$$

Hence $\hbar\omega$ is bounded:

$$\varepsilon_b + \frac{\hbar^2}{2m^*}(-2k_F q + q^2) < \hbar\omega < \varepsilon_b + \frac{\hbar^2}{2m^*}(2k_F q + q^2)$$

The quasi-elastic peak will thus have a width given approximately by $(\hbar^2/m^*)k_F q$. The spreading is a consequence of the Fermi motion of the target nucleon. The effects of the nucleon interactions are crudely taken into account through the use of the effective mass. Examples of the quasi-elastic peak for three target nuclei are given in Fig. 2.19. The reader can check that the width is given approximately by $(\hbar^2/m)k_F q$.

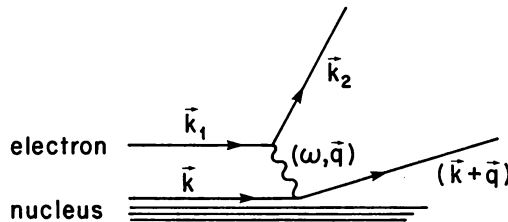


FIG. 2.18. Diagram for the $(e, e' p)$ process.

The inclusive differential cross section for the $(e, e'x)$ reaction can be obtained directly from (2.111). It is

$$\frac{d\sigma}{d\Omega_2 dE_2} = \sigma_M \left[\frac{q_\mu^4}{q^4} R_L + \left(\frac{1}{2} \frac{q_\mu^2}{q^2} + \tan^2 \frac{\theta}{2} \right) R_T \right] \quad (2.117)$$

where

$$R_L = \sum |\langle f | \rho(\mathbf{q}) | i \rangle|^2 \delta(E_i - E_f) \quad (2.118a)$$

and

$$R_T = \sum [|\langle f | j_1 | i \rangle|^2 + |\langle f | j_{-1} | i \rangle|^2] \delta(E_i - E_f) \quad (2.118b)$$

In these equations the sum is taken over all final states designated by f and averaged over the initial states designated by i . The delta function indicates that only those final states that conserve energy are to be included in the sum.

The sum includes an integral over the continuum in the case of particle emission. For example, for the case of proton emission, $(e, e'p)$,

$$R_L = \int \sum |\langle f_N | \rho(\mathbf{q}) | i \rangle|^2 \delta \left(\hbar\omega - \frac{\hbar^2}{2m} \kappa^2 - (E_N - E_A) - E_R \right) \frac{d\kappa}{(2\pi)^3} \quad (2.119)$$

where $\hbar\kappa$ is the momentum of the emitted proton and E_R is the recoil energy. The sum is now over *residual* nuclear states, which in the case of closed-shell nuclei, are one-hole states. $E_N - E_A$ is the excitation energy of those states. To obtain the *exclusive* cross section, one drops the integral, and dividing (2.117) by $d\mathbf{\kappa}$ one obtains an expression for $d\sigma/(d\Omega_2 dE_2)(d\Omega_\kappa dE_\kappa)$.

Employing the model illustrated in Fig. 2.18, (2.119) becomes

$$R_L = \int \sum |\langle f_N | \rho(\mathbf{q}) | i \rangle|^2 \delta \left(\frac{\hbar^2 k^2}{2m^*} + \hbar\omega - \varepsilon_b - \frac{\hbar^2 (\mathbf{k} + \mathbf{q})^2}{2m^*} \right) \frac{d\mathbf{k}}{(2\pi)^3} \quad (2.120)$$

Note the shift from $d\mathbf{\kappa}$ to $d\mathbf{k}$ which is possible in the model because κ and \mathbf{k} are linearly related. But \mathbf{k} refers to the initial nucleon momenta, so that R_L depends on the nucleon momentum distribution. A first overview of the quasi-elastic process is obtained by using the Fermi-gas model. Then

$$R_L = \frac{3Z}{4\pi k_F^3} \int_0^{k_f} d\mathbf{k} \theta(k_F - k) \delta \left(\frac{\hbar^2 k^2}{2m^*} + \hbar\omega - \varepsilon_b - \hbar^2 \frac{(\mathbf{k} + \mathbf{q})^2}{2m^*} \right) \quad (2.121)$$

where $\theta(x)$ is the unit function, $\theta(x) = 1$, $x > 0$, $\theta(x) = 0$, $x < 0$. The integration can be readily carried out. The results are given by deForest and Walecka (66) or Donnelly and Walecka (75). Here we note only that for large $q(> 2k_F)$, R_L is proportional to $1/q \{ 1 - [(\hbar\omega - \varepsilon_b)m^*/k_F q + q/2k_F]^2 \}$, a parabolic function of $(\hbar\omega - \varepsilon_B)$.

Calculations by Moniz, Sick, et al. (71) using the Fermi-gas model with ε_b and k_F empirical parameters have been compared with the experimental results (the target nucleus is ^{12}C) shown in Fig. 2.19. The agreement is excellent and the empirical values of ε_b and k_F reasonable (see Fig. I.3.4). However, when the longitudinal and transverse cross sections are separately compared with experiment, this nice agreement disappears. That comparison [Ciofi degli Atti and Salmè (84)] is shown in Figs. 2.20 and 2.21. One sees (the dotted-dashed curve) that the Fermi gas model overestimates the longitudinal cross section by a large factor; agreement with the transverse cross section is good. When a more realistic nuclear model is employed (i.e., the Hartree-Fock model) and final state interactions of the emerging nucleon are included (the solid line), excellent agreement with the longitudinal cross section is obtained.

The expression (2.121) exhibits the property of *scaling* [see West (75); Sick, Day, and McCarthy (80); Sick (87)]. The δ -function factor can be rewritten as follows:

$$\begin{aligned} \delta\left(\frac{\hbar^2 k^2}{2m^*} + \hbar\omega - \varepsilon_b - \frac{\hbar^2(\mathbf{k} + \mathbf{q})}{2m^*}\right) &= \delta\left(\hbar\omega - \varepsilon_b - \frac{\hbar^2 q^2}{2m^*} - \frac{\hbar^2}{m^*} \mathbf{k} \cdot \mathbf{q}\right) \\ &= \frac{m^*}{\hbar^2 q} \delta\left(\frac{m^*}{\hbar^2 q} (\hbar\omega - \varepsilon_b) - \frac{q}{2} - k_{\parallel}\right) \\ &= \frac{m^*}{\hbar^2 q} \delta(y - k_{\parallel}) \end{aligned} \quad (2.122)$$

where k_{\parallel} is the component of \mathbf{k} parallel to \mathbf{q} and

$$y \equiv \frac{m^* (\hbar\omega - \varepsilon_b) - q^2/2}{\hbar^2 q} \quad (2.123)$$

$$\begin{aligned} &= \frac{m^*}{2\hbar^2} \frac{[\sqrt{2(\hbar\omega - \varepsilon_b)} - q][\sqrt{2(\hbar\omega - \varepsilon_b)} + q]}{q} \\ &\xrightarrow[\omega \rightarrow \infty]{q \rightarrow \infty} \frac{m^*}{2\hbar^2} [\sqrt{2(\hbar\omega - \varepsilon_b)} - q] \end{aligned} \quad (2.124)$$

Inserting (2.122) into (2.121) for R_L , we observe that qR_L is a function of y only. Thus all experiments performed at identical values of y by choosing the appropriate ω and q should, according to the Fermi model, have identical values of qR_L .

Although the results above are instructive, it is necessary to go beyond the Fermi gas model and employ a more accurate description of the nucleus. Toward that end we rewrite R_L as follows:

$$\begin{aligned} R_L &= \sum \langle i | \rho^\dagger(\mathbf{q}) f \rangle \langle f | \rho(\mathbf{q}) | i \rangle \delta(E_i - E_f) \\ &= \sum \langle i | \rho(\mathbf{q}) \delta(E_i - H) | f \rangle \langle f | \rho(\mathbf{q}) | i \rangle \end{aligned} \quad (2.125)$$

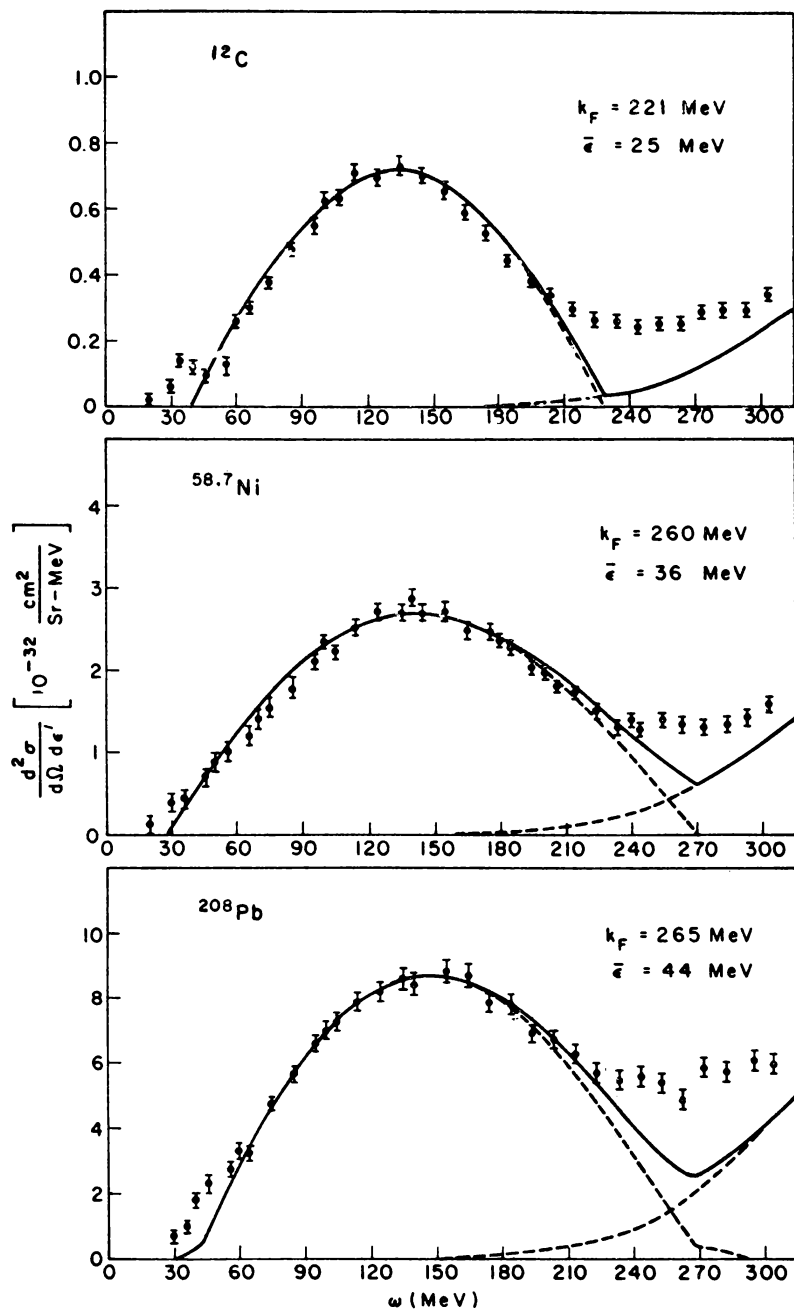


FIG. 2.19. Cross sections for quasi-elastic electron scattering. The electron's energy is 500 MeV. The scattered electron is observed at 60° . The solid lines are the results of Fermi-gas calculations with parameters indicated on the figure. [From Moniz, Sick, et al. (71).]

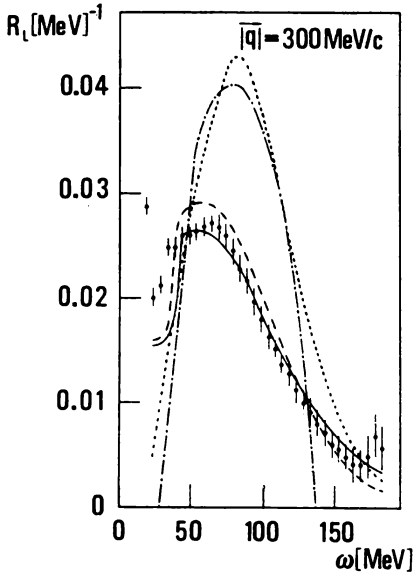


FIG. 2.20. Experimental and theoretical longitudinal response functions. Dotted curve, Hartree-Fock results without final-state interaction; dashed curve, Hartree-Fock results with final-state interaction, optical model potential real, solid curve, Hartree-Fock results with final-state interaction, optical model potential complex; Dashed-dotted curve, Fermi-gas result. [From Ciofi degli Atti and Salmè (84).]

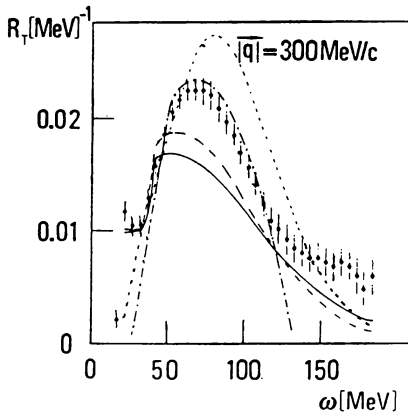


FIG. 2.21. Same as Fig. 2.20 for the transverse response function. [From Ciofi degli Atti and Salmè (84).]

The Hamiltonian can be decomposed into the Hamiltonian H_N for the residual nucleus plus the Hamiltonian H_0 for the emerging nucleon, including its interaction with the residual nucleus:

$$H = H_0 + H_N$$

where

$$H_0 = T + V$$

At this point it is convenient to make approximations that are valid in the high-energy regime. A similar set of approximations are described in Chapter II on multiple scattering. First we replace V , which is in fact a many-body operator, by an effective optical potential of the nucleon moving in the field of the residual nucleus. Second, H_N is replaced by an average energy $\bar{\epsilon}$, the excitation energy of the residual nucleus. Finally, the initial energy E_i is taken to be the ground-state energy of the target nucleus, taken to be zero, plus the energy transferred by the incident electrons to the nuclear system $\hbar\omega$. With these assumptions, R_L becomes

$$R_L = \sum_f \langle i | \rho^\dagger(\mathbf{q}) \delta(\hbar\omega - \bar{\epsilon} - H_0) | f \rangle \langle f | \rho(\mathbf{q}) | i \rangle$$

Performing the sum over the final states yields

$$R_L = \langle i | \rho^\dagger(\mathbf{q}) \delta(\hbar\omega - \bar{\epsilon} - H_0) \rho(\mathbf{q}) | i \rangle \quad (2.126)$$

Using the identity

$$\text{Im} \frac{1}{\hbar\omega - \bar{\epsilon} - H_0 + i\epsilon} = -\frac{1}{\pi} \delta(\hbar\omega - \bar{\epsilon} - H_0) \quad (2.127)$$

one has

$$R_L = -\frac{1}{\pi} \text{Im} \left\langle i \left| \rho^\dagger(\mathbf{q}) \frac{1}{\hbar\omega - \bar{\epsilon} - H_0 + i\epsilon} \rho(\mathbf{q}) \right| i \right\rangle \quad (2.128)$$

We now approximate the Green's function in this expression by its eikonal limit [see Gurvitz and Rinat (87)]:

$$\left\langle \mathbf{r} \left| \frac{1}{\hbar\omega - \bar{\epsilon} - H_0 + i\epsilon} \right| \mathbf{r}' \right\rangle = -\frac{im}{\hbar^2 K} e^{iK(z-z')} \delta(\mathbf{b} - \mathbf{b}') \theta(z - z') e^{(1/2iK) \int_z^\infty U(\zeta, \mathbf{b}) d\zeta} \quad (2.129)$$

where

$$K^2 = \frac{2m}{\hbar^2} (\hbar\omega - \bar{\epsilon}) \quad \text{and} \quad U = \frac{2m}{\hbar^2} V$$

Note. To derive this result, note that

$$\left\langle \mathbf{r} \left| \frac{1}{\hbar\omega - \bar{\epsilon} - H_0 + i\epsilon} \right| \mathbf{r}' \right\rangle = G(\mathbf{r}, \mathbf{r}')$$

satisfies

$$\left(\hbar\omega - \bar{\epsilon} + \frac{\hbar^2}{2m} \nabla^2 - V \right) G = \delta(\mathbf{r} - \mathbf{r}') = \delta(z - z') \delta(\mathbf{b} - \mathbf{b}).$$

Let

$$G = e^{iK(z-z')} g$$

Then approximately (neglecting $\nabla^2 g$ compared to $2K \partial g / \partial z$)

$$2iK \frac{\partial g}{\partial z} - U g = \frac{2m}{\hbar^2} \delta(z - z') \delta(\mathbf{b} - \mathbf{b})$$

Equation (2.129) is obtained by integrating this first-order equation.

Inserting (2.129) and

$$\rho(\mathbf{q}) = \sum_{\mathbf{r}_i} e^{i\mathbf{q} \cdot \mathbf{r}_i} \Rightarrow Z e^{i\mathbf{q} \cdot \mathbf{r}}$$

into (2.128) for R_L , one finds that

$$R_L = \frac{mZ^2}{\pi\hbar^2 K} \text{Re} \int d\mathbf{r} \int d\mathbf{r}' \rho(\mathbf{r}, \mathbf{r}') e^{i\mathbf{q} \cdot (\mathbf{r}' - \mathbf{r})} e^{iK(z-z')} \delta(\mathbf{b} - \mathbf{b}') \theta(z - z') e^{(1/2iK) \int_z^z d\zeta U(\zeta, \mathbf{b})}$$

where $\rho(\mathbf{r}, \mathbf{r}')$ is the density matrix:

$$\rho(\mathbf{r}, \mathbf{r}') = \int \psi^*(\mathbf{r}, \mathbf{r}_2, \dots) \psi(\mathbf{r}', \mathbf{r}_2, \dots) d\mathbf{r}_2 \dots$$

[see (2.88) et seq.].

Carrying out the integrations over \mathbf{b} and choosing the z direction to be along \mathbf{q} , we have

$$R_L = \frac{mZ^2}{\pi\hbar^2 K} \text{Re} \left[\int_{-\infty}^{\infty} d\mathbf{b} dz \int_{-\infty}^{\infty} dz' \rho(z, \mathbf{b}; z' \mathbf{b}) e^{i(K-q)(z-z')} \theta(z - z') e^{-(i/2K) \int_z^{z'} U d\zeta} \right] \quad (2.130)$$

Scaling no longer prevails since the final factor that reflects the final-state interaction is not a function of $K - q$. The exponent can be expanded in a series in $(K - q)/q$, so that scaling is approached when $(K - q)/q \ll 1$. The simple Fermi-gas model leading to (2.121) requires further approximation. More accurately, the quasi-elastic inclusive electron scattering probes the density matrix $\rho(z, \mathbf{b}; z' \mathbf{b})$.

Problem. Using expansion, (2.88) shows that in the absence of final-state interaction effects

$$\begin{aligned}
 R_L &= \text{Re} \int d\mathbf{b} \int_{-\infty}^{\infty} dz \int_{-\infty}^{\infty} dz' \rho(z, \mathbf{b}; z' \mathbf{b}) e^{i(K-q)(z-z')} \theta(z-z') \\
 &= \sum \kappa_\lambda \text{Re} \frac{1}{2\pi i} \int d\mathbf{b} \int_{-\infty}^{\infty} \frac{dt}{t+i\epsilon} |\bar{\omega}_\lambda(t+K-q, \mathbf{b})|^2 \\
 &= -\frac{1}{2} \sum \kappa_\lambda \int d\mathbf{b} |\bar{\omega}_\lambda(K-q, \mathbf{b})|^2 \\
 &= -\frac{1}{8\pi^2} \sum \kappa_\lambda \int d\mathbf{s} |\Omega_\lambda(K-q, \mathbf{s})|^2
 \end{aligned}$$

where

$$\bar{\omega}_\lambda(K-q, \mathbf{b}) = \int_{-\infty}^{\infty} dz e^{i(K-q)z} \omega_\lambda(z, \mathbf{b})$$

and

$$\Omega_\lambda = \int e^{-i\mathbf{s} \cdot \mathbf{b}} e^{i(K-q)z} \omega_\lambda(z, \mathbf{b}) d\mathbf{r}$$

In addition, scaling is no longer possible when relativistic effects are taken into account [see Alberico et al (88)]. Nevertheless, it is clearly exhibited experimentally, as one can see from Fig. 2.22. Scaling is observed for $y < 0$ but is not obtained for $y > 0$. Similar results have been obtained for ${}^4\text{He}$, ${}^{12}\text{C}$, ${}^{27}\text{Mg}$, and ${}^{197}\text{Au}$ [Day et al. (88)]. The lack of scaling for $y > 0$ is presumably because the reaction mechanism for large energy transfers is no longer primarily the ejection of a single nucleon.

Note. The potential U in (2.130) is obtained by fitting the elastic scattering data. It is a possibly useful property of the eikonal approximation that one can express the exponential involving U in terms of the nuclear scattering amplitude of a nucleon moving in the \mathbf{q} direction. We recall from Chapter II [Eq. (II.5.8)] that the *elastic* scattering amplitude is, in the eikonal approximation, given by

$$f(\mathbf{Q}) = -\frac{1}{4\pi} \int d\mathbf{r} e^{i\mathbf{Q} \cdot \mathbf{r}} U(\mathbf{r}) e^{-(i/2K) \int_{-\infty}^{\infty} U(\zeta, \mathbf{b}) d\zeta} \quad (2.131)$$

Using the Fourier integral theorem, one can invert the equation to obtain

$$U(\mathbf{r}) e^{-(i/2K) \int_{-\infty}^{\infty} U(\zeta, \mathbf{b}) d\zeta} = -\frac{4\pi}{(2\pi)^3} \int d\mathbf{Q} f(\mathbf{Q}) e^{-i\mathbf{Q} \cdot \mathbf{r}}$$

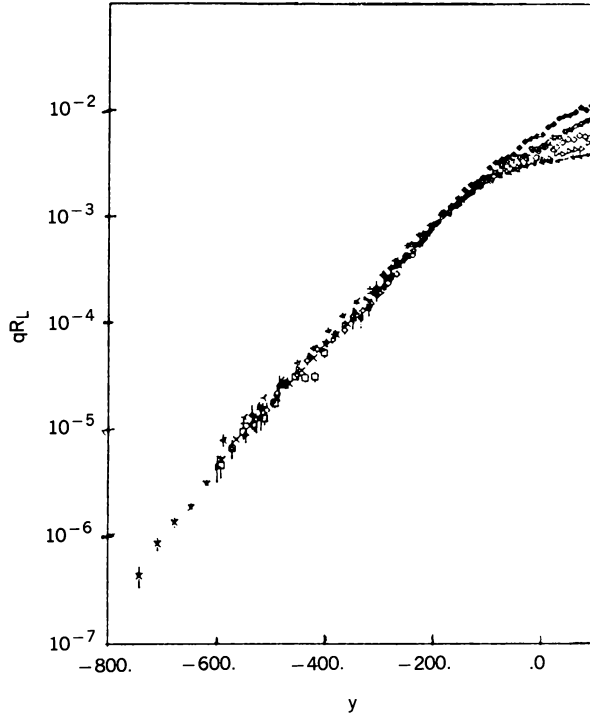


FIG. 2.22. See (2.123) et seq. [From Sick (81).]

To remove the prefactor $U(\mathbf{r})$, integrate both sides of the equation from zero to z . One obtains

$$2iK[e^{-(i/2K)\int_{-\infty}^z U(\zeta, \mathbf{b})d\zeta} - e^{-(i/2K)\int_{-\infty}^0 U(\zeta, \mathbf{b})d\zeta}] = -\frac{4\pi i}{(2\pi)^3} \int d\mathbf{Q} f(\mathbf{Q}) e^{-i\mathbf{Q}\cdot\mathbf{b}} \frac{e^{-iQ_L z} - 1}{Q_L}$$

so that

$$e^{-(i/2K)\int_{-\infty}^z U(\zeta, \mathbf{b})d\zeta} = e^{-(i/2K)\int_{-\infty}^0 U(\zeta, \mathbf{b})d\zeta} - \frac{1}{(2\pi)^2 K} \int d\mathbf{Q} f(\mathbf{Q}) e^{-i\mathbf{Q}\cdot\mathbf{b}} \frac{e^{-iQ_L z} - 1}{Q_L}$$

where Q_L is the component of \mathbf{Q} in the \mathbf{q} direction. The desired quantity

$$e^{-(i/2K)\int_{-\infty}^z U(\zeta, \mathbf{b})d\zeta} = \frac{e^{-(i/2K)\int_{-\infty}^0 Ud\zeta} - [1/(2\pi)^2 K] \int d\mathbf{Q} f(\mathbf{Q}) e^{-i\mathbf{Q}\cdot\mathbf{b}} (e^{-iQ_L z} - 1)/Q_L}{e^{-(i/2K)\int_{-\infty}^0 Ud\zeta} - [1/(2\pi)^2 K] \int d\mathbf{Q} f(\mathbf{Q}) e^{-i\mathbf{Q}\cdot\mathbf{b}} (e^{-iQ_L z'} - 1)/Q_L} \quad (2.132)$$

From this equation one obtains

$$e^{-(i/2K)\int_{-\infty}^0 U(\zeta, \mathbf{b})d\zeta} - \frac{1}{(2\pi)^2 K} \lim_{z' \rightarrow \infty} \int d\mathbf{Q} f(\mathbf{Q}) \frac{e^{-iQ_1 z'} - 1}{Q_1} = 1$$

or

$$e^{-(i/2K)\int_{-\infty}^0 U(\zeta, \mathbf{b})d\zeta} = 1 - \frac{i}{4\pi K} \int d\mathbf{Q} f(\mathbf{Q}_T, 0) e^{-i\mathbf{Q} \cdot \mathbf{b}} \quad (2.133)$$

where \mathbf{Q}_T is the component of \mathbf{Q} perpendicular to \mathbf{q} . Substituting in (2.132) yields the desired expression:

$$\begin{aligned} & e^{-(i/2K)\int_x^z U(\zeta, \mathbf{b})d\zeta} \\ &= \frac{1 - (i/4\pi K) \int d\mathbf{Q}_T f(\mathbf{Q}_T, 0) e^{-i\mathbf{Q} \cdot \mathbf{b}} - (1/4\pi^2 K) \int d\mathbf{Q} f(\mathbf{Q}) e^{-i\mathbf{Q} \cdot \mathbf{b}} [(e^{-iQ_1 z} - 1)/Q_1]}{1 - (i/4\pi K) \int d\mathbf{Q}_T f(\mathbf{Q}_T, 0) e^{-i\mathbf{Q} \cdot \mathbf{b}} + (1/4\pi^2 K) \int d\mathbf{Q} f(\mathbf{Q}) e^{-i\mathbf{Q} \cdot \mathbf{b}} [(e^{-iQ_1 z'} - 1)/Q_1]} \end{aligned} \quad (2.134)$$

Another procedure valid at high energy begins with the relation

$$G = G_0 + G_0 \mathcal{T} G_0$$

where $G^{-1} = E + i\varepsilon - H$ and $G_0^{-1} = E + i\varepsilon - H_N$, $H = H_N + V$, and \mathcal{T} is the transition matrix for the scattering of a proton by the $(A-1)$ nucleus. If in the second term one approximates G_0 by its energy on the energy-shell component, \mathcal{T} will involve reaction amplitudes whose corresponding cross sections can be obtained from experiment.

J. The Reaction $(e, e'N)^\dagger$

The reaction discussed in the preceding section is referred to as an *inclusive* reaction since only the emerging electron is observed. Effectively, therefore, all possible final states contribute to the cross section. In this section the reaction $(e, e'N)$, where N is a nucleon, is considered. This is an *exclusive* reaction since only one final system is observed. Such measurements are coincidence experiments; that is, both the final electron and ejected nucleon momenta and energy are measured. The experimental arrangement is illustrated schematically in Fig. 2.23. The shaded plane is the scattering plane containing the incident \mathbf{k}_i and final momenta \mathbf{k}_f of the electron. The unshaded plane contains the momentum transfer \mathbf{q} and the emergent proton whose momentum makes an angle θ_p with respect to \mathbf{q} . The angle between the two planes is ϕ_p . In a typical experiment the energies of the emerging electron and proton are measured.

[†]Dieperink and DeForest (75); DeForest (67); Co' et al. (87).

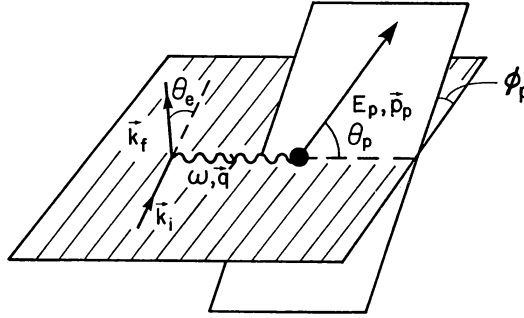


FIG. 2.23. Diagram for the $(e, e'p)$ reaction.

Their sum will not equal the incident electron energy since some of the energy has gone into the excitation of the residual nucleus. The difference

$$E_m = \hbar\omega - E_p - (E_{A-1}^{(f)} - E_A) - E_R \quad (2.135)$$

is referred to as the missing energy or the removal energy. Here E_R is the recoil energy of the residual nucleus, while $E_{A-1}^{(f)} - E_A$ is the excitation energy for the excitation of a final state E_f of the $A - 1$ nucleus. If the cross section is plotted as a function of the missing energy, one will see relatively sharp peaks which can be identified with single hole state. An example is presented in Fig. 2.24.

In addition, one can also determine the cross section as a function of the missing momentum. In the Born approximation in which the emerging proton wave function is taken as a plane wave with momentum \mathbf{p} , the longitudinal response function, the important factor in these experiments becomes

$$R_L = \sum_f |\phi_f(\mathbf{p}_p - \mathbf{q})|^2 \delta(\hbar\omega - E_p - (E_{A-1}^{(f)} - E_A) - E_R) \quad (2.136)$$

where $\phi_f(\mathbf{p}_p - \mathbf{q})$ is the wave function of the hole state of the final nucleus in momentum space. This result suggests that determining the cross section in the energy domain where the delta function condition is satisfied will yield the momentum distribution of the hole state. Note that $\mathbf{p}_p - \mathbf{q}$ is the recoil momentum of the target nucleus. It is also referred to as the missing momentum p_m . This is illustrated in Fig. 2.25. We see the characteristic shapes of a p and an s single-particle nucleon wave function emerges. Note the differing ranges of E_m , the missing energy for the two cases. The dotted-dashed curve follows from (2.136) using the Elton-Swift (67) wave function. A better approximation to R_L uses the DWA. The matrix element $\langle f | \rho | i \rangle$ is then given by

$$\langle f | \rho | i \rangle = \sum_i \int \langle \psi_f | \Psi_i \rangle e^{i\mathbf{q} \cdot \mathbf{r}_i} \chi^{(-)*}(\mathbf{r}_p) d\mathbf{r}_p \quad (2.137)$$

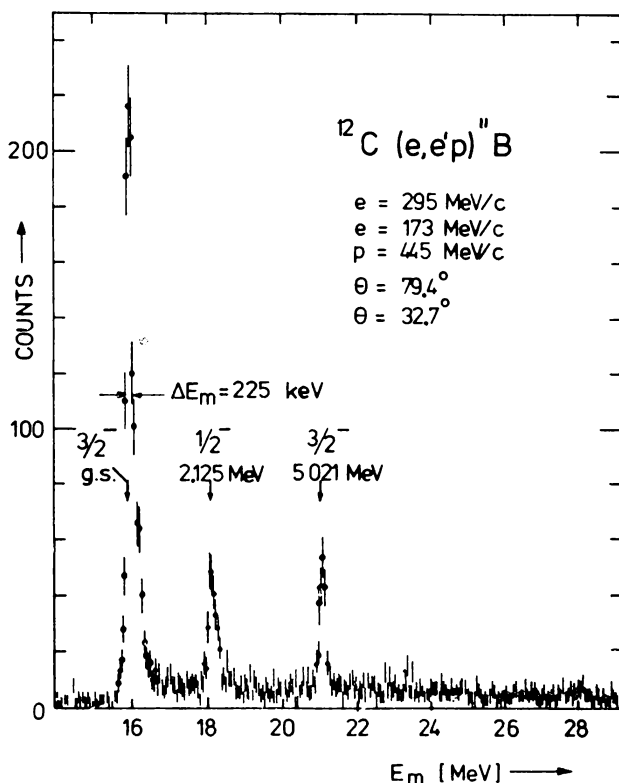


FIG. 2.24. Missing energy (E_m) spectrum of the reaction $^{12}\text{C}(e, e'p)^{11}\text{B}$ showing an energy resolution of 225 keV. Excited states in the residual nucleus ^{11}B are indicated. [From de Vries (84).]

where $\chi^{(-)*}$ is the appropriate distorted wave for the emerging proton with a final momentum of \mathbf{p}_p . The factor $\langle \psi_f | \Psi_i \rangle$, in which integrations over all variables but \mathbf{r}_i are carried out, also appears in the DWA expression for the pickup (p, d) or ($d, {}^3\text{He}$) process [see (VII.3.4)]. However (2.137) differs from that expression in that the perturbing potential for the pickup process is a short-ranged nucleon–nucleon two-body potential v_{oi} in the notation of Chapter VII, which is to be compared with $e^{i\mathbf{q}\cdot\mathbf{r}_i}$. Therefore, substantially different properties of the overlap $\langle \psi_f | \Psi_i \rangle$ are probed in the two reactions. In the pickup reaction it is mostly the surface region of the nucleus that is involved, while in the ($e, e'p$) case the interior plays an important role. For a detailed study of this comparison, see deWitt–Huberts (87).

There are two noteworthy results. One is that the shapes of the overlap $\langle \psi_f | \Psi_i \rangle$ wave function as determined from the ($e, e'p$) and ($d, {}^3\text{He}$) reactions are in good agreement. Second, the predicted cross sections in both cases require

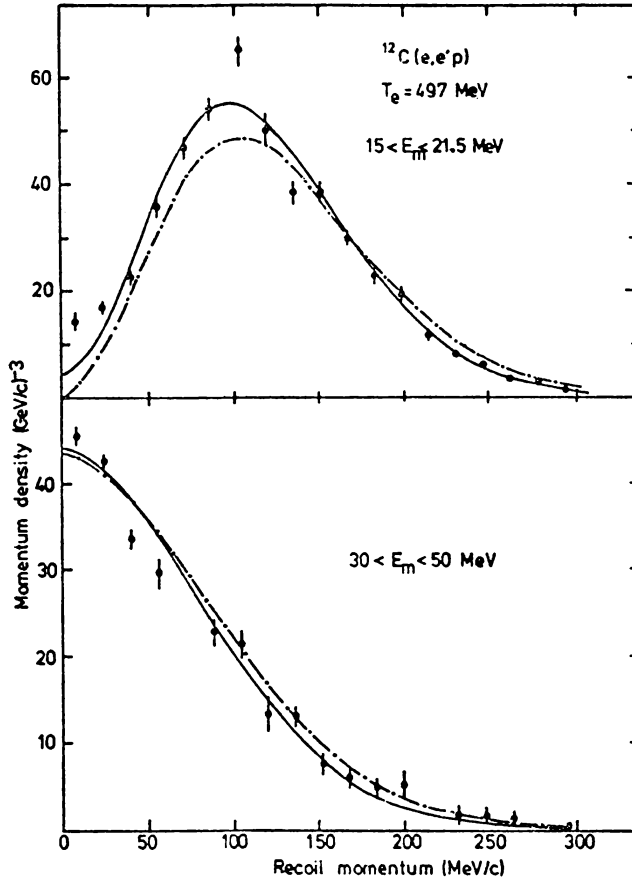


FIG. 2.25. Momentum distributions for the $(e, e'p)$ reaction on ^{12}C in two different regions of removal energy, E_m , corresponding to knock-out from the $0p$ and $0s$ shells. The calculated results using DWIA (PWIA) are given by the solid (dotted-dashed) curves and have been normalized to the experimental data. [From Dieperink and DeForest (75).]

spectroscopic factors (the probability that the overlap can be described by a single-particle wave function) considerably less than unity.

The correction resulting from the use of a distorted wave function is small. We recall from Chapter V that distorting effects of the optical potential are minimal when the proton energy is in the range 150 to 300 MeV.

Note. Assuming a valence model for the target nucleus, one can show that the exchange terms produced by the Pauli exclusion principle are zero. Let

$$\Psi_i(\mathbf{r}_p, \mathbf{r}_1, \mathbf{r}_2, \dots) = \mathcal{A} u(\mathbf{r}_p) \psi_f(\mathbf{r}_1, \mathbf{r}_2, \dots)$$

The wave function ψ_f is the antisymmetrized wave function for the $Z - 1$ system. The function u carries the normalization. The final state

$$\Psi_f = \mathcal{A}\chi^{(-)}(\mathbf{r}_p)\psi_f(\mathbf{r}_1, \mathbf{r}_2, \dots)$$

Antisymmetrization has not been included in (2.137) since it is automatically guaranteed by the symmetry of $\sum_i e^{i\mathbf{q}\cdot\mathbf{r}_i}$ and the antisymmetry of Ψ_i . The proof of the result that we will leave to the reader is a consequence of the condition

$$\langle u(\mathbf{r}_1) | \psi_f(\mathbf{r}_1, \mathbf{r}, \dots) \rangle = 0$$

where the integration is carried out over \mathbf{r}_1 .

The hole state that is formed by the proton removal is not an eigenstate of the nuclear Hamiltonian. As revealed by a high-resolution experiment, it fragments into several separate states. The hole state acts as a doorway state to these. It therefore becomes possible to apply the doorway state formalism developed in Chapter III. From (III.4.16) we have the doorway state \mathcal{T} matrix

$$\langle \mathcal{T}_{fi} \rangle_{\text{doorway}} = \frac{\langle \phi_f | H_{PD} \psi_d \rangle \langle \psi_d | H_{DP} \psi_i \rangle}{E - E_d + \frac{1}{2}i\Gamma_d^\downarrow} \quad (2.138)$$

where we have assumed that the entire width Γ_d^\downarrow is the result of fragmentation of the one-hole state. One must now take the absolute square of $\langle \mathcal{T}_{fi} \rangle$ and sum over final residual nuclear states within the width Γ_d^\downarrow . An energy average over narrow resonances $\psi_d^{(+)}$ is implied [see the discussion leading to (VII.5.22)]. The result is

$$|\langle \mathcal{T}_{fi} \rangle|^2 = \frac{1}{2\pi} \frac{\Gamma_d^\downarrow |\langle \psi_d | H_{DP} \psi_i \rangle|^2}{(E - E_d)^2 + (\Gamma_d^\downarrow)^2/4}$$

where

$$\psi_d \simeq \psi_f^* \chi^{(-)*} \quad (2.139)$$

according to (2.137). Thus in the response function one should replace the energy delta function by

$$\frac{1}{2\pi} \frac{\Gamma_d^\downarrow}{(E - E_d)^2 + \frac{1}{4}\Gamma_d^2} \quad (2.140)$$

in order to obtain the results obtained when averaging over the states into which the hole state fragments. Note that Γ_d is a function of the energy. [See Orland and Schaeffer (78) for more details.] A comparison with experiment is

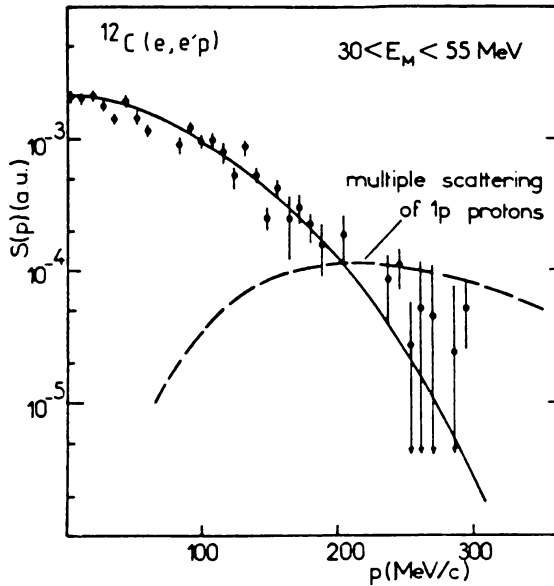


FIG. 2.26. Rescattering effects in the $^{12}\text{C}(e, e'p)$ reaction. In the separation energy region corresponding to the $1s$ shell, the contribution of $1p$ protons is estimated. [From Mougey (80).]

shown in Fig. 2.26. For a review of the experimental situation, see Mougey (80) and deWitt-Huberts (87).

This is where we will end the discussion of electron-induced reactions. Much more in the way of exclusive experiments will be done as CW electrons accelerators become operational. For example, referring to Fig. 2.23, measurement of the dependence on the angle ϕ_p will lead to further information on the nuclear matrix elements of various components of the currents. [See, e.g., (3.13) in the paper by Co' et al. (87).] and therefore to new types of response functions beyond R_L and R_T . The use of polarized electrons will yield relative phases of the nuclear matrix elements [see Donnelly (88)]. Importantly, measurement of the parity violating transitions will permit stringent tests of the "standard" theory of the electro-weak interactions. We shall not discuss the EMC effect [see Jaffe (88) and Close (88)], which appears to indicate a change in the structure of the nucleons in the nuclear environment. At least that is one interpretation. But this phenomenon is, at this moment of writing, not clearly understood experimentally and theoretically. Finally, I should mention the clear evidence for exchange currents obtained by electron scattering from ^3H and ^3He , which have not been discussed because the nuclear two- and three-body systems are not included in this volume. Nevertheless, we include two figures showing the effect of exchange currents and nucleon excitation to the Δ on the electric and magnetic form factors for ^3H and ^3He (Figs. 2.27 and 2.28).

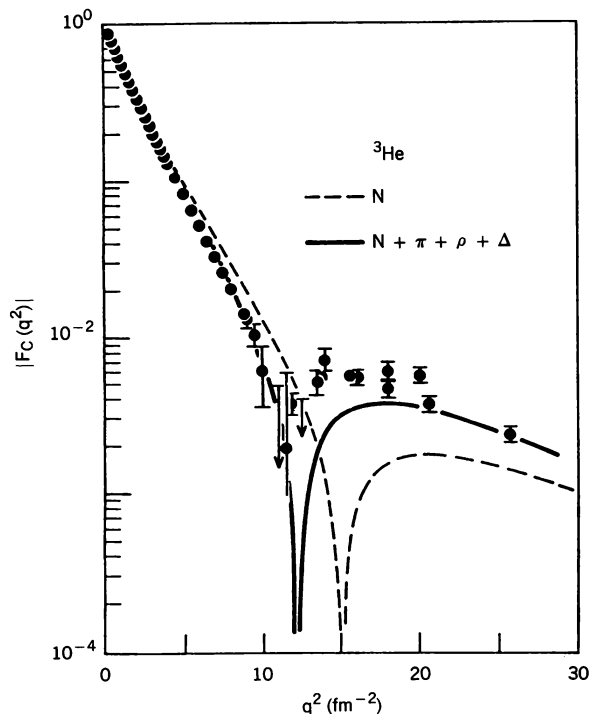


FIG. 2.27. Charge form factor of ^3He . The dashed curve gives the impulse approximation results. The solid curve includes the effects of meson exchange contributions. [From Hodjuk, Sauer, and Strueve (83).]

3. MEDIUM-ENERGY PROTON-NUCLEUS SCATTERING

The application of the theory of multiple scattering to the scattering of protons by nuclei was discussed briefly in Section II.8. We summarize the pertinent formulas using the KMT formalism.[†] The effective potential $V_{\text{opt}}^{(1)}(\mathbf{q})$, $\mathbf{q} = \mathbf{k} - \mathbf{k}'$ is given by (II.4.30)

$$V_{\text{opt}}^{(1)} = \frac{A-1}{A} \left\langle 0 \left| \sum_i t_i \right| 0 \right\rangle = (A-1) \langle 0 | t_1 | 0 \rangle \quad (3.1)$$

[†]The eikonal method is often used. However, comparison with the KMT results for 800-MeV protons (see Fig. 3.1) shows that in the lowest order the eikonal method overshoots the diffraction maxima and minima at the larger angles, especially for the polarization observables. A more careful treatment of the eikonal method beyond the first order is required. The eikonal approximation is also found to be in error in inelastic scattering [see Ray and Hoffmann (84)]. However, great improvement in the eikonal results can be obtained if higher-order corrections are made [Wallace (73a, 73b); Rosen and Yennie (64); Wallace and Friar (84)].

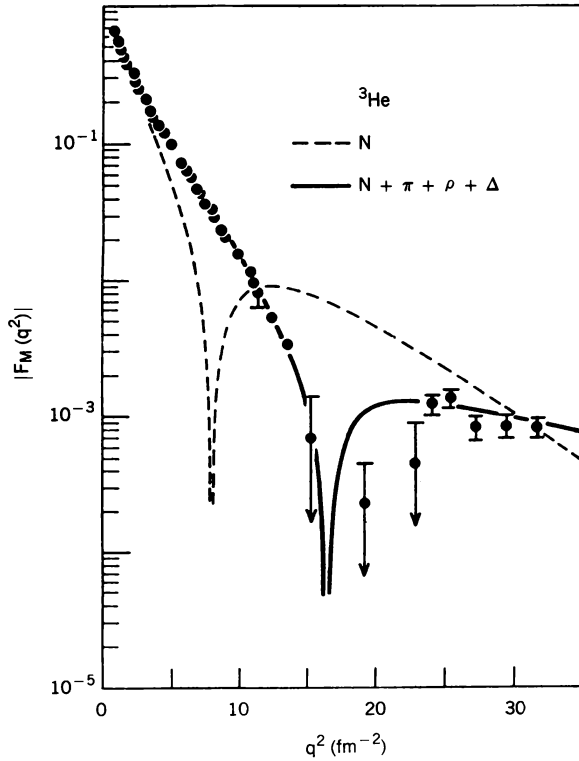


FIG. 2.28. Magnetic form factor of ${}^3\text{He}$. (See caption for Fig. 2.27.)

The quantity t_i is the nucleon–nucleon transition amplitude, $|0\rangle$ is the ground state of the target, while A is the number of nucleons. In general, $V_{\text{opt}}^{(1)}$ is a nonlocal operator $V_{\text{opt}}^{(1)}(\mathbf{r}, \mathbf{r}')$. However, assuming locality [see (II.4.38)] for the transition operator t_i , $V_{\text{opt}}^{(1)}$ becomes local [Eq. (II.4.39)]. The local optical potential $v_{\text{opt}}^{(1)}$ is then [Eq. (II.4.40)],

$$v_{\text{opt}}^{(1)}(\mathbf{r}) = (A - 1) \langle 0 | t(\mathbf{r} - \mathbf{r}_1) | 0 \rangle \quad (3.2)$$

while

$$\int e^{i\mathbf{q}\cdot\mathbf{r}} v_{\text{opt}}^{(1)} d\mathbf{r} = \tilde{v}_{\text{opt}}^{(1)}(\mathbf{q}) = (A - 1) \langle 0 | e^{i\mathbf{q}\cdot\mathbf{r}_1} \tilde{t}(\mathbf{q}) | 0 \rangle \quad (3.3)$$

The optical potential is to be used in a nonrelativistic Schrödinger equation. The resultant scattering amplitude is multiplied by $(A/A - 1)$ [see (II.4.10)] to obtain the predicted amplitude. The superscript on $v_{\text{opt}}^{(1)}$ indicates that it is the first term in an expansion. The second term is given by (II.4.44). It depends explicitly on correlations. For most studies and except for the lightest nuclei,

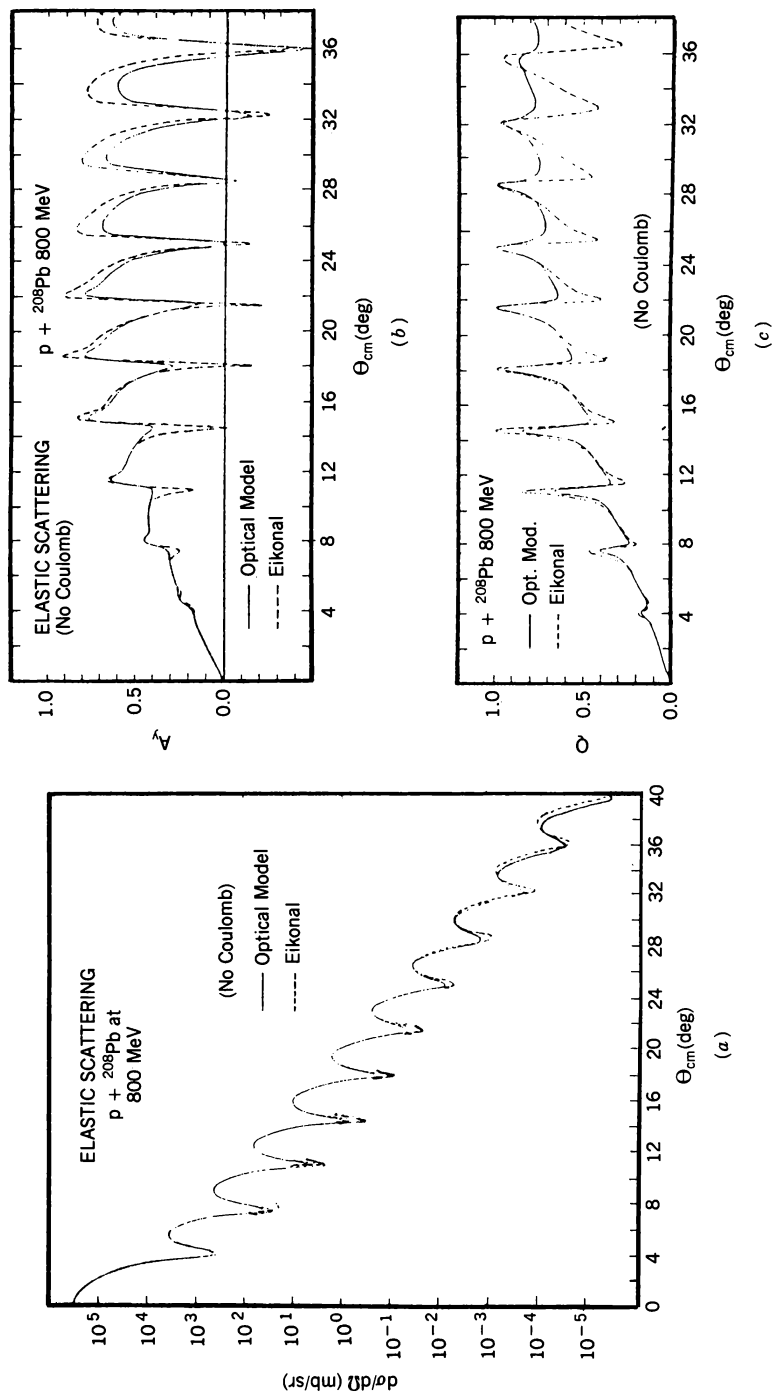


FIG. 3.1. 800-MeV $p + {}^{208}\text{Pb}$ elastic scattering: (a) differential cross section; (b) analyzing power; (c) spin rotation. [From Ray (83).]

this second term does not significantly affect the predicted angular distributions. However, the polarization observables are more sensitive to the correlations. The nucleon-nucleon transition matrix t_i is given in the nucleon-nucleus center-of-mass frame by (II.8.4)

$$t_i(\mathbf{k}, \mathbf{k}') = A_i + B_i \boldsymbol{\sigma}_0 \cdot \boldsymbol{\sigma}_i + C_i (\boldsymbol{\sigma}_0 + \boldsymbol{\sigma}_i) \cdot (\mathbf{q} \times \mathbf{Q}) + D_i (\boldsymbol{\sigma}_0 \cdot \mathbf{Q})(\boldsymbol{\sigma}_i \cdot \mathbf{Q}) + E_i (\boldsymbol{\sigma}_0 \cdot \mathbf{q})(\boldsymbol{\sigma}_i \cdot \mathbf{q}) \quad (3.4)$$

where $\mathbf{q} = \mathbf{k} - \mathbf{k}'$ and $\mathbf{Q} = \frac{1}{2}(\mathbf{k} + \mathbf{k}')$. The subscript i refers to the struck nucleon in the target nucleus and the subscript 0 refers to the incident nucleon. The coefficients A_i , B_i , and so on, are functions of q^2 and the energy of the incident nucleon. These coefficients also depend on the isospin, for example,

$$A_i = A_+ + A_- \boldsymbol{\tau}_0 \cdot \boldsymbol{\tau}_i \quad (3.5)$$

The connection between the coefficients A_i , and the coefficients A'_i , and so on, appropriate to the nucleon-nucleon center-of-mass reference system is given by (II.8.5). We shall not repeat them here. One often parametrizes the coefficients A'_i as follows:

$$A' = A(0)e^{-\alpha q^2} \quad (3.6)$$

where α and A are complex functions of the energy. A table of these coefficients is given in Chapter II (Table II.8.1) for a nucleon kinetic energy L_{lab} of 1 GeV. Coefficients appropriate at other energies are given Wallace (81).[†] Note that the transformation from the nucleon-nucleon to the nucleon-nucleus reference frame is valid only at small angles. Moreover, there is an ambiguity described in the problem following (II.7.2). Finally, we remark that using the form given by (3.6) involves values of A , and so on, which for large values of q are not observable in nucleon-nucleon scattering. (See the discussion in Section II.7.) Extrapolation from nucleon-nuclear scattering to these off-the-energy-shell values is obtained by fitting the energy dependence of the coefficients $A(0)$ and α and then continuing that dependence to the required values of the energy. Another procedure, using the Breit frame, leads to (II.7.20), in which $\tilde{t}(\mathbf{k}, \mathbf{k}')$ is replaced by

$$\tilde{t}\left(\frac{\mathbf{Q}(1 + 1/A) + \mathbf{q}}{2}, \frac{\mathbf{Q}(1 + 1/A) - \mathbf{q}}{2}\right)$$

evaluated at the energy $T_{\text{lab}}^{(\text{eff})} = (1/2m)(Q^2(1 + 1/A)^2 + q^2)$. In most of the results to be reported below, only the A and C coefficients enter into $v_{\text{opt}}^{(1)}$, since the spin of the target nuclei selected is zero. The bilinear terms in spin (B, D, E, F) do contribute to the second-order terms. However, they are generally neglected in the calculation of second-order effects.

[†]Note that Wallace's D is proportional to our E and his E to our D .

Despite many caveats referred to above, the agreement of the first-order multiple scattering theory with elastic scattering of protons by spin-zero nuclei at sufficiently high energy is excellent, as one can see from Fig. II.8.2. This is because the nucleon–nucleus amplitude is not sensitive to the details of the transition matrix for nucleon–nucleon scattering for relatively small values of q . The first-order potential is a product of the nucleon–nucleon \tilde{t} and the nuclear $\tilde{\rho}$. Since \tilde{t} is generated by a short-range force, it will change slowly with q . On the other hand, $\tilde{\rho}(\mathbf{q})$ will be sharply peaked at $q = 0$, with the consequence that only values of \tilde{t} near $q = 0$ will be important. The cross section near $q = 0$ will then be a diffraction pattern given by $\tilde{\rho}(\mathbf{q})$ whose minima and maxima reflect the value of the nuclear radius. Their positions are stable against the inclusion of various effects, such as those generated by the second-order potential. Many effects are present for larger-angle scattering. In addition to correlations, there are the corrections arising from the various approximations used to obtain the simple formula (3.1) and of course the uncertainties in $\tilde{\rho}(\mathbf{q})$ and $\tilde{t}(\mathbf{q})$. A systematic treatment of the correlations, including those originating in the Pauli exclusion principle, in the center-of-mass correlation and in the spin and space correlations in the target nucleus has been given by L. Ray and G. W. Hoffmann and their associates. [See, for example, Ray (79); see also Chaumeaux, Layly, and Schaeffer (78)] Ray (79) improves upon the treatment of the Pauli correlations by Boridy and Feshbach (77) by letting k_F , the Fermi energy, be a function of r reflecting the spatial dependence of the density, which in a local density approximation is directly related to k_F . The major effect of these correlations is to increase the cross section at the diffraction maxima by an amount that increases with q and decreases with A (see Table 3.1).

The relative importance of the various correlations at the maxima is shown in Table 3.2. We see from the table that the most important correlation effect is produced by the Pauli exclusion principle. Finally, Hoffmann et al. (81) have pointed out the importance of the spin-orbit coupling that arises from the interaction of the magnetic moment of the incident proton and the Coulomb field of the target nucleus. Approximately the interaction is given by

$$H_{\text{m.d.}} = -\frac{\partial \phi}{\partial r} \frac{\mu_0 \hbar c}{2E} (\boldsymbol{\sigma} \cdot \mathbf{l}) \quad (3.7)$$

TABLE 3.1 Percent Increase in Cross Section at Diffraction Maxima

Max.	^{40}Ca	^{116}Sn	^{208}Pb
1	13	8	6
2	18	13	10
3	20	17	14
4		21	18
5			23

Source: Ray (79).

TABLE 3.2 Relative Importance of the Various Correlation Corrections^a

Nucleus	Correction (%)				
	Pauli	SRD	PSR-I	cm	Pauli-S.O.
⁴⁰ Ca	85	10	-2.1	11.0	-3.9
¹¹⁶ Sn	91.3	11.6	-2.4	5.2	-5.7
²⁰⁸ Pb	92.2	11.7	-2.8	3.4	-4.5

^a(1) Pauli, because of the exclusion principle; (2) SRD, short-range correlation; (3) PSR-I, interference between Pauli and short-range; (4) cm, corrections for transformation from nuclear center of mass to proton-nucleus center of mass; (5) Pauli-S.O., Pauli spin-orbit interference. Values are the percentages of the total increase in the height of the maxima in the angular distribution.

where ϕ is the nuclear electrostatic potential and μ_0 is the proton magnetic moment.[†] The comparison with experiment of the calculated angular distribution, including only A and C terms of (3.4), second-order terms, and magnetic moment effects, are shown in Fig. 3.2. The incident protons have an energy of 800 MeV; the target nuclei are ¹⁶O, ⁴⁰Ca, and ²⁰⁸Pb. The proton density is taken from electron scattering while the neutron density is calculated according to the following recipe:

$$\rho_n(r) = \rho_p(r) + [\rho_n(\mathbf{r}) - \rho_p(\mathbf{r})]_{\text{HFB}} \quad (3.8)$$

where the densities within brackets is taken from Hartree-Fock-Bogoliubov calculations [Dechargé et al. (81)]. Agreement is good except that as is especially noticeable in the lead case, the predicted diffraction oscillations are out of phase with experiment at the larger scattering angles.

One need not use (3.8) but rather determine the neutron density from experiment. A check on the method used is obtained by comparing the proton density difference obtained using polarized elastic scattering with that obtained using electron elastic scattering from ⁴⁸Ca and ⁵⁴Fe. In first approximation the neutron densities are the same, so that the differences in the proton densities can be obtained. The results are shown in Fig. 3.3. Agreement is quite good, especially in the region of large r when both experiments have smaller uncertainties. At smaller r the uncertainties are much larger, so that the agreement is less significant. Examples of the neutron densities determined by proton scattering in comparison with that obtained from Negele's density matrix expansion (DME) are shown in Fig. 3.4. Reasonable agreement is obtained.

[†]Hoffmann et al. (81) use a more accurate expression which is valid relativistically and takes the nucleon form factors into account.

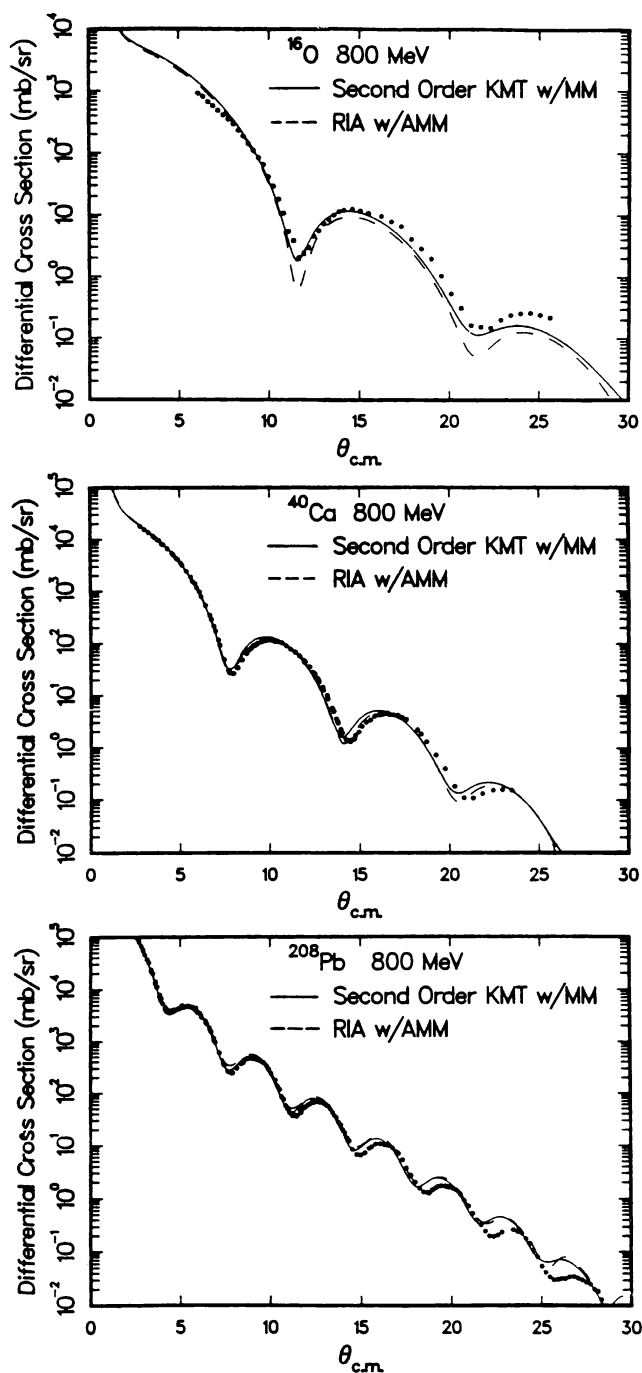


FIG. 3.2. The 800-MeV $p + ^{16}\text{O}$, ^{40}Ca and ^{208}Pb elastic differential cross section compared to the nonrelativistic and relativistic predictions (RIA). MM refers to the magnetic moment correction. A in AMM stands for anomalous. [From Ferguson, Barlett, et al. (86).]

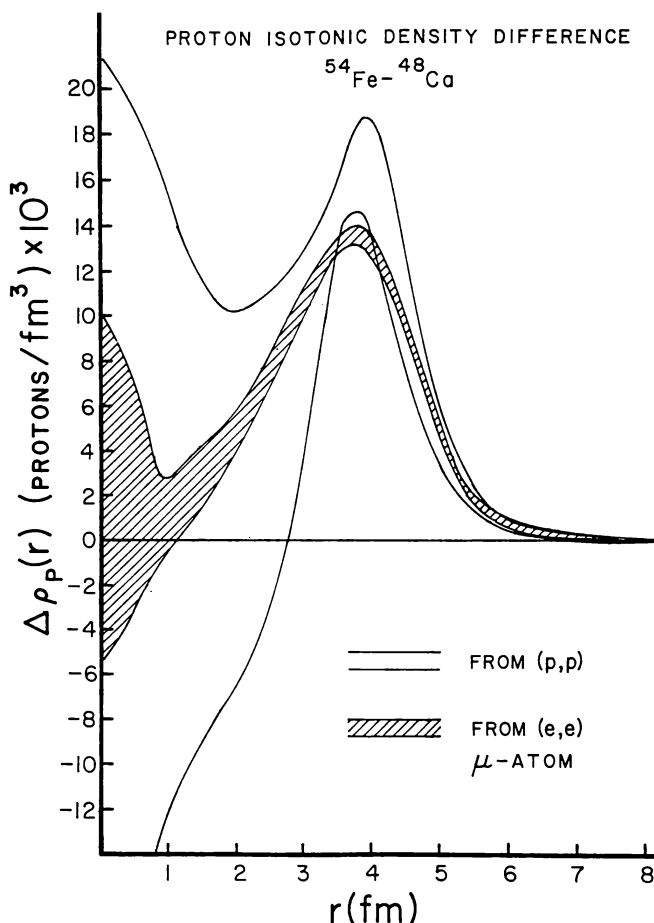


FIG. 3.3. Comparison of the proton density differences between Fe and Ca obtain by analysis of 800-MeV proton elastic scattering (outer band) with that obtained by electromagnetic measurements (inner shaded band). [From Ray and Hoffmann (83).]

We consider next the two independent polarization observables, Q , the spin rotation, and A_y , the analyzing power, which by time reversal equals P in (V.2.52). These provide a more subtle test of our understanding of the elastic scattering of protons by nuclei. In particular, they are more sensitive in the angular regions covered by the minima in the angular distributions. In Fig. 3.5 we present first-order KMT calculations of the analyzing power, the second-order KMT (i.e., including correlations), and finally, calculations that include the magnetic moment effect [Eq. (3.7)] designated by MM . The data points are obtained with polarized 800-MeV proton beams available at LAMPF. The target nuclei are ^{16}O , ^{40}Ca , and ^{208}Pb . We see that the correlation effects

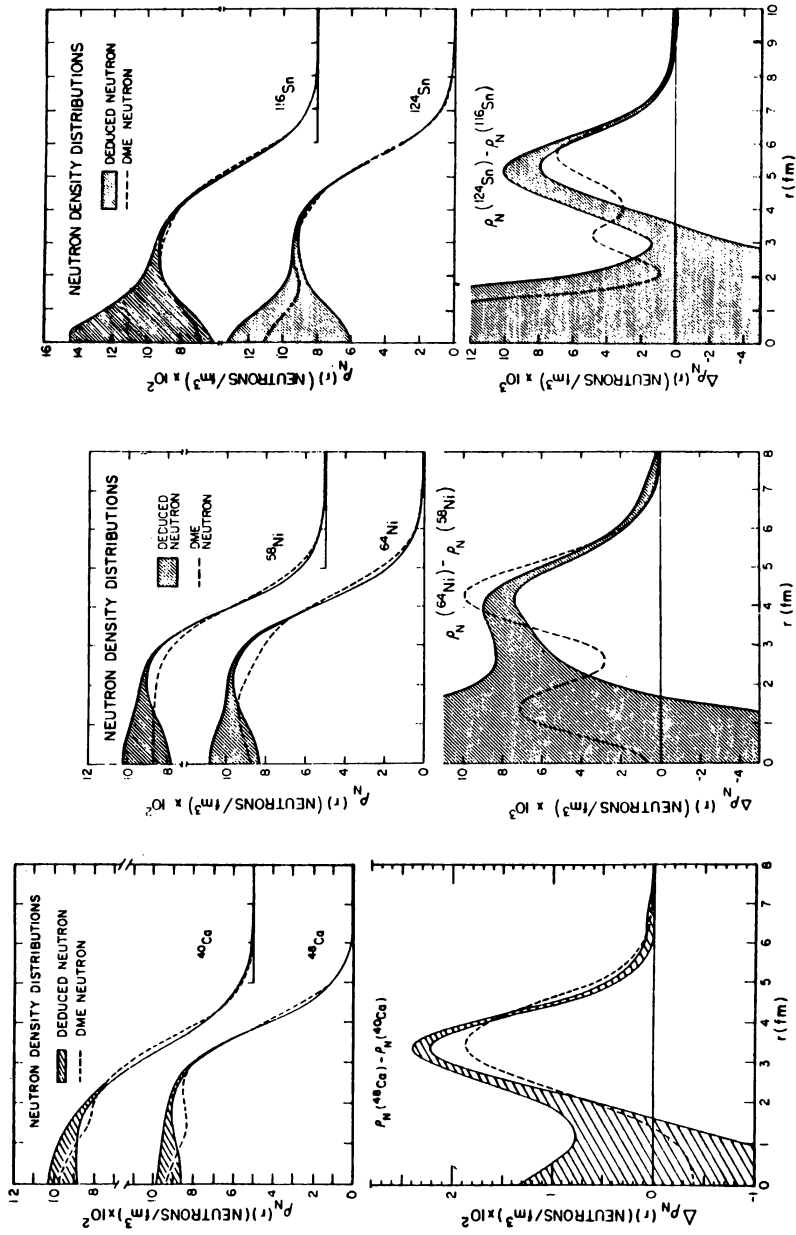


FIG. 3.4. Point neutron density distributions for ^{40}Ca , ^{58}Ni , ^{64}Ni , ^{116}Sn , and ^{124}Sn deduced from second-order KMT analysis (shaded bands) and predicted by the density matrix approach (dashed curves DME) of Negele. [From Ray (79).]

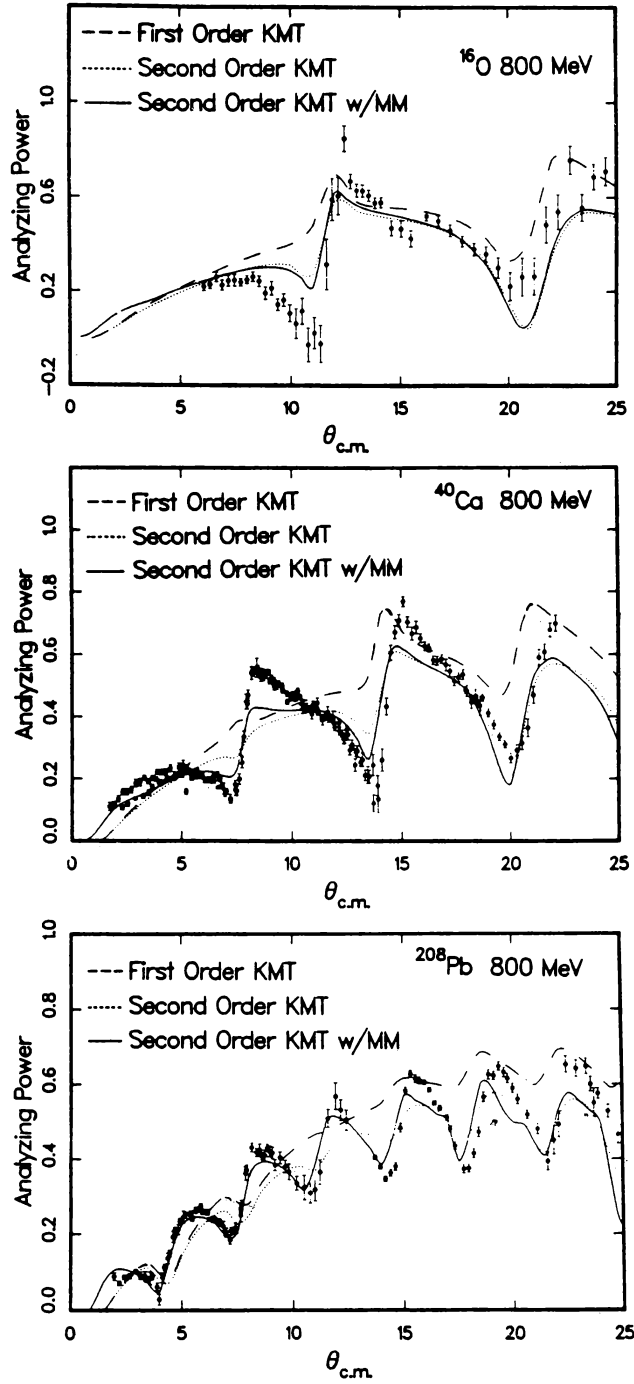


FIG. 3.5. The 800-MeV $p + ^{16}\text{O}$, ^{40}Ca and ^{208}Pb elastic analyzing power data compared to various nonrelativistic impulse approximation predictions. [From Ferguson, Barlett, et al. (86).]

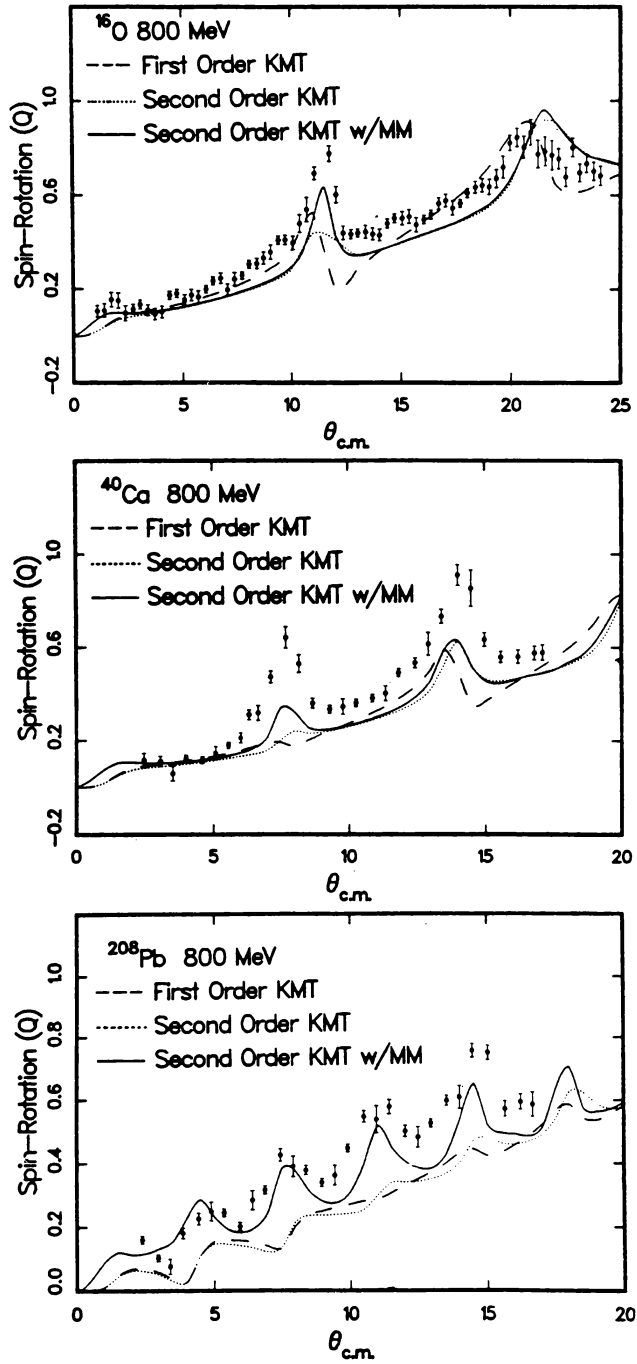


FIG. 3.6. The 800-MeV $p + ^{16}\text{O}$, ^{40}Ca and ^{208}Pb spin-rotation data compared to various nonrelativistic impulse approximation predictions. [From Ferguson, Barlett, et al. (86).]

are quite large and for the case of ^{16}O are sufficient to bring the calculation and experiment into substantial agreement. For ^{40}Ca and especially for ^{208}Pb , the magnetic moment effect plays an important role. Generally, the first-order KMT does not give sufficient structure; terms “proportional” to ρ^2 and the magnetic moment modification of the spin-orbit term are necessary. Both of these act to break the correlation between the numerator in the expression for the polarization and the angular distribution that is in the denominator. A similar story prevails for the spin-rotation parameter Q , as illustrated by Fig. 3.6. In these cases correlation effects are not significant; the improvement on KMT is largely carried by the magnetic moment interaction. The agreement with the data is quite good, although there are substantial deviations in the Q for the ^{40}Ca target.

These polarization tests of the KMT theory are incomplete, since the effects of the spin-spin terms in the t matrix may be appreciable [Feshbach (90)]. However, detailed calculations that would show how these effects affect the polarization observables are not available [except for a calculation of Q for ^4He by Parmentola and Feshbach (82)].

Another approach to nucleon-nucleus scattering is referred to as the *relativistic impulse approximation*. We shall only sketch this procedure. For more details and references, we refer the reader to a review by Wallace (87). Very briefly, a relativistic transition operator for the nucleon-nucleon interaction is taken to be

$$t_D = f_s + f_v \gamma_\mu^{(1)} \gamma_\mu^{(2)} + f_t \sigma_{\mu\nu}^{(1)} \sigma_{\mu\nu}^{(2)} + f_a \gamma_5^{(1)} \gamma_\mu^{(1)} \gamma_5^{(2)} \gamma_\mu^{(2)} + f_{ps} \gamma_5^{(1)} \gamma_5^{(2)} \quad (3.9)$$

The equivalent Schrödinger form, t_s , is obtained from the equation

$$\begin{aligned} & \bar{u}_1(\mathbf{k}'_1, s'_1) \bar{u}_2(\mathbf{k}'_2, s'_2) t_D u_1(\mathbf{k}_1, s_1) u_2(\mathbf{k}_2, s_2) \\ &= \chi_1^\dagger(\mathbf{k}'_1, s'_1) \chi_2^\dagger(\mathbf{k}'_2, s'_2) t_s(\mathbf{k}_1, \mathbf{s}_1) \chi_1(\mathbf{k}_1, s_1) \chi_2(\mathbf{k}_2, s_2) \end{aligned} \quad (3.10)$$

where $u(\mathbf{k}, s)$ is the four-component plane wave solution of the Dirac equation and $\chi(\mathbf{k}, s)$ is a two-component Pauli plane wave spinor. The process described by (3.10) is one in which particle 1 makes the transition from momentum \mathbf{k}_1 , spin s , to momentum \mathbf{k}'_1 , spin s'_1 with a similarly indicated change for particle 2. For a detailed discussion of this transformation, see McNeil, Ray, and Wallace (83) and Ray and Hoffmann (85). The resulting amplitude must be folded into the appropriate nuclear density functions. These must be relativistic in origin and are obtained from relativistic theories of the nucleus such as those proposed by Walecka [Serot and Walecka (86) or Celenza and Shakin (86)]. The first of these is a σ (scalar)- ω (vector) model treated by a mean field approximation. The second is a relativistic Breuckner-Hartree-Fock approximation starting with a relativistic nucleon-nucleon force taken from a meson exchange model. The resulting one-body Dirac equation describing nucleon-nucleus scattering

is, according to Ray and Hoffmann (85),

$$\left\{ c\boldsymbol{\alpha} \cdot \mathbf{p} + \beta(mc^2 + U_s(r)) + [U_v(r) + U_{\text{Coul}}(r)] - i\beta\boldsymbol{\alpha} \cdot \hat{\mathbf{r}} \left[2U_T(r) + \frac{\kappa_p}{2m} \frac{\partial}{\partial r} U_{\text{Coul}}(r) \right] \right\} \phi = E\phi. \quad (3.11)$$

In this equation U_s , U_v , and U_T are the scalar, vector, and tensor potentials, κ_p is the proton anomalous magnetic moment, and E is the total relativistic energy of the proton in the proton–target nucleus center-of-mass frame. It is found that U_T has a small effect on the scattering so that it is omitted in the calculations reported below. Equation (3.11) is remarkably similar to the relativistic model discussed in Chapter V. The results obtained with the RIA agree with the empirical results of that model as demonstrated in Fig. 3.7. With these assumptions one obtains the angular distributions of Fig. 3.2, labeled RIAw/AMM. The agreement with experiment is better than KMT for the target nuclei ^{40}Ca and ^{208}Pb but not as good as KMT for target nucleus ^{16}O . In Fig. 3.8 we compare the predictions of the analyzing power, and Fig. 3.9, the spin rotation, is given for the relativistic theory. From Fig. 3.8 we see that

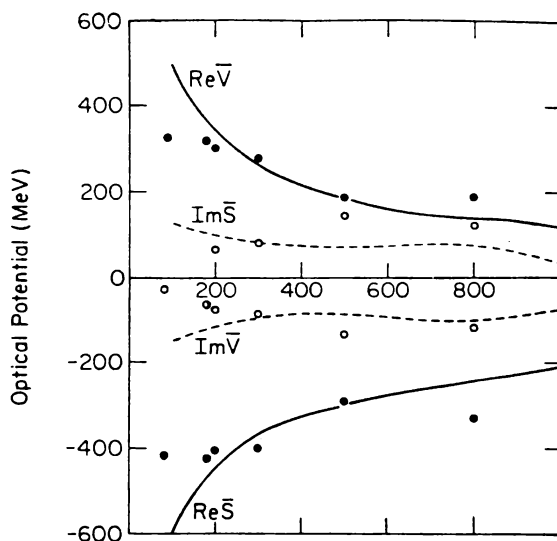


FIG. 3.7. Isospin averaged scalar vector (\bar{V}) potential at nuclear matter density as a function of the proton kinetic energy. Solid and dashed lines are the predictions of the relativistic impulse approximation. Filled and open circles are the phenomenological values for the real and imaginary potentials found by fitting proton scattering data using the Dirac equation. [From Wallace (87).]

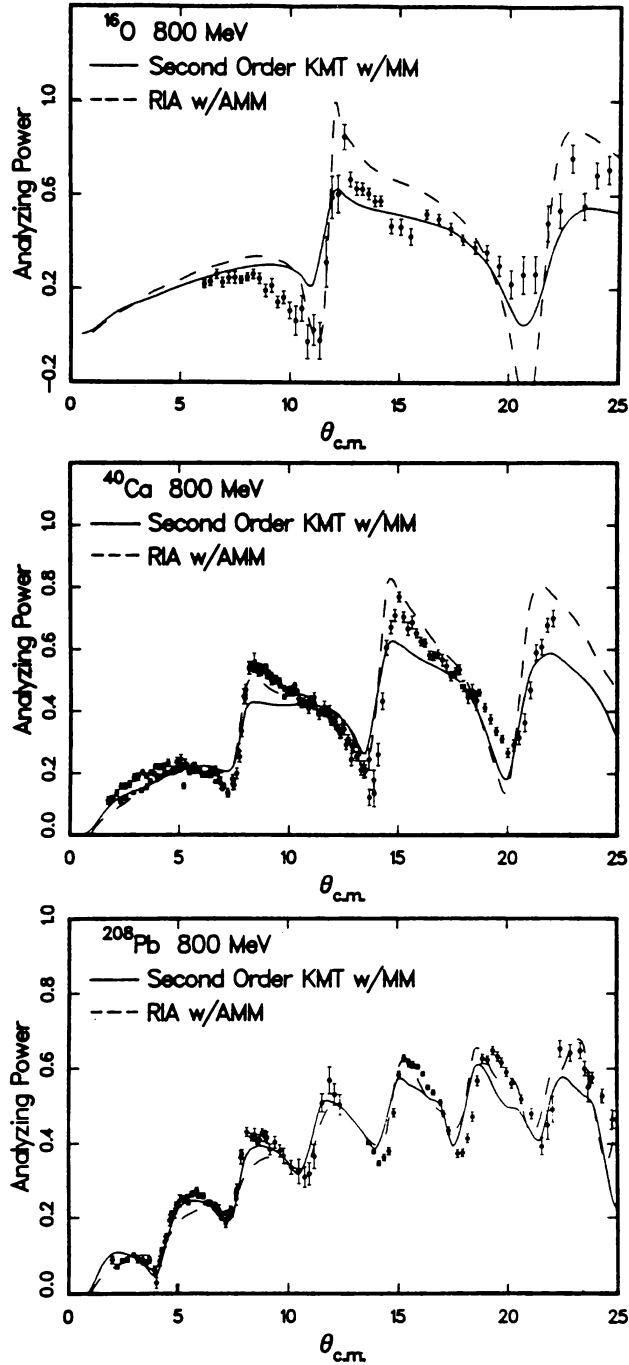


FIG. 3.8. The 800-MeV $p + ^{16}\text{O}$, ^{40}Ca and ^{208}Pb elastic analyzing power data compared to the nonrelativistic and relativistic impulse approximation predictions. [From Fergerson, Bartlett, et al. (86).]

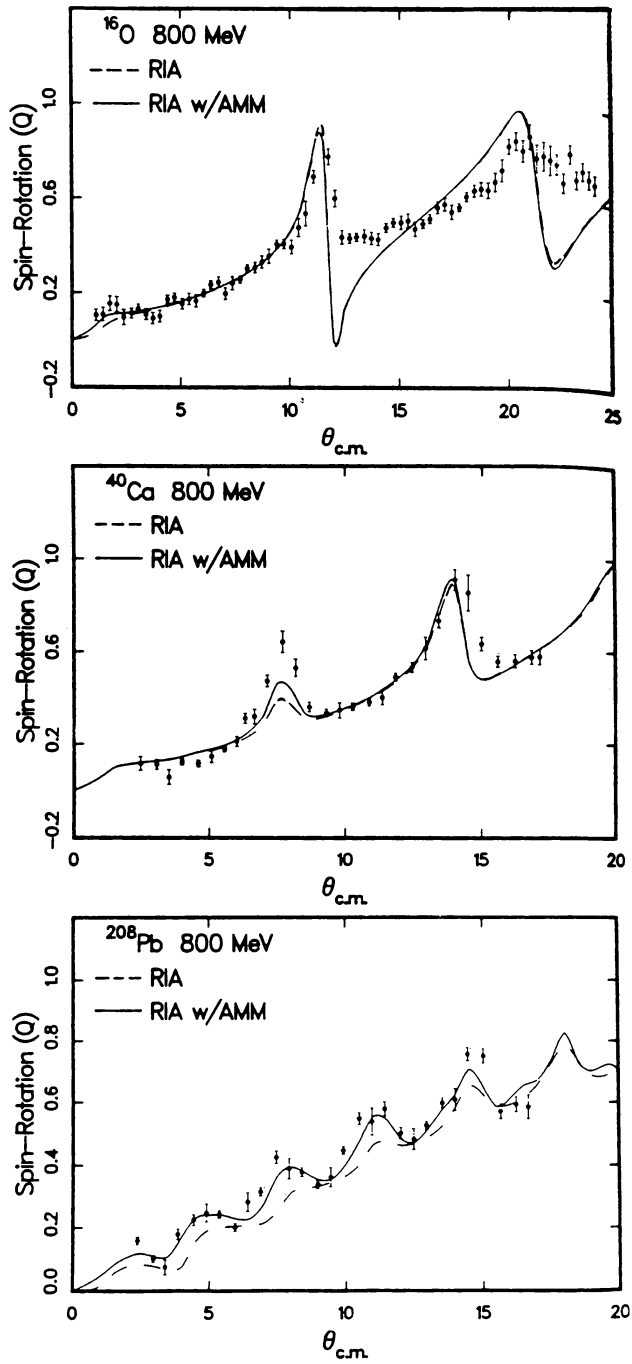


FIG. 3.9. The 800-Mev $p + ^{16}\text{O}$, ^{40}Ca , and ^{208}Pb spin-rotation data are compared to relativistic impulse approximation predictions. [From Ferguson, Bartlett et al. (86).]

RIA and KMT differ from experiment in differing ways, but it would be difficult on this basis to choose one above the other. In Fig. 3.9 the RIAW/AMM result differs considerably from the ${}^{16}\text{O}$ experiment, with which second-order KMT/MM is in substantial agreement (see Fig. 3.6). Agreement with ${}^{40}\text{Ca}$ and ${}^{208}\text{Pb}$ data is good. Overall the sharp difference in the ability of the KMT and RIA models to match the data, especially that of the rotation spin parameter, is not repeated at 800 MeV.

The second-order corrections to RIA are severe. This is because one can add many terms to t_D [Eq. (3.9)] that will not contribute to the positive energy projection, (3.10). As a consequence, t_s is ambiguous [Adams and Bleszynski (84)] since these additional terms can contribute to the second-order potential. No information on their strength is available from the nucleon–nucleon amplitude. According to Tjøn and Wallace (85, 87), t_D can contain 56 terms for each isospin. Tjøn and Wallace reduce the number of independent terms by invoking relations obtained from a relativistic theory of the nucleon–nucleon interaction. They thus obtain a fit to nuclear forces as well as to medium-energy nucleon–nucleon scattering.

4. PROTON ${}^4\text{He}$ ELASTIC SCATTERING AND THE EFFECT OF ISOBAR EXCITATION[‡]

The angular distribution of 1-GeV protons scattered by ${}^4\text{He}$ is shown in Fig. I.15.2 in deShalit and Feshbach (74). The experimental points shown are not correct, as shown by subsequent experiments [Geaga et al. (77); Courant et al. (79)]. The strong diffraction minimum is filled in so that the angular distribution is flat in the neighborhood of 20° and then drops off quite rapidly. It is not possible to explain these results using only the first-order KMT potential. This is primarily because to that order the angular distribution is given by the Fourier transform of the density $\rho(\mathbf{q})$ for ${}^4\text{He}$. But $\rho(\mathbf{q})$ is quite accurately determined by electron scattering. It is thus essential to consider the second-order term:

$$\begin{aligned} \langle \mathbf{k} | V^{(2)} | \mathbf{k}' \rangle &= (A-1)^2 \int \frac{d\mathbf{k}''}{(2\pi)^3} \int \frac{d\mathbf{k}'''}{(2\pi)^2} \{ \langle 0 | \tilde{t}_1(\mathbf{k} - \mathbf{k}'') \tilde{t}_2(\mathbf{k}''' - \mathbf{k}') | 0 \rangle \\ &\quad - \langle 0 | \tilde{t}_1(\mathbf{k} - \mathbf{k}'') | 0 \rangle \langle 0 | \tilde{t}_2(\mathbf{k}''' - \mathbf{k}') | 0 \rangle \} \\ &\quad \times \langle \mathbf{k}'' | \frac{1}{E - \bar{\epsilon} - V^{(1)} - K} | \mathbf{k}''' \rangle \end{aligned} \quad (4.1)$$

Here $\tilde{t}_1(\mathbf{k} - \mathbf{k}'')$ is the t matrix for the scattering of the proton by the nuclear nucleon labeled by the subscript. Matrix elements are taken with respect to the

[‡]Wallace (80); Parmentola and Feshbach (82).

ground state, $|0\rangle$. In the propagator, E is the energy, $\bar{\epsilon}$ an average excitation energy, $V^{(1)}$ the first-order potential, and K the kinetic energy operator for the incident proton in the nucleon–nucleus center-of-mass system. When the effect of $V^{(2)}$ is evaluated (as, indeed, one must because of the center-of-mass correlations), including dynamical and Pauli correlations and including the entire expression for the nucleon–nucleon matrix, (3.4), using the Wallace–Alexander parametrization (Table II.8.1) there are substantial changes but the diffraction minimum remains.

A possible remedy suggested by Ikeda (72) and exploited by Alexander and Wallace (72) is isobar excitation, which can also contribute to $V^{(2)}$. In this process the incident proton in scattering by a nucleon is transformed into a Δ and in its second scattering deexcited to a proton. Note that the second scattering must involve a second and different nucleon to avoid double counting. De-excitations by the nucleon that produced the excitation have already been included in the nucleon–nucleon transition. Thus in (4.1), $\tilde{t}_1 \tilde{t}_2$ should be rewritten

$$\tilde{t}_1 \tilde{t}_2 = \tilde{t}_1(NN_1 \rightarrow NN_1) \tilde{t}_2(NN_2 \rightarrow NN_2) + \tilde{t}_1(NN_1 \rightarrow \Delta N_1) \tilde{t}_2(\Delta N_2 \rightarrow NN_2) \quad (4.2)$$

The second term is new. The amplitude $f(NN_1 \rightarrow \Delta N_1)$ corresponding to $\tilde{t}(NN_1 \rightarrow \Delta N_1)$ in the nucleon–nucleon reference frame is parametrized by

$$f(NN_1 \rightarrow \Delta N_1) = f(0) e^{-\Delta q^2} \boldsymbol{\sigma}_1 \cdot \mathbf{S} \boldsymbol{\tau}_1 \cdot \mathbf{T} \quad (4.3)$$

where \mathbf{S} and \mathbf{T} are $\frac{3}{2}$ spin and isospin operators ($S^2 = \frac{15}{4}$). In principle, f should be chosen so as to yield the observed cross section for Δ production in nucleon–nucleon scattering. At 1 GeV the isobar production cross section is substantial (~ 22 mb). A fit to the data in the form given by (4.3) has been obtained by Chadwick et al. (62). Parmentola takes

$$f(0) = 7iD'_{pp}(0)$$

$$\Delta \simeq \delta_{pp}$$

with

$$B'_- = D'_- = E'_- = 0$$

that is, assuming that B' , D' and E' do not depend on isospin yields (Fig. 4.1).

Two points should be noted. One is that a corollary of the isobar excitation is the existence of three-body forces in nuclei. The impact on our understanding of the binding energy of nuclei, especially the three-body systems, has not been calculated. Second, since the expectation value of (4.3) with respect to spin is zero for zero-spin nuclei, one will find that the isobar addition to $V^{(2)}$ for zero-spin nuclei will decrease like $1/A$ with increasing A . It thus will not be of importance for the angular distributions for proton–nucleus scattering for the heavier nuclei.

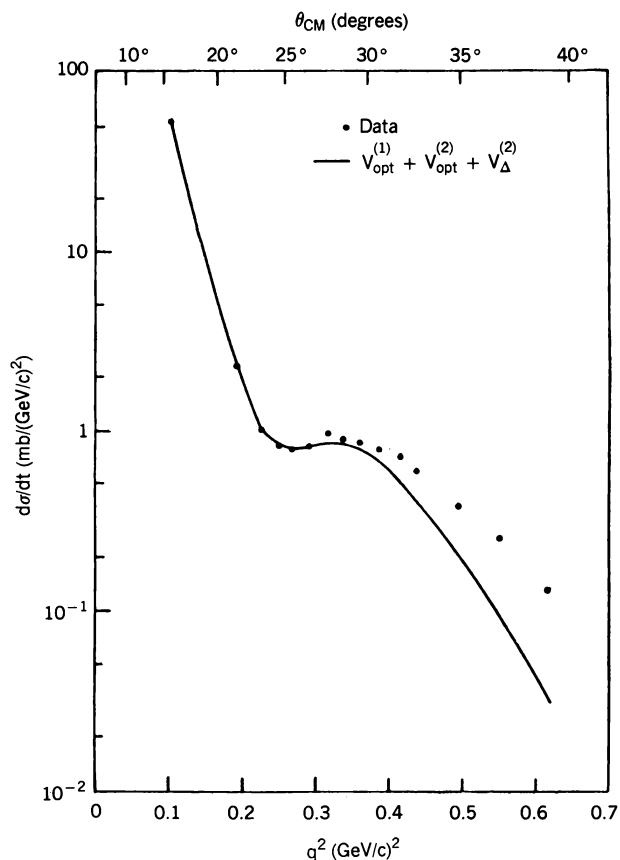


FIG. 4.1. Elastic differential p - ${}^4\text{He}$, $E(p) = 1.03$ GeV cross section compared to the predictions of multiple scattering theory including the effects of the isobar Δ . [From Parmentola and Feshbach (82).]

5. REACTIONS INDUCED BY MEDIUM-ENERGY PROTONS

Reactions, such as inelastic scattering, quasi-elastic scattering, and particle transfer, have all been treated theoretically using the DWA of Chapter V and VI. The matrix element between the initial $|a\rangle$ and $|b\rangle$ nuclear states is given by [see (3.1)]

$$\mathcal{V}_{ba} = \frac{A-1}{A} \langle b | \sum_i t_i | a \rangle \quad (5.1)$$

To obtain the \mathcal{T} matrix for the reaction one calculates the matrix element \mathcal{V}_{ba} between the initial state of the projectile and the final state of the emerging

system. The reader is referred back to Chapters V and VI for the details. There is one simplification: namely, for forward scattering and production one can neglect the Pauli principle between the projectile and target.

The DWA has been applied successfully to inelastic scattering leading to excitation of collective levels [see, for example, Chaumeaux, Layly, and Schaeffer (78) and Blanpied, Ritchie, et al. (88)]. The potential \mathcal{V}_{ba} may be expressed in terms of the transition density:

$$\begin{aligned}\mathcal{V}_{ba} &= \int d\mathbf{r}_1 \cdots d\mathbf{r}_A \psi_b^*(\mathbf{r}_1 \cdots \mathbf{r}_A) \frac{A-1}{A} \sum t_i(\mathbf{r}_i, \mathbf{r}_0) \psi_a(\mathbf{r}_1 \cdots \mathbf{r}_A) \\ &= (A-1) \int d\mathbf{r}_1 \rho_{ba}(\mathbf{r}_1) t_1(\mathbf{r}_1, \mathbf{r}_0)\end{aligned}\quad (5.1')$$

where

$$\rho_{ba}(\mathbf{r}_1) = \int \psi_b^*(\mathbf{r}_1 \cdots \mathbf{r}_A) \psi_a(\mathbf{r}_1 \cdots \mathbf{r}_A) d\mathbf{r}_2 \cdots \quad (5.2)$$

If we employ only the component of t_1 independent of the proton spin, the angular momentum transfer in the reaction will be orbital. If the angular momentum transfer is l , the only component of the ρ_{ba} that will be effective is proportional to $Y_{lm}(\mathbf{r}_1)$, leading to the definition

$$\rho_{ba,l}(r_1) = \int Y_{lm}^*(\mathbf{r}_1) \rho_{ba}(\mathbf{r}_1) d\hat{\mathbf{r}}_1 \quad (5.3)$$

The quantities $\rho_{ba}(\mathbf{r}_1)$ and $\rho_{ba,l}(r_1)$ are referred to as transition densities. The proton transition density can be determined from inelastic electron scattering. High-energy proton scattering will permit the additional study of the neutron transition density. Ray and Hoffmann (83) use two forms for the transition density

$$\rho_{ba,l} = \xi_l f'(r) \quad (5.4)$$

where ξ_l is a parameter and f is given by the forms

$$f(r) = \frac{1}{1 + e^{(r-c)/z}} \quad \text{two parameters} \quad (5.5)$$

or

$$f(r) = \frac{1 + wr^2/c^2}{1 + e^{(r^2 - c^2)/z^2}} \quad \text{three parameters} \quad (5.6)$$

The parameters now include c , z , and w . The constants in each of these forms are chosen as to give a best fit to the data. The consequent $f_{ab,l}$ can then be

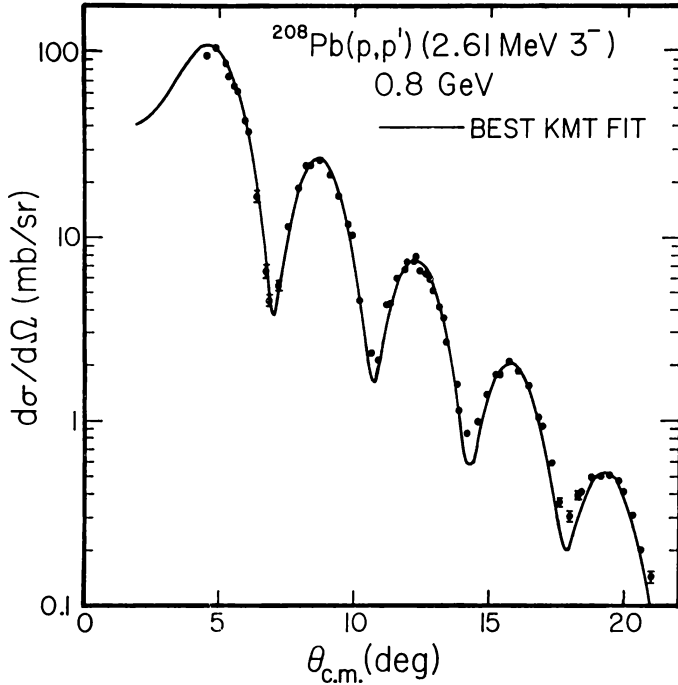


FIG. 5.1. Experimental data and best KMT fit for 800-MeV (p, p') to the 2.61-MeV 3^- state in ^{208}Pb . [From Ray and Hoffmann (83).]

compared with the results of a microscopic calculation. The best fit using the two-parameter form for the reaction $^{208}\text{Pb}(p, p')$ exciting the 2.6-MeV, 3^- level in lead is shown in Fig. 5.1. The fit is excellent. A similar fit is obtained with the three-parameter form. However, these do not give identical neutron transition densities, as one can see from Fig. 5.2. As one can anticipate, the two transition densities are identical in the surface region but differ substantially in the interior, indicating the insensitivity of the experimental data to the interior values. This insensitivity is a consequence of the absorption of the incident proton wave.

One can go beyond the DWA and use, for example, the method of coupled channels described in Chapter VII. Such a treatment is useful and practical when the excited levels are collective. It has been applied to such excitations in a series of papers by Blanpied et al. with moderate success. References to these articles are given in Blanpied (88). One noteworthy feature uncovered by these investigations is the need to increase the number of channels in the calculation as the angular range increases. Other methods make use of the Glauber representation and group properties of the exponential $\exp(-\int V dx)$. Bassichis, Feshbach, and Reading (11) treat the vibrational case, while Ginocchio

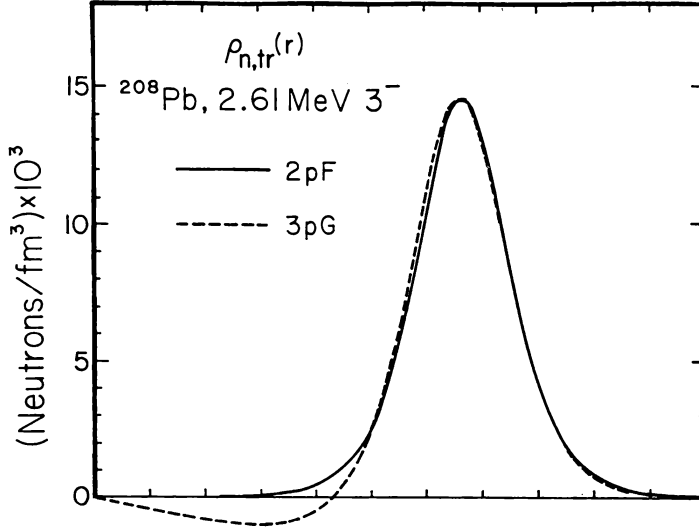


FIG. 5.2. Deduced neutron transition density for the 2.61 MeV 3^- state in ^{208}Pb . The two-parameter Fermi (2pF) and three-parameter (3pG) forms are shown. [From Ray and Hoffmann (83).]

et al [see the review by Ginocchio and Wenes (86)] generalize to deformed nuclei using the Hamiltonian of the interacting boson model.

It is expected that there is a close relation between the elastic and inelastic cross sections in high-energy reactions when the excited states are low-lying collective models. One should recall that connection established by Austern and Blair (65) at lower energies (see Chapter V). At the higher energies under consideration in this chapter it is again possible to express the inelastic scattering cross section for excitation of a collective state in terms of the elastic scattering cross section. Use is made of the eikonal approximation to the initial and final state projectile wave functions and of the Tassie (56) parametrization of the matrix element, which is appropriate for collective state excitation. That approximation yields [see (II.5.7)]

$$\psi_f^* \psi_i = e^{i\mathbf{q} \cdot \mathbf{r}} e^{i\chi} \quad (5.7)$$

where

$$\chi = -\frac{i}{2K} \int_{-\infty}^{\infty} U(\mathbf{b}, z') dz' \quad (5.8)$$

But from (II.4.30.)

$$U = -4\pi(A-1)\rho(f(0))$$

where $f(0)$ is the scattering amplitude evaluated at 0° . From the optical theorem

$$\sigma_T = \frac{4\pi}{k} \text{Im } f(0^\circ) \quad (5.9)$$

so that

$$f(0) = \frac{k}{4\pi} \sigma_T(r + i) \quad (5.10)$$

where r is the ratio of $\text{Re } f$ to $\text{Im } f$. Then

$$\begin{aligned} i\chi &= -\frac{\sigma_T}{2}(1 - ir)(A - 1) \int_{-\infty}^{\infty} \rho(z, \mathbf{b}) dz = -g(\mathbf{b}) = -\gamma t(b) \\ t(b) &\equiv \int_{-\infty}^{\infty} \rho(z, \mathbf{b}) dz \end{aligned} \quad (5.11)$$

The amplitude for inelastic scattering exciting a level with spin L , z projection M , and parity π is

$$f_{\text{in}}(0^\pi, 0 \rightarrow I^\pi, M) = -\frac{1}{4\pi} \frac{E + mc^2}{\hbar^2 c^2} \int e^{i\mathbf{q} \cdot \mathbf{r} - g(\mathbf{b})} \langle I^\pi M | V | 0^\pi 0 \rangle d\mathbf{r} \quad (5.12)$$

Following the discussion of Amado, Lenz, McNeil, and Sparrow (80), one notes that because of the transformation properties of $|I^\pi, M\rangle$ and $|0^\pi, 0\rangle$, it follows that

$$A \langle I^\pi M | t(\mathbf{r}, \mathbf{r}_1) | 0^+ 0 \rangle \equiv \langle I^\pi M | V | 0^+ 0 \rangle = f_I(r) P_{IM}(\vartheta) e^{iM\varphi} \quad (5.13)$$

where P_{IM} are the associated Legendre polynomials. In addition, Amado, Lenz, McNeil, and Sparrow (80) use the Tassie parametrization (56), where

$$f_I = \lambda_I r^{I-1} \frac{d\rho}{dr} \quad (5.14)$$

The parameter λ_I can be related to the transition probabilities (BEI) obtained from an analysis of inelastic electron scattering using the Tassie form [see, e.g., Heisenberg, McCarthy, and Sick (71)]. Substituting (5.13) and (5.14) in (5.12), replacing approximately $\mathbf{q} \cdot \mathbf{r}$ by $\mathbf{q} \cdot \mathbf{b}$, and integrating over φ yields

$$\begin{aligned} f_{\text{in}}(0^+, 0 \rightarrow I^\pi, M) &= -\frac{1}{2} \lambda_I \frac{E + mc^2}{\hbar^2 c^2} i^{-M} \int_0^\infty J_M(qb) b db e^{-g(b)} \\ &\times \int_{-\infty}^\infty dz \left(r^{I-1} \frac{d\rho}{dr} \right) P_{IM}(\vartheta) \end{aligned} \quad (5.15)$$

Note that P_{IM} is a polynomial in $z^n b^{I-n}/r^I$; n is odd if $(I+M)$ is odd, even if $(I+M)$ is even. Multiplying by $r^{I-1} d\rho/dr$ yields $z^n b^{I-n}[(1/r)(d\rho/dr)]$. The integrand in the z integral of (5.15) is thus odd if n is odd and thus will vanish for odd $(I+M)$. This result was obtained earlier in (V.4.20). We shall now restrict the discussion to the $I=1$ case for illustrative purposes. The details for the general values of I are given in Amado, Lenz, McNeil, and Sparrow (80) and the review article by Amado (85). We are then concerned with only $f_{in}(0^+, 0 \rightarrow 1^-, \pm 1)$. For $M=1$, we need $P_{11} = -(3/8\pi)^{1/2} b/r$, so that

$$f_{in}(0^+, 0 \rightarrow 1^-, M) = \frac{1}{2i} \lambda_1 \frac{E + mc^2}{\hbar^2 c^2} \left(\frac{3}{8\pi} \right)^{1/2} \int_0^\infty J_1(qb) e^{-g(b)} b^2 db \int_{-\infty}^\infty dz \frac{1}{r} \frac{d\rho}{dr}$$

The z integral can be reduced by noting that $(1/r)(d\rho/dr) = (1/z) d\rho/dz$ and

$$\frac{\partial}{\partial b} \int_{-\infty}^\infty dz \rho(\sqrt{z^2 + b^2}) = b \int_{-\infty}^\infty dz \frac{1}{r} \frac{d\rho}{dr}$$

Therefore,

$$\begin{aligned} f_{in}(0^+, 0 \rightarrow 1^-, 1) &= \frac{1}{2i} \lambda_1 \frac{E + mc^2}{\hbar^2 c^2} \left(\frac{3}{8\pi} \right)^{1/2} \frac{1}{\gamma} \int_0^\infty db J_1(qb) e^{-g(b)} b \frac{dg}{db} \\ f_{in}(0^+, 0 \rightarrow 1^-, 1) &= \frac{1}{2i} \lambda_1 \frac{E + mc^2}{\hbar^2 c^2} \left(\frac{3}{8\pi} \right)^{1/2} \frac{1}{\gamma} \int_0^\infty b db J_1(qb) \frac{d}{db} (1 - e^{-g(b)}) \end{aligned}$$

Integrating by parts yields

$$f_{in}(0^+, 0 \rightarrow 1^-, 1) = \frac{i}{2} \lambda_1 \frac{E + mc^2}{\hbar^2 c^2} \left(\frac{3}{8\pi} \right)^{1/2} \frac{q}{\gamma} \int_0^\infty b db J_0(qb) (1 - e^{-g(b)})$$

But the elastic scattering amplitude is

$$f^{el} = ik \int_0^\infty J_0(qb) (1 - e^{-g(b)}) b db$$

so that

$$f_{in}(0^+, 0 \rightarrow 1^-, 1) = \frac{1}{2} \lambda_1 \left(\frac{3}{8\pi} \right)^{1/2} \frac{E + mc^2}{\hbar^2 c^2} \frac{q}{\gamma k} f^{(el)}$$

Finally, adding in the $M = -1$ case, we obtain[†]

$$\sigma_{in}(0^+ \rightarrow 1^-) = \frac{3}{16\pi} \frac{q^2}{k^2} \left(\frac{\lambda_1}{\gamma} \frac{E + mc^2}{\hbar^2 c^2} \right)^2 \sigma_{el} \quad (5.16)$$

[†]This equation and (5.17) differ from the Amado et al. result because of differing normalizations.

Amado, Lenz, McNeil, and Sparrow (80) have derived the relationship between the elastic and inelastic cross section for arbitrary L . It is

$$\sigma_{\text{in}}(0^+ \rightarrow I^\pi) = \left(\frac{\lambda_I}{\gamma}\right)^2 \frac{2I+1}{4\pi} B_0^{2(I-1)} \left(\frac{q}{k}\right)^2 \left(\frac{E+mc^2}{\hbar^2 c^2}\right)^2 e^{2\pi a \Phi_I / R} \sigma_{\text{el}} \left(\theta + \frac{\Phi_I}{kR}\right) \quad (5.17)$$

where $R + i\pi a = B_0 e^{i\phi}$ and $\Phi_I = (I-1)\phi + \eta$, where $\eta = 0$ for odd L and $\pi/2$ for even L , where ρ is given by $\rho_0[1 + \exp((r-R)/a)]^{-1}$. Comparison of (5.17) with experiment is illustrated in Fig. 5.3. Excellent agreement is obtained. [See also Feshbach and Boridy (74) for the KMT result.] The success of Tassie expression (5.14) indicates that the interactions responsible for the inelastic scattering occur in the surface. This is not surprising since the central potential is so strongly absorptive (see Fig. II.8.1).

Amado (85) also discusses the properties of the polarization parameters for elastic scattering. These turn out to be sensitive to the radial dependence of the spin-orbit terms. A difference in the radial dependence given by the nuclear density results in substantial differences in the polarization. We have already observed this phenomena earlier in this chapter (see Section 3). There one found

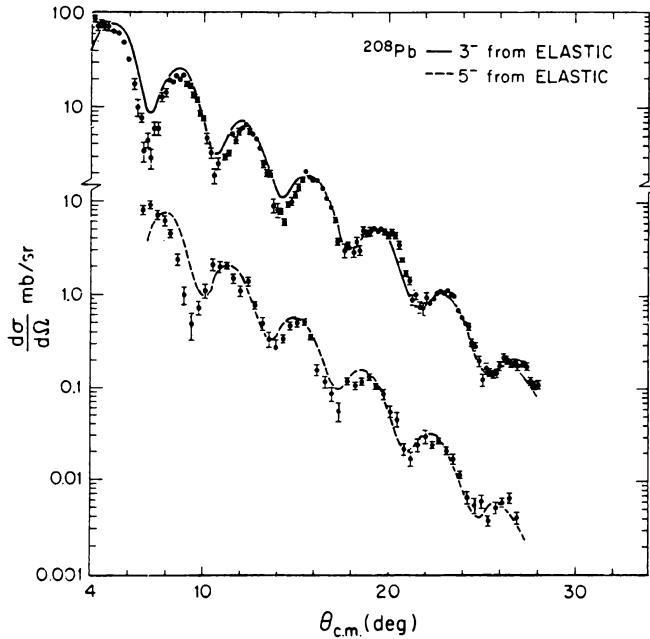


FIG. 5.3. Inelastic cross sections obtained from elastic scattering data (solid lines) compared with experiment. [From Amado (85).]

that adding in the interaction between the proton magnetic moment and the Coulomb field of the nucleus introduced oscillations into the asymmetry, for example, which brought the predictions in line with experiment. The reason for this sensitivity lies in the fact that the polarization parameters are ratios of various measured quantities to the differential cross section. For given interaction there can be correlations between the angular dependence of the numerator and that of the denominator. For example, at low energies there is the result obtained by Hüfner and de Shalit (65) that the polarization is proportional to the angular derivative of the angular distribution. At the higher energies, the nonoscillating behavior of the asymmetry (or Q) at the smaller angle must be a consequence of such a correlation. Adding in the magnetic moment Coulomb interaction or modifying the radial dependence in Amado's discussion destroyed the correlation since the angular distribution is not substantially modified by these changes. The oscillations of the numerator and the denominator are no longer in phase, so that new oscillations appear.

6. THE $(p, 2p)$ REACTION[‡]

The objectives of the studies of this process are similar to those of the study of the $(e, e'p)$ reaction—namely, to obtain information with regard to the hole state formed upon ejection of a target proton. In addition, one can hope to form some insight into the effect of the nuclear medium on the proton–proton interaction. There are substantial differences from the electron-induced reaction. Most important is the strong absorptive proton–nucleus interaction, which is to be compared with that of the relatively weak electron–nucleus interaction. In addition, the electron–proton interaction differs in character from that governing the proton–proton system.

The development to be presented here is suggested by the procedure used to discuss the $(e, e'p)$ reaction discussed earlier in this chapter. This is not the traditional procedure. I refer the reader to the reviews by Barrett and Jackson (77) and Kitching, McDonald, Maris, and Vasconcellos (85) for a description of that procedure. The model to be used is shown in Fig. 6.1 (compare with

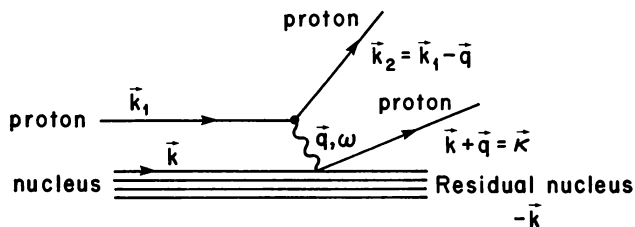


FIG. 6.1. The $(p, 2p)$ reaction.

[‡]Barrett and Jackson (77); Kitching, McDonald, Maris, Vasconcellos (85).

Fig. 2.17). The incident proton with momentum \mathbf{k}_1 interacts with a target proton with momentum \mathbf{k} whose momentum and energy are increased by \mathbf{q} and $\hbar\omega$, respectively. The scattered incident proton has the momentum $\mathbf{k}_2 = \mathbf{k}_1 - \mathbf{q}$. The residual nucleus will have a momentum of $-\mathbf{k}$ but may be excited to an energy ε . The model assumes that we are dealing with a single-step direct reaction. Conservation of energy requires that

$$\hbar\omega = \frac{\hbar^2}{2m}k_1^2 - \frac{\hbar^2}{2m}(\mathbf{k}_1 - \mathbf{q})^2 = \frac{\hbar^2}{m}(\mathbf{k}_1 \cdot \mathbf{q}) - \frac{\hbar^2}{2m}q^2 \quad (6.1)$$

and

$$\hbar\omega = \varepsilon + \frac{\hbar^2}{2m}(\mathbf{k} + \mathbf{q})^2 - \frac{\hbar^2 k^2}{2m} \quad (6.2)$$

By measuring \mathbf{k}_2 and $(\mathbf{k} + \mathbf{q})$, one can obtain ε . Figure 6.2 shows a plot of the cross section versus ε for the reaction $^{16}\text{O}(p, 2p)^{15}\text{N}$, for incident proton energy of 460 MeV. The hole states $s_{1/2}^{-1}$, $p_{1/2}^{-1}$, and $p_{3/2}^{-1}$ are clearly visible. A summary of the results obtained using a variety of targets is shown in Fig. 6.3.

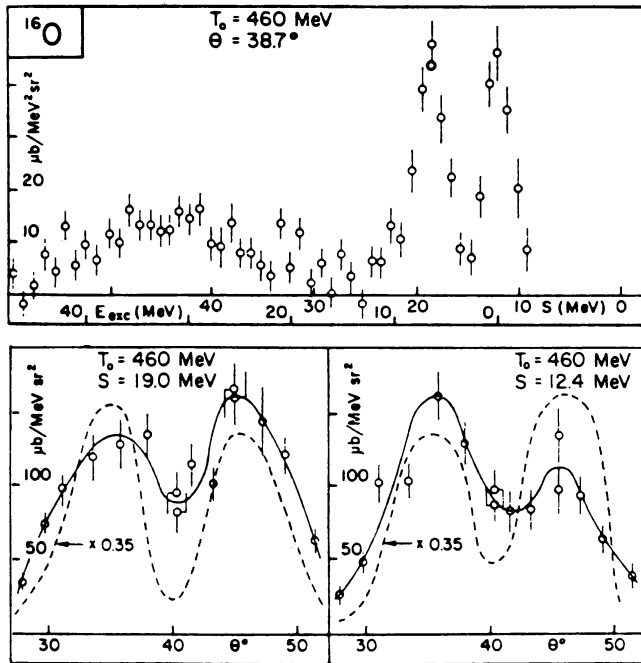


FIG. 6.2. Energy spectrum and angular correlations for the reaction $^{16}\text{O}(p, 2p)^{15}\text{N}$. The dashed lines are calculated results multiplied by the indicated factor. [From Kitching, McDonald, Maris, and Vasconcellos (85).]

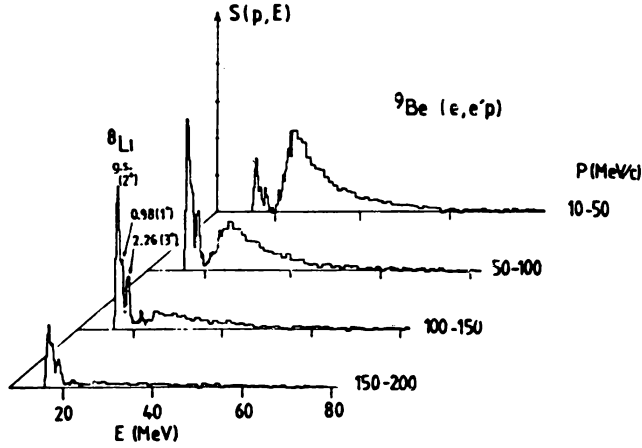


FIG. 6.3. Momentum distributions for the reaction ${}^9\text{Be}(e, e'p){}^8\text{Li}$. The p and s states are at $E \approx 15$ and 25 MeV, respectively. [From Kitching, McDonald, Maris, and Vasconcellos (85).]

The cross section for the inclusive $(p, 2p)$ process is

$$\begin{aligned} \frac{d^2\sigma}{dE_2 d\Omega_2} &= \left[\frac{\mathcal{E}^2 - m^2 c^4}{2\pi \hbar^2 c^2 E_L^{(p)}} \right]^2 \\ &\times \sum_f |\langle \chi_f^{(-)}(\mathbf{k}_2) \phi^{(-)}(\mathbf{\kappa}) \Psi_f | (A-1) \hat{\rho}(\mathbf{q}) t(\mathbf{q}) | \chi_i^{(+)}(\mathbf{k}_1) \Psi_i \rangle|^2 \\ &\times \delta(E_i - E_f) \end{aligned} \quad (6.3)$$

where \mathcal{E} is the energy of the incident proton $E_L^{(p)}$ plus the proton rest mass mc^2 , $E_i - E_f = E_L^{(p)} - (\hbar^2/2m)k_2^2 - (\hbar^2/2m)\kappa^2 - \varepsilon$, neglecting the recoil kinetic energy of the residual nucleus. The initial and final nuclear wave functions are Ψ_i and Ψ_f , respectively. If we drop the spin-dependent terms in $t(\mathbf{q})$ and assume that $t(\mathbf{q})$ varies so slowly that it can be removed from the matrix element in (6.3), we have

$$\begin{aligned} \frac{d^2\sigma}{dE_2 d\Omega_2} &= \left[\frac{\mathcal{E}^2 - m^2 c^4}{2\pi \hbar^2 c^2 E_L^{(p)}} \right]^2 |\langle \chi_f^{(-)} t(\mathbf{q}) \chi_i^{(+)} \rangle|^2 (A-1)^2 \\ &\times \sum |\langle \phi^{(-)}(\mathbf{\kappa}) \Psi_f | \hat{\rho} \Psi_i \rangle|^2 \delta(E_i - E_f) \end{aligned}$$

The first two factors can be combined to give an effective pp cross section, $d\sigma_{\text{eff}}^{(pp)}/dE_2 d\Omega_2$. It is not identical to the free proton-proton cross section since χ_i and χ_f are distorted waves as a consequence of their interaction with the target and residual nuclei, respectively. The factor that remains is just R_L , the

longitudinal response function of (2.118a). Therefore,

$$\frac{d^2\sigma}{d\Omega_2 dE_2} = \frac{d^2\sigma_{\text{eff}}^{(p,p)}}{d\Omega_2 dE_2} (A-1)^2 R_L \quad (6.4)$$

relating the inclusive $(e, e'P)$ and $(p, 2p)$ cross sections. If one includes the spin-dependent terms, one will obtain other response functions which are also present in the expression for $(e, e'p)$ polarization parameters.

7. RELATIVISTIC HEAVY IONS

In this section we consider the collision of heavy ions with nuclei with energies of the order of 1 GeV/A. These experiments have been for the most part performed at the Bevalac, the heavy-ion accelerator at the Lawrence Berkeley Laboratory, which produces beams of heavy ions with a maximum energy of 2.1 GeV/A. In Section 8 we briefly discuss collisions of protons and heavy ions with energies in the hundreds of GeV/A range. These are referred to as *ultra-relativistic heavy ions*.

Experimentally, two types of collisions could be differentiated, the *peripheral* and the *central*. In the first of these, the fragments move with nearly the same velocity as the incident projectile, and nearly in the forward direction in the laboratory reference frame. These fragments were ejected from the incident projectile by its interaction with the target nucleus. The impact parameter for these collisions are relatively large; the momentum transfer relatively small. The central collision is characterized by a high multiplicity, as one would intuitively expect. This is illustrated by Fig. 7.1, obtained by the internuclear cascade method. We see that high multiplicity is present for relatively small impact parameters, the nuclei “exploding” upon collision. This multiparticle final state involving many particles is a new feature that makes its appearance at relativistic energies (and at ultrarelativistic energies for even nucleon–nucleon collisions).

A. Peripheral Collisions

Peripheral collisions will be discussed first. As we shall see, this is essentially a low-energy phenomenon that can be understood rather directly in terms of small energy and momentum transfers to the projectile nucleus. Let us summarize the experimental facts obtained by experiments performed at the Bevalac facility. Experiments were performed with a beam of energetic projectiles (e.g., ^{16}O) at energies of 1.05 GeV/A and 2.1 GeV/A. Inclusive cross sections, that is, cross sections for the production of a particular nuclear fragment without a determination of the correlated production of other fragments, were measured. The results obtained are most simply expressed with respect to the projectile frame of reference defined as that frame in which the incident projectile is at rest and the target nuclei effectively form the incident beam.

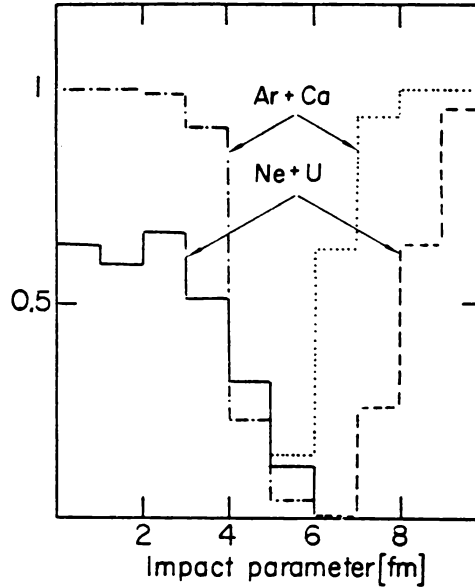


FIG. 7.1. Ratio of the multiplicity-selected proton inclusive cross section to the total proton inclusive cross section as a function of impact parameter. The solid line represents the $\sigma_{m \geq 20}/\sigma_{\text{tot}}$ ratio for $^{20}\text{Ne} + ^{238}\text{U}$ at $E/A = 400$ MeV and the dashed line represents the ratio $\sigma_{m \leq 8}/\sigma_{\text{tot}}$ for the same reaction. The dashed-dotted line represents the ratio $\sigma_{m \geq 20}/\sigma_{\text{tot}}$ for $^{40}\text{Ar} + ^{40}\text{Ca}$ at $E/A = 1050$ MeV and the dotted line represents the ratio $\sigma_{m \leq 5}/\sigma_{\text{tot}}$ for the same reaction. [From Yariv and Fraenkel (81).]

1. In the projectile frame, the momentum of a fragment is relatively small. For example, if the target nucleus is Pb, its momentum in the projectile frame is $208 \times 2.9 \sim 601$ GeV/c when the projectile has an energy of 2.1 GeV/A. The longitudinal-momentum, p_L , distribution of ^{10}Be fragments produced by fragmentation of the projectile, ^{12}C , in the projectile frame is shown in Fig. 7.2. We see that the ^{10}Be average longitudinal momentum is only about 50 MeV/c, while the dispersion of the p_L distribution is about 100 MeV/c, which should be compared with the 601,000 MeV/c carried by the Pb nucleus. Thus a very small fraction (10^{-4}) of the momentum of the lead nucleus is transferred to the projectile.
2. The distribution, $\omega(p_L, \mathbf{p}_T)$, in the longitudinal, p_L , and transverse, \mathbf{p}_T , components of the momentum is Gaussian in each. Empirically, one finds that

$$\omega(p_L, \mathbf{p}_T) \sim \exp \left\{ - \left[\frac{1}{2\sigma_L^2} (p_L - \bar{p}_L)^2 + \frac{1}{2\sigma_T^2} p_T^2 \right] \right\} \quad (7.1)$$

where as mentioned above, \bar{p}_L is generally several tens of MeV/c.

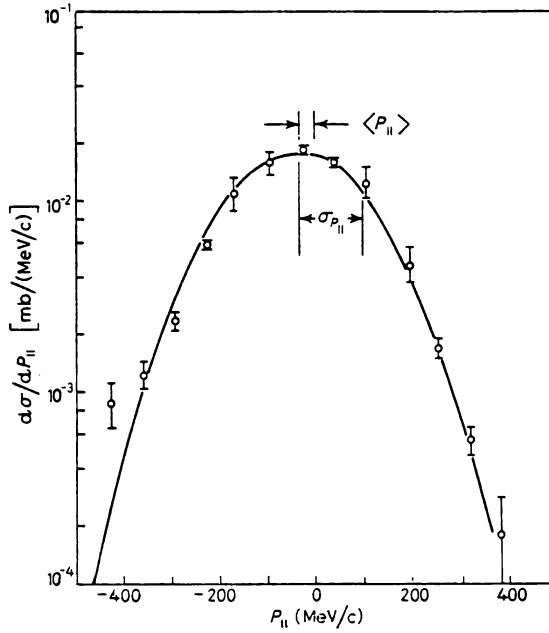


FIG. 7.2. Longitudinal-momentum distribution in the projectile frame of reference of the ^{10}Be fragments produced by the fragmentation of a ^{12}C projectile with an energy of 2.1 GeV/nucleon. [From Greiner, Lindstrom, et al. (75).]

3. The angular distribution is approximately isotropic, that is,

$$\sigma_L \simeq \sigma_T \quad (7.2)$$

However, because of the much greater experimental difficulty in the determination of the transverse momenta, (7.2) must be considered as approximate.

4. The dispersion, σ_L , is empirically independent of A_T (the target mass number), depending only on A_F (the fragment mass number) and A_P (the projectile mass number). This is a first example of independence of the projectile fragmentation of A_T .
5. A second is given by the fact that the branching ratio for the relative probability for the production of a fragment type is independent of the target nucleus. The cross section for the production of a fragment F , upon the collision of a target T with a projectile P , is found to be

$$\sigma_{PT}^{(F)} = \sigma_{PT} \frac{\gamma_P^{(F)}}{\gamma_P} \quad \text{where} \quad \sum_F \gamma_P^{(F)} = \gamma_P \quad (7.3)$$

The ratio multiplying σ_{PT} is the branching ratio for the production of fragment F .

6. The inclusive cross section σ_{incl} is proportional to the radius of the interaction. Empirically,

$$\sigma_{\text{incl}} \sim A_P^{1/3} + A_T^{1/3} - 0.8 \quad (7.4)$$

7. Cross sections and σ_L at 1.05 and 2.1 GeV/ A are approximately the same, indicating within this energy range, independence with respect to the energy (see Fig. 7.3).
8. The momentum distribution of the emerging protons is not Gaussian. It is better described by an exponential, $\exp(-p/p_0)$, where $p_0 \sim 65 \text{ MeV}/c$.

We shall now discuss the momentum distribution of the fragments.

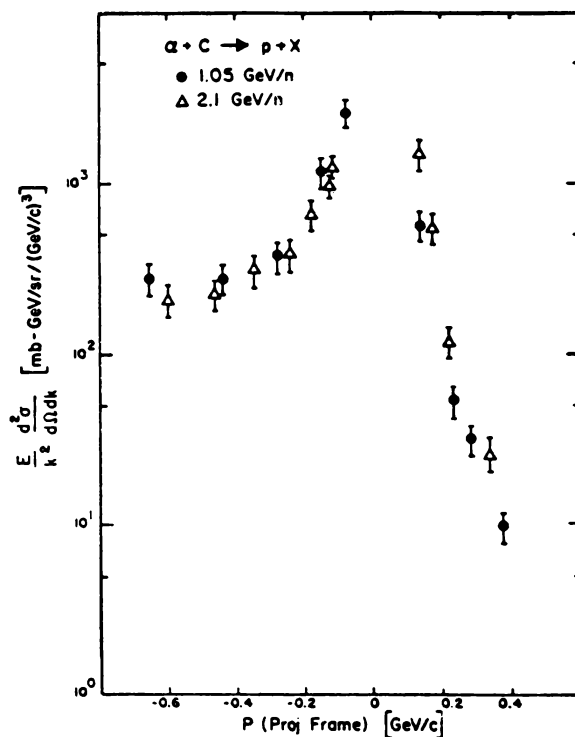


FIG. 7.3. Lorentz invariant cross section for an α beam of indicated energies fragmenting to protons versus the proton momentum in the projectile rest frame. [From Schroeder (76).]

Momentum Distribution of Projectile Fragments. The model we use was suggested by Feshbach and Huang (73). The derivation employed below follows essentially that of Goldhaber (74b). The model assumes that the fragment of mass number A_F is formed from the projectile of mass A_P by removing the binding of a group of A_F nucleons. The net momentum \mathbf{P}_F of the fragment is then obtained by adding up the momentum of each of these nucleons. The value of \mathbf{P}_F will vary according to which group of A_F nucleons is selected from the projectile giving rise to a distribution in \mathbf{P}_F . If the mean-square momentum of a nucleon in the projectile is $\langle p^2 \rangle$, the mean-square value of \mathbf{P}_F is, according to a simple statistical consideration,[†] given by $A_F \langle p^2 \rangle$. The distribution in \mathbf{P}_F , following again from statistical considerations, is Gaussian[§] at least in the neighborhood of the maximum of the distribution. This occurs near $P_F = 0$, since the average momentum of the fragments is so close to zero. Note that this model automatically assumes that the projectile fragment distribution does not depend on the nature of the target.

Suppose then that the projectile breaks up into fragments of mass number A_i , so that

$$\sum A_i = A_P \quad (7.5)$$

Let the momentum of each fragment be \mathbf{P}_i . Assume that the distribution of momenta for the i th fragment depends only on \mathbf{P}_i , and is Gaussian. Then the momentum distribution, ω , for a given set of A_i , is

$$\omega(\mathbf{P}_1, \mathbf{P}_2, \dots) \sim \prod_i \exp \left[-\frac{\frac{2}{3} P_i^2}{A_i \langle p^2 \rangle} \right] \quad (7.6)$$

To obtain the observed inclusive momentum distribution, we must integrate over all momenta except that of the observed fragment, say A_1 , subject to the condition

$$\sum_i \mathbf{P}_i = 0 \quad (7.7)$$

As shown by experiment, the average momentum of a projectile fragment in the projectile frame of reference is very small, justifying (7.7) to some extent.

[†]Assume that $\mathbf{P}_F = \sum \mathbf{p}_\mu$, where \mathbf{p}_μ are the momenta of the nucleons making up the fragment. Then $P_F^2 = \sum p_\mu^2 + \sum_{\mu \neq \nu} \mathbf{p}_\mu \cdot \mathbf{p}_\nu$. Averaging over the momentum distribution of the projectile nucleons, we find that $\langle \sum_{\mu \neq \nu} \mathbf{p}_\mu \cdot \mathbf{p}_\nu \rangle = 0$. Hence

$$\langle P_F^2 \rangle = \left\langle \sum_\mu p_\mu^2 \right\rangle = A_F \langle p^2 \rangle$$

[§]This result follows simply from the assumption that the momentum distribution is symmetric about the maximum.

Hence the single-fragment distribution, $\omega(\mathbf{P}_1)$, is given by

$$\omega(\mathbf{P}_1) = \int \omega(\mathbf{P}_1, \mathbf{P}_2, \dots) \delta(\sum \mathbf{P}_i) d\mathbf{P}_2 \dots \quad (7.8)$$

This integral may be easily performed to yield

$$\omega(\mathbf{P}_1) \sim \exp\left(-\frac{P_1^2}{2\sigma^2}\right) \quad (7.9)$$

where

$$\sigma^2 = \frac{1}{3} \langle p^2 \rangle \frac{(A_P - A_F)}{A_P} A_F \quad (7.10)$$

If we adopt the Fermi-gas model as a description of the projectile nucleus,

$$\frac{1}{3} \langle p^2 \rangle = \frac{1}{5} p_F^2 \quad (7.11)$$

where p_F is the Fermi momentum.

The experimental results are shown in Fig. 7.4. As can be seen from the figure, the dependence of σ^2 on A_P and A_F , given by (7.10), is verified by experimental data. However, those data yield a value for p_F [according to (7.10)] equal to 190 Mev/c, whereas the value of p_F determined from quasi-elastic electron scattering is, for ^{16}O , given by 225 MeV/c. As suggested by Hüfner, this discrepancy may occur because fragmentation occurs only after the emission of a number of nucleons. The fragmenting nucleus is not ^{16}O but a lighter nucleus with a correspondingly lower value of p_F .

The distribution given by (7.6) can also be used to calculate the angular correlation between two fragments, A_1 and A_2 , which exists in virtue of (7.7). One obtains

$$\omega(\mathbf{P}_1, \mathbf{P}_2) \sim \exp\left[-\frac{2}{3\langle p^2 \rangle} \frac{1}{A_P - A_1 - A_2} \left(P_1^2 \frac{A_P - A_2}{A_1} + P_2^2 \frac{A_P - A_1}{A_2} + 2\mathbf{P}_1 \cdot \mathbf{P}_2\right)\right]$$

This implies a greater probability for the two fragments to go off in opposite directions. Determination of this angular correlation would provide a test of the independence hypothesis as formalized by (7.6). It appears, however, to be very difficult to carry out this experiment.

The Nuclear Weizsäcker–Williams Method [Feshbach and Zabek (77)]. The Weizsäcker–Williams method relates the reaction cross section induced by a charged particle to that induced by a distribution of photons. The electromagnetic field of a rapidly moving charged particle can be shown to be

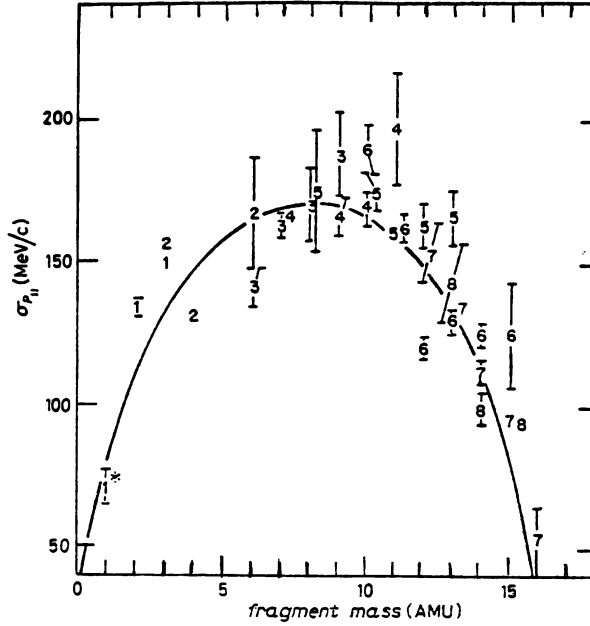


FIG. 7.4. Target averaged values of the dispersion σ of the longitudinal-momentum distribution in the projectile frame. The plotted numeral gives the charge of the fragment. The projectile is ^{16}O with an energy of 2.1 GeV/nucleon. The solid line is a best fit using (7.10). [From Greiner, Lindstrom, et al. (75).]

approximately equivalent to a beam of photons with the frequency distribution

$$n(\omega) d\omega = \frac{2}{\pi} (Z\alpha)^2 \frac{d\omega}{\omega} \quad (7.12)$$

where Z is the charge of the particle and α is the fine-structure constant. The cross section for the reaction induced by a charged particle is then given in terms of the cross section $\sigma_\gamma(\omega)$ for the photon-induced reaction by

$$\sigma = \int n(\omega) \sigma_\gamma(\omega) d\omega = \frac{2}{\pi} (Z\alpha)^2 \int \frac{\sigma_\gamma(\omega)}{\omega} d\omega \quad (7.13)$$

In this section a theory of the fragmentation of a relativistic heavy-ion projectile will be developed. The expression for the cross section which will be obtained will have a structure similar to that of (7.13), so that the theory will be referred to as the *nuclear Weizsäcker–Williams method*.

The projectile reference frame will be used. In that frame it will be assumed that the target nucleus travels without deviation and without internal excitation

in a straight line. This assumption is indicated by experimental result (1), which demonstrates that the momentum transferred to the projectile nucleus by the target nucleus is small. It is identical with the assumptions made in developing the electromagnetic Weiszäcker–Williams result. However, after the target nuclei have penetrated into the projectile a distance λ approximately equal to a nucleon mean free path, a strong collision with large momentum transfer will occur. This collision will not contribute to the process being considered, since the reaction products will fall outside the small forward cone where the fragments were detected. This competitive process is taken into account by assuming that the probability of finding the target nucleus intact attenuates during the collision with a scale measured by the mean free path λ .

It is assumed that the collision is peripheral. This result is implied very directly by experimental result 6, as given by (7.4). The mean free path λ used is the value valid on the surface region of the interacting nuclei.

A qualitative description of the consequences of these assumptions can be given. The projectile nucleon feel a pulse of force as the target nucleus passes by. The duration of the pulse, τ , is given by the scale, λ , Lorentz contracted to λ/γ , divided by the velocity of the projectile, v , which is very close to c , the velocity of light. Thus

$$\tau \sim \frac{\lambda}{\gamma v} \quad (7.14)$$

where

$$\gamma = \left(1 - \frac{v^2}{c^2}\right)^{-1/2} = \frac{E}{mA_T}$$

where v is the velocity of the target and E its energy. From the duration of the pulse one can calculate the maximum[†] energy transfer $\hbar\omega_c$ that can occur:

$$\hbar\omega_c \sim \frac{\hbar}{\tau} = \frac{\gamma \hbar v}{\lambda} \quad (7.15)$$

For a target energy of 2.1 GeV/ A and $\lambda = 1.75$ fm, the maximum energy transfer is found from this equation to be 365 MeV. We see immediately that we are in fact dealing with a comparatively low-energy phenomenon. There will be other effects to be discussed below, which will reduce the maximum energy transfer to even considerably lower values.

Following an argument of Guet, Soyeur, Bowlein, and Brown (89), one can establish a relation between the energy transfer $\hbar\omega$ and the longitudinal momentum transfer $\hbar q_L$. Let E_i and p_i be the initial four-momentum of the

[†]By “maximum” we shall mean the value of $\hbar\omega$ at which the cross section is $1/e$ of its value for very small values of $\hbar\omega$.

target and E_f and p_f its corresponding final four momentum, so that

$$\hbar\omega = E_i - E_f$$

and

$$\mathbf{q} = \mathbf{p}_i - \mathbf{p}_f$$

Then one can immediately obtain

$$\frac{\mathbf{p}_i \cdot \mathbf{q}}{E_i} - \hbar\omega = \frac{-(\hbar\omega)^2 + q^2 + (M_f^2 - M_i^2)}{E_i}$$

For sufficiently large E_i and small momentum and energy transfer, one can neglect the terms on the right-hand side of this equation so that

$$\frac{\mathbf{p}_i}{E_i} \cdot \mathbf{q} \simeq \hbar\omega$$

or

$$q_L \simeq \frac{\hbar\omega}{v} \quad (7.16)$$

The error in approximation leading to (7.16) is on the order of $\hbar\omega/E_i$ and therefore small.

The maximum value of transverse-momentum transfer, $\hbar q_T$, is determined by the transverse scale of the target density, namely a , the parameter measuring the thickness of the nuclear surface. The maximum transverse-momentum transfer is thus

$$\hbar q_{T,c} \sim \frac{\hbar}{a}$$

For $a \sim 0.6$ fm, $\hbar q_{T,c}$ is about 333 MeV/c.

In addition to these cutoffs in q_T and q_L , which come from the shape of the interacting nuclei, additional cutoffs that have a dynamic origin must be taken into account. The most obvious of these is the momentum transfer, which the nucleon–nucleon potential will allow before a substantial reduction in the amplitude will occur. From the empirical expression for the nucleon–nucleon amplitude, we find that the nucleon–nucleon potential produces a momentum cutoff, for both the transverse and longitudinal components, of 370 MeV/c.

The two factors so far described, the geometric factor and the potential factor, when combined, yield a momentum cutoff for both components of about 260 MeV/c.

Finally, it is necessary to consider the ability of the projectile nucleus to absorb the energy $\hbar\omega$ and the momentum $\hbar q$. If the energy is absorbed by a single nucleon, it will be very far off the energy shell. If it absorbs the full energy

$\hbar\omega$, it will have a momentum $\sqrt{2m\hbar\omega}$. This, however, is very much larger than the momentum transferred, which, as we have seen, is on the order of $\hbar\omega/c$, that is,

$$\sqrt{2m\hbar\omega} \gg \frac{\hbar\omega}{c}$$

or

$$\sqrt{\frac{\hbar\omega}{2mc^2}} \ll 1 \quad (7.17)$$

This inequality is satisfied by the $\hbar\omega$ of interest, that is, $\hbar\omega < 260 \text{ MeV}$. The absorbing nucleon must therefore interact with a second nucleon in the projectile. This absorption by two nucleons can proceed because it is then possible to conserve both momentum and energy. The momenta of the two nucleons will be opposite and nearly equal, so that the total momentum is small, but the total energy will be a sum of the energies of each nucleon.

The probability for two-nucleon absorption will therefore depend critically on the correlation length r_c , the mean distance between the first nucleon and the second. From the uncertainty principle, the lifetime of the nucleon absorbing the momentum and energy is on the order of $1/\omega$. This nucleon moves with a velocity equal to $\sqrt{(2/m)\hbar\omega}$ and thus covers in the time $1/\omega$ the distance $\sqrt{2\hbar/m\omega}$. This distance must be of the order of or greater than r_c :

$$\left(\frac{2\hbar}{m\omega}\right)^{1/2} > r_c$$

or

$$\hbar\omega < \frac{2\hbar^2}{mr_c^2} \quad (7.18)$$

If we take r_c as $1/2(\hbar/m_\pi c)$, one-half of the pion Compton wavelength, this inequality becomes

$$\hbar\omega < 165 \text{ MeV} \quad (7.19)$$

Combining this result with the geometric and interaction potential gives a longitudinal-momentum cutoff of $139 \text{ MeV}/c$, of the same order as the experimental value. It also implies a maximum value of the energy that can be transferred to the projectile equal to 139 MeV . This energy is split between the two absorbing nucleons, so that the cutoff energy for one of these nucleons is approximately 70 MeV and the cutoff momentum on the order of $70 \text{ MeV}/c$.[†]

[†]It has been suggested by Goldhaber that in addition to the two-nucleon mechanism, there is the possibility of nucleon excitation to form a Δ . However, the momentum change would then be on the order of $300 \text{ MeV}/c$. This combined with the other factors would yield a cutoff of $190 \text{ MeV}/c$, which would be too large to explain the fragmentation data. However, as Guet, Soyeur, Bowlein, and Brown (89) have shown, it is an important mechanism for pion production.

The low value of the momentum transferred ($\sim \hbar\omega/c$) indicates that the angular distribution of the nucleons will be roughly isotropic in the projectile frame. In the collision of the two nucleons as discussed above, their final linear momentum is $\hbar\omega/c$, so that their angular momentum lh is on the order of $(\hbar\omega/c)r_c$. Hence

$$l \leq \frac{\hbar\omega r_c}{\hbar c} \quad (7.20)$$

Inserting a maximum value for $\hbar\omega$ of 139 MeV and $r_c = 0.7$ fm yields

$$l \leq 0.5 \quad (7.21)$$

demonstrating that for nearly all values of $\hbar\omega$ the angular distribution of the nucleon pair will be isotropic.[‡]

These qualitative considerations provide a simple explanation of the projectile fragmentation as a consequence of the action of the “fringing field” of the target nucleus as it moves past the projectile. Our principal conclusion is that the process is essentially a low-energy phenomenon. The energy of the nucleon pairs produced is predicted to have the observed order of magnitude. These nucleons will deposit energy within the projectile nucleus and by that means fragmenting it. The net maximum momentum that can be transferred is calculated to be of the experimental order of magnitude. A rough isotropy is also predicted. Energy dependence in the GeV/A range is weak, since the energy occurs only in the geometric cutoff given by (7.15). As observed, the cutoff energy is changed by only a few percent when the heavy-ion energy is changed from 2.1 GeV/A to 1.05 GeV/A, since the dynamical conditions, (7.18), and the limits imposed by the nucleon–nucleon potential are energy independent in this range of energy. Finally, it should be observed that none of the cutoff conditions depend on the target nucleus. This does indicate that the width of the momentum distribution of the fragments is independent of the target. It is obviously a necessary condition for showing that the branching ratios are target nucleus independent. The quantitative calculation we report below shows that indeed the nucleon spectrum, and therefore the projectile fragmentation, are target independent.

We turn now to the nuclear Weizsäcker–Williams method. The projectile frame of reference will be used so that the incident system is the target nucleus. As in the Coulomb case, the target nucleus is assumed to continue to move in a straight line along the incident direction. It is also assumed that the interaction provided by the long-range component of the nuclear field, the *fringing field*, is weak. We may therefore use first-order perturbation theory.

[‡]Actual calculation shows, in fact, that this estimate is overgenerous and that the maximum value of l is considerably smaller than that given by (7.21).

Let the coordinates of the target nucleus relative to its center of mass be given by ξ_T and its internal wave functions by $\chi(\xi_T)$. Similarly, the coordinates of the projectile nucleus relative to its center of mass are given by ξ_P and its internal wave functions by $\psi(\xi_P)$. The vector between the center of mass of each of the nuclei, \mathbf{r} , has components z and \mathbf{b} , where z is in the direction of motion of the target nucleus and \mathbf{b} is transverse to that direction.

The wave function of the system has the following form:

$$\psi = \chi_0(\xi_T) \sum_{\alpha} \psi_{\alpha}(\xi_P) \Phi_{\alpha}(\mathbf{r}, t) e^{-i/\hbar E_{\alpha} t} \quad (7.22)$$

where χ_0 is the ground-state target wave function, and ψ_{α} describes the internal states of the projectile and E_{α} their energies. The function Φ_{α} is the wave function for the relative motion of the target and projectile. Inserting (7.22) into the time-dependent Schrödinger equation yields an equation for Φ_{β} :

$$\begin{aligned} \frac{i\hbar \partial \Phi_{\beta}}{\partial t} &= \sum_{\alpha} \langle \chi_0 \psi_{\beta} | V | \psi_{\alpha} \chi_0 \rangle \Phi_{\alpha} e^{i\omega_{\alpha\beta} t} \\ \omega_{\alpha\beta} &\equiv E_{\beta} - E_{\alpha} \end{aligned} \quad (7.23)$$

We now insert the assumption that the z component of the velocity of the target nucleus is unchanged during the course of the collision:

$$\Phi_{\beta} = u(z, t) \phi_{\beta}(\mathbf{b}, t) \quad (7.24)$$

with

$$|u|^2 = \delta(z - vt) \quad \int |u|^2 dz = 1 \quad (7.25)$$

Inserting (7.24) into (7.23) yields

$$\frac{i\hbar \partial \phi_{\beta}}{\partial t} = \sum_{\alpha} \langle \psi_{\beta} | (V \rho_T |u|^2) \psi_{\alpha} \rangle \phi_{\alpha}(\mathbf{b}, t) e^{i\omega_{\alpha\beta} t} \quad (7.26)$$

where

$$(V \rho_T |u|^2) = \int V |\chi_0|^2 |u|^2 d\xi_T dz \quad (7.27)$$

We use first-order perturbation theory to solve (7.26), that is, we assume that ϕ_{α} on the right-hand side of (7.26) has its initial value

$$\phi_{\alpha} = \delta_{\alpha i} \quad (7.28)$$

The probability $P_{\beta i}$ that the projectile makes a transition from its initial state

ψ_i to a final state ψ_β is

$$P_{\beta i} = \frac{2\pi}{\hbar^2} |F_\beta(\omega_{\beta i})|^2 \quad (7.29)$$

where $\hbar\omega_{\beta i}$ is the energy transfer and

$$F_\beta(\omega) = \langle \phi_\beta | \psi_\beta | U | \phi_i | \psi_i \rangle \quad (7.30)$$

The function U is

$$U(\mathbf{b}, \xi_p, \omega) = \frac{\gamma}{2\pi} \int dt e^{i\omega t} \int dz \int d\xi_T \rho_T(\mathbf{b}_T, \gamma z_T) |u|^2 V \quad (7.31)$$

where

$$\gamma = \frac{1}{\sqrt{1 - v^2/c^2}}$$

The factor γ in (7.31) takes into account the relativistic contraction of length. Inserting (7.25) for $|u|^2$ and integrating over time yields

$$U(\mathbf{b}, \xi_p, \omega) = \frac{\gamma}{2\pi v} \int dz e^{-i\omega z/v} \int d\xi_T \rho_T(\mathbf{b}_T, \gamma z_T) V \quad (7.32)$$

Taking V to be a central potential acting between a nucleon in the target and a nucleon in the projectile summed over all pairs, V has the general form

$$V = V(\mathbf{r} + \xi_T - \xi_p) \quad (7.33)$$

Let

$$\zeta = z + z_T - z_p$$

$$\boldsymbol{\beta} = \mathbf{b} + \mathbf{b}_T - \mathbf{b}_p$$

Then

$$U(\mathbf{b}, \xi_p, \omega) = \frac{\gamma}{2\pi v} e^{i\omega z_p/v} \int d\zeta \int d\xi_T e^{i\omega(\zeta - z_T)/v} \rho_T(\mathbf{b}_T, \gamma z_T) V(\zeta, \boldsymbol{\beta}) \quad (7.34)$$

demonstrating that the longitudinal momentum transferred to a projectile nucleon is $\hbar\omega/v$. Finally, from (7.30) it is necessary to evaluate $\langle \phi_\beta | U | \phi_i \rangle$. Taking ϕ_i from (7.28) and

$$\phi_\beta = e^{i\mathbf{k} \cdot \mathbf{b}} \quad (7.35)$$

where \mathbf{k} is the transverse momentum transfer, one obtains

$$\langle \phi_\beta | U | \phi_i \rangle = \frac{1}{2\pi v} e^{i(\omega z/v - \mathbf{k} \cdot \mathbf{b}_p)} \tilde{\rho}_T\left(\mathbf{k}, -\frac{\omega}{\gamma v}\right) \tilde{V}\left(-\mathbf{k}, \frac{\omega}{v}\right) \quad (7.36)$$

where the tilde indicates the Fourier transform, so that

$$\tilde{V}\left(-\mathbf{k}, \frac{\omega}{v}\right) = \int V(\boldsymbol{\beta}, \zeta) e^{-i\mathbf{k} \cdot \boldsymbol{\beta} + i\omega\zeta/v} d\boldsymbol{\beta} d\zeta \quad (7.37)$$

As a consequence of these results the matrix element $F_{\beta i}$ factorizes into a product of two terms, one of which depends only on the properties of the projectile, the other on those of the target.

$$F_{\beta i} = F_{\beta i}^{(P)}\left(-\mathbf{k}, \frac{\omega}{v}\right) F^{(T)}\left(\mathbf{k}, \frac{\omega}{v}\right)$$

where

$$F^{(T)}\left(\mathbf{k}, \frac{\omega}{v}\right) \equiv \frac{1}{2\pi v} \tilde{\rho}_T\left(\mathbf{k}, -\frac{\omega}{\gamma v}\right) \tilde{V}\left(-\mathbf{k}, \frac{\omega}{v}\right) \quad (7.38)$$

$$F^{(P)}(\mathbf{q}) \equiv \langle \psi_\beta | e^{i\mathbf{q} \cdot \boldsymbol{\xi}_p} | \psi_i \rangle \quad \mathbf{q} = \left(-\mathbf{k}, \frac{\omega}{v}\right) \quad (7.39)$$

The projectile factor involves a sum over the projectile nucleon coordinates and thus equals the projectile transition density. $F^{(T)}$ is independent of the transition induced in the projectile. From the point of the projectile, the target acts as a source of “phonons” with momentum \mathbf{q} and energy $\hbar\omega$. The total cross section is obtained by integrating the probability that a transition from ψ_i to ψ_β is induced by a phonon of momentum \mathbf{q} over the number density of such phonons. Thus

$$\sigma_T = \frac{1}{\hbar^2} \int \rho_\beta dE_\beta d\mathbf{k} d\omega \left| F_{\beta i}^{(P)}\left(-\mathbf{k}, \frac{\omega}{v}\right) \right|^2 \left| F^{(T)}\left(\mathbf{k}, \frac{\omega}{v}\right) \right|^2 \delta(\omega - \omega_{\beta i}) \quad (7.40)$$

where ρ_β is the density of final states. We have therefore referred to this procedure as the nuclear Weiszäcker–Williams method.

We shall not develop this procedure further, as all that is required is the calculation of $F^{(T)}$ and $F^{(P)}$. For details the reader is referred to the original articles [Feshbach and Zabek (77); Feshbach (81)]. It is found that the anisotropy of the angular distribution is governed by a small parameter:

$$\frac{1}{4} \left(\frac{mc^2}{\hbar c} \right) \left(\frac{\hbar\omega r_c}{\hbar c} \right)^4$$

which equals 0.068 for $r_c = 0.7$ fm and $\hbar\omega = 140$ MeV. The cross section is proportional to $A_T^{1/3}$. It is sensitive to the value of the correlation length, r_c . Reasonable values are obtained for $r_c \sim 0.7$.

To obtain the partial cross sections, the two particles ejected by the phonon are followed using cascade theory. Finally, one must add the effect of a single particle ejection for the total branching ratio. Good agreement with experiment is obtained [Feshbach (81)]. This process has also been treated as an “abrasion–ablation” process by Hüfner (75) and collaborators. The method described here has been generalized by Guet, Soyeur, Bowlein, and Brown (89) and used to discuss subthreshold pion production in ^{12}C – ^{12}C collisions at a projectile energy of 95 MeV/A.

B. Central Collisions[†]

A number of different theoretical descriptions of the central, high-multiplicity collisions have been proposed. Some of these such as the fireball–firestreak thermal models [Westfall, Gosset, et al. (76); Myers (78)] and the hydrodynamic models [Amsden, Harlow, and Niu (77); Amsden, Goldhaber, Harlow, and Niu (78); Stöcker and Greiner (86)] presume the existence of thermal equilibrium. Others, such as Koonin (77), have shown that a significant fraction of the observed cross section is a consequence of direct knockout of a preequilibrium nature. Classical or semiclassical procedures are employed by the models of Hüfner and Knoll (77), Wilets et al. (77), Bodmer and Panos (77), and finally the internucleon cascade mode of Yariv and Fraenkel (79,81) and Cugnon (80,81). We shall limit the discussion below to a description of the internuclear cascade model, an important technique that permits detailed calculation of many of the observed phenomena. None of the models are completely successful, but the internucleon cascade does quite well for many situations. Perhaps its most significant failure is the prediction of the directed flow momenta, which it underestimates by a factor of 2 while the hydrodynamic model errs by its overestimate of the flow by a factor of 2 [Stöcker and Greiner (86); Cugnon (82)].

The internuclear cascade (INC) follows the passage of a nucleon (or group of nucleons) through a target nucleus assuming two-body collisions. In one method [Chen et al. (68); Yariv and Fraenkel (79,81)] the target nucleus is represented by a continuous fluid whose density is obtained, for example, from electron scattering. The probability that a target nucleon has a momentum \mathbf{p} at a point \mathbf{r} is given by the Fermi-gas distribution corresponding to the density $\rho(\mathbf{r})$. Attention is focused on the projectile motion during the time it could travel a distance $\bar{\lambda}/n$, where $\bar{\lambda}$ is an estimated mean free path and n is on the order of 20. The first step is randomly to select a nucleon from the Fermi gas, which is to interact with the projectile nucleon. The next step is to determine whether an interaction occurs within the distance $\bar{\lambda}/n$. Toward that end the probability of such a collision $P(\bar{\lambda}/n)$ is calculated and compared to a random number ζ . If ζ is less than P , an interaction is assumed to have occurred. If $\zeta > P$, no interaction is said to have occurred and the projectile is advanced by a distance $\bar{\lambda}/n$ and the process is repeated. If there has been an interaction, it will have

[†]Cugnon (82).

taken place at a distance from the beginning of the interval given by $\zeta/\bar{\lambda}$. At this point the direction of travel of the particle is determined from the known nucleon–nucleon angular distribution by a technique similar to that described above for deciding if an interaction has taken place, that is, the probability for scattering through a given angle randomly selected is compared with a random number. The final energies of the colliding nucleons can then be calculated. If the energy of either of the particles is below the Fermi energy, the interaction is forbidden so that the momentum of the projectile is unchanged. One now repeats the process with another Fermi-sea nucleon to see if an interaction takes place in the remainder of the interval. If the energies of both particles are above the Fermi energy, the collision is allowed. Their momenta are determined from the selected scattering angle. The process is then repeated for each nucleon. As the cascade develops, the density in the Fermi seas is reduced. Yariv and Fraenkel (79) consider two possible consequent rearrangements. In the *fast rearrangement*, the density of the target is instantaneously reduced. In the *slow arrangement* a “hole” of volume $1/\rho$ is punched around the position of the collision. No more interactions are allowed within this volume. Empirically, slow arrangement yields results that are in better agreement with experiment. The entire procedure is repeated until statistical significance is obtained.

Several features are sometimes included in the calculation. Pion production and absorption proceeding through the Δ baryon resonance is one. In another, the nucleons are assumed to be traveling in a potential well so that the nucleon paths between collisions are no longer straight lines. Collisions among the cascade particles, as well as formation of composite systems, may (or may not) be included.

In the calculations by Cugnon (81), Stevenson (78), Bondorf et al. (76), and Halbert (81), the continuum distribution for the target is dropped. Each of the nucleons on the target and projectiles is positioned randomly within spheres, representing the target and projectile nuclei. Their momenta are chosen randomly using the Fermi gas model. The projectile is given the beam velocity. The projected nucleons are assumed to move in straight lines between collisions. When the minimum relative distance is smaller than $\sqrt{\sigma_{\text{tot}}/\pi}$, the nucleons are assumed to scatter. Here σ_{tot} is the total nucleon–nucleon cross section at their center-of-mass energy. It is evident that in both of these procedures the nucleon correlations in both the target and projectile are neglected.

The motion of the nucleons in the INC simulation is classical. A necessary condition for its validity is that the cascade and projectile nucleon wavelengths are much smaller than the internucleon distance r_{12} .

$$\frac{\hbar}{p_{\text{lab}}} \ll r_{12}$$

This condition will not be met by the low-energy cascade nucleons generated by the incident projectile. The calculation of the low-energy part of the spectrum

will thus be unreliable. A second condition requires that the mean free path must be large compared to the interaction range r_c :

$$\lambda \gg r_c$$

Here r_c is defined by $\sigma_{\text{tot}} = \pi r_c^2$. Since $\lambda = 1/\rho\sigma_{\text{tot}}$, this condition becomes

$$\pi r_c^3 \rho \ll 1$$

This condition is well satisfied for normal nucleon densities. Finally, nucleon correlations are reflected in nucleon momenta which exceed the limits of the Fermi gas. As a consequence, one may expect an inability to match the data at the high-energy end of the energy spectrum. A similar remark may be made with respect to the angular distribution.

The invariant nucleon cross section is related to the calculated one-body distribution function, f_1 , by

$$E \frac{d^3\sigma}{dp^3} = \lim_{t \rightarrow \infty} \int_0^{b_{\text{max}}} 2\pi b db \int d\mathbf{r} E f_1(\mathbf{r}, \mathbf{p}, b, t) \quad (7.41)$$

An example of a comparison with experiment is shown in Fig. 7.5. The agreement is very good except for the low-energy part of the spectrum, where INC underestimates the cross section for $E < 80$ MeV. Evaporation of the residual nuclei has not been included in the calculation. The effect of including the interaction between cascade particles is small.

Another example is provided by Cugnon and Vandermulen (85) as shown in Fig. 7.6. We see that at 800 MeV/A the angular distribution is far from isotropic. This is because a considerable fraction of the proton distribution is a consequence of a single collision. As the number of collisions increase, the angular distribution will become more isotropic. For the Ca + Ca case at 800 MeV/A, isotropy is achieved for $n \lesssim 6$. The probability distribution for the number n of collisions is shown in Fig. 7.7 for the Ca + Ca collision. The mean value is 3.24. Of course, the probability for a large n is very small for peripheral collisions.

A second observable is the correlation between two protons, as given by

$$C(\mathbf{p}_1, \mathbf{p}_2) = \lim_{t \rightarrow \infty} \frac{\int 2\pi b db \int \int d\mathbf{r}_1 d\mathbf{r}_2 f_2(\mathbf{r}_1, \mathbf{p}_1; \mathbf{r}_2, \mathbf{p}_2; b, t)}{\int 2\pi b db \int d\mathbf{r}_1 f_1(\mathbf{r}_1, \mathbf{p}_1; b, t)} \quad (7.42)$$

where f_2 is the two-body distribution function. In the Nagamiya et al. (79) experiment, the correlation between a proton emitted at a “telescope” angle and an second particle in the angular range $35^\circ < \theta < 45^\circ$ is studied. The ratio C is defined to be the ratio of such in the scattering plane correlations for the azimuthal angle $\phi = 180^\circ \pm \Delta\phi$ ($\Delta\phi = 10^\circ$), to the out-of-plane correlations

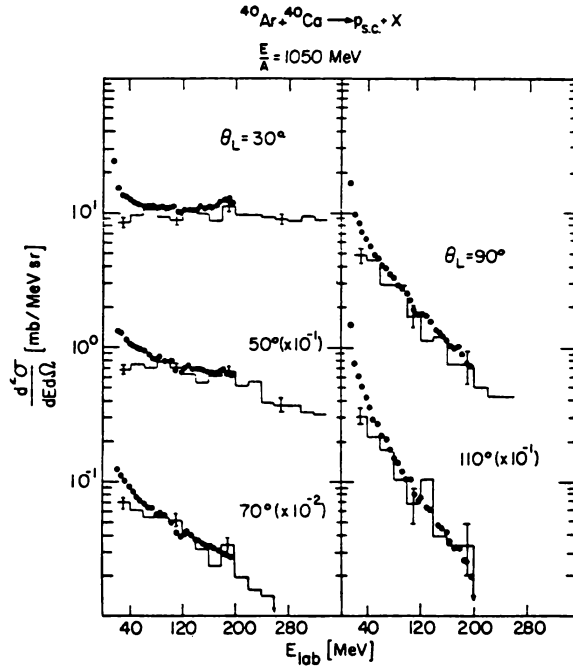


FIG. 7.5. Inclusive double-differential cross section for the emission of nucleon charges in the reaction $^{40}\text{Ar} + ^{40}\text{Ca}$ at a bombarding energy of $E/A = 1050$ MeV. The histograms show the calculated results, including the effects of interaction between the cascade particles. [From Yariv and Fraenkel (81).]

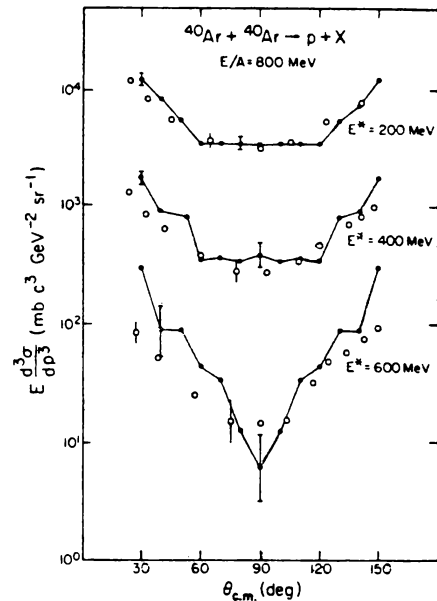


FIG. 7.6. Invariant inclusive proton cross section as a function of the center-of-mass angle for the $^{40}\text{Ar} + ^{40}\text{Ar}$ system at 800 MeV/nucleon. [From Cugnon and Vandermuelen (85).]

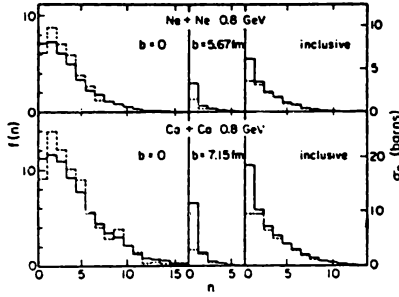


FIG. 7.7. Probability distribution for the number n of collisions that the particles have undergone. The full lines refer to the nucleons. Left, zero impact parameter; center, large impact parameter; right, average overall impact parameters. [From Cugnon and Vandermuelen (85).]

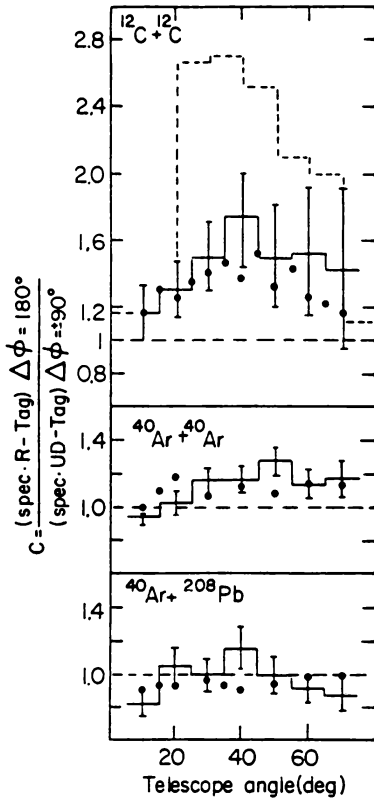


FIG. 7.8. Ratio, C , of "in-plane" ($\Delta\phi = 180^\circ$) to "out-of-plane" ($\Delta\phi = \pm 90^\circ$) tow-particle correlations as a function of the polar (telescope angle). The second particle is detected at a polar angle of $10 \pm 5^\circ$, $\Delta\phi$ is the difference in the azimuthal angle of the two particles. The histograms are calculated. The solid-line ones include the effects of interaction between the cascade particles, the dashed-line ones do not. [From Yariv and Fraenkel (81).]

($\phi = \pm 90^\circ + \Delta\phi$). The results of the INC calculation and a comparison with experiment are shown in Fig. 7.8. The calculated results *when the interaction between cascade particles is included* are in good agreement with experiment. The ratio C is close to unity (except for the $^{12}\text{C} + ^{12}\text{C}$ collision), indicating a degree of thermalization.

Other observables include the momentum tensor $Q_{\mu\nu}$ and the related quantity

the thrust, T . For an event, $Q_{\mu\nu}$ is given by

$$Q_{\mu\nu} = \sum_i \gamma(p_i) p_i^\mu p_i^\nu \quad (7.43)$$

where i runs over the fragments and μ, ν designate the Cartesian coordinates. The weights $\gamma(p_i)$ are to be chosen. When $\gamma(p_i)$ is taken to be $1/A_i$, where A_i is the mass number of the fragment, the resultant $Q_{\mu\nu}$ is independent of the degree of clusterization.

The thrust, T , is given by

$$T = \min_{\mathbf{n}} \frac{\sum |\mathbf{p}_i \cdot \mathbf{n}|}{\sum |\mathbf{p}_i|} \quad (7.44)$$

where the unit vector \mathbf{n} is chosen to as to minimize this ratio. The direction of the thrust is given by \mathbf{n} . The values for the thrust angle (the calculated thrust lies in the reaction plane for collisions between equal nuclei) are given in Fig. 7.9 as calculated by INC [Bertsch and Cugnon (81)] and using hydrodynamics [Kapusta and Strottman (81)]. As expected, the INC calculation predicts a flow that is much more in the forward direction. Experimental indications of collective flow is given in the paper by Gustafson, Gutbrod, et al. (84). In Fig. 7.10 the frequency distribution $dN/d\cos\theta$ as a function of flow angle θ is plotted for various multiplicities for reactions involving heavy ions at 400 MeV/A. The flow angle is defined as the angle between the beam direction and the major axis of the ellipsoid given by $Q_{\mu\nu}$ of (7.43), with weights $\gamma(p_i) = 1/2A_i$, where A_i is the mass of the fragment. We observe that as the multiplicity increases (impact parameter decreases), the frequency distribution has a maximum at a finite angle, while the INC calculations have their maxima at 0° . The parallel component of the projectile momentum is reduced during the collision, and the momentum acquires a small perpendicular momentum on the order of 50 MeV/c. The origin of this discrepancy is not yet clear. Is it because of the approximation (e.g., the Fermi-gas description of the colliding nuclei) of the INC procedure, or is it because of the omission of collective modes of motion by the INC? For a recent discussion, see Aichelin, Cugnon, et al. (89).

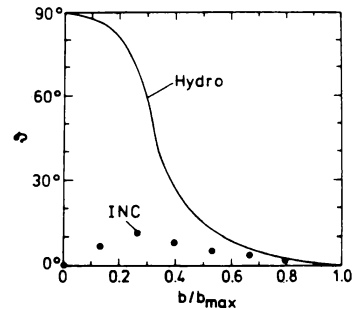


FIG. 7.9. Thrust angle as given by a hydrodynamic calculation (full line) and by the inter nuclear cascade (dots). [From Cugnon (82).]

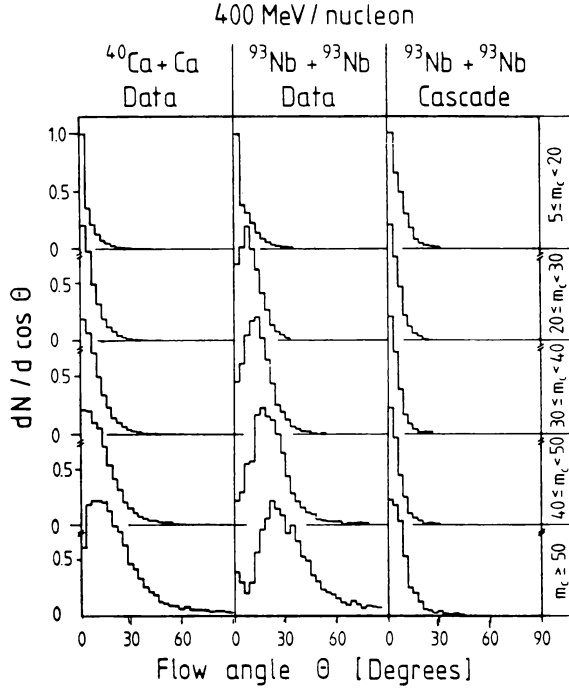


FIG. 7.10. Frequency distributions of the flow angle θ for two sets of data and a cascade calculation for different multiplicity bins. For the case of Ca the multiplicities are half the indicated values. [From Gustafsson, Gutbrod, et al. (84).]

8. COLLISIONS AT ULTRARELATIVISTIC ENERGIES

In this section the collision of ultrarelativistic projectiles, with energies greater than several GeV/nucleon, with nucleon is briefly considered. Experiments in which the projectile has an energy of up to several hundred GeV have been reported. This field is in its infancy. There are many results that are still not understood and much more experimentation and theoretical studies are needed.

A. Lorentz Transformation

In the relativistic regime, the Lorentz transformation is especially important. The Lorentz transformation to a frame moving with a velocity v (we shall use units in which the velocity of light, c , is unity) in the position z direction is [Morse and Feshbach (53 p. 94)]

$$\begin{aligned} z' &= z \cosh \xi + t \sinh \xi \\ t' &= z \sinh \xi + t \cosh \xi \end{aligned} \quad (8.1)$$

where

$$\cosh \xi \equiv \frac{1}{\sqrt{1-v^2}} \quad \sinh \xi = \frac{v}{\sqrt{1-v^2}} \quad \xi = \frac{1}{2} \ln \frac{1+v}{1-v}. \quad (8.2)$$

Under a second boost with velocity v' ,

$$\begin{aligned} z'' &= z' \cosh \xi' + t' \sinh \xi' \\ t'' &= z' \sinh \xi' + t' \cosh \xi' \end{aligned}$$

Substituting from (8.1) for z' and t' , one finds, for example,

$$z'' = z \cosh(\xi + \xi') + t \sinh(\xi + \xi')$$

Thus the effect of two sequential boosts of v and v' can be obtained by addition of the corresponding ξ parameters.

This result is even more apparent if one introduces the *light cone variables*,

$$z_+ \equiv x + t \quad z_- = x - t \quad (8.3)$$

Under a Lorentz transformation,

$$z'_+ = e^{\xi} z_+ \quad z'_- = e^{-\xi} z_- \quad (8.4)$$

Finally, the trajectory of a free particle

$$z - ut = 0$$

can be written in terms of the light cone variables as

$$z_- = -\frac{1-u}{1+u} z_+ = -e^{-2\mu} z_+ \quad (8.5)$$

where

$$\mu = \frac{1}{2} \ln \frac{1+u}{1-u}$$

If we consider the motion in a moving frame of velocity v , (8.5) becomes

$$z'_- = -e^{-2(\mu-\xi)} z'_+ \quad (8.6)$$

B. Rapidity

Suppose that we have a particle of mass M_p and total energy (including rest mass) E_L incident on a target of mass M_T at rest. In the zero-momentum frame,

inaccurately referred to as the center-of-mass frame, the total energy \sqrt{s} , that is, the energy of the projectile and the target, is given by

$$s = 2E_L M_T + M_T^2 + M_P^2 \quad (8.7)$$

If E_L is sufficiently large,

$$\sqrt{s} \simeq \sqrt{2E_L M_T} \quad (8.8)$$

The result that the energy in the center-of-mass frame increases as the square root of the energy in the laboratory frame has led to the development of accelerators in which beams of opposite momenta collide.

The kinematics of the collisions can be treated most expeditiously through use of the rapidity variable, y , defined by [compare with (8.3)]

$$\begin{aligned} E + p_{\parallel} &= \mu e^y & E - p_{\parallel} &= \mu e^{-y} \\ E &= \mu \cosh y & p_{\parallel} &= \mu \sinh y \end{aligned} \quad (8.9)$$

The quantity p_{\parallel} is the component of the momentum in the z direction. To obtain μ , note that $(E + p_{\parallel})(E - p_{\parallel}) = \mu^2 = E^2 - p_{\parallel}^2 = m^2 + p_{\perp}^2$, where p_{\perp}^2 is the *transverse momentum*

$$p_{\perp}^2 = p^2 - p_{\parallel}^2$$

Therefore,

$$\mu = \sqrt{m^2 + p_{\perp}^2} \quad (8.10)$$

and μ is referred to as the *transverse mass*. From (8.9) one finds that

$$y = \frac{1}{2} \ln \frac{E + p_{\parallel}}{E - p_{\parallel}} = \ln \frac{E + p_{\parallel}}{\mu} \quad (8.11)$$

Under a Lorentz transformation in the z direction

$$\begin{aligned} p' &= p_{\parallel} \cosh \xi + E \sinh \xi \\ E' &= p_{\parallel} \sinh \xi + E \cosh \xi \end{aligned}$$

or

$$\begin{aligned} E' + p'_{\parallel} &= e^{\xi}(E + p) = \mu e^{(\xi + y)} \\ E' - p'_{\parallel} &= e^{-\xi}(E - p) = \mu e^{-(\xi + y)} \end{aligned}$$

Therefore, the rapidity in the new frame, y' , is

$$y' = \xi + y \quad (8.12)$$

As a consequence, rapidity difference are invariant with respect to boosts in the z direction:

$$y'_2 - y'_1 = (y_2 + \xi) - (y_1 + \xi) = y_2 - y_1 \quad (8.13)$$

As an example, let us use these results to describe the transformation to the center of mass when a proton of energy E_L and momentum p_L is incident on a proton at rest. The center-of-mass system is defined as one in which the protons have equal but opposite momenta. We therefore require that

$$p'_{\text{cm}} = m \sinh(y - \xi) = m \sinh \xi$$

Therefore,

$$\xi = \frac{y}{2} \quad (8.14)$$

The total energy is then given by

$$\sqrt{s} = E = 2m \cosh \frac{y}{2} \quad (8.15)$$

and

$$s = 4m^2 \cosh^2 \frac{y}{2} = 2m^2(1 + \cosh y) = 2m(m + E_L) \quad (8.16)$$

which agrees with (8.7) for $M_T = M_L = m$.

The Lorentz invariant phase space volume $d\mathbf{p}/E$ has a simple form when expressed in terms of y :

$$\begin{aligned} \frac{d\mathbf{p}}{E} &= d\mathbf{p}_\perp \frac{dp_\parallel}{E} = d\mathbf{p}_\perp \frac{\mu \cosh y dy}{E} \\ &= d\mathbf{p}_\perp dy \end{aligned} \quad (8.17)$$

The Lorentz invariant cross section is thus

$$\frac{E d\sigma}{d\mathbf{p}} = \frac{d\sigma}{d\mathbf{p}_\perp dy} \quad (8.18)$$

In the laboratory frame the projectile will initially have a momentum $p = p_\parallel$, $p_\perp = 0$, while the target's initial momentum is zero. The corresponding rapidities in the limit in which the masses are very much smaller than the corresponding energies are

$$y_T = 0 \quad y_P = \ln \frac{2p_L}{M_P}$$

In the center-of-mass frame,

$$y_T = -\frac{1}{2} \ln \frac{2p_L}{M_T} \quad y_P = \frac{1}{2} \ln \frac{2M_T p_L}{M_P^2}$$

In the frame in which the projectile is at rest and the target is in motion

$$y_T = -\ln \frac{2p_L}{M_P} \quad y_P = 0$$

It is often the case that measurements yield only the angle with respect to the incident direction, ϑ , along which a secondary particle is traveling. The relation of that angle with y will now be obtained. Consider the quantity

$$\frac{E - p_{\parallel}}{p_{\perp}} = \frac{\mu e^{-y}}{p_{\perp}}$$

The left-hand side of this equation can be written

$$\frac{1}{p_{\perp}} (\sqrt{p^2 + m^2} - p_{\parallel}) \simeq \frac{1}{p_{\perp}} \left(p - p_{\parallel} + \frac{1}{2} \frac{m^2}{p} \right)$$

The right-hand side to the same order is

$$\frac{1}{p_{\perp}} \sqrt{m^2 + p_{\perp}^2} e^{-y} \simeq e^{-y} \left(1 + \frac{1}{2} \frac{m^2}{p_{\perp}^2} \right)$$

Collecting terms and using $p_{\parallel}/p = \cos \vartheta$ and $p_{\perp}/p = \sin \vartheta$ yields

$$y \simeq -\ln \tan \frac{\vartheta}{2} + \frac{m^2}{p_{\perp}^2} \cos \vartheta \quad (8.19)$$

The pseudo-rapidity η is defined to be

$$\eta \equiv -\ln \tan \frac{\vartheta}{2} \quad (8.20)$$

The quantity η approximates y if m^2/p_{\perp}^2 is sufficiently small. The error is large for soft collisions when the secondary particles is a proton.

The rapidity, y , depends only upon the longitudinal velocity:

$$y = \frac{1}{2} \ln \frac{1 + v_{\parallel}}{1 - v_{\parallel}} \quad (8.21)$$

where

$$v_{\parallel} = \frac{p_{\parallel}}{E}$$

A change in y by 1 unit corresponds to a change in v_{\parallel} , for $v_{\parallel} \sim 1$, of

$$\delta v_{\parallel} = 6.4(1 - v_{\parallel}) \quad (8.22)$$

In a reaction, the peripheral collision will result in the fragmentation of the projectile (even if it is a proton!). The fragments will be traveling with approximately the same velocity as the projectile; that is, they will acquire relatively little transverse momentum. Experimentally, $\langle p_{\perp} \rangle \lesssim 350 \text{ MeV}/c$ (see the later discussion). The target will also fragment, contributing to the particle distribution for y close to the target rapidity. The region in y to which the proton fragmentation makes a contribution is experimentally on the order of 2 units, as ascertained from p - p ISR experiments at CERN. The corresponding Δy for nuclear fragmentation is on the order of 3 units. A clear separation of the fragments occurs only at sufficiently high energy. If, for example, the projectile is a 15-GeV proton, the value of y for the projectile is only 3.47. In this case the two contributions from target and projectile will overlap. When the energy is 200 GeV, the projectile y is 6.06, so that a central region which is a consequence of a more central collision will be visible.

C. Proton–Nucleus Collisions[†]

A complete understanding of the interaction of multi-GeV protons with nuclei is very far from being achieved. The experimental attack on the problem is for the most part just beginning. Similarly, the theoretical concepts required still remain to be identified. However, a few features have emerged. These will be the subject of this subsection.

Before proceeding to this task, it would be useful to note two characteristics of the proton–proton collisions. The first is the multiplicity plotted in Fig. 8.1. We note that the multiplicity rises slowly with beam momentum, rising from about 3 at 20 GeV/ c to about 10 at 10³ GeV/ c . Most of the particles observed are charged pions of both signs. To get the total multiplicity, including the neutral pions, one must multiply the charged pion multiplicity by $\frac{3}{2}$.

The second point of interest is the transverse momentum of the protons and pions produced in a p - p collision. The average value $\langle p_T \rangle$ of pions is shown in Fig. 8.2 as a function of rapidity. The $p + p \rightarrow \pi + X$ channel is the principal inelastic channel. The maximum transverse momentum of the pions produced in the reaction is about 350 MeV/ c . More than one pion is produced, as one can see from Fig. 8.1. At $p = 100 \text{ GeV}/c$, the number of charged particles is

[†]Busza and R. Ledoux (88); McCubbin (88); J. Hüfner and Klar (84); Klar and Hüfner (85).

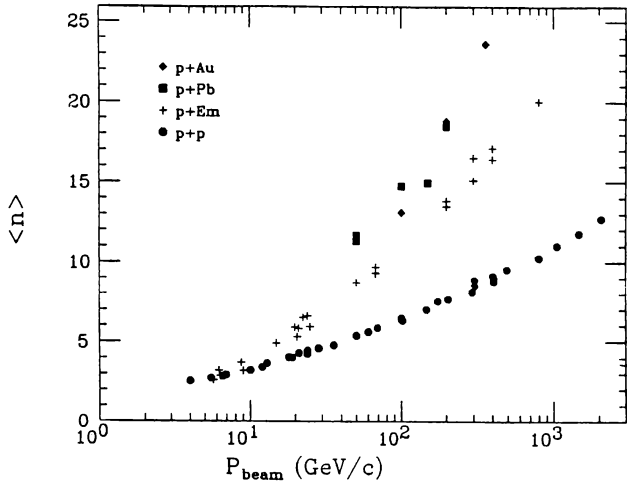


FIG. 8.1. The mean number of charged particles ($\langle n \rangle$) as a function of beam momentum. Em refers to an emulsion target. [From Busza and Ledoux (88).]

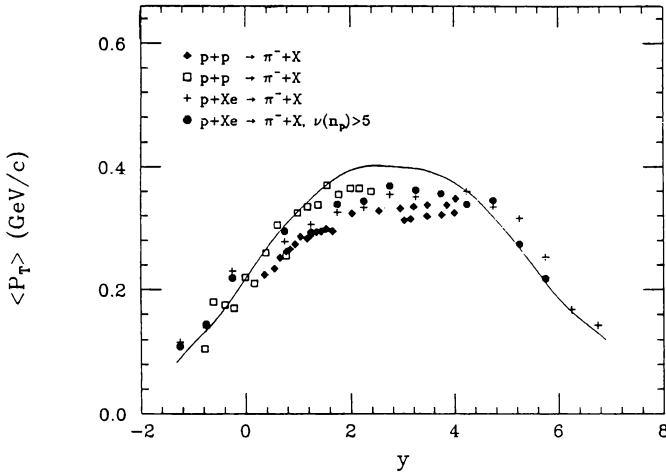


FIG. 8.2. The $\langle p_T \rangle$ of π^- as a function of y for $p + p$ and $p + \text{Xe}$ collisions. [From Busza and Ledoux (88).]

6.37 ± 0.05 , $v > 0.7$. These are thought to be mostly charged pions. To include π^0 , we multiply the charged particle multiplicity by $\frac{3}{2}$ to obtain 9.6. Taking the mass of each pion to be 137 MeV with a momentum of 350 MeV/c (see Fig. 8.2), assuming that the angular distribution is roughly isotropic in the center-of-mass reference frame yields an average energy per pion of 376 MeV. The total excitation energy of the radiating projectile proton in the proton-proton center

of mass is $0.376 \times (9.6)$ or 3.6 GeV at $p_L = 100 \text{ GeV}/c$ (or $E_{\text{cm}} = \frac{1}{2}\sqrt{s} = 6.9 \text{ GeV}$). More than one-half of the available kinetic energy is converted into nucleon excitation. The excited nucleon has total energy of 4.5 GeV .

For the most part, $p + p$ collisions are “soft.” “Hard” collisions involve pion momenta much beyond $400 \text{ MeV}/c$. For these cases involving a close collision, one may expect hadron jets to be produced. However, the probability for such close collisions is relatively low, as one can see from Fig. 8.3.

What happens when a proton strikes a nucleus? Naively (and incorrectly), one might believe that the proton strikes several nucleons, producing about 10 relatively energetic pions in the target frame of reference per collision. These pions would also generate secondaries, and so on. On this basis one would expect a very large number of emerging charged particles per incident proton. Table 8.1 and Fig. 8.4, where the multiplicity of charged particles with $v > 0.7$ is tabulated, demonstrate that this is very far from the truth. Multiplicities are small, rising to a factor of about 2.5 for U relative to the multiplicity for a p - p collision. Note that the same result holds when the incident hadron is a kaon or a pion. Parenthetically, the variable \bar{v} is defined as the average thickness of a nucleus in units of the mean free path (Fig. 8.4) for absorption of the incident proton:

$$\bar{v} = \frac{A\sigma_{\text{inel}}(p + \text{nucleon})}{\sigma_{\text{inel}}(p + \text{nucleus})} \quad (8.23)$$

Empirically, $\bar{v} = 0.7A^{0.31}$ for protons and $0.74A^{0.25}$ for pions. The variable \bar{v} is a rough measure of the number of collisions made by the indicated hadron

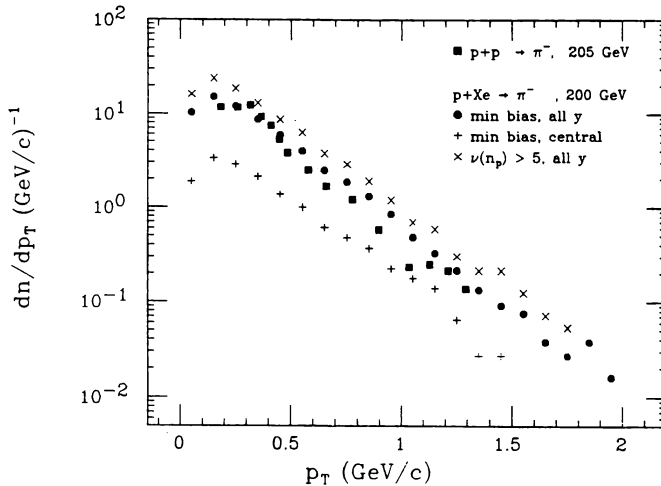


FIG. 8.3. The π^- transverse momentum distributions from $p + p$ and $p + \text{Xe}$ collisions. [From Busza and Ledoux (88).]

TABLE 8.1 Average Multiplicities of Relative Charged Particles Produced in 100-GeV/c Hadron-Nucleon Collisions

Target	Projectile	Average Multiplicity
C	π^+	7.86 ± 0.15
	K^+	6.92 ± 0.33
	p	7.72 ± 0.16
Cu	π^+	10.29 ± 0.26
	K^+	8.89 ± 1.10
	p	11.00 ± 0.32
Pb	π^+	13.21 ± 0.30
	K^+	12.92 ± 0.79
	p	14.75 ± 0.38
U	π^+	14.57 ± 0.39
	K^+	12.93 ± 1.33
	p	15.94 ± 0.50
Hydrogen (bubble chamber)	π^+	6.62 ± 0.07
	K^+	6.65 ± 0.31
	p	6.37 ± 0.06

Source: Elias, Busza, et al. (78).

in passing through the nucleus. As one can see from Fig. 8.4 for small laboratory angles, the ratio to hydrogen is unity for all elements. If one extends the laboratory angle to 100° , the ratio rises to values of less than 2. In Fig. 8.5 we show the ratio of the multiplicity in pA collisions to that in $p-p$ collisions for 100-GeV/c protons. The ratio is a linear function v :

$$\frac{\langle n_a \rangle}{\langle n_p \rangle} = 1 + 0.3(v - 1) \quad (8.24)$$

The absence of cascading can be understood as a relativistic effect [Goldhaber (74a)]. The incident proton on striking a nucleon of the target nucleus will form an excited system. Because of the relativistic time dilation its lifetime will be very much longer than its rest-frame lifetime, which is of the order of 1 fm/c. In fact, as we shall see, the mean distance it would travel before decaying is very much larger than the nuclear radius. It therefore will not decay before its collision with a second nucleon. This collision will change its excitation energy somewhat. This process continues until the proton leaves the nucleus and then decays. Cascading induced by the decay of the excited nucleon thus does not occur.

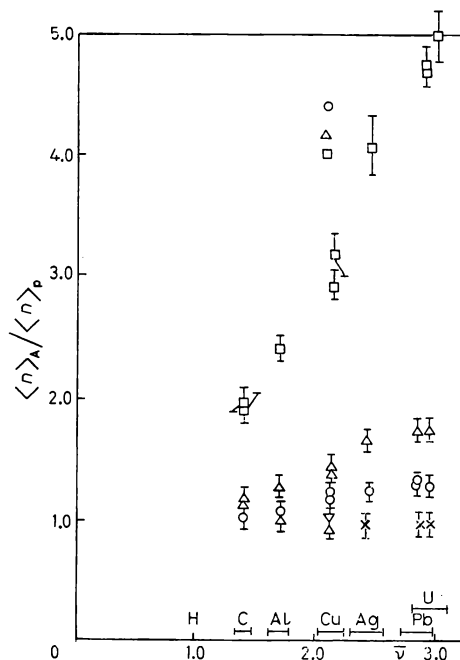


FIG. 8.4. Angular dependence of the ratio of the multiplicity for the indicated target nuclei with the multiplicity for a hydrogen target: $\times 0^\circ < \theta_{lab} < 3.5^\circ$, $\circ 0^\circ < \theta_{lab} < 26^\circ$, $\triangle 0^\circ < \theta_{lab} < 110^\circ$, $\square 26^\circ < \theta_{lab} < 110^\circ$; MIT π -A data. [From Elias, Busza, et al. (78); Elias et al. (80).]

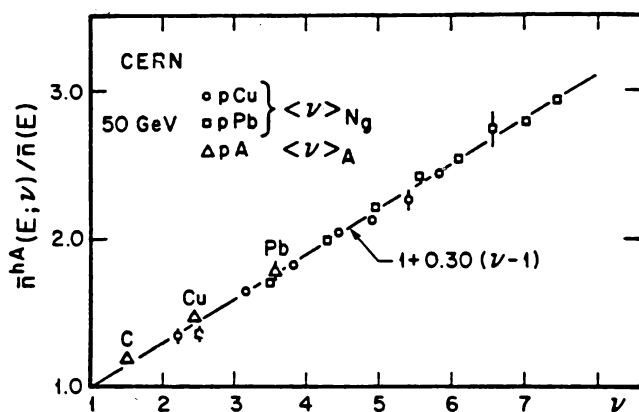


FIG. 8.5. Ratio of the multiplicity of produced particles in pA collisions divided by the multiplicity in pp collisions as a function of $\bar{\nu}$ and $\bar{\nu}(n_p)$. [From Ledoux, Bloomer, and Huang (86).]

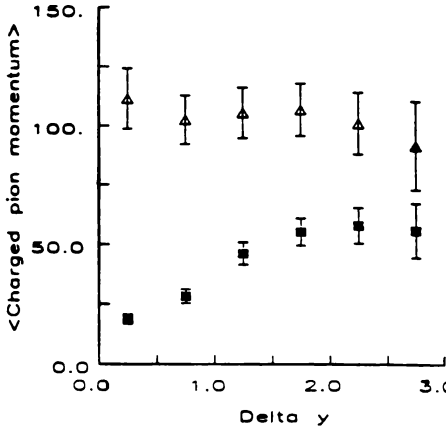


FIG. 8.6. Results from the reactions $p + A$ and $\bar{p} + A$ at 100 GeV/c, showing the momentum (in GeV/c) of charged pions (■) and the total momentum of the leading baryon plus 1.5 times the charged pion momentum (Δ). [From Busza and Ledoux (88).]

Let us look at this process in more detail. We make use of three experimental facts. The first is that in a proton–proton collision the incident proton in the rest frame loses 2 units of rapidity [Busza and Ledoux (88)]. The rapidity of a 100-GeV proton is 5.362, so that after the collision $y - 2 = 3.362$, corresponding to an energy loss of 86%. Second, as we have seen (Table 8.1), the numbers of charged pions emitted is 6.37. This is to be multiplied by 1.5 to take the neutral pion production into account, yielding 9.56 as the number of pions. Moreover, the secondaries produced by the proton fragmentation are mostly pions, as demonstrated by Fig. 8.6. The energy loss of the proton consists of the energies of these pions and the recoil energy transmitted to the target nucleon plus the pions emitted by it. We shall assume that the recoil energy is about 3.5% (this can be checked later and a correction calculated). Hence the energy per pion is 7.64 GeV, where the target nucleon pions have been assigned an energy of 1 GeV per pion. Finally, we recall that the average transverse pion momentum is 350 MeV/c, so that its transverse mass is 0.377 GeV.

Let a pion in the center-of-mass system have a rapidity σ . Note that proton and target nucleon have a rapidity of $y/2$ and $-y/2$, respectively, where $y = 5.362$. Then the pion energy, including the proton pion and a target nucleon pion energy in the laboratory frame, is

$$\begin{aligned}
 8.64 &= \mu \left[\cosh \left(\sigma + \frac{y}{2} \right) + \cosh \left(\sigma - \frac{y}{2} \right) \right] \\
 &= 2\mu \cosh \sigma \cosh \frac{y}{2}
 \end{aligned} \tag{8.25}$$

In this equation μ is the pion transverse mass. From (8.25) we find that

$$\sigma = 1.016 \tag{8.26}$$

The projectile pion rapidity in the laboratory frame is $y/2 + \sigma = 3.7$, close to rapidity of the final proton, 3.362. Its energy is 7.61 GeV. The target pion rapidity is $y/2 - \sigma = 1.66$, with an energy of 1.03 GeV. The corresponding longitudinal momenta are 7.60 GeV/c and 0.96 GeV. Since the transverse momentum is 0.350 GeV/c, the target nucleon pions are emitted at an average angle of 20° . They will thus not make a very significant contribution to the forward angle pion multiplicity but will affect the larger angle contributions. Finally, we calculate the difference in the velocities of the projectile pions and the nucleon assigning a rapidity of 3.362 to the proton and 3.7 to the pion.

$$v_p - v_\pi \equiv \delta v \simeq 2e^{-2y_p}(1 - e^{-2(y_\pi - y_p)}) = 1.2 \times 10^{-3}$$

In traveling the distance of a nuclear radius R , the separation of the projectile nucleon and the projectile pions will be $\delta v \times R$, which for a nucleus of radius of 6 fm is 7.2×10^{-16} fm. In other words, the pions will be “inside” the proton projectile. Thus the pions will not separate from projectile proton until the system is far outside the nucleus. The effect of only the first collision has been considered, but it is clear that subsequent collisions will not affect this result.

We have assumed that the system is on the energy shell after the collision and before the second collision. This is not at all obvious. If it is not, one must treat the collision with all the nucleons in the path of the projectile. A simple nonrelativistic calculation [Feshbach (83)] shows that this effect will not change the results above (i.e., the decay outside the nucleus), but there can be substantial quantitative differences. A more sophisticated theory has been published by Gottfried (74b), which yields (8.19) with the $\frac{1}{3}$ factor.

Empirically, the loss of rapidity of the projectile in colliding with a nucleus is of the order of 3 units [Busza and Ledoux (88)], so that a 1200-GeV proton has a final energy of 5 GeV. Most of that loss of energy is in pions emitted outside the nucleus. Most of the very energetic pions are generated by the first collision.

Another outstanding feature of the proton–nucleus interaction is the energy independence of the rapidity distributions in the target and projectile fragmentation regions. This is illustrated in Figs. 8.7 and 8.8. There are emulsion data, so that the target nuclei are Ag and Br. “Shower particles” correspond to single charged relativistic secondaries ($\beta > 0.7$). The incident protons have energies of 200, 400, and 800 GeV. The explanation is straightforward. As we have just described, most of these secondaries are generated in the first proton–nucleon collision (see Table 8.1). Combine this with the experimental result that such energy independence is observed in proton–proton collisions and we have the result of energy independence for proton–nucleus collisions. This behavior is referred to as *limiting fragmentation*. It is interesting to note that the projectile fragmentation in nucleus–nucleus collisions at a few GeV/A discussed in Section 7 is also energy independent.

One final comment is suggested by the rapidity distributions for different targets as shown in Fig. 8.9. We see a strong target dependence. Let $dn/d\eta \sim A^\alpha(\eta)$. From the data one finds $\alpha(\eta) > 0.3$ for $\eta \leq 1.5$ [Elias *et al.* (80)]. Second,

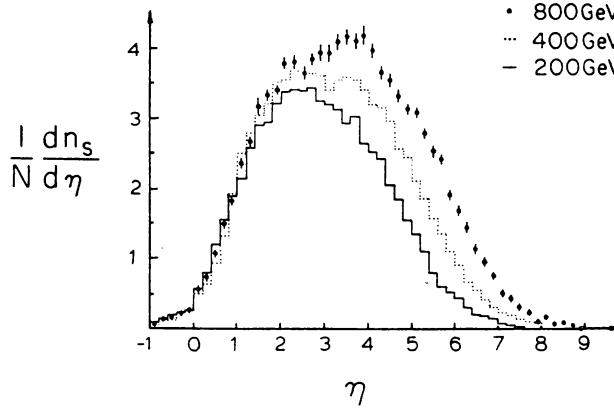


FIG. 8.7. Inclusive pseudorapidity distribution of shower particles in the laboratory frame at 200, 400, and 800 GeV. [From Abduzhamilov et al. (87).]

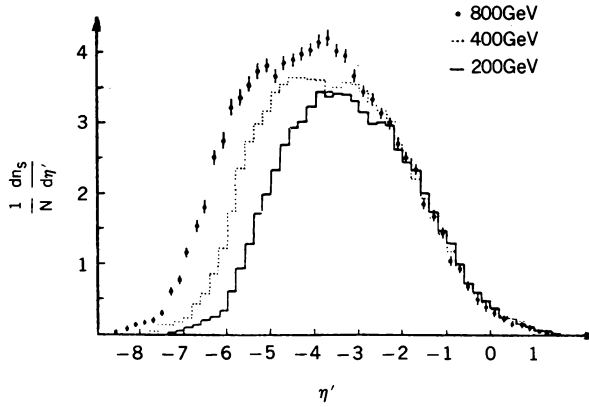


FIG. 8.8. Inclusive pseudorapidity distribution of shower particles in the projectile rest frame at 200, 400, and 800 GeV. [From Abduzhamilov et al. (87).]

we note that

$$\frac{dn}{d\eta} = \frac{1}{\sigma_{\text{inel}}} \frac{d\sigma}{d\eta} \quad (8.27)$$

where σ is the cross section for producing n secondaries. Since $\sigma_{\text{inel}} \sim A^{0.7}$,

$$\frac{d\sigma}{d\eta} = A^{0.7+\alpha}$$

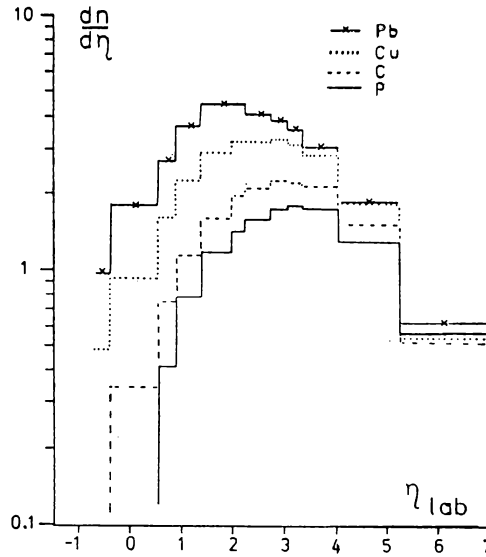


FIG. 8.9. $dn/d\eta$ versus η at 200 GeV on four different targets. [From McCubbin (89).]

The exponent is greater than unity, which indicates the presence of multiple scattering with associated cascading. The effect of such multiple scattering is larger for the larger nuclei.

D. Nucleus–Nucleus Collision[†]

Interest in the collision of ultrarelativistic particles (protons and nuclei) has been motivated by the prediction of QCD (quantum chromodynamics) lattice gauge calculations that a quark–gluon plasma will be formed when the temperature of nuclear matter exceeds roughly 200 MeV. Above that temperature nuclear matter “melts” into quarks and gluons. More accurately, there is a combination of density and temperature at which such a transition occurs, as illustrated in Fig. 8.10. It is hoped that such densities and temperatures can be obtained through the collision of very energetic nuclei. Experiments are now being conducted at BNL (~ 15 GeV/A) and at CERN (~ 200 GeV/A) with fixed targets and beams as heavy as Si. BNL will soon be able to provide Au beams and CERN is planning a Pb injector. For the more distant future, a collider, RHIC (relativistic heavy ion collider), providing 100-GeV/A beams, has been proposed by BNL. The study of a new form of matter, the quark–gluon plasma, would not only test QCD but it would be of great importance for cosmology as well. Soon after the “big bang,” before hadronization, the matter in the

[†]Satz (88).

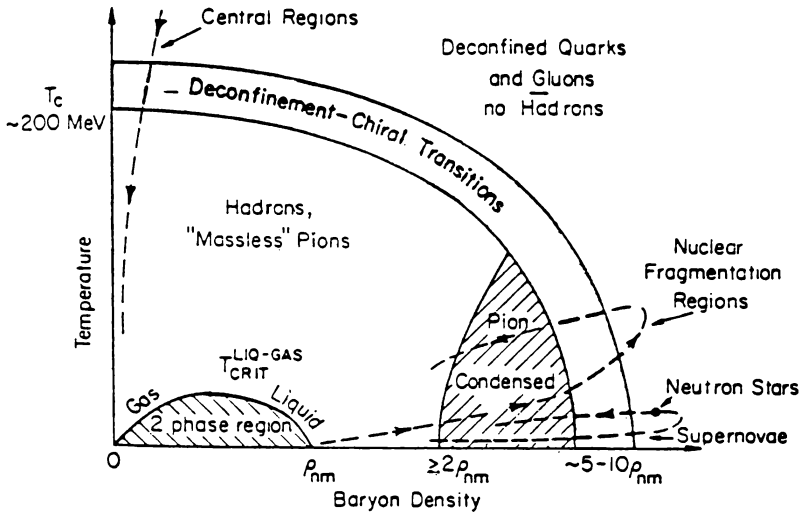


FIG. 8.10. Phase diagram of nuclear matter in the baryon density, temperature plane showing regions of hadronic and deconfined matter. Normal nuclear matter density ρ_{nm} is 0.16 fm^{-3} . [From Baym (87).]

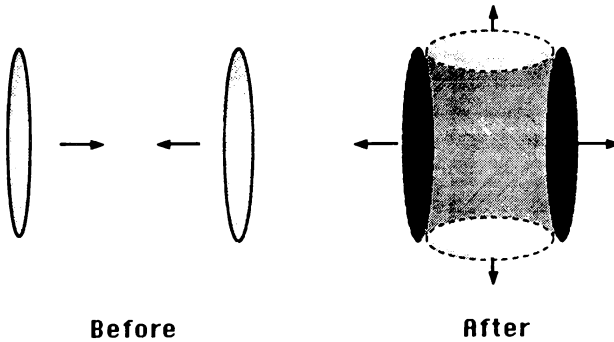


FIG. 8.11. Collision of two nuclei with relativistic energies. [From Matsui (88).]

universe would form a quark–gluon plasma, which as the universe cools would condense into nucleons and nuclei.

The collision of two nuclei is pictured as follows. In the center-of-mass system, because of the Lorentz contraction, the nuclei will be disks approaching each other at a velocity close to the velocity of light. As they pass through each other, energy will be deposited in each of the nuclei as a consequence of nucleon–nucleon collisions. In addition, the volume between the nuclei will contain mostly pions and will be for the most part baryon free (see Fig. 8.11). Each of these domains, the baryon-rich nuclear volumes or the baryon-free one, is a candidate for the formation of the quark–gluon plasma. The questions, whose

answer is uncertain, include: Are the density and the temperature big enough, and will that condition last for a long enough time? Will enough energy be deposited in either domain to raise the temperature to a large enough value?

The formulations of a reaction theory that describes the collision and development of the quark-gluon plasma and its equilibration is a major challenge to the theorists. One badly needs accurate evaluations of the phenomena which would signal the formation of the plasma. Several such phenomena have been proposed, such as the anomalous K/π ratio relative to its value in p - p collisions and the suppression of the formation of J/ψ particles. For an introductory review of the present situation, see Matsui (88).

CHAPTER X

PION AND KAON INTERACTIONS WITH NUCLEI[†]

1. INTRODUCTION

Pion and kaon interactions with nuclei provide a novel set of circumstances not covered in Chapters VII to IX. The pion–nucleon system shows (see Fig. 1.1) a strong resonance called the Δ , of mass 1.232 GeV and width 115 MeV. This is an excited state of the nucleon whose spin J is $\frac{3}{2}$, and whose isospin T is $\frac{3}{2}$. We shall call it a particle despite its short lifetime, given by $\hbar/\Gamma = 1.7 \text{ fm}/c = 0.59 \times 10^{-23} \text{ s}$. When a pion, whose energy is near the resonance energy, strikes a nucleus, the formation of the Δ is highly likely, creating thereby a Δ –nucleon hole state in the target nucleus. In this energy domain the Δ –hole state will act as an isolated doorway state [Kisslinger and Wang (73, 76)] through which all pion–nucleus reactions will proceed. We are familiar with such doorway states. Some examples include the isobar analog resonance, the Gamow–Teller resonance, and the electric dipole resonance, which can be described as collective proton particle–neutron hole states and proton particle–proton hole states, respectively. Although the Δ – h configuration is similar in character to these nuclear examples, there is one very significant difference. In the present case, the Δ is itself a resonance in the pion–nucleon system. Many of the pion–nucleon data can be explained if it is assumed that the reaction under study proceeds through the resonance Δ . Thus the theory of pion–nuclear reactions to be developed in this chapter begins with an analysis of the pion–nucleon resonant state. Introducing it into the nucleus permits us to study the impact of the nuclear medium on its properties and thus on the properties of the Δ .

[†]Eisenberg and Koltun (80); Ericson and Weise (88); Moniz and Lenz (90).

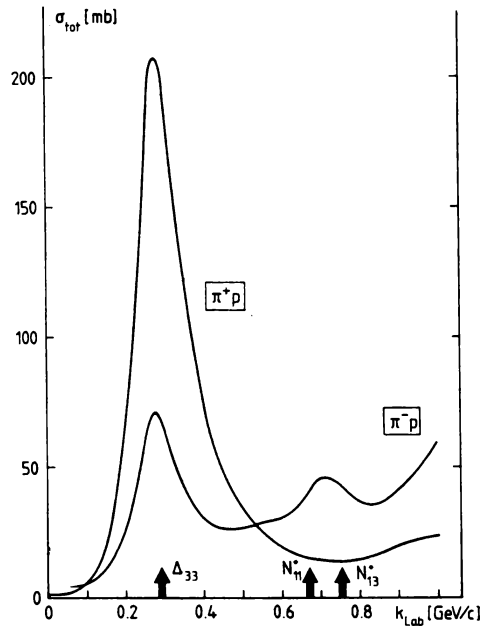


FIG. 1.1. Pion-nucleon total cross sections. [From Ericson and Weise (88).]

This pivotal role is played by the Δ within a restricted energy domain. It is not dominant near threshold nor at high energies. Like other projectiles, discussed in Chapter IX, the pion at high energies can induce inelastic and quasi-elastic scattering. The reaction theory used in these cases is quite straightforward and we shall discuss only inelastic scattering here. We shall, however, discuss charge exchange reactions, which are a special feature of pion reactions. These include the single charge exchange reaction (SCX)

$$\pi^+ + {}_Z A \rightarrow \pi^0 + (Z+1)A \quad (1.1)$$

$$\pi^- + {}_Z A \rightarrow \pi^0 + (Z-1)A \quad (1.2)$$

and the double charge exchange reaction (DCX)

$$\begin{aligned} \pi^+ + {}_Z A &\rightarrow \pi^- + (Z+2)A \\ \pi^- + {}_Z A &\rightarrow \pi^+ + (Z-2)A \end{aligned} \quad (1.3)$$

The SCEX reaction has its analog in

$$p + {}_Z A \rightarrow n + (Z+1)A \quad (1.4)$$

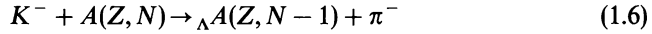
which might be thought of as a reaction in which a π^+ is transferred to the target nucleus. There is no well-studied corresponding nuclear reaction for the DCEX reaction. The DCEX reaction is of special interest, because it is thought to involve a two-step process involving in each step a change in charge (e.g., $\pi^- \rightarrow \pi^0 \rightarrow \pi^+$). Such a two-step process is sensitive to correlations in the target nucleus since it involves successive interactions with two nucleons of the target.

The pion is a boson. As a consequence, it can be created or destroyed. The elementary interaction is, for example,



It was by comparing these two reactions and using detailed balance that the intrinsic spin of the pion was found to be zero. These elements, the absorption and production of pions, must of course be taken into account in any theory of pion–nuclear collision.

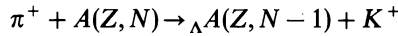
The strangeness exchange reaction by means of which hypernuclei are formed will be a major focus of the section on kaon–nuclear interactions. In this reaction



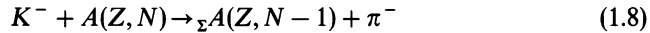
a neutron in the target nucleus is converted into Λ via the elementary reaction



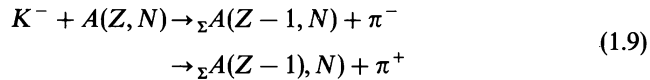
Hypernuclei have also been formed through the inverse reaction:



The formation of the Σ hypernucleus through the reactions



and



is more problematic. If it exists, one must understand why the strong interaction transition



does not immediately convert it into a Λ hypernucleus if the Λ is captured by the host nucleus or, as is likely, results in the Λ simply leaving the nucleus with no hypernuclear formation.

The Λ hypernucleus has received considerable study, revealing several important aspects of the Λ -nucleon interaction, such as charge symmetry breaking, a weak spin-orbit force as compared to the nucleon-nucleon case, and the need for a three-body (Λnn) repulsive interaction. In addition, in the Λ hypernucleus one can study the weak interaction

$$\Lambda + n \rightarrow n + n \quad (1.11)$$

The free-space decay of the Λ ,

$$\Lambda \rightarrow n + \pi \quad (1.12)$$

is reduced, especially in the heavier nuclei, because of the Pauli principle. The energy of the nucleon produced in the decay equation (1.12) is much less than the Fermi energy; most of the kinetic energy is carried by the pion so that there may not be an unoccupied level for the nucleon to occupy.

Investigations of hypernuclei have been hampered by the lack of adequate facilities. This is not the case for pion physics, where the intense beams at Los Alamos (LAMPF) at SIN near Zürich and at TRIUMF at Vancouver have been available since the late 1960s.

2. PION-NUCLEON SYSTEM

A. The Pion

The three pions π^+ , π^0 , and π^- form an isospin triplet ($T=1$). They have zero spin and odd parity. The mass of the charged pions is 139.6 MeV. The mass of the neutral pion is 135.0. The lifetime of the charged pions is 2.6×10^{-8} s, that of the π^0 is 8.4×10^{-17} s. The form factor for the charged pion has been determined from the scattering of the high-energy pions by the electron in a hydrogen atom. Its root mean-square charge radius is

$$\langle r_\pi^2 \rangle^{1/2} = (0.66 \pm 0.01) \text{ fm} \quad (2.1)$$

B. Isospin Symmetry

The pion-nucleon interaction is, except for the Coulomb and mass effects, isospin invariant. This means that the combined system can have an isospin of $\frac{3}{2}$ and $\frac{1}{2}$. Any system composed of a pion and nucleon $|\pi n\rangle$ can be decomposed into states of a definite isospin:

$$|\pi n\rangle = \sum_{T, T_3} |T, T_3\rangle \langle T T_3 | 1 t_\pi; \frac{1}{2} t_n \rangle \quad (2.2)$$

Therefore,

$$\begin{aligned}
 |\pi^+ p\rangle &= |\tfrac{3}{2}, \tfrac{3}{2}\rangle = \Delta^{++} & Q=2 \\
 |\pi^+ n\rangle &= \frac{1}{\sqrt{3}}[|\tfrac{3}{2}, \tfrac{1}{2}\rangle + \sqrt{2}|\tfrac{1}{2}, \tfrac{1}{2}\rangle] = \frac{1}{\sqrt{3}}[\Delta^+ + \sqrt{2}|\tfrac{1}{2}, \tfrac{1}{2}\rangle] & Q=1 \\
 |\pi^0 p\rangle &= \frac{1}{\sqrt{3}}[\sqrt{2}|\tfrac{3}{2}, \tfrac{1}{2}\rangle - |\tfrac{1}{2}, \tfrac{1}{2}\rangle] = \frac{1}{\sqrt{3}}[\sqrt{2}\Delta^+ - |\tfrac{1}{2}, \tfrac{1}{2}\rangle] & Q=1 \\
 |\pi^0 n\rangle &= \frac{1}{\sqrt{3}}[\sqrt{2}|\tfrac{3}{2}, -\tfrac{1}{2}\rangle + |\tfrac{1}{2}, -\tfrac{1}{2}\rangle] = \frac{1}{\sqrt{3}}[\sqrt{2}\Delta^0 + |\tfrac{1}{2}, -\tfrac{1}{2}\rangle] & Q=0 \\
 |\pi^- p\rangle &= \frac{1}{\sqrt{3}}[|\tfrac{3}{2}, -\tfrac{1}{2}\rangle - \sqrt{2}|\tfrac{1}{2}, -\tfrac{1}{2}\rangle] = \frac{1}{\sqrt{3}}[\Delta^0 - \sqrt{2}|\tfrac{1}{2}, -\tfrac{1}{2}\rangle] & Q=0 \\
 |\pi^- n\rangle &= |\tfrac{3}{2}, -\tfrac{3}{2}\rangle = \Delta^- & Q=-1
 \end{aligned} \tag{2.3}$$

where Q is the charge of each system.

One can invert these relations and thus express the $T=\frac{3}{2}$ state, the Δ , in terms of the pion-nucleon system. We find that

$$\begin{aligned}
 \Delta^{++} &= |\pi^+ p\rangle & T_3 = \tfrac{3}{2} \\
 \Delta^+ &= \frac{1}{\sqrt{3}}[|\pi^+ n\rangle + \sqrt{2}|\pi^0 p\rangle] & T_3 = \tfrac{1}{2} \\
 \Delta^0 &= \frac{1}{\sqrt{3}}[\sqrt{2}|\pi^0 n\rangle + |\pi^- p\rangle] & T_3 = -\tfrac{1}{2} \\
 \Delta^- &= |\pi^- n\rangle & T_3 = -\tfrac{3}{2}
 \end{aligned} \tag{2.4}$$

Any isospin invariant operator will be diagonal in isospin space:

$$\langle TT_3 | O | T', T'_3 \rangle = O_T \delta(T, T') \delta(T_3, T'_3) \tag{2.5}$$

The transition matrix \mathcal{T} is such an operator. Therefore,

$$\langle \pi^+ p | \mathcal{T} | \pi^+ p \rangle = \mathcal{T}_{3/2} \tag{2.6a}$$

$$\langle \pi^- p | \mathcal{T} | \pi^- p \rangle = \tfrac{1}{3}\mathcal{T}_{3/2} + \tfrac{2}{3}\mathcal{T}_{1/2} \tag{2.6b}$$

$$\langle \pi^0 n | \mathcal{T} | \pi^- p \rangle = \frac{\sqrt{2}}{3}(\mathcal{T}_{3/2} - \mathcal{T}_{1/2}) \tag{2.6c}$$

The amplitudes $\mathcal{T}_{3/2}$ and $\mathcal{T}_{1/2}$ are functions of the spin and energy and momentum variables. By comparing the possible reaction cross sections, one can obtain the two amplitudes. Because of the linear relation between the total cross section and the imaginary part of \mathcal{T} , we have from (2.6)

$$\begin{aligned}\sigma(\pi^+ p) &= \sigma_{3/2} \\ \sigma(\pi^- p) &= \frac{1}{3}\sigma_{3/2} + \frac{2}{3}\sigma_{1/2}\end{aligned}\quad (2.7)$$

where the subscripts indicate the isospin channel.

It may be convenient to parametrize the isospin dependence of $\hat{\mathcal{T}}$ by

$$\hat{\mathcal{T}} = a + b \mathbf{t}_n \cdot \mathbf{T}_\pi \quad (2.8)$$

where a and b are functions of spin, energy, and momentum variables. The quantity a is referred to as the *isoscalar* component, b the *isovector*. The vector \mathbf{t}_n is the isospin operator acting on the nucleon

$$\mathbf{t}_n = \frac{1}{2}\boldsymbol{\tau}_n \quad t_n^2 = \frac{3}{4} \quad (2.9)$$

The vector \mathbf{T} acts on the pion with the normalization

$$T_\pi^2 = 2 \quad (2.10)$$

since the pion has an isospin, $T = 1$. Since $\mathbf{T} = \mathbf{T}_\pi + \mathbf{t}_n$ is conserved, one can show that

$$\begin{aligned}\mathbf{T}_\pi \cdot \mathbf{t}_n &= \frac{1}{2}(\hat{T}^2 - 2 - \frac{3}{4}) \\ &= \begin{cases} \frac{1}{2} & T = \frac{3}{2} \\ -1 & T = \frac{1}{2} \end{cases}\end{aligned}\quad (2.11)$$

Parenthetically, one can construct the projection operators on to the $T = \frac{3}{2}$ and $\frac{1}{2}$ states, respectively. They are

$$P_{3/2} = \frac{2}{3}(1 + \mathbf{T}_\pi \cdot \mathbf{t}_n) \quad (2.12)$$

$$P_{1/2} = \frac{1}{3}(1 - 2\mathbf{T}_\pi \cdot \mathbf{t}_n) \quad (2.13)$$

Using (2.9), one finds from (2.6) that

$$\mathcal{T}_{3/2} = a + \frac{b}{2} \quad \mathcal{T}_{1/2} = a - b \quad (2.14)$$

The total cross sections for the two most readily available reactions are

$$\begin{aligned}\sigma(\pi^+ p) &= \sigma_{3/2} \\ \sigma(\pi^- p) &= \frac{1}{3}\sigma_{3/2} + \frac{2}{3}\sigma_{1/2}\end{aligned}\quad (2.15)$$

Coulomb effects modify these results.

C. Pion-Nucleon Scattering

The most striking feature of pion-nucleon scattering is the Δ resonance. This occurs when the momentum of the pion in the center-of-mass system is 230 MeV/c ($k = 1.15 \text{ fm}^{-1}$), corresponding to a mass of 1.232 GeV. The peak cross sections show clearly that the resonant cross sections are for a $T = \frac{3}{2}$ state. Assuming that at the resonance peaks $\sigma_{3/2} \gg \sigma_{1/2}$, one finds from (2.15) and (2.7) that

$$\sigma(\pi^+ p)/\sigma(\pi^- p)/\sigma(\pi^0 n \leftarrow \pi^- p) = (1/\frac{1}{3}/\frac{2}{9})$$

at resonance. This result is in agreement with experiment (see Fig. 1.1). Second, one can also determine the spin at the resonance. The resonant cross section for $(\pi^+ p)$ scattering, assuming no inelasticity is given by $2\pi/k_{cm}^2(2J+1) = 19\text{fm}^2 = 190\text{mb}$ for $J = \frac{3}{2}$, confirming that the Δ^{++} is $J = \frac{3}{2}$ state, and the inelasticity is small. The resonance must occur in the $l = 1$, p -wave channel yielding a unique angular distribution. The amplitude for the scattering of a zero-spin particle by a particle of spin $\frac{1}{2}$ is given for each isospin channel according to (V.2.44) by

$$\hat{f} = A + B\boldsymbol{\sigma} \cdot \mathbf{n} \quad \mathbf{n} = \frac{\mathbf{k}_i \times \mathbf{k}_f}{|\mathbf{k}_i \times \mathbf{k}_f|} \quad (2.16)$$

where

$$A = \frac{1}{k} \sum_l [(l+1)f_l^{(+)} + lf_l^{(-)}]P_l(\cos \vartheta) \quad (2.17)$$

and

$$B = \frac{i}{k} \sum_l [f_l^{(+)} - f_l^{(-)}]P_l^{(1)}(\cos \vartheta) \quad (2.18)$$

$$P_l^{(1)}(\cos \vartheta) = \sin \vartheta \frac{d}{d(\cos \vartheta)} P_l(\cos \vartheta)$$

The quantities $f_l^{(+)}$ and $f_l^{(-)}$ are the partial wave amplitudes for the $j = l + \frac{1}{2}$ and $j = l - \frac{1}{2}$ states. In terms of phase shifts, $f_l^{(+)}$ is

$$f_l^{(+)} \equiv \frac{1}{2ik} (e^{2i\delta_l^+} - 1) \quad (2.19)$$

with a similar expression for $f_l^{(-)}, \delta_l^{(+)}$ will be complex if there is any inelasticity. The differential cross section is

$$\frac{d\sigma}{d\Omega} = \frac{1}{k^2} [|A|^2 + |B|^2] \quad (2.20)$$

The total integrated cross section is

$$\sigma = \frac{4\pi}{k^2} \sum [(l+1)|f_l^{(+)}|^2 + l|f_l^{(-)}|^2]$$

The polarization parameters \mathbf{P} and Q are

$$\mathbf{P} = 2 \frac{\text{Re } AB^*}{|A|^2 + |B|^2} \mathbf{n} \quad Q = \frac{2 \text{Im } AB^*}{|A|^2 + |B|^2} \quad (2.20')$$

For the Δ^{++} resonance, $l = \frac{1}{2}$, $J = \frac{3}{2}$, so that

$$\frac{d\sigma}{d\Omega} = \frac{1}{k^2} |f_l^{(+)}|^2 (4 \cos^2 \vartheta + \sin^2 \vartheta) \quad (2.21)$$

in agreement with experiment (see Fig. 2.1). At 0° , $d\sigma/d\Omega = 30$ mb at resonance. It will be noted that as the pion energy deviates from resonance, the angular distributions are no longer symmetric about 90° . This is because of the presence of nonresonant amplitudes, for example coming from $\mathcal{T}_{1/2}$. The low-energy behavior of the phase shift is given by the limit

$$\delta_{2T,2J}^{(L)} \rightarrow a_{2T,2J}^{(L)} q^{2L+1} \quad q \rightarrow 0 \quad (2.22)$$

For S waves, a is referred to as the scattering length; for P waves a has the dimensions of a volume and therefore could be called the *scattering volume*. The numerical values for a are [Moniz and Lenz (91)]

$$\begin{aligned} a_{3,1}^S &= (-0.092 \pm 0.002) m_\pi^{-1} \\ a_{1,1}^S &= (0.170 \pm 0.004) m_\pi^{-1} \end{aligned} \quad (2.23)$$

and

$$\begin{aligned} a_{3,1}^P &= (-0.043 \pm 0.004) m_\pi^{-3} \\ a_{3,3}^P &= (0.214 \pm 0.004) m_\pi^{-3} \\ a_{1,1}^P &= (-0.082 \pm 0.006) m_\pi^{-3} \\ a_{1,3}^P &= (-0.029 \pm 0.005) m_\pi^{-3} \end{aligned} \quad (2.24)$$

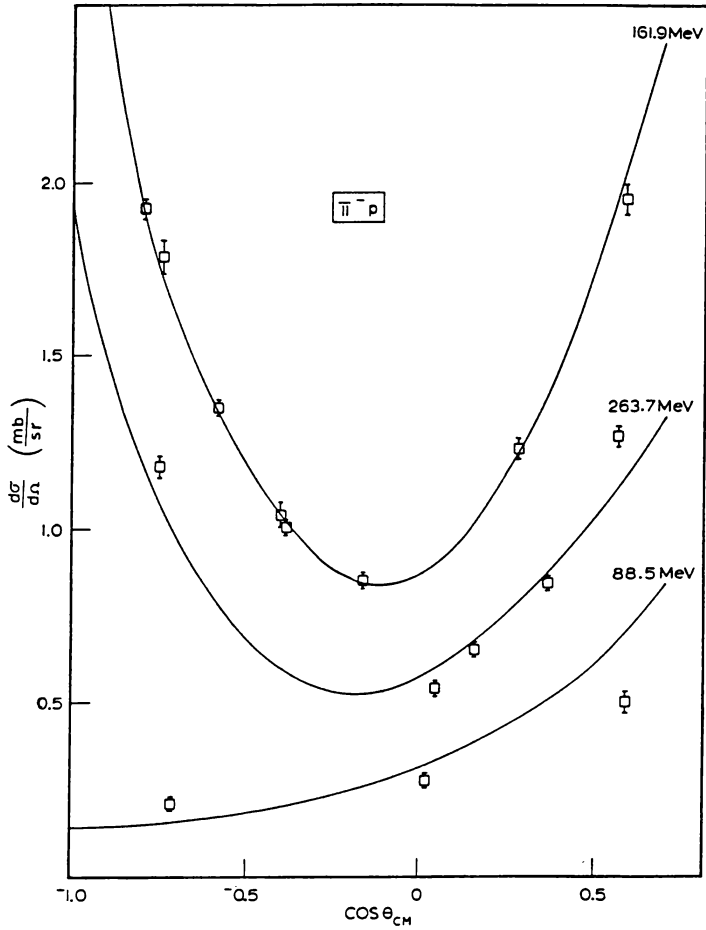


FIG. 2.1. Angular distributions for $\pi^- p$ scattering. [From Rowe, Solomon, and Landau (78).]

We note that the nonresonant P -wave amplitudes are negative, corresponding to a relatively weak repulsion. Moreover, the isoscalar quantity in (2.8) is very small for S waves. Using

$$a_s = \frac{2}{3}a_{3,1}^S + \frac{1}{3}a_{1,1}^S$$

we obtain $a_s = -0.0046 m_\pi^{-1}$.

At higher energies, the empirical phase shifts as determined by Rowe, Solomon, and Landau (78) are presented in Figs. 2.2 to 2.4. The curves are labeled by $L_{2T,2S}$. The phase shift $\delta(P_{33})$ rises rapidly from zero through $\pi/2$, the resonance value of δ . The phases $\delta(P_{13})$ and $\delta(P_{31})$ are increasingly negative.

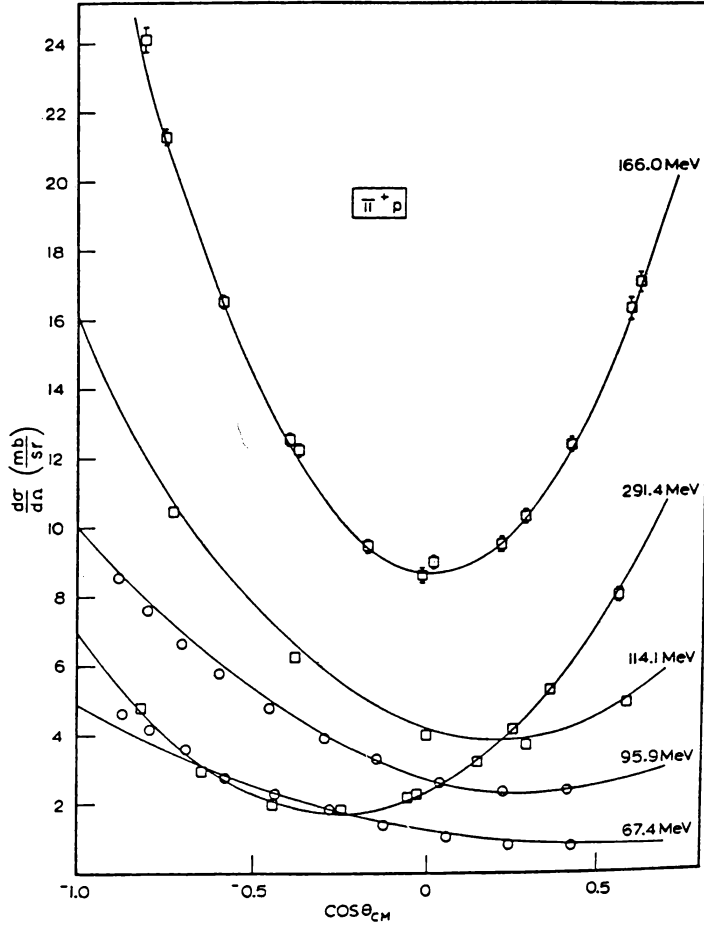


FIG. 2.2. Angular distributions for $\pi^+ p$ scattering. [From Rowe, Solomon, and Landau (78).]

The phase shift $\delta(P_{11})$ ($T = \frac{1}{2}s - \frac{1}{2}$) turns about and crosses the real axis, becoming positive and rising rapidly, indicating the effect of a resonance at a mass of 1.440 ± 80 MeV.

Rowe, Solomon, and Landau (78) have given a useful parametrization of the phase shifts for pion energies less than 400 MeV. It is

$$\tan \delta_l = \left(\frac{k}{m_\pi}\right)^{2l+1} \left[b + c \left(\frac{k}{m_\pi}\right)^2 + d \left(\frac{k}{m_\pi}\right)^4 \right] + x \left(\frac{k}{k_0}\right)^{2l+1} \frac{\Gamma_0 \sqrt{s_0}}{s_0 - s} \quad (2.25)$$

where k and s are the πn center-of-mass momentum and (energy)², respectively.

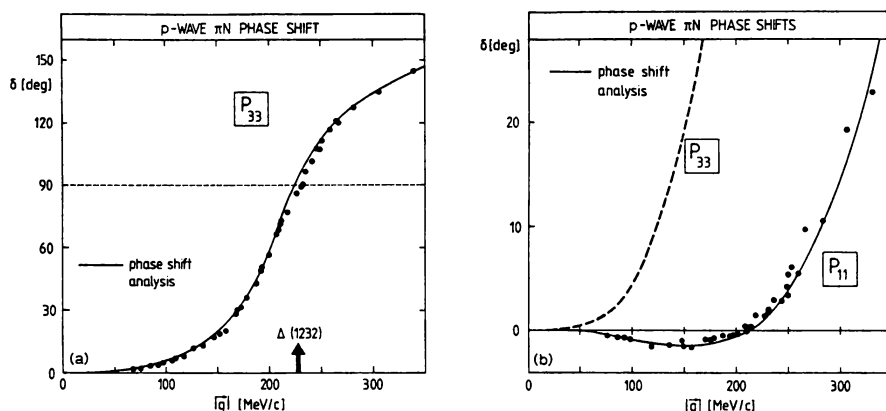


FIG. 2.3. Empirical pion-nucleon p -wave phase shifts versus center-of-mass momentum $|q|$ [Rowe, Solomon, and Landau (78). [From Ericson and Weise (88).]

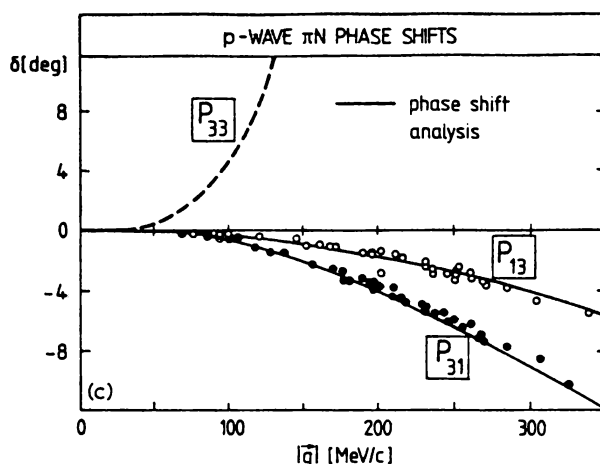


FIG. 2.4. Empirical pion-nucleon p -wave phase shifts versus center-of-mass momentum $|q|$ [Rowe, Solomon, and Landau (78). [From Ericson and Weise (88).]

The resonance form is meaningful only for the P_{33} and P_{11} phases. The values of the parameters are given in Table 2.1.

Principally because of the Coulomb interaction, isospin symmetry is broken. The masses of the Δ 's are not all equal, nor are their widths equal. For example, $M(\Delta^0) - M(\Delta^{++}) = 2.7 \pm 0.3$ MeV and $\Gamma(\Delta^0) - \Gamma(\Delta^{++}) = 6.6 \pm 1.0$ MeV [Pedroni, Gabathuler, et al. (78)].

Inelastic pion-nucleon reactions occur when pions are produced. The threshold energy for the $\pi n \rightarrow \pi\pi n$ reaction is about 179 MeV in the laboratory

TABLE 2.1 Parameters for (2.26)

	x	$\sqrt{s_0}$ (GeV)	k_0 (GeV/c)	Γ_0 (GeV)	b (10^{-2})	c (10^{-3})	d (10^{-4})
S_{11}	0.44	1.550	0.477	0.105	16.8 ± 0.75	-35.4 ± 5.4	27 ± 11
S_{31}	0.31	1.655	0.550	0.170	-11.2 ± 0.20	-30.7 ± 1.1	21 ± 2
P_{11}	0.61	1.435	0.393	0.230	-5.71 ± 0.54	25.4 ± 2.1	-29 ± 3
P_{13}	0.23	1.815	0.656	0.255	-1.31 ± 0.08	1.22 ± 0.32	-0.4 ± 0.3
P_{31}	0.22	1.850	0.678	0.200	-2.91 ± 0.08	3.45 ± 0.27	-1.5 ± 0.2
P_{33}	0.99	1.233	0.228	0.116	11.4 ± 0.30	-15.4 ± 2.1	7.2 ± 2.1

Source: Rowe, Solomon, and Landau (78).

reference frame. It appears that many of the data for this reaction can be understood under the assumption that the final state is a two-body state, of which one body is an isobar. For example, the two-body state could be a $\pi + \Delta$, or a 2π isobar, such as the spin 1 ρ or the spin 0 σ plus a nucleon. Such a hypothesis can be tested by calculating the ratios of the production of various possible two-pion + nucleon final states, using the isospin properties of the isobars and comparing with experiment. For example, suppose that the reaction is

$$\pi^- + p \rightarrow \begin{cases} \pi^+ \pi^- p \\ \pi^0 \pi^0 n \\ \pi^- \pi^0 p \end{cases} \quad (2.26)$$

Suppose that the reaction can be described as leading to $\Delta^+ \pi^-$, $\Delta^0 \pi^0$, and $\Delta^- \pi^+$ states with the subsequent decay of the Δ^+ , Δ^- , and Δ^0 . Using the isospin Clebsch–Gordan coupling coefficients and for simplicity considering only the $T = \frac{1}{2}$ channel, one finds that

$$|T, T_3\rangle = |\tfrac{1}{2}, -\tfrac{1}{2}\rangle = \sqrt{\tfrac{1}{6}}(\Delta^+ \pi^- - \sqrt{2}\Delta^0 \pi^0 + \sqrt{3}\Delta^- \pi^+) \quad (2.27)$$

Now using (2.4), which expressed the Δ^+ , Δ^0 , Δ^- in terms of nucleon + pion amplitudes, one can obtain the branching ratios for the three final states of (2.26), namely,

$$\sigma_{1/2}(\pi^+ \pi^- n) / \sigma_{1/2}(\pi^0 \pi^- p) / \sigma_{1/2}(\pi^0 \pi^0 n) = 5/2/2 \quad T = \tfrac{1}{2}$$

which can be compared with experiment.

Problem. Consider the $T = \frac{3}{2}$ channel. Show that $|\frac{3}{2}, -\frac{1}{2}\rangle = \sqrt{\frac{1}{15}}[-\sqrt{8}\Delta^+ \pi^- + \Delta^0 \pi^0 + \sqrt{6}\Delta^- \pi^+]$. Calculate the cross section ratio for the three reactions of (2.26).

D. The Isobar Description of the Δ

We shall not enter into the dynamics underlying the properties of the Δ . Suffice it to say that it is the simplest excitation of the three-quark system, whose ground state is the nucleon. In this excitation the spin of a quark is flipped while the isospin ($d \rightleftharpoons u$ quarks) may also change. Our goal in this section is to obtain a consistent description of the Δ , which will prove to be useful when we consider π -nucleus scattering.

The expression for the \mathcal{T} matrix for resonant scattering for an isolated resonance has been derived in Chapter III [Eq. (III.2.18)]. We recall that one proceeds by dividing the Hilbert space in two through the use of the projection operators P and $Q = 1 - P$, where the space subtended by P contains the incident and exit channels. Then as seen from Chapter III, the \mathcal{T} matrix is given by

$$\mathcal{T} = \mathcal{T}_P + \left\langle \psi_f^{(-)} H_{PQ} \frac{1}{E - H_{QQ} - W_{QQ}} H_{QP} \psi_f^{(+)} \right\rangle \quad (2.28)$$

where $H_{PQ} \equiv PHQ$, and so on, and

$$W_{QQ} = H_{QQ} \frac{1}{E^{(+)} - H_{PP}} H_{PQ} \quad (2.29)$$

\mathcal{T}_P is the nonresonant scattering in P space, that is, a consequence of the Schrödinger equation

$$(E - H_{PP})\psi = 0 \quad (2.30)$$

In the case of a single isolated resonance, one chooses Q to contain only one state—the resonant state Φ . Then

$$\mathcal{T} = \mathcal{T}_P + \mathcal{T}_R = \mathcal{T}_P + \frac{\langle \psi_f^{(-)} H_{PQ} \Phi \rangle \langle \Phi H_{QP} \psi_i^{(+)} \rangle}{E - \langle \Phi H \Phi \rangle - \langle \Phi H_{QP} [1/(E^+ - H_{PP})] H_{PQ} \Phi \rangle} \quad (2.31)$$

In the application to pion-nucleon scattering, we shall limit the discussion to the $\pi^+ + p \rightarrow \Delta^{++}$ resonance. The results for other channels can be obtained from isospin invariance. The state vector Φ is $\Delta(\mu_\Delta)$, where μ_Δ is the z component of the Δ spin of $\frac{3}{2}$. The operator H_{QP} couples the Δ to the pion-nucleon states of P space. We take it to be given by

$$H_{QP} = gh(k^2) \mathbf{k} \cdot \mathbf{S}^\dagger \quad (2.32)$$

where g is a coupling constant, $h(k^2)$ is a form factor, $h(0) = 1$, \mathbf{k} is the center of mass relative momentum of the pion-nucleon system, and \mathbf{S}^\dagger is referred to

as the transition spin operator. The form given by (2.32) is determined by angular momentum and parity invariance. One recalls that the pion is a *pseudoscalar* spin-zero particle. Hence the interaction must itself transform like a pseudoscalar. The transition operator S^\dagger converts a nucleon of spin- $\frac{1}{2}$, z component μ_n into a Δ of spin- $\frac{3}{2}$, z component μ_Δ . It therefore has the matrix elements

$$\langle \frac{3}{2}\mu_\Delta | S^\dagger | \frac{1}{2}\mu_n \rangle \equiv \sum_\mu (1\mu\frac{1}{2}\mu_n | \frac{3}{2}\mu_\Delta) \mathbf{e}_\mu \quad (2.33)$$

where

$$\begin{aligned} \mathbf{e}_{\pm 1} &= \mp \frac{1}{\sqrt{2}}(\hat{\mathbf{a}}_1 \pm \hat{\mathbf{a}}_2) \\ \mathbf{e}_0 &= \hat{\mathbf{a}}_3 \end{aligned} \quad (2.34)$$

Here $\hat{\mathbf{a}}_i$ are three perpendicular unit vectors. From this result we have

$$\begin{aligned} S^\dagger &= \mathbf{e}_1 \left[\left| \frac{3}{2} \right\rangle \langle \alpha + \sqrt{\frac{1}{3}} \left| \frac{1}{2} \right\rangle \langle \beta \right] + \mathbf{e}_{-1} \left[\sqrt{\frac{1}{3}} \left| -\frac{1}{2} \right\rangle \langle \alpha + \left| -\frac{3}{2} \right\rangle \langle \beta \right] \\ &+ \mathbf{e}_0 \sqrt{\frac{2}{3}} \left[\left| \frac{1}{2} \right\rangle \langle \alpha + \left| -\frac{1}{2} \right\rangle \langle \beta \right] \end{aligned} \quad (2.35)$$

where $|\cdot\rangle$ refers to the state vector $|\frac{3}{2}\mu_\Delta\rangle$. We have tabulated only μ_Δ . The states α and β are the $+\frac{1}{2}$, $-\frac{1}{2}$ spin states of the nucleon, respectively. In component form,

$$\begin{aligned} S_1^\dagger &= -\frac{1}{\sqrt{2}} \left[\left| \frac{3}{2} \right\rangle \langle \alpha + \sqrt{\frac{1}{3}} \left| \frac{1}{2} \right\rangle \langle \beta \right] + \frac{1}{\sqrt{2}} \left[\sqrt{\frac{1}{3}} \left| -\frac{1}{2} \right\rangle \langle \alpha + \left| -\frac{3}{2} \right\rangle \langle \beta \right] \\ S_2^\dagger &= -\frac{i}{\sqrt{2}} \left[\left| \frac{3}{2} \right\rangle \langle \alpha + \sqrt{\frac{1}{3}} \left| \frac{1}{2} \right\rangle \langle \beta \right] - \frac{i}{\sqrt{2}} \left(\sqrt{\frac{1}{3}} \left| -\frac{1}{2} \right\rangle \langle \alpha + \left| -\frac{3}{2} \right\rangle \langle \beta \right) \\ S_3^\dagger &= \sqrt{\frac{2}{3}} \left[\left| \frac{1}{2} \right\rangle \langle \alpha + \left| -\frac{1}{2} \right\rangle \langle \beta \right] \end{aligned} \quad (2.36)$$

We now define the product $S_i S_j^\dagger$ by

$$S_i S_j^\dagger = \sum S_i | \mu_\Delta \rangle \langle \mu_\Delta | S_j^\dagger \quad (2.37)$$

This operator acts only on the nucleon spinors. One may show using (2.36) that

$$S_i S_j^\dagger = \frac{2}{3} \delta_{ij} - \frac{1}{3} \sigma_i \sigma_j$$

and

$$S_i^\dagger S_j = \frac{2}{3} \delta_{ij} + \frac{1}{3} \sigma_i \sigma_j \quad (2.38)$$

From (2.38) we have the useful result

$$\begin{aligned} \mathbf{A} \cdot \mathbf{S} \mathbf{S}^\dagger \cdot \mathbf{B} &= \frac{2}{3} \mathbf{A} \cdot \mathbf{B} - \frac{1}{3} (\boldsymbol{\sigma} \cdot \mathbf{A}) (\boldsymbol{\sigma} \cdot \mathbf{B}) \\ &= \frac{1}{3} \mathbf{A} \cdot \mathbf{B} - \frac{1}{3} i \boldsymbol{\sigma} \cdot (\mathbf{A} \times \mathbf{B}) \end{aligned} \quad (2.39)$$

Note that a similar development can be made in isospin space where the $T = \frac{1}{2}$ nucleon is transformed to a $T = \frac{3}{2}\Delta$.

We return to the numerator, N , of \mathcal{T}_R in (2.31), which can be written using (2.32) as follows:

$$\hat{N} = g^2 \sum_{\mu_\Delta} h(k'^2) (\mathbf{k}' \cdot \mathbf{S}) |\Delta(\mu_\Delta)\rangle \langle \Delta(\mu_\Delta) | (\mathbf{k} \cdot \mathbf{S}^\dagger) h(k^2)$$

or

$$\hat{N} = \frac{g^2}{3} h(k^2) h(k'^2) [\mathbf{k}' \cdot \mathbf{k} - i\boldsymbol{\sigma} \cdot (\mathbf{k}' \times \mathbf{k})] \quad (2.40)$$

To complete the calculation of the numerator N , one must take the matrix element of \hat{N} between appropriate initial and final nucleon spinors. The form factor $h(k^2)$ measures the overlap of the incident and final pion-nucleon wave function with the Δ wave function. The resonance denominator D in (2.31) is given by (E = total energy)

$$D(E) = E - \bar{m}_\Delta - \frac{g^2}{3} \int \frac{d\mathbf{k}}{(2\pi)^3} \frac{h^2(k^2)\kappa^2}{E^{(+)} - m - m_\pi - \kappa^2/2\mu} \quad E^{(+)} = E + i\varepsilon \quad (2.41)$$

where $\bar{m}_\Delta = \langle \Delta | H | \Delta \rangle$, μ is the pion-nucleon reduced mass (units $\hbar = c = 1$). The real part of the integral will combine with the parameter \bar{m}_Δ to yield the Δ mass, m_Δ . The imaginary part of the integral equals twice the width of the Δ resonance. The ratio N/D , given by (2.40) and (2.41), is the Breit-Wigner result, describing the Δ .

The discussion above is nonrelativistic. The relativistic generalization adopted by Hirata, Koch, Lenz, and Moniz (78, 79) and by Horikawa, Thies, and Lenz (80) replaced $D(E)$ by a form obtained from the Blankenbecler-Sugar reduction of the Bethe-Salpeter equation. According to Moniz and Lenz (91), the $D(E)$ of (2.41) should be replaced by

$$D(s) = s - \bar{m}_\Delta^2 - \frac{2g^2}{3} \int \frac{d\kappa}{(2\pi)^3} (\omega_\kappa + E_\kappa) \frac{m_\pi m}{\omega_\kappa E_\kappa} \frac{\kappa^2 h^2(\kappa^2)}{s^{(+)} - (\omega_\kappa + E_\kappa)^2} \quad (2.42)$$

where

$$\omega_\kappa^2 \equiv m_\pi^2 + \kappa^2 \quad E_\kappa^2 = m^2 + \kappa^2$$

and s is the square of the invariant energy. Both expressions for D , (2.41) and (2.42), include only pion-nucleon scattering in the expression for the W_{QQ} term. Other inelastic processes, such as $\pi + n \rightarrow \pi + \pi + n$ or $\pi + n = \gamma + n$, can also contribute to the Δ width but are not significant at or near the resonance energy.

Problem. Take the nonrelativistic limit of (2.42) and compared with (2.41)

The width can be obtained from the singularity in (2.42):

$$\text{Im } D = \frac{1}{3\pi} g^2 \int d\kappa (\omega_\kappa + E_\kappa) \frac{m_\pi m}{\omega_\kappa E_\kappa} \kappa^4 h^2(\kappa^2) \delta(s - (\omega_\kappa + E_\kappa)^2)$$

The argument of the δ function is zero when κ^2 equals κ_0^2 , where

$$\kappa_0^2 = \frac{1}{4s} [s - (m - m_\pi)^2][s - (m + m_\pi)^2] \quad (2.43)$$

Therefore,

$$\text{Im } D = \frac{g^2}{3\pi} (\omega_{\kappa_0} + E_{\kappa_0}) \frac{m_\pi m}{\omega_{\kappa_0} E_{\kappa_0}} \frac{\kappa_0^4 h^2(\kappa_0^2) \omega_{\kappa_0} E_{\kappa_0}}{2\kappa_0 (\omega_{\kappa_0} + E_{\kappa_0})^2}$$

or

$$\text{Im } D = \frac{1}{6\pi} g^2 \frac{m_\pi m}{\sqrt{s}} \kappa_0^3 h(\kappa_0^2) \quad (2.44)$$

In the laboratory frame, the width and $\text{Im } D$ are related by

$$\Gamma = \left(\frac{1}{m} \right) \text{Im } D \quad (2.45)$$

A good fit to the resonance phase shifts is obtained, according to Moniz and Lenz (91), with

$$h(k^2) \equiv \frac{1}{1 + k^2/\alpha^2} \quad (2.46)$$

when $\alpha = (0.56 \text{ fm}^{-1})$, $\bar{m}_\Delta = 1384 \text{ MeV}$, and $g = 8.72/m_\pi$.

3. PION-NUCLEUS SCATTERING

The scattering of pions by nuclei involves a number of novel features, compared to reactions induced by projectiles considered so far in this volume. At low energies ($E_\pi < 80 \text{ MeV}$) the pion-nucleon interaction is weak and multiple scattering theory is used to understand the results. The optical model potential contains significant nonlocal contributions in addition to the customary central and spin-orbit potentials. In the kinetic energy range 80 to 400 MeV, Δ resonance formation is the dominant mode and an isobar-doorway state model is appropriate. It is this last feature that is of interest to the theory of reactions, for it provides an observable example of the impact of the nuclear medium on the propagation of a short-lived system through that medium.

A. Low Energy: $E_\pi < 80 \text{ MeV}$

Multiple scattering theory (see Chapter II) has been used to obtain the form of the pion-nucleon optical potential in this energy range. Since multiple scattering theory is a high-energy approximation, its validity for the scattering of low-energy pions whose wavelength/ 2π is on the order or larger than the internuclear distance in the nucleus must be justified. The first-order (and higher-order) optical potential

$$V^{(1)} = \frac{A-1}{A} \sum_{i=1}^A \langle 0 | t_i | 0 \rangle \quad (3.1)$$

depends directly on the pion-nucleon scattering. To fit the data the parameters describing pion-nucleon scattering must be modified, replaced by effective parameters. These modifications are ascribed to higher-order effects which are said to describe the impact of the medium on the pion-nucleon interaction. It is, however, not correct to employ the multiple scattering second-order potential $V^{(2)}$ to determine those effects. In the derivation, presented in Chapter II, of $V^{(2)}$ the approximation is made in which the nuclear Hamiltonian, H_N , in the propagator is replaced by a constant. This is equivalent to the fixed scatterer approximation (or $m_\pi/m \rightarrow 0$), which is not valid at these energies. However, we shall use $V^{(2)}$ to indicate the form of the media modification, adjusting its parameters as well as those of $V^{(1)}$ to obtain a fit for experiment. The results are physically meaningful since these parameters vary slowly with respect to nucleus and energy.

At low energy the scattering amplitude f_i for pion-nucleon scattering in the center-of-mass pion nucleon frame can be parametrized as follows:

$$f_{\pi n}(\mathbf{k}_{cm}, \mathbf{k}'_{cm}) = b'_0 + c'(\mathbf{k}_{cm} \cdot \mathbf{k}'_{cm}) + id'\boldsymbol{\sigma} \cdot (\mathbf{k}_{cm} \times \mathbf{k}'_{cm}) \quad (3.2)$$

where b' depends on isospin

$$b' = b'_0 + b'_1(\mathbf{T}_\pi \cdot \boldsymbol{\tau})$$

and similarly for parameters c' and d' . [Note that t of (2.8) = $\tau/2$.] The coefficients b' , c' , d' depend on energy and momentum transfer $\mathbf{q} = (\mathbf{k} - \mathbf{k}')$. At threshold ($E_\pi = 0$) the coefficients have the following values [Ericson and Weise (88)]:

$$\begin{aligned} b'_0 &= -0.010(3)m_\pi^{-1} & b'_1 &= -0.091m_\pi^{-1} \\ c'_0 &= 0.208(3)m_\pi^{-3} & c'_1 &= 0.175(2)m_\pi^{-3} \\ d'_0 &= -0.190(2)m_\pi^{-3} & d'_1 &= -0.069(2)m_\pi^{-3} \end{aligned} \quad (3.3)$$

The c' term, the p -wave scattering amplitude, is clearly dominant, demonstrating the importance of the Δ resonance even at very low energies. From the results

$(\mathbf{T}_\pi \cdot \boldsymbol{\tau})|\pi^+ p\rangle = 1$ and $(\mathbf{T}_\pi \cdot \boldsymbol{\tau})|\pi^+ n\rangle = -1$, we see that the $\pi^+ + p$ scattering spin averaged amplitude is $c'_0 + c'_1 = 0.38m_\pi^{-3}$, and the $\pi^+ + p$ amplitude is given by $c'_0 - c'_1 = 0.03m_\pi^{-3}$. We therefore expect that π^+ nuclear scattering will be more sensitive to the proton distribution, while the opposite will be the case for π^- scattering.

We shall need the transition matrix t_i in the pion-nucleon center-of-mass frame, in terms of $f_{\pi n}$ in (3.2). This relation is given by (II.7.16). It is

$$t_{\pi A} = -2\pi \frac{k_L}{k_{\text{cm}} E_L} \frac{1 + 2E_L/Am + (m_\pi/Am)^2}{(1 + m_\pi^2/AmE_L)(1 + E_L/Am)} f_{\pi n} \quad (3.4)$$

where k_L is the pion momentum in the laboratory frame, E_L the corresponding energy including its rest mass, and Am the mass of the target nucleus. In addition, it is necessary to transform the momenta \mathbf{k}_{cm} and \mathbf{k}'_{cm} to the pion-nucleon frame momenta, \mathbf{k} and \mathbf{k}' .

We consider the transformation from the reference frame in which the incident pion has a momentum of \mathbf{k} and the target nucleon a momentum of $-\mathbf{k}/A$ to the frame in which the pion and nucleon have momenta of \mathbf{k}_{cm} and $-\mathbf{k}_{\text{cm}}$, respectively. For all but the lightest nucleus, the pion energy in the first of these frames equals the pion laboratory energy, E_L . The boost in velocity \mathbf{v} in units of c required to transform to the nucleon-pion center-of-mass frame is determined by the Lorentz transformation:

$$k_{\text{cm}} = \gamma(k - vE_L) = \gamma\left(\frac{k}{A} + mv\right) \quad (3.5)$$

This yields

$$v = \left(1 - \frac{1}{A}\right) \frac{k}{m + E_L} \quad (3.6)$$

For the maximum pion kinetic energy considered (80 MeV), $v^2 = 0.0245$. Hence in (3.5), one may safely put $\gamma = 1$, so that

$$\mathbf{k}_{\text{cm}} = \mathbf{k} \left[1 - \frac{E_L(1 - 1/A)}{m + E_L} \right] = \mathbf{k} \frac{m + E_L/A}{m + E_L} \simeq \mathbf{k} \frac{m}{m + E_L} \quad (3.7)$$

Similarly,

$$\mathbf{k}'_{\text{cm}} = \mathbf{k}' - \frac{\mathbf{k}(1 - 1/A)E'_L}{E_L + m} \quad (3.8)$$

We thus obtain

$$\mathbf{k}_{\text{cm}} \times \mathbf{k}'_{\text{cm}} = \frac{m}{m + E_L} (\mathbf{k} \times \mathbf{k}') \quad (3.9)$$

Evaluating $\mathbf{k}_{\text{cm}} \cdot \mathbf{k}'_{\text{cm}}$ takes more work but one finds that to $O(k^2/m^2, k'^2/m^2)$,

$$\mathbf{k}'_{\text{cm}} \cdot \mathbf{k}_{\text{cm}} \simeq \frac{m}{m + E_L} \mathbf{k} \cdot \mathbf{k}' - \frac{k^2 m E_L}{(m + E_L)^2} \left(1 - \frac{1}{A}\right)$$

Note that

$$k^2 = \frac{1}{2}(\mathbf{k} - \mathbf{k}')^2 + \mathbf{k} \cdot \mathbf{k}' + \frac{1}{2}(\mathbf{k} - \mathbf{k}') \cdot \left(\frac{\mathbf{k} + \mathbf{k}'}{2}\right)$$

We drop the last term on the assumption that it will average to zero and/or because it is zero on the energy shell. Inserting the approximate result into the equation for $\mathbf{k}_{\text{cm}} \cdot \mathbf{k}'_{\text{cm}}$ and using the notation

$$\mathbf{k} - \mathbf{k}' = \mathbf{q}$$

one obtains

$$\mathbf{k}_{\text{cm}} \cdot \mathbf{k}'_{\text{cm}} = \left(\frac{m}{m + E_L}\right)^2 \left[\mathbf{k} \cdot \mathbf{k}' - \frac{E_L}{2m} q^2 \right] \quad (3.10)$$

Substituting (3.9) and (3.10) into (3.2) and (3.4) yields

$$t_{\pi A} = b + c \left[(\mathbf{k} \cdot \mathbf{k}') - \frac{E_L}{2m} \left(1 - \frac{1}{A}\right) q^2 \right] + id\boldsymbol{\sigma} \cdot (\mathbf{k} \times \mathbf{k}') \quad (3.11)$$

where the coefficients b, c, d are proportional to $b', c',$ and d' of (3.2). They are functions of the momentum transfer and the energy.

Inserting (3.11) into (3.1) yields

$$V(\mathbf{r}, \mathbf{r}') = \frac{A-1}{(2\pi)^6} \int d\mathbf{k} \int d\mathbf{k}' e^{i\mathbf{k} \cdot \mathbf{r}} \rho(\mathbf{q}) t_{\pi A} e^{-i\mathbf{k}' \cdot \mathbf{r}'} \quad (3.12)$$

Assuming that the coefficients $b, c,$ and d vary slowly with q allows us to replace them by their value at $q = 0$, $b^{(0)}$, $c^{(0)}$, and $d^{(0)}$. The integration in (3.12) can then be performed easily. For example, consider the $\mathbf{k} \cdot \mathbf{k}'$ term:

$$\begin{aligned} V_p &= c^{(0)} \frac{A-1}{(2\pi)^6} \int d\mathbf{k}' \int d\mathbf{k} e^{i\mathbf{k} \cdot \mathbf{r}} \mathbf{k} \cdot \mathbf{k}' \rho(\mathbf{k} - \mathbf{k}') e^{-i\mathbf{k}' \cdot \mathbf{r}'} \\ &= c^{(0)} \frac{A-1}{(2\pi)^6} \nabla \cdot \nabla' \int d\mathbf{k} \int d\mathbf{k}' e^{i\mathbf{k} \cdot \mathbf{r}} \rho(\mathbf{k} - \mathbf{k}') e^{-i\mathbf{k}' \cdot \mathbf{r}'} \\ &= c^{(0)} (A-1) (\nabla \cdot \nabla') \delta(\mathbf{r} - \mathbf{r}') \rho(\mathbf{r}) \end{aligned} \quad (3.12')$$

Acting on $\psi(\mathbf{r}')$ yields

$$\int V_p(\mathbf{r}, \mathbf{r}') \psi(\mathbf{r}') d\mathbf{r}' = -c^{(0)}(A-1) \nabla \cdot \rho \nabla \psi \quad (3.13)$$

Hence the first term in the multiple scattering series is

$$V^{(1)} = (A-1) \left[b^{(0)} \rho - c^{(0)} \nabla \cdot \rho \nabla - c^{(0)} \frac{E_L}{2m} (\nabla^2 \rho) + d^{(0)} \boldsymbol{\sigma} \cdot \mathbf{l} \frac{1}{r} \frac{\partial \rho}{\partial r} \right] \quad (3.14)$$

where in the last term ρ has been assumed to be spherical, a function of r only. Potential $V^{(1)}$ is known as the *Kisslinger potential*.

It was pointed out in the preceding section that the form we have used in developing $V^{(1)}$, (3.2), should be modified as follows [see (2.32)]:

$$c' \rightarrow c' h(k) h(k'), \quad \text{where } h(k_{\text{cm}}) = \frac{1}{1 + k_{\text{cm}}^2 / \alpha^2} \quad \alpha = 0.56 \text{ fm}^{-1} \quad (3.15)$$

Using this form, it is possible, with some approximation, to carry through the calculation leading to (3.12). One obtains

$$V'_p = c^{(0)}(A-1) \nabla \cdot \nabla' \left(\rho \left(\frac{\mathbf{r} + \mathbf{r}'}{2} \right) \frac{\alpha^3}{8\pi} e^{-\alpha|\mathbf{r} - \mathbf{r}'|} \right)$$

so that

$$\int V'_p(\mathbf{r}, \mathbf{r}') \psi(\mathbf{r}') d\mathbf{r}' = -c^{(0)}(A-1) \nabla \cdot \int \rho \left(\frac{\mathbf{r} + \mathbf{r}'}{2} \right) \frac{(\alpha')^3}{8\pi} e^{-\alpha'|\mathbf{r} - \mathbf{r}'|} \nabla' \psi(\mathbf{r}') d\mathbf{r}' \quad (3.16)$$

where

$$\alpha' = \alpha \cdot \frac{m + E_L}{m}$$

The quantity $(\alpha'^3/8\pi) e^{-\alpha'|\mathbf{r} - \mathbf{r}'|}$ is a spread-out delta function becoming a delta function as $\alpha' \rightarrow \infty$. To obtain some feeling as to when the introduction of the form factor $h(k)$ is important, replace $\psi(\mathbf{r}')$ by $e^{i\mathbf{k} \cdot \mathbf{r}'}$, ρ by a constant ρ_0 . The integral in (3.16) then equals

$$i\mathbf{k} e^{i\mathbf{k} \cdot \mathbf{r}} \frac{\rho_0}{(1 + k^2/\alpha'^2)^2} \quad (3.17)$$

which is to be compared with $i\mathbf{k}\rho_0$ obtained from (3.13). Using the value of $\alpha' = 0.69 \text{ fm}^{-1}$, (3.16), one sees that the factor $1/[(1 + k^2/\alpha'^2)]^2$ becomes important at relatively low energies.

The Lorentz–Lorentz Effect. The Kisslinger potential, (3.14), is the first-order term in the multiple scattering series for the optical potential. We shall now consider higher-order terms, or more physically the effects of correlations. Following Eisenberg and Koltun (80), the second-order term involving pair correlations will be considered first. We have remarked earlier on the approximations involved, but the result will provide us with a form that will be useful in obtaining the semiempirical optical potential.[†] We shall use (II.4.43) at zero energy. One further approximation will be made, namely $V^{(1)}$ and $\bar{\varepsilon}$, in (II.4.27) for the inverse of the propagator will be dropped. With these modifications one obtains

$$\tilde{V}_{\text{opt}}^{(2)}(\mathbf{k}, \mathbf{k}') = (A - 1)^2 \int \frac{d\mathbf{k}''}{(2\pi)^3} \tilde{t}(\mathbf{k}, \mathbf{k}'') \frac{1}{-(1/2\mu)k''^2 + i\varepsilon} t(\mathbf{k}'', \mathbf{k}') \tilde{C}(\mathbf{k}'' - \mathbf{k}, \mathbf{k}' - \mathbf{k}'') \quad (3.18)$$

where $\mu = E_L m / (m + E_L)$. We consider only the effect of the P -wave term, so that (3.18) becomes

$$\tilde{V}_{\text{opt}}^{(2)}(\mathbf{k}, \mathbf{k}') = -2\mu c^2 (A - 1)^2 \int \frac{d\mathbf{k}''}{(2\pi)^3} (\mathbf{k} \cdot \mathbf{k}'') (\mathbf{k}'' \cdot \mathbf{k}') \frac{1}{(k''^2/2\mu) - i\varepsilon} \tilde{C}(\mathbf{k}'' - \mathbf{k}, \mathbf{k}' - \mathbf{k}'')$$

One can decompose the numerator into a “monopole” and a “quadrupole” term:

$$(\mathbf{k} \cdot \mathbf{k}'') (\mathbf{k}'' \cdot \mathbf{k}') = \frac{1}{3} \mathbf{k} \cdot \mathbf{k}' (k'')^2 + [(\mathbf{k} \cdot \mathbf{k}'') (\mathbf{k}'' \cdot \mathbf{k}') - \frac{1}{3} (\mathbf{k} \cdot \mathbf{k}') (k'')^2] \quad (3.19)$$

Dropping the quadrupole term [see Warszawski, Gal, and Eisenberg (78)], $\tilde{V}^{(2)}$ becomes

$$\tilde{V}^{(2)}(\mathbf{k}, \mathbf{k}') = -\frac{1}{3} (2\mu) (A - 1)^2 c^2 (\mathbf{k} \cdot \mathbf{k}') \int \frac{d\mathbf{k}''}{(2\pi)^3} \tilde{C}(\mathbf{k}'' - \mathbf{k}, \mathbf{k}' - \mathbf{k}'') \quad (3.20)$$

Introducing the Fourier transform of \tilde{C} yields

$$\begin{aligned} \tilde{V}^{(2)}(\mathbf{k}, \mathbf{k}') &= -\frac{1}{3} (2\mu) (A - 1)^2 c^2 (\mathbf{k} \cdot \mathbf{k}') \int d\mathbf{r}_1 e^{i(\mathbf{k}' - \mathbf{k}) \cdot \mathbf{r}_1} C(\mathbf{r}_1, \mathbf{r}_1) \\ &= \frac{1}{3} 2\mu (A - 1)^2 c^2 (\mathbf{k} \cdot \mathbf{k}') \int \rho^2(\mathbf{r}_1) e^{i(\mathbf{k}' - \mathbf{k}) \cdot \mathbf{r}_1} d\mathbf{r}_1 \end{aligned} \quad (3.21)$$

[†]An optical analogy makes use of the fact that long-wavelength electromagnetic interactions with matter are, as in the case of the $\mathbf{k} \cdot \mathbf{k}'$ term of (3.11), dipole in nature. Therefore, there should be a term in the optical potential that is similar to the Clausius–Massotti term in the index of refraction for electromagnetic waves. This analogy has been exploited particularly by Madga and Torlief Ericson (66). [See also the most recent discussions by Ericson and Weise (88).] For a more extensive bibliography on the derivation of the Lorentz–Lorentz and other density-dependent effects, such as that induced by ρ -meson excitation [Baym and Brown (75)], see Eisenberg and Koltun (80).

Transforming to coordinate space and including the first-order P -wave contribution, one obtains

$$V_p(\mathbf{r}) = -(A-1)c_0 \nabla \cdot [\rho - \frac{1}{3}(A-1)2\mu c_0 \rho^2] \nabla \quad (3.22)$$

Eisenberg and Koltun (80) calculate the next-order term, making it plausible that

$$V_p(\mathbf{r}) = -(A-1)c_0 \nabla \cdot \frac{\rho}{1 + \frac{1}{3}2\mu(A-1)c_0 \rho} \nabla \quad (3.23)$$

This should replace the $c^{(0)}$ term in (3.14). One should bear in mind that the form factors $h(k)$ have not been inserted and that only a subset of the higher-order terms has been summed. The cross-terms with the nonresonant components of $V^{(1)}$ have not been included, for example. Finally, (3.14) suitably modified by (3.23) does not contain absorption effects. The constants b, c , and so on, are nearly real in this energy range, indicating, as expected, that the inelastic and quasi-elastic cross sections are small. The Pauli principle plays an important role here.

The significant absorption reaction is the $\pi(2n) \rightarrow 2n$. Of course, there is the single-step process $\pi + n \rightarrow n$, but this involves a large momentum mismatch; that is, the energy of the final nucleon yields a larger momentum than that provided by the incident pion and the Fermi motion of the target nucleon. A more likely process is thought to be absorption of the pion by two nucleons which would go off in opposite directions with equal momenta (or nearly equal if the incident pion has some kinetic energy). The probability of this process is proportional to the (density)², since two nucleons are involved. These terms are introduced phenomenologically, so that $V^{(1)}$ reads

$$V = (A-1) \left\{ b^{(0)}\rho + B^{(0)}\rho^2 - \nabla \cdot \frac{c^{(0)}\rho + AC^{(0)}\rho^2}{1 + \xi(2\mu)(A-1)[c^{(0)}\rho + AC^{(0)}\rho^2]} \nabla - \frac{1}{2} \nabla^2 \left[\frac{E_L}{m} c^{(0)}\rho + \frac{E_L}{2m} AC^{(0)}\rho^2 \right] \right\} \quad (3.24)$$

where the spin-orbit terms have been omitted. The empirical parameter ξ replaces the factor of $\frac{1}{3}$ in (3.23). $B^{(0)}$ and $C^{(0)}$ are complex. Thus even when $b^{(0)}$, $c^{(0)}$, and $d^{(0)}$ are taken from pion-nucleon scattering, we are left with five empirical parameters whose values are obtained by fitting the experimental data.

The factors $b^{(0)}$ and $c^{(0)}$ parametrize the pion-nucleon t matrix. To obtain these in terms of the pion-nucleon scattering amplitude $f_{\pi n}$, we make use of (3.4). Dropping the recoil terms, (3.4) becomes

$$t_{\pi A} = -2\pi \frac{k_L}{k_{\text{cm}} E_L} f_{\pi n} = -\frac{2\pi}{E_L} \left(1 + \frac{E_L}{m} \right) f_{\pi n} \quad (3.25)$$

Each of the quantities in (3.3) must therefore be multiplied by $-2\pi/E_L(1 + E_L/m)$. However, the parameter $B^{(0)}$ should contain the factor $(1 + E_L/2m)$ since the interaction is with two nucleons. According to (3.10), the parameter c' of (3.2) should be multiplied by $(m/m + E_L)^2$ upon transforming to the laboratory reference frame. Putting all these factors together yields

$$\begin{aligned}
 V = & -\frac{2\pi}{E_L} \left\{ \left(1 + \frac{E_L}{m} \right) b' \rho + \left(1 + \frac{E_L}{2m} \right) B' \rho^2 \right. \\
 & - \nabla \cdot \frac{\frac{1}{1 + E_L/m} c' + \frac{A}{1 + E_L/2m} C'}{1 + 4\pi\xi(A - 1) \left[\frac{c'}{1 + E_L/m} + \frac{AC'}{1 + E_L/2m} \right]} \\
 & \left. - \frac{1}{2} \frac{E_L}{m} \nabla^2 \left(\frac{c'}{1 + E_L/m} + \frac{1}{2} \frac{AC'}{1 + E_L/2m} \right) \right\} \quad (3.26)
 \end{aligned}$$

The effect of the form factors $h(k^2)$ has not been included in (3.26). This potential is then inserted into the Klein-Gordon equation,

$$[\nabla^2 + (E_L - V_C)^2 - 2E_L V - m_\pi^2] \vartheta = 0$$

where V_C is the Coulomb potential and terms proportional to $(V)^2$ have been dropped. The results of Ericson and Weise (88) for the parameters b'_0 , b'_1 , c'_0 , c'_1 , and so on, are presented in Table 3.1.

The quantity $(b'_0)_{\text{eff}}$ is $b_0 - (1 - m_\pi/m)[b_0^2 + 2b_1^2]\langle 1/r \rangle$, with $\langle 1/r \rangle$ taken to be $0.91 m_\pi$. The term subtracted from b_0 is a second-order multiple scattering correction. These results should be compared with the values given in (3.3). The agreement with experiment is illustrated in Fig. 3.1. The predicted reaction cross sections are shown in Fig. 3.2.

TABLE 3.1 Low-Energy Optical Model Parameters

	π Atom	$T_\pi = 50$ MeV	Units
$(b'_0)_{\text{eff}}$	-0.03	$-0.04 + 0.004i$	m_π^{-1}
b'_1	-0.09	-0.09	m_π^{-1}
c'_0	0.23	$0.25 + 0.01i$	m_π^{-3}
c'_1	0.15	$0.16 + 0.005i$	m_π^{-3}
ξ	0.47	0.47	
B'	$0.002 + 0.05i$	$-0.005 + 0.03i$	m_π^{-4}
AC'	$0.04 + 0.12i$	$0.05 + 0.07i$	m_π^{-6}

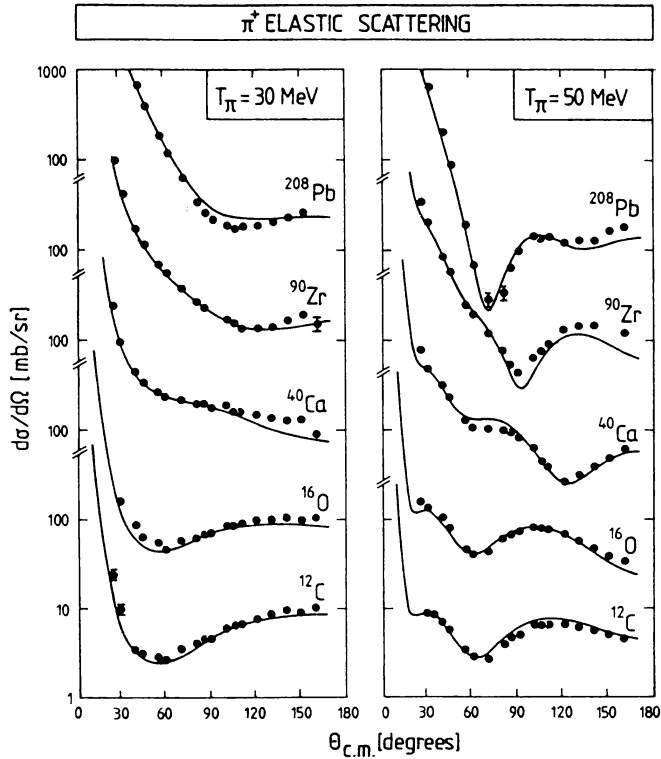


FIG. 3.1. Angular distributions for π^+ elastic scattering on various nuclei at $T_\pi = 30$ and 50 MeV [Carr, McManus, and Strickler (82)]. [From Ericson and Weise (88).]

B. Pion Energy 80–400 MeV; The Resonance Region

The dominant physical process in this energy range is the absorption of the incident pion by one of the nucleons in the target nucleus, forming a Δ . The Δ propagates through the nucleus, colliding with other nucleons. The Δ eventually decays into a nucleon + pion, leaving the nucleus in the ground state (elastic scattering) or excited (inelastic scattering). In an equivalent description the pion is absorbed by the target nucleus, forming a Δ -hole state, that is, a system consisting of $A - 1$ nucleons plus a Δ . This state acts as a doorway to more complex states, such as the $\Delta - n - 2$ hole state, and generally to Δ -hole plus multiparticle-hole states.

These two descriptions are equally valid. However, the first suggests a multiple scattering description, while the second suggests a doorway state description. In this volume we describe the latter, first proposed by Kisslinger and Wang (73, 76) and further exploited by Hirata, Koch, Lenz, and Moniz (78, 79) and Horikawa, Thies, and Lenz (80). A critical review of this area, including an

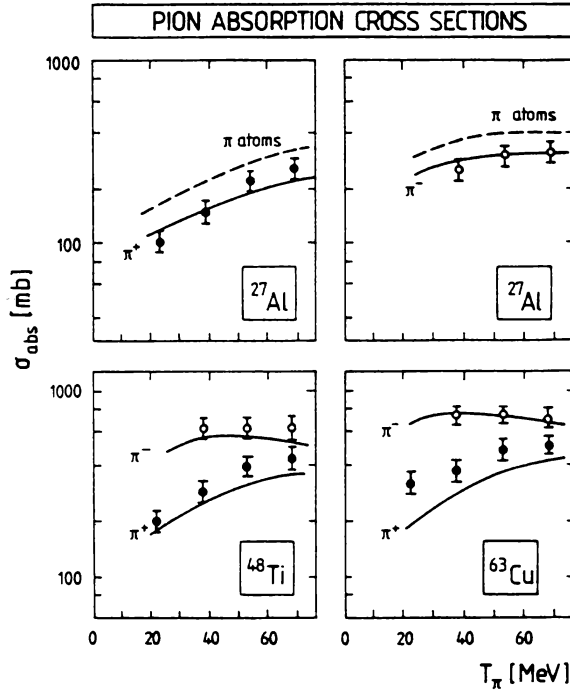


FIG. 3.2. Pion absorption cross sections for various nuclei as a function of energy [Carr, McManus, and Strickler (82)]. [From Ericson and Weise (88).]

analysis of both approaches, is being prepared by Lenz and Moniz (91). The reader is referred to this article for a discussion of the multiple scattering description together with an extensive list of references.

In the language of Chapter III, P space contains the states of A baryons, containing a maximum of one Δ and at least one but no more than one pion. As usual, the other degrees of freedom are contained in Q space. Perhaps the most important term in Q space is the two-pion + baryon system, which is generated by the reaction ($\pi n \rightarrow \pi\pi n$). The Hamiltonian H_{PP} we shall use is

$$H = \tilde{H}_A + h_\pi^0 + H' \quad (3.27)$$

where

$$\begin{aligned} \tilde{H}_A = & H_n^0 + H_\Delta^0 + V_A(n) + V_A(\Delta) + H(n\Delta \rightarrow nn) + H(\pi n \rightarrow \Delta) \\ & + \text{hermitian conjugates of the last two terms} \end{aligned} \quad (3.28)$$

The quantities h_π^0 , H_n^0 , and H_Δ^0 contain the mass and kinetic energy operators. The single-particle potentials $V_A(n)$ and $V_A(\Delta)$ approximate in shell model fashion the potential in which a nucleon or the Δ move. The term $H(n\Delta \rightarrow nn) + H(nn \rightarrow n\Delta)$

describes a Δ -nucleon collision in which the Δ is deexcited to a nucleon, and vice versa, a process that in nucleon-nucleon scattering leads to the production of a Δ . The last term $H(\pi n \rightarrow \Delta)$ describes the formation of a Δ by absorption of the pion by a nucleon, or vice versa, the decay of the Δ into a pion + nucleon.

We define a set of mutually orthogonal projection operators P_π , P_A , and P_Δ . The first of these, P_π , projects onto the space, consisting of the states of A nucleons and one pion. Thus

$$P_\pi H P_\pi = h_\pi^0 + H_A \equiv H_\pi \quad (3.29)$$

where

$$H_A = \sum_i (T_i + U_i) \quad \Sigma U_i = V_A(n) \quad (3.30)$$

and

$$h_\pi^0 = T_\pi + m_\pi \quad (3.31)$$

The operator P_A projects onto a space containing only nucleons, so that

$$P_A H P_A = H_A \quad (3.32)$$

Finally, the operator P_Δ projects onto a space containing one Δ and $(A-1)$ nucleons:

$$P_\Delta H P_\Delta = \Delta m + \sum_i (H_i^{A-1} + T_{\Delta,i} + V_{\Delta,i}) \equiv H_\Delta \quad (3.33)$$

where $\Delta m = m_\Delta - m_n$, and the subscript i in the sum denotes the nucleon, which has been converted into a Δ . The sum $\sum V_{\Delta,i} = V_A(\Delta)$. The nondiagonal terms are

$$P_\Delta H P_\pi = H(\pi n \rightarrow \Delta) = \sum_i \hat{g}_i \equiv H_{\Delta\pi} \quad (3.34)$$

and

$$P_\Delta H P_A = H(\Delta n \rightarrow nn) = \sum_{i < j} v_{\Delta n}(i, j) \equiv H_{\Delta A} \quad (3.35)$$

The operator $H_{\Delta\pi}$ describes the absorption of a pion to form a delta. The operator \hat{g}_i is given by (2.32):

$$\hat{g}_i \equiv gh(k^2) \mathbf{k} \cdot \mathbf{S}_i^\dagger \quad (3.36)$$

Finally, $H_{\Delta A}$ is $H(n\Delta \rightarrow nn)$. The corresponding wave functions

$$P_\pi \Psi = \psi_\pi \quad P_A \Psi = \psi_A \quad P_\Delta \Psi = \psi_\Delta \quad (3.37)$$

satisfy the Schrödinger equations (Ψ is the exact state vector)

$$(E - H_\pi)\psi_\pi = H_{\pi\Delta}\psi_\Delta \quad (3.38a)$$

$$(E - H_A)\psi_A = H_{A\Delta}\psi_\Delta \quad (3.38b)$$

$$(E - H_\Delta)\psi_\Delta = H_{\Delta A}\psi_A + H_{\Delta\pi}\psi_\pi + H_{\Delta Q}\psi_Q \quad (3.38c)$$

$$(E - H_Q)\psi_Q = H_{Q\Delta}\psi_\Delta \quad (3.38d)$$

where $Q\Psi \equiv \psi_Q$ contains all the channels, such as the Δ -hole, many p - h states not subtended by $P_\pi + P_A + P_\Delta$ (i.e., $Q = 1 - P_\pi - P_A - P_\Delta$). We have made the strong doorway state hypothesis, that only ψ_Δ connects to Q space. By the process of elimination one can obtain the transition matrix of various reactions. First, let us obtain a description of ψ_Δ . We “solve” (3.38a):

$$\psi_\pi = \phi_\pi^{(+)} + \frac{1}{E^+ - H_\pi} H_{\pi\Delta}\psi_\Delta$$

where $\phi_\pi^{(+)}$ is the incident pion-nuclear wave function. Second, from (3.38b) we find that

$$\psi_A = \frac{1}{E^+ - H_A} H_{A\Delta}\psi_\Delta$$

Hence

$$\begin{aligned} & \left(E - H_\Delta - H_{\Delta A} \frac{1}{E^+ - H_A} H_{A\Delta} - H_{\Delta\pi} \frac{1}{E^+ - H_\pi} H_{\pi\Delta} - H_{\Delta Q} \frac{1}{E^+ - H_Q} H_{Q\Delta} \right) \psi_\Delta \\ & = H_{\Delta\pi} \phi_\pi^{(+)} \end{aligned} \quad (3.39)$$

To simplify the appearance of these equations, introduce the definitions

$$H_{\Delta A} \frac{1}{E - H_A} H_{A\Delta} \equiv W_\Delta^{(A)} \quad (3.40a)$$

$$H_{\Delta\pi} \frac{1}{E - H_\pi} H_{\pi\Delta} \equiv W_\Delta^{(\pi)} \quad (3.40b)$$

and

$$H_{\Delta Q} \frac{1}{E - H_Q} H_{Q\Delta} \equiv W_\Delta^{(Q)} \quad (3.40c)$$

Equation (3.39) becomes

$$(E - H_\Delta - W_\Delta)\psi_\Delta = H_{\Delta\pi}\phi_\pi^{(+)} \quad (3.41)$$

where

$$W_{\Delta} = W_{\Delta}^{(A)} + W_{\Delta}^{(\pi)} + W_{\Delta}^{(Q)} \quad (3.42)$$

Inserting (3.41) into (3.38) yields expressions for the ψ_{π} and ψ_A . From ψ_{π} one can obtain the \mathcal{T} matrix for π -nucleus scattering

$$\mathcal{T}_{\pi\pi} = \mathcal{T}_{\pi\pi}^P + \left\langle \phi_{\pi}^{(-)} H_{\pi\Delta} \frac{1}{E^{(+)} - H_{\Delta} - W_{\Delta}} H_{\Delta\pi} \phi_{\pi}^{(+)} \right\rangle \quad (3.43)$$

where $\mathcal{T}_{\pi\pi}^P$ is the amplitude for nonresonant reactions. One can also obtain the amplitude for π absorption, assuming the absence of nonresonant terms:

$$\mathcal{T}_{ab} = \left\langle \psi_A^{(-)} H_{A\Delta} \frac{1}{E^{(+)} - H_{\Delta} - W_{\Delta}} H_{\Delta\pi} \phi_{\pi}^{(+)} \right\rangle \quad (3.44)$$

where $\psi_A^{(-)}$ is an excited state of the target nucleus in the continuum, usually a $2p-2h$ state.

Each of the components of W_{Δ} corresponds to a physical process. The operator $W_{\Delta}^{(A)}$ describes a process in which the Δ is converted into a nucleon, thereby forming the target nucleus again. This is followed by propagation and recovery of the Δ . We shall refer to it as *absorption*. The operator $W_{\Delta}^{(\pi)}$ describes the decay of the Δ into a π + nucleon, forming the target nucleus plus a pion. This is followed by propagation and reabsorption of the pion to form the Δ .

To evaluate $\mathcal{T}_{\pi\pi}$ or \mathcal{T}_{ab} , it is necessary to determine the states of the operator $H_{\Delta} + W_{\Delta}$. Not all the states, of course: rather, that state which is most strongly excited by the incident pion. The principal component is presumed to be a Δ -hole state. We shall therefore look for that linear combination of Δ -hole states which diagonalize (approximately, of course) $H_{\Delta} + W_{\Delta}$. This is the doorway state. Toward that end we shall examine and approximate W_{Δ} .

Consider first $W_{\Delta}^{(\pi)'}$, where the prime indicates that we have removed the incident channel; that is, the intermediate states will only be those in which the target nucleus is excited. If P_0 is the projection operator for the nuclear ground state and $Q_0 = 1 - P_0$ is its complement, then

$$W_{\Delta}^{(\pi)'} = H_{\Delta\pi} Q_0 \frac{1}{E - H_{\pi}} H_{\pi\Delta} \quad (3.45)$$

Inserting (3.34), we have

$$W_{\Delta}^{(\pi)'} = \sum_{i,j} \hat{g}_i^{\dagger} Q_0 \frac{1}{E - H_{\pi}} \hat{g}_j \quad (3.46)$$

where i and j indicate the nucleon which is converted into a Δ (and vice versa).

We separate the diagonal and nondiagonal contributions:

$$W_{\Delta}^{(\pi)'} \equiv W_D^{(\pi)} + W_{ND}^{(\pi)} \quad (3.47)$$

where

$$W_D^{(\pi)} = \sum \hat{g}_i^\dagger Q_0 \frac{1}{E - H_\pi} \hat{g}_i \quad (3.48)$$

This term corresponds to the case where the system returns to a Δ -hole configuration while W_{ND} involves a final system consisting of a Δ - p - $2h$ configuration. The latter, W_{ND} , is referred to as the *rescattering* term.

Similarly, $W_{\Delta}^{(A)}$ can be broken up into a term in which the Δ - h configuration is preserved and a term in which the final system involves the Δ - p - $2h$ configuration, so that

$$W_{\Delta}^{(A)} = W_D^{(A)} + W_{ND}^{(A)} \quad (3.49)$$

Hence the denominator in (3.43) can be rewritten

$$E^{(+)} - H_{\Delta} - W_{\Delta} = E^{(+)} - H_{\Delta} - W'_D - W^{(Q)} \quad (3.50)$$

where

$$W'_D = W_D^{(\pi)} + W_D^{(A)} \quad (3.51)$$

and

$$W^{(Q)} = W_{\Delta}^{(Q)} + W_{ND}^{(\pi)} + W_{ND}^{(A)} \quad (3.52)$$

The decomposition could have been introduced at an earlier stage [Eq. (3.38)] by the addition of suitable projection operators or through use of the multistep theory of Chapter VII. Physically, one should note that the Δ - p - $2h$ state can be generated either through the rescattering term or through $W_{ND}^{(A)}$. Both mechanisms must be considered when the generation of a Δ - p - $2h$ configuration is important, as it is in the case of double charge exchange ($\pi^- \rightarrow \pi^+$).

To make the Pauli-blocking effect explicit, we replace Q_0 in (3.48) by $1 - P_0$, where P_0 is the projection onto occupied levels. Thus

$$W_D^{(\pi)} = \sum \hat{g}_i^\dagger \frac{1}{E - H_\pi} \hat{g}_i + W_{PB}^{(\pi)} \quad (3.53)$$

where

$$W_{PB}^{(\pi)} \equiv - \sum \hat{g}_i \frac{P_0}{E - H_\pi} \hat{g}_i \quad (3.54)$$

Equation (3.50) is therefore

$$E^{(+)} - H_{\Delta} - W_{\Delta} = E^{(+)} - H_{\Delta} - w_{\Delta} - W_{PB}^{\pi} - w_{gs} - W^{(Q)} \quad (3.55)$$

where

$$w_{\Delta} = \sum g_i^{\dagger} \frac{1}{E - H_{\pi}} g_i + W_{\Delta}^{(A)} \quad (3.56)$$

and

$$w_{gs} = H_{\Delta\pi} P_0 \frac{1}{E - H_{\pi}} H_{\pi\Delta} \quad (3.57)$$

But

$$\begin{aligned} H_{\pi} &= T_{\pi} + m_{\pi} + H_A \\ &= T_{\pi} + m_{\pi} + T_i + U_i + H_{A-1} \\ &\simeq T_{\Delta} + U + H_{A-1} + m_{\pi} \end{aligned} \quad (3.58)$$

In the last equation the pion-nucleon center-of-mass kinetic energy has been replaced by the Δ kinetic energy T_{Δ} and U is now the average Δ -nucleus potential. Because the nuclear wavefunctions are antisymmetrized, the sum in (3.56) can be replaced by a single term. This is identical with the similar term appearing in the denominator of (2.31) except that H_{PP} is now given by H_{π} as approximated by (3.58). Therefore,

$$\sum_i \hat{g}_i^{\dagger} \frac{1}{E - H_{\pi}} \hat{g}_i = \Sigma(E - T_{\Delta} - U - H_{A-1} - m_{\pi}) \quad (3.59)$$

where Σ is defined by

$$\Sigma(E) \equiv H_{QP} \frac{1}{E^+ - H_{PP}} H_{PQ}$$

from (2.31).

The denominator of (3.43) becomes

$$\begin{aligned} E^{(+)} - H_{\Delta} - W_{\Delta} &= E^{(+)} - H_{\Delta} - W_D^{(A)} \\ &\quad - \Sigma(E - T_{\Delta} - U - H_{A-1}) - W_{PB}^{(\pi)} - W^{(Q)} - w_{gs} \end{aligned}$$

To make further progress, we linearize Σ by expanding $E - \Sigma$ about its zero, $E - E_R + i\Gamma/2$. We obtain

$$\begin{aligned} E^{(+)} - H_{\Delta} - W_{\Delta} &= E - E_R(E) + \frac{i\Gamma(E)}{2} \\ &\quad - \gamma(E - T_{\Delta} - \mathcal{U} - H_{A-1}) - W_{PB}^{(\pi)} - W^{(Q)} - w_{gs} \end{aligned} \quad (3.60)$$

where

$$\gamma = 1 + \left(\frac{\partial \Sigma}{\partial E} \right)_{E=E-E_R+i\Gamma/2} \quad (3.61)$$

and

$$\mathcal{U} = U + \frac{1}{\gamma} W_D^{(A)}$$

The expression

$$\mathcal{H} = \gamma(T_\Delta + \mathcal{U} + H_{A-1}) + W_{PB}^{(\pi)} + W^{(Q)} \quad (3.62)$$

is the Δ -nucleus interaction. Medium modifications are given by γ and $W_{PB}^{(A)} + W^{(Q)}$. In the notation of Feshbach (82),

$$W^{(Q)} \equiv \hat{W}^\downarrow \quad (3.63)$$

and

$$w_{gs} \equiv \hat{W}^\uparrow \quad (3.64)$$

where \hat{W}^\downarrow is the spreading operator and \hat{W}^\uparrow the escape operator.

Expression (3.66) is now in a form that makes a phenomenological approach possible. One adopts the optical model strategy by replacing \hat{W}^\downarrow with a spreading potential composed of central and spin-orbit terms:

$$\hat{W}^\downarrow = W_0 \rho(r) + 2\mathbf{L}_\Delta \cdot \boldsymbol{\Sigma}_\Delta V_{LS}^{(0)} \mu r^2 e^{-\mu r^2} \quad (3.65)$$

where $\boldsymbol{\Sigma}_\Delta$ is the spin- $\frac{3}{2}$ operator for the Δ . The matrix elements of other terms \hat{W}^\uparrow and $W_{PB}^{(\pi)}$ can be evaluated in the Δ -hole basis. For details, see Hirata, Koch, Lenz, and Moniz (79).

Doorway States. We now turn to the problem of obtaining the eigenstates of

$$\mathcal{H} \equiv H_\Delta + W_\Delta = \gamma(T_\Delta + \mathcal{U} + H_{A-1}) + W_{PB}^{(\pi)} + \hat{W}^\downarrow \quad (3.66)$$

as given in (3.62). The potential \mathcal{U} is taken by Hirata, Koch, Lenz, and Moniz (79) to be proportional to the nucleon density with a depth of 55 MeV. The remaining parameters are W_0 , $V_{LS}^{(0)}$, and μ . The method used by these authors and Horikawa, Thies, and Lenz (80) was suggested by the results they obtained when the eigenfunctions of \mathcal{H} were determined using harmonic oscillator wave functions. It was found that the contribution of one particular eigenfunction dominated the \mathcal{T} matrix for elastic scattering. Moreover, the overlap of this wave function, D , with the state developed by the first interaction was large; that is,[†]

$$\frac{|\langle \tilde{D} | \hat{g} \psi_\pi^{(+)} \rangle|^2}{|\langle \psi_\pi^{(+)} | \hat{g}^\dagger \hat{g} \psi_\pi^{(+)} \rangle|^2} = 0.9 \quad (3.67)$$

[†]In the notation of Chapter III this ratio is

$$\frac{|\langle \Phi_d H_{dp} \psi^{(+)} \rangle|^2}{|\langle \psi^{(+)} | H_{pd} H_{dp} | \psi^{(+)} \rangle|^2}$$

Here \tilde{D} is the adjoint to the D used because \mathcal{H} is complex and $\psi^{(+)}$ is the scattering solution of (3.38a). This result suggested the use of the Lanczos method [Morse and Feshbach (53, p. 1155); see also Whitehead, Watt, Cole, and Morrison (77)]. Let

$$D_0 = \hat{g}\psi_\pi^{(+)} \quad (3.68)$$

Then D_1 is generated by

$$D_1 = \mathcal{H}D_0 - \frac{\langle \tilde{D}_0 \mathcal{H}D_0 \rangle}{\langle \tilde{D}_0 D_0 \rangle} D_0 \quad (3.69)$$

Note the orthogonality:

$$\langle \tilde{D}_0 D_1 \rangle = 0$$

State D_2 is obtained by operating on D_1 and orthogonalizing with respect to D_0 and D_1 :

$$D_2 = \mathcal{H}D_1 - \frac{\langle \tilde{D}_1 \mathcal{H}D_1 \rangle}{\langle \tilde{D}_1 D_1 \rangle} D_1 - \frac{\langle \tilde{D}_0 \mathcal{H}D_1 \rangle}{\langle \tilde{D}_0 D_0 \rangle} D_0 \quad (3.70)$$

$$\langle \tilde{D}_0 D_2 \rangle = \langle \tilde{D}_1 D_2 \rangle = 0 \quad (3.71)$$

One continues this process obtaining the general expression for the n th iterate D_n :

$$D_n = \mathcal{H}D_{n-1} - \frac{\langle \tilde{D}_{n-1} \mathcal{H}D_{n-1} \rangle}{\langle \tilde{D}_{n-1} D_{n-1} \rangle} D_{n-1} - \frac{\langle \tilde{D}_{n-2} \mathcal{H}D_{n-1} \rangle}{\langle \tilde{D}_{n-2} D_{n-2} \rangle} D_{n-2} \quad (3.72)$$

D_n is not only orthogonal to D_{n-1} and D_{n-2} but to D_{n-3} , D_{n-4} as well. One can show (this is left as an exercise) that

$$\langle \tilde{D}_\beta \mathcal{H}D_\alpha \rangle = 0 \quad \text{unless } \beta = \alpha, \quad \alpha \pm 1 \quad (3.73)$$

The three-term recurrence formula (3.72) thus generates an orthogonal set. To obtain the eigenvalue of \mathcal{H} , one expands the eigenfunction ψ_Δ in terms of the iterates D_n :

$$\psi = \sum a_n D_n \quad (3.74)$$

Operating with \mathcal{H} on ψ , we find that

$$\mathcal{H}\psi = \sum a_n \mathcal{H}D_n = \left[a_{n-1} + \frac{\langle \tilde{D}_n \mathcal{H}D_n \rangle}{\langle \tilde{D}_n D_n \rangle} a_n + \frac{\langle \tilde{D}_{n+1} \mathcal{H}D_{n+1} \rangle}{\langle \tilde{D}_n D_n \rangle} a_{n+1} \right] D_n \quad n > 0 \quad (3.75)$$

and

$$\mathcal{H}\psi = \left[\frac{\langle \tilde{D}_0 \mathcal{H} D_0 \rangle}{\langle \tilde{D}_0 D_0 \rangle} a_0 + \frac{\langle \tilde{D}_0 \mathcal{H} D_1 \rangle}{\langle \tilde{D}_0 D_0 \rangle} a_1 \right] D_0 \quad n=0 \quad (3.76)$$

The eigenvalue problem $\mathcal{H}\psi = \varepsilon\psi$ yields

$$a_{n-1} + \left[\frac{\langle \tilde{D}_n \mathcal{H} D_n \rangle}{\langle \tilde{D}_n D_n \rangle} - \varepsilon \right] a_n + \frac{\langle \tilde{D}_n \mathcal{H} D_{n+1} \rangle}{\langle \tilde{D}_n D_n \rangle} a_{n+1} = 0 \quad n > 0 \quad (3.77)$$

To “solve,” let

$$R_n \equiv \frac{a_{n-1}}{a_n}$$

Then (3.77) becomes

$$R_n = \left[\varepsilon - \frac{\langle \tilde{D}_n \mathcal{H} D_n \rangle}{\langle \tilde{D}_n D_n \rangle} \right] - \frac{\langle \tilde{D}_n \mathcal{H} D_{n+1} \rangle}{\langle \tilde{D}_n D_n \rangle} \frac{1}{R_{n+1}} \quad (3.78)$$

The solution of the equation for R_1 is the continued fraction:

$$R_1 = \varepsilon - \frac{\langle \tilde{D}_1 \mathcal{H} D_1 \rangle}{\langle \tilde{D}_1 D_1 \rangle} - \frac{\langle \tilde{D}_1 \mathcal{H} D_2 \rangle}{\langle \tilde{D}_1 D_1 \rangle} \times \frac{1}{\left[\varepsilon_1 - \frac{\langle \tilde{D}_2 \mathcal{H} D_2 \rangle}{\langle \tilde{D}_2 D_2 \rangle} \right] - \frac{\langle \tilde{D}_2 \mathcal{H} D_3 \rangle}{\langle \tilde{D}_2 D_2 \rangle} \frac{1}{\left[\varepsilon - \frac{\langle \tilde{D}_3 \mathcal{H} D_3 \rangle}{\langle \tilde{D}_3 D_3 \rangle} \right] - \dots}} \quad (3.79)$$

One can also obtain an expression for R_1 from (3.76):

$$R_1 = \frac{\langle \tilde{D}_0 \mathcal{H} D_1 \rangle / \langle \tilde{D}_0 D_0 \rangle}{\varepsilon - \langle \tilde{D}_0 \mathcal{H} D_0 \rangle / \langle \tilde{D}_0 D_0 \rangle} \quad (3.80)$$

Equating (3.80) with (3.79) yields an equation for ε . There are many solutions for ε , each corresponding to an eigenstate of \mathcal{H} . To obtain the wave function corresponding to each ε , we need the expansion coefficients a_n . These are given by

$$\frac{a_n}{a_0} = \frac{1}{R_n} \cdot \frac{1}{R_{n-1}} \dots \frac{1}{R_1}$$

One can also obtain a continued fraction expression for the \mathcal{T} matrix for elastic scattering. From (3.43) and (3.68) we have

$$\mathcal{T}_{\pi\pi} = \langle \tilde{D}_0 G D_0 \rangle \quad (3.81)$$

where

$$G = \frac{1}{\mathcal{E} - \mathcal{H}} \quad (3.82)$$

The complex energy $\mathcal{E} = E - E_R(E) + i\Gamma(E)/2$. Define the matrix element

$$G_{n0} \equiv \langle \tilde{D}_n G D_0 \rangle \quad (3.83)$$

so that $G_{00} = \mathcal{T}_{\pi\pi}$. We can therefore rewrite (3.82) as follows:

$$\mathcal{E} G_{n0} - \Sigma \langle \tilde{D}_n \mathcal{H} D_v \rangle G_{v0} = \delta_{n0}$$

Because of (3.73) this becomes

$$[\mathcal{E} - \langle \tilde{D}_n \mathcal{H} D_n \rangle] G_{n0} = \langle \tilde{D}_n \mathcal{H} D_{n-1} \rangle G_{n-1,0} + \langle \tilde{D}_n \mathcal{H} D_{n+1} \rangle G_{n+1,0} + \delta_{n0} \quad (3.84)$$

The solution of this set of equations has been obtained earlier in this volume. Let

$$\mathcal{H}_{nm} \equiv \langle \tilde{D}_n \mathcal{H} D_m \rangle$$

Then

$$G_{00} = \frac{1}{\mathcal{E} - \mathcal{H}_{00} - \frac{\mathcal{H}_{01}\mathcal{H}_{10}}{\mathcal{E} - \mathcal{H}_{11} - \frac{\mathcal{H}_{12}\mathcal{H}_{21}}{\mathcal{E} - \mathcal{H}_{12} - \frac{\mathcal{H}_{23}\mathcal{H}_{32}}{\mathcal{E} - \mathcal{H}_{33} - \dots}}}} \quad (3.85)$$

This is an exact solution of the elastic scattering problem.

It is also possible to obtain an expression for a reaction. Let us consider as an example the case of inelastic scattering to a state $\phi_{\pi,\alpha}$. The \mathcal{T} matrix is then

$$\mathcal{T}_{\alpha 0}^{\text{inel}} = \langle \phi_{\pi\alpha}^{(-)} \hat{g}^\dagger G D_0 \rangle \quad (3.86)$$

Expanding $G D_0$ in terms of D_n yields

$$\mathcal{T}_{\alpha 0}^{\text{inel}} = \sum_n \frac{\langle \phi_{\pi\alpha}^{(-)} \hat{g}^\dagger D_n \rangle}{\langle \tilde{D}_n D_n \rangle} G_{n0} \quad (3.87)$$

From (3.84)

$$G_{n0} = \frac{1}{\mathcal{E} - \mathcal{H}_{nn} - \frac{\mathcal{H}_{n,n+1}\mathcal{H}_{n+1,n}}{\mathcal{E} - \mathcal{H}_{n+1,n+1} - \frac{\mathcal{H}_{n+1,n+2}\mathcal{H}_{n+2,n+1}}{\mathcal{E} - \mathcal{H}_{n+2,n+2} - \cdots}}} \quad (3.88)$$

This expression can be inserted into (3.87) to obtain the inelastic transition amplitude. As one can see from (3.87), $\mathcal{T}^{\text{inel}}$ will be especially large if $\hat{g}\phi_{\pi\alpha}$ has a strong overlap with the incident doorway state.

The convergence of the continued fractions has been studied by Lenz, Moniz, and Yazaki (80). They consider a number of model scattering problems. The convergence to the exact partial wave amplitude and the forward scattering amplitude is determined by the parameter $\mu = (k - \kappa)R$, where $k - \kappa$ is the momentum difference outside and inside the interaction region and R is the radius of that region. Iterations up to a number equal to $|\mu|$ leads to high accuracy. This number is ≤ 5 for pion-nucleon scattering in both the high- and low-energy limits. For light nuclei $|\mu| \sim 1$, which is a great simplification. The convergence of the nonforward amplitude involves a second parameter $\xi = qR$, where q is the momentum transfer. If $\xi \leq |\mu|$, then $|\mu|$ determines the number of iterations. If $\xi > |\mu|$, more iterations are needed. One word of caution: These criteria are generalizations obtained from the study of specific models, the square well, and the Woods-Saxon potential and may not be valid for other situations.

An illustrative example is provided by the potential suggested by pion-nucleus scattering in the resonance region:

$$V(r) = \frac{4\pi\rho_0}{R} \frac{\Gamma/2}{E - E_R + i\Gamma/2} f(r)$$

where $f(r)$ is either a square well of radius R or a Woods-Saxon well:

$$f(r) = \frac{1}{1 + e^{(r-R)/a}}$$

Lenz, Moniz, and Yazaki (80) take $R = 1.12A^{1/3}$, $\rho_0 = 0.17 \text{ fm}^{-3}$, $\Gamma = 110 \text{ MeV}$, $E_R = 190 \text{ MeV}$, $A = 16$, k the pion-nucleus relative momentum in units of \hbar , 1.5 fm^{-1} , and $a = 0.53 \text{ fm}$. Table 3.2 shows the rate of convergence for these two types of wells for the $L = 0$ wave. N is the iterate number.

The wave function also converges rapidly, as is demonstrated by Fig. 3.3. Another example is given by Hirata, Koch, Lenz, and Moniz (79) for $E_{\pi^+} = 163 \text{ MeV}$, $\pi^- {}^{16}\text{O}$ scattering. \hat{W}^\dagger is given by the first term in (3.65). The mean potential, \mathcal{U} , is taken to be proportional to $\rho(r)$ with a depth of 55 MeV . The results are shown in Table 3.3. The exact result was obtained by a straightforward diagonalization of \mathcal{H} using harmonic oscillator wave functions. We see that

TABLE 3.2 $\mathcal{T}_{L=0}$

N	Square Well	Woods-Saxon
0	$-0.0031 + 0.5461i$	$0.0322 + 0.4961i$
1	$-0.0441 + 0.4172i$	$0.0120 + 0.4256i$
2	$-0.0410 + 0.4172i$	$0.0144 + 0.4298i$
3	$-0.0410 + 0.4172i$	$0.0144 + 0.4298i$

TABLE 3.3

N	$\mathcal{T}_{L=0}$	ε	$\mathcal{T}_{L=4}$	ε
0	$0.155 + 0.490i$	$-53.1 - 154.5i$	$0.060 + 0.280i$	$13.9 - 14.4i$
1	$0.159 + 0.372i$	$-68.7 - 138.5i$	$0.062 + 0.246i$	$-2.7 - 17.7i$
2	$0.154 + 0.381i$	$-68.7 - 138.0i$	$0.059 + 0.251i$	$-3.4 - 22.7i$
"Exact"	$0.154 + 0.381i$	$-68.7 - 138.0i$	$0.059 + 0.250i$	$-3.5 - 23.1i$

convergence for \mathcal{T}_L is very good in both cases. Accurate values of ε are obtained for $L=0$ after two iterates. Three iterates are needed for ε when $L=4$, as the value with one iterate is nowhere near the exact answer.

The contribution of the various components of $\text{Im } \varepsilon$ are shown in Fig. 3.4. (The qualitative results are not changed by the inclusion of the spin-orbit term in Eq. (3.65) [see Horikawa, Thies, and Lenz (80).] We see that the escape width, $\text{Im } W^\uparrow$, also referred to as the rescattering term, dominates. The Pauli blocking term does reduce the width substantially, but this is more than made up by $\text{Im}(W^\uparrow + W^\downarrow)$.

This theory has been applied to a number of reactions for which the Δ resonance is important. Background terms that do not involve the Δ must be added. The elastic scattering of π^- by ^{16}O at 114 and 240 MeV is shown in Fig. 3.5. The agreement is good and the need for the spin-orbit term is quite clearly demonstrated. The agreement is not quite as good for ^{12}C , where substantial deviations at back angles are recorded. Comparison has also been made with ^4He data [Horikawa, Thies, and Lenz (80)] and with Pb data [Karaoglu and Moniz (86)]. The empirical values of the parameters of the spreading potential W_0 , $V_{LS}^{(0)}$, and μ , (3.65), are given in Fig. 3.6 and Table 3.4.

TABLE 3.4 Parameters $V_{LS}^{(0)}$ and μ for the Spin-Orbit Potential

	$\mu (\text{fm}^{-2})$	$V_{LS}^{(0)} (\text{MeV})$
$\pi^+ + ^4\text{He}$	0.25	$-4.6 - 1.8i$
$\pi^- + ^{12}\text{C}$	0.35	$-10 - 4i$
$\pi^- + ^{16}\text{O}$	0.3	$-10 - 4i$

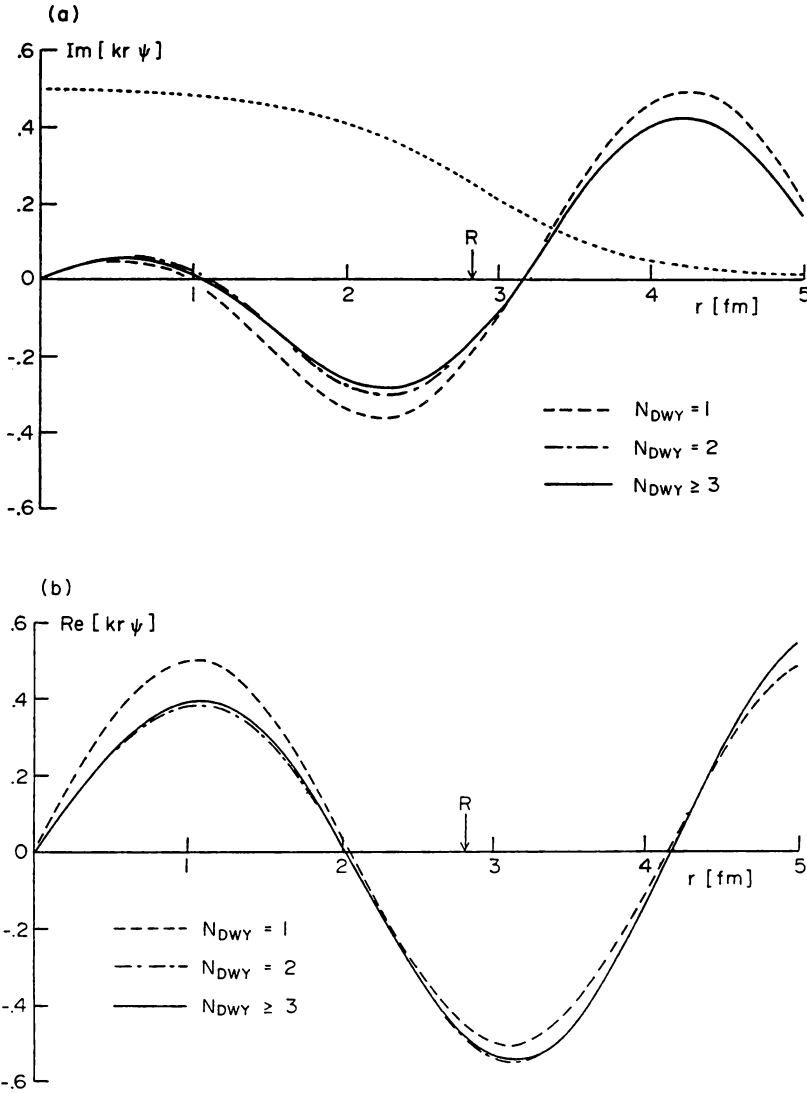


FIG. 3.3. *S*-wave scattering wave function for a Woods-Saxon potential with strength appropriate to intermediate energy pion-nucleus scattering. The (a) imaginary and (b) real parts of the wave function are shown for different numbers of doorway states. The dotted line in (a) shows the shape of the Woods-Saxon potential. [From Lenz, Moniz, and Yazaki (80).]

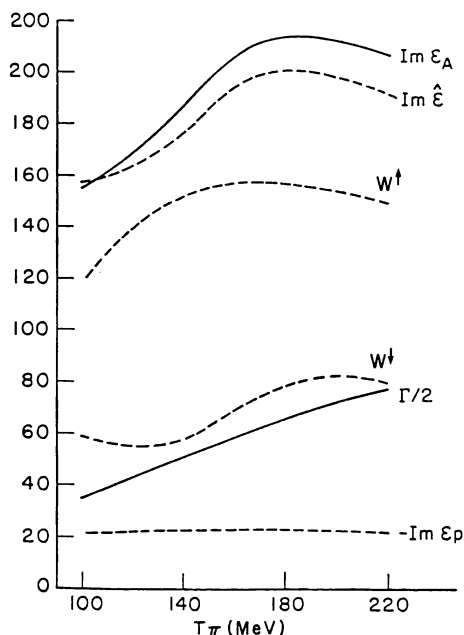


FIG. 3.4. Decomposition of the imaginary part of the doorway expectation value of the isobar-hole Hamiltonian. The eigenvalue of the leading eigenstate is denoted by $\hat{\epsilon}$, and Γ is the free-space isobar width.

The isobar-doorway model has been applied to inelastic scattering [Lenz, Thies, and Horikawa (82); Takaki (86)] and to nuclear photoabsorption and Compton scattering [Koch, Moniz, and Ohtsuka (84)]. Inelastic scattering and charge exchange scattering are discussed in the following sections. These provide tests of the isobar-doorway model which differ from those made by elastic scattering. The model has been successful, although some puzzles do remain, particularly at back angles. The overall result is that medium effects are very important. As a consequence, the DWA method is not successful in describing reactions in this energy range.

Reviews of the isobar-doorway model have been published by Moniz (78a, b). A review is now being prepared by Lenz and Moniz (91) which will contain a critical analysis of the various methods that have been used. Another approach to the isobar-doorway model is given by Oset with Weise (79). Other procedures are used by Wilkin (79), Lee and Ohta (82), Lee and Kurath (80), Johnson (86), and Liu and Shakin (77, 79).

Inelastic Scattering [Lenz, Thies, and Horikawa (82); Hirata, Lenz, and Thies (83); Takaki (86)]. The excitation of a nucleus by a pion whose energy is in the

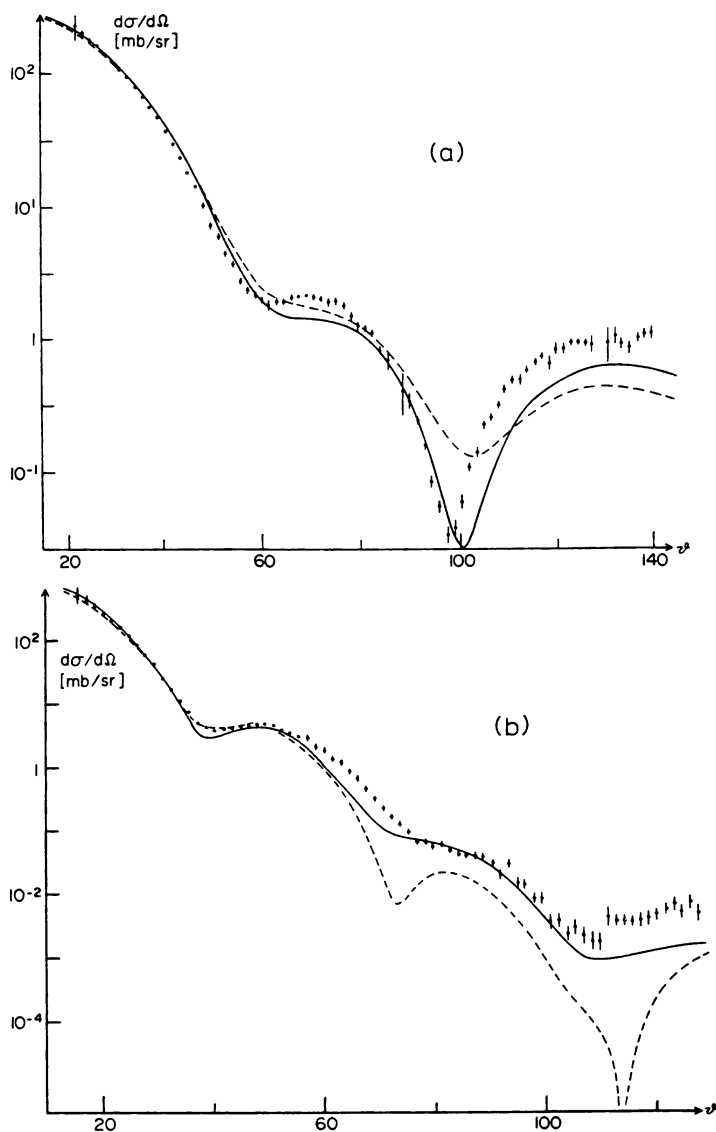


FIG. 3.5. π - ^{16}O scattering at 114 and 240 MeV, solid lines, spin-orbit term included (see Fig. 3.6 and Table 3.4 for the strength of central and spin-orbit term); dashed line, without spin-orbit potential ($W_0 = 2 - i55$ at 114 MeV and $W_0 = -12 - i35$ at 240 MeV, $V_{LS} = 0$). [From Horikawa, Thies, and Lenz (80).]

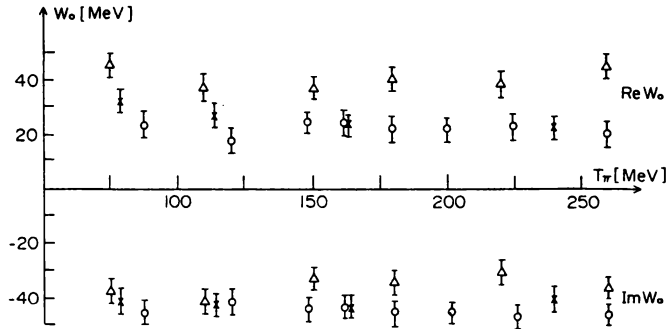


FIG. 3.6. Strength of central part of the spreading potential π - ^4He (triangles), π - ^{12}C (circles) and π - ^{16}O (crosses). [From Horikawa, Thies, and Lenz (80).]

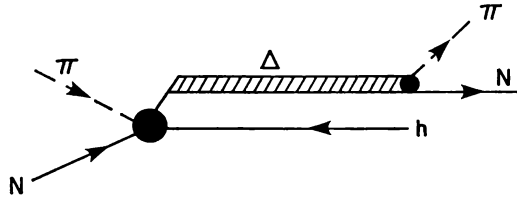


FIG. 3.7. Pion particle-hole excitation.

resonance region is the subject of this section. We consider only those contributions made when the intermediate state involves the Δ . As mentioned earlier, there may be contributions from the nonresonant components of the π - N reaction. The obvious first-order contribution involves the formation of the Δ -hole state. The Δ decays back into a pion plus nucleon so that the residual nucleus has a p -hole (p = particle) excitation. This is illustrated by Fig. 3.7. The amplitude for this process is

$$\mathcal{T}_{fi} = \left\langle \psi_{\pi f}^{(-)} H_{A\Delta} \frac{1}{E - \mathcal{H}_{\Delta}} H_{\Delta A} \psi_{\pi i}^{(+)} \right\rangle \quad (3.89)$$

The DWIA approximation [Lenz, Thies, and Horikawa (82)] consists in using the Δ -hole Hamiltonian for \mathcal{H}_{Δ} and the elastic scattering wave functions as modified by the Δ resonance described in the preceding section. The quantity $H_{\Delta A}$ is defined by (3.36) and \mathcal{H}_{Δ} is defined by (3.62). The amplitude equation (3.89) in the DWIA approximation has been studied thoroughly by Lenz, Thies, and Horikawa (82). We are able here to point out a few salient features of their analysis of inelastic π scattering. *Incidentally, most of these remarks apply equally well to elastic scattering.*

We first note that for p - h excitations,

$$\begin{aligned} H_{A\Delta}H_{\Delta A} &= g^2 h(k) \left[\sum_{i < j} \mathbf{S}_i \cdot \mathbf{k} S_j^\dagger \cdot \mathbf{k}' \right] h(k') \\ &= g^2 h(k) \left[\sum_i \mathbf{S}_i \cdot \mathbf{k} S_i^\dagger \cdot \mathbf{k}' \right] h(k') \end{aligned} \quad (3.90)$$

In this expression, \mathbf{k} is the center-of-mass momentum/ \hbar for the system consisting of a pion and a target nucleon. In the laboratory frame, \mathbf{k} in (3.90) must be replaced by

$$\mathbf{k} \rightarrow \mathbf{k} - \alpha \mathbf{K} \quad (3.91)$$

and similarly for \mathbf{k}' . The vector \mathbf{K} is the momentum of the nucleon/ \hbar , while α is E/mc^2 , where E is the total energy of the pion in the laboratory frame and m is the nucleon mass. The term proportional to α is referred to as the “recoil” term. The “static” limit is obtained by placing $\alpha = 0$. Equation (3.90) becomes approximately

$$H_{A\Delta}H_{\Delta A} = g^2 h(k)h(k') \sum_i \mathbf{S}_i \cdot (\mathbf{k} - \alpha \mathbf{K}) S_i^\dagger \cdot (\mathbf{k}' - \alpha \mathbf{K}') \quad (3.92)$$

Using (2.39), that is,

$$\mathbf{A} \cdot \mathbf{S} \mathbf{S}^\dagger \cdot \mathbf{B} = \frac{1}{3} \mathbf{A} \cdot \mathbf{B} - \frac{1}{3} i \boldsymbol{\sigma} \cdot (\mathbf{A} \times \mathbf{B})$$

one obtains

$$H_{A\Delta}H_{\Delta A} = \frac{1}{3} g^2 h(k)h(k') \sum_i \{ (\mathbf{k} - \alpha \mathbf{K}) \cdot (\mathbf{k}' - \alpha \mathbf{K}') - i \boldsymbol{\sigma}_i \cdot [(\mathbf{k} - \alpha \mathbf{K}) \times (\mathbf{k}' - \alpha \mathbf{K}')] \} \quad (3.92')$$

The initial wave function can be factored as follows:

$$\psi_{\pi i}^{(+)} = \chi_i^{(+)} \Psi_i \quad (3.93)$$

where Ψ_i is the wave describing the target nucleus depending only on the internal coordinates. The function $\chi_i^{(+)}$ is the pion-nucleon elastic scattering wave function. Similarly,

$$\psi_{\pi f}^{(-)} = \chi_f^{(-)} \Psi_f$$

Therefore,

$$\mathcal{T}_{fi} = \langle \chi_f^{(-)} t_{fi} \chi_i^{(+)} \rangle \quad (3.94)$$

where

$$t_{fi} = \left\langle \Psi_f H_{A\Delta} \frac{1}{E^* - \mathcal{H}_\Delta} \mathcal{H}_{\Delta A} \Psi_i \right\rangle \quad (3.95)$$

and $E^* = E - E_r + i\Gamma/2$.

Neglecting for the moment the nonlocality indicated by the propagator, we see from (3.92) that t_{fi} will involve the longitudinal density matrix,

$$\rho_{fi} = \left\langle \Psi_f \left| \sum_{\kappa=1}^A \delta(\mathbf{r} - \mathbf{r}_\kappa) (1 + \frac{1}{2}\tau_z(\kappa)) \right| \Psi_i \right\rangle = \frac{3}{2}\rho_{fi}^p + \frac{1}{2}\rho_{fi}^n \quad (3.96)$$

and the spin density,

$$\mathbf{S}_{fi} = \left\langle \Psi_f \left| \sum_{\kappa=1}^A \delta(\mathbf{r} - \mathbf{r}_\kappa) \boldsymbol{\sigma}(\kappa) (1 + \frac{1}{2}\tau_z(\kappa)) \right| \Psi_i \right\rangle \quad (3.97)$$

The factor $(1 + \frac{1}{2}\tau_z)$ gives the 3:1 ratio between the $T = \frac{3}{2}$ isospin total cross sections for $(\pi^+ p)$ and $(\pi^+ n)$. In (3.96) ρ_{fi}^p and ρ_{fi}^n are the proton and neutron density matrices.

Introducing the nonlocality by a first-order expansion of the orbital particle-hole wave functions introduces another set of nuclear operators. These include the convection current

$$\mathbf{j}_{fi}(\mathbf{r}) = \frac{1}{2m} \left\langle \Psi_f \left| \sum_{\kappa=1}^A (1 + \frac{1}{2}\tau_z(\kappa)) [\mathbf{p}(\kappa)\delta(\mathbf{r} - \mathbf{r}_\kappa) + \delta(\mathbf{r} - \mathbf{r}_\kappa)\mathbf{p}(\kappa)] \right| \Psi_i \right\rangle \quad (3.98)$$

and a dyadic

$$\vec{\vec{U}}_{fi}(\mathbf{r}) = \frac{1}{2m} \left\langle \Psi_f \left| \sum_{\kappa=1}^A (1 + \frac{1}{2}\tau_z(\kappa)) [\mathbf{p}(\kappa)\boldsymbol{\sigma}(\kappa)\delta(\mathbf{r} - \mathbf{r}_\kappa) + \delta(\mathbf{r} - \mathbf{r}_\kappa)\mathbf{p}(\kappa)\boldsymbol{\sigma}(\kappa)] \right| \Psi_i \right\rangle \quad (3.99)$$

These quantities ρ_{fi} , \mathbf{S}_{fi} , \mathbf{j}_{fi} and $\vec{\vec{U}}_{fi}$ are probed by inelastic pion scattering. Combined with electron scattering, they will yield the neutron particle density, spin density, and current density matrices as well as the spin flux tensor $\vec{\vec{U}}$. Note that the vectors $\mathbf{k}(\kappa)$ are momentum operators acting on the nucleon wave functions.

The modifications because of nonlocality and recoil (whose neglect through closure for the propagator and putting $\alpha = 0$ leads to the “static” solution) are substantial. The calculations involve (1) distorted wave functions for the pions as obtained by the methods discussed earlier, and (2) nucleon and hole orbital wave functions. They are required to yield the transition and spin density matrices as determined from electron scattering. In Fig. 3.8a we show the cross

sections for excitation of the 2^+ state (4.44 MeV) in ^{12}C by ρ_{fi} (longitudinal excitation) under various approximations. We see the large differences between the closure and full Δ - h calculations. In Fig. 3.8b a similar comparison is made for the 3^- state at 9.64 MeV. The match of the full calculation (the longitudinal excitation dominates) is not quantitatively satisfactory, although qualitative aspects are reproduced. We show just the case of the 2^+ excitation in Fig. 3.8c. In the resonance region the calculations do agree reasonably well up to the region of the second maximum. Large discrepancies are found for large momentum transfers. This is possibly not surprising since a similar difficulty exists for elastic scattering. Lenz, Thies, and Horikawa (82) believe that the cause of the discrepancy lies in the Δ -nucleus interaction as described by the spreading potential.

Hirata, Lenz, and Thies (83) point out that the mean field description of the Δ - h spreading potential may be an oversimplification. They propose a model in which the Δ interacts with the nuclear nucleons via a two-body interaction. This interaction can excite one of the nucleons, so that a possible intermediate state consists of a Δ - h plus a p - h state. This is illustrated in Fig. 3.9. Of course, higher-order multistep intermediate states Δ - h , $v(p-h)$, where v is an integer are possible.

The amplitudes corresponding to Figs. 3.7 and 3.9 add up to give the \mathcal{T} matrix:

$$\begin{aligned} \mathcal{T} = & \left\langle \psi_{\pi f}^{(-)} \left| H_{A\Delta} \frac{1}{E^* - \mathcal{H}_\Delta} H_{\Delta\Delta} \right| \psi_{\pi i}^{(+)} \right\rangle \\ & + \left\langle \psi_{\pi f}^{(-)} \left| H_{A\Delta} \frac{1}{E^* - \tilde{\mathcal{H}}_\Delta} \tilde{t}_{\Delta N} \frac{1}{E - \mathcal{H}_\Delta} H_{\Delta A} \right| \psi_{\pi i}^{(+)} \right\rangle \end{aligned} \quad (3.100)$$

where $\tilde{t}_{\Delta N}$ is the component of the Δ - N interaction, which results in further nuclear excitation. The quantity $(1/E^* - \tilde{\mathcal{H}}_\Delta)$ is the propagator for the Δ - h , p - h system, and $E^* = E - E_R + i\Gamma/2$.

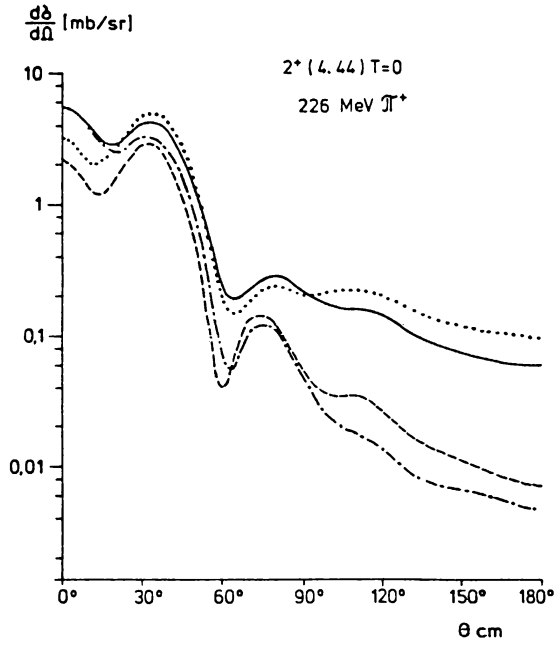
Equation (3.100) is an example of the amplitude for the multistep direct process described in Chapter VI. The higher-order multistep components are not included. An estimate of their importance using the statistical approach of Chapter VI has not been made.

The Hamiltonian in (8.39) is given by [see (3.53) and (2.60)]

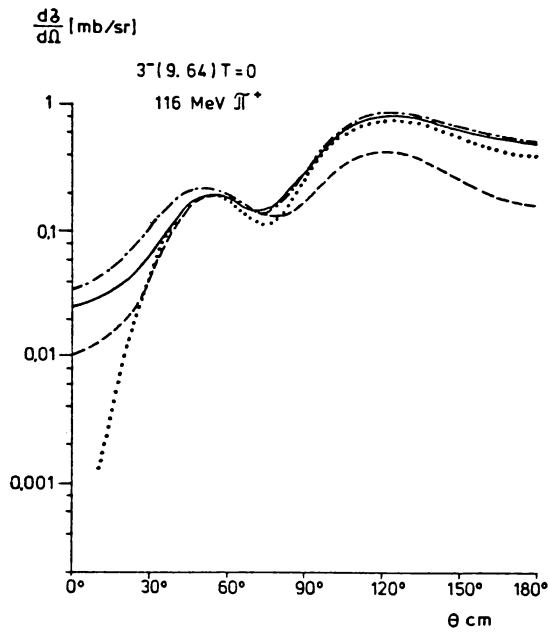
$$H_\Delta = \gamma(T_\Delta + \mathcal{U} + H_{A-1}) + W_{PB}^{(\pi)} + W^{(Q)} \quad (3.101)$$

Hirata, Lenz, and Thies (83) and Takaki (86) replace the spreading potential $W^{(Q)} + \gamma\mathcal{U}$ by a sum of two-body potentials instead of using the mean field as given in (3.65); that is,

$$W^{(Q)} + \gamma\mathcal{U} = \sum \tau(\Delta, i) \equiv t_{\Delta N} = \tilde{t}_{\Delta N} + W_D^{(\pi)} \quad (3.102)$$

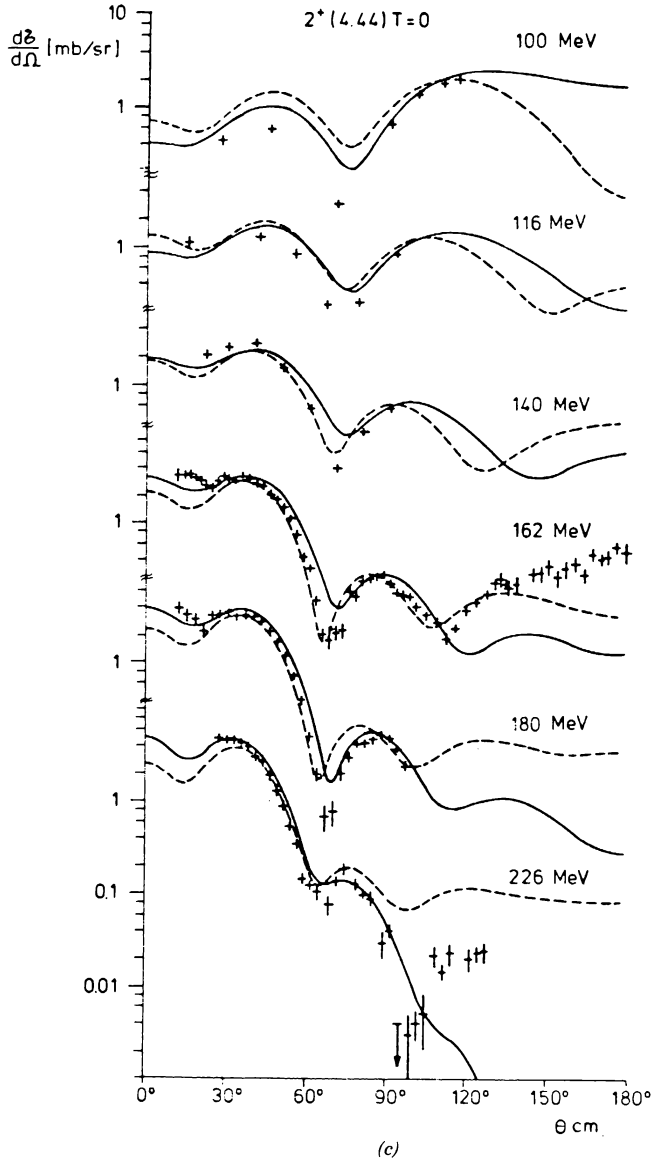


(a)



(b)

FIG. 3.8. (a) Comparison of various approximations to the Δ Green's function in the transition operator for excitation of the 2^+ (4.44 MeV) $T=0$ state by 226 MeV π^+ (pure longitudinal parameterization). Dotted curve; closure approximation; solid curve, free



Δ (kinetic energy only); dashed curve, including central Δ -nucleus potential; dashed-dotted curve, full Δ - h calculation, including Pauli terms and spin-orbit potential. The distorted π wave functions always correspond to the full Δ - h calculation. (b) Like (a), but 3^- (9.64 MeV) $T=0$ state, pure longitudinal parameterization, 116-MeV π^+ . (c) Differential cross sections for the 2^+ (4.44 MeV) $T=0$ excitation for various pion energies. Solid curves: Δ - h calculations, dashed curves: closure approximation. [From Lenz, Thies, and Horikawa (82).]

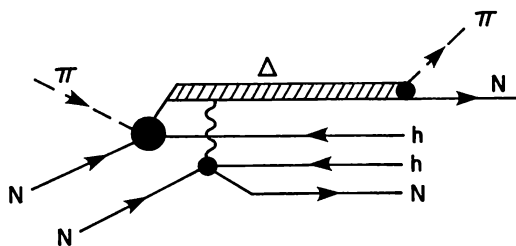


FIG. 3.9. Pion two-particle/two-hole excitation.

The potential $t_{\Delta N}$ contains the diagonal rescattering term [see (3.48)], which does not contribute to the production of the more complex nuclear states. The remainder $\tilde{t}_{\Delta N}$ is the interaction that appears in (3.100). Takaki (86) parametrizes $\tilde{t}_{\Delta N}$ as follows:

$$\tilde{t}_{\Delta N} = \sum_{i, S_{\Delta}, T_{\Delta}} C(S_{\Delta}, T_{\Delta}) \delta(\mathbf{r}_{\Delta} - \mathbf{r}_i) P(S_{\Delta}) P(T_{\Delta}) \quad (3.103)$$

where S_{Δ} and T_{Δ} are the spin and isospin of the interacting Δ - p pair, while $P(S_{\Delta})$ and $P(T_{\Delta})$ are the corresponding projection operators. Since the Δ spin is $\frac{3}{2}$ and the nucleon spin is $\frac{1}{2}$, S_{Δ} can be either 2 or 1. The same holds for T_{Δ} , so that (3.103) contains four complex parameters, $C(11)$, $C(12)$, $C(21)$, and $C(22)$. One relation exists among them: namely, that the mean field that follows from (3.102) agrees with the empirical mean field, W^{\dagger} [Eq. (3.65)]. The comparison is obtained by taking the diagonal value of $t_{\Delta N}$ in the single-doorway-state approximation. This result, together with fit of the inelastic data for the $(\pi^+, {}^{12}\text{C})$ reaction, permits the determination of the values of $C(S_{\Delta}, T_{\Delta})$. Finally, Takaki approximates \mathcal{H}_{Δ} by \mathcal{H}_{Δ} . Results for the excitation of the 1^+ , $T=0$ (12.72 MeV) and the 1^+ , $T=1$ (15.11 MeV) levels in ${}^{12}\text{C}$ are shown in Fig. 3.10 and for the 2^+ , $T=0$ (4.4 MeV) level and the 3^- , $T=0$ (9.6 MeV) levels in Fig. 3.11. The values of $C(S_{\Delta}, T_{\Delta})$ obtained from fitting 1^+ excitations are used in the calculation of the 2^+ and 3^- excitations. Qualitative agreement is good, especially at small angles, but there are strong differences from experiment at the back angles at 162 and 266 MeV. At 100 MeV, the full calculations are in good agreement with experiment. One also sees that by taking into account the more complex excitation, Δ - h , p - h , it becomes possible to fit the ratio $\sigma(T=0)/\sigma(T=1)$ as a function of the energy. The disagreement with the data is significant since this model correctly predicts the elastic and total cross sections. We speculate that full agreement with the data will not be attained until more complex excitations are included in the calculation.

Single (SCX) and Double (DCX) Charge Exchange Scattering. An example of an SCX reaction is

$$\pi^+ + {}_Z A \rightarrow {}_{Z+1} A + \pi^0 \quad (3.104)$$

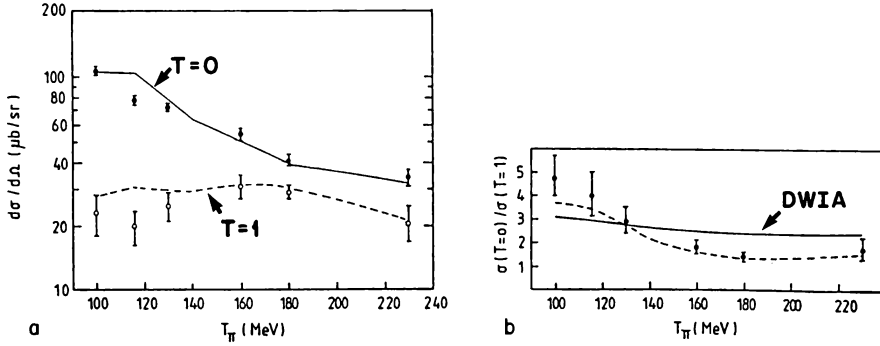


FIG. 3.10. Excitation functions for the $1^+ T=0$ (12.71 MeV) and $T=1$ (15.11 MeV) excitations. Solid and dashed lines correspond to the full calculations for $T=0$ and $T=1$, respectively. [From Takaki (86).]

It is closely related to the (p, n) reaction as the residual nucleus is identical for both. In the latter case, a most salient feature is the formation of the isobar analog of the target nucleus. We may expect that the reaction (3.104) will also excite the isobar analog states. This is illustrated by Fig. 3.12. With DCX, other giant resonances, such as the electric dipole and double isobar analog states, can also be excited (see Fig. 3.13). Thus once the dynamics of SCX reaction is understood, one should be able to gain further understanding of these resonances. Similarly, the (π^-, π^0) reaction is the image of the (n, p) reaction and would be useful in the study of the nucleus $(Z-1, N+1)$.

The isobar analog resonance can be discussed phenomenologically by using the Lane equation (Chapter V). A similar procedure can be followed here where following the papers of M. Johnson, E. R. Siciliano, and their colleagues [Siciliano, Cooper, Johnson, and Leitch (86), for example], one writes for the potential

$$V = V_0 + V_1(\mathbf{T}_\pi \cdot \mathbf{T}_A) + V_2(\mathbf{T}_\pi \cdot \mathbf{T}_A)^2 \quad (3.105)$$

where V_0 , V_1 , and V_2 are referred to as the scalar, vector, and tensor potentials. \mathbf{T}_π and \mathbf{T}_A are the isospin operators for the pions and nucleus, respectively. Equation (3.105) is the extension, to charge exchange reactions, of the pion optical potential described earlier [see (3.26)]. This potential was used to describe the elastic and total cross sections and involves terms quadratic in ρ (the density) which are a consequence of medium effects. Once one distinguishes between the neutron and proton components of ρ , these quadratic terms lead directly to a tensor contribution to V . It should also be noted that (3.105) contains the most complicated dependence on \mathbf{T}_π . To confirm this, we need only to recall[†] that

$$(\mathbf{T}_{\pi i})^3 = \mathbf{T}_{\pi i}$$

[†]More completely, $[\mathbf{T}_{\pi i}, \mathbf{T}_{\pi j}] = i\mathbf{T}_{\pi k}$; i, j, k cyclical and $\mathbf{T}_{\pi i} \mathbf{T}_{\pi j} \mathbf{T}_{\pi k} + \mathbf{T}_{\pi k} \mathbf{T}_{\pi j} \mathbf{T}_{\pi i} = \delta_{ij} \mathbf{T}_{\pi k} + \delta_{kj} \mathbf{T}_{\pi i}$

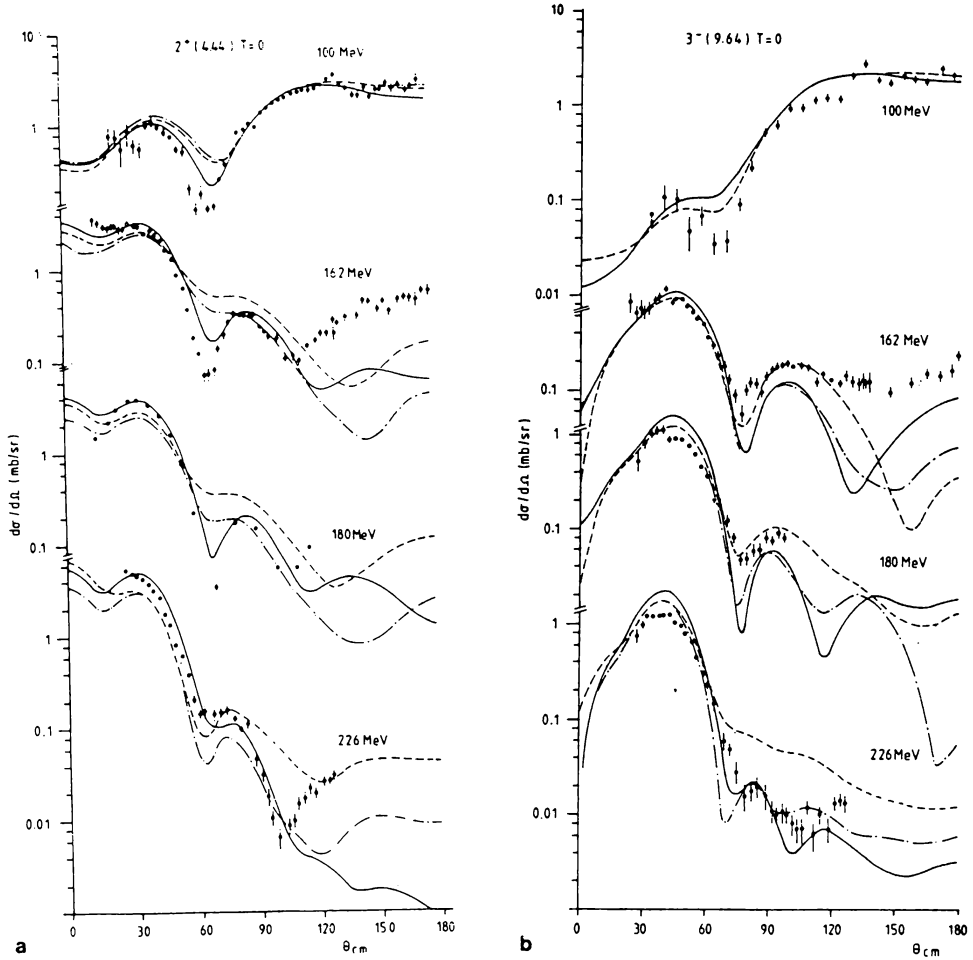


FIG. 3.11. Differential cross sections for (a) the $2^+ T=0$ (4.4 MeV) and (b) the $3^- T=0$ (9.6 MeV) excitations for various pion energies. Solid lines correspond to the DWIA calculation, and dashed lines to the full calculation. [From Takaki (86).]

where $T_{\pi i}$ is the i th component of \mathbf{T} . We emphasize that the tensor term is present as a consequence of the effect of the medium on pion-nucleon interaction. An analysis of the origin of this term will show that it depends on nuclear structure, on Pauli and on both short-range and long-range pair and higher-order correlations.

The solution of the Klein-Gordon equation with the V of (3.105) is relatively straightforward. One can determine the uncoupled equations for each of the

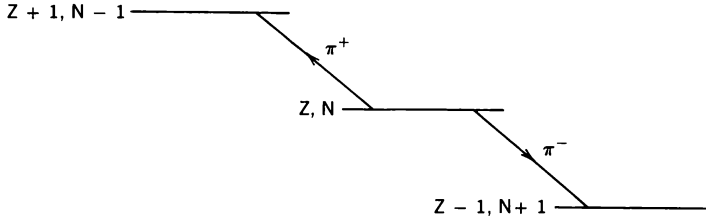


FIG. 3.12. Charge exchange reactions.

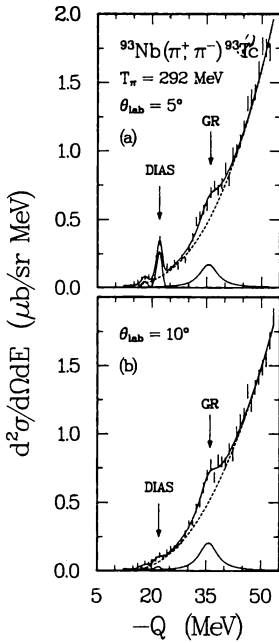


FIG. 3.13. Double-differential cross section spectrum for (π^+, π^-) reaction on a ^{93}Nb target at $T_\pi = 292$ MeV: (a) $\theta_{\text{lab}} = 5^\circ$; (b) $\theta_{\text{lab}} = 10^\circ$. The arrows indicate the fitted location of the DIAS and the giant resonance (GR). Short vertical lines represent statistical uncertainty of the data. The dashed line is the fitted background. DIAS, double isobar analog resonance. [From Mordechai, Auerbach, et al. (89).]

three possible isospins of the system $T = T_A \pm 1$ and $T = T_A$. Since

$$\mathbf{T} = \mathbf{T}_\pi + \mathbf{T}_A$$

one can immediately obtain the values of $\mathbf{T}_A \cdot \mathbf{T}_\pi$ that appear in (3.105). One obtains

$$\mathbf{T}_\pi \cdot \mathbf{T}_A = \frac{1}{2} [T(T+1) - T_\pi(T_\pi+1) - T_A(T_A+1)] \quad (3.106)$$

Recall that $T_\pi = 1$ and $T_A = \frac{1}{2}(N - Z)$. From the solutions $\psi(T_A + 1)$, $\psi(T_A)$, and $\psi(T_A - 1)$, one can obtain the amplitudes for SCX and DCX. The wave function for the π^+ nucleus system, $\psi_+(T_\pi, T_{\pi z}; T_A, T_{Az})$, is given in terms of the three

solutions $\psi(T_A + 1)$, $\psi(T_A)$, and $\psi(T_A - 1)$ by

$$\begin{aligned}\psi_+(1, 1; T_A, -T_A) = & (1, 1; T_A, -T_A | T_A + 1, 1 - T_A) \psi(T_A + 1) \\ & + (1, 1; T_A, -T_A | T_A, 1 - T_A) \psi(T_A) \\ & + (1, 1; T_A, -T_A | T_A - 1, 1 - T_A) \psi(T_A - 1)\end{aligned}$$

or

$$\begin{aligned}\psi_+(1, 1; T_A, -T_A) = & \sqrt{\frac{1}{(2T_A + 1)(T_A + 1)}} \psi(T_A + 1) \\ & + \sqrt{\frac{1}{T_A + 1}} \psi(T_A) + \sqrt{\frac{2T_A - 1}{2T_A + 1}} \psi(T_A - 1)\end{aligned}\quad (3.107)$$

The states $\psi(T_A + 1)$, and so on, must be chosen so that ψ_+ asymptotically consists of an incident plus outgoing wave. The outgoing wave will contain π^+ , π^0 , and π^- components corresponding to elastic (or inelastic) SCX and DCX scattering. To obtain the DCX, one needs the wave function for π^0 plus the residual nucleus with isospin T_R , z component T_z . This wave function is

$$\begin{aligned}\psi_0(1, 0; T_R, T_z) = & (1, 0; T_R, T_z | T_A + 1, T_z) \psi(T_A + 1) + (1, 0; T_R, T_z | T_A, T_z) \psi(T_A) \\ & + (1, 0; T_R, T_z | T_A - 1, T_z) \psi(T_A - 1)\end{aligned}\quad (3.108)$$

In the case of “elastic” scattering,

$$\begin{aligned}\psi_0(1, 0; T_A, 1 - T_A) = & 2 \sqrt{\frac{T_A}{(2T_A + 1)(T_A + 1)}} \psi(T_A + 1) \\ & + \frac{T_A - 1}{\sqrt{T_A(T_A + 1)}} \psi(T_A) - \sqrt{\frac{2T_A - 1}{T_A(2T_A + 1)}} \psi(T_A - 1)\end{aligned}\quad (3.109)$$

Experimentally, *elastic* scattering to the nucleus $(T_A, 1 - T_A)$ does not occur because of the presence of the isobar symmetry breaking Coulomb interaction. The residual nucleus in state ψ_0 is the isobar analog state of the target nucleus. The double isobar analog state is generated by the (π^+, π^-) reaction. It is the residual nucleus in state ψ_- :

$$\begin{aligned}\psi_-(1, -1; T_A, 2 - T_A) = & \sqrt{\frac{T_A(2T_A - 1)}{(T_A + 1)(2T_A + 1)}} \psi(T_A + 1) \\ & - \sqrt{\frac{2T_A - 1}{T_A(T_A + 1)}} \psi(T_A) + \sqrt{\frac{1}{T_A(2T_A + 1)}} \psi(T_A - 1)\end{aligned}\quad (3.110)$$

Returning to (3.108), the asymptotic boundary condition for ψ_0 is that it contains only an outgoing wave. The same boundary condition applies to the π^- + residual nucleus wave function, ψ_- , generated by the DCX reaction. These boundary conditions together with the boundary conditions for ψ_+ determine the amplitudes of $\psi(T_A + 1)$, $\psi(T_A)$, and $\psi(T_A - 1)$ and thus the reaction amplitudes.

In the absence of the Coulomb interaction, the transition matrix \mathcal{T} can also be written in the same form given in (3.105),

$$\mathcal{T} = t_0 + t_1(\mathbf{T}_\pi \cdot \mathbf{T}_A) + t_2(\mathbf{T}_\pi \cdot \mathbf{T}_A)^2 \quad (3.111)$$

For “elastic” scattering this equation yields the relationships [Koltun and Singham (89)]

$$\begin{aligned} \mathcal{T}_{11} &= t_0 - T_A t_1 + T_A(T_A + 1)t_2 & \pi^+ \rightarrow \pi^+ \\ \mathcal{T}_{01} &= \sqrt{T_A}(t_1 - T_A t_2) & \pi^+ \rightarrow \pi^0 \\ \mathcal{T}_{-11} &= \sqrt{T_A(2T_A - 1)}t_2 & \pi^+ \rightarrow \pi^- \end{aligned} \quad (3.112)$$

Equation (3.110) implies a connection between π^+ - and π^- - or π^0 -induced reactions. For example,

$$\mathcal{T}_{-1, -1} = t_0 + T_A t_1 + T_A^2 t_2 \quad \pi^- \rightarrow \pi^- \quad (3.113)$$

These relations will be valid for high energies and light nuclei, where the isospin symmetry-breaking Coulomb interaction is least important. They should fail substantially for low-energy incident pions and heavy target nuclei.

In the high-energy limit, one can establish the relation between V_0 , V_1 , and V_2 of (3.105) and t_0 , t_1 , and t_2 of (3.110) by using the eikonal approximation. From (II.5.11) we have

$$\mathcal{T}_{el} = \frac{2\pi i \hbar^2 k}{\mu} \int_0^\infty b db J_0(2kb \sin \frac{1}{2} \theta) (e^{i\chi} - 1) \quad (3.114)$$

where

$$\chi = v_0 + v_1(\mathbf{T}_\pi \cdot \mathbf{T}_A) + v_2(\mathbf{T}_\pi \cdot \mathbf{T}_A)^2 \quad (3.115)$$

and

$$v_i(b) = -\frac{\mu}{\hbar^2 k} \int_{-\infty}^{\infty} V_i(\mathbf{b}, z) dz$$

These nonrelativistic results can be modified to satisfy relativistic kinematics by using the Klein-Gordon equation [see (II.7.2)]. One can evaluate $e^{i\chi}$ through

use of the recurrence relations [Siciliano, Cooper, Johnson, and Leitch (86)]

$$(\mathbf{T}_\pi \cdot \mathbf{T}_\pi)^3 = -2(\mathbf{T}_\pi \cdot \mathbf{T}_A)^2 + (\mathbf{T}_\pi \cdot \mathbf{T}_A)(\mathbf{T}_A^2 - 1) + \frac{1}{2}\mathbf{T}_\pi^2 \mathbf{T}_A^2 \quad (3.116)$$

and

$$(\mathbf{T}_\pi \cdot \mathbf{T}_A)^4 = (\mathbf{T}_\pi \cdot \mathbf{T}_A)^2(\mathbf{T}_A^2 + 3) + \mathbf{T}_\pi \cdot \mathbf{T}_A[2 + \mathbf{T}_A^2(\frac{1}{2}\mathbf{T}_\pi^2 - 2)] - \mathbf{T}_\pi^2 \mathbf{T}_A^2 \quad (3.117)$$

Note that $\mathbf{T}_\pi^2 = T_\pi(T_\pi + 1) = 2$ and $\mathbf{T}_A^2 = T_A(T_A + 1)$. One finds that

$$e^{iv_1(\mathbf{T}_\pi \cdot \mathbf{T}_A)} = Ae^{-iv_1} + Be^{iv_1 T_A} + Ce^{-iv_1(T_A + 1)} \quad (3.118)$$

where

$$C = \frac{\mathbf{T}_A \cdot \mathbf{T}_\pi}{T_A(2T_A + 1)} [\mathbf{T}_A \cdot \mathbf{T}_\pi - T_A] \quad (3.119a)$$

$$B = \frac{\mathbf{T}_A \cdot \mathbf{T}_\pi}{(T_A + 1)(2T_A + 1)} [\mathbf{T}_A \cdot \mathbf{T}_\pi(T_A + 1)] \quad (3.119b)$$

and

$$A = 1 - B - C = 1 - \frac{(\mathbf{T}_A \cdot \mathbf{T}_\pi)^2}{T_A(T_A + 1)} \quad (3.119c)$$

For the v_2 term one obtains

$$e^{iv_2(\mathbf{T}_\pi \cdot \mathbf{T}_A)} = ae^{iv_2} + be^{iv_2 T_A^2} + ce^{iv_2(T_A + 1)^2} \quad (3.120)$$

where

$$c = \frac{(1 + \mathbf{T}_A \cdot \mathbf{T}_\pi)(\mathbf{T}_A \cdot \mathbf{T}_\pi - \mathbf{T}_A)}{(2T_A + 1)T_A} \quad (3.120a)$$

$$b = \frac{(1 + \mathbf{T}_A \cdot \mathbf{T}_\pi)(\mathbf{T}_A \cdot \mathbf{T}_\pi + T_A + 1)}{(2T_A + 1)(T_A + 1)} \quad (3.120b)$$

$$a = 1 - \frac{(2T_A + 1)(\mathbf{T}_\pi \cdot \mathbf{T}_A)^2 + 3(\mathbf{T}_\pi \cdot \mathbf{T}_A)}{T_A(2T_A + 1)(T_A + 1)} \quad (3.120c)$$

The quantity e^{ix} is

$$e^{ix} = e^{iv_0} \cdot e^{iv_1(\mathbf{T}_\pi \cdot \mathbf{T}_A)} \cdot e^{iv_2(\mathbf{T}_\pi \cdot \mathbf{T}_A)^2}$$

We note that the second factor contains both absorptive and regenerative terms. It is necessary, to conserve unitarity, that the net be absorptive, which condition limits the values of v_1 and therefore of V_1 . We shall not continue

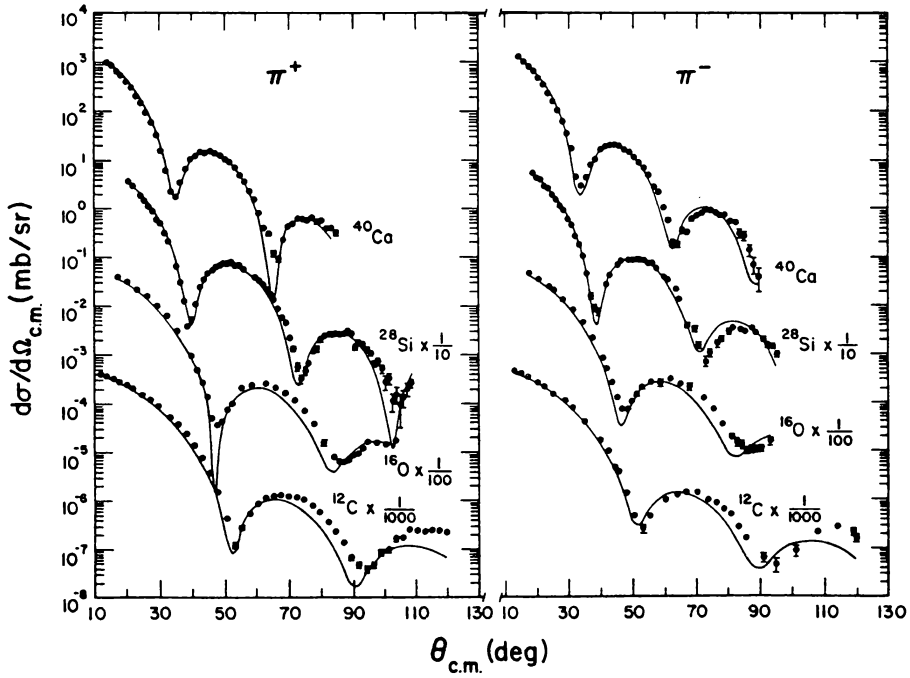


FIG. 3.14. Comparison of theoretical π^+ and π^- elastic scattering cross sections to data at $T_\pi = 164$ MeV for ^{16}O , ^{28}Si , ^{40}Ca , and ^{12}C . [From Greene, Harvey, et al. (84).]

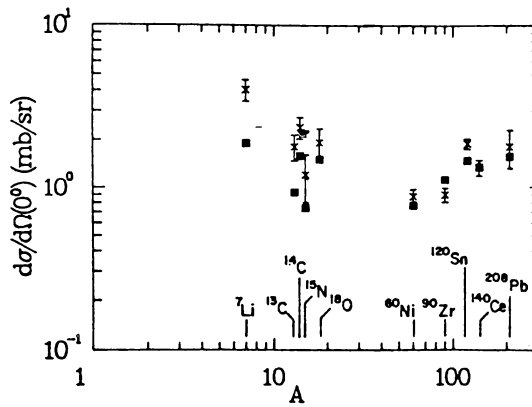


FIG. 3.15. Comparison of theoretical single charge exchange $d\sigma/d\Omega(0^\circ)$ to data at $T_\pi = 165$ MeV. The \times represent data and the \blacksquare represent theoretical result. [From Greene, Harvey, et al. (84).]

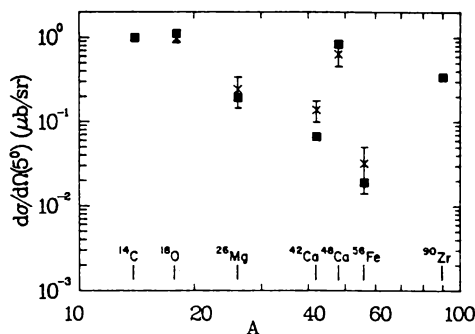


FIG. 3.16. Comparison of theoretical double charge exchange $d\sigma/d\Omega(5^\circ)$ to data at $T_\pi = 164$ MeV. The \times represent data and the \blacksquare represent theoretical results. [From Greene, Harvey, et al. (84).]

with development, as exploration of these results has not been made. They do demonstrate the possible importance of the vector and tensor components of V .

The phenomenological theory using potential equation (3.105) has been used by Greene, Harvey, et al. (84) to analyze pion single and double charge exchange scattering to isobaric analog states, and elastic scattering in the resonance region ($E_\pi = 164$ MeV). Suffice it to say that agreement with experiment is obtained as illustrated by Fig. 3.14 for elastic scattering, Figs. 3.15 and 3.16 for SCX and DCX. The DCX angular distribution obtained for ^{18}O and ^{26}Mg and when

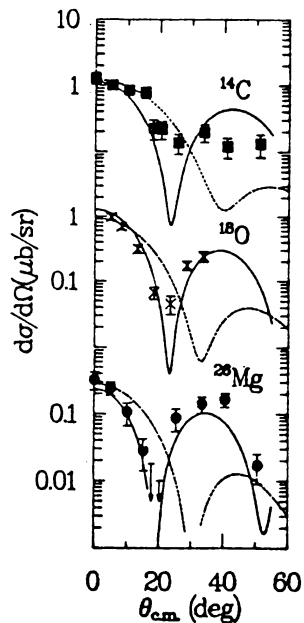


FIG. 3.17. Comparison of theoretical double charge exchange angular distributions to data at $T_\pi = 164$ MeV. The dashed curves are the lowest-order result. [From Greene, Harvey, et al. (84).]

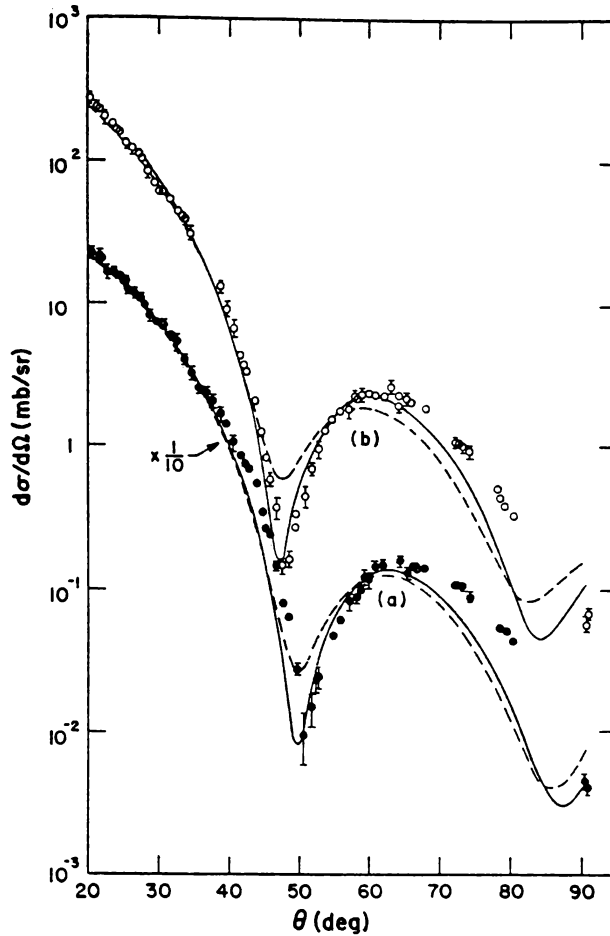


FIG. 3.18. Comparison of theoretical π^+ (a) and π^- (b) elastic scattering cross section from ^{14}C to data at $T_\pi = 164$ MeV. The solid and dashed curves are, respectively, results with and without the isospin-dependent terms in $U^{(2)}$. [From Greene, Harvey, et al. (84).]

the target nucleus is ^{14}C is shown in Figs. 3.17 and 3.18. This illustrates the importance of the tensor term, V_2 , in (3.105). One technical result of importance is the finding of Siciliano, Cooper, Johnson, and Leitch (86) that the plane wave approximation for the pion wave functions is inadequate.

The DCX reaction proceeds along two possible paths. In one a π^+ , for example, scatters from a nucleon becoming a π^0 . The π^0 then scatters a second time, becoming a π^- . This process is referred to as *sequential*. In the Δ - N interaction, the π^+ is absorbed by a target nucleon, forming a Δ^+ . The Δ^+ interacts with the nucleus via $t_{\Delta N}$ [see (3.102)], becoming a Δ^0 , which then decays into a π^- and a proton. Calculations of the DCX reaction at low pion

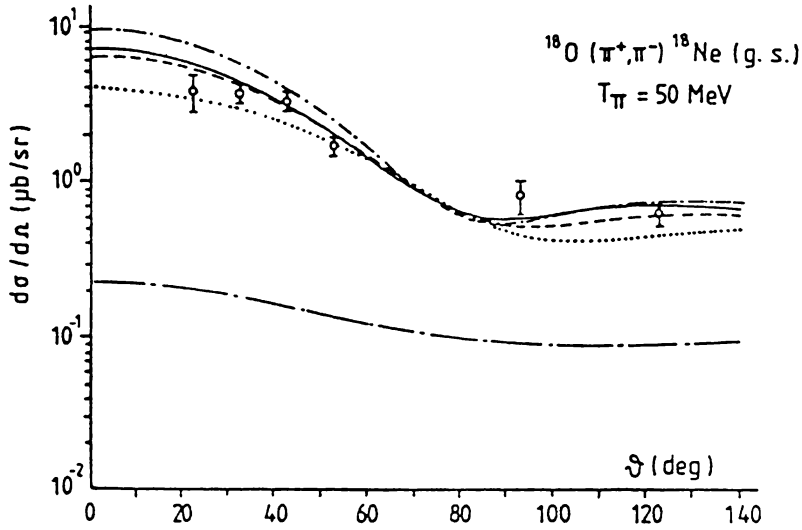


FIG. 3.19. $^{18}\text{O}(\pi^+, \pi^-)^{18}\text{Ne}(\text{g.s.})$ differential cross section: full sequential (solid curve), sequential, but keeping only the $J=0$ intermediate nuclear state (dotted-long-dashed curve), with Δ - N interaction of strength $\delta v = 0.5 - 1.0i$, $0.2 - 2.8i$, $1.0 + 0.4i \text{ fm}^2$ (dashed, dotted, and dotted-dashed curves, respectively). [From Karapiperis (89).]

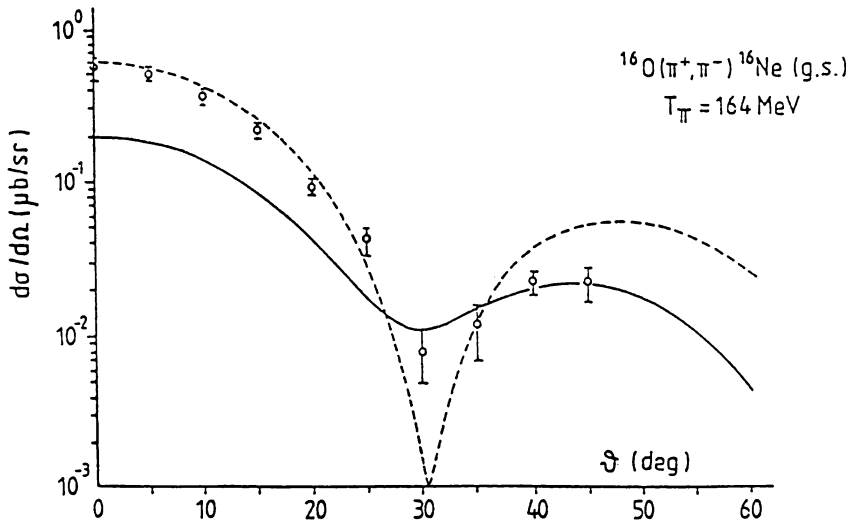


FIG. 3.20. Same as in Fig. 3.19 but for the reaction $^{16}\text{O}(\pi^+, \pi^-)^{16}\text{Ne}(\text{g.s.})$. [From Karapiperis (89).]

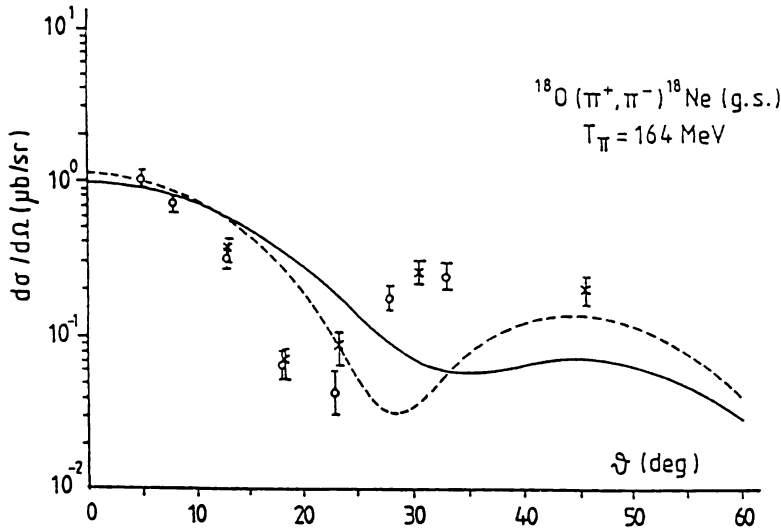


FIG. 3.21. $^{18}\text{O}(\pi^+, \pi^-)^{18}\text{Ne}(\text{g.s.})$ differential cross section: sequential (solid curve) and with Δ - N interaction of strength $\delta v = 2.0 - 0.4i \text{ fm}^2$ (dashed curve). [From Karapiperis (89).]

energies where the sequential process dominates ($\sim 50 \text{ MeV}$) have been successful. But calculations in the resonance region in the isobar hole model are not. For an analysis, see Karapiperis and Kobayashi (87) and Karapiperis (89). For an analysis from another point of view, see Siciliano, Johnson, and Sarafian (90). The isobar-hole model uses the analysis described earlier for elastic and inelastic scattering. The results for 50-MeV $^{18}\text{O}(\pi^+, \pi^-)^{18}\text{Ne}(\text{g.s.})$ are satisfactory. See Fig. 3.19. We see that the Δ - N process is relatively unimportant. Distortion effects are very important. At the higher energies good agreement is obtained for the $^{16}\text{O}(\pi^+, \pi^-)^{16}\text{Ne}(\text{g.s.})$. See Fig. 3.20. However, there is strong disagreement with the angular distribution in the reaction $^{18}\text{O}(\pi^+, \pi^-)^{18}\text{Ne}$ (Fig. 3.21), which is as yet unresolved. Disagreement with the $^{14}\text{C}(\pi^+, \pi^-)^{14}\text{O}(\text{g.s.})$ is also present. Reasons for these disagreements include possibly inadequate nuclear wave functions and the oversimplified form of $t_{\Delta, N}$, (3.105). The importance of nuclear structure has been emphasized by Auerbach, Gibbs, and Piasetsky (87) and Auerbach, Gibbs, Ginocchio, and Kaufmann (88).

4. KAON-NUCLEUS INTERACTION

The kaon is a pseudoscalar (odd parity, spin zero) boson. There are four varieties, the K^+ , K^0 , K^- , and \bar{K}^0 . The antiparticle of the K^+ is K^- , and of the K^0 , \bar{K}^0 . This differs from the photon and π^0 , which are identical with their antiparticles. The mass of the K^+ and K^0 are, respectively, 493.71 MeV and 497.70 MeV. The

K^0 and K^+ (and the K^- , \bar{K}^0) form an isospin- $\frac{1}{2}$ system. The kaon is a “strange” particle in that it has an additional internal quantum number of *strangeness* S . We shall use *hypercharge* Y rather than S , where

$$Y = B + S \quad (4.1)$$

and B is the baryon number. This permits a symmetrical classification of the bosons and fermions as illustrated by Fig. 4.1. The axes are the value of the z component of the isospin, T_3 , and Y . One observes that the fermion analog of the (K^0, K^+) isodoublet is the nucleon isodoublet; that of the pion isospin one system is the Σ isospin one system. The Σ^\pm mass is 1189.37 MeV and the Σ^0 mass is 1192.47 MeV. Finally, the (K^-, K^0) doublet is mirrored by the Ξ doublet, with the mass of the Ξ^- equal to 1321.29 MeV and the mass of the Ξ^0 1314.9 MeV. The masses of the isosinglet Λ^0 and η^0 are 1115.60 and 548.8 MeV, respectively. The spin of each of the particles in Fig. 4.1a is zero, while the spin of the particles in Fig. 4.1b is $\frac{1}{2}$. The particles in Fig. 4.1a are said to form the pseudoscalar octet, while those in Fig. 4.1b form the baryon spin- $\frac{1}{2}$ octet. This classification based on SU(3) symmetry is a generalization of the SU(2) isospin symmetry of the nucleon system. If SU(2) symmetry were exact, the neutron and proton would have the same mass and each would be an example of the nucleon. If SU(3) symmetry were exact, the masses of all the particles in Fig. 4.1a would be identical and one would refer to them as states of one particle, the pseudoscalar boson. Similarly, Fig. 4.1b represents a spin- $\frac{1}{2}$ baryon. As the masses are not the same, SU(3) symmetry is broken.

It will be useful for us to give the quark description of these particles. We shall need only the u (up), d (down), and s (strange) quarks and their antiparticles. These quarks are spin- $\frac{1}{2}$ fermions. The properties of these quarks are given in Table 4.1. In Table 4.2 we list the combinations for the various particles shown in Fig. 4.1. Note that the antiparticles of a quark q is written \bar{q} .

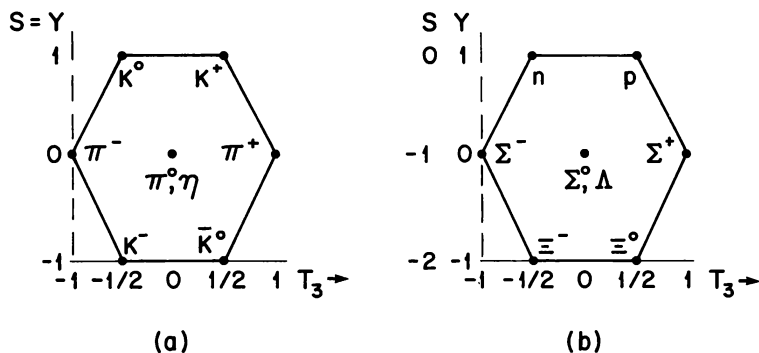


FIG. 4.1.

TABLE 4.1 Properties of the u , d , and s Quarks

Flavor	Charge	Strangeness	T_3	Baryon Number, B	Y
u	$\frac{2}{3}e$	0	$\frac{1}{2}$	$\frac{1}{3}$	$\frac{1}{3}$
d	$-\frac{1}{3}e$	0	$-\frac{1}{2}$	$\frac{1}{3}$	$\frac{1}{3}$
s	$-\frac{1}{3}e$	-1	0	$\frac{1}{3}$	$-\frac{2}{3}$
\bar{u}	$-\frac{2}{3}e$	0	$-\frac{1}{2}$	$-\frac{1}{3}$	$-\frac{1}{3}$
\bar{d}	$\frac{1}{3}e$	0	$\frac{1}{2}$	$-\frac{1}{3}$	$-\frac{1}{3}$
\bar{s}	$\frac{1}{3}e$	1	0	$-\frac{1}{3}$	$\frac{2}{3}$

TABLE 4.2 Quark Composition of Hadrons

Baryons		Bosons ^a	
p	(uud)	K^+	$(u\bar{s})$
n	(udd)	K^0	$(d\bar{s})$
$\Sigma\Lambda$	$(uds), (uus), (dds)$	π, η	$(\bar{u}d)(\bar{u}u)(\bar{d}d)(u\bar{d})$
		\bar{K}^0	$(\bar{d}s)$
Ξ	$(uss), (dss)$	K^-	$(\bar{u}s)$

^aThis list omits the $(\bar{s}s)$ combination, leading to the existence of another particle, the η' . In fact, both the η and η' contain the $\bar{s}s$ combinations: $\eta = 1/\sqrt{6}(u\bar{u} + d\bar{d} - 2s\bar{s})$ and $\eta' = 1/\sqrt{3}(u\bar{u} + d\bar{d} + s\bar{s})$. Within the SU(3) framework we are using, the η is included in Fig. 4.1a octet, while the η' is regarded as a singlet.

This quark description must be used with some care. The *constituent quarks*, as they are sometimes called, are quasi-particles, as their environment is rich with quark-antiquark pairs as well as gluons. Moreover, we have not assigned spin and still another internal degree of freedom, called *color*. All this is presumably a consequence of *Quantum Chromodynamics* (QCD). We shall not describe that theory here, as we shall be concerned only with qualitative considerations. The interested reader will find the details in a number of references [Gottfried and Weisskopf (84, 86); Close (79); Gasirowicz (66), Lee (81)]. The reader should confirm that the isospin of the baryons and bosons can be deduced from the isospin of the constituent quarks.

The conservation of isospin in the strong interactions is expanded by the additional requirement of the conservation of strangeness. The latter condition is illustrated by the fact (for example) that $\pi^- + p \rightarrow K^+ + \Sigma^-$ is allowed but $\pi^- + p \rightarrow K^- + \Sigma^+$ is forbidden. More compactly, the strong interactions are SU(3) symmetric [i.e., the strong interactions commute with the generators of the SU(3) group]. From the quark point of view, for sufficiently low-energy phenomena one need consider only the u , d , and s quarks. The other known quarks, the c (charm) and b (bottom), are much more massive than the u , d ,

and s . The c mass is 1.5 GeV and the b mass 5 GeV greater than the mass of the u and d .

SU(3) symmetry is broken. The masses of the members of the spin- $\frac{1}{2}$ octet and of the pseudoscalar boson octet differ substantially. In terms of the constituent quarks, the mass of the strange quark, s , is about 150 MeV greater than the mass of the up and down quarks, whose masses are equal. This heavier mass for the strange quark provides much of the observed mass differences. In addition, the spin- and color-dependent forces between quarks generated by the exchange of colored gluons provide additions to the mass of the composites. This interaction also breaks symmetry since these exchange forces are mass dependent. These, together with the larger mass of the s quark, suffice to explain the mass spectrum of both the spin- $\frac{1}{2}$ baryons and the pseudoscalar bosons. [See Close (78) for the details.]

At large distances the baryon-baryon interaction is generated by the exchange of bosons [the singlet η' , the pseudoscalar, and the vector (ρ , ω , etc.)]. Because of the difference in the boson masses, there will be strong symmetry breaking. For example, the one-boson exchange ΛN nucleon interaction, because of isospin conservation, involves the exchange of a kaon, while the pion mediates ΣN interaction (see Fig. 4.2). Since the mass of the kaon is larger than that of the pion, the ΛN interaction will have a range much shorter than that of the ΣN interaction. At small interparticle distances, the six-quark system must be considered. One would speculate that symmetry breaking would be weaker in this case. It has also been speculated that the $\Sigma N \rightarrow \Lambda N$ transition matrix element breaks SU(3) symmetry weakly [Dover and Feshbach (87, 90)].

The antiparticle of the K^0 , \bar{K}^0 is not identical with K^0 , differing in this respect from the π^0 or the photon γ for which the particle-antiparticle equality does prevail. This unique property of the K^0 system has important consequences. It surfaces in the pionic decays of the kaons. These violate conservation of strangeness and are therefore governed by the weak interactions. These (as well as the strong interactions) conserve CP , although neither C nor P is separately conserved. We recall the C is the operator that converts a particle into an antiparticle, while P is the parity operator that gives the effect of reflecting all the spatial coordinates ($\mathbf{r} \rightarrow -\mathbf{r}$) in a state. Since $C^2 = P^2 = 1$,

$$CPK^0 = e^{i\phi} \bar{K}^0$$

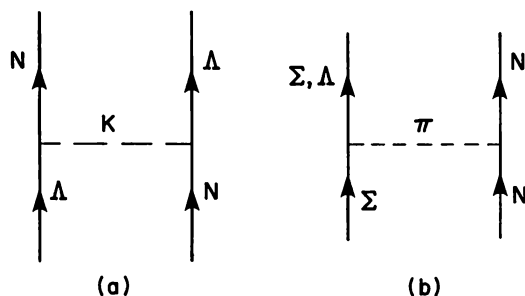


FIG. 4.2.

and

$$CP\bar{K}^0 = e^{-i\phi}K^0$$

We use the customary convention, $\phi = 0$, so that

$$\begin{aligned} CPK &= \bar{K}^0 \\ CP\bar{K}^0 &= K^0 \end{aligned} \quad (4.2)$$

Photons are odd under C . Since π^0 decays into two photons

$$C\pi^0 = \pi^0$$

so that the π^0 is an eigenstate of C . But the π^0 is a pseudoscalar, so that

$$CP\pi^0 = -\pi^0$$

We now consider the weak decay of the kaons into $\pi\pi$ and $\pi\pi\pi$. Since the spin of the kaon is zero, the two pions are in an $l = 0$ orbital state. The intrinsic parity of the two pions is $+1$ and the orbital state is even under parity. Thus the parity of the two-pion final state is even. If the two pions are π^0 's, the operator C will not affect them. If they are a π^+ and π^- , C will interchange them. However, they are in a relative $l = 0$ orbit and their state is thus unchanged by C . Hence the two pion state formed by the decay of the kaon has even CP .

Consider next the three-pion system $\pi^0\pi^0\pi^0$. Our conclusion will be valid for kaon decays involving charged pions. Since they are bosons and their total spin is zero, they are in a spatially symmetric state (i.e., the exchange of any two will not affect the three-pion wave function. Under these circumstances the spatial parity of the three-pion system is even but the intrinsic parity of each is odd, so that finally the parity is odd. Since $C = 1$ for each of the pions, CP for the three-pion decay is odd.

Since the weak interaction is CP invariant, K^0 and \bar{K}^0 are not eigenstates of H , the total Hamiltonian, $H_{\text{strong}} + H_{\text{weak}}$. The eigenstates of H are

$$\begin{aligned} K_1 &= \frac{1}{\sqrt{2}}(K^0 + \bar{K}^0) \\ K_2 &= \frac{1}{\sqrt{2}}(K^0 - \bar{K}^0) \\ K^0 &= \frac{1}{\sqrt{2}}(K_1 + K_2) \\ \bar{K}^0 &= \frac{1}{\sqrt{2}}(K_1 - K_2) \end{aligned} \quad (4.3)$$

The state K_1 is even under CP , while K_2 is odd. The K_1 will therefore decay into two pions and the K_2 will decay into three pions. Thus if K^0 is produced in a reaction, its composition will change with time. If

$$\begin{aligned} HK_1 &= \left(m_1 - \frac{i\Gamma_1}{2}\right)K_1 \\ HK_2 &= \left(m_2 - \frac{i\Gamma_2}{2}\right)K_2 \end{aligned} \quad (4.4)$$

then

$$K^0(t) = \frac{1}{\sqrt{2}}(e^{-im_1t - \Gamma_1 t/2} K_1 + e^{-im_2t - \Gamma_2 t/2} K_2) \quad (4.5)$$

Note that (4.4) holds only in the rest frame of K_1 and K_2 . The short lifetime \hbar/Γ_1 is 0.89×10^{-10} s, while the long lifetime \hbar/Γ_2 is 0.52×10^{-7} s. We see from (4.5) that the mixture of $S = 1$ and $S = -1$ changes with time. Eventually, $K_0 \rightarrow K_2$ with equal amplitudes for K_0 and \bar{K}_0 . Moreover, the amplitudes of the K_1 and K_2 components can be obtained by measuring the ratio of 2π to 3π decays. From this result, using (4.5), the mass difference between K_1 and K_2 can be determined. It equals 3.52×10^{-6} eV.

Suppose that a beam of neutral kaons are incident on a nucleus. These kaons will all be in the K_2 state if a sufficient time has elapsed from the time of production. But the K_0 and \bar{K}_0 components of K_2 will scatter differently with amplitudes f and \bar{f} , respectively. The kaon wave function will then become

$$\begin{aligned} K_2 &\rightarrow \frac{1}{\sqrt{2}}(fK^0 - \bar{f}\bar{K}^0) \\ &= \frac{1}{2}[(f - \bar{f})K_1 + (f + \bar{f})K_2] \end{aligned} \quad (4.6)$$

As a consequence of the scattering, some K_1 has been produced. This phenomenon is referred to as *regeneration* [Pais and Piccioni (55)]. The incident beam particles could only decay into three pions. After the scattering, two-pion decay can also occur because of the presence of K_1 in (4.6). By measuring the two- and three-pion decays, one can determine the amplitudes f and \bar{f} .

The discussion above is not entirely correct, for it is found that the long-lived kaon, which is referred to as K_L , decays into *both* 3π and 2π final states (Christenson, Cronin, Fitch, and Turlay (64)). Thus CP cannot be conserved. K_L must be a linear combination of K_1 and K_2 :

$$K_L = \frac{1}{\sqrt{1 + \varepsilon^2}}(K_2 + \varepsilon K_1) \quad (4.7)$$

The particle K_S , which has a short lifetime, is given by

$$K_S = \frac{1}{\sqrt{1 + \varepsilon^2}}(K_1 + \varepsilon K_2) \quad (4.8)$$

The measured value of ε is $(1.6)(1 + i) \times 10^{-3}$. Up to this time, no other system has exhibited CP violation. Since ε is small, for most of the phenomena to be discussed we can disregard the differences between K_L and K_2 and K_S and K_1 :

$$K_L \simeq K_2 \quad K_S \simeq K_1$$

A. Kaon–Nucleon Scattering[†]

The study of kaon–nucleon reactions is far from achieving the completeness that we have seen to exist in the pion case. The associated phenomenology is therefore less secure. But there are some broad features that are understood qualitatively and in some cases quantitatively, which are of importance for an understanding of kaon-induced nuclear reactions. *Many of the numerical values given in the discussion must be regarded as tentative.*

The reactions induced by K^- beams incident on the nucleon are qualitatively different from those induced by K^+ beam. This can be seen in Figs. 4.3 and 4.4. One observes the complex structure of the K^- total cross section. These are a consequence of a number of resonances that are tabulated in Tables 4.3 and 4.4 for the energy range considered in Fig. 4.3.

In these tables the column labeled $L_{T,2J}$ gives the possible spatial configuration for each of these composite particles. The column labeled “dominant channel” indicates the most probable decay modes and therefore the most likely

TABLE 4.3

$T = 0$	$L_{T,2J}$	$\Gamma(\text{MeV})$	Dominant Channel	Mass (MeV)
Λ (1405 MeV)	S_{01}	40 ± 1	$\bar{K}N$	1405 ± 5
Λ (1520)	D_{03}	15.6 ± 1	$\bar{K}N, \Sigma\pi$	1519.5 ± 1.0
Λ (1600)	P_{01}	50 – 250	$\Sigma\pi, \bar{K}N$	1560 – 1700
Λ (1670)	S_{01}	25 – 50	$\Sigma\pi$	1660 – 1680
Λ (1690)	D_{03}	50 – 70	$\Sigma\pi, \bar{K}N$	1685 – 1695
Λ (1800)	S_{01}	200 – 400	$\bar{K}N$	1720 – 1850
Λ (1810)	P_{01}	50 – 250	$\Sigma\pi$	1750 – 1850
Λ (1820)	F_{05}	70 – 90	$K^*(892)N$	1815 – 1825
Λ (1830)	D_{05}	60 – 110	$\Sigma\pi$	1810 – 1830

Source: “Review of Particle Properties,” Particle Data Group, *Phys. Lett. B* 204(1988).

[†]Dover and Walker (82); Arndt and Roper (85); Dalitz, McGinlay, Belyca, and Anthony (82).

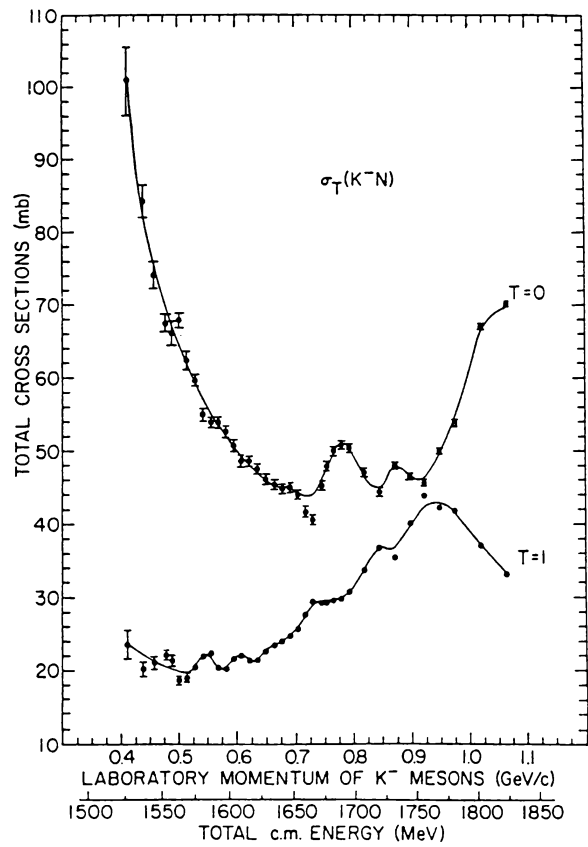


FIG. 4.3. Total K^- -nucleon cross sections for isospin $T = 0$ and $T = 1$. [From Carroll, Chiang, et al. (76).]

TABLE 4.4

$T = 1$	$L_{T,2J}$	Γ (MeV)	Dominant Channel	Mass (MeV)
$\Sigma^* (1385)$	P_{13}	36 ± 1	$\Lambda\pi$	1382.8 ± 0.4
$\Sigma^0 (1385)$				1383.7 ± 1.0
$\Sigma^- (1385)$				1387.2 ± 0.6
$\Sigma (1660)$	P_{11}	40 – 200	$\bar{K}N$	1630 – 1690
$\Sigma (1670)$	D_{13}	40 – 80	$\Sigma\pi$	1665 – 1685
$\Sigma (1750)$	S_{11}	60 – 160	$\bar{K}N, \Sigma\eta$	1730 – 1800
$\Sigma (1775)$	D_{15}	105 – 135	$\bar{K}N, \Lambda\pi$	1770 – 1780

Source: "Review of Particle Properties," Particle Data Group, *Phys. Lett B* 204 (1988).

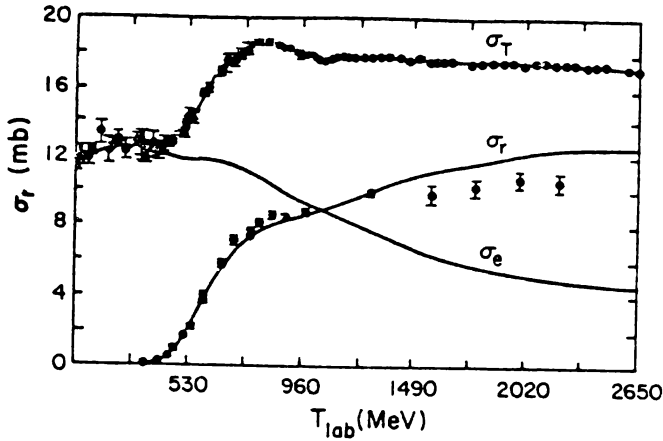


FIG. 4.4. Total (σ_T), inelastic (σ_r), and elastic (σ_e) K^+p cross sections. [From Arndt and Roper (85).]

production reactions. The $K^*(892)$ is a spin-1 particle with the same strangeness as the K . It is a member of the spin-1 octet that includes the ρ as a member. One can conclude from the rich spectrum seen in these tables that the $\bar{K}N$ system is strongly interactive.

The picture for the K^+N system is strikingly different, as we can see from Fig. 4.4. The total cross section for $K^+ + N$ is relatively constant up to a kaon laboratory kinetic energy of about 0.4 GeV ($p_L = 0.745$ MeV/c, $E_{cm} = 1.674$ GeV), after which there is a relatively steep rise up to about 0.8 GeV in the laboratory, after which it is relatively constant. Below 0.4 GeV, $\sigma_T \sim 1.2$ mb, while for energies greater than 0.8 GeV, $\sigma_T \sim 1.7$ mb. The last is the sum of a decreasing elastic cross section, σ_e , and a rising reaction cross section, σ_r . Three resonances are reported by Arndt and Roper (85), who find the evidence for $Z^*(1780)$ as strong; there are two other resonances listed as “highly probable” (see Table 4.5). In the “*Review of Particle Properties*,” these resonances are considered to be uncertain. The difference between the NK and $\bar{K}N$ systems can be qualitatively understood by considering the quark structure in each case. The kaon, \bar{K} , is made up of $\bar{u}s$, while the nucleon, say the proton, contains two u ’s and one d . The \bar{u} in the kaon and the u in the proton can annihilate, going off, for example,

TABLE 4.5

$T = 1$	$L_{T,2J}$	Γ (MeV)
$Z^*(1780)$	P_{13}	280
$Z^*(1725)$	P_{11}	180
$Z^*(2161)$	D_{15}	320

as a pion leaving behind usd , a Λ or Σ^0 . When the incident kaon is K^+ , which is a $u\bar{s}$ system, no such annihilation can occur and we are left with a five-quark system $uuud\bar{s}$. This system ($uuu = \Delta^{++}$, $d\bar{s} = K^0$) suggests the existence of an inelastic channel ΔK . Its threshold (for $K^+\Delta^+$) is 1725.67 MeV near to one of the Z^* resonances. One expects that the probability of forming a five-quark resonance in the low-energy domain is much less probable than that of forming a three-quark resonance.

B. The KN System[†]

The reactions that are relevant are:

	$K + N \rightarrow K + N$
Elastic	$K^+ + n \rightarrow K^+ + p$
	$K_L^0 + p \rightarrow K_S^0 + p$
	$K + N \rightarrow K + N + \pi$
Inelastic	$K + N \rightarrow \Delta + K$
	$K + N \rightarrow K^* + N$
	0.305 GeV/ c
Threshold (p_{cm})	0.466
	0.552

In these equations N can be either a neutron or a proton and K, K^+ , or K^0 . Let $f_2^{(1)}$ be the amplitude in the $T = 1$ channel and $f_2^{(0)}$ be the amplitude in the $T = 0$ channel for $Y = 2$. Then from isospin conservation, one obtains

$$f(K^+p \rightarrow K^+p) = f_2^{(1)} \quad (4.9a)$$

$$f(K^+n \rightarrow K^+n) = \frac{1}{2}(f_2^{(1)} + f_2^{(0)}) \quad (4.9b)$$

$$f(K^+n \rightarrow K^0p) = \frac{1}{2}(f_2^{(1)} - f_2^{(0)}) \quad (4.9c)$$

If $f_0^{(1)}$ and $f_0^{(0)}$ are the amplitudes for $Y = 0$, then

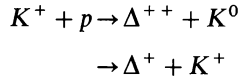
$$f(K_L^0p \rightarrow K_S^0p) = \frac{1}{4}(f_2^{(1)} + f_2^{(0)} - 2f_0^{(1)}) \quad (4.10)$$

Similarly,

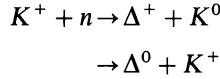
$$\sigma(K^+ + n \rightarrow \Delta + K) = \frac{1}{5}\sigma(K^+ + p \rightarrow \Delta + K) \quad (4.11)$$

[†]Corden, Cou, et al. (82); Arndt and Roper (85).

In this reaction



and



From (4.11) we conclude that Δ production by K^+ in nuclei will be sensitive to the proton distribution. In the regeneration reaction amplitude, (4.10), $f_0^{(1)}$ is obtained from K^-p elastic scattering data, while $f_2^{(1)}$ is given by elastic K^+p scattering. Thus from the measurement of $f(K_L^0 p \rightarrow K_S^0 p)$ together with K^-p and K^+p elastic scattering data, one can obtain the $T=0$, $Y=2$ amplitude. Much of the same information can be obtained from elastic scattering of K^+ by neutrons [Eq. (4.9b)] and from charge exchange scattering [Eq. (4.9c)].

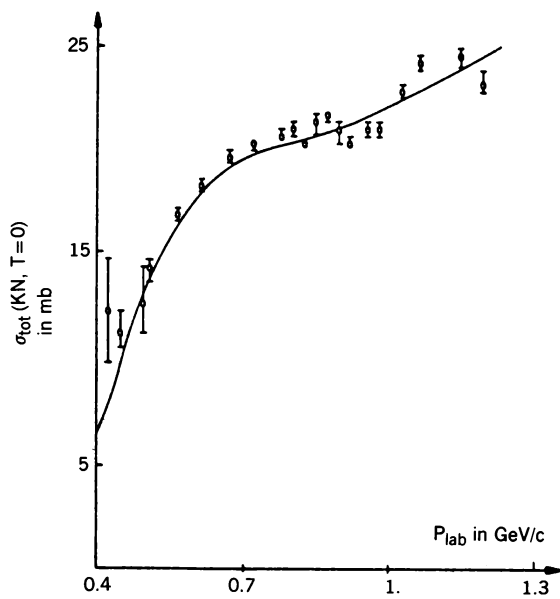
Since we are dealing with the scattering of a spin-zero particle (K) by a spin- $\frac{1}{2}$ particle (N), the partial wave analysis of the scattering and polarization is identical with that described earlier in this chapter from an analysis of pion-nucleon scattering. The scattering amplitude is (see 2.16)

$$\hat{f} = f + i\boldsymbol{\sigma} \cdot \mathbf{n}g \quad (4.12)$$

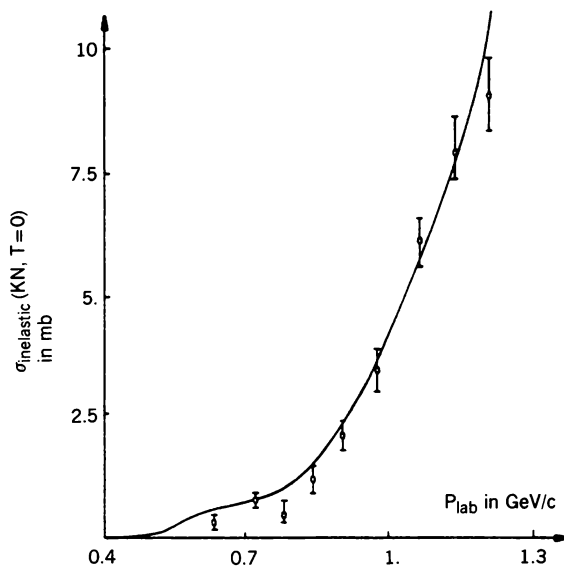
where f and g are functions of the center-of-mass energy and the spherical angles ϑ and φ , while \mathbf{n} is a unit vector perpendicular to the scattering plane. The expressions for the scattering cross section, the polarization, and the spin rotation parameter in terms of f and g are given by 2.20 and 2.20'. We recall that two phase shifts are associated with each value of the angular momentum, $\delta_{l+1/2}$ and $\delta_{l-1/2}$. The relations given by (4.9) are satisfied by both f and g of (4.12).

The $T=1$ total and inelastic cross section is given in Fig. 4.4. This is supplemented in Fig. 4.5 by the $T=0$ total and inelastic cross sections, in Fig. 4.6 by the $K_L^0 p \rightarrow K_S^0 p$ cross section, in Fig. 4.7 by the $K^+ n \rightarrow K^0 p$ cross section, and by Fig. 4.8 giving the angular distribution for $K^+ p$ ($T=1$) elastic scattering for a range in K^+ momentum.

The elastic cross section is isotropic up to K^+ laboratory momentum of 800 MeV/c, corresponding to the dominance of the partial wave $L_{T,2J} = S_{11}$. Above 800 MeV/c higher values of L must be added as the angular distribution becomes anisotropic. Coulomb interference at small angles indicate that the S_{11} amplitude is repulsive. We observe that the charge exchange scattering $K^+ n \rightarrow K^0 p$ is important only in the neighborhood of K^+ momentum equal to 800 MeV/c. Note that $K^+ n$ scattering and charge exchange scattering must be deduced from K^+ collisions with deuterons.



(a)



(b)

FIG. 4.5. Total (σ_{tot}) and inelastic ($\sigma_{\text{inelastic}}$) cross sections for KN scattering. [From Corden, Cox, et al. (82).]

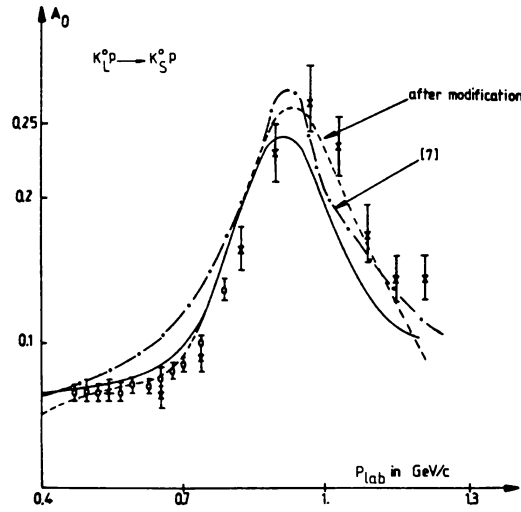


FIG. 4.6. Cross section for $K_L^0 \rightarrow K_S^0 p$. The preferred fit is given by the solid line. [From Corden, Cox, et al. (82).]

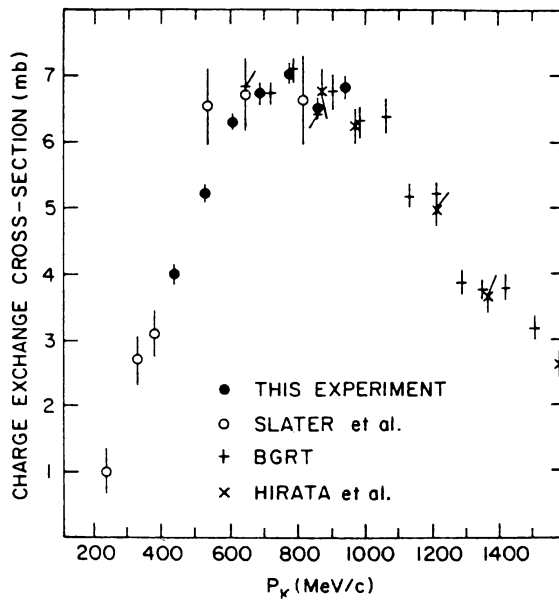


FIG. 4.7. Cross section for $K^+ n \rightarrow K^0 p$ charge exchange. [From Darnerell, Hotchkiss, et al. (85).]

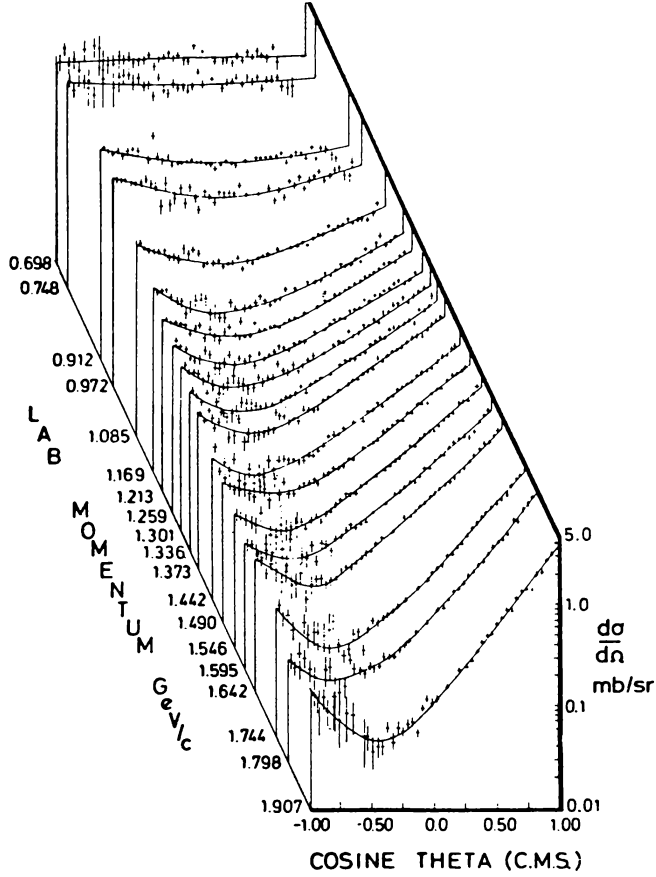


FIG. 4.8. Differential cross sections for K^+p elastic scattering. Below 700 MeV/c angular distribution is nearly isotropic. $S_{1/2}$, $T = 1$ channel dominates. [From Charles, Cowan, et al. (77); Charles, Cowan (72).]

The data at low energies can be summarized in terms of scattering length a , and effective range r , for S -wave scattering and scattering volume for the P -wave amplitudes. The effective range expansion is

$$k^{2l+1} \cot \delta = \frac{1}{a} + \frac{1}{2} r k^2 \quad (4.13)$$

For isospin $T = 1$ and S wave,

$$\begin{aligned} a_L(T, 2J) &= a_S(1, 1) \simeq -0.309 \pm 0.002 \text{ fm} \\ r_L(T, 2J) &= r_S(1, 1) \simeq 0.32 \pm 0.02 \text{ fm} \end{aligned} \quad (4.14)$$

where we use the data of Cameron et al. (74). For the P -wave amplitudes

$$\begin{aligned} a_P(1, 1) &= -0.021 \text{ fm} \\ a_P(1, 3) &= 0.013 \text{ fm} \end{aligned} \quad (4.15)$$

For $T = 0$,

$$\begin{aligned} a_S(0, 1) &\sim -0.035 \text{ fm} \\ a_P(0, 1) &\sim 0.086 \text{ fm} \\ a_P(0, 3) &\sim -0.019 \text{ fm} \end{aligned} \quad (4.16)$$

where we have used the data of Martin (75). A summary of the data is given by Dover and Walker (82). From their summary we see that there is agreement among various experiments on the signs and magnitude of a (two significant figures) and r (one significant figure) for $T = 1$. For $T = 0$ there is no agreement on sign. As regards magnitude, there is agreement that the $T = 0$ scattering lengths and volumes are small and are considerably smaller than the comparable $T = 1$ quantities.

At higher energies a phase-shift analysis for $T = 1$ has been made by Arndt and Roper (85). Their analysis led to claims of the three resonances listed in Table 4.5. Their match with the data is shown in Figs. 4.4 and 4.9. Of special interest are the P_{13} amplitudes shown in Fig. 4.10 and the corresponding Argand diagram Fig. 4.11. We see that the P_{13} resonance is strongly inelastic, as it differs sharply from the bounding circle valid for elastic scattering.

Note on the Argand Diagram. We write the S matrix

$$S = e^{2i\delta} \frac{E - E_r - i\Gamma'/2}{E - E_r + i\Gamma/2} = e^{2i\delta} \frac{E - E_r - i\Gamma/2 + i\Delta/2}{E - E_r + i\Gamma/2}$$

where δ is the potential scattering phase shift, E_r the resonance energy, Γ the width, and $\Delta = \Gamma - \Gamma'$. When the scattering is elastic, $\Gamma' = \Gamma$ and $\Delta = 0$. The transition amplitude is taken to be

$$\mathcal{T} = \frac{(S - 1)}{2i}$$

If $S = e^{2i\delta}$, $\mathcal{T} = \sin \delta e^{i\delta}$. Letting

$$\tan \phi = \frac{\Gamma}{2(E - E_r)}$$

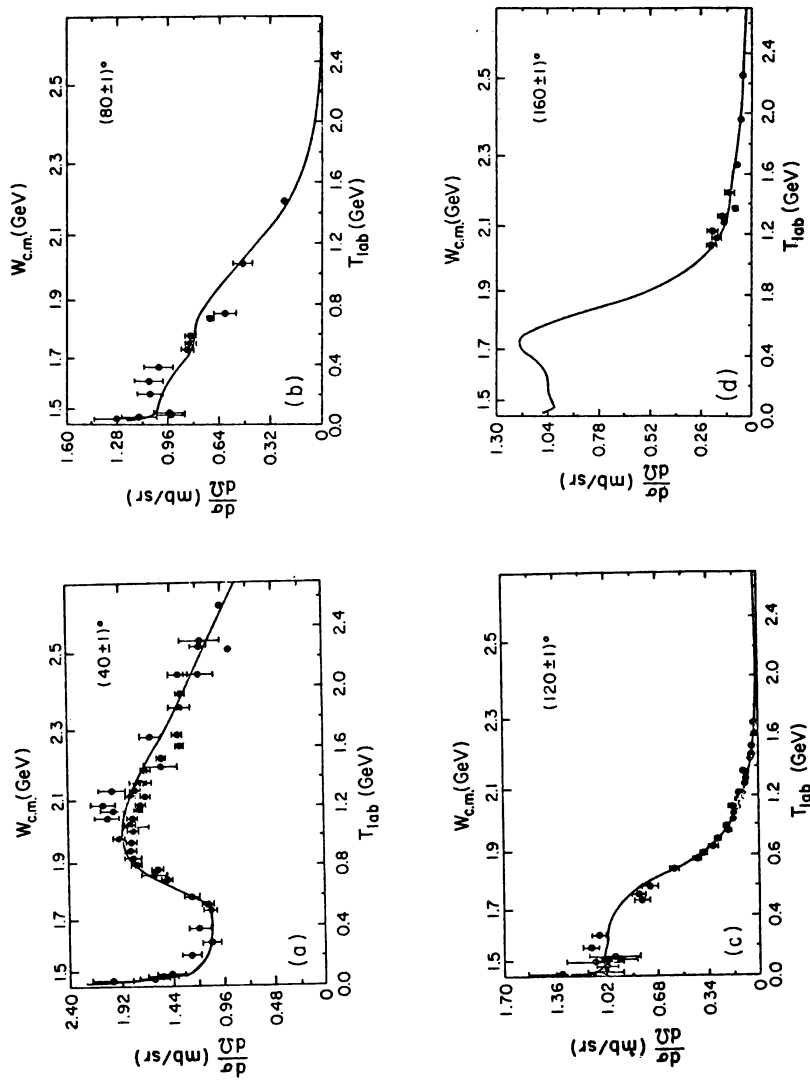


FIG. 4.9. Representative differential cross section data together with Arndt and Roper's predictions for $K^+ p$ scattering. [From Arndt and Roper (85).]

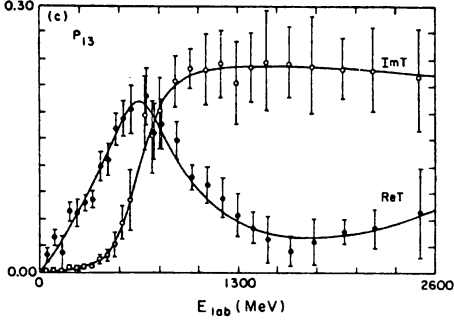


FIG. 4.10. P_{13} scattering amplitude. [From Arndt and Roper (85).]

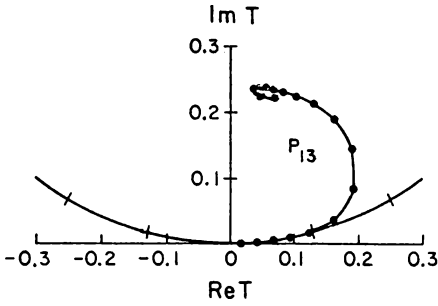


FIG. 4.11. Argand diagram for P_{13} amplitude. [From Arndt and Roper (85).]

one finds that

$$\operatorname{Re} \mathcal{T} = -\sin(\phi - \delta) \cos(\phi - \delta) + \frac{\Delta}{4H} \cos(\phi - 2\delta) \quad (4.17a)$$

$$\operatorname{Im} \mathcal{T} = \sin^2(\phi - \delta) - \frac{\Delta}{4H} \sin(\phi - 2\delta) \quad (4.17b)$$

$$|\mathcal{T}|^2 = \sin^2(\phi - \delta) - \frac{\Delta}{2H} \sin(\phi - \delta) \cos \delta + \frac{\Delta^2}{16H^2} \quad (4.17c)$$

where

$$H = \left[(E - E_r)^2 + \frac{\Gamma^2}{4} \right]^{1/2}$$

Consider first the simplest case ($\delta = 0$, $\Delta = 0$), so that

$$\operatorname{Re} \mathcal{T} \rightarrow -\sin \phi \cos \phi = -\frac{1}{2} \sin 2\phi$$

$$\operatorname{Im} \mathcal{T} = \sin^2 \phi = \frac{1}{2}(1 - \cos 2\phi)$$

Therefore,

$$(\operatorname{Re} \mathcal{T})^2 + (\operatorname{Im} \mathcal{T} - \frac{1}{2})^2 = \frac{1}{4}$$

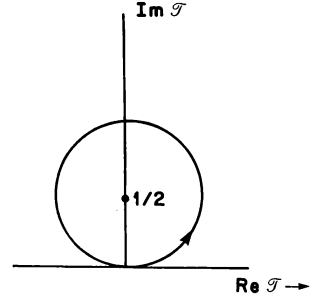


FIG. 4.12. Argand diagram.

A plot in which the horizontal axis is $\text{Re } \mathcal{T}$ and the vertical axis is $\text{Im } \mathcal{T}$ will be a circle of radius $\frac{1}{2}$ with the center on the vertical axis at $\frac{1}{2}$ (Fig. 4.12). For E negatively infinite, $\phi = 0$, and $\text{Re } \mathcal{T} = 0$ and $\text{Im } \mathcal{T} = 0$. As E increases, one travels counterclockwise, reaching the top of the circle at the resonance energy, $E = E_r$, where $\phi = \pi/2$, so that $\text{Re } \mathcal{T} = 0$ and $\text{Im } \mathcal{T} = 1$.

The second case is the most common, $\delta = 0$, Δ finite;

$$\text{Re } \mathcal{T} = -\sin \phi \cos \phi + \frac{\Delta}{4H} \cos \phi$$

$$\text{Im } \mathcal{T} = \sin^2 \phi - \frac{\Delta}{4H} \sin \phi$$

$$|\mathcal{T}|^2 = \sin^2 \phi - \frac{\Delta}{2H} \sin \phi + \frac{\Delta^2}{16H^2}$$

At resonance $\phi = \pi/2$,

$$|\mathcal{T}|^2 = \left(1 - \frac{\Delta}{4H}\right)^2 = \left(1 - \frac{\Delta}{2\Gamma}\right)^2 \quad (4.18)$$

so that the locus of $\text{Re } \mathcal{T}$, $\text{Im } \mathcal{T}$, will be in the interior of the circle. Moreover, at resonance

$$\text{Re } \mathcal{T} = 0 \quad (4.19)$$

From Fig. 4.11 one sees that the amplitude for the P_{13} partial wave does approach the $\text{Im } \mathcal{T}$ axis. The extrapolated value of $\text{Im } \mathcal{T}$ at $\text{Re } \mathcal{T} = 0$ is about 0.25 or $\Delta/\Gamma = 1$. The partial wave reaction cross section is

$$\sigma_r = \frac{\pi}{k^2} (1 - |S|^2) (2J + 1)$$

Inserting the expression for $|S|$, one finds that

$$1 - |S|^2 = \frac{\frac{1}{4}(2\Gamma\Delta + \Delta^2)}{(E - E_r)^2 + \Gamma^2/4}$$

At $E = E_r$,

$$1 - |S|^2 \rightarrow \frac{2\Delta\Gamma + \Delta^2}{\Gamma^2} = 2\frac{\Delta}{\Gamma} + \left(\frac{\Delta}{\Gamma}\right)^2$$

relating Δ/Γ to the inelasticity seen in (4.18).

C. The $\bar{K}N$ Reaction[†]

Because of the existence of the Λ^0 at 1405 MeV and the Σ at 1385 MeV, this reaction is much more complex than the KN reaction. Note that the mass of the $\bar{K}p$ system is 1431.9 MeV, so that a conversion of the $\bar{K}p$ system to $\pi\Sigma$ or a $\pi^0\Lambda^0$ is energetically possible. Therefore, in addition to elastic scattering,

$$K^- + p \rightarrow K^- + p$$

we also have the open channels

$$K^- + p \rightarrow \pi^0\Lambda^0 + 180 \text{ MeV}, \quad T = 1$$

$$K^- + p \rightarrow \pi\Sigma + 100 \text{ MeV}, \quad T = 1, 0$$

as well as the charge exchange scattering channel,

$$K^- + p \rightarrow \bar{K}^0 + n$$

Isospin invariance connects the cross sections for these reactions:

$$\sigma(K^- n \rightarrow \pi^- \Lambda) = 2\sigma(K^- p \rightarrow \pi^0 \Lambda) \quad (4.20)$$

and

$$\sigma(K^- n \rightarrow \pi^- \Sigma^0) = \sigma(K^- p \rightarrow \pi^+ \Sigma^-) + \sigma(K^- p \rightarrow \pi^- \Sigma^+) - 2\sigma(K^- p \rightarrow \pi^0 \Sigma^0) \quad (4.21)$$

The analysis of this experimental data was pioneered by Dalitz and Tuan (60), who made use of the \mathcal{N} matrix (see Chapter III, p. 169, and Appendix A). The

[†]Note that \bar{K} can refer to either K^- or \bar{K}^0 .

\mathcal{K} matrix is related to the \mathcal{T} and S matrices are follows:

$$\mathcal{K} = \mathcal{T} + i\pi\mathcal{K}\delta(E_i - E_f)\mathcal{T} = \mathcal{T} + i\pi\mathcal{T}\delta(E_i - E_f)\mathcal{K} \quad (4.21a)$$

$$S = 1 - 2\pi i\delta(E_i - E_f)\mathcal{T} \quad (4.21b)$$

$$S = \frac{1 - i\pi\delta(E_i - E_f)\mathcal{K}}{1 + i\pi\delta(E_i - E_f)\mathcal{K}} \quad (4.21c)$$

From (4.21c) we note that the unitarity of the S matrix implies that \mathcal{K} is Hermitian. Second, because of time reversal invariance, \mathcal{K} is real.

Equation (4.21a) is simplified greatly if it is restricted to a given partial wave. Then \mathcal{K} and \mathcal{T} become matrices involving the various channels. For $T = 0$,

$$\mathcal{K} = \begin{pmatrix} \kappa_{NN} & \kappa_{N\Sigma} \\ \kappa_{N\Sigma} & \kappa_{\Sigma\Sigma} \end{pmatrix} \quad T = 0 \quad (4.22)$$

where

$$\kappa_{NN} \equiv \langle N\bar{K} | \mathcal{K} | N\bar{K} \rangle$$

and

$$\kappa_{N\Sigma} = \langle \Sigma\pi | \mathcal{K} | N\bar{K} \rangle \quad (4.23)$$

It is necessary to insert the diagonal matrix elements of $\delta(E_i - E_f)$ for the two channels. Those matrix elements will depend on the normalization convention for the states involved. For $l=0$, a spatial wave, the diagonal matrix for $\delta(E_i - E_f)$ is taken to be[†]

$$\hat{\rho} \equiv -\frac{1}{\pi} \begin{pmatrix} k_N & 0 \\ 0 & k_\Sigma \end{pmatrix} \quad (4.24)$$

Equation (4.21a) [and similarly for (4.21b) and (4.21c)] becomes

$$\mathcal{K} = \mathcal{T} + i\pi\mathcal{K}\hat{\rho}\mathcal{T}$$

or

$$\mathcal{T}^{-1} = \mathcal{K}^{-1} + i\pi\hat{\rho}$$

More generally for $l > 0$, k_i on the right-hand side of (4.23) is replaced by k_i^{2l}

[†]The minus sign in (4.24) is chosen so as to come into agreement with the Dalitz–Tuan choice for \mathcal{K} and \mathcal{T} , which are the negatives of the \mathcal{K} and \mathcal{T} used in this volume.

by Arndt, Roper, and Steinberg (78). For the S partial wave the cross section is

$$\sigma = \frac{2\pi}{k^2 |\mathcal{T}_{fi}|^2} \quad (4.25)$$

For the $T = 1$ case, the \mathcal{K} matrix involves three channels, so that

$$\mathcal{K} = \begin{pmatrix} \kappa_{NN} & \kappa_{N\Sigma} & \kappa_{N\Lambda} \\ \kappa_{\Sigma N} & \kappa_{\Sigma\Sigma} & \kappa_{\Sigma\Lambda} \\ \kappa_{\Lambda N} & \kappa_{\Lambda\Sigma} & \kappa_{\Lambda\Lambda} \end{pmatrix} \quad (4.26)$$

and

$$\hat{\rho} = -\frac{1}{\pi} \begin{pmatrix} k_N & 0 & 0 \\ 0 & k_\Sigma & 0 \\ 0 & 0 & k_\Lambda \end{pmatrix} \quad (4.27)$$

Dalitz, McGinley, Belyca, and Anthony (82) parameterize \mathcal{K}^{-1} by an effective range expansion [Ross and Shaw (60, 61)]:

$$\mathcal{K}_T^{-1} = M_T + R_T k^2 \quad (4.28)$$

where k is the center-of-mass momentum in the K^-p channel. The results obtained by Dalitz, McGinley, Belyca, and Anthony (82) using the column labeled new data in their Table 1 are in units of fermis:

$$\begin{aligned} T = 0: \quad & \kappa_{NN} = -1.863, \quad \kappa_{N\Sigma} = -0.955, \quad \kappa_{\Sigma\Sigma} = -0.382 \\ T = 1: \quad & \kappa_{NN} = 0.26, \quad \kappa_{N\Sigma} = -0.99, \quad \kappa_{\Sigma\Sigma} = 0.81 \\ & \kappa_{N\Lambda} = 0.29, \quad \kappa_{\Sigma\Lambda} = 0.44, \quad \kappa_{\Lambda\Lambda} = -0.55 \end{aligned} \quad (4.29)$$

From the results for \mathcal{K} , one can obtain \mathcal{T} and in the low-energy approximation the scattering length [see (4.13)]

$$k \cot \delta_0 \rightarrow \frac{1}{a + ib}$$

The values of a for isospin 1, a_1 , and for isospin 0, a_0 , and similarly for b are [Dalitz, McGinley, Belyca, and Anthony (82)]

$$\begin{aligned} a_0 &= -1.57 \text{ fm} & a_1 &= 0.1075 \text{ fm} \\ b_0 &= 0.70 \text{ fm} & b_1 &= 0.57 \text{ fm} \end{aligned} \quad (4.30)$$

Note that in contrast to the KN scattering length, the scattering length for the

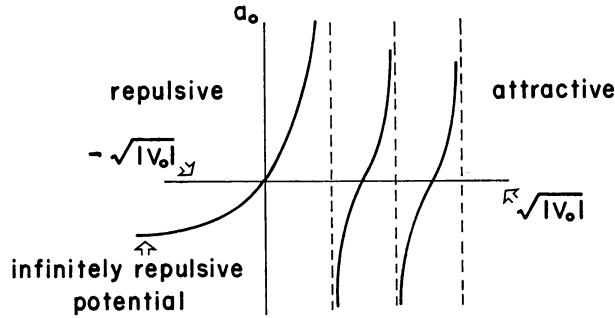


FIG. 4.13

$\bar{K}N$ is complex because absorption into other channels ($\Sigma\pi$ and $\Lambda\pi$) is possible even at threshold.

Note. For systems with bound states such as the $\bar{K}N$, the sign of the scattering length does not necessarily indicate the attractive or repulsive nature of the interaction. For a potential model, the dependence of the scattering length on the strength of the potential V_0 is illustrated in Fig. 4.13. From this figure we see that a positive S -wave scattering length does correspond to attraction. However, a negative scattering length can correspond to either an attractive or repulsive potential. For a weak interaction as is the case for the KN system, a negative a_0 does correspond to a repulsion. For the $\bar{K}N$ system, since there is a $T = 0$ (1405) bound state, a_0 must take on a value in the attractive half-plane.

The $T = 1$ scattering length is relatively small and positive. The interaction is therefore relatively weakly attractive. For both the $T = 0$ and $T = 1$ cases the absorption is strong.

The \mathcal{K} -matrix method can be carried out for each partial wave. This analysis was used by Arndt and Roper (85) in their analysis of K^+ reactions. Gopal et al. (77) employ a multichannel analysis. The total and elastic scattering K^-p cross section are shown in Figs. 4.14 and 4.15. The charge and strangeness exchange cross sections are given in Figs. 4.16 to 4.18. The analysis of Gopal et al. (77) is used in constructing some of these cross sections. Included in these figure are the cross sections averaged over a Fermi-gas nucleon distribution. These are defined as follows. Let $\rho(k)$ be the Fermi-gas distribution normalized by

$$2 \int_0^\infty dk k^2 \rho(k) = 1$$

Let

$$\left(\frac{d\sigma}{d\Omega_L}(p_k, k, 0) \right)_0$$

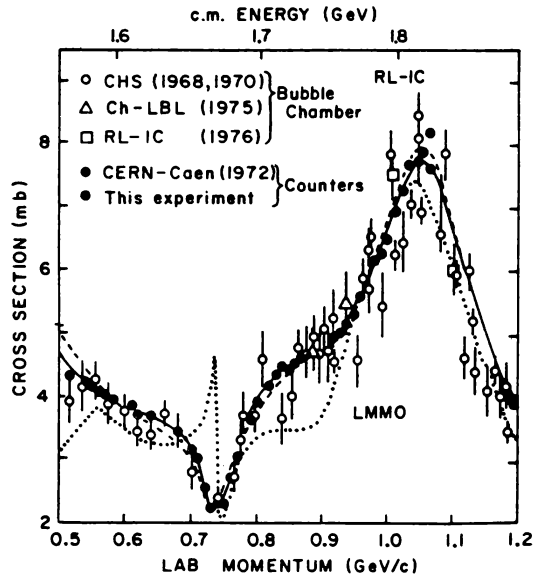


FIG. 4.14. Cross section for the charge exchange reaction $K^-p \rightarrow \bar{K}^0n$. [From Alston-Garnjost et al. (77, 78, 80).]

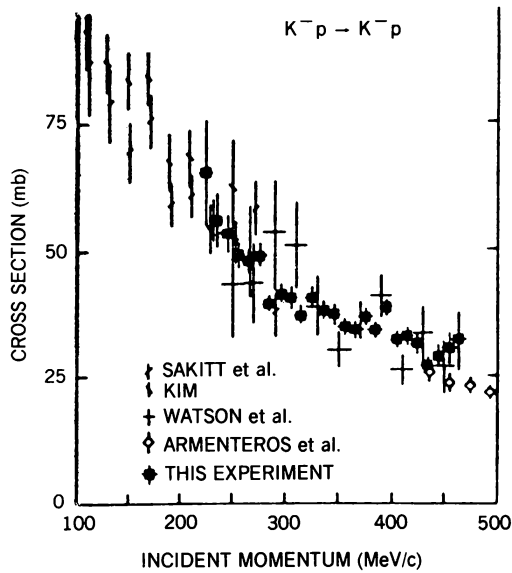


FIG. 4.15. Elastic cross section for $K^-p \rightarrow K^-p$. [From Mast, Alston-Garnjost, et al. (76).]

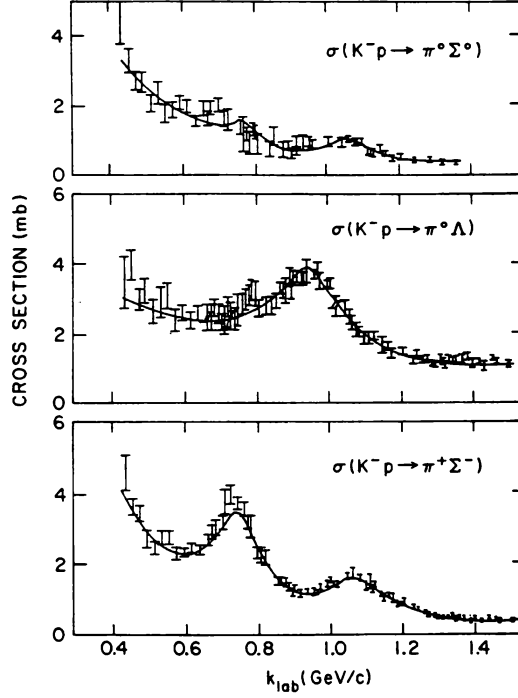


FIG. 4.16. Total cross sections for the reactions $K^-p \rightarrow \pi^0 \Sigma^0$, $\pi^0 \Lambda$ and $\pi^+ \Sigma^-$. [From Dover and Walker (82).]

be the differential cross section for the scattering into the incident direction. This is a function of the kaon momentum p_k , the nucleon momentum k , and x the cosine of the angle between \mathbf{p}_k and \mathbf{k} . Then

$$\left\langle \left(\frac{d\sigma}{d\Omega_L} \right)_{0^+} \right\rangle_{\text{av}} = \int_0^\infty dk k^2 \rho(k) \int_{-1}^1 dx \left(\frac{d\sigma}{d\Omega_L}(p_k, k, x) \right)_{0^+} \quad (4.31)$$

and

$$\langle f_L(0) \rangle_{\text{av}} = \int_0^\infty dk k^2 \rho(k) \int_{-1}^1 dx f_L(0) \quad (4.32)$$

where f_L is the reaction amplitude. Averaging smooths the strong fluctuations with energy of the free-space cross section and amplitude. The later is a consequence of the resonances in the $\bar{K}N$ system.

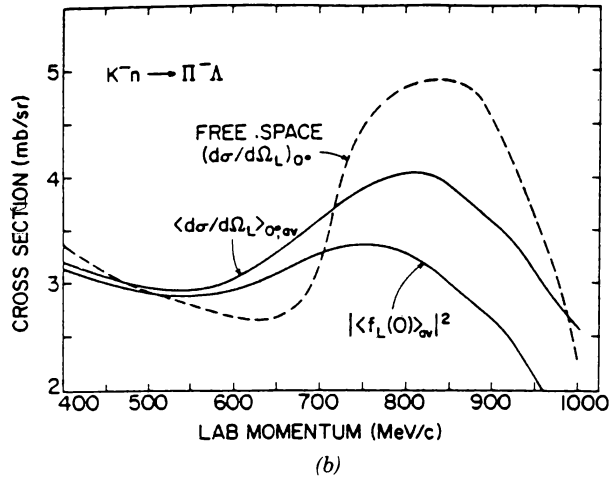
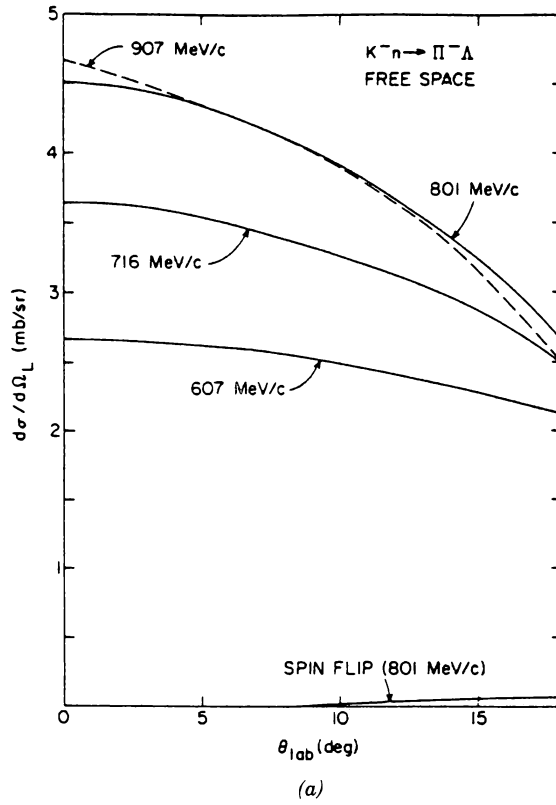


FIG. 4.17. (a) Laboratory differential cross sections for $K^-n \rightarrow \pi^-\Lambda$ [Gopal et al. (77)]; (b) Fermi-averaged forward $K^-n \rightarrow \pi^-\Lambda$ cross sections. [From Dover and Walker (82).]

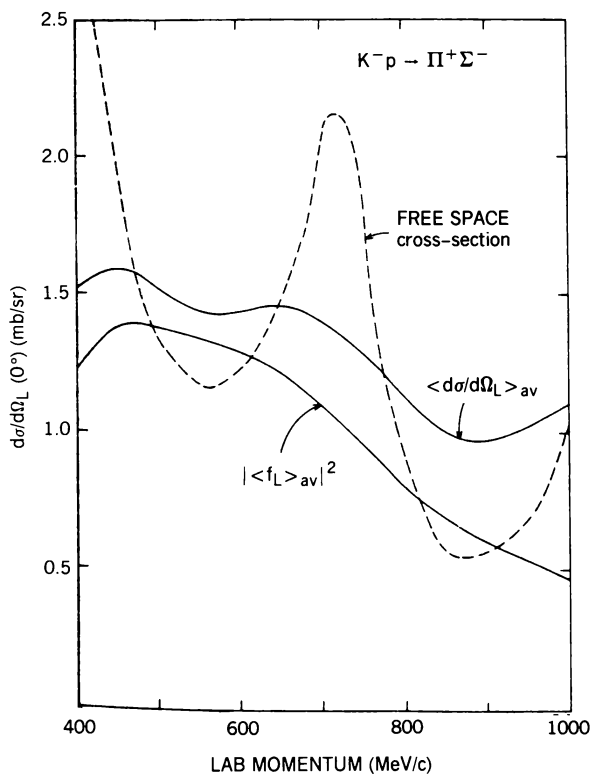


FIG. 4.18. Fermi-averaged $K^-p \rightarrow \pi^+\Sigma^-$ laboratory cross section [Gopal et al. (77)]. [From Dover and Walker (82).]

Dover and Walker (82) use

$$\rho(k) = \frac{\rho_0}{1 + e^{(k - k_0)/\Delta(k)}} \quad (4.33)$$

$$k_0 = 100 \text{ MeV}/c \quad \Delta(k) = 50 \text{ MeV}/c$$

as suggested by Allardyce et al. (73).

D. K^+ -Nucleus Scattering[†]

The K^+ -nucleus scattering is of considerable interest because of the relative weak KN interaction. As a consequence, the K^+ can penetrate much farther into the nucleus than, for example, a nucleon. We have earlier commented on

[†]Coker, Lumpe, and Ray (85); Siegel, Kaufmann, and Gibbs (84, 85).

the fact that because of the strong nucleon–nucleon interaction, high-energy nucleon–nucleus scattering reveals mostly surface properties of the density distribution of nucleons in the nucleus. K^+ –nuclear scattering could be exploited to determine the properties of these distribution in the nuclear interior. Combined with the proton distributions obtained from elastic electron–nucleus scattering, one would have a complete picture of both nucleon distributions.

There are additional simplifications. Because of the weak KN interaction, the first order, ρt , in the multiple scattering series should be sufficient. Second, because the K has a zero spin, the analysis of experiment should prove to be more easily performed.

Elastic scattering K^+ –nucleus scattering have been performed with the ^{12}C and ^{40}Ca nuclei [Marlow, Barnes, et al. (82)]. The momentum of the K^+ beam is 800 MeV/c. The results are shown in Fig. 4.19. The solid lines are first-order optical model ρt calculations [Rosenthal and Tabakin (80); Marlow, Barnes, et al. (82)] based on the KN phase shifts given by Martin (75). It is, of course, necessary to transform these from the kaon–nucleon reference frame to the K –nucleus one. The agreement in the ^{40}Ca case is good. In the ^{12}C case the theoretical curve lies below the experimental one. The total cross sections reflects this difference. (see Fig. 4.20) The deviation from theory may be because of experimental artifacts (such as normalization of the cross section, errors in the measurement of angles, energy spread in the incident beam, etc.). There is after all just one experiment. These are analyzed by Siegel, Kaufmann, and Gibbs (84) with the conclusion that agreement with theory is possible. In addition, there may be errors in the KN phase shifts used, although the agreement with the $K^+ ^{40}\text{Ca}$ results indicate these are not major. By comparing the $K^+ ^{12}\text{Ca}$ results with the K^+ deuterium scattering, the effects of such errors are reduced. The suggestion has been made by Siegel, Kaufmann, and Gibbs (85) that within the nucleus there is an increase of the $S_{11}KN$ phase shift from that given by Martin. Two explanations have been offered. Siegel, Kaufmann, and Gibbs (85) suggest that the effect arises from an increase of nucleon size because of an increase in the confinement radius of the nucleon inside the nucleus. This is suggested by the EMC effect [Aubert et al. (83); Bodek et al. (83); see Close (88a) for a review of this effect.] Brown, Dover, Siegel, and Weise (88) ascribe this increase to the change in the mass of the ρ and ω which mediate the K^+ reaction in the nuclear medium. This leads to an optical potential that depends nonlinearly on the nucleon density giving rise to an increased repulsion (over the first-order ρt) and a decreased effective nuclear radius. The agreement with experiment is shown in Fig. 4.21. The parameter λ describes the change in mass of the ρ and ω in the nuclear medium,

$$\frac{m_V^2(p)}{m_V^2(0)} = 1 - \frac{\lambda\rho}{\rho_0}$$

In this equation V can be either ρ or ω , and ρ_0 is the equilibrium nucleon

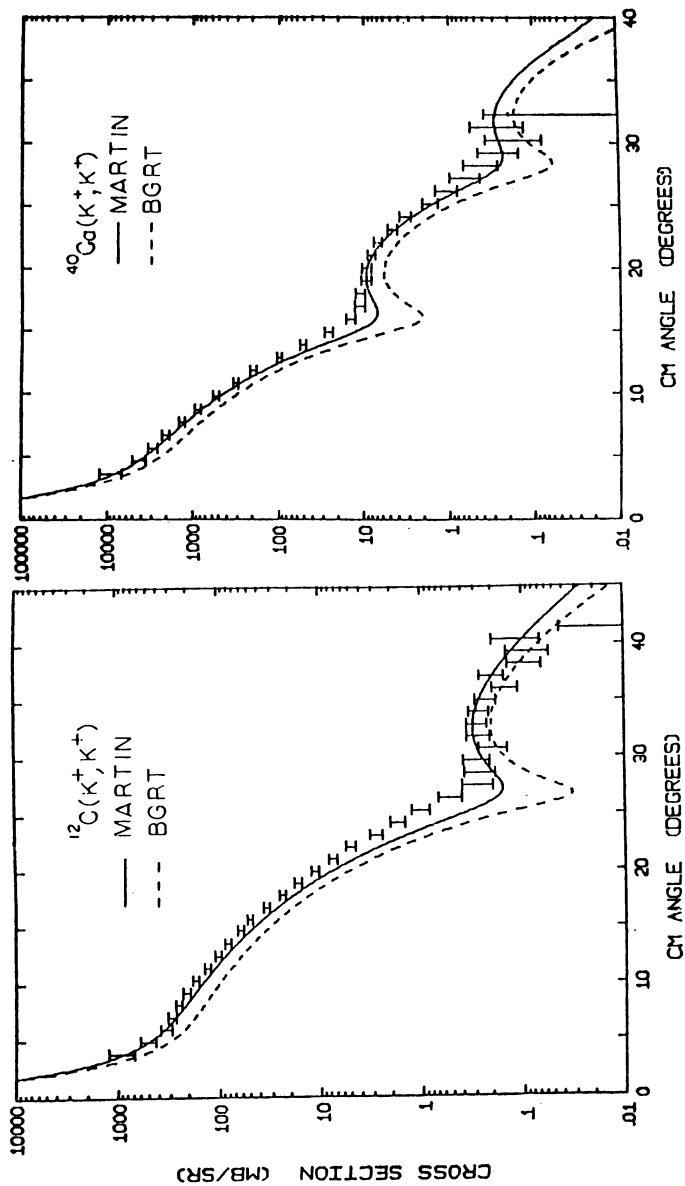


FIG. 4.19. Elastic scattering differential cross section for $K^+ + ^{12}\text{C}$ and $K^+ + ^{40}\text{Ca}$ at 800 MeV/c. [From Marlow, Barnes, et al. (82).]

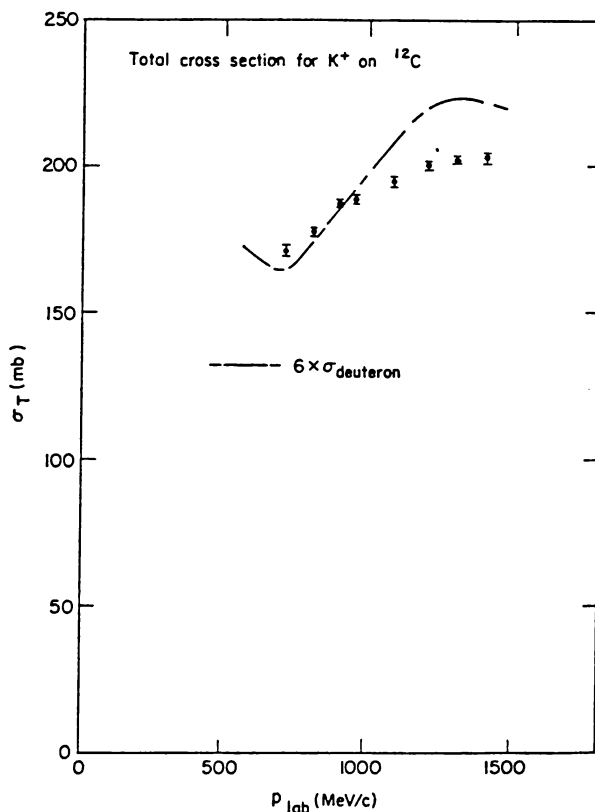


FIG. 4.20. Total cross section for K^+ scattering by ^{12}C . σ_{deuteron} is the cross section for K^+ scattering by ^2H . [From Siegel, Kaufmann, and Gibbs (84).]

density. According to these authors there is little effect of this density dependence on the $K^+ + ^{40}\text{Ca}$ elastic cross section.

Assuming that the ρt first-order term suffices for the heavier nuclei, one can ask for the sensitivity of the K^+ nucleus scattering to the nucleon density distribution [Coker, Lumpe, and Ray (85)]. These authors use the Martin phase shifts. This is illustrated by Figs. 4.22 and 4.23 for elastic scattering by Pb. The solid lines give the percentage change from a standard nucleon distribution induced by a Gaussian addition to the exterior surface or tail region of the neutron density. The dotted-dashed line gives the cross section for proton elastic scattering. We see that as predicted the K^+ projectile provides more information since the proton does not successfully penetrate into the nuclear interior.

Similar results are obtained for inelastic scattering using the DWIA. According to Dover and Walker (82), the dominant amplitude for a closed shell $J=0$, $T=0$ nucleus involves no spin, $\Delta S=0$, or isospin $\Delta T=0$, change.

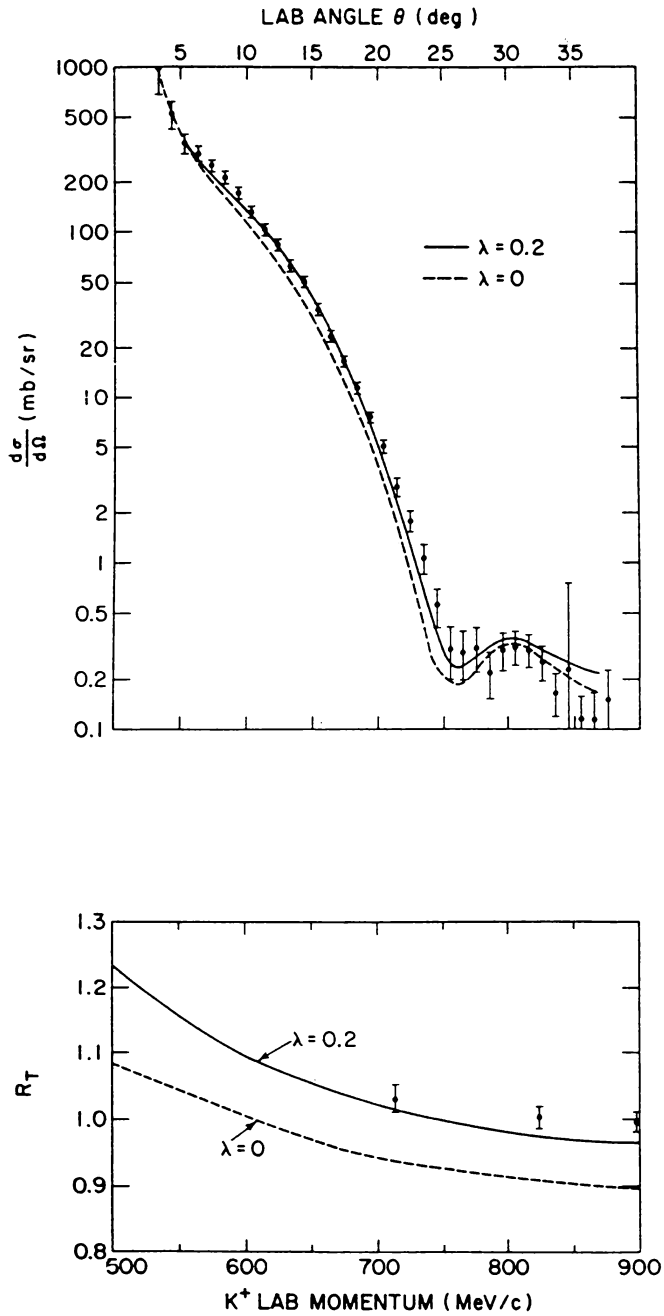


FIG. 4.21. Angular distribution for $K^+ + {}^{12}\text{C}$ elastic scattering at 800 MeV/c is shown at top; at the bottom, the total cross section ratio. [From Brown, Dover, Siegel, and Weise (88).]

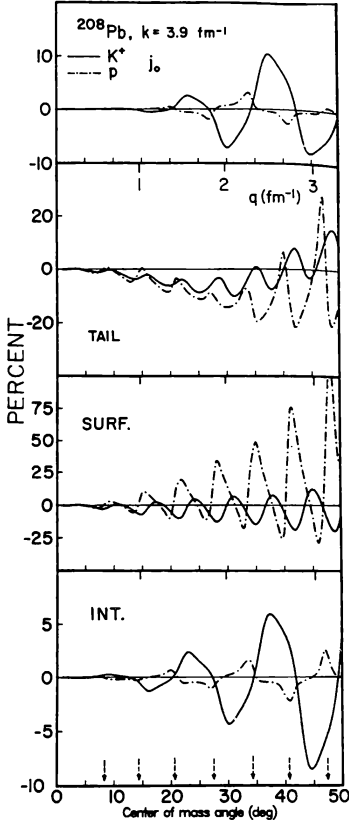


FIG. 4.22. Percent changes in the K^+ ^{208}Pb and p ^{208}Pb because of perturbations of the neutron density. Arrows indicate minima in the proton angular distribution. $E_k = 442$ MeV; $E_p = 297$ MeV. (j_0 = damped interior wiggle). [From Coker, Lumpe, and Ray (85).]

Coker, Lumpe, and Ray (85) use the DWIA formalism to compute the excitation of the collective 3^- level in Pb using the transition potential

$$U_{\text{trans}} = \frac{\beta}{\sqrt{2L+1}} \left[R \frac{d}{d\tau} U_{\text{opt}} + (V_H + iW) e^{-[r-(r_0)/a_0]^2} \right] \quad (4.34)$$

where β is the deformation parameter, U_{opt} is given by ρt , and the last term is an interior perturbation. The results are shown in Fig. 4.24, where again the solid line are K^+ induced and the dotted-dashed ones the proton induced. Again we see that the K^+ inelastic reaction is much more sensitive than the proton-induced reaction. More experiments are needed!

E. K^- –Nuclear Scattering

As in the case of K^+ scattering, the ρt first-order optical potential yields cross sections in substantial agreement with experiment when the kaon wavelength is

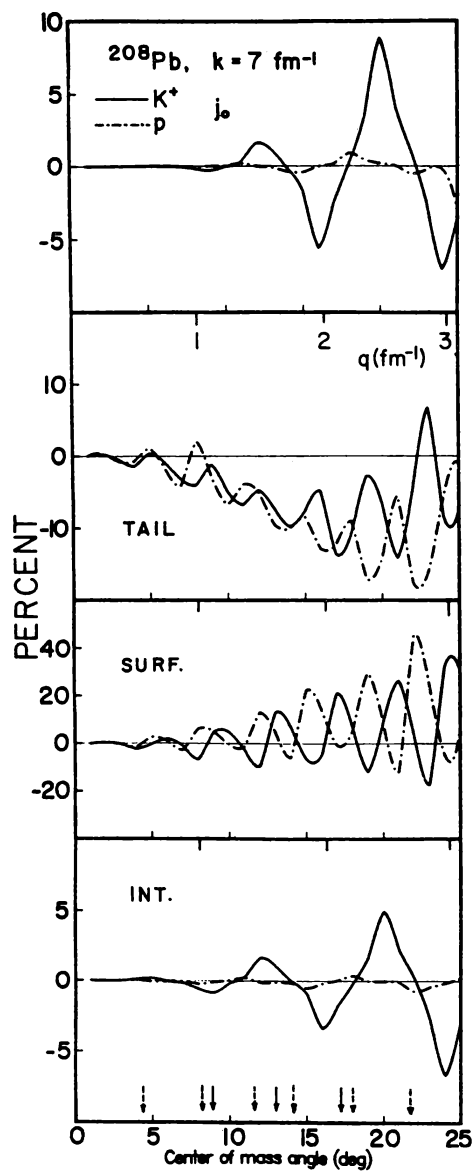


FIG. 4.23. Same as Fig. 4.22 except that $E_k = 991 \text{ MeV}$ and $E_p = 800 \text{ MeV}$. [From Coker, Lumpe, and Ray (85).]

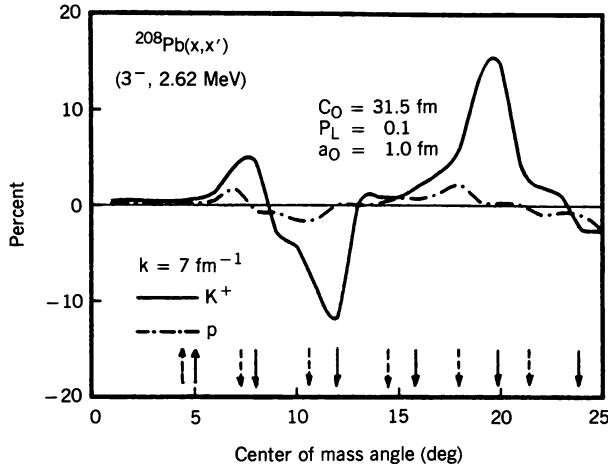


FIG. 4.24. Percent change in K^+ - and p -induced inelastic differential cross section for ^{208}Pb resulting from an interior perturbation in transition potential. [From Coker, Lumpe, and Ray (85).]

sufficiently small. This is seen in Fig. 4.25, where $p_k = 800 \text{ MeV}/c$ and $\lambda = 1/4 \text{ fm}$. The K^-N phase shifts used for t are those of Gopal et al. (77). Evidence for an anomaly in the $K^- + ^{12}\text{C}$ scattering is not as strong as in the analogous $K^+ + ^{12}\text{C}$ case.

At low energies, the $t\rho$ optical potential fails badly. If one were to use the $T = 0$ K^-N scattering length [Eq. (4.30)], the $t\rho$ potential would be repulsive, whereas we know from the existence of bound $\bar{K}N$ states listed in Table 4.3 that the $K^- + N$ interaction, and therefore the $K^- + \text{nucleus}$ interaction, is attractive. A much more sophisticated approach similar to that of Mahaux and his collaborators, who use a Bruckner-Hartree-Fock approach (see Chapter IV), is required.

Theoretical studies of the inelastic K^- scattering by nuclei are described by Dover and Walker (82). The results are similar to those obtained for K^+ inelastic scattering. Again the cross section is dominated by the $\Delta S = \Delta T = 0$ transition interaction. Hence one expects that the normal-parity, nonisospin flip states will be preferentially excited. Good agreement is obtained for the excitations of the 4.4- and 9.6-MeV levels on ^{12}C using nuclear density as determined by electron scattering. The agreement with a collective model [see (4.83)] is poor (see Fig. 4.26).

Dover and Walker (82) point to usefulness of the (K^-, \bar{K}^0) reaction, since in that case we have $\Delta T = 1$. [Compare with (p, n) reaction] This reaction converts a proton into a neutron. For $T = 0$ nuclei only $T = 1$ states will be excited. For a $T \neq 0$ nucleus, the $T_>$ states would be easily identified.

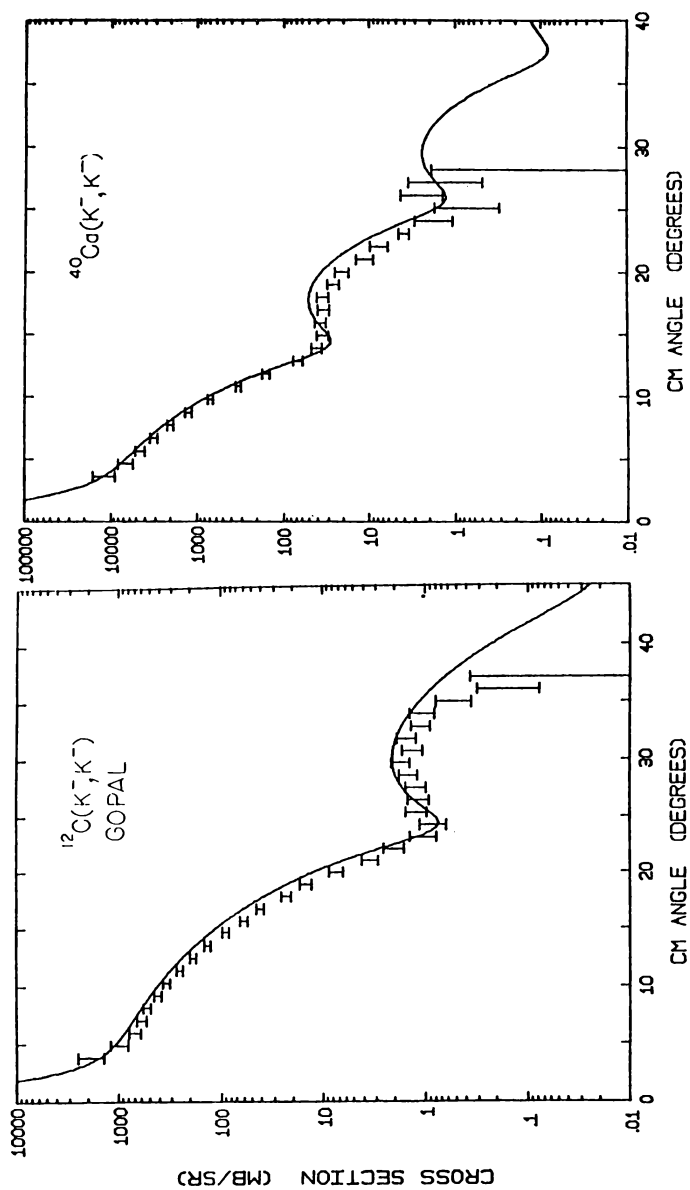


FIG. 4.25. Elastic scattering of K^- by ^{12}C and ^{40}Ca . Curves are first-order optical model calculations using Gopal (77) free-space K^-N amplitudes. [From Dover and Walker (82).]

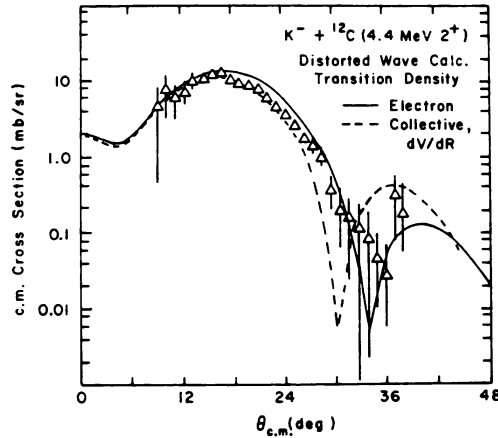


FIG. 4.26. Inelastic K^- scattering at 800 MeV/c to first 2^+ level in ^{12}C . [From Dover and Walker (82).]

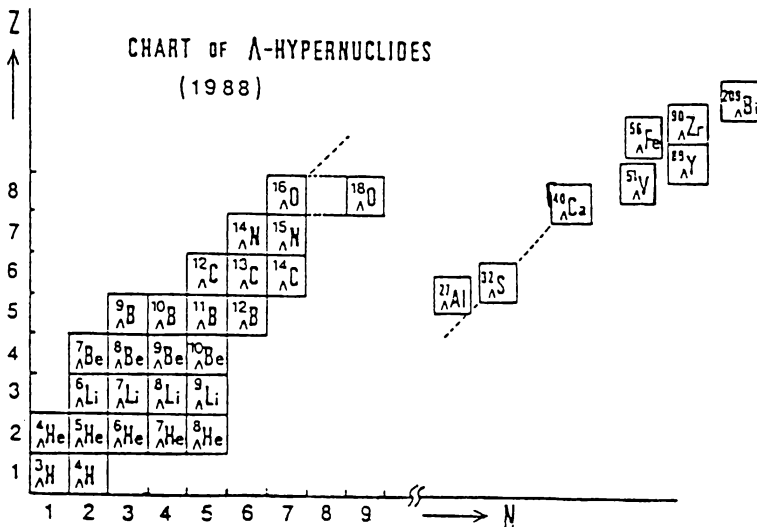


FIG. 4.27. Chart of observed Λ hypernuclei as of 1988. [From Bando (89).]

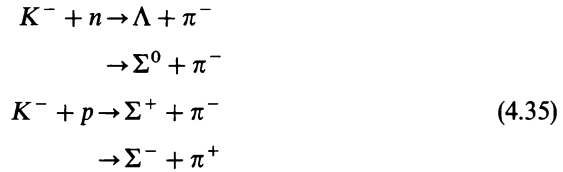
F. The Strangeness Exchange Reaction and Hypernuclei

By using the (K^-, π^-) or (π^+, K^+) reaction a nucleon in the nucleus is converted into a hyperon. Under appropriate conditions the hyperon is bound to the residual nucleus to form a hypernucleus. A (K^-, K^+) reaction could lead to the formation of a doubly strange ($S = -2$) hypernuclei. The Λ hypernuclei which have been observed are shown in Fig. 4.27. The existence of Σ hypernuclei

[Bertini et al. (84, 85); Walcher (88)] is controversial. These are very interesting systems since the Λ has approximately the same mass (Λ mass = 1115.6 MeV) as the nucleon, has the same spin, but has a zero isospin. The simplest assumption is that the Pauli exclusion principle does not limit the Λ , so that it can occupy orbits in the host nucleus which are forbidden to a nucleon.[†] As a consequence, new low-lying states that would not be present in the target nucleus will make their appearance.

Lambda hypernuclei were first observed in nuclear emulsions [Davis and Sacton (67)]. They have also been observed in the capture of K^- particles in Coulomb orbits about the carbon nucleus [C. Vandervelde-Wiquet, J. Sacton and J. H. Wickens (77)], forming a kaonic atom. Experimental opportunities were expanded substantially when it was shown that a small momentum transfer (K^-, π^-) reaction leading to the formation of a hypernucleus was possible. A review of the experiments using this reaction has been made by Povh (76, 78). Most recently, experiments at BNL have employed the (π^+, K^+) reaction, permitting the excitation of states in the large A hypernucleus, not as accessible with the (K^-, π^-) reaction.

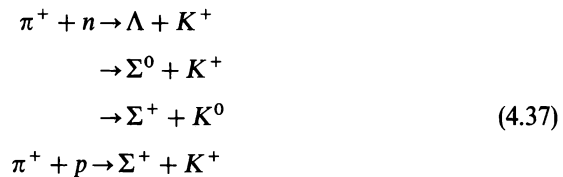
The underlying physical processes using kaon beams of interest in the production of hypernuclei are



where we have limited the reactions to ones in which the final pion is charged. Another possible reaction is radiative capture:



Using π^+ beams, the pertinent reactions are



[†]This is not completely true since the u and d quarks in the Λ and the u and d quarks in the nucleon do satisfy the Pauli principle. One of the investigations that is of fundamental importance will be to determine the effect of the Pauli principle satisfied by the quarks on the spectra of hypernuclei. In particular, this would depend on the degree of deconfinement of the quark.

The small momentum strangeness exchange reaction $n(K^-, \pi^-)\Lambda$ is possible because the mass of the K^- plus nucleon is about 178 MeV greater than that of the mass of the $\pi + \Lambda$. Consider the case when a K^- strikes a neutron at rest. Then there is a “magic momentum” for which the Λ is at rest and π^- moves in the forward (0°) direction. The equation determining this momentum is

$$m_n + \sqrt{m_K^2 + p^2} = m_\Lambda + \sqrt{m_\pi^2 + p^2}$$

or

$$E_K = \sqrt{m_K^2 + p^2} = \frac{m_K^2 - m_\pi^2 + (m_\Lambda - m_n)^2}{2(m_\Lambda - m_n)} \quad (4.38)$$

For values of the kaon momentum that differ from the value obtained from (4.38), about 531 MeV/c, the momentum transfer to the Λ when the pion is observed at 0° can be small. This is illustrated in Fig. 4.28, where we see that the momentum transfer, $q(0)$, is less than the Fermi momentum over the entire range in the momentum p_K of the incident kaon. Much the same can be said for the $K^- + n \rightarrow \Sigma^0 + \pi^-$ reaction, for which the magic momentum is about 284 MeV/c:

$$m_n + \sqrt{m_K^2 + p^2} = m_\Sigma + \sqrt{m_\pi^2 + p^2}$$

or

$$E_K = \sqrt{m_K^2 + p^2} = \frac{m_K^2 - m_\pi^2 + (m_\Sigma - m_n)^2}{2(m_\Sigma - m_n)}$$

Thus when the K^- with the momenta shown in Fig. 4.28 strikes a nucleus and one studies the case where the pion goes off in the forward direction, it is very likely that the Λ will “stick” to the residual nucleus so that a hypernucleus is formed. In the simplest example of this reaction, a neutron in the nucleus is replaced by the Λ and the wave function of the system is not changed. For this

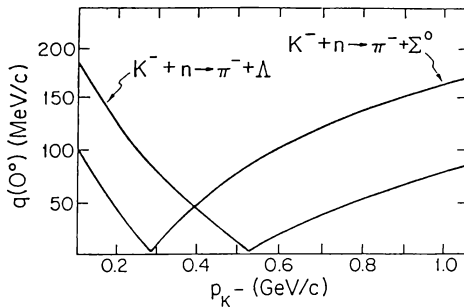


FIG. 4.28. Kinematics of the (K^-, π^-) reaction.

reason the reaction is referred to as a “substitutional” reaction. The angular momentum change is $\Delta l = 0$. When the emitted π^- is observed at angles greater than zero, $\Delta l = 1$ and $\Delta l = 2$ transitions become possible. Examples of the production of hypernuclei states by the (K^-, π^-) are shown in Fig. 4.29. The sharp peaks in the pion spectrum correspond to states in the hypernucleus.

The (K^-, π^-) reaction is not as useful for excitation of the low-lying Λ hypernuclear states for the heavier nuclei principally because the single-particle

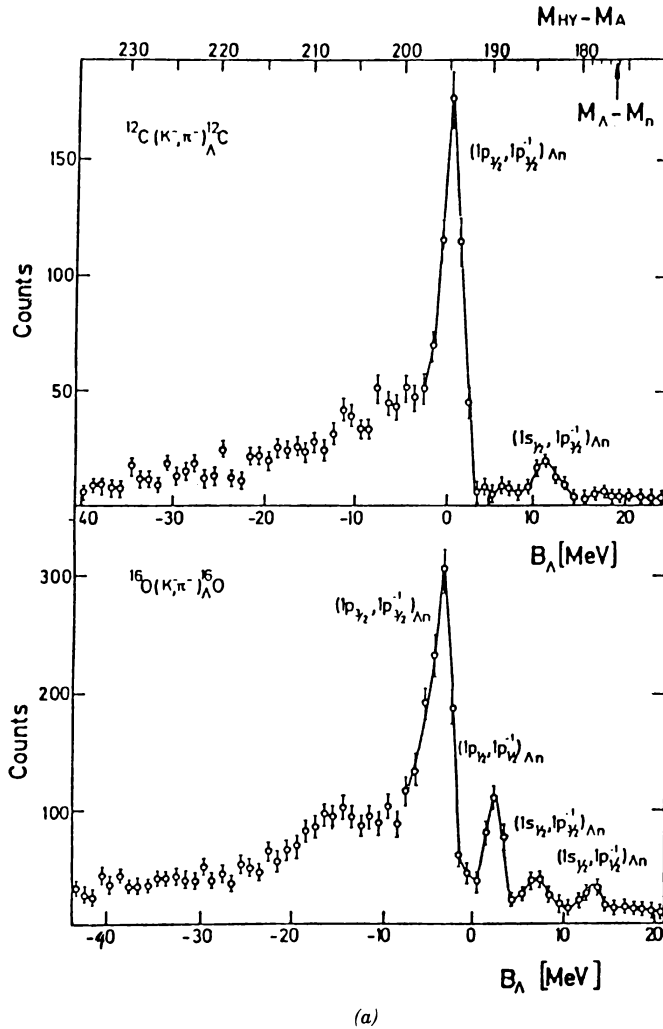
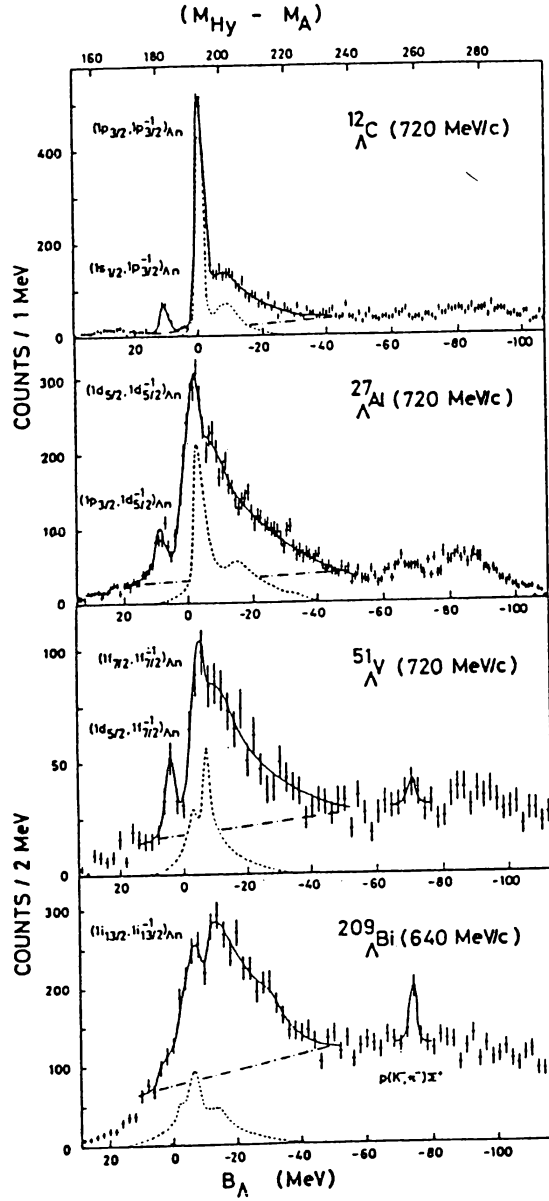


FIG. 4.29. (a) Production of hypernuclei ^{12}C , ^{16}O by the K^-, π^- reaction. [From Brückner, Granz, et al. (76).]; (b) Production of hypernuclei ^{12}C , ^{27}Al , ^{51}V , ^{209}Bi . [From Bertini, Bing, et al. (81).]



(b)

FIG. 4.29. (Continued)

neutron orbits have a large angular momentum, therefore requiring a large momentum change to generate a low-angular-momentum Λ orbit. This momentum change could, in principle, be obtained by examining the pion spectrum at large angles. But then the cross section is very much reduced.

The (K^-, π^-) has a number of innate difficulties. First, the incident K^- beam is accompanied by many more negative pions. Second, K^- decays and this compresses all the experimental dimensions. Moreover, the K^- decays into negative pions. The net resolution for the BNL experiments is a few MeV. Interpretation of the results is not easy since the K^- and π^- are strongly interacting. However, as we shall see, this difficulty is overcome by a careful DWA calculation.

Some of these restrictions are lifted in the (π^+, K^+) reaction. The momentum

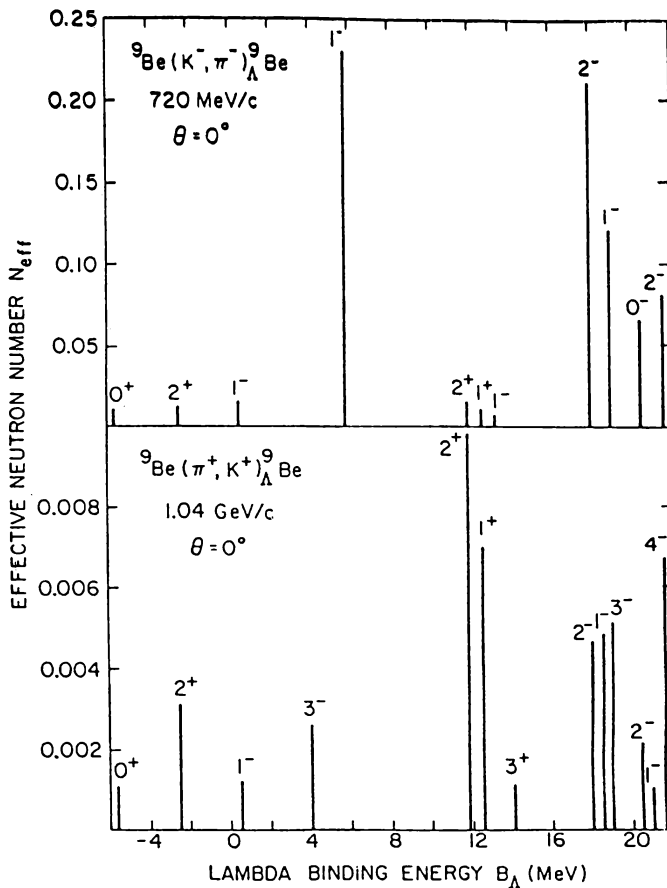


FIG. 4.30. Theoretical comparison of the production of ${}^9_{\Lambda}\text{Be}$ hypernucleus using (K^-, π^-) and (π^+, K^+) reactions. [From Yamada, Ikeda, et al. (88).]

transfer is large. For $p_K = 1050 \text{ MeV}/c$, $q \geq 250 \text{ MeV}/c$. The cross sections for the formation of a hypernucleus are, of course, reduced, but this is compensated by the large pion intensity available in the incident beam. Interpretation is somewhat simpler since the K^+ -nucleon interaction is relatively weak. Finally, the fact that the K^+ decays does not affect the experimental background. In fact, the decay is used to identify the K^+ . The two reactions are complementary, as can be seen from Fig. 4.30, so that both experiments are needed to obtain a complete spectrum.

An example of the production of Λ hypernuclear states by the (π^+, K^+) reaction is shown in Fig. 4.31. In both examples, Figs. 4.29 and 4.31, the peaks are correlated with states in the hypernucleus. These are doorway states, which would fragment if experiments with sufficient resolution could be performed.

To determine the indicated configurations requires a calculation since there is much overlap in the experimental cross section. The DWA is used. That approximation has been discussed in Chapter V. Since no new principles are involved, we shall not discuss the details of the calculation in this chapter. The reader is referred to Auerbach, Baltz, et al. (83) and Hufner, Lee, and Weidenmüller (74a, 74b, 79) for the detailed discussion.

The input into the DWA calculation for the (K^-, π^-) reaction requires (1) a wave function for the K^- nucleus system, (2) a wave function for the π^- nucleus system, (3) a wave function for the target neutron, (4) the Λ -host nucleus wave function, and (5) the transition matrix element converting $K^- + \text{neutron}$ into

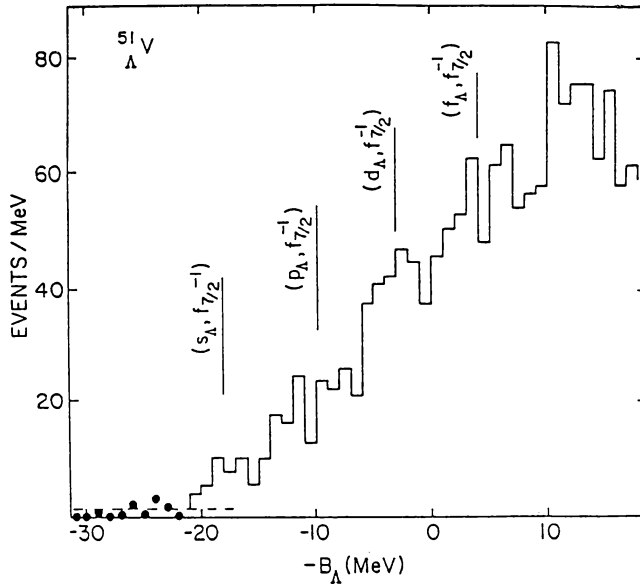


FIG. 4.31. Production of Λ hypernuclear states in $^{51}_{\Lambda}\text{V}$ using the (π^+, K^+) reaction. [From Chrien (88).]

TABLE 4.6 Potentials for π^- , K^- Elastic Scattering at $p_K = 800 \text{ MeV}/c$

Reaction	$V_0(\text{MeV})$	$W_0(\text{MeV})$	$r_0(\text{fm})$	$a_0(\text{fm})$	rms radius (fm)
$K^+ - {}^{12}\text{C}$	24.4	41.4	1.075	0.375	2.36
$\pi^- + {}^{12}\text{C}$	0.9	50.9	0.926	0.44	2.32
$K^- + {}^{40}\text{Ca}$	23.57	18.69	1.182	0.49	3.63

$\pi^- + \Lambda$. The first two of these is obtained by first adjusting the parameters in a simple Woods–Saxon potential so as to give the K^- –nucleus and π^- –nucleus elastic scattering. (The last should be the π^- –hypernucleus scattering.) The wave function is obtained from a solution of the Klein–Gordon equation assuming that potential to be the fourth component of a four-vector potential, neglecting the square of the potential in the Klein–Gordon equation. (See Chapter II for a discussion.) The resulting parameters are given in Table 4.6. The Woods–Saxon form is

$$U(r) = -(V_0 + iW_0)/f(r)$$

$$f(r) = 1 + \exp\left(\frac{r - r_0 A^{1/3}}{a_0}\right)$$

These potentials were used throughout the p -shell. The neutron and Λ wave functions were obtained by again using the Woods–Saxon form but adjusting so as to obtain the correct binding energy for the orbit in question. The parameters, r_0 and a_0 were taken to be 1.15 fm and 0.63, respectively. Parenthetically, we note that according to Auerbach, Baltz, et al. (83), the eikonal approximation for these wave functions does not suffice quantitatively, especially for $\Delta l = 0$ reactions.

The transition matrix element for the reaction $K^- + n \rightarrow \pi^- + \Lambda$ is taken to be

$$\langle \mathbf{r}_\pi, \mathbf{r}_\Lambda | v | \mathbf{r}_k, \mathbf{r}_n \rangle = V_T \delta(\mathbf{R}_{\pi\Lambda} - \mathbf{R}_{Kn}) \delta(\mathbf{r}_{\pi\Lambda} - \mathbf{r}_{Kn}) \delta(\mathbf{r}_{Kn}) \quad (4.39)$$

where V_T depends on isospin. The vectors $\mathbf{R}_{\pi\Lambda}$ and \mathbf{R}_{Kn} give the positions of the center of mass of the $\pi\Lambda$ and Kn , respectively. The first δ function in (4.39) assures conservation of momentum in the $Kn \rightarrow \pi\Lambda$ reaction. The second term assumes that the interaction is local, while the last δ function is the zero-range approximation often used in the DWA. The strength V_T is given by the t matrix for $\bar{K}N \rightarrow \pi\Lambda$ at 0° . This must be transformed to the laboratory and averaged over a Fermi gas [see (4.31) and (4.32)]. The wave functions for the p shell core and the p -shell initial state were taken from Cohen and Kurath (65) using the POT interaction [see Fig. IX.4.1 in deShalit and Feshbach (74)]. The basis wave functions used to describe the hypernucleus is simply the core wave function Ψ_c times the Λ orbital ψ_Λ combined to yield the total angular

momentum J and isospin T . The wave function Ψ_c can refer to the ground state or excited states of the core. This representation for the hypernucleus wave function is called the *weak coupling approximation*. To obtain agreement with experiment it is necessary to introduce some residual Λ - N interaction [see Millener, Gal, Dover, and Dalitz (85)].

Qualitatively [and this is shown in the detailed analysis of Auerbach, Baltz, et al. (83)], one expects that the cross section will be proportional to the cross section for the pickup process [e.g., (p, d)], in which the picked-up particle is the neutron that is to be replaced by a Λ to produce a neutron hole. This is very useful since in some cases this pickup cross section has been measured.

We illustrate with the calculations for $^{13}\text{C}(K^-, \pi^-)^{13}_{\Lambda}\text{C}$. The energy-level diagram for the core nucleus, ^{12}C , and the resultant spectrum for $^{13}_{\Lambda}\text{C}$ are indicated by the dashed line shown in Fig. 4.32. If we combine the 0^+ ground state of ^{12}C with an $l=1\Lambda$ orbital, we obtain in the weak coupling basis a $\frac{1}{2}, \frac{3}{2}$ hypernuclear state that can be split by a spin-orbit coupling. Similarly, the 2^+ state of ^{12}C when combined with the Λ yields the upper three levels, which can be further split into six levels. The brackets [441], [54] give the number of

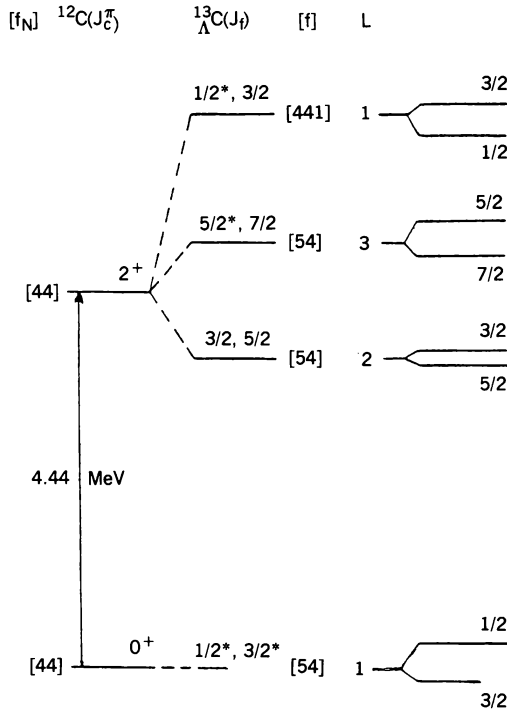


FIG. 4.32. $^{12}\text{C}(O^+, 2^+) \otimes p_{\Lambda}$ spectrum. States that dominate in the 10- and 16-MeV peaks are marked with an asterisk. $\mathcal{L} = J_c + l_{\Lambda}$, where J_c is the core spin and l_{Λ} is the Λ angular momentum. [From Auerbach, Baltz, et al. (83).]

particles in each orbit. In ^{12}C we have four neutrons and four protons in $p_{3/2}$ orbits. Thus the spatial symmetry [54] is forbidden for nucleons by the Pauli principle. The substitutional reaction can thus lead only to the [441] states.

The DWA results for the various possible transitions $p_n \rightarrow s_\Lambda$, $\Delta l = 0, 2$, $p_n \rightarrow p_\Lambda$, $\Delta l = 1$, and so on, are shown in Fig. 4.33 and in Table 4.7. As is clear from Fig. 4.33, it should be relatively easy to pick out the $\Delta l = 0$ $p_n \rightarrow p_\Lambda$ transition. However, before the $p_n \rightarrow s_\Lambda$ $\Delta l = 1$ transition can be extracted, it is necessary to unfold the $\Delta l = 0$ cross section. The $\Delta l = 2$ transition requires unfolding both the $\Delta l = 0$ and $\Delta l = 1$ cross sections before it will be visible quantitatively.

The experimental results for $^{13}\text{C}(K^-, \pi^-)^{13}_\Lambda\text{C}$ are compared to theory in Fig. 4.34. Theory and experiment agree quite well. As expected, the $\Delta l = 0$ and $\Delta l = 1$ transitions dominate at small angles ($\theta_{\text{lab}} = 4^\circ$). At high excitation energies the $\Delta l = 1$ transitions to (sd) Λ orbitals become visible. The $\Delta l = 2$ transition is appreciable only at $\theta_{\text{lab}} = 15^\circ$. The dominant transition is the $\Delta l = 1$,

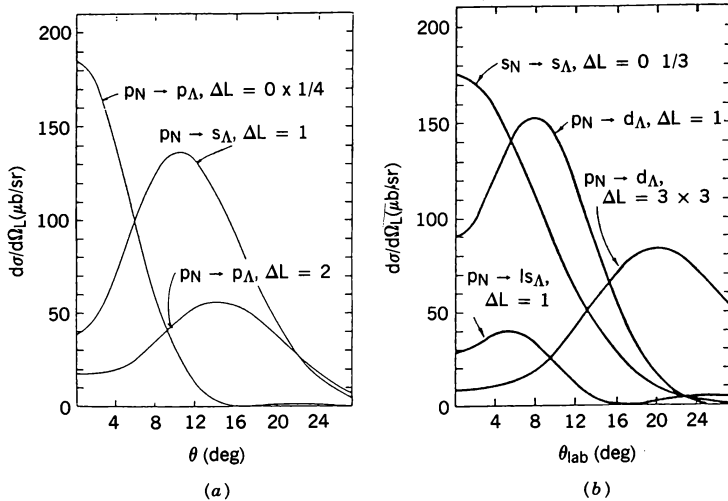


FIG. 4.33. Laboratory cross section for the (K^-, π^-) reaction on a ^{13}C target. In (a) $p_n \rightarrow p_\Lambda$ and $p_n \rightarrow s_\Lambda$. In (b) $s_n \rightarrow s_\Lambda$ and $p_n \rightarrow s_\Lambda$ and d_Λ . The K^- momentum is 800 MeV/c. [From Auerbach, Baltz, et al. (83).]

TABLE 4.7 Differential Cross Sections in $\mu\text{b/st}$,
 $p_k = 530 \text{ MeV/c}$, $^{13}\text{C}(K^-, \pi^-)^{13}_\Lambda\text{C}$

	θ_{cm}	4°	10°	15°
$p_n \rightarrow p_\Lambda$	$\Delta l = 0$	708	375	109
$p_n \rightarrow p_\Lambda$	$\Delta l = 2$	9.1	12.6	32.8
$p_n \rightarrow s_\Lambda$	$\Delta l = 1$	19.8	78.8	113

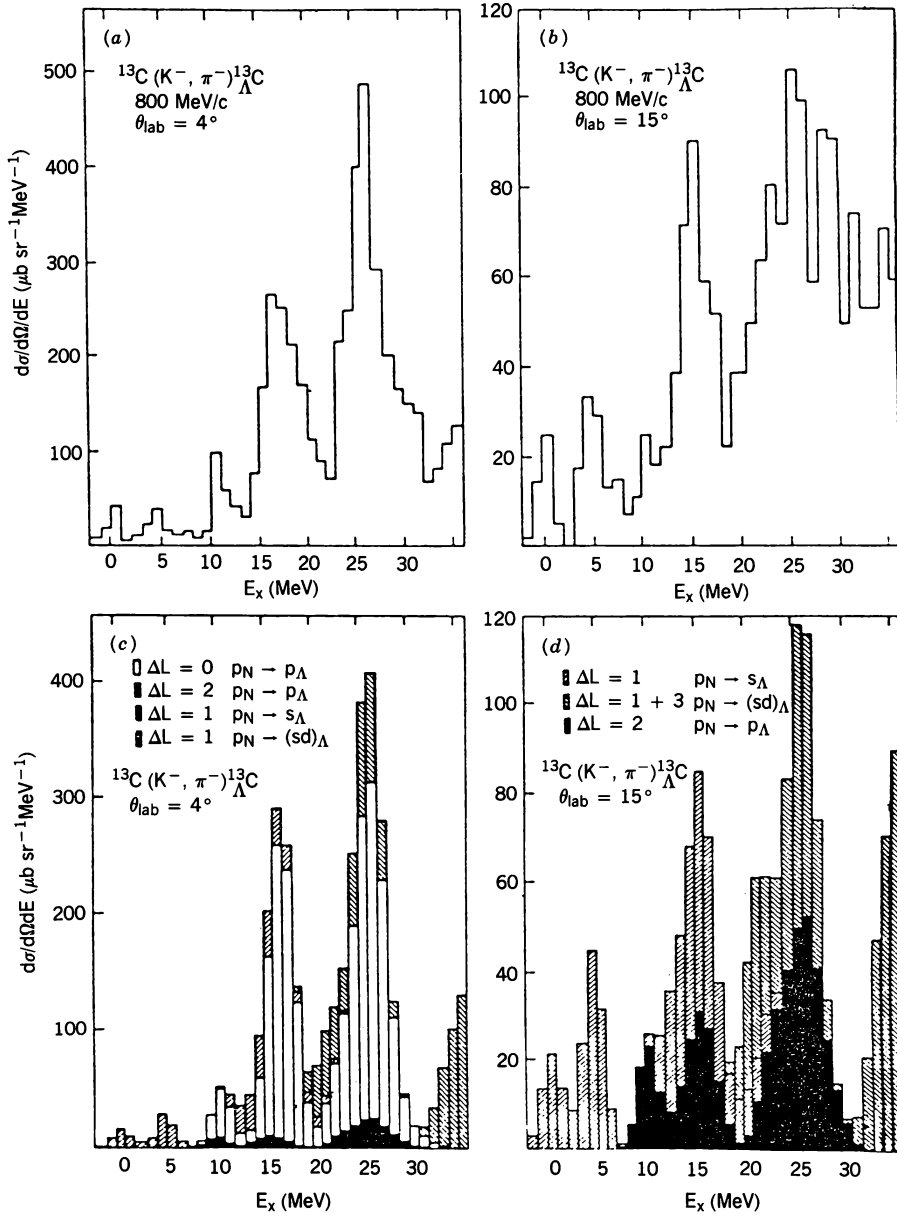


FIG. 4.34. Comparison of experiment and theory for the reaction $^{13}\text{C}(K^-, \pi^-)^{13}\text{C}_\Lambda$. [From Auerbach, Baltz, et al. (88); May et al. (81).]

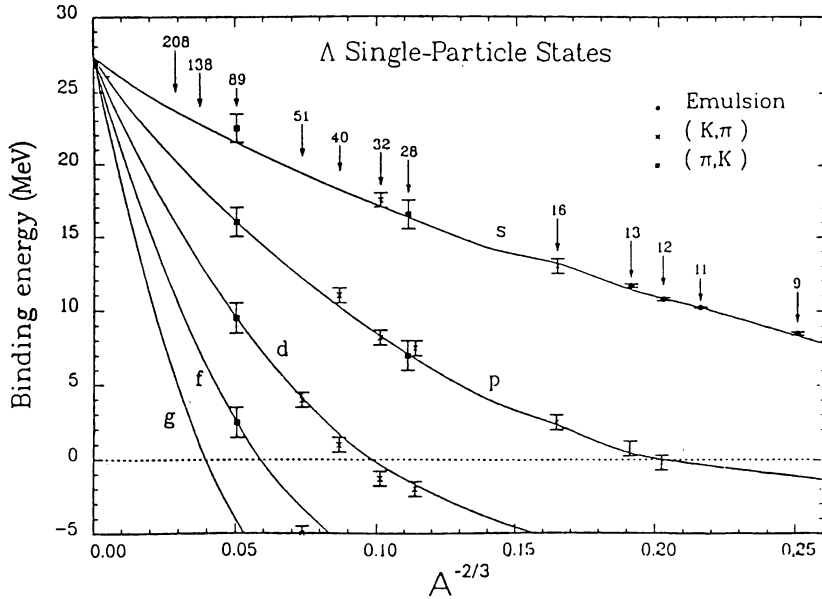


FIG. 4.35. Λ single-particle states. The solid lines are theoretical. [From Millener, Dover and Gal (88).]

$p_n \rightarrow s_\Lambda$. Coupling the s_Λ to the ^{12}C core (ground and excited states) yields the states populating the peaks at 0, 5, and 12 to 16 MeV. Coupling the p_Λ to the ^{12}C core yields the starred states shown in Fig. 4.32. These states will occur at excitation energies about 10 MeV (the energy difference between s_Λ and p_Λ) greater than the values for s_Λ hypernuclei.

A similar analysis has been performed for other target nuclei by Auerbach, Baltz, et al. (83) and for the states seen in the (π^+, K^+) reaction (Fig. 4.31) by Millener, Dover, and Gal (80). The conclusions that can be drawn include: (1) the ΛN spin-orbit potential is small; and (2) the effective mean field potential is nonlocal and density dependent. The single-particle states that have been determined are shown in Fig. 4.35. Because the Λ interacts relatively weakly with the host nucleus, one obtains a very clearly observed set of single-particle states. They are doorway states, which would fragment if the energy resolution were to be improved. These Λ shell-model states provide a direct justification of the mean-field concept.

G. Σ Hypernuclei[†]

Candidates for Σ hypernuclear states have been seen for $A = 4$ [Hayano et al. (89)], $A = 6$ [Piekarczyk et al. (82); Kneis (83)], $A = 7$ [Bertini (79)], $A = 9$ [Bertini

[†]Millener, Dover, and Gal (89).

(80); Mayer (80)], and $A = 12$ [Yamazaki et al. (85); Bertini et al. (84); Peng (82)]. On the other hand, contradictory experiments have seen no evidence for narrow Σ peaks in $A = 7$ [Hungerford (86); Tang et al. (88)], $A = 12$ [Iwasaki (87)], and $A = 16$ [Piekarczyk et al. (82)].

The existence of long-lived Σ hypernuclei with widths of the order of 5 to 10 MeV was not expected because of the strong $\Sigma N \rightarrow \Lambda N$ conversion. Dover and Gal (80), using the optical model with $\text{Im}V = -\langle v\sigma \rangle_{\text{av}} \rho(r)/2$, obtain the following values for the width of single-particle Σ states:

$$\begin{aligned} {}^{13}_{\Sigma}\text{C}: \quad \Gamma_{1s} &\approx 23 \text{ MeV}, \quad \Gamma_{1p} \approx 13 \text{ MeV} \\ {}^{41}_{\Sigma}\text{Ca}: \quad \Gamma_{1s} &\approx 28 \text{ MeV}, \quad \Gamma_{1p} \approx 23 \text{ MeV}, \quad \Gamma_{1d} \approx 18 \text{ MeV} \end{aligned}$$

The width decreases with increasing orbital angular momentum because of the angular momentum barrier, which reduces the overlap of the Σ with the nucleons of the core. Several mechanisms have been proposed. Stepien-Rudzka and Wycech (81), Johnstone and Thomas (83), and Dabrowski and Rosynek (81, 82, 85, 86) have studied the effects of Pauli blocking and nuclear binding. Auerbach (87) has considered many-body effects Gal and Dover (82) point out that the transition $\Sigma N \rightarrow \Lambda N$ is dominated at low energies by $T = \frac{1}{2}$, ${}^3S_1 \rightarrow {}^3D_1$ transitions. If one neglects the 1S_0 contribution, the transition operator for the $\Sigma + \text{nucleus} \rightarrow \Lambda + \text{nucleus}$ transition is

$$\mathcal{T} = \sum_i v(\mathbf{r}_i - \mathbf{r}_{\Sigma}) \left(\frac{3}{4} + \frac{1}{4} \boldsymbol{\sigma}_i \cdot \boldsymbol{\sigma}_{\Sigma} \right) \left(\frac{1}{3} - \frac{1}{3} \mathbf{t}_{\Sigma} \cdot \mathbf{t}_i \right)$$

where \mathbf{t}_{Σ} is the isospin operator for the Σ where $t_{\Sigma}^2 = 2$. This does lead to a reduction in width for some levels for light nuclei.

Finally, we mention the mechanism proposed by Dover and Feshbach (87, 90), who suggest that SU(3) symmetry breaking of the baryon–baryon interaction occurs only in the diagonal components. For the nondiagonal components responsible for the $\Sigma \rightarrow \Lambda$ transition, SU(3) symmetry is conserved. In analogy with the SU(2) isobar analog states, where the Coulomb symmetry-breaking interaction has small non diagonal components and relatively large diagonal matrix elements, these authors propose that the Σ hypernuclear states are SU(3) analog states.

There are several other suggestions, which are discussed by Millener, Dover, and Gal (89) in their review article, to which the reader is referred. Needless to say, more experiments are needed!

APPENDIX A

SCATTERING THEORY

H AND V HERMITIAN

Lippman–Schwinger Equation

$$\psi^{(+)} = \phi + \frac{1}{E^{(+)} - H_0} V \psi^{(+)} \quad (1)$$

$$= \phi + \frac{1}{E^{(+)} - H} V \phi \quad (2)$$

where

$$H_0 \phi = E \phi$$

and

$$E^{(+)} = E + i\eta \quad \eta \rightarrow 0^+ \\ \psi^{(-)} = \phi + \frac{1}{E^{(-)} - H_0} V \psi^{(-)} \quad (3)$$

$$= \phi + \frac{1}{E^{(-)} - H} V \phi \quad (4)$$

where

$$E^{(-)} = E - i\eta \quad \eta \rightarrow 0^+ \\ \psi^{(+)}(\mathbf{k}_i, \mathbf{r}) = \psi^{(-)*}(-\mathbf{k}_i, \mathbf{r}) \quad (5)$$

\mathcal{T} Matrix

$$\mathcal{T}_{fi} = \langle \psi_f^{(-)} V \phi_i \rangle = \langle \phi_f \mathcal{T}(E^{(+)}) \phi_i \rangle \quad (6)$$

$$= \langle \phi_f V \psi_i^{(+)} \rangle \quad \text{when } E_f = E_i \quad (7)$$

$$\mathcal{T}(E) = V + V \frac{1}{E - H_0} \mathcal{T}(E) \quad (8)$$

$$= V + V \frac{1}{E - H} V \quad (9)$$

Reaction Probability/Time

$$w_{fi} = \frac{2\pi}{\hbar} |\mathcal{T}_{fi}|^2 \delta(E_f - E_i)$$

For comparison with experiment, one must average over the initial states (e.g., spin) and sum over final states. The sum over final energies is the integral

$$d\bar{w}_{fi} = \int \rho_f dw_{fi} dE_f = \frac{2\pi}{\hbar} |\mathcal{T}_{fi}|^2 \rho_f \quad E_f = E_i \quad (10)$$

where ρ_f is the density of states at E_f and $\phi_{f,i} = \exp[i(\mathbf{k}_{f,i} \cdot \mathbf{r})]$.

Cross Section

$$\frac{d\sigma}{d\Omega} = \frac{w_{fi}}{j_i}$$

where j_i is the incident current.

Let $H = H_0 + V_0 + V_1$; then

$$\mathcal{T}_{fi} = \langle \phi_f V_0 \chi_i^{(+)} \rangle + \langle \chi_f^{(-)} V_1 \psi_i^{(+)} \rangle \quad (11)$$

where

$$(H_0 + V_0)\chi = E\chi$$

Single Channel

$$\rho_f = \left(\frac{1}{2\pi}\right)^3 k_f^2 \frac{dk_f}{dE} = \left(\frac{1}{2\pi}\right)^3 \frac{\mu}{\hbar^2} k_f \quad (12)$$

where

μ = reduced mass

$$j_i = \frac{\hbar k_i}{\mu} \quad (13)$$

$$\frac{d\sigma}{d\Omega} = \frac{1}{(2\pi)^2} \frac{\mu^2 k_f}{\hbar^4 k_i} |\mathcal{T}_{fi}|^2$$

Scattering Amplitude

$$f_{fi} = -\frac{1}{2\pi} \frac{\mu}{\hbar^2} \mathcal{T}_{fi} \quad (14)$$

The appearance of these formulas depends on the normalization of ϕ_i . For example, let

$$\phi_i = \sqrt{\rho_i} e^{i\mathbf{k}_i \cdot \mathbf{r}} \quad \text{and} \quad \phi_f = \sqrt{\rho_f} e^{i\mathbf{k}_f \cdot \mathbf{r}}$$

Then

$$\bar{w}_{fi} = \frac{2\pi}{\hbar} |\mathcal{T}_{fi}|^2$$

and

$$\frac{d\sigma}{d\Omega} = \frac{(2\pi)^4}{k_i^2} |\mathcal{T}_{fi}|^2 \quad (15)$$

It is important to ascertain the normalization of $\phi_{i,f}$, $\psi_i^{(+)}$, and $\psi_f^{(-)}$.

S Matrix

$$S_{fi} = \langle \psi_f^{(-)}, \psi_i^{(+)} \rangle = \langle \phi_f, S\phi_i \rangle \quad (16)$$

$$SS^\dagger = S^\dagger S = 1 \quad (17)$$

$$S = 1 - 2\pi\mathcal{T}\delta(E_f - E_i) \quad (18)$$

$$\mathcal{T}_{if}^* - \mathcal{T}_{fi} = 2\pi i \sum_g \mathcal{T}_{gf}^* \mathcal{T}_{gi} \quad (E_f = E_i = E)$$

Single-Channel

$$\mathcal{T}^*(\mathbf{k}_i, \mathbf{k}_f) - \mathcal{T}(\mathbf{k}_f, \mathbf{k}_i) = 2\pi i \rho \int \mathcal{T}^*(\mathbf{k}_g, \mathbf{k}_f) \mathcal{T}(\mathbf{k}_g, \mathbf{k}_i) d\Omega_g \quad (19)$$

or

$$f(\mathbf{k}_f, \mathbf{k}_i) - f^*(\mathbf{k}_i, \mathbf{k}_f) = \frac{ik}{2\pi} \int f^*(\mathbf{k}_g, \mathbf{k}_f) f(\mathbf{k}_g, \mathbf{k}_i) d\Omega_g \quad (20)$$

where in both Eq. (19) and Eq. (20)

$$E_f = E_i = E$$

Generally,

$$\sigma_{\text{tot}} = \frac{4\pi}{k} \text{Im} f(0^\circ) \quad (21)$$

This equation holds even when H is not Hermitian.

\mathcal{K} Matrix

Let

$$\psi^{(0)} = \phi + \mathcal{P} \frac{1}{E - H_0} V \psi^{(0)}$$

where \mathcal{P} symbolizes the principal value of the integral.

$$\begin{aligned} \mathcal{P} \frac{1}{E - H_0} &= \frac{1}{2} \left[\frac{1}{E^{(+)} - H_0} + \frac{1}{E^{(-)} - H_0} \right] \\ \mathcal{K}_{ba} &\equiv \langle \phi_b, V \psi_a^{(0)} \rangle \end{aligned} \quad (22)$$

The operator \mathcal{K} is defined by

$$\mathcal{K}_{ba} = \langle \phi_b, \mathcal{K} \phi_a \rangle \quad (23)$$

$$\mathcal{K} = V + V \frac{\mathcal{P}}{E - H_0} \mathcal{K} \quad (24)$$

$$\psi^{(0)} = \psi^{(+)} (1 + i\pi \mathcal{K}) \quad (25)$$

$$\psi^{(+)} = \psi^{(0)} (1 - i\pi \mathcal{T}) \quad (26)$$

$$\mathcal{K} = \mathcal{T} + i\pi \mathcal{T} \mathcal{K} = \mathcal{T} + i\pi \mathcal{K} \mathcal{T} \quad \text{Heitler integral equation} \quad (27)$$

or

$$\mathcal{T} = \frac{\mathcal{K}}{1 + i\pi \mathcal{K}} \quad (28)$$

$$S = \frac{1 - i\pi \mathcal{K}}{1 + i\pi \mathcal{K}} \quad (29)$$

K is Hermitian,

$$\mathcal{K}_{ba} = \langle \phi_b, V_0 \chi_a^{(0)} \rangle + \langle \chi_b^{(0)}, V_1 \psi_a^{(0)} \rangle \quad (30)$$

where

$$\begin{aligned} \chi_a^{(0)} &= \phi_a + \frac{\mathcal{P}}{E - H_0} V_0 \chi_a^{(0)} = \phi_a + \frac{\mathcal{P}}{E - H_0 - V_0} V_0 \phi_a \\ \psi_a^{(0)} &= \phi_0 + \frac{\mathcal{P}}{E - H_0 - V_0} V_1 \psi_a^{(0)} \end{aligned}$$

Dispersion Relations

Subject to the condition that $\int |V(\mathbf{r})| d\mathbf{r}$ is bounded

$$\operatorname{Re} f(0^\circ) = f_{\text{Born}}(0^\circ) - \frac{2\pi\hbar^2}{\mu} \sum \frac{N_b^2}{E + \varepsilon_b} + \frac{1}{4\pi^2} \mathcal{P} \int_0^\infty \frac{k' \sigma_{\text{tot}}(E')}{E' - E} dE' \quad (31)$$

where ε_b are the binding energy of the bound states whose normalized wave function asymptotically satisfy

$$\psi_b \rightarrow N_b e^{-\kappa_b r/r} \quad \kappa_b = \sqrt{\frac{2\mu}{\hbar^2} \varepsilon_b} \quad (32)$$

H AND V NOT HERMITIAN[†]

Equation (4) is replaced by

$$\psi^{(-)} = \phi + \frac{1}{E^{(-)} - H^\dagger} V^\dagger \phi \quad (33)$$

In addition, two new functions need to be defined:

$$\tilde{\psi}^{(+)} = \phi + \frac{1}{E^{(+)} - H^\dagger} V^\dagger \phi \quad (34)$$

$$\tilde{\psi}^{(-)} = \phi + \frac{1}{E^{(-)} - H} V \phi \quad (35)$$

The function $\tilde{\psi}^{(+)}$ is the wave function for a regenerative potential V^\dagger of V is absorptive. We note that

$$\langle \tilde{\psi}_a^{(+)}, \psi_b^{(+)} \rangle = \delta_{ab} \quad \langle \psi_a^{(-)}, \tilde{\psi}_b^{(-)} \rangle = \delta_{ab} \quad (36)$$

[†]Feshbach (85).

The S matrix remains as defined by (16). We define

$$\tilde{S}_{ba} = \langle \tilde{\psi}_b^{(+)}, \tilde{\psi}_a^{(-)} \rangle = \langle \phi_b, \tilde{S} \phi_a \rangle \quad (37)$$

Then

$$S\tilde{S} = \tilde{S}S = 1 \quad (38)$$

If

$$\tilde{\mathcal{T}}_{ba} = \langle \tilde{\psi}_b^{(+)} V \phi_a \rangle = \langle \phi_b V \tilde{\psi}_a^{(-)} \rangle \quad E_a = E_b$$

then

$$\tilde{S}_{ba} = \delta_{ba} + 2\pi i \delta(E_a - E_b) \tilde{\mathcal{T}}_{ba} \quad (39)$$

$$\tilde{\mathcal{T}} - \mathcal{T} = 2\pi i \mathcal{T} \tilde{\mathcal{T}} = 2\pi i \tilde{\mathcal{T}} \mathcal{T} \quad (40)$$

If

$$\mathcal{T}^{(e)} = \frac{1}{2}(\tilde{\mathcal{T}} - \mathcal{T})$$

and

$$\mathcal{T}^{(0)} = \frac{1}{2}(\tilde{\mathcal{T}} + \mathcal{T})$$

then for $q = 0$,

$$\mathcal{T}^{(0)} = \mathcal{T}_{\text{Born}} + \frac{1}{\pi i} \mathcal{P} \int \frac{dE'}{E - E'} \mathcal{T}^{(e)}(E') + \text{sum over bound states}$$

Let

$$\tilde{\mathcal{K}}_{ba} = \langle \phi_b V \tilde{\psi}_a^{(+)} \rangle = \langle \phi_b \tilde{\mathcal{K}} \phi_a \rangle \quad (41)$$

Then

$$\tilde{\mathcal{K}} = \mathcal{K}$$

$$\tilde{S} = \frac{1 + i\pi \mathcal{K}}{1 - i\pi \mathcal{K}} \quad (42)$$

\mathcal{K} is not Hermitian.

Single Channel

$$\psi^{(+)} \xrightarrow[r \rightarrow \infty]{r} \frac{1}{r} (e^{-ikr} - S(k)e^{ikr})$$

$$\tilde{\psi}^{(-)} \xrightarrow[r \rightarrow \infty]{r} \frac{1}{r} (e^{ikr} - \tilde{S}(k)e^{-ikr})$$

For a potential $V + iW$,

$$f(\mathbf{k}_f, \mathbf{k}_i) - f^*(\mathbf{k}_i, \mathbf{k}_f) = \frac{ik}{2\pi} \int d\Omega_g f^*(\mathbf{k}_g, \mathbf{k}_f) f(\mathbf{k}_g, \mathbf{k}_i) - \frac{i}{2\pi} \int \psi^{(+)*}(\mathbf{k}_f, \mathbf{r}) \frac{2\mu}{\hbar^2} W \psi^{(+)}(\mathbf{k}_i, \mathbf{r}) d\mathbf{r} \quad (44)$$

Phase-Shift Analysis

Scattering of a spinless particle by a spinless nucleus. Central potential

$$f(\vartheta, \varphi) = \frac{1}{2ik} \sum (2l+1) P_l(\cos \vartheta) (e^{2i\delta_l} - 1) \quad (45)$$

$$\langle l'm' | S | lm \rangle = S_l \delta(l, l') S(m, m')$$

$$S_l = e^{2i\delta_l} \quad (46)$$

$$\mathcal{T}_l = -\frac{1}{\pi} e^{i\delta_l} \sin \delta_l \quad (47)$$

$$\sigma_{el} = \frac{4\pi}{k^2} \sum_l (2l+1) |S_l - 1|^2 \quad (48)$$

$$\sigma_a = \frac{\pi}{k^2} \sum (2l+1) [1 - |S_l|^2] \quad (49)$$

If $\delta_l = \xi_l + i\eta_l$,

$$|S_l - 1|^2 = 1 - 2e^{-2\eta_l} \cos 2\xi_l + e^{-4\eta_l} \quad (50)$$

$$1 - |S_l|^2 = 1 - e^{-4\eta_l} \quad (51)$$

Transmission Factor

$$T_l = 1 - |S_l|^2 \quad (52)$$

Zero-Energy Limit (Uncharged Particles)

$$S_l \rightarrow O(k^{2l+1}) \quad (53)$$

$$T_l \rightarrow O(k^{2l+1}) \quad (54)$$

Effective Range

$$k^{2l+1} \cot \delta_l = -\frac{1}{a_l} + \frac{1}{2} k^2 r_l \quad (55)$$

$a_l \equiv$ scattering length

$r_l \equiv$ effective range

For $l=0$, a_0 and r_0 have the dimension of a length. $l=1$, a_l , and r_l have the dimensions of a volume. In Chapter X on kaon-nucleus interactions, the minus sign on the right-hand side (55) is dropped.

Effective Volume

$$\frac{\tan \delta_l}{k^{2l+1}} = -a_l - \frac{1}{2}k^2 v_l \quad (56)$$

For $l=0$, v_l has the dimensions of a volume.

Elastic Scattering of a Spin Zero by a Spin- $\frac{1}{2}$ System

$$\begin{aligned} \hat{f}(k, \vartheta) &= A(k, \vartheta) + B(k, \vartheta) \boldsymbol{\sigma} \cdot \mathbf{n} \\ \mathbf{n} &= \frac{\mathbf{k}_i \times \mathbf{k}_f}{|\mathbf{k}_i \times \mathbf{k}_f|} \end{aligned} \quad (57)$$

where $\hbar \mathbf{k}_i$ = incident momentum and $\hbar \mathbf{k}_f$ = final momentum.

$$\begin{aligned} A(k, \vartheta) &= \frac{1}{2ik} \sum_0^\infty [(l+1)(e^{2i\delta_l^{(+)}} - 1) + l(e^{2i\delta_l^{(-)}} - 1)] P_l(\cos \vartheta) \\ B(k, \vartheta) &= \frac{1}{2k} \sum_1^\infty (e^{2i\delta_l^{(+)}} - e^{2i\delta_l^{(-)}}) P_l^{(1)}(\cos \vartheta) \\ P_l^{(1)} &= \sin \vartheta \frac{d}{d(\cos \vartheta)} P_l(\cos \vartheta) \end{aligned} \quad (58)$$

where asymptotically ($r \rightarrow \infty$),

$$\psi(j = l \pm \frac{1}{2}) \rightarrow \sin \left(kr - \frac{l\pi}{2} + \delta_l^{(\pm)} \right) \quad (59)$$

$$\left(\frac{d\sigma}{d\Omega} \right)_{\text{unpol}} = |A|^2 + |B|^2 \quad (60)$$

$$\sigma_{\text{tot}}^{\text{el}} = \frac{\pi}{k^2} \sum_{l=0}^\infty \{ (l+1) |e^{2i\delta_l^{(+)}} - 1|^2 + l |e^{2i\delta_l^{(-)}} - 1|^2 \} \quad (61)$$

$$\mathbf{P} = \text{polarization} = \frac{\text{tr } \hat{f}^\dagger \boldsymbol{\sigma} f}{\text{tr } \hat{f}^\dagger \cdot \hat{f}} = 2 \frac{\text{Re } AB^*}{|A|^2 + |B|^2} = 2P\mathbf{n} \quad (62)$$

$$\left(\frac{d\sigma}{d\Omega} \right)_{\text{pol}} = \left(\frac{d\sigma}{d\Omega} \right)_{\text{unpol}} [1 + P_p P_{\mathbf{n}_p} \cdot \mathbf{n}] \quad (63)$$

where $P_p \mathbf{n}_p$ is the beam polarization,

$$Q = \frac{2 \operatorname{Im} AB^*}{|A|^2 + |B|^2} \quad (64)$$

Coulomb Wave Function: Elastic Scattering

$$\left(\nabla^2 + k^2 - \frac{2\eta k}{r} \right) \psi(\mathbf{r}) = 0 \quad \eta = \frac{Z_1 Z_2 e^2}{\hbar v} \quad v = \text{velocity}$$

$$\psi(\mathbf{r}) = \Gamma(1 + i\eta) e^{-(1/2)\pi\eta} e^{ikz} F(-i\eta; 1; ik(r-z))$$

$$F(a, b; \xi) = 1 + \frac{a}{b} \xi + \frac{1}{2!} \frac{a(a+1)}{b(b+1)} \xi^2 + \dots \quad (65)$$

$$\psi \rightarrow e^{i[kz + \eta \ln k(r-z)]} - \frac{\eta}{k(r-z)} \frac{\Gamma(1+i\eta)}{\Gamma(1-i\eta)} e^{i(kr - \eta \ln k(r-z))} \quad (66)$$

$$f = -\frac{\eta}{2k \sin^2 \frac{1}{2} \vartheta} e^{-i\eta \ln \sin^2 (1/2) \vartheta + 2i\sigma_0} \quad (67)$$

$$e^{2i\sigma_0} = \frac{\Gamma(1+i\eta)}{\Gamma(1-i\eta)} \quad (68)$$

$$\text{Rutherford cross section} = \frac{\eta^2}{4k^2} \sin^4 \frac{\vartheta}{2} \quad (69)$$

Partial Wave Expansion

$$\psi_{lm} = Y_{lm} \frac{F_l(r)}{kr}$$

where F_l = regular spherical Coulomb wave function,

$$F_l'' + \left[k^2 - \frac{2\eta k}{r} - \frac{l(l+1)}{r^2} \right] F_l = 0$$

$$F_l = \frac{2^l e^{-(1/2)\pi\eta} |\Gamma(l+1+i\eta)|}{(2l+1)!} e^{-ikr} (kr)^{l+1} F(l+1-i\eta; 2l+2; 2ikr)$$

$$\rightarrow \sin \left(kr - \eta \ln 2kr - \frac{l\pi}{2} + \sigma_l \right) \quad kr \rightarrow \infty$$

$$\rightarrow C_l (kr)^{l+1}$$

$$e^{2i\sigma_l} = \frac{\Gamma(l+1+i\eta)}{\Gamma(l+1-i\eta)} \quad (70)$$

$$\psi = \frac{1}{kr} \Sigma (2l+1) i^l e^{i\sigma_l} F_l(r) P_l(\cos \theta) \quad (71)$$

G_l = irregular spherical Coulomb wave function

$$\rightarrow \cos \left(kr - \eta \ln 2kr - \frac{l\pi}{2} + \sigma_l \right) \quad kr \rightarrow \infty$$

$$G_l \rightarrow \frac{1}{(2l+1)C_l} (kr)^{-l} \left[1 + \begin{cases} O(\eta kr \ln kr) & l=0 \\ O\left(\frac{\eta}{l} kr\right) & l \neq 0 \end{cases} \right] \quad kr \rightarrow 0$$

$$C_l = \frac{2^l e^{-\pi\eta/2} |\Gamma(l+1+i\eta)|}{(2l+1)!} \quad \sigma_l = \sigma_0 + \sum_{t=1}^l \tan^{-1} \frac{\eta}{t} \quad (72)$$

$$C_0^2 = \frac{2\pi\eta}{e^{2\pi\eta} - 1} \quad (73)$$

$$C_l^2 = \frac{(1+\eta^2)(4+\eta^2)\cdots(l^2+\eta^2)2^{2l}}{(2l+1)^2[(2l)!]^2} C_0^2 \quad (74)$$

For properties of these functions and numerical values, see Chapter 14 (p. 537 et seq.) of *Handbook of Mathematical Functions*, M. Abramovitz and I. A. Stegun, eds., National Bureau of Standards (U.S. Government Printing Office, Washington, D.C., 1964).

The solutions of the field-free equations

$$\frac{d^2 u}{d\zeta^2} + \left[1 - \frac{l(l+1)}{\zeta^2} \right] u = 0 \quad (75)$$

of interest are

$$u_l = \zeta j_l(\zeta)$$

$$v_l = \zeta n_l(\zeta)$$

$$w_l^{(+)} = v_l + iu_l = i\zeta h_l(\zeta) \quad (76)$$

where j_l , n_l , and h_l are the spherical Bessel, Neumann, and Hankel functions:

$$u_l \xrightarrow{\zeta \rightarrow 0} \frac{\zeta^{l+1}}{(2l+1)!!} \quad v_l \xrightarrow{\zeta \rightarrow 0} \frac{(2l-1)!!}{\zeta^l} \quad (77)$$

$$\xrightarrow{\zeta \rightarrow \infty} \sin\left(\zeta - \frac{l\pi}{2}\right) \quad \xrightarrow{\zeta \rightarrow \infty} \cos\left(\zeta - \frac{l\pi}{2}\right) \quad (78)$$

$$w_l \xrightarrow{\zeta \rightarrow 0} v_l \quad (79)$$

$$\xrightarrow{\zeta \rightarrow \infty} e^{i(\zeta - l\pi/2)} \quad (80)$$

$$\begin{aligned}
u_0(\zeta) &= \sin \zeta & v_0 &= \cos \zeta \\
u_1(\zeta) &= \frac{\sin \zeta}{\zeta} - \cos \zeta & v_1 &= \frac{\cos \zeta}{\zeta} + \sin \zeta \\
u_2(\zeta) &= \left(\frac{3}{\zeta^2} - 1 \right) \sin \zeta - \frac{3}{\zeta} \cos \zeta & v_2 &= \left(\frac{3}{\zeta^2} - 1 \right) \cos \zeta + \frac{3}{\zeta} \sin \zeta \quad (81)
\end{aligned}$$

$$w_0^{(+)} = e^{i\zeta} \quad w_1^{(+)} = \frac{1 - i\zeta}{\zeta} e^{i\zeta} \quad w_2^{(+)} = \frac{3 - 3i\zeta - \zeta^2}{\zeta^2} e^{i\zeta} \quad (82)$$

Recurrence relations satisfied by u_l, v_l , and $w_l^{(+)}$:

$$\frac{2l+1}{\zeta} u_l = u_{l-1} + u_{l+1} \quad (2l+1)u'_l = (l+1)u_{l-1} - lu_{l+1} \quad (83)$$

APPENDIX B

CROSS SECTIONS; VECTOR AND TENSOR POLARIZATIONS[†]

In the following it will be assumed that the target has zero spin and the projectile a spin of S . This is a useful choice since many of the target nuclei have zero spin. But it is also totally general since it applies to the channel spin representation, in which the spin of the projectile and target are combined and then combined with the relative orbital angular momentum, \mathbf{l} :

$$\mathbf{S} = \mathbf{S}_T + \mathbf{S}_P$$

and

$$\mathbf{J} = \mathbf{l} + \mathbf{S}$$

\mathbf{S}_T and \mathbf{S}_P are the target and projectile spins, respectively.

Let the reaction amplitude be

$$f(\alpha_i SM_i \rightarrow \alpha_f SM_f) = \langle SM_f | \hat{F}(\alpha_f, \alpha_i) | SM_i \rangle \quad (1)$$

In this equation M_i and M_f are components of \mathbf{S} along an arbitrary direction. The parameters α and α' are the remaining quantum numbers needed to specify the initial and final states, including the relative momenta $\hbar \mathbf{k}_f$ and $\hbar \mathbf{k}_i$ for the final nucleus plus emergent particle and the initial nucleus plus projectile, respectively.

[†]Kerman (62).

CROSS SECTIONS AS TRACES

$$\sigma_{\text{tot}} = \frac{1}{2S+1} \text{tr } \hat{F}^\dagger \hat{F} \quad (2)$$

where the trace is performed with respect to all the variables,

$$\frac{d\sigma}{d\Omega} = \frac{1}{2S+1} \text{tr } \hat{F}^\dagger P_f \hat{F} P_i \quad (3)$$

where P_f and P_i are projection operators

$$\begin{aligned} P_f &= |\hat{\mathbf{k}}_f\rangle \langle \hat{\mathbf{k}}_f| \\ P_i &= |\hat{\mathbf{k}}_i\rangle \langle \hat{\mathbf{k}}_i| \end{aligned}$$

so that, for example,

$$\langle \hat{\mathbf{k}} | P_f | \hat{\mathbf{K}} \rangle = \delta(\hat{\mathbf{k}} - \hat{\mathbf{k}}_f) \delta(\hat{\mathbf{k}}_f - \hat{\mathbf{K}}) \quad (4)$$

For orbital angular momentum states $|lm\rangle$,

$$\langle lm | P_f | l'm' \rangle = (-1)^{l-m} \sum_{LM} Y_{LM}^* \begin{pmatrix} l & L & l' \\ -m & M & m' \end{pmatrix} (l \| Y_L \| l') \quad (5)$$

Let

$$\hat{F} = \sum_{l'l'J\mu} |l'SJM\rangle f_J(l', l) \langle l'SJM| \quad (6)$$

where

$$|l'SJM\rangle = \sum (lm; Sm_s | JM) |lm\rangle |Sm_s\rangle$$

and f_J also depends upon S . Then

$$\hat{F}(m_i \rightarrow m_f, \mathbf{k}_i \rightarrow \mathbf{k}_f) = \sum_{\substack{\lambda J \\ l, l' \\ \mu}} \mathcal{B}_{\lambda\mu}(l', l) i^{l'-l} (-1)^{J+m_f} f_{JS}(l', l) \begin{Bmatrix} l' & S & J \\ S & l & \lambda \end{Bmatrix} (Sm_i S - m_f | \lambda\mu) \quad (7)$$

where

$$\mathcal{B}_{\lambda\mu}(l', l) = \sqrt{\frac{2l+1}{4\pi}} Y_{l'\mu}(\hat{\mathbf{k}}_f) (l'\mu | 0 | \lambda\mu) \quad (8)$$

The z -axis has been taken along the incident projectile direction \mathbf{k}_i . The

differential cross section is

$$\begin{aligned} \frac{d\sigma}{d\Omega_f} = & \frac{1}{2S+1} \sum_{\substack{L, J_1, J_2 \\ l_1, l_1' \\ l_2, l_2' \\ \mu}} (-1)^{J_1 - J_2} f_{J_1}(l_1', l_1) f_{J_2}^*(l_2', l_2) P_L(\cos \vartheta) \\ & \times (l_1 S J_1 \parallel Y_L \parallel l_2 S J_2)(l_2' S J_2 \parallel Y_L \parallel l_1' S J_1) \end{aligned} \quad (9)$$

POLARIZATION TENSORS: $T_{\lambda\mu}(\hat{\mathbf{S}})$

$$T_{\lambda\mu}^\dagger(\hat{\mathbf{S}}) = (-1)^\mu T_{\lambda, -\mu}(\hat{\mathbf{S}}) \quad \lambda \leq 2S \quad (10)$$

normalization

$$\langle S \parallel T_{\lambda\mu}(\hat{\mathbf{S}}) \parallel S \rangle = \sqrt{2S+1} \quad (11)$$

$$\langle S\sigma \parallel T_{\lambda\mu} \parallel S\sigma' \rangle = (S\sigma'; \lambda\mu \parallel S\sigma) \quad (12)$$

$$T_{00} = 1$$

$$T_{10} = \frac{S_z}{\sqrt{S(S+1)}} \quad T_{1, \pm 1} = \frac{\mp (S_x \pm iS_y)}{\sqrt{2S(S+1)}} \quad (13)$$

$$T_{20} = \frac{3S_z^2 - S(S+1)}{\sqrt{S(S+1)(2S+3)(2S-1)}}$$

Expectation value of $T_{\lambda\mu}$ in the final state averaged over an unpolarized initial state,

$$\langle \overline{T_{\lambda\mu}} \rangle = \frac{1}{2S+1} \text{tr} \hat{F}^\dagger P_f T_{\lambda\mu} \hat{F} P_i \quad (14)$$

$$\begin{aligned} &= \frac{1}{(2S+1)\sqrt{4\pi}} \sum (-1)^{J_2 - J_1} Y_{L'M'}^*(\hat{\mathbf{k}}_f) \frac{(L'M'; \lambda, \mu \parallel L0)}{\sqrt{2L+1}} \\ &\quad \times (l_1 S J_1 \parallel Y_L \parallel l_2 S J_2)(l_2' S J_2 \parallel T_\Lambda(L', \lambda) \parallel l_1' S J_1) \\ &\quad \times f_{J_1}(l_1', l_1) f_{J_2}^*(l_2', l_2) \end{aligned} \quad (15)$$

where

$$\begin{aligned} T_\Lambda(L', \lambda) &= (Y_{L'} \otimes T_\lambda)^\Lambda \\ T_{\Lambda, M} &= \sum_{q, M'} (L' - M'; \lambda q \parallel \Lambda, M) Y_{L' - M'} T_{\lambda q} \end{aligned} \quad (16)$$

SPIN- $\frac{1}{2}$ PROJECTILE

Let the polarization induced by a scatterer on an unpolarized beam be

$$\mathbf{P}_s = P_s \mathbf{n}_s$$

where \mathbf{n}_s is a unit vector normal to the scattering plane:

$$\mathbf{n}_s = \frac{(\mathbf{k}_i \times \mathbf{k}_f)}{|\mathbf{k}_i \times \mathbf{k}_f|} \quad (17)$$

where \mathbf{k}_i is the incident direction and \mathbf{k}_f the final direction of the spin- $\frac{1}{2}$ projectile.

The cross section for the scattering of a beam with polarization $P\mathbf{n}$ by the scatterer above is

$$\sigma_{0s} = \sigma_0(1 + PP_s \mathbf{n} \cdot \mathbf{n}_s) \quad (18)$$

where σ_0 is the cross section for an unpolarized beam.

The general expression for the scattering of a polarized beam with polarization \mathbf{P} is

$$\begin{aligned} \sigma_s \mathbf{P}_s = \sigma_{0s} \{ & \mathbf{n}[P_{0s} + D_s \mathbf{n} \cdot \mathbf{P}] + (\mathbf{n} \times \hat{\mathbf{k}}_f)[A_s \hat{\mathbf{k}}_i \cdot \mathbf{P} + R_s(\mathbf{n} \times \hat{\mathbf{k}}_i) \cdot \mathbf{P}] \\ & + \hat{\mathbf{k}}_f[A'_s(\hat{\mathbf{k}}_i \cdot \mathbf{P}) + R'_s(\mathbf{n} \times \hat{\mathbf{k}}_i) \cdot \mathbf{P}] \} \end{aligned} \quad (19)$$

TIME-REVERSAL INVARIANCE

$$A = -R' \quad (20)$$

If the incident beam is unpolarized,

$$\mathbf{P}_s = \mathbf{n}P_{0s} \quad (21)$$

If the polarization of the incident beam is in the \mathbf{n} direction,

$$\mathbf{P}_s = \mathbf{n}(P_{0s} + PD_s) \quad (22)$$

D_s is the depolarization. Under time-reversal invariance, $-1 + 2P_s \leq D_s \leq 1$:

$$D_s = 1 \quad \text{spin 0 target} \quad (23)$$

$$Q_s = -[A_s \cos \vartheta + R_s \sin \vartheta] = \frac{2 \operatorname{Im} A^* B}{|A|^2 + |B|^2} \quad \text{spin 0 target} \quad (24)$$

$$Q'_s = R_s \cos \vartheta - A_s \sin \vartheta = |A|^2 - |B|^2 \quad \text{spin 0 target} \quad (25)$$

$$P_s = \frac{2 \operatorname{Re} A^* B}{|A|^2 + |B|^2} \quad \text{spin 0 target} \quad (26)$$

$$\left(\frac{d\sigma}{d\Omega} \right)_{\text{unpol}} = |A|^2 + |B|^2 \quad \text{spin 0 target} \quad (27)$$

BIBLIOGRAPHY

We list below the references that have proven useful or supplement our discussion in an important way. Reviews that present the most recent descriptions are found in *AIP Conference Proceedings*, *Advances in Nuclear Physics*, *Annual Review of Nuclear and Particle Science*, *Physics Reports*, and *Reviews of Modern Physics*. Conference reports are a valuable source of information. The International Conference on Nuclear Physics, in which the entire field is reviewed, has been held in 1980 (Berkeley), 1983 (Florence), 1986 (Harrogate), and 1989 (São Paulo). The conferences on Particles and Nuclei (PANIC), which review advances in intermediate-energy physics, have been held in 1981 (Versailles), 1984 (Heidelberg), 1987 (Kyoto), and 1990 (Cambridge, USA). Nucleus–nucleus collisions have been discussed in conferences in 1982 (East Lansing), 1985 (Visby), and 1988 (St. Malo). Many meetings on more specialized aspects are held every year. They are too numerous to be listed here. We mention only *Proceedings of the International School of Physics “Enrico Fermi,”* and the publication of “schools” at Les Houches, at Erice, and at the International Center for Theoretical Physics at Trieste.

General references that were broadly useful are listed below. More specialized sources are referenced at the beginning of most of the sections of this volume.

GENERAL REFERENCES

- Austern, N., *Direct Nuclear Reaction Theories* (John Wiley & Sons, New York, 1970).
Barrett, R. C. and D. F. Jackson, *Nuclear Sizes and Structure* (Clarendon Press, Oxford, 1977).

- Blatt, J. M., and V. F. Weisskopf, *Theoretical Nuclear Physics* (John Wiley & Sons, New York, 1952).
- Bohr, A., and Ben R. Mottelson, *Nuclear Structure* (W.A. Benjamin, New York, 1962).
- Bromley, D. A., ed., *Treatise on Heavy Ion Science* (Plenum Press, New York, 1984).
- deShalit, A., and H. Feshbach, *Theoretical Nuclear Physics*, Vol. 1 (John Wiley & Sons, New York, 1974).
- Dietrich, K., M. DiToro, and H. J. Mang, eds., *Proceedings of the Winter College on Fundamental Nuclear Physics* (World Scientific, Singapore, 1985).
- Eisenberg, J. M., and W. Greiner, *Excitation Mechanisms of the Nucleus* (North-Holland, Amsterdam, 1970).
- Marmier, P., and E. Sheldon, *Physics of Nuclei and Particles* (Academic Press, New York, 1969).
- Satchler, J. R., *Direct Nuclear Reactions* (Clarendon Press, Oxford, 1983).

REFERENCES

- Abduzhamislov, A., et al., *Phys. Rev. D* **35**, 3537 (1987).
- Abe, Y., in *Nuclear Molecular Phenomena*, N. Cindro, ed. (North-Holland, Amsterdam, 1978).
- Abul-Magd, A., and J. Hüfner, *Z. Phys. A* **277**, 379 (1976).
- Abul-Magd, A., J. Hüfner, and B. Schürmann, *Phys. Lett.*, **60B**, 327 (1976).
- Acheson, L. K., *Phys. Rev.* **82**, 488 (1951).
- Adams, D., and M. Bleszynski, *Phys. Lett.* **136B**, 10 (1984).
- Agassi, D., and C. M. Ko, and H. A. Weidenmüller, *Ann. Phys. (NY)* **107**, 140 (1977); **117**, 404 (1979).
- Agassi, D., and H. A. Weidenmüller, *Phys. Rev. C* **22**, 147 (1975).
- Agassi, D., G. Montzouranis, and H. A. Weidenmüller, *Phys. Rev.* **22**, 145 (1975).
- Aichelin, J., *Phys. Rev. C* **33**, 537 (1986).
- Aichelin, J., and G. Bertsch, *Phys. Rev. C* **31**, 1730 (1985).
- Aichelin, J., J. Cugnon, Z. Fraenkel, K. Fraenkel, C. Gale, M. Gyulassy, D. Kean, C. M. Ko, J. Randrup A. Rosenbaum, H. Stöcker, G. Welke, and J. Q. Wu, *Phys. Rev. Lett.* **62**, 1461 (1989).
- Alberico, W. M., A. Molinari, T. W. Donnelly, E. L. Kronenberg, and J. W. van Orden, *Phys. Rev.* **38**, 1801 (1988).
- Alder, K., A. Bohr, T. Huus, B. Mottelson, and A. Winther, *Rev. Mod. Phys.* **28**, 432 (1956).
- Alexander, Y., and S. J. Wallace, *Phys. Rev. Lett.* **38**, 1272 (1972).
- Allardyce, B. W. et al., *Nucl. Phys. A* **209**, 1 (1973).
- Almqvist, E., D. A. Bromley, and J. A. Kuehner, *Phys. Rev. Lett.* **4**, 515 (1960); *Proceedings of the Second Conference on Heavy Ion Interactions* A. Zucker, F. T. Howard, and E. C. Halbert, eds. (John Wiley & Sons New York, 1960).
- Alston-Garnjost, M., R. P. Hamilton, R. W. Kinney, D. L. Pollard, R. D. Tripp, H. Nicholson, and D. M. Lazarus, *Phys. Rev. Lett.* **38**, 1003, 1007 (1977); *Phys. Rev. D* **18**, 182 (1978); **17**, 2216 (1978); **21**, 1191 (1980).

- Amado, R. D., *Adv. Nucl. Phys.* **15**, 1 (1985).
- Amado, R. D., F. Lenz, J. A. McNeil, and D. A. Sparrow, *Phys. Rev. C* **22**, 2094 (1980).
- Amsden, A. A., A. S. Goldhaber, F. H. Harlow, and J. R. Nix, *Phys. Rev. C* **17**, 2080 (1978).
- Amsden, A. A., F. H. Harlow, and J. R. Nix, *Phys. Rev. C* **15**, 2059 (1977).
- Arima, A., in *Clustering Aspects of Nuclear Structure and Nuclear Reactions*, Conference Proceedings 47, W. T. H. Van Oers, J. P. Svenne, J. S. C. McKee, and W. R. Falk, eds. (American Institute of Physics, New York, 1978).
- Arima, A., and F. Iachello, *Phys. Rev. Lett.* **35**, 1069 (1975); **40**, 385 (1978).
- Arima, A., and F. Iachello *Ann. Phys. (NY)* **99**, 273 (1976); **111**, 201 (1978); **123**, 468 (1979).
- Arima, A., Y. Horikawa, H. Hyuga, and T. Zuzuki, *Phys. Rev. Lett.* **40**, 1001 (1978).
- Arima, A., and S. Kubono, in *Treatise on Heavy Ion Science*, Vol. 1, D. A. Bromley, ed. (Plenum Press, New York, 1984).
- Arndt, R. A., and D. Roper, *Phys. Rev. D* **31**, 2230 (1985).
- Arndt, R. A., L. D. Roper, and P. H. Steinberg, *Phys. Rev. D* **18**, 3278 (1978).
- Arnold, L. G., B. C. Clark, R. L. Mercer, and P. Schwandt, *Phys. Rev. C* **23**, 1949 (1981).
- Arnold, L. G., et al., *Phys. Rev. C* **25**, 936 (1982).
- Ascutto, R. J., and N. K. Glendenning, *Phys. Rev.* **181**, 1396 (1969).
- Ascutto, R. J., N. K. Glendenning, and B. Sørensen, *Nucl. Phys. A* **183**, 60 (1972).
- Ascutto, R. J., C. H. King, L. J. McVay, and B. Sørensen, *Nucl. Phys. A* **226**, 454 (1974).
- Ascutto, R. J., and E. A. Seglie, *Treatise on Heavy Ion Science*, Chapter 5, Vol. 1, D. A. Bromley, ed. (Plenum Press, New York, 1984).
- Aubert, J. J., et al. (European Muon Collaboration), *Phys. Lett.* **123B**, 275 (1983).
- Auerbach, N., *Phys. Rev. C* **35**, 1798 (1987).
- Auerbach, E. H., A. J. Baltz, C. B. Dover, A. Gal, S. H. Kahana, L. Ludeking, and D. J. Millener, *Ann. Phys. (NY)* **148**, 381 (1983).
- Auerbach, N., and C. Dover, *Phys. Rev. Lett.* **17**, 1184 (1966).
- Auerbach, N., A. Gal, J. Hüfner, and A. K. Kerman, *Rev. Mod. Phys.* **44**, 48 (1972).
- Auerbach, N., W. R. Gibbs, J. N. Ginocchio, and W. B. Kaufmann, *Phys. Rev. C* **38**, 1277 (1988).
- Auerbach, N., W. R. Gibbs, and E. Piasetsky, *Phys. Rev. Lett.* **59**, 1076 (1987).
- Austern, N., *Ann. Phys. (NY)* **15**, 299 (1961).
- Austern, N., *Direct Nuclear Reaction Theories* (John Wiley & Sons, New York, 1970).
- Austern, N., in *The Interaction Between Medium Energy Nucleons in Nuclei—1982*, H. O. Meyer, ed. (American Institute of Physics, New York, 1983).
- Austern, N., and J. S. Blair, *Ann. Phys. (NY)* **33**, 15 (1965).
- Austern, N., Y. Iseri, M. Kamimura, M. Kawai, G. Rawitscher, and M. Yahiro, *Phys. Rep.* **154**, 126 (1987).
- Austern, N., and C. M. Vincent, *Phys. Rev. C* **20**, 2523 (1974).
- Austin, S., L. Avaldi, R. Bonetti, and L. Colli-Milazzo, *Phys. Lett.* **94B**, 463 (1980).
- Avaldi, L., R. Bonetti, and L. Colli-Milazzo, *Phys. Lett.* **94B**, 463 (1980).
- Ayik, S., and J. N. Ginocchio, *Nucl. Phys. A* **234**, 13 (1974).
- Ayik, S., and W. Nörenberg, *Z. Phys. A* **309**, 121 (1982).

- Baba, H. *Nucl. Phys. A* **159**, 625 (1970).
- Babinet, R., L. G. Moretto, J. Galin, R. Jared, J. Moulton, and S. G. Thompson, *Nucl. Phys. A* **258**, 172 (1976).
- Balian, R., M. Rho, and G. Ripka, eds., *Theory of Interactions in Nuclear Physics with Heavy Ions and Mesons* (North-Holland, Amsterdam, 1977).
- Balian, R., and M. Veneroni, *Ann. Phys. (NY)* **135**, 270 (1981).
- Baltz, A. J., P. D. Bond, J. D. Garrett, and S. Kahana, *Phys. Rev. C* **12**, 136 (1975).
- Bando, H., *Suppl. J. Phys. Soc. Jpn.* **58** (1989).
- Bang, J. M., and J. S. Vaagen, *Z. Phys. A* **297**, 233 (1980).
- Baranger, M., and M. Vénérioni, *Ann. Phys. (NY)* **114**, 123 (1978).
- Barker, J. R., and D. G. Sarantities, *Phys. Rev. C* **9**, 607 (1984).
- Barnes, C. A., in *Fusion Reactions Below the Coulomb Barrier*, Lecture Notes in Physics 219, S. M. Steadman, ed. (Springer-Verlag, Berlin, 1985).
- Barrett, R. C., and D. F. Jackson, *Nuclear Size and Structure* (Clarendon Press, Oxford, 1977).
- Barschall, H. H., *Phys. Rev.* **86**, 431 (1952).
- Bassichis, W. H., H. Feshbach, and J. F. Reading, *Ann. Phys. (NY)* **68**, 462 (1971).
- Bates, *Linear Accelerator Certificate Proposal for a CW Upgrade* (1984).
- Batty, C. J., *Nucl. Phys. A* **178**, 17 (1981).
- Bauhoff, W., H. V. von Geramb, and G. Pella, University of Hamburg internal report (1980).
- Baym, G., in *Proceedings of the International Nuclear Physics Conference—1986*, J. L. Dunell, J. M. Irvine, and G. C. Morrison, eds. (Institute of Physics, Bristol, England, 1987).
- Baym, G., and G. E. Brown, *Nucl. Phys. A* **247**, 395 (1975).
- Bayman, B., *Phys. Rev. Lett.* **25**, 1768 (1970); *Nucl. Phys. A* **168**, 1 (1971).
- Bear, K., and P. E. Hodgson, *J. Phys. G Nucl. Phys.* **4**, L287 (1978).
- Becchetti, F. D., Jr., and G. W. Greenlees, *Phys. Rev.* **182**, 1190 (1969).
- Beckerman, M., in *Fusion Reactions Below the Coulomb Barrier*, Lecture Notes in Physics 219, S. M. Steadman, ed. (Springer-Verlag Berlin, 1985).
- Bell, J. S., in *Lectures on the Many-Body Problem*, E. R. Caianello, ed. (Academic Press, New York, 1962), p. 91.
- Belote, T. A., N. Anyas-Weiss, J. A. Becker, J. C. Cornell, P. S. Fischer, P. N. Hudson, A. Menchaca-Rocha, A. D. Panigistou, and D. K. Scott, *Phys. Rev. Lett.* **30**, 450 (1973).
- Bernard, V., and N. Van Giai, *Lecture Notes in Physics* **89**, 118 (1978); *Nucl. Phys. A* **327**, 397 (1979).
- Bertini, R., in *Meson–Nuclear Physics*, AIP Conference Proceedings 54, E. V. Hungerford, ed. (Amer. Inst. of Physics, New York, 1979).
- Bertini, R., O. Bing, P. Birien, W. Brückner, H. Catz, A. Chaumeaux, J. M. Durand, M. A. Faessler, T. J. Ketel, K. Kilian, B. Mayer, J. Niewisch, B. Pietrzyk, B. Povh, H. G. Rotter, and M. Uhrmacher, *Phys. Lett.* **90B**, 375 (1980).
- Bertini, R., B. Bing, P. Birien, K. Braune, W. Brückner, H. Catz, A. Chameaux, M. A. Faessler, R. W. Frey, D. Garreta, T. J. Ketel, K. Kilian, B. Mayer, J. Niewisch, B.

- Petrzyk, B. Povh, H. G. Bitter, and H. Uhrmacher, *Nucl. Phys. A* **360**, 315 (1981).
- Bertini, R., P. Birien, K. Braune, W. Brückner, G. Bruge, H. Catz, A. Chaumeaux, J. Ciborowski, H. Döbbeling, J. M. Durand, R. W. Frey, D. Garreta, S. Janouin, T. J. Ketel, K. Kilian, H. Kneis, S. Majewski, B. Mayer, J. C. Peng, B. Povh, R. V. Ransome, R. Szwed, T. A. Shibata, A. Thiessen, M. Treichel, M. Uhrmacher, and Th. Walcher, *Phys. Lett.* **136B**, 29 (1984); *Phys. Lett.* **158B**, 19 (1985).
- Bertozzi, W., *Nucl. Phys. A* **374**, 109c (1982).
- Bertozzi, W., J. Friar, J. Heisenberg, and J. W. Negele, *Phys. Lett.* **41B**, 408 (1972).
- Bertsch, G., J. Borysowicz, H. McManus, and W. G. Love, *Nucl. Phys. A* **284**, 399 (1977).
- Bertsch, G., and J. Cugnon, *Phys. Rev. C* **24**, 2514 (1981).
- Bertsch, G., and R. Schaeffer, *Nucl. Phys. A* **277**, 509 (1977).
- Bethe, H. A., *Rev. Mod. Phys.* **9**, 69 (1937).
- Betts, R. R., S. B. Diczienzo, and T. F. Peterson, *Phys. Lett.* **100B**, 117 (1981).
- Biedenharn, L. C., *J. Math. Phys.* **31**, 287 (1953).
- Bijken, R., A. E. L. Dieprink, O. Scholten, and R. E. Spanhoff, *Nucl. Phys. A* **344**, 207 (1980).
- Bilpuch, E. G., A. M. Lane, G. E. Mitchell, and J. D. Moses, *Phys. Rep. C* **28**, 145 (1976).
- Bilpuch, E. G., N. H. Prochnow, R. Y. Cusson, H. W. Newson, and G. E. Mitchell, *Phys. Lett.* **35B**, 303 (1971).
- Bjerggaard, J. H., O. Hansen, O. Nathan, R. Chapman, and S. Hinds, *Nucl. Phys. A* **131**, 481 (1969).
- Bjorken, J. D., and S. Drell, *Relativistic Quantum Mechanics* (McGraw Hill, New York, 1964).
- Bjornholm, S., *Nucl. Phys. A* **387**, 51c (1982).
- Blann, M., in *Intermediate Processes in Nuclear Reactions*, N. Cindro, P. Kališić, and T. Mayer-Kuckuk, eds. (Springer-Verlag, Heidelberg, 1972).
- Blann, M., *Annu. Rev. Nucl. Sci.* **25**, 123 (1975).
- Blann, M., R. R. Doering, A. Galonsky, D. M. Patterson, and F. E. Serr, *Nucl. Phys. A* **257**, 15 (1976).
- Blann, M., and F. M. Lanzafame, *Nucl. Phys. A* **142**, 559 (1970).
- Blanpied, G. S., B. G. Ritchie, M. L. Barlett, R. W. Fergerson, G. W. Hoffmann, J. A. McGill, and B. H. Wildenthal, *Phys. Rev. C* **38**, 2180 (1988).
- Bloch, C., *Phys. Rev.* **93**, 1094 (1954).
- Bloch, C., *Nucl. Phys.* **4**, 503 (1957).
- Bloch, C., *Varennia Lectures 1965 Course XXXVI* (Academic Press, New York, 1966).
- Bloch, C., in *Ecolé d'Ete des Houches—Physique Nucleaire* (Gordon & Breach, New York, 1968).
- Bloch, C., in *Statistical Properties of Nuclei*, J. B. Garg, ed. (Plenum Press, New York, 1972).
- Bloch, C., and V. Gillet, *Phys. Lett.* **16**, 62 (1965); **18**, 58 (1965).
- Block, B., and H. Feshbach, *Ann. Phys. (NY)* **23**, 47 (1963).
- Blomquist, J., *Phys. Lett.* **28B**, 22 (1968).
- Bodek, A., et al., *Phys. Rev. Lett.* **50**, 1431 (1983); **51**, 534 (1983).
- Bodmer, A. R., *Proc. Phys. Soc. London A* **66**, 1041 (1953).
- Bodmer, A. R., and C. N. Panos, *Phys. Rev. C* **15**, 1342 (1977).

- Boguta, J., *Nucl. Phys. A* **372**, 386 (1981).
- Bohannon, G., L. Zamick, and E. Moya deGuerra, *Nucl. Phys. A* **234**, 278 (1980).
- Bohigas, O., and J. Flores, *Phys. Lett.* **34B**, 261 (1971), **35B**, 383 (1971).
- Bohigas, O., and H. A. Weidenmüller, *Annu. Rev. Nucl. Particle Sci.* **38**, 421 (1988).
- Bohigas, O., R. Haq, and A. Pandey, in *Nuclear Data for Science and Technology*, K. H. Böckhoff, ed. (Reidel, Dordrecht, 1983).
- Böhning, M., *Z. Naturforsch.* **21a**, 881 (1966).
- Bohr, A., and B. R. Mottelson, *Nuclear Structure*, Vol. II (W A. Benjamin, New York, 1962).
- Bonazzota, G. C. et al., *Phys. Lett.* **53B**, 297 (1974); *Phys. Rev. Lett.* **34**, 683 (1975).
- Bonche, P., B. Grammatico, and S. E. Koonin, *Phys. Rev. C* **17**, 1700 (1978).
- Bonche, P., S. E. Koonin, and J. W. Negele, *Phys. Rev. C* **13**, 1226 (1976).
- Bondorf, J. P., H. T. Feldmeier, S. Garpman, and E. C. Halbert, *Z. Phys.* **279**, 385 (1976).
- Bonetti, R., M. Camnasio, L. Colli-Milazzo, and P. E. Hodgson, *Phys. Rev. C* **24**, 71 (1981).
- Bonetti R., M. B. Chadwick, P. E. Hodgson, B. V. Carlson, and M. S. Hussein, *Physics Reports* **202**, 173 (1991).
- Bonetti, R., L. Colli-Milazzo, A. de Rosa, G. Inghima, E. Perillo, M. Sandoli, and F. Shakin, *Phys. Rev. C* **21**, 816 (1980).
- Bonetti, R., L. Colli-Milazzo, and M. Melanotte, *Lett. Nuovo Cimento* **31**, 33 (1981).
- Bonetti, R., L. Colli-Milazzo, and M. Melanotte, *Phys. Rev. C* **27**, 1003 (1983).
- Bonetti, R., L. Colli-Milazzo, L. Doda, and P. E. Hodgson, *Phys. Rev. C* **26**, 2417 (1982a).
- Bonetti, R., L. Colli-Milazzo, M. Melanotte, A. de Rosa, G. Inghima, E. Perillo, M. Sandoli, V. Russo, and F. Shakin, *Phys. Rev. C* **25**, 717 (1982b).
- Bonetti, R., and L. Columbo, *Phys. Rev. C* **28**, 980 (1983).
- Boridy, E., and H. Feshbach, *Ann. Phys. (NY)* **109**, 468 (1977); *Phys. Lett.* **50B**, 433 (1974).
- Borysowicz, J., and J. H. Hetherington, *Phys. Rev. C* **7**, 2293 (1973).
- Boussy, A., *Nucl. Phys. A* **290**, 324 (1977).
- Braun-Munzinger, P., in *Proceedings of the Conference on Nuclear Structure with Heavy Ions*, R. A. Ricci and C. Villi, eds. (Italian Physical Society, Bologna, 1986).
- Braun-Munzinger, P., in *Resonant Behavior of Heavy Ion Systems*, G. Vourvopolous, ed. (Greek Nat'l Printing Off., Athens, 1981).
- Breit, G., *Phys. Rev.* **34**, 553 (1929).
- Brieva, F. A., H. V. Geramb, and J. R. Rook, *Phys. Lett.* **79B**, 177 (1978).
- Brieva, F. A., and J. R. Rook, *Nucl. Phys. A* **291**, 299 (1977); **297**, 206 (1978).
- Brink, D. M., *Phys. Lett.* **40B**, 37 (1972).
- Brink, D. M., *Semi classical Methods in Nucleus-Nucleus Scattering* (Cambridge University Press, Cambridge, 1985).
- Brink, D. M., in *Nuclear Physics with Heavy Ions and Mesons*, R. Balian, M. Rho, and G. Ripka, eds. (North Holland, Amsterdam, 1977).
- Brink, D. M., and R. O. Stephen, *Phys. Lett.* **5**, 77 (1963).
- Brink, D. M., R. O. Stephen, and N. W. Tanner, *Nucl. Phys.* **54**, 577 (1964).
- Brody, T. A., J. Flores, J. B. French, P. A. Mello, A. Pandey, and S. S. M. Wong, *Rev. Mod. Phys.* **53**, 385 (1981).
- Broglia, R. A., O. Hansen, and C. Riedel, *Adv. Nucl. Phys.* **6**, 287 (1973).

- Broglia, R. A., S. Landowne, R. A. Malfliet, V. Rostokin, and A. Winther, *Phys. Rep. C* **11**, 3 (1974).
- Broglia, R. A., and A. Winther, *Phys. Rep. C* **4**, 155 (1972).
- Broglia, R. A., and A. Winther, *Heavy Ion Reactions* (Addison-Wesley Reading Mass 1981).
- Bromley, D. A., in *Nuclear Molecular Phenomena*, N. Cindro, ed. (North-Holland, Amsterdam, 1978).
- Bromley, D. A., ed., *Treatise on Heavy Ion Science* (Plenum Press, New York, 1984).
- Brown, B. A., in *Proceedings of the International Nuclear Physics Conference*, J. L. Durell, J. M. Irvine, and G. C. Morrison, eds. (Institute of Physics, Bristol, England, 1986).
- Brown, G. E., *Many-Body Problems* (North-Holland, Amsterdam, 1972).
- Brown, G. E., C. B. Dover, P. B. Siegel, and W. Weise, *Phys. Rev. Lett.* **60**, 2723 (1988).
- Brückner, W., B. Granz, D. Ingham, K. Kilian, U. Lynen, J. Newisch, B. Pietrzyk, B. Povh, and H. G. Schroeder, *Phys. Lett.* **62B**, 486 (1976); **79**, 157 (1978).
- Brussard, P. J., and H. A. Tolhoek, *Physica* **23**, 955 (1957).
- Burzynski, S., M. Baumgartner, H. P. Gubler, J. Jourdan, H. O. Meyer, G. R. Plattner, H. W. Roser, and I. Sick, *Nucl. Phys. A* **399**, 130 (1983).
- Busza, W., and R. Ledoux, *Annu. Rev. Nucl. Part. Sci.* **38**, 119 (1988).
- Cameron, W., et al., *Nucl. Phys. B* **78**, 93 (1974).
- Carr, J. H., H. McManus, and K. Stricker, *Phys. Rev. C* **25**, 952 (1982).
- Carroll, A. S., I. H. Chiang, T. F. Kycia, K. C. Lo, P. O. Mazur, D. N. Michael, P. M. Mockett, D. C. Rahm, and R. Rubenstein, *Phys. Rev. Lett.* **37**, 806 (1976).
- Carruthers, P., and F. Zachariasen, *Rev. Mod. Phys.* **55**, 245 (1987).
- Cassing, W., and W. Nörenberg, *Nucl. Phys. A* **401**, 467 (1983).
- Cavedon, J. M., *Phys. Rev. Lett.* **49**, 978 (1982).
- Cèlenza, L. S., and C. M. Shakin, *Relativistic Nuclear Physics* (World Scientific, Singapore, 1986).
- Chadwick, G. B., G. B. Collins, P. J. Duke, T. Fujii, N. C. Hein, M. A. R. Kemp, and F. Turkot, *Phys. Rev.* **128**, 1823 (1962).
- Chandra, H., and U. Mosel, *Nucl. Phys. A* **298**, 151 (1978).
- Chang, F. S., J. B. French, and T. H. Thio, *Ann. Phys. (NY)* **66**, 137 (1971).
- Chao, W. Q., F. Hachenberg, and J. Hüfner, *Nucl. Phys. A* **384**, 24 (1982).
- Charles, B. J., I. M. Cowan, T. R. M. Edwards, W. M. Gibson, A. R. Gillman, R. S. Gilmore, M. H. Gledhill, C. M. Hughes, J. Malos, A. C. McPherson, J. C. Slaeman, V. J. Smith, R. J. Tapper, B. McCartney, G. C. Oades, D. L. Ward, P. D. Wroath, G. A. Beck, M. Coupland, and S. G. F. Frank, in *Proceedings of the Conference on Baryon Resonances*, E. C. Fowler, ed. (Purdue University Press, West Lafayette, Ind., 1973); *Nucl. Phys. B* **131**, 7 (1977).
- Charles, B. J., I. M. Cowan, T. R. M. Edwards, W. M. Gibson, A. R. Gillman, R. G. Gilmore, M. H. Gledhill, C. M. Hughes, J. Malos, V. J. Smith, R. J. Tapper, B. McCartney, G. C. Oades, D. L. Ward, P. D. Wroath, G. A. Beck, M. Coupland, S. G. F. Frank, *Phys. Lett.* **40B**, 289 (1972).
- Chaumeaux, A., V. Layly, and R. Schaeffer, *Ann. Phys. (NY)* **116**, 247 (1978).
- Chen, Z., Z. Fraenkel, G. Friedlander, J. R. Grover, J. M. Miller, and Y. Shimamoto, *Phys. Rev.* **166**, 949 (1968).

- Cheston, W. B., *Phys. Rev.* **83**, 1118 (1951).
- Chiang, H., and J. Hüfner, *Phys. Lett.* **84B**, 397 (1979).
- Chrien, R. E., *Nucl. Phys. A* **478**, 705c (1988).
- Christenson, J. H., J. W. Cronin, V. L. Fitch, and R. Turlay, *Phys. Rev. Lett.* **13**, 138 (1964).
- Cianguaru, G., *Phys. Rev. C* **30**, 349 (1984).
- Cianguaru, G., C. C. Chang, H. D. Holmgren, A. Nadasen, and P. G. Roos, *Phys. Rev. C* **29**, 1289 (1984).
- Cindro, N., in *Nuclear Molecular Phenomena*, N. Cindro, ed. (North-Holland, Amsterdam, 1978a).
- Cindro, N., *J. Phys. G Nucl. Phys.* **4**, L23 (1978b).
- Cindro, N., and W. Greiner, *J. Phys. G Nucl. Phys.* **9**, L175 (1983).
- Ciofi degli Atti, C., and C. Salmé, in *Perspectives in Nuclear Physics at Intermediate Energies*, S. Boffi, C. Ciofi degli Atti and M. M. Giannini, eds. (World Scientific, Singapore, 1984).
- Clark, B. C., S. Hama, and R. L. Mercer, in *The Interaction Between Medium Energy Nucleons in Nuclei—1982*, H. O. Meyer, ed. (American Institute of Physics, New York, 1983).
- Clementel, E., and C. Villi, *Nuovo Cimento* **4**, 595 (1956).
- Close, F. E., *An Introduction to Quarks and Partons* (Academic Press, New York 1979).
- Close, F. E., *Nucl. Phys. A* **478**, 407c (1988).
- Co', G., A. M. Lallena, and T. W. Donnelly, *Nucl. Phys. A* **469**, 684 (1987).
- Coceva, C., F. Corvi, P. Giacobbe, and M. Stefanon, in *Statistical Properties of Nuclei*, J. B. Garg, ed. (Plenum Press, New York, 1972).
- Cohen, B., *Concepts of Nuclear Physics* (McGraw-Hill Book Company, New York, 1971).
- Cohen, S., and D. Kurath, *Nucl. Phys.* **73**, 1 (1965).
- Cohen, S., F. Plasil, and W. J. Swiatecki, *Ann. Phys. (NY)*, **82**, 557 (1974).
- Coker, W. R., J. D. Lumpe, and L. Ray, *Phys. Rev. C* **31**, 1412 (1985).
- Colli, L., U. Facchini, I. Iori, G. Marazzan, and A. M. Sona, *Nuovo Cimento* **13**, 730 (1959).
- Cook, C. F., and T. Bonner, *Phys. Rev.* **94**, 651 (1954).
- Corden, M. J., G. F. Cox, D. P. Kelsey, C. A. Laurence, P. M. Watkins, O. Harmon, H. M. Lévy, and G. W. London, *Phys. Rev. D* **25**, 720 (1982).
- Cormier, T. M., J. Applegate, G. M. Berkowitz, P. Braun Munziger, *Phys. Rev. Lett.* **38**, 940 (1977).
- Cormier, T. M., C. J. Jackenski, L. L. Lee, Jr., J. Barette, and H. W. Wegner, *Phys. Rev. Lett.* **40**, 924 (1978).
- Cosman, E. R., R. J. Ledoux, M. J. Bechara, C. E. Ordonez, and H. A. Al-Juwair, in *Heavy Ion Reactions*, H. A. Eberhard, ed. (Springer-Verlag, Berlin, 1982).
- Cota, E., J. Flores, P. A. Mello, and E. Yépez, *Phys. Lett.* **53B**, 32 (1974).
- Cotanch, S. R., *Phys. Lett.* **57B**, 123 (1975).
- Cotanch, S. R., and C. M. Vincent, *Phys. Rev. C* **14**, 1739 (1976).
- Courant, H., K. Einsweiler, T. Joyce, H. Kagan, Y. I. Madisi, M. L. Marshak, B. Mossberg, E. A. Peterson, K. Ruddick, T. Walsh, G. J. Igo, R. Talaga, A. Wriekat, and R. Klem, *Phys. Rev. C* **19**, 104 (1979).

- Cowan, T., H. Backe, M. Begemann, K. Bethge, H. Bakemeyer, H. Folger, J. S. Greenberg, H. Green, A. Gruppe, Y. Kido, M. Klüver, D. Schwalm, J. Schweppe, K. E. Steibing, N. Trautman, and P. Vincent, *Phys. Rev. Lett.* **54**, 1761 (1983).
- Cranberg, L., T. A. Oliphant, J. S. Levin, and C. D. Zafaratos, *Phys. Rev.* **159**, 969 (1967).
- Cugnon, J., *Nucl. Phys. A* **387**, 191c (1982).
- Cugnon, J., *Phys. Rev. C* **22**, 1885 (1980).
- Cugnon, J., *Phys. Rev. C* **23**, 2094 (1981).
- Cugnon, J., and J. Vandermuelen, in *Winter College on Fundamental Nuclear Physics*, K. Dietrich, M. di Toro, and H. J. Mang, eds. (World Scientific, Singapore, 1985).
- Curr, R. M., *Proc. Phys. Soc. London Ser. A* **68**, 156 (1955).
- Dabrowski, J., and J. Rozynek, *Phys. Rev. C* **23**, 1706 (1981); *Proceedings of the International Conference on Hypernuclei and Kaon Physics*, B. Povh, ed. (Max Planck Institut für Kernphysik, Heidelberg, 1982); *Nucl. Phys. A* **450**, 349c (1986).
- Daehnick, W. W., J. D. Childs, and Z. Vrcelj, *Phys. Rev. C* **21**, 2253 (1980).
- Dalitz, R. H., and A. Gal, *Phys. Rev. Lett.* **36**, 362, 628 (1976).
- Dalitz, R. H., J. McGinley, C. Belyea, and S. Anthony, in *Proceedings of the International Conference on Hypernuclear and Kaon Physics*, B. Povh, ed. (Max-Planck Institut für Kernphysik, Heidelberg, 1982).
- Dalitz, R. H., and S. F. Tuan, *Ann. Phys. (NY)* **3**, 307 (1960).
- Darnerell, C. J. S., M. J. Hotchkiss, F. Wickens, K. R. Bentley, J. D. David, J. D. Dowell, R. J. Homer, C. McLeod, T. J. McMahon, H. B. van der Raay, and J. G. Rhoades, *Nucl. Phys. B* **94**, 374 (1975).
- D'Auria, J. M., M. J. Fluss, G. Herzog, L. Kowalski, J. M. Miller, and R. C. Reedy, *Phys. Rev.* **174**, 1409 (1968).
- Davies, K. T. R., K. R. S. Devi, S. E. Koonin, and M. R. Strayer, in *Treatise on Heavy Ion Science*, D. A. Bromley, ed. (Plenum Press, New York, 1984).
- Davies, K. T. R., V. Maruhn-Rezwani, S. E. Koonin, and J. W. Negele, *Phys. Rev. Lett.* **41**, 632 (1978).
- Davies, K. T. R., K. R. Sandhya Devi, and M. R. Strayer, *Phys. Rev. C* **20**, 1372 (1979).
- Davis, D. H., and J. Sacton, in *High Energy Physics*, Vol. II, E. M. S. Burhop, ed. (Academic Press, New York, 1967).
- Davydov, A. S., and G. F. Filippov, *Nucl. Phys.* **8**, 237 (1958).
- Dearnley, G., W. R. Gibbs, R. B. Leachman, and P. C. Rogers, *Phys. Rev.* **139B**, 1170 (1965).
- deBoer, J., in *Treatise on Heavy Ion Science*, D. A. Bromley, ed. (Plenum Press, New York, 1984).
- Dechargé, J., M. Girod, D. Gogny, and B. Grammaticos, *Nucl. Phys. A* **358**, 203c (1981).
- Dechargé, J., and D. Gogny, *Phys. Rev. C* **21**, 1568 (1980).
- Dechargé, J., and L. Sips, *Nucl. Phys. A* **407**, 1 (1983).
- DeForest, T., Jr., and J. D. Walecka, *Adv. Phys.* **15**, 1 (1966).
- DeJager, C. S., H. DeVries, and C. DeVries, *Atomic Data and Nuclear Data Tables* **14**, 470 (1974).

- Delic, G., and B. A. Robson, *Nucl. Phys. A* **232**, 493 (1974).
- de Rosa, A., G. Inghima, E. Rosato, M. Sandoli, R. Bonetti, and L. Milazzo-Colli, *J. Phys. G Nucl. Phys.* **4**, 271 (1978).
- deShalit, A., and H. Feshbach, *Theoretical Nuclear Physics*, Vol. 1 (John Wiley & Sons, New York, 1974).
- Devi, K. R. Sandhya, and M. R. Strayer, *Phys. Lett.* **77B**, 135 (1978).
- DeVries, R. M., *Phys. Rev. C* **8**, 951 (1973).
- deVries, C., in *Perspectives in Nuclear Physics at Intermediate Energies*, S. Boffi, C. Ciofi degli Atti, and M. M. Giannini, eds. (World Scientific, Singapore, 1984).
- deWitt-Huberts, P. K. A., in *Proceedings of the International Nuclear Physics Conference at Harrogate—1986* (Institute of Physics, Bristol, England, 1987).
- Dhar, A. K., B. S. Nelson, K. T. R. Davies, and S. E. Koonin, *Nucl. Phys. A* **364**, 105 (1981).
- Dickens, J. K., R. M. Drisko, F. G. Perey, and G. R. Satchler, *Phys. Lett.* **15**, 337 (1965).
- Dickens, J. K., F. G. Perey, and R. G. Silva, in *International Nuclear Physics Conference*, R. L. Becker, C. D. Goodman, P. H. Stelson, and A. Zucker, eds. (Academic Press, New York, 1967).
- Dieperink, A. E. L., and T. DeForest, Jr., *Annu. Rev. Nucl. Sci.* **25**, 1 (1975).
- Dietrich, K., in *Proceedings of the Winter College on Fundamental Nuclear Physics*, K. Dietrich, M. diToro, and H. J. Mang, eds. (World Scientific, Singapore, 1985).
- Dirac, P. A. M., *Proc. Cambridge Phil. Soc.* **26**, 376 (1930).
- Döhnert, L., *Ann. Phys. (NY)* **62**, 442 (1971); thesis, MIT (1968).
- Donnelly, T. W., in *International School of Intermediate Energy Nuclear Physics* (July 1988).
- Donnelly, T. W., and A. S. Raskin, *Ann. Phys. (NY)* **169**, 247 (1986).
- Donnelly, T. W., and I. Sick, *Rev. Mod. Phys.* **56**, 461 (1984).
- Donnelly, T. W., and J. D. Walecka, *Annu. Rev. Nucl. Sci.* **25**, 329 (1975).
- Døssing, T., and A. S. Jensen, *Nucl. Phys. A* **222**, 493 (1974).
- Dover, C. B., and H. Feshbach, *Phys. Rev. Lett.* **59**, 2539 (1987); *Ann. Phys. (NY)* **198**, 321 (1990).
- Dover, C. B., D. J. Millener, and A. Gal, *Phys. Rep.* **184**, 2 (1989).
- Dover, C. B., and G. E. Walker, *Phys. Rep.* **89**, 1 (1982).
- Dresner, L., in *Proceedings of the International Conference on Neutron Interactions with Nuclei*, Columbia University report CU-175 (1957).
- Dudek, J., and W. Nazarewicz, *Phys. Rev. C* **31**, 298 (1985).
- Dyson, F. J., *J. Math. Phys.* **3**, 140 (1962); **3**, 157 (1962); **3**, 66 (1962).
- Dyson, F. J., and M. L. Mehta, *J. Math. Phys.* **4**, 701 (1963).
- Eberhard, K., ed., *Resonances in Heavy Ion Collisions* (Springer-Verlag, Berlin, 1982).
- Eisenberg, J., and W. Greiner, *Nuclear Theory*, Vol. 2 (North-Holland, Amsterdam, 1970).
- Eisenberg, J. M., and D. S. Koltun, *Theory of Meson Interactions with Nuclei* (John Wiley & Sons, New York, 1980).
- Elias, J. E., W. Busza, C. Halliwell, D. Luckey, L. Votta, and C. Young, *Phys. Rev. Lett.* **41**, 285 (1978).

- Elias, J. E., W. Busza, C. Halliwell, D. Luckey, P. Swartz, L. Votta, and C. Young, *Phys. Rev. D* **22**, 13 (1980).
- Elton, L. R. B., *Proc. Phys. Soc. London A* **66**, 806 (1953).
- Elton, L. R. B., *Nucl. Phys.* **89**, 69 (1966).
- Elton, L. R. B., and A. Swift, *Nucl. Phys. A* **94**, 52 (1967).
- Engelbrecht, C. A., and H. A. Weidenmüller, *Phys. Rev. C* **8**, 859 (1973).
- Erb, K. A., R. R. Betts, D. L. Hanson, M. W. Sachs, R. L. White, P. P. Tung, and D. A. Bromley, *Phys. Rev. Lett.* **37**, 670 (1976).
- Erb, K. A., R. R. Betts, D. L. Hanson, M. W. Sachs, R. L. White, P. P. Tung, and D. A. Bromley, *Phys. Rev. Lett.* **58**, 337 (1977).
- Erb, K. A., and D. A. Bromley, *Phys. Rev. C* **23**, 2781 (1981).
- Erb, K., and D. A. Bromley, in *Treatise on Heavy Ion Science* (Plenum Press, New York, 1984).
- Erb, K. A., C. Olmer, D. Hansen, M. W. Sachs, R. Stokstad, and D. A. Bromley, in *Proceedings of the International Conference on Nuclear Physics, Munich 1973*, J. de Boer and H. G. Mang, eds. (North-Holland, Amsterdam, 1973).
- Ericson, M., and T. E. O. Ericson, *Ann. Phys. (NY)* **36**, 323 (1966).
- Ericson, T., *Nucl. Phys.* **11**, 430 (1959).
- Ericson, T., *Nucl. Phys.* **17**, 250 (1960a).
- Ericson, T., *Phys. Rev. Lett.* **5**, 481 (1960b).
- Ericson, T., *Phil. Mag. Suppl.* **9**, 425 (1960c).
- Ericson, T., *Ann. Phys. (NY)* **23**, 390 (1963).
- Ericson, T., and T. Mayer-Kuckuk, *Annu. Rev. Nucl. Sci.* **16** (1966).
- Ericson, T., and V. Strutinsky, *Nucl. Phys.* **8**, 284 (1958).
- Ericson, T., and W. Weise, *Pions and Nuclei* (Clarendon Press, Oxford, 1988).
- Erskine, J. R., W. W. Buechner, and H. A. Enge, *Phys. Rev.* **128**, 720 (1962).
- Estrada, L., and H. Feshbach, *Ann. Phys. (NY)* **23**, 123 (1963).
- Euteneuer, H., J. Friedrich, and N. Volgler, *Nucl. Phys. A* **298**, 452 (1978).
- Fantoni, S., B. L. Friman, and V. Pandharipande, *Phys. Lett.* **104B**, 89 (1981).
- Feld, B. J., *Models of Elementary Particles* (Blaisdell, Waltham, 1969).
- Feller, W., *An Introduction to Probability Theory and Its Applications*, Vol. I (John Wiley & Sons, New York, 1968).
- Feng, D. H., T. Tamura, T. Udagawa, J. Lynch, and K. S. Low, *Phys. Rev. C* **14**, 1484 (1976).
- Feng, D. H., T. Udagawa, and T. Tamura, *Nucl. Phys. A* **274**, 262 (1976).
- Ferguson, R. W., M. L. Bartlett, G. W. Hoffmann, J. A. Marshall, E. C. Milner, G. Pauletta, L. Ray, J. F. Amann, K. W. Jones, J. B. McClelland, M. Gazzaly, and G. J. Igo, *Phys. Rev. C* **33**, 239 (1986).
- Feshbach, H., *Phys. Rev.* **84**, 1206 (1951).
- Feshbach, H., *Phys. Rev.* **88**, 295 (1952).
- Feshbach, H., *Ann. Phys. (NY)* **5**, 357 (1958a).
- Feshbach, H., *Annu. Rev. Nucl. Sci.* **8**, 49 (1958b).

- Feshbach, H., in *Nuclear Spectroscopy*, F. Ajzenberg-Selove, ed. (Academic Press, New York, 1960).
- Feshbach, H., *Ann. Phys. (NY)* **19**, 287 (1962).
- Feshbach, H., *Ann. Phys. (NY)* **43**, 410 (1967a).
- Feshbach, H., in *Interaction of High Energy Particles with Nuclei*, T. E. O. Ericson, ed. (Academic Press, New York, 1967b).
- Feshbach, H., in *In Honor of Philip M. Morse*, H. Feshbach and U. Ingard, eds. (MIT Press, Cambridge, Mass., 1969).
- Feshbach, H., in *Proceedings of the International Conference on Nuclear Physics, Munich, 1973*, J. de Boer and H. J. Mang, eds. (North-Holland, Amsterdam, 1973).
- Feshbach, H., *J. Phys. (Paris) Colloq.* **37**, C5-177 (1977).
- Feshbach, H., in *Physics of Medium Light Nuclei*, F. Blasi and R. A. Ricci, eds. (Editrice Compositori, Bologna, 1977).
- Feshbach, H., in *Themes in Contemporary Physics* S. Deser, H. Feshbach, R. J. Finkelstein, K. A. Johnson, and P. C. Martin, eds. (North-Holland, Amsterdam, 1979).
- Feshbach, H., in *From Nuclei to Particles*, Proceedings of the International School of Physics "Enrico Fermi," A. Molinari, ed. (North-Holland, Amsterdam, 1981).
- Feshbach, H., in *Asymptotic Realms of Physics*, A. A. Guth, K. Huang, and R. L. Jaffe, eds. (MIT Press, Cambridge, Mass., 1983).
- Feshbach, H., *Ann. Phys. (NY)* **159**, 150 (1985).
- Feshbach, H., in *Proceedings of the International School of Physics, Enrico Fermi Course XCI*, A. Molinari and R. A. Ricci, eds. (North-Holland, Amsterdam, 1986), p. 116.
- Feshbach, H., in *Ericson Festschrift*, *Nucl. Phys. A* **518**, 1 (1990).
- Feshbach, H., and W. A. Friedman, in *Spectroscopic and Group Theoretical Methods in Physics*, F. Bloch, ed. (North-Holland, Amsterdam, 1968).
- Feshbach, H., A. Gal, and J. Hüfner, *Ann. Phys. (NY)* **66**, 20 (1971).
- Feshbach, H., and K. Huang, *Phys. Lett.* **47B**, 300 (1973).
- Feshbach, H., and A. K. Kerman, in *Preludes in Theoretical Physics*, A. DeShalit, H. Feshbach, and L. van-Hove, eds. (North-Holland, Amsterdam, 1966).
- Feshbach, H., A. K. Kerman, and S. Koonin, *Ann. Phys. (NY)* **125**, 429 (1980).
- Feshbach, H., A. K. Kerman, and R. H. Lemmer, *Ann. Phys. (NY)* **41**, 230 (1967).
- Feshbach, H., and J. R. Lamarsh, *Phys. Rev.* **104**, 1633 (1956).
- Feshbach, H., D. C. Peaslee, and V. F. Weisskopf, *Phys. Rev.* **71**, 145 (1947).
- Feshbach, H., C. E. Porter, and V. F. Weisskopf, *Phys. Rev.* **90**, 166 (1953); **96**, 448 (1954).
- Feshbach, H., and D. R. Yennie, *Nucl. Phys.* **37**, 150 (1962).
- Feshbach, H., and M. Zabeck, *Ann. Phys. (NY)* **107**, 110 (1977).
- Field, G. M., R. Bonetti, and P. E. Hodgson, *J. Phys. G* **12**, 93 (1986).
- Fink, H. J., W. Scheid, and W. Greiner, *Nucl. Phys. A* **188**, 259 (1972).
- Fleissbach, J., *Z. Phys. A* **288**, 211 (1978).
- Fleissbach, J., and H. Mang, *Nucl. Phys. A* **263**, 75 (1976).
- Fletcher, N. R., J. D. Fox, G. J. Kekalis, G. R. Morgan, and G. A. Norton, *Phys. Rev. C* **13**, 1172 (1976).

- Fletcher, N. B., and A. D. Frawley, in *Resonant Behavior of Heavy Ion Systems*, G. Vourvopoulos, ed. (Greek National Printing Office, Athens, 1981).
- Ford, J. L., K. S. Toth, G. R. Satchler, D. C. Hensley, L. W. Owen, R. M. DeVries, R. M. Gaedke, P. J. Riley, and S. T. Thornton, *Phys. Rev. C* **10**, 1429 (1974).
- Frahn, W. E., *Nucl. Phys.* **66**, 357 (1965).
- Frahn, W. E., *Nucl. Phys.* **75**, 557 (1966).
- Franey, M. A., J. S. Lilley, and W. R. Phillips, *Nucl. Phys. A* **324**, 93 (1979).
- French, J. B., P. A. Mello, and A. Pandey, *Ann. Phys. (NY)* **113**, 277 (1978).
- French, J. B., and S. S. M. Wong, *Phys. Lett.* **33B**, 449 (1970), **35B**, 5 (1971).
- Frenkel, J., *Sov. Phys.* **9**, 533 (1936).
- Friar, J. L., and J. W. Negele, *Nucl. Phys. A* **212**, 93 (1973).
- Friar, J. L., and J. W. Negele, *Nucl. Phys. A* **240**, 301 (1975a).
- Friar, J. L., and J. W. Negele, *Adv. Nucl. Phys.* **8**, 219 (1975b).
- Friar, J. L., and M. Rosen, *Ann. Phys. (NY)* **87**, 289 (1974).
- Friedrich, J., and F. Lenz, *Nucl. Phys. A* **183**, 523 (1972).
- Friedlander, E., and H. H. Heckman, in *Treatise on Heavy Ion Science*, D. A. Bromley, ed. (Plenum Press, New York, 1985).
- Friedman, W. A., *Ann. Phys. (NY)* **45**, 265 (1967).
- Friedman, W., M. S. Hussein, K. W. McVoy, and P. Mello, *Phys. Rep.* **77**, 47 (1981).
- Friedman, W. A., and W. G. Lynch, *Phys. Rev. C* **28**, 950 (1983).
- Friedman, F. L., and V. F. Weisskopf, in *Niels Bohr and the Development of Physics*, W. Pauli, L. Rosenfeld, and V. F. Weisskopf, eds. (Pergamon Press, London, 1955).
- Frois, B., J. B. Bellicaid, J. M. Cavedon, M. Huet, P. LeConte, P. Ludeau, A. Nakoda, Phan Xyan Ho, and I. Sick, *Phys. Rev. Lett.* **38**, 152 (1977).
- Frois, B., *Nucl. Phys. A* **396**, 409c (1983).
- Frois, B., and C. N. Papanicolas, *Annu. Rev. Nucl. Particle Sci.* **37**, 133 (1987).
- Frölich, H., T. Shimoda, M. Ischara, K. Nagatani, T. Udagawa, and T. Tamura, *Phys. Rev. Lett.* **42**, 1548 (1979).
- Fujiwara, M., Y. Fujita, I. Katayama, S. Morinobu, T. Yamazaki, H. Ikegami, S. I. Hayakawa, and K. Katori, *Nucl. Phys. A* **410**, 137 (1983).
- Fulbright, H. W., U. Strohbusch, R. G. Markham, R. A. Lindgren, G. C. Morrison, S. C. McGuire, and C. L. Bennett, *Phys. Lett.* **53B**, 449 (1975).
- Fulmer, C. B., G. R. Satchler, E. E. Gross, F. E. Bertrand, C. D. Goodman, D. C. Hensley, J. R. Wu, N. M. Clarke, and M. F. Steeden, *Nucl. Phys. A* **356**, 235 (1981).
- Gadioli, E., and L. Milazzo-Colli, in *Intermediate Processes in Nuclear Reactions*, N. Cindro, P. Kulišić, and T. Mayer-Kuckuk, eds. (Springer-Verlag, Heidelberg, 1973).
- Gal, A., and C. B. Dover, *Phys. Lett.* **110B**, 428 (1982).
- Gal, A., and C. B. Dover, *Phys. Rev. Lett.* **44**, 379 (1980).
- Galin, J., *J. Phys. (Paris) Colloq. C* **5**, **37**, 83 (1976).
- Galin, J., B. Gatty, D. Gaerreau, C. Rousset, U. Schlotthauer-Voos, and X. Tarrago, *Phys. Rev. C* **9**, 1113 (1974).
- Gasiorowicz, S., *Elementary Particle Physics* (John Wiley & Sons, New York, 1967).
- Gaudin, M., *Nucl. Phys.* **25**, 447 (1961).

- Geaga, J. V., M. M. Gazzely, G. J. Igo, J. B. McClelland, M. A. Nasser, A. L. Sagle, H. Spinka, J. B. Carroll, V. Perez-Mendez, and E. T. Whipple, *Phys. Rev. Lett.* **38**, 1265 (1972).
- Gilat, J., E. R. Jones, and J. M. Alexander, *Phys. Rev. C* **7** (1973).
- Gillet, V., A. M. Green, and E. A. Sanderson, *Phys. Lett.* **11**, 44 (1964).
- Gillet, V., A. M. Green, and E. A. Sanderson, *Nucl. Phys.* **88**, 321 (1966).
- Ginocchio, J. N., and G. Wenes, in *Nuclear Structure, Reactions and Symmetries*, R. A. Meyer and V. Paar, eds. (World Scientific, Singapore, 1986).
- Glas, D., and U. Mosel, *Phys. Rev. C* **10**, 2620 (1974); *Nucl. Phys. A* **237**, 429 (1975).
- Glasgow, W., and D. G. Foster, *Phys. Rev. C* **3**, 604 (1971).
- Glashauser, C., and J. Thirion, *Adv. Nucl. Phys.* **2**, 79 (1969).
- Glauber, R. J., in *Lectures in Theoretical Physics*, Vol. I, W. E. Brittan and L. G. Dunham, eds. (Interscience, New York, 1959).
- Glendenning, N. K., *Rev. Mod. Phys.* **47**, 659 (1975).
- Glendenning, N. K., D. R. Hendrie, and O. N. Jarvis, *Phys. Lett.* **26B**, 131 (1968).
- Gobbi, A., R. Wieland, L. Chua, D. Shapira, and D. A. Bramley, *Phys. Rev. C* **7**, 30 (1973).
- Gogny, D. *Lect. Notes Phys.* **108**, 88 (1979).
- Goldberger, M. L., *Phys. Rev.* **74**, 1269 (1948).
- Goldberger, M., and K. M. Watson, *Collision Theory* (John Wiley & Sons, New York, 1964).
- Goldhaber, A. S., *Phys. Rev. Lett.* **33**, 47 (1974a).
- Goldhaber, A. S., *Phys. Lett.* **53B**, 306 (1974b).
- Gopal, G. P., et al., *Nucl. Phys. B* **119**, 362 (1977).
- Gottfried, K., in *High Energy Physics and Nuclear Structure*, G. Tibell, ed. (North-Holland, Amsterdam, 1974a).
- Gottfried, K., *Phys. Rev. Lett.* **32**, 957 (1974b).
- Gottfried, K., and V. F. Weisskopf, *Concepts of Particle Physics*, (Clarendon Press, Oxford, Vol. I, 1984; Vol. II, 1986).
- Greene, S. J., C. H. Harvey, P. A. Seidl, R. Gilman, E. R. Siciliano, and M. B. Johnson, *Phys. Rev. C* **30**, 2003 (1984).
- Greenlees, G., *Phys. Rev. C* **2**, 1063 (1970).
- Greenlees, G. W., V. Hnizdo, O. Karban, J. Lowe, and W. Makofake, *Phys. Rev. C* **2**, 1063 (1970).
- Greenlees, G. W., M. W. Makofake, and G. J. Pyle, *Phys. Rev. C* **1**, 1145 (1970).
- Greenlees, G. W., G. J. Pyle, and Y. C. Tang, *Phys. Rev.* **171**, 1115 (1968).
- Greenwood, L. R., K. Katori, R. E. Malmin, T. H. Braid, J. C. Stoltzfus, and R. H. Siemssen, *Phys. Rev. C* **6**, 2112 (1972).
- Gregoire, C., Ngô, E. Tomasi, B. Remaud, and F. Scheuter, *Nucl. Phys. A* **387**, 37c (1982).
- Greiner, D. E., P. J. Lindstrom, H. H. Heckman, B. Cork, and F. S. Beiser, *Phys. Rev. Lett.* **75**, 152 (1975).
- Greiner, W., and W. Scheid, *J. Phys. (Paris) Colloq. C* **32**, 6–91 (1971).
- Griffin, J. J., *Phys. Rev. Lett.* **17**, 478 (1966).
- Griffin, J. J., *Phys. Lett.* **24B**, 5 (1967).

- Grimes, S. M., J. D. Anderson, B. A. Pohl, J. W. McClure, and C. Wong, *Phys. Rev. C* **3**, 645 (1971); **4**, 605 (1971).
- Gross, D. H. E., and H. Kalinowski, *Phys. Rep.* **45**, 175 (1978).
- Grotch, H., and D. R. Yennie, *Rev. Mod. Phys.* **41**, 350 (1969).
- Grover, J. R., and R. J. Nagle, *Phys. Rev. B* **134**, 1248 (1964).
- Gruppelaar, H., and G. Ruffo, *Nucl. Sci. Eng.* **62**, 756 (1977).
- Guet, C., M. Soyeur, J. Bowlein, and G. E. Brown, Saclay PhT/88-160 (1989).
- Gurvitz, S. A., J. P. Dedonder, and R. D. Amado, *Phys. Rev. C* **19**, 142 (1979).
- Gurvitz, S. A., and A. S. Rinat, *Phys. Rev. C* **35**, 696 (1987).
- Gustafsson, H. A., H. H. Gutbrod, B. Kolb, H. Löhner, B. Lidewigt, A. M. Poskanzer, T. Renner, H. Riedesel, H. G. Ritter, A. Warwick, F. Weik, and H. Wieman, *Phys. Rev. Lett.* **52**, 1590 (1984).
- Hadjuk, O., P. Sauer, and W. Strueve, *Nucl. Phys. A* **405**, 620 (1983).
- Hahne, F. J. W., *Nucl. Phys. A* **104**, 545 (1967); **106**, 660 (1968).
- Halbert, E. C., *Phys. Rev. C* **23**, 295 (1981).
- Halbert, M. L., F. E. Durham, C. D. Moak, and A. Zucker, *Nucl. Phys.* **47**, 353 (1964).
- Hanson, D. L., R. G. Stokstad, K. A. Erb, C. Olmer, and D. A. Bromley, *Phys. Rev. C* **9**, 929 (1974).
- Harar, S., in *Nuclear Molecular Phenomena*, N. Cindro, ed. (North-Holland, Amsterdam, 1978).
- Hardy, G. H., and S. Ramanujan, *Proc. Math. Soc. (London)* **42**, 75 (1918).
- Harvey, M., in *Proceedings of the Second International Conference on Clustering Phenomena in Nuclei*, USDERA report ORO-4856-26 (1975).
- Hauser, W., and H. Feshbach, *Phys. Rev.* **87**, 366 (1952).
- Hayano, R. S., T. Ishikawa, M. Iwasaki, H. Oata, E. Takada, H. Tamura, A. Sakaguchi, M. Aoki, and T. Yamazaki, *Phys. Lett.* **231B**, 355 (1989).
- Heckman, N. H., D. E. Greiner, P. J. Lindstrom, and F. S. Beiser, *Phys. Rev.* **28**, 926 (1972).
- Heeringa, W. H., H. Postma, H. Dobiasch, R. Fischer, H. O. Klages, R. Maschuur, and B. Tietnitz, *Phys. Rev. C* **16**, 1389 (1977).
- Heisenberg, J. H., *Comm. Nucl. Part. Phys.* **13**, 267 (1984).
- Heisenberg, J. H., in *Electron Scattering in Nuclei*, C. N. Papanicolas, L. S. Cardman, and R. A. Eisenstein, eds. (American Institute of Physics, New York, 1987).
- Heisenberg, J. H., J. S. McCarthy, and I. Sick, *Nucl. Phys. A* **164**, 353 (1971).
- Heisenberg, J. H., and I. Sick, *Phys. Lett.* **32B**, 249 (1970).
- Henning, W., F. L. H. Wolfs, J. P. Schiffer, and K. E. Rehm, *Phys. Rev. Lett.* **58**, 318 (1987).
- Hillis, D. L., J. D. Garrett, O. Christensen, B. Fernandez, G. B. Hagemann, B. Herskind, B. B. Bock, and J. Folkmann, *Nucl. Phys. A* **325**, 216 (1979).
- Hillman, M., and J. R. Grover, *Phys. Rev.* **185**, 1303 (1969).
- Hirata, M., *Phys. Rev. C* **24**, 1604 (1981).
- Hirata, M., J. H. Koch, F. Lenz, and E. J. Moniz, *Ann. Phys. (NY)* **116**, 247 (1978); **120**, 205 (1979).
- Hirata, M., F. Lenz, and M. Thies, *Phys. Rev. C* **28**, 785 (1983).

- Hirata, M., F. Lenz, and K. Yazaki, *Ann. Phys. (NY)* **108**, 116 (1977).
- Hodgson, P. E., *Nuclear Heavy Ion Reactions* (Clarendon Press, Oxford, 1978).
- Hodgson, P. E., *Growth Points in Nuclear Physics*, Vol. 2 (Pergamon Press, Oxford, 1980).
- Hodgson, P. E., *Rep. Prog. Phys.* **50** (1987).
- Hodgson, P. E., *Nuovo Cimento* **81A**, 250 (1984).
- Hoffmann, G. W., L. Ray, M. Barlett, W. R. Coker, J. McGill, G. S. Adams, G. J. Igo, F. Irom, A. T. M. Wang, C. A. Whitten, Jr., R. L. Boudrie, J. F. Amann, C. Glashauser, N. M. Hintz, G. S. Kyle, and G. S. Blanpied, *Phys. Rev. C* **24**, 541 (1981).
- Hoffman, H. M., J. Richert, and J. W. Tepel, *Ann. Phys. (NY)* **90**, 391 (1975).
- Hoffman, H. M., J. Richert, J. W. Tepel, and H. A. Weidenmüller, *Ann. Phys. (NY)* **90**, 403 (1975).
- Holbrow, C. H., and H. H. Barschall, *Nucl. Phys.* **42**, 269 (1963).
- Holler, Y., A. Kaminsky, R. Langkau, W. Scobel, M. Trabandt, and R. Bonetti, *Nucl. Phys. A* **442**, 79 (1985).
- Hooper, M. B., *Nucl. Phys.* **76**, 449 (1966).
- Horikawa, Y., N. Thies, and F. Lenz, *Nucl. Phys. A* **345**, 386 (1980).
- Horiuchi, H., *Suppl. Prog. Theor. Phys.* **62**, 90 (1977).
- Horowitz, C. J., *Phys. Lett.* **117B**, 153 (1982).
- Horowitz, C. J., and B. D. Serot, *Nucl. Phys. A* **368**, 503 (1981).
- Huang, K., *Statistical Mechanics*, 2nd ed. (John Wiley & Sons, New York, 1987).
- Huby, R., M. Y. Refai, and G. R. Satchler, *Nucl. Phys.* **9**, 94 (1958).
- Hüfner, J., *Phys. Rep.* **21**, 1 (1975).
- Hüfner, J., and A. deShalit, *Phys. Lett.* **15**, 52 (1965).
- Hüfner, J., and A. Klar, *Phys. Lett.* **145B**, 167 (1984).
- Hüfner, J., and J. Knoll, *Nucl. Phys. A* **290**, 460 (1977).
- Hüfner, J., S. Y. Lee, and H. A. Weidenmüller, *Phys. Lett.* **49B**, 409 (1974); *Nucl. Phys. A* **234**, 429 (1974).
- Hüfner, J., K. Schäfer, and B. Schürmann, *Phys. Rev. C* **12**, 1988 (1975).
- Huizenga, J. R., in *Statistical Properties of Nuclei*, J. B. Garg, ed. (Plenum Press, New York, 1972).
- Huizenga, J. R., A. N. Behkamu, R. W. Atcher, J. S. Sventek, H. C. Britt, and H. Friesleben, *Nucl. Phys. A* **223**, 589 (1974).
- Huizenga, J. R., and J. R. Birkelund, *University of Rochester Report UR-NSRL 261*, (1982).
- Huizenga, J. R., and L. G. Moretto, *Annu. Rev. Nucl. Sci.* **22**, 427 (1972).
- Humblert, J., and L. Rosenfeld, *Nucl. Phys.* **26**, 529 (1961).
- Hungerford, E., *Nucl. Phys. A* **450**, 157c (1986).
- Hurwitz, H., Jr., and H. A. Bethe, *Phys. Rev.* **81**, 898 (1951).
- Hussein, M., and K. W. McVoy, *Phys. Rev. Lett.* **43**, 1645 (1979).
- Hynes, M. V., H. Miska, B. Norum, W. Bertozzi, S. Kowalski, F. N. Rod, C. P. Sargent, T. Sasanuma, W. Turchinefz, and B. L. Berman, *Phys. Rev. Lett.* **42**, 1444 (1979).

- Iachello, F., *Ann. Phys. (NY)* **52**, 16 (1969).
- Iachello, F., *Phys. Rev. C* **23**, 2278 (1981).
- Ichimura, M., E. Takoda, T. Yamaya, and K. Nagatami, *Phys. Lett.* **101B**, 31 (1981).
- Ikeda, M., *Phys. Rev. C* **6**, 1608 (1972).
- Imanishi, B., *Phys. Lett.* **27B**, 267 (1968); *Nucl. Phys. A* **125**, 33 (1969).
- Imanishi, B., M. Ichimura, and M. Kawai, *Phys. Lett.* **52B**, 267 (1974).
- Iseri, Y., Ph.D. thesis, Kyushu University (1985).
- Iwasaki, M., Ph.D. dissertation, Tokyo University (1987).
- Jacob, G., and Th. A. Maris, *Rev. Mod. Phys.* **45**, 6 (1973).
- Jacob, M., and G. C. Wick, *Ann. Phys. (NY)* **7**, 404 (1959).
- Jaffe, R. L., *Nucl. Phys. A* **478**, 3c (1988).
- Jaffe, R. J., and F. E. Low, *Phys. Rev. D* **20**, 2105 (1979).
- Jaminon, M., in *The Interaction Between Medium Energy Nucleons in Nuclei—1982*, H. O. Meyer, ed. (American Institute of Physics, New York, 1983).
- Jeukenne, J. B., A. Lejeune, and C. Mahaux, *Phys. Rep. C* **23**, 616 (1981).
- Jeukenne, J. B., A. Lejeune, and C. Mahaux, *Phys. Rep. C* **15**, 10 (1977); **16**, 80 (1977).
- Joachain, C., *Quantum Collision Theory* (North-Holland, Amsterdam, 1975).
- Johnson, C. H., A. Galonsky, and J. P. Ulrich, *Phys. Rev.* **109**, 1243 (1958).
- Johnson, M. B., in *From Nuclei to Stars*, A. Molinari, ed. (North-Holland, Amsterdam, 1986).
- Johnson, R. C., N. Austern, and M. H. Lopes, *Phys. Rev. C* **26**, 348 (1982).
- Johnson, R. C., and P. J. R. Soper, *Phys. Rev. C* **1**, 976 (1970).
- Johnstone, J. A., and A. W. Thomas, *Nucl. Phys. A* **392**, 409 (1983).
- Kahana, S., and A. J. Baltz, *Adv. Nucl. Phys.* **9**, 1 (1977).
- Kallne, J., and Fagerstrom, *Physica Scripta* **11**, 79 (1979).
- Kapur, P. I., and R. Peierls, *Proc. Roy. Soc. A* **166**, 277 (1937).
- Karaoglu, B., and E. J. Moniz, *Phys. Rev. C* **33**, 974 (1986).
- Karapiperis, T., in *Second LAMPF International Workshop on Pion Double Charge Exchange* (August 1989).
- Karapiperis, T., and M. Kobayashi, *Ann. Phys. (NY)* **177**, 1 (1987).
- Kato, K., and Y. Abe, *Yukawa Hall Kyoto RIFP-700* (May 1987).
- Kato, K., S. Okate, and Y. Abe, *Structure of $^{12}\text{C} + ^{16}\text{O}$ Molecular Bands*, preprint (June 1985).
- Kawai, M., A. K. Kerman, and K. W. McVoy, *Ann. Phys. (NY)* **75**, 156 (1975).
- Kelly, J. J., Thesis, MIT (1981).
- Kelly, J. J., in *The Interaction Between Medium Energy Nucleons in Nuclei—1982*, H. O. Meyer, ed., (American Institute of Physics, New York, 1983).
- Kerman, A. K., Los Alamos Scientific Lab. Report (1962).
- Kerman, A. K., *Lectures in Theoretical Physics*, Vol. VIII, (University of Colorado Press, Boulder, Colo., 1966).
- Kerman, A. K., and S. E. Koonin, *Ann. Phys. (NY)* **100**, 332 (1976).

- Kerman, A. K., H. McManus, and R. Thaler, *Ann. Phys. (NY)* **8**, 551 (1959).
- Kerman, A. K., and A. Sevgen, *Ann. Phys. (NY)* **102**, 570 (1976).
- Kirouac, G. J., in *Nuclear Cross-Sections and Technology*, R. A. Schrock and C. D. Bowman, eds. (National Bureau of Standards, Washington, D.C., 1975).
- Kisslinger, L., and W. L. Wang, *Phys. Lett.* **30**, 1071 (1973); *Ann. Phys. (NY)* **99**, 374 (1976).
- Kitching, P., W. J. McDonald, Th. A. Maris, and C. A. Z. Vasconcellos, *Adv. Nucl. Phys.* **15**, 43 (1985).
- Klar, A., and J. Hüfner, *Phys. Rev. D* **31**, 491 (1985).
- Kneis, H., Ph.D. dissertation, University of Heidelberg (1983).
- Kobos, A. M., and R. S. MacIntosh, *Ann. Phys. (NY)* **123**, 296 (1979).
- Koch, J. H., E. J. Moniz, and N. Ohtsuka, *Ann. Phys. (NY)* **154**, 99 (1984).
- Kocher, D. C. and W. Haeberli, *Nucl. Phys. A* **196**, 225 (1972).
- Koltun, D. S., and M. K. Singham, *Phys. Rev. C* **39**, 704 (1989).
- Konda, Y., Y. Abe, and T. Matsuse, *Phys. Rev. C* **19**, 1356 (1979).
- Konnerth, D., W. Dünneweber, W. Harig, W. Trautmann, W. Trombek, W. Zippen, D. Habs, W. Hennerici, H. J. Hennrich, R. Kroth, A. Lazzarini, R. R. Repnow, V. Metag, and R. S. Simon, *Phys. Rev. Lett.* **55**, 588 (1985).
- Konobeevskii, E. S., R. M. Musaelyan, V. I. Popov, and I. V. Surkova, *Sov. J. Part. Nucl.* **13**, 124 (1982); *Nucl. Phys.* **13**, 124 (1982).
- Koonin, S. E., *Phys. Rev. Lett.* **39**, 680 (1977).
- Koonin, S. E., *Prog. Part. Nucl. Phys.* **4**, 283 (1979).
- Koonin, S. E., K. T. R. Davies, V. Maruhn-Rezwani, H. Feldmeier, S. J. Krieger, and J. W. Negele, *Phys. Rev. C* **15**, 1359 (1977).
- Koonin, S. E., B. Flanders, H. Flocard, and M. S. Weiss, *Phys. Lett.* **77B**, 13 (1978).
- Korotky, S. K., K. A. Erb, S. J. Willett, and D. A. Bromley, *Phys. Rev. C* **20**, 1014 (1979).
- Kovar, D. G., D. F. Gessamen, T. H. Braid, Y. Eisen, W. Henning, T. R. Ophel, M. Paul, K. E. Rehm, S. J. Sanders, P. Sperr, J. P. Schiffer, S. L. Tabor, S. Vidgor, B. Zeidman, and F. W. Prosser, Jr., *Phys. Rev. C* **20**, 1350 (1979).
- Krappe, H. J., R. J. Nix, and A. J. Sierk, *Phys. Rev. C* **20**, 992 (1979).
- Kretschmer, W., and M. Wangler, *Phys. Rev. Lett.* **41**, 224 (1978).
- Krieger, S. J., and K. T. R. Davies, *Phys. Rev. C* **20**, 167 (1979).
- Kruse, H., B. V. Jacak, J. J. Molitous, G. D. Westfall, and H. Stöcker, *Phys. Rev. C* **31**, 1770 (1985).
- Kumar, K., *Phys. Lett.* **29B**, 25 (1969).
- Kumar, K., Ch. Lagrange, M. Girod, and B. Grammaticos, *Phys. Rev. C* **31**, 762 (1985).
- Lacombe, M., B. Loiseau, J. M. Richard, R. Vinh Mau, J. Côté, P. Pirés, and R. de Tourreil, *Phys. Rev. C* **21**, 861 (1980).
- Lamarsh, J. T., and H. Feshbach, *Phys. Rev.* **104**, 1633 (1965).
- Lambert, E., and H. Feshbach, *Ann. Phys. (NY)* **76**, 80 (1973).
- Landon, H. H., and V. L. Sailor, *Phys. Rev.* **98**, 1267 (1955).
- Lane, A. M., *Phys. Rev. Lett.* **8**, 171 (1962); *Nucl. Phys.* **98**, 1524 (1955).
- Lane, A. M., and D. Robson, *Phys. Rev.* **151**, 774 (1966).

- Lane, A. M., and R. G. Thomas, *Rev. Mod. Phys.* **30**, 257 (1958).
- Lane, A. M., R. G. Thomas, and E. P. Wigner, *Phys. Rev.* **98**, 693 (1955).
- Lane, A. M., and C. F. Wandel, *Phys. Rev.* **98**, 1524 (1955).
- Larsson, S. E., G. Leander, I. Ragnarson, and N. G. A. Denius, *Nucl. Phys. A* **261**, 77 (1976).
- Lax, M., *Rev. Mod. Phys.* **23**, 287 (1951).
- Layly, V., and R. Schaeffer, *Phys. Rev. C* **17**, 1145 (1978).
- Leander, G., and S. E. Larsson, *Nucl. Phys. A* **239**, 93 (1975).
- Ledoux, R. J., M. Bloomer, and H. Z. Huang, in *Hadronic Matter in Collision*, P. Carruthers and D. Strottman, eds. (World Scientific, Singapore, 1986).
- Ledoux, R. J., C. E. Ordonez, M. J. Bechara, H. A. Al-Tuwain, G. Lavelle, and E. R. Cosman, *Phys. Rev. C* **30**, 566 (1984).
- Lee, H. K., and H. McManus, *Phys. Rev.* **161**, 1087 (1967).
- Lee, L. L., Jr., A. Marinov, C. Mayer-Borick, J. P. Schiffer, R. H. Bassel, R. M. Drisko, and G. R. Satchler, *Phys. Rev. Lett.* **14**, 261 (1965).
- Lee, L. L., and J. P. Schiffer, *Phys. Rev. B* **136**, 405 (1964).
- Lee, L. L., J. P. Schiffer, B. Zeidman, G. R. Satchler, G. R. Drisko, and R. H. Bassel, *Phys. Rev. B* **136**, 971 (1964).
- Lee, T. D., *Particle Physics and Introduction to Field Theory* (Harwood, New York, 1981).
- Lee, T. S. H., and D. Kurath, *Phys. Rev. C* **23**, 293 (1980).
- Lee, T. S. H., and K. Ohta, *Phys. Rev. C* **25**, 3043 (1982).
- Lefort, M., *Rep. Prog. Phys.* **39**, 129 (1976a).
- Lefort, M., in *Nuclear Spectroscopy and Nuclear Reactions with Heavy Ions* (LXII Corso Editrice Compositori, Bologna, 1976b).
- Lefort, M., and Ch. Ngô, *Ann. Phys.* **3**, 5 (1978).
- Lemmer, R. H., and C. M. Shakin, *Ann. Phys. (NY)* **27**, 13 (1964).
- Lenz, F., E. J. Moniz, and K. Yazaki, *Ann. Phys. (NY)* **129**, 842 (1980).
- Lenz, F., and E. J. Moniz, private communication, to be published.
- Lenz, F., M. Thies, and Y. Horikawa, *Ann. Phys. (NY)* **140**, 266 (1982).
- Levin, F. S., and H. Feshbach, *Reaction Dynamics* (Gordon & Breach, New York, 1973).
- LeVine, M. J., A. J. Baltz, P. D. Bond, J. D. Garrett, S. Kahana, and C. E. Thorn, *Phys. Rev. C* **10**, 1603 (1974).
- Liou, H. I., H. S. Camarda, S. Wynchank, M. Slogowitz, C. Haken, F. Rahn, and J. Rainwater, *Phys. Rev. C* **5**, 974 (1972).
- Liu, L. C., *Phys. Rev. C* **17**, 1787 (1978).
- Liu, L. C., and C. M. Shakin, *Phys. Rev. C* **16**, 333 (1977); **19**, 129 (1979).
- Love, W. G., *Nucl. Phys. A* **312**, 160 (1978).
- Love, W. G., and M. A. Franey, *Phys. Rev. C* **24**, 1073 (1981).
- Love, W. G., A. Scott, F. T. Baker, W. P. Jones, and J. D. Wiggins, Jr., *Phys. Lett.* **73B**, 277 (1978).
- Lu, C. C., L. C. Vaz, and J. R. Huizenga, *Nucl. Phys. A* **190**, 222 (1972).
- Mahaux, C., in *Common Problems in Low and Medium Energy Nuclear Physics*, B. Castel, B. Goulard, and F. C. Khanna, eds. (Plenum Press, New York, 1978).

- Mahaux, C., and H. Ngô, *Phys. Lett.* **100B**, 285 (1981).
- Mahaux, C., and H. A. Weidenmüller, *Annu. Rev. Nucl. Part. Phys.* **29**, 1, (1979).
- Mahaux, C., and H. A. Weidenmüller, *Shell Model Approach to Nuclear Reactions* (North-Holland, Amsterdam, 1969).
- Malmin, R. E., J. W. Harris, and P. Paul, *Phys. Rev. C* **18**, 163 (1978).
- Mantzouranis, G., *Phys. Rev. C* **121**, 2018 (1976).
- Mantzouranis, G., D. Agassi, and H. Weidenmüller, *Phys. Lett.* **57B**, 220 (1970).
- Mantzouranis, G., H. Weidenmüller, and D. Agassi, *Z. Phys. A* **276**, 145 (1976).
- Margolis, B., and V. F. Weisskopf, *Phys. Rev.* **107**, 641 (1957).
- Marlow, D., P. Barnes, N. Collela, S. Dytman, R. E. Eisenstein, R. Grace, F. Takeutchi, W. Wharton, S. Bart, D. Hancock, R. Hackenberg, E. Hungerford, W. Mayes, L. Pinsky, T. Williams, R. Chrian, H. Palevsky, and R. Sutter, *Phys. Rev. C* **25**, 2619 (1982).
- Marmier, P., and E. Sheldon, *Physics of Nuclei and Particles* (Academic Press, New York, Vol. I, 1969; Vol. II, 1970).
- Marshak, R. E., *Phys. Rev.* **82**, 313 (1951).
- Martin, B. R., *Nucl. Phys. B* **94**, 413 (1975).
- Maruhn, J. A., in *Proceedings of the Winter College on Fundamental Nuclear Physics*, K. Dietrich, M. diToro, and H. J. Mang, eds. (World Scientific, Singapore, 1985).
- Maruhn, J. A., and W. Greiner, in *Treatise on Heavy Ion Science*, D. A. Bromley, ed. (Plenum Press, New York, 1985).
- Mast, T. J., M. Alston-Garnjost, R. O. Bangerter, A. S. Babaro-Galtieri, F. T. Solmitz, and R. D. Tripp, *Phys. Rev. D* **14**, 13 (1976).
- Matsui, T., *Nucl. Phys. A* **488**, 535c (1988).
- Matsuse, T., A. Arima, and S. M. Lee, *Phys. Rev. C* **26**, 2338 (1982).
- May, M., et al., *Phys. Rev. Lett.* **47**, 1106 (1981).
- Mayer, B., *Nulkeoniki* **25**, 439 (1980).
- McCauley, G. P., and G. E. Brown, *Proc. Phys. Soc. (London)* **71**, 893 (1958).
- McCubbin, N. A., *Nucl. Phys. A* **458**, 585c (1988).
- McEllistrem, M. G., in *Neutron-Nucleus Collisions*, J. Rappaport, R. W. Finley, S. H. Guinnes, and F. D. S. Dietrich, eds. (American Institute of Physics, New York, 1985).
- McKinley, W. A., Jr., and H. Feshbach, *Phys. Rev.* **74**, 1759 (1948).
- McNeil, J. A., L. Ray, and S. J. Wallace, *Phys. Rev. C* **27**, 2123 (1983).
- Mello, P. A., *Notas Fis. Unam.* **1**, 1 (1978).
- Mello, P. A., and H. Feshbach, *Phys. Lett.* **39B**, 461 (1972).
- Menet, J. J. H., E. E. Gross, J. J. Malinify, and A. Zucker, *Phys. Rev. C* **4**, 1114 (1971).
- Meyer, H. O., P. Schwandt, G. L. Moake, and P. P. Singh, *Phys. Rev. C* **23**, 616 (1981).
- Meyer-Berkhout, U., K. W. Ford, and A. E. S. Green, *Ann. Phys. (NY)* **8**, 119 (1959).
- Michaud, G., and E. W. Vogt, *Phys. Lett.* **30B**, 85 (1969); *Phys. Rev. C* **5**, 350 (1972).
- Migdal, A. B., *Theory of Finite Fermi Systems* (John Wiley & Sons, New York, 1967).
- Millener, D. J., C. B. Dover, and A. Gal, *Phys. Rev. C* **38**, 2700 (1988).
- Millener, D. J., C. B. Dover, and A. Gal, *Phys. Rep.* **198**, 1 (1989).
- Millener, D. J., A. Gal, C. B. Dover, and R. H. Dalitz, *Phys. Rev. C* **31**, 499 (1985).

- Miller, D. W., R. K. Adair, C. K. Bockelman, and S. E. Darden, *Phys. Rev.* **88**, 83 (1952).
- Miller, J. M., in *Statistical Properties of Nuclei*, J. B. Garg, ed. (Plenum Press, New York, 1972).
- Mitchell, G. E., in *Theory and Applications of Moment Methods in Many Fermion Systems*, B. J. Dalton, J. P. Vary, S. A. Williams, and S. M. Grimes, eds. (Plenum Press, New York, 1980).
- Mittelman, M. H., *Ann. Phys.* **20**, 430 (1964).
- Moldauer, P. A., *Phys. Rev.* **123**, 968 (1961).
- Moldauer, P. A., *Nucl. Phys.* **47**, 65 (1963).
- Moldauer, P. A., *Phys. Rev.* **135**, B642 (1964).
- Moldauer, P. A., *Phys. Rev. C* **11**, 426 (1975a).
- Moldauer, P. A., *Phys. Rev. C* **12**, 744 (1975b).
- Moldauer, P. A., *Nucl. Phys. A* **344**, 185 (1980).
- Möller, P., and R. J. Nix, *Nucl. Phys. A* **272**, 502 (1976).
- Mon, K. K., and J. B. French, *Ann. Phys. (NY)* **95**, 90 (1975).
- Moniz, E. J., in *Theoretical Methods in Medium Energy and Heavy Ion Physics*, K. McVoy and W. Friedman, eds. (Plenum Press, New York, 1978).
- Moniz, E. J., in *Nuclear Physics with Heavy Ions and Mesons*, R. Balian, M. Rho, and G. Ripka, eds. (North-Holland, Amsterdam, 1978).
- Moniz, E. J., R. R. Whitney, J. R. Ficenec, R. D. Kephart, and W. P. Trower, *Phys. Rev. Lett.* **26**, 445 (1971).
- Mordechai, S., N. Auerbach, S. Greene, C. L. Morris, T. M. O'Donnell, H. T. Fortune, G. Liu, M. Burlein, A. Wuosmaa, S. H. Yoo, and C. F. Moore, *Phys. Rev. C* **40**, 850 (1989).
- Moretto, L. G., *Nucl. Phys. A* **182**, 641 (1972a).
- Moretto, L. G., *Nucl. Phys. A* **185**, 145 (1972b).
- Moretto, L. G., and R. Schmitt, *J. Phys. (Paris) Colloq. C* **5**, 37, 109 (1976).
- Moretto, L. G., R. Stella, and V. Caramella-Crespi, *Energ. Nucl.* **17**, 436 (1970).
- Morgenstern, J., R. N. Alves, J. Julien, and C. Samour, *Nucl. Phys. A* **123**, 561 (1969).
- Morse, P. M., and H. Feshbach, *Methods of Theoretical Physics* (McGraw-Hill, New York, 1953).
- Morrison, P., in *Experimental Nuclear Physics*, Vol. II, E. Segrè, ed. (John Wiley & Sons, New York, 1953).
- Mosel, U., in *Treatise on Heavy Ion Science*, D. A. Bromley, ed. (Plenum Press, New York, 1984).
- Moses, J. D., H. W. Newson, E. G. Bilpuch, and G. E. Mitchell, *Nucl. Phys. A* **175**, 556 (1971).
- Mott, N. F., *Proc. Roy. Soc. A* **124**, 426 (1929); **135**, 429 (1932).
- Mott, N. F., and H. S. W. Massey, *The Theory of Atomic Collisions* (Oxford University Press, Oxford, 1949).
- Mougey, I., in *Electron and Pion Interactions with Nuclei at Intermediate Energies*, W. Bertozzi, S. Costa, and C. Schaerf, eds. (Harwood, New York, 1980).
- Moya de Guerra, E., *Phys. Rep.* **138**, 293 (1986).
- Moya de Guerra, E., and F. Villars, *Nucl. Phys. A* **285**, 297 (1977).

- Mülhans, K., E. Müller, K. Neegård, and U. Mosel, *Phys. Lett.* **105B**, 329 (1981).
- Murdock, D. P., and C. J. Horowitz, *Phys. Rev. C* **35**, 1442 (1987).
- Myers, W. D., *Nucl. Phys. A* **296**, 177 (1978).
- Nadasen, A., P. Schwandt, P. P. Singh, W. W. Jacobs, A. D. Bacher, P. T. Debevec, M. D. Kaitchuk, and J. T. Meek, *Phys. Rev. C* **23**, 1023 (1981).
- Nagamiya, S., L. Anderson, W. Brückner, O. Chamberlin, M. C. Lemaire, S. Schnetzer, G. Shapiro, H. Steiner, and I. Tanihata, *Phys. Lett.* **81B**, 147 (1979).
- Namboodiri, M. N., E. T. Chulick, and J. B. Natowitz, *Nucl. Phys. A* **263**, 491 (1976).
- Negele, J. W., *Phys. Rev. C* **1**, 1260 (1970).
- Negele, J. W., in *Theoretical Methods in Medium Energy and Heavy Ion Physics*, K. W. McVoy and W. A. Friedman, eds. (Plenum Press, New York, 1978).
- Negele, J. W., *Rev. Mod. Phys.* **54**, 913 (1982).
- Negele, J. W., and D. Vautherin, *Phys. Rev. C* **5**, 1472 (1972).
- Negele, J. W., and D. Vautherin, *Phys. Rev. C* **11**, 1031 (1975).
- Negele, J. W., and K. Yazaki, *Phys. Rev. Lett.* **47**, 71 (1981).
- Nerenson, N., and S. E. Darden, *Phys. Rev.* **94**, 1678 (1954); **89**, 775 (1953).
- Nix, J. R., and A. J. Sierk, *Phys. Rev. C* **15**, 2072 (1977).
- Nörenberg, W., in *Proceedings of the Winter College on Fundamental Nuclear Physics*, K. Dietrich, M. diToro, and H. J. Mang, eds. (World Scientific, Singapore, 1985).
- Ohmura, T., B. Imanishi, G. Ichimura, and M. Kawai, *Prog. Theor. Phys.* **41**, 391 (1970); **43**, 347 (1970).
- Okazaki, A., S. E. Darden, and R. B. Walton, *Phys. Rev.* **93**, 461 (1954).
- Olmer, C., in *The Interaction Between Medium Energy Nucleons in Nuclei—1982*, H. O. Meyer, ed. (American Institute of Physics, New York, 1983).
- Orland, H., and R. Schaeffer, *Nucl. Phys. A* **299**, 442 (1978).
- Oset, E., and W. Weise, *Nucl. Phys. A* **329**, 365 (1979); **368**, 375 (1981); **319**, 477 (1977).
- Ottenstein, N., S. J. Wallace, and J. A. Tjøn, *Phys. Rev. C* **38**, 2272, 2289 (1988).
- Owen, L., and G. R. Satchler, *Phys. Rev. Lett.* **25**, 1720 (1970).
- Pais, A., and O. Piccioni, *Phys. Rev.* **100**, 1483 (1955).
- Pal, M. K., in *Proceedings of the Winter College on Fundamental Nuclear Physics*, K. Dietrich, M. diToro, and H. J. Mang, eds. (World Scientific, Singapore, 1985).
- Pandey, A., *Ann. Phys. (NY)* **119**, 170 (1979).
- Pandey, A., *Ann. Phys. (NY)* **134**, 110 (1981).
- Pandharipande, V. R., N. Papanicolas, and J. Wambach, *Phys. Rev. Lett.* **53**, 1133 (1984).
- Park, J. Y., W. Scheid, and W. Greiner, *Phys. Rev. C* **10**, 967 (1974).
- Parmentola, J., and H. Feshbach, *Ann. Phys. (NY)* **139**, 314 (1982).
- Passatore, G., *Nucl. Phys. A* **95**, 694 (1967); **110**, 91 (1968).
- Passatore, G., in *Nuclear Optical Model Potential* (Springer-Verlag, Heidelberg, 1976).
- Patterson, D. M., R. R. Doering, and A. Galonsky, *Nucl. Phys. A* **263**, 261 (1976).
- Pedroni, E., K. Gabathuler, J. J. Domingo, W. Hert, P. Schwaller, et al., *Nucl. Phys. A* **300**, 321 (1978).

- Peng, J. C., in *Proceedings of Second LAMPF II Workshop*, Report LA-9272-C, H. A. Thiessen, et al., eds. (1982).
- Perey, F. G., *Phys. Rev.* **131**, 745 (1963).
- Perey, F. G., and B. Buck, *Nucl. Phys.* **32**, 353 (1962).
- Perey, C. M., and F. G. Perey, *Atomic Data and Nuclear Data Tables* **17**, 1 (1974).
- Perey, F. G., and D. S. Saxon, *Phys. Rev.* **10**, 107 (1964).
- Petrovich, F., and W. G. Love, *Nucl. Phys. A* **354**, 449c (1981).
- Petrovich, F., H. McManus, V. A. Madsen, and J. Atkinson, *Phys. Rev. Lett.* **22**, 895 (1969).
- Petrovich, F., D. Stanley, and J. J. Bevelacqua, *Phys. Lett.* **71B**, 259 (1977).
- Picklesimer, A., P. C. Tandy, R. M. Thaler, and D. H. Wolfe, *Phys. Rev. C* **30**, 1861 (1984).
- Picklesimer, A., and R. M. Thaler, *Phys. Rev. C* **23**, 42 (1981).
- Piekarz, H., S. Bart, R. Hackenberg, A. D. Hancock, E. V. Hungerford, B. Mayes, K. Sekharan, J. Piekarz, M. Deutsch, R. Chrien, S. Chen, M. LeVine, D. Maurizio, M. May, H. Palevsky, Y. Xu, P. D. Barnes, B. Bassalleck, R. Eisenstein, R. Grace, C. Maher, P. Pile, R. Rieder, W. Wharton, and R. L. Stearns, *Phys. Lett.* **110B**, 428 (1982).
- Podgoretsky, M. I., *J. Exp. Theor. Phys.* **44**, 695 (1963).
- Poppalardo, G., *Phys. Lett.* **13**, 320 (1964).
- Porter, C. F., *Statistical Theory of Spectra: Fluctuations* (Academic Press, New York, 1965).
- Porter, C. F., and N. Rosenzweig, *Ann. Acad. Sci. Fennicae* **AVI 44** (1960).
- Porter, C. F., and R. G. Thomas, *Phys. Rev.* **104**, 483 (1956).
- Povh, B., *Rep. Prog. Phys.* **39**, 824 (1974).
- Povh, B., *Ann. Rev. Nucl. Part. Sci.* **28**, 1 (1978).
- Pühlhofer, F., *Nucl. Phys. A* **280**, 267 (1977).
- Racah, G., *Phys. Rev.* **84**, 910 (1951).
- Rae, W. D. M., *Notas Fis. Unam* **10**, 283 (1987).
- Rae, W. D. M., and S. Marsh, *Phys. Lett.* **161B**, 251 (1985).
- Ray, L., *Phys. Rev. C* **19**, 1855 (1979).
- Ray, L., in *The Interaction Between Medium Energy Nucleons in Nuclei—1982*, H. O. Meyer, ed. (American Institute of Physics, New York, 1983).
- Ray, L., and G. W. Hoffmann, *Phys. Rev. C* **27**, 2133 (1983).
- Ray, L., and G. W. Hoffmann, *Phys. Rev. C* **31**, 538 (1985).
- Rehm, K. E., A. H. van den Berg, J. J. Kolata, D. G. Kovar, W. Kutschera, G. Rosner, G. S. F. Stephans, and J. L. Yntema, Argonne Nat'l. Lab. report Phy-4689-HI-85 (1985).
- Rehm, K. E., F. L. H. Wolfs, A. M. Vanden Berg, and W. Henning, *Phys. Rev. Lett.* **55**, 280 (1985).
- Reising, R. F., G. L. Bate, and J. R. Huizenga, *Phys. Rev.* **141**, 1161 (1966).
- Rhoades-Brown, M. J., P. Braun-Munzinger, M. Prakash, and S. Sen, in *Fusion Reactions Below the Coulomb Barrier*, Lecture Notes in Physic 219, S. M. Steadman, ed. (Springer-Verlag, Berlin, 1985).

- Ribe, F. L., in *Fast Neutron Physics*, J. B. Marion and J. L. Fowler, eds (John Wiley & Sons, New York, 1963).
- Robson, D., *Phys. Rev. B* **137**, 505 (1965).
- Robson, D. in *Isospin in Nuclear Physics*, D. H. Wilkinson, ed. (North-Holland, Amsterdam, 1969).
- Robson, D., and A. M. Lane, *Phys. Rev.* **161**, 982 (1967).
- Rosen, L., T. G. Beery, A. S. Goldhaber, and E. H. Auerbach, *Ann. Phys. (NY)* **34**, 96 (1965).
- Rosen, L., and L. Stewart, *Phys. Rev.* **99**, 1052 (1955).
- Rosen, M., and D. R. Yennie, *J. Math. Phys.* **5**, 1505 (1964).
- Rosenthal, A. S., and F. Tabakin, *Phys. Rev. C* **22**, 711 (1980).
- Rosenzweig, N. in *Statistical Physics* (W. A. Benjamin, New York, 1963).
- Rosenzweig, N., *Phys. Rev.* **105**, 950 (1957); **108**, 817 (1957).
- Ross, M. and G. Shaw, *Ann. Phys. (NY)* **9**, 391 (1960); **13**, 147 (1961).
- Rost, E., *Phys. Rev.* **154**, 994 (1967).
- Rothaas, H., in *Modern Trends in Elastic Electron Scattering* Proc. of Conf. Amsterdam (1978).
- Rowe, G., M. Solomon, and R. H. Landau, *Phys. Rev. C* **18**, 584 (1978).
- Saito, S., *Prog. Theor. Phys.* **40**, 893 (1968); **41**, 705 (1969).
- Sakai, H., K. Hosono, M. Matsusko, S. Nagamachi, K. Okada, K. Maeda, and H. Shimizu, *Nucl. Phys. A* **344**, 416 (1980).
- Salnikov, O. A., G. N. Lovichikova, G. V. Kotelnikova, A. N. Trefanov, and N. I. Fetisov, *Yad. Fiz* **12**, 1132 (1970); *Sov. J. Nucl. Phys.* **12**, 620 (1971).
- Sandorfi, A. M., and M. T. Collins, in *Resonances in Heavy Ion Collisions*, K. Eberhard, ed. (Springer-Verlag, Berlin, 1982).
- Santos, F. D., *Nucl. Phys. A* **212**, 341 (1973).
- Satchler, G. R., *Phys. Lett.* **7**, 55 (1963).
- Satchler, G. R., *Nucl. Phys. A* **91**, 75 (1967).
- Satchler, G. R., in *Isospin in Nuclear Physics*, D. H. Wilkinson, ed. (North-Holland, Amsterdam, 1969).
- Satchler, G. R., *Phys. Lett.* **59B** 167 (1975).
- Satchler, G. R., *Direct Nuclear Reactions* (Oxford University Press, New York, 1983).
- Satpathy, L., P. Sarangi, and A. Faessler, *J. Phys. G* **12**, 201 (1986).
- Satz, H., *Nucl. Phys. A* **488**, 511c (1988).
- Schaeffer, R., in *Selected Aspects of Heavy Ion Reactions*, M. Martenot, C. Ngô, and P. Gugenberger, eds. (North-Holland, Amsterdam, 1982).
- Scheid, W., H. F. Fink, and H. Müller, in *Proceedings of the Conference on Intermediate Processes in Nuclear Reactions* (Springer-Verlag, Heidelberg, 1973).
- Scheid, W., W. Greiner, and R. Lemmer, *Phys. Rev. Lett.* **25**, 176 (1970).
- Schiffer, J. P., *Rev. Mod. Phys.* **36**, 1065 (1964).
- Schiffer J. P., *Suppl. J. Phys. Soc. Jpn.* **24** (1968).
- Schiffer, J. P., and L. L. Lee, *Phys. Rev.* **107**, 640 (1957).

- Schiffer, J. P., and L. L. Lee, *Phys. Rev.* **109**, 2098 (1958).
- Schiffer, J. P., L. L. Lee, R. H. Davis, and F. W. Prosser, Jr., *Phys. Rev.* **107**, 547 (1957).
- Schnitzer, H. J., *Rev. Mod. Phys.* **37**, 666 (1964).
- Schroeder, L. S., *L.B.L. Preprint LBL-3082* (1976).
- Schröder, W. U., J. R. Birkelund, J. R. Huizenga, K. L. Wolf, and V. E. Viola, Jr., *Phys. Rep.* **45**, 301 (1978).
- Schröder, W. U., and J. Huizenga, *Treatise on Heavy Ion Science*, D. A. Bromley, ed. (Plenum Press, New York, 1984).
- Schwandt, P., in *The Interaction Between Medium Energy Nucleons in Nuclei—1982*, H. O. Meyer, ed. (American Institute of Physics, New York, 1983).
- Schwinger, J. S., *Phys. Rev.* **73**, 407 (1948).
- Schwinger, J., *Phys. Rev.* **75**, 898 (1949a).
- Schwinger, J., *Phys. Rev.* **76**, 790 (1949b).
- Scott, D. K., B. G. Harvey, D. L. Hendrie, U. Johnke, L. Klaus, C. F. Maguire, J. Mahoney, Y. Yerrien, K. Yagi, and N. K. Glendenning, *Phys. Rev. Lett.* **34**, 895 (1975).
- Serot, B. D., and J. D. Walecka, *Adv. Nucl. Phys.* **16**, 327 (1986).
- Seth, K. K., J. A. Biggerstaff, P. D. Miller, and G. R. Satchler, *Phys. Rev.* **164**, 1450 (1967).
- Shakin, C. M., in *The Interaction Between Medium Energy Nucleons in Nuclei—1982*, H. O. Meyer, ed. (American Institute of Physics, New York, 1983).
- Shapiro, I. S., in *Proceedings of the International School of Physics “Enrico Fermi” Course XXXVII*, T. E. O. Ericson, ed. (Academic Press, New York, 1967).
- Sherr, R., and F. P. Brady, *Phys. Rev.* **124**, 1928 (1961).
- Siciliano, E. R., M. D. Cooper, M. B. Johnson, and M. J. Leitch, *Phys. Rev. C* **34**, 267 (1986).
- Siciliano, E. R., M. B. Johnson and H. Sarafian, *Ann. Phys. (NY)* **203**, 1 (1990).
- Sick, I., *Nucl. Phys. A* **218**, 509 (1974).
- Sick, I., in *Electron Scattering in Nuclear and Particle Science*, C. M. Papinicas, L. S. Cardman, and R. A. Eisenstein, eds. (American Institute of Physics, New York, 1987).
- Sick, I., D. Day, and J. S. McCarthy, *Phys. Rev. Lett.* **45**, 871 (1980).
- Sick, I., and J. S. McCarthy, *Nucl. Phys. A* **150**, 631 (1970).
- Siegel, P. B., W. B. Kaufmann, and W. R. Gibbs, *Phys. Rev. C* **30**, 1256 (1984); **31**, 2184 (1985).
- Siegert, A. J. F., *Phys. Rev.* **56**, 750 (1939).
- Simoni, M., *Phys. Lett.* **52B**, 279 (1974).
- Singh, P. P., R. E. Segel, L. Meyer-Schützmeister, S. S. Hanna, and R. G. Allas, *Nucl. Phys.* **65**, 577 (1965).
- Siwek-Wilczyński, K., and J. Wilczyński, *Nucl. Phys. A* **264**, 115 (1976).
- Siwek-Wilczyńska, K., and J. Wilczynski, *Phys. Rep.* **45**, 175 (1978).
- Slanina, D., and H. McManus, *Nucl. Phys. A* **116**, 271 (1968).
- Smith, R. D., and S. J. Wallace, *Phys. Rev. C* **32**, 1654 (1985).
- Sparrow, P. A., *Ann. Phys. (NY)* **91**, 157 (1975).
- Spencer, J. E., and A. K. Kerman, *Phys. Lett.* **38B**, 289 (1972).
- Spinka, H., and H. Winkler, *Nucl. Phys. A* **233**, 456 (1974).

- Steadman, S. M., ed., *Fusion Reactions Below the Coulomb Barrier*, Lecture Notes in Physics **219** (Springer-Verlag, Berlin, 1985).
- Stepien-Rudzka, W., and S. Wycech, *Nucl. Phys. A* **362**, 349 (1981).
- Stevenson, J. D., *Phys. Rev. Lett.* **41**, 1702 (1978).
- Stock, R., R. Bock, P. David, H. H. Duham, and T. Tamura, *Nucl. Phys. A* **104**, 136 (1967).
- Stöcker, H., R. Y. Cusson, J. A. Maruhn, and W. Greiner, *Phys. Lett.* **101B**, 379 (1981).
- Stöcker, H., and W. Greiner, *Phys. Rep.* **137**, 278 (1986).
- Stokstad, R. G., in *Treatise on Heavy Ion Science*, Vol. III D. A. Bromley, ed. (Plenum Press, New York, 1985).
- Strayer, M., R. Y. Cusson, A. S. Umar, P. G. Reinhard, D. A. Bromley, and W. Greiner, *Phys. Lett.* **135B**, 261 (1984).
- Swiatecki, W. J., *Nucl. Phys. A* **376**, 275 (1982).
- Takaki, T., *Ann. Phys. (NY)* **166**, 1 (1986).
- Takeda, G., and K. M. Watson, *Phys. Rev.* **94**, 1087 (1954).
- Takeda, G., and K. M. Watson, *Phys. Rev.* **97**, 1336 (1955).
- Tamura, T., *Rev. Mod. Phys.* **37**, 679 (1965).
- Tamura, T., *Phys. Rep.* **14**, 60 (1974).
- Tamura, T., T. Udagawa, D. H. Feng, and K. K. Kan, *Phys. Lett.* **66B**, 109 (1977).
- Tamura, T., T. Udagawa, and H. Lenske, *Phys. Rev. C* **26**, 379 (1982).
- Tang, L. G., E. Hungerford, T. Kishimoto, B. Mayes, L. Pinsky, S. Bort, R. Chrien, P. Pile, R. Sutter, P. Bornes, G. Diebold, G. Franklin, P. Hertzog, B. Quinn, J. Seydour, J. Szymanski, T. Fukda, and R. Stearns, *Phys. Rev. C* **38**, 846 (1988).
- Tassie, L. T., *Aust. J. Phys.* **9**, 407 (1956).
- Teichmann, T., and E. P. Wigner, *Phys. Rev.* **87**, 123 (1952).
- Tapel, J. W., *Z. Phys. A* **273**, 59 (1975).
- Tepel, J. W., H. M. Hoffman, and H. A. Weidenmüller, *Phys. Lett.* **49B**, 1 (1974).
- Thies, M., *Nucl. Phys. A* **382**, 434 (1982).
- Thomas, R. G., *Phys. Rev.* **97**, 224 (1955).
- Thouless, D. J., *Nucl. Phys.* **21**, 225 (1961).
- Tjønn, P. O., I. Espe, G. B. Hagemann, B. Herskind, and D. L. Hillis, *Phys. Lett.* **72B**, 439 (1978).
- Tjønn, T. A., and S. J. Wallace, *Phys. Rev. C* **32**, 267 (1985).
- Tjønn, T. A., and S. J. Wallace, *Phys. Rev. C* **35**, 280 (1987).
- Tonozuka, I., and A. Arima, *Nucl. Phys. A* **323**, 45 (1979).
- Tucker, A. B., J. T. Wells, and W. E. Meyerhoff, *Phys. Rev. B* **137**, 1181 (1965).
- Twin, P. J., B. M. Nayako, A. H. Nelson, J. Simpson, M. A. Bentley, H. Cranmer-Gordon, P. D. Forsyth, D. Howe, A. R. Mokhtar, J. D. Morrison, J. F. Sharpey-Shafer, and G. Slotten, in *Proceedings of the International Nuclear Physics Conference*, Vol. I (Harrogate, England, August, 1986).
- Twin, P. J., et al., *Phys. Rev. Lett.* **57**, 811 (1986).
- Tyrén, H., S. Kullander, O. Sunderg, R. Ramachandran, P. Isaacson, and T. Berggren, *Nucl. Phys.* **79**, 321 (1966).

- Überall, H., *Electron Scattering from Complex Nuclei* (Academic Press, New York, 1971).
- Uehling, E. and G. Uhlenbeck, *Phys. Rev.* **43**, 552 (1933).
- Ullo, J., and H. Feshbach, *Ann. Phys. (NY)* **82**, 156 (1974).
- Umar, A. S., and M. R. Strayer, *Phys. Lett.* **171B**, 353 (1986).
- Umar, A. S., M. R. Strayer, R. Y. Cusson, P. G. Reinhard, and D. A. Bromley, *Phys. Rev. C* **32**, 172 (1985).
- Vager, Z., *Phys. Lett.* **36B**, 269 (1971).
- van de Hulst, H. C., *Light Scatteing by Small Particles* (John Wiley & Sons, New York, 1957).
- Vandenbosch, R., *Phys. Lett.* **87B**, 183 (1979).
- Vandenbosch, R., *Proceedings of the Symposium on High Spin Phenomena in Nuclei*, Report ANL/Phy-79-4 (Argonal National Laboratory, 1979).
- Vandenbosch, R., and A. J. Lazzarini, *Phys. Rev. C* **23**, 1074 (1981).
- Van der Berg, A. M., W. Henning, L. L. Lee, K. T. Lesko, K. E. Rehm, J. P. Schiffer, G. S. F. Stephans, F. L. H. Wolfs, and W. S. Freeman, *Phys. Rev. C* **37**, 178 (1988).
- Van der Velde-Wiquet, C., J. Sacton, and J. H. Wickens, *Nuovo Cimento A* **38** 178 (1977).
- Villars, F., *Nucl. Phys. A* **285**, 269 (1977).
- von Geramb, H. V., in *The Interaction Between Medium Energy Nucleons in Nuclei-1982*, H. O. Meyer, ed. (American Institute of Physics, New York, 1983).
- von Geramb, H. V., F. A. Brieva, and J. R. Rook, in *Microscopic Optical Potentials*, H. V. von Geramb, ed. (Springer-Verlag, Berlin, 1979).
- von Geramb, H. V., and K. Nakano, in *The Interaction Between Medium Energy Nucleons in Nuclei-1982*, H. O. Meyer, ed. (American Institute of Physics, New York, 1983).
- von Witsch, W., P. von Brentano, T. Mayer-Kuckuk, and A. Richter, *Nucl. Phys.* **80**, 394 (1966).
- Vourvopolous, G., *Resonant Behavior of the Heavy Ion Systems* (Greek National Printing Office, Athens, 1981).
- Walcher, T., *Nucl. Phys. A* **479**, 63c (1988).
- Walecka, J. D., *Ann. Phys. (N.Y)* **83**, 491 (1974).
- Wallace, S. J., *Ann. Phys. (NY)* **78**, 190 (1973a).
- Wallace, S. J., *Phys. Rev. D* **8**, 1846 (1973b).
- Wallace, S. J., *Adv. Nucl. Phys.* **12**, 135 (1981).
- Wallace, S. J., *Annu. Rev. Nucl. Part. Sci.* **37**, 267 (1987).
- Wallace, S. J., and Y. Alexander, *Phys. Lett.* **90B**, 346 (1980).
- Wallace, S. J., and J. L. Friar, *Phys. Rev. C* **29** 956 (1984).
- Walt, M., R. L. Becker, A. Okazaki, and R. E. Fields, *Phys. Rev.* **89**, 1271 (1953).
- Warszawski, J., A. Gal, and J. M. Eisenberg, *Nucl. Phys. A* **294**, 321 (1978); **312**, 253 (1978).
- Watanabe, S., *Nucl. Phys.* **8**, 484 (1958).
- Watson, K. M., *Phys. Rev.* **89**, 575 (1953).
- Watson, K. M., *Phys. Rev.* **105**, 1388 (1957).
- Watson, K. M., *Phys. Rev.* **30**, 565 (1958).

- Weisskopf, V. F., *Phys. Rev.* **52**, 295 (1937).
- Weisskopf, V. F., *Phys. Today* **14**, 18 (1960).
- Weisskopf, V. F., and D. H. Ewing, *Phys. Rev.* **57**, 472 (1940).
- West, G. B., *Phys. Rep. C* **18**, 264 (1975).
- Westfall, G. D., J. Gosset, P. J. Johanson, A. M. Poskanzer, W. G. Meyer, H. H. Gutbrod, A. Sandoval, and R. Stock, *Phys. Rev. Lett.* **37**, 1202 (1976).
- Whitehead, R. R., A. Watt, B. J. Cole, and I. Morrison, *Adv. Nucl. Phys.* **9** (Plenum Press N.Y. 1977).
- Wigner, E. P., *Phys. Rev.* **40**, 749 (1930).
- Wigner, E. P., and L. Eisenbud, *Phys. Rev.* **72**, 29 (1947).
- Wilcke, W. W., J. R. Birkelund, A. D. Ha, J. R. Huizenga, W. U. Schroeder, V. E. Viola, K. L. Wolf, and A. C. Mignerey, *Phys. Rev. C* **22**, 128 (1980).
- Wilczyński, J., *Phys. Lett.* **47B**, 484 (1973).
- Wilets, L., E. M. Henley, and A. D. MacKellar, *Nucl. Phys. A* **282**, 361 (1977).
- Wilkin, C., *Nucl. Phys. A* **220**, 621 (1979).
- Wilmore, D., and P. E. Hodgson, *Nucl. Phys.* **55**, 673 (1964).
- Wilmore, D., and P. E. Hodgson, *Use of Nuclear Theory in Neutron Data Evaluation* (International Center for Theoretical Physics, Trieste, 1975).
- Wolf, K. L., and C. T. Roche, in *Proceedings of the Symposium on Macroscopic Features of Heavy Ion Collisions* (Argonne National Laboratory, 1976), [Report ANL/Phy-76, Vol. I] p. 295.
- Wong, C. Y., *Phys. Lett.* **42B**, 186 (1972); *Phys. Rev. Lett.* **31**, 766 (1973).
- Woods, R. D., and D. S. Saxon, *Phys. Rev.* **95**, 577 (1954).
- Xuetian, T., *Phys. Lett.* **104B**, 99 (1981).
- Yahiro, M., Ph.D. thesis, Kyushu University (1985).
- Yahiro, M., Y. Iseri, M. Kamimura, and N. Makano, *Phys. Lett.* **141B**, 19 (1984).
- Yamada, Y., K. Ikeda, H. Bando and T. Motoba, *Phys. Rev. C* **38**, 854 (1988).
- Yamazaki, T., T. Ishikawa, K. H. Tanaka, Y. Akiba, M. Iwasaki, S. Ohtake, H. Tamura, M. Nakajima, T. Yamanaka, I. Arai, T. Suzuki, F. Naito, and R. S. Hayano, *Phys. Rev. Lett.* **54**, 102 (1985).
- Yamazaki, T., M. Kondo, and S. Yamato, *J. Phys. Soc. (Jpn.)* **18**, 620 (1963).
- Yang, C. N., *Phys. Rev.* **74**, 764 (1948).
- Yariv, Y., and Z. Fraenkel, *Phys. Rev. C* **20**, 2227 (1979); **24**, 488 (1981).
- Yennie, D. R., D. G. Ravenhall, and R. N. Wilson, *Phys. Rev.* **95**, 500 (1954).
- Zachariasen, F., in *Semi-classical Description of Atomic and Nuclear Collisions*, J. Band and J. deBoer, eds. (Elsevier Science Publications, New York, 1983).
- Zamick, L., *Phys. Rev. Lett.* **40**, 381 (1978).
- Zamick, L., E. Klemt, and J. Speth, *Nucl. Phys. A* **245**, 365 (1975).
- Zyskind, J. L., J. M. Davidson, M. T. Esat, M. H. Sapiro, and R. H. Spearn *Nucl. Phys. A* **301**, 179 (1978).

INDEX

- Abrasion–ablation, 781
- Absorption, nucleon, 17, 178, 361
 - pion, 830
- Adiabatic approximation, 77, 414, 419
 - limit to TDHF, 662
- Analog state, *see also* Doorway states
 - isobar, 397, 460, 849
 - $SU(3)$, 64
- Analyzing power, 482, 747
- Angular distribution
 - in elastic scattering, 357
 - in evaporation region, 27
 - in heavy ion reactions, 579
 - maximum complexity, 65, 233
 - in reactions, 231
 - for statistical theory, 300
 - symmetry about 90° , 34, 235
- Angular momentum barriers, 41
 - dependent potentials, 355
 - distribution, 27, 270, 274
 - limiting, 573
 - window, 481, 604, 676
- Annihilation, 19
- Anomalous dispersion, 151
- Antisymmetrization
 - in heavy ion reactions, 613
 - and projection operators, 195
 - and Schrödinger equation, 206
 - in transfer reactions, 466
- Argand diagram, 873
- Asymmetric rigid rotator, 519
- Atoms, kaonic and pionic, 17
- Autocorrelation, 252
- Average cross sections, 337
 - S -matrix, 186
- Averaging, 175
 - Box, 176
 - Lorentzian, 176
- Axial vector current, 62
- Barriers, 41, 244
- Baryons, 861
 - baryon number, 6
- BBGKY hierarchy, 648
- Bessel functions, 915
- Bethe–Goldstone equation, 95, 377
- Blair’s phase rule, 412
- Bloch, Mahaux, Weidenmüller reaction
 - theory, 226
- Bohr independence hypothesis, 24, 29, 305
- Born approximation, 47
- Bose statistics, 65
- Boundary condition model, 226
- Box average, 176

Note: Italicized numbers indicate more detailed discussion of the subject.

- Breit kinematics, 129, 743
- Breit–Wigner formula, 164, 618
- Brink kinematic conditions, 603
- Brueckner–Hartree–Fock approximations, 343, 443
- Capture, radiative, 19
- $^{12}\text{C} + ^{12}\text{C}$ level density, 624
 - resonances, 241, 613, 628
 - and superdeformation, 627
- $^{12}\text{C} + ^{16}\text{O}$ resonances, 613
- Cascading, 795
- Center-of-mass correlation, 121
- Center-of-mass frame, 8
- Central collisions, 767, 781
- Central limit theorem, 251
- Chaining, 526
- Channel coupling, 232, 511
- Channels, closed and open, 157
- Charge exchange reactions, 396
 - double pion induced DCX, 16, 804
 - kaon induced, 869
 - single pion induced SCX, 16, 804
- Classical differential cross section, 561
- Closest approach, 561
- Cluster transfer, 571, 607
- Clutching model, 667
- Coherence energy, 256
- Complexity, 524
 - theorem, 65, 233
- Compound elastic scattering, 313, 320
- Compound nucleus, 6, 45
 - reactions, 24, 338, 579
 - resonance, 23, 38, 164, 618
- Configuration mixing, 722
- Conservation
 - baryon number, 6
 - charge, 6
 - current, 345
 - hypercharge, 7, 861
 - isospin, 7
 - lepton number, 7
 - nucleons, 6
 - in TDHF, 660
- Continued fraction, 835
- Continuity, equation of, 651
- Correlations, 6, 81
 - center-of-mass, 121
 - in fluctuation cross section, 252
 - for inelastic scattering, 433
 - in nucleon-nucleus scattering, 145
 - pair, 71, 76
 - Pauli, 122
 - third order, 73
 - two proton, 783
- Coulomb barrier, 41
 - excitation, 49, 555
 - parameter, 41, 243, 561, 595
- Coulomb scattering, classical, 560
 - cross section, 690
 - electrons, 688
 - polarization, 690
 - $m/E \rightarrow 0$, 691
- Coulomb wave function, for electrons, 689
 - eikonal, 692
 - non-relativistic, 914
 - partial wave expansion, 914
- Coupled channels, 509
 - applications, 517, 759
 - Born approximation (CCBA), 34, 522
- CP violation, 862
- Cross section, 907, 917
- Cusps, 245
- Deep inelastic collision, 22, 566, 588
 - diffusion theory, 633
 - orbiting, 593
 - strong focusing, 591
- Deflection angle, 565
- Deformation, 575
- Deformed nucleus, scattering by, 417, 518, 706
- Density, 67, 69, 377
 - charge density, 700, 704, 713
 - neutron density, 745, 887
- Density matrix, 199, 377
 - eigenvalues of, 201
 - in second quantization, 222
- Density of particle-hole states, 542
- Depolarization, 301, 920
- Deuteron-nucleus interaction
 - adiabatic approximation, 496
 - coupled equations, 497
 - optical model, 488
 - three-body model, 494
 - Watanabe potential, 496
- Differential cross section, classical, 561
- Diffraction, 109
 - Fraunhofer, 562
 - Fresnel, 562
 - in inelastic scattering, 414
- Diffusion theory for heavy ion collision, 633
 - cross section, 639
 - Fokker–Planck equation, 637
 - mass asymmetry, 641
- Dirac equation, 388, 685, 751
- Direct reactions, 22, 67. *See also* Distorted wave approximation

- effect on statistical theory of reactions, 314
- and specificity, 40
- Dispersion relationship, 160, 910
 - correction, 688
 - in infinite nuclear matter, 349
- Distorted wave approximation (DWA), 23
 - exchange effects, 429
 - and heavy ion reactions, 613
 - higher order, 509
 - and inelastic scattering, 422, 758
 - strong absorption limit, 427
 - for transfer reactions, 463
- Distribution function, 644
 - Liouville's theorem, 646
- Doorway states, 179
 - effect of direct coupling, 187
 - effect on fine structure, 192
 - exit, 190
 - in heavy ion resonances, 619
 - in hypernuclei, 899
 - hypothesis, 180
 - in nucleon-nucleus scattering, 365
 - in pion induced reactions, 58, 833
 - strong assumption, 184
 - Δ -hole state, 803
- Double charge exchange (DCX), 852
 - sequential, 857
- (d, p) reaction, 458. *See also* Transfer reactions
 - polarization and analyzing power, 483
- Dynamic deformation model, 519
- Edge effect in averaging, 177
- ($e, e'N$), 734
- Effective range, 477, 912
 - volume for s -wave, 913
- Eigenvalues of the density matrix, 201
 - of the reactance matrix, 170
- Eikonal, *see* Semi-classical approximation
- Elastic scattering, 11, 333
 - adiabatic approximation, 78
 - amplitude, 75, 79
 - angular distribution, 358
 - energy average, 172
 - phase shift analysis, 357, 913
 - polarization, 359
 - spin rotation, 360
- Electric dipole resonance, 3. *See also* Doorway states
- Electron excitation, 46
- Electron scattering, 684
 - Coulomb, 688
 - current induced, 714, 708
 - by deformed nuclei, 706
 - effect of finite nuclear size, 690
 - magnetic elastic, 720
 - by ^{206}Pb and ^{205}Tl , 704
 - quasi-elastic, 724
 - by spin-0 nuclei, 685
- Elongation, 575
- EMC effect, 739, 885
- Endoergic, 10
- Energy average
 - box, Lorentzian, 176
 - edge effect, 177
 - and optical model, 174, 184
- Energy-dependent potential, 99, 340
- Energy resolution, 2
- Energy transfer, 11, 684
- Equilibrium, 27
- Ericson fluctuations, 250, 298, 614
- Escape width, 38, 182
- Evaporation, 27
 - angular distribution, 301
 - energy spectrum, 325
- Exchange current and charge, 680, 719
- Exchange effects in the DWA, 429
- Exchange folding potential, 378
- Exchange scattering, 197
- Exclusive cross-section, 734
- Exit doorways, 190
- Extra push, 575
- Fermi β -ray matrix element, 62
 - gas model, 13
 - for optical model potential, 351
 - momentum, 13
 - motion, 124
- Fine structure
 - effect of doorway states, 191
 - effect of single particle resonance, 192
- Finite range deviations, 257
- Finite size effects in (t, p) reactions, 607
- Fission, 575
 - fast, 572
- Fluctuations, 23, 250, 303, 337
 - autocorrelations in, 252
 - Ericson, 250
 - in level density, 269
 - probability distribution, 251
- Fokker-Planck diffusion equation, 637
- Folding potential, 86, 375
 - direct and exchange, 378
- Formalism invariance, 209
- Form factor, 48, 102, 695
 - elastic, 48
 - inelastic, 102
 - nucleon, 695

- Fragmentation, 21, 767
 - limiting, 798
 - momentum distribution, 771
- Frame center-of-mass, 8
 - laboratory, 7
- Fraunhofer diffraction, 562
- Fresnel diffraction, 562
- Friction model, 597
- Frozen nucleus, 76, 92
- Fusion, 568, 570
 - incomplete, 571
 - sub-barrier, 587
- Gamow solutions, 220
- Gamow–Teller β -ray matrix element, 62
- Gauge invariance, 719
- Gaussian orthogonal ensemble, 287
- Geramb–Bauhoff interaction, 447
- Giant resonances, 179. *See also* Doorway states
- Glauber approximation, 111, 759
- G -matrix, 443
- Grazing, 561, 624
- Hauser–Feshbach theory, 309, 319, 579, 616
- Heat flux, 652
- Heavy ions, 55, 554
 - and level density, 624
 - relativistic, 767
 - resonances, 613
 - super deformation, 627
 - ultra-relativistic, 787
- Heavy particle stripping, 431
- Helicity coupling scheme, 232
- Hypercharge, 7, 860. *See also* strangeness
 - exchange, 16, 805
- Hypernucleus, 16, 59
 - Λ , 805, 893
 - Σ , 805, 904
 - $^{13}_{\Lambda}\text{C}$, 901,
 - magic momentum, 895
 - single particle states, 904
 - weak coupling, 904
- Hyperons, 861
- Impact parameter, 107, 409, 561
- Inclusive cross-section, 14
- Incomplete fusion, 571
- Independent particle model, level density, 263
- Inelastic scattering, 12, 407, 756
 - adiabatic approximation, 419
 - Blair phase-rule, 412, 417
 - by deformed nuclei, 418
 - diffractive, 414
 - DWA, 422
 - eikonal approximation, 409
 - exchange effects, 429
 - interaction potentials, 436
 - multiple scattering, 80
 - pion-nucleus, 840
 - surface reaction, 408
 - vibrational nuclei, 417
- Infinite nuclear matter, 343, 346, 444
- Interacting Boson model, 519
- Interaction potentials, 436
 - G -matrix method, 443
 - $M3Y$, 436
 - multipole series, 513
 - and saturation, 437
- Interaction time, 22, 36, 256, 507, 596
 - intermediate, 31
 - and kinetic energy loss, 602
 - and number of stages, 636
- Interference between resonance and prompt
 - amplitude, 235
- Intermediate energy reactions
 - $E < 100$ MeV, 371
 - $100 \text{ MeV} < E < 200$ MeV, 381
 - > 200 MeV, 382
- Intermediate interaction time, 31
- Intermediate structure, 36, 179. *See also* Doorway states
- Internuclear cascade, 781
 - angular distribution, 783
 - correlations, 783
- Intruder states, 283
- Isobar analog resonances, 397, 460, 852
- Isospin
 - conservation, 7
 - distribution, 276
 - extension of the optical model, 397
 - projection operators, 805
 - symmetry, 63, 64, 806
- Kaon, 859
 - CP symmetry, 862
 - K_L , 864
 - K_S , 865
 - regeneration, 864
 - weak decay, 863
- Kaon-nucleon interaction, 865
 - charge exchange, 869
 - \mathcal{K} -matrix analysis, 877
 - KN , 866, 868
 - $\bar{K}N$, 877
 - K^+p angular distribution, 872
 - scattering length, 872

- Kaon-nucleus interaction
 - inelastic scattering, 887
 - K^+ -nucleus scattering, 884
 - K^- -nucleus scattering, 889
 - "magic momentum", 895
 - optical potential, 885
- Kapur and Peierls theory of reactions, 213
- Kawai, Kerman, and McVoy theory, 250, 299, 316
- Kinematic conditions, Brink, 603
- Kinematics, 6
 - relativistic, 125
- Kisslinger potential, 822
- KMT method for multiple scattering, 90, 740
- Knock on, 431
- Lanczos method, 834
- Lane optical model, 399
- Level density, 25, 260
 - angular momentum distribution, 27, 270, 280
 - for $^{12}\text{C} + ^{12}\text{C}$ system, 624
 - effect of residual interaction, 279
 - fluctuations, 269
 - for independent particle model, 263
 - isospin distribution, 276
 - odd-even effect, 279
 - of particle-hole states, 542
 - for rotational nuclei, 275
- Liouville's theorem, 646
- Lippman-Schwinger equation, 906
- Local density approximation, 383, 390, 451
- Longitudinal cross section, 727
- Lorentz, Boltzmann equation, 648
- Lorentz, Boltzmann, Uhlenbeck, and Uehling method (LBUU), 644
 - applications, 655
- Lorentzian average, 176
- Lorentz transformation, 787
- Lorenz-Lorentz effect, 823
- Low-energy scattering, 360
- Magnetic elastic electron scattering, 720
 - by ^{25}Mg , 722
 - by ^{17}O , 721
- Magnetic moment, Coulomb interaction, 695, 744
- Magnetization current, 718
- Mahaux and Weidenmüller theory of reactions, 226
- Many-body forces, 283
- Mass asymmetry, 641
- Mass, effective, 13, 343
- $M3Y$ interaction potential, 438
- Mean free path, 86
- Microscopic theory of reactions, 227
- Mixing, external, 402
- Model independence, 697
- Momentum-dependent potential, 340
 - matching, 482
 - tensor, 785
- Momentum transfer, 11
 - longitudinal, 774
 - transverse, 775
 - zero, 59
- Mott cross section, 688
- Multichannel optical model, 333, 509
- Multiple scattering, 74
 - elastic scattering, 84, 96
 - formal theory, 90
 - inelastic scattering, 102
 - kinematics, 125
 - spin-dependence, 100
- Multiplicity, γ -ray, 577
 - in proton-proton collisions, 792
- Multipole excitations, 709
- Multipole series for interaction potential, 513
- Multistep compound reactions, 506, 534
 - applications, 548
 - chaining, 526
 - cross section, 539
 - and heavy ions, 570, 657
 - isospin conservation, 63
 - random phase approximation, 527
- Multistep direct reactions, 29, 505, 509, 528
 - applications, 544
 - cross section, 533
 - and heavy ions, 55, 570, 657
- Neutron density, 141, 745
 - form factor, 697
 - resonance, 240
- Nonlocal potentials, 99, 339, 353
- Nonorthogonality, 346
 - in transfer reactions, 471
- Nuclear reactions
 - angular distribution, 231
 - complexity, 233
 - elastic, 333
 - formal theory, 149
 - inelastic, 407
 - multistep, 505
 - parity conservation, 233
 - statistical theory, 297
 - transfer, 455
- Nucleon-nucleon transition matrix, 743
- Optical model
 - angular momentum-dependent, 355
 - derivation, 172

- Optical model (*Continued*)
 deuteron-nucleus, 488
 energy-dependence, 99, 340
 folding model, 86, 375
 imaginary part, 350, 353
 isospin extension, 397
 momentum dependence, 340
 multichannel, 333
 multiple scattering, 84, 96
 nucleon-nucleus, 333
 Perey-Buck, 372
 pion-nucleus, 825, 851
 relativistic, 387
 single-channel, 336
 surface absorption, 365
 Woods-Saxon, 356
 Optical theorem, 337, 909
 Optics, physical, 56
 Optimal approximation, 142
 Orthogonality, 429, 465
 Over completeness, 198
 Overlap, 188, 466, 482
 Overlapping resonances, 164, 211, 248
- Pair correlation, 71, 76
 Pair production in heavy ion collisions, 558
 Parity conservation, 233
 Particle-hole states, density of, 542
 excitations, 444
 Particle transfer, 17. *See also* Transfer reactions
 Partition sum, 261
 Pauli principle, 117, 195, 737
 correlations, 121
 in heavy ion collisions, 656
 in hypernuclei, 61
 and optical model, 351
 in transfer reactions, 467
 Perey-Buck potential, 372
 Perey effect, 346, 486
 Peripheral collisions, 767
 momentum distribution, 771
 Phase shift analysis, 357, 912
 angular distribution, 357
 cross section, 359
 polarization, 359
 spin rotation, 360
s-wave effective range, 912
 Phase space, 645
 Physical optics, 56
 Pickup, 17, 523. *See also* Transfer reactions
 Pion, 16, 58, 806
 Pion-nucleon system, 806
 isospin symmetry, 806
 scattering, 809
 scattering amplitude, 818
 scattering length, 810
 scattering volume, 810
 Pion-nucleus system, 818
 absorption, 830
 doorway state, 833
 inelastic scattering, 840
 Kisslinger potential, 822
 Lorentz-Lorenz effect, 823
 optical model, 825, 851
 rescattering, 831
 resonance region, 826
 single and double charge exchange, 848
 Poisson distribution of energy level spacing, 287
 Polarization in (*d*, *p*) reaction, 458, 482
 in elastic scattering, 359
 in nucleon-nucleus scattering, 747, 763
 Schwinger scattering, 400
 in statistical theory of reactions, 301
 Porter-Thomas distribution of widths, 294, 302
 Post-prior representation, 473
 Potentials, local and nonlocal, 99, 339
 angular momentum-dependent, 355
 energy and momentum-dependent, 340
 scalar, vector and tensor, 752
 surface absorption, 365
 Potential scattering, *see* Prompt amplitude
 Precompound reactions, 506, 526, 572
 Pre-equilibrium, *see* Precompound reactions
 Pressure tensor, 652
 Profile function, 116
 Projection operators
 and antisymmetrization, 195
 for transfer reactions, 469
 Prompt amplitude, 195, 236
 interference with resonance, 235
 separation from fluctuating amplitude, 250
 Proton-⁴He elastic scattering, 132, 755
 Proton-nucleus scattering, high energy, 682, 740
 induced reactions, 759
 polarization, 747
 ultra-relativistic collisions, 782
 Proton-proton collisions at ultra-relativistic energies, 792
 (*p*, 2*p*), 764
 Pseudo rapidity, 791
- Quantum chromodynamics, 861
 Quantum transport, 653
 Quark-gluon plasma, 801
 Quarks, 860

- Quasi-elastic scattering, 134, 566, 591, 680
 - for electrons, 724
 - for heavy ions, 602
 - longitudinal and transverse cross sections, 727
 - ($p, 2p$), 764
 - scaling, 727
- Q -value, 10
- window, 605

- Radiative tail, 681
- Radii, nuclear, rms from electron scattering, 699, 705
- Random phase hypothesis
 - for multistep reactions, 527
 - for statistical theory of reactions, 298
- Rapidity, 788
- Reactance matrix, 169, 909
 - eigenvalues of, 170
 - and the S -matrix, 170, 210
- Reaction formalisms
 - Bloch, Mahaux, and Weidenmüller, 224
 - boundary condition model, 226
 - formal theory, 149
 - invariance of, 209
 - Kapur and Peierls, 213
 - microscopic theory, 221
 - \mathcal{R} -matrix, 215, 229
 - \mathcal{A} -matrix, 219
 - statistical theory, 231
- Reaction probability/time, 907
- Reactions, angular distribution, 231
- Reference level, 279
- Regeneration, 865
- Relativistic heavy ions, 767
 - central collision, 781
 - peripheral collisions, 767
- Relativistic impulse approximation, 751
- Relativistic optical model, 387, 752
- Rescattering, 831
- Resonances
 - compound nucleus, 161, 231
 - doorway state, 179
 - giant, 179
 - heavy ion, 241, 613
 - interference with the prompt amplitude, 235
 - isolated, 234
 - overlapping, 248
 - single particle, 192
 - width, 156, 163
 - Δ -hole, 803
- Resonance scattering of light by atoms, 151
- Response functions, 726, 730, 735, 766
- \mathcal{R} -matrix theory, 215
- Rotational nuclei, level density for, 275
 - inelastic scattering by, 417, 518
- RPA, 658

- Saddle point, in fission, 575
- Saturation, 437
- Scaling, 727
- Scattering
 - deuteron, 488
 - elastic, 333
 - electron, 684
 - inelastic, 407, 756
 - intermediate energies, 371
 - low energy, 360
 - pion, 825, 851
 - proton, 132, 333, 682, 740, 755, 788
- Scattering amplitude, 908
- Scattering length, 361, 810
 - dependence on potential strength, 880
 - volume 810
- Schwinger polarization scattering, 400
- Selection rules and symmetry, 34
- Semi-classical approximation, 103
 - elastic scattering, 107
 - in heavy ion reactions, 613
- Semi-infinite slabs, collision of, 664
- Sharp cutoff model, 583
- Single charge exchange (SCX), 16, 804
- Single channel optical model, 336, 911
- Single-channel scattering, 907
- Single-particle resonance
 - effect on fine structure, 192
 - states in hypernuclei, 904
- Single-step reactions, 22, 31
 - for transfer reactions, 464
- S -matrix, 164, 167, 209, 908
 - average, 186
 - for non-Hermitian Hamiltonian, 910
 - and the reactance matrix, 170
- S -matrix reaction theory, 219
- Source term method, 523
- Space-time symmetries, 7
- Spacing of energy levels, 286
 - Poisson distribution, 287
 - Wigner distribution, 287
 - Wishart distribution, 292
- Specificity and direct reactions, 40
 - and symmetry, 61
 - and transfer reactions, 455
- Spectator, 74
 - approximation in transfer reactions, 476
 - in heavy ion collisions, 657
- Spectroscopic factor, 53, 460, 479, 737
- Spin cutoff, 274, 280

- Spin density, 844
- Spin flux tensor, 844
- Spin one, 849
- Spin-orbit coupling scheme, 232, 511
- Spin-orbit interaction, 435
 - Λ -nucleon, 61
 - optical model, 349, 379
- Spin rotation, 360, 395, 747
- Spreading potential, 833
- Spreading width, 38, 182
- Square well, 108
- Static limit in inelastic pion scattering, 843
- Statistical theory of
 - compound nuclear reactions, 24, 296
 - doorway state reactions, 34
 - multistep reactions, 39, 505
- Statistical theory of reactions, 296
 - angular distribution, 300
 - applications, 321
 - effect of direct reactions, 314
 - Hauser–Feshbach theory, 30, 319
 - isotropy, 301
 - polarization, 301
 - random phase hypothesis, 298
- Strangeness, *see also* Hypercharge
 - conservation, 861
 - current, 63
 - exchange of, 805, 893
- Strength function, 189, 362, 369
- Stretched configuration, 720
- Stripping, 17, 52, 463. *See also* Transfer reactions
 - of heavy particles, 431
- Strong focusing angular distribution, 591
- Sub-barrier fusion, 587
- Sum rule, 82
- Superdeformation, 558, 627
- Superfluous states, 198, 204
 - in transfer reactions, 468
- Surface reactions, 50, 455
 - absorption, 58
- $SU(3)$, 64
 - analog states, 64
 - symmetry, 860
- Symmetry and specificity, 61
 - breaking, 64, 400, 862
 - and selection rules, 61
 - space time, 7, 61
- Tassie parametrization, 761
- Temperature, nuclear, 26, 261, 325
 - and excitation energy, 266
 - in heavy ion collisions, 652
- Tensor interaction, 379, 435
- Three-body model, 494
- Three-body forces, 756
- Threshold behavior of cross sections, 242
- Thrust, 786
- Time delay, 22, 165. *See also* Interaction time
- Time-dependent Hartree–Fock (TDHF), 658
 - adiabatic limit, 662
 - clutching model, 667
 - collision of semi-infinite slabs, 664
 - conservation, 660
 - initial conditions, 663
 - two-dimensional frozen approximation, 670
- Time reversal, 7, 920
- Time scale in heavy ion reactions, 573
- \mathcal{T} -matrix, 907
- Transfer reactions, 455
 - antisymmetry, 466
 - applications, 475
 - DWA amplitude, 463
 - overlap, 466, 482
 - three-body model, 494
 - zero range approximation, 485
- Transition axial vector current, 62
 - charge density, 48, 709
 - density, 758
 - multipole moment, 49
 - probability per unit time, 907
 - spin operator, 816
- Transmission factor, 186, 243, 306, 338, 367, 912
- Transverse cross section, 727
- Two-body potential, effective, 376
- Two-body random Hamiltonian ensemble, 287
- Two-body transfer, 17, 455. *See also* Transfer reactions
- Two-dimensional frozen approximation, 670
- Two potential theorem, 165
- Two-step reactions, 505
- Ultra-relativistic energies, 787
- Unitarity, 107, 167
- Vibrational nuclei, inelastic scattering by, 417, 518
- Watanabe potential, 496
- Weizsäcker–Williams method
 - electromagnetic, 49, 557
 - nuclear, 772, 780
- Widths, 242
 - of doorway state, 36
 - effect of fluctuations, 311, 330
 - partial, 163
 - Porter–Thomas distribution, 294
 - of a resonance, 156
 - χ^2 distribution, 286, 296

- Wigner distribution of energy level spacings, 287
 - function, 653
- Wilczyński plot, 592
- Wine-bottle shape, 395
- Wishart distribution of energy level spacings, 292
- Wolfenstein parameters, 133, 743
- Woods–Saxon potential, 356
- Yrast line, 274
- Zero momentum transfer, 895
- Zero range approximation, 485
- Δ , 58, 803
- Δ -hole state, 58, 803, 833
- η meson, 860
- Λ baryon, 860
 - hypernuclei, 905
 - nucleon interaction, 862
 - nucleon spin orbit interaction, 61
 - resonances, 865
- Ξ baryon, 860
- ρ meson, 1
 - change in mass, 885
- Σ baryon, 860
 - hypernuclei, 905
 - resonances, 866

ISBN 0-471-05750-9